Proceedings of 10th International Workshop on Laser Ranging Instrumentation

第十届国际激光测距会议论文集

Compiled and Edited by
Yang Fumin, Chen Wanzhen

Shanghai Observatory , Chinese Academy of Sciences
Shanghai , China
November 11-15,1996
中国科学院上海天文台
中国 上海

10th International Workshop on Laser Ranging Instrumentation, Shanghai, Nov. 11-15 1996

Proceedings of the Tenth International Workshop on Laser Ranging Instrumentation
Shanghai, China
November 11-15, 1996

TABLE OF CONTENTS

Forward

The Tenth International Workshop on Laser Ranging Instrumentation was successfully held in the Convention Center, Chinese Academy of Sciences in Shanghai, China on November 11-15, 1996. This was the first time for the Workshop to be held in Asia.

We are very pleased to have 110 participants from 18 countries to attend the Workshop. We are grateful to the members of the Program Committee, especially to John Luck and Peter Shelus for their many suggestions to the Workshop agenda. Many thanks to Mike Pearlman, John Degnan, Ben Greene, Hiroo Kunimori and all session chairpersons for their valuable supports to the organization of the Workshop.

The agenda of the Workshop is included in the Proceedings. Comparing with the content, you may find some changes: some authors have not submitted their papers, while a few authors prefer to give some new papers. We collect all those good papers in the Proceedings.

A special thank go to the Astronomical Committee, Chinese Academy of Sciences and Chinese Astronomical Society for their financial supports to the Workshop.

Thanks also go to many colleagues of mine for their hard work during the Workshop and the preparation of the Proceedings publication, especially to Chen Wanzhen, Tan Detong, Xiao Chikun, Zhang Zhongping and Liu Nailing.

YANG Fumin

Chairman

10th International Workshop on Laser Ranging Instrumentation

List of Participants of 10th Laser Workshop

Shanghai, November 11-15, 1996

Al-ghamdi, Attieh A
Institute of Astronomy and Geophysics
SALRO
P. O. BOX 6086
Riyadh 11442
SAUDI ARABIA
Tel: 966-1-4813325
Fax: 966-1-4813523
E-mail: alghamdi@kacst.edu.sa

Araki, Shintaro
S & A, Ltd.
8-26-2 Konandai, Konan-ku,
Yokohama 244
JAPAN
Fax: 81-45-881-7364

Balodis, Janis
Institute for Geodesy and Geoinformation
University of Latvia
19 Boulevard Rainis, LV-1586 Riga
LATVIA
E-mail: slr_jb@laima.acad.latnet.lv

Banni, Aldo
Cagliari Astronomica Station
Loc.Poggio dei Pini, Strada 54
09012 Capoterra
ITALY
Tel: 39-70-725246
Fax: 39-70-725425
E-mail: banni@ca.astro.it

Beutler, Gerhard
Astronomical Institute of Berne
Sidlerstrasse 5
CH-3012 Berne
SWITZERLAND
Tel: 41-31-6318591
Fax: 44-31-6313869
E-mail: gurtner@aiub.unibe.ch

Bock, Olivier
I.G.N (National Geographic Institute)
2 avenue Pasteur
94160 Saint Mande,
FRANCE
Tel: 331-43988392
Fax: 331-43988581
E-mail: bock@icare.ign.fr

Burmistrov, Vladimir
Russian Institute of Space Device Eng.
53 Aviamotornaya Street
Moscow 111024
RUSSIA
E-mail: natali@ricimi.msk.su

Carter, David
NASA/ Goddard Space Flight Center
Code 921.0
Greenbelt, MD 20771

USA
Tel: 301-286-6319
Fax: 301-286-0213
E-mail: dcarter@eibl.gsfc.nasa.gov

Chen, Wanzhen
Shanghai Observatory
Chinese Academy of Sciences
80 Nandan Rd, Shanghai   200030
CHINA
Tel: 86-21-64386191
Fax: 86-21-64384618
E-mail: yangfm@center.shao.ac.cn

Chen, Zongping
Geo Forschungs Zentrum (GFZ)
Telegrafenberg A 17
D-14473, Potsdam
GERMANY
E-mail: prd@dfd.dlr.de

Dahl, Leigh
Electro Optic Systems Pty Limited
55A Monaro St. Queanbeyan NSW 2620
AUSTRALIA
Tel: 61 6 299 2470
Fax: 61 6 299 7687
E-mail: eos@netinfo.com.au

Decker, Winfield
AlliedSignal Technical Services Corp.
7515 Mission Drive,
Lanham, MD 20706
USA
Tel: 301-805-3993
Fax: 301-805-3974
E-mail: DeckerW@thorin.atsc.allied.com

Degnan, John J.
NASA/Goddard Space Flight Center
Crustal Dynamic Project Center
Code 920.1
Greenbelt, MD 20771-0001
USA
Tel: 301-286-8470
Fax: 301-286-0213
E-mail: degnan@cddis.gsfc.nasa.gov

Dunn, Peter
Hughes STX Corporation
Suite 400,
7701 Greenbelt Road
Greenbelt, MD 20770
USA
E-mail: pdunn@stx.com

Eanes, Richard
Center for Space Rsearch
University of Texas at Austin
3925 W. Braker Ln, Suite 200
Austin, Texas 78759-5321
USA

Tel: 512-471-4267
Fax: 512-471-3570
E-mail: eanes@utcsr.ae.utexas.edu

Elphick, Mark
Orroral Observatory
Auslig, PO Box 2,
Belconnen ACT 2616,
AUSTRALIA
Tel: 61 6 2357111
Fax: 61 6 2357103
E-mail: markelphic@auslig.gov.au

Fan, Chunbo
Changchun Satellite Observatory
Chinese Academy of Sciences
Jing Yue Tan, Changchun 130117
CHINA
Tel: 86-431-4511337
Fax: 86-431-4513550
E-mail: zhxh@mail.jlu.edu.cn.

Fujita , Masayuki
Ocean Research Laboratory
Hydrographic Department of Japan
5-3-1 Tsukiji, Chuo-ku, Tokyo 104
JAPAN
Tel: 81-3-3541-4387
Fax: 81-3-3541-4387
E-mail: mfuji@cue.jhd.go.jp

Gaignebet, Jean
OCA/CERGA
Avenue Copernic
F 06130-Grasse
FRANCE
Fax: 33-93-40-53-33
E-mail: gaignebet@obs-azur.fr

Gao, Yue
Electro Optic Systems Pty Limited
55A Monaro St. Queanbeyan NSW 2620
AUSTRALIA
Tel: 61 6 299 2470
Fax: 61 6 299 7687
E-mail: eos@netinfo.com.au

Glotov, Vladimir
Russian Space Agency,
Mission Control Center
RUSSIA
Tel: 7-095-513-44-75
Fax: 7-095-274-00-25
E-mail: navserv@mcc.rsa.ru

Gong, Xiangdong
Shanghai Observatory
Chinese Academy of Sciences
80 Nandan Rd, Shanghai   200030
CHINA
Tel: 86-21-64386191
Fax: 86-21-64384618

E-mail: yangfm@center.shao.ac.cn

Greene, Ben
Electro Optic Systems Pty Limited
55A Monaro St. Queanbeyan NSW 2620
AUSTRALIA
Tel: 61 6 299 2470
Fax: 61 6 299 7687
E-mail: eos@netinfo.com.au

Greene, Lyn
Electro Optic Systems Pty Limited
55A Monaro St. Queanbeyan NSW 2620
AUSTRALIA
Tel: 61 6 299 2470
Fax: 61 6 299 7687
E-mail: eos@netinfo.com.au

Gurtner, Werner
Astronomical Institute, University of Berne
Sidlerstrasse 5
CH-3012 Berne
SWITZERLAND
Tel: 41-31-6318591
Fax: 41-31-6313869
E-mail: gurtner@aiub.unibe.ch

Hamal, Karel
Czech Technical University
Brehova 7,
115 19 Prague 1
CZECH REPUBLIC
Tel: 42-2-85762246
Fax: 42-2-85762252
E-mail: prochazk@mbox.cesnet.cz

Hatat, Jean-Louis
OCA/CERGA, LLR Station
Avenue Copernic
F 06130-Grasse
FRANCE
E-mail: hatat@obs-azur.fr

He, Huijuan
Shanghai Institute of Optics and Fine
Mechanics,
Chinese Academy of Sciences
PO Box 8211, Shanghai
CHINA
Tel: 86-21-59534890
Fax: 86-21-59528885

Huang, Chengli
Shanghai Observatory
Chinese Academy of Sciences
80 Nandan Rd, Shanghai   200030
CHINA
Tel: 86-21-64386191
Fax: 86-21-64384618
E-mail: jwj@center.shao.ac.cn

Huang, Li
Shanghai Observatory
Chinese Academy of Sciences
80 Nandan Rd, Shanghai   200030
CHINA
Tel: 86-21-64386191

Fax: 86-21-64384618
E-mail: yangfm@center.shao.ac.cn

Husson, Van
AlliedSignal Technical Services Corporation
7515 Mission Drive, .
Lanham, MD 20706
USA
Tel: 301-805-3981
Fax: 301-805-3974
E-mail: HussonV@thorin.atsc.allied.com

Jackson, Suzanne
Orroral Observatory
Auslig, PO Box 2,
Belconnen ACT 2616,
AUSTRALIA
Tel: 61 6 2357111
Fax: 61 6 2357103
E-mail: suzyj@auslig.gov.au

Jiang, Hu
Shanghai Observatory
Chinese Academy of Sciences
80 Nandan Rd, Shanghai   200030
CHINA
Tel: 86-21-64386191
Fax: 86-21-64384618
E-mail: jh@center.shao.ac.cn

Jin, Honglin
Changchun Satellite Observatory
Chinese Academy of Sciences
Jing Yue Tan, Changchun 130117
CHINA
Tel: 86-431-4511337
Fax: 86-431-4513550
E-mail: zhxh@mail.jlu.edu.cn.

Jin, Wenjing
Shanghai Observatory
Chinese Academy of Sciences
80 Nandan Rd, Shanghai   200030
CHINA
Tel: 86-21-64386191
Fax: 86-21-64384618
E-mail: jwj @center.shao.ac.cn

Kirchner, Georg
Austrian Academy of Sciences
Observatory Lustbuhel
Lustbuhelstr. 46
A-8042 Graz
AUSTRIA
Tel: 43-316-4673-51
Fax: 43-316-462678
E-mail: kirchner@flubiw01.tu-graz.ac.at

Koidl, Franz
Austrian Academy of Sciences
Observatory Lustbuhel
Lustbuhelstr. 46
A-8042 Graz
AUSTRIA
Tel: 43-316-4673-51
Fax: 43-316-462678
E-mail: kirchner@flubiw01.tu-graz.ac.at

Kokurin, Yuri
Lebedev Physical Institute
Leninsky Prospect 53
Moscow 117924
RUSSIA
Tel: 007-095-132-0729
Fax: 007-095-938-2551
E-mail: kokurin@fian.crimea.ua

Kolbl, Josef
Electro Optic Systems GmbH
Hermann-Gcib-Strasse 18
D-93053 Regensburg
GERMANY
Fax: 49 9 41 781222

Kunimori, Hiroo
Communications Research Laboratory
4-2-1 Nukuikita
Koganei, Tokyo 184
JAPAN
Tel: 81-423-27-7565
Fax: 81-423-27-6664
E-mail: kuni@crl.go.jp

Liang, Ersheng
Changchun Satellite Observatory
Chinese Academy of Sciences
Jing Yue Tan, Changchun 130117
CHINA
Tel: 86-0431-4511337
Fax: 86-0431-4513550
E-mail: zhxh@mail.jlu.edu.cn

Lin, Qinchang
Guangzhou Satellite Station
Chinese Academy of Sciences,
Wushan, Guangzhou, 510640
CHINA
Tel: 86-020-87707002
E-mail: gzgsos@public.guangzhou.gd.cn

Liu, Nailing
Chinese Academy of Surveying and
Mapping
16 Beitaiping Rd, Beijing 100039
CHINA
Tel: 86-010-682122777-255
Fax: 86-010-68218654
E-mail: wangtq@sun.ihep.ac.cn

Liu, Zhi
Changchun Satellite Observatory
Chinese Academy of Sciences
Jing Yue Tan, Changchun 130117
CHINA
Tel: 86-0431-4511337
Fax: 86-0431-4513550
E-mail: zhxh@mail.jlu.edu.cn

Luceri, Vincenza
Nuova Telespazio S.p.A.
Centro di Geodesia Spaziale
PO Box 155
75100 Matera
ITALY

Tel: 39-835-377231
Fax: 39-835-334951
E-mail: luceri@asimt0.mt.asi.it

Luck, John
Orroral Observatory
Auslig
PO Box 2, Belconnen ACT 2616,
AUSTRALIA
Tel: 61 6 235-7111
Fax: 61 6 235-7103
E-mail: johnluck@auslig.gov.au
        orroral@auslig.gov.au

Maberry, Michael
Observatory Foreman
Lure Observatory, University of Hawaii
PO Box 209
Kula, Hawaii 96790
USA
E-mail: mike@lure.ifa.hawaii.edu

Mangin, Jean
OCA/CERGA, LLR Station
Avenue Copernic
F 06130-Grasse
FRANCE
Fax: 33-93 40 53 33
E-mail: mangin@obs-azur.fr

Maurice, Laplanche
OCA/CERGA
Avenue Copernic
F 06130-Grasse
FRANCE
Fax: 33-93 40 53 33

Mcgarry, Jan
NASA/ Goddard Space Flight Center
Crustal Dynamic Project Center
Code 920.1, NASA
Greenbelt, MD 20771-0001
USA
Tel: 01-301-286-5020
Fax: 01-301-286-0213
E-mail: mcgarry@cddis.gsfc.nasa.gov

Moore, Christopher
Electro Optic Systems Pty Limited
55A Monaro St. Queanbeyan NSW 2620
AUSTRALIA
Tel: 61 6 299 2470
Fax: 61 6 299 7687
E-mail: eos@netinfo.com.au

Morozov, Sergey
Space system Control Office
Russian Space Agency
42, Schepkin st.
Moscow 129090
RUSSIA
Tel: 095 975 4585
Fax: 095 251 8702

Murata, Masaaki
National Aerospace Laboratory
7-44-1 Jindaiji-Higashi

Chifu, Tokyo 182
JAPAN
Tel: 81-422-47-5911(ext.2527)
Fax: 81-422-42-0566
E-mail: murata@nal.go.jp

Murdoch, Alan
AlliedSignal Technical Services Corp.
7515 Mission Drive,
Lanham, MD 20706
USA
Tel: 301-805-3993
Fax: 301-805-3974
E-mail: MurdocA@thorin.atsc.allied.com

Mureddu, Leonardo
Cagliari Astronomica Station
Loc.Poggio dei Pini, Strada 54
09012 Capoterra
ITALY
Tel: 39-70-725246
Fax: 39-70-725425
E-mail: mureddu@ca.astro.it

Neubert, Reinhart
Geo Forschungs Zentrum (GFZ)
Telegrafenberg A 17
D-14473, Potsdam
GERMANY
Tel: 49-331-288-1153
Fax: 49-331-288-1111
E-mail: neub@gfz-potsdam.de

O'Gara, Daniel
Project Manager
Lure Observatory, University of Hawaii
PO Box 209
Kula, Hawaii 96790
USA
Tel: 808 878 1217
Fax: 808 878 2852
E-mail: ogara@lure.ifa.hawaii.edu

Offierski, Jacek W.
Delft University of Technology
Faculty of Geodetic Engineering
Satellite Geodesy Group
Thijsseweg 11
2629 JA DELFT
THE NETHERLANDS
Tel: 31-152785277
Fax: 31-152783711
E-mail: joffi@geo.tudelft.nl

Otsubo, Toshimichi
Communications Research Laboratory
4-2-1 Nukui-kita,
Koganei, Tokyo 184
JAPAN
Tel:
Fax: 81-423-27-7933
E-mail: otsubo@crl.go.jp

Paradiso, Michele
Nuova Telespazio S.p.A.
Centro di Geodesia Spaziale
PO Box 155

75100 Materra
ITALY
Tel: 39-835-377290
Fax: 39-835-334951
E-mail: paradiso@asimt0.mt.asi.it

Paris, J.
OCA/CERGA
Avenue Copernic
F 06130-Grasse
FRANCE

Parkhomenko, Natalia
Russian Institute of Space Device
Engineering
53 Aviamotornaya Street
Moscow 111024
E-mail: natali@ricimi.msk.su
RUSSIA

Paunonen, Matti
Finnish Geodetic Institute
Geodeetinrinne 2
FIN - 02431 Masala
FINLAND
Tel: 358-9-264994
Fax: 358-9-264995
E-mail: geodeet@csc.fi

Pavlis, Erricos
NASA/Goddard Space Flight Center
Space Geodesy Branch,
Code 926
Greenbelt, MD 20771-0001
USA
Tel: 301-286-4880
Fax: 301-286-1760
E-mail: epavlis@helmert.gsfc.nasa.gov

Pearlman, Michael R
Harvard-Smithsonian
Center for Astrophysics
60 Garden Street
Cambridge, MA 02138
USA
Tel: 617-495-7481
Fax: 617-495-7105
E-mail: pearlman@cfa.harvard.edu

Pen, Bibo
Institute of Geodesy and Geophysics,
Chinese Academy of Sciences
54 Xudong Rd, Wuhan 430077
CHINA
Tel: 86-27-6813841
Fax: 86-27-6813841
E-mail: bobby@asch.whigg.ac.cn

Pham Van, Jacqueline
OCA/CERGA, LLR Station
Avenue Copernic
F 06130-Grasse
FRANCE
Fax: 33-93 40 53 33
E-mail: phamvan@ocar01.obs-azur.fr

Pierron, Francis
OCA/CERGA
Avenue Copernic
F 06130-Grasse
FRANCE
E-mail: pierron@obs-azur.fr

Pop, Eugen
Astronomical Institute of Berne
Sidlerstrasse 5
CH-3012 Berne
SWITZERLAND
Tel: 41-31-6318591
Fax: 44-31-6313869
E-mail: gurtner@aiub.unibe.ch

Prochazka, Ivan
Czech Technical University
Brehova 7
115 19 Prague 1
CZECH REPUBLIC
Tel: 42-2-85762246
Fax: 42-2-85762252
E-mail: prochazk@mbox.cesnet.cz

Qu, Feng
Chinese Academy of Surveying and
Mapping
16 Beitaiping Rd, Beijing 100039
CHINA
Tel: 86-10-68212277-255
Fax: 86-10-68218654
E-mail: wangtq@sun.ihep.ac.cn

Schiavone, Franco
Nuova Telespazio S.p.A.
Centro di Geodesia Spaziale
PO Box 155
75100 Matera
ITALY
Tel: 39-835-377230
Fax: 39-835-334951
E-mail: laser@asimt0.mt.asi.it

Schillak, Stanislaw
Space Research Centre
Polish Academy of Sciences
Astrogeodynamical Observatory
Borowiec, ul. Drapalka 4
Kornik ,62-035
POLAND
Tel: 48-61-170187
Fax: 48-61-170219
E-mail: sch@cbk.poznan.pl
        laser@cbk.poznan.pl

Schreiber, Ulrich
Technische Universitaet Muenchen
Fundamentalstation Wettzell
D-93444 Koetzting
GERMANY
Tel: 49- 9941 603-113
Fax: 49- 9941 603-222
E-mail: schreiber@wettzell.ifag.de

Seemueller, Wolfgang
DGFI, Abt.I

Marstallplatz 8
D-80539 Munchen
GERMANY
Tel: 49- 9941 603-113
Fax: 49- 9941 603-222
E-mail: seemueller@dgfi.badw-
        muenchen.de

Selden, Mike
AlliedSignal Technical Services Corp.
7515 Mission Drive,
Lanham, MD 20706
USA
Tel: 301-805-3993
Fax: 301-805-3974
E-mail: SeldenM@thorin.atsc.allied.com

Shargorodski, Vladimir
Secretary of Russian Representation of
WPLTN
53 Aviamotornaya Street
Moscow 111250
RUSSIA
E-mail: vladimir@vshar.msk.ru

Shargorodsky, Victor
Russian Institute of Space Device Eng.
53 Aviamotornaya Street
Moscow 111250
RUSSIA
Tel: 095 273 3344
Fax: 095 273 4535
E-mail: natali@ricimi.msk.su

Shelus, Peter
McDonald Obsevatory
Dept of Astronomy
University of Texas-Austin
Austin TX 78712
USA
E-mail: pjs@astro.as.utexas.edu

Sinclair, Andrew
Royal Greenwich Observatory
Madingley Road
Cambridge CB3 0EZ
UK
Fax: 44-1223-374700
E-mail: ats@ast.cam.ac.uk

Sperber, Peter
Institute for Applied Geodesy
Fundamentalstation Wettzell
D-93444 Koetzting
GERMANY
Tel: 49 9941 603205
Fax: 49 9941 603222
E-mail: sperber@wettzell.ifag.de

Sun, Zhanao
Shanghai Institute of Optics and Fine
Mechanics, Chinese Academy of Sciences
PO Box 8211, Shanghai
CHINA
Tel: 86-021-59534890
Fax: 86-021-59528885

Suzaki, Yasuji
Telecommunications Division Hitachi, Ltd.
216 Totsuka-cho, Totsuka-ku
Yokohama 244
JAPAN
Fax: · 81-45-881-7364

Tan, Detong
Shanghai Observatory
Chinese Academy of Sciences
80 Nandan Rd, Shanghai 200030
CHINA
Tel: 86-21-64386191
Fax: 86-21-64384618
E-mail: tdt@center.shao.ac.cn

Tawadros, Maher Y.
Helwan Institute of Astronomy and
Geophysics,
el Marsed street, Helwan, Cairo
EGYPT
Tel: 002 02 782683
Fax: 002 02 782683
E-mail: satellite2@frcu.eun.eg

Titterton, Paul
EOO, Inc
269 North Mathilda Ave
P.O. Box 60339
Sunnyvale, CA 94086
USA
Tel: 408-738-5390
Fax: 408-738-5399
E-mail: eooinc@aol.com

Torre, Jean-Marie
OCA/CERGA, LLR Station
Avenue Copernic
F 06130-Grasse
FRANCE
E-mail: torre@ocar-azur.fr

Van der Kraan, Rien
TNO Institute of Applied Physics(TPD)
PO Box 155 , 2600 AD Delft
THE NETHERLANDS
Tel: 31 15 2692000
Fax: 31 15 2692111

Van Loon, Danny
Delft University of Technology
Kootwijk Observatory for Satellite Geodesy
Thijsseweg 11
2629 JA DELFT
THE NETHERLANDS
Tel: 31 15 2788137
Fax: 31-15 2782526
E-mail: vanloon@geo.tudelft.nl

Varghese, Tom
AlliedSignal Technical Services Corp.
7515 Mission Drive,
Lanham, MD 20706
USA
Tel: 301-805-3993
Fax: 301-805-3974
E-mail: VargheT@thorin.atsc.allied.com

Vassilev, Vladimir
Russian Institute of Space Device
Engineering
53 Aviamotornaya Street
Moscow 111024
RUSSIA
Tel: 095 2732911
E-mail: natali@ricim.msk.su

Visser, Huib
TNO Institute of Applied Physics(TPD)
PO Box 155, 2600 AD Delft
THE NETHERLANDS
Tel: 31 15 2692000
Fax: 31 15 2692111

Wang , Yanjie
Electro Optic Systems Pty Limited
55A Monaro St. Queanbeyan NSW 2620
AUSTRALIA
Tel: 61 6 299 2470
Fax: 61 6 299 7687
E-mail: eos@netinfo.com.au

Wang, Tanqiang
Chinese Academy of Surveying and
Mapping
16 Beitaiping Rd, Beijing 100039
CHINA
Tel: 86-10-68212277-255
Fax: 86-10-68218654
E-mail: wangtq@sun.ihep.ac.cn

Wang, Wu
Yunnan Observatory,
Chinese Academy of Sciences
Kunming 650011
CHINA
Tel: 86-871-3911347
Fax: 86-871-3911845
E-mail: yozsx@public.km.yn.cn

West, Owen
School of Surveying and Land Information
Curtin University of Technology
GPO Box U 1987
Perth 6001
West AUSTRALIA
Fax: 61 9 257 1892

Wetzel, Scott
AlliedSignal Technical Services Corp.
7515 Mission Drive,
Lanham, MD 20706
USA
Tel: 301-805-3993
Fax: 301-805-3974
E-mail: WetzelS@thorin.atsc.allied.com

Wood, Roger
NERC Satellite Laser Ranger Facility,
Herstmonceux Castle Hailsham
East Sussex BN27 1RP

UK
Tel: 44 (01323) 833888
Fax: 44 (01323) 833929
E-mail: rw@gxvf.rgo.ac.uk

Wu, Jie
National University of Defense Technology
303 Changsha, Hunan province, 410073
CHINA
Tel: 86-731-4516759

Xia, Zhizhong
Institute of Seismology,
State Seismological Bureau
Xiao Hong Shan, Wuhan 430071
CHINA
Tel: 86- 27-7863456
Fax: 86- 27-7884662
E-mail: hbwh@public.sta.net.cn

Xiao, Chikun
Shanghai Observatory
Chinese Academy of Sciences
80 Nandan Rd, Shanghai   200030
CHINA
Tel: 86-21-64386191
Fax: 86-21-64384618
E-mail: yangfm@center.shao.ac.cn

Xiong, Yaoheng
Yunnan Observatory,
Chinese Academy of Sciences
Kunming 650011
CHINA
Tel: 86-871-3911347
Fax: 86-871-3911845
E-mail: yozsx@public.km.yn.cn

Xu, Yongping
Shanghai Observatory
Chinese Academy of Sciences
80 Nandan Rd, Shanghai   200030
CHINA
Tel: 86-21-64386191
Fax: 86-21-64384618
E-mail: yangfm@center.shao.ac.cn

Yamaguchi, Tetsuro
Denoh System, Ltd.
202 SunCourt Totsuka
167-1 Totsuka-Cho, Totsuka-ku
Yokohama 244
JAPAN
Fax: 81-45-865-7364?

Yan, Haojian
Shanghai Observatory
Chinese Academy of Sciences
80 Nandan Rd, Shanghai   200030
CHINA
Tel: 86-21-64386191
Fax: 86-21-64384618
E-mail: yhj@center.shao.ac.cn

Yang, Fumin
Shanghai Observatory
Chinese Academy of Sciences
80 Nandan Rd, Shanghai   200030
CHINA
Tel: 86-21-64386191
Fax: 86-21-64384618
E-mail: yangfm@center.shao.ac.cn

Ye, Shuhua
Shanghai Observatory
Chinese Academy of Sciences
80 Nandan Rd, Shanghai   200030
CHINA
Tel: 86-21-64386191
Fax: 86-21-64384618
E-mail: ysh@center.shao.ac.cn

Zhang, Yufeng
Xi'an Research Institute of Surveying
and Mapping
1 Middle Yanta Road, Xi'an 710054
CHINA
Tel: 86-29-5534996
Fax: 86-29-5525310

Zhang, Zhongping
Shanghai Observatory
Chinese Academy of Sciences
80 Nandan Rd, Shanghai   200030
CHINA
Tel: 86-21-64386191
Fax: 86-21-64384618
E-mail: zzp@center.shao.ac.cn

Zhao,You
Changchun Satellite Observatory
Chinese Academy of Sciences
Jing Yue Tan, Changchun 130117
CHINA
Tel: 86-431-4511337
Fax: 85-431-4513550
E-mail: zhxh@mail.jlu.edu.cn

Workshop Agenda

TENTH INTERNATIONAL WORKSHOP
ON LASER RANGING INSTRUMENTATION

Sunday, November 10, 1996

9:00-22:00   Registration/Orientation (Hope Hotel)

21:30-23:30   Program Committee/Session Chairperson Meeting

Co-Chairpersons: Yang Fumin, Shanghai Observatory

Michael Pearlman, Harvard/SAO

Monday, November 11

9:00- 9:40   Welcome and Opening

9:40-12:00   Scientific Achievements and Applications

Chairperson: Richard Eanes, UTX/CSR

1. Application of SLR to Temporal Variations of the Gravity Field and Earth Orientation

    R. Eanes, UTX/CSR

2. Science from Lunar Laser Ranging

    P. Shelus, UTX/McDonald Observatory

3. Applications of Accurate SLR Station Positioning

    P. Dunn for the GSFC SLR Analysis Group

4. SLR Contributions to the Mean Gravity Field

    E. Pavlis for the GSFC/DMA Gravity Group

5. Analysis of Non-gravitational Forces on the Etalon Satellites from a 2.5-year Orbital Arc

    G. Appleby, RGO

6. Compact Laser Transponders for Interplanetary Ranging and Time Transfer

    J. Degnan , NASA/GSFC

7. A Wide Angle Airborne Laser Ranging System for Millimeter Accuracy Subsidence

    Measurements   O. Bock, M. Kasser (ESGT), Ch. Thom (IGN), France

8. Lidar System for Emergency Detection and Environmental Monitoring of the City Air

    E. Andruschak, V. Vassiliev, V. Shargorodsky, A. Kozyrev, RISDE, Russia

9. Proposition for a New SLR Methodology Using CW or Long Pulse Lasers (poster)

    M. Kasser (ESGT), Ch. Thom (IGN), France

10. Short Message " Invitation to SLR Stations for Work with a Satellite Equipped with

    Retroreflectors and GPS/GLONASS Receiver" Which Will Be Launched in the Near

    Future. (poster)   V.Vassiliev, V.Shargorodsky, RISDE, Russia

11. Preliminary Report on ADEOS/RIS Laser Tracking Experiments (poster)

    H.Kunimori, T.Goto, H.Nojiri CRL, M.Sawabe, N.Ogawa, M.Maeda NASDA, Japan

13:30-15:30	Station Performance Evaluation
	Chairperson: Michael Pearlman, Harvard/SAO
15:30-15:45	Break
15:45-17:30	Station Performance Evaluation (continued)
	Chairperson: Michael Pearlman, Harvard/SAO
17:45-19:00	Buffet reception
19:10-22:00	Huangpu River Cruise (for volunteers)

Tuesday, November 12

8:30-10:00   **New Fixed Stations**

Chairperson: Hiroo Kunimori, CRL, Japan

1. The New Laser and Astrometric Telescope in Zimmerwald

   W. Gurtner, E. Pop, J. Utzinger, T. Schildknecht, Astronomical Institute, University of Berne, Switzerland, J. Barbe, G.I.E. Telas, Cannes, France

2. The Use of High-Precision Absolute Optic-Electronic Axis-Angular Encoder in SLR System,   Fan Cunbo,et.al Changchun Observatory, China

3. The Matera Laser Ranging Observatory: Current Status

   Giuseppe Bianco (ASI, Center for Space Geodesy, Matera, Italy)

   Michael D. Selden ATSC, USA

4. Keystone SLR System

   Hiroo Kunimori ,Communications Research Laboratory ,

   and Ben Greene, Electro Optic Systems

5. Laser Ranging From The Naval Research Laboratory at the USAF Starfire Optical Range: an Update

   G. Charmaine Gilbreath,   U. S. Naval Research Laboratory   and Mark A. Davis, Alan Murdoch, Scott L. Wetzel, AlliedSignal Technical Services Corporation

6. Upgrading the SLR Station Katsively (poster)

   V.Ignatenko,L.Kokurin,F.Lobanov,N.Sukhanovski,N.Triapitsin

   Lebedev Physical Institute, Russia

7. Status Report of Borowiec SLR, 1994-1996 (poster)

   Stanislaw Schillak, J.Bartoszak, Space Research Center of Polish Academy of Sciences Astrogeodynamical Observatory, Poland

10:00-10:30   **Break**

10:30-12:00   **New Mobile Stations**

Chairperson: Ulrich Schreiber, Wettzell, Germany

1. FTLRS: Report on the Corsica Campaign

   F.Pierron, OCA/CERGA, France

6. A New Generation of Laser Ranging Satellite for Sub-Millimeter Ranging.

   B. Greene (EOS), V. Shargorodsky, M. Fujita, H. Kunimori.

7. The TiPS Mission, Past, Present and Future.

   S. Wetzel and 14 others, ATSC, USA

8. Variations in L1L2-Topex Bias from a Point of View of Spacecraft and Ground Systems

   Peter Dunn (Hughes STX), Tom Varghese(ATSC), USA

9. Brief Report of Calculation of Refined Mathematical Model of the Satellite WPLTN-1-fizeau (poster)   V.Burmistrov,V.Shargorodsky,V.Vassiliev , N.Soyuzova

   Russian Institute of Space Device Engineering

10. Study of Retroreflectors with Two-spot Reflection Pattern at Sloped Light Incidence

    (poster)   V.Burmistrov,V.Shargorodsky,V.Vassiliev,N.Soyuzova

    Russian Institute of Space Device Engineering

11. An Analysis of Polarization Effects in SLR Retroreflectors (poster)

    Kasser, ESGT/CNAM, France

18:00-22:00   **CSTG SLR/LLR Subcommission General Meeting**

        Chairperson: John Degnan, NASA/GSFC

Wednesday, November 13

8:30-10:30   **Detectors and Spectral Filters**

        Chairperson: Georg Kirchner, Graz, Austria

1. The Test Performance of F4129f MCP-PMT at Changchun Station

   Liu Zhi, Zhao You, Zhang Xinghua, Fan Cunbo, China

2. (1) Increasing Satellite Laser Ranging System at Lure Observatory

   Mike Maberry, Lure Observatory, University of Hawaii, USA

   (2) How to Get GPS Data with a 400 mm (16 inch) Telescope.

   Zane, D. O'Gara Lure Observatory, University of Hawaii, USA

3. Advancements to Enhance Satellite Laser Ranging to Satellites with Low Optical Links

   Howard Donovan, Alan Murdoch, Mark Levy, Thomas Oldham, Brion

   Conklin, Bart C Clarke, R.Eichinger, Tom Varghese, (ATSC),

   John Degnan (NASA/GSFC)

4. Receiver and Timing Upgrades at NRL@SOR

   Alan Murdoch et.al   ATSC, USA

5. SPAD Detectors for Ranging with Sub-mm Bias. (two speakers)

   1). Ivan Prochazka, K.Hamal   Czech Technical University

   2). Ben Greene, EOS

6. SPAD Time Walk Compensation.

   G.Kirchner, F. Koidl, Observatory Lustbuhel, Austria

2. Report on the SALRO

   Attieh A Al Ghamdi, Saudi Arabia

3. TIGO Project : Concept, Status, Plans - First Results

   P.Sperber, A.Boer, R.Dassing, H.Hase, W.Schluter, H.Seeger, R.Kilger

   IfAG, Fundamentalstation Wettzell, Germany

4. A Transportable Laser Ranging System in China

   Xia Zhizhong, Institute of Seismology, Wuhan, China

5. Keystone Mobile Station

   B.Greene, EOS, Australia

13:30-14:30 **Lunar Laser Ranging**

Chairperson: Peter Shelus, McDonald Observatory, USA

1. Adaptive Ridge Regression: the Multicollinearity and Its Remedy in Lunar Laser Ranging

   Huang C.L., Jin W.J. and Xu Huaguan, Shanghai Observatory

2. Expected Results from the Analysis of LLR Data

   Ulrich Schreiber, J.Mueller, Wettzell, Germany

3. OCA/CERGA LLR: Status and Accuracy

   Jean-Francois Mangin,   OCA/CERGA, LLR Station , France

4. The Impact of Technology on-LLR at MLRS

   Peter J. Shelus, Jerry R. Wiant, Randall L. Ricklefs, Arthur L. Whipple and Judit

   G. Rie,   McDonald Observatory, University of Texas-Austin, USA

5. Millimetrie Lunar.Laser Ranging at OCA

   E. Samain, J.F. Mangin , J. D. Chabandie,   OCA/CERGA, LLR Station, France

6. Compensation of a Laser Beam Propagation for the LLR

   Feng Hesheng , Xiong Yaoheng , Yunnan Observatory , China

14:30-16:30 **Target Design, Signature and Biases**

Chairperson: Andrew Sinclair, RGO, UK

1. Amplitude Corrections to Delay Measurements.

   J.McK. Luck, Orroral Observatory, Australia

2. Accuracy of Satellite Laser Ranging

   S.Schillak, Space Research Center of Polish Academy of Sciences

   Astrogeodynamical Observatory, Poland

3. Laser Reflector Design for the CHAMP Satellite

   R.Neubert, Geo Forschungs Zentrum(GFZ), Germany

4. Dependence of Ajisai's Center-of-Mass Correction on Laser Ranging System

   Toshimichi Otsubo, Jun Amagai and Hiroo Kunimori, CRL, Japan

5. Remote Sensing of Atmospheric Parameters

   U. Schreiber, Wettzell, Germany

13:30-19:00   **Buses leave for Sheshan station tour (SLR, VLBI, GPS, PRARE)**

20:30-22:00   **WPLTN Plenary Meeting (open)**

          Chairperson: Ben Greene, EOS, Australia

Thursday, November 14

8:30-10:00   **Timing Devices and Calibration**

          Chairperson: John Luck, AUSLIG, Australia

1. Instrumentation Development and Calibration for the Matera Laser Ranging Observatory

    M.Selden, C.Steggerda, R.Stringfellow, D.McClure, C.B.Clark, G.Bianco ATSC, USA

2. Multi-Counter Operation

    G.Kirchner, F.Koidl Austrian Academy of Sciences, Observatory Lustbuhel, Austria

3. Femtosecond Timing of Electronic Pulses

    B.Greene, L.Dahl, J.Kolbl, EOS, Australia

4. Timing System Aspects

    U.Schreiber, Wettzell, Germany

5. Short Distance Calibration

    G.Kirchner, F.Koidl Austrian Academy of Sciences, Observatory Lustbuhel, Austria

6. Portable SLR Calibration Standard

    I.Prochazka, K.Hamal (Czech Technical University), H.Kunimori, B.Greene

10:00-10:30   **Break**

10:30-12:00   **Multiwavelength Ranging/Streak Cameras**

          Chairperson: Jean Gaignebet, CERGA, France

1. Streak Camera Limitations and New Timing Ideas

    J. Gaignebet, CERGA, France

2. An Electronic Streak Camera" with High Sensitivity and 15ps Resolution

    B.Greene, EOS

3. The Circular Scan- SC Experiment of the WLRS

    U.Schreiber , Wettzell, Germany

4. Water Vapor Correction of Two Color SLR

    R.Neubert, GFZ, Germany

5. Atmospheric Dispersion Monitoring Using $0.53\mu m$ and $1.54\mu m$ Satellite Laser Ranging.

    B.Greene (EOS), H.Kunimori, K.Hamal

6. Second Harmonic Generator Based T/R Switch

    K.Hamal (Czech Technical University), B.Greene

13:30-15:30   **System Automation and Operational Software**

          Chairperson: Jan Mcgarry, NASA/GSFC

1. Deficiencies of the IRV Model for the GPS Satellites, and Some Possible Solutions ,

7. Large Aperture Germanium Detector Package for Picosecond Photon Counting in 0.5 to 1.6 um Range.   Ivan Prochazka, K. Hamal, B. Greene , H. Kunimori

8. Testing Ge-APD's for Ranging Application in a Cryogenic Environment
Ulrich Schreiber, Wettzell, Germany

10:30-10:45   Break

10:45-11:30   Laser Technology Development

Chairperson: Karel Hamal, Czech Technical University

1. Cr:LiSAF/Ti:Sapphire Based Solid State Laser System for Two Color SLR
P.Sperber,.. IfAG, Wettzell, Germany

2. Lasers for kHz Satellite Ranging with Millimetre Precision and Accuracy
Yue Gao, Ben Greene, Yanjie Wang, EOS

3. Optimal Design of Passively Q-switched Microlaser Transmitters for SLR
J.J. Degnan, NASA/ GSFC

4. Eyesafe Raman Lasers
K.Hamal,... Czech Technical University

5. A Compact Modified SFUR Passively Mode-locked Nd: YAG Laser for SLR
Sun Zhan'ao, Yang Xiangchun, Zhu Xiaolei ,Wu Zhaoqing
Shanghai Institute of Optics and Fine Mechanies
Yang Fumin, Chen Wanzhen and Xiao Chikun, Shanghai Observatory

11:30-12:30   Eyesafe Systems

Chairperson: Ivan Prochazka, Czech Technical University

1. Short Review on Eyesafe SLR Techniques
B.Greene,.. EOS

2. Integration of SLR Radar into the Geophysical Laboratory Environment
Tom Varghese, Roger Allshouse, Howard Donovan, Don Patterson, Rich
Savaal, Alan Murdoch, ATSC

3. SLR2000: an Inexpensive, Fully Automated, Eyesafe Satellite Laser Ranging System
J.Degnan,.. NASA/GSFC

4. Correlation Processing Approach for Eyesafe SLR2000
P.J.Titterton,.. EOO Inc, USA

5. SLR2000 Performance Simulations
J.McGarry, NASA/GSFC

6. Eyesafe Satellite Laser Ranging Using Raman Shifter Nd:YAG Laser
B.Greene,.. EOS

7. Integration of SLR Radar into the Geophysical Laboratory Environment
Tom Varghese, Roger Allshouse, Howard Donovan, Don Patterson,
Rich Savaal, Alan Murdoch (ATSC)

Haojian Yan and Chugang Feng, Shanghai Observatory, China

3. The Question of Measuring Error Distribution in SLR Data

 Wu Jie, Li Zhengxin, Zhang Zhongping, Yang Fumin, Tan Detong

 Shanghai Observatory, China

4. Full-rate vs. Normal Points: Two Ways of Managing SLR Data

 G. Bianco, R. Devoti, M. Fermi, V. Luceri, P. Rutigliano, C. Sciarretta

 Nuova Telespazio S.p.A.Centro di Geodesia Spaziale, Italy

5. The Fast Computing the Spherical Harmonic Perturbation on Artificial Satellite and the
 Recurrence Equations of the Coefficients of the Earth's Gravity

 Lin Qinchang, Guangzhou Satellite Station, Chinese Academy of Sciences

·6. LRA Signature Assessment from TOPEX Precision Orbits.

 P.J. Dunn, T. Varghese and G.M. Appleby, RGO

 Hughes STX Corporation, USA

7. Synchronous Satellite Laser Ranging for Millimeter Baselines.

 T. Herring (MIT), H. Kunimori(CRL) , B. Greene(EOS)

. 8. Work Organization and Some Results of the Data Analysis on Satellite Laser Ranging
 at Russian Mission Control Center (poster)

 V.Glotov , V.Polyakov, V.Pochukaev, Mission Control Center, Russia

9. Discussion over Orbit Determination of Satellite Ajisai

 Jiang Hu, Feng Chugang, Shanghai Observatory, China

19:00-   **Workshop Banquet**

Friday, November 15

 8:30-10:00   **Panel #1: Colocation between Techniques**

         Chairperson: Gerhard Beutler   (Astronomical Institute of Berne)

10:00-10:30   **Break**

10:30-12:00   **Panel #2: Height Changes with mm Accuracy**

         Chairperson: Peter Dunn (Hughes STX)

13:30-15:00   **Workshop Summary and Resolutions**

         Chairperson: Ben Greene (EOS)

15:00-15:30   **Business Meeting**

         Chairperson: Ye Shuhua (Shanghai Observatory)

15:30-16:00   **Break**

16:00-18:00   **CSTG Steering Committee (by invitation)**

         Chairperson: John Degnan (NASA/GSFC)

A.T. Sinclair, Royal Greenwich Observatory.

2. The GFZ/D-PAF Orbit Prediction System with Emphasis on the Low Flyer GFZ-1
   Zongping Chen, GFZ/D-PAF

3. Matera Laser Ranging Observatory Software System
   Michael Selden, ATSC

4. X Window Based Graphical User Interface for a Laser Ranging Control System
   Jacek W. Offierski, Delft University of Technology

5. Real-time Correction of SLR Range Measurements for the Return Amplitude Induced
   Bias of the Multi-Channel Plate PMT/TC-454 DSD Discriminator Receive System,
   Dan O'Gara, University of Hawaii

6. Combined Digital Tracking System
   Ivan Prochazka, Czech Technical University

7. Automation of Borowiec SLR
   S. Schillak, Space Research Center of Polish Academy of Sciences

8. Upgrading the NASA SLR Network for the 21st Century
   David Carter, NASA/GSFC

15:30-16:00 **Break**

16:00-16:30 **System Automation and Operational Software (continued)**

Chairperson: **Jan Mcgarry**

9. NASA Single Operator Automation Project (SOAP)
   Winfied M. Decker, ATSC

10. Automated Quality Control of Data from the NASA SLR Network
    Van S Husson, ATSC

11. Automated and Remotely Operated SLR Systems
    Ben Greene, EOS

12. A Method to Improve the Precision of Low Orbit Satellite Prediction (poster)
    Lin Qinchang, Guangzhou Satellite Station, Chinese Academy of Sciences
    Yang Fumin, et al, Shanghai Observatory

13. RGO Predictions and Time Bias Functions
    Roger Wood, Royal Greenwich Observatory

14. Precaution for Thunder Storm in Beijing SLR station (poster)
    Wang Tanqiang, Liu Nailing,   Beijing SLR Station, China

16:30-18:00 **Data Analysis and Models**

Chairperson: **Vincenza Luceri, Matera, Italy**

·1. Analysis of HTLRS Data at Marine Fiducial Points in Japan
    Masayuki Fujita (Hydrographic Department of Japan)

2. New Mapping Function of the Tropospheric Refraction in SLR

Science Achievements

and

Applications

The Science Derived from Lunar Laser Ranging

Peter J. Shelus
McDonald Observatory/Department of Astronomy/Center for Space Research
University of Texas at Austin
Austin, TX 78712-1083
USA

Abstract

This paper deals with lunar laser ranging and the science that is derived from it. The LLR data that have been gathered for more than a quarter of a century fill an important niche in Astronomy. They form a foundation for many fundamental astronomical disciplines and provide the grist for a multi-disciplinary analysis mill, the benefits of which are found in such areas as the solid Earth sciences, geodesy and geodynamics, Solar System ephemerides, terrestrial and celestial fundamental reference frames, lunar physics, general relativity, and gravitational theory. They contribute to our knowledge of the precession of the Earth's spin axis, the lunar induced nutation, polar motion and Earth rotation, the determination of the Earth's obliquity to the ecliptic, the intersection of the celestial equator and the ecliptic, lunar and solar solid body tides, lunar tidal deceleration, lunar physical and free librations, and energy dissipation in the lunar interior. They provide vital input into the lunar surface cartographic and surveying system. They determine Earth station and lunar surface retroreflector location and motion, mass of the Earth-Moon system, lunar and terrestrial gravity harmonics and Love numbers, relativistic geodesic precession, and the equivalence principle of general relativity.

1.0 Introduction

Positional astrometry has always played an important role in Astronomy. It contributes to our knowledge of reference frames, time keeping, position on the Earth, rotation of the Earth, positions and motions of the major and minor planets and natural satellites, proper motions and parallaxes of stars. Providing the base for the distance scale of the universe, it provides us with a better understanding of the Earth, the Solar System, the local solar neighborhood, the Milky Way Galaxy, the local group, the hierarchy of galactic clustering, the universe itself. Originating with naked-eye observations using the crudest of instruments and progressing to the filar micrometer and the photographic plate, there has been a steady evolution to more accurate and precise instrumentation, reduction, and analysis. Today we have CCD imaging, optical interferometry, very long baseline interferometry (VLBI), artificial satellite ranging (SLR), lunar laser ranging (LLR), the Global Positioning System (GPS) as well as radar and spacecraft Doppler. In addition, the availability of powerful and inexpensive desktop computers and workstations has provided a vast increase in our analytical capabilities. All of this gives us a better understanding of the universe around us. Each new step depends upon the successes of the past and leads to a better future. LLR is one of the most modern and exotic of the astrometric techniques that are used in basic scientific studies. The analysis of the constantly changing Earth-Moon distance, using different observatories on the Earth and different retroreflectors on the Moon, provides for a wide array of terrestrial, lunar, solar system, and relativistic science [Bender, et al 1973; Mulholland, 1980; Dickey, et al 1994; Nordtvedt, 1996].

2.0 Observation to science

Observations without science are meaningless. By applying a procedure that can be called "dynamic parameter improvement" [Mulholland, 1976], to a set of LLR measurements, one can obtain as much information about the dynamics of the site from which the observations are being

made as about the dynamics of the target itself and the universe around us. This procedure requires that not only the set of measurements be available for analysis but also, for each one of those measurements, a prediction of what that measurement would have been if the universe acted in conformity with some specific, well-defined model. Let us begin with a convenient definition of the topocentric distance, r, between an observing station and some target on the Moon. In vector form,

r = R(geocenter-selenocenter) - R(geocenter-observatory) + R(selenocenter-reflector).

This can be approximated in scalar form, by dotting the station vector into the remaining part, i.e.,

$$r = R_1 - \rho \cos (\delta) \cos (H) - z \sin (\delta),$$

where R_1 is the geocentric distance to the target, ρ is the perpendicular distance of the station from the Earth's spin axis; z is the perpendicular distance of the station from the Earth's equatorial plane; δ is the declination of the target; and H is the local hour angle of the target. Although this is a simple looking equation, it is a complicated function of the time. And, the LLR measurement is not simply one of distance, it is a measurement of an out-and-back time interval. Therefore, it is necessary to use this equation in an iterative scheme to obtain the prediction for a two-way transit time, τ, with the Earth and the Moon each being in motion; we cannot just use an instantaneous distance. In any event, the evaluation of a predicted transit time for any given laser firing, requires the knowledge and application of a gravitational and relativistic theory, all of the motions affecting the station and the target, precession and nutation, polar motion and Earth rotation, lunar libration, the elastic deformations of the Earth and the Moon, models of atmospheric refraction, as well as the nominal body-fixed coordinates of the telescope and the target, just to mention a few. The increase in our knowledge comes from comparing our predicted transit times with the ones that we have measured. Were prediction and observation to agree, our model would be accurately representing the universe. It is the residual between prediction and observation that allows us to study the workings of the universe. As already mentioned, to evaluate the above equation and then to use it to predict a transit time requires that we have estimated values for a large number of physical parameters, e.g., the masses, radii, internal make-up, and gravitational harmonics of the Earth and the Moon, the value of the Gravitational constant, the locations of the telescope on the Earth and the corner retroreflectors on the Moon, and many others. Further, for each of these parameters, κ_i, one must have a partial derivative $\delta\tau/\delta\kappa_i$, i.e., the manner in which the transit time, τ, would vary, were we to change the value of only that particular parameter in our model. Each observation then provides an equation of condition of the form

$$\Delta t = \Sigma (\delta t/\delta\kappa_i) \Delta\kappa_i$$

and this system of equations of condition can be reduced by a suitable regression algorithm to provide improvements to the estimated values of each of the various parameters, κ_i. Table 1 lists some of the more important parameters derived using LLR data. Following that table are short descriptions of some of scientific disciplines being addresses via LLR scientific analyses.

Table 1. Parameter values derived from LLR

Parameter	Value
Gravitational Physics and relativity parameters	
Principal of Equivalence parameter, E	$(3.2 \pm 4.6) \times 10^{-13}$
Parameterized Post-Newtonian (PPN) superposition parameter, β	1.003 ± 0.005
Parameterized Post-Newtonian (PPN) curvature parameter, γ	1.000 ± 0.005
Deviation from the expected geodetic precession, K_{GP}	-0.003 ± 0.007

3

Change in gravitational constant (G-dot)/G $(1 \pm 8) \times 10^{-12}/yr$

Geophysical Parameters

GM_{EARTH} $398,600.443 \pm 0.004 \ km^3/s^2$

Luni-solar precession constant at year 2000 $50.3845 \pm 0.0004 \ arcsec/year$

   18.6-year nutation corrections

      In-phase terms

$\Delta\varepsilon$	2.8 ± 1.1 marcsec		$\sin \varepsilon \ \Delta\psi$	-2.9 ± 1.4 marcsec

      Out-of-phase terms

$\Delta\varepsilon$	0.6 ± 1.3 marcsec		$\sin \varepsilon \ \Delta\psi$	0.5 ± 1.0 marcsec

n-dot secular acceleration of the moon

   Total $-25.88 \pm 0.5 \ arcsec/century^2$

   Diurnal term $-4.04 \pm 0.4 \ arcsec/century^2$

   Semidiurnal term $-22.24 \pm 0.6 \ arcsec/century^2$

   Lunar contribution $+0.40 \ arcsec/century^2$

   Increase semimajor axis rate $3.82 \pm 0.07 \ cm/year$

Lunar parameters

Love number, k_2 0.0302 ± 0.0012

Normalized moment of inertia, C/MR^2 0.3940 ± 0.0019

Dissipation parameters

Q	26.5 ± 1.0		k_2/Q	0.001136 ± 0.000016

Second-degree moment differences

$\beta_L = (C - A)/B$	$631.72 \pm 0.15 \times 10^{-6}$	$\gamma_L = (B - A)/C$	$227.88 \pm 0.02 \times 10^{-6}$

Low-degree gravitational harmonics

J_2	$204.0 \pm 1.0 \times 10^{-6}$	J_3	$8.66 \pm 0.16 \times 10^{-6}$
C_{22}	$22.5 \pm 0.11 \times 10^{-6}$		
C_{31}	$32.4 \pm 2.4 \times 10^{-6}$	S_{31}	$4.67 \pm 0.73 \times 10^{-6}$
C_{32}	$4.869 \pm 0.025 \times 10^{-6}$	S_{32}	$1.696 \pm 0.009 \times 10^{-6}$
C_{33}	$1.73 \pm 0.05 \times 10^{-6}$	S_{33}	$-0.28 \pm 0.02 \times 10^{-6}$

3.0 Real-Time Earth Orientation Parameters

The attempt to model all of the Earth's motions affects many scientific disciplines. Although precession and nutation were well observed by the 19th century, it was not until the turn of this century that the irregularities in the Earth's rotation and the phenomenon of polar motion were clearly recognized. By the 1960's, largely from optical observations, augmented by artificial satellite Doppler measurements, 5-day mean values for each component of the polar motion were believed accurate to ± 40 cm and angular position of the Earth accurate to ± 0.03 arcseconds. From its inception in the late 1960's, LLR was a source for accurate Earth rotation and polar motion information. Project EROLD (Earth Rotation from Lunar Distances) was conceived in 1974 under the auspices of COSPAR. The first series of LLR results for Universal Time was published in the Annual Report of the Bureau Internationale de l'Heure (BIH) for 1978. Project MERIT (Monitor Earth Rotation and Intercompare Techniques) was held in the early 1980's and LLR played a fundamental role in that campaign to pave the way for the replacement of the BIH with the International Earth Rotation Service (IERS) in the 1990's. Now, co-mingled with results from SLR, VLBI, and GPS, LLR monitors the rotational characteristics of the Earth at the few millisecond of arc level. Although often not as dense as data from some of the other techniques, LLR data is often the most timely data type, enhancing the predicative capabilities of the USNO's NEOS Earth Orientation predictions.

3.1 Solar System Dynamics

The Moon's orbit around the Earth is strongly perturbed by the Sun. This perturbation gives rise to a rich spectrum of range signatures that, in turn, give sensitivity to a wide variety of Solar System parameters. The LLR data set provides a dramatic improvement compared to classical

optical data in the accuracy with which the lunar orbit can be known. For example, the lunar orbit orientation is determined at least two orders of magnitude more accurately and the radial component is determined at least four orders of magnitude more accurately than previously, through the use of the LLR data type. In fact, the radial distance variations are determined slightly better than the present 2-3 cm LLR range accuracy and the angular rate uncertainty is no more than 0.15 milliseconds of arc per year. The lunar orbital components that have the greatest uncertainties are the mean distance, presently 0.4 m (due to correlation with the retroreflector coordinates in the mean Earth direction) and the orientation of the lunar orbital plane with respect to the Earth's equator, 1.5 milliseconds of arc (3 m at the Earth-Moon separation)

The strong influence of the Sun on the Moon's orbit also permits LLR data to be used efficiently to determine the mass ratio $Mass_{Sun}/(Mass_{Earth} + Mass_{Moon})$ as well as the relative orientation of the Earth-Moon system orbit around the Sun. The actual size of the Earth-Moon orbit is determined by the gravitational constant multiplying the sum of the masses of the Earth and the Moon, with the Moon's orbit being perturbed from a simple Keplerian ellipse by the Sun. The two largest solar perturbations for the Moon, the monthly and semimonthly variations in distance, are determined from LLR data to a few cm. This corresponds to a 10^{-8} relative accuracy in the value of the mass ratio in question. Further, the analysis of LLR observations allows the relative geocentric positions of the Sun and the Moon to be determined to within 1 millisecond of arc. Since planetary positions are determined with respect to the Earth's orbit around the Sun, the geocentric position of the Moon and the heliocentric positions of the planets can be made internally consistent in their relevant orientation. Because LLR stations are located on a spinning Earth, the orientation of the Earth's equatorial plane is determined relative to both the lunar orbit plane and the ecliptic plane of the heliocentric Earth-Moon orbit. Thus, LLR data is sensitive to the mutual orientation of the planes of the Earth's equator, the lunar orbit, and the ecliptic. Hence, it locates the intersection of the ecliptic and equatorial planes (the dynamical equinox) and determines the angle between them (the obliquity of the ecliptic). This process allows the orienting of the planetary ephemerides onto the fundamental astronomical reference frame at the millisecond of arc level.

Of course, all of these accuracies are degraded when one extrapolates outside the span of observations. This means that a continual supply of high quality measurements and analysis are required to maintain and enhance these results. Using LLR data alone and in combination with the other modern observing techniques provides for the very best results available.

3.2 Relativity and Gravitational Physics

LLR has contributed greatly to Solar System tests of general relativity and gravitational theories. The Moon proves to be especially valuable for this because the ratio of non-gravitational to gravitational forces acting upon it is very small. LLR now establishes the definitive limit for both the strong and the weak equivalence principles[Williams, et al 1996], requiring that the ratio of gravitational mass to inertial mass be exactly unity. Therefore, all bodies must fall with the same acceleration in an external gravitational field, with the gravitational self-energy contributing equally to the gravitational and inertial masses. Although the Equivalence Principle was tested in the laboratory, until the coming of the LLR technique, it has not been tested for bodies large enough to have a significant fraction of their masses coming from gravitational self-energy. Roughly 4.6×10^{-10} of the Earth's mass derives from its gravitational self-energy; the corresponding fraction for the Moon is 1.9×10^{-11}. Considering the orbit of the Moon around the Earth, a violation of the Equivalence Principle would cause the orbit of the Moon about the Earth-Moon barycenter to be polarized in the direction of the Sun, the signature of which would have a synodic period of 29.53 days. This is the so-called Nordtvedt effect [Nordtvedt, 1988]. Today,

LLR analyses give $(M_G/M_I - 1) = (2 \pm 5) \times 10^{-13}$, the best current test of the Strong Equivalence Principle available. With feasible improvements in LLR data accuracy and with a longer span of data, further improvement is assured.

Another important test of gravitational physics is that coming from the measurement of the relativistic precession of the lunar orbit, i.e., geodetic precession. This was first predicted by deSitter in 1916. This effect should cause a precession of the entire lunar orbit with respect to the inertial frame of the Solar System by some 19 milliseconds of arc per year. The LLR data are sensitive to this effect mainly through the excess precession of the lunar perigee above and beyond that due to the Newtonian effects of the Sun, the Earth, and the other planets. Early LLR reductions agreed with the predictions of General Relativity to within 2%. More recent solutions give a difference of -0.3 ± 0.9% from the expected value. At the present time the leading source of error in this result is an uncertainly in J_2, the primary lunar oblateness term. New, more, and better observations will be invaluable.

LLR data also provide information concerning the possible change of the gravitational constant, G, with time, because of the lunar orbit's sensitivity to the solar longitude. Adding cosmological interest to this situation is the suggestion that very large changes in G may have occurred during an inflationary phase in the early history of the universe. Estimates of limits on the rate of change of G currently range from $|(dG/dt)/G|$ ² 1×10^{-11} to 0.4×10^{-11} per year. The LLR value is presently $(0.1 \pm 0.8) \times 10^{-11}$ per year [Williams, et al 1996]. Other independent determinations can be made from Viking lander tracking data and binary pulsar data. The best results on G-dot will undoubtedly depend upon the analysis of a combination of all of these data types.

3.3 Lunar Science

The analysis of LLR data certainly provides an especially large amount of information about the dynamics and the internal structure of the Moon. Selenocentric reflector surface coordinates, moment of inertia ratios, as well as the second and third degree lunar gravity harmonics are determined with quite high accuracy using LLR data. The reflector coordinates, together with the ALSEP radio transmitter coordinates, serve as the fundamental control points for lunar surface cartography. The changing apparent distances, as monitored by LLR, between the several reflectors and the Earth provide information on the lunar physical librations and solid body tides. Values of the lunar gravity harmonics, the moments of inertia and their differences, the lunar Love number, k_2 (which measures the tidal change in the moments of inertia and gravity), and variations in the lunar physical librations are all related to the Moon's structure, mass distribution, and internal dynamics and, therefore, give us great insight into a much better understanding the lunar interior. Presently, the most accurate estimate of the lunar moment of inertia is obtained from a combination of moment of inertia differences determined by the LLR solutions and the lunar gravity field coefficients coming from lunar satellite Doppler observations and LLR.

The lunar mass distribution also perturbs the lunar orbit that, in turn, produces a secular precession in the lunar node and perigee directions. Lunar seismic data suggest a core and a mantle, with little definitive evidence of a core. The existence of a lunar core, as well as whether it is solid or liquid, are important questions for which the lunar polar moment, as derived from LLR results, can help set limits. Information concerning the apparent tidal distortion of the Moon and the mean direction of its spin axis can be inferred from the lunar librations, measured by LLR. However, because of insufficient LLR data accuracy and volume, complications exist in the interpretation of results. Better accuracy and greater amounts of multi-corner data are needed, since key answers depend on very small signatures. If the Moon were a perfectly rigid body, the mean direction of its spin axis would precess with the orbit plane. LLR data show that the true

spin axis is actually displaced from this expected direction. The two dissipative terms are due to solid and liquid dissipation. The presence of a fluid core with a turbulent boundary layer appears to be a plausible interpretation. However, the direct separation of the competing dissipative terms is difficult The differential signature arises in the lunar orbit acceleration, and separation requires an independent estimate of n-dot, due to the Earth's tidal friction. In principle, the difference in n-dot could be detected by comparing the total n-dot measured by LLR with n-dot predicted from artificial satellite measurements of ocean tides. Unfortunately, the present determinations are not yet precise enough to discriminate between alternatives.

The LLR data show an apparent rotational free libration in longitude for the Moon with a 2.9 year period and a 1.4 arcsecond amplitude. The free-plus-forced blend has a 1.8 arcsecond amplitude and is quite tricky to separate. Recently, also strongly seen in the LLR data, is a 74 year elliptical wobble of the lunar pole with semiaxes 3 by 8 arcseconds. Theoretically, separate from the lunar librations that are driven by the time-varying torques of the Earth, the Sun, and the other planets, i.e., the forced physical librations, three modes of free librations exist. One of these theoretical modes is a 2.9 year oscillation in lunar rotation speed. Without suitable recent exciting torques, and because of substantial dissipation, the amplitudes of all lunar free librations should be damped to zero. However, the observed 2.9 year free libration is complicated because two very small forcing terms in the lunar orbit, close to the resonance frequency for the free libration, are amplified to mimic the observed free libration. Numerically integrated lunar rotational motions have been compared to semi-analytic calculations of the forced angular motions in an attempt to separate out the free libration. Seismic events on the Moon would be insufficient to explain the observed amplitude. Other studies have been carried out to investigate whether the apparent free libration might have been excited by recent impacts on the Moon. Such excitation would have required an impact in very recent times by an object large enough to leave a crater with a 10 km diameter. A third free libration mode, much smaller than the others, i.e., only 0.02 arcseconds in magnitude, has only been recently detected; its small size nearly completely excludes impacts as being an important stimulating mechanism. As another possibility, Eckhardt has suggested that passes though weak resonances have occurred for the lunar rotation in the geologically recent past that can perhaps stimulate free librations in longitude. Another plausible explanation appears to be core-boundary effects, similar to those that are believed to account for the decade time-scale fluctuations in the Earth's rotation. This can oly be determined with more and better LLR data that can irrefutably define the third mode of libration and extend the span of measurement of the 74 year wobble.

3.4 Geodynamics

The classic geodynamical results from LLR derive from the long term study of the variation of the Earth's rotation, the determination of the constants of precession and nutation of the Earth, LLR observing station coordinates and motions, the Earth's gravitational coefficient, and solid-body and ocean tides that accelerate the motion of the Moon. LLR observations supplement and complement the results being obtained from other space-based observing techniques, but with an almost three decade long span of data, LLR data exceeds that available from any other space geodetic technique. The very accurate value of the LLR-derived Sun/(Earth + Moon) mass ratio can be combined with the solar GM and the lunar GM (from lunar-orbiting spacecraft) to give the Earth's GM in an geocentric reference frame with an accuracy of 1 part in 10^8. Within the uncertainties, this value is quite compatible with that derived from SLR.

Tidal dissipation of energy on the Earth causes a misalignment of the Earth's tidal bulge to the Earth-Moon line. This bulge exerts a secular torque that causes both the Moon to increase its distance from the Earth and the Earth's rotation rate to decrease. The resulting change has been

seen in the geological record. With respect to specific Earth tides, the span and accuracy of the LLR data is such that the diurnal and semi-diurnal tides can be resolved from the amplitude of the 18.6 year along-track tidal perturbation. Due to the gravitational attraction of the Sun, Moon, and other planets the Earth's spin axis precesses and nutates in space. These motions depend on the flattening of the Earth, its moment of inertia, the flattening of the core-mantle interface, the Earth's anelasticity, as well as ocean and solid body tides. Both LLR and VLBI analyses indicate that significant corrections are required to the standard precession and nutation models. The almost 30 year span of LLR data is a distinct advantage when attempting to separate precession and the 18.6 year nutation correction. Joint VLBI and LLR solutions [Charlot, et al 1995] combine the strength of the LLR data for long period terms and the high resolution of the VLBI data for shorter periods.

4.0 Summary

A great deal of science has been accomplished using LLR data over the past 30 or so years. We expect that a great deal more will be accomplished in the future. LLR analysis efforts in the fields of relativity and gravitational theory are continuing to reduce the uncertainty of the Principle of Equivalence parameter, the relativistic precession of the lunar orbit, as well as the rate of change of the gravitational constant; today, LLR provides the only high accuracy testing of a significant number of relativistic and gravitational theory parameters. Further, within the lunar sciences, significant LLR analytical effort is being applied to studies of the lunar interior, especially those that deal with the dissipation of rotational energy in the Moon, the shape of the lunar core-mantle boundary, the lunar Love number k_2, and the free librations of the Moon. Finally, in geodynamics, LLR analytical efforts will continue to contribute to studies that deal with fundamental coordinate frames, the variation of the Earth's rotation, precession, nutation, and the tides.

Because of the passive nature of the lunar reflectors and the steady improvement in observing equipment, the LLR data type will continue to provide for state-of-the-art results in many disciplines of Astronomy. Similar to other astrometric techniques, LLR is broad ranging in results and its gains are steady as its data base continues to be extended. As a basic astronomical data

type, longevity and continuity must be assured. It is interesting to note that we are approaching the 30th anniversary of the first emplacement of a reflector package on the lunar surface. LLR remains the only active Apollo experiment and it is still marching at the forefront of science with its ever expanding results. During these times of austerity, it is important to cite examples of efficient and cost-effective progress of research. LLR, and the science it is able to produce, is a source of special pride within the scientific community.

5.0 Acknowledgments

6.0 References

Bender, P. L., Currie, D. G., Dicke, R. H., Eckhardt, D, H., Faller, J. E., Kaula, W. M., Mulholland, J. D., Plotkin, H. H., Poultney, S. K., Silverberg, E. C., Wilkinson, D. T., Williams, J. G., and Alley, C. O., 1973, Science, 182, 229.
Charlot, P., Sovers, O. J., Williams, J. G., and Newhall X X, 1995, Astronomical Journal, 109,

418.

Dickey, J. O., Bender, P. L., Faller, J. E., Newhall, X X, Ricklefs, R. L., Ries, J. G., Shelus, P. J., Veillet, C., Whipple, A. L., Wiant, J. R., Williams, J. G., and Yoder, C. F. 1994, Science, 265, 482.

Mulholland, J. D., 1976, Scientific Applications of LLR, J. D. Mulholland, Ed., Reidel, Dordrecht, Netherlands, 9.

Mulholland, J. D., 1980, Reviews of Geophysics and Space Physics, 18, 3.

Nordtvedt, K., 1996, Physics Today, 49, No. 5, 26.

Williams, J. D., Newhall, X X, and Dickey, J. O., 1996, Physical Review D, 53, 6370.

Applications of Accurate SLR Station Positioning

Peter Dunn for the GSFC SLR Analysis Group

Introduction

The technical applications of SLR data cover a variety of scientific areas. The satellite position defined by a network of SLR stations enables us to improve the gravity model of the Earth and to investigate other force model effects on the orbit. The network also defines high resolution Earth orientation parameters from observations of geodetic satellites in stable orbits, such as the LAGEOS and ETALON constellations, and the scale of the measurements allows very accurate definition of the center of mass of the Earth, as well as the dimensions of the planet and its gravitational constant. This paper will describe some accomplishments of SLR analysis in the field of station and network positioning, which includes the determination of the velocity of the most accurate SLR Observatories.

Geomagnetic Time Scale Revisions

The SLR-defined global and regional kinematic velocity models have suggested that the relative velocities of SLR stations on the stable interiors of tectonic plates were about five percent slower than those expected from the NUVEL-1 geophysical model (Smith et l.,1990). This observation supports the recent revision of the Potassium/Argon-defined paleomagnetic time scale based on astro-geochronology, which forms the basis of the NUVEL-1A model (Demets et al.,1994). The correlation with NUVEL-1A computed by by the GSFC SLR group for a recent global solution is shown in Figure 1 as the solid line: it has a slope of 0.970 =/- 0.034, whereas the comparison with NUVEL-1 has a slope of 0.928 +/- 0.032. The SLR velocities in this solution are thus still 3 percent slower than the prevailing geophysical model, but with an uncertainty which suggests marginal significance. The correlation measures are influenced by the choice of stations to represent stable plate interiors, and rely on the assumption of uniform motion over the differing observation spans for the chosen stations.

The motion of the Easter Island station on the Nazca plate with respect to neighbouring stations on the Pacific plate is the largest of all plate pairs, and the results in Figure 1 suggest that it's velocity is slower than the NUVEL-1A value. There is emerging evidence from GPS observations (Heflin et al., 1994) that supports the SLR velocity at Easter Island as slower than the geophysical prediction. This calls into question the validity of the choice of this station as representative of a stable plate interior, or could also suggest that the NUVEL-1A model for the behavior of the Nazca Plate should be re-addressed. SLR observations collected around the Gulf of California analysed by Dunn et al. (1995) have confirmed the early indications from GPS observations (Dixon et al, 1992.) that the Gulf is extending faster than predicted by the Gulf rise spreading rates. DeMets (1995) has conducted a reappraisal of these seafloor spreading lineations which contradicts the assumption that Baja California has been rigidly coupled to the Pacific plate since 3.6 Ma. DeMets concludes that PA-NA motion is now 4 mm/year faster than that predicted by the 3 Myear average of NUVEL-1A, and this faster rate is closer to the rate determined from the space geodetic measurements. We can thus see how the space measurements can check and even challenge the integrity of the latest geophysical models.

Evidence for Regional Deformation

The SLR velocity model has indicated that several other areas exhibit regional deformation which should not be considered as representative of stable plate interiors. The successful

deployment of transportable systems with the WEGENER campaign in the Mediterranean has confirmed the expected extension in the Aegean, and the SLR geodynamic observations can now be combined with earthquake moment tensors for regional seismic risk assessment (Jackson et al, 1994). The direction of the motion of SLR observatories located behind island arcs in Simosato, Japan and at Arequipa, Peru is aligned with that of the subducting plate; Robaudo and Harrison (1993) have concluded that strain expected to be relieved at the trench is carried over onto the over-riding plate, to be compensated by a mechanism for which a model has yet to be developed.

SLR Measurements of the Vertical

The definition of horizontal position and velocity is easier than that of the vertical component because tracking geometry is strong enough that the effects of orbital and instrumental errors on station latitude and longitude largely cancel over the time span of the orbital arc. A modern laser system can be calibrated to a ranging accuracy of a few millimeters (Degnan, 1993) and atmospheric refraction errors for the optical measurements are unaffected by the variable water vapor component. The positioning accuracy of the SLR systems has progressively improved as the instruments were up-graded and the network expanded. This progress will continue with the deployment of advanced stations: MLRO (Varghese et al., 1992), TIGO (Sperber et al., 1994), SALRO (Wetzel et al. 1994), SLR2000 (McGarry, et al.1996) and positioning capability can be further enhanced by measurements to new, stable satellite targets. The contribution of LAGEOS II has been particularly helpful in the definition of the vertical component of station position, by reducing the influence of orbit force model errors on a station's height estimate, as the second satellite improves the tracking geometry.

Station Height Resolution

The best current SLR systems provide range measurements with an accuracy at their noise level of one to three millimeters. The LAGEOS position determined from these observations is limited by force and Earth model errors to a few centimeters, and the position determined at a station is dependent on the quality of the instrumentation. Since daily monitoring of the vertical is limited by visibility constraints, the best use of the currently available laser data is in defining longer period motion on the scale of months and years and in detecting coherent signals with known spectral characteristics, such as the tidal response of the Earth.

The vertical resolution of a modern SLR station can be seen in the plots of height values shown in Figure 2, which were determined in monthly arcs of LAGEOS I and II data as part of a global solution conducted by the GSFC SLR analysis group. The scatter in height estimates for independent solutions for the Yarragadee laser is listed in the Figure as 7 mm, although formal errors for a simultaneous solution from both satellites' data are as low as one or two millimeters for strong cases. The total spread of heights determined in the two-satellite solution is about twenty millimeters, but the systematic nature of the height variation suggests that this spread is not a good three sigma error estimate. The scatter can be reduced to 6 mm if the effect of atmospheric pressure loading is modelled (VanDam and Wahr, 1987), as this can amount to several millimeters amplitude with an annual period at Yarragadee. The relatively abrupt change in height seen at GGAO in January 1994 is also observed in the TOPEX/Poseidon orbit analysis, and is thus unlikely to be caused by satellite mis-modeling. It could be due to thermal loading in the region, caused by the formation of a permafrost layer during a particularly heavy winter. Unfortunately, the GPS receiver at the GGAO site was affected by the severity of the weather and there are no GPS results available to compare during this period. The variation in the monthly height of RGO shows strong systematic trends, and suggests that the random fluctuations occur at the millimeter level during some periods.

11

GeoCenter Determination

Mass redistribution in the atmosphere, hydrosphere, cryosphere, and atmosphere causes the center of mass of the Earth to move relative to the geocenter defined by the observing network. Earth orientation and geocenter are both influenced by tidal and wind-driven ocean mass change, variations in atmospheric pressure, and large earthquakes. Watkins et al. (1995) have shown that geocenter motions determined with LAGEOS observations exhibit annual and semi-annual signals of two to four millimeter amplitude, and Pavlis (1995) and Anderson (1995) have also demonstrated that variations of the geocenter due to ocean tides can be resolved with sub-millimeter accuracy at some tidal frequencies.

The geocenter resolution which can be reached with the data from the best SLR observatories with regular tracking data from LAGEOS I and II is shown in Figure 5. The estimates were made as part of the global solution for station motion, Earth orientation and orbit parameters conducted by the GSFC Laser Ranging Group (Kolenkiewicz et al, 1996). The equatorial components of geocenter motion can be resolved with an rms variation of 5 mm in the x direction, in the Greenwich meridian, and with 3 mm scatter in the y direction. The motion is restricted to an area of 2.4 cm by 2.2 cm, and most of this variation occurs within a block which is only one centimeter square. The polar component is not as well resolved as the equatorial component from satellite observations, and the scatter of the z-component about a mean position is 11 millimeters. The structure in the geocenter motion is caused by Earth mass redistribution, but measured with a network which is not geographically balanced. Improved resolution of these global parameters will become possible as the SLR network expands and is supplemented by automatic, low maintenance continuously tracking systems like SLR2000.

Tidally driven geocenter motion

Variations in the geocenter caused by the lack of symmetry of the ocean tides have been described by Schwiderski (1980), Brosche and Wuensch(1993) and Ray et al. (1994). Watkins and Eanes (1993) have extended the approach they originally adopted to determine coherent nearly diurnal and semi-diurnal variations in the Earth's orientation to include geocenter variations affecting the SLR network. The three year data span of LAGEOS II observations has enabled us to combine this information with that of LAGEOS I to make an accurate assessment of the tidal spectrum, which can be compared with the theoretical models, as well as that developed by Watkins and Eanes. The comparison of tidal coefficients in Figure 6 shows the values in each model for the Z-component in M2, which is the strongest
signal in the spectrum, and the extent to which the difference between the results from LAGEOS I and LAGEOS II can be used to qualify those from the combined solution.

SLR Positioning in the Future

The unique capabilities of SLR systems can be exploited to make important contributions to geodetic science and geodynamics, and we anticipate advances in positioning techniques to produce a variety of valuable products. These will include time series of height estimates at each SLR station which are free of the influence of instrument error, and which can be used for monitoring regional characteristics of the Earth in the vicinity of the station, calibrating the atmospheric pressure loading response of a spherically stratified Earth, or an Earth with assumed lateral crustal inhomogeneities. Furthermore, events and trends in these vertical measurements which indicate stress in the crust can be used to anticipate Earth movement and other natural hazards. An SLR-determined geocenter time series will accurately reflect the common signal in the position variation of the best SLR stations in the network and will define a reference system for monitoring Earth/ocean/atmosphere interactions. In order to reach this goal, coefficients of the

ocean tidal geocenter variation must be determined, taking advantage of the atmospheric loading and Earth tidal modelling results, and with error characteristics calibrated using independent estimates from LAGEOS I and II data.

The combination of space technologies of SLR, VLBI, GPS, DORIS and PRARE systems will enable us to compute a reference system which will provide the accurate long-term stability necessary for rigorous monitoring of important Earth processes in four dimensions. Improved knowledge of the motion in space of geodetic tracking sites is integral to our understanding of global and regional dynamic processes at work within the Earth, including the contemporary behavior of the Earth's major plates, deformation along plate boundaries, and deformation within plate interiors. Combining data from various space geodetic networks to form solutions for site motions will provide the detailed description of global and regional tectonics required to derive more detailed models of the kinematics of the lithosphere and to better understand the mechanisms which drive the plates, produce deformation, and trigger earthquakes. The resulting inertially oriented, accurately scaled reference frame will enhance our ability to accurately model and monitor processes which link the Earth, the oceans and the atmosphere.

REFERENCES

Anderson, P. H., Measuring rapid variations in Earth orientation, geocenter and crust with satellite laser ranging, Bulletin Geodesique, 69, 233-243, 1995.

Brosche, P, and J. Wunsch, Variations of the solid Earth's center of mass due to oceanic tides, Astron. Nachr., 314, 87-90, 1993.

Degnan, J. J., Millimeter accuracy Satellite LASER ranging: a review AGU Geodynamics Series, V.23, pp. 133-162, 1993.

DeMets, C., A reappraisal of seafloor spreading in the Gulf of California: Implication for the transfer of Baja California to the Pacific plate and estimates of Pacific-North America motion, Geophys. Rsch. Lett., 22, 1995.

DeMets, C., R. G. Gordon, D. F. Argus, and S. Stein, Effect of recent revision to the geomagnetic reversal time scale: on estimates of current plate motions, Geophys. Rsch. Lett., 21, 20, pp, 2191 2194, 1994.

Dixon, T. H., G. Gonzalez, S. M. Lichten, D. M. Tralli, G.E. Ness and J. P. Dauphin, Preliminary determination of Pacific-North America relative motion in the sourther Gulf of California using the Global Positiong System, Geophys. Rsch. Lett., 18, 20, pp, 861-864, 1991.

Dunn, P. J., J. W. Robbins, J. M. Bosworth, and R. Kolenkiewicz, Crustal deformation around the gulf of California, Geophys. Rsch. Lett., 23, 2, pp, 193 196, 1996.

Heflin, M., D. Jefferson, Y. Vigue, M. Watkins, F. Webb, J. Zumberge, and G. Blewitt, GPS Times Series: January 22, 1991 - April1, 1994, JPL Interoffice Memo, November 23, 1994.

Jackson, Haines and Holt, A comparison of satellite laser ranging and seismicity data in the Aegean region, Geophys. Res. Lett., 21, pp. 2849-2852,1994.

Kolenkiewicz, R., D. E. Smith, P. J. Dunn, M. H. Torrence and E. C. Pavlis, Geodynamics from LAGEOS I and II, Eos Trans., 77, 17, 1996.

McGarry, J. F. , J. J. Degnan, B. Conklin, P. J. Titteton, Sr., and P. J. Dunn, Automated tracking for advanced satellite LASER ranging systems, SPIE Proc. 2739, April, 1996.

Pavlis, E. C., TRF Determined From Multiple Space Techniques, Eos Trans., 76, 17, 1995.

Ray, R. D., B. F. Chao, B. V. Sanchez and R. S. Nerem, Some geodetic alications of the new Topex/Poseidon oceanic tide models, Eos Trans., 75. 44. 1994.

Robaudo, S, and C. G. A. Harrison, Plate tectonics from SLR and VLBI global data, Combinations of Space Geodesy in Geodynamics; Crustal Dynamics, AGU Geodynamics Series, V.23, pp. 51 72, 1993.

Schwiderski, E. W., Ocean tides, Part I: Global ocean tidal equations, Marine Geod., 3, 161-216, 1980.

Smith, D,E,, R. Kolenkiewicz, P.J. Dunn, J.W. Robbins, M.H. Torrence, S.M. Klosko, R.G. Williamson, E.C. Pavlis, N.B. Douglas, and S.K. Fricke, Tectonic motion and deformation from satellite laser ranging to LAGEOS, J. Geophys. Res., 95, 22013-22041, 1990.

Sperber, P., The Transportable Integrated Geodetic Observatory (TIGO), Ninth International Workshop on Laser Ranging Instrumentation, Canberra, Australia, November, 1994.

vanDam, T. M. and J. A. Wahr, Displacements of the Earth's surface due to atmospheric loading: effects on gravity and baseline measurements, J. Geophy. R., 92, 1281-1286, 1987.

Varghese, T., W. Decker, H. Crooks and G. Bianco, Matera laser ranging observatory (MLRO): an overview, Proc. Eighth International Workshop on Laser Ranging Instrumentation, Annapolis, Maryland, May, 1992.

Watkins, M. M., D. N. Dong, J. O. Dickey, M. B. Heflin, R. J. Eanes and S. Kar, Observations of Seasonal Translations Between the Earth's Mass Center and Lithosphere, Eos Trans., 76, 17, 1995.

Watkins, M. M. and R. J. Eanes, Long Term Changes in the Earth's Shape, Rotation, and Geocenter, Adv. Space Res., 13, 11, 11251-11255, 1993.

Wetzel, S., J. Horvath, V. Husson, G.Su, B. Greene and J. Guilfoyle, The ALRO/MOBLAS-7 Collocation Results, Ninth International Workshop on Laser Ranging Instrumentation, Canberra, Australia, November, 1994.
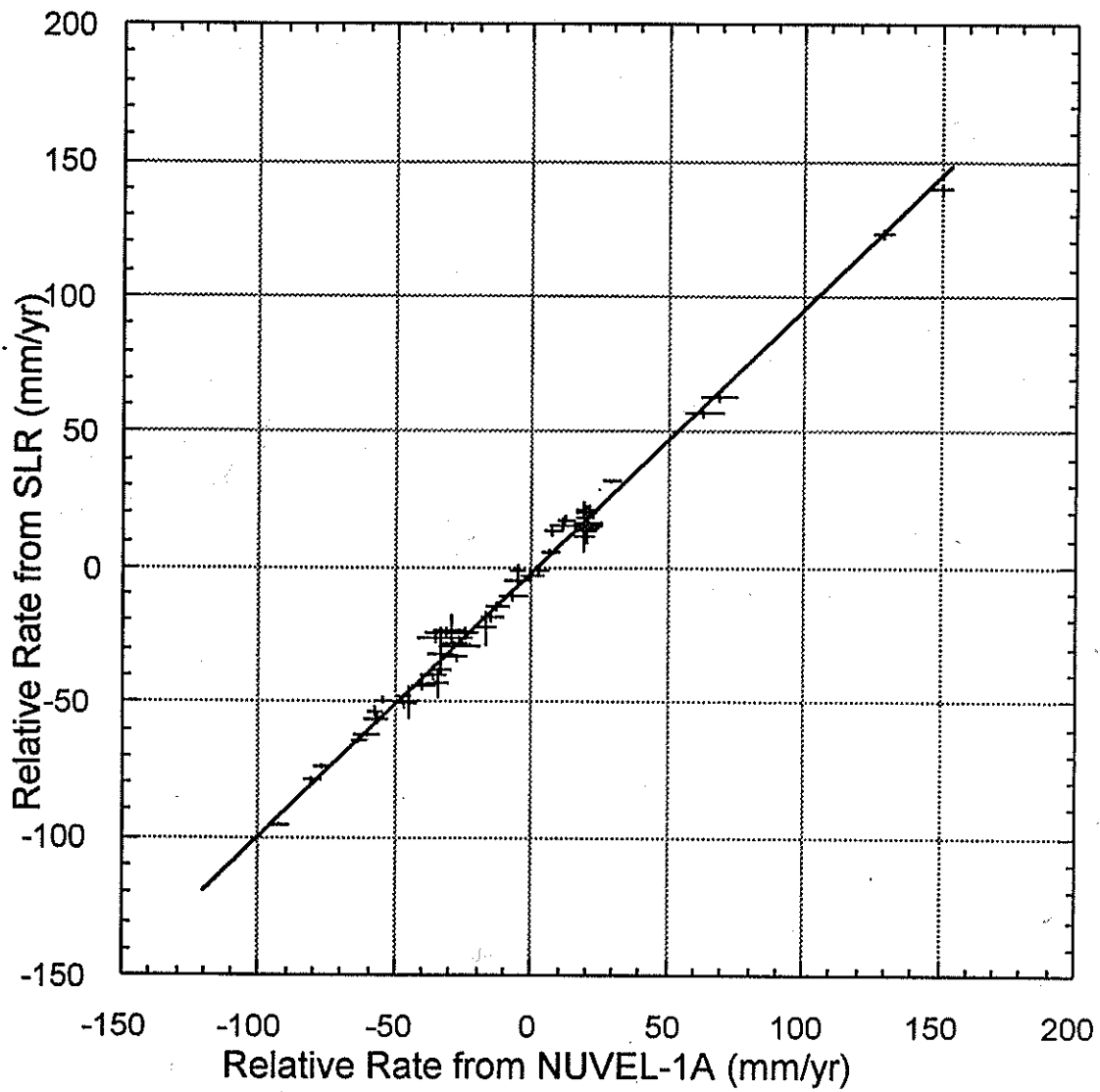
Figure 1: The correlation between the geophysical model NUVEL-1A and an SLR global solution has a slope of 0.970 +/- 0.034. The correlation with NUVEL-1 gave a slope of 0.928 +/- 0.032.
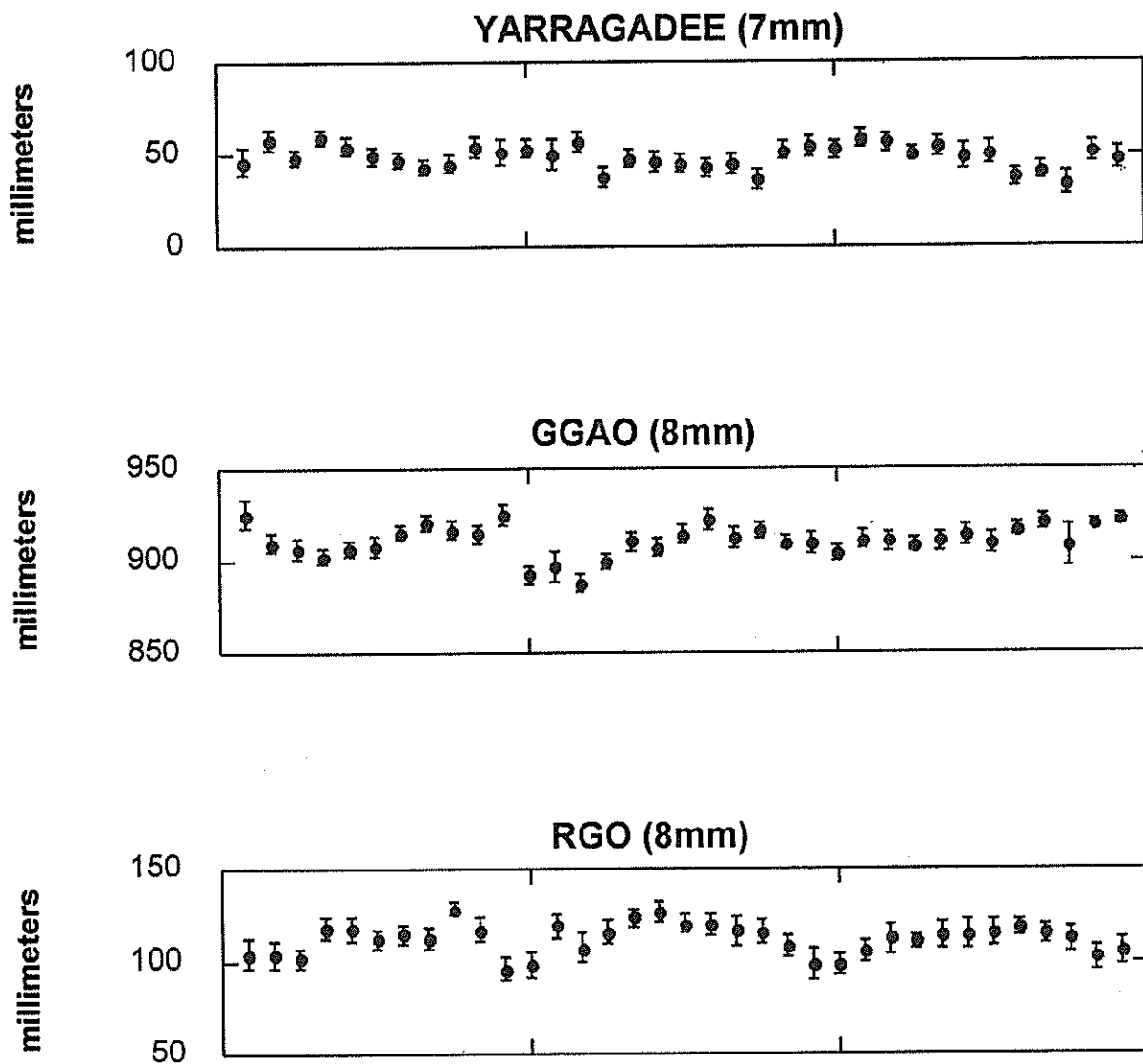
Figure 2: Monthly height values for the stations in Western Australia, at Greenbelt, Maryland, and on the south coast of England exhibit systematic signals, with a local scatter of 2 or 3 mm. The frame titles give the scatter to a mean height estimate.
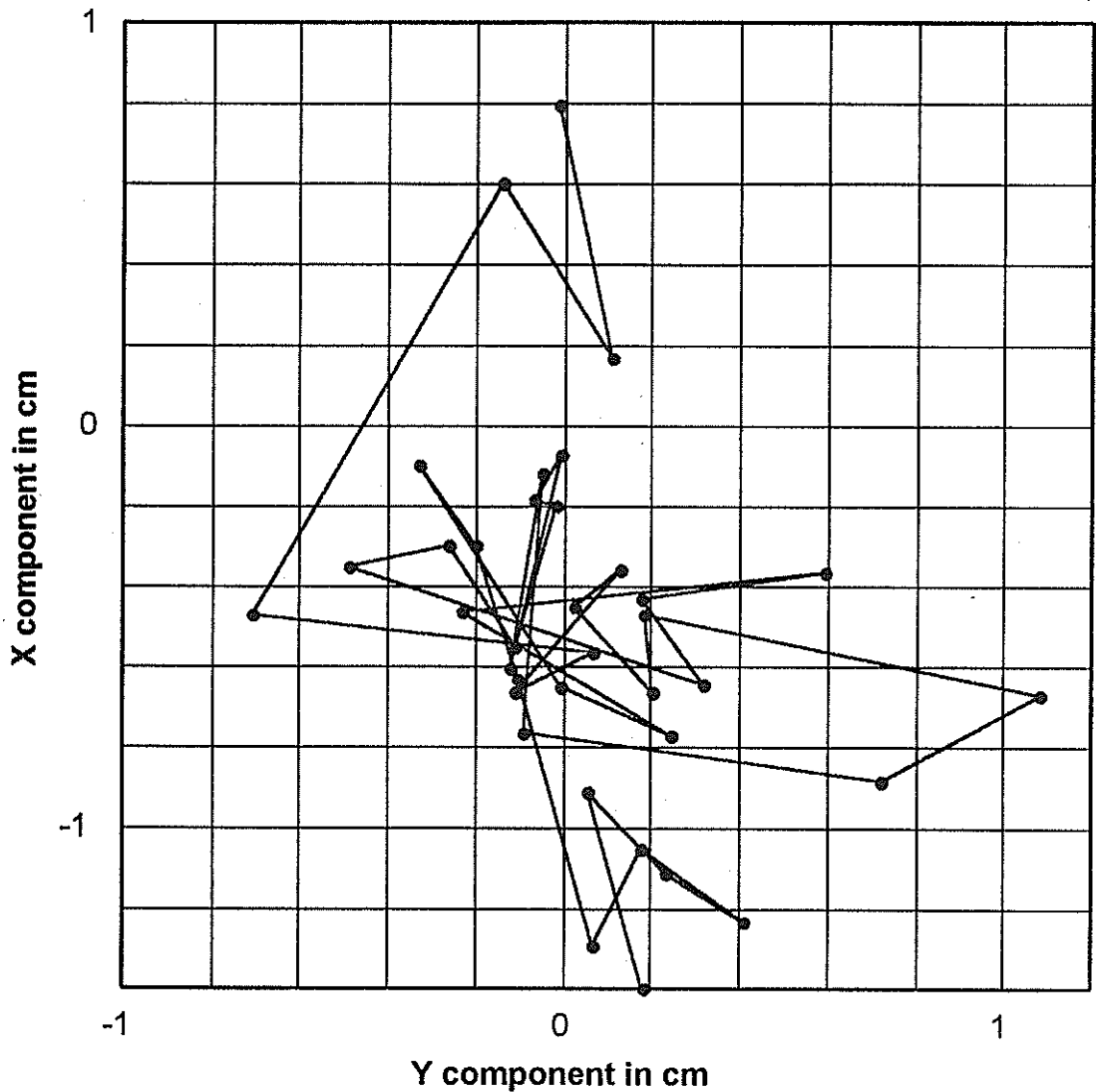
Figure 3: Geocenter estimates from a global solution using SLR observations from LAGEOS 1 and II show a 5 mm RMS scatter in x and 3 mm scatter in y. The motion is restricted to an area of 2.4 cm by 2.2 cm, which is the size of a domestic postage stamp (U.S. or Chinese): most of the variation occurs within a block which is only one centimeter square.
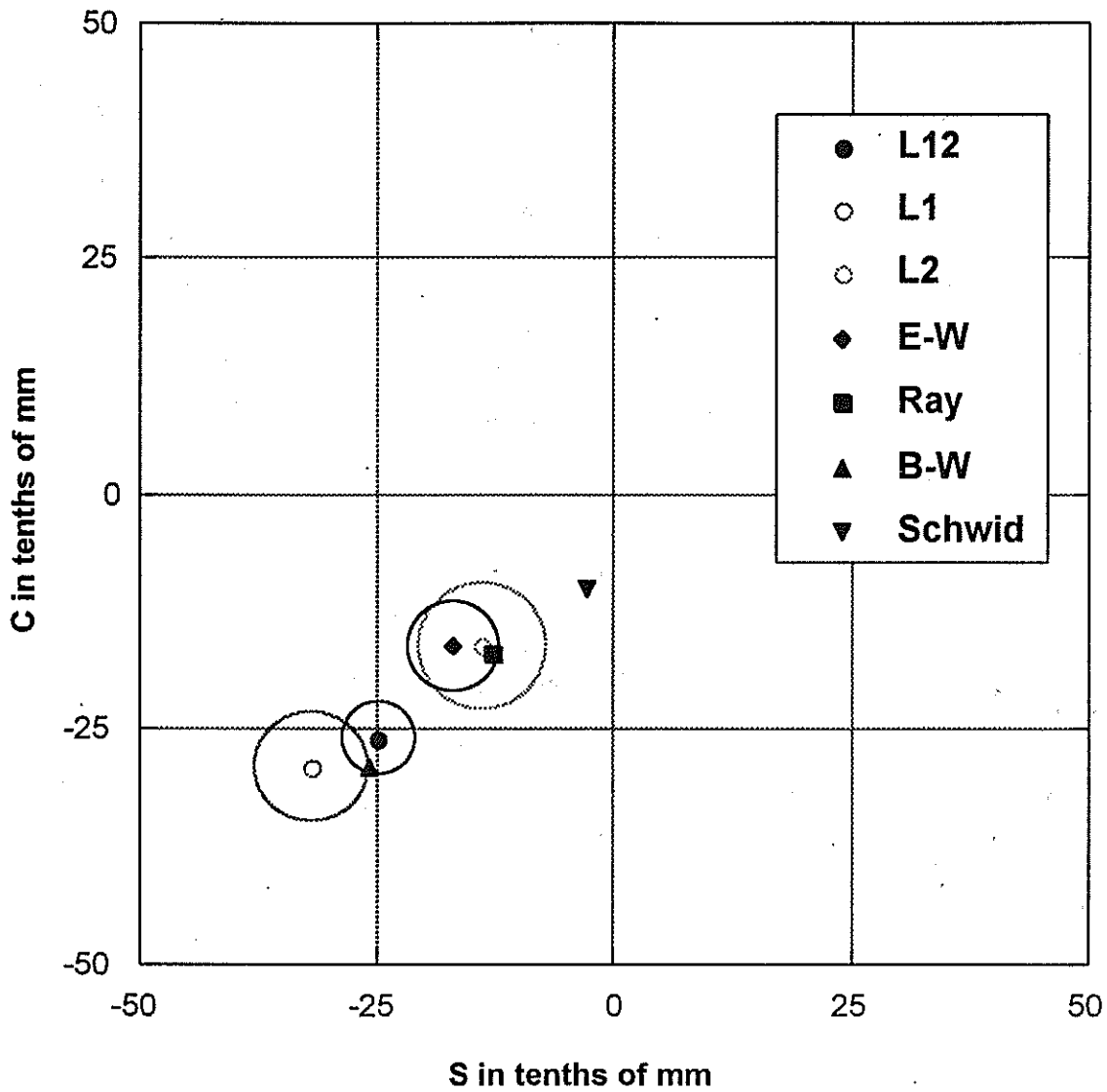
Figure 4: Tidal coefficients for geocenter variations of the Z-component predicted by three theoretical models at the M2 frequency are compared with measured values from CSR (diamond) and with GSFC solutions using LAGEOS I, LAGEOS II (open circles), and a LAGEOS I/II combination (closed circle)

Quality Checks within the EUROLAS Cluster

G.M. Appleby
Royal Greenwich Observatory,
Madingley Road,
Cambridge CB3 0EZ,
England

1 Introduction

The cluster of European satellite laser ranging stations (EUROLAS) provides a unique opportunity to monitor the precision and accuracy of the observations routinely carried out by a group of high-precision systems. Analysis of simultaneously tracked passes has the potential to identify at the centimeter level subtle biases in the measurements of one station with respect to others, and provide early warning of possible system degradation. On behalf of the EUROLAS stations, the Royal Greenwich Observatory (RGO) has begun a feasibility study to determine whether such a technique can add significant new information on potential observational bias to that already available on a routine weekly basis from the Center for Space Research, University of Texas. The strategy that we adopted is to compute month-long orbits and fit them to sets of on-site Lageos and Lageos-2 normal points, using the RGO SLR analysis package SATAN. Passes within the data sets that were tracked simultaneously by two or more Eurolas stations are then used to form short-arc corrections to the orbit, and residuals from the corrected orbit used to monitor observational bias. The results in numerical and graphical form from the monthly long-arc and from the Eurolas short-arc solutions are made available to the tracking and analysis community via the World Wide Web, ideally within a few days of the end of each month. The results are accessible via the Web pages of the RGO (http://www.ast.cam.ac.uk/RGO)

This paper describes the methods used and results to date, and points to potential further development.

2 Monthly Solutions

30-day orbits of Lageos-1 and Lageos-2 are fitted to the normal point data available through the CDDIS, using tracking station coordinates and velocities taken from the ITRF94 solution. We adjust the initial state vectors of the satellites, a solar radiation coefficient and empirical along-track acceleration, and also solve for corrections to the initial set of Earth rotation parameters, which are taken from the IERS Bulletin A results. We finally achieve a post-fit residual rms of about 6 cm for both satellites, where rejection of outliers is carried out at about a 3-sigma (20 cm) level. The series of post-solution range

residuals for each station provides a graphic indication of the general health of the system; any systematic trends or out-lying points indicate some bias in the range or epoch measurement, or transient fault in the on-site noise filtering process. Shown in Figure 1 are four typical sets of range residuals from a fitted orbit of Lageos-2 for 1997 February. The residual scale is +/- 1m, and deliberately no data editing has been carried out when generating the plots. Any residuals that were greater in size than one meter have been set equal to 1m for the plots. Included in the plots are the means and standard deviations of the residuals that were accepted for the orbital fitting process.

2.1 Discussion

From several months of such analyses, we find that some stations performed significantly better than others. The best stations produce almost no outliers, have residual mean values close to zero and residual standard deviations of around 30-40mm, which principally reflects the precision of the 30-day orbital model. However some stations do show clear bias and often produce significant numbers of out-lying points. There is also evidence that such bias values are sometimes different for each pass. Of course it is inevitable that the data produced by a large number of disparate systems will be variable in precision; some stations do not have access to the highest precision interval counters, or the shortest laser pulses or the fastest detectors. However, it is considered vital that all stations make every effort to eliminate systematic bias from their data, since it cannot be right that the analyst should have to estimate in some cases large pass-by-pass bias as well as the geodetic or geophysical parameters which he seeks. It is also very important that the numbers of outlying points are reduced considerably, since such data lead to great difficulty for orbit determination, particularly if the tracking data is sparse, or the initial orbit poorly known. We feel that the availability of these simple residual plots may act as a stimulus for improvement.

We could use these residuals to solve for station range and time bias values. However, measurement bias determined in this way may be corrupted by imperfections in the force model used, thus limiting the effectiveness of the long-arc solution for precise determination of system bias.

3 Short-Arc Solutions

We can remove much of the effect of force model error by using a short arc technique to solve both for corrections to the long-arc orbit and for station range and time bias. The method used here is that developed at RGO (Sinclair, 1989) and requires that at least two stations quasi-simultaneously track a given satellite pass. For each of the short-arcs that pass this criterion, we use a constrained six-parameter model to correct the orbit in the along-track, cross-track and radial directions, and also to solve if required for station range and time bias. We now use this method to analyse Lageos-1 and Lageos-2 observations made by the EUROLAS Cluster of stations. We take a core set of the best Eurolas stations, find the passes of Lageos-1 and Lageos-2 that were tracked by two or more of these stations, and use their observations in an iterative solution to correct the original long arc orbit, for the duration of each of the passes. Typical values of the post-fit residual rms are at the 1 or 2 cm level. We then compute residuals from these improved orbits for all the Eurolas stations that were tracking the passes, and finally carry out a simultaneous solution for orbit corrections and time and range bias for selected stations. To complement these numerical results, we plot for each pass the range residuals for all the tracking stations prior to the final solution for range and time bias. In this way, we can visualize those stations whose observations stand off from the corrected orbit. We consider that biases at the level of one or two cm can be routinely determined by this method. However, we do emphasize that all such residuals are with respect to the coordinate of the stations given in the ITRF94 solutions; deliberately no adjustments to those coordinates have been carried out. Such a re-adjustment will be the aim of further work on this topic. Shown in Figure 2 are four sets of residuals derived from this short-arc technique. All residuals that are greater than the range of the plot axes (± 10cm) are set equal to ± 10cm, and thus appear at the limits of the plot. The versions of the plots presented on the WWW are colour-coded with a key to identify residuals with station numbers; as a guide to station identification for the results shown in monochrome in Figure 2, we change with tracking station the symbols used to plot the points, from a
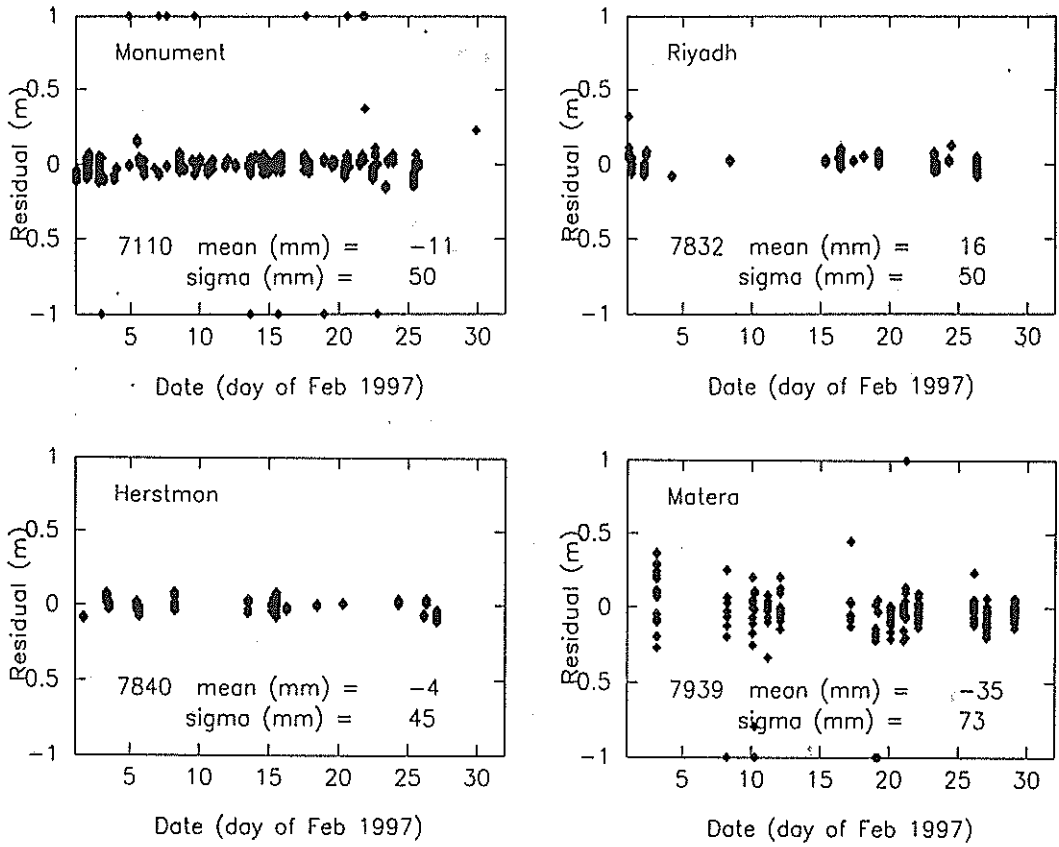
Figure 1: Range residuals from month-long Lageos-2 orbit.
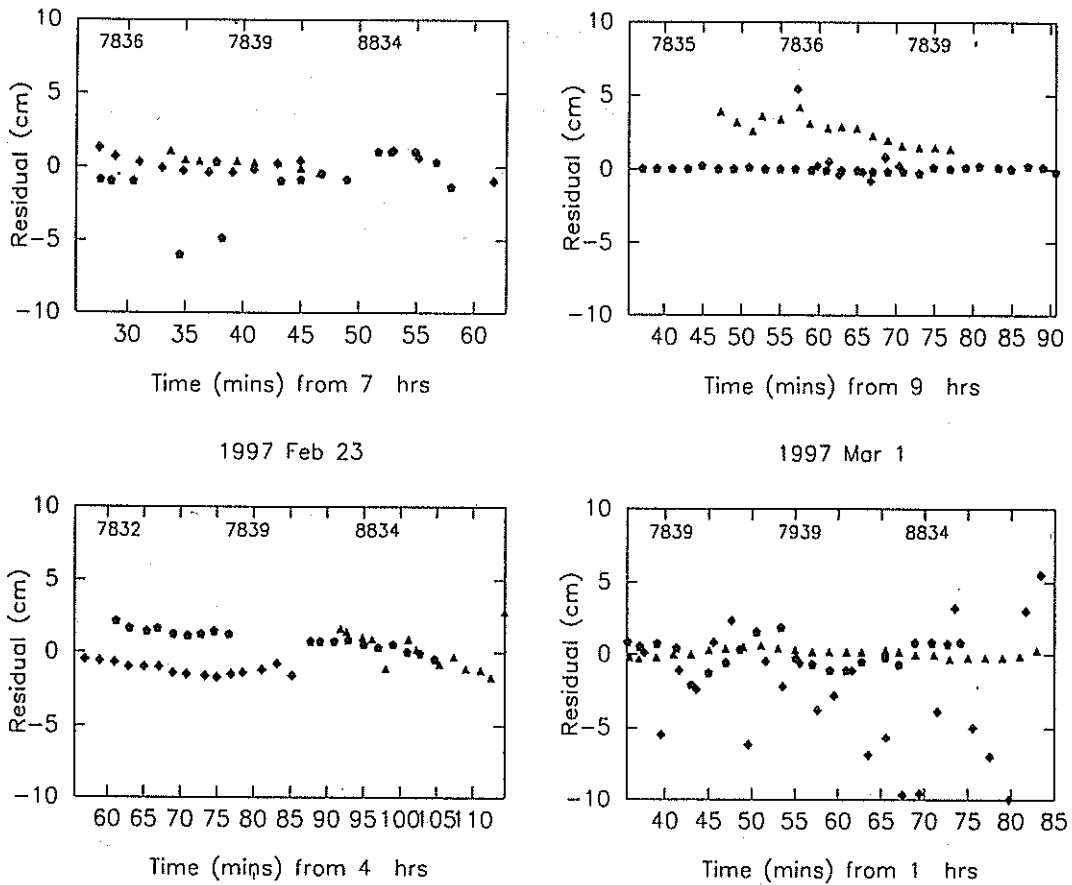
Figure 2: Range residuals from short-arc solutions.

triangle for the first station in the key, to a square for the next, to a pentagon for the next and so on.

3.1 Discussion

The plots show that most of the residuals are small, with occasional out-lying points, and occasional clear bias in the measurements from one or more stations. Also clear is the different precision achieved amongst the cluster of stations. We consider that at the very least the method clearly identifies individual out-lying points at the level of a few cm, and should thus be useful for stations wishing to trace the cause of such problems.

The power of the method is illustrated by the pass observed by the three stations 7835 Grasse, 7836 Potsdam and 7839 Graz on 1997 February 10, where post-solution residuals are shown in the second plot of Figure 2. Observations from Potsdam and Graz were used initially to correct the long-arc orbit for the duration of the 50-minute pass, and then observations from all three stations were used to solve additionally for time and range bias for those stations. A single out-lying point was identified for Potsdam, and for Grasse we determined a significant range-bias (28 ± 1mm) and time-bias ($-7 \pm 1 \mu$s). We note that the weekly analyses carried out at the University of Texas assume for Grasse a constant range bias of 30mm, in good agreement with our result for this single pass. As a further check on our procedure, we took the observations from all three stations and used them to solve for corrections to the orbit. The resulting residuals showed significant trends, confirming that the method is sensitive to bias in one or more of the sets of observations, and cannot absorb such bias into meaningful corrections to the orbit.

We have also carried out a similar short-arc analysis for four NASA stations working in the USA. The stations involved are 7080 MLRS at McDonald, 7105 Moblas 7 at GGAO, 7110 Moblas 4 at Monument Peak and 7210 at Mt Haleakala, Hawaii. At present, we have used only Lageos-1 for this analysis. The arcs tend to be shorter than those tracked by the European stations because of the greater inter-site distances between the NASA stations, but in general the agreement between the systems is very good. Results from these solutions are also available on the WWW.

4 Further Development

To be of maximum use to the tracking community, and to complement the work carried out by the University of Texas, we consider that these results should be available very soon after the observations have been made. Ultimately we plan to generate automatically short-arc solutions as soon as suitable observations from the EUROLAS cluster are available. In this way system problems can be rapidly identified, ideally before the data are made available to the analysis community. We will also consider analysing data from other lower or higher satellites, in order to distinguish constant range bias from scale error, such as might arise from a frequency error in the time-of-flight measurement device. A preliminary analysis using residuals from Lageos-1, Lageos-2, Etalon-1 and Etalon-2 to solve simultaneously for orbital corrections and station bias has suggested for example that station 7236 Wuhan has a scale measurement error of some 75mm per Mm. Such a method using Stella, Ajisai, Topex/Poseidon and Lageos has been successfully applied by

Eanes, Bettadpur and Reis (1996), and we feel that the short arc technique described here could also make a contribution to this particular investigation.

5 References

Eanes, R.J., S.V. Bettadpur, J.C. Reis. 1996. Multi-Satellite Laser Range Residual Analysis for Quality Control of the SLR Network. In Proc. Ninth International Workshop on Laser Ranging Instrumentation, Vol 1, pp 131-146, Canberra.

Sinclair, A.T. 1989. The determination of station coordinates and baselines from the 1986 and 1987 WEGENER/MEDLAS data by global and short-arc solutions. Fourth international conference on the WEGENER/MEDLAS project, Schevenin

COMPACT LASER TRANSPONDERS
FOR INTERPLANETARY RANGING AND TIME TRANSFER

John J. Degnan
NASA Goddard Space Flight Center
Greenbelt, MD 20771 USA

ABSTRACT

A conceptual design for a laser transponder, capable of precision ranging and time transfer to spacecraft orbiting about or on the surface of the inner planets of the solar system , is described. The proposed transponder, designed to operate in conjunction with the SLR2000 satellite laser ranging system, makes use of two key SLR2000 subsystems - a high repetition rate Q-switched microlaser transmitter and a correlation range receiver (CRR) which simultaneously provides centimeter precision ranging and subarcsecond level pointing corrections, even in a high background noise environment. A third important element is an ultraminiature laser-diode pumped cesium atomic clock developed by Westinghouse Corporation for the Advanced Research Projects Agency (ARPA).

The proposed transponder optical head contains a small (15 cm diameter) telescope and a low power (300 mW) microlaser transmitter and is designed to mount on the microwave communications antenna of a planetary lander or orbiter. It is assumed that the microwave communications link provides the initial crude pointing (to $\pm$ 0.3° or about 10% of the microwave beamwidth); this allows the transponder optical head to be mounted on either a two-axis tilt table or gimbal mount of limited angular range. The onboard CRR, combined with a quadrant detector, provides subarcsecond pointing angle corrections during two-way transponder operations. We demonstrate through analysis that a 2 Khz Asynchronous Transponder/ SLR2000 system, operating between Mars and Earth, is capable of recording up to several thousand two way measurements per minute and several tens of thousands of one way measuements per minute. Two way measurements allow determination of the range and the time offset between the ground and spaceborne clocks whereas one way ranges help to maintain a common boresight between the Mars and Earth-based systems and enable temporal locking as well. Decimeter accuracy interplanetary range measurements and subnanosecond clock offset determinations can easily be achieved. Improved accuracies may be possible if a ground-based maser is used to drive the SLR2000 system and "discipline" the spacecraft clock. Based on past experience with the Viking lander on Mars, current microwave system precisions appear to be limited at the few meter level. Furthermore, unlike microwaves, the absolute accuracy of an optical link is not affected by uncertainties in propagation delays induced by the interplanetary solar plasma.

1. INTRODUCTION

Lunar laser ranging (LLR) has been routinely achieved by only three stations over the past 28 years since Apollo 11 carried the first passive retroreflector array to the Moon in July, 1969 [1]. For good reasons, all LLR stations (McDonald Observatory in Texas, Grasse in France, and HOLLAS on Mt. Haleakala in Hawaii) were located at astronomical sites with above average atmospheric "seeing", and they typically employed the largest telescopes and most powerful lasers in the SLR network . In spite of these advantages, the mean signal strength is still well below a single photoelectron because of the familiar R^4 dependence of signal strength on range. The signal return rates from the Moon are sufficiently low that lunar operations are only carried out at night using special post-detection Poisson filtering techniques which extract the range signal from background noise [2] although it should be mentioned that the McDonald Laser Ranging System (MLRS) has recently demonstrated a strong lunar capability with a relatively modest telescope aperture (76 cm) and laser energy (on the order of 100 mJ) [3]. The scientific information extracted from centimeter accuracy LLR data has been enormous and includes ultraprecise measurements of the lunar ephemeris and librations, insights into the internal makeup of the Moon, as well as important tests of General Relativity and its associated metrics [1]. The

ability to extend these precise range measurements to the inner planets, or to spacecraft in orbit about the Sun, would certainly result in a similar array of important scientific results.

The most precise ranging to another planet was achieved when the radio telescopes of the NASA Deep Space Network (DSN) were in communication with the Viking Lander on Mars. This two-way microwave link resulted in measurements at the subdecameter level with 3 meters precision being the best internal consistency ever reported [4]. However, absolute range accuracies over interplanetary distances are limited by the presence of the interplanetary solar plasma which, like the similarly charged ionosphere, can have a significant impact on the propagation delay at microwave frequencies. Light frequencies, on the other hand, are much too high to be affected by the charged solar plasma, and therefore transmission media-dependent range errors are largely limited to propagation delays in the Earth and ,in the case of a Lander, planetary atmospheres which are on the order of a centimeter or less. Furthermore, the shorter optical wavelengths allow the transmitted energy to be propagated in tight, few arcsecond divergence beams resulting in larger photon fluxes and smaller collecting and transmitting apertures at both ends of the link. On the down side, much improved pointing is required to take advantage of the reduced divergence.

Although modern SLR systems, using picosecond pulse lasers and high bandwidth receivers, are capable of few mm ranging precisions and 50 picosecond time transfer between remote clocks over typical near-Earth satellite distances, extending these unique capabilities to the inner planets and beyond requires that we solve a number of important new technical issues. First of all, to overcome a prohibitively large R^4 loss, we must abandon our usual single-ended SLR station and utilize two-way laser links which we will refer to generically as "transponders". The use of microwave or laser transponders had previously been proposed for lunar ranging [5].

2. LASER TRANSPONDERS

In the simplest and most familiar transponder scheme, the ground station sends out a pulse which is detected at the spacecraft and triggers a response pulse which is in turn received by the ground station. We will refer to this as an "echo transponder". With this type of transponder, one can subtract the delay between the received and transmitted pulses at the spacecraft from the overall roundtrip time-of-flight (TOF), as measured by the ground station, to compute a range to the spacecraft. The transponder delay is either known a priori from careful preflight calibration or measured onboard the spacecraft and transmitted via microwave communication link to the ground station. The signal return rate at the ground station is then equal to the fire rate of the laser multiplied by the probability that pulses are detected at both ends of the link. This simple approach works very well when there is in a high probability of detection on both ends of the link, i.e. when both the uplink and downlink are strong and pointing uncertainties are small compared to the transmitted beamwidths. For example, an echo transponder would work quite well in conjunction with the SLR2000 ground station over lunar distances since the photon fluxes are high and well above the threshold for detection due to the smaller R^2 losses (see Figure 3). A one inch telescope aperture on the Moon would collect hundreds of SLR2000 photons per pulse in spite of its low output energy on the order of 150 µJ. However, over interplanetary distances, it is worthwhile considering an alternative approach, the "asynchronous laser transponder", which can operate effectively even when mean signal strength and detection probabilities are relatively small.

In the asynchronous laser transponder, shown in Figure 1, the ground and spacecraft lasers both fire independently at a common predetermined rate, R. The times of departure and arrival of the outgoing and incoming pulses are recorded at each end of the link and timetagged with respect to their respective system clocks. There are four possible outcomes within a given "transponder cycle" of period $\tau_c = 1/R$.
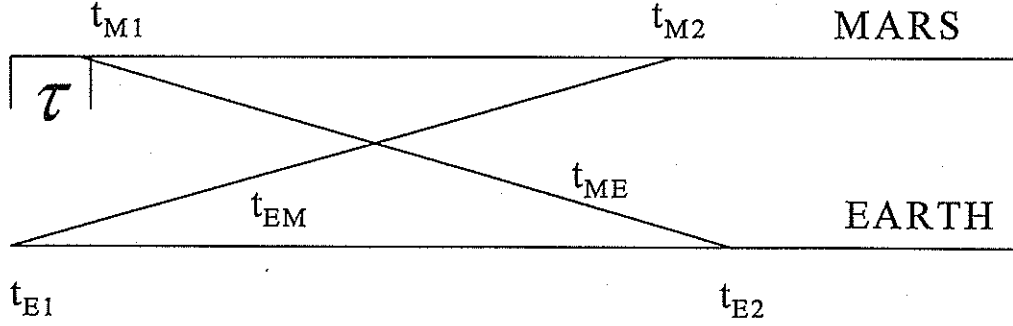
Figure 1: Timing diagram for an asynchronous laser transponder on Mars exchanging pulses with an Earth station. A pulse leaves the Earth station at time t_{E1}, travels to Mars in a time t_{EM}, and arrives at Mars at time t_{M2}. During the same transponder cycle, a pulse is transmitted from Mars at time t_{M1}, travels to Earth in a time t_{ME}, and arrives on Earth at time t_{E2}. Times of departure and arrival are referenced to that terminal's clock, and the Mars values are transmitted to Earth over the microwave communications link. The quantity τ is the time interval between the departure of pulses from the Earth and Mars stations within the same transponder cycle (500 μsec time bin for a 2 KHz system) and, combined with the outgoing pulse times, provides the offset between the ground and spacecraft clocks.

(1) No incoming pulses are detected at either terminal = $(1-P_s)(1-P_g)$
(2) An incoming pulse is detected only at the ground station = $P_g(1-P_s)$
(3) An incoming pulse is detected only at the spacecraft = $P_s(1-P_g)$
(4) Incoming pulses are detected at both ends of the link = P_gP_s

We will refer to outcome (1) as a "null event", to (2) and (3) as "one-way events", and (4) as a "two way event". Two way events allow the post facto calculation of an instantaneous spacecraft range and spacecraft clock offset via the equations:

$$R=\frac{c}{2}\left(t_{ME}+t_{EM}\right)=\frac{c}{2}\left[\left(t_{E2}-t_{E1}\right)+\left(t_{M2}-t_{M1}\right)\right] \tag{1}$$

$$\tau=\frac{\left[\left(t_{E2}-t_{E1}\right)-\left(t_{M2}-t_{M1}\right)\right]}{2\left(1+\frac{\overset{\bullet}{R}}{c}\right)} \tag{2}$$

where the intervals $\left(t_{E2}-t_{E1}\right)$ and $\left(t_{M2}-t_{M1}\right)$ are measured by the Earth and spacecraft rang receivers respectively. In (1) and (2), R and τ are the instantaneous range and clock offset at the point in time when the "photon world lines" marked t_{EM} and t_{ME} in Figure 1 cross each other.

In (2), the small correction term, $\overset{\bullet}{R}/c$, corresponding to the instantaneous range rate between the Earth station and the spacecraft divided by the speed of light, can be estimated from planetary ephemerides or the microwave communications link or iteratively solved for from the laser range data.

Null events provide no useful information and can be ignored. At a minimum, one way events provide a means of acquiring and tracking (in both angle and time) the opposite terminal togreatly improve the probability of a two way event. Combined with one-way events observed in the opposite terminal during other transponder cycles, they may permit accurate interpolation of range and clock offsets between two way events.

3. MEASUREMENT ACCURACY

Unlike artificial satellite ranging, clock effects can dominate interplanetary ranging errors with interplanetary pulse transit times on the order of several minutes. From Equations (1) and (2), the errors in the measured range and clock offsets due to a constant frequency offset error in the Earth and spacecraft clocks are

$$\Delta R = \frac{c}{2}\left[\Delta\left(t_{E2}-t_{E1}\right)+\Delta\left(t_{M2}-t_{M1}\right)\right] \approx \frac{R}{2}\left[\frac{\Delta f_E}{f_E}+\frac{\Delta f_M}{f_M}\right] \tag{3}$$

and

$$\Delta\tau = \frac{\left[\Delta\left(t_{E2}-t_{E1}\right)-\Delta\left(t_{M2}-t_{M1}\right)\right]}{2\left(1+\frac{\dot{R}}{c}\right)} \approx \frac{R}{2c\left(1+\frac{\dot{R}}{c}\right)}\left[\frac{\Delta f_E}{f_E}-\frac{\Delta f_M}{f_M}\right] \tag{4}$$

We see from the latter equations that the fractional error in range is equal to the average of the fractional errors in the two clocks whereas the fractional error in the spacecraft clock offset is proportional to the difference between the fractional errors in the two clocks. The variance in the range and offset measurements is in turn given by

$$\langle \Delta R^2 \rangle \approx R^2\left[\frac{\langle \Delta f_E^2 \rangle}{f_E^2}+\frac{\langle \Delta f_M^2 \rangle}{f_M^2}\right] \tag{5}$$

and

$$\langle \Delta\tau^2 \rangle \approx \left(\frac{R}{2c\left(1+\frac{\dot{R}}{c}\right)}\right)^2\left[\frac{\langle \Delta f_M^2 \rangle}{f_M^2}+\frac{\langle \Delta f_E^2 \rangle}{f_E^2}\right] \tag{6}$$

for two independent free-running clocks.

Thus, the single shot ranging precision and time transfer will be limited by the less accurate of the ground and spaceborne clocks. If both clocks were of maser quality (1 x 10^{-15} over time intervals of several minutes), clock instabilities would introduce submillimeter errors over distances of 1 AU and range accuracy would be limited at the cm level by uncertainties in the atmospheric propagation path as in SLR. If the spaceborne clock had the stability of a good rubidium (1x10^{-12}), as discussed in the next section, decimeter single shot range accuracies would result. With respect to single shot time transfer, the latter clock would introduce errors on the order of 250 picoseconds.

4. A TRANSPONDER CONCEPTUAL DESIGN BASED ON SLR2000

Laser and receiver technology being developed for SLR2000 lends itself extremely well to the interplanetary transponder problem because the system is designed to operate in daylight at mean signal levels as small as .0001 photoelectrons [6,7].As a result, few demands are placed on either the ground or space segments with regard to size, weight, or prime power in order to accomodate high power lasers or large optical telescopes and their equally large pointing gimbals.

A conceptual design for an asynchronous laser transponder, capable of decimeter precision ranging and subnanosecond time transfer to spacecraft orbiting about, or on the surface of, the inner planets of the solar system , is described in Figure 2. The transponder, which is designed to operate in conjunction with the SLR2000 satellite laser ranging system, makes use of two key SLR2000 subsystems - a high repetition rate Q-switched microlaser transmitter [8] and a correlation range receiver (CRR) which simultaneously provides centimeter precision ranging and subarcsecond level pointing corrections, even in a low signal-to-noise environment [6]. A third important element is an ultraminiature laser-diode pumped cesium atomic clock [9] developed by Westinghouse Corporation for the Advanced Research Projects Agency (ARPA) which weighs only 60 grams and has a spatial volume of 25 cm^3, a power consumption of only 300 mW, and the performance of a good rubidium time reference (i.e. 1 part in 10^{12} over several minute intervals typical of interplanetary light transit times).

The microlaser is anticipated to be very lightweight and could be designed to operate at about 15% optical efficiency with only a few watts of prime power to the pump diodes. A flight-qualified event timer, the major component of the CRR, has been developed by the Smithsonian Astrophysical Observatory (SAO). It has a 10 picosecond resolution, weighs less than 1 Kg, and consumes about 9.25 Watts of prime power [10]. With the exception of the flight computer, which is expected to consume on the order of 7 Watts, the other transponder components in Figure 3 consume little or no power, and it is therefore not unreasonable to propose an interplanetary laser transponder weighing a few Kg and consuming less than 20 Watts of power.

The transponder optical head contains a small (15 cm diameter) telescope and a low power microlaser transmitter and is designed to mount on the microwave communications antenna of a planetary lander or orbiter. It is assumed that the microwave communications link provides the initial crude pointing to about ± 0.3° or roughly 10% of the microwave beamwidth for a nominal one meter antenna operating in X-band (7.9 GHz). This allows the transponder optical head to be mounted on either a two-axis tilt table or gimbal mount of limited angular range. These can be driven by simple stepper motors.

The distance between Earth and Mars is routinely known to about 100 meters using ephemerides provided by the Jet Propulsion Laboratory [4], and, as mentioned previously, microwave communications to the lander reduces this uncertainty below 10 meters. Thus, if we knew when the pulse left the opposite terminal, the pulse arrival time uncertainties would be between 100 nsec and 1 μsec , similar to the range gates used by SLR2000 in acquiring artificial satellites in daylight. However, due to the asynchronous nature of the link, the pulse departure time from the opposite terminal is generally not known a priori (although prior successful transponder experiments can greatly narrow the range of search if the laser fire times are tied to their respective clocks). At night, the relatively narrow transponder field of view defined by the microwave antenna pointing uncertainty can be monitored for incoming pulses by an integrating CCD array in the telescope focal plane which views the Earth through a narrowband 532 nm filter. A rapid buildup of photoelectron counts within one or more localized pixels in the approximate 200 by 200 pixel array indicates the presence of a beam from Earth and provides an intermediate
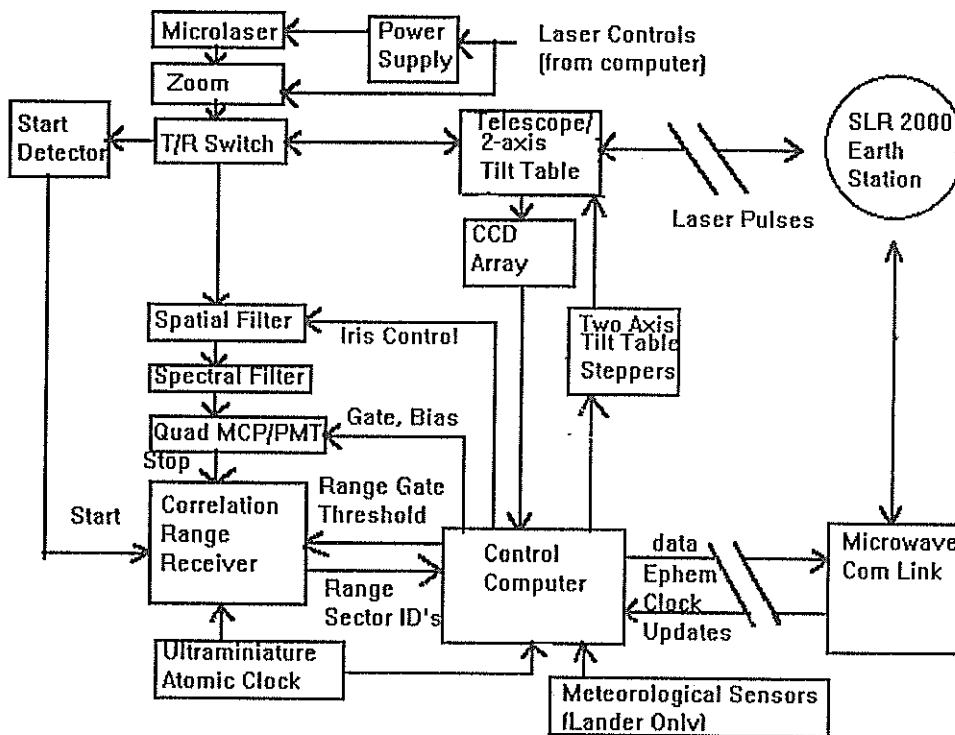
Figure 2: Block diagram of an Asynchronous Laser Transponder working in tandem with an SLR2000 Earth Station.

level of pointing correction at the few arcsecond level which places the Earth station within the transponder beam. In daylight, one can add an optical gating mechanism, if necessary, to reduce background noise . In the worst case,a terminal in daylight conditions must conduct a temporal scan of the range gate over the 500 μsec cycle time (in few microsecond increments) in order to acquire and lock onto the opposite terminal. Fortunately, the Earth station pointing can be quite accurate due to a combination of precise ephemerides, routine star calibrations, and accurate mount modelling.

The Q-switched microlaser emits 150μJ, 140 psec pulses at a repetition rate of 2 KHz through the 15 cm telescope which reduces the transponder beam divergence to about 40 μrad (2X diffraction limit). During transponder operations, the onboard CRR, with input from the quadrant timing detector, provides fine pointing angle corrections at the subarcsecond level [6] and keeps the small transponder telescope pointed at the Earth source while the ground-based SLR2000 receiver performs a parallel function using the incoming transponder pulses as a guide.

5. EXAMPLE: EARTH-MARS LINK USING SLR2000 AS A BASE STATION

We now consider the example of SLR2000 ranging to a transponder on the surface of Mars. Among the inner planets, this represents a worst case scenario since the distance between Earth and Mars varies between 0.52 and 2.52 astronomical units (between 80 and 380 Million Km). The output energies of both Nd:YAG microlasers are set at 150 μJ per pulse, the maximum eyesafe energy allowed for an Earth-based telescope aperture of 40 cm. With a repetition rate of 2 KHz, this corresponds to an average output power at the green 532 nm wavelength of 300 mW. On the transponder end, where there are (presumably) no eye safety issues , the radiation exits through a relatively small 15 cm transmit/receive aperture. The full angle beam divergence at both ends of

the link is assumed to be the SLR2000 value of 40 microradians. We have also assumed a rather conservative value for the detector quantum efficiency (20%) and realistic values for the throughput of the transmit (80%) and receive (54%) optics and the atmospheric channel (70%) on each end of the link. We further assume that the threshold is set at one photoelectron at both ends of the link resulting in a probability of detection given by Poisson statistics

$$P_D = 1 - e^{-n_s} \approx n_s \qquad (7)$$

where n_s is the mean signal level (different at the two terminals due to the different collecting aperures)and the approximation holds for $n_s \ll 1$. Over the range of Earth-Mars distances, mean signal n_s varies from about 0.1 to about .005 pe/pulse for the Mars terminal and about a factor of seven higher at the Earth terminal due to its larger telescope. Thus, the Earth terminal records about seven times more one way eventsthan the Mars terminal.
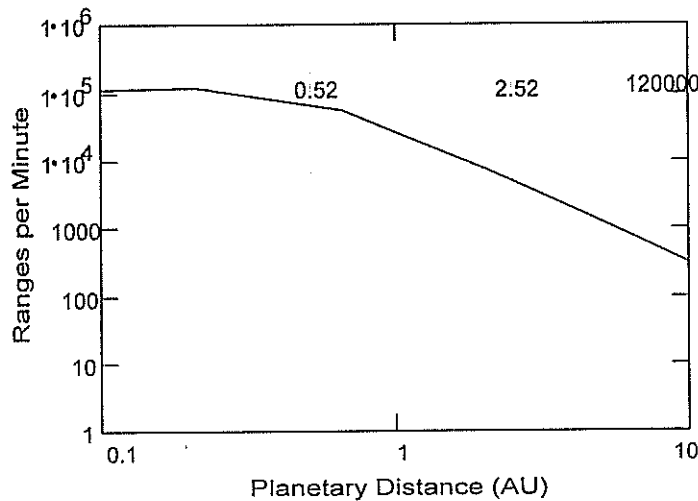
Figure 3: The number of "two-way" events (dashed line) and the number of non-null events (solid line) per minute as a function of range in AU. The Mars-Earth distance varies between 0.52 and 2.52 AU and represents a worst case for the inner solar system. The SLR2000 laser fire rate is 120,000 pulses per minute (2 KHz).

In Figure 3, the number of "two way" events per minute is represented by the curved dashed line whereas the curved solid line represents the summed rate of "two-way" and "one-way" ("non-null") events. The SLR2000 laser fire rate of 120,000 pulses per minute is indicated by the horizontal dashed line near the top of the graph and is included for reference. The two verical dashed lines represent the extremes of the Earth-Mars distance. We note from the figure that the number of "two-way" events varies from several thousand per minute at its nearest approach to Earth (0.52 AU) to about 20 per minute as Mars moves to the opposite side of the Sun from Earth (2.52 AU). Similarly, the number of "non -null" events (sum of one-way and two-way events) falls from several tens of thousands per minute to several thousand per minute. This high "non-null" rate should allow both the ground and space-based systems to effectively lock onto each other with respect to both pointing angle and range gate. Note that, with the simple "echo transponder" discussed previously, the ground station would only record events at the "two-way" rate since the "echo transponder" only fires a pulse upon detecting a pulse from Earth. Thus, an "echo transponder" makes it much more difficult for the Earth station to actively lock onto the spacecraft laser relative to the asynchronous case, although, as mentioned previously, open loop pointing to the spacecraft should be relatively accurate.

6. SUMMARY

We have demonstrated through analysis that a compact, low power Asynchronous Laser Transponder working with the SLR2000 system, each operating at 2 KHz rates between Mars and Earth, is capable of recording up to several thousand two way measurements per minute and several tens of thousands of one way measurements per minute. Two way measurements allow precise determination of the range and the time offset between the ground and spaceborne clocks whereas one way ranges help to maintain a common boresight between the Mars and Earth-based systems and can potentially provide other useful information. Due to interplanetary light travel times which are several orders of magnitude longer than is typical for artificial satellites, the absolute accuracy of the range and clock offset measurements is determined more by the frequency accuracy and stability of the ground and spaceborne clocks than by errors in the range vernier or propagation delays in the transmission channel, which are typically at the subcentimeter level. Decimeter accuracy interplanetary range measurements and subnanosecond time transfer would appear to be easily achievable with the conceptual system described here. If a ground-based maser were used to govern the SLR2000 timing and to "discipline" the onboard ultraminiature atomic clock, significantly greater accuracies might be achieved. Based on past experience with the Viking lander on Mars, current microwave system precisions appear to be limited at the few meter level. Furthermore, unlike microwaves, the absolute accuracy of an optical link is not affected by uncertainties in propagation delays induced by the interplanetary solar plasma.

REFERENCES

1. Dickey, J. O. , P. L. Bender, J. E. Faller, X. X. Newhall,R. L. Ricklefs, J. G. Ries, P. J. Shelus, C. Veillet, A. L. Whipple, J. R. Wiant, J. G. Williams, and C. F. Yoder, "Lunar laser ranging: a continuing legacy of the Apollo Program", Science, 265, pp. 482-490, 1994

2. Abbott, R. I., P. J. Shelus, R. Mulholland, and E. Silverberg, "Laser Observations of the Moon: Identification and Construction of Normal Points for 1969-1971", The Astronomical Journal, 78, pp. 784-793 , 1973.

3. Shelus, P. J., J. R. Wiant, R. L. Ricklefs, A. L. Whipple, and J. G. Rie, "The impact of technology on LLR at MLRS", these Proceedings

4. Lemoine, F. J., NASA Goddard Space Flight Center, private communication.

5. Bender, P. L., J. E. Faller, J. L. Hall, J. J. Degnan, J. O. Dickey, X.X. Newhall, J. G. Williams, R. W. King, L. O. Machnik, D. O'Gara, R. L. Ricklefs, P. J. Shelus, A. L. Whipple, J. R. Wiant, and C. Veillet, "Microwave and Optical Lunar Transponders", in Astrophysics from the Moon, AIP Conf. Proc. Series, (American Institute of Physics New York) April, 1990.

6. Degnan, J. J. , J. McGarry, T. Zagwodzki, P. Titterton, H. Sweeney, H. Donovan, M. Perry, B. Conklin, W. Decker, J. Cheek, A. Mallama, and P. Dunn, "SLR2000: An inexpensive, fully automated, eyesafe satellite laser ranging system", these proceedings.

7. McGarry, J., "SLR2000 Performance Simulations", these proceedings

8. Degnan, J. J., "Optimal Design of Q-switched Microlaser Transmitters for SLR", these proceedings.

9. Lieberman , I. and H. Nathanson, Westinghouse Corporation, Pittsburgh, PA, USA, private communication.

10. Mattison, E., Smithsonian Astrophysical Observatory, Cambridge, Massachusetts, USA, private communication.

A Wide Angle Airborne or Spaceborne
Laser Ranging Instrumentation
for Millimeter Accuracy Subsidence Measurements

O. BOCK and M. KASSER
Ecole Supérieure des Géomètres & Topographes, 18 allée Jean Rostand, 91025 EVRY Cedex, France

Ch. THOM
Institut Géographique National, Laboratoire d'Optoélectronique et de Microinformatique, 2 avenue Pasteur, BP 68, 94160 Saint Mandé, France.

I. INTRODUCTION

A wide-angle airborne laser ranging system is under investigation at IGN [i, ii]. This system is intended to achieve a new geodesy technique, based on aerial multilateration. Extension to a spaceborne system is also considered. The technique should have the capability of detecting height displacements of ground-based benchmarks with sub-millimeter accuracy in a very short time (a few hours). It would be particularly adapted to the daily monitoring of a network of typically 100 benchmarks, extending over an area of 10 by 10 km. For instance, it would be adequate for estimating surface effects induced from fluid withdrawal or solid extraction [iii]. But it can be extended to periodic monitoring of more general geophysical processes where a millimeter accuracy of the vertical component is required, e.g., tectonics, volcanology, and geology. Assuming that some benchmarks are fixed, i.e., that they are far away from the deformation area, only relative locations are to be considered since one is interested in displacements not locations.

Airborne or spaceborne laser ranging systems, with the ranging system onboard, appear as attractive solutions for monitoring large networks of ground-based retroreflectors. Several such systems have been studied during the last fifteen years [iv, v, vi]. But the use of multi-beam, servo-controlled, pointing systems made them rather complicated and they were, in a first time, transformed into single narrow beam systems and, finally, abandoned. Using a wide-angle beam simplifies considerably the instrumentation while needing a proper signal processing, in order to identify which reflectors are measured. In order to assess the accuracy of such a system, we have developed a first instrument made several terrestrial experiments.

In section 2 of this paper, we describe the principle of wide-angle aerial and spatial multilateration. Such techniques are based on simultaneous distance measurements, achieved, in our case by the use of a wide angle laser beam. The instrumentation and its associated signal processing is presented in section 3. In section 4 we analyze the main error sources : atmospheric effects, laser effects, and effects from the detection electronics (signal-strength related biases, electrical noise, and temporal jitters). In section 5 we present experimental results, obtained from three different terrestrial experiments. Finally, in section 6 we propose an optimization of the current instrumentation, to fulfill the requirements for airborne and also spaceborne configurations.

II. PRINCIPLE OF WIDE-ANGLE AERIAL AND SPATIAL MULTILATERATION

The aerial or spatial multilateration technique is based on range measurements, to a network of ground based benchmatrks, performed from an airborne or spaceborne platform

(Figure 1). By using an inverse method, benchmarks can then be positioned, with an accuracy depending only on the accuracy and number of measurements and the geometrical configuration. Typically, the single-shot ranging accuracy is a few centimeters, and requires negligible biases.

We investigated this technique a few years ago, by a numerical simulation approach, based on the assumption that an ad hoc instrument could be developed to fulfill these requirements. We found that the objective of a vertical precision of 1 mm could be achieved, using a least-squares adjustment method, with some requirements on measurements. A priori locations of the aircraft and the benchmarks have to be known within a few decimeters. This requirement is not critical because it is used only as a first trial of a few iterations. On the other hand, the accuracy of relative distances and the number of measurements are critical. They must respectively be, for example, a few centimeters and a few thousands per retroreflector. The a priori locations are easily achievable by GPS techniques, e.g., Differential-Trajectography for the aircraft, and Rapid-Static for the ground based benchmarks. Note that the complete network survey for a priori locations has only to be performed once, before the first aerial survey. Posterior surveys can simply use the previous results.
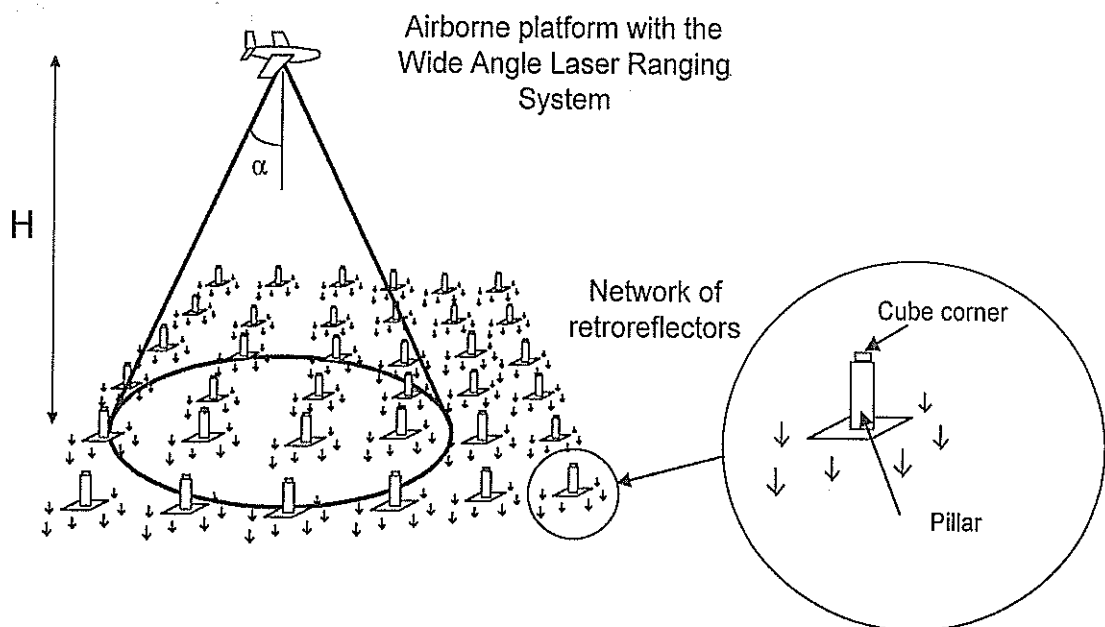
Figure 1: View of a typical airborne configuration, over a ground-based retroreflector network.

The use of a widely diverging laser beam (± 15 ° around nadir), illuminating the network of ground-based optical cube corners, seems a good solution to this problem. For one pulse transmitted by the laser, several echoes (typically ten) are retroreflected. By estimating precisely their times-of-flight and correcting for the mean refraction effect we achieve simultaneous range measurements and create strong constraints on both the coordinates of the laser source with respect to the network of reflectors, and between the coordinates of the reflectors. Note also that, the more the laser beam is divergent, the best is the horizontal accuracy of the positioned benchmarks. But since we are mostly interested in the vertical component, the range measurements are preferably done in a moderate field with around nadir. Atmospheric refraction effects are thus not critical to correct. By a proper modeling of both direct and inverse problems, one can also add other unknowns to the fundamental model, like a range bias fluctuating from shot to shot. By taking into account such a range bias, one has only to estimate arrival times of the laser echoes. The associated ranges are then called pseudo-distances, as in GPS where the transmitter

and receiver clocks are not synchronized. Relative pseudo-distances become then fundamental observations. Modeling the range bias has two interesting consequences. Firstly, it relaxes the constraints on refraction index correction as only differential variations need to be corrected. Secondly, it allows to record the detected signal only during the time window where echoes are expected. The amount of static memory of the recorder (digital oscilloscope, cf. next section) can thus be reduced.

III. INSTRUMENTATION AND SIGNAL PROCESSING

A. Instrumentation

A block diagram of the wide angle laser ranging system is illustrated in Figure 2. The mode-locked Nd:YAG laser transmitter (modified Quantel, from the Mobile Satellite Laser Station, Observatoire de la Côte d'Azur, Grasse, France) is based on a stable cavity with uniform reflectivity mirrors, aperture for TEM_{00} mode selection, passive Q-switch (saturable absorber) and active mode-locking (acousto-optic modulation). Mode-locking produces a train of 100 psec pulses in an average waveform of 70 nsec (FWHM), of which one pulse is extracted and amplified up to 100 mJ by a double-pass Nd:YAG amplifier. The pulse repetition frequency is 10 Hz.

The wide-angle beam is produced by whether a diverging lens or a ground glass plate, and is typically 15° at half-angle. But, in order to reduce irradiance fluctuations produced by speckle patterns, a diverging lens is preferred [vii]. For each laser shot, multiple echoes, arising from the network of retroreflectors, are detected and their waveforms are recorded. The photodetector is composed of a large area (1 cm^2) PIN photodiode (EG&G, YAG 444). The long transit-time of the photodiode (about 6 nsec), combined with a high transimpedance amplifier (3000 V/A gain, 50 MHz bandwidth), produces electrical response pulses of typically 13 nsec (FWHM), with a 4 nsec leading edge. The electrical signal is sampled by a digital oscilloscope (Lecroy 7200), with a 1 nsec period, and stored, whether in central memory of the oscilloscope or on the hard-drive of a host computer (Fieldworks 7500, PC) in real-time by GPIB. Note that the hardware of our system is much simpler than earlier proposed airborne and spaceborne systems [iv, v, vi], and also than current SLR systems [viii]. In return, the digitized signal has to be processed properly to retrieve the times-of-flight of laser pulses.
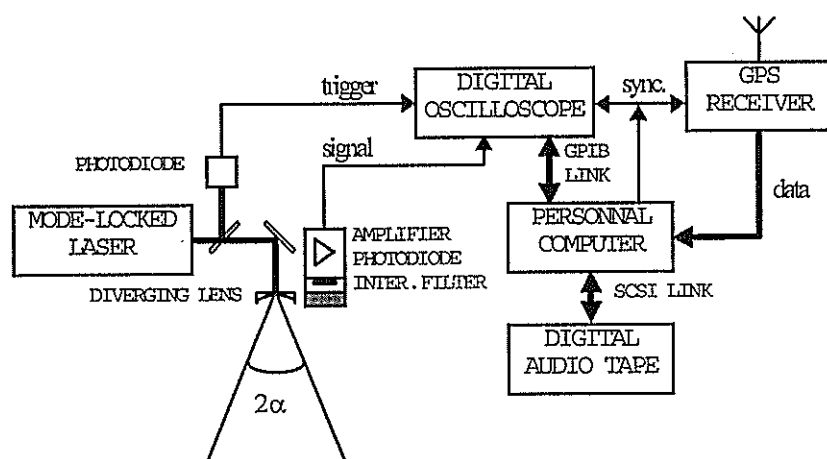
Figure 2 : Block diagram of the wide-angle airborne laser ranging instrument. A fixed GPS receiver (not shown) is also required at a ground station for differential trajectography.

B. Signal processing

The signal processing is composed of two steps. Firstly, measured echoes have to be properly identified, i.e., detected pulses have to be assigned reflector numbers. Therefore, the range bias is roughly estimated by correlating the measured signal with a Dirac comb composed of delta-functions at the approximate arrival times, calculated from a priori locations. The resulting range bias is accurate within one sampling interval, i.e., 1 nsec (15 cm), which is far enough for detecting 13 nsec FWHM pulses. Remember that the residual range bias is accurately estimated during the global inversion. Secondly, times of arrival of the detected pulses are estimated with an accuracy of, say, 100 psec (15 mm). To achieve this, one can implement either sub-optimum methods, or optimum methods, e.g., minimum mean-square error and maximum likelihood methods. We analyzed several ones, such as leading-edge threshold detection, center-of-gravity, cross-correlation and deconvolution. The first two belong to the sub-optimum estimator class, while the last two are two implementations of the same optimum method. Table 1 compares the theoretical precision of these methods.

Estimation method	Leading edge	Center-of-gravity	Cross-correlation
Single-shot accuracy	42 psec (6.3 mm)	29 psec (4.3 mm)	23 psec (3.4 mm)

Table 1 : Theoretical single-shot precision, i.e., standard deviation or estimation error in presence of additive noise, of several time-of-arrival estimators. Signal and noise characteristics are representative of the current instrumentation, assuming an electrical SNR of 100.

When combining the approximate range bias, i.e., the time of departure of the laser pulse, and the estimated times of arrival of the reflected pulses, one has a set of simultaneous "pseudo" times-of-flight. Here again, "pseudo" refers to the fact that only relative times-of-flight are known with the proper accuracy. When converting these times to distances, with the help of an atmospheric refraction model, e.g. [ix], one gets a set of simultaneous pseudo-distances. Therefore, we consider only relative distances.

Cross-correlation is an efficient pseudo-range estimator for individual pulses. But in operational configurations several pulses are reflected simultaneously. Pulse-superimposition, when reflectors are close in distance, produce then biases because pulse shapes are altered. In order to take into account the mutual effect of pulses, it is necessary to estimate simultaneously all the echoes in the oscilloscope trace. Therefore, we implemented a deconvolution method, fitting pulses of a synthetic trace on every measured trace by a least-squares adjustment. The reference pulses of the synthetic trace must be close, in their waveforms, to the real pulses. Therefore, we use an average measured pulse. Note that this method is, on a mathematical point of view, equivalent to the cross-correlation, with a reference function equal to the average measured pulse. In a second step we perform a sorting of the ranges estimated, rejecting all ranges closer than 4 m to another range. In this way we avoid to use estimations from pulses which may be affected by superimposition effects or even which may be wrongly affected a reflector number.

IV. ERROR SOURCES IN WIDE ANGLE LASER RANGING

A. Atmospheric effects

The first error source stems from atmospheric refraction. Since we are interested in relative distances, only differential refraction effects have to be corrected, i.e., stemming from the part of atmosphere between the reflectors. When using local meteorological measurements, one is able to correct for this effect with an accuracy of a few mm with a spherical shell model [ix]. In a typical application, these parameters are necessary in order to correct for tropospheric effects of

.GPS measurements, at the reference, ground based, station and in the aircraft. It is thus necessary to relate the atmospheric parameters at the reflectors of the network to these meteorological measurements. This can be done with the help of basic thermodynamics. Deviations of local parameters from this model, especially in the boundary layer, should lead to biases lower than 1 mm. On the other hand, turbulence produces also path length fluctuations. The strength of this effect can be evaluated by the path length structure function [x]. It should remain below the millimeter level both in the case of the terrestrial experiments presented in section 5 and in the case of a typical airborne experiment. In the general case, refraction effects can thus be neglected.

A second effect, induced by atmospheric turbulence, is irradiance fluctuations, or scintillation. Phase perturbations of the propagating optical wave induce interference effects and, therefore, intensity, phase and angle-of-arrival fluctuations at a point receiver. In weak turbulence regime, intensity statistics are governed by a log-normal probability density function (pdf) [xi], whereas in strong regime, the pdf become rather exponential [xii]. We can therefore expect, in aerial, and even more in spatial, configurations near unity scintillation contrasts. The main effect of these fluctuations is a reduction of the number of simultaneous measurements above a fixed SNR threshold. The impact of the remaining atmospheric induced scintillation, on the constraints created by the measured pseudo-distances on the multilateration problem, is one of the next effects to be analyzed. A statistical analysis of this phenomenon would be useful to optimize instrumental parameters, such as beam divergence, pulse repetition frequency, and aerial survey duration or number of satellite passes.

B. Laser beam effects

Wavefront distortions in laser beams have been well known to the SLR community, because they are among the most limiting phenomena at the instrumentation [xiii]. Biases up to a few nanoseconds have been reported in Q-switched lasers [xiii]. We have also investigated two different laser transmitters and measured biases reaching half the pulsewidth at the edge of the beam [ii]. The first laser was an unstable cavity resonator, with super-gaussian mirrors (Quantel, Brillant), transmitting a 4 nsec, 350 mJ pulse. The second laser was the mode-locked laser, described in section 3. We showed that our mode-locked laser produces biases, in the near-field, of about 100 psec (15 mm) at the edge of the beam ($1/e^2$ intensity), or 50 psec (7.5 mm) at FWHM, while for the unstable cavity laser, biases reach 2 nsec at the edge [ii]. Mode-locked lasers have the advantage of producing a smooth temporal waveform pulse and low far-field angular biases thanks to the transverse mode stability achieved by the long build-up of the beam. Nevertheless, there exist some . other means of achieving picosecond laser pulses, with consequently low wavefront distortion, such as pulse compression techniques, e.g., backward Stimulated Brillouin Scattering [xiv]. But such devices have not yet been evaluated.

C. Signal strength related biases in the detection stage

The second, deterministic, error source is a temporal bias depending on the signal · magnitude, stemming from both the photodiode and the amplifier. As the signal magnitude fluctuates, this effect increases the bias and the standard deviation of range measurements. A characterization of the detection stage revealed this effect was present predominantly in the amplifier but was not significant in the photodiode. A linear relationship, with a slope of 0.5 m/V, has been reported [vii]. It can thus be corrected on individual range measurements, knowing their amplitude. Without correction, biases of almost 20 cm may arise, whereas corrected data exhibit a gaussian scatter of a few cm standard deviation [vii].

D. Electrical noise in the detection stage

Electrical noise in the detection stage is mainly composed of additive Gaussian noise from the photodetector, amplifier and oscilloscope. The predominant noise in the photodiode is shot-

36

noise stemming from the received laser pulses, solar background illumination, and dark current. The solar irradiance is reduced by an interference filter of large bandwidth (20 nm at 1.064 µm), allowing transmission of the wide angle beams. This current is, with the dark current, generally negligible with respect to the signal photocurrent. Thus, only shot-noise produced by the laser pulses has to be considered. The total shot-noise is about 70 µV for a 100 mV signal magnitude at the output of the amplifier. Electrical noise in the amplifier is mainly produced by active components, such as bipolar transistors. It reaches 260 µV rms for a 95 MHz bandwidth. The oscilloscope produces electrical noise and quantization effects, though the second effect is negligible. We measured typical values of 230 µV, rms, at 5 mV/div.

We compared photodiode shot-noise, amplifier noise and oscilloscope noise, for caliber ranging from 5 mV/div. to 500 mV/div., and assuming the detected signal is of 5 divisions magnitude (in order to compute the photodiode shot-noise) [vii]. Since the electrical noise in the oscilloscope is roughly proportional to the caliber, it is always superior to the photodiode shot-noise. The amplifier noise becomes predominant only for weak signals. The noise spectral density has to be considered, since in bipolar transistor devices, such as amplifiers and oscilloscopes, it is generally not constant. On the other hand, since non-stationary noise, e.g., shot-noise, can be neglected with respect to the other noise sources, the overall noise can be assumed stationary.

We analyzed the variance, σ^2, of the cross-correlation time-of-arrival estimator in presence of additive gaussian noise [vii]. The ranging precision, i.e., standard deviation, can be put into form

$$\sigma \approx \frac{K}{SNR}$$

where $SNR = \dfrac{a}{\sigma_n}$ is the signal-to-noise ratio, $\sigma_n^{\ 2}$ the noise variance, a the magnitude of the measured pulses, and K a waveform dependent parameter [vii]. Parameter K can be related to the rise time and fall time of the impulse-response of the detection stage. Thus, for a typical value of $K = 0.3$ m, an SNR of 100 yields a ranging accuracy of 3 mm, independently of other error sources.

E. Temporal jitters

Time-of-arrival uncertainty of single photons is a fundamental temporal limitation. But, in our system, the detected laser pulse contains typically 10^4 photons, this effect can thus be neglected. On the other hand, the digital signal is affected by a temporal uncertainty with respect to the sampling grid of the oscilloscope. We evaluated this uncertainty, which is also an estimate of the sampling clock stability, to be at a few picoseconds level, over a typical 10 µsec interval. It can, therefore, be neglected. In order to analyze the effect of the signal sampling, we performed numerical simulations. A careful modeling of the instrumentation yielded a dispersion of 20 psec (3 mm).

F. Budget of error sources

Error source	Type	Order of magnitude	Conditioning parameters
1. ATMOSPHERE			
Mean refraction correction	systematic	< 1 mm, 1 °C deviation	Micro-meteorological effects
Pathlength fluctuations	random	0.8 mm, $C_n^2 = 10^{-14}$ m$^{-2/3}$	Turbulence structure constant, C_n^2
Scintillation	random	shot-to-shot SNR fluctuations	C_n^2 and SNR
2. LASER			
Wavefront distortion	systematic	< 1 cm, 100 psec FWHM laser	Cavity mode build-up

Electronic noise	random	3 mm, SNR=100	K, SNR
Magnitude related biases in the amplifier	systematic	negligible, after numerical correction	Correction model
Sampled signal aliasing	random	< 3 mm, 1 nsec sampling	sampling period, detection response-time
4. WIDE-ANGLE RANGING			
Pulse superimposition	systematic	negligible, when using deconvolution estimator and proper data sorting	Reference-pulse waveform, instrumental pulse discrimination

Table 2 : Summary of error sources limiting the ranging accuracy

Table 2 summarizes the accuracy limitation from the error sources described in the previous sub sections. We can assume from this analysis that cm accuracy is achievable with the current system. In the next section we present an experimental verification of this assumption.

V. RANGING PERFORMANCE EVALUATION FROM TERRESTRIAL EXPERIMENTS

In order to assess for the ranging accuracy of the developed instrument we performed three terrestrial experiments, differing by pathlength, instrumental configurations and turbulence regimes. For each experiment, we evaluated the standard deviation for relative range estimations and compared it to the theoretical precision, predicted by the above equation of σ. The theoretical precision gives an estimate of the single-shot accuracy of a sequence of measurements, characterized by its accuracy-constant K, and its SNR. Since standard deviations do not reveal biases in relative-distances, we also performed repeatability tests. Therefore, we computed mean relative distances and error bars for several samples of 100 measurements. Discrepancies between mean relative distances and error bars, with respect to the overall mean value, were used as an indicator of biases. The results and main characteristics of these experiments have been presented in [vii]. We summarize then in Table 3.

The first experiment validated the proposed instrument, composed of a mode-locked laser with a low impulse-response photodetector, and cross-correlation as time-of-arrival estimator. The standard deviation of relative distances, defined as single-shot accuracy, was better than 8 mm (SNR around 30). Biases, estimated by means of the above-mentioned repeatability test, were about 4 mm (SNR around 30). The second experiment showed that, when employing a transimpedance amplifier, the instrument still achieves centimeter precision, even for very low SNRs (e.g., 5.4 cm for SNR=5). The third experiment confirmed these performances at even longer distances, up to 1 km. Note that in the last experiment a diverging lens was used to achieve the beam divergence.

Exp.	Number of meas./seq.	SNR	K (m)	standard deviation σ_ρ (mm)	repeatability $\Delta\rho$ (mm)
1	43 - 100	33 - 91	0.16 - 0.29	3.6 - 7.8	< +/- 4.0
2	23 - 70	5 - 62	0.24	4.6 - 54	
3	6 - 25	15 - 36	0.72	22 - 60	< +/- 20

Table 3 : Summary of the main characteristics of three terrestrial experiments and the achieved accuracy (standard deviation and repeatability).

Figure 3 illustrates the relationship between single-shot accuracy and SNR, from data of the three terrestrial experiments. One can note that good agreement is found between measured and predicted values, even for high SNRs. This is due to the fact that amplifier biases are properly corrected. This is a fundamental assumption. Moreover, in these experiments the pulse shape

control and noise spectral distribution were identified as critical to keep low values of K and thus high ranging precision.
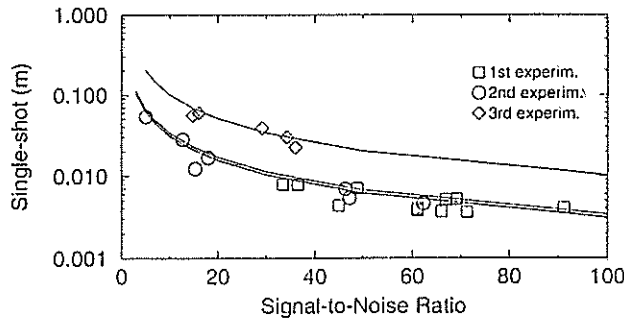
Figure 3 : Comparison of measured and predicted single-shot precision, versus SNR, for three terrestrial experiments. Note that, for $K = 0.22$ m, SNRs above 5 produce a 7 cm single-shot precision.

In fact, the second experiment of Figure 3 was intended to test the performance of the inverse method of our multilateration technique from real data. It was implemented as a reduction of a typical aerial configuration to a two-dimensional terrestrial configuration. This experiment was conducted near Paris, in December 1995. After computation of the experimental range data, we found a relative positioning accuracy between 1 and 4.4 mm, rms, on the radial component, and between 1.8 cm and 7.8 cm on the transverse component [xv].These results are compatible with theoretical predictions from the covariance matrix and with numerical simulations, validating thus both the instrumentation and the simulation models. On the basis of these results, an aerial experiment simulation showed that the vertical component of retroreflectors could be estimated with a sub-mm accuracy, providing the instrumentation was adapted to the longer range constraint. An optimization of the present system is therefore proposed below.

VI. SYSTEM OPTIMIZATION

A. Aerial configuration

In a typical aerial configuration, i.e. 10 km altitude, the current instrumentation yields a SNR of 1.3 and a single-shot ranging accuracy of 21 cm. In order to satisfy the requirement of at least 3 cm ranging accuracy, we have to optimize the current instrumentation. This can be achieved by means of minimizing σ^2. As a first approach three different, though related, parameters can be considered. The first is the signal strength. Optimization could thus be achieved by maximizing the link budget (through the receiver surface or responsivity), or the amplifier gain, or by reducing the response-time of the detection stage. The second is the overall electronic noise. Since it stems mostly from amplifier, this element should be optimized, e.g., by reducing the bandwidth. The third parameter is K. It can be lowered by reducing the response-time of the photodetector. When expressing σ^2 as a function of instrumental parameters, we identified the fundamental and independent parameters conditioning the ranging accuracy as being : amplifier gain, photodetector surface, and photodetector transit time. A further parameter can be investigated : the detector technology (APD vs. PIN photodiode).

1. Amplifier gain

Assuming the predominant noise source is the transimpedance amplifier, the SNR varies as the square-root of the gain, i.e., feed-back resistance. By taking into account the convolution effect of the impulse-response, for high gain, i.e., low bandwidth, the response is inversely

39

proportional to the gain, the accuracy is thus reduced. Identically, for low gain, i.e. high bandwidth, the fall-time of the impulse-response becomes independent of gain. The accuracy is therefore also reduced. An optimum gain near 1400 ohms can be found (see Figure 4), but the accuracy improvement is small. On must thus conclude that the amplifier gain can hardly be optimized.
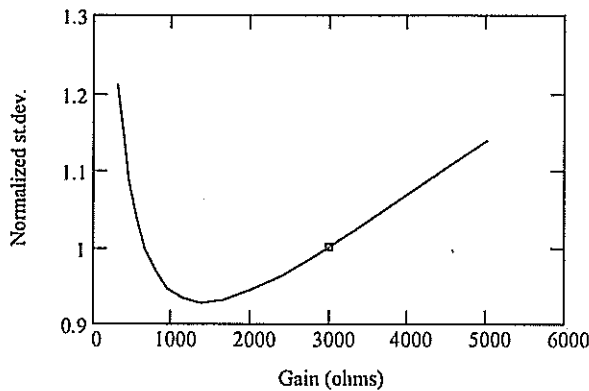
Figure 4 : Normalized accuracy (with respect to the current instrumentation, shown by the small box) vs. gain of the transimpedance amplifier

2. Photodetector surface

The photodetector surface must be high so as to keep an acceptable figure for the link budget with large field optics. But an increase of this surface produces an increase of the junction capacitance and, consequently, a reduction of the bandwidth. Finally, the accuracy becomes independent of the photodetector surface, for high values. Conversely, for low values the junction capacitance is no more a limiting parameter. Decreasing the surface just decreases the link budget and, therefore, the ranging accuracy. Hence, this parameter does not exhibit an optimum like the previous one (see Figure 5). A nearly asymptotic accuracy optimum could be achieved with a $10 \, cm^2$ photosensitive surface detector. But this requirement seems rather unrealistic. Photodetector surface can, therefore, hardly be optimized.
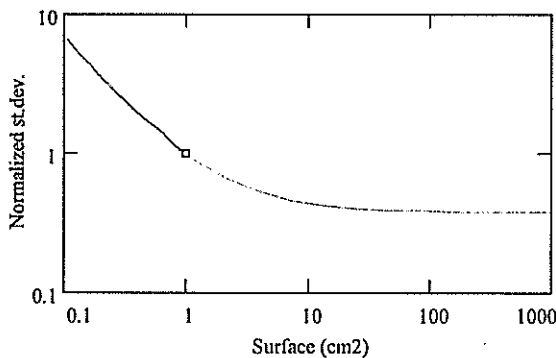
Figure 5 : Normalized accuracy vs. photodetector surface.

3. Photodetector transit time

Reduction of the photodetector transit time can be achieved, on a technological point of view, by reducing the width of the intrinseque zone (for a PIN structure). But the quantum efficiency is then consequently reduced. Again, this parameter does not exhibit any optimum and can hardly be improved (see Figure 6). But, once again, the current system is already near the optimum.
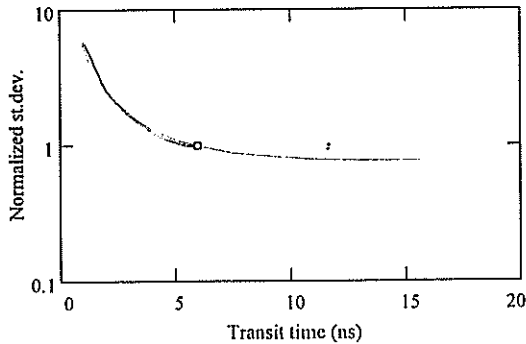
Figure 6 : Normalized accuracy vs. photodetector transit time.

4. Photodetector technology

Finally, there is an other fundamental parameter that we did not consider in the above optimization : the photodetector technology. The absorption coefficient of Si (of which the current PIN photodiode is made) is of 21 cm^{-1} at 1.064 µm whereas for Ge, it is about 10^4 cm^{-1}. But this latter technology is known as producing stronger electronic noise [xvi]. For InGaAs, sensitivities of 0.7 A/W are possible at 1.064 µm, but it seems that available detectors are limited to nearly 3 mm diameters. Actually, the best way to improve the current instrumentation seems to be the use of large photosensitive surface APDs. Such devices, with diameters up to 16 mm, are proposed by Advanced Photonix, for example. With a moderate avalanche gain of 100, a single-shot ranging accuracy of 1 cm should be achievable for an aerial configuration at 10 km altitude.

B. Spatial configuration

On the other hand, a spaceborne system would need a more fundamental revision of the instrumentation. To meet higher altitude requirements, the use of a telescope seems necessary and possible since, for the same network areas, the field of view is now much narrower, e.g., 0.01 rad. Velocity aberration correction can be achieved by the use of spoiled cube corners, but with a loss in the link budget amounting to a factor of 36. In order to achieve centimeter ranging accuracy, the instrumentation should be based on a 30 cm telescope, 1 J laser, 10 cm retroreflectors, 5 mm diameter APD of 10 A/W responsitivity, and 10,000 gain transimpedance amplifier. Actually, the single-shot ranging accuracy would then be between 2.3 cm and 5.3 cm from center to the half-width of the laser beam. A rough pointing system would also be necessary, in order to acquire data from an extended part of the orbit.

In this configuration, atmospheric effects are slightly different. On the transmission point of view, cirrus clouds have to be taken into account. Like for all spaceborne optical applications, cloud cover is a main limitation to the feasibility of surveys. Operational parameters, such as laser repetition frequency and spatial reflector density, have therefore to be carefully chosen in order to achieve the desired positioning accuracy from a single satellite passage. Concerning turbulence aspects, the dynamic layer is now located far away from the laser source. The main consequence on the link budget is that beam spreading and scintillation are stronger. For the same reasons, the pdf of scintillation becomes exponential, i.e., with unity intensity contrast. The effects of these error sources are still under investigation. But since the instrumental models have now been validated experimentally, they can be applied in numerical simulations of aerial and spatial configurations of the proposed positioning technique.

VII. CONCLUSION

A wide-angle laser ranging system, intended to achieve a new geodesy technique based on aerial or spatial multilateration, has been presented. A first instrumentation has been fully

validated on several terrestrial experiments. Results are compatible with theoretical predictions, related to the electrical SNR. An optimization for airborne experiments of the current instrument has been proposed. It consists mainly on replacing the PIN photodiode by a large aperture APD. This solution is now under investigation, with the aim of conducting an airborne experiment during 1997. From link budget considerations, an extension to a future spaceborne configuration seems also possible. But therefore, a more classical instrumentation, using a telescope, would be necessary.

ACKNOWLEDGMENTS

REFERENCES

[i] M. Kasser and IGN, "Method for determining the spatial coordinates of points, applications of said method to high prescision topography, system and optical device for carrying out said method", US Patent 774,038, 1991

[ii] O. Bock, C. Thom, M. Kasser and D. Fourmaintraux : Development of a new airborne laser subsidence measurement system, aiming at mm-accuracy, Proceedings of the Fifth International Symposium on Land Subsidence (FISOLS-95), The Hague 16-20 October 1995, Balkema Publisher

[iii] D. Fourmaintraux, M. Flouzat, M.J. Bouteca, M. Kasser, (1994) Improved subsidence monitoring methods. SPE, paper 28095, Int. Symp. SPE-ISRM Eurock'94, Balkema Publisher

[iv] W. D. Kahn, J. J. Degnan and T. S. Englar, Jr : The airborne Laser Ranging System, Its Capabilities and Applications, Nasa Tech. Memo. 83984, Sept. 1982, Goddard Space Flight Center, Greenbelt, Maryland

[v] H. Lutz, W. Krause and G. Barthel : High-Precision Two-Colour Spaceborne Laser Ranging System for Monitoring Geodynamic Processes, 33rd Congress of the International Astronautical Federation, Paris, France, September 1982

[vi] S. C. Cohen, J. J. Degnan, J. L. Bufton, J. B. Garvin, J. B. Abshire : The Geoscience Laser Altimetry/Ranging System, IEEE Tr. on Geoscience and Remote Sensing, Vol. GE 25, No. 5, Sept. 1987

[vii] O. Bock, Ch. Thom, M. Kasser & J. Pelon, Ranging Performance Evaluation of the Wide-Angle Laser Ranging System, IEEE Tr. on Geoscience and Remote Sensing, to be published

[viii] J. J. Degnan : Millimeter Accuracy Laser Ranging : A Review, Geodynamics Serie volume 25, Contributions of Space Geodesy to Geodynamics: Technology, American Geophysical Union, 1993

[ix] J. W. Marini and C. W. Murray : Correction of laser range tracking data for atmospheric refraction at elevation angles above 10 degrees, GSFC, Nasa Technical Memo, Nov. 1973

[x] V. I. Tatarskii : Wave propagation in a turbulent medium, (translated by R.A. Silverman) McGraw-Hill, New-York 1961

[xi] M. E. Gracheva, A. S. Gurvich, S. S. Kashkarov and VI. V. Pokasov : Similarity Relations and Their Experimental Verification for Strong Intensity Fluctuations of Laser Radiation, Topics in Applied Physics, Vol. 25 : Laser Beam Propagation in the Atmosphere, Ed. J. W. Strohbehn, Springer-Verlag, 1978

[xii] J. W. Strohbehn : Modern Theories in the Propagation of Optical Waves in a Turbulent Medium, Topics in Applied Physics, Vol. 25, Laser Beam Propagation in the Atmosphere, Ed. J.W. Strohbehn, Springer-Verlag, 1978

[xiii] J. J. Degnan : Satellite Laser Ranging : Current Status and Future Prospects, IEEE Tr. on Geoscience and Remote Sensing, Vol. GE-23, No. 4, July 1985

[xiv] V. Kubecek, K. Hamal, I. Prochazka, R. Buzelis, A. Dement'ev, Optics Commun., Vol. 73, No. 3, 1989

[xv] O. Bock, M. Kasser Ch. Thom, & J. Pelon, "Precise Relative Positioning by Wide - Angle Laser Ranging", submitted to IEEE Tr. on Geoscience and Remote Sensing

[xvi] H. Melchior : Demodulation and photodetection techniques, Laser Handbook, Ed. F.T. Arecchi & E.O. Schultz-Dubois, North-Jolland Publishing Company, Amsterdam, 1972.

PROPOSITION FOR A NEW SLR METHODOLOGY USING CW OR LONG PULSE LASERS

M. Kasser, ESGT / CNAM, 18 Allée Jean Rostand, 91 025 EVRY Cedex, France
Fax : +331 69 36 74 21
C. Thom, LOEMI / IGN, BP 68, 94 160 Saint- Mandé, France

INTRODUCTION

The main goals of SLR, as an operational orbitographic tool or as a scientific one, derive from its capability to determine artificial satellite orbits with a centimetric accuracy. From the orbit one may deduce information of very high importance concerning earth rotation parameters, earth gravity field and its temporal variations, and a very high quality absolute positioning. In this area, SLR could be a very good candidate, if not the best on a long term basis, to provide millimetric absolute altimetry for studies concerning minute altitude variations (mountains formation, tectonic subsidences and surrexions, post-glacial rebound, oceanic loading over continental margins, etc...).

The main limitations of SLR in terms of accuracy, by descending order of importance, are probably : (i) the quite inhomogeneous repartition of SLR stations in the world, (ii) the technology of SLR that lets some important biases uncorrected, (iii) target temporal signatures, and (iv) tropospheric delay uncertainties.

Concerning (i), we observe regular improvements, but there will always be some basic limitations (due to semi-permanent cloud coverage in some parts of the world, for example). Concerning (iii), the models have considerably improved and some technological possibilities not yet used exist (Kasser & Lund 1994). And concerning (iv), the correction to look for is quite low if the pressure is correctly measured at the station (Kasser 1992), and in any case it is expected soon that two-colour ranging (Prilepin 1957) will achieve automatic corrections at the millimetre level. Thus we have worked on the point (ii), i. e. how to remove any sort of instrumental bias.

To achieve this goal we have looked for the solutions used by early geodesists with electronic distance measurements (EDM). These type of instruments have been explored through a wide range of different technologies, with only a small number of scientific publications as most of the knowledge in this domain is industrial and thus not disclosed. Nevertheless we know, from the publication of patents, what technologies are used :

- Use of pulsed diode lasers (long pulses, typically 200 ns), with the same detection for the start and return pulses, and a statistical reduction of the decimetric single shot r.m.s. up to one millimetre,

- Continuous modulation of light beams (often not coherent ones), with an efficient phase measurement over periods up to a few seconds, and a systematic internal calibration removing the biasses due to ageing of components and thermal effects,

- For the highest precision EDM (Mekometer, Geomensor, Terrameter), an electro-optical device is used to modulate twice the laser beam, one before and the other after the free space propagation, and then the accuracy may be below one tenth of millimetre, due to a totally bias-free operation.

This last solution has been explored in order to check its transposability to SLR. In some way it is complicated, but it has been found that it could be used with only minor modifications of existing stations.

PRINCIPLE OF THE METHODOLOGY PROPOSED

Today the highest precision EDM is a laser one, named Mekometer after its invention by MM. Froome and Bradsell (NPL, Teddington, UK) and now produced by LEICA (Switzerland) as Mekometer ME 5000 and by COM-RAD as the Geomensor. This type of instrument uses an extremely interesting laser modulation method, invented by Dr. Froome in the sixties, which allows to avoid completely any systematic errors. It relies upon the use of a Potassium Di Hydrogen Phosphate crystal, called KDP for ease. The KDP is optically an anisotropic crystal.

From one point, let us draw for each direction of the space a vector whose length is equal to the refraction index experienced by the electric field of the electromagnetic wave (called *polarisation vector*). If the medium is isotropic, the end of this vector is on a sphere. For the KDP, without any electric field applied, it is on a revolution ellipsoid. This sort of crystal is said *uniaxe*, the large axis is called z, and x and y are chosen parallel to the crystallographic axes. The electro-optic effect in such a crystal is the following : if we apply an electric field along z axis, the indexes along x and y are modified with the law :

$$n_y = n_0 - n_0^3 r_{63} E$$
$$n_x = n_0 + n_0^3 r_{63} E$$

where r_{63} means an electro-optical constant of the crystal and n_z , that represents the index of refraction along z axis, is different from n_x and n_y, and is independent from E. The modulator of the Mekometer uses such a "longitudinal" modulation, E being parallel to z axis.
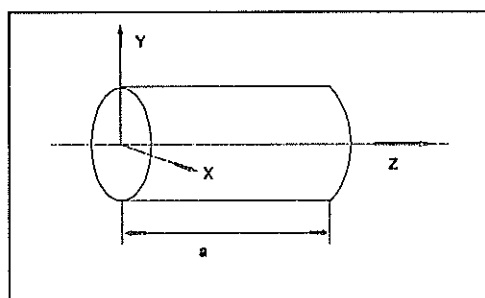
The section of the ellipsoid of refraction index in the xOy plane, that is a circle for E = 0, becomes :

With $E \neq 0$, if we enter the crystal along z axis, with the polarisation **P** at 45° of **Ox** and **Oy** directions (directions called neutral axes of the crystal because an incoming polarisation along one of these planes is not modified during the propagation), we decompose **P** into P_x and P_y that do not travel at the same speed (refraction indexes along x and y are different as soon as E is different from zero). The difference of phase R between the components of the electromagnetic wave P_x and P_y is at the exit of the crystal expressed by : $R = 4\pi n_0^3 r_{63} E.a/\lambda$, λ being the wavelength of **P**.

Y

E > 0

E = 0

X

E < 0

Lignes neutres
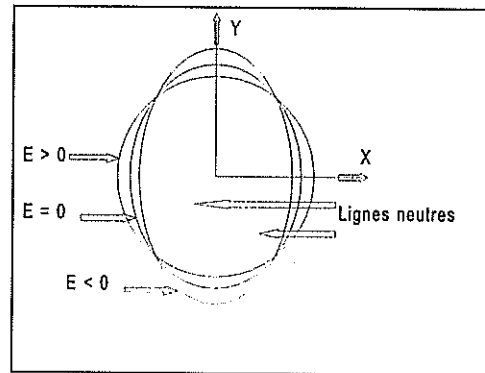
That way, with $R = \pi/2$, the resulting polarisation from P_x and P_y at the end of the crystal is perpendicular to the initial orientation of **P** (for $R = \pi/4$, **P** describes a circle at an angular speed of $2\pi c/\lambda$ rd/s). Thus generally, we note that the emitted light has an elliptic polarisation changing at the frequency **f** of modulation of the electric field **E**.

When the modulated laser light comes back from the reflector located at the far end of the line, it is sent back through the same crystal, experiencing the same alternative high frequency electric field **E**. Let us suppose that the total optical path **L** between the output of the crystal and its second input (close to half the distance to be measured) is equal to an integer number of modulation wavelengths plus half a wavelength. The laser light will see at the first passage in the crystal indexes n_1 and n_2 along the x and y projections of **P**. But when it will cross the crystal for the second time, the value of **E** will be the opposite of that during the first passage, so that the crystal indexes will now be n_2 and n_1 along x and y axes. And if we compute the total optical paths for polarisation along x and y axes, we find that they are exactly equal. It means that the outcoming polarisation is perfectly parallel to the initial incoming one : If at the output we observe the polarisation orthogonal to the input direction, in this very precise situation where $L = (K + 1/2) . c/f$ (K integer), the output signal intensity is null. And it is easy to see that for any other value of **L**, this intensity has a value following a cycle, whose shape is close to a sinusoid when **E** does not reach too high figures, and still cyclic but more complicated beyond e. g. one kilovolt.

General description of the "Mekometer" Geodetic EDM

The ME 5000 is working so as to detect the values of **f** for which the null return intensity occurs, then with such a set of measured values, it computes the integer **K** and then **L**. And if the value of **K** is provided to the instrument before the measure, the sequence is much faster. The light source employed is a He-Ne laser ; It allows to reach ranges up to 10 km if necessary, although for such distances, the excellent precision of the instrument is limited by the atmospheric index uncertainty.

The input end of the crystal is mechanically disposed at the exact intersection of the two axes of the instrument : that way, the zero error, to be added to the measurement to get the distance, is constant and depends only of the geometrical centring device employed for the reflector.

The accuracy is excellent (the instrumental standard deviation is close to 0.1 mm + 0.1 mm/km), due to the fact that this is a null measurement, for which no electronic drift of any type will influence the result. The 0.1 mm/km is only due to the frequency standard, and may be considerably improved if necessary, but this would be useless for terrestrial measurements where

the refraction index is hardly known to the 1 mm/km level.

HOW COULD SUCH A TECHNOLOGY BE USED FOR SLR ?

The main differences between SLR and an EDM are :

- A link budget that is fairly low (10^{-15} for example), which requires the use of powerful lasers (which in turn implies pulsed lasers, like YAG),

- A distances that varies all the time long during the flight of the satellite over the station.. If Z is the zenith angle of the satellite, the apparent speed from the station is $k.\sin Z$, and the value for k is for example 2.6 km/s for Lageos, and 6.7 km/s for Starlette.

- Very long distances, which requires a very high quality oscillator (typically 10^{-11}), but that is now quite easy to obtain.

- A return signal that is frequency shifted due to the Doppler effect, because of the radial component of the relative speed of the satellite.

- The polarisation signature of the cube-corner retroreflectors which is quite complicated, and generally close to a quarter-wave plate (Kasser & Goupil 1996).

We have evaluated two different solutions in terms of modulation :

1/ A variable frequency, synthesised accurately from the ephemeris of the satellite and allowing a "fringe" movement (i.e. the passage to 0 of the intensity detected after the second passage in the crystal) quite steady, allowing for a very comfortable detection (e. g. at 100 Hz).

2/ On another hand, a fixed frequency and a measurement of the "fringe" movement in a much larger range. The elements we have used to perform simulations have been the following :

- Use of a YAG laser at 1.06 :m, 5 ns pulses at 10 Hz

- Atmospheric scintillation giving a random modulation of the return signal from 0 to 100 %.

- Intensity varying in $\mathbf{D}^{-4}$.

- A satellite like Lageos, with a tracking since $\mathbf{Z < 45°}$

- An overall modulation efficiency of 90 %

- A mean value of measurements for normal points each 15 s

The measuring equipment is composed of the following instruments :

- The YAG laser that receives the polarisation modulation at a fixed frequency. The KDP is in a tuned cavity, modulated with a peak voltage close to $V_{8/2}$, with its entrance as close as possible to the intersection of the axes of the telescope.

- The return signal is driven through the modulator once again and a polarizer to an avalanche photodiode optimal for YAG. The signal observed is a series of pulses, slightly

widened by the detection (e. g. 10 ns), and is amplified up to 0.5 V peak.

- The signal is then sampled by a 1 Gech/s oscilloscope, and the data and the related timing are transferred to a computer.

- The processing consists, for each period of integration used for one "normal point", in a correlation between received signals and theoretical curves corresponding to the a priori orbits provided by ephemeris.

The simulations performed show that the measurement noise is below the millimetre level, and on another hand no measuring bias is possible. Since the two-pass modulation process provides a curve that, although periodical is not purely sinusoidal and thus has a significant amount of 3rd harmonic, it is necessary to perform a correlation on the mean frequency and another on the third harmonic. In parallel an absolute chronometry is performed on the sampled pulses (with a modest precision, close to 0.1 m) in order to measure the integer number of half-wavelength of the frequency of modulation at a given moment.

If we compare with a classical SLR station, this new technology requires only a few modifications :

- On the laser, neutralisation of the mode-locking to go back to nanosecond pulses as energetic as possible.

- Installation of a modulator, fed by a synthesiser driven by an atomic oscillator, with a power amplification allowing to reach in a cavity a voltage close to $V_{\lambda/2}$. This crystal must be located as close as possible to the intersection of the mechanical axes of the telescope. The same crystal will be used to modulate the return signal.

- After the detection and the amplification, use of a fast sampling digital oscilloscope, linked to the computer.

The optimal frequency to be used in an exploratory configuration could be 500 MHz, frequency where power amplification is not too difficult, and where $\lambda/2 = 30$ cm allowing for an easy determination of the ambiguity figure in the measured distance. The following drawing provides a general scheme of a SLR station using this technology.

Interesting alternatives would be to use either a powerful CW laser (e. g. an Argon one), or a very different type of pulsed laser, optimised for very energetic but long pulses (relaxed injected YAG for example), or on another hand with short pulses at a high pulse rate (e. g. Cu vapour). The main technological problem to solve will be the modulator. KDP is not suitable for high peak optical power, and it is not able to bear an important HF power during a semi-CW duty cycle. Thus some possibilities must be explored :

- Lithium tantalate or lithium niobate instead of KDP, for their behaviour at high energy levels and their mechanical strength. But in large size such crystals are quite expensive. This type of crystal would have to be used in a cavity tuned on the central frequency of the synthesiser, used as an impedance transformer.
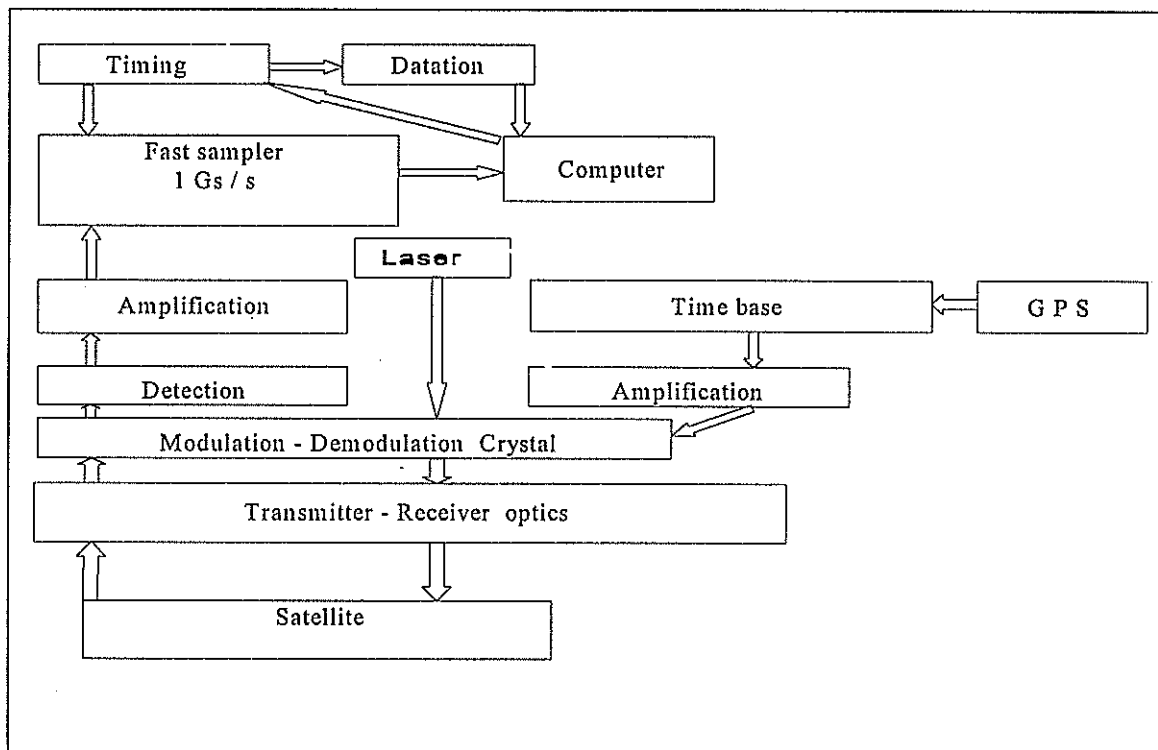
- Considering the uncertainties about the depolarisation due to the cube corner retroreflectors used on satellites, another situation must be explored, using two successive intensity modulations of the beam, as if in the previous situation presented here we would have used an intermediate polarising plate just after the first modulation and thus before the second one. The signal-to-noise ratio will be lower, but the first modulation could be obtained directly in the YAG laser, between the pilot and the amplifiers, at a low energy level. The only other drawback of such a configuration seems to be the geometric separation between the first and the second modulators, probably not very difficult to keep stable at the 0.1 mm level.

CONCLUSION

The methodology we present here is not new at all, and its main advantage relies on the fact that the detection has no requirement at all in terms of temporal jitters, it works at a very low speed so as to perform - more or less - just photometry measurements, and not timing measurements. Its use in geodesy since late sixties has been constant for very high precision distances, and excepted for the high power HF aspects, it is very simple to get operational.

We expect to have the possibility to test as soon as possible the instrumentation described here as a temporary modification of an existing SLR station (it would be advisable to start with a station benefiting of a large collecting area in order to work with a strong link budget). The problem of the elimination of the calibration and of any measuring bias seems possible, using a technical solution that has been proved as very efficient for EDMs for more than 20 years. Nevertheless, the question of the modulator has to be solved, and our first tests have shown that it was not a minor point. We hope that this new possibility will be evaluated by other teams and at least that a good solution (this one or any other one) will be found to remove any biases in SLR. Major scientific

goals will then be accessible, and especially we expect a significant improvement on the vertical component precision of the SLR stations co-ordinates.

49

BIBLIOGRAPHY

Prilepin, 1957. Aerial surveying and cartography, Trans. Inst. of Geodesy, URSS (114), pp. 127-130

Kasser, 1992. Improvement of SLR accuracy, a possible new step. *Proceedings of the 8th International Workshop on SLR Instrumentation, Annapolis, Nasa publication 3214, pp 8-23 to 8-29*

Kasser, Lund, 1994. A new concept of spatial retroreflectors for high precision satellite laser ranging. *Ninth International Workshop On Laser Ranging Instrumentation. 7-11 November 1994, Camberra, Australia*

Kasser, Goupil, 1996. The polarisation behaviour of cube corner retroreflectors used in slr satellites. *Tenth International Workshop On Laser Ranging Instrumentation. 11-15 November 1996, ShangaV, China*

Laser Ranging Performance Evaluation

Global SLR Performance Evaluation

Van S. Husson
AlliedSignal Technical Services Corporation
NASA SLR Program
7515 Mission Dr.
Lanham, Md 20706

1.1.1 Introduction

Global SLR system performance is currently measured in several different areas. The major areas of performance evaluation are data products, data quality, and data quantity. The goal of performance assessment is to identify any data problem in the global network as soon as possible in order that the cause of the problem can be corrected.

Currently, SLR data centers, analyst centers, and the stations assess system performance. Both data and analyst centers perform some redundant and unique evaluation functions. For example, data format adherence is usually verified by both data centers and analyst centers. But data accuracy can only be determined by analyst centers or data centers with orbit determination capabilities.

Historically, LAGEOS data have been the primary dataset that has been used for measuring system performance. This is because LAGEOS is in a very stable orbit and has a robust historical global dataset. Due to the dramatic increase in satellite missions the past six years and recent improvements in precision orbit determination of other satellites, like TOPEX/Poseidon, performance assessment can no longer be limited to just LAGEOS.

The globally recommended approach to performance assessment presented at the Shanghai SLR Workshop is to migrate this activity from the data centers and analyst centers to the field stations to the largest extent possible. AlliedSignal Technical Services Corporation (ATSC) has demonstrated [Husson et al., 1994] that problem identification at the system is not only feasible, but it can be successfully done if the system has been methodically characterized [Pearlman, 1984] and tested.

The current level of performance in the global SLR community is as diverse as the countries that have SLR ranging capability. The diversity in performance is caused primarily by the differences in configuration (i.e. hardware, software, operational procedures, and tracking philosophy); differences in funding levels; and differences in technical understanding. In the rest of this white paper, we will address the major groups that do performance assessment; address the three major areas of performance evaluation and define system performance goals that each system can and should strive to achieve.

1.1.2 Performance Assessment Centers

Currently, there are three main types of SLR performance assessment centers (data centers, analyst centers and the SLR systems). The SLR global data operational centers are the NASA Crustal Dynamics Data Information System (CDDIS), the European Data Center (EDC), and NASA/ATSC. Historically, the primary analyst centers have been Center for Space Research (CSR) at University of Texas NASA/STX, NASA/STX, Delft .

Institute for Earth-Oriented Space Research of the Delft University of Technology and NASA/ATSC. There are also at least another 15-20 analyst centers that are becoming very active in the global community on performance evaluation reporting.

The assessment activities of the data centers include verifying format adherence; monitoring timeliness of normal point data delivery; and generating and distributing regular data quantity reports. The analyst centers also verify format adherence and generate regular data quality and data quantity reports. Currently, some but not all field systems have some capability of evaluating their own data quality.

1.1.3 Data Products

In the early and mid 1990's four SLR data products (full-rate data, full-rate normal points, quicklook sampled data and quicklook normal points) in a variety of formats (MERIT II, SAO, NASA and CSTG) were supported and managed by the global SLR data centers.

1.1.3.1 History

The Subcommission on Satellite Laser Ranging (SLR) and Lunar Laser Ranging (LLR), a subcommission of the International Coordination of Space Techniques for Geodesy and Geodynamics (CSTG), has played an active role in streamlining global data operations, which were necessitated by global budget constraints. At the Berne, Switzerland SLR/LLR CSTG subcommission meeting in December 1995, it was agreed that only a single primary data product would continue to be supported by the global community. This data product would be CSTG normal points. In April 1996, MERIT II full-rate data was discontinued and most stations have stopped providing it to the appropriate data center(s).

1.1.3.2 Field Generated Normal Points

When the CSTG normal point format was originally proposed in 1988, a resolution was passed to keep the new format as close to MERIT II format as possible, but the new format had to satisfy telex line constraints. Both formats did contain the necessary information (i.e. calibration correction, meteorological conditions, time-tags, and time-of-flights) to use the data. In addition in 1988, there was no intention to cease the collection and archiving of full-rate data, and so there was no need for critical information about the structure of SLR full-rate data (i.e. skew and kurtosis) be in the CSTG normal point format.

Note: Skew and kurtosis cannot be reconstructed from the normal points.

Changing the CSTG format were proposed by NASA/ATSC at the Canberra SLR Workshop in 1994 to address these issues. The SLR CSTG decided then, that changing the normal point format at that time would be too costly and time consuming and thus would be addressed at a future date. Now 2+ years have expired and this item is still open.

The global transition to CSTG normal points has been slow. As of January 1996, all SLR systems are providing CSTG normal points. This marks the first time in history that this has occurred. There are still a number of minor CSTG normal points violations, but these are not significant and usually do not impact the use of the data. The definitions of some

of the fields in the CSTG normal point format are being updated by the SLR/LLR CSTG Format Working Group to help remove any ambiguities in the interpretation of these fields.

1.1.3.3 Data Flow

The SLR/LLR CSTG recommends that stations forward their normal point data to the appropriate data center within 24 hours. This is difficult for some stations with limited internet accessibility. The preferred standardized method of transmitting SLR data is via File Transfer Protocol (FTP).

Currently, most stations either have a direct or dial-up internet connectivity. A few stations do not have normal point generation capability. These systems transmit their full-rate to their central facility where the full-rate data is analyzed and normal points are produced. However, this is not the recommended approach because this can cause unacceptable delays of several days or more in the delivery of the normal points.

Currently, ATSC and EDC are the only two data centers that receive normal points directly from the international SLR network. The NASA network and some stations in the Western Pacific Laser Tracking Network (WPLTN) send their data to ATSC. The EUROpean LASer (EUROLAS) network and the other stations in the WPLTN network send their normal point data to the EDC. Currently, the NASA CDDIS stills archives any MERIT II full-rate data that it receives.

1.1.4 SLR Data Quality

SLR data quality performance can be subdivided into precision and accuracy. Precision is usually measured in the terms of a single pass or pass segment, whereas, accuracy is measured over a much longer time interval (i.e. weeks, months, years).

1.1.4.1 Precision

The precision of a system is dependent upon the system's hardware, the tracking philosophy (i.e. single-photoelectron vs. multi-photoelectron), and the satellite array. The precision is usually computed as the single shot RMS of a pass or as the normal point pass RMS. For passes that have only a few normal points, computing the normal point RMS is not meaningful. Typically normal point RMS are 4-5 times lower than their respective single shot RMS. For example, if a system has a 1 or 3 centimeter LAGEOS single shot RMS, then its normal point RMS is typically 2-3 millimeters or 6-8 millimeters, respectively.

Historically, system precisions have been based on LAGEOS, because of it's long history and most systems have LAGEOS ranging capability. Most systems get better precision on satellites with just several corner cubes (i.e. ERS-2, Stella, ADEOS, etc.), because the satellite signature is less pronounced.

The single shot RMS is computed as part of the process of the formation of normal point and therefore is one performance parameter than is best done in the field. A system with a very good precision can have accuracy problems (i.e. a system with 1 centimeter precision may have a 20 centimeter range bias) . Data precision is excellent overall from

the international network (see Figure 1), but data accuracy and data stability are still an issue and a significant problem and one of the primary motivations for writing this paper.

SLR Data Precision
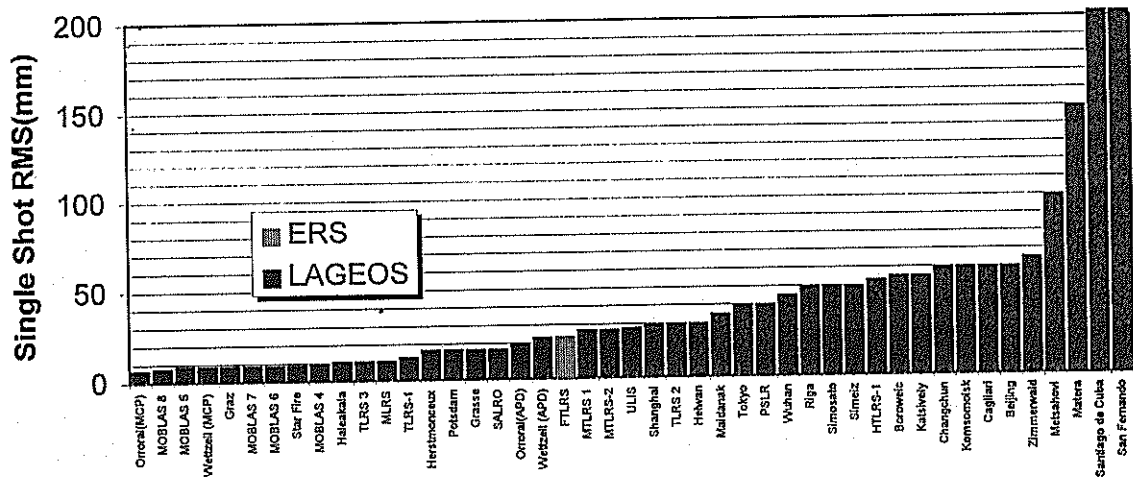
Figure 1. Global Single Shot RMS's

Note: ERS precision values are used for stations that do not have LAGEOS ranging capability.

1.1.4.2 Accuracy

Data accuracy can be measured by several different analysis techniques (long arc, short arc and geometric). Each technique has it's own strengths and limitations. Currently, absolute system accuracy is virtually impossible to measure below the 1-2 cm level. Absolute system accuracy is not only limited by the system's hardware, but is also limited by the accuracy of the geophysical models, atmospheric models, station position determination and satellite signature effects.

The most important factor in data accuracy is not the fact that a system has a near zero range bias, but is that the system range bias is constant both in the short and long term. It is very easy to model a constant bias, but virtually impossible to model a dynamic bias.

1.1.4.3 Long Arc Techniques

Currently, LAGEOS and TOPEX long arc RMS fits of several days are typically 1-2 centimeters and 3-4 centimeters, respectively. As part of the long arc technique, range bias and time bias can be computed. Richard Eanes's weekly LAGEOS report, available via email or the World Wide Web (WWW) contains range and time bias results on a pass-by-pass basis. The Uniform Resource Locator (URL) for CSR analyst results is http://ftp.csr.utexas.edu/slr.html.

For stations that have had stable performance for an extended period of time (i.e. greater than one year) and produce an adequate amount of data (i.e. >200 LAGEOS passes a year), the limitation on LAGEOS range bias and time bias determination are 1-2 cm and

10-20 microseconds, respectively. These levels of problem identification can not be determined on a pass-to-pass basis, but can be determined by aggregating bias results from several passes over short periods of time. The accuracy of range bias determination is maybe no better than 5 centimeters for stations that have never had stable performance for an extended period of time.

1.1.4.4 Short Arc Techniques

Another technique that is used in measuring system performance is a short arc fit to simultaneous data. Graham Appleby from Royal Greenwich Observatory, in September 1996, has semi-automated this technique for LAGEOS and publishes the results via the WWW. The URL is http://www.ast.cam.ac.uk/~gma/bias.html. This technique can identify biases between stations at the 1 centimeter level; however, there a far fewer simultaneous LAGEOS passes than total LAGEOS passes. The largest problem in the SLR analysis community is the lack of a standardized output (i.e. station coordinates, station performance analysis information, etc.). The SLR/LLR CSTG Analyst Centers Working Group was formed at the Shanghai SLR workshop to address this problem.

LAGEOS is still the best satellite for determining system performance using long and short arc techniques and the WWW is currently the preferred medium for publishing SLR analysis results.

1.1.4.5 Geometric

Geometric techniques depend upon quasi-simultaneous data like the short arc technique described above and therefore the technique is limited due to the reduction of available data to work with. Quasi-simultaneous means that two or more stations tracking the same satellite with the tracking time periods overlapping, and tracking does not have to be synchronized. One advantage of the geometric technique is any satellite can be used without loss in accuracy of the results. They are two types of geometric analysis techniques, one for stations that are very close in proximity (i.e. <100 meters), called collocation, and one for stations that are very far apart (i.e. >1000 kilometers). Both geometric techniques require MERIT II full-rate data. Normal point data does not currently support this analysis application.

1.1.4.5.1 Collocation

From a strictly system hardware perspective, the best demonstration and best technique for determining potential system accuracy is collocation. Collocations at NASA/ATSC since the mid 1980's (see Figure 2) have demonstrated that systems are capable of mm level repeatibilities both in the short term (i.e. within a pass and from day to day) and long term (i.e. up to several months). The primary collocation analysis technique that has been accepted by the SLR community is Polyquick, which was developed by ATSC in the early 1980's.

Polyquick is a truly geometric technique that does not have any modeling problems that long and short arc techniques have. Polyquick has been successful in identifying not only

bias problem, if the bias is larger than 2 centimeters. For this reason, Polyquick and long arc analysis are complimentary collocation analysis techniques. Also in the early 1990's, ATSC used Polyquick in verification of the normal points algorithms used by the global community by comparing normal point data to their corresponding full-rate data.

NASA/ATSC Collocation Results
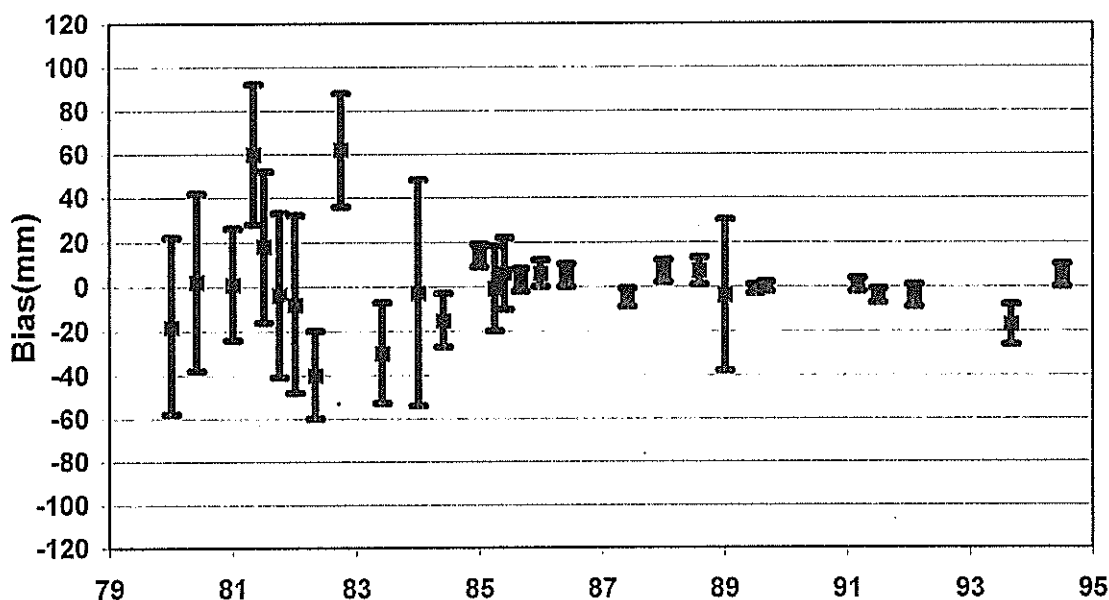
Figure 2. Collocation Results

1.1.4.5.2 Tetrahedrons

The other geometric technique, where stations are not in close proximity, we will call tetrahedrons to distinguish it from collocation analysis. Tetrahedrons requires at least quasi-simultaneous data from at least four stations and does not require synchronous ranging. Quasi-simultaneous means returns only need to be within seconds of each other, not nanoseconds. .This technique also requires an initial estimate of station positions to the several cm level. NASA/ATSC proved this concept can work and be used as a quality control tool in 1991 using historical simultaneous LAGEOS, Etalon, and low satellite data from the NASA and EUROLAS networks [Degnan et al., 1991]. LAGEOS and Etalon are visible over 12% and 25% of the globe, respectively, at any given time. NASA/ATSC found it best to use up to six stations versus four and then intercompare all the possible combinations of four of the six systems.

The reason synchronous ranging is not required is because the interpolation techniques are very accurate (i.e. sub-millimeter) and the added advantage of interpolation is truly simultaneous data can be generated at any frequency without the stations having synchronous ranging capability. Another advantage of interpolation is the RMS scatter of individual measurements is essentially eliminated or dramatically reduced in the interpolation process. Reducing the RMS scatter of individual truly synchronized ranges is still required in synchronous ranging analysis.

1. The stations can not be surveyed by traditional surveying techniques and therefore station   coordinates is an error source.
2. The geometry of the stations and the station absolute accuracies is critical to the convergence of four ranges to a single point.
3. The seeing conditions are not the same for the stations and the chances for simultaneous data is greatly reduced.
4. Solid earth tides need to be applied and is a source of error.
5. There will not be much simultaneous data on low earth orbiting satellites.

1.1.5 SLR Data Quantity

Another important parameter in system performance is the amount of data that a system produces (see Figure 3). Many diverse factors determine the data gathering capability of a system. The three primary factors that determine data quantity are the funding support, the weather, and the inherent ranging capability of the system.

Comparing tracking statistics is not fair because of the first two factors, funding support and weather. Some stations only have funding support for an 8 hour tracking period (i.e. single shift) and for maybe only part of the year, while other stations have funding support for 24 hour operations (i.e. 3 shifts), 365 days a year. The weather is the largest weakness of SLR and can vary significantly from location to location. Also, system with different ranging capabilities can and are affected by weather conditions differently (i.e. all systems are not equal).

System ranging capabilities (see Figure 4) can be analyzed as a function of ranging to a satellite as certain altitudes (i.e. Low Earth Orbiting LEO, LAGEOS, or high) and as a function of daytime ranging capability.

1.1.6 Definition of a High Performance System

During the Shanghai SLR Workshop, Mike Pearlman from SAO defined a high performance system. A high performance system is a system that has a stable bias at the 1-2 cm level; has day and night ranging capability on Low Earth Orbiting (LEO) satellites, LAGEOS, and high satellites; and produces 400 LAGEOS passes/year and 1000 LEO passes/year.

1.1.7 References

Degnan J, Conklin B, Bucey S, Husson V, Decker W, "Baselines from Orbit-Free Geometric SLR Solutions", 1991.

Husson V, Horvath J, and Su G, "NASA Automated Quality Control", Proceedings of the Ninth International Workshop on Laser Ranging Implementation, Canberra, Australia, Nov 1994.

Pearlman M, "Laser System Characterization", Smithsonian Astrophysical Observatory, Proceedings of the Fifth International Workshop on Laser Ranging Implementation, Sep 84.

Global SLR Data Volume (October 1, 1995 through September 30, 1996)

System	Tips (Ralph)	Tips (Norton)	GFZ-1	ERS-1	ERS-2	Star-lette	Stel-la	Re-surs	Fi-zeau	Topex	Ajisai	Lag1	Lag2	Eta1	Eta2	Glo63	Glo65	Glo66	Glo67	GPS 35	GPS 36	Pass Total
Yarragadee (M5)	24		196	291	349	382	315	43	172	523	505	467	439	100	42	187			203	74	22	4334
Monument Peak	13		152	220	213	423	191	59	207	447	495	403	366	77	51	153	1			204	122	86	3883
Haleakala	18		77	195	253	308	240	57	131	333	396	326	365	185	107	173				192	171	142	3669
Herstmonceux	50	42	255	233	330	320	318			490	357	445	294	44	46	37				52	26	15	3354
Ororal	5		56	198	240	406	225	18	113	337	459	377	298	15	12	45	7	20		38	4	1	2874
Quincy	38	3	77	145	218	383	203	63	126	463	362	309	247	11	11	36				83	3		2781
Graz	11		177	244	326	269	237	33	60	384	280	303	181	46	35	24				38	12	16	2676
Wettzell (WLRS)	1	3		105	143	243	137	5	42	395	352	408	294	129	96	76				113	79	45	2666
Arequipa	7		31	221	272	266	248	29	153	378	403	170	218										2396
Potsdam	32	21	323	192	267	183	178			369	205	239	146							2	3	1	2161
Grasse	13	10	189	246	343	224	216			363	231	103	88										2026
Greenbelt (M7)	46		47	87	135	241	111	50	91	193	243	213	178	3	2	40	22	52		56	9	5	1824
McDonald	14			125	164	154	125	11	52	360	269	195	170	9	12	15				9	15	12	1711
Greenbelt (M6)	3	1	32	100	120	198	83	7	60	162	180	153	143	3	18	33	1	1		20	15	3	1336
Riga (LS-105)	53	53	135	186	254					49		130	84			2				1	5	4	958
Maidanak			25	103	149					111		140	97	39	70	64				80	19	12	909
Metsahovi	25			97	160	38	87	27	56	222	92	14	10			1							829
Simosato			10	59	55	86	59			92	218	81	81	3	20								764
Changchun	16			58	78	82	77	11	18	108	94	119	71	12	13								757
Matera	1			48	64	89	37	1	5	107	99	95	94										640
San Fernando			1	63	77	73	64	20	24	115	189		1										627
Beijing	5		2	17	26	74	15	5	5	136	236	23	16										560
Borowiec	1		12	47	64	27	33	5	20	103	83	76	31										502
Santiago			6	53	74	55	24	1	7	110	103	14	42										489
Shanghai				13	22	38	15			63	136	61	80	6	14	6				3			467
Santiago de Cuba			24	80	63	41	16			61	54	2	4										346
Komsomolsk			6	15	24					85		64	50	11	21	22				19	1	8	326
**Riyadh					5	50	8			27	34	59	78	1	2					7	4		276
Cagliari	1	1	1	28	35	11	12			43	51	29	35										247
Mendeleevo			2	49	74					97													222
Holwan				15	35	20	34	3	3	39	43	3	1										196
Wettzell (MT1)	3		5	10	15	5	7	3	2	20	7	49	41										167
Yarragadee (PSLR)			2	12	15	21	7		2	18	34	30	13										154
Tokyo				5	1	11	9			18	39	10	22	2	1	7				2			127
Wuhan	1			2	5	6	4		3	11	31	12	25		2	1				1			104
Katsively				13	12					11	4	26	9	4	1	3				11			94
Simelz				8	9	5	3			16	19	17	6							1			84
**Riga (ULIS)	7	3		3		3				3													19
**Grasse (FTLRS)				1		1	4			2	1												9
Totals	388	137	1843	3586	4692	4733	3346	451	1362	6864	6304	5165	4318	700	676	926	31	73	1136	562	372	47,552

Figure 3. Global SLR Data Volume

Note: ** Indicates a new system or a system that has relocated within this period.

Global System Capabilities (November 1996)

Location and/or System Name	Pad ID	Network	Shifts	LEO Capability	LAGEOS Capability	GPS Capability	Lunar Capability	Internet Connectivity
Maidanak 1, Uzbekistan	1863	WPLTN	inactive	night/day	night	n/a	n/a	n/a
Maidanak 2, Uzbekistan	1864	WPLTN	1.5	night/day	night	night	n/a	dedicated
Evpatoria, Ukraine	1867	EUROLAS	inactive	night/day	night	n/a	n/a	n/a
Komsomolsk-na-Amure, Russia	1868	WPLTN	1.5	night/day	night	night	n/a	dial-up
Balkash, Russia	1869	EUROLAS	inactive	night/day	night	n/a	n/a	n/a
Mendeleevo, Russia	1870	WPLTN	1.5	night/day	n/a	n/a	n/a	dial-up
Sarapul, Russia	1871	WPLTN	inactive	night/day	n/a	n/a	n/a	n/a
Simeiz, Ukraine	1873	EUROLAS	2	night/day	night	n/a	n/a	dial-up
Riga, Latvia	1884	EUROLAS	1	night/day	night/day	night	n/a	dial-up
Riga, Latvia (ULIS)	1885	EUROLAS	1	night/day	night/day	night	n/a	dial-up
Katsively, Ukraine	1893	EUROLAS	1	night/day	night	n/a	n/a	dial-up
Santiago De Cuba	1953	EUROLAS	1	night/day	night	n/a	n/a	dial-up
McDonald Observatory, Texas	7080	NASA	2	night/day	night/day	night/day	night	dedicated
Yarragadee, Australia (MOBLAS 5)	7090	NASA	2	night/day	night/day	night/day	n/a	dial-up
Greenbelt, Maryland (MOBLAS 7)	7105	NASA	3	night/day	night/day	night/day	n/a	dedicated
Greenbelt, Maryland (48 inch)	7106	NASA	1	night/day	night/day	n/a	n/a	dedicated
Quincy, California (MOBLAS 8)	7109	NASA	2	night/day	night/day	night/day	n/a	dedicated
Monument Peak, California (MOBLAS 4)	7110	NASA	3	night/day	night/day	night/day	n/a	dedicated
Haleakala, Hawaii	7210	NASA	2	night/day	night/day	night/day	n/a	dedicated
Wuhan, China	7236	WPLTN	1.5	night/day	night	n/a	n/a	dial-up
Changchun, China	7237	WPTLN	1.5	night/day	night	n/a	n/a	dial-up
Beijing, China	7249	WPLTN	1.5	night/day	night	n/a	n/a	dial-up
Tokyo, Japan	7308	WPLTN	1	night/day	night/day	n/a	n/a	dedicated
Arequipa, Peru (TLRS-3)	7403	NASA	2	night/day	night/day	n/a	n/a	dial-up
Santiago, Chili (TLRS-2)	7404	NASA	2	night/day	night	n/a	n/a	dedicated
Cagliari, Italy	7548	EUROLAS	1	night/day	night	n/a	n/a	dedicated
Wettzell, Germany (MTLRS-1)	7597	EUROLAS	1	night/day	night/day	n/a	n/a	site dependent
Metsahovi, Finland	7805	EUROLAS	2	night/day	night	n/a	n/a	dial-up
Borowelc, Poland	7811	EUROLAS	1	night/day	night	n/a	n/a	dedicated
San Fernando, Spain	7824	EUROLAS	1	night/day	n/a	n/a	n/a	dial-up
Helwan, Egypt	7831	EUROLAS	1	night/day	night	n/a	n/a	dial-up
Riyadh, Saudi Arabia	7832	WPLTN	2	night/day	night/day	night/day	night	dial-up
Grasse, France	7835	EUROLAS	2	night/day	night/day	night	n/a	dedicated
Potsdam, Germany	7836	EUROLAS	3	night/day	night/day	night	n/a	dedicated
Shanghai, China	7837	WPLTN	1.5	night/day	night/day	n/a	n/a	dial-up
Simosato, Japan	7838	WPLTN	2	night/day	night/day	n/a	n/a	dedicated
Graz, Austria	7839	EUROLAS	1.5	night/day	night/day	night/day	n/a	dedicated
Herstmonceux, U. K.	7840	EUROLAS	2.5	night/day	night/day	night/day	n/a	dedicated
Orroral, Australia	7843	WPLTN	2	night/day	night/day	night/day	n/a	dedicated
Yaragadee, Australia (PSLR)	7847	WPLTN	inactive	night/day	night	n/a	n/a	site dependent
Ajaccio, Corsica, France (FTLRS-1)	7848	EUROLAS	1	night/day	n/a	n/a	n/a	site dependent
Albuquerque, New Mexico	7884	US Military	1.5	night/day	night/day	night/day	n/a	dedicated
Greenbelt, Maryland (MOBLAS 6)	7918	NASA	1	night/day	night/day	night/day	n/a	dedicated
Greenbelt, Maryland (TLRS-4)	7920	NASA	inactive	night/day	night/day	n/a	n/a	n/a
Matera, Italy (SAO-1)	7939	EUROLAS	3	night/day	night	n/a	n/a	dedicated
Kootwijk, Netherlands (MTLRS-2)	8833	EUROLAS	inactive	night/day	night/day	n/a	n/a	site dependent
Wettzell, West Germany (WLRS)	8834	EUROLAS	3	night/day	night/day	night/day	night	dedicated
Matera, Italy (TLRS-1)		NASA	inactive	n/a	night/day	n/a	n/a	n/a
Japan (HTLRS-1)		WPLTN	1	night/day	night/day	n/a	n/a	site dependent

Note: n/a means no ranging capability or non applicable

Figure 4. Global System Capabilities as of November 1996

SLR Data Usage, Applications, Performance and Requirements

Michael Pearlman
Smithsonian Astrophysical Observatory
Cambridge, MA, USA

Data Usage and Applications

The SLR analysis centers were recently surveyed to ascertain:

> Who is using the SLR data?
> What applications are they studying?
> What satellites are they using?
> Are they satisfied with the data?
> What is missing (volume, accuracy, consistency, geographic location, etc)?
> What should the network be providing to meet current requirements?

The responses to the surveys showed that more than 25 analysis groups are now using laser ranging data for a wide range of applications including: solid earth sciences, precision orbit determination for altimetry and navigation, lunar science and related relativity, atmospheric and weather sciences, and calibration of other distance measuring techniques such as GPS, GLONASS, Doris, and PRARE (see Table 1). Solid Earth science areas of study include: structure of the static gravity field, modelling of the time-varying gravity field, tides, Earth rotation and polar motion, crustal motions, and Earth mass (Gm) and relativity. Some of the most challenging applications are now centered around measurement of the vertical for hazard assessment and studies of post-glacial uplift and the response of the Earth's crust to seasonal changes in barometric pressure.

SLR data on all of the retroreflector satellites currently included on the CSTG list of priorities are being used by analysis groups for science and precision orbit applications, or to support special experiments such as TiPS or ADEOS/RIS. LAGEOS I and II provide the fundamental reference system for all other SLR applications, so they constitute a critical element in the tracking schedule for all SLR stations. Six additional satellites are planned for launch in 1997. Always of particular interest are satellites at new inclinations that will assist in further separation of the harmonics of the gravity field and its time varying components.

Current Performance

A number of the SLR stations are routinely providing large quantities of high quality data. Thirteen stations tracked 2000 - 5000 passes during 1996 and provided normal points with cm or better precision (source: CDDIS; also see the following paper by Van Husson). Several of these stations that had experienced range bias stability problems in the past have improved their performance. Many of the stations in the global network, however, tracked less than 1000 passes per year (a third of the 40 stations tracked less than 500) and many had range bias stability

problems of several cm. or more. The major issues as reported in the survey of the analysis groups were (see Table 2):

1. large disparity among stations in data quantity and data quality;.
2. incomplete geographic distribution;
3. large temporal gaps (lapses in data from individual stations); and
4. incomplete and inaccessible system configuration information

Although bias free performance is preferable, a fixed range bias can be accommodated by the analysts for most applications. Difficulty arises from frequent system changes that are not adequately calibrated. The strongest advice to the stations is:

1. leave the systems in a stable configuration, avoiding changes unless absolutely necessary; and

2. when changes must be made, the transition must be accompanied by very careful calibration and documentation of the change.

In addition, we need to:

1. strengthen network quality assurance; and

2. establish on-line, up-to-date engineering/configuration files on each station.

Requirements

Network Configuration

For global reference requirements, the SLR community needs to provide the equivalent of at least a dozen high performance SLR stations, well distributed in latitude and longitude. Some of these "stations" may be provided by "clusters" of SLR sites, as in Europe, China, and Japan where SLR sites are in place for more localized studies, but may also serve to share tracking responsibilities, expand temporal coverage, and overcome the vagaries of weather. This "cluster concept" has been discussed by Prof. Gerhard Beutler later in this report.

The current SLR network has some serious geographic gaps, but station relocations now underway or under serious consideration will help fulfill the global requirement. The MOBLAS-8 system is in the process of being relocated to Tahiti, and serious planning is underway regarding the relocation of MOBLAS-6 to South Africa, TLRS-4 to India, and MTLRS-2 to Indonesia.

Still in need of attention is the improvement in equipment and operations of the Russian and Chinese SLR systems which would play a very important geographic role in the global reference network.

Station Performance Expectation

The SLR global reference network should be comprised of "high performance" stations operations. As a guideline, "high performance" stations should provide:

1. routine day and nighttime ranging;

    2. high and low satellites coverage
    3. minimum data quantity of:

        a. 1500 passes per year on all satellites
        b. 200 passes per year on LAGEOS

    4. stable range bias (<1 cm) over a period of a year
    5. punctual data delivery (within 24 hours)
    6. strict format compliance
    7. up-to-date configuration information
    8. up-to-date calibration information

The analysis centers routinely evaluate data and issue reports on data quality by station.
The operations centers have routinely worked with the field stations to diagnose and remedy performance problems. However, the stations must recognize that the evaluation of station performance begins at the station, where the knowledge on the system resides and the source of information is most immediate. Please keep in mind:

    1. There is no substitute for careful, on-site engineering and calibration testing of system performance, and

    2. Keep the system configuration constant; change things only when necessary.

It is pretty clear that only data from systems that are stable or whose configuration changes are easily traceable and well calibrated will be used in the analysis activities.

SLR Analysis Survey Results

SLR User Organizations

AIUB[t]
ASI[t]
AUSLIG
Auston University[t]
CRL
DGFI
DUT[t]
GFZ/DLR[t]
GRGS/CNES and OCA[t]
IfAG Potsdam[t]
MIT/Lincoln Labs[t]
NAL[t]
NASA GSFC[t]
NASA JPL
NRL
NSWC
RAS[t]
RGO[t]
Shanghai Observatory[t]
Univ. of Bologna
Univ. of MD
Univ. of Padova[t]
Univ. of Southampton[t]
Univ. of TX/CSR[t]
USAF
+Others

[t]responded to survey

Satellites Used

AJISAI

ERS-1/2

ETALON-1/2

GFZ-1

GPS-35/36

GLONASS

LAGEOS-1/2

STARLETTE

STELLA

TOPEX

Areas of Investigation

Altimetry and Calibration
Atmospheric Density
Earth Rotation/Polar Motion
Earth Tides
Fundamental Physics
Gravity Field and Long Period Variations
Long Period Aerodynamics/Gas Surface Interactions
Non-Gravitational Acceleration and Perturbations
Ocean Tides
Orbital Analysis
Performance Assessment
Precise Orbits for Altimetry and SAR
Precise Orbits for Calibration of Satellite Surveillance Radars
Position/Motion/Velocity
Technique Comparison/ Combination

SLR Analysis Survey on the WWW: http://cddis.gsfc.nasa.gov/cstg/slr_analysis.html

Table 1

General Comments

- **Data quality:**
  - Large disparity in data quality among stations
  - Often, data of poor quality are worse than no data at all
  - Too many systems with poor data quality

- **Data Volume:**
  - Tracking coverage from some stations is very sporadic and sparse
  - Some stations do not provide a minimum level of contribution
  - Tracking gaps of more than ten days are a problem
  - Weeks with less than 100 LAGEOS passes are sparse
  - Much more data required on ETALON-1 and -2, GPS-35/36, and GLONASS
  - Significant amount of bad ETALON data
  - GFZ-1 data is insufficient
  - STELLA and STARLETTE often marginal (but still useful)

- **Geographic Coverage:**
  - Better geographic coverage needed in the Southern hemisphere, Russia, and China

- **Temporal Coverage:**
  - Tracking gaps over weekends are a problem
  - LAGEOS-1 and -2 data is adequate for three-day resolution, but inadequate for one-day resolution
  - More data on STELLA, STARLETTE, and AJISAI required for one-day resolution of higher order perturbations

- **Local Surveys:**
  - More reliable local surveys and more information about the surveys and local eccentricities required

- **Operational Follow-up:**
  - Lack of communications with some stations regarding problems

- **Satellites:**
  - More satellite targets of high quality needed

Table 2

Station Performance Evaluation
BOROWIEC SLR (7811)

S.SCHILLAK

SPACE RESEARCH CENTRE
OF POLISH ACADEMY OF SCIENCES
BOROWIEC ASTROGEODYNAMICAL OBSERVATORY
62-035 KÓRNIK, POLAND
tel: +48-61-170-187
fax: +48-61-170-219
e-mail: sch@cbk.poznan.pl

New since last Workshop:
- new control computer PC-486 with new real-time software
- new satellite tracking system > better pointing accuracy
- automation of predictions calculations
- automation of post pass data handling
- camera CCD

New in the near future:
- transmitting telescope
- photomultiplier HAMAMATSU H5023
- Time Interval Counter STANFORD SR-620
- shorter laser pulse (35 ps)

Data quality control:

a) on-site;
    single shot RMS
    residuals distribution control
    normal points RMS
    calibration residuals distribution and means
    calibration pre-post

b) off site;
    LAGEOS Range Bias and Time Bias (CSR Reports) (Fig.)
    LAGEOS Raw RMS (CSR Reports)
    LAGEOS Raw RMS (DUT Reports)
    ERS Raw RMS (GFZ Reports)

Improvements of data quality control:

a) on site;
    graund target calibration improvement (second target)
    control of return signal strength

b) off site;
    TOPEX and AJISAI Range Bias
    Residuals for every normal point

BOROWIEC SLR RANGE BIAS - CSR
1995
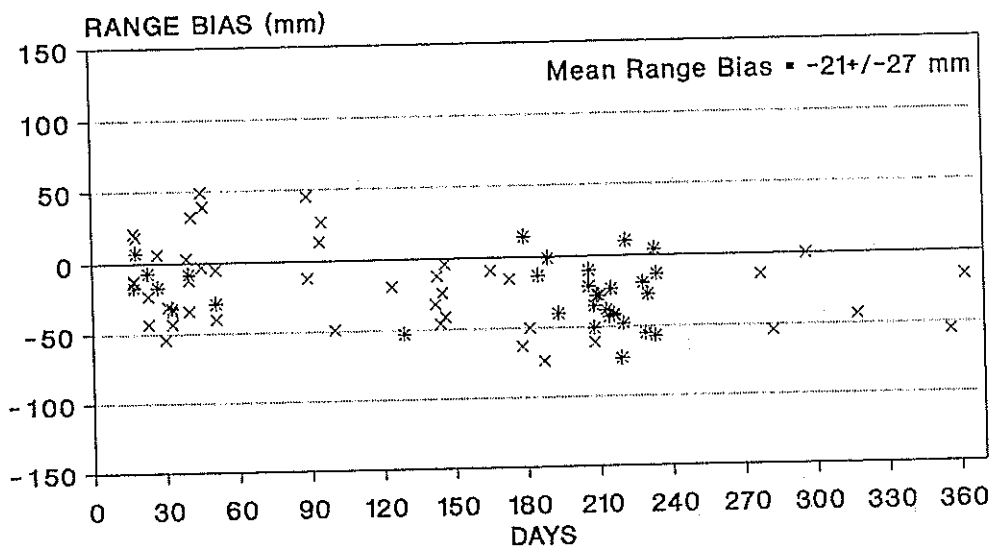
RANGE BIAS (mm)

Mean Range Bias = -21+/-27 mm

DAYS

× LAGEOS-1   * LAGEOS-2

Range Bias from weekly Reports of Center for Space Research
University of Texas at Austin

BOROWIEC SLR RANGE BIAS - CSR
1996
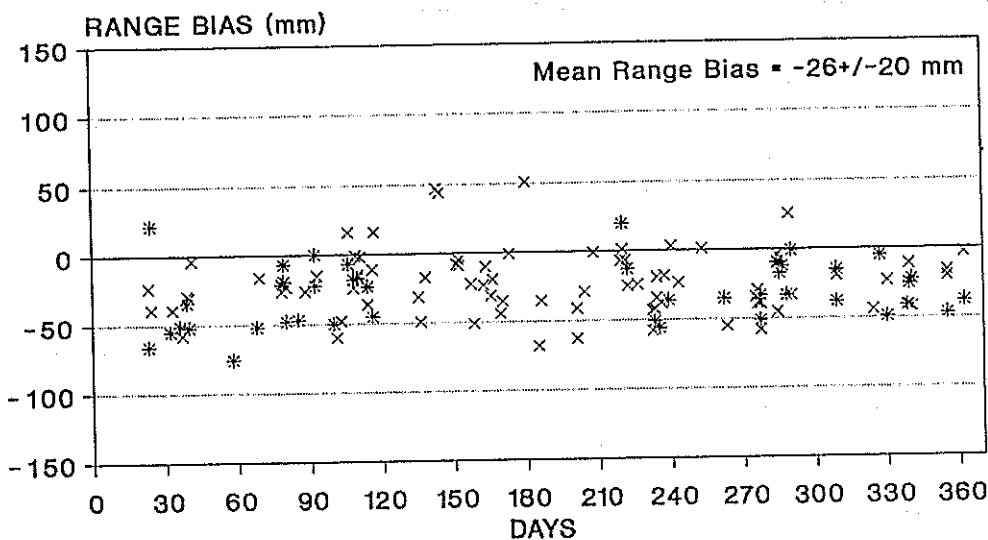
RANGE BIAS (mm)

Mean Range Bias = -26+/-20 mm

DAYS

× LAGEOS-1   * LAGEOS-2

Range Bias from weekly Reports of Center for Space Research
University of Texas at Austin

Global SLR: Recognition, Identification, and Resolution of Data Problems.

Tom Varghese, AlliedSignal, 7515 Mission Drive, Lanham, Maryland 20706, USA.
e-mail: varghet@thorin.atsc.allied.com.

The processes within the global SLR community can be significantly improved to realize the full potential of the technique and the resources expended. At the present time, the global SLR systems belong to several classes with varying attributes. The differences in the system behavior are clearly demonstrated in the ranging performance as well as the data problems they exhibit. The data often shows significant instability and inconsistency. We have achieved quite a bit of improvement in the last few years. However, we must accomplish more and is well within the reach of the current technology and processes that we can implement.

The quality of the data is strongly coupled to the station hardware/software performance as well as operational procedures. It is observed that, there is insufficient quality control of data in many stations before the data leaves for the use of the scientific community. Even when problems are identified by the user community, the problem resolution is not always expedient or even attempted. It is extremely important that quality control become a critical part of the station operational and maintenance procedures.

It is common knowledge that there is increasing fiscal pressures on the SLR budget within the global community. This leaves insufficient resources for major hardware or software changes in many stations. Under these conditions, we must explore ways of getting the best scientific value for our data through minimal changes of the systems engineering. A number of improvements can be incorporated by adapting new processes or modifying existing ones.

The instability of station performance is a noticeable characteristic within the SLR data. It must be recognized that the stability of station performance is much more important than sporadic good performance as we are looking for long term answers. Since no science question is solved in one satellite pass or passes within a few days, the long term stability and accuracy must be the top priority of all data producers. Last but not least, there is sparse data coming from several stations. It goes without saying that such data does not impact the global solution and such stations become poor contributors within the framework of the global SLR analysis and solution. Thus minimum standards for data quality and quantity must be met by each station.

How can we improve and where do we go from here? We must define an approach that is simple and can be embraced by the entire community without intruding into the autonomy of the stations. The stations must have access to the "knowledge" required towards doing a great job with their systems. Once this is available, the following

practices may be adopted towards improving the data quality while ensuring adequate data quantity.

- Perform frequent validation of the engineering performance of the system to verify data quality as well as to detect problems.
- improve the on-station QC capability to screen data problems before it becomes a problem for the analysis community.
- Adopt well defined and successful processes from the best practices within the SLR community to facilitate on-station QC efforts.
- expedite data problem resolution when identified by the analyst and take measures to prevent them or obtain early warning prior to becoming a problem.

As indicated earlier, an approach to implement this is to "capture and exploit" the current knowledge and experience in the global SLR community. Having an on-line access to "current SLR systems configuration and the performance characteristics of the data relevant modules " is fundamental to expedient data problem resolution. This will provide the baseline knowledge required for closer interaction between the data users and data producers and timely resolution of problems.

The accompanying slides capture the key points of the proposed approach and outlines a mechanism to accomplish the above goal. The formation of an international engineering data panel is proposed that will frequently examine unresolved engineering problems. This group will also foster close ties between the data users and data producers.

A well coordinated approach is critical to achieve the maximum potential of SLR towards producing the highest quality data. The existing SLR "knowledge" infrastructure needs to be enhanced to handle the additional information that the station needs to facilitate expedient data resolution. The stations must also enhance its knowledge base about the system performance and document it properly for current and future reference. The station must understand the cause of its problem when it occurs and identify it either explicitly or by examination or in consultation within the community. It must also find ways to solve the problem and hopefully prevent them in the future.

In summary, the stations have the ultimate responsibility for their data. It must exploit all available knowledge within the Global SLR community to produce the highest quality data possible for the scientific community. The proposed Global SLR Engineering Data Panel and the improved process steps and information defined in the slides in this document are means to facilitate and accomplish the above goal.

Global SLR: Recognition, Identification, and Resolution of Data Problems

- Improve the global SLR data quality (accuracy and stability) and data quantity.
- Expedite data problem resolution
- establish a **standardized approach** from best practices.
- improve the **on-station QC capability** to screen data problems.

Approach:

- "**Capture and exploit**" the current knowledge and experience in the global SLR community.

d:\varghese\...\conference\shanghai\data001.ppt 3/17/97   1

AlliedSignal
AEROSPACE

Global SLR: Current Information flow

| Operations Data | → | Data Center | → | SLR Data Analysis Community |
| SLR Station | | Data Screening | | Analysis: Results, Data Problems Feedback |

d:\varghese\...\conference\shanghai\data001.ppt 3/17/97   2

AlliedSignal
AEROSPACE

70
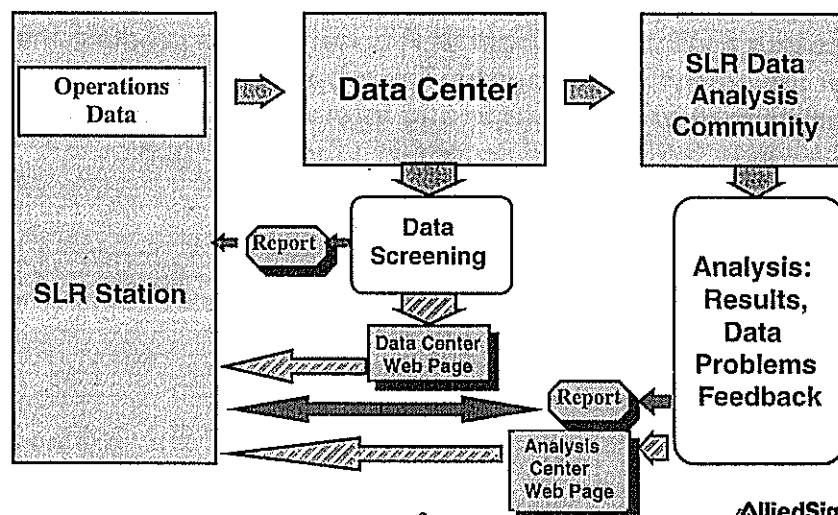
Global SLR: On-station Data Processing, Testing and QC

Operational Data:

- Normal Point Data
- Station Local Survey Data
- Data problems "reported by the station" to the data centers.

Engineering Data /Results

- No engineering test data or results relevant to operational performance is currently maintained in the Data Center.

WHAT ARE WE MISSING?

- on-line access to "current SLR systems configuration"; fundamental to expedient data problem resolution.
- station HW/SW performance data.
- framework for closer interaction between data users and data producers.

AlliedSignal AEROSPACE

d:\varghese\...\conference\shanghai\data001.ppt 3/17/97   3

Global SLR : FeedBack provided by Data Centers (CDDIS, EDC,...) to the Stations

Data Centers provides the following feedback to the stations.

FORMAT COMPLIANCE:

–Verify compliance with data formats; "minimal problem" within the global SLR Data.

DATA ACKNOWLEDGEMENT:

–provides feedback to the stations on the amount of data received by the Data Center from the respective stations

–DATA ANALYSIS FEEDBACK:

–some "engineering" feedback provided by data centers to the stations

AlliedSignal AEROSPACE

d:\varghese\...\conference\shanghai\data001.ppt 3/17/97   4

Global SLR : Feedback provided by the analysis community.

CSR:<weekly Report on each **L1, L2 pass based on 3-day arc.**

- **Satellite Data:** Good Obs, single shot RMS*, RMS to an orbit, Precision Estimate of NP, Range Bias, Time Bias, Modeled Bias, Pass Duration, Edited Obs
- **Calibration Data:** Mean*, Std. Dev*., Cal. shift*.

Delft: <weekly Report on **L1, L2 based on 10 day arc.**

- **satellite data:** RMS to an orbit, Range, Time Bias (problem passes), good/bad passes, statistics on day/ night passes, geometric distribution for transportable (TLRS, PSLR, MTLRS) systems, adjustment to station co-ordinates.

Herstmonceux: < monthly graphics dispaly based on daily solutions>

- **satellite Data:** Range Bias and Std. Dev. , intercomparison of stations using short arc analysis of simulatneous passes.

AlliedSignal
AEROSPACE

Global SLR

What information do we need in the future?

AlliedSignal
AEROSPACE

Global SLR: What information do we need to maintain in the future ?

- SLR system **"current baseline configuration and performance"** data.
- **Data center feedback.**
- **Analyst feedback** on station performance.
- **Lessons learned:** History of Past problems and their solutions.
- **Information on** New Technologies, methods, solutions, results,..

AlliedSignal
AEROSPACE

Global SLR : SLR System "Baseline Performance Data"

SLR System Modular Verification
- Timing and Frequency Devices; < Epoch and Event time>
  [Stability (Drift), Accuracy, Precision]
- Detectors *[Stability (Drift), Accuracy, Precision]*
- Signal Processing Devices; *[Stability (Drift), Accuracy, Precision]*

SLR Subsystem Verification:
- Timing Subsystem *[Stability, Accuracy, Precision]*
- Meteorological Sensors *[Stability, Accuracy, Precision]*
- Local Survey: *Cal Targets, Internal Cal, Telescope eccentricity [Stability, Accuracy]*

System Verification:

AlliedSignal
AEROSPACE

73

Global SLR: Information needed from the Analysis Community

Data Center:
- Format compliance, Data Acknowledgement
- Out-of-bound parameters

Analysts: < multiple satellite solutions for each station>
- **Precision:** RMS fit to a global arc, NP precision, single shot RMS
- **Observations:** Total, Edited, Day/Night
- **Bias:** Modeled Range, Time Bias, Observed Range, Time Bias
- **Stability:** Short term(3 month) and long term(=>6 months) Stability.
- **Systematic signatures:** short term, long term.
- **Station co-ordinates**
- **data assessment:** quantity, quality, adequacy, geometry, significance
- **Others:** barometric pressure, calibration delays, cal. shift, precision.

Global SLR: Examples of Lessons learned

(NASA Collocations:)
- **Rigorous characterization** of modules and subsystems critical to data.
- **Accurate survey** to eliminate range bias, height dependence, and azimuth dependence errors.
- **Meteorological Closure** especially barometer with national and international standards.
- **Epoch Timing Closure** with UTC.
- **Robust Calibration Procedures** for signal strength, system non-linearities, etc.
- Capability to **verify system behavior** at all satellite ranges.
- Short **stable calibration** targets.
- **Stable clock** frequency.
- **monitoring** of station parameters for out-of-bound values.

Global SLR: Proposed Framework to Solve Data Problems

Operations Data ⇨ Data Center CDDIS, EDC,.. ⇨ SLR Data Analysis Community

Engg. Data ⇨

<SLR Station>

Data Screening Results

Data Analysis: Results, Problems

SLR Data Analysis, Results, Knowledge : <Web Site>

Data Review Panel
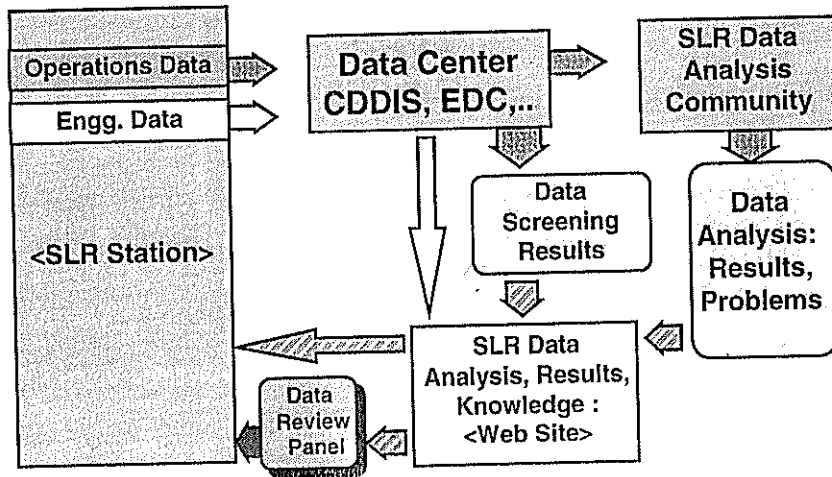
AlliedSignal
AEROSPACE

Global SLR : Proposed Approach for Expedient "Recognition, Identification, and Resolution" of Data Problems

- **SLR stations** take full responsibility for the Generation and maintenance of high quality SLR data; stations will maintain its engineering and configuration data file up-to-date and maintain the integrity of the system.
- The **SLR analysis community** in concert with the **data centers** provide appropriate and timely feedback to the stations on the quality and quantity of the data as well as the data problems.
- The operational **SLR stations** expedite the solution of data problems and make "changes" to the stations with proper rationale and close coordination with the user community.
- **The SLR community** share information collectively to solve common data related problems.

AlliedSignal
AEROSPACE

New Fixed Station

THE NEW LASER AND ASTROMETRIC TELESCOPE
IN ZIMMERWALD

W. Gurtner, E. Pop, T. Schildknecht, J. Utzinger
Astronomical Institute
University of Berne
CH-3012 Berne
Switzerland

·U. Wild
Federal Office of Topography
CH-3084 Wabern
Switzerland

J. Barbe
G.I.E. Télas
F-06322 Cannes
France

1. THE OLD SLR SYSTEM

From 1984 till April 1995 a Satellite Laser Ranging Telescope was routinely operated in Zimmerwald by the Astronomical Institute of the University of Berne, during the last few years substantially supported by the Federal Office of Topography.

The telescope was designed and mostly built in-house. It consisted of a Cassegrain receiving telescope of 50 cm aperture and a separate transmitting Galilei telescope which collimated the laser beam with a factor of about five.

The telescope also comprised a ISIT TV camera that used the 50 cm primary mirror of the receiving telescope to allow optical guiding of all sunlit targets during the night.

To test developments in the area of CCD image processing, object recognition, position, and orbit computation of optically tracked targets the TV camera was occasionally replaced by a CCD camera.

The laser used was a Quantel Nd:YAG laser allowing 10 observations per second.

The system, especially the telescope, had some serious limitations:

- Due to difficult and unstable axis alignments between the transmitting and receiving telescope and the limited tracking accuracy it was not possible to narrow the field of view enough for daylight tracking

- The energy budget of the whole system did not allow ranging to high-orbit targets such as GPS, Glonass, and Etalon satellites

- Rapid switching from one satellite to another (pass interleaving) was not possible

- The single-shot accuracy was not adequate anymore. An upgrade to a SPAD detector was not possible because of the bad definition of the optical axes and the limited optical imaging quality

- The Nd:YAG laser has been in operation for more than 10 years, it has practically reached its service life

2. REQUIREMENTS OF THE NEW SYSTEM

In 1991 the SLR group of the Astronomical Institute compiled a detailed list of requirements of a new system that was submitted to six possible telescope manufacturers.

The most important question to answer was: Is it possible and feasible to design and manufacture a telescope for both SLR and astrometric (CCD) observations?

The following requirements were formulated:

2.1 Satellite Laser Ranging

- ranging from low orbiting satellites up to geostationary satellites

- a few millimeters single shot accuracy

- both night- and daytime operation

- pass interleaving, i.e. rapid switching from one satellite to another (requirement affecting the system **and** the dome)

- fully automated operation, on-site operator is necessary only to handle exception conditions

- prepared for two colors

- 10 to 20 deg minimum elevation (requirements for the dome)

- visual tracking support possible
  - large field of view (> 0.5 deg)
  - small object tracking

2.2 Astronomical Observations

- high-precision tracking for
  - zero velocity objects (geostationary satellites)
  - slow objects (minor planets)
  - fast moving objects (low orbiting satellites)

$\rightarrow$ two tracking ranges
1) 0 - 1 arcmin/sec; exposure time: several minutes
2) 0 - 1 degree/sec; exposure time: a few 1/10 sec

- high image resolution: ca. 1" per CCD pixel

- small object tracking (a few cm diameter)

- derotation of the field of view

- fast switching from one experiment to another (i.e. several ready to use camera ports with individual focal reductors)

2.3 General Requirements

- Simultaneous SLR and astrographic operation must be possible. A certain reduction in performance (e.g. imaging qualities, laser cadence) however is acceptable

- Switching from SLR mode to pure astrographic mode and vice versa can be done within a few seconds

- The telescope has to fit into the existing building

In parallel we also evaluated

- a laser system

- a station computer

- electronic equipment for the signal processing

Four out of the six manufacturers came up with a coarse concept study and cost estimate. We decided to continue negotiations with G.I.E. Télas, France (a joint venture between the two French companies Aerospatiale and Framatome) and ordered a detailed design study to be realized during 1992.

The results of the first evaluation phase showed that it seemed to be possible to combine the two major tasks (SLR and CCD observations) on the same telescope.

However, the requirements for pass interleaving and low minimum elevation lead to the conclusion that the old dome had to be replaced with a new design, fortunately still fitting onto the existing building.

The following institutions are financing the the new system:

- The Federal Office of Topography
- The University of Berne (Canton of Berne)
- The Department for Civil Engineering of the Canton of Berne
- The Swiss National Science Foundation

The telescope was ordered at Télas in March 1994 and the final Design Review took place end of October 1994.

3. THE NEW ZIMLAT TELESCOPE

The telescope has a 1 m primary mirror and a 30 cm secondary mirror in a Richey-Chretien configuration.

The optical part of the telescope has a Nasmith path to 4 different positions for cameras, each one with its own focal reductor:

Port	Camera	Reductor	Field of view	Focal length
1	CCD Camera	CO1	13 '	4 m
2	CCD Camera	CO2	40 '	4 m
3	CCD Camera	CO3	13 '	8 m
4	TV Camera	FR	45 '	1.2 m

The cameras are radially mounted on motorized slides on a vertical instrument platform fixed at one end of the horizontal axis. A computer-controlled deflection mirror (DM) at the center of the platform selects the camera port to be used. The platform can be rotated around this axis for field of view derotation according to different strategies (elevation-coupled, declination-coupled, along-track-coupled).

The requirement of fast switching between various satellites asked for rather high slew rates and accelerations. Technical reasons didn't allow a 180° range for the elevation axis (which would have allowed an even faster switching and an easier tracking at near zenith). This restriction could be compensated by a relatively high maximum velocity in azimuth:

- Azimuth   < 30°/s ;   10°/s² ;   ± 270°
- Elevation   < 15°/s ;   5°/s² ;   -2° to +90°

The confirmed tracking accuracies are:

- 2 arcsec absolute
- few 1/10 arcsec relative

The laser beam is guided into the telescope through a coudé path and a beam splitter (DBS) mounted in the horizontal axis of the telescope. The laser beam is expanded into a ring shape by means of an axicon (two conical lenses), and it leaves the telescope concentrically around the secondary mirror. The ring diameter is about 35 cm (inner) and 50 cm (outer), respectively.

The receiving path uses the area around the laser ring and it is separated from the transmitted beam through a 45°-mirror with a center hole for the beam. This design does not need a rotating mirror as transmit/receive switch, and the transmitted laser beam does not change its position within the telescope during the tracking. The latter fact facilitates in-pass calibration and beam direction control through retroreflectors.

All the optical components are prepared for two-color ranging (beamsplitter, coudé mirrors, mirrors and lenses on the detector table).

The tracking of sun-lit laser satellites can be checked during night time with the ISIT TV camera mounted on the instrument platform in port number 4. The transmitted laser beam can be seen on the TV screen as a spot (a small part of the beam is reflected into the camera by a very small corner cube reflector mounted on the spider of the secondary mirror).

Although an additional optical component (P1-P2) between the dichroic beam splitter (DBS) and the deflection mirror (DM) has been inserted to decrease the negative effect of the beam splitter, it can be lifted pneumatically to allow completely undisturbed optical observations with each one of the CCD cameras on the instrument platform.

First tests showed that the switching from one satellite to another can be done within 10 to 20 seconds (depending on the relative positions), the time for (re-)acquisition, i.e. until returns are confirmed by the realtime filter, not included.

The following table shows a possible scenario for pass-interleaving automatically generated by the station computer:

```
 -------------------------------------------------------------------------------------
  # Satellite 07:46:47                         08:03:17                      08:19:17
 -------------------------------------------------------------------------------------
 01 STARLETTE ###++#++#+++++------------------------------------------------------
 02 LAGEOS-2  -------+++++#++++#++++#++++#++++++++++++#++++#++++###+++++###++
 03 LAGEOS    ----++++++++++##++++++###++++++++#++++##++++++++++##+++++###++++++##
 04 TOPEX     -------------------+##++#++##+++-----------------------------
 05 ERS-1     ----------------------++##++#++#-------------------
 06 STELLA    ---##++#++##--------------------------------------------------
 07 GPS-35    --+++++++++++++++##+++++++++++++++++++++++++##++++#++++++##+++++
 ------------------------------- 1 char = 30 seconds ----------------------
```

Figure 1: Tracking Scenario (# = actually tracked)

4. THE LASER

The evaluation of a new laser system finally concentrated on two systems: Either a "classic" Nd:YAG system of a Titanium Sapphire system that has never been used for satellite ranging till now.

We decided to take the risk and order more or less a prototype Titanium Sapphire system One of the major reasons for this choice is the fact that its primary wavelength (846 nm) gives best performances with avalanche diodes. The second harmonic (423 nm) still offers good performance for both photomultipliers and diodes.

The laser was manufactured by BM Industries, France. Shortly after our command the Institute for Applied Geodesy, Wettzell, Germany also ordered a similar laser at BMI for their TIGO system.

The system consists of a diode pumped Cr:LiSAF oscillator and three Ti:Al$_2$O$_3$ amplifiers (pumped by a Nd:YAG laser).

The laser experienced some delay in production, it could only be delivered end of January 1996.

The laser basically performs very well. However, we find the power-up procedures very complicated. Currently improvements are being developed. We also found some stability problems with the beam direction, the reasons of which are not yet clear.

5. CALIBRATION

The old telescope used an internal path for calibration. By setting the range gate accordingly we could easily switch between satellite ranging and calibration. Usually after each 6th satellite observation a calibration measurement was inserted. We are trying to incorporate a similar design into the new system, as well. However, due to the nearly identical transmit and receive path we are more disturbed by the backscatter of the transmitted beam, so we have to extract more energy for calibration to be above the noise level of the backscattered light.

We extract energy from the transmitted beam and re-insert it into the receiving path where the metric relation to the reference "point" (i.e. the horizontal axis) is easy to realize, namely at the end of the tube, approximately at the height of the secondary mirror.

By inserting a calibration filter (mounted on a pneumatically driven slide on the reception table) the light is attenuated to the proper (if necessary single photon) level.

For independent checks we also have external targets (in 10 and 400 m distance) determined through precise terrestrial surveying.

6. RECEIVING PATH

Down to the t/r switch (45°-mirror with center hole) the receiving path is identical with the transmit path (although the transmitted beam only uses a small part of the full aperture).

Two pin holes of different diameters for field of view limitations can be swapped pneumatically into the receiving path.

When using a photomultiplier as detector we have to protect it from the backscatter of the transmit beam, otherwise it produces unacceptable noise during more than 10 milliseconds after the start pulse. Currently we are using a fast shutter with an opening time of three to four milliseconds.

The receiving path is split into two branches for the two wavelengths by a beam splitter. Each branch has a Fabry-Perrot filter and additional 5 nm filters right in front of each detector. Each branch has three ports for three detectors, two ports each can be remotely selected through pneumatically driven 3-stage 45°-mirrors with 0%, 50/50%, and 100% transmission.

Currently we have one Hamamatsu photomultiplier and two Tchec SPADs as detectors available.

See Figure 4.

7. CONTROL SYSTEM

7.1 General System Control (VAXstation)

The overall computer control of the new system is executed by a VAXstation 4000 running under VMS.

Many of the programs, especially those for prediction generation, general data handling, data screening and data exchange, previously running on a MicroVAX for the old system, could be moved to the VAXstation without much modification.

The following major tasks are run on the VAXstation:

- Administration of incoming orbital element and time bias mails
- Computation of weekly pass lists
- Computation of pass predictions (lists of satellite positions)
- SLR observations (tracking and data acquisition)
- Data preprocessing (calibration corrections, data screening, normal point generation)
- Data reformating (Quick-Look format generation)
- Mailing of quick look data files (through the university's Alpha cluster)

The SLR Observation Program automatically generates the observation scenario for a certain time period (e.g. the next two hours), connects to and controls the telescope PC and the PC controlling the CAMAC Interface System and other equipment, controls the aircraft detection radar, various installations and equipment (like the dome opening, met sensors), checks the Air Traffic Control data (see below), and interacts with the observer.

7.2 Telescope PC

The telescope is controlled by a 486 PC programmed mostly in Fortran with a few assembler and C library routines for special input/output.

The control program runs in two modes:

- a manual (interactive) mode, where the operator can directly control the telescope for "offline-" positioning, star tracking and star calibration, and telescope device control (focusing, movement of optical components, sun cover, power on/off of cameras etc, filter wheel control)

- a remotely controlled mode where the VAXstation sends specific commands to be executed. All functions defined for interactive mode can also be executed through remote control.

The PC contains a special microprocessor card (PMAC) for the drive control of the three telescope axes (azimuth, elevation, instrument platform).

The PC communicates with the telescope devices through several microprocessors (MicroDACs) using a serial line bus system.

7.3 CAMAC PC

The old MicroVAX could directly control the CAMAC interface system by bypassing the standard VMS QIO system. This "trick" is not possible on the new VAXstation, leading to unacceptably long communication cycle times with the individual CAMAC modules. Now the CAMAC control is done by a PC, avoiding the necessity of fast (microsecond) response times for the VAX and simultaneously reducing the command and data transfer to and from the VAX to a reasonable amount.

The PC uses two special interfaces, one for the CAMAC control, one for a realtime clock for system synchronization. The latter is synchronized to GPS time by an IRIG-B time signal generated by a Truetime GPS receiver.

Communication with a MicroDAC microprocessor is done through a standard serial interface.

7.4 CCD Computers

Each CCD camera for astronomical applications is controlled by a special computer. Realtime communications with the station computer will be performed through the local area network in the same way as the communication between the PCs and the VAX (see below).

7.5 Realtime Communication

The realtime transfer of commands and data between the VAXstation and the PCs, (and the CCD camera computers), formally also between programs running simultaneously on the VAXstation, is performed through the local area network (Ethernet) using the TCP/IP basic routines (to open sockets, to connect to a foreign host or to accept incoming calls, to send and receive data packages, and to close connections). These subroutines ("socket library") are available on all major platforms and can easily be called by our Fortran programs.

Current implementations of the TCP/IP libraries are: PC/TCP by FTP Software Inc for the PCs and TCPWare by Process Software Corporation for the VAXstation.

All this communication is organized in client/server relations. One end of a communication link (usually the PCs) acts as a server, i.e. the program opens a "listening" socket and accepts incoming calls from the other end (usually the VAXstation). When the communication link has been established, the data and command transfer is controlled by the client and is done in records of ASCII strings following a message format specially designed for this purpose.

The communications are usually performed ten times per second, i.e. in the same frequency as the basic observation rates.
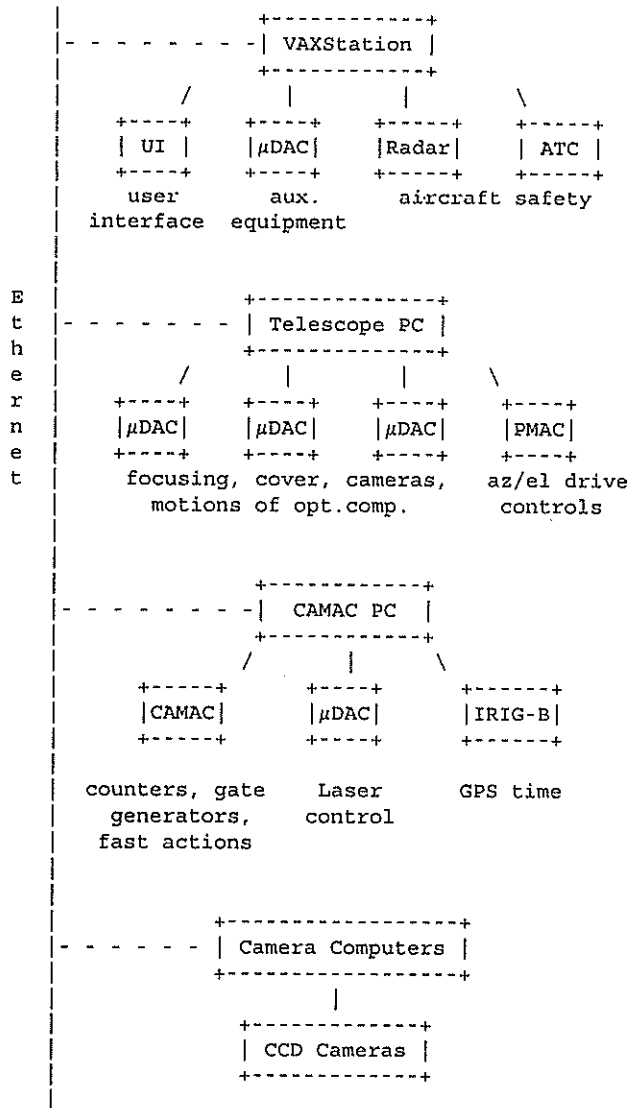
```
|              +------------+
|- - - - - - -| VAXStation |
|              +------------+
|        /        |        |        \
|    +----+    +----+    +-----+    +-----+
|    | UI |    |µDAC|    |Radar|    | ATC |
|    +----+    +----+    +-----+    +-----+
|    user      aux.       aircraft safety
|  interface  equipment
|
|
E |              +--------------+
t |- - - - - -  | Telescope PC |
h |              +--------------+
e |        /        |        |        \
r |    +----+    +----+    +----+    +----+
n |    |µDAC|    |µDAC|    |µDAC|    |PMAC|
e |    +----+    +----+    +----+    +----+
t |    focusing,  cover,  cameras,   az/el drive
|       motions of opt.comp.          controls
|
|
|              +------------+
|- - - - - - -| CAMAC PC   |
|              +------------+
|        /        |        \
|    +------+    +----+    +------+
|    |CAMAC |    |µDAC|    |IRIG-B|
|    +------+    +----+    +------+
|
|   counters, gate    Laser     GPS time
|     generators,    control
|    fast actions
|
|
|              +-------------------+
|- - - - - -  | Camera Computers  |
|              +-------------------+
|                       |
|              +-------------+
|              | CCD Cameras |
|              +-------------+
|
```

Figure 2: Zimmerwald Control System

7.6 Aircraft Safety

As the system does not operate in an eye-safe mode we have to avoid any interferences of the laser beam with aircraft. Until now we had to get the permission for each pass to observe by the Air Traffic Control a few minutes before the pass. Permission was granted when no aircraft were within a certain radius around the observatory. As the old system could only be used during the night when air traffic was not too heavy, these restrictions were not too serious.

With the new system which will allow daylight operation and with air traffic steadily increasing this solution is not adequate anymore.

The new system contains two components to avoid interference:

- A commercially available boat radar. We replaced the single antenna axis by a microprocessor-driven az/el mount to point the radar parallel to the laser beam. The radar beam width is about

20 deg in azimuth and 2 deg in elevation. Whenever an aircraft is detected, the control electronics disables the laser within a few milliseconds. The radar is capable of aircraft detection up to a range of 10-15 km, which is enough for low-altitude aircraft flying under visual flight rules (helicopters, small planes, etc).

- Positional data of aircraft within a certain radius around our observatory are made available to us in realtime through a dedicated telephone link by the Swiss Air Traffic Control. The data contain positions of transponder-equipped aircraft down to a certain minimum altitude level only. The VAXstation continuously compares the positions of the aircraft with the laser beam and disables the laser whenever an interference could happen.

8. CURRENT STATUS

The telescope without optics arrived, exactly following the original schedule, early July 1995. Due to the very late arrival of substantial parts of the system (laser in January 1996, primary, secondary, and tertiary mirrors end of April 1996) full system tests could only start mid 1996. The first ranges to a terrestrial target were collected in July, the first returns from a satellite (Starlette) succeeded on August 29.

The axicon turned out to be a serious problem: The first one was not of sufficient precision, the ring increased in diameter with the distance. Another axicon, produced by a different manufacturer, also turned out to be of minor quality, it didn't produce a clean ring. A replacement of the first one has a center hole of too large a diameter, so that the laser beam divergence can not be varied within the specified limits. Now the second manufacturer is trying a new approach.

Currently we are ranging as a test without the axicon, using the laser beam shifted off-axis to exit the telescope next to the secondary mirror. Unfortunately the beam position now rotates around the secondary mirror depending on the telescope pointing direction so that no in-pass calibration can be done.

First ranges up to the Lageos satellites sent to the data centers were collected on December 19, 1996. Until February 4, 1997 all major satellites up to Glonass (still without the two GPS satellites) were observed at least once, but during night time only.

9. CONCLUSION

The new Zimmerwald Laser and Astrometric Telescope (ZIMLAT), together with the new Titanium Sapphire laser, the new control system, ranging electronics, and CCD cameras, will be the up-to-date and state-of-the-art basis for the observational activities of the Astronomical Institute in the area of satellite laser ranging (with substantial support by the Federal Office of Topography) and astrometric observations (optical tracking of satellites and other objects, space debris search) for the next twenty years. First tests, both with the SLR and the CCD systems, were performed in 1996. The routine observations will be started early 1997, first during night time only, afterwards in daylight, too.
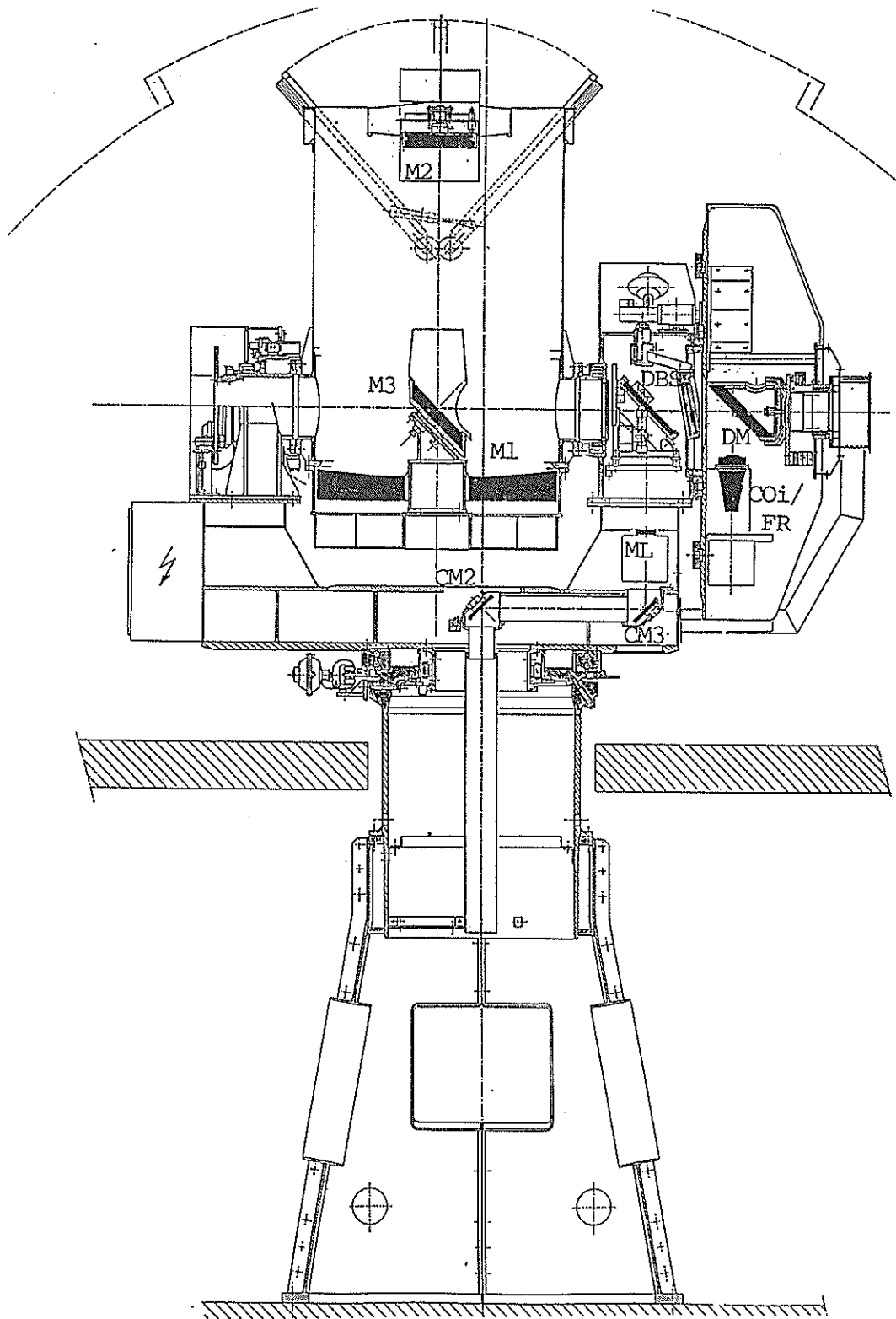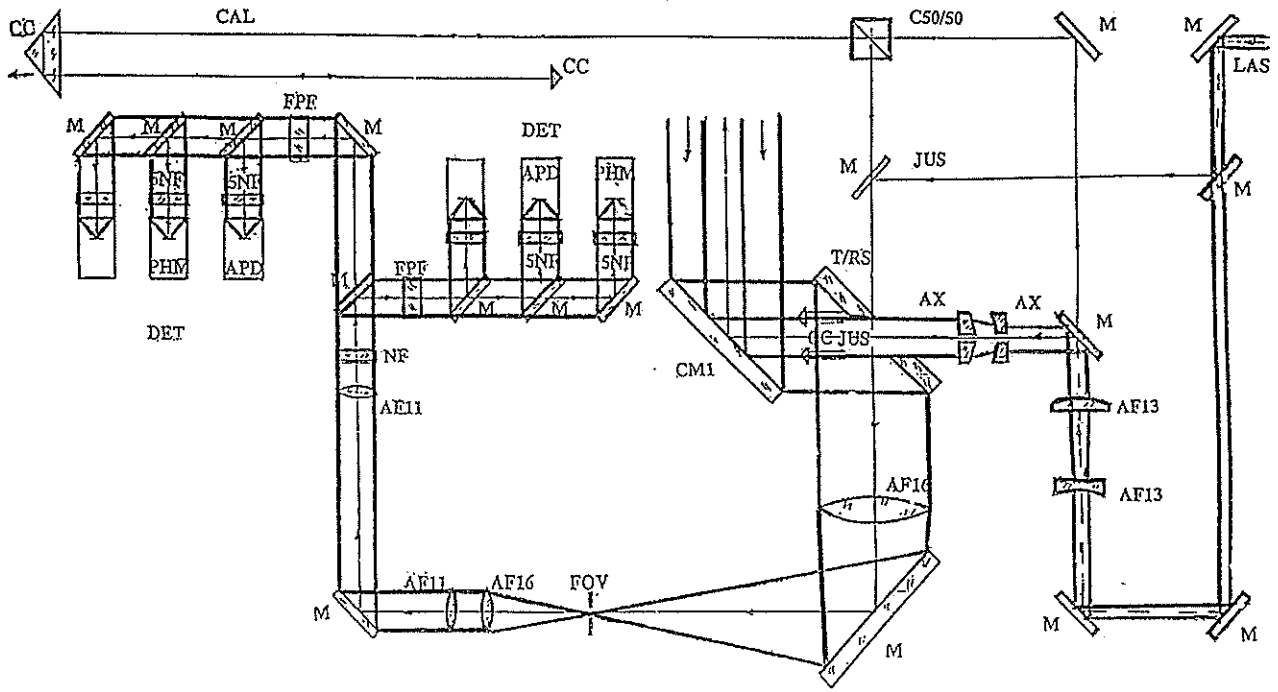
Figure 3: The ZIMLAT Telescope Optics
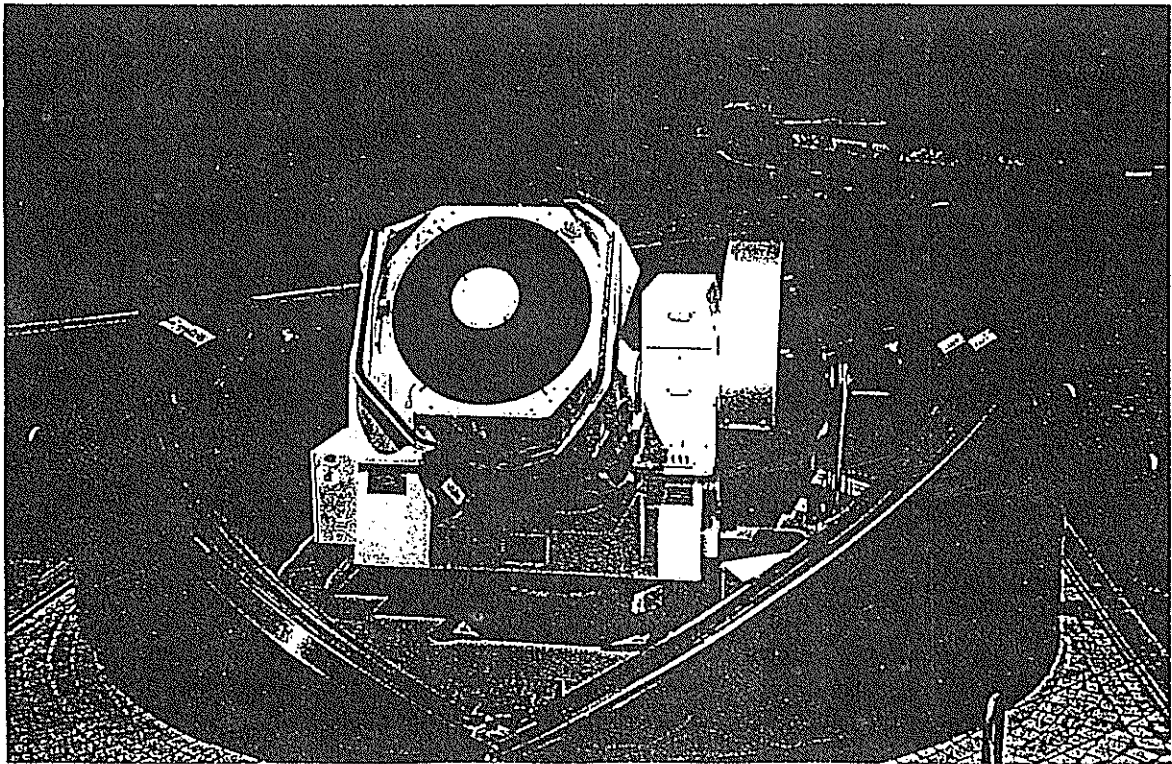
Figure 4: ZIMLAT Transmit/Receive Path

Figure 5: ZIMLAT Dome and Telescope

The Current Status and Development of Changchun SLR System

**Liu Zhi, Fan Cunbo, Chen Haiyan, Zhang Xinghua, Liu Chengzhi,
Shi Jianyong, Li Yinzhu, Gong Yan, Jin Honglin, Zhao You**

**Changchun Artificial Satellite Observatory
Chinese Academy of Sciences**

ABSTRACT

This paper introduces the current status of Changchun SLR system and its development. It includes the characteristics of the system, the new developments and the developments in the near future. It also shows some problems which need to be solved.

1. Introduction

The third generation of Satellite Laser Ranging (SLR) systems in Changchun observatory has been completed with single shot accuracy of 5-7 centimeter since 1988. But it was not in operation routinely because the components of the original system were unstable. In 1991, we changed the computer control system and adopted a HP 5370B counter routinely. The obtained SLR data have been drastically increasing and 1000 passes data have been obtained this year.

2. Description of the SLR system

The main components of the SLR system are described as follows.

2.1 Laser

An active-passive model-locked Nd:YAG laser made by the North China Research Institute of Optic-electronics is used to generate a 532 nm/second harmonic with 200 ps width optical pulses. The laser has output energy of 100 mj per pulse. The laser firing is controlled by the real-time tracking system, typically 5 pps repetition rate adopted.

2.2 Transmitting path

The laser pulse is guided to the Coude optical path via several 45^0 bending HR mirrors. Before entering the Coude optical path, a small portion of energy of the pulse is separated to a high speed photodiode to generate a signal to start the time interval unit. The rest is guided to a 15 cm diameter transmitting telescope via Coude optical path and transmitted to satellites.

2.3 Receiving path

The laser pulse reflected from the satellite returns into the main telescope with a 60 cm diameter, and then reflected by a dichoic mirror and go into photomultiplier tube. The received light other than 532 nm pass through the dichoic mirror and guided to an ICCD camera for observing satellites.

2.4 Telescope

The telescope at Changchun station is the same as Shanghai station also made by Changchun Institute of Optics and Fine Mechanics. The aperture of the main telescope is 60 centimeters. the main telescope has an azimuth-elevation mount. The maximum speed of azimuth is 12 deg/sec and that of elevation is 5 deg/sec. The maximum accelerations are 10 deg/sec/sec and 5 deg/sec/sec respectively. The azimuth-elevation encoders have a resolution of 1.2 arcsecond.

2.5 Receiving system

The receiving system is composed of photomultiplier tube (PMT GDB49A, China-made), discriminator(TC454) and time interval unit (HP5370B).

The photomultiplier converts photons into photoelectrons and multiplies them. The discriminator accepts an input pulse from PMT and generates a regulated output pulse. The purpose of time interval unit is to measure the flight time of the optical pulse.

2.6 Controlling system

All of the operations in Changchun SLR system are completely controlled by a AST286 computer. There is a controlling card in it. Its main functions include laser firing, range gate controlling, telescope real-time tracking, data collection.

The computer is also used to predict the satellite positions and ranges and pre-process the obtained SLR data.

2.7 Timing system

The timing system consists of a rubidium frequency standard and a GPS receiver. The rubidium frequency standard generates a 5MHz signal which is for time interval unit. The frequency is also doubled to 10MHz for station clock. The GPS receiver gives a second pulse which is used to synchronize the station clock to UTC.

2.8 Terrestrial ranging

The terrestrial ranging is adopted to calibrate the system delay. A corner cube reflector is installed on a mountain building. One way distance is 1268.6215m. The laser energy is controlled and very small receiving aperture is adopted during terrestrial ranging in order to simulate the actual satellite ranging.

3. The current development

The SLR data of Changchun observatory had some problems before April 11, 1996. It was suspected that the rubidium frequency standard did not work well. So air-conditioners were installed at the beginning of this year and a new power-supply with higher stability has been adopted to supply the power to the rubidium frequency standard since April. After doing these, the SLR system became more stable and the data became much better.

In order to improve ranging accuracy, a microchannel plate (MCP)PMT is planned to substitute the photomultiplier tube (PMT) for ranging. Several experiments of ranging to the satellites have been done and the data of satellites LAGEOS-1,2 with an accuracy of less than 2cm have been obtained. For low orbit satellites, the accuracy of obtained data sometimes is about 3cm. The MCP has not been routinely used until now, because some technical problems have not been solved.

In order to improve the tracking accuracy and stability, a new encoder electronics with higher precision has been used since mid-April, 1996. It has a resolution of 0.15 arcsecond.

4. Future plan

In order to obtain more data and utilize the whole capability of current SLR system, the SLR system in Changchun observatory is planned to be operated in day time. So some new developments must be done in the near future.

In order to reduce background noise in day-time ranging, the returned pulse should be guided to the receiver via spectral and spatial filters.

Modeling the telescope's mount and optical alignment should be done to improve pointing accuracy within a reasonable range for day-time ranging. This will also be necessary to observe the unseen satellites which are passing through the earth shadow.

A new serving system is also planned to be installed to substitute the old one in order to avoid the tracking problems.

References

(1) J.J.Degnan, "Satellite laser ranging: Current status and future prospects", IEEE Trans Geosci. Remote Sensing, Ge-23, 4, pp.398-413, Jul. 1985.
(2) H.Kunimori et al., "New development of satellite laser ranging system for highly precision space and time measurements", Journal of Communications Research Laboratory, 38, 2, pp.303-317, July 1991.

Matera Laser Ranging Observatory Software System

Matthew Bieneman, C. Bart Clarke, J. Michael Heinick, David McClure, Bhashyam Nallappa, Michael Selden

AlliedSignal Technical Services Corporation
Greenbelt, Maryland

Dr. Giuseppe Bianco
ASI
Matera, Italy

Abstract

The MLRO software has been developed as an object-oriented multi-processor distributed system. A team of software engineers have been working to develop this advanced environment. The software will be described and an update on the progress of its development will be provided. This paper will describe both the methodology used for the software development as well as some of the new features of the MLRO software system.
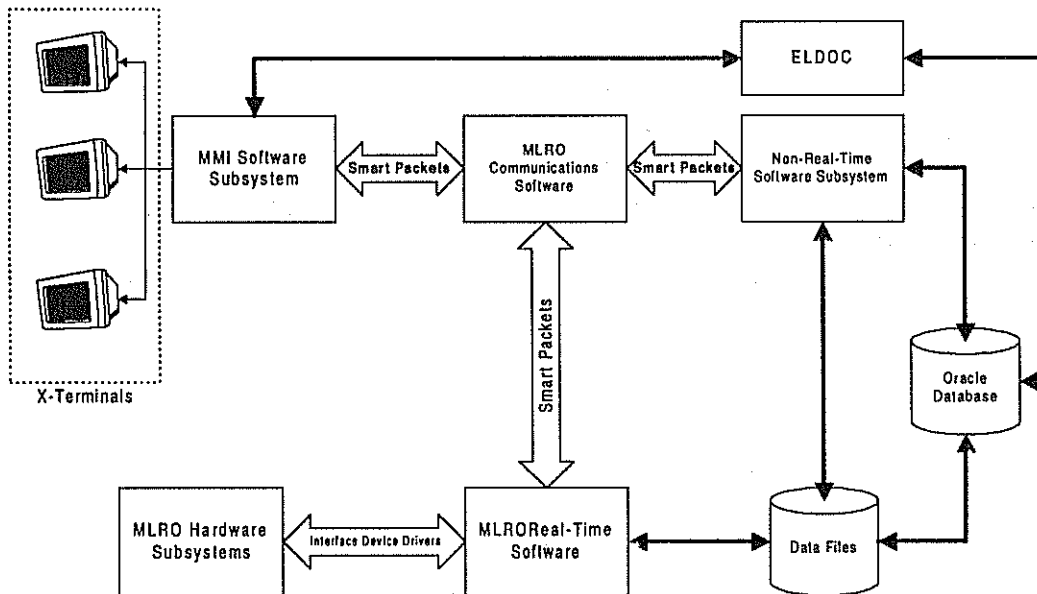
MLRO Software System

The MLRO software system was designed with several important goals. Some of these are specific to the MLRO, but many are focused on improving the ATSC software engineering capabilities. Some of these goals include:

- Meeting the functional requirements of the MLRO software system.
- Providing the foundation to the MLRO system to allow for future system improvements such as:
    - ⟹ high-speed (kHz) ranging operations,
    - ⟹ automation,
    - ⟹ two-color ranging,
    - ⟹ astronomy,
    - ⟹ and other special applications.

- Providing for easy software maintenance and for customer additions to the system functions.
- Developing a set of generic modules (class libraries) which can be used by AlliedSignal to produce real-time control systems on any computer with a C++ compiler and for any application (SLR, manufacturing and quality control, traffic-management, or any other type of work we might do). This will allow us to develop software systems for future customers **very rapidly** and at a reduced price and risk to the customers.
- Operator control through an X-Windows interface with widgets and tools that comply with Motif standards where possible. These applications should also be portable to the maximum extent possible.
- Development of the Non-Real-Time (Data Processing and Analysis) software to allow for easy maintenance and functional flexibility.
- Developing software to support ATSC's custom-built instruments.

Software Description

The MLRO software is divided into five subsystems. These are: 1) real-time control and data acquisition, 2) non-real-time data processing and analysis, 3) electronic on-line hypertext documentation, 4) Man-Machine Interface (MMI) software (which uses the X-Windows graphical interface), and 5) the communications software which acts as the software backbone. A diagram depicting this software system is illustrated in Figure 1.


Figure 1: MLRO Software Block Diagram
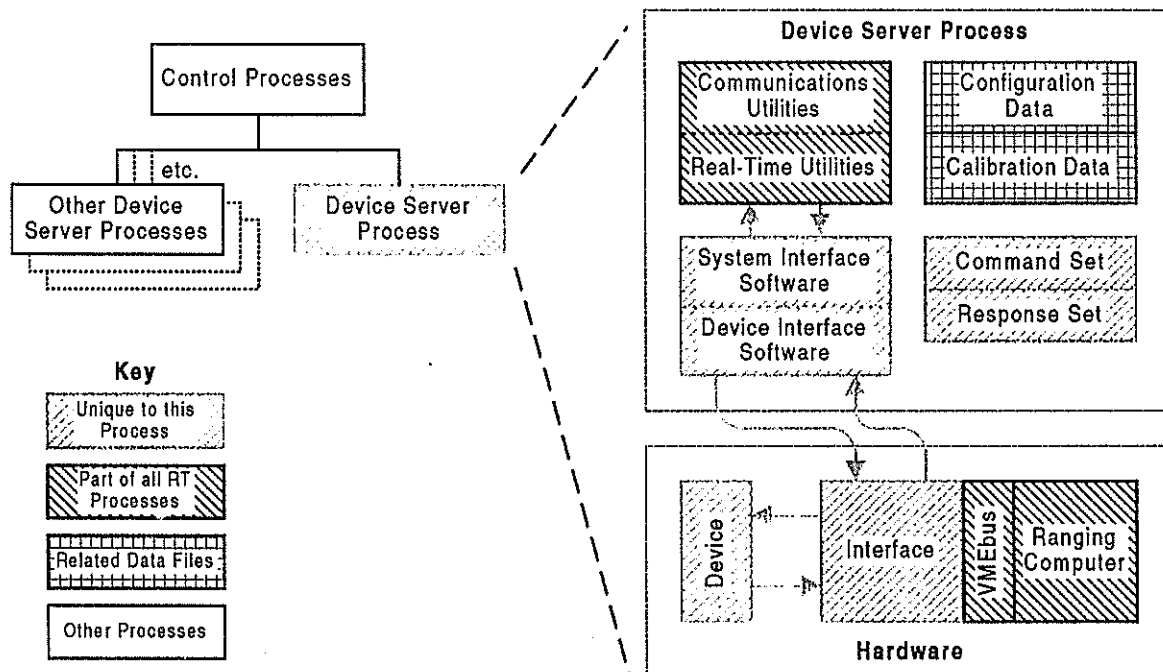
Real-Time Software

The real-time object-oriented software performs the data acquisition, control and real-time modeling of systematic non-linearity for the various hardware units. Real-time feedback is provided to the MMI software subsystem to allow personnel to monitor the data or to adjust system parameters. Data acquired during laser ranging operations is stored to disk and can be accessed by the data processing (Non-Real-Time) subsystem.

The real-time software allows for laser ranging applications, calibration and modeling of laser ranging instrumentation, and automated diagnostics and simulations for the MLRO system and various subsystems. The real-time applications are linked to a series of X-Windows applications to allow for real-time user interaction with the instrumentation and real-time feedback about the data acquired and the system status.

The real-time software is built on a layered approach with hardware and device-drivers at the lowest level, device server processes (or daemons) and control processes at the intermediate level and main processes at the highest level. A diagram depicting this relationship is illustrated in Figure 2. The real-time daemons (device server processes) are composed of elements (class library objects) produced during the initial development phase of the MLRO project (called the MLRO "real-time utilities") and process-specific data structures like command and response sets and configuration data. Control processes use the daemons and are themselves combined to perform various applications (like laser ranging, calibrations, etc). These relationships are illustrated in Figure 3.
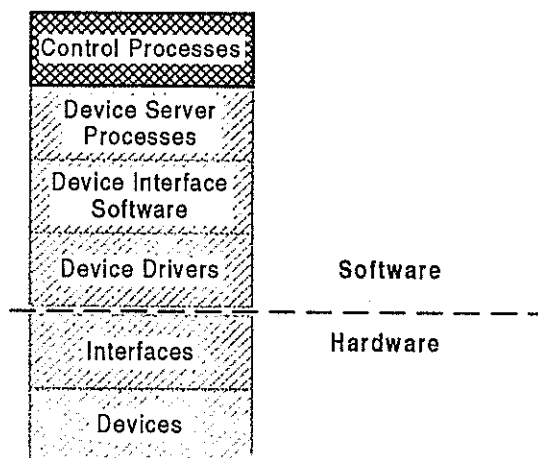
Figure 2: Real-Time Architecture

Figure 3: Interrelationship among Real-Time Processes

Non-Real-Time Software

The Non-Real-Time software performs the data processing, system scheduling, predictions, and analysis functions. The software takes maximum advantage of the Oracle database as a central data repository to store important information like scheduling input parameters, system parameters, satellite characteristics, ground target information, special applications information (like instrument calibrations, scientific data, etc.), satellite pass summary data, and long-term trend analysis data. This information is used by virtually all NRT applications and provides unparalleled configuration management, precluding errors caused by multiple copies of important data and allows the capability to generate reports about the information and its evolution. The Non-Real-Time software includes the following components:

Scheduler

The system scheduler, which allows for scheduling of events including satellites, interlaced satellite segments, lunar ranging, calibrations, and other special events. The software will determine the schedule by assessing the relative priority and other associated parameters of each available event. Among these parameters are minimum and maximum tracking time restrictions, elevation restrictions, and any special optimization parameters selected by the user. These optimization parameters include fine-interleaving optimization, geodetic (sky coverage) optimization, altimetric (high elevation) optimization, and ascending/descending optimization. The scheduler is interfaced to an oracle database

which it shares with the prediction software and the data analysis software. It is also interfaced to a set of X-Windows applications which allow the user to interface with the software parameters and to view the various schedules and satellite coverage plots.

Single-Pass Analysis Software (SPAS)

SPAS is derived from the analysis software that has been used by ATSC to process SLR data for years. This software was significantly improved for modularity and to allow for the enhanced system capabilities and accuracy that the MLRO provides. SPAS uses an Oracle database to store important processing parameters and to store summary information about satellite pass events for long-term reports and analysis. SPAS is linked with a number of X-Windows applications to allow for user interaction with the data processing parameters and to view the data graphically. SPAS can be run manually, or scheduled to run automatically as data is acquired.

Lunar Ranging Analysis

ATSC is adapting lunar software provided by Dr. Christian Veillet of Centre d'Etudes et de Recherches Geodynamiques et Astronomiques (CERGA) to enhance the MLRO lunar ranging capability. The software is being incorporated within the framework of the scheduling, prediction and data processing strategy and a number of X-Windows applications are being developed to support data processing.

Prediction Software

The MLRO prediction software produces satellite or lunar predictions for both scheduling and tracking purposes. The software may be run automatically at given time intervals or manually for one-time predictions. The software can produce satellite predictions using NORAD elements, Tuned IRVs, or GEODYN ephemerides. When GEODYN ephemerides are used, the software produces a new ephemeris (using GEODYN) by either propagating an existing ephemeris forward in time or by producing updated orbit information using new satellite ranging data. Lunar predictions are produced using JPL ephemerides files. The prediction software uses X-Windows applications to modify the various prediction parameters and to activate the prediction process.

Collocation Analysis Software

The MLRO collocation analysis software is derived from the software used for NASA collocations. The software has been improved for modularity and a set of X-Windows applications are being developed to provide interaction with the summary results. The collocation results are stored in an Oracle database for trend analysis and graphical summary.

Long-Term Trend Analysis

The MLRO long-term trend analysis (LTTA) software is being developed to allow for monitoring of the MLRO system performance over an extended period of time. This software will allow for monitoring of system-level, as well as instrument-level

performance. A set of X-Windows applications are being developed to allow for interaction with the data stored in the LTTA Oracle database.

ELDOC

The Electronic (On-Line) documentation system is a stand-alone UNIX-based set of applications developed for ATSC by Dataspazio Company in Rome, Italy. The subsystem uses Prologue, Oracle, and Knowledge Management System (KMS) to provide the context-sensitive on-line documentation and the MLRO configuration control management tools.

Internal Communications Software

The communications subsystem allows the various MLRO applications to communicate with each other, regardless of the relative physical locations of the applications.

All of the real-time processes, and the MMI software, communicate with each other using a standardized, object-oriented mechanism. Each process using this mechanism has assigned to it a service name, which allows the communications subsystem to find it. Each computer also has a unique cpu identifier. Each process has (automatically) assigned to it a shared memory block and a semaphore. The shared memory block contains a queue of commands and data directed to that process, and the semaphore is used to control access to that queue.

As an example, the Meteorological Daemon has a service name 'METD'. For a process to send a command it calls SendTo ('METD'). The communications software will attempt to find the process with the identifier 'METD'. If it is on the same computer, the command is delivered to that process immediately to that process's queue. If 'METD' is not found on the same computer, the command is immediately delivered to the process 'DATQ'. This is a special process (called gateway) which transmits data to other computers. In either case, the commanding process can resume its real-time duties without slowing for communications transmission time.

This mechanism maximizes performance and is easy to use in application programs, because it automatically decides whether to use the interprocess communications subsystem or the interprocessor communications program (gateway). Client applications only need to know the service name of the process that they want to communicate with. Server applications only need to call the Reply( ) method to have data automatically sent back to the client.

Man-Machine Interface (MMI) Software

Man Machine Interface are used on the MLRO project to allow the operator to interface with the system for virtually all of the MLRO applications including:

Operation
- Laser Ranging
- Calibration
- Simulations
- Diagnostics
- Verification
- System Alarms and Errors
- Scheduling

Data Analysis
- Single Pass Analysis Software (Satellite and Lunar)
- Prediction
- Collocation Analysis
- Long Term Trend Analysis
- ELDOC support

The MMI is primarily designed using Motif. Commercial Vendors like DataViews were used to implement non-Motif parts of the project.

The MMI is divided into two domains, Real Time MMI and Non Real Time MMI. The MMI applications run on the HP-UX machine. During real time computing, the MMI acts as a client to the data sent by the real time machine. The data transfer and updating of the screen is dependent on the real time event being processed. The MMI sends commands and data to the real time system and in turn receives data and status messages. Non Real Time MMI involves display of graphs and plots along will interaction with the ORACLE database. The operator can, through standard Motif forms, send SQL queries to the ORACLE database and in turn receive data and error messages which are displayed by the form. These screens are used by the operator to create, update and delete various parameters. The analysis software also allows the operator to view graphs and plots. Most of the MMI applications are written in C++. Classes are used so that the applications are reusable.

Software Environment

The MLRO software system is hosted on five computers these include two Hewlett Packard UNIX workstations (an HP J200 workstation and an HP 715/100 workstation) and three Hewlett Packard real-time VME computers (HP 743 RT). Each of the HP743 workstations is roughly equivalent to a 715 / 66 MHz UNIX workstation. The two UNIX workstations host the HP-UNIX operating system and the three real-time machines host the Hewlett-Packard HP-RT real-time operating system which is a POSIX-compliant UNIX-like operating system originally based on the *LYNX* kernel, but modified and improved by HP. A diagram of the MLRO computing subsystem is illustrated in Figure 4. The system has been configured to allow for expanded capability. Each real-time computer

has ample excess capacity to support added functionality, but our plan is to add new functions in a modular fashion to provide a certain level of orthoganality between machines and functions. It should be noted that the software is designed to be portable to other platforms and could all be run on a single computer.
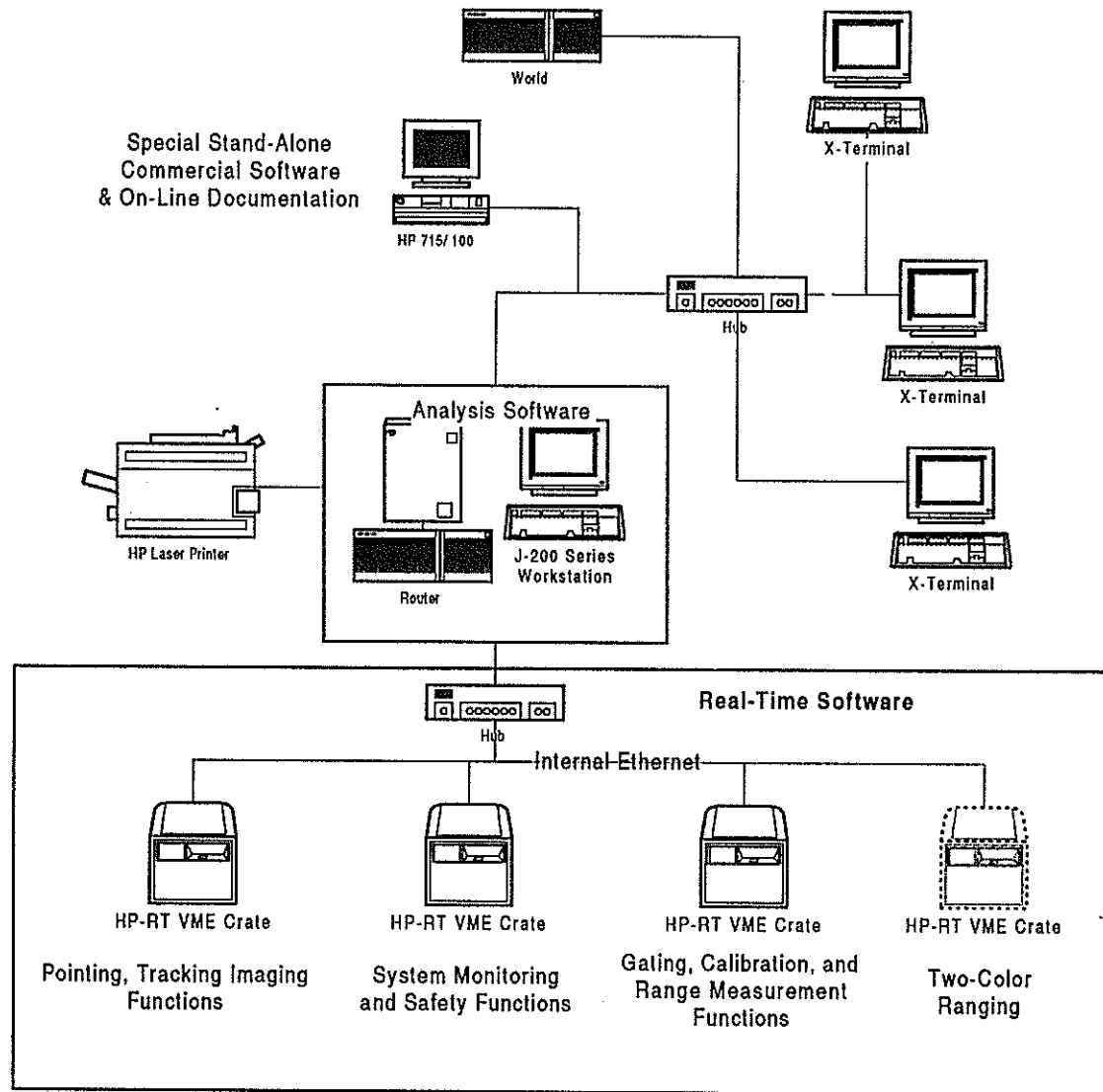
Figure 4: MLRO Computing Environment

Software Development Methodology

To meet these needs, ATSC chose to use an object-oriented approach to all new software developed. Some of the MLRO software was derived from existing FORTRAN applications and routines that have existed for many years. These "legacy applications" were debugged, improved for functional expandability, but not transformed into C++ objects.

The nature of an object-oriented approach (especially one where C++ class libraries are constructed) is that development is done in a highly non-linear fashion. For the first year most of the development time was spent creating building-blocks that would be used to assemble the various daemons and processes that compose the MLRO Real-Time software subsystem. In addition to these developments we found it necessary to create several drivers, which were not available for the chosen operating system. These included a frame-grabber driver, a GPIB (IEEE-488) driver, and several low-level routines to operate instruments using parallel digital I/O and analog I/O.

The benefits of an object-oriented approach include:
* Maintainability: An increase in the maintainability and upgradability of the software since the applications are built from a common set of class-library objects. If a common unit is changed in one place, the change is automatically propagated throughout the software system.
* Talent Sharing: Since the application developers use common building blocks, the application developers are able to share the talent of the highest-level system programmer. They need not know system-level functions, or even object-oriented programming.
* New projects: Since the class libraries contain generic (very simple) functions which have already been shown to work and to be integrated, new applications can be developed rapidly. The application developer can assemble special (custom) applications or systems in a matter of a few days, rather than months or years.

Summary

The MLRO software system has been designed and developed to be a highly flexible object-oriented software and computing environment. The development philosophy and objectives have been for a long-term benefit to both the customer and to AlliedSignal. For FORTRAN-based applications, existing software has been improved to be more modular and modified to make extensive use of Oracle database software. The system uses an X-Windows interface and an advanced communications subsystem to allow for an easy upgrade to remote operation or full automation.

Crimean Laser Observatory of the Lebedev Physics Institute.

Yu.V. Ignatenko, Yu.L.Kokurin, V.V. Kurbasov, V.F. Lobanov, A.N. Sukhanovski, V.N. Triapitsin.

Upgrading the SLR station Katziveli

Summary

The current state of the SLR station Katziveli is described, as well as plans for upgrade of this station. The upgrade includes a use of a new laser transmitter (30 mJ/40ps/10Hz) and better timing, angle measurement, and receiver components. It is expected, that after finishing the modernization, planned for the year 1997, the ranging accuracy will be 1 - 2 cm RMS, approximately 3 times better than before.

SLR station Katziveli became operational in August 1984 with the observations of LAGEOS During subsequent few years we attempted to bring the parameters of the station to the level necessary for laser ranging of the Moon. Due to technical and financial difficulties this work was interrupted in 1990.

Routine observations of the geodynamical satellites were started in 1988 and continued up to present. By 1990 the station has reached the 3rd generation level. Since then, the RMS of the individual measurements has been about 5 cm for the satellites with orbits from 700 km to 40,000 km.

During the period of 1990 to 1995 due to insufficiency of funding no upgrade to the station has been made, and the station was used with extreme economy of its resources. Namely, the number of observations was reduced to approximately 500 per year. Also, the energy and repetition rate of the laser were lowered. Now, average numbers of the individual measurements per pass for different satellites are:

- For LAGEOS 2,2 - about 400
- For ETALON 1,2 - about 160
- For low - orbit satellites - about 150

With full use of the station resourses (as up to 1990) we could easily do 2000 - 3000 sessions per year with a few thousand points per pass. In order to increase the number of observations and their accuracy, as well as to provide observations at to day time, it was necessary to fundamentally upgrade the station. this became possible only in 1995 when INTAS has granted us a special funding. In 1995 - 1997 it is intended to purchase the following equipment:

- Intel Pentium TM-based computers with necessary peripherals, which will replace outdated AT-286's;
- SVee-6 GPS-receiver by Trmible;
- RI2V rotary encoders for both axes of the telescope, by Zeiss, Jena;
- Hamamatsu H5023 photo multipliers;
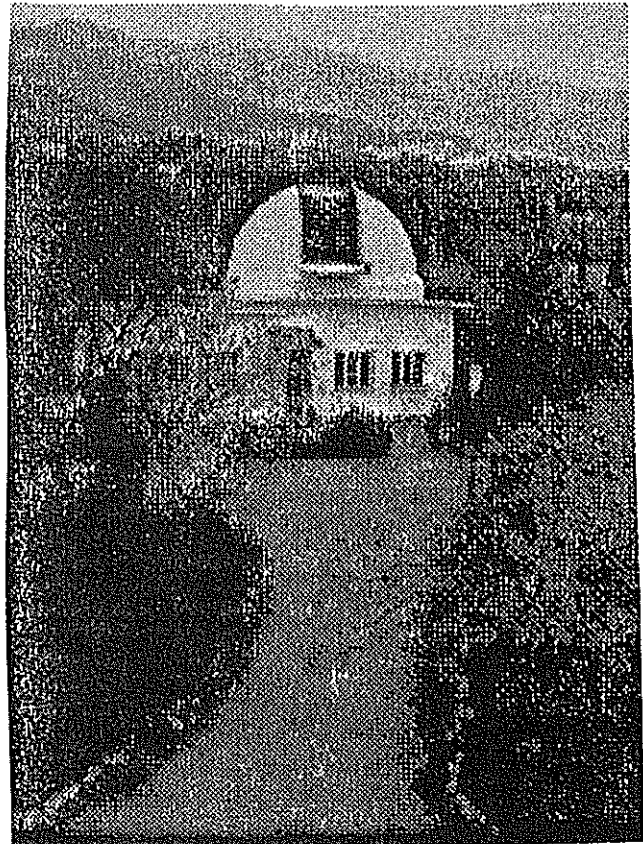
- SR-620 event timer.

The computers, GPS-receiver and rotary encoders have already been purchased and installed at the station. Besides, we aim to build a new laser transmitter using basic parts of the existing "Pulsar - 2M" laser. This work will be done under the contract with "Dynamic" company (Kiev, Ukraine). The new laser should have the following parameters:

- Pulse length: 40ps;
- Pulse energy: 30 mJ;
- Repetition rate: 10 Hz.

We are planning to finish upgrading the station in 1997. The expected improvement of the accuracy should bring the RMS to 1-2 cm level. Also, with the new encoders, we hope to get a real potential for day time observations.
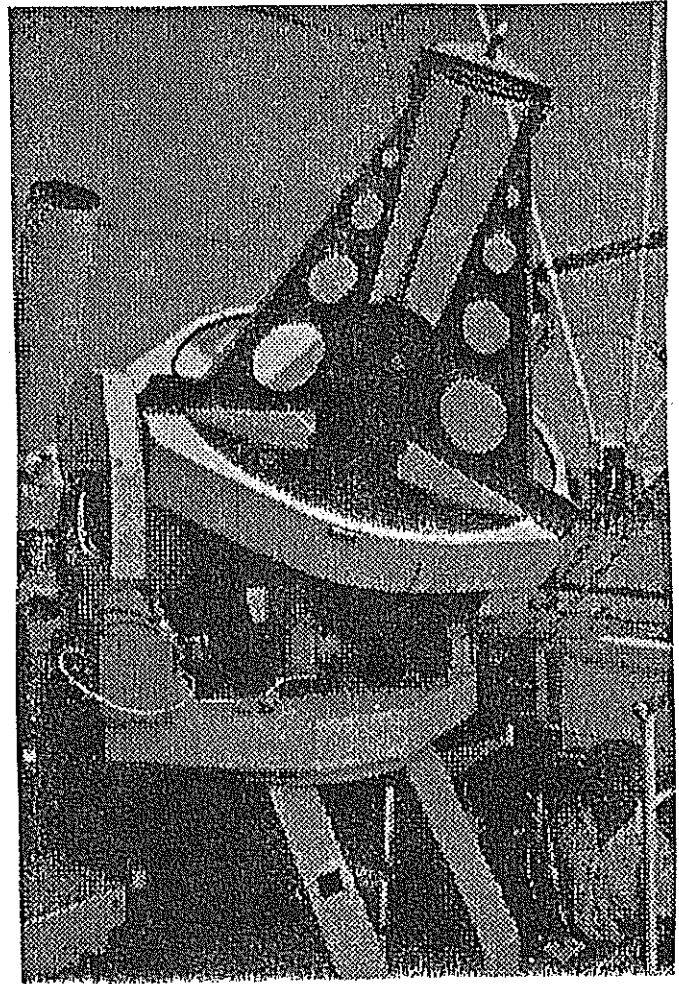
STATUS REPORT ON BOROWIEC SLR
1994-1996

S.SCHILLAK, J.BARTOSZAK, E.BUTKIEWICZ
D.SCHILLAK, S.ZAPAŚNIK

SPACE RESEARCH CENTRE
OF POLISH ACADEMY OF SCIENCES
BOROWIEC ASTROGEODYNAMICAL OBSERVATORY
62-035 KÓRNIK, POLAND
tel: +48-61-170-187
fax: +48-61-170-219
e-mail: sch@cbk.poznan.pl

ABSTRACT. The report mentions the improvements and modernisation which have been introduced at the Borowiec SLR since the last workshop. In the end of 1994, a new main computer PC-486 with real time software was installed. The first return signals from a satellite with this computer were recorded in December 1994. A new tracking system has been introduced and the pointung accuracy of the telescope is now a few times better. The subsequent aim is automation of the system and reduction of the staff on duty to a single person crew. Thanks to improvements of the system, it can trace more satellite passes and record more return signals per a single pass. At present installation of a telescope emitting a narrower laser beam is under way. It will permit tracking of GPS, GLONASS and ETALON satellites. In the nearest future due to the installation of a new detector, time interval counter, and shortening of the laser pulse width, the single shot precision will be probably about 1 to 2 cm.

The main improvements at the Borowiec SLR within the last two years were replacement of a minicomputer MERA-400 by a PC-486, exchange of interfaces and the telescope control system. This changes opened further possibilities of upgrading and automation of the system. Consequently, a significant improvement of the quality and quantity of results was noted in 1996. The nearest future the efforts will concentrate on improvement of the accuracy of the system.

1. A new control system.
    The works related to exchange of computers were undertaken in 1994 (Schillak et al., 1996a). Care was taken to introduce the new computer and the control system in such a way so that observations could be continued. A new real time program was written which controls the system (STR) - its schematic presentation is included in "Automation of the Borowiec SLR" in these Proceedings. The first test observations were carried out in December 1994, when return signals from a few satellites were recorded. Regular observations were started from February 21, 1995. After a one month break in May 1995 when it was necessary to go back to MERA-400, since June 13, 1995 all observations have been made with the new system. The main problem which hindered obtaining good results was the continuous tracking system of the telescope. Having tested from June to the end of August many variants of the system work, it was eventually abandoned and a new step by step system was chosen as it proved the most accurate tracking for the heavy mount in Borowiec. A scheme of the currently used system is

shown in Fig. 1. A PC-386 is used as an interface of the system and it is connected via a high speed line with the main PC-486 unit.

2. The tracking accuracy.

The return to the step by step tracking system meant coming back the unsolved problem of the mount delay depending on the satellite velocity. The accuracy of tracking fast satellites was limited even to 5 arcmin, which significantly obstructed tracking of invisible satellites. From October 1995 the works on mathematical model of these delays have begun. The control program has been modified to facilitate introduction of a satellite into the centre of the field of view and enable read out of the azimuth and altitude corrections with reference to the emphemeris data. Realisation of this task was delayed because of the invisibility of satellites in winter. With the coming of spring the model was gradually improved and the accuracy of the telescope tracking was a few times increased. It is reflected by the increased number of return signals per a satellite pass, see Fig. 2. After completion of the works on the model, in July 1996 this value reached on the average over 1000 returns per pass.

Table 1. Results of Borowiec SLR - 1995

SATELLITE	PASSES	RETURNS	RETURNS/ PASS	SP RMS cm	NP RMS cm
LAGEOS-1	49	9850	201	5.5	2.6
LAGEOS-2	37	6766	183	5.3	2.3
ERS-1	49	10126	207	3.3	1.8
ERS-2	45	8746	194	3.4	1.9
TOPEX	98	95105	970	4.3	1.6
STELLA	25	5335	213	3.3	1.8
STARLETTE	19	2327	122	3.3	1.8
METEOR-3	45	8901	198	3.6	2.2
AJISAI	59	60882	1032	4.0	1.4
TOTAL	426	208038	488	4.1	1.9

Table 2. Results of Borowiec SLR - 1996

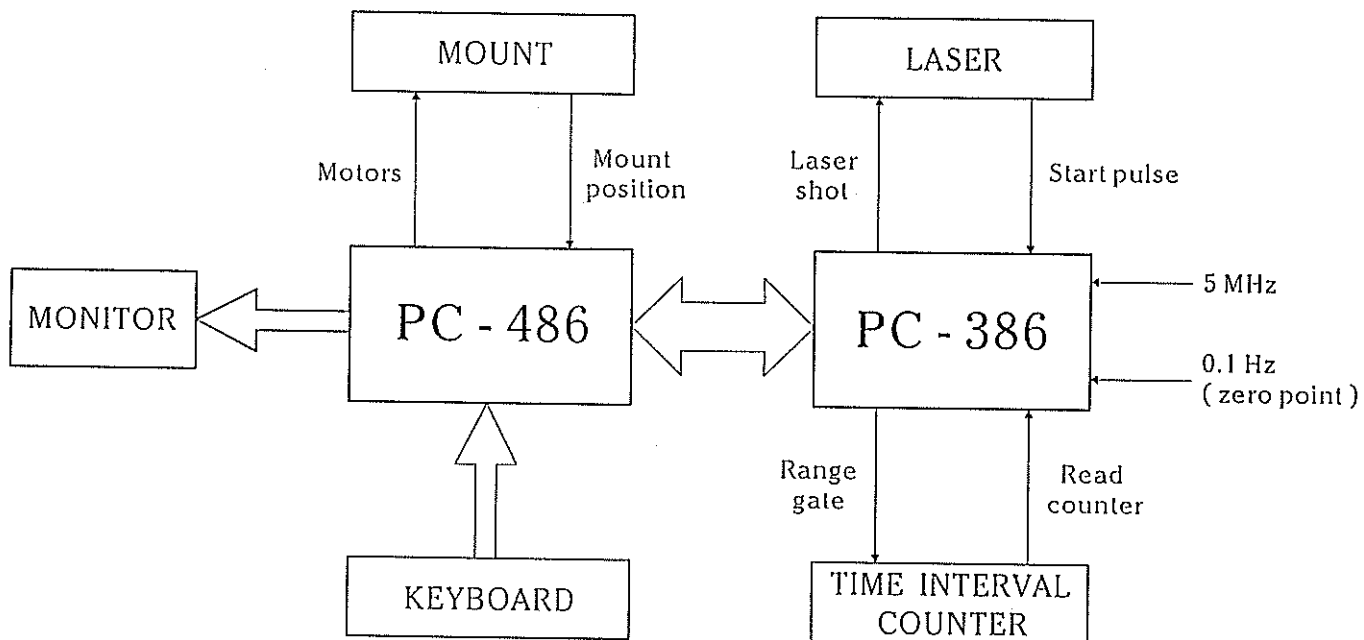| SATELLITE	PASSES	RETURNS	RETURNS/ PASS	SP RMS cm	NP RMS cm
LAGEOS-1	91	36274	399	5.7	2.0
LAGEOS-2	50	23616	472	5.7	2.0
ERS-1	39	25288	648	3.2	1.1
ERS-2	62	28520	460	3.4	1.3
TOPEX	98	207100	2113	4.1	1.0
STELLA	34	10866	320	3.2	1.5
STARLETTE	27	11386	422	3.6	1.6
AJISAI	59	133325	1932	3.8	0.9
RESURS	5	928	186	3.6	2.1
FIZEAU	20	2687	134	3.8	2.0
GFZ-1	16	3333	208	3.7	2.0
TiPS	5	471	94	6.3	3.0
TOTAL	516	483794	938	4.3	1.5

Fig. 1

BOROWIEC SLR   RETURNS/PASS
1995-1996
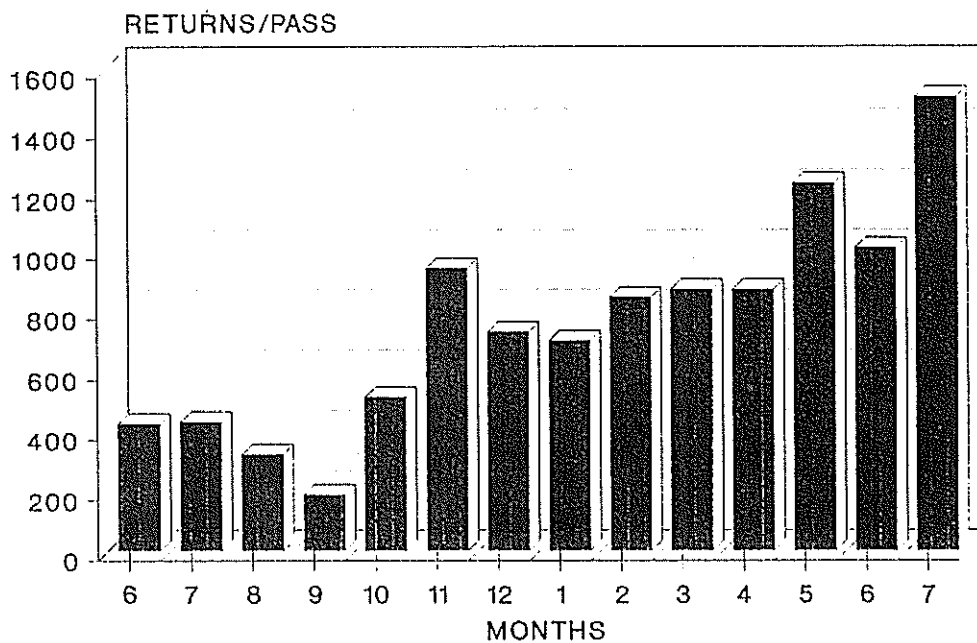
Fig. 2
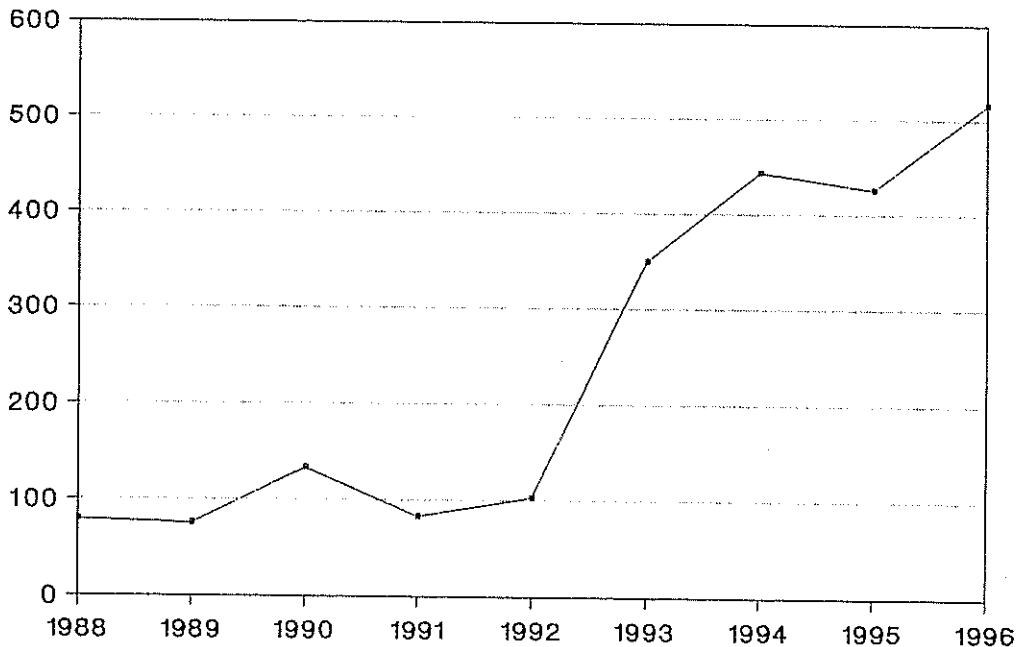
NUMBER OF PASSES: 1988-1996
BOROWIEC SLR - 7811

Fig. 3

3. Results of observations.

Introduction of a new computer and tracking system has led to substantial improvement of the quality and quantity of results. The increase of the number of observations from 1988 till the end of 1996 is shown in Fig. 3. Results of the observations carried out in 1995 and 1996 are collected in Tables 1 and 2, from which a significant increase in the number of return signals and improvement of the normal point precision for each satellite is visible. Introduction of a new computer and improvement of the tracking accuracy did not affect the single shot precision (Figs. 4 and 5) whose enhancement is expected as a result of the works began in the end of 1996.

4. Automation of the system.

An important task under realisation for the last two years is automation of the system. The project is discussed in detail in "Automation of the Borowiec SLR" within the same Proceedings. Connection of the main control computer to the Internet in November 1995 proved much beneficial for the process of the system automation.

5. Plans for the future.

In the nearest 3 years the introduction of the following improvements at Borowiec SLR is planned:
- increase of a single shot precision to 1-2 cm is expected after installation of a HAMAMATSU H5023 photomultiplier, time interval counter STANFORD SR-620, and shortening of the laser pulse to 35 ps,
- reduction of the range bias as a result of installation of the second target or inner calibration, enhancement of the accuracy of pressure read out, measurement of the return signal amplitude,
- increase of the number of observations through automation of the system and reduction of the staff on duty to a single operator, performance of daily observations, extension of observation
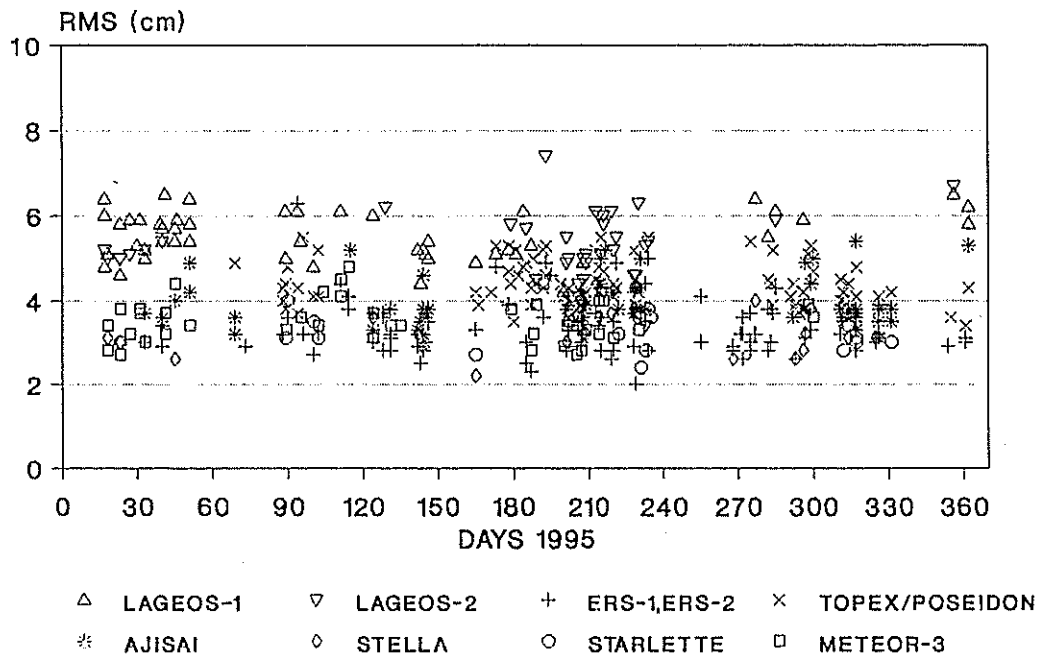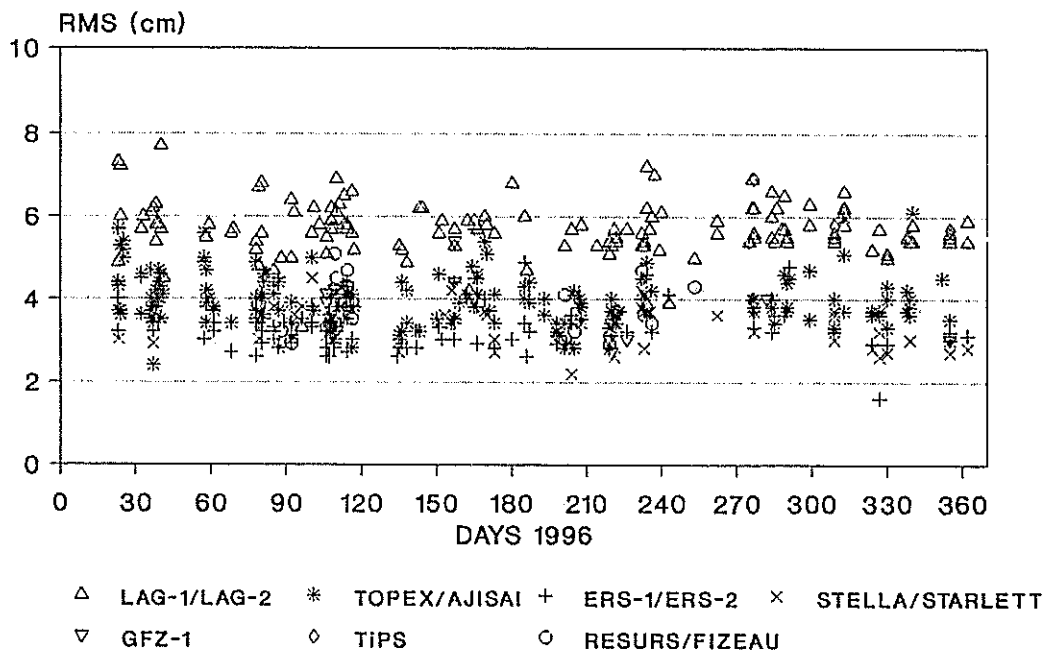
107

PASS RMS Vs TIME   BOROWIEC SLR

RMS (cm)

DAYS 1995

| Δ | LAGEOS-1 | ▽ | LAGEOS-2 | + | ERS-1,ERS-2 | × | TOPEX/POSEIDON |
| * | AJISAI | ◇ | STELLA | ○ | STARLETTE | □ | METEOR-3 |

Fig. 4

PASS RMS Vs TIME   BOROWIEC SLR

RMS (cm)

DAYS 1996

| Δ | LAG-1/LAG-2 | * | TOPEX/AJISAI | + | ERS-1/ERS-2 | × | STELLA/STARLETT |
| ▽ | GFZ-1 | ◇ | TiPS | ○ | RESURS/FIZEAU | | |

Fig. 5

time for 7 days a week and starting the observations of high orbiting satellites such as GPS, GLONASS, ETALON.

6. Borowiec -2 SLR.

For the last two years efforts have been made to install a system Borowiec-2 in Tunisia. From April to the end of June 1995, test observations were performed with this system in Borowiec, obtaining results for 25 passes (Schillak, 1996 b). Results of these observations confirmed that the system is ready for installation. The necessary changes (laser) and complementations will be made after the final decision as to the system installation in Tunisia. The Tunisian side bought the grounds on which the Geodynamical Station will be built and made architectural design of the Station building.

References 1995-1996.

Schillak S., 1995, Borowiec Laser Station-Operational Report 1994, *Publ. of Space Research Centre of the Polish Academy of Sciences*, Borowiec, January 1995, Poland, pp. 1-38.

Rutkowska M., Romay Merino M.M., Schillak S., Dow J.H. ,1995, Improvement of the SLR Borowiec station position in the global network ITRF91, *Adv. in Space Res.*, Vol. 16, No 12, pp. 97-100.

Schillak S., Butkiewicz E., Bartoszak J., Schillak D., Zapaśnik S., 1995, The satellite laser ranging performed at Borowiec with accuracy to a few centimeters, *Artificial Satellites, Planetary Geodesy-No 25*, Vol. 30, No 2-3, Warsaw, Poland, pp. 103-113.

Schillak S., 1995, The accuracy and precision of the Satellite Laser Ranging Systems, *Artificial Satellites, Planetary Geodesy-No 25*, Vol. 30, No 2-3, Warsaw, Poland, pp. 115-121,

Schillak S., Latka J.K., Bartoszak J., Butkiewicz E., Schillak D., Zapaśnik S., 1996a, Status Report on the Borowiec Laser Ranging Systems, *Proc. of the 9 th International Workshop on Laser Ranging Instrumentation*, Canberra (Australia), 1994.11.07-11, Vol. 1, Australian Goverment Publishing Service, Canberra, Australia, pp. 264-272.

Schillak S., Butkiewicz E., Latka J.K., Dybczyński P., Baranowski R., Frączyk P., Sczaniecki L., 1996, Software of the Borowiec-2 SLR System, *Artificial Satellites, Planetary Geodesy No 26*, Vol. 31, No 1, Warsaw, Poland, pp. 71-80.

Schillak S., 1996b, Borowiec Laser Station-Operational Report 1995, *Publ. of Space Research Centre of the Polish Academy of Sciences*, Borowiec, January 1996, Poland, pp. 1-40.

Schillak S., 1996, Satellite Laser Ranging in Poland 1976-1996, *Artificial Satellites, Planetary Geodesy No 28*, Vol. 31, No 3, Warsaw, Poland, pp. 163-177.

The Laser Ranging System of Yunnan Observatory(YLRS) and its Status

Yunnan Observatory   China

Jiang Chongguo   Xiong Yaoheng
Wang Wu   Feng Hesheng

October 1996

I. Introduction

Yunnan Observatory is situated in the middle of Yun-Gui Plateau, southwest China. It has the latitude 25° N, the longitude 102° E and the altitude 2030m. Initially the project of the YLRS was proposed in 1985. The project was not carried into effect because of financial problem. The group rebuilt the 1.2m telescope and worked on other project, but still did not give up the goal of SLR and LLR.   In April 1996, the Chinese Academy of Sciences examined the proposal of YLRS and offered partial funds to set up SLR station. Up to now we have already had:
1. Telescope
2. Imaging system for pointing calibration
3. Laser
4. Transmit/Receive optics
5. Receiver(PMT)
6. Software of satellite prediction and data pre-processing

The electronic hardwawe for   transmit control, transmit/receive switch, range gate, time control,   interface, and the software for observation and system control are being modificated and will   soon be finished.   We lack 'still   the time system and the counter. It is estimated that the system can be completed in a few months.

II. YLRS Overview

The YLRS is shown as F1 and F2.
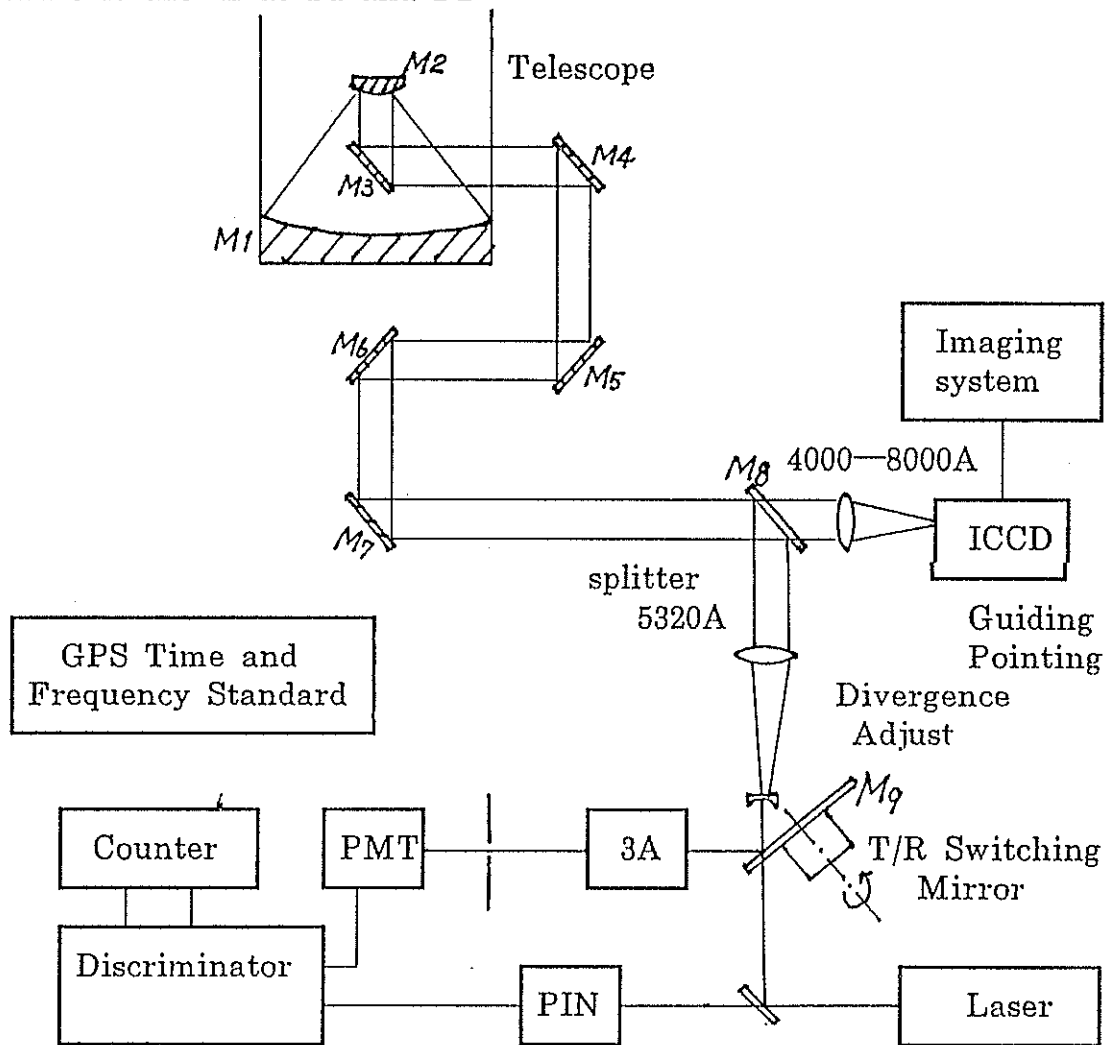
F1. YLRS Diagram
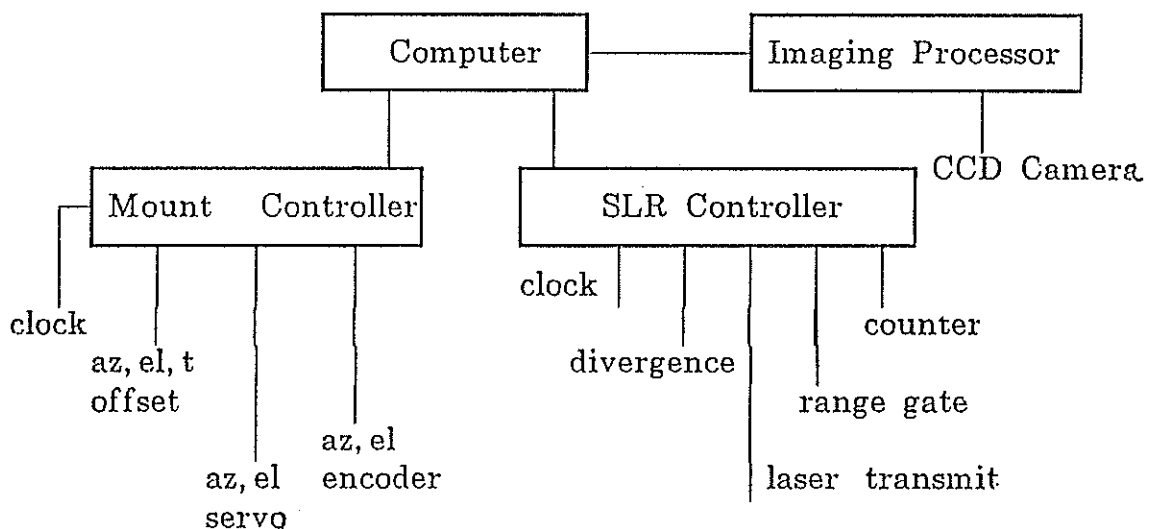
F2. YLRS Control Diagram

The YLRS Specifications is as follows:
1. Ranging Ability: 800~>20000 km
2. Accuracy: 3~4 cm
3. Repetition Rate: 4 Hz
4. Divergence: 0.01~0.4 mrad
5. Operating Time: Day and Night

III. Telescope

The telescope has the Az–Alt configuration. In resent years it was successfully used for the experiment of "real time correction of the atmospherical turbulence for stars " (adaptive optics).
It indicated that the telescope has especially good pointing accuracy. As a result of good pointing and tracking performance, relative larger apeture, and more stable Coude optics, it is expected that the YLRS is especially suitable to day and night ranging of the long distance satellites, such as Lageos, Etalon, GPS35, 36...

The characteristics of the telescope are as follows:
1. effective apeture: 1060 mm
   (It can use both in transmit and receive)
2. configuration: Az—Alt
3. transmission mode: friction transmission directly drived by torque motors
4. resolution of the encoder: 0.″36
5. pointing accuracy: ±1″ (R.M.S)
6. tracking accuracy: ±1—3″ (for lageos, etalon...)

IV. Laser

This is the active and passive mode-locked Nd: YAG laser, manufactured in Beijing. The laser consist of an oscillator and three stage amplifier.

The characteristics of the laser are as follows:
1. wavelength: 0.532 nm
2. energy per pulse: 150 mj (max. 200mj)
3. pulse duration: 200 ps
4. repetition frequency: 4 Hz
5. divergence: 0.8±0.2 mrad
6. output beam diameter: 10 mm
7. output laser mode: TEMoo

Active/Passive   Mode-Locked Oscillator
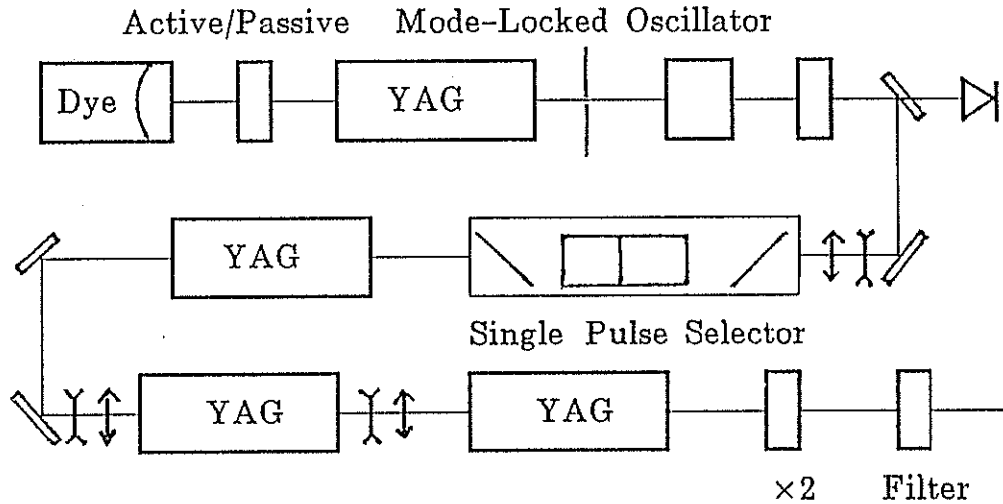
F3.   Nd:YAG laser diagram

V.   Time and Time Interval   Measurement

The   time   system   of   Yunnan   Observatory is   based   on   the   rubidium
time   and   frequency   standard   calibrated   by Loran-C receiver. These
old   devices   have   worked for   over   20 years   and   will   stop   the
routine   service   by   end   of   this   year. We plan to   use   much more
reliable   GPS timing   sysem.

For   flying   time   interval   measurement, time interval counter   model
SR620 is   selected.   It   has   a   resolution   of   20ps   and   an   accuracy
of better   than   100ps.   F4   is   the   diagram   of   flying   time interval
measurement. The   range   gate   has   a   resolution   of   0.1 μs,   gate
width   of   0.1us~6 ms   and   minimum   range of   0~3 s.
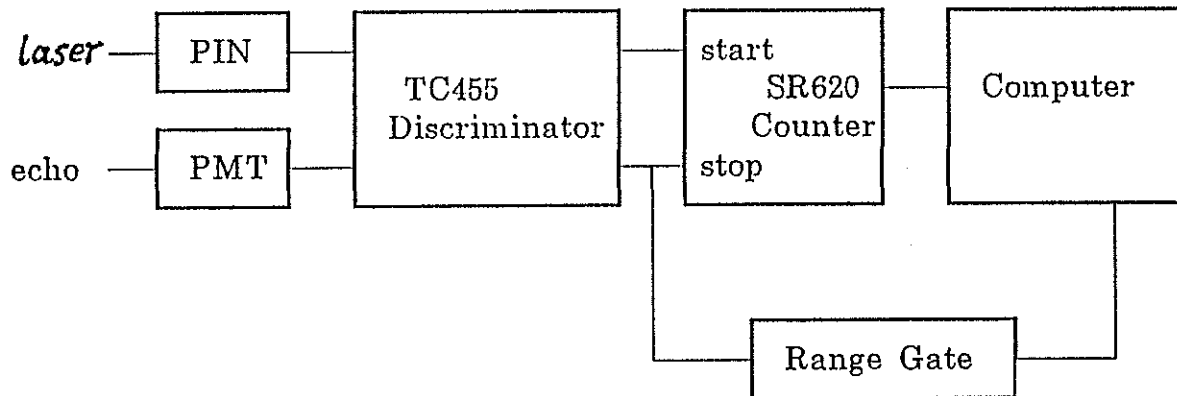
F4.   Flying   Time Interval   Measurement

VI. T/R Switch and Receiver

The YLRS has the same optic path for both transmit and receive. These are mirrors M1~M8 of 1.2 m telescope (see F1) and two matching mirrors. The rotating mirror M9, drived by a stepping motor, switchs between transmit and receive.

To the receiver of the YLRS, PMT (RCA 8850) is used at first. The avalanche diode with transistor cooler will be developed later to improve the performance of the system.

VII. Imaging and Guiding System

M8 in F1 is the dichroic beam splitter. While the laser beam is almost totally reflected, the beam of other wavelength will transmit the splitter. The CCD camera and imaging device are installed for sky mapping to correct the pointing errors of the telescope. After imaging processing, precise positions of stars (about 0.1 arc sec.) can be measured. It is convenient to use an ICCD camera here for guiding of satellites.

THE SIMEIZ (N 1873) SLR STATION.

L.S. Stirberg (Crimean Astrophysical Observatory)
S.K. Tatevian (Institute of Astronomy, Moscow)

The Simeis satellite laser station (N 1873) is equipped with a laser ranger system, based on the 1-m telescope of the CRIMEA type. The installation of the station was made in 1989 jointly by the Institute of Astronomy and the Lebedev's Physical Institute. The initial single-shot precision of the system was 20-25 cm. In 1991-1993, to satisfy the IERS requirements, a modification of the laser system was undertaken by the Institute of Astronomy (INASAN) and the Simeis laser group. The laser transmitter and the time counter were replaced, and a new control PC (an IBM provided by the GFZ/Potsdam) was added. Specially developed software was also installed.

Simeiz SLR system Description.

Mount configuration	Azimuth-Elevation, Coude system for transmitted and received beams.
Movement drive	2 axis stepping motors and 2 driving motors of constant currents are used.
Tracking speeds	Azimuth - max 3.4 deg/sec Elevation - max 3.4 deg/sec

The Elevation-Azimuth telescope movement is provided by the two step-motors and two small constant current motors, installed in parallel, to increase the tracking velocity limit. Axes of the step and constant current motors are connected by a special belt gear. There is no need for an additional power supply for constant current motors, since they receive power through the dividing capacitors and diodes of the step motor resistances. When the frequency of the step motor pulses is increased, the capacitors let current pass to the diodes, and the constant current motors start working. The higher the frequency, the larger the current to the motors. This makes it possible to increase the velocity of the telescope movement to 4 deg/sec.

1.2 Laser Transmitter
- -

Type of laser	Nd: YAG, Q - switched
Laser wavelength	532 nm
Pulse width	250 -350 ps
Output energy	100 - 120 mj (satellite)
Repetition rate	1 Hz
Output beam divergence	6 - 50 arcsec (adjustable)

1.3 Receiving System

Optics	Spherical mirror, diameter 1 m effective area 0.72 sq. m
Optical filter	4 nm, 60% transmission
Photomultiplier	FEU-79, rise time 0.5 ns, (since June, 1996 - C31034A PMT)
Mode	Single PE detection

The receiving-transmitting systems are controlled by the same PC/386.

1.4 Ranging Electronics

Time interval counter	PC-500
Discretion	25 ps
Resolution	100 ps
Calibration	Short external path (fiber optics)

1.5 Time and Frequency System

Frequency standard	Rubidium 3 e-12
Synchronization	TV
Resolution interval	0.1 ns counter

The new software includes a real-time tracking program, IRV and ORBMESSE predictions, graphic images of tracking passes at the screen, analysis programs and polynomial filtering.

In the receiving system there is a device for automatic recording of the energy of photomultipliers pulses for every range measurement.This makes it possible to correct measurements in real-time for amplitude variations due to the effects of multi-photons pulses. The dynamic range of the signal energy control system is 35 db. To avoid nonlinearity in the response of the PC-500 counter, it is necessary to record the time of a start pulse relative to the 5 MHz base frequency. The time registration precision of the counter is 1 ns. As a result of the SLR system upgrading (changes of the laser transmitter and time interval counter, measurements of return pulse energy, new software and data filtering), the ranging precision has been improved to 5-9 cm. The new laser transmitter will support considerably better ranging precision, but the FEU-79 photomultiplier, which we are presently using, gives a significant jitter(0.2-0.4 ns) and the PC-500 counter has limitations in resolution.Data is filtered using a polynomial fit with a rejection of no more than 15 % of measurements. The data are sent to the European Data Center (Munich) within 10 hours. The Simeiz station observes 150-300 passes per year. The data yield is limited by the instrument performance and weather conditions. The satellites observed include: ERS-1 and 2, LAGEOS 1 and 2, TOPEX-Poseidon, Ajisai, Starlette, Stella, Etalon 1 and 2, and GFZ-1.

Perspective: We plan to upgrade the SLR system and replace the time counter, photomultiplier and some other units with the help of a Grant received jointly with SAO from the Civilian Research and Development Foundation (CRDF), USA, in 1996.

STATUS OF THE SIMEIZ SLR STATION.

1. The Simeiz SLR(1873) station was established in 1989 with the ranging system based on the CRIMEA type 1-m telescope. Since then almost all of the components of the laser system, except of the telescope mount, have been replaced. Since 1993 the station may be considered as a second generation semiautomatic system with visual guiding (night tracking only) and a single shot precision of 6-8 cm.

Upgrading of the Simeiz (N 1873) SLR station. (Oct. 1996)

	1989	1996
Laser transmitter:		
pulse length	2.5 - 3.0 ns	0.25 - 0.3 ns
output energy	0.03 - 0.05 J	0.07 - 0.12 J
Time interval counter:		
resolution	1.0 ns	0.025 ns
precision	0.7 ns	0.015 ns
Control computer	" Chekan" and MERA-400 computers.	PC(ibm) 386, new S/W for system control.
Recording of measurements	magnetic and perforated-tape	Floppy-disks
Software		Software modification for the automatic guiding and data control.
Measurements of the received pulses energy	No	since 1991
Precision	14-22 cm	6-8 cm

2. a) The energy of the received calibration pulses is measured and used to correct satellite range data.

b) Polynomial filtering, 15 % of the outliers are admitted.

>> c) Results of the data orbital control, which are available by E-Mail from the SLR analyses centers, take about a week to reach the station, which makes it impossible to make effective use of this information for daily data corrections.<<

3. " Special" effect.

A nonlinearity in the PS-500 time interval counter was discovered. It was shown that if a transmitting pulse is rigidly tied to the base frequency of 5 MHz, the mean square error of the range measurements is 0.03 ns. If an impulse is emitted randomly in time, the RMS will increase by an order of magnitude. This effect was found when calibration of the PS time counter with a 100 m cable was made. To avoid this interpolator problem, a special method is used: the position of the START pulse is measured relatively to the 5 MHz frequency with 1 ns accuracy; then these data are used for data correction.

New Mobile Systems

Report on Saudi Arabian Laser Ranging Observatory (SALRO)

Attieh A. AL- Ghamdi
Research Institute of Astronomy and Geophysics (RIAG)
King Abdulaziz City for Science and Technology (KACST)
P. O Box 6086, Riyadh 11442, Saudi Arabia
e-mail: ALGHAMDI@KACST.edu.SA

ABSTRACT

*Saudi Arabian Laser Ranging Observatory (SALRO) "state-of-the-art"
laser ranging system is described. The system meets the .SLR system
performance specification. SALRO is now on mission support and
every available satellite is tracked when weather and
serviceability allow. The SALRO normal point analysis results for
August and September 1996 is discussed and shown to be 3.6 mm
(RMS) for LAGEOS satellite.*

1. INTRODUCTION

atellite Geodesy is a powerful tool for the study of the earth's kinetic and dynamics [1,2]. The rapid progress in laser technology and its applications to satellite ranging has considerably improved the accuracies to the subcentimeter level.

In the last 30 years many Satellite Laser Ranging systems have been installed on most of the global plates. Saudi Arabian Laser Ranging Observatory (SALRO) is the first SLR system to be installed on the Arabian plate. The purpose of the SALRO project is to open an access to the study of the Arabian Plate tectonic motion, which is extremely important because the availability of SALRO data to the SLR community will compliment the existing contemporary relative plate tectonic motions of the Arabian to Eurasian, Australian, South American, North American, Pacific, Nazca, and Caribbean plates.

The SALRO system was designed and developed in Australia by Electro Optic Systems Pty limited (EOS)and has completed testing at NASA, GSFC, USA. The SALRO has been installed in the Solar Village approximately 40 km north-west of Riyadh and operated by Research Institute of Astronomy and Geophysics (RIAG) of King Abdulaziz City for Science and Technology (KACST).

The SALRO uses a 0.75 meter telescope to transmit and receive optical signals from satellites equipped with corner cube retroreflectors. The SALRO laser operates at a wavelength of 532 nm with energy of 100 mJ and generates a pulse-width of 100 ps at a rate of 10 Hz. The SALRO system is easily managed by a single operator, excluding the aircraft observer. The software utilises both VDU and graphics from the telescope flexure analysis, real-time ranging, and post-ranging data analysis functions, aiding and accelerating the operator and analysts comprehension of the systems performance.

The multi-stop epoch timing is used to measure range time-of-flight with picosecond accuracy. Open ended coupling of its

"state of the art" technologies positions SALRO to meet the emerging developments in fully automated, multicolour, high repetition rate, subcentimeter Satellite Laser Ranging.

The following description of the SALRO system (see **appendix A**) also includes some results of satellites observations from August and September 1996, respectively.

2. Collocation, Site, and Survey

The system underwent comprehensive collocation tests with the NASA network standard, MOBLAS7, prior to its arrival in Riyadh. Extensive analysis of field data at Riyadh, Saudi Arabia (see the map in **figure (1)**)conducted by three NASA-sponsored groups (*Allied Signal Technical Services Corporation, Hughes STX Corporation, and the University of Texas Center for Space Research*) have demonstrated that the LAGEOS (prime source of geodetic reference) data taken at Riyadh is comparable in quality to that of other high quality SLR systems. The SALRO system ranks among the best SLR stations in terms of data quality.

The SALRO is sited in rocky landscape i.e. no sand, with minimal airborne dust, and the elevation is approximately 790 m above the sea level with latitude 24^0 54'.638 and longitude 46^0 24'.025 (see **figure (2)**) . The first-order survey data is shown in **table (1)**. The SALRO system (**figure (3)**) was installed on a specially-prepared, and very stable concrete PAD. Retroreflectors mounted to three permanent calibration piers are being used to monitor the stability of the system before and after each satellite pass. SALRO is operating and maintaining by the KACST staff. A special building at the site is used to house the staff and support the SALRO operations where a local Area Network (LAN) was installed in the building.

One error source is an apparent large (~ 2.5 cm) discrepancy between the surveyed distance to the south monument pier and the distance determined by the SALRO data. The site survey must be repeated to resolve the calibration range ambiguities among the piers. The tests at the site conducted with the three calibration targets (West, East, South) suggested a system delay which varied with azimuth. The West target, at a distance of 200 m from the station is normally used for routine system delay calibration. The East and South targets are located 400 m and 800 m respectively from the station. The system delay computed from the South and East targets showed biases of 25 mm and 50 mm respectively relative to the West target. To resolve the issue, a special test was conducted using the retroreflector on the telescope spider array which demonstrated that azimuth biases introduced by the system were less then ± 2 mm [3].

COORDINATES			ELEV.
POINT	NORTHING	EASTING	
T-1	2755938.111	641328.533	790.241
T-2	2755786.457	641341.140	790.033
T-3	2755633.808	641378.178	798.336
T-4	2755310.543	641314.045	789.336
T-5	2755199.949	641334.847	791.142

T-6	2755428.911	641659.929	787.884
T-7	2755612.044	641565.593	789.085
0	2755813.540	641422.980	793.196
P-1	2755013.565	641422.916	792.491
P-2	2756013.609	641769.452	790.049
P-3	2755908.545	641258.467	793.763

Table (1). Coordinates and Elevations of the SALRO site.

3. SYSTEM DESCRIPTION

Figure (4) illustrate the interior layout of the SALRO trailer. The SALRO trailer consists of four sections:
- 5 Meter Dome, with 30" Contraves Telescope.
- Coude' Room, contain laser system, Transmitter, and Receiver.
- Control Room, work station for operation contain computers, Handpaddle, Printers ..etc.

- Facilities Room, contain MPACS Rack, Computer Rack, Control Rack, Electrical Distribution, ACU#1 CTRL, ACU#2 CTRL ..etc.

3.1 Dome and Telescope

The 5.1 meter diameter Dome was manufactured by observa-Dome Laboratories of Jackson, Mississippi. The Dome has single slit opening, composed of laterally moving half doors for fast performance. The rotation is unrestricted at about 5 degrees per second, with slip rings for power allowing control of the slit at any azimuth. The Dome is totally automated during ranging and star tracking operations i.e. initializing, slit opening, tracking, parking and slit closure.

The SALRO Telescope design embraces the needs of a traditional Astronomical observing platform to the specific requirement of an SLR system. The SALRO telescope is a CONTRAVES Inc. manufactured item, and is based on the standard MOMS mount. The coude path allows the full telescope aperture to be utilised for both transmit and receive. There is an adjustable secondary mirror for precise focus setting under software control (a computer readable thermistor returns tube temperature to account for thermal expansion in the telescope tube).The SALRO telescope, also provided by an indexed rotating tertiary mirror, allows the Nasmyth 2 port to be used for astronomical observations. To enhance tracking and imaging (photographic) of multiple stellar objects the telescope's also enhanced by a computer controlled derotating stage on the Nasmyth 2 port. By this way it keeps their angular relationship intact. One more enhancement is that the telescope optics are coated with enhanced aluminum with a silicon oxide over-coat for protection and to prolong the time between re-aluminising.

The control electronics reside in the facilities room. The system is the Model 30H MPACS (Modular Precision Angular Control System) and its features include position and rate driving modes and chassis display of encoder position readouts with 0.0001

degree granularity. Off-mode-stops the telescope with out requiring commands for unique positions.

It is also provided with an external computer and local keypad command/data input facilities. Another feature is the fast slew rate in both axes, reducing the traditional ranging zenith keyhole. The last feature is the high bandwidth for precise computer control at very high rates [4].

3.2 CUODE' ROOM

3.2.1 Laser and Receive/Transmit Systems

The block diagram of the SLR laser system at SALRO is shown in figure (4). The laser source consists of a Nd: YAG laser Quantal YAG 501C series modified by EOS for SLR operations. The laser has an active/active mode-locked oscillator with 80 ps minimum (80-250 ps, normally 110 ps) pulse-width and 1064 nm wavelength. Two amplifiers combine to produce in excess of 110 mJ per pulse at a repetition rate in excess of 10 Hz when needed. The frequency slicer is a Quantal solid-state slicer model SPSH-11 with H.V avalanche board and double pockle cell. It is vastly superior to the old Krytron slicer and needs no maintenance at all. The SALRO slicer is further enhanced by the EOS option of external trigger.

This trigger is locked to the Active-Active oscillator trigger ensuring that the same pulse is taken every time (i.e no pulse jumping, which happens frequently with the optical feedback system).

The result is a highly stablized output. Doubled output of 532 nm beam light is generated from the second Harmonic Generator (SHG) using KD*P nonlinear crystal. The output laser light has an approximate divergence of 80 arcseconds (~ 400 micro radians). The system gives oscillator stability of 4%, output power stabilities of 5% and also provides a permanently stable pulse slicing trigger via the A/A circuit.

When the MCP detector is in use and the discriminator module has its walk characteristics optimized over a large input range, signal strengths for terrestrial (eyesafe) versus satellite ranging are matched to maintain calibration. When the SPAD is in use, by virtue of its single photon detection ability, and optical "splash" any prior signal to the internal calibration event will stop the detector, thus leading to unreliable results, real time calibrations have therefore been replaced by the standard NASA pre and post calibrations method of SYSTEM DELAY determination.

Table (2) shows the output power measured with the laser set after oscillator, 1st Amp., 2nd Amp., and SHG, for 100 ps and 250 ps. The short term RMS fluctuation in the power at the laser beam after oscillator, 1st Amp., 2nd Amp., and SHG over 1 minute period give values of 1%, 1.4%, 2.1%, and 1.2% RMS respectively. Signal strength matching is achieved by utilizing ND filters in the transmit path to maintain single photon return rates for all targets. Single photon ranging is defined by the SPAD manufacturer's as being approximately 25-30% return rate. In practice attenuation of the laser transmission for terrestrial ranging is set between ND 4.0 TO ND 5.0, depending on current atmospheric conditions.

	OUTPUT POWER (mw) for 100 ps	OUTPUT POWER (mw) for 250 ps
OSCILLATOR	65	73
FIRST AMPLIFIER	135	160
SECOND AMPLIFIER	.2500	2900
SH GENERATION	1100	1500

Table (2). shows the output power measured with the laser set after oscillator, 1st Amp., 2nd Amp., and SHG, for 100 ps and 250 ps.

During operations utilizing the MCP detector, the real time calibration target can be a retro reflecting cube either on the receiver table, or mounted on the telescope secondary spider. The receiver table source is more stable because the full outgoing laser beam is sampled, whereas when the spider source is in place only a very small percentage of the outgoing diameter is sampled. Two problems can rise when utilizing the spider calibration retro:
a) The vagaries of the laser fringe patterns effect the percentage of signal arriving at the spider retro due to the high/trough pattern.
b) Even though totally internally reflective cubes are used, there is a polarizing component that reduces the returning signal, at some positions of rotation.
There are two racks in the Coude' Room; the Laser Rack and Receiver Rack. Each rack has independent cooling, controlled via thermostat sampling the return air temperature. Temperature stability is not as critical in the coude' room as in the facilities room since the electronics and optics are more stable than, say, the timing vernier in the CAMAC crate and the MPACS electronics.

The laser temperature is controlled via a twin chiller set located beneath the laser table. This set-up maintains the temperature of water used in the standard continuum heat exchange unit and is controlled via (adjustable) Evaporator Pressure Regulator valve on each chiller, thus the temperature is always above local dew point. This essential feature prevents condensation from forming on any sensitive optical surface [4].

3.3 Control Room

3.3.1 Software

The HP A900 has been installed with the standard vendor maintained operating system. The software operating on this computer includes:
1- Timing system calibrations
2- Pass alert and prediction packages (programs ALERT AND PDICT) which take as input UTX IRNs, ATSC TIVs, orbital elements and MIT lunar ephemera's. PDICT can also apply time bias corrections to its predicated pointing and ranges.

3- Star tracking and mount calibration analysis package, with graphical output.
4- Real-time range data acquisition software system for terrestrial, satellite (>500 km one-way) and lunar ranging real time operator feedback.
5- Graphics based engineering range editing/processing package that include:
  a) Standard sample quick-look data files
  b) Normal point generation according to the community accepted   algorithm
  c) MERIT II full rate data files
  d) Feedback time bias data for the prediction   package
  e) Graphical output to a variety of devices e.g. laser printer etc.
6- A variety of utilities for fixing corrupt range files, extracting diagnostic data etc.

The IBM compatible Vectra PC is used for the following:

1- HP graphics TERMINAL (EMULATED)
2- Data communications and file transfer
3- Word processing, spread sheet and database applications on commercial packages [4].

4. Facilities Room

The MPACS interface provides a means for diagnostic, utility and operational software to communicate with the telescope control system providing absolute positioning and tracking of satellite, lunar and stellar objects in real time. Additional features include 10 Mhz time base clock, derotator control with

5. COMMUNICATIONS

One significant limitation to station throughput, not foreseen when the various development contracts were put in place, is communications between the HP mainframe and the outside world. This one point was more and more of a headache as the SALRO has progressed through its scrutiny by the advisory panel, and progressed from an engineering system into a production system. The packages provided in the EOS system work well, though the engineering processing package was unacceptably labor intensive for a production site. NASA offered KACST their standard packages, and in some respects these packages have shown themselves superior, but they operate only on a high-speed PC. PCs were connected to the HP via 192K band serial link, and therefore transfer of prediction files to the HP, and transfer of formatted range data from the HP, added a significant operational overhead. In addition, Data processing was automated and routine, but took over 20 minutes to process a LAGEOS pass. To reduce this unproductive time, several sources have recommended that KACST invest in a LAN for the HP/PC network at the Solar Village. For high productivity and to reduce the data transfer bottleneck KACST has implemented a Local Area Network (LAN), where the HP A900 was connected with 3-PCs inside the main staff building, so that analysis data can be transferred and processed much more quicker.

A satellite laser ranging station requires telecommunications media that can really support the timely receipt and transmission of vital data needed for its functions. Daily access to satellite orbital position prediction and time bias information is needed for telescope pointing. The efficiency of the station depends on the format of this information and the manner by which it is transmitted. Similarly, an SLR station needs modes for the timely transmission of the acquired data to Data Centers. Most stations in the global laser network use the internet to perform these functions. SALRO also needs this capability. During SALRO test operations, there were limitations that significantly hampered station productivity and time lines of data distribution. Recently KACST has implemented a direct Internet link at the SALRO offices in Riyadh which has been connected to the SALRO site by PC Modem. An internet access was arranged, so that we may send from KACST offices.

6. Results

The system is now on mission support and every available satellite is tracked when weather and serviceability allow. The number of passes obtained in this period is very good and further successes are assured as the staff of the SALRO become more familiar and competent with the system. Establishment of INTERNET at SALRO offices facilitate the two way transfer of satellite orbit predications and data.

Tables (3) and (4) show the SALRO observations for August and September 1996, respectively. We have received the normal point results from *ATSC*. The analysis starts on the 5_{th} August through 30_{th} September 1996, but because of intermittent communications problems there are 2 days of data missing. There

are 83 passes in the 23 days period in August. Basically the results are quite encouraging, with a new system, new crew and especially when all these pass results are obtained by SPAD.

SATELLITE	TOTAL HITS	PASSES	AVERAGES	RMS
LAGEOS1	102665	27	3802	1.59
LAGEOS2	111190	32	3473	1.62
AJISAI	35317	25	1412	1.73
TOPEX	35177	29	1313	1.47
ERS2	1936	7	276	1.20
STARLETTE	13474	22	612	1.22
STELLA	122	1	122	1.43
GLONASS67	17850	7	2550	6.51
ETALON1	2667	1	2667	3.19
GPS35	1943	2	972	1.35

Table (3). SALRO observations for August 1996.

SATELLITE	TOTAL HITS	PASSES	AVERAGES	RMS
LAGEOS1	60051	28	2144	1.66
LAGEOS2	151520	42	3607	1.64
AJISAI	58340	35	1667	1.95
TOPEX	15709	16	982	1.8
EUROS2	1159	4	290	1.12
STARLETTE	14448	19	760	1.31
STELLA	1233	3	411	1.22
GLONASS63	6259	2	2086	----
GLONASS67	16584	6	2764	4.37
ETALON1	127	1	127	2.34
FIZEAU	280	1	280	----

Table (4). SALRO observations for September 1996.

Figure 6.a and 6.b show the first data returns obtained in the Arabian Peninsula for LAGEOS-1 and AJISAI satellites respectively. Both these passes were obtained using the Czech Republic 100 micrometer SPAD.

7. Conclusion:

The SALRO meets the satellite Laser Ranging (SLR) system performance specifications and configured for fully automated, high repetition rate, subcentimeter Laser Ranging. The performance of the system, as evidenced by LAGEOS normal point precision (RMS) of 3.6 mm and a near zero range bias, placing it highly in the global SLR network.

8. Acknowledgments

my dept to the KACST people who contributed to SALRO (past and present); thank you Dr. A. Alqadhi, Dr. M. Alsuwyeel, Dr. F. Noor, Dr. A. Neiazi, Dr. M. Al-dail, S. Alsa'ab, A. Al-khashlan, F. Alsa'eid, F. Alhusain, Z. Almustafa. I also wish to thank the staff of EOS led by Dr. B. Greene, special thanks to John Guilfoyle for his extraordinary effort to bring SALRO to the current status.

9. References

1   Smith, D.E., R. Kolenkiewicz, P. Dunn, J. W. Robbins, M. H. Torrence, S. M. Klosko, R. G. Williamson, E.   C. Pavlis, N.   B. Douglas, and S. K. Fricke,   "Tectonic Motion and Deformation   from Satellite Laser Ranging to LAGEOS". *J. Geophys. Res.*, 95,   22, 013-22, 041, 1990.

2   Harrison, C. G. A., and N. B. Douglas, "Satellite Laser Ranging and geological constraints on plate motion". *Tectonics*,   9, 935-952, 1990.

3   "SALRO FAT Review Board Report", SALRO, Riyadh, 20-23 July 1996.

4   a)"PRELIMINARY ACCEPTANCE BOARD REVIEW AND BRIEFING DOCUMENT", SALRO, Riyadh, 12 SEPTEMBER 1994.
     b)"SALRO ACCEPTANCE TEST PLAN", by EOS PTY Limited, 22 February, 1995.

5   Greene, B., personal communication, EOS pyt Limited, Australia.

Appendix (A)

SALRO PERFORMANCE SPECIFICATIONS

TELESCOPE

Aperture	:	75 cm, both transmit and receive
Configuration	:	Alt/Azimuth
Optics	:	Coude configured for transmit and receive
Drive	:	DC Torque Motors
Pointing Accuracy	:	1 arc second RMS
Position Readout	:	to 0.5 arc seconds, both axes
Slew Rate	:	20 degrees/second (azimuth)
		5 degrees/second (elevation)
Acceleration	:	5 degrees/sec/sec (azimuth)
	:	3 degrees/sec/sec (elevation)
Sky Access	:	to 95% elevation, all azimuths
Working Foci	:	Coude (Nasmyth 1)
	:	Derotator (Nasmyth 2)

LASER

Type	:	Nd:YAG, Continuum (Quantal) YAG501C
Oscillator	:	Active/Active ML (80 ps minimum pulsewidth
Wavelength	:	532 nm
Pulse width	:	80-250 ps, nominal 110 ps
Repetition Rate	:	1 to 15 Hz
Pulse Energy	:	85 mJ/80 ps
		110 mJ/100 ps
		125 mJ/250 ps

START DETECTOR

Photo diode	:	Fast Optical Switch Detector, Czech Technical University

RECEIVER

PMTs	:	MCP (ITT 4129F)
	:	Single Photon Avalanche Diode (SPAD) Czech Technical University
Filters	:	10 Angstrom and 1.5 Angstrom

STATION TIMING

Primary Standard	:	HP5061B Cesium Beam
Secondary Standard	:	FTS 1050A Quartz Oscillator
Time Transfer	:	FTS 8400 GPS Satellite Receiver

RANGING TIMING

Resolution	:	5 picoseconds
Random Error	:	10 picoseconds RMS (single event)
Systematic Error	:	1 picosecond RMS

CALIBRATION

Modes available	:	Terrestrial Target (for Pre/Post pass)
	:	Real-Time (feedback)

COMPUTERS

	:	HP-A900 System
	:	HP Vectra 386

WEATHER SENSOR

	:	Temperature (5)
		Humidity (1)

Pressure (1)
Wind speed (1)
Wind direction (1)
Lighting conductor (1), for connection to
ground mat where available

FACILITY

: 13mx3m (approximately) relocatable observatory
with astronomical dome. The prime mover for
relocating the observatory is not included

PERFORMANCE

: SLR:5mm normal point in 2 minutes
SLL: 1 cm normal point in 20 minutes
: SALRO shall be meet or exceed the following
overall system performance requirements for
ranging to the Laser Geodynamics Satellites
(LAGEOS1&2):
1. Single-Shot Ranging Precision shall be one
centimeter (RMS) or better when:
a. Magnitude 3 stars are visible at the site
to the unaided eye, and
b. seeing is better than 6 arc seconds.
2. Minimum Precision for two minutes normal
points shall be 0.5 centimeter or better,
3. Systematic errors shall be less than one
centimeter for 95% of the two minutes
normal points,
4. The data yield shall, at a minimum, be 50
returns per normal point for 67% of the time
the satellite is above the ranging horizon,
and
5. The SALRO shall be capable of ranging during
both the day and the night.
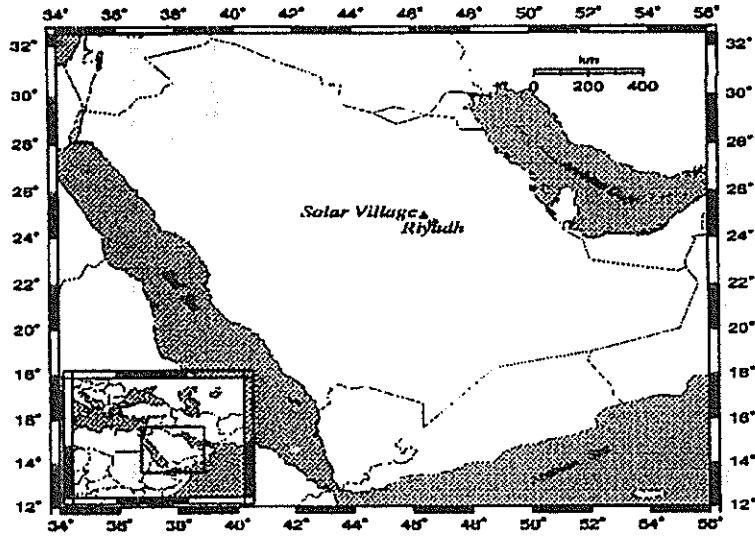
Figure (1). SALRO sited in the Solar
Village 45 km northwest of Riyadh in the
Arabian plate.
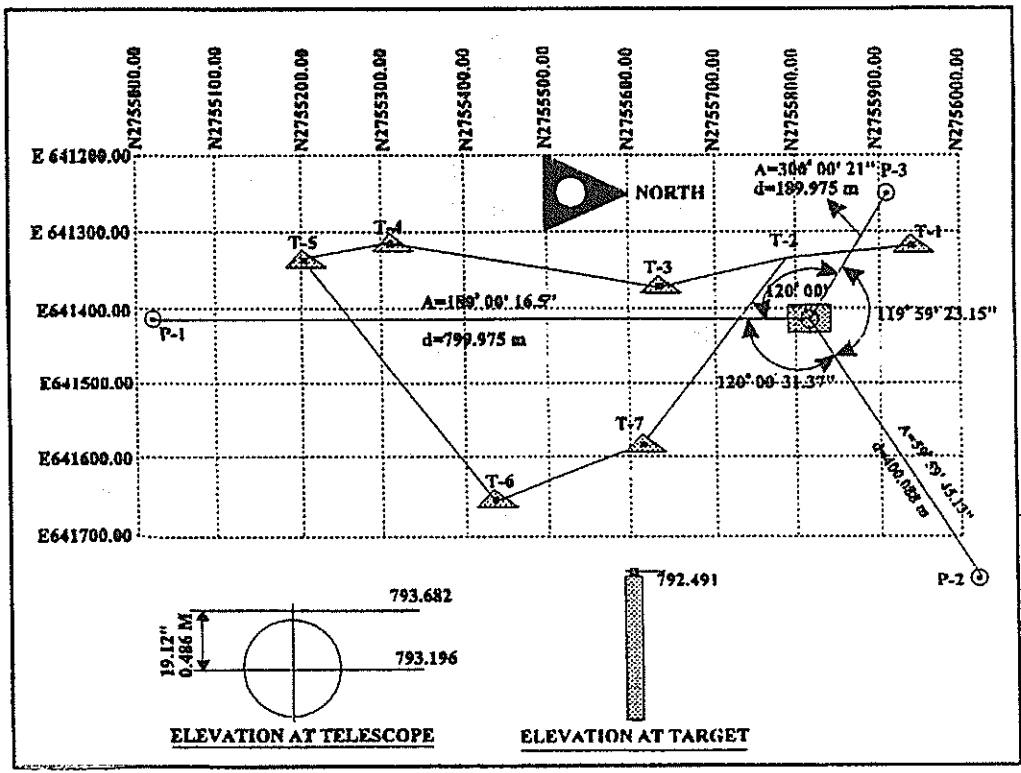
<u>**Figure (2). The site network- first order survey.**</u>

131
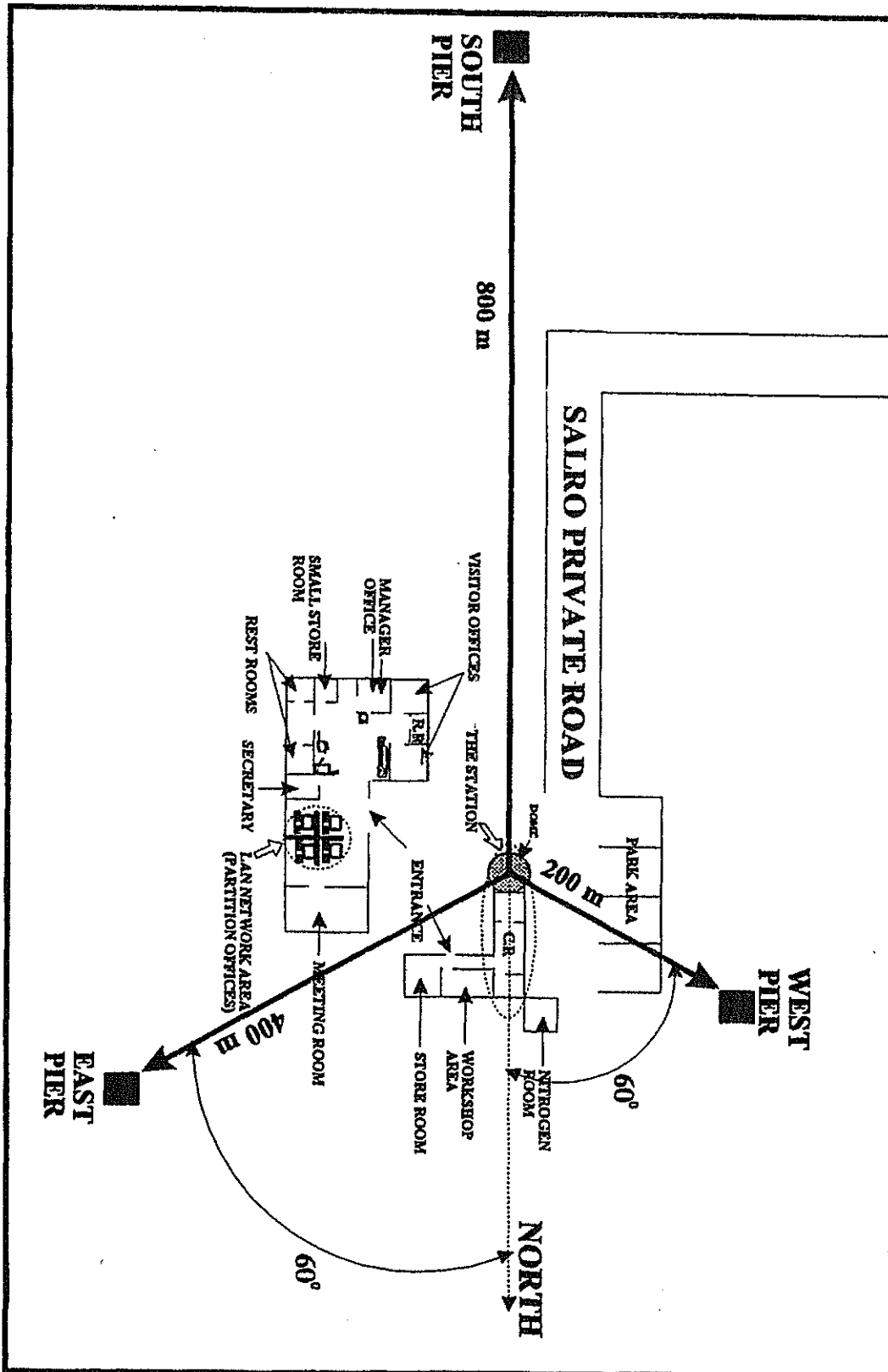
Figure (3) Salro Site Construction

132
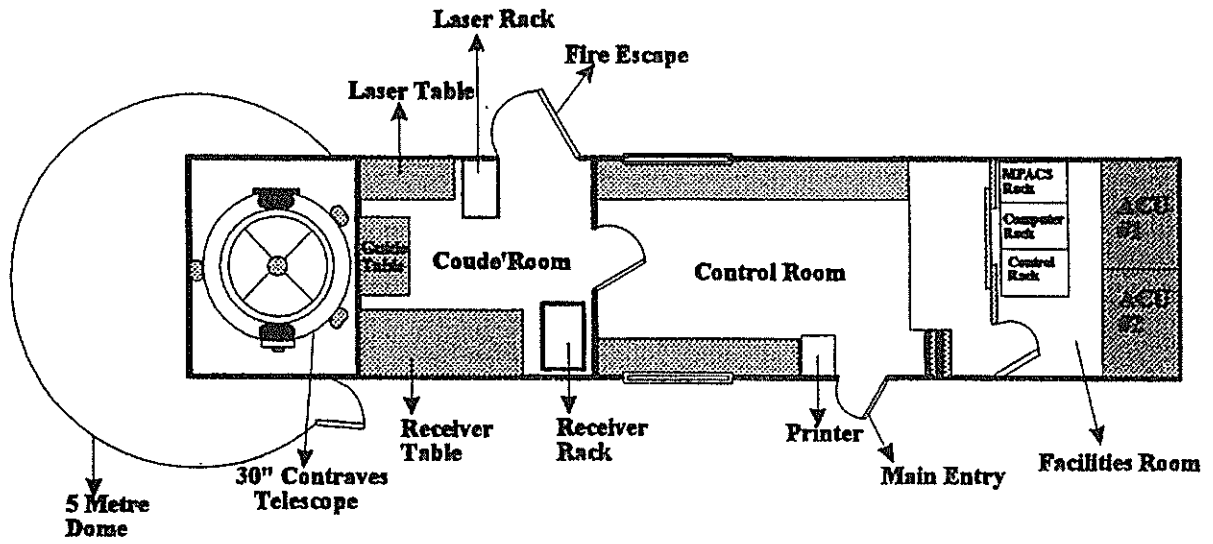
Figure (4) Schematic diagram of the SALRO system-an overall view.
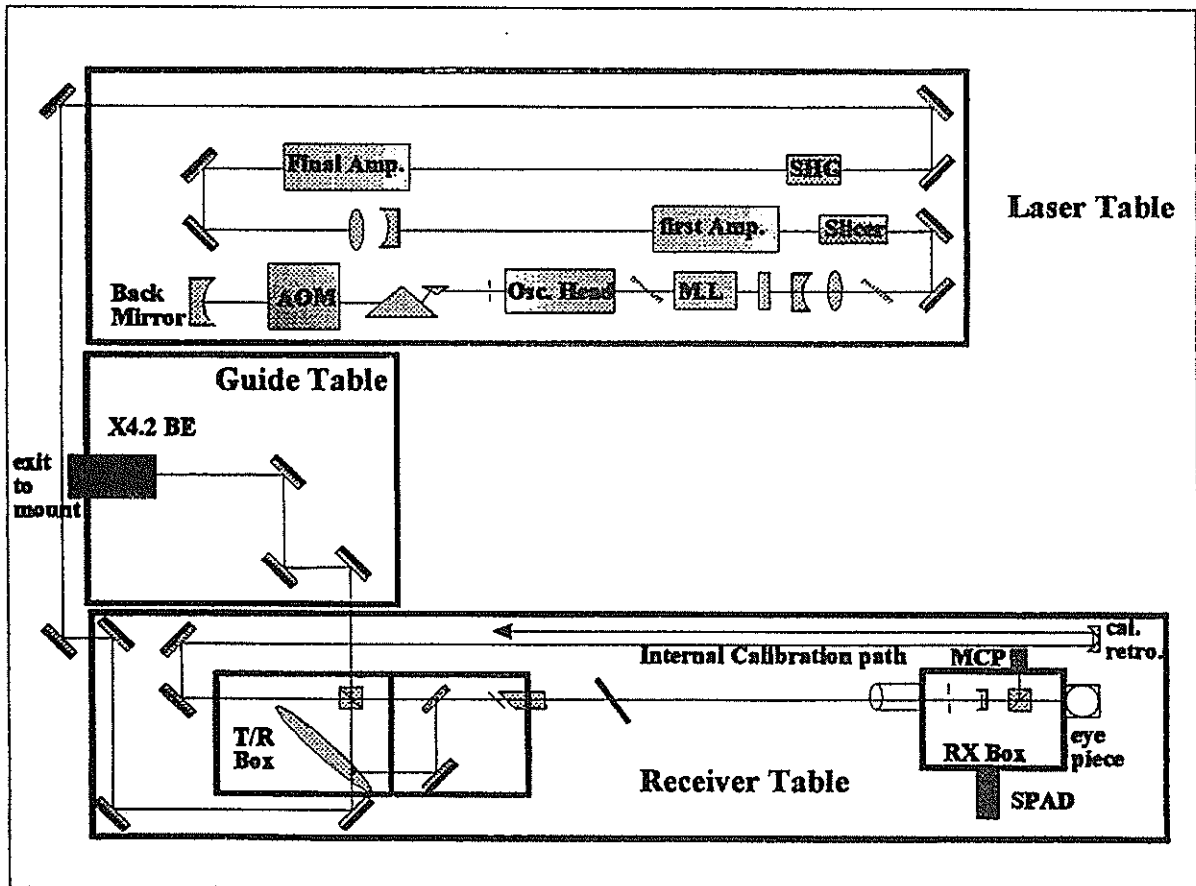
Figure ((5). Coude' Room Optical Layout
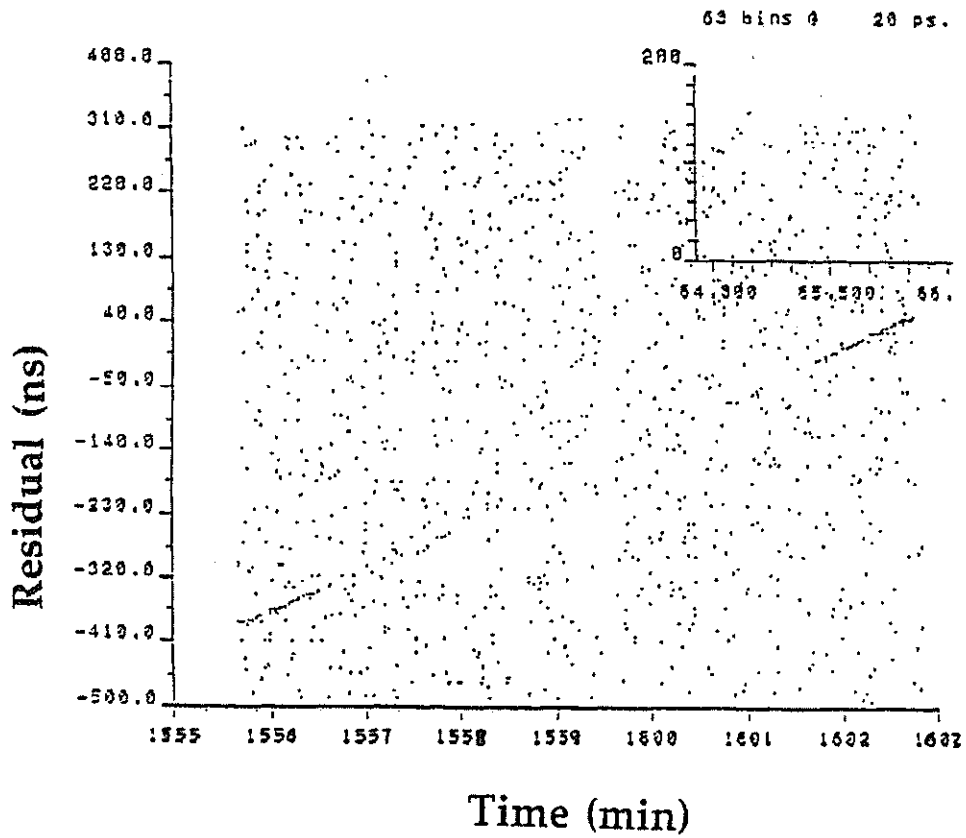
Figure (6.a). The data shows the first satellite ranging on the arabian Peninsula by SALRO. The data collected is from the LAGEOS-1 satellite using SPAD detection system.
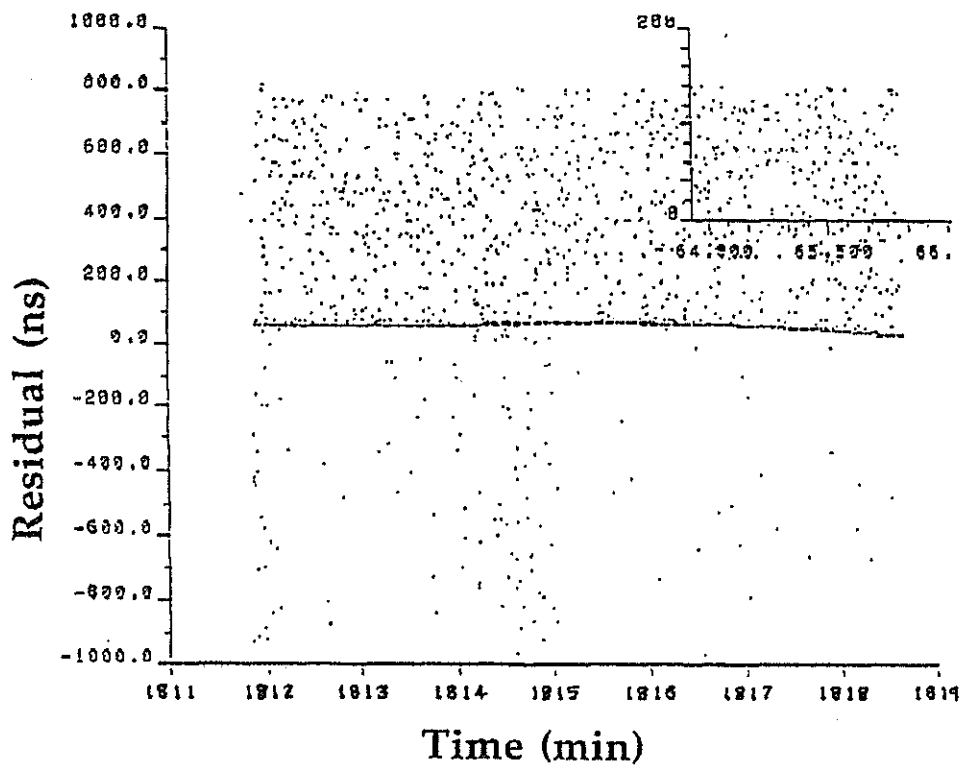
Figure (6.b). First data collected from AJISAI satellite by SALRO using SPAD detection system.

TIGO-Project: Concept-Status-Plans

P. Sperber, A. Böer, R. Dassing, H. Hase, W. Schlüter
Institut für Angewandte Geodäsie
Fundamentalstation Wettzell
D-93444 Kötzting

R. Kilger
Forschungseinrichtung Satellitengeodäsie der TU München
Fundamentalstation Wettzell
D-93444 Kötzting

Abstract: This paper will give a short overview about the concept, the actual status and the plans of the Transportable Integrated Geodetic Observatory (TIGO).

Currently all components of the observatory are assembled at the Fundamental Station Wettzell. During 1997 and 1998 the observatory will operate for a test period in Wettzell, then it will be used abroad as a fundamental station for the densification of the network of observatories realizing the terrestrial reference frame.

1.   Introduction and Concept

TIGO is the acronym for "Transportable Integrated Geodetic Observatory". TIGO will consist of the relevant instruments for geodetic space techniques such as for VLBI, for SLR and GPS as well as other relevant sensors as a gravity meter, a seismograph and meteorological sensors. TIGO integrates the advantages of the different techniques and acts as a fundamental station /1,2,3,4,5/. The whole observatory is housed in standard sea-containers for transportation. During 1995 a platform for TIGO has been built at the Fundamental Station Wettzell (figure 1) in order to assemble and to test the whole equipment. In 1995 the 6 m-radiotelescope and 4 of 5 transport and laboratory containers (figure 2, 3) have been delivered. As soon as the MK IV Data Acquisition Terminal (DAT) becomes available in 1997 the VLBI module will be operational.

The motivation to build a transportable fundamental station for geodesy and geodynamics results from the need for a better global distribution of reference stations that are representing the terrestrial reference frame. The objective is to densify the terrestrial reference frame and to optimize the geographical distribution by transportable devices.

For geodynamical research a globally distributed network of fundamental stations is required to obtain precise and reliable results. This coordinated network of Fundamental Stations will define and realize a terrestrial reference frame and maintain the reference frame with respect to the extraterrestrial reference frame represented by quasars. Therefore it is possible to determine the position and the motion of Earth in the Universe. For this purpose a permanent, complementary and redundant spectrum of observable being sensitive to the rotation of Earth and the crustal motion have to be provided. TIGO is designed to make measurements on sites in the southern hemisphere (for at least 1-2 years per site) with all actual available geodetic sensors. Each module is new designed with a high degree of automatisation.

2.   Status

2.1.   Platform for TIGO

TIGO requires a prepared platform, in order to mount the radiotelescope on it and to setup the SLR-telescope. A platform was built at Wettzell within 6 weeks in 1995. The specification of the platform consists of:

-        concrete fundament (10 x 10 x 1,5 m³) for the radiotelescope containing a special steel construction to fix the radiotelescope,

-        concrete fundament (3.5 x 3.5 x 1.5 m³) for the SLR module,

-        concrete fundament to setup 5 TIGO containers,

-        separated underground cable channels for either power or signal cables,

-        grounding network to earth all instruments and containers,

-        dehydration tubes.

The sixth container with six 25 kW power generators will be located in a sufficient distance to minimize problems due to the emission and vibration of the generators.

2.2.   VLBI Module

The 6m Offset antenna for the VLBI module (specifications in Table 1) was delivered in 1995 and tested in 1996. Due to the delay of the Mark IV Data Acquisition Terminal until 1997, the telescope is tested with parts of the Mark III terminal of the Wettzell VLBI System.

OFFSET ANTENNA with S/X-FEEDHORN

Diameter	6 m single offset
f/D	0.3629
Surface Accuracy	0.4 mm
Azimuth velocity	6 deg. per second
Elevation velocity	3 deg. per second

	Frequencies	Efficiency
S-Band	2.216 ... 2.350 GHz	64% (spec.) ... 67%
X-Band	8.108 ... 9.036 GHz	68% (spec.) ... 71%

Antenna Noise Temperature (45 deg. El., clear sky, 300K)

Antenna Noise	27K (S-Band)	24K (X-Band)
Ohmic Noise	26K (S-Band)	26K (X-Band)
Total Noise	53K (S-Band)	50K (X-Band)

Helium Cooled S/X-Receiver via NASA-GSFC
MK IV Data Acquisition Terminal and Field Unit via NASA
Set up time in Field < 2 days
Antenna, Receiver delivered in 1996 # MK IV expected in 1997

Table 1: Specifications of the TIGO VLBI Module

2.3. Basic Module

Three containers of TIGO are used for the basic module, in which five subsystems, which are important for the operation of the main modules or give additional information for the data analysis, are integrated.

> Precise Satellite Microwave Systems, which includes 5 GPS receivers (IGS standard receiver and a GPS array around TIGO for local control survey). GLONASS, PRARE and Doris receivers will be placed on request.

- In Situ Observations consisting of a superconducting gravity meter, seismometer, meteorology sensors (pressure, humidity, temperature, rain, wind speed, water vapour radiometer) and a time & frequency system (hydrogen-masers and cesium-clocks).

- The central control computer will directly control most of the subsystems of the basic module and work as data storage and distribution system for all modules.

- LAN and WAN communication facilities will be available. All modules will be connected over a LAN to exchange of data and to control/operate TIGO from one terminal. Dependent on the possibilities of the site, the WAN will be realized by direct Internet connection, telephone line or INMARSAT data transmission.

- A powersystem consisting of six 25 kW Diesel generators and a solar power system (220 V, 48 V, 24 V, 12 V) will provide TIGO with electrical power in operation and standby mode.

2.3.   SLR Module

The SLR module (specifications in Table 2) is currently in the final assembly and test status at TPD, TNO Institute of Applied Physics in Delft /6,7,8/. Telescope, Optics and Laser have passed the test procedures. These components are currently integrated and assembled with the control system consisting of the electronics, timing facilities and software.
Preparations are ongoing at the Technical University Delft to place the SLR-module on a pad for final testing and acceptance (Demonstration of ranging to all satellites). The delivery of the system to Wettzell is expected in summer 1997.
The telescope in the opened cart and the cart with telescope in the container (transport configuration) is shown in Figure 4, 5. The laser system is shown in Figure 6.

3.   Operational Plans

After integration and test operation of the complete observatory at Wettzell in 1997/1998 the system will go into field operation. A small workshop at Wettzell is planned for 1997 to discuss the best sites for TIGO. The necessity for additional sites in the southern hemisphere is obviously shown in Figure 7, where the distance of SLR-, VLBI- and Fundamental Stations to their closest neighbour is plotted and the remote regions with distances of more than 4000 - 5000 km to the next station are marked with crosses /3/. In field TIGO has to be operated in close cooperation with a partner of the host country.

Overall Specifications	Telescope Specifications
Subcentimeter Ranging Accuracy	Folded Lens Telescope without central obscuration Diameter: 500 mm
Range from 0 up to 40000 km	Aberration Correction for 847 nm and 423.5 nm
Two-Color System	Max. Field of View: 4 arcmin
High Automatic Operation	Optical Efficiency: 75%
50cm Telescope for Transmit and Receive	Material: Static Part: Granite Tube : Stainless Steel Fixations : Titanium
High Efficiency in Transmit/Receive	Mass: 1700 kg
Internal and External Calibration	Pointing Accuracy: better than 2 arcsec RMS
Cr:LiSAF/Titan Sapphire Laser	Speed: 6 deg/s (Elevation) 15 deg/s (Azimuth)
3 Detector Ports (SPAD)	Encoders: 21 bit absolute accuracy: 0.8 arcsec
# Set up Time < 2 days # Delivery: begin 1997	Size of Mount: Height : 2 m Diameter: 1.3 m

Table 2: Specifications of the TIGO SLR Module

4. Summary

The Transportable Integrated Geodetic Observatory TIGO is currently assembled at Wettzell and will be ready for test operation in summer 1997. The observatory combines a complete set of state-of-the-art geodetic measurement techniques to form a fundamental station for geodesy and geodynamics.

The system will improve the global distribution of stations significantly when it starts field operation in the southern hemisphere.
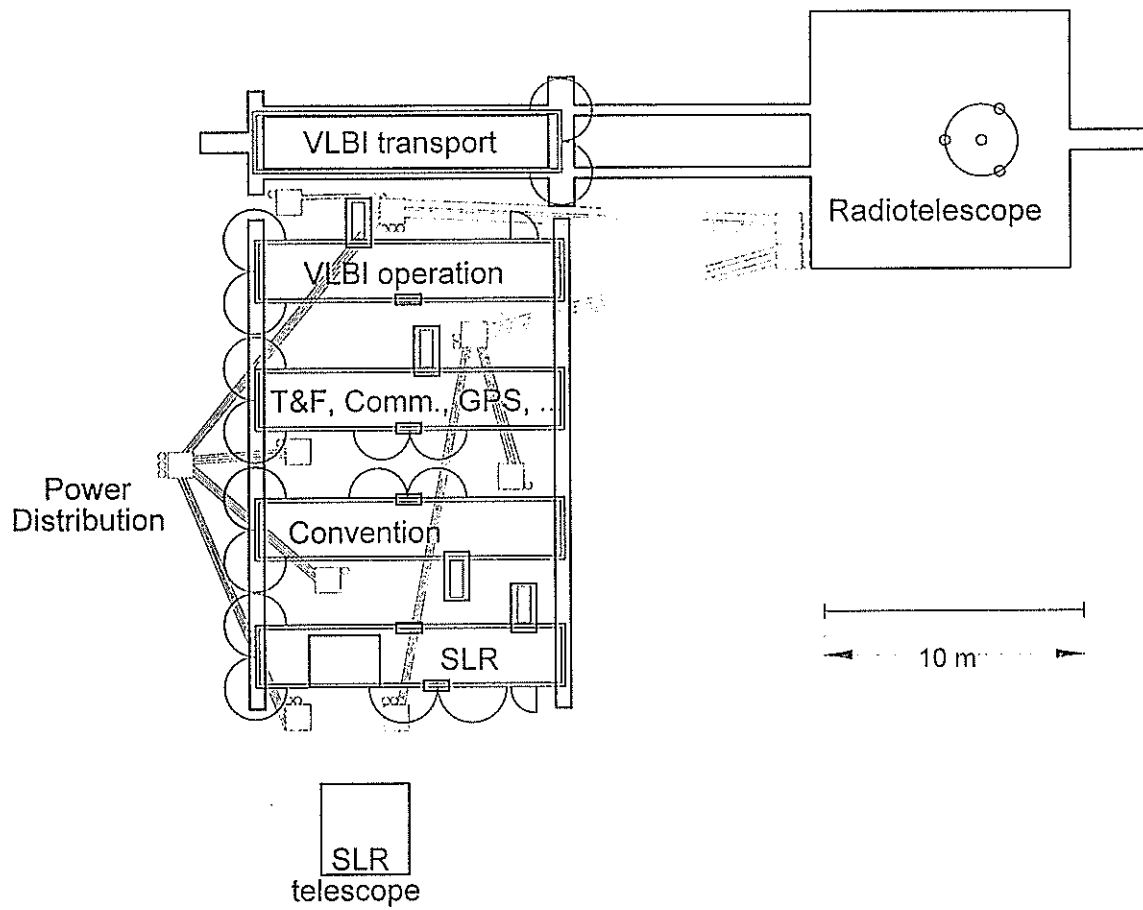
Figure 1: Schematic of the TIGO platform designed for Wettzell
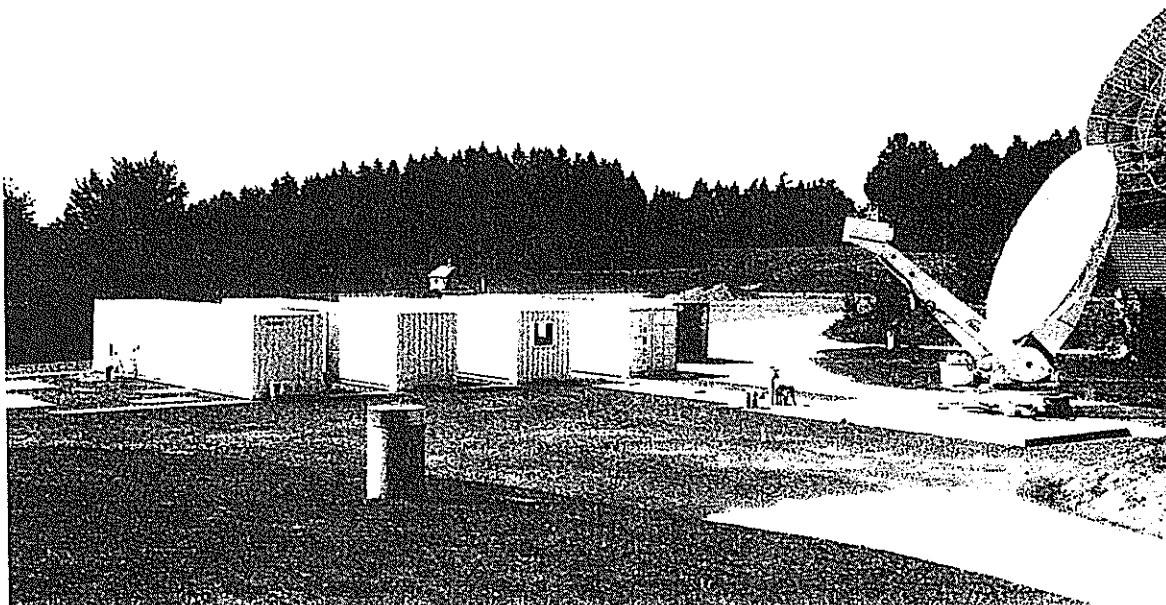
Figure 2: Four of five TIGO laboratory container and VLBI antenna
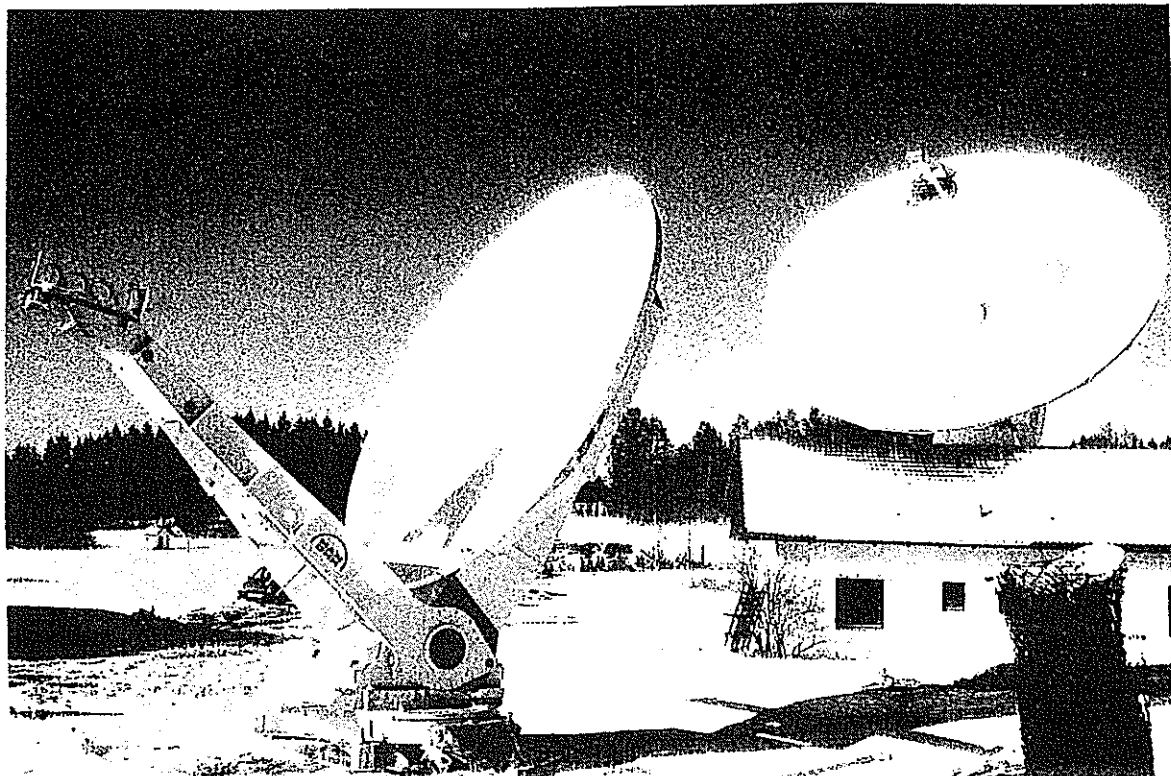
Figure 3: 6 m VLBI antenna in front of the 20 m VLBI antenna at Wettzell
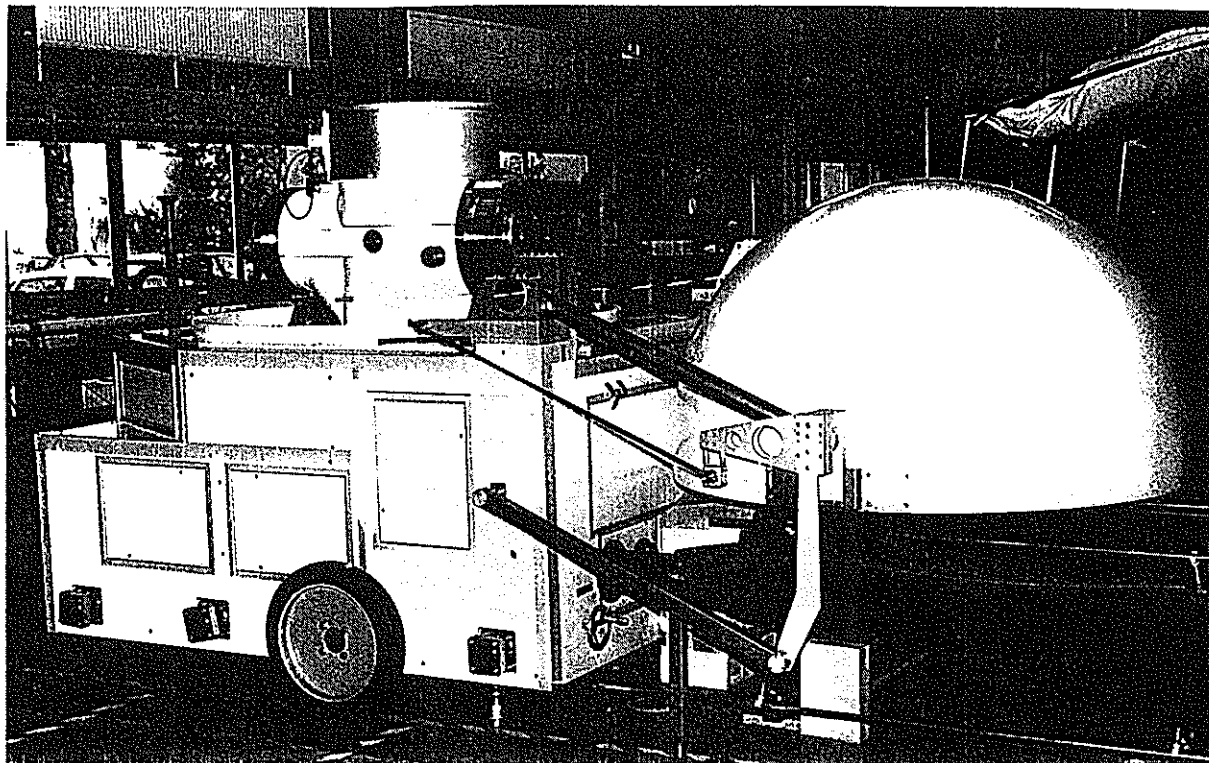
Figure 4: TIGO SLR Telescope in the open cart (ranging configuration)
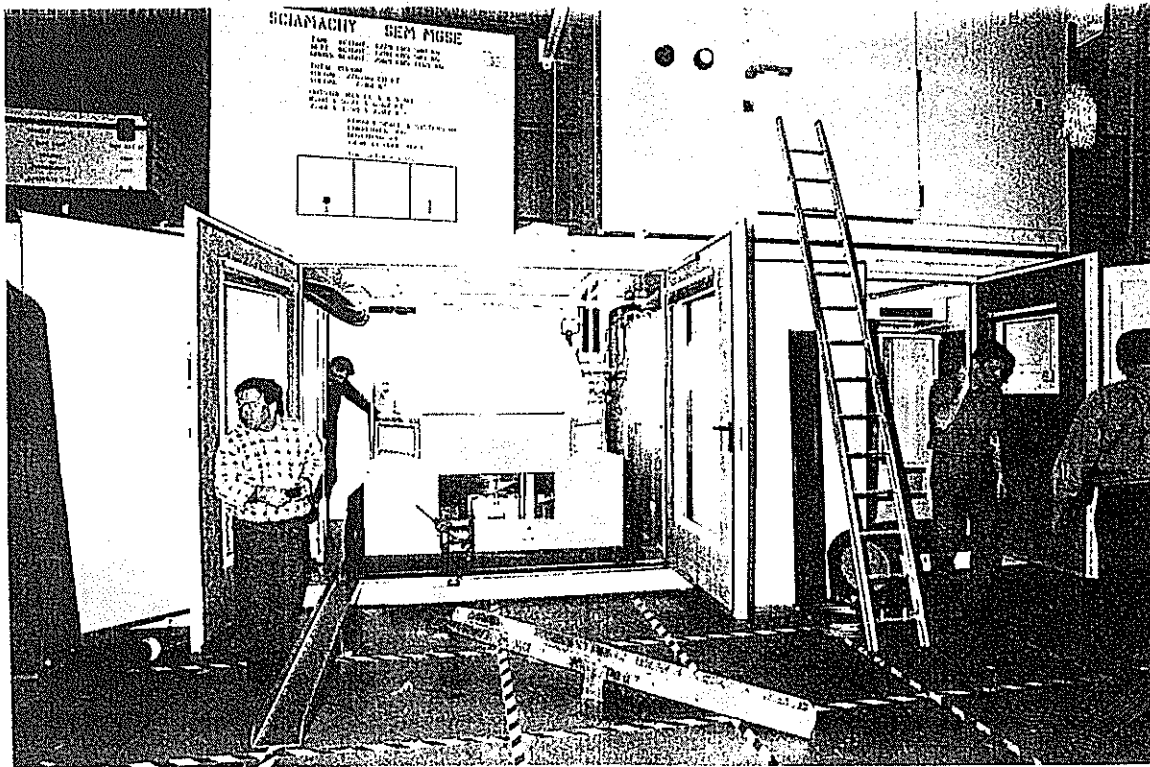
Figure 5: TIGO SLR cart in the container (transport configuration)
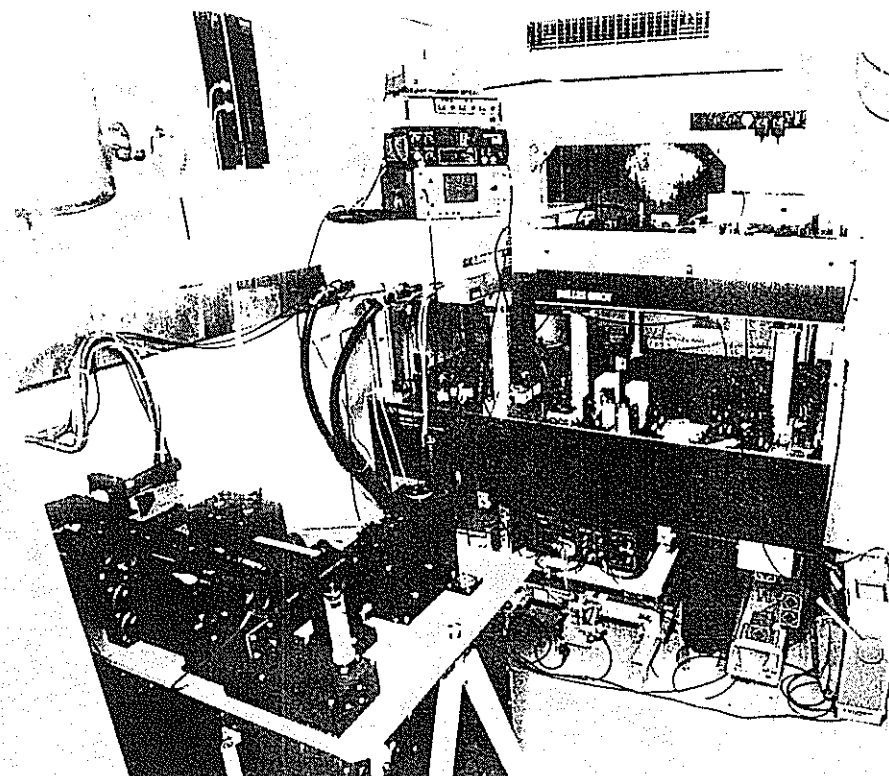
Figure 6: Ti:Sapphire Laser System in the optics room of the SLR container
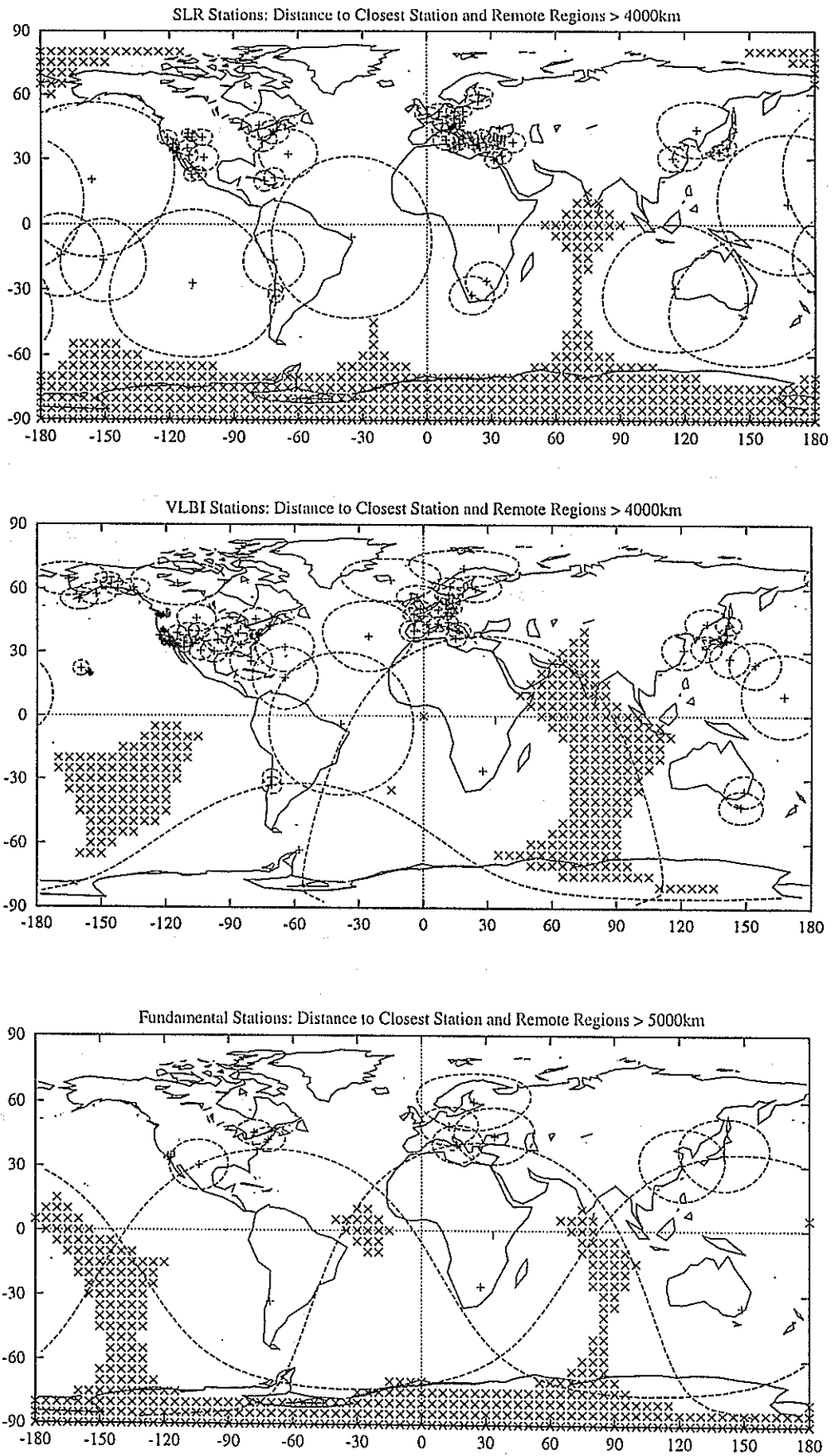
Figure 7: Worldwide distribution of SLR, VLBI and Fundamental Stations (ITRF 93) and their distance to the closest neighbour

143

References:

/1/   Seeger H., Schlüter W., Dassing R., Böer A., Hase H. Sperber P., Kilger R.,
        TIGO Transportable Integrated Geodetic Observatory - A Fundamental
        Station for Geodetic Research, XXI General Assembly of the IUGG, Boulder
        (1995)

/2/   W. Schlüter, A. Böer, R. Dassing, H. Hase, P. Sperber, R. Kilger, "The
        Transportable Integrated Geodetic Observatory-Status of the System",
        Dynamics of Solid Earth (DOSE), Pasadena, (1995)

/3/   H. Hase, W. Schlüter, A. Böer, R. Dassing, P. Sperber, R. Kilger,
        "Status of the TIGO Project", Proceedings of the 4th Asia Pacific Telescope
        Workshop, Sydney, (1996) (in print)

/4/   W. Schlüter, A. Böer, R. Dassing, H. Hase, R. Kilger, E. Reinhart, B. Richter,
        W. Riepl, U. Schreiber, H. Seeger,   P. Sperber, "Die Fundamentalstation
        Wettzell", Verlag des Instituts für Angewandte Geodäsie, Beiträge zum J. J.
        Baeyer-Symposium, Berlin-Köpenick; Deutsche Geodätische Kommission,
        Reihe E, Heft Nr. 25, (1996) 143

/5/   W. Schlüter, A. Böer, R. Dassing, H. Hase, R. Kilger, P. Sperber, "Status
        of the TIGO Project", IAG/CSTG working group on IUGG Fundamental
        Reference and Calibration Network, Baltimore, (1996)

/6/   P. Sperber, A. Böer, U. Hessels, W. Schlüter, "TIGO-SLR Module: Status",
        Proceedings of the 10th International Workshop on Laser Ranging
        Instrumentation, Shanghai (1996)

/7/   P. Sperber, A. Böer, F. Estable, F. Falcoz, E. Pop, L. Vigroux,
        "Cr:LiSAF/Ti:Sapphire based solid state Laser System for Two Color Satellite
        Laser Ranging", Proceedings of the 10th International Workshop on Laser
        Ranging Instrumentation, Shanghai, (1996)

/8/   P. Sperber, A. Böer, U. Hessels, U. Schreiber, "Two Color Satellite Laser
        Ranging using a   Cr:LiSAF/Ti:Sapphire Picosecond Laser System",
        Society for Optical and Quantum Electronics, Proceedings of the Conference
        on Lasers'96, Portland, (1996), in print

TIGO SLR Modul: Status

P. Sperber, A. Böer, R. Dassing, U. Hessels, W. Schlüter
Institut für Angewandte Geodäsie
Fundamentalstation Wettzell
D-93444 Kötzting

Abstract. This paper gives a short overview about the status of the different subsystems of the new Satellite Laser Ranging Module for the Transportable Integrated Geodetic Observatory (TIGO).

In the moment the module is at TPD (Delft) for final assemblage and is expected to start with test ranging in spring 1997.

1.   Introduction

During the last years Satellite Laser Ranging (SLR) using picosecond Nd:YAG Lasers achieved an accuracy of better than one cm. At this accuracy more emphasis has to be placed on the influence of satellite geometry and atmospheric dispersion causing errors up to a few cm. The control and refinement of these models can be done with multiple wavelength ranging /1, 2/. Taking into account the difference in the refractive index, the atmospheric transmission and the sensitivity of single photon detectors, best results are expected with wavelengths around 425 nm and in the near Infrared. This paper reports about the setup of a SLR system, expecially designed for two-color ranging.

The system is based on a Cr:LiSAF/Ti:Sapphire picosecond laser system, a 50 cm compact Lens Telescope and a flexible and powerful controlsystem realized on a Dec Alpha workstation and a transputer network. The whole SLR-Module is installed in a 40 ft standard seacontainer.

2.   Overview

This chapter gives a short overview about the specifications and about the status of the different subsystem container, laser, telescope and control system.

2.1. The TIGO SLR Container

2.1.1 Mechanical description

The TIGO Satellite Laser Ranging module is installed in a standard 40 feet sea container (see figure 1). This allows an easy transportation by train, truck or ship without using a special vehicle.
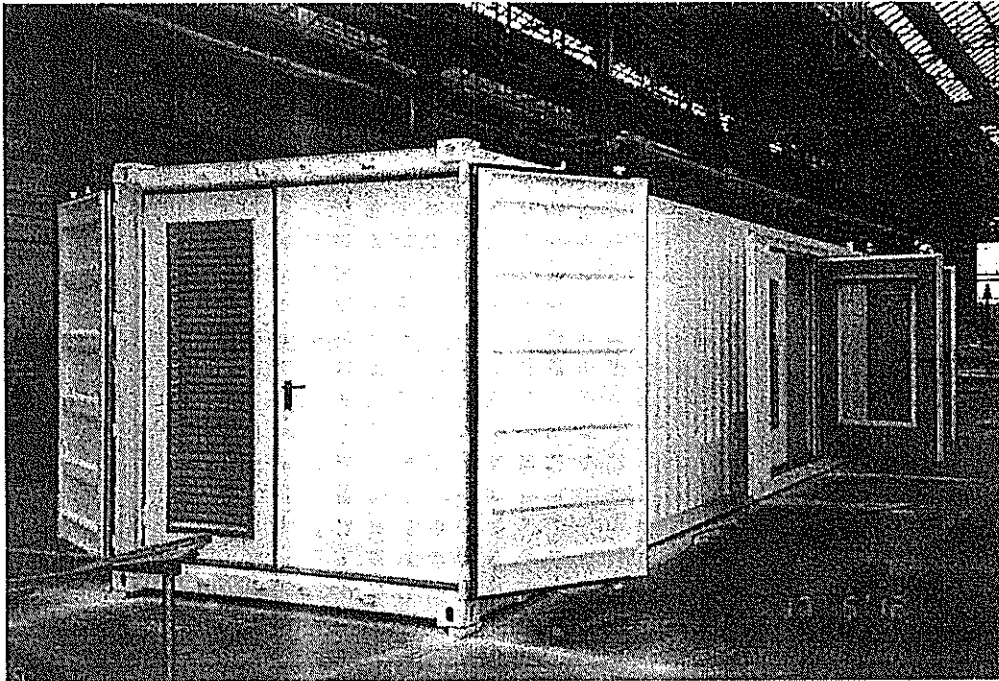
Figure 1: The SLR Container under construction
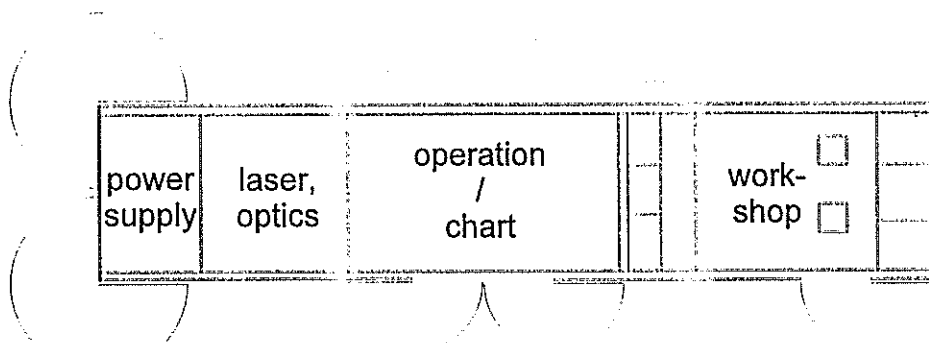
Figure 2: Sketch of the SLR container

The container is divided into four rooms as shown in figure 2. The first room is not air conditioned and houses the main electrical junction supply and the power supplies for the Ti:Sapphire laser. The Ti:Sapphire laser and the Transmit/Receive optics are

installed in the second room. As the requirements are constant temperature and dry and clean air, this room is highly isolated. An air condition provides nearly constant temperature and constant humidity. The air is kept clean by having a little over pressure in the room and by an additional air filter system. There are holes in the floor, which allows the laser table and the Transmit/Receive unit to stand on the concrete ground to avoid instability to the optics. The third room is the operators room with the controll system. This room is also air conditioned. A window in the door allows to observe the telescope during operation. When the SLR module has to be transported, the telescope is placed and fixed in this room. During operation, the telescope is placed in front of this room on a concrete plattform as shown in figure 3 /3/.
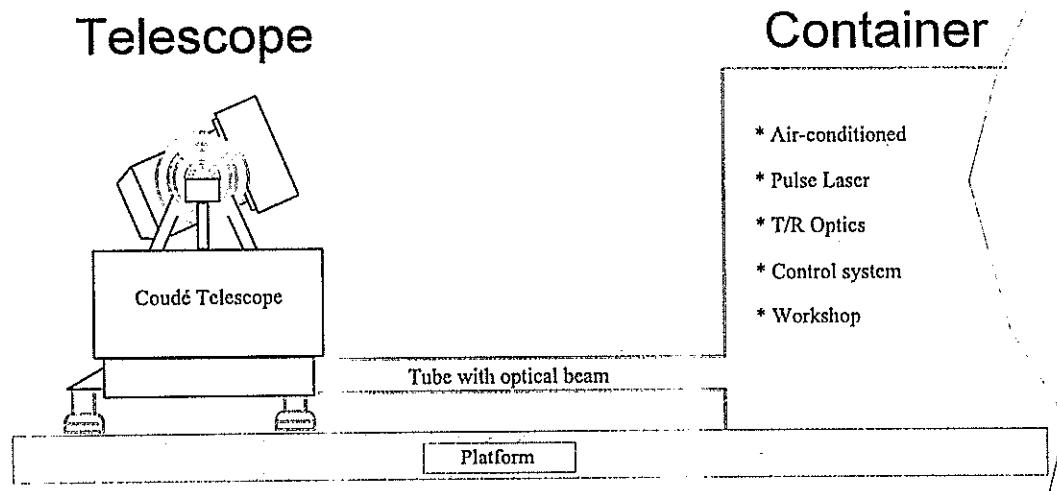
Figure 3: SLR configuration during operation

The last room is housing the air compressor and is used as a workshop and a storage room for spare parts and maintenance equipment.

2.1.2 Electronic description

In the SLR container three completely separated main power supplies are installed. One permanent, clean supply for sensitive instruments like detectors, clocks, encoder, etc. and one permanent supply for airconditioning, light, computers and other instruments producing noise in the net. The third supply is used for the direct measurement equipment like laser and telescope motors and is switched on only during measurement.

The whole power cabling is done with shielded cables. All circuits are protected against over voltage and over current to provide a safety and reliable operation.

2.2. Laser System

The Laser was especially designed for this application by B.M. Industries /4, 5/ in Paris/France. It is based on a diode pumped cw-modelocked Cr:LISAF oszillator generating pulses between 50 ps and 150 ps. A chain of Nd:YAG pumping Ti:Sapphire amplifiers. The system (figure 4) produces pulses with 10 Hz repetition rate at 847 nm and 423.5 nm with a pulse energy of 30 mJ at each wavelength.
The detailed optical setup is shown in figure 5, the specifications are summarized in Table 1.
The Cr:LiSAF Oszillator is longitudinally pumped by a Laser Diode, a Lyot Filter is used to adjust the wavelength, a Fabry Perot Etalon is used for the selection of the pulse duration (without Etalon the oszillator produces pulses below 20 ps). The pulses are amplified with 10 Hz repetitionrate in one regenerative and two multipass Ti:Sapphire amplifiers. The amplifiers are pumped by a two channel q-switched Nd:YAG Laser.
After second harmonic generation the pulses at 847 and 423.5 nm are sent to the telescope. The returned photons from the satellite are detected with three single photon avalanche diodes (two at 847 nm, and at 423.5 nm), (SPAD /6/).

The laser is operational since summer 1996.
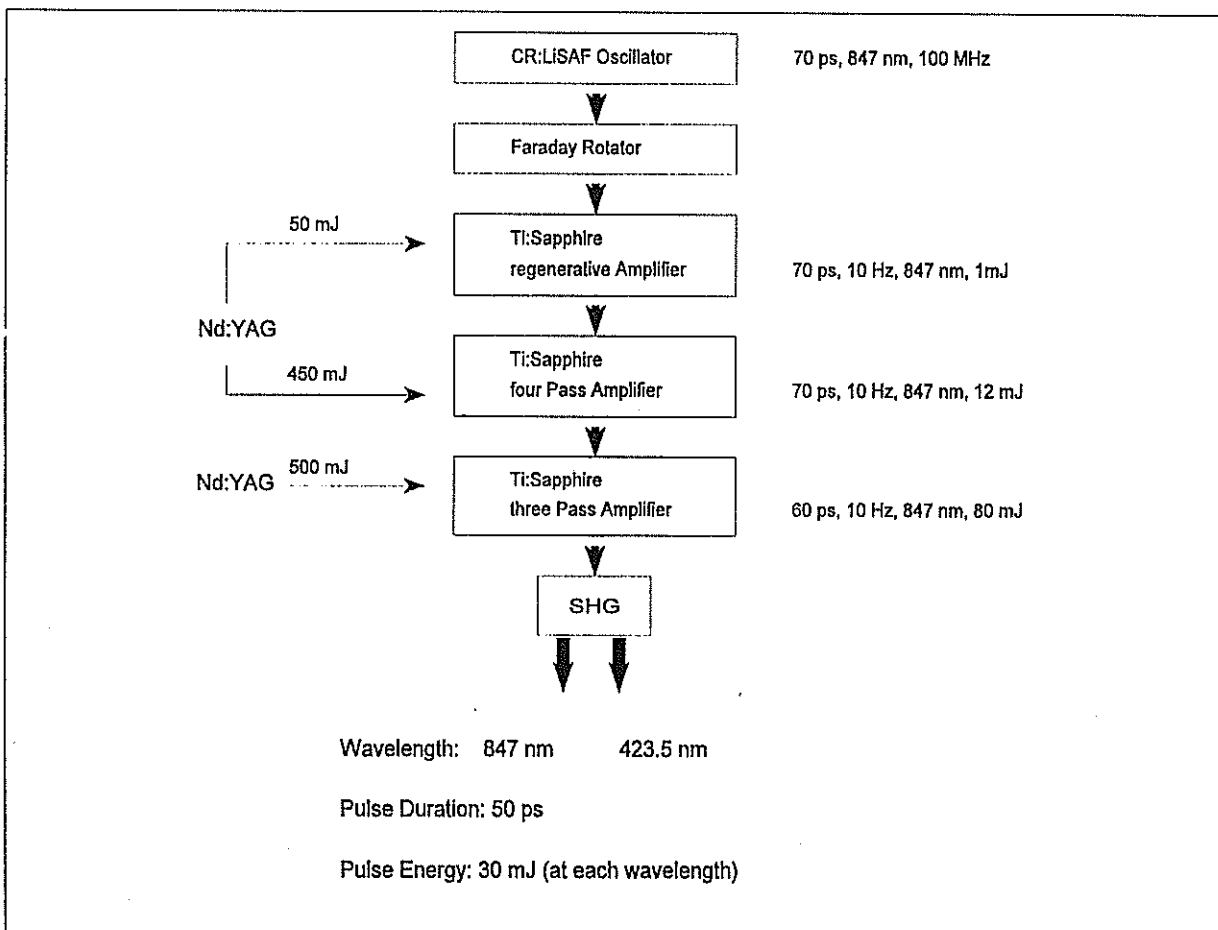
Figure 4: Block Diagram of the Cr:LiSAF/Ti:Sapphire Laser System

Cr:LiSAF oscillator	
Active medium	Cr^{3+}:LiSAF
Typical output power	> 5 mW
Tuning range	820 - 900 nm
Operating wavelength	847/846* nm
Spectral width	< 0.5 A
Repetition rate	100 MHz
Spatial mode	TEM$_{oc}$
Polarisation	Linear horizontal
Pulse duration	variable 60/100* ps

Regenerative amplifier	
Active medium	Titanium:Sapphire (Ti^{3+}:Al$_2$O$_3$)
Tuning range	750 - 850 nm
Operating wavelength	847/846* nm
Repetition rate	10 Hz
Pump energy	40 mJ
Output energy (1)	> 2 mJ at 10 Hz
Spatial mode	TEM$_{oo}$
Beam divergence	< 1.5 mrad
Pulse duration (FWHM) (2)	< 100 ps
Output polarisation	Linear vertical

(1) Measured just at the output of the regenerative oscillator. The cavity is then unseeded.
(2) For the seeded cavity only. This specification depends on the oscillator specifications.

Multipass preamplifier	
Active medium	Titanium:Sapphire
Tuning range	750 - 850 nm
Operating wavelenght	847/846* nm
Repetition rate	10 Hz
Pass number	4
Pump energy	200 mJ
Input energy	> 2 mJ
Output energy	> 25 mJ
Typical average power	> 250 mW at 10 Hz
Spatial mode	Single transverse
Beam divergence	< 1 mrad
Pulse duration (2)	< 100 ps
Output polarisation	Linear horizontal

Multipass amplifier	
Active medium	Titanium:Sapphire
Tuning range	750 - 850 nm
Operating wavelenght	847/846* nm
Repetition rate	10 Hz
Pass number	3
Pump energy	400 mJ
Input energy	> 25 mJ
Output energy	> 65 mJ
Typical average power	> 650 mW at 10 Hz
Spatial mode	Single transverse
Beam divergence	< 1 mrad
Pulse duration (2)	< 100 ps
Output polarisation	Linear horizontal

(2) Specification depends on the oscillator specifications

Table1: Specifications of the Cr:LiSAF/Ti:Sapphire Laser System
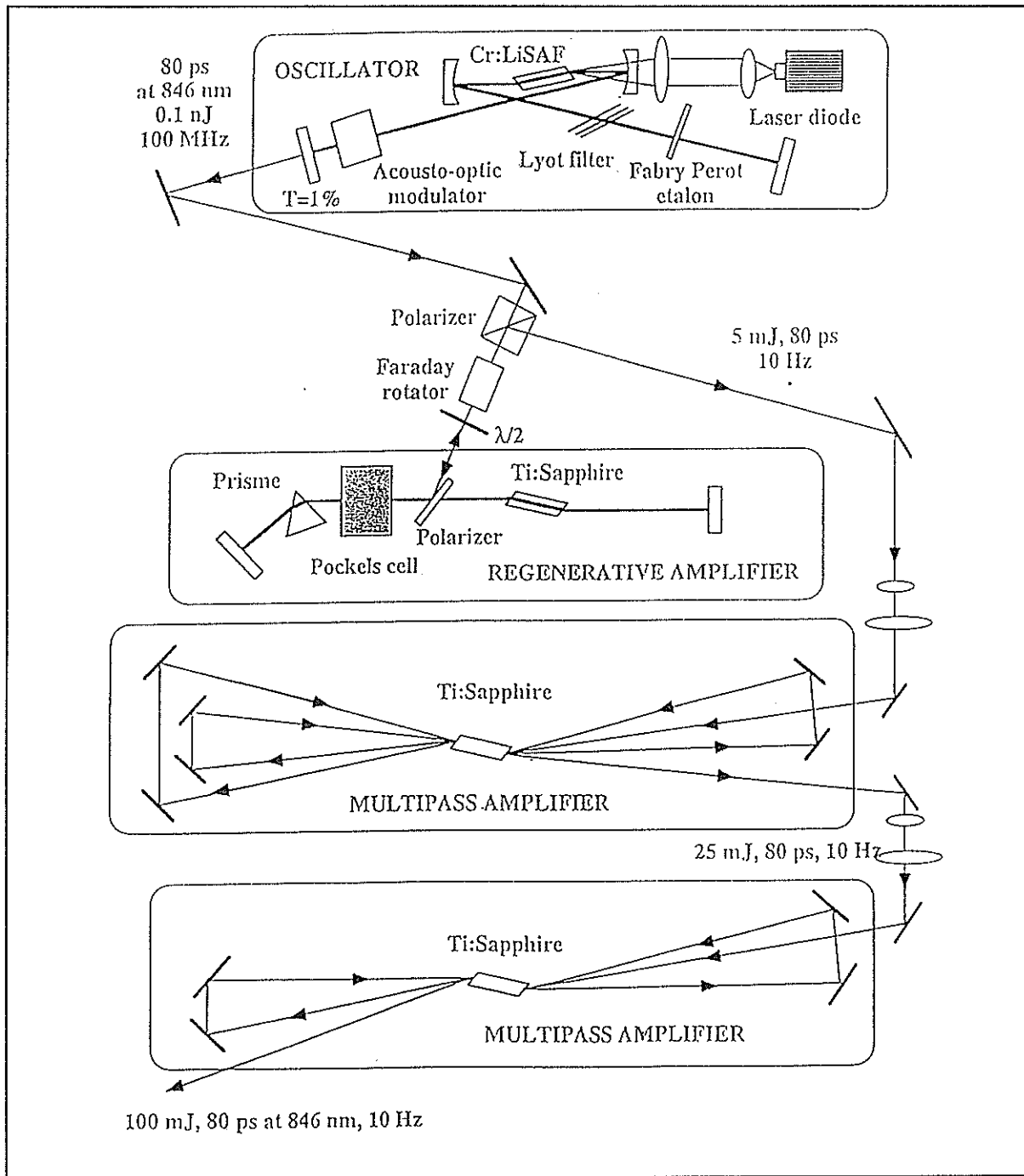
Figure 5: Detailed optical setup of the Laser System

2.3. Telescope

The design of the telescope is based on a further development of the MTLRS-1 telescope /3, 7/.

The 50 cm lens telescope with excellent optical efficiency is installed in a small cart. During transport this cart is fixed in the container, during measurement the cart with the telescope is moved to a concrete pad near the container.

Due to the design of the folded lens telescope (figure 6), central obscuration of the beam is avoided. The transmit / receive switch is realized by aperture sharing, this means the laser is fired through the central part of the telescope (18 % of telescope area), the outer circle (82 % of telescope area) is used for receiving photons.
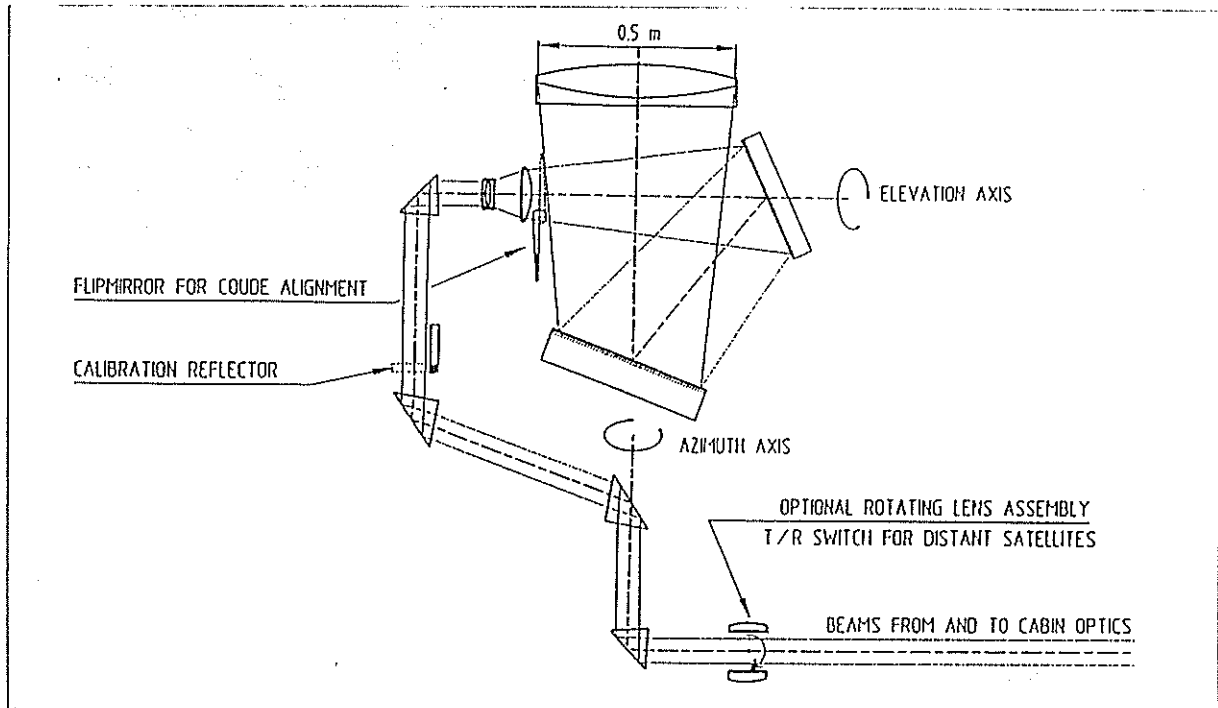
Figure 6: Telescope Optics

The telescope is supported by three adjustable feet on the TIGO platform. These three feet are mounted on a large ring-shaped granite component (out of one single block of granite), that forms the main part of the static structure of the telescope mount.

The main advantages of the granite component in the static part of the mount are:

- good top surface finish and flatness (better than 4 µm over the entire diameter) to form the static part of an air-bearing that determines the direction of the azimuth axis of the telescope
- good stiffness
- good thermal and temporal stability
- corrosion resistant.

The telescope and cart in operational and transport configuration is shown in figure 7. The telescope was finished in december 1996 with the installation of the big coated optics.

151
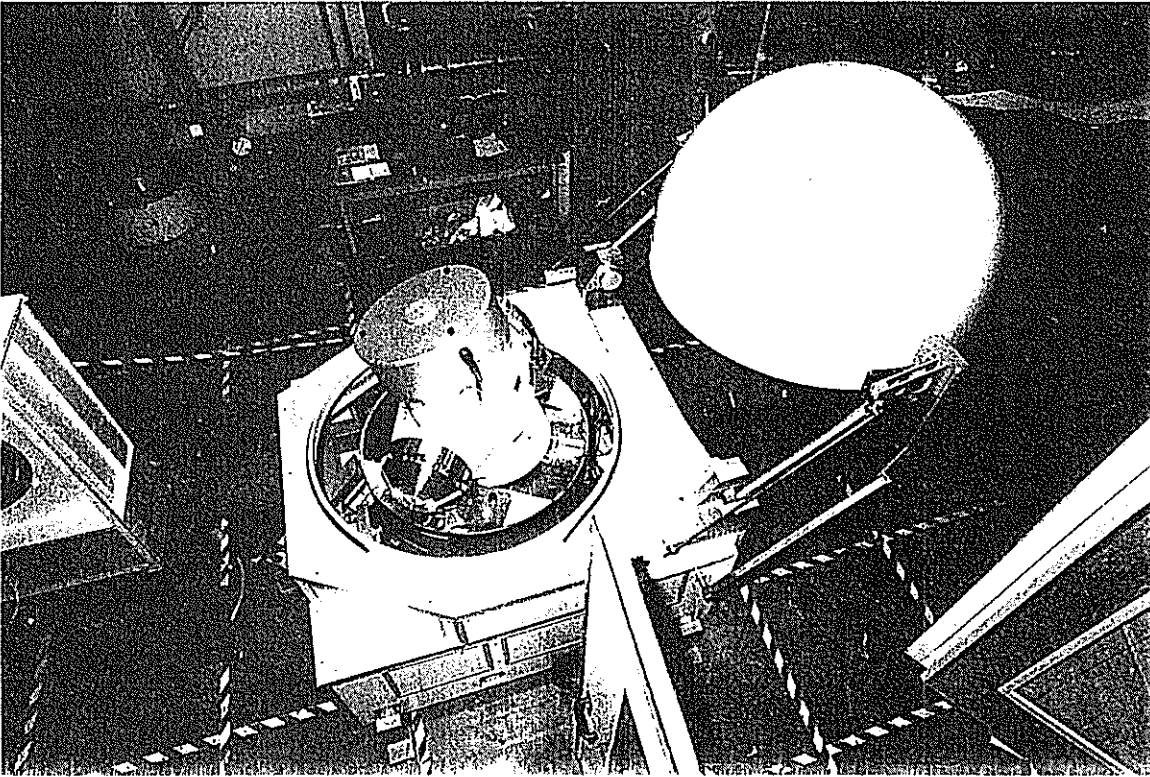
Figure 7a: TIGO SLR Telescope in the open cart (ranging configuration)
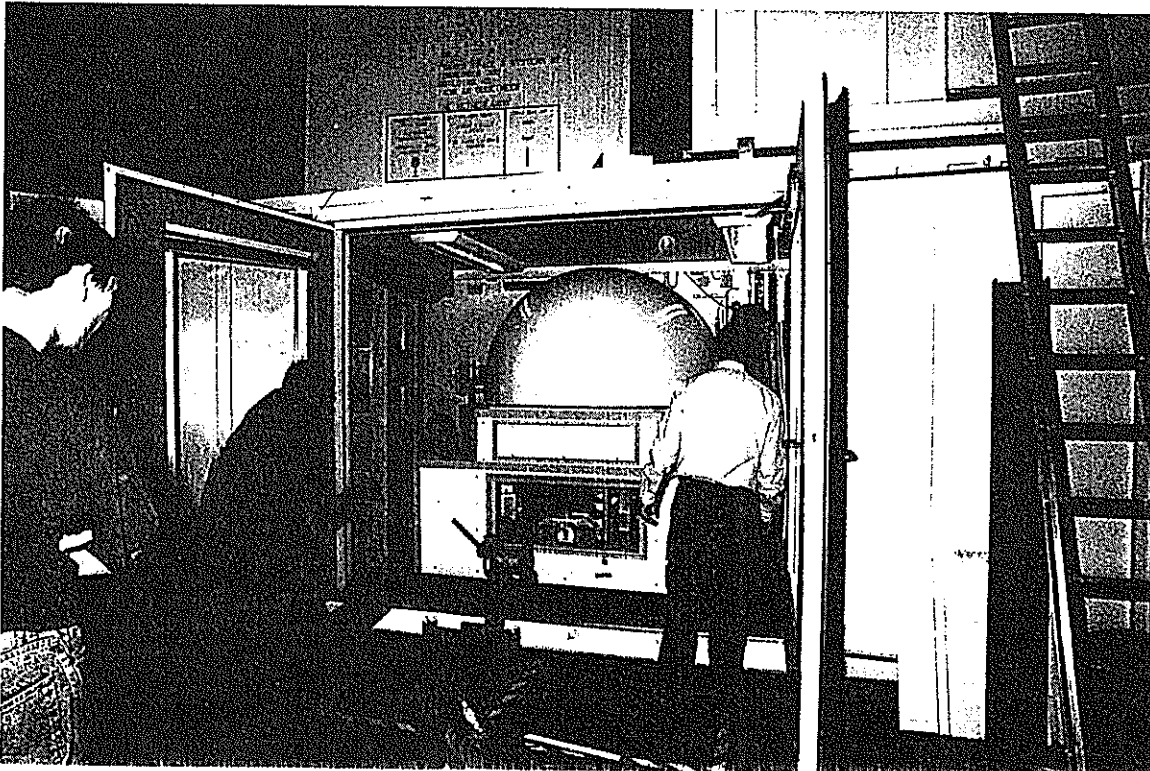
Figure 7b: TIGO SLR cart in the container (transport configuration)

2.4 The Control System

2.4.1 System Architecture

The control system for the Tigo SLR module consists of a workstation and a real time controller /8/. The operator uses a completely graphical program to work with the laser ranging system. The real time controller controlls directly all functions of the instrument. An overview of the global architecture is given in figure 8.
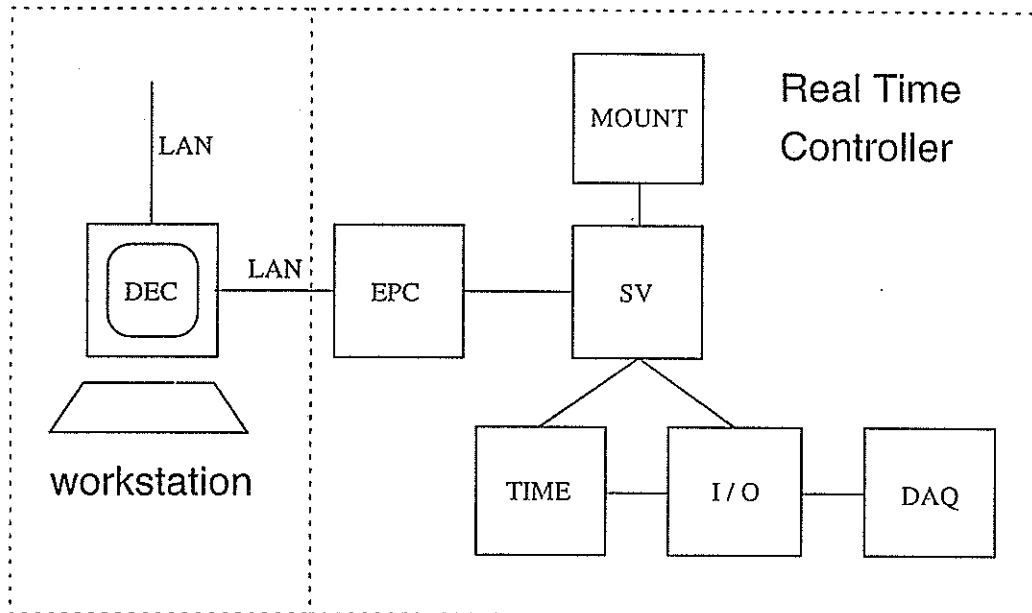
Figure 8: Architecture overview of the SLR controller

2.4.2 The workstation

The main task for the workstation is to run the graphical user interface program. This user interface provides everything to operate the complete SLR module. That means it is not only used to do the real tracking work, but also takes care on nearly all other tasks for Satellite Laser Ranging.

The first thing which must be done, is to setup the parameters for initialisation and installation. Therefor a window based, especially developed editor can be used to edit the associated data bases. Furtheron a star observation program is implemented to do the site installation and to determine the mount model (figure 9).
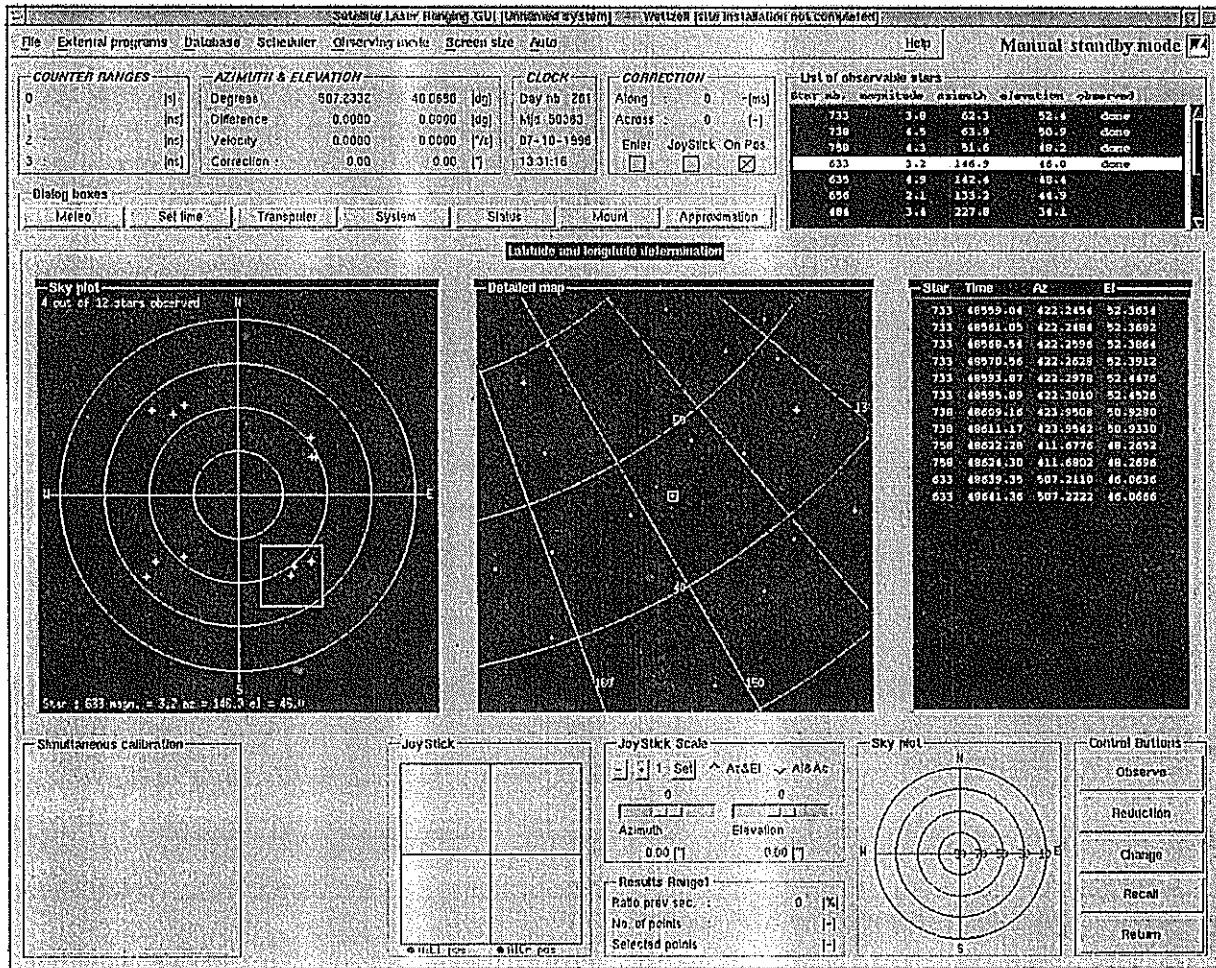
Figure 9: The graphical user interface during site installation

It is very convenient to use the implemented backgroud tasks, which automatically provides the latest IRV values and calculates the predictions. During real tracking the operator can switch between two displays. One showes the detected photons in the expected time gate and the other displays the values in histograms to have a "real time impression" on the quality of the data. See figure 10 and 11.
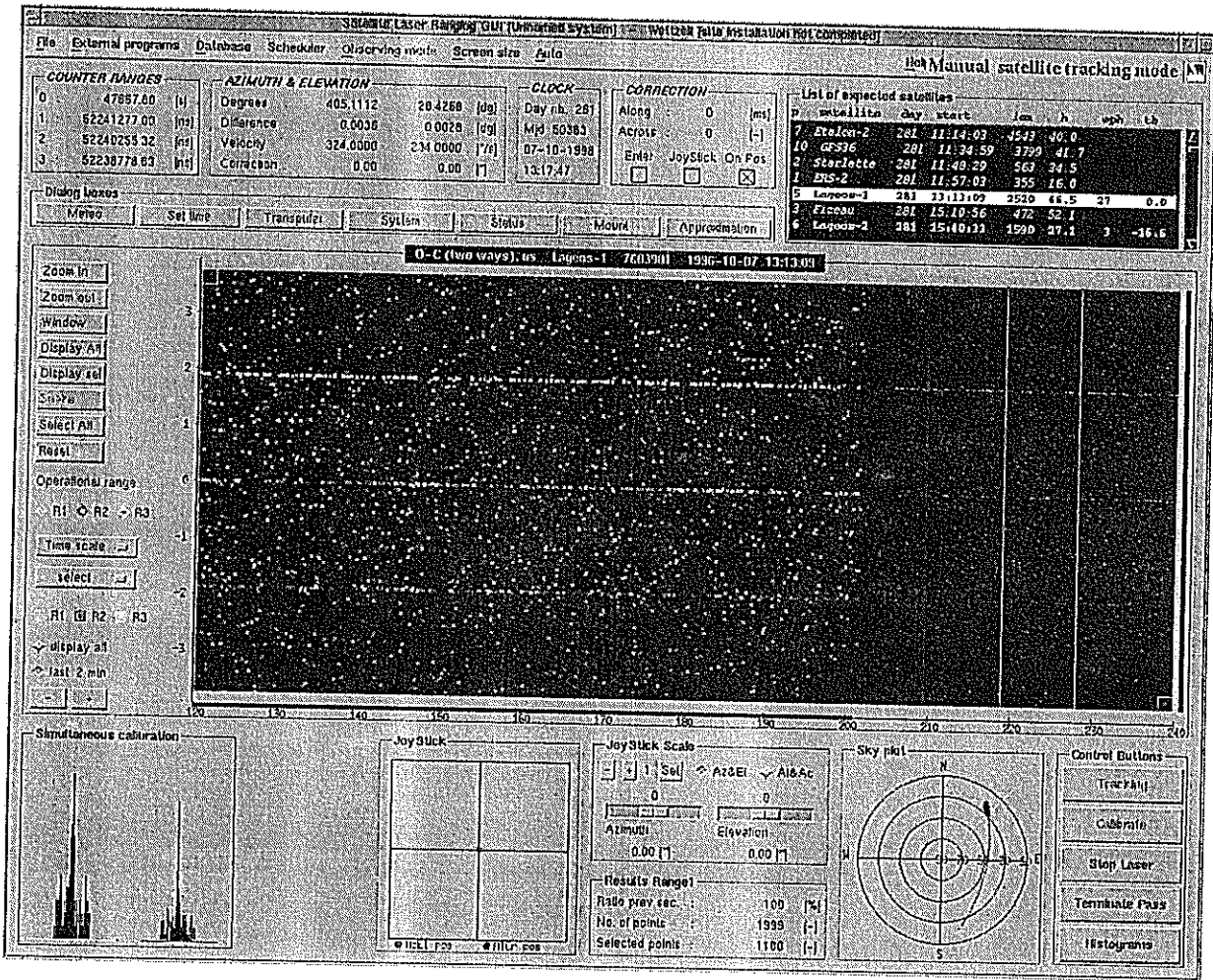
Figure 10: The graphical user interface in normal tracking mode
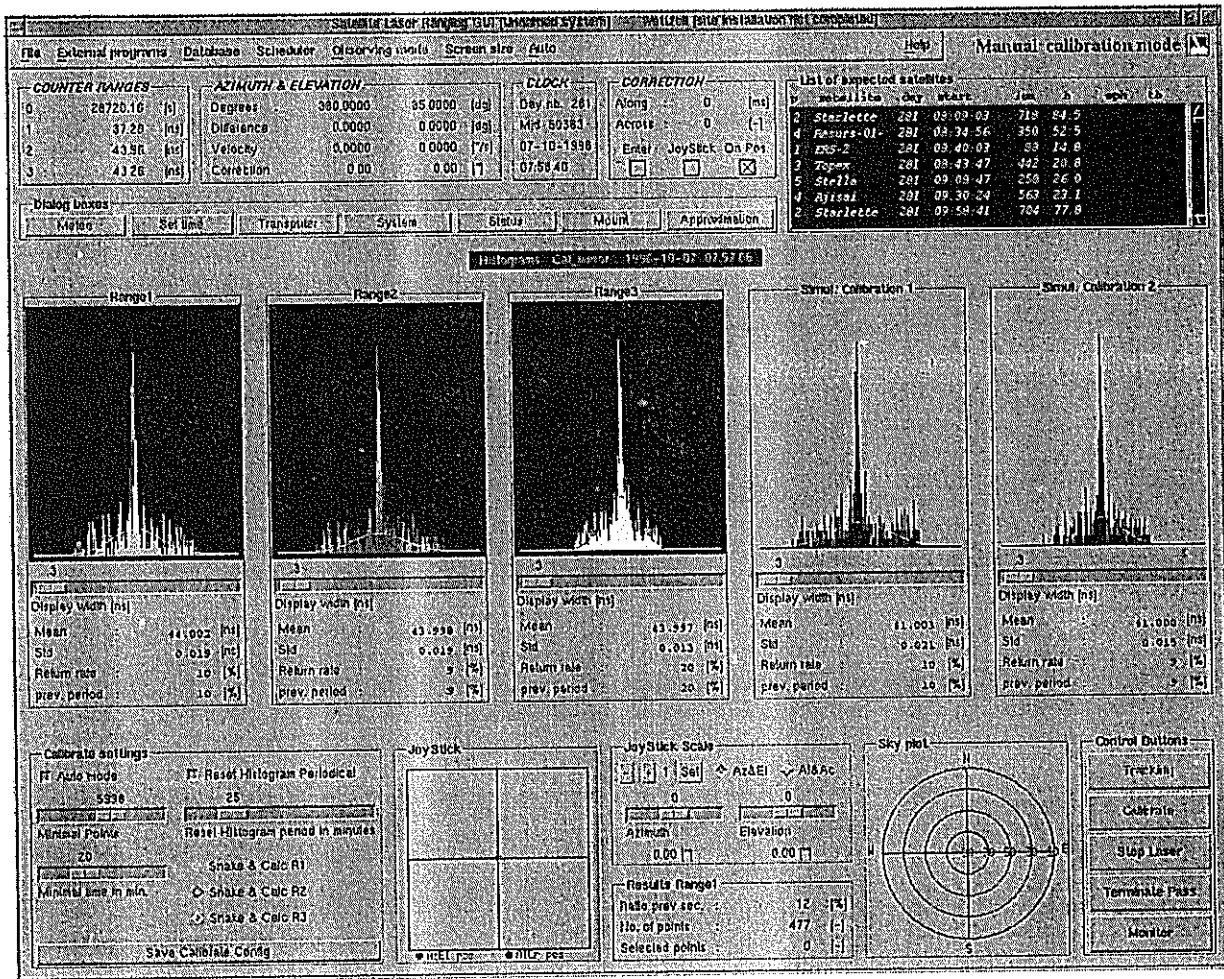
Figure 11: Measured data in form of histogramms

After tracking the grahpical user interface program can be used to evaluate the measured data. The purpose of this graghical user interface is to make the normal "tracking work" as easy as possible. The administration of the system however requires the knowlegde of an expert.

2.4.3   The Real Time Controller

The Real Time Controller controls directly all functions of the instrument. It is implemented by using five transputer boards and an embedded Personal Computer (PC). One transputer board, the supervisor board, has global tasks and routes the communication stream from the user interface on the workstation to each transputer board. The other four transputer boards, the time board, the mount board, the I/O board and the data aquisition board are controlling special functions of the instrument. On the time board all tasks are executed that are associated with the measurement of accurate time intervals. The software controls and reads out the hardware status that is needed for the generation of signals with very accurate timing. On the mount board all tasks, related with the positioning of the telescope are executed. The I/O board carries out the sysnchronous tasks which have strict timing constraints, like controlling the counters or the photo detectors. On the data aquisition board all asynchronous tasks with no strict timing constraints are executed such as reading out the temperatur sensors.

The embedded PC acts as an interface between the graphical user interface running on the workstation and the real time control system of the instrument. It contains the boot code for the real time controller and performs some elementary maintenance functions by using a touch screen. The embedded PC can also maintain a system log with all command issued to and responsed from the real time controller. The communication between the PC and the workstation is done by an ethernet interface, using the TCP/IP protocol. To transfer the data transfer from the PC to the real time controller and vice versa a special interface with a special serial transputer protocol is used.

3.   Overall System Status

All the main subsystems except the control software (data analysis and tracking routines are not yet implemented) were ready and tested in Dec. 1996. The final assemblage started in Oct. 1996 and should be finished at the beginning of 1997. In Nov./Dec. 1996 the system was able to make the first calibration measurements at 423.5 nm (figure 12), showing the good operation of laser, electronics, optics and detectors. The system will by moved to a test pad in Delft in spring 1997 to perform the acceptance test (ranging to all satellites), the delivery to Wettzell is expected in summer 1997.
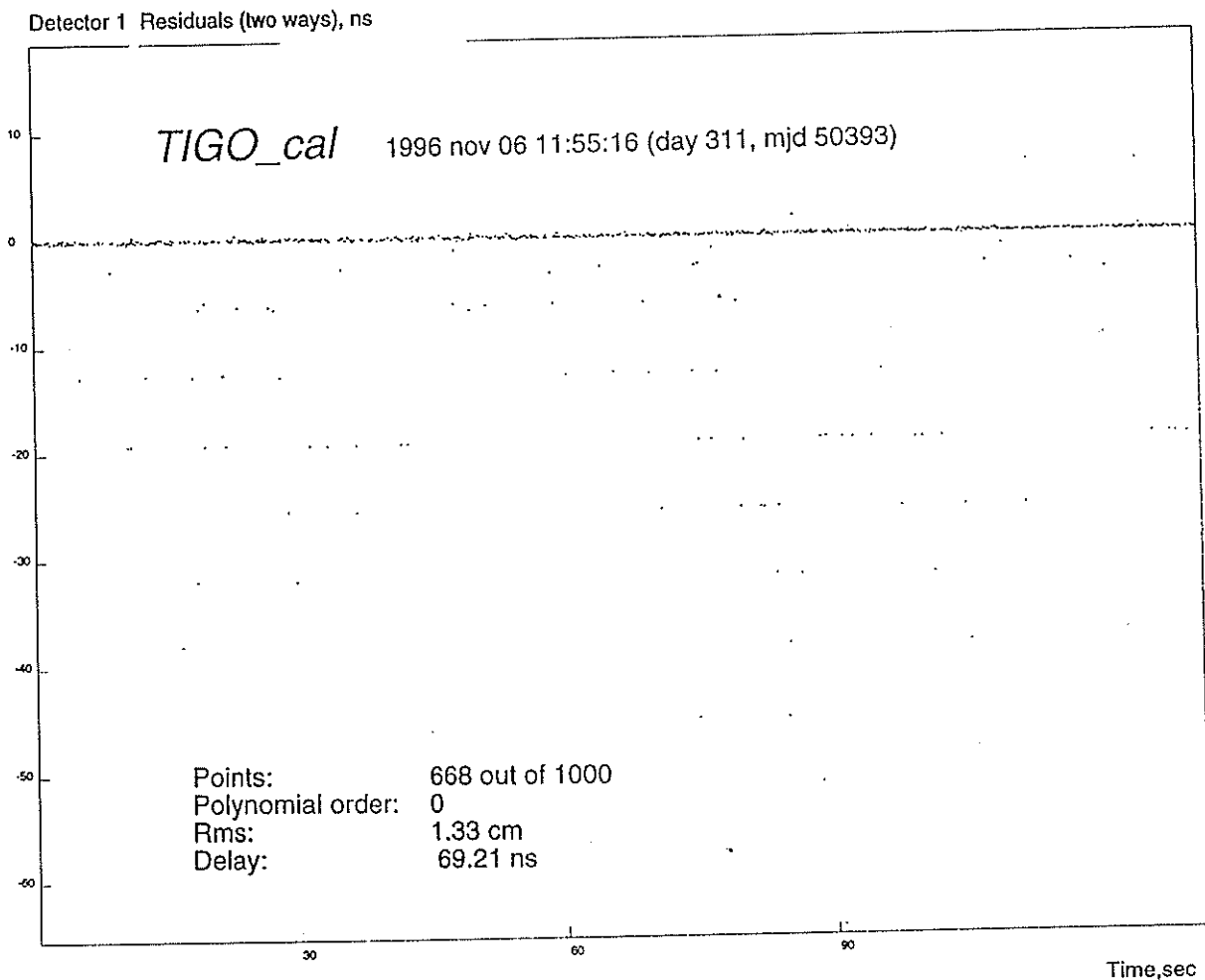
Figure 12: First Calibration at 423.5 nm with the TIGO SLR Module

References:

/1/ Kirchner G., Koidl F., Hamal K., Prochazka I., Multiple Wavelength Ranging in Graz, Australian Government Publishing Service, Proceedings of the 9th International Workshop on Laser Ranging Instrumentation, Canberra (1994) 609

/2/ Degnan I. I., Millimeter Accurancy Satellite Laser Ranging: A Review, Geodynamics Series Vol. 25, Contributions of Space Geodesy to Geodynamics, Americal Geophysical Union, Washington (1993) 125

/3/ Braakman H., van der Kraan M., Visser H., van der Zwaan B., Sperber P., TIGO-SLR Opto-Mechanical Configuration, Australian Government Publishing Service, Proceedings of the 9th International Workshop on Laser Ranging Instrumentation, Canberra (1994) 198-206

/4/ P. Sperber, A. Böer, F. Estable, F. Falcoz, E. Pop, L. Vigroux, "Cr:LiSAF/Ti:Sapphire based solid state Laser System for Two Color Satellite Laser Ranging", Proceedings of the 10th International Workshop on Laser Ranging Instrumentation, Shanghai (1996)

/5/ P. Sperber, A. Böer, U. Hessels, U. Schreiber, "Two Color Satellite Laser Ranging using a Cr:LiSAF/Ti:Sapphire Picosecond Laser System", Society for Optical and Quantum Electronics, Proceedings of the Conference on Laser'96, Portland (1996), in print

/6/ Prochazka, K. Hamal, B. Sopko, G. Kirchner in Conference on Lasers and Electro-Optics, Vol. 7, 1990 OSA Technical Digest Series (Optical Society of America, Washington, DC, 1990)

/7/ Braakman H., van der Kraan M., Visser H., van der Zwaan B., Sperber P., Transmit / Receive Two-Color Unit for TIGO, Australian Government Publishing Service, Proceedings of the 9th International Workshop on Laser Ranging Instrumentation, Canberra (1994) 407-415

/8/ Vermaat E., Offierski J. W., Otten K. H., Beek W., van ES C., Sperber P., Transputer Based Control System for MTLRS, NASA Conference Publication 3214, Proceedings of the 8th International Workshop on Laser Ranging Instrumentation, Annapolis (1992) 12-40

A Transportable Laser Ranging System in China (CTLRS)

Xia Zhizhong, Cai Qingfu, Ye Wenwei,
Guo Tangyong, Wang Linhua
Institute of Seismology,State Seismological Bureau
Xiao Hong Shan, Wuhan 430071,China

Abstract

In order to set up a state geodesy control network and to monitor crustal movement, since 1993 Institute of Seismology, State Seismological Bureau and Xi'an Institute of Surveying and Mapping have cooperated to develop a transportable satellite laser ranging system. The system is composed of a Nd:YAG mode-locked laser, a telescope mount, receiving electronics equipment, time and frequency standard, and a computer etc. The repetition rate of the laser is 1-5pps, the wavelength is 532nm and the main pulse energy is 30mj. The diameter of the receiving telescope is 35cm. All these equipments can be installed in a vehicle consisted of two rooms, its loaded weight is 3.5 tons. The single shot ranging accuracy of the system will reach 2-4cm for LAGEOS and other satellites. The system will be completed in 1996 and put into operation in 1997. This paper provided with the technical details of the system and the results of the testing observation.

Key words: Satellite laser ranging-TLRS

Introduction

Since 1980's, the 3rd generation satellite laser ringing network has been set up in Shanghai, Wuhan, Changchun, and Beijing in China. Each station can observe satellite ETALON, LAGEOS, ERS-1, TOPEX, etc. in generally, the single shot accuracy can reach 5cm. All stations joined the international cooperative project of NASA and WPLTN. But the geographical distribution of the stations is not even, there aren't observation station in the western part of China. Thus, in order to set up a space geodesy network with reasonable distribution and monitor crustal movement beneficially in China. Since 1993 Institute of Seismology and Xi'an Institute of surveying and mapping have cooperated to develop a transportable laser ranging system which is suitable for China. The system can observe LAGEOS etc. We hope the ranging precision can reach 2-4cm. In 1995 the CTLRS has been entered in to the stage of the assembly and the adjustment. It is estimated that the system will be completed in 1996 and come into operation in next year.

System Configurations

1. Laser

The laser is a frequency doubled and passively mode-locked (SFUR) Nd:YAG system that produces a mode-locked pulse train with a repetition rate of 1-5pps. The Laser consist of a pumping oscillator followed by a pulse slicer, an amplifier and an optical second-harmonic. The oscillator transmits a mode-loked pulse train which included five to seven pulses, the slicer selects 2-3 pulse from the pulse train. The main pulse has 30 mj energy with wavelength 532nm and about 60ps width. The diameter of the output laser beam is 8mm. The laser transmitter assembly is located on a table under the mount, the volume of the table is 320x260x1320mm. This laser is developed by Shanghai Institute of Optics and Fine Mechanics.

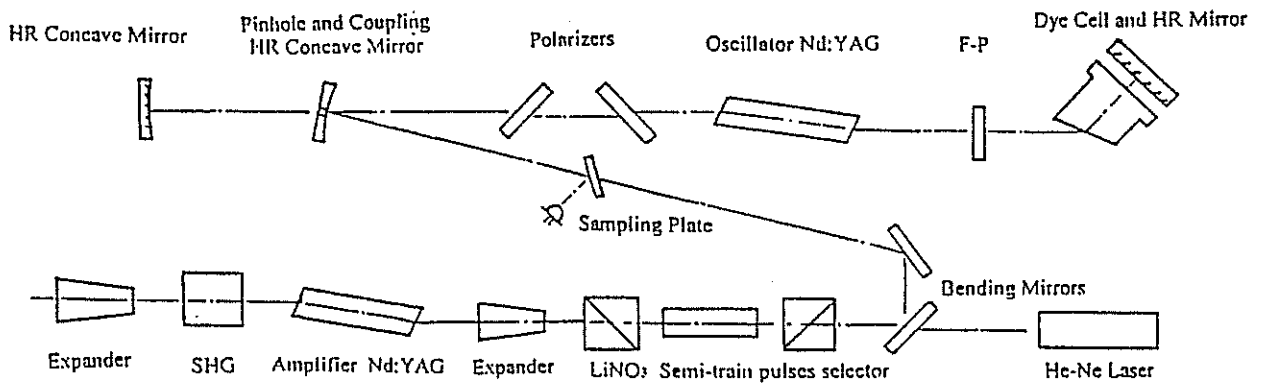The optical diagram of the laser is given in figure 1.
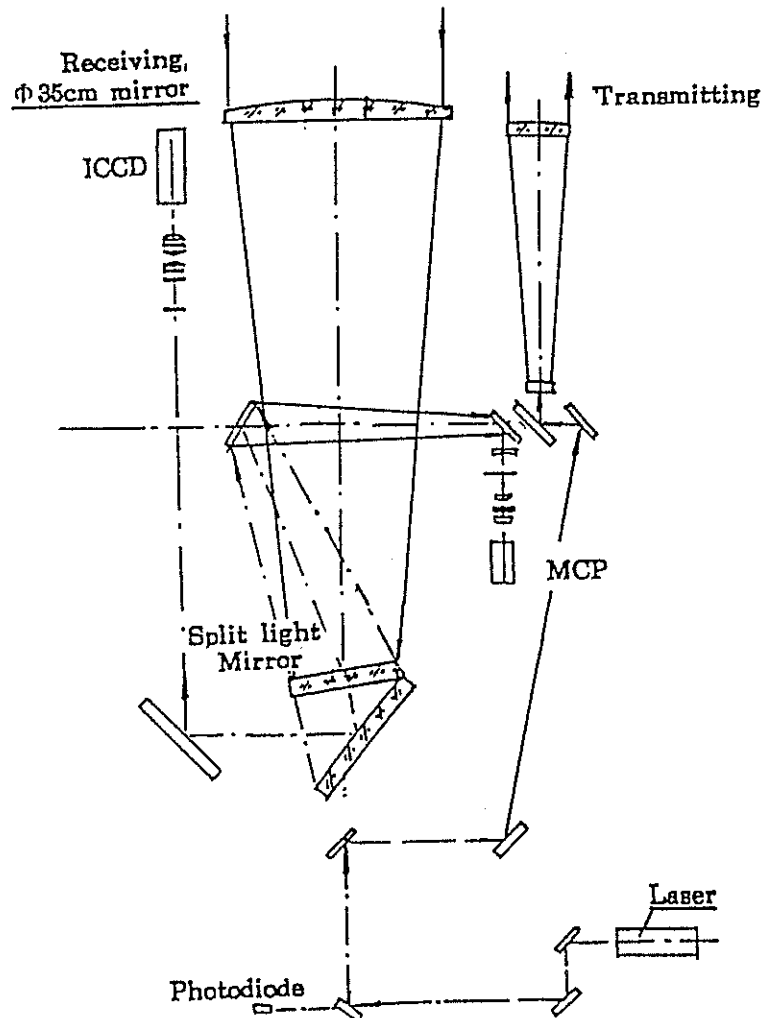
Fig.1 The optical diagram of the Nd:YAG laser

Fig.2 The optical block diagram of the system

2.mount

A horizontal structure with two axes is used for the mount. The optical block diagram of the system is shown in figure 2. The elevation and the azimuth axes are driven by DC-torque motor and controlled by both a tachometer and a synchronistic inductor (resolution 1 arcsec). The ranges of the azimuth and the elevation axes are ± 270 deg. and -10 deg. to +190 deg. respectively. The tracking angular velocities are from sidereal to 2 deg/s for elevation and 15 deg/s for azimuth. The estimation of the tracking accuracy is within 10 arcsec.

2.1 Transmitting optics

The laser pulse beam transmitted from Nd:YAG laser with diameter 8mm is expanded to about 80mm by two beam expanders and reflected in a Coude path along the azimuth and elevation axes by the mirrors. The divergence for output laser light is controlled from 100 μ rd to 1 mrd by a motor. In order to measure the ground target for calibration, an attenuator for output laser beam is installed in the Coude path.

2.2 Receiving optics

The aperture of the receiving telescope is 35cm and the focal length is 2.3m. The returned light from satellite is splitted in two ways by a split mirror. One light beam with the wavelength 532nm goes to a micro-channel-plate photomultiplier tube along the Coude path and the another (except 532nm) goes to a television with an image intensifier for guiding satellite.

3. Receiving electronics equipment

In order to detect returned signal and to measure the flight time, the receiving electronics equipment includes a MCP photomultiplier, (Hamamatsu R2566U-07) two amplifiers(B&H DC3003A), a constant fraction discriminator (TENNELEC TC454) and a time interval counter (Stanford Research system SR620 resolution 25ps). The external frequency standard of the counter is provided by a Rubidium clock. The MCP-PMT has a gain of 5x10E5 (TYP) and a rise time of 100ps, the quantum efficiency is 6% at 532nm of the wavelength. The start pulse is detected by a photodiode (Hamamatsu S-2381 with 200ps risetime) behind the first mirror in the Coude path.

4. time and frequency standard

A model TTR-6A NAVSTAR GPS Synchronized Time and Frequency standard (Allen Osborne Associates, Inc) is used as time and frequency standard for TLRS. This equipment contains a Rubidium clock which supplies a 10 MHz signal with the stability of 1x10E-11, the timing accuracy of corrected 1pps output is about 100ns. The TTR-6A GPS receiver also includes a navigation, or position and program for refining local coordinates.

5. Control and computer

An IBM PC 486 computer has been used in the transportable laser ranging system as control center. Real-time clock range gate controller, data acquisition and laser shooting controller etc. are integrated on two extending circuit boards to be installed on the extension slots of IBM PC computer. Software regarding calculation of prediction, data processing, numerical track guiding,software managing etc. are all transplanted to this computer. While working , the telescope isautomatically guided towards the satellite by the track control part with the calculating

result from ephemeris. In order to improve tracking accuracy, the tracking parameter (UTC time, azimuth, elevation O-C etc.) can be displayed and corrected in real-time during the observation, so that some of the status of the system and computed results are shown on the CRT colorfully and in picture.

6. Transportable manner

All equipments of CTLRS are installed in a vehicle which has loading capacity of 3.5 tons. This vehicle is divided into two rooms. The receiving electronic control and computer, time and frequency standard equipments etc. are set up in the front room with a air conditioner. The mount and laser are installed in the another one located at the back the vehicle. While working, the roof of the vehicle can be moved off and the mount and laser are jacked up by four jacks. The size of the vehicle is 2.3x3.0x6.4m. Figure 3 shows the schematic diagram of the mobile SLR system.

The overview of the mount and receiving electronics, control computer, time and frequency standard equipments of CTLRS are given in figure 4.

Testing observation of the CTLRS

Since 1995 the CTLRS has been entered into the stage of the assembly and the adjustment. the first returns from TOPEX were obtained in July 24,1996. The number of ranges is about 205 and the RMS of residuals to observation range minus prediction range for polynomials fitting is 6.1cm(Fig.5). We also have observed successfully LAGEOS satellite in Aug.5. The number of ranges for this pass and the ranging accuracy is about 122 and 6.5cm respectively(Fig.6). Because we are afraid to damage the MCP photomultiplier, the PM2233 PMT is used in the testing stage as a receiving equipment, so the ranging accuracy only reached about 6-7cm.

Now the improvement of this system is further carried on by us. It can estimate that the all equipments will be completed in 1996 and put into the operation in next year.

Reference

[1] Xia Zhizhong et al. A Technical Scheme for The Transportable Satellite laser ranging system. 1992.12 Wuhan (in Chinese)

[2] Xia Zhizhong et al. New progress of Ranging Technology at Wuhan SLR station. Proceedings of Symposium on Eight International Workshop on Laser Ranging Instrumentation Annapolis U.S.May,1992.

[3] Sasaki M. Completion of a transportable laser ranging station (HTLRS). Data Report of Hydrographic Observation. Maritime Safety Agency Tokyo. Japan No.1,March 1988.
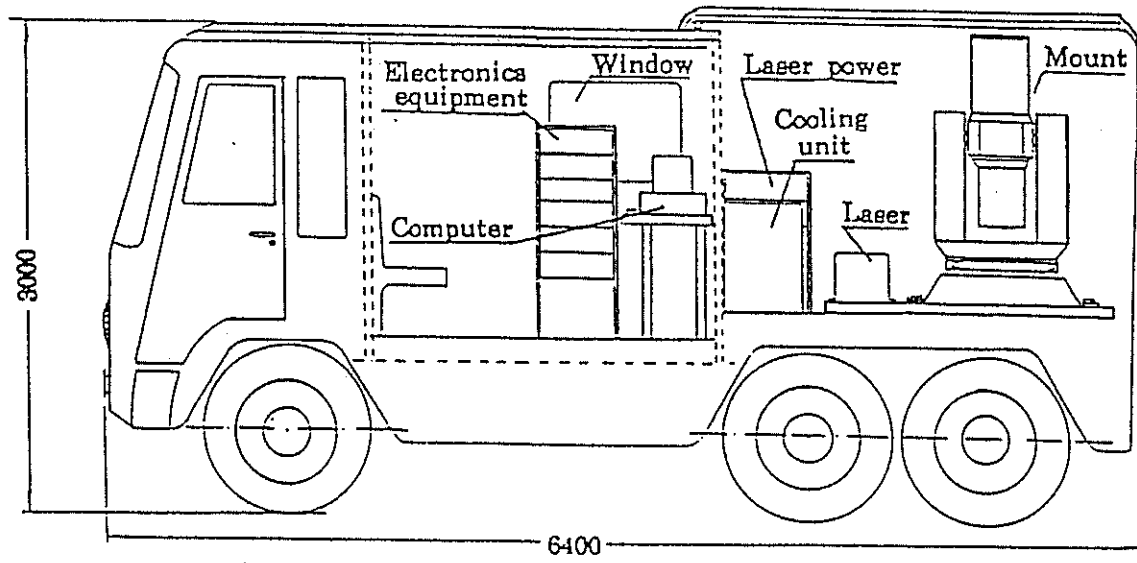
Fig. 3 The schematic diagram of the CTLRS

Fig.4 The overview of the mount and receiving electronics, control computer, time
and frequency standard equipments of CTLRS

STATION MOBILE   SATELLITE TOPEX   N=205
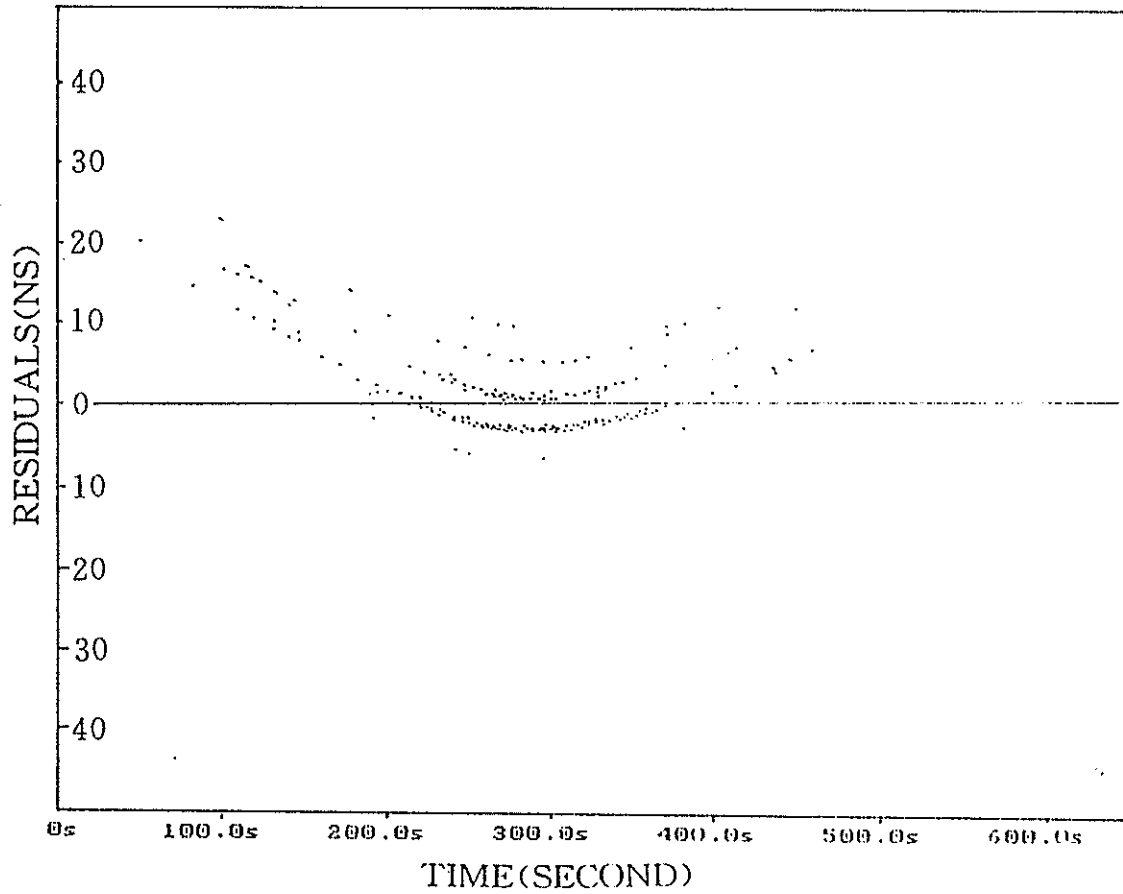DATA 1996. 07. 24   TIME:12. 08(UTC) RMS=6. 1CM
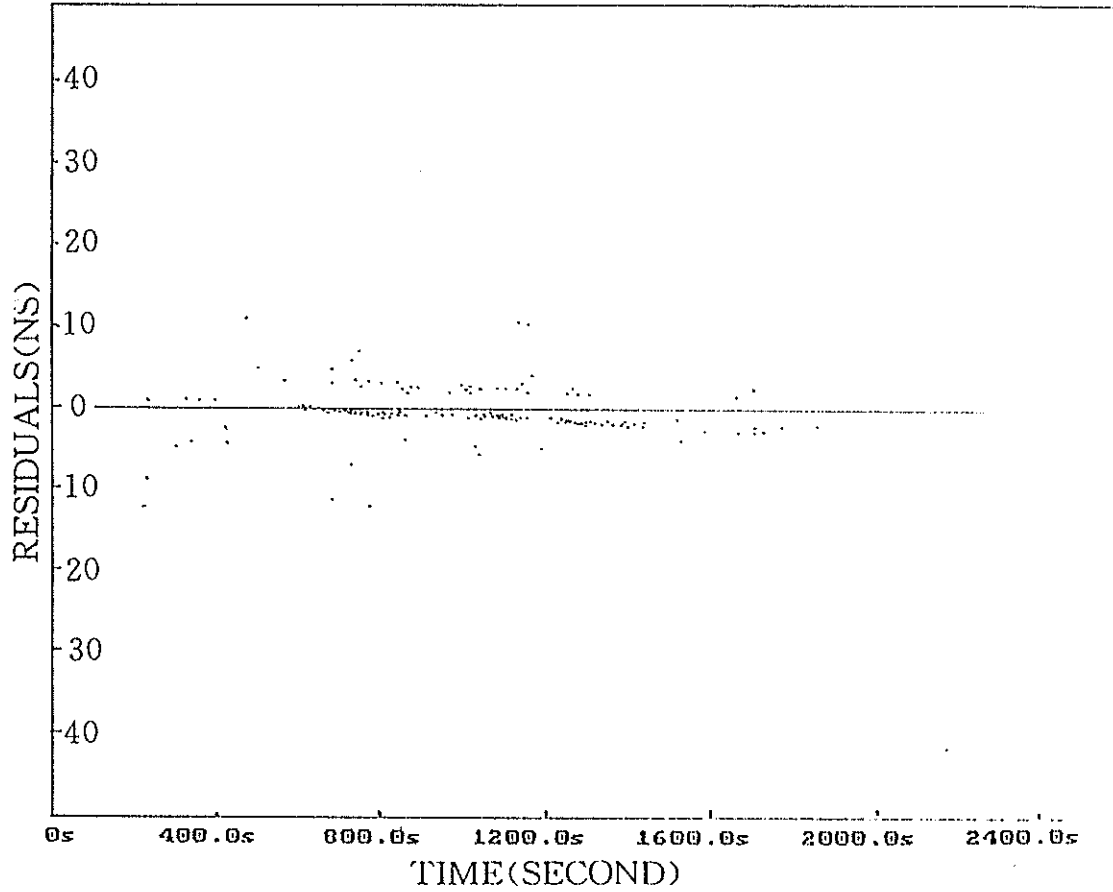
Fig.5   Testing results of ranging to TOPEX

Fig.6 Testing results of ranging to LASEOS-2

Lunar Laser Ranging

Adaptive Ridge Regression: the Multicollinearity and its Remedy – a Case in Lunar Laser Ranging

[1] Chengli HUANG , Wenjing JIN, and Huaguan XU

Shanghai Observatory, Academia Sinica,
80 Nandan Road, Shanghai 200030, P.R.China
E-mail:jwj@center.shao.ac.cn

Abstract. The multicollinearity among regression variables is a common phenomenon in astronomy data reduction. The case of determining Earth Orientation Parameters by Lunar Laser Ranging(LLR) is discussed in this paper. It is pointed out that there exists serious multicollinearity between these two regression variables at the last stage of LLR data reduction in which the Universal Time(UT) and the variation of latitude ($\Delta\phi$) at observing site are solved from the post-fit residuals. As a remedy, a new method, Adaptive Ridge Regression(ARR), as well as the method to choose the departure constant θ, is suggested and applied in this paper. It is proved that ARR method is effective to reduce the multicollinearity and makes the regression coefficients more stable than that by standard least square fits, especially when there is serious multicollinearity.

Key words: adaptive ridge regression — multicollinearity — lunar laser ranging

1. Introduction

As one of the new techniques to determine Earth Orientation Parameter(EOP), Lunar Laser Ranging(LLR) can provide highly accurate Universal Time(UT) frequently and regularly. The accuracy of UT from LLR depends upon not only the measurements but also the mathematical method and physical models adopted in the reduction (*Huang 1992*). The difference of the UT results by pre-residual and post-residual has been discussed by *Wang (1985)*. In order to overcome the imperfections of adopted physical models in calculating the theoretical delay and the uncertainty of the adopted initial value which can induce an obvious systematic deviation in UT, the post-residual are used for solving UT and $\Delta\phi$ except for rapid service. And the related problem on the terrestrial and lunar reference frame has also been discussed by *Huang et al. (1996)*. Because there are only four LLR stations and the common observation of more than two stations is rare, it is common to use LLR data obtained at a single station data for solving UT and $\Delta\phi$.

Nevertheless, the number of normal points of a single station is small and their time span of observation at one night is short, the parameters to be solved are usually related to each other(*Huang, et al., 1993*). At this time, we say that there exists multicollinearity among the regression parameters to be estimated, and then we should be careful in chosing the proper parameters into the observation equa-

---

tions.

In fact, the multicollinearity among regressors is a common phenomenon in astronomy data reduction, and there are different methods to solve the problem in different fields. In this paper, we discuss the case of LLR and introduce the Adaptive Ridge Regression (ARR) method in the following sections. It is proved that ARR is an effective method to reduce the multicollinearity and makes the regression coefficients more stable.

2. LLR data reduction

Generally, LLR data can be processed by two steps. First, corrections of more than fifty parameters and post-fit residuals are obtained from least square adjustment of the whole available measurements. These parameters include geocentric coordinates of observatories, precession, nutation, the orbit of the Moon around the Earth and some lunar parameters such as third-degree potential harmonics, Love number, fractional moment of inertia differences, rotation dissipation and selenocentric coordinates of reflectors. In the second step, UT and the variation of latitude $\Delta\phi$ at observing site are solved from the post-fit residuals at a single station. The observation equation in the second step can be written as(*Jin et al.,1985*)

$$\Delta\rho_i = (\frac{\partial\rho}{\partial UT})_i \Delta UT + (\frac{\partial\rho}{\partial\phi})_i \Delta\phi + \sum_j (\frac{\partial\rho}{\partial K_j})\Delta K_j \tag{1}$$

Where, the partial derivatives:

$$\begin{cases} (\frac{\partial\rho}{\partial UT})_i = R cos\phi cos\delta_i sinH_i \\ \\ (\frac{\partial\rho}{\partial\phi})_i = R(sin\phi cos\delta_i cosH_i - cos\phi sin\delta_i) \end{cases} \tag{2}$$

in which (R,ϕ) are the geocentric radius and latitude of station, and (δ_i, H_i) are the declination and time angle of the Moon at time t_i.

The time span used in the second step is short (about 3 hours), so the last term in equation (1) can be considered as a constant.

3. The multicollinearity between regressors, ΔUT and $\Delta\phi$

During the past two decades, the problem of multicollinearity has received considerable attention. Multicollinearity exists when the multiple regressor variables are truly not independent, but rather, display redundant information(*Myers 1986*). Generally, we write the observation equation as follows:

$$Y = XB + E \tag{3}$$

where, Y, X, B and E denote weighted vector of observations (O-C), weighted design matrix, vector of the coefficients to be estimated and error term respectively.

It is well known that if X is less than full rank in the weighted least-squares fit, the matrix $X'X$ is singular and the normal equations no longer have a unique solution. In practice, this case of exact multicollinear data rarely occurs, but due to the presence of a near linear relationship among the multiple regressors, the near-multicollinear data frequently arises(*Souchay et al., 1995*).

Consequently, there are two important effects of multicollinearity, not readily illustrated by the foregoing. One is the instability of the regression coefficients which are very much dependent on the particular data set which generated them; the other is that the estimated coefficients may vary by large amounts and perhaps change sign.

When more than two regressors are taken into account, the simple correlations could be low and yet multicollinearity could be serious due to intercorrelations. Nonetheless, when only two regressors are considered, as is the case here, their multicollinearity degenerates into collineation.

In practice, there are many quantities which serve as multicollinearity diagnoses and evaluate the extent of the multicollinearity problem. For example, the simple correlations coefficients among the regressor variables is the most simple diagnosis and is often used; variance inflation factors(VIFs) represent the extent of inflation that each regression coefficient goes beyond the ideal condition in which the correlation matrix is a unit. So, VIFs are more accurate, at certain extent, than the simple correlations coefficients. In addition, the system of eigenvalues of $X'X$, including the eigenvalues, eigenvectors and the related condition numbers of the correlation matrix(*Maddala,1977*), is also a formal diagnostic tool. At times, the functions of these three diagnoses are equivalent to each other. In this paper, the simple correlation coefficients and VIFs are used to show the severity of collineation between ΔUT and $\Delta\phi$.

3.1. The simple correlation coefficients in a simulated observation

Assuming that the declination of the Moon, δ, is constant in the time span of observation, the simple correlation between ΔUT and $\Delta\phi$ can be obtained from equation (2):

$$r_{12} = \frac{\sum_{k=1}^{NP}(\sin H_k - \overline{\sin H})(\cos H_k - \overline{\cos H})}{\sqrt{\sum_{k=1}^{NP}(\sin H_k - \overline{\sin H})^2}\sqrt{\sum_{k=1}^{NP}(\cos H_k - \overline{\cos H})^2}} \tag{4}$$

Where, NP is the total number of normal points obteained from one telescope per night.

From equation (4), r_{12} is related to the time angles of retro-reflector H_k. If all observations are strictly symmetric with respect to meridian, it can be proved that r_{12} is always equal to 0.0, or r_{12} lies on (-1.0 +1.0).

A simulated observation is presented in this paper: Supposing there are five well-distributed normal points (NP=5), the time angle of the middle observation $H_0 = -0^h.10$, the total time span is 1 hour, then the time angle of other four observations are $H_{-2} = -0^h.60$, $H_{-1} = -0^h.35$, $H_{+1} = +0^h.15$ and $H_{+2} = +0^h.40$, the simple correlations,r_{12}, between ΔUT and $\Delta \phi$ is then calculated to be 0.56. Similarly, taking different central time angle H_0 and different time span of observation, the corresponding correlation coefficients r_{12} are listed in Table I.

Table I. The correlation coefficients of different H_0 and different observation span (NP=5)

$H_0(hour)$	S P A N (hour)										
	1.0	1.2	1.4	1.6	1.8	2.0	2.2	2.4	2.6	2.8	3.0
-0.1	0.56	0.49	0.43	0.39	0.35	0.32	0.29	0.27	0.25	0.23	0.22
-0.2	0.80	0.75	0.69	0.64	0.60	0.56	0.52	0.49	0.45	0.43	0.40
-0.3	0.90	0.86	0.82	0.78	0.74	0.71	0.67	0.64	0.61	0.58	0.55
-0.5	0.96	0.94	0.92	0.90	0.88	0.86	0.83	0.81	0.78	0.76	0.74
-0.7	0.98	0.97	0.96	0.94	0.93	0.92	0.90	0.89	0.87	0.85	0.83
-1.0	0.99	0.98	0.98	0.97	0.96	0.95	0.95	0.94	0.93	0.91	0.90
-1.5	0.99	0.99	0.99	0.98	0.98	0.98	0.97	0.97	0.96	0.95	0.95
-2.0	1.00	0.99	0.99	0.99	0.99	0.98	0.98	0.98	0.97	0.97	0.96
-2.5	1.00	1.00	0.99	0.99	0.99	0.99	0.98	0.98	0.98	0.97	0.97
-3.0	1.00	1.00	0.99	0.99	0.99	0.99	0.99	0.98	0.98	0.98	0.97

It can be concluded from Table I that

(1) the farther the distance between the central time angle of observation H_0 and meridian is, the larger r_{12}; and

(2) the longer the time span is, the smaller r_{12}.

Additionally, with the same time span and the same central time angle of observation, increasing or decreasing the number of normal points NP makes r_{12} vary little; making the central time angle of observation the opposite sign with the same other conditions makes r_{12} the opposite sign, too.

Nonetheless, because the practical observations are far from symmetric and well-distributed and the central time angles are also usually far from meridian, the practical correlation coefficients are often very large. This can be reflected in the VIFs of practical observation data in the following section.

3.2. Variance Inflation Factors(VIF)

The VIF of the ith coefficient is defined by (*Neter et al,1983*)

$$(VIF)_i = (1 - r_i^2)^{-1} \qquad (i = 1, 2, ..., p-1) \tag{5}$$

where, r_i^2 is the complex coefficient of the regressor variable x_i against the remain (p-2) regressor variables, the $x_j (j \neq i)$.

It is easy to see that VIF involves the notion of multiple association. If the ith regressor variable has a strong linear association with the remaining regressors, r_i^2 is near unity, $(VIF)_i$ will be very large. They supply us with a numerical indication of which coefficients are adversely affected and of how the extent is, so VIFs represent a considerably more productive approach for detection than do the simple correlation values.

When $p - 1 = 2$, i.e., there are only two regressor variables, as the case here, the situation becomes clear and easy to deal with. At this time, r_i becomes the simple correlation coefficient r_{12} between $\Delta\phi$ and ΔUT. The relationship between VIFs and r_{12} is

$$(VIF)_1 = (VIF)_2 = 1/(1 - r_{12}^2) \tag{6}$$

Unfortunately, there is not a universal value of VIF which can tell us whether there is multicollinearity, but it is practically believed that if any VIF exceeds 10(equally, r_{12} larger than 0.95), there is reason for at least concern.

As an example and a test, the 1060 LLR normal points during Jan.7, 1995 and Dec.27,1995 are used, they are divided into 206 groups which were observed at the same telescope and retro-reflector in the same night, while about half groups are deleted because they are fewer than three normal points or they are obvious outliers. As a result, only 104 groups remained. Finally, their VIFs of ΔUT or $\Delta\phi$ are plotted in Figure I.

It is necessary to point out here that, in order to reduce the truncation error in the calculation of $(X'X)^{-1}$, the variables(X_1 and X_2) and Y have been previously transformed to X_1', X_2' and Y', by related transformation:

$$\begin{aligned}
Y_i' &= \frac{1}{\sqrt{n-1}}\left(\frac{Y_i - \overline{Y}}{S_y}\right) \\
X_{i1}' &= \frac{1}{\sqrt{n-1}}\left(\frac{X_{i1} - \overline{X_1}}{S_1}\right) \\
X_{i2}' &= \frac{1}{\sqrt{n-1}}\left(\frac{X_{i2} - \overline{X_2}}{S_2}\right)
\end{aligned} \tag{7}$$

where, the values under overline represent their mean value, and the S_y, S_1 and S_2 are the root mean square error of Y, X_1 and X_2 respectively.

It is shown from figure I that many of the VIFs are greater than 100 (equally, the simple correlation coefficients r_{12} are greater than 0.99). So, the collineation should be regarded as serious.

4. Adaptive Ridge Regression: The Method and Its Result

In order to overcome the so-called ill-condition situations where correlations between the various parameters in the model cause the $X'X$ matrix in equation (3) to be close to singular, giving rise to an unstable parameter estimates which, for example, have the wrong sign or are much larger than physical or practical considerations, there are several numerical methods available to obtain a better conditioning and to reduce the model to one of full rank. For example, there are principal component regression(*Hotelling et al., 1933*), latent root regression(*Webster et al., 1974*), stepwise regression(*Berk, 1977*), ridge regression(RR)(*Hoerl 1962; Weisberg 1985*) and so on. *Huang et al.(1993)* has attemoted for the first time to adopt RR method in LLR, which is proved to be effective.

Generally, in the RR method, another matrix, $(X'X + \theta I_t)$, is used to replace the original normal equations coefficient matrix $X'X$, where θ is the departure constant and positive, in practice, it usually lies on $(0,1)$; I_t is the normalized matrix. RR becomes the least square estimation when $\theta = 0.0$. Consequently, the ridge regression estimation of the parameters **B** is

$$\beta = (X'X + \theta I_t)^{-1}Y$$

(8)

In fact, RR is a biased estimation. Alternately, it adds a constraint to the parameter estimation, so RR is somewhat controversial and, indeed, is often criticized by many statistical researchers, especially concerning its usage. Sometimes, the use of RR is unnecessary and even incorrect. But there is a situation in which RR can be used as a useful and exactly appropriate treatment of the problem. This situation is that the values of the regression parameters are unlikely to be large from prior theoretical knowledge or from a practical point of view (*Draper & Smith 1981*). Furthermore, people will probably prefer to use an estimation which is of small bias with high precision rather than to use one which is unbiased with very low precision because the probability of the former, with which the estimation distributes in the confidence region of the true value, is far greater than that of the latter.

Our LLR data reduction is just this case. We adopt the EOP(UT and polar coordinates) series from IERS Bulletin as initial values, so the regressor variables to be estimated are the deviations of UT from the IERS values. From a practical and theoretical point of view, the initial EOP value of IERS can be considered as appropriate "true" value. Their discrepancy should not be very large, especially when there is serious multicollinearity. So, now that it has been detected that there is serious multicollinearity, adding a constraint to the parameter estimation and adopting RR method are reasonable and appropriate.

However, it is difficult in RR to choose the value of θ. The choice of θ is essentially equivalent to an expression of how big one believes those parameters to be.

So, as for this problem, the benevolent see benevolence and the wise see wisdom—different people have different views, and it depends on the condition, under which the problem is discussed. Usually, it is determined by experience or manually with certain arbitrariness.

Here, we put an adaptive method for choice of θ:

$$\theta_k = (p-1)(rms)_{k-1} / \sum_{i=1}^{p-1}(\sigma_i^2 \beta_i^2)_{k-1} \tag{9}$$

Where, (p-1) is the number of parameters in the model which is 2 in this case, θ_k is the departure constant in the kth iteration; $(rms)_{k-1}, \sigma_{k-1}$ and β_{k-1} are the root mean square of residual, root mean square error and the estimated value of parameter β_i in the $(k$-$1)$th iteration, respectively. It is an iterative process, the criteria to end the iteration is determined by the author for various special purposes; for instance, the resulted root mean square error of estimated parameter may be asked by an author to be smaller than a value. If $k = 1$, the iteration is processed only once, this is just the general RR method based on the standard weighted least squares fit.

There are two benefits from equation (9):

(1) the intensity of constraint can vary according to the severity of multi-collinearity. The more Severe the multicollinearity is, the more the constraint; by contrast, if there is not multicollinearity, θ will be zero, it returns to general least square estimation. This is just the concept of RR method, and

(2) the information of the resulted rms and root mean square error of estimated parameters can serve as feedback information for the choice of θ directly and in time.

4.1. Results

The LLR post-residuals during 1995 are used again to calculate the UT and $\Delta\phi$ by ARR model. The root mean square deviation(RMSD) of estimated UT by standard least squares fit(LS) and by ARR model are plotted in Figure (2a) and (2b), respectively. The deviation of UT results, by LS and by ARR, from the UT value of EOP(IERS)C04 are also plotted in Figure (2c) and (2d), respectively. It is obvious that

(1) the RMSD of the results by ARR model is smaller than that by LS, so, ARR is effective to reduce the RMSD, especially when RMSD is too large in which the multicollinearity usually occurs and

(2) the deviation of UT from EOP(IERS)C04 by ARR are smaller than that by LS.

So, ARR can make the results more stable and make the probability, with which the resulted UT locates inside the distribution region of EOP(IERS)C04, greater than that by LS, especially when there is serious multicollinearity.

5. Concluding Remarks

Adding a constraint will make the resulting system have a rotation. Generally speaking, all observation and reduction are biased. There is not any system which is absolute. There may be a departure with a constant term and a liner term or some periodic terms between two different systems. These two systems can be linked by transformation, so it is irrelevant whether one system is regared as effective as the preferred system. Additionally, in order to evaluate one system, it is not enough to note only the difference between this system and another reference system, even though the latter is considered as an absolute one; it is also necessary to investigate the internal stability of this system.

The correlation coefficients of simulation and VIFs of practical observation have shown the existence of serious collineation problems, which makes the result instable and unreliable. As a proper remedy, the ARR method, an improved form of RR, as well as the method to choose the departure constant θ, is suggested in this paper. It is proved that ARR is effective to reduce the multicollinearity and get satisfied results.
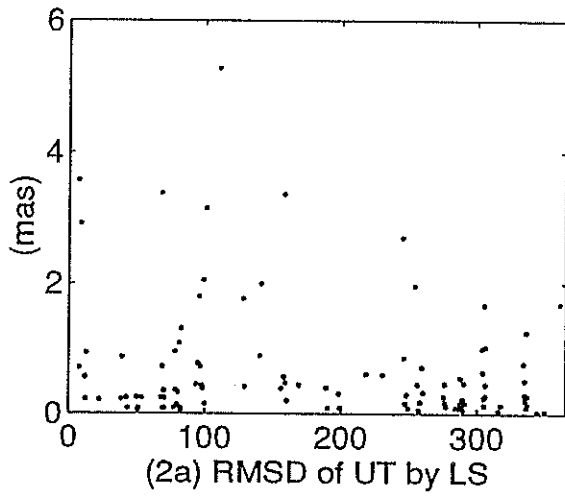
Acknowldgement

Reference

Berk, K., 1977, Tolerance and condition in regression computations, *J. Am. Statist. Assoc.*, **72**, 863-866

Draper, N.R. and Smith, H., 1981, Applied Regression analysis, John Wiley & Sons, Inc., New York, 313-324

Hoerl, A.E., 1962, Application of ridge analysis to regression problems, *Chem. Eng. Prog.*, **58**, 54-59

Hoerl, A.E., Kennard, R.W., and Baldwin, K.F., 1975, Ridge regression: some simulations, *Comm. Statist.*, **4**, 105-123

Hotelling, H., 1933, Analysis of a complex of statistical variables into principal components, *J. Ed. Psych.*, **24**, 417-441, 489-520

Huang, C.L.,1992, Improvment of the models in lunar laser ranging, M.S. Degree Thesis

Huang, C.L., Xu H.G., and Jin W.J., 1993, On the methods of determination of UT from LLR, *Annals of Shanghai Observatory, Academia Sinica*, **14**, 110-117

Huang, C.L., Jin, W.J., and Xu, H.G., 1996, The terrestrial and lunar reference frame in lunar laser ranging, *Journal of Geodesy* (accepted)

Jin, W.J., and Wang Q.G., 1985, Determination of ERP with LLR and discussion of the influence of the adopted parameters, *Proceedings of the international conference on earth ratation and terrestrial reference frame*, 287

Maddala, G.S., 1977, Econometrics, eds. Mc Graw Hill

Myers , R.H., 1986, Classical and moden regression with applications, PWS Publishers, Boston, 218-275

Neter, J., Wasserman, W., and Kutner, M.H, 1983, Applied Linear regression models, Richard D.Irwin, Inc.,

Souchay, J., Feissel, M., Bizouard C., Capitaine N., and Bougeard, M., 1995, Precession and nutation for a non-rigid earth: comparison between theory and VLBI observation, *Astron. Astrophys.*, **299**, 277-287

Wang, 1985, M.S. degree thesis.

Webster, J.T., Gunst, R.F., and Mason, R.L., 1974, Latent root regression analysis, *Technometrics*, **16**, 513-522

Weisberg, S., 1985, Applied Linear regression, John Wiley & Sons, Inc., New York, 196-225

Xu H.G., Jin W.J., and Huang C.L., 1996, The secular acceleration of the Moon determined from lunar laser ranging data, *Earth, Moon and Planets*, **73**, 101-106

Figure I. VIF of UT

(2a) RMSD of UT by LS

(2b) RMSD of UT by ARR

(2c) deviation from IERS by LS

(2d) deviation from IERS by ARR
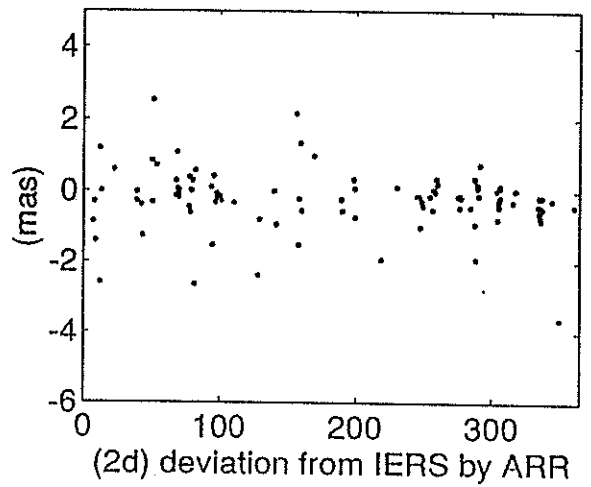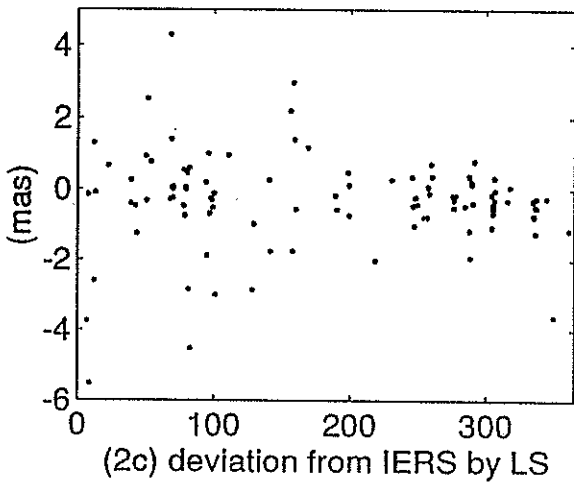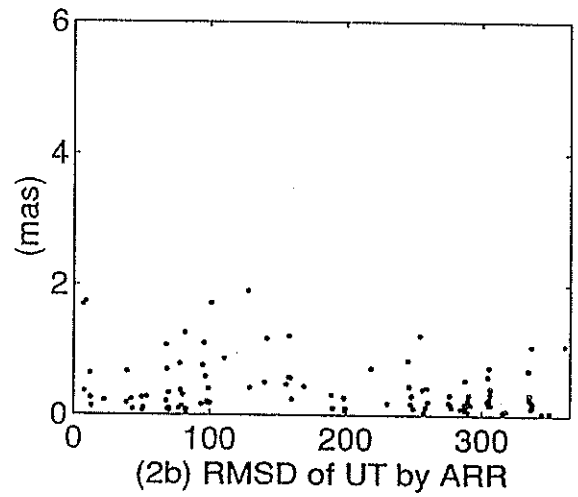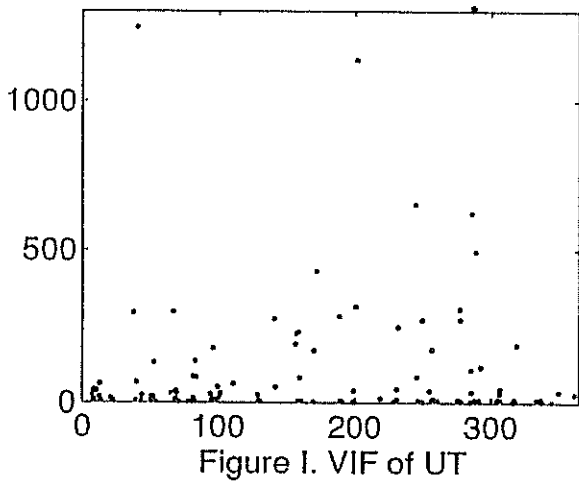
Expected Results from the Analysis of LLR Data

J. Müller
Institut für Astronomische und Physikalische Geodäsie
Technische Universität München
D-80290 München, Germany
Email: jxmx@alpha.fesg.tu-muenchen.de

U. Schreiber
Forschungseinrichtung Satellitengeodäsie
Fundamentalstation Wettzell
D-93444 Kötzting, Germany

Abstract

Lunar Laser Ranging provides an excellent tool for testing metric theories of gravitation. Remarkable results have been obtained by analyzing the lunar observations over the past 27 years. However the realistic errors of the relativistic parameters (of others too) are by a factor 3 (or more) larger than the formal standard errors resulting from the global fit. This discrepancy can be reduced by an improved observation strategy and by a more accurate analysis model.

1. Introduction

Since the beginnig of Lunar Laser Ranging (LLR) in 1969, the data have been used for the determination of relativistic quantities and parameters describing the dynamics of the Earth-Moon system. In fact, one important reason for setting up the LLR experiment has been the chance to test EINSTEIN's theory: if there exists a violation of the strong equivalence principle, the lunar orbit about the Earth would be polarised towards the Sun (NORDTVEDT effect) which can be measured by LLR ([1]).

Several analysis centers determined relativistic quantities like the NORDTVEDT parameter η, metric parameters (γ, β, α_1), a time variation of the gravitational constant $\dot{G}/G$ and others (see e.g. [5], [4], [2], [3]). It is obvious that the realistic errors derived in some tricky way are much larger than the formal errors obtained from the adjustment of the unknown parameters. The results for the relativistic quantities determined at our institute are given in table 1. The realistic errors are up to a factor 3 - 5 (one about 10) worse compared to the formal ones. The reason for the difference is the insufficient theoretical model, but also the non-ideal distribution of the observations. Therefore both analysts and observers can contribute to an improvement of the LLR results. This will be shown for the NORDTVEDT effect.

Table 1: Realistic errors for the relativistic quantities

parameter	realistic error
geod. prec. Ω_{GP} ["/cy]	$\leq 1.5 \cdot 10^{-2}$
metric par. γ	$\leq 6 \cdot 10^{-3}$
metric par. β	$\leq 5 \cdot 10^{-3}$
Nordtvedt par. η	$\leq 1 \cdot 10^{-3}$
time var. grav.const. $\dot{G}/G$ [yr^{-1}]	$\leq 5 \cdot 10^{-12}$
Yuk. coupl.const. $\alpha_{\lambda=4 \cdot 10^5\,\mathrm{km}}$	$\leq 1 \cdot 10^{-11}$
spec. relativity $\zeta_1 - \zeta_0 - 1$	$\leq 1.5 \cdot 10^{-4}$
infl. of dark matter δg_c [cm/s^2]	$\leq 3 \cdot 10^{-14}$
preferred frame effect: α_1	$\leq 9 \cdot 10^{-5}$
preferred frame effect: α_2	$\leq 2.5 \cdot 10^{-5}$

Furthermore, the precision of the observations has improved remarkably[1] since the beginning in 1969 (figure 1). One goal should be to transfer this increase of accuracy as good as possible to the quantities to be determined by the analysis of LLR data.
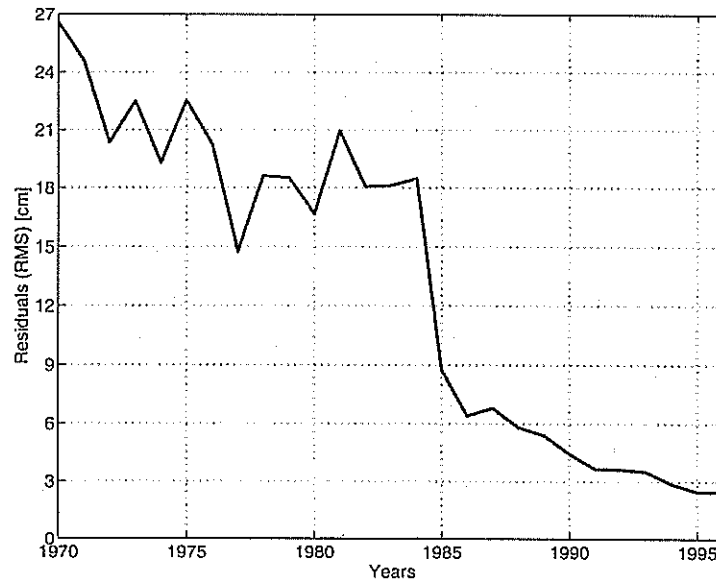

Figure 1: RMS Residuals (observed - computed Earth-Moon distance)

2. Expected results for the NORDTVEDT parameter

The NORDTVEDT effect which describes how a violation of the strong equivalence priniple would appear in the Earth-Moon system, can be understood as follows: the silicate Moon is attracted by the Sun in a different way as the nickel-iron Earth which leads to a shift of the lunar orbit towards the Sun[2]; see figure 2.

---

[1] A precision of 3 mm for a single normal point seems possible.

[2] In contrast, EINSTEIN, also NEWTON state that all bodies/matter will be attracted gravitationally in
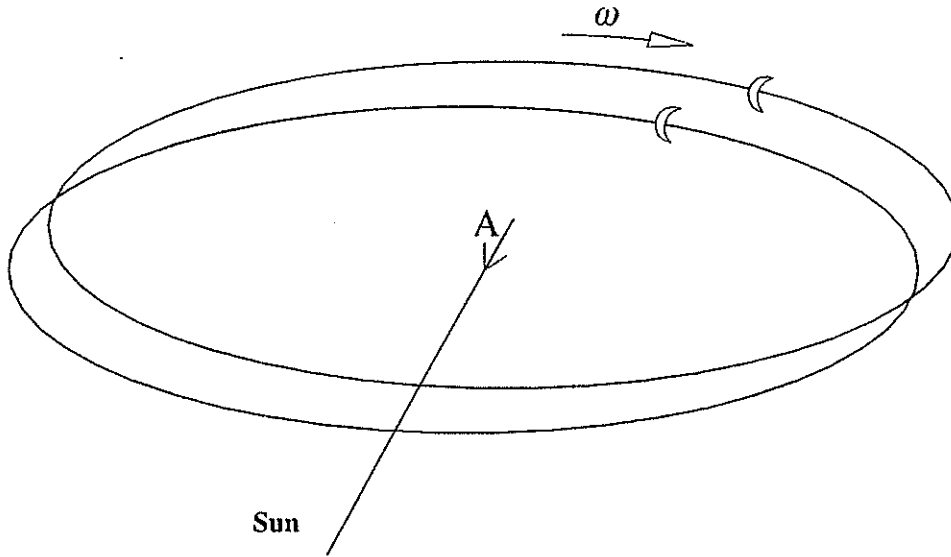
Figure 2: NORDTVEDT effect

This effect can be modelled by

$$\Delta r_{Earth-Moon} = 12.8\,\eta\cos(\omega\,t)\,[\mathrm{m}] = A\cos(\omega\,t). \tag{1}$$

ω is the synodic frequency (angular velocity of the Moon). The amplitude A can be determined with a realistic error of 1.3 cm, whereas the formal error becomes only about 3 mm. One should try to achieve this 3 mm as realistic error. To see how to reach this goal one can look on figure 3.

There the lunar residuals (observed - computed Earth-Moon distance) are plotted as a function of their angular distance from the nearest New Moon[3]. The residuals are weighted and averaged over 10 degree blocks. E.g. for 25° we took observations between 20° and 30°. The residuals plotted at 175° are based theoretically on measurements between 170° and 180°. In fact there are only observations available which were performed during some lunar eclipse (Full Moon) which means they belong all to 179,...°.

What can be seen? The residuals are much worse near New and Full Moon. But the observations during lunar eclipses are better than those taken for 165° (much noise by reflected photons from the surface of the Moon). Bad residuals can mean bad theoretical model or bad observations or both.

The smoother curve (dashed) is designated with 'Nordtvedt effect'. It shows how the NORDTVEDT effect appears in such a plot, if one does not model it in the analysis program resp. does not solve for the amplitude of the synodic frequency. It was computed by adding a signal as (1) to the computed range using our largest error value (that 1.3 cm, the realistic error) for the amplitude A. The post-fit residuals have been compared to those post-fit residuals where this effect was not considered. The dashed curve in figure 3 shows the difference between the post-fit residuals of both fits.

---

the same way.

[3]For the following discussion, only the observations since 1986 are used where more than one observatory are tracking the Moon and the precision of the observations are much better since before (figure 1).
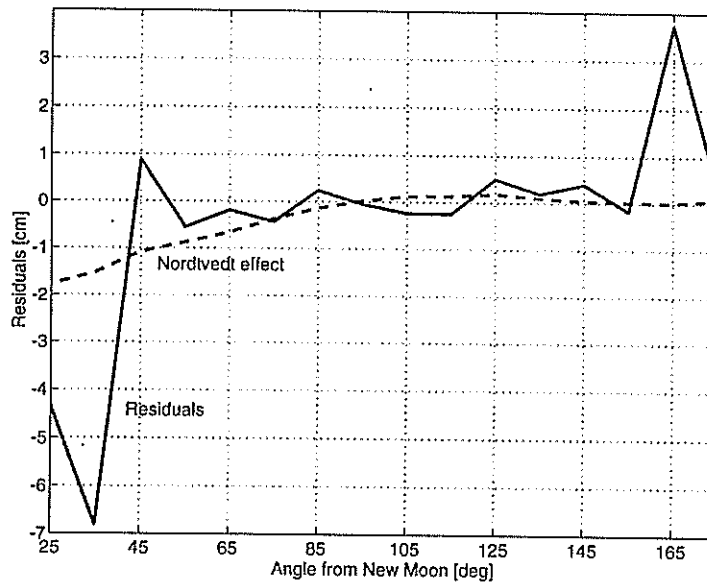
Figure 3: Weighted Residuals (solid line) and NORDTVEDT effect (dashed line) as a function of the angular distance from the nearest New Moon

It can be clearly seen that such a large NORDTVEDT effect can not be found in the observations and if at all it is caused by the bad observations (or bad model) near New Moon.
A further error source is given by the less accurate observations in the seventies which are neglected for the computation of the residuals in figure 3; but for the determination of the realistic error of the NORDTVEDT parameter all measurements since 1970 have been used. Therefore it would be certainly advantageous to neglect the old observations when investigating the NORDTVEDT effect, but it would be very disadvantageous for the determination of $\dot{G}/G$ which can be just well determined from the very long period of observations.
Figure 4 supports the arguments of figure 3. Near New and Full Moon, one has not only bad but even much less observations. It means one observes only a small part of the lunar orbit with many observations and a large part is only observed marginally. Then it is difficult to improve the theoretical model in such areas if one has only less observations. One can not decide what an improvement is at all.
Measurements near New Moon have to be performed in low elevations in most cases to avoid perturbing light from the Sun. But just this fact (low elevations) provides the possibility to investigate elevation-dependent effects (e.g. caused by the atmosphere) which could still be modelled insufficiently. And such an insufficient modeling could be responsible for the increase of the residuals near New Moon. If analysts would get more observations in these areas they could search for errors in their models with more success.

3. Conclusions

The future tasks follow automatically: the theoretical model has to be improved up to mm level (to be done by the analysts); one needs more good observations especially near New
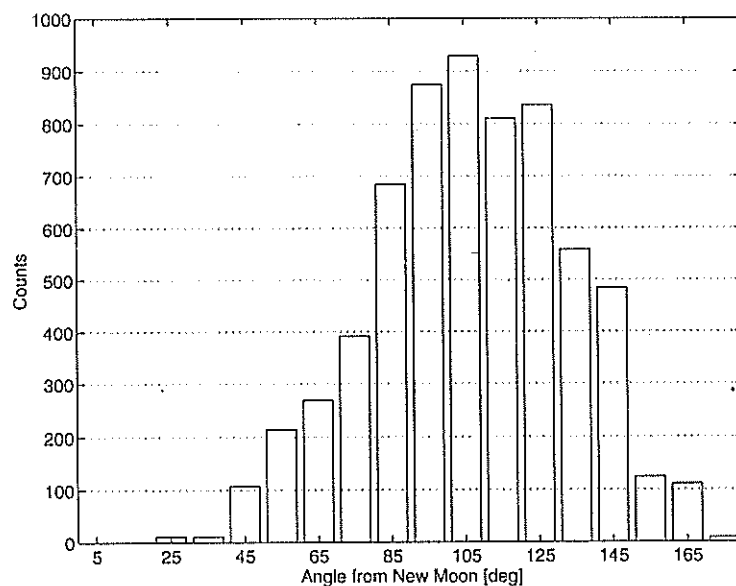
Figure 4: Distribution of lunar observations as a function of the angular distance to the nearest New Moon

and Full Moon. Taking both actions together one can extract much more information from the LLR data as now. One can improve the accuracies of the solve-for parameters; the NORDTVEDT parameter can be determined with a realistic error of a factor 3 better than now. Similar results can be expected for the other parameters.

References

[1] K. Nordtvedt: Testing relativity with laser ranging to the Moon. Phys. Rev., Vol. 170, 1186 (1968)

[2] J. Müller, M. Schneider, M. Soffel, H. Ruder: Determination of Relativistic Quantities by Analyzing Lunar Laser Ranging Data. Proceedings of the 7th Marcel Grossmann Meeting on General Relativity, Stanford, July 1994 (to appear)

[3] J. Müller, D. Vokrouhlický, K. Nordtvedt: An improved constraint on the α_1 PPN parameter from lunar motion. Phys. Rev. D, Vol. 54, 5927 (1996)

[4] J. Dickey et al.: Lunar Laser Ranging: A Continuing Legacy of the Apollo Program. Science, Vol. 265, 482 (1994)

[5] J. Williams, S. Newhall and J. Dickey: Relativity Parameters Determined from Lunar Laser Ranging. Phys. Rev. D, Vol. 53, 6730 (1996)

The Impact of Technology on Lunar Laser Ranging at MLRS -

Peter J. Shelus
McDonald Observatory/Department of Astronomy/Center for Space Research
University of Texas at Austin
Austin, TX 78712-1083
USA

Abstract

Lunar laser ranging observing operations at McDonald Observatory have evolved markedly over the almost 30 years of activity. These included software and hardware changes as well as logistical and administrative ones. Each change ws designed to provide for improvemnet in either data quantity or quality or both. Some were successful; some were not. The prersent paper presents the latest set of changes at the MLRS and their effects.

1.0 Introduction

At McDonald Observatory, the use of two different ranging systems has led to different quantities and qualities of laser ranging data over the history of the experiment. The original McDonald 2.7-m system was a lunar only one. It was built around ruby laser technology, using rather long, powerful laser pulses and slow firing rates, i.e., 3-6 joule/pulse, 3-6 nanosecond pulse-length, 1/3-1 hertz. The later system, the MLRS, was a joint lunar and artificial satellite system. It was built around Nd-YAG laser technology, using shorter, less powerful laser pulses and much more rapid firing rates, i.e., 120 millijoules/pulse, 100-400 picosecond pulse-lengths, 10 hertz. Laser ranging data accuracy, to first order and with everything else being equal, scales inversely with laser pulse length, thus the shorter pulse length of the Nd-YAG laser has led to almost a factor four improvement in the accuracy of the ranges. Since the total weight of a set of observations scales linearly with data accuracy, but only as the inverse square of the number of observations, the later data sets are much better.

2.0 The present McDonald SLR/LLR station

Since 1991, we have pursued an aggressive and a substantial lunar upgrade for the MLRS. The effort has enjoyed a most remarkable success.

- The lunar data rate for the MLRS has been increased by almost an order of magnitude.
- LLR data accuracy and precision has been at least doubled.
- The number of UT-0 Earth orientation points has increased by almost a factor six.
- For the first time since 2.7-m operations in the mid-1980's, McDonald Observatory LLR operations are obtaining, on a routine basis, significant amounts of multi-corner data, i.e., ranges to more than one lunar surface retroreflector during a single observing session.
- During 1995 the MLRS actually exceeded the best years of 2.7-m operations, in terms of data volume, and this has continued through 1996.
- MLRS data quality greatly exceeds that of the 2.7-m system.
- SLR/LLR operational status has been maintained at all times throughout the upgrade.
- The MLRS continued as one of the best SLR stations in the world.

Figure 1 illustrates the spendid multi-terget capabilities of the MLRS, together with the vast increases in data volume obtained for both SLR and LLR operations over the past several years. Figure 2 illustrates the improved LLR data quality and quantity characteristics of the MLRS, compared to that of the original 2.7-m system.
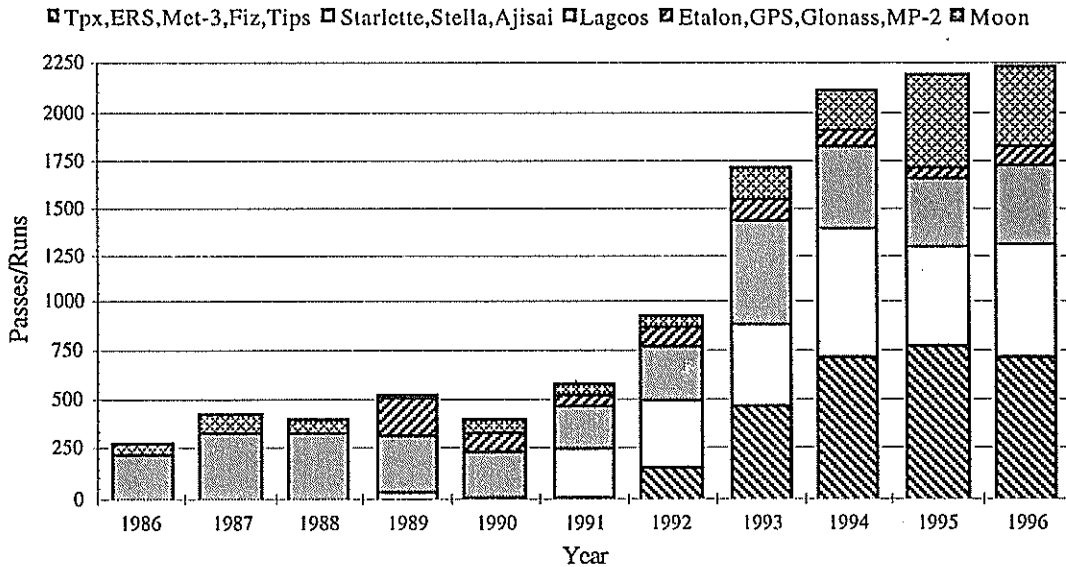
3.0 The MLRS LLR upgrade

Figure 1. MLRS laser ranging Data Throughput

-- Auto-Guiding and Image Enhancement: an integrated hardware and software system that accepts real-time, video signals as input and performs real-time image processing to produce raw and filtered tracking error signals to the control computer for automatic guiding.

-- Avalanche Photo-Diode: in receive path, similar to that used at OCA, should provide a noticeable increase in sensitivity due to better quantum efficiency as well as improved accuracy and precision due to better jitter characteristics.

-- Control Computer: replaces the original MLRS 15 year old Data General NOVA system with a LynxOS based, X-windows, real-time UNIX system running on PC hardware.
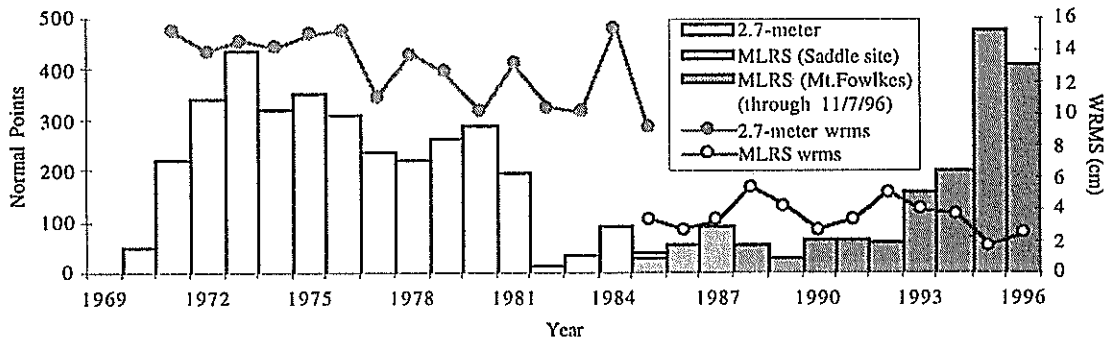

Figure 2. Number of normal points and weighted RMS of post-fit residuals for McDonald LLR observations.

4.0 Conclusions

A series of enhancements at the MLRS has produced significant gains in LLR data quantity and quality. The multi-purpose MLRS (SLR & LLR), with a 0.75-m aperture at a good site, is now competitive with the larger, dedicated LLR station at OCA. With a thoughtful and planned use of resources, significant amounts of both SLR and LLR observations can be obtained simultaneously with excellent results. A selected sub-set of appropriate SLR stations perhaps should examine the possibility of making LLR observations at some small level.

5.0 Acknowledgments

The Lunar Laser Ranging Network and the Lunar Data Gathered ...
... Are they Sufficient?

Peter J. Shelus
McDonald Observatory/Department of Astronomy/Center for Space Research
University of Texas at Austin
Austin, TX 78712-1083
USA

Abstract

Success with the analysis of any data type depends critically upon the quality and the quantity of those data. Over the past several years, the present SLR/LLR laser tracking network has become responsible for the monitoring of an increasingly large number of Earth-orbiting targets. Therefore, in this era of vastly shrinking resources, it is becoming increasingly mandatory to assess specific data requirements for the types of scientific analysis that are to be performed. In this paper we consider the lunar laser ranging data type. We ask the questions as to the types of science that are being done, as well as the quality and quantity of data that is required. We then consider the present network of LLR capable stations and determine the adequacy, or the lack thereof, of the present LLR data products.

1.0 Introduction

The resources of the world-wide laser ranging community are increasingly being brought under greater pressure. The number of Earth-orbiting targets that require observing support is growing and the shrinking of financial support mandates that ever greater cost efficiencies be obtained. It is therefore absolutely necessary that we begin monitoring a set of cost/benefit parameters to maximize the amount of science being performed per unit cost. In the present paper we examine those laser ranging stations that are lunar capable, the quantity and quality of the data that can be gathered by them, as well as the types of science that are able to be pursued. We will evaluate those results and assess overall LLR network strengths and weaknesses.

2.0 The lunar data yield

At the present time only two stations in the laser ranging network are routinely capable of ranging to the Moon. They are the French station at the Observatoire de la Cote d'Azur near Grasse (OCA) and the United States station at McDonald Observatory near Fort Davis, Texas (MLRS). The lunar data yield from those two stations over the past four years are shown in Table 1. Those data are broken down into the number of normal points and the number of minutes of LLR data that were observed annually, the number of nights throughout the year when LLR data were taken, and the number of UT-0 Earth rotation points computed using LLR data.

3.0 Lunar science

The lunar science that is being addressed by the general analytical community, using the LLR data type, is specifically addressed in another paper in these workshop proceedings. However, for the purposes of this paper, we wish to consider the following types of LLR-related science, together with an estimate of the quality and the quantity of the data that is required:

Lunar structure (probing the lunar core and mantle)
 Round-robin, multi-reflector sub-cm normal points in a 1 hour span
 Data should be obtained at least several times (3-5) per month

Spacecraft navigation and Solar System ephemeris generation (where is the Earth?)
 Several (5-10) sub-cm normal points distributed throughout a month
 Data should be obtained every month

General relativity & gravitation (Nordtvedt effect, geodetic precession, G-dot)
 Sub-cm data covering all lunar phases
 Data should be obtained every lunation

Earth Orientation (looking for sub-daily signals)
 Several sub-cm normal points (5 or more) within a 2 hour span
 Data should be obtained as many days as possible during a month

Table 1

MLRS/OCA Lunar Laser Ranging Data Throughput (1993-1996)

		MLRS				OCA			
		1993	1994	1995	1996	1993	1994	1995	1996
LLR	Ap 11	3	25	34	38	53	55	59	50
Normal	Ap 14	8	17	54	34	53	44	49	57
Points	Ap 15	151	160	383	337	433	499	457	485
	Lnk 2	1	3	6	1	12	17	12	15
	Total	163	205	477	410	551	615	577	607
Lunar	Ap 11	12	158	392	405	1,296	1,695	1,710	1,377
returns	Ap 14	55	131	830	454	1,526	1,119	1,562	2,046
	Ap 15	1,589	1,583	7,445	5,986	14,450	23,424	21,679	29,644
	Lun 2	2	8	32	4	132	407	194	197
	Total	1,668	1,880	8,699	6,849	17,404	26,645	25,145	33,264
Minutes	Ap 11	28	382	428	565	561	484	513	432
of	Ap 14	141	242	688	506	485	383	432	505
LLR Data	Ap 15	1,953	2,122	5,059	4,260	4,156	4,603	4,296	4,544
	Lnk 2	3	40	75	11	105	142	104	123
	Total	2,125	2,776	6,250	5,343	5,307	5,612	5,345	5,604
Nights	Ap 11	2	16	21	24	27	23	24	26
LLR Data	Ap 14	5	12	29	20	26	17	24	27
Taken	Ap 15	56	61	104	89	75	71	65	66
	Lnk 2	1	3	4	1	11	9	8	6
UTO pts.	Ap 15	26	30	65	52	49	44	47	49

4.0 The data statistics

The four usable lunar surface retroreflectors comprise a large quadrilateral on the Moon's surface. Because of the its aspherical mass distribution and the gravitational attraction of the Sun and planets (forced librations) and departures of the its angular position from an equilibrium state (free librations), the Moon experiences departures from uniform rotation. Both forced and free librations are apparent in LLR data. These complex angular motions of the Moon about its center of mass can be separated with high accuracy using differential range measurements to the several retroreflectors. This provides a powerful tool to probe the interior of the Moon and its structure. It becomes of paramount importance that ranges to the several retroreflectors be obtained close in time so that the differential measures can be formed. Figure 1 shows observation times and (O - C) residuals for two recent LLR runs, one on April 10, 1996 at OCA (on the left) and another on September 22, 1996 at MLRS (on the right), where the data yield satisfies the data requirements for probing the interior structure of the Moon. During each of these runs, successive multi-reflector normal points were obtained during relatively short intervals of time.
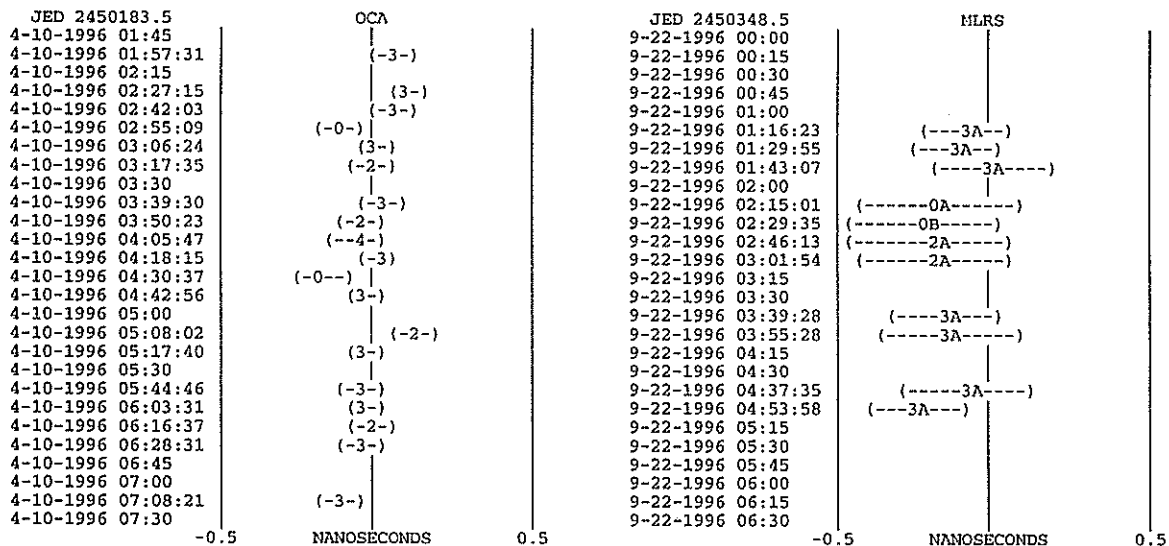
```
 JED 2450183.5                OCA                  JED 2450348.5                MLRS
4-10-1996 01:45      |                            9-22-1996 00:00      |                            |
4-10-1996 01:57:31   |         (-3-)              9-22-1996 00:15      |                            |
4-10-1996 02:15      |                            9-22-1996 00:30      |                            |
4-10-1996 02:27:15   |           (3-)             9-22-1996 00:45      |                            |
4-10-1996 02:42:03   |         (-3-)              9-22-1996 01:00      |                            |
4-10-1996 02:55:09   (-0-)|                       9-22-1996 01:16:23   |    (---3A--)               |
4-10-1996 03:06:24   (3-)                         9-22-1996 01:29:55   |    (---3A--)               |
4-10-1996 03:17:35   (-2-)                        9-22-1996 01:43:07   |    (----3A----)            |
4-10-1996 03:30      |                            9-22-1996 02:00      |      |                     |
4-10-1996 03:39:30   (-3-)                        9-22-1996 02:15:01   (------0A------)              |
4-10-1996 03:50:23   (-2-)                        9-22-1996 02:29:35   (------0B-----)               |
4-10-1996 04:05:47   (--4-)                       9-22-1996 02:46:13   (-------2A-----)              |
4-10-1996 04:18:15   (-3)                         9-22-1996 03:01:54   (------2A-----)               |
4-10-1996 04:30:37   (-0--)|                      9-22-1996 03:15      |      |                     |
4-10-1996 04:42:56   (3-)                         9-22-1996 03:30      |                            |
4-10-1996 05:00      |                            9-22-1996 03:39:28   |    (----3A---)              |
4-10-1996 05:08:02   |  (-2-)                     9-22-1996 03:55:28   |    (-----3A-----)           |
4-10-1996 05:17:40   (3-)                         9-22-1996 04:15      |                            |
4-10-1996 05:30      |                            9-22-1996 04:30      |      |                     |
4-10-1996 05:44:46   (-3-)                        9-22-1996 04:37:35   |    (-----3A----)            |
4-10-1996 06:03:31   (3-)                         9-22-1996 04:53:58   (---3A---)                    |
4-10-1996 06:16:37   (-2-)                        9-22-1996 05:15      |                            |
4-10-1996 06:28:31   (-3-)                        9-22-1996 05:30      |                            |
4-10-1996 06:45      |                            9-22-1996 05:45      |                            |
4-10-1996 07:00      |                            9-22-1996 06:00      |                            |
4-10-1996 07:08:21   (-3-)|                        9-22-1996 06:15     |                            |
4-10-1996 07:30      |                            9-22-1996 06:30      |                            |
               -0.5  NANOSECONDS      0.5                         -0.5  NANOSECONDS         0.5
```

Figure 1. Multi-reflector LLR data from OCA and MLRS .

Spacecraft navigation, both manned and unmanned, is a vital tool that allows us to perform in situ examinations of many objects in the Solar System. Because any probe must initially depart from the Earth, it is necessary that the position of the Earth within the Solar System, as a function of time, be known with maximum precision and accuracy. The LLR data type provides that required accuracy and precision uniquely. However, because errors grow quickly when one extrapolates beyond the range of a data set, it is important that a continuous set of LLR observations be available to maintain this required precision and accuracy. Table 2, showing only MLRS monthly normal point yields, reveals that, at least since early 1993, the spacecraft navigation and Solar System ephemeris requirements for LLR are easily being fulfilled. In fact, we see that several ten's of LLR normal points are being routinely gathered each and every month. Even better monthly statistics exist for the OCA station.

Table 2

Monthly Statistics for MLRS LLR Normal Points

	1987	1988	1989	1990	1991	1992	1993	1994	1995	1996
January	18	5	1	7	0	0	7	14	22	22
February	13	1	0	7	9	1	3	14	34	31
March	13	15	0	2	2	1	5	7	60	26
April	1	6	0	0	1	5	10	18	25	26
May	10	8	8	2	3	8	21	12	38	56
June	1	21	0	8	7	4	28	17	44	37
July	4	3	0	4	8	3	12	0	32	60
August	0	10	0	0	2	0	19	47	7	10
September	11	7	6	12	10	19	14	29	41	52
October	16	11	3	13	11	6	12	7	61	27
November	3	4	11	2	8	6	18	21	65	31
December	6	0	7	14	7	7	18	20	48	32

The five histograms of Figure 2 illustrate the distribution of LLR normal points with respect to the classical fundamental arguments of the lunar theory. Flat, long-term data distributions are especially important for the relativistic and gravitational science being pursued with LLR data. With almost 30 years of data in hand, the distribution of LLR observations with respect to the lunar mean anomaly I (a monthly period), the solar mean anomaly I' (an annual period), and the argument of the latitude F, are reasonably flat. Further, much more than one full period of LLR data exists for the 18.6 year period of the mean longitude of the ascending node of the lunar orbit, Ω, even though the distribution itself is not exactly flat. However, it is the mean elongation of the Moon from the Sun, D, that renders the greatest problem for LLR data distribution. This phenomena speaks to the extreme difficulty that is associated with obtaining lunar ranges at the new and full moon phases and the consequent preferential scheduling of LLR observing time at the quarters, when ranges are most easy to obtain.
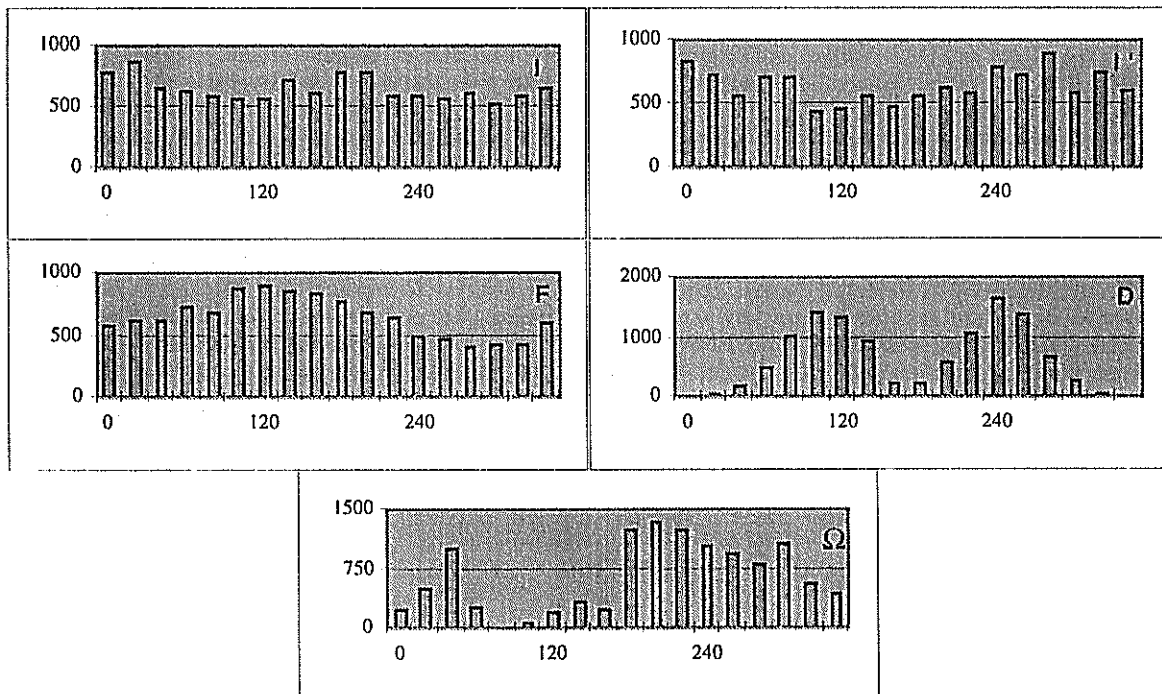
Figure 2. Distribution of LLR observations with respect to the fundamental arguments of the lunar motion.

Together with other space-based techniques, e.g., SLR, VLBI, microwave, and GPS, LLR contributes important information about the variations of the Earth's rotation, including precession and nutation. Also, in a unique sense, LLR determines the intersection of the Earth's equatorial plane with the plane of the Moon's orbit as well as the angle between them. From these, the equivalent quantities for the Earth's orbit can be found. The resulting dynamical equinox and obliquity of the ecliptic can then be used to tie the Solar System reference frame to that determined from the Earth's rotation. Since VLBI observations can tie the Earth rotation frame accurately and precisely to an inertial frame based upon distant radio sources, the Solar System frame can then be tied to that same inertial frame. Illustrating the density and the continuity of the LLR observations that contribute to these types of tasks, Figure 3 depicts both the OCA and MLRS-derived UT-0 points that were computed during the past 600 days using LLR observing observations.
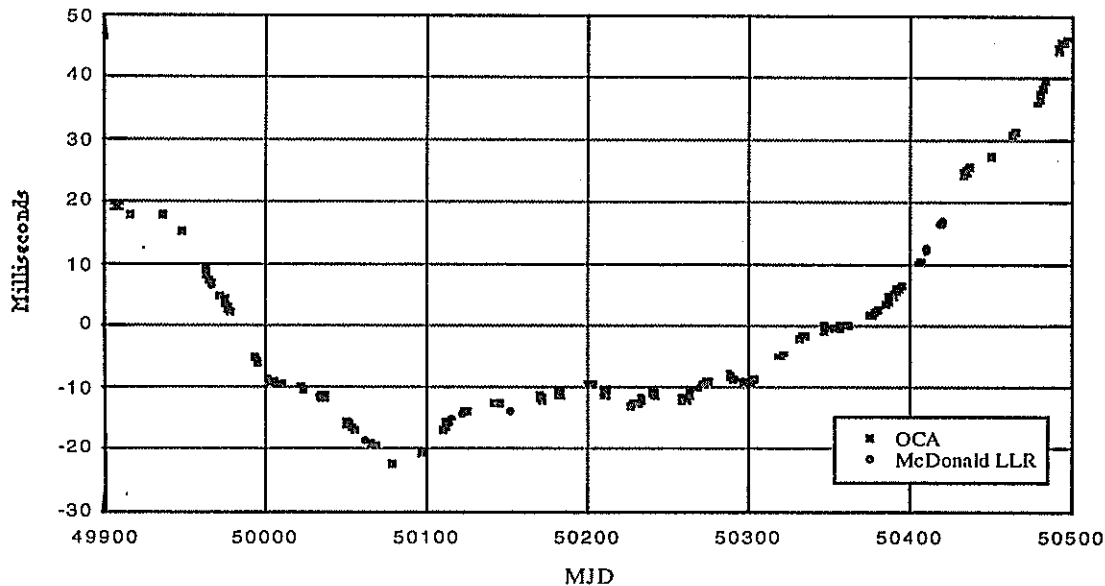
Figure 3. UT-2R -TAl results (with slope removed)

5.0 Summary and conclusion

On the positive side, an objective assessment of the situation shows that the present LLR network, consisting only of the MLRS and OCA stations, is doing remarkably well. LLR data density and accuracy, as well as multi-reflector data, when it is obtained, is quite good. On the negative side, the present LLR-capable part of the SLR network is just barely adequate. Any two-station network is going to be especially vulnerable to weather, equipment, and funding problems. Gaps in data acquisition can be common. Also, of paramount importance for the additional benefit of the LLR data type, the routine generation of sub-cm data must be strongly advocated.

Looking to the future, good effort is already being applied within LLR, especially at OCA, to make routine sub-cm LLR data acquisition a reality. There also must be much more effort applied to obtaining more comprehensive lunar phase coverage. It has been shown in the past that LLR data can be obtained at and near full Moon. However, the difficulty of the task requires additional stations over which the effort might be spread. Further, on account of the Moon's proximity to the Sun, performing LLR observations near the new Moon phase can be quite dangerous, both to equipment as well as to personnel. Can the development and implementation of absolute telescope pointing and better "bright sky" technologies ameliorate some of this danger?

The obvious conclusion is that OCA and MLRS are doing a remarkable job with respect to LLR observations. OCA continues as primarily an LLR-only station. MLRS continues in its part-time LLR mode, while continuing to be one of the most prolific data producers in the world of SLR data. A few other, part-time, LLR-capable stations could help to eliminate weather and equipment problems as well as to spread out the effort that is required for the more difficult tasks. A final comment is that at least one southern hemisphere LLR-capable SLR station should be sought.

6.0 Acknowledgments

Millimetric Lunar Laser Ranging
O.C.A./C.E.R.G.A.

J.F.Mangin ; J.E.Chabaudie ; D.Feraudy ; P.Fridelance ; M.Furia ; M.Glentzlin ;
A.Journet ; J.Pham Van ; E.Samain ; J.M.Torre ; G.Vigouroux .

Status and accuracy

A new manager for the French L.L.R. station :

- In September 1996, Christian VEILLET left the C.E.R.G.A. to join the staff of the Canada, France, Hawaii Telescope.

- Jean-François MANGIN is the new manager. (email : MANGIN@OBS-AZUR.FR).

Status of the millimetric L.L.R. station :

Status : laser

- The Y.A.G. laser emits a train with 3 pulses at about 10 Hz. Each pulsewidth is 130 ps. The train energy is about 600 mJ. The time interval between the first and the second pulse is 1.6 ns, and between the second and the third is 2.5 ns. It will be possible, in the future, to work with 4 pulses with a pulsewidth of 90 ps ; the train energy will be the same.

Status : filtering

- Spatial filter : In general, we works with 15 arc second in dark and 7 or 10 arc second in light (this depends on the seeing).

- Spectral filter : We use two filters, the first is a Fabry-Perot filter 1.2 A°, finesse 50, followed by a large filter 60 A° . The total transmission is 60%.

- Temporal filter : The electronic and computer gate is usually 100 ns wide. For satellite ranging it is possible to increase the gate to 2 µs.

Status : datation

- Start time : The detector at the emission is an infrared InGaAs pin diode (C30617 RCA). It works with a large number of photoelectrons, therefore the precision is better than 10 ps.

- Return time : The return detector is a silicon A.P.D. (Silicon sensor: SSOAD-230) working in single photoelectron. It is used at a temperature -50° C. The continuous voltage is -138 V (breakdown = -142 V for this using temperature) and the geiger voltage is -150 V added to the continuous voltage. The geiger pulsewidth is 2µs, but the beginning is 80 ns before predicted return from the Moon. In that case the precision is 35 ps.

- Event timing system : This system is constituted by two event timing modules and one clock generator module connected to a caesium clock. We use one event timing module for the start

time and one for the calibration-target time or for the Moon-return time. The interval time accuracy is 7 ps.

Accuracy analysis :

Standard deviation :

- The standard deviation is between 60 ps and 200 ps, often below 100 ps. It depends on the laser, on the lunar reflector size and on the Moon libration. The event timers and detectors precision are of little effect on the standard deviation.

- For medium series (100 echoes in 10 min and st. dev. = 100 ps), the normal point precision should be 10 ps without atmospheric effect.

Accuracy test :

- In our station we range simultaneously, with the same laser pulse, a local target within the telescope and the reflector on the Moon.

- By calibration of the local corner cube we have an accurate measurement of the pulse flight time.

- In our case we emit a pulse train (3 pulses) and the accuracy of the distances measured between the pulses gives a good idea of the best accuracy that could be achieved on the Moon for comparable returns rates. Of course the atmospheric effect is not taken in account.

- The following plot shows the accuracy of the distance measured, between two pulses, on a local target, during seven hours. The st. dev. is 8 ps for 30 normal points.
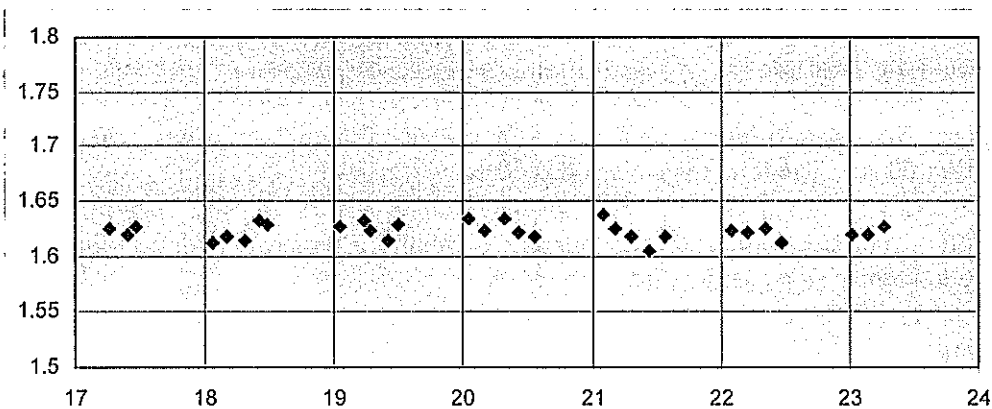
Last results

- Since 24 July 1995, the station works with a millimetric accuracy, there were 93 nights with the following results :
  ref. 0 TRA   2501 echoes in 87 normal points
  ref. 2 FMR   2734 echoes in 78 normal points
  ref. 3 HAD 42966 echoes in 714 normal points
  ref. 4 LK2   345 echoes in 25 normal points

Returns per lunar month

Normal points per lunar month

Returns distribution per lunar month

191
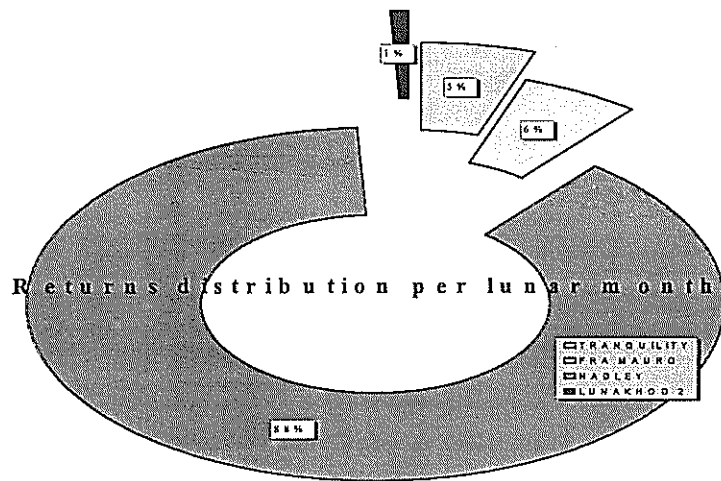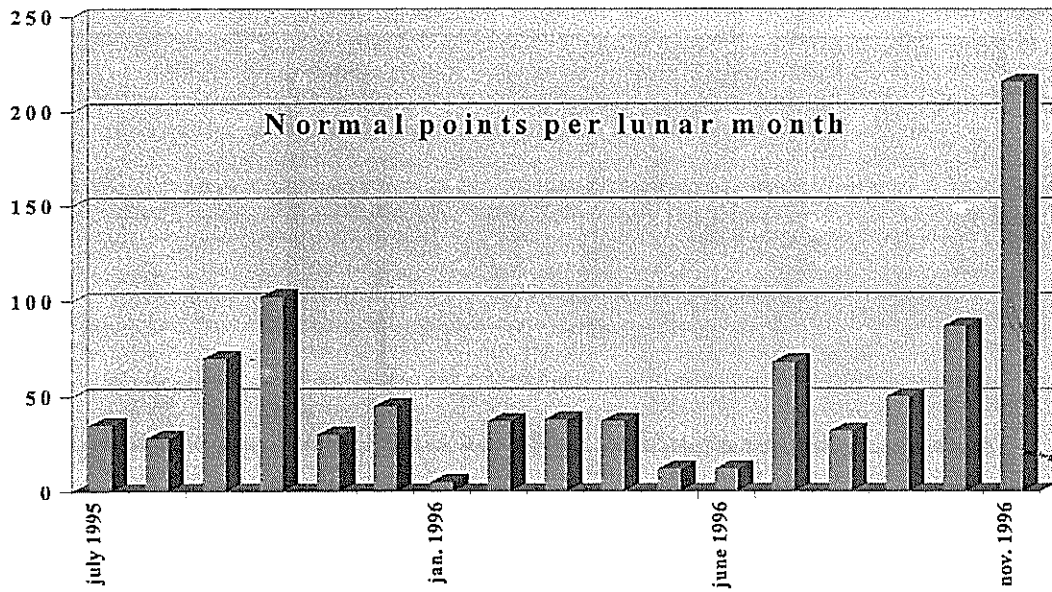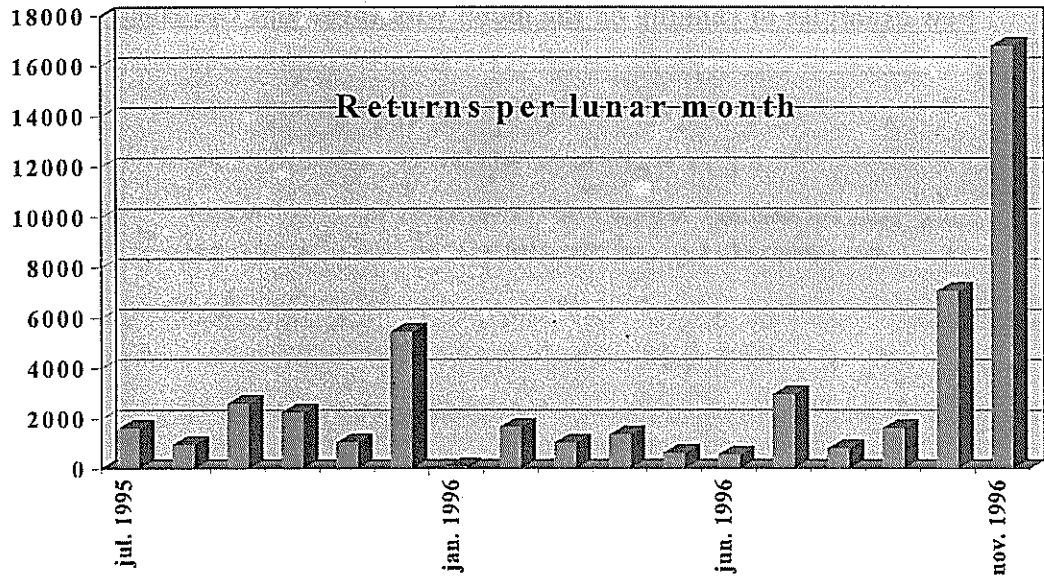
Few examples of ranging on the moon with three and two laser pulses
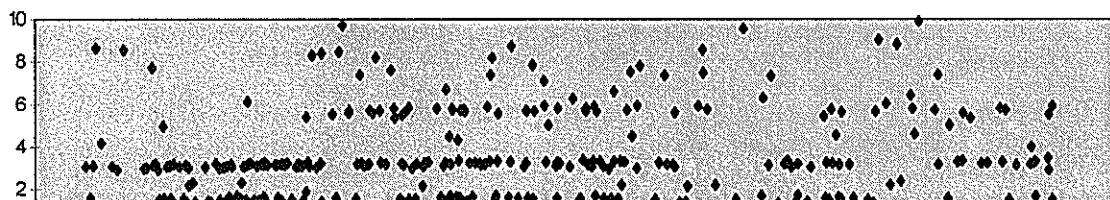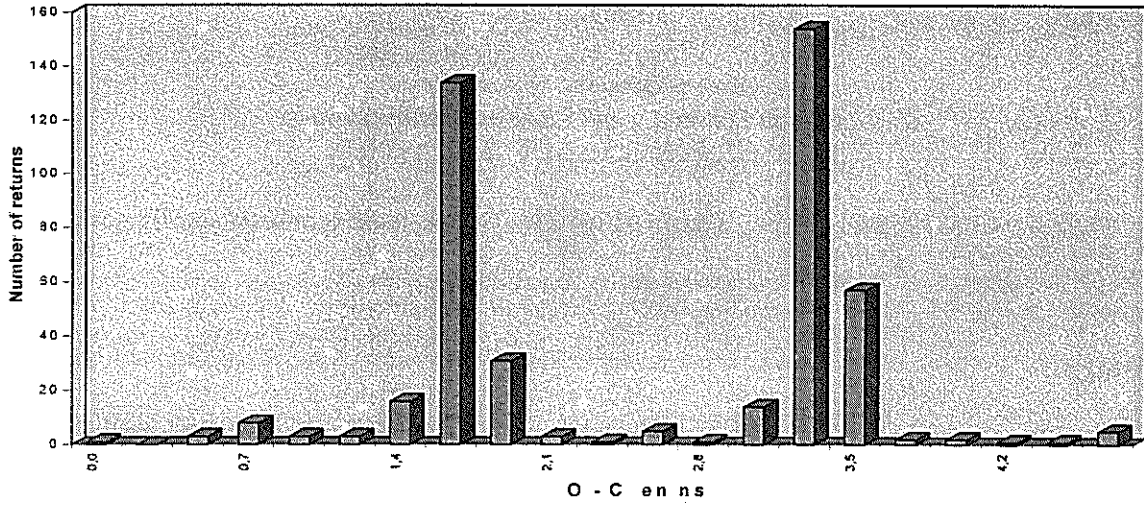
One good night with many returns serials on the four reflectors.
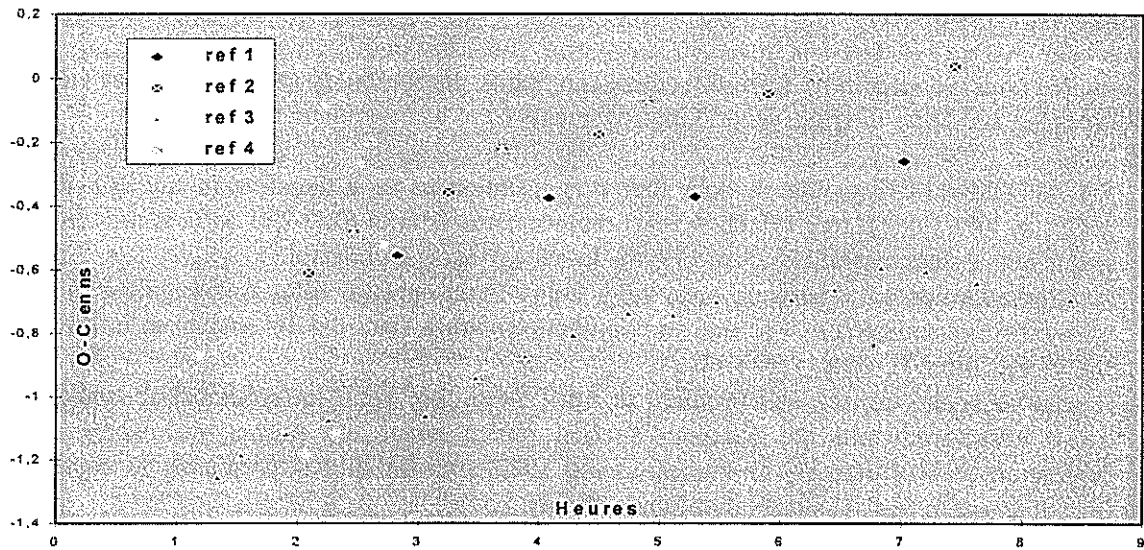
PROSPECTS FOR LLR AT ORRORAL

J.McK. Luck

Orroral Geodetic Observatory
Australian Surveying and Land Information Group
PO Box 2, Belconnen ACT 2616, Australia

Phone: +61 (6) 235-7111   Fax: +61 (6) 235-7103 E-mail: johnluck@auslig.gov.au

History

A series of successful observations was achieved using the 1.5 metre telescope at Orroral in 1979-81, when the mount was equatorial and the laser was a 3 ns pulsewidth ruby laser at 3-5 Hz, mounted on the side of the telescope tube.

In 1982 under a grant from NASA, the telescope mount was converted to X-Y with fast slewing and artificial satellite tracking capability, the ruby laser was replaced with a standard frequency-doubled Nd:YAG laser at 10 Hz, and the control system upgraded to HP1000-series computers [Luck,1992]. Incontrovertible lunar echoes were received on several nights in 1985 [Luck and Greene,1985]. None have been received since.

Recent Developments

In order to improve sensitivity towards routine ranging to geostationary satellites such as OPTUS, GPS ranging and lunar ranging, several improvements have been implemented.

- An APD SP-114 from Ulrich Schreiber was installed as an alternative to the ITT F4129f MCP, in July 1993 [Luck,1994]. Several replacements later, a SSO-230 APD is now in place and is being characterised [Jackson,1996]. Its sensitivity is wonderful.
- A Stigma Optics 1.3 Angstrom bandwidth Fabry-Perot spectral filter was installed in 1994, with 60% transmission at 532 nm, in conjunction with a standard 10 Angstrom interference 'blocking' filter. It works very well.
- A new secondary mirror was installed in April 1996, to correct for spherical aberration and coma introduced into the Ritchey-Chretien optics when the primary-secondary mirror separation was unalterably shortened in the 1982 upgrade. It has produced no significant improvement in SLR results or star image quality, so far.
- A Differential Image Motion Monitor (DIMM), based on an 11-inch Celestron telescope, has been acquired [Wood et al,1995]. It is to be used for testing the "seeing" inside and outside the dome.
- The operating software has recently been tested using an up-to-date lunar ephemeris provided by Randy Ricklefs, and it all seems to work satisfactorily.

Future Plans

Several short-term projects are under way, especially replacement of a burnt lens in the Coude Path, restoring telescope pointing quality, and restoring laser quality and power.

Other enhancements to be considered would be shortening of the immensely long Coude path to the receiver and rationalisation of its convolutions, replacement of the refractive optics, and installation of an X-Y Offset Guiding Stage [cf Shelus et al,1994]. But there is no budget for such enhancements.

Orroral will continue to attempt lunar ranging as a target of opportunity whenever it is considered that sufficient numbers of sub-systems are near-optimal to warrant the effort.

Acknowledgements

References

Jackson, S (1996): "Effects of Common Gating Schemes on SPAD/APD Bias", These Proceedings.

Luck , J.McK and B.A.Greene (1985): "Report from Orroral", Proc. International Conference on Earth Rotation and the Terrestrial Reference Frame, July 31-August 2 1985, Columbus, Ohio, pp 257-273.

Luck, J.McK (1992): "Performance of the Upgraded Orroral Laser Ranging Sytem", Proc. 8th International Workshop on Laser Ranging Instrumentation, NASA Conf.Publ.3214, p 11-6 ff.

Luck, J.McK. (1994): "Laser Ranging Support for TV Time Transfer Using Geostationary Satellites", Proc. 8th European Frequency and Time Forum, March 9-11,1994, Weihenstephan, Germany, Vol.1, pp 341-355.

Shelus, P., R.L.Ricklefs, G.G.Ries, A.L.Whipple and J.R.Wiant (1994): "Lunar Laser Ranging at McDonald Observatory: An Upgrade to Start the 2nd Quarter Century", Proc. 9th International Workshop on Laser Ranging Instrumentation, Canberra, Australia, 7-11 November 1994, Vol.1, pp 295.

Wood, P.R., A.W.Rodgers and K.S.Russell (1995): "Seeing Measurements at Freeling Heights and Siding Spring Observatory", Publ. Astron. Soc. Aust., Vol.12 No.1, 1995, pp.97-105.

Compensation of Laser Beam Propagation for the LLR

Feng Hesheng,   Xiong Yaoheng

Yunnan Observatory, Chinese Academy of Sciences
P.O.Box 110, Kunming, Yunnan Province 650011, P.R.China

ABSTRACT

We present a new idea to the Laser Ranging technique, especially for the Lunar Laser Ranging. Using Adaptive Optics technique, like Deformable Mirror, Tip-Tilt Mirror and Laser Guide Star, to the Lunar Laser Ranging, we believe that the efficiency of the echo will be improved obviously.

Keywords: Lunar Laser Ranging, Adaptive Optics

1. INTRODUCTION

There are many limitation facts to achieve LLR successfully. The earth's atmospheric turbulence that disturbs a transmitted laser beam from a ground station and causes the laser wavefront distortion and increases the laser beam divergence is also a main fact.

Kunming laser ranging station, which is situated at the south-west of the China, now is shakedown and calibration, and will be put into operation in the beginning of the next year. The first goal is the satellite laser ranging (SLR). Because the telescope's aperture in this system is larger than 1 meter (1.2m), and the telescope has a ±1″ pointing accuracy and has a better than 1″ tracking stability, it is very suitable for using this telescope to the lunar laser ranging (LLR). This is the second goal for our station. Moreover, using 1.2m telescope in 1989, the Institute of Optics and Electronics, Chinese Academy of Sciences, cooperated with our group, did an adaptive optical image compensation experiment [1]. Furthermore, in the end of this century, a 61 actuators' adaptive optics system with laser guide star will be set up on the telescope. So it is possible for our station to consider using adaptive optics technique to the LLR.

The development motives of the adaptive optics (AO) originated from two field requirements: high resolution imaging and powerful laser beam propagation through the atmosphere. Adaptive high resolution imaging technique is going to be used widely in the ground-based telescopes. For compensation techniques of a laser beam propagation in the atmosphere, the U. S JPL now is considering applying it to the long-range laser communication by using 3.5m telescope of Air Force Phillips Lab., which will send out a compensated laser beam to the moon's Apollo retroreflectors and then detect the return light from the moon [2]. It seems reasonable for us to propose to use this technique for the long-range laser ranging, especially for the LLR. Using AO techniques to compensate atmosphere effects, it can be expect to improve the laser beam's energy concentration and increase both the intensity and the efficiency of the echo that return from the moon retroreflector.

2. PLAN OVERVIEW

In view of many difficulties and less success for the traditional LLR, the applied object of the AO technique ought mainly to the LLR. Moreover, in the last decade many high orbit satellites that we can use them as research steps have been launched into the space, such as Lageos 1, 2; Etalon 1, 2; GPS 35, 36 etc. Because these satellites are very faint, we can not use themselves as a guide star for the wavefront detection. Though the moon is a bright extended source, it is not very possible for us to find a suitable reference target near the retroreflector (within the isoplanatic angle). Therefore, we ought to use an artificial light source in the plan. There is another small aperture telescope that is coaxial to the 1.2m telescope as a transmitter telescope for the laser guide star (Fig.1). Transmitted laser that is for the laser guide star can be focused at an altitude less than 15km on the sky and formed an artificial beacon that uses Rayleigh scattering off air molecules in the stratosphere. The 1.2m telescope that is using for the laser ranging receives the light that comes from the laser guide star and gives the wavefront sensor a signal of the wavefront distortion that is used to control a deformable mirror or a tip-tilt mirror to compensate the laser beam which is about to be transmitted for the laser ranging at the same time.

It is well known that an artificial star can not provide the information of the globe wavefront tilt. Only considering our goal is not for the high resolution imaging but for the laser ranging, we can neglect effects of the tilt and only compensate effects of the higher order wavefront distortion, which will improve the energy concentration of a transmitted laser beam that is for the LLR. At the Yunnan Observatory, under a typical condition: $r_0 = 12cm$, for a 1 meter aperture telescope, according to [3]

$$\sigma_m = 0.6(\frac{\lambda}{D_0})^{1/6}(\frac{\lambda}{r_0})^{5/6}$$

The amount of the tilt induced by the atmosphere is only about $0.''3$. However, the seeing induced by the atmospheric turbulence decreases to about more then $1''$. Moreover, because the laser device itself that uses for the laser ranging has a given divergence, about 0.8 mrad, and though through the beam expander and the telescope reduction, about 100 times, the laser device has still a $1.''5$ divergence. So the whole transmitted laser beam is not less than $2''$. Adaptive optics can have a real-time compensation not only for the laser beam divergence induced by the atmospheric turbulence, but also for the laser beam itself and the static error effects of the telescope optical transmission system at the same time.

After an atmospheric compensation for the star light, the 61 actuators' adaptive optics system at the Yunnan Observatory in future will have $0.''2$ FWHM for its star image. We can not have an extravagant hope to reduce the laser beam that is transmitted to the moon to such small level. Because photon numbers that are transmitted to the moon retroreflector is inverse proportion to the square of the laser beam divergence, through partial reduction, if we can reduce an uncorrected laser beam divergence with $2''$ to 1/3 of this number, the echo intensity will increase one order. The prospect is very considerable.

3. DISCUSSIONS

1. As mentioned above, after realizing the wavefront compensation of a transmitted laser beam, the light energy concentration transmitted to the target can be improved effectively and is expected to less than 1″. Right now, the pointing accuracy of the telescope becomes a more prominent problem. Although the pointing accuracy of our 1.2m telescope has been achieved ±1″ (RMS) level now, it still needs to improve the pointing accuracy further for satisfying such a requirement. We think it is possible because the telescope has a very good axial stability that can be achieved ±0.1″ [4]. The principal problem is to improve the accuracy of the axial encoder, especially for the resolution of the digitizer. The resolution of the digitizer is 0.″36 in using now, equal to 22 bits. Further improvement is possible. For example, it is said that the measuring angle resolution for the MMT mount is 26 bits.

2. Because of using a laser guide star for the wavefront detection, we can not measure the globe wavefront tilt induced by the atmosphere. For the laser ranging, it is unable to compensate the transmitted laser beam wobble induced by the atmospheric turbulence. But as mentioned before, this typical amount at the Yunnan Observatory is ±0.″3 and has a statistical property that its average value is zero. Though unable to compensate this amount, when the absolute pointing accuracy of the 1.2m telescope is increased to a given level, such as better than 0.″5, it has still a high probability to hit the target. As mentioned above, we expect that the FWHM of a transmitted laser beam is about 0.″5 — 1″ after the compensation of the adaptive optical techniques.

3. Although in our system we do not compensate the tilt of the transmitted laser beam induced by the atmospheric turbulence, we need still to use a tip-tilt mirror that is used frequently in the adaptive optical technique and need to use it firstly. It may have three functions:
(1) correction the disturbance of the wind power for the telescope pointing accuracy;
(2) correction the servo-control system deviation of the telescope;
(3) correction the system error of the direction variation of the laser beam.

We expect that after using a tip-tilt mirror as the first step of the adaptive optics application for the LLR, the rate of the wave-echo will be improved obviously.

4. REFERENCES

1. Wenhan Jiang, et al. 1995, Opt.Eng., Vol.34, No.1, P.15.
2. R. Fugate, 1994, May 20, BMD Monitor, P.7.
3. F. Roddier, 1981, Progress in Optics, Vol. XIX, P.281.
4. Feng Hesheng, et al. 1991, Publications of Yunnan Observatory, No.4, P.1.

Telescope

Laser for LGS

Control Module

Laser Beam Jitter Sensor

Laser for LLR

Rotating Disk

Detector

LLR/LGS Dichroic

Beam Splitter

Wavefront Sensor

Beam Expander

ICCD

Imaging Processing

Tip-Tilt Mirror

Deformable Mirror
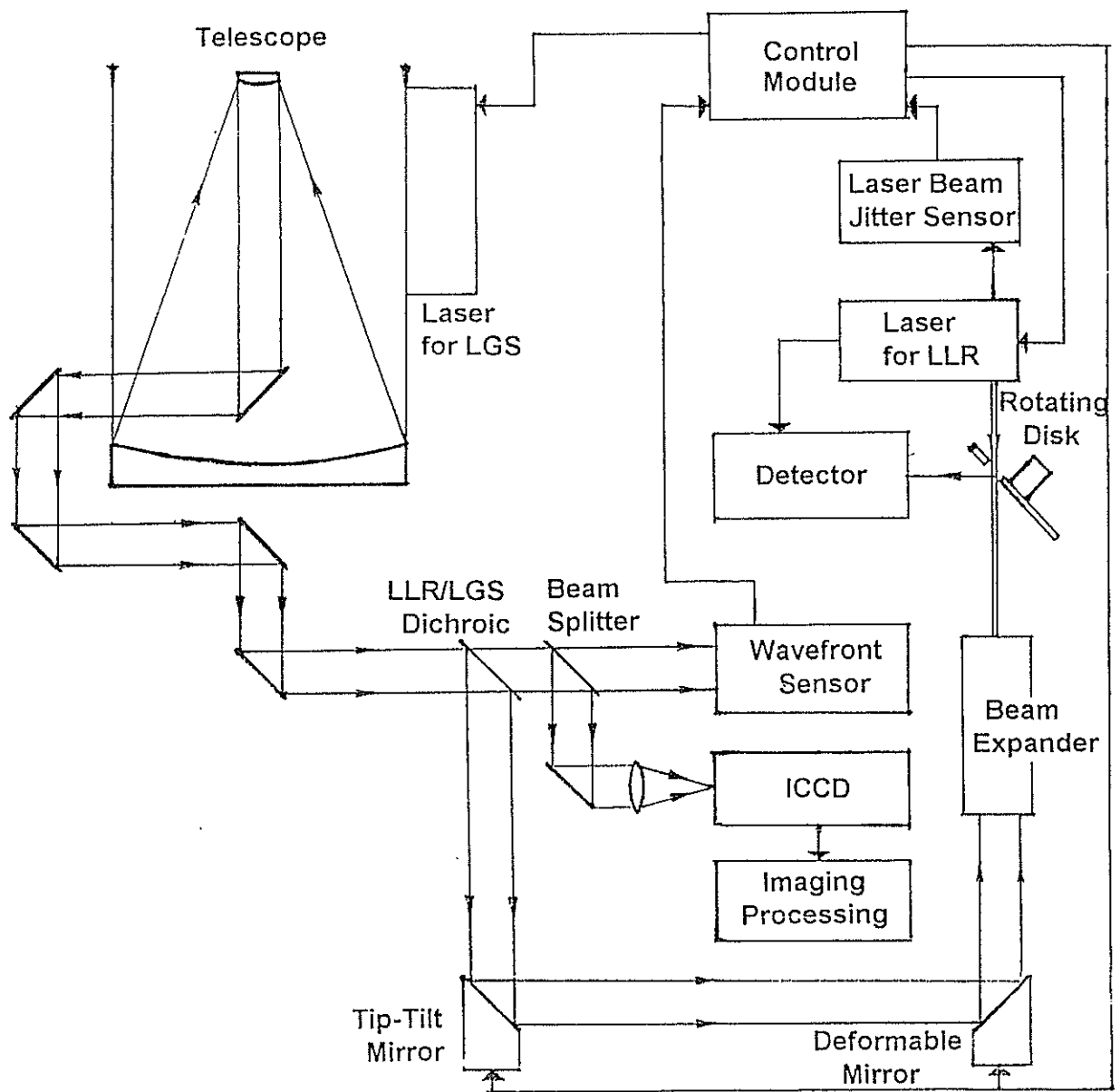
Fig.1. Compensated LLR System Diagram

Target Design, Signature and Biases

AMPLITUDE CORRECTIONS TO DELAY MEASUREMENTS

John Luck, Tom Stamp, Mark Elphick and Suzanne Jackson

Orroral Geodetic Observatory
Australian Surveying and Land Information Group
PO Box 2, Belconnen ACT 2616, Australia

Phone: +61 (6) 235-7111
Fax: +61 (6) 235-7103
E-mail: johnluck@auslig.gov.au

Abstract

The relationship between delay variations and received signal strength has been calibrated for the MCP in use at Orroral, and the resulting linear formula is routinely applied to all satellite measurements on a shot-by-shot basis. The calibration is effected by varying several parameters such as MCP voltage, PLZT polarization and pointing while ranging to the ground target and the real-time external calibration target. This procedure has resulted in substantial improvement in station performance especially on the stronger satellites. Fitting a cubic polynomial over a limited amplitude range can give even better results.

The procedure has also proved to be a valuable diagnostic tool.

1. Introduction

It is well known that the propagation delay in a laser ranging system depends upon the intensity of light hitting the detector, and voltage applied to the detector. It is one of the functions of the discriminator to eliminate - as far as possible - the delay variations arising from such amplitude variations coming from the detector. A great deal of effort, and mystic art, goes into setting up the discriminator in stations using MCP-type detectors. Nevertheless, delay variations remain which affect adversely the precision and accuracy of ranging results, especially for very 'bright' targets such as TOPEX/POSEIDON and AJISAI which yield uncontrollably large fluctuations in received intensity.

The relationship between delay variation and amplitude variation has been calibrated by measuring these quantities as the intensity of return signal from local calibration targets, and MCP voltage, are varied in a controlled manner. It has been found that substantial improvements in satellite r.m.s., and some improvement in range biasses, result.

2. Experimental Configuration

The equipment used is exactly the same as used in normal ranging to satellites and to ground targets. It is described in Table 1. The physical arrangements are as shown in [Luck,1994]. The "PLZT" operates for the calibration targets "Spider" and "Rock" but not for satellites, and is varied by the operator during ranging to equalize (approximately) the signal strengths being received from both "Spider" and the satellite at the time.

Being a polarization-induced attenuator, the transmission T of the PLZT is given by:

$$T = A + B \sin^2(\pi P/2000)$$

where A and B do not need to be known, and P is the setting between 0 and 1000 which controls the voltage applied to the PLZT. The amplitude from the MCP nominally doubles for each 100 volt increase in its applied voltage M.

As the parameters P and M are varied, the following observables are measured every shot:

s: Signal strength from Charge Digitizer, in arbitrary counts (0-1024)
c: Real-Time ("Spider") Calibration delay, in nanoseconds
r: Ground target ("Rock") delay residual, O-C, in nanoseconds.

TABLE 1 : Equipment Configuration for Amplitude Dependence Calibration

Ground Target:	50mm solid retroreflector on a "Rock" 1.1km distant
Real-Time Target:	20mm solid retroreflector mounted on telescope "Spider" vanes
Variable Filter:	"PLZT", electrically controlled crossed polarizing ND filter
Detector:	ITT F4129f z-plate "MCP" PMT
Discriminator:	Tennelec 454 CFD cascaded according to NASA setup
Charge Monitor:	LeCroy 2249A ADC "Charge Digitizer", accessed via CAMAC Dataway
Event Timer:	LeCroy 2229A TDC, modified, accessed via Electro Optic Systems MRCS

3. Linear Model for Calibration

The calibration model adopted in November 1995 has the following form for each return 'i':

$$c_i = c_0 + a.(s_i - 130)$$

$$r_i = r_0 + a.(s_i - 130)$$

where s, c and r are defined above, c_0 and r_0 are the estimated values when the signal strength reads 130 - which was the average value observed from LAGEOS I & II passes over the previous twelve months - and the most important estimated value is 'a', the slope in nanoseconds/count. The observation equations are coupled through the solution parameter 'a', so are solved together by the method of least squares.

Subsequently, the range 'x' nanoseconds on every shot 'j' is corrected by:

$$x_j(corrected) = x_j - a.(s_j - 130).$$

3.1 Cubic Model

A cubic model of the following form has been tested but not implemented:

$$c_i = c_0 + a.(s_i - 130) + b.(s_i - 130)^2 + c.(s_i - 130)^3$$

$$r_i = r_0 + a.(s_i - 130) + b.(s_i - 130)^2 + c.(s_i - 130)^3$$

4. Results

Figure 1 shows how the signal strength (amplitude) measurements vary as the parameters P (PLZT setting, in counts) and M (MCP volts) are varied, from a session of ground target ranging in which each setting was held for one minute, yielding approximately 250 returns per setting. It is clear that, particularly for the Ground Target, the $\sin^2 P$ law for the PLZT applies approximately, until the signal strength exceeds 500 counts.
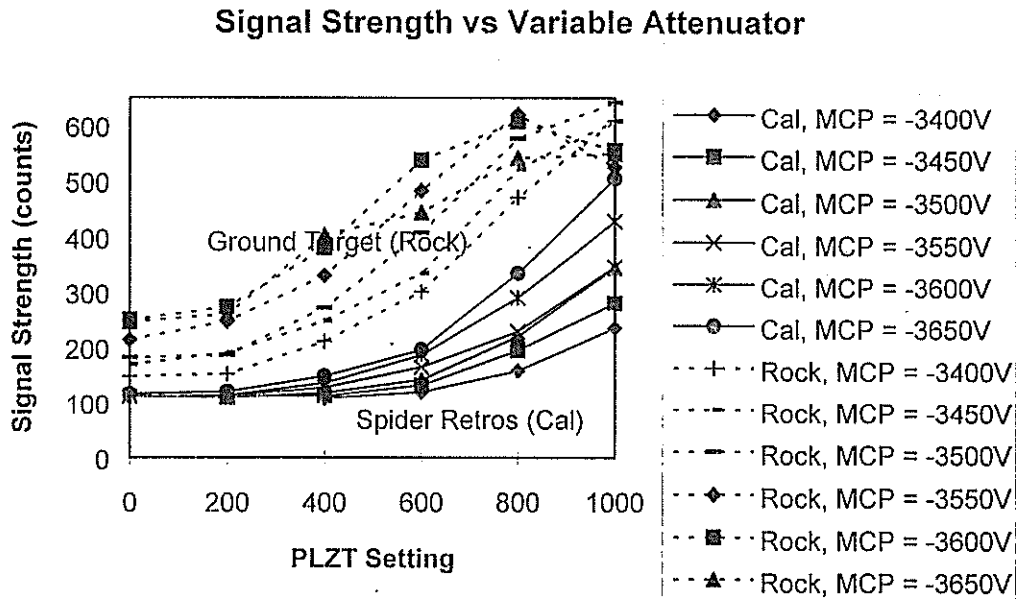
Figure 1: Amplitude variation as PLZT setting and MCP volts are varied systematically.

In Figure 2, the corresponding effects on propagation delay are plotted, relative to an arbitrary zero point. There is a very large increase in delay for large PLZT settings and high MCP volts, ie when signal strength exceeds 500 counts.
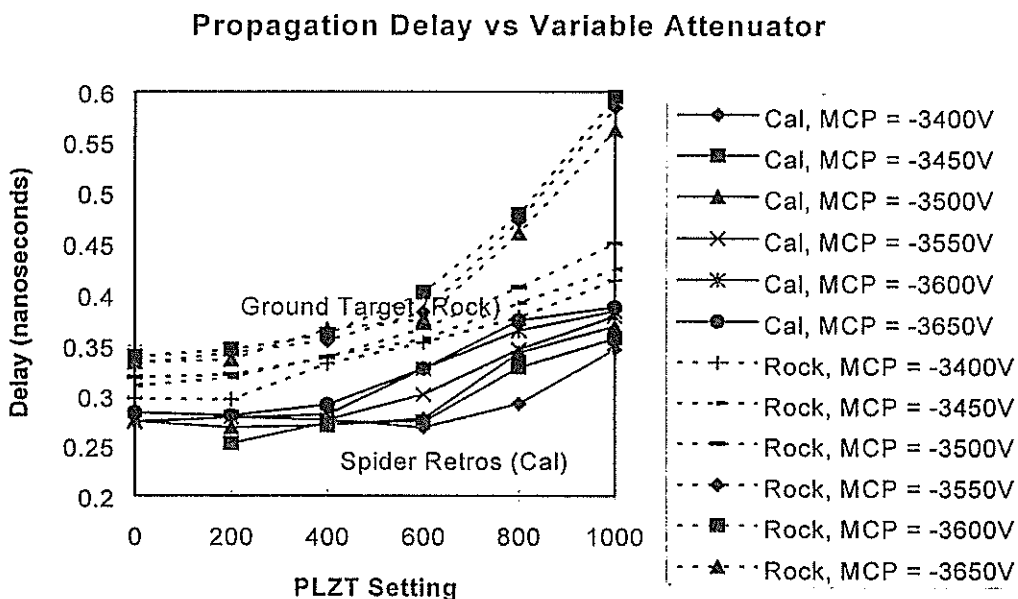
Figure 2: Propagation delay variation as PLZT setting & MCP volts are varied systematically.

4.1 Linear Model Fit

The linear model was then fit to the Delay vs. Signal Strength data implicit in Figures 1 and 2. The residuals from the fit are shown in Figure 3. Note that, for clarity in the graph, 1000 counts have been added to the Signal Strength values for the Rock residuals on the right-hand side of the graph - they really overlap the points for the Spider in the left-hand half. Obviously, some points above 520 counts (shown as 1520 counts) should have been deleted - they are the same points showing non-standard behaviour in Figures 1 and 2.

AMPLITUDE DEPENDENCE - 963092346.linear
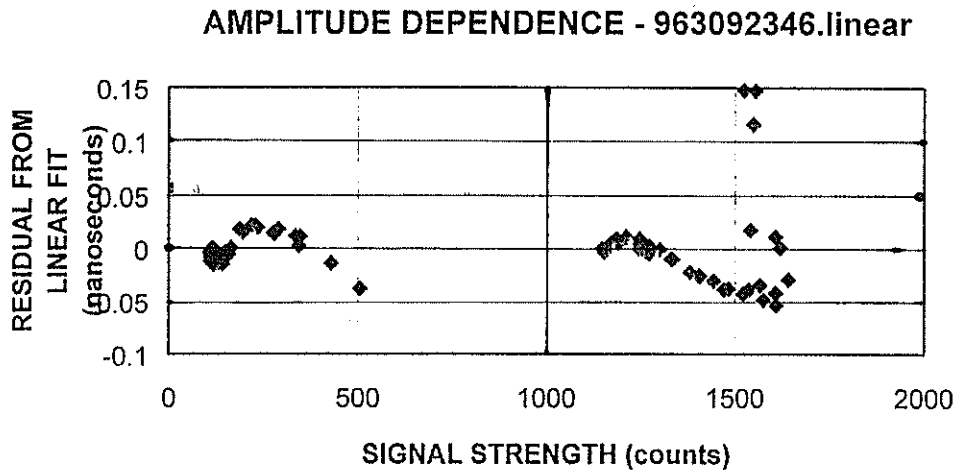
Figure 3: Residuals from linear fit to amplitude calibration data. Note that ground target data has been shifted to the right by 1000 counts, for clarity.

A similar procedure was followed for a set of calibration data observed in October 1995. Its linear solution yielded:

$a = 0.409$ picoseconds/count :- adopted on 26 November 1995
r.m.s. of residuals about the fit = 15 picoseconds.

4.2 Cubic Model Fit

Figure 4 shows the results when the cubic model is fitted through the previous data set, restricted to signal strengths less than 520 counts. Again, the Rock values have 1000 counts artificially added for graphing clarity. The r.m.s. of the residuals is now 6 ps. The repeatability of this result has not yet been established, so it has not been adopted.

AMPLITUDE DEPENDENCE - 963092346.cubic
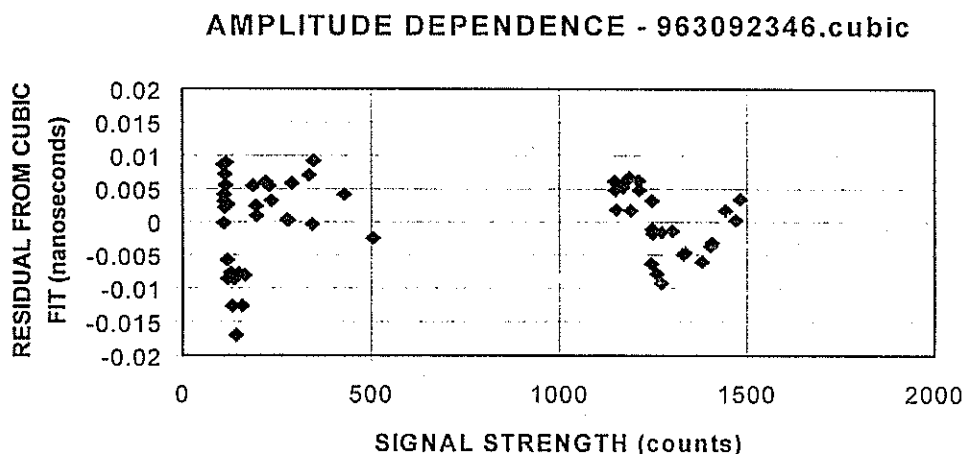
Figure 4: Residuals from a cubic fit to amplitude calibration data, restricted to signal strengths less than 520 counts. Note that ground target data has been shifted to the right by 1000 counts, for clarity.

4.3 A Pathological Case

A set of data taken on a previous occasion is displayed in Figure 5. Something is wrong!

AMPLITUDE DEPENDENCE: 9629408
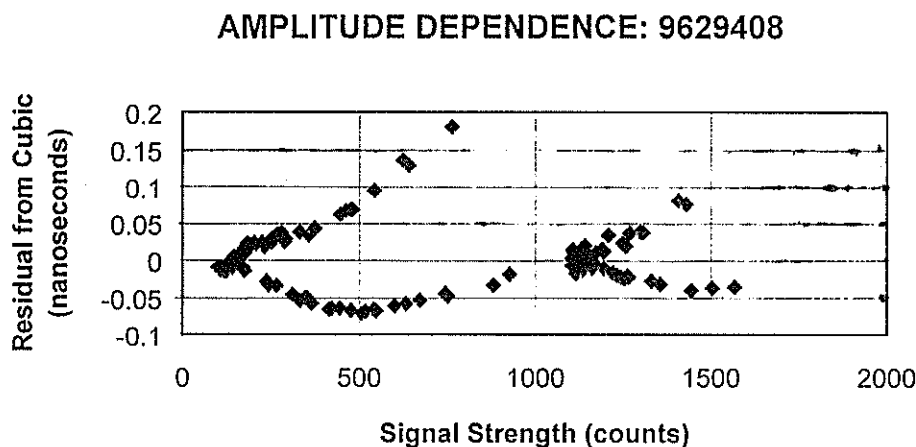
Figure 5: Residuals from a cubic fit to some pathological data. Note that ground target data has been shifted to the right by 1000 counts, for clarity.

It turns out that, due to a malfunction of a Ledex flip mirror, the beam was hitting the edge of the MCP aperture, not the centre. This type of analysis, plus careful examination of the shapes of the curves in Figures 1 and 2, have proved to be very useful diagnostic tools.

5. Effect on Precision and Range Bias

Application of the linear model correction has reduced the Orroral LAGEOS r.m.s. from about 70 ps single-shot to typically 45 ps. As expected, little effect has been noted on the range biasses for LAGEOS as reported in the University of Texas Center for Space Research's weekly analyses because the model has been normalised to LAGEOS results and the amplitude variation is small, anyway.

Topex/Poseidon range biasses improved considerably as a result [Dunn,1996]. Figure 6 illustrates a pronounced move towards zero and much smaller scatter of range biasses from Cycle 118 which started on 95 Nov 17, about when the new algorithm was implemented. These data from the TOPEX Precision Orbit Determination Group do not contain the spurious height rate of 9.3mm/year previously attributed to Orroral. Dunn's data also shows a decrease in the Normal Point r.m.s. from 15mm to 9mm from the same date.

Orroral Range Biasses from TOPEX
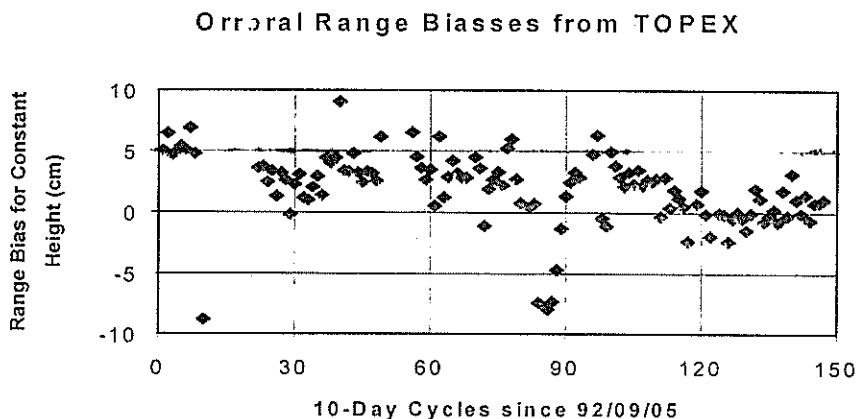
Figure 6: Orroral range biasses from Topex/Poseidon data [Dunn,1996]. The new algorithm was introduced at Cycle 118.

6. Summary and Conclusions

The linear model has been adopted with confidence in its applicability because of the controllability and repeatability of the calibration experiments which use identical equipment and configurations as in normal ranging operations. It has produced substantial improvements to r.m.s. of ranging results, both for single-shot and normal-point estimations. Range biasses from TOPEX/POSEIDON have reduced and tightened noticeably.

The adopted value for the slope coefficient is 0.409x10^{-3} nanoseconds/count. It was implemented on 26 November 1995.

The calibration procedure should be repeated at regular intervals, both because the constants need to be verified, and because the procedure highlights malfunctions in the ranging system.

An improved model obtained by fitting a cubic polynomial instead of a straight line, and by restricting amplitudes to certain admissible limits, can reduce the r.m.s. error from this source to 6 ps. It will undoubtedly be introduced in due course.

7. References

Dunn, P.J. (1996): Private communication - Topex data.

Luck, J.McK (1992): "Performance of the Upgraded Orroral Laser Ranging System", Proc. 8th International Workshop on Laser Ranging Instrumentation, Annapolis, MD, NASA Conf.Publ. 3214, p.11-6 ff.

ACCURACY OF THE SATELLITE LASER RANGING

S.SCHILLAK

SPACE RESEARCH CENTRE
OF POLISH ACADEMY OF SCIENCES
BOROWIEC ASTROGEODYNAMICAL OBSERVATORY
62-035 KÓRNIK, POLAND
tel: +48-61-170-187
fax: +48-61-170-219
e-mail: sch@cbk.poznan.pl

ABSTRACT. Accuracy of laser measurements is one of the most important parameters of SLR systems which determines the reliability and thus usefulness of results. It is of particular significance in determination of coordinates in the geodynamic projects. Accuracy includes contributions of two components: random error and systematic biases, and care should be taken to keep them as low as possible. The paper discusses contributions due to main sources of single shot RMS including: laser pulse width, detector time spreading, precision of time interval counter and electronic systems. Systematic bias combines the effects of the atmosphere, standard frequency inaccuracy (range bias and time bias), calibration system (the problem of the mean level of return pulses), accuracy of meteorological read out, target distance and position of the reference point. The effects of the photons distribution in front of the detector such as range bias dependence on the signal strength and pulse attenuation, and skewness in the residuals distribution were the subjects of particular interest.

The main aim of satellite laser ranging is determination of a distance between a stable point of the telescope and the satellite mass centre. This distance should be measured with a maximum accuracy, that is our results should be as close as possible to the real distance between these points. Each process of physical measurement is charged with two kinds of errors: random ones (precision) and systematic biases.

1. Precision.

The ideal measurements give a normal distribution of deviations. Other distributions can be expected when the effect of an experiment is asymmetrical or our experiment is disturbed by certain physical phenomena. In such situations the problem appears of a systematic bias as a difference between the peak value and the mean in the distribution of deviations. Table 1 gives contributions of the main sources of random errors in the satellite laser ranging which are the width of a laser pulse, jitter of the detector and precision of the electronics. The contributions due to these sources have been estimated for the best parameters of SLR systems in 1996 and for the corresponding parameters expected to be achieved in the year 2000. The contribution of the laser pulse width has been estimated taking into account the distribution of photons in front of the detector for the single-photoelectron level and the standard deviation of this distribution in centimetres. The standard deviation of the detector time spreading was assessed assuming that the detector jitter for a single-photoelectron pulse is 3σ. The standard deviation of errors due to the electronics (mainly the time interval counter or event timer) can be found experimentally (inner calibration without the detector) and the result is usually in agreement with technological specification of the instrument. In general we know the precision on site

immediately after the satellite pass, and then sources of significant random errors can be found for each station. This RMS can be additionaly reduced by assuming normal points as means in certain time intervals.

Table 1. PRECISION
(Single Shot RMS)

ERRORS SOURCES	THE BEST SYSTEM 1996	NEAR FUTURE
WIDTH OF THE LASER PULSE - 35 ps => 20 ps	±1.7 mm	±1.0 mm
DETECTOR'S JITTER 100 ps => 25 ps	±5.0 mm	±1.2 mm
ELECRONIC'S JITTER 25 ps => 10 ps	±3.7 mm	±1.5 mm
TOTAL SINGLE POINT RMS	±6.4 mm	±2.2 mm
TOTAL NORMAL POINT RMS	±0.6 mm	±0.2 mm

Table 2. SYSTEMATIC BIASES

ERRORS SOURCES	THE BEST SYSTEM 1996	NEAR FUTURE
ATMOSPHERIC PROPAGATION	±5 mm	±2 mm
METEOROLOGICAL MEAS.	±1 mm	±1 mm
SATELLITE CENTRE OF MASS	±2 mm	±1 mm
SIGNAL STRENGTH VARIATION	±3 mm	±2 mm
TEMPORAL VARIATION	±2 mm	±1 mm
CALIBRATION PATH	±1 mm	±1 mm
CALIBRATION PATH - METEO	±1 mm	±1 mm
MOUNT ECCENTRICITIES	±1 mm	±1 mm
TOTAL	±6.8 mm	±3.7 mm

Table 3. MAIN PROBLEMS

ATMOSPHERE MODEL => TWO-COLOR RANGING

SATELLITE CENTER OF MASS => NEW TYPES OF CUBE CORNERS

CALIBRATION METHOD => SIGNAL STRENGTH
SATELLITE = CALIBRATION

PRECISION UPGRADING => BETTER DETECTORS
NEW TIME INTERVAL COUNTERS (<10 PS)
SHORTER LASER PULSE

ORBITAL METHOD => ACCURACY BETTER THAN 1 CM

COST => NEW GENERATION AUTOMATIC
STATIONS

MAX. ACCURACY
NOW = ±9 mm => FUTURE = ±4 mm

2. Systematic biases.

Identification and determination of systematic errors is much more difficult. The information on the contribution of systematic biases can be obtained after analysis of the satellite orbit, and unfortunately, the contribution of the errors following from the orbital method is significant particularly for the best stations. The main sources of systematic deviations are specified in Table 2. The problems related to the accuracy of measurements and the proposed ways of their elimination are illustrated in Table 3. The most important problem is the atmospheric delay which is probably greater than 5 mm but unfortunately, this effect has been rather poorly recognised. The use of two- or multi-colour measurements can reduce the contribution of this effect to about 2 mm, however, high cost and technological difficulties inhibit realisation of this task . The other systematic biases are relatively small and not so difficult to establish. Among them particular attention should be paid to the effects of varying the strength of the return signal. This effect is particularly important for photomultipliers and avalanche photodiodes where it is known as the time walk.

3. Signal strength variation.

Systematic bias related to the varying strength of the return signal originates from two sources: a distribution of photons in front of the detector and the amplitude of the return signal. The second source is related to the types of the detector and discriminator used and is discussed in detail in a few other papers in these Proceedings. The mean distribution of photons in front of the detector, for a gaussian laser pulse of full width of 200 ps and a few levels of the signal strength is illustrated in Fig. 1. For a weak signal the detector start is delayed and when the calibration is not at a similar level the results will be charged with range bias. In order to avoid this problem particular care should be taken to control the strength of the return signal during the calibration and satellite observation. For the multi-photoelectron method the effect will be more pronounced because of changes in the signal strength during the satellite pass and difficulties in establishing a proper mean calibration amplitude. For the single-photoelectron

method the situation will be more stable. Moreover, the use of an attenuator eliminates inner pulses and the probability of range bias occurrence diminishes.

Another effect due to a distribution of photons in front of the detector is the skewness of the pulse. This effect appears for weak single photoelectron pulses (Fig. 2), as the probability of the detector start by photons on the right - hand side is greater (greater number of photons) than by those on the left. Consequently, the distribution of deviations is asymmetrical. For strong pulses this effect is very small so in practice it can be neglected. The contributions due to all the effects related to the varying strength of the signal can be reduced by the use of shorter laser pulses.

The effects related to the varying strength of the return signal have been assessed on the basis of laser observation data from Borowiec SLR collected in October 1996. The passes of LAGEOS are divided into two populations, those with weak signals (12 passes, less than 300 returns per pass) and strong signals (11 passes, about 700 returns per pass), see Figs. 3a and b, respectively. For weak signals the skewness and the difference between the peak value and the mean (12mm) are clearly visible, whereas for strong signals these effects do not appear. A similar analysis was performed for the distribution of calibrations for exactly the same passes, see Figs. 4a and b. The results are similar which means that the level of the calibration signal is similar to that of the observed signal, consequently, the range bias of results of the laser ranging in Borowiec is not caused by the effects of this kind. The effect of the signal attenuation is noticeable in the passes of TOPEX/ POSEIDON. For LAGEOS we do not use the attenuator while for low satellites we use 8dB attenuation. In the case of the latter, RMS is lower and the distributions of deviations for the observations (Fig. 5a) and calibrations (Fig. 5b) are close to the normal one without the skewness and significant differences between the peak and the mean. However, the calibrations are a bit too good.
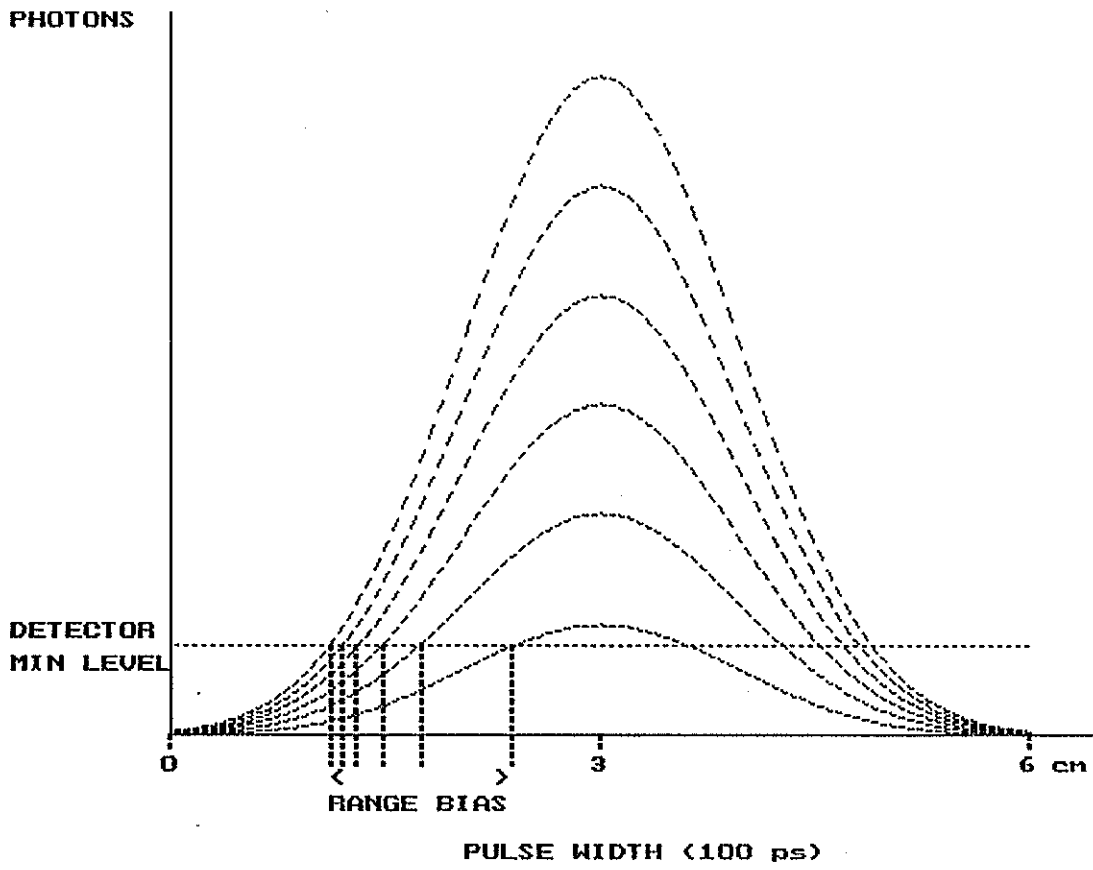
Fig. 1

Fig. 2

RESIDUALS DISTRIBUTION
STATION: BOROWIEC   SATELITTE: LAGEOS   12 PASSES


```
No. Pts    = 3400
Pts/pass   =  283
RMS        = 5.93 cm
Skew       = 0.02
Kurt       = 2.67
peak-mean=-12.0 mm
```

a)

RESIDUALS DISTRIBUTION
STATION: BOROWIEC   SATELITTE: LAGEOS   11 PASSES


```
No. Pts    = 7626
Pts/pass   =  693
RMS        = 5.57 cm
Skew       = 0.00
Kurt       = 2.66
peak-mean=-0.0 mm
```

b)
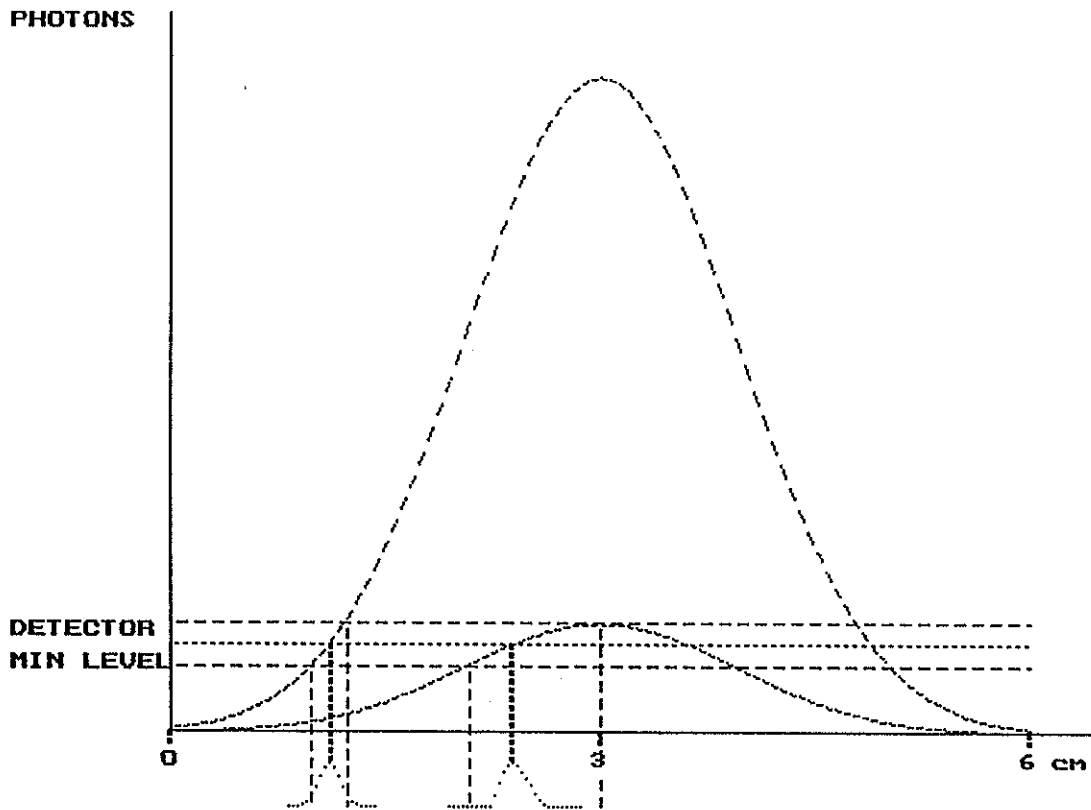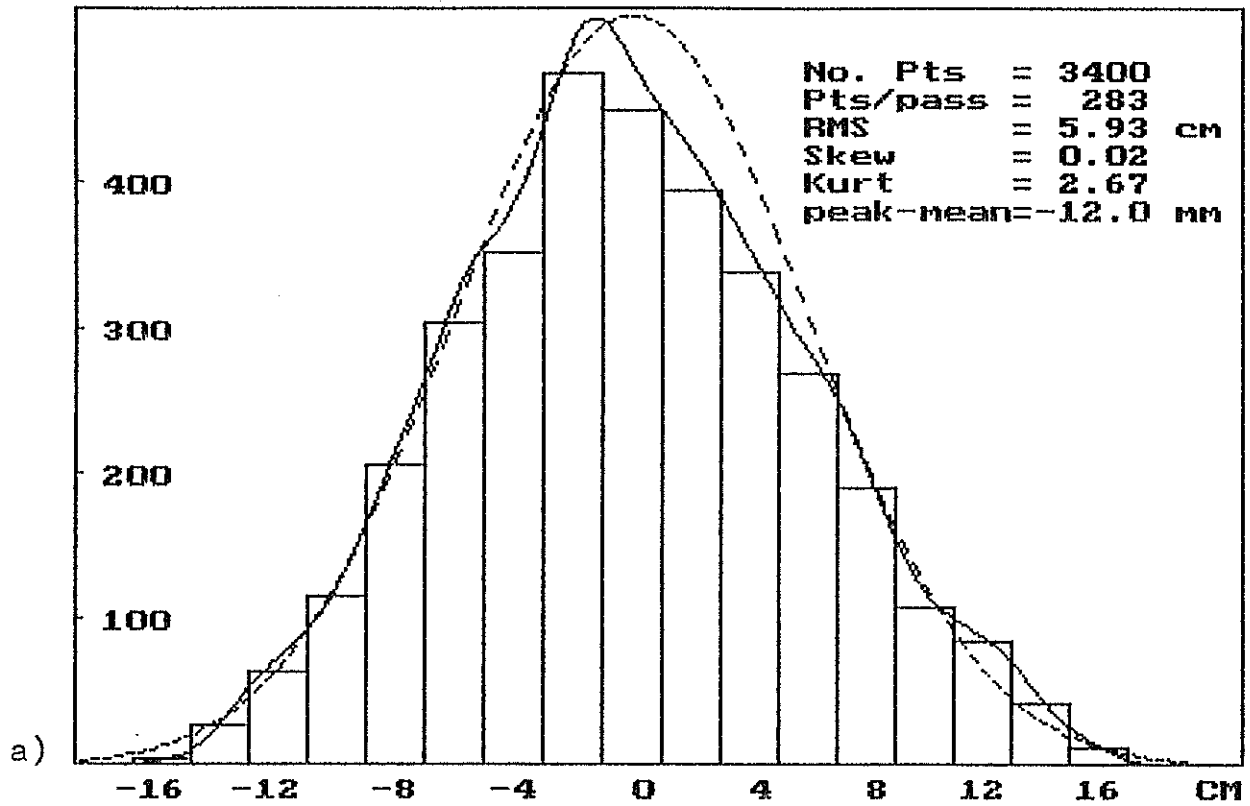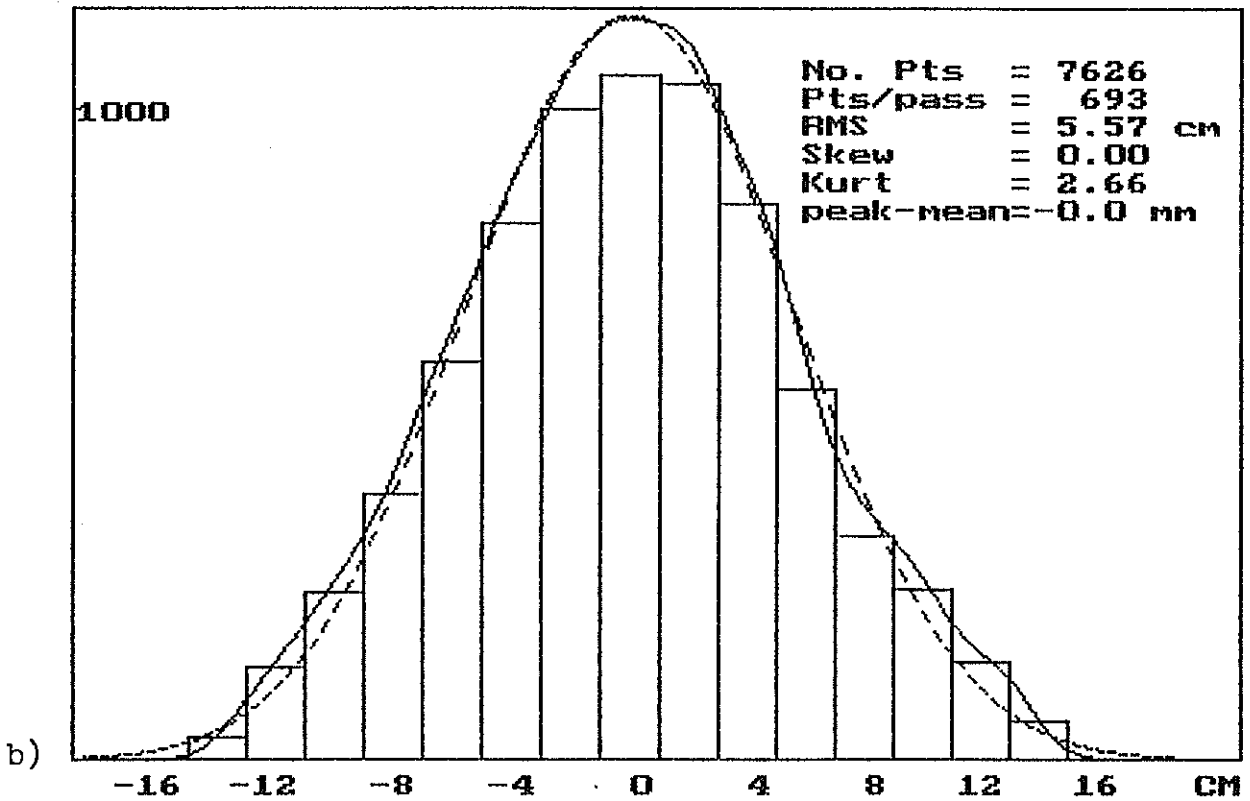
Fig. 3

RESIDUALS DISTRIBUTION
STATION: BOROWIEC   CALIBRATION   23 SERIES

No. Pts = 2015
Pts/ser =   87
RMS   = 4.92 cm
Skew   = 0.01
Kurt   = 2.98
peak-mean=-12.0 mm

a)
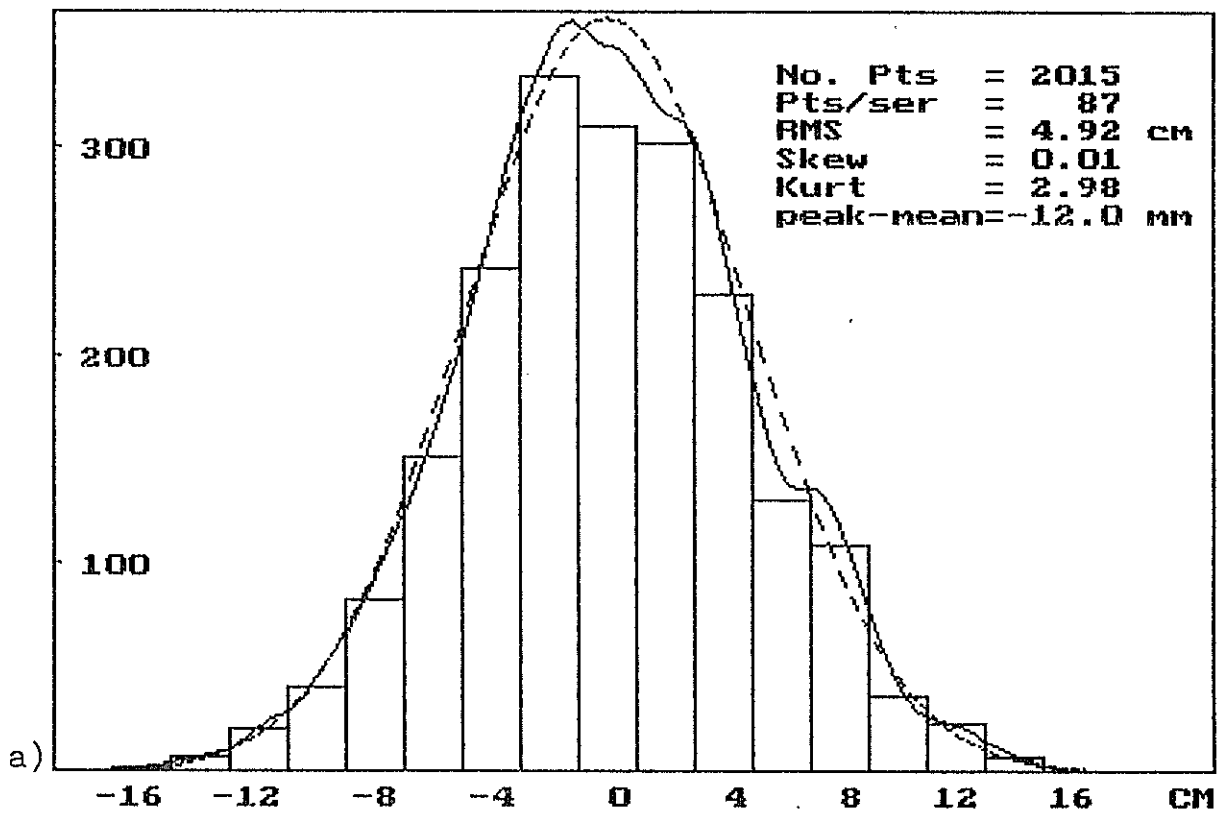
RESIDUALS DISTRIBUTION
STATION: BOROWIEC   CALIBRATION   20 SERIES
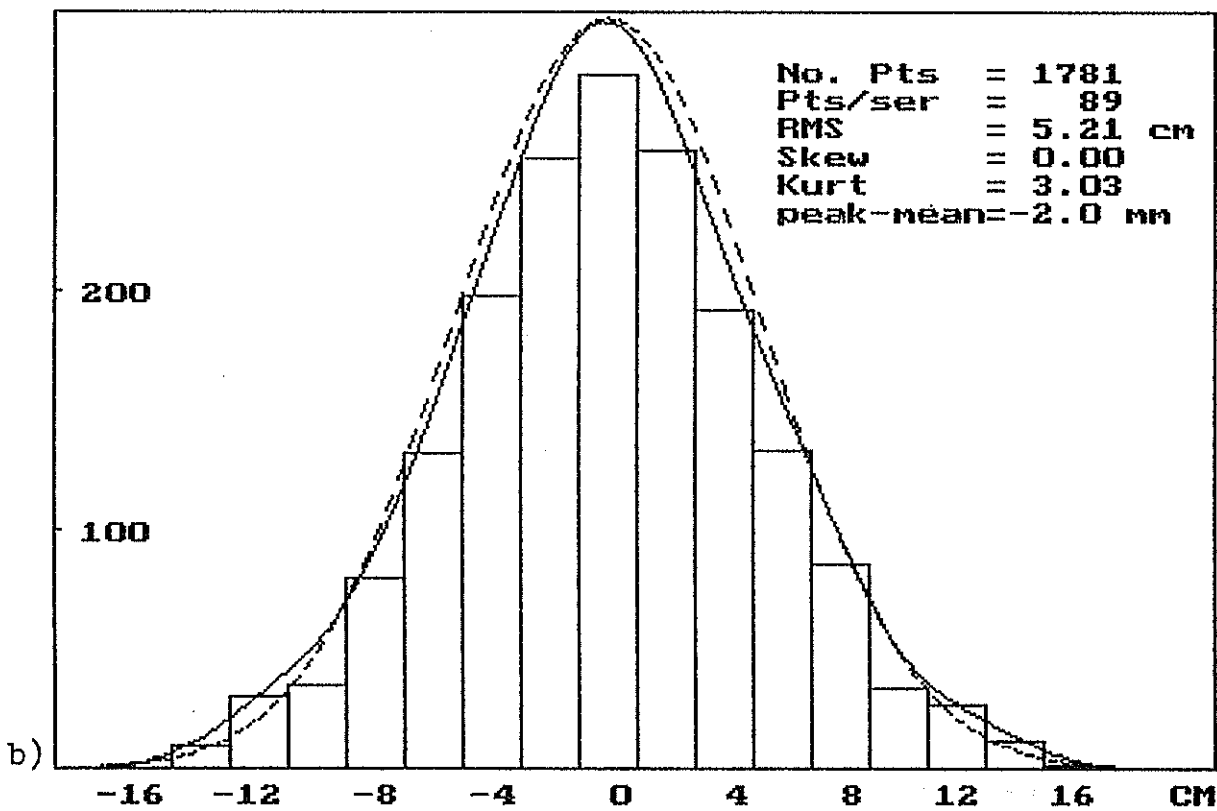
No. Pts = 1781
Pts/ser =   89
RMS   = 5.21 cm
Skew   = 0.00
Kurt   = 3.03
peak-mean=-2.0 mm

b)

Fig. 4

214

RESIDUALS DISTRIBUTION
STATION: BOROWIEC   SATELITTE: TOPEX   12 PASSES

No. Pts   = 24622
Pts/pass = 2051
RMS   = 3.85 cm
Skew   = 0.00
Kurt   = 2.73
peak-mean=-2.0 mm

a)
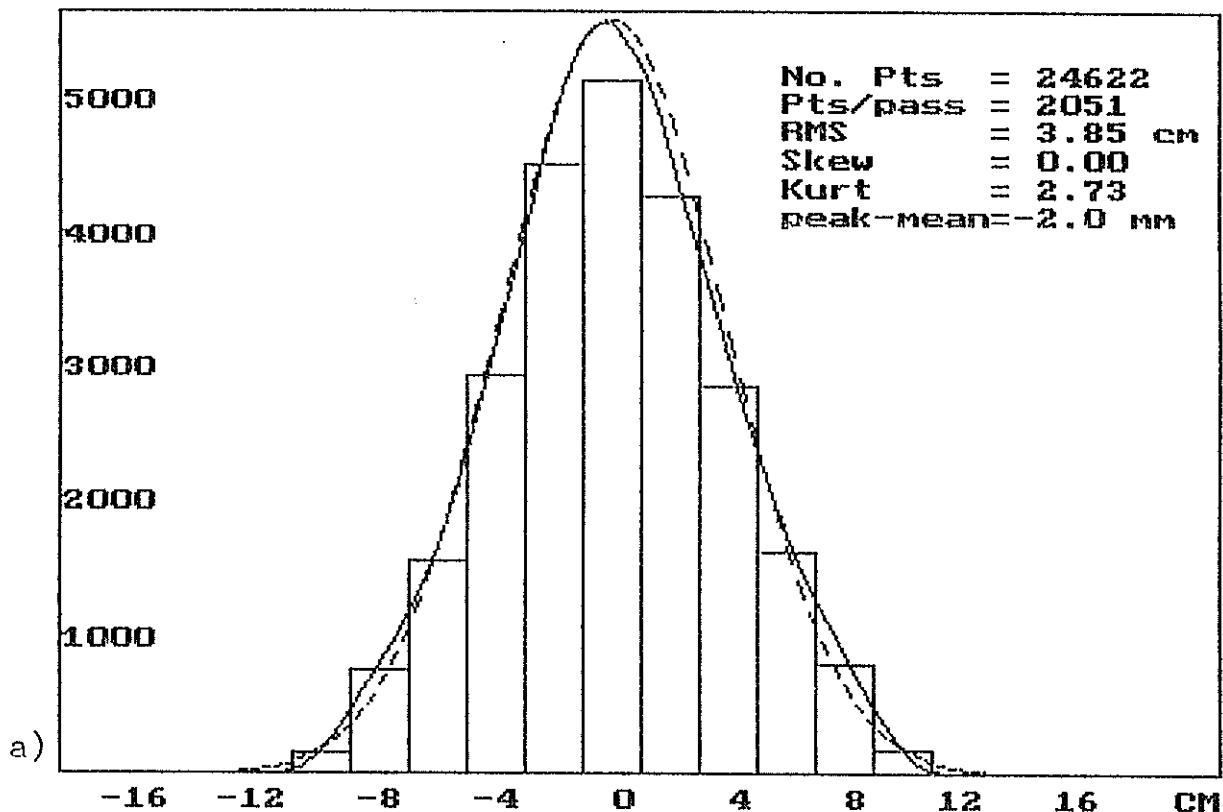
RESIDUALS DISTRIBUTION
STATION: BOROWIEC   CALIBRATION   24 SERIES

No. Pts   = 2257
Pts/ser   =   94
RMS   = 3.23 cm
Skew   = 0.00
Kurt   = 3.12
peak-mean=-6.0 mm

b)
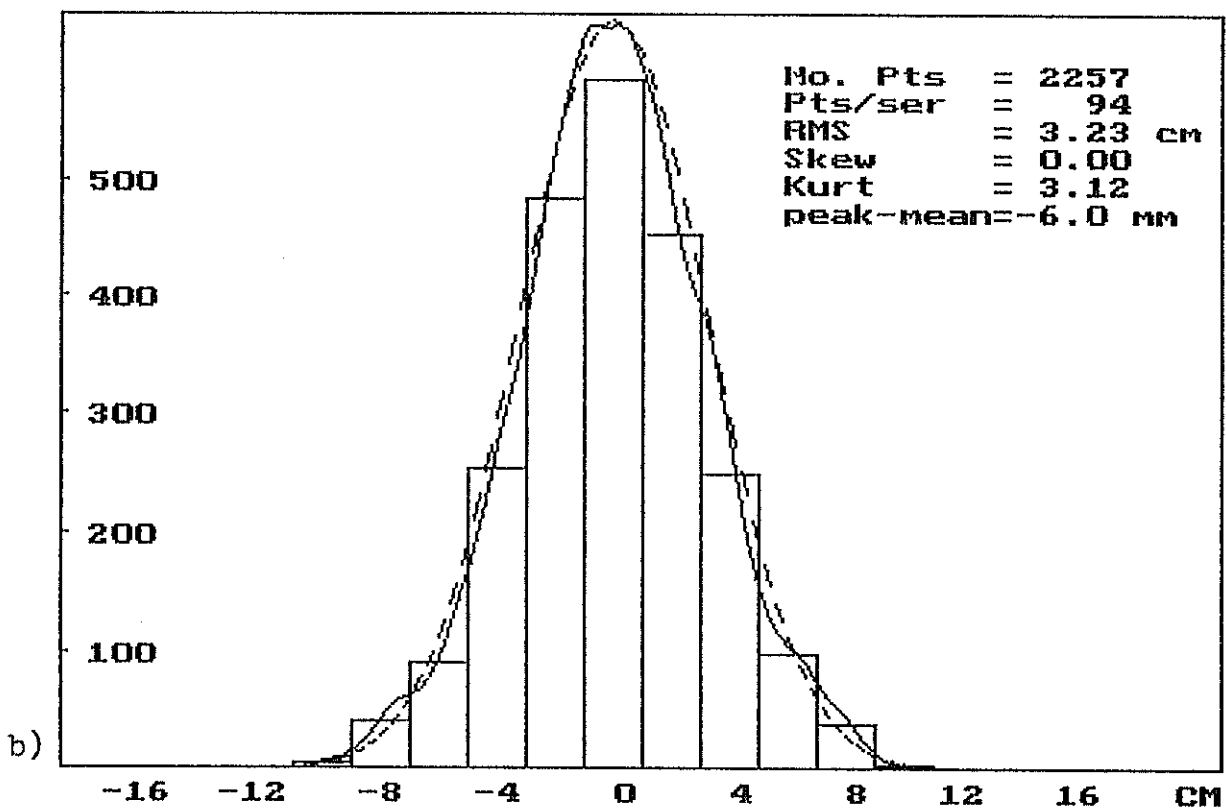
Fig. 5

Preliminary Design of the Laser Reflector Array for the CHAMP Satellite

Reinhart Neubert
GeoForschungsZentrum Potsdam, Div.1: Kinematics and Dynamics of the Earth
Telegrafenberg A17, D-14473 Potsdam, Germany
Tel.: (49)-331-288-1153, Fax.: (49)-331-288-1111, e-mail: neub@gfz-potsdam.de

Introduction:

The CHAMP mission is dedicated to the study of the Earth's gravity field, magnetic and electric fields as well as for sounding of the atmosphere [10]. The high resolution accelerometer will give the unique possibility to measure the non-gravitational forces acting on the surface of the satellite. The result could be an accuracy improvement of the derived geoid undulations at about 1000 km wavelength by one order of magnitude compared to the present knowledge.
Main data source for the orbit determination will be an advanced space-born GPS receiver providing full global coverage. Laser ranging will be used as a supporting and independent data source for orbit determination. Its limitation is the rather poor global and temporal coverage but the SLR data are free from ambiguities and directly related to the terrestrial reference frame.
The CHAMP satellite (Fig.1) shall be launched in mid 1999 into a near circular polar (83°) orbit with 470 km altitude above ground. It is expected that the altitude will go down to 300 km after about 5 years and then decay very fast.
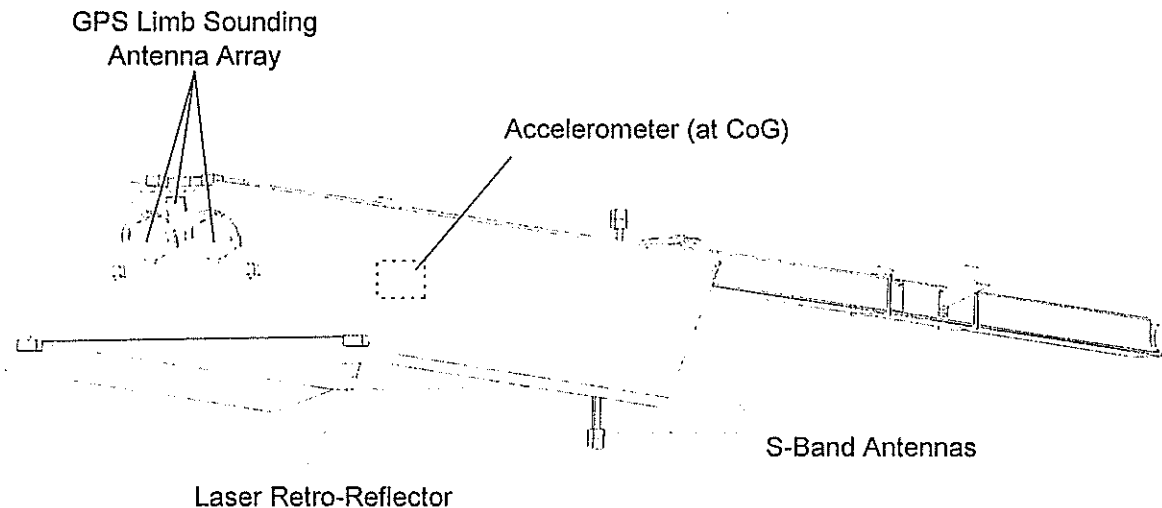
Fig.1 : Schematic drawing of the CHAMP satellite

Design philosophy of the reflector

The first requirement of the laser reflector is to enable the worldwide SLR station network to track the satellite with a resolution of about 1 cm. This can be fulfilled quite easily using a small array of standard design like the ERS-1 reflector for instance. Recent improvements of the SLR technology suggest to make the reflector suited for very high resolution ranging. Especially there is a lack of targets for demonstrating the power of the dispersion method (two-colour ranging).

An ideal target would be a single cube corner reflector but because of its limited angular field it is not well suited for very low orbiting satellites. An example of this type is the special purpose RIS reflector [5] on ADEOS. Another approach for spherical (rotating) satellites, proposed by Degnan [2], uses a high number of evenly distributed cube corners with a drastically reduced field of view. The first realization of this idea will be the WPLTN-1 satellite [8] with only one prism visible at any orientation. The drawback of this design is the strong fading: in about 50 per cent of the orientations the signal will be extremely weak or zero but this is tolerable for the goals of the WPLTN-1 project.

In the case of CHAMP we prefer a more simple and compact design similar to the concept of the GLRS-R reflector [6],[7]. It consists of four prisms only. This concept implies the use of the full unrestricted angular field of the cube corners to get sufficient coverage..

Estimation of the Ranging Performance

The following calculations of the performance parameters assume the use of standard quartz prisms with 19.1mm vertex and 45 degrees inclination of the front faces. The radial distance of the centers of the front faces of each prism from the symmetry axis of the array has been set to 33 mm.

The most interesting performance parameters are the variation of the signal strength and the location of the effective reflection plane (range correction). Special attention has to be paid to the influence of aberration and diffraction.

Basic relations

Signal Strength

The signal variation is mainly governed by the effective reflecting aperture, diffraction, the range and the atmospheric transmission. The dependence of the active reflecting aperture of a cube corner with circular front face can be approximated by a linear relation [3]. In addition the far field diffraction pattern is changing because the shape of the active area becomes more and more elliptical with increasing angle of incidence. If the station would be always in the centre of the far field, the combined effect can be approximated by the simple relation:

$$I(\alpha) = \left| 1 - \frac{\alpha}{\alpha c} \right|$$

Eq.1

where the cut-off angle αc is about 0.85 radians. Actually the station is not in the maximum of the far field in general because of velocity aberration. Nevertheless we are using the simple Eq.1 for this preliminary study. The real intensity can be weaker by as much as a factor of three to four. In addition we take the the R^{-4} dependence on range and the clear sky transmission [3] into account in the computation of the relative signal strength.

Range Correction

The range correction of the array refers to some reference point which can be defined arbitrarily.

We are using the intersection of the optical axes of the cube corners as a reference point. The reduction from this point to the centre of mass of the satellite can be done very precisely because of CHAMP's attitude stabilization. The range correction for a particular single prism to the reference point can be expressed by:

$$\Delta R = D \cdot \cos(\alpha) \quad L \quad n^2 \quad \sin(\alpha)^2 \qquad \cos(\alpha) = (\underline{N} \cdot \underline{C})$$

Eq.2

where D is the distance from the reference point to the centre of the front face, α the angle of incidence, L the vertex length an n the refractive index. The angle of incidence can be obtained from the scalar product of the unit vectors $\underline{N}$ (normal to the front face) and $\underline{C}$ (line of sigth direction).

Velocity Aberration

The angular displacement vector of the returning beam due to aberration can be expressed by the vector relation (first order approximation):

$$\underline{ab} = \frac{2 \cdot v}{c} \cdot (\underline{V} - (\underline{V} \cdot \underline{C}) \cdot \underline{C})$$

Eq.3

In this formula $\underline{V}$ and $\underline{C}$ are unit vectors parallel to the satellite velocity and the laser beam, v and c the absolute values of the velocities. The aberration vector is coplanar with $\underline{V}$ and $\underline{C}$ and orthogonal to $\underline{C}$.
The absolute value of the aberration is given by:

$$|\underline{ab}| = \frac{2 \cdot v}{c} \cdot \sin(\delta) \qquad\qquad \cos(\delta) = (\underline{V} \cdot \underline{C})$$

Eq.4

It has been suggested that the aberration is smaller for a moving prism because of the Fizeau effect and will be zero for a special value of the refractive index [11]. Return energy measurements using specially designed reflectors seem to confirm this prediction [12]. However, the special relativity theory does not predict such an effect. This can be seen easily when using a reference frame moving with the satellite. In this system the usual optical formulas for refraction and reflection are applicable. But the incoming laser beam as well as the apparent position of the station are shifted. The refractive index of the prism has no influence on aberration within the frame of special relativity. To explain the strong returns observed in the Fizeau experiments one has to look for some other effect. Possibly atmospheric distortion is responsible.
To be on the safe side, we decided to take the classical aberration into account in the case of the GFZ-1 satellite and for CHAMP as well.

Results

Let us first get an overview of the angular fields of the individual cube corners using Fig.2.
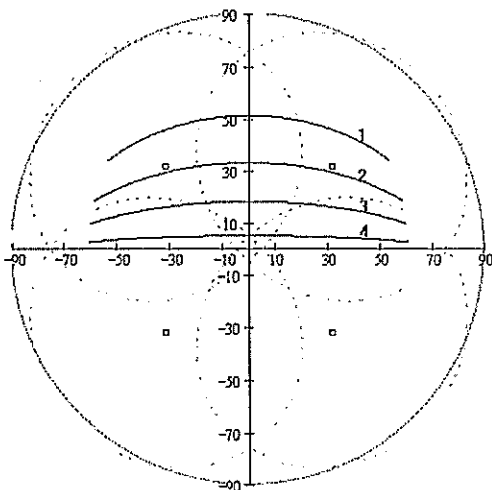
Fig.2: Polar plot of the angular fields of the cube corners.
Origin: Nadir direction.
Radial : Angle between Nadir and line of sight
Peripheral: Azimuth of line of sight (no scale printed)
Angular positions of the cube corner optical axes are
indicated by small boxes
Dotted curves surrounding the boxes: loci of the cut-off
Curves 1 to 4 : Angular tracks of the laser beam direction for passes with a culmination elevation of 32.4°, 53.7°, 70.0° and 84.5°, respectively.
The velocity vector is directed from left to right

From Fig.2 it can be seen that there is some overlap but regions where only one prism is contributing are existing as well.

For the visualization of the performance characteristics we use two representations:
a) mapping the parameters over the relative location between the station and the sub-satellite point
b) plotting the time dependence of the relevant parameters assuming circular orbits of different culmination elevation

Signal Strength

Fig.3 a,b are examples of the first representation. In these graphs the following coordinate system is used: Let the z-axis be directed from the geocentre to the satellite, the x-axis from the geocentre parallel to the
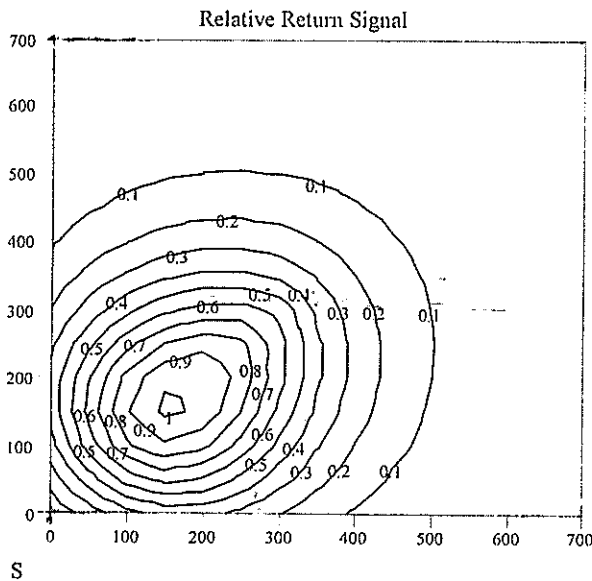
Fig. 3a: Relative signal strength over the station position . Origin: Sub-satellite poin The scale is in km
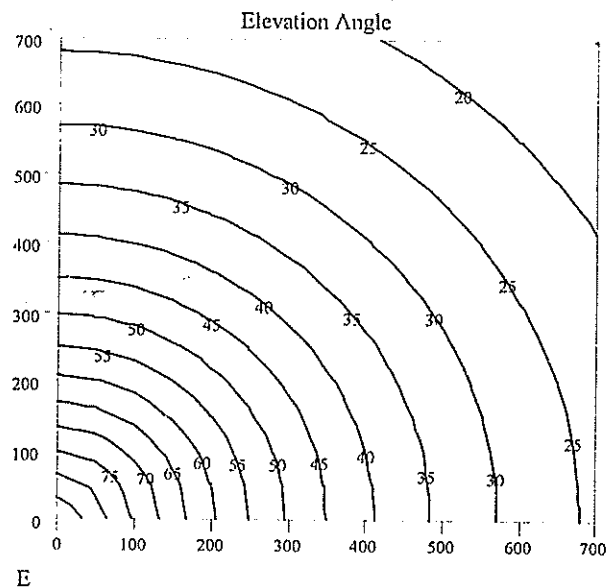
Fig.3b: Elevation angle over the relative station position.

satellite velocity and the y-axis orthogonal to both. Let the station coordinates vary on a spherical Earth. The coordinates x and y of the station are now used as the independent variables in Fig.5. That means that the origin corresponds to the sub-satellite point and x and y are the orthogonal distances of the station from the line geocentre to the satellite.

Fig.3a is a map of the relative signal of one prism. Only one quadrant is represented to avoid confusion .

Fig.3b maps the elevation angle in the same representation to enable cross-reference to this quantity.

In the following Fig.4 a..d we plot the relative signal versus time of all the individual cube corners. From these plots it can be seen that for more than 50 per cent of the total observation time one prism is responding only. Strong crosstalk between the reflectors are observed at very high elevation passes.

a) El=32.7°

b) El=53.7°

c) El=70.0°

d) El=84.5°
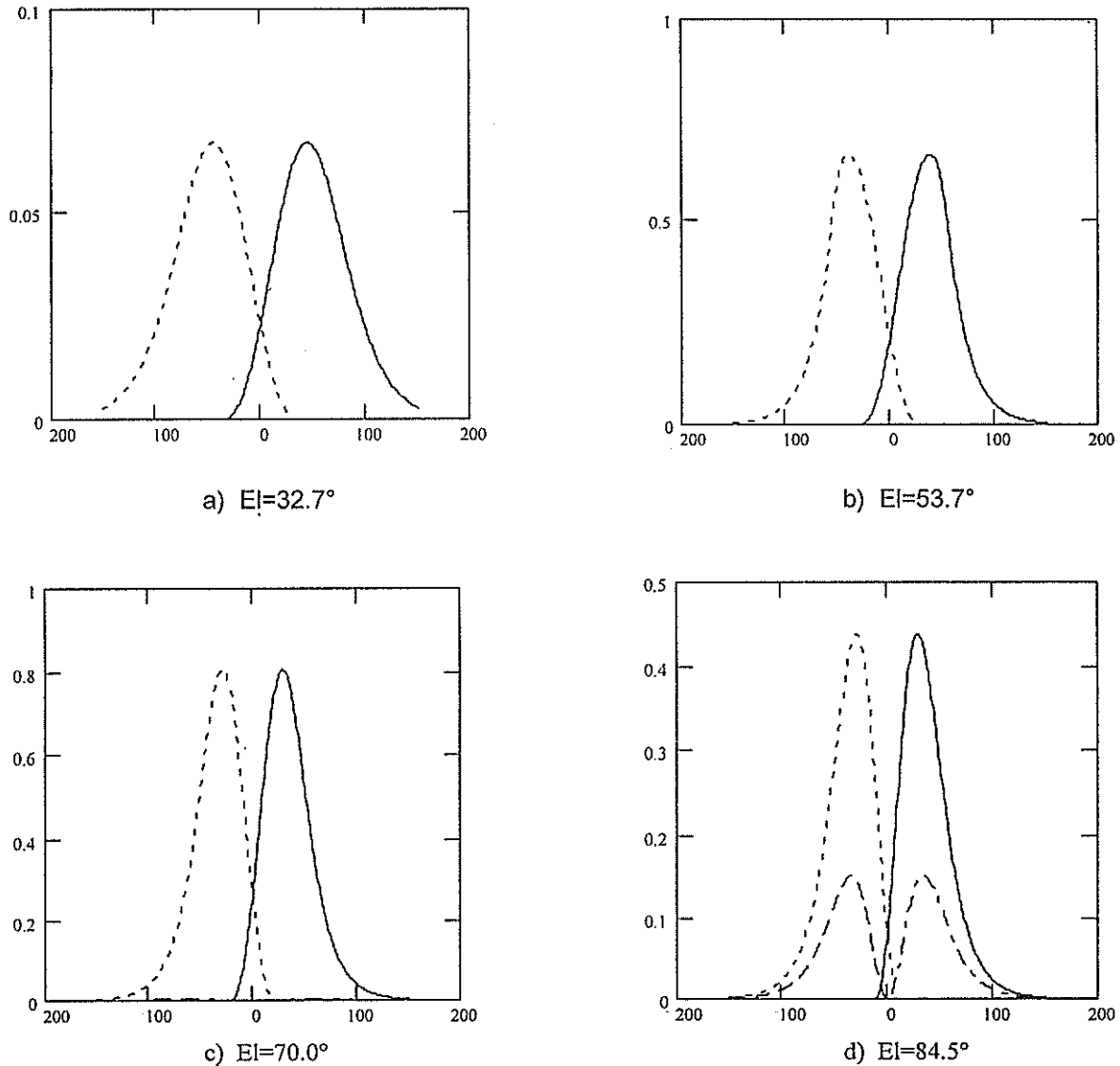
Fig.4 a...d: Signal strength versus time for passes with different elevation at culmination. Time scale is in seconds. The vertical scale is relative to the expected signal of GFZ-1 for 54° elevation.

Range Correction

The range correction for each prism can be easily obtained from Eq.2. If more than one prism is contributing, the weighted mean can be used as the range correction. This definition is correct for a single photon system working at very low signal level. The majority of observations will be single prism responses however. In this case the range correction does not depend on the receiving system, provided that the calibration is done at the same signal level as the satellite returns, or the ranges are properly corrected for signal level.

In Fig.5 we plot the mean range correction versus time for the 4 test orbits. As can be seen, the range correction is very weakly dependent from the orientation except for near culmination. This is not a source of error because the orientation of the satellite and, therefore, the actual range correction are known at any time. If the model error of the orbit exceeds 10 mm, then the range correction can be replaced by a constant value of about 15 mm.
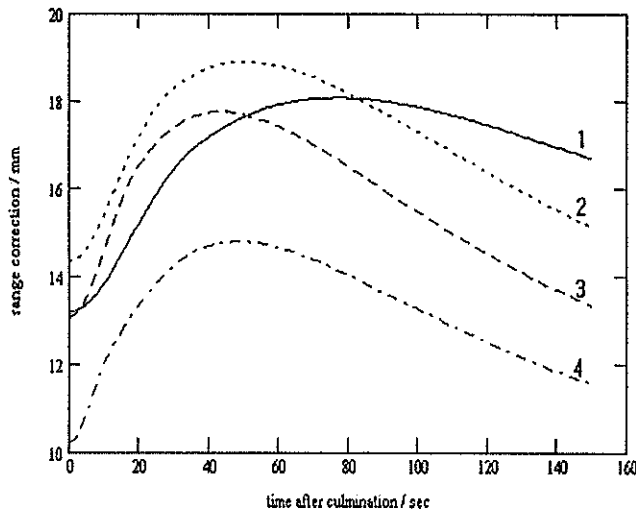
Fig.5: Effective range correction versus time for circular passes
time scale: sec; vertical scale: mm
The tracks 1 to 4 correspond to the elevations at culmination of 32.7°, 53.7°, 70.0° and 84.5°, resp.

The effective range correction is the weighted mean of the single cube values. It differs from the single cube correction near culminatation or for high elevation passes (>70°).

Aberration and Diffraction

Although the orbital velocity is constant for a circular orbit, the aberration vector varies[*] both in its orientation and length. This is represented in Fig.6. It can be seen that there is a transversal component except when the station is on the x-axis (zenith pass) or on the y-axis (culmination). The simplest way to match the reflector to this situation is to use a small offset of one of the dihedral angles of each prism. The result is a two-spot far field diffraction pattern. The splitting must be adjusted in such a way, that one of the lobes is approximately directed to the apparent place of the station.
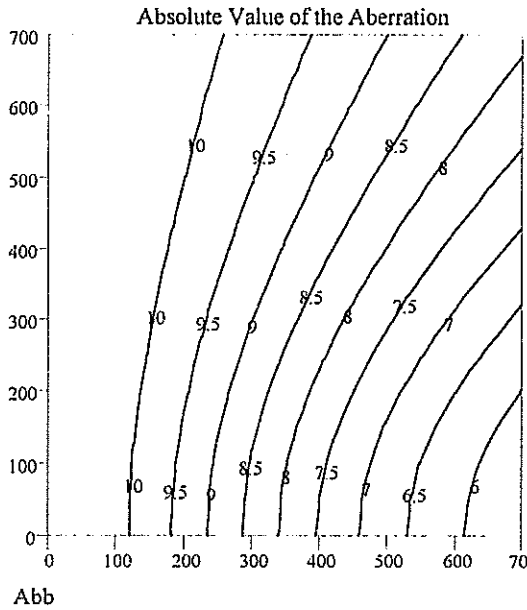
Fig.6a: Absolute value of the aberration vector over the relative station position
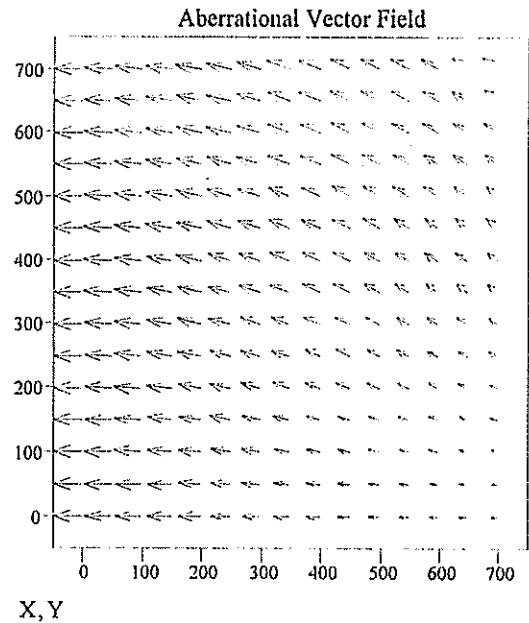
Fig.6b: Projection of the aberration vectors onto the x-y-plane

221

Because of the varying aberration the two lobes must have a certain width. Small prisms have a sufficient natural width of the far field because of diffraction. If necessary, a small spherical distortion can be added to optimize the field. Full optimization has to consider the dependence of the far field from orientation [4]. Most pronounced changes of the pattern occur when both lobes overlap. In this case the maximum tends to be in the centre as can be seen in Fig 7 for a 28° rotation in the plane of the spots. Similar patterns have been observed experimentally by Burmistov et al. [9].
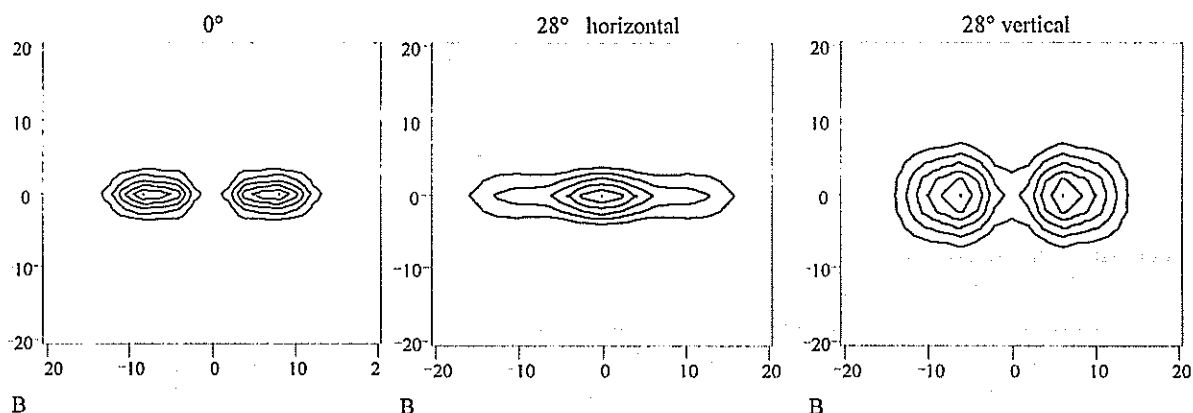
Fig.7: Computed far field patterns for normal incidence and inclined by 28° in two orthogonal directions
The geometrical splitting of the lobes at normal incidence has been set to 16". The lowest level contour lines correspond to 17% of the maximum.

References:

[1] D.A.Arnold: Method of Calculating Retroreflector-Array Transfer Functions,
    Smithsonian Astrophysical Observatory Special Report No. 382 (1978)

[2] J.J.Degnan: Millimeter Accuracy Satellites for Two- Colour Ranging
    Proc. 8th Workshop on Laser Ranging Instr., Annapolis, p.7-36....7-51 (1992)

[3] J.J.Degnan: Millimeter Accuracy Satellite Laser Ranging: A Review Geodynamics Series Volume 25:
    Contribution of Space Geodesy to Geodynamics: Technology, p.133-162, 1993

[4] A.Minato, N.Sugimoto, Y.Sasano: Optical Design of Cube Corner Retroreflectors Having
    Curved   Mirror Surfaces, Appl. Opt. Vol.31, No.28, p.6015-6020, (1992)

[5] N.Sugimoto, A.Minato: Optical Characteristics of the Retroreflector in Space for the
    Advanced Earth Observing Satellite, Optical Review, Vol.3, No.2, p.62-64 (1996)

[6] G.Lund: New Perspectives for High Accuracy SLR with Second Generation Geodesic
    Satellites Proc. 8th Workshop on Laser Ranging Instr., Anapolis, p.7-56....7-64, (1992)

[7] G.Lund: GLRS-R 2-Colour Retroreflector Target Design and Predicted Performance
    Proc. 8th Workshop on Laser Ranging Instr., Anapolis, p.13-17....13-32 (1992)

[8] B.Greene, V.Shargorodsky, M.Fujita, H.Kunimori: A New Generation of Satellite for Sub-
    Millimeter Ranging, these Proceedings

[9] V.Burmistov, V.Shargorodsky, V.Vasiliev, N.Soyuzova: Study of Retroreflectors with Two-
    Spot Reflection Pattern at Sloped Light Incidence,   these Proceddings

[10] Ch.Reigber, R.Bock, Ch.Förste, L.Grunwaldt, N.Jakowski, H.Lühr, P.Schwintzer, C.Tilgner:
     CHAMP Phase B, Executive Summary, GFZ Scientific Technical Reports STR96/13,
     (Nov. 1996)

[11] V.Vasiliev, V.Grishmanovskij, L.Pliev, T.Startsev: Effect of Motion of the Optical Medium
     in Optical Location, JETP Lett., Vol.55, No.6, March 1992, p.316-320

[12] V.Vasiliev, L.Gusev, J.J.Degnan, V.Shargorodsky: Experimental Verification of the Fizeau
     Effect   Influence on the Reflected Beam Direction in Satellite Laser Ranging, Proc. 10th
     Workshop on Laser Ranging Instr., Canberra, Nov. 7-11, 1994, p.147-157

Dependence of Ajisai's Center-of-mass Correction on Laser Ranging System

Toshimichi Otsubo *(otsubo@crl.go.jp)*,

Jun Amagai and Hiroo Kunimori

Communications Research Laboratory / Tokyo

4-2-1 Nukui-kita, Koganei, Tokyo, 184 Japan

1. Introduction

The size of geodetic satellites has become one of the limiting factors in laser ranging precision, and it is called the "satellite signature" effect. In this paper, we focus on the satellite signature of the Japanese geodetic satellite "Ajisai" and its center-of-mass correction values. Ajisai was launched in 1986 and it is still one of the most frequently tracked satellites according to a NASA CDDIS data summary.

The value of 101 cm for a 200 ps pulse width laser in the pre-launch analysis (Sasaki, 1987) has been the only standard for its center-of-mass correction, even though various laser ranging systems are currently in operation and their performance has improved considerably. According to Sinclair (1995), the Lageos' center-of-mass correction for the single-photon system differs several millimeters from its standard value. The bigger Ajisai is considered to be more dependent on laser ranging systems.

In this paper, the return pulse shape from the Ajisai is simulated and Ajisai's center-of-mass values are determined for several system configurations. The range biases for multi-photon stations and single-photon stations are then estimated by an orbital analysis.

2. Simulation of return pulse shape

The specifications of the Japanese geodetic satellite Ajisai are listed in Table 1 and its external appearance is shown in Figure 1. Most of its surface is covered by mirrors to reflect sunlight, and the sets of corner-cube reflectors (CCR) are scattered sparsely between the mirrors. Therefore, the return pulse shape varies significantly according to the laser incident angle to Ajisai.

We can evaluate the satellite signature effect of Ajisai only by a computer simulation since Ajisai is already orbiting in space. In this section, the return pulse for each incident angle is simulated.

However, when we start simulating the return pulse from Ajisai using a detailed specification, two critical problems are found:

(1) All CCRs are installed so that its front face is located at 1.053 m from the center-of-mass with a tolerance of 5 mm.

(2) The angles between CCR faces have an error of about 2 arcseconds.

It is difficult to discuss the signature effect at 1 mm or better because of limitation (1). Calculation of the far field diffraction pattern would be meaningless with an error as large as (2). However, even if each simulated return pulse does not model the real one because of these limitations above, the statistical behavior is considered to follow our simulation. In this study, it is therefore assumed that the installation was done with no error and that the far field diffraction pattern is simple.

The CCR installed on Ajisai is shown in Figure 2. Let us consider the strength of the return pulse reflected by CCR here. The back face is not coated, and the reflectance of CCR is dependent on the azimuth angle especially when the incident angle is wide (Figure 3). (In the pre-launch analysis, the reflectance is uniformly treated as zero when the incident angle > 17 deg, which is corrected in this study.) Each vertex of the front face is cut as long as 8.5 mm, which makes the calculation of the effective reflection area complex (Figure 4). Although we gave up modeling the far field diffraction pattern, the diffracted area is spread in inverse proportion to the effective reflection area of

Launch	August 12, 1986 by NASDA
COSPER ID	8606101
Diameter	2.15 m
Mass	685 km
Number of CCRs	1436 (120 sets)
Optical index of CCR	1.46 (fused silica)
Number of mirrors	318
Orbit altitude	1485 km
Orbit inclination	50.01 deg.

Table 1. Specifications of Ajisai.
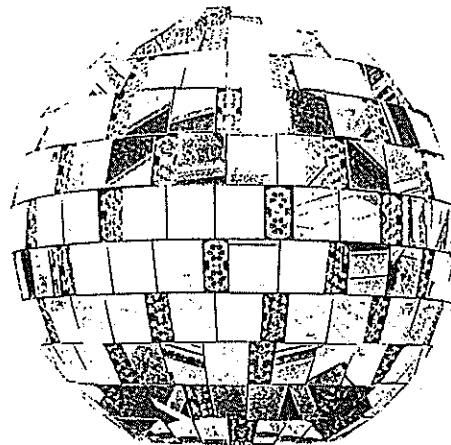
Figure 1. Outlook of Ajisai.

Dimensions mm	
Flatness tolerance	$\lambda/10$
Angle between faces	$90° \pm 2''$
Material	Fused silica
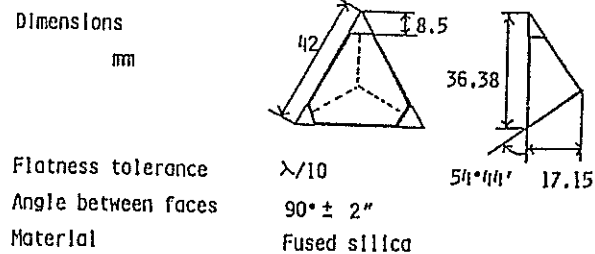
Figure 2. Ajisai's corner cube reflector.
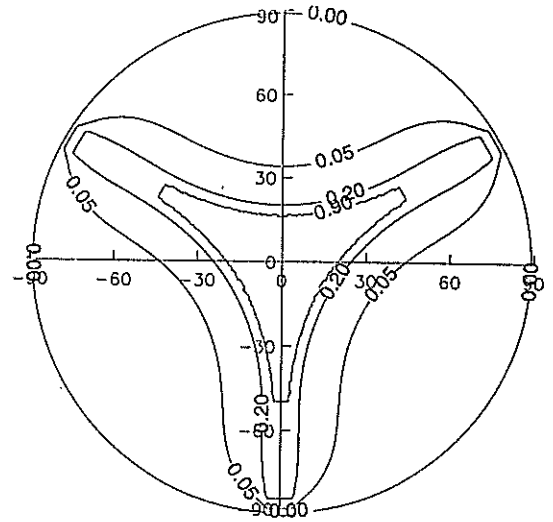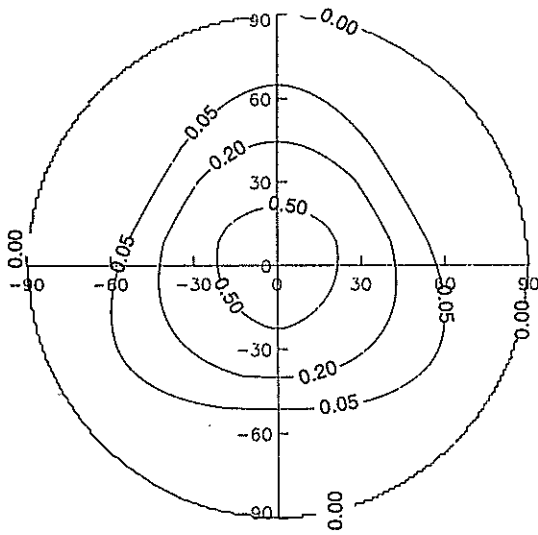
Figure 3. Effective reflection area of Ajisai CCR. (Area of the front face without vertex cut is 1.)

Figure 4. Reflectance of Ajisai CCR. It is calculated as the product of double refraction at the front face and triple reflection at the back face.
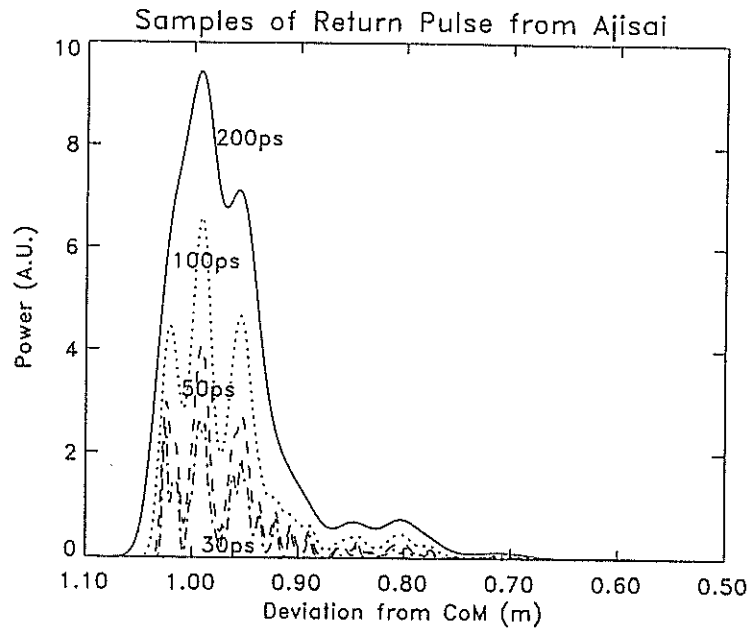
Figure 5. A sample of return pulse shape from Ajisai (Latitude= +13.5 deg and Longitude=-19.5 deg in Ajisai reference frame).

CCR. The return strength is hence in proportion to the effective reflection area for the diffraction effect. Then the relative return pulse strength for a CCR is given as:

$$(strength) \propto (effective \ reflection \ area)^2 \times (reflectance).$$

A return pulse shape from Ajisai is given as a simple sum of the contribution from each CCR as the diffraction pattern is neglected here. When an incident angle for Ajisai is taken, the delay and the return intensity for each CCR are calculated and the contribution of each is totaled.

225

We generate return pulse shapes taking 10267 incident angles equally around Ajisai with the interval of about 2 degrees. The incident laser pulses are assumed to be a Gaussian distribution with pulse widths (FWHM) of 200 ps, 100 ps, 50 ps and 30 ps. A sample is shown in Figure 5; the return pulse ranges more than 40 cm, the deformation of the pulse is simple for a 200 ps laser, but complex for a 50 ps and 30 ps laser with many peaks.

3. Center-of-mass corrections

3.1. Multi-photon System

Most laser ranging stations are now operated as the return echo is detected as a pulse, i.e., at a multi-photon level. The combination of a micro-channel plate photomultiplier (MCP) and a constant fraction type discriminator (CFD) is popularly used in current laser ranging stations. In this study, both the MCP and the CFD are assumed to work ideally.

The center-of-mass correction for this multi-photon system is calculated here. Figure 6 is a sample of the dependence on the incident angle, taking a laser pulse width of 100 ps; (a) and (b) are graphs for Ajisai's upper hemisphere and lower hemisphere. The center-of-mass correction varies about 3 cm from peak to peak. The vague pattern of the 120-degree azimuth interval in Figure 6 is caused by the arrangement of sunlight reflection mirrors; that is, three mirrors in each row are identical.

Ajisai CoM correction (MCP; Upper Hemisphere)   Ajisai CoM correction (MCP; Lower Hemisphere)

(a) upper hemisphere   (b) lower hemisphere
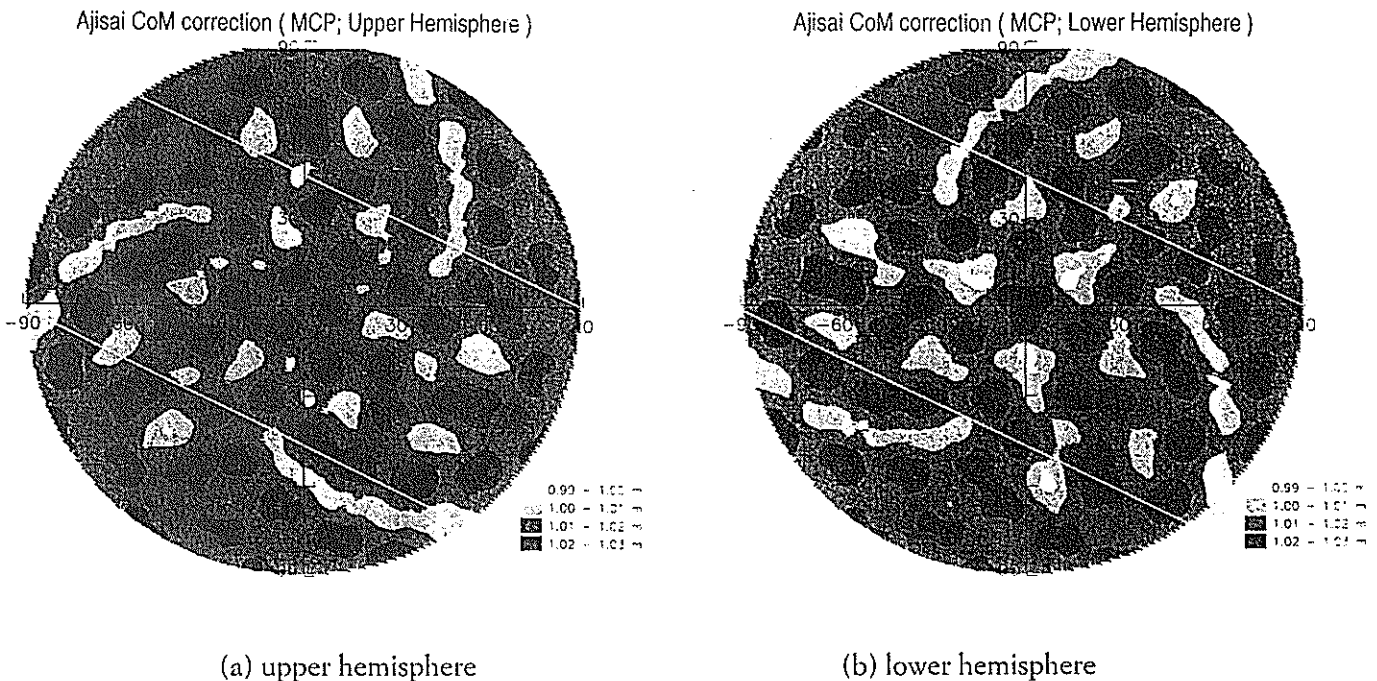
Figure 6. Ajisai's center-of-mass correction for a multi-photon system with respect to the incident angle.
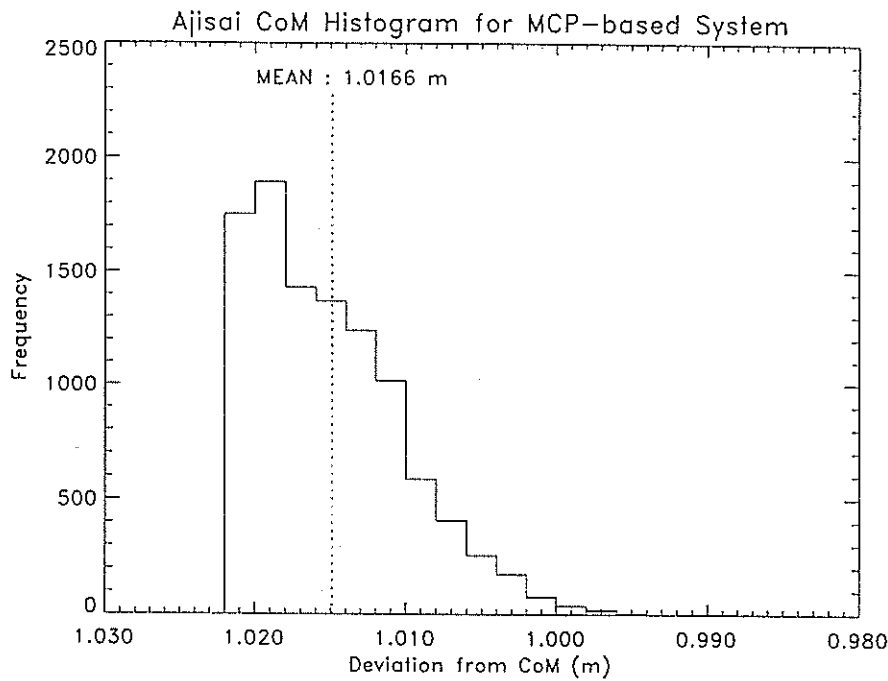
Figure 7. A histogram of Ajisai's center-of-mass correction for a multi-photon system (100 ps laser pulse width).

A histogram of the center-of-mass correction values for 10267 incident angles is plotted in Figure 7 for a 100 ps laser. It represents the distribution of full-rate data residuals under the condition that Ajisai is shot adequately and uniformly from every direction, and that the tracking operation is done with no systematic error. In other words, the rms of the full-rate data residuals cannot be better than that of Figure 7; 5.4 mm for a 100 ps laser. The results for 200 ps -- 30 ps pulse widths are listed in Table 2. The pre-launch value, 1.01 m, which was derived for a 200 ps laser, agrees well with our result for a 200 ps laser, 1.0103 m, although the effective digit of the pre-launch value is not clear. The shorter the laser pulse width is, the longer the center-of-mass correction becomes. We must take notice of its dependence on the laser pulse width since it might cause cm-level bias because of the system configuration.

We should comment that the MCP response time or any jitters also limit the laser ranging precision, and its behavior in the leading edge becomes important if the laser pulse width is sufficiently shorter than it. Hence the value for the

Laser pulse width (FWHM)	Center-of-mass correction and rms (m)
200 ps	1.0103 (0.0060)
100 ps	1.0166 (0.0054)
50 ps	1.0199 (0.0049)
30 ps	1.0211 (0.0047)

Table 2. Ajisai's center-of-mass correction for a multi-photon system with respect to the laser pulse width.

30 ps laser in Table 2 might not be realistic in current stations even if such a short pulse laser is available.

3.2. Single-photon System

Several stations have adopted a single-photon avalanche diode (SPAD) recently (ex. Herstmonceux, Graz, Wettzell, Orroral, Riyadh, Tokyo) and it seems Herstmonceux is now the only station which regularly uses a SPAD for Ajisai ranging at the single-photon level.

The return epoch cannot be determined for each shot, but its statistical behavior can be estimated. The return pulse shape like Figure 5 is the probability distribution for the SPAD system as long as the signal strength is kept at a single-photon level. It is of no use to examine each return pulse shape, but the residual distribution will follow the "average" pulse shape (Figure 8) if the data amount is sufficient. Figure 8 is a sum of the 10267 simulated pulse shapes for incident laser pulses, at 200 ps -- 30 ps. It should be emphasized that the mean is almost a constant --- 0.9712 m, independent of laser pulse width.

Because the distribution in Figure 8 is apparently larger than the current system noise and because it is skewed, the pre-processing procedure will reject a certain part of the distribution tail. The data clipping method is currently different from station to station but most of them adopt a Gaussian fitting with 2 -- 3 x rms clipping criteria. We repeat 2.0, 2.5 and 3.0 x rms clipping and determine its
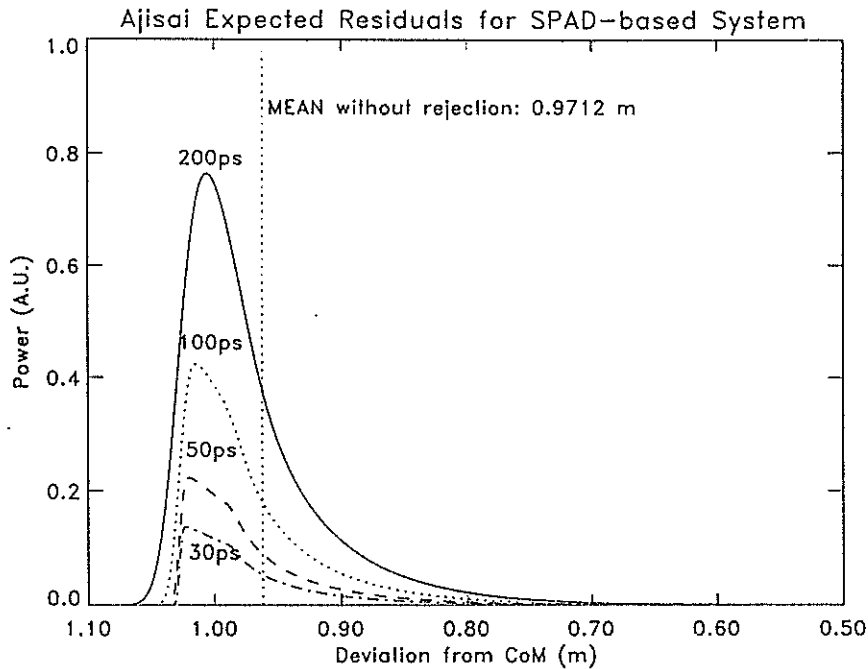
Figure 8. Ajisai's residual distribution for an ideal single-photon system.
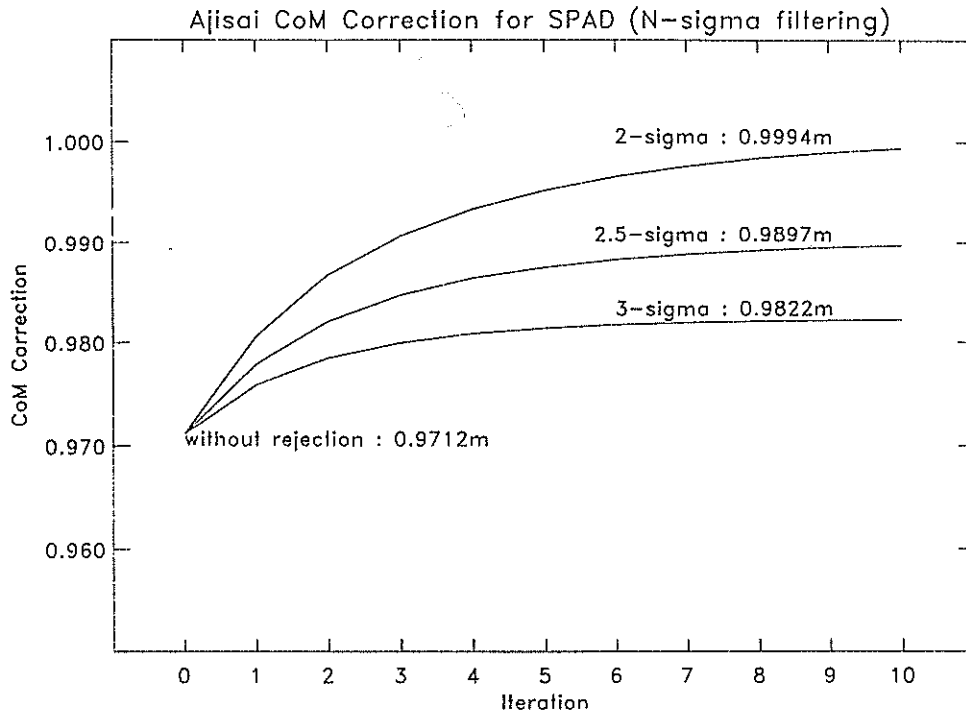
Figure 9. Shift of Ajisai's center-of-mass correction for a single-photon system with respect to the noise rejection criteria.

convergence value (Figure 9). A bias of about 2 cm would appear between a 2.0 x rms clipping and 3.0 x rms according to the graph. Ajisai's center-of-mass correction for single-photon detection is robust with respect to the incident laser pulse width, but sensitive on the noise rejection procedure.

4. Range bias estimation – preliminary results

Using the laser ranging data analysis software CONCERTO (Otsubo, 1994), a series of short-arc analysis was performed between September 1995 and August 1996. The on-site normal point data set is taken from the NASA CDDIS QL directory, and the standard value 1.01 m is used as Ajisai's center-of-mass correction. The station coordinates and the range bias are estimated every 15 days whereas the orbital elements and force coefficients (C_R and C_D) are estimated every day.

The range bias for a multi-photon system with a 100 ps laser should be -6.6 mm and that for a single-photon system with a 3 x rms clipping should be +27.8 mm, according to the discussion in the previous section.

The estimated range biases are plotted in Figure 10 (a) and (b). A sample of multi-photon system, Quincy 7109, is shown in figure (a) and that of Herstmonceux 7840 representing a single-photon system is given in (b). The range bias of Quincy scatters around zero, so the standard value
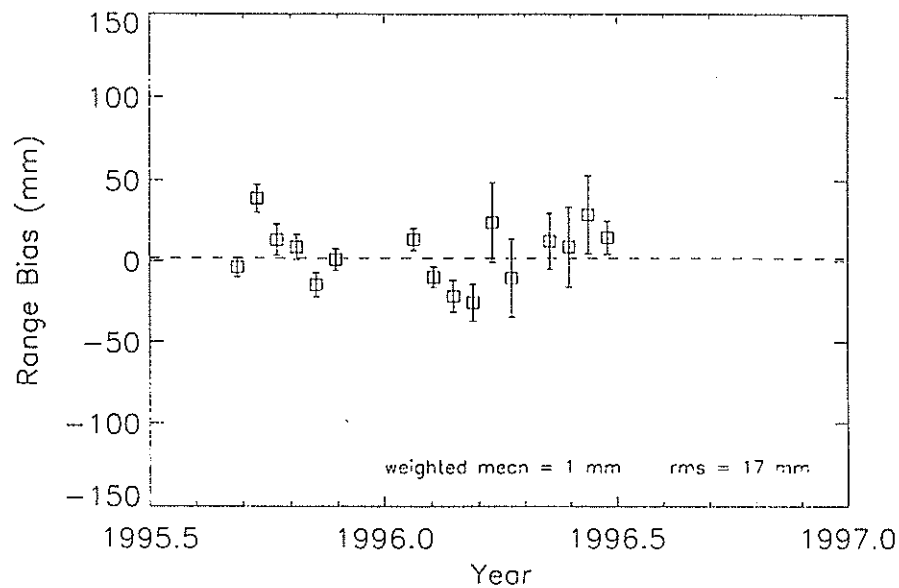
(a) Quincy 7109
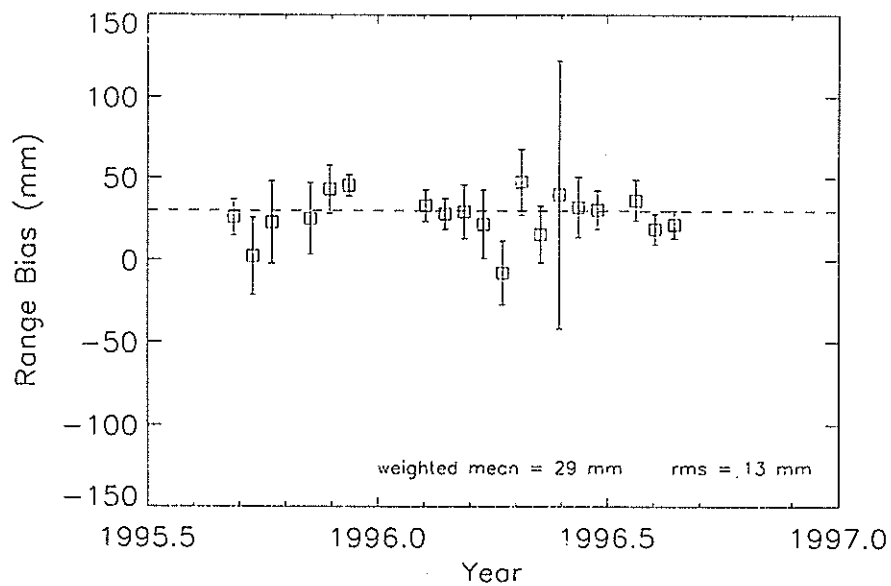
(b) Herstmonceux 7840

Figure 10.   The Ajisai's range bias estimated by CONCERTO.

1.01 m seems appropriate.   On the other hand, the mean of Herstmonceux's range bias is +29 mm agreeing well with our model.

We cannot conclude yet that the system dependence of center-of-mass correction is detected from orbital analysis.   This is firstly because the range bias results above are not separated from the system bias, and secondly because the data set is preliminary without the error correction (such as that listed in DATA BITS AND BYTES in "CDDIS BULLETIN").

5. Conclusion

Ajisai's center-of-mass correction should be treated as a *variable* not a constant. To determine the value accurately, we must take account of

- ☐ The laser pulse width and the timing response of detector (for a multi-photon system)

- ☐ The data clipping criteria (for a single-photon system)

for each laser ranging station. The correction values are derived with the following new viewpoints compared to the pre-launch analysis:

- ☐ The azimuth angle dependence of each CCR's reflectance is considered.

- ☐ Short pulse width lasers are extended up to 30 ps.

- ☐ Single-photon system is modeled with a variety of noise rejection criteria.

The range bias estimation of Ajisai is promising for detecting the system dependence of its center-of-mass correction.

In future work, the relation between the center-of-mass correction and Ajisai's spin motion will be researched. The simultaneous detection by an MCP and a SPAD will help our research. The study here can also be applied to smaller satellites.

Acknowledgment

References

G. M. Appleby, P. Gibbs, "Monitoring potential range biases in single-photon SLR systems," Proceedings of 9th International Workshop on Laser Ranging Instumentation, 1, 92-102, 1994.

G. M. Appleby, "Centre of mass corrections for Lageos and Etalon for single-photon ranging systems," Proceedings of Annual EUROLAS meeting, 18-26, 1995.

P. O. Minott, T. W. Zagwodzki, T. Varghese, M. Seldon, "Prelaunch optical characterization of the Laser Geodynamic Satellite (LAGEOS 2)," NASA Technical Paper, 3400, 1993.

R. Neubert, "An analytical model of satellite signature effects," Proceedings of 9th International Workshop on Laser Ranging Instumentation, 1, 82-91, 1994.

T. Otsubo, H. Kunimori, B. Engelkemier, F. Takahashi, "Error control of numerical integration in SLR analysis software CONCERTO," Journal of Geodetic society of Japan, 40, 4, 347-355, 1994.

M. Sasaki, H. Hashimoto, "Launch and observation program of the experimental geodetic satellite of Japan," IEEE Tranactions on Geoscience and Remote Sensing, 25, 5, 526-533, 1987.

A. T. Sinclair, R. Neubert, G. M. Appleby, "The Lageos centre of mass correction for different detection techniques," Proceedings of Annual EUROLAS meeting, 31-36, 1995.

Remote Sensing of Atmospheric Parameters

Ulrich Schreiber, Birgit Bardorf, Stefan Riepl
Forschungseinrichtung Satellitengeodäsie
Fundamentalstation Wettzell
D - 93444 Kötzting
Germany

Karl Heinz Haufe
Institut für Angewandte Geodäsie
Fundamentalstation Wettzell
D-93444 Kötzting
Germany

Abstract

A model for the refractive index of the atmosphere along the line of sight is used [1] to reduce the measurements to real ranges. However, these corrections are based on model assumptions dependent on values for pressure, temperature and humidity, taken on the ground in the vicinity of the ranging station. From dispersion measurements of the atmosphere by simultaneous dualcolor ranging some evidence for small model errors was found [2]. It is assumed, that these errors arise from inadequate modelling of the water vapor content. This content is measured by a meteorological sensor close to the ground and might not be representative for the lower troposphere around the station. Meteorological temperature inversion effects are also not properly been accounted for. Remote sensing techniques promise to fill a gap. Instantaneous profiles of the water vapor content in the troposphere in the vicinity of the tracking stations can be obtained using Raman scattering from the water vapor. This paper reports the technology employed and the results obtained.

1. INTRODUCTION

Laser Ranging in general can be considered as a special form of a lidar application. One would like to use the existing backscattered light from the ranging laser pulse for the determination of the atmospheric parameter of interest. Since water vapor was identified as being the important parameter to determine [2]. a profile of the water vapor content of up to 5 km around the tracking station could ultimately allow the model of refraction correction to be refined by replacing profile assumptions with real data. A Raman scattering experiment [3] serves this purpose. The outgoing laser pulse of $\lambda = 532nm$ interacts elasically, as well as inelastically with the water vapor in the atmosphere. The Raman shifted echo then can be detected at the wavelength $\lambda = 660nm$. The amplitude and shape of the detected lidar echo reflects the amount and distribution of the water contained in

the atmosphere. A Raman lidar presents a few specific experimental difficulties which need to be overcome.

- The Raman echo is very weak, therefore it needs a very sensitive detection scheme. This is not unlike the LLR application

- The elastic backscattered Rayleigh- and Mie- signal is theoretically between 4 and 8 orders of magnitude higher. This requires efficient optical blocking of the laser frequency at the detection unit of the lidar experiment.

Laser ranging in general is a very demanding technology, operating on extremely low signal levels depending on the distance and structure of the target. Any additional experiment hooked to the existing setup therefore must not interfere with the primary ranging task. Since there was no extra funding for this experiment, the setup described had to be fitted to the existing instrumentation and is far from optimal.

2. THE LIDAR EXPERIMENT USING SINGLE STOP DETECTION

The telescope of the WLRS [4, 5] has a guiding station, which assists tracking mainly during the lunar ranging application. This guiding station uses the same telescope as the ranging equipment. The light which is guided from the telescope to the receiver passes through an interference filter. The laser frequency is reflected towards the ranging detector, while the other spectral components pass through this filter and enter the guiding station. Since the Raman shifted backscattered laser echo lies within the passband of the interference filter, the detector for the lidar experiment must go to the guiding station during the Raman experiments. A narrowband spectral filter together with an edge filter was used to ensure total blocking of the elastic backscatter components, the attenuation being more than 9 orders of magnitudes. The complete setup was discussed in detail in [4], however Figure 1 shows the block diagram of the electronic part. An avalanche diode detected the firing of the laser on the optical bench and started a Time Interval Counter. A delay generator switched an avalanche photodiode into the geiger mode after the laser pulse left the telescope. Any backscattered Raman shifted photon causing a breakdown in the detector stops the Counter again. From the time elapsed one can take the distance of the

scatterer, before the measurement is repeated on the next shot of the laser 100 ms later. The advantage of this technique is the fact, that the full sensitivity of avalanche photodiodes can be used. However a drawback is the slow repetition rate for this statistical approach, due to limitations in the laser and the high dark count rate caused by the intrinsic noise of silicon avalanche photodiodes. Cooling this device down to $-32°C$ helps, but does not eliminate the problem. Lidar experiments were carried out for both Rayleigh and Raman scattering, in order to analyse the properties of this experimental setup. Figure 2 summarises this work. The plot of countrates versus range in the Rayleigh scattered case should be at least 4 orders of magnitude greater than in the Raman scattered case. For reasons that are still unknown, it was found that the elastic scattering experiment was roughly 4 orders of magnitude weaker than expected. This does not seem to be a general property of the experimental setup, since the inelastic scattering case yielded the expected results. It is

interesting to note that the count rate increases for long ranges in this experiment. This was attributed to a high concentration of water vapor in a higher layer of the atmosphere, because clouds formed rapidly, shortly after the measurement. A general drawback of this approach is the fact that a measurement, integrating over 10 000 shots, takes roughly 15 minutes to be carried out. This is to long to be of practical value.

3. THE LIDAR EXPERIMENT USING MULTI STOP DETECTION

In order to increase the data yield, the setup was modified so that the avalanche diode was gated on and off rapidly. A direct negative consequence is in addition to the thermally induced noise counts, the contribution coming from afterpulsing of the detector. On the other hand more than one echo can be collected per laser shot. When an avalanche process occurs, it is passively quenched due to the design of the driving circuit. However it still takes time for the electrons to disappear from the avalanche region. If the gate is switched on before all carriers have left this avalanche regime, another breakdown is generated. Since this additional source for noise counts must be avoided, the recovery time of the avalanche diode was estimated experimentally. A comparatively short gate of $1\mu s$ and a off- time of the same duration were a good compromise. The short gate keeps the thermally induced dark count rate low, while $1\mu s$ is just enough for the diode to quench properly and avoid afterpulsing. Time Interval Counters are not suitable for this multigate application. Since exact timing is not an issue in lidar applications, the following approach has been chosen. Every 250 ns one out of 4 Flipflops is activated. When a pulse from the breakdown of the lidar detector reaches this circuit, the currently active Flipflop reverses its logical state, to mark a bin. This information in turn is stored in a shift register before the next gate of the sequence comes on. After a total of 250 gates, the shift register content is analysed by a computer and the recorded events are converted to a range information again. Figure 3 sketches the principle of this approach.

This concept was tested in a Rayleigh type of lidar experiment by pointing the telescope at a cloud layer. Figure 4 shows a plot of the ranges obtained versus the time interval over which the experiment was carried out. One can clearly see the lower cloud boundary at a range of about $5\mu s$. The clear section below $3\mu s$ is devoid of counts as it is within the dead time of of this experiment. This plot gives a good impression of the cloud movements during this measurement, since the lower boundary changed a lot with time. Converting these measurements to countrates and plotting them together with the theoretically calculated lidar equation show a very good agreement as one can see from figure 5 when the low sensitivity of the WLRS as a Rayleigh lidar system is taken into account by a constant scaling factor of 3×10^{-4} for all ranges. The hump, where measurement and lidar equation disagree is caused by the lower cloud boundary. The presence of clouds of course was not included in the calculations.

The data from the Raman scattering experiment was treated in similiar fashion. Figure 6 also shows a comparision between a measurement and the lidar equation. Again a constant scaling factor was required to match measurement and calculation, thus accounting for a lack of sensitivity. However for the Raman case this factor is only 0.15 as oposed to 3×10^{-4} for the Rayleigh case. Apart from this general lack of sensitivity a good agreement between

model and measurement is evident. These scaling factors remain about constant, when different datasets are compared to the lidar model.

Some other datasets however do not agree so well with the model. Figure 7 gives an example of such a measurement. At around a distance of 500 m the lidar equation and the measured profile match quite well again. However for shorter ranges, one can see a significant discrepancy due to a countrate which is in excess of the usual values. A situation like this was not met very often, however it did happen from time to time. In some cases the disagreement was larger for short ranges as in the example above, while in other cases the discrepancy showed up at the far end. (See also figure 2 for this effect.)

4. CONCLUSIONS

Dualcolor laser ranging measurements have indicated that the water vapor content of the atmosphere is not sufficiently well modelled by using an assumed atmospheric profile and a value from a ground measurement which, for various reasons, is not representative for the atmosphere around the tracking station for various reasons. The basic idea is to use remote sensing techniques to obtain a full water vapor profile simultaneously with the range measurements to satellite. The temperature profile can be assessed likewise if it turns out to be of importance. As far as it is understood today, the atmospheric pressure profile does not require additional attention, since it is easier to model at the the resolution currently required.

In order to transform the measured countrate into a vertical water vapor profile the rescaled countrates were put into the lidar equation, which was solved for the parameter water vapor. Figures 8 and 9 show such profiles. The WLRS was firing to the bottom of a cloud during this measurement. Clearly one can see how the humidity increases, when the laser hits the cloud. This effect is even more pronounced when the same profile is converted to partial pressure of water vapor. Although this result was surprisingly good, the whole technique is far from being calibrated and routine. However, it could be shown that this approach is successful, specially under the circumstances. that no extra funding was available to support the work.

The goal behind the experiment reported here was to demonstrate, that lidar capabilities can be added to a ranging station and that it makes sense to do so. It made use of the telescope, the high power Nd:YAG laser system and the high detector sensitivity available from avalanche photodiodes operated in the geiger mode. Advantage was taken of the large amount of effort that went into the design of highly sensitive detection devices, suitable for lunar ranging. A big disadvantage for this work however was the fact, that the WLRS is operated in a monostatic configuration. This caused a lot of problems for the detection section, because direct backreflections of the transmit laser beam from parts of the telescope were many orders of magnitude brighter, than the atmospheric backscatter. It is expected that for the more common bistatic tracking stations a far better sensitivity will be achieved.
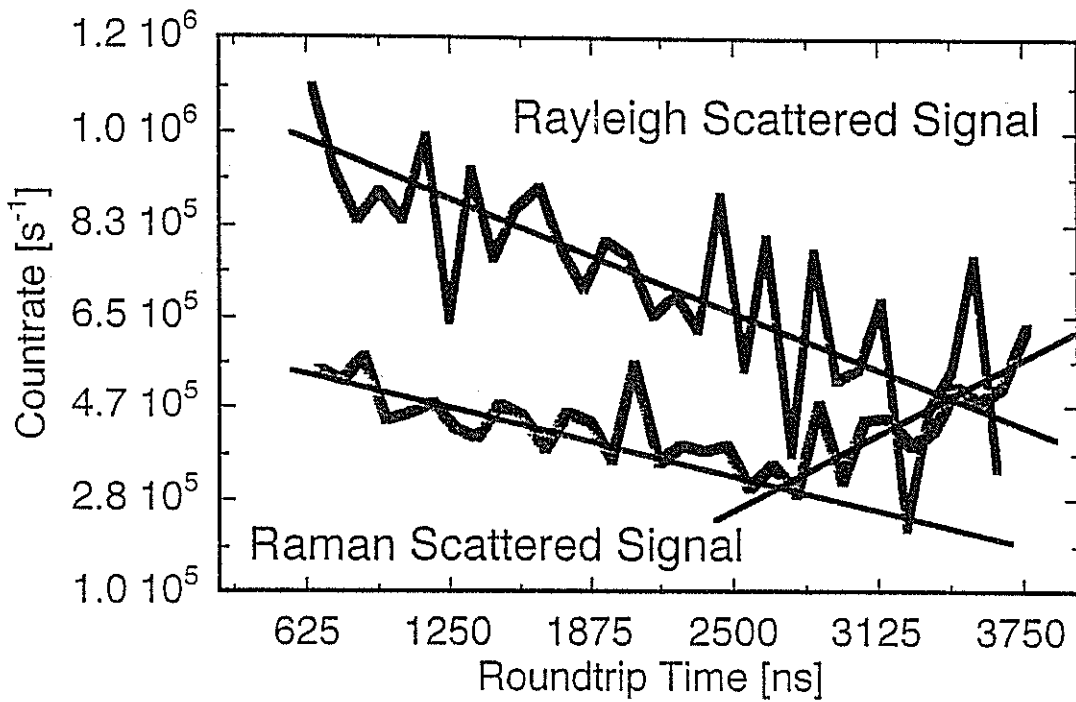
Figure 2: Histogram of countrates versus range of both a Rayleigh- (Mie-) and a Raman-scattering experiment. The elastic echo rate is roughly 4 magnitudes weaker than theoretically expected. The inelastic scattered signal is close to the expectations. The increase in the countrate towards long distances can be attributed to water vapor, since clouds formed rapidly shortly after this measurement
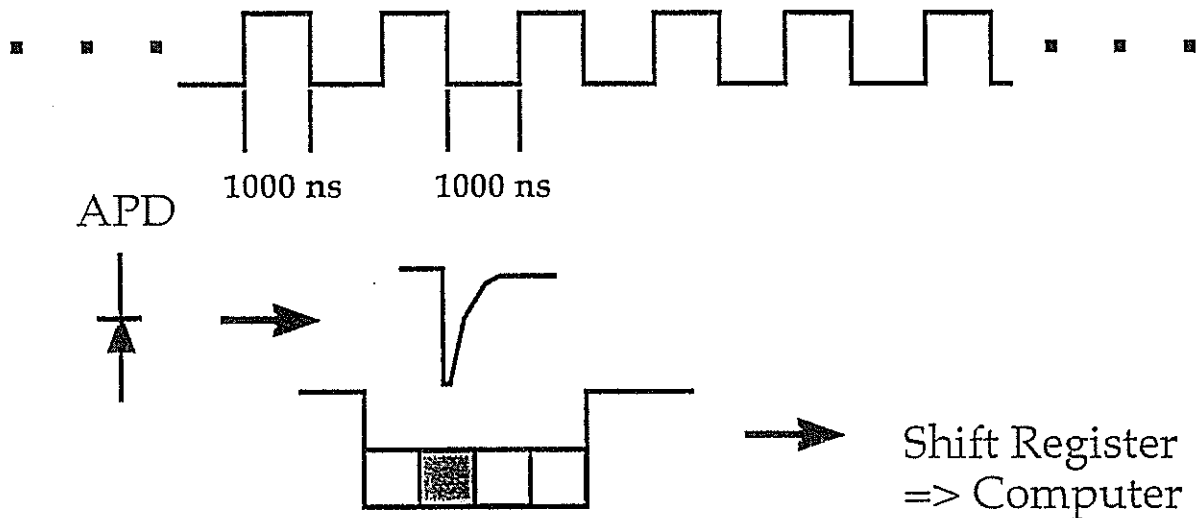

Figure 3: Rough sketch of the operating principle of the multigate detection scheme. Per laser shot there are 250 gates of $1\mu s$ width. Each gate is subdivided by 4 giving a range resolution of approximately 10 m

References

[1] J. W. Marini, C. W. Murray Jr.; *Correction of satellite tracking data for atmospheric refraction at elevations above 10 degrees*; NASA-TM-X-70555,(1973)

[2] U. Schreiber, St. Riepl; "Measuring atmospheric dispersion employing avalanche photo diodes", *Lidar Techniques for Remote Sensing, Chr. Werner, Editor*, Proc. SPIE 2310, **25**, (1994)

[3] A. Ansmann, M. Riebesell. U. Wandinger, C Weitcamp, E. Voss, W. Lahmann, W. Michaelis; "Combined Raman elastic- backscatter lidar for vertical profiling of moisture, aerosol extinction, backscatter and lidar ratio", *Appl. Phys. B* **55**, 18-28, (1992)

[4] U. Schreiber, R. Mayer, S. Riepl, K. H. Haufe; "Integrating LIDAR capabilities into Satellite Laser Ranging Operation", *Lidar Techniques for Remote Sensing, Chr. Werner, Editor*, Proc. SPIE 2581, (1995)

[5] R. Dassing, W. Schlüter, U. Schreiber; "Status Report on The New Wettzell Laser Ranging System (WLRS)", *Proceedings Of 7th International Workshop on Laser Ranging Instrumentation*, Matera. 1989
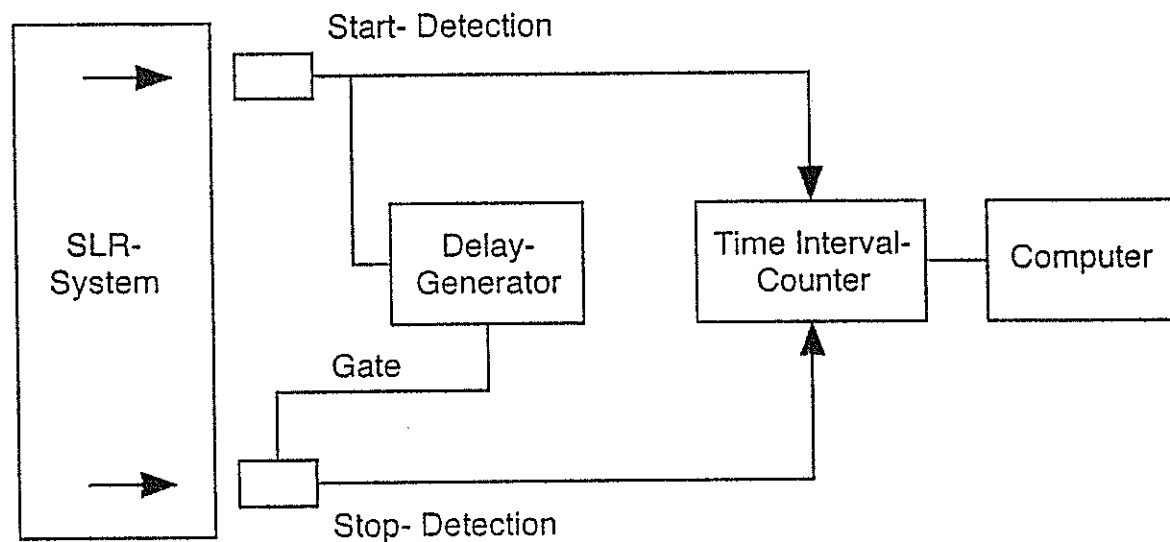
Figure 1: The block diagram of the experimental setup employed. The firing of the laser was detected by a photodiode and started the Time Interval Counter.The stop event was taken from the lidar detector. A delay generator avoided the recording of spurious reflections of the laser beam inside the telescope
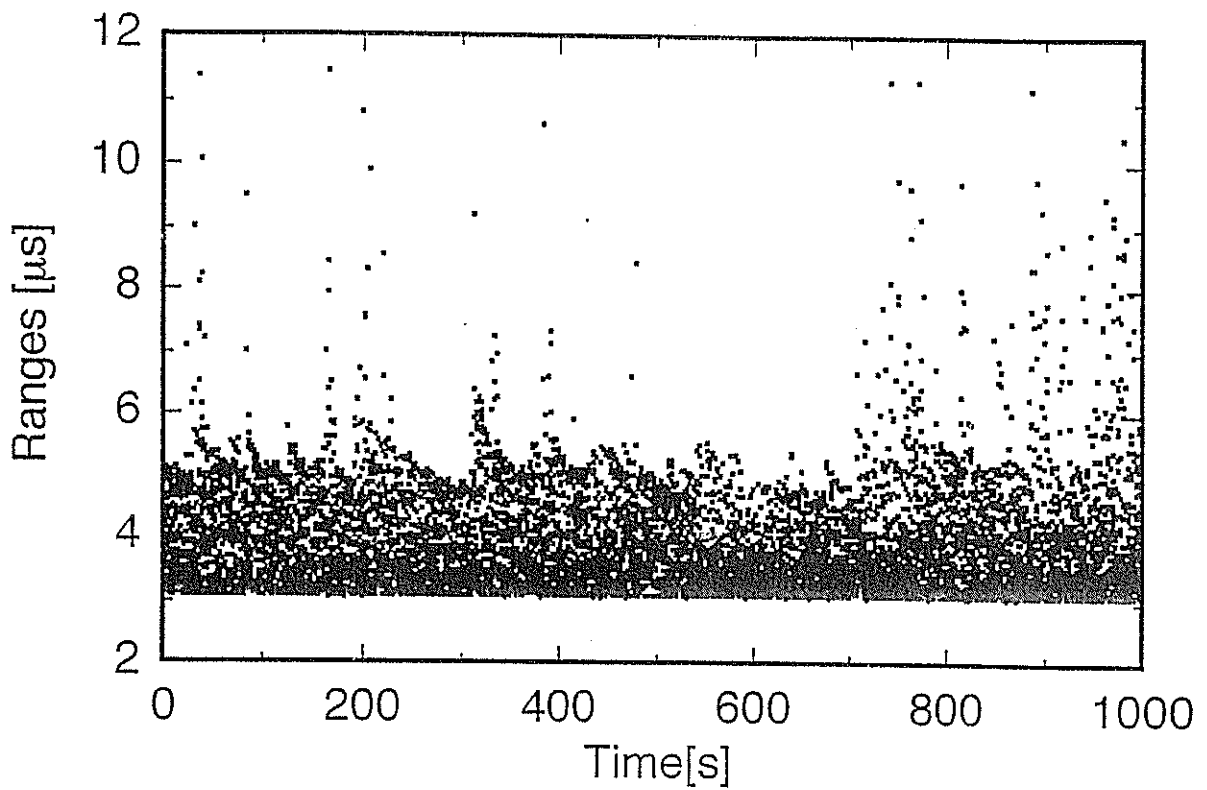
Figure 4: Plot of ranges versus time in the experiment, for an elastic backscatter lidar measurement. The telescope is pointing to a lower cloud boundary, which can be clearly identified at a range at around $5\mu s$. The dynamic changes of the cloud structure are also obvious
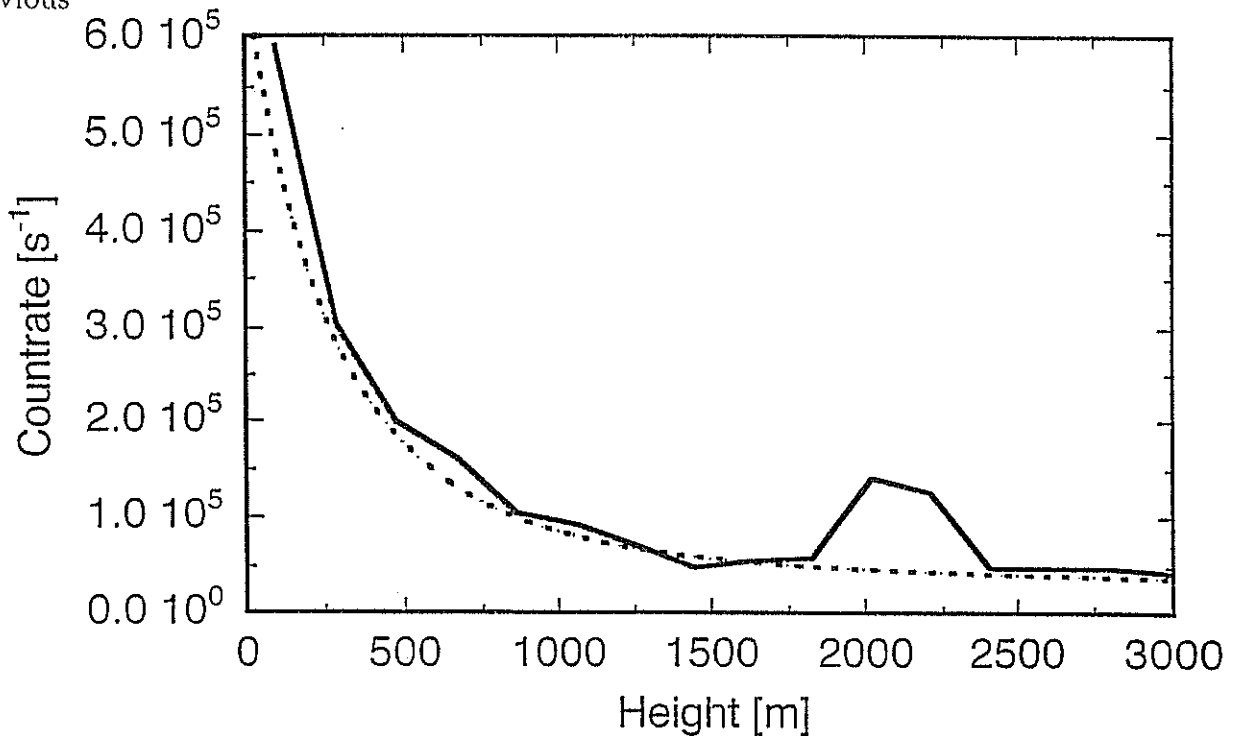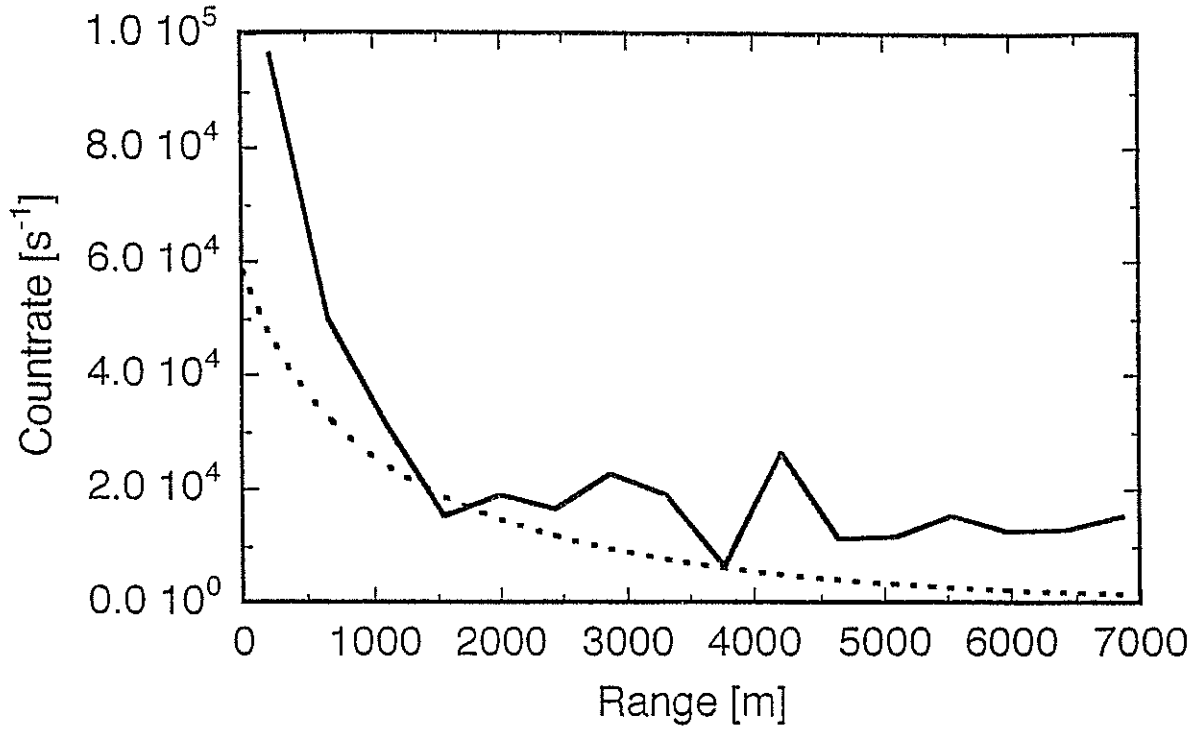

Figure 5: The countrate of the above shown measurement over range along with the calculated contribution from the lidar equat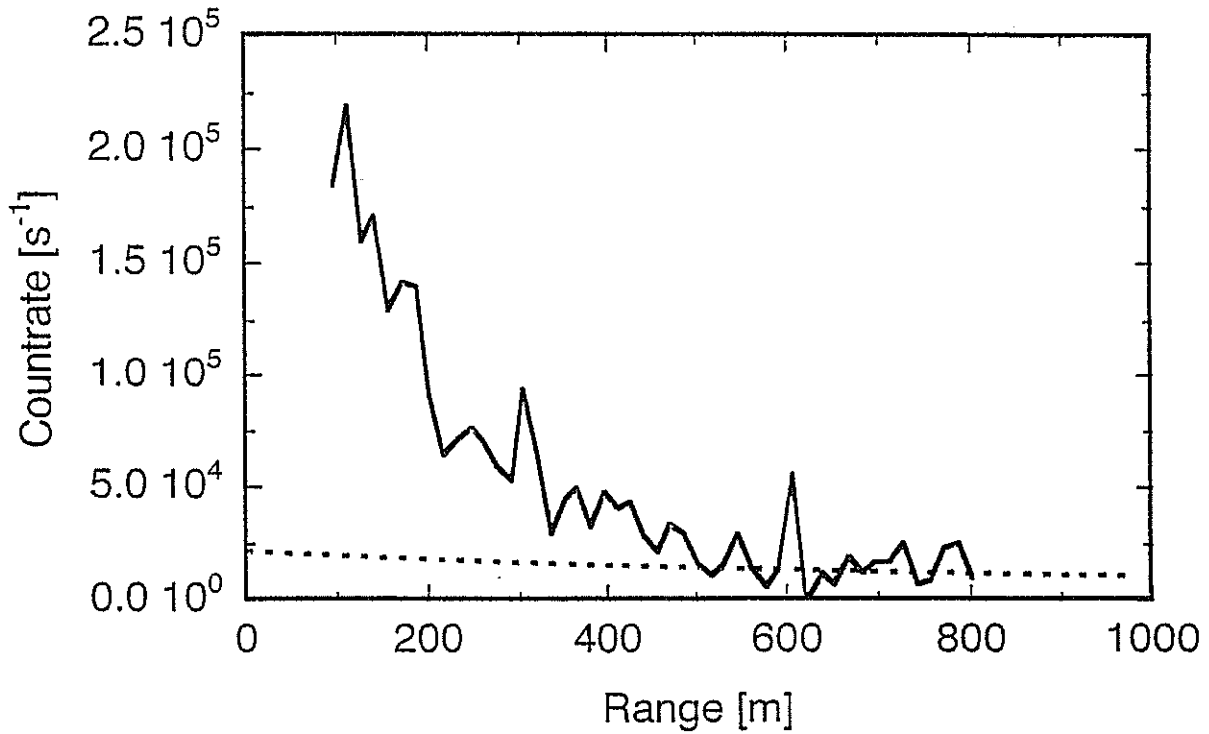ion. There is a good agreement between measurement and model. The hump, which does not show up in the calculations is caused by the lower cloud boundary

Figure 6: The countrate of a Raman measurement over range along with the calculated contribution from the lidar equation. There is a good agreement between measurement and model

Figure 7: The countrate of another Raman measurement over range along with the calculated contribution from the lidar equation. The agreement between measurement and model is poor for short ranges
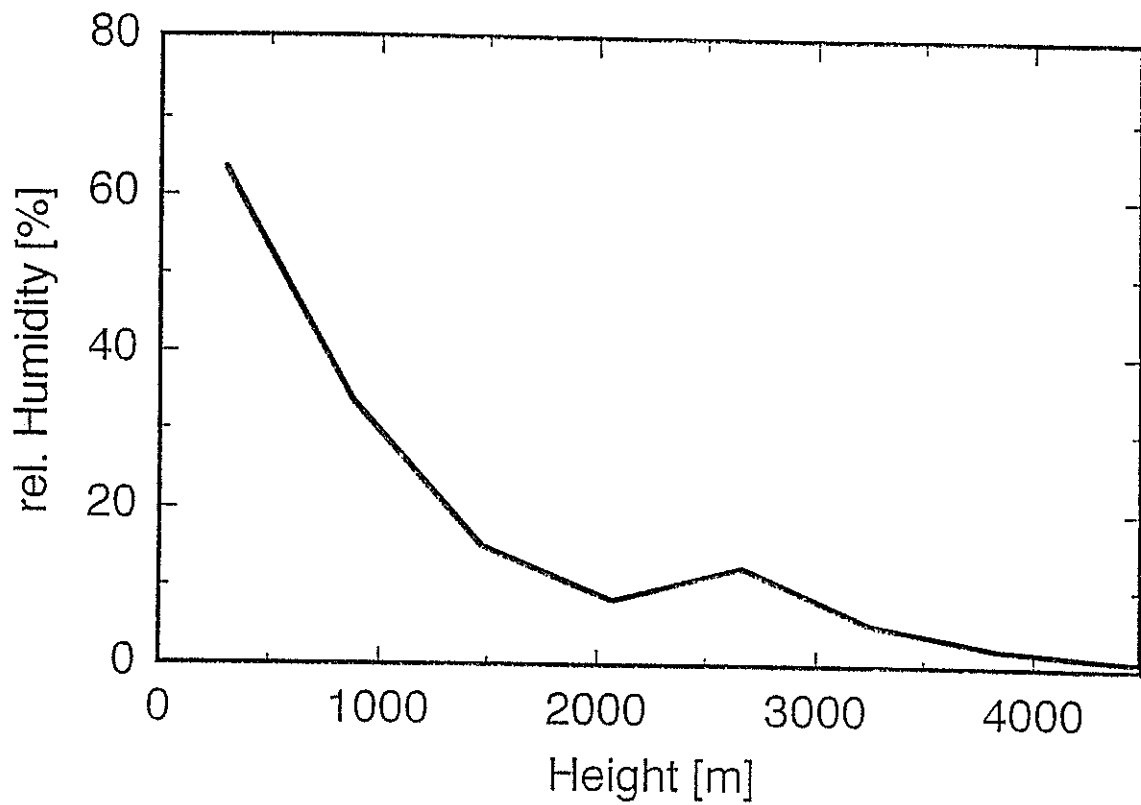
Figure 8: A vertical profile of relative Humidity around the WLRS for this given experiment. The telescope was pointing into a cloud, which showes up as a source of additional water at a distinct range
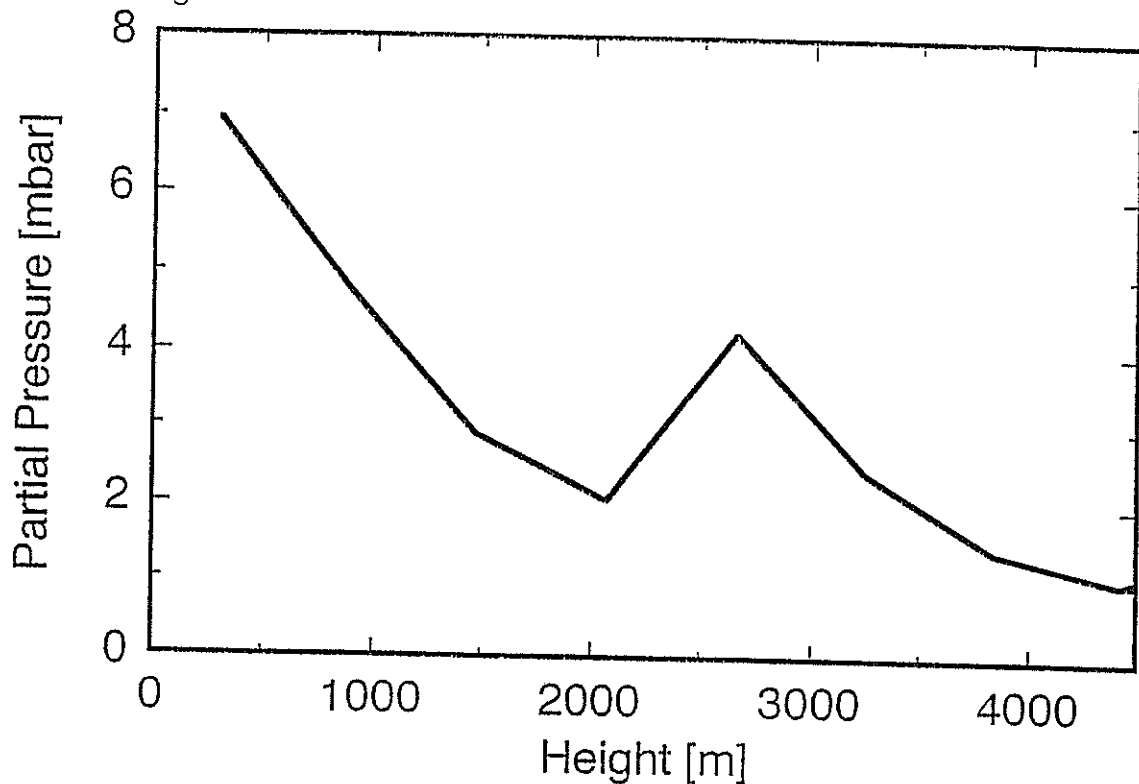
Figure 9: The same vertical profile of Humidity around the WLRS, converted into partial pressure of water vapor. In this plot the cloud shows up more dramatically

ON-ORBIT MEASUREMENT OF TOPEX IMPULSE RESPONSE: ASSESSMENT OF COHERENT INTERACTION AND VERIFICATION OF RANGE CORRECTION

THOMAS VARGHESE*, THOMAS W. ZAGWODZKI, JAN F. MCGARRY, JOHN J. DEGNAN.
BRION CONKLIN*
NASA/Goddard Space Flight Center, Greenbelt, Maryland 20771, USA.
*AlliedSignal, 7515 Mission Drive, Lanham, Maryland 20706, USA.
e-mail: varghet@thorin.atsc.allied.com.

The orbit precision of Topex is at the level of ~3cm. This is a remarkable accomplishment considering the fact that Topex is an active satellite with a large laser retroreflector array (LRA). If the observed station range biases (0.5 -1.5 cm) can be eliminated or reduced to the level of a few millimeters (mm), the accuracy of the Topex orbit can be improved substantially. Indeed, it can be made comparable to that of Lageos. The accurate knowledge or verification of the satellite center of mass (CM) is thus critical to resolving any questions concerning the range biases and the accuracy of the orbit.

The CM correction is deduced from the impulse response (IR) of the satellite and is estimated using far field diffraction theory. The Topex Precision Orbit Determination (POD) team (JPL, NASA GSFC, SAO, AlliedSignal) for the CM determination decided to use the incoherent superposition approach to compute the satellite response. This is for reasons of computational ease for deducing the satellite response for various laser and receiver configurations. The coherent case would have entailed computing the individual satellite impulse response for a large number of random phases and then deducing a mean IR from these instantaneous responses of the satellite. In fact, the incoherent case is a limiting case of the coherent superposition when the pulse width and the contributing number of cubes are large.

The coherent interaction of short laser pulses can generate fairly complex waveforms from a satellite that has a large LRA with close spacing. Short picosecond (<30 ps) pulses are capable of mapping this characteristic when used in conjunction with a high resolution (~2 ps) streak camera receiver system. Such a capability allows accurate on-orbit temporal mapping of the satellite and thereby the determination of the satellite IR. It will also allow to verify the impact of coherent interaction and its effect on the magnitude of the range correction to the CM of the satellite.

It was proposed to the JPL project office in 1992 that it would be extremely beneficial to have a direct on-orbit measurement to verify the actual performance. This will help to alleviate any concerns or questions regarding the accuracy of the FFDP model and make the model robust by validating it with experimental data. This activity was not funded and was pursued by NASA Space Geodesy project office within the constraints of its fiscal budget.

NASA GSFC 48 inch telescope facility has the infrastructure to support these measurements. The optically calibrated streak camera based receiver system in this facility has a resolution of ~ 1.5 ps and an accuracy of ~ 1 ps. This allows to determine the temporal variations accurately. A number of measurements at 532 nm were conducted in the past to collect the data to support this investigation. This paper highlights the initial results of this ongoing measurement and analysis.

The preliminary results show that the satellite return pulse temporal structure varied considerably for short laser pulse width such as 30 ps. For a short input pulse, the number of cubes contributing to the resulting pulse envelope is quite small. The composite waveform thus generated, does not enjoy the benefit of the statistical averaging for the various temporal locations defining the pulse envelope, unlike a wide pulse. The phase variations from shot to shot will, therefore, produce varying temporal and amplitude structure. The features illustrated in several slides indicate the variability seen in the experimental waveforms and is indicative of the coherent interaction.

These measurements can also provide insight into the actual on-orbit LRA thermal conditions. There may be an impact on CM correction from the variations in the FFDP resulting from the thermal gradients due to the partial solar loading / shading of the LRA. We expect to collect more data in the future to make further investigation of this interesting problem and discern the behavior of the FFDP under different solar loading conditions..

TOPEX TEMPORAL RESPONSE:
ON-ORBIT MEASUREMENT

Background:

- Topex **LRA model** (and CM correction) is quite **complex.**

- Model is built on the **incoherent superposition** of the computed intensities of the FFDP of 192 single cubes. Coherent model may change the CM correction.

- **No Integrated experimental measurement** was possible in the laboratory for the LRA due to its large diameter.

- **Laboratory FFDP** measurement of a number of cubes and trays were performed at GSFC. **Variability of the FFDP** was observed experimentally among the trays and the cubes.

- **On-orbit behavior** may be different due to the space environment <low temp, selective sunloading,...>

△lliedSignal AEROSPACE

TOPEX: COMPUTED IMPULSE RESPONSE
Inc. Ang. (angle wrto nadir) = 10 Degree

ROW = 5, COLUMN = 17	ROW = 24, COLUMN = 5

TOPEX TEMPORAL RESPONSE:
COHERENT INTERACTION

- The **coherent interaction** between short pulses depends on the **spatio-temporal overlap** between the pulses.
- Coherent interaction results in the **vector addition** of the amplitudes.
- The **resultant amplitude** (and therefore the intensity) depends on the **phase characteristics** and the number of pulses contributing to the process.
- The **resultant temporal structure** can be quite **complex** depending on the number of pulses and spacing.
- **Shot-to-shot variability** can be significant depending on the above factors.

AlliedSignal
AEROSPACE

TOPEX TEMPORAL RESPONSE:
COHERENT INTERACTION

"A(t) " is the instantaneous amplitude of the reflected pulse from a cube. "σ" is the gaussian half width of the pulse. "ϕ" is the resultant phase on reflection from the cube. "δt " is the temporal offset of the reflection plane of the cube with respect to the cube closest to the source of the wavefront. "I" is the resultant intensity from the entire array computed using coherent or incoherent superposition. "m" is the index for the discrete time and "j" that for the cubes.

$$A_1(t) = |a_1|\exp(-(t + \delta t_0)^2 / 2\sigma^2)\exp(\pm i\phi_1)$$

$$A_2(t) = |a_2|\exp(-(t + \delta t_1)^2 / 2\sigma^2)\exp(\pm i\phi_2)$$

. . . . .

$$A_n(t) = |a_n|\exp(-(t + \delta t_{n-1})^2 / 2\sigma^2)\exp(\pm i\phi_n)$$

TOPEX TEMPORAL RESPONSE:
FACTORS AFFECTING LRA COHERENT INTERACTION

- The **diffracted outputs** from the cubes of the Topex LRA can produce a **complex temporal structure** to the waveforms.
- **Satellite** motion is essentially **frozen** during the time of a picosecond pulse.
- **Pulse to Pulse variability** from the satellite is a function of several key parameters:
    - **number of contributing cubes**
    - **effective separation between the cubes wrto a plane wave.**
    - **laser pulse temporal characteristics**
    - **FFDP of the individual cubes.**

AlliedSignal
AEROSPACE

TOPEX TEMPORAL RESPONSE:
Computed vs Measurement

OBJECTIVES:
- Examine the **differences between computed and measured waveforms** for various azimuths and elevation.
- Assess the Impact if any on the the range correction to the CM of the satellite.
- Verify and validate or modify the current CM correction values.
- Examine the differences between coherent and incoherent superposition.

AlliedSignal
AEROSPACE

TOPEX: Computation of the Temporal Response

- Determine the "Location" in the FFDP for the observing station based on the **orbit from "Geodyn"** and and the **spacecraft attitude from spacecraft telemetry data.**
- Compute the **LRA impulse response** based on that location.
- **Compute the Az, El angles** corresponding to the intensities at specific nadir angle values for the LRA <0,5,10,....55>
- **Generate pulses with random phases** and assign the phases using a random number generator.
- Assuming a randomly phased array, determine the **integrated response of the LRA using coherent superposition** of the intensities of 192 cubes.
- Compute an **average waveform.**

AlliedSignal
AEROSPACE

TOPEX: COMPUTED WAVEFORM:
Inc. Ang. = 10 Degree; Laser Pulse= 30ps;
Incoherent Superposition

AlliedSignal
AEROSPACE

247
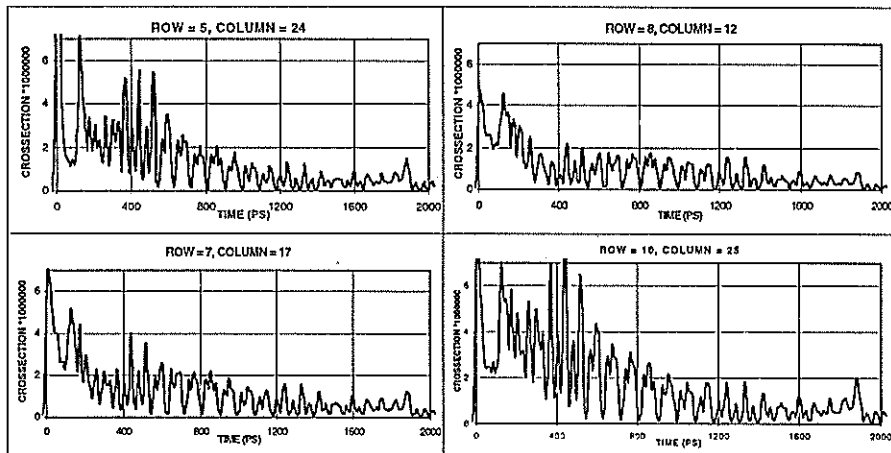
TOPEX: : Analysis of the Temporal Response

- Compute the **Average Experimental Waveform.** Time interval to be detrmined based on the pulse to pulse variations and the amount of data.
- **Compare and Contrast** the **average experimental waveforms** at different Azimuth And Elevation Angles With That Deduced From the **theoretical** Model.
- Compute the response of the tracking stations by **convolving the experimental waveforms** with the temporal response of the Ranging detectors employed.
- Compute the **range correction differences.**

AlliedSignal
AEROSPACE

TOPEX: : Measurement of the Temporal Response

- **Measure** the on-orbit **"impulse response"** of the satellite.
- Ideally, one would like to have a very short laser pulse, e.g., <10 picosecond laser for a satellite like Topex.
- Short **picosecond (<30ps) laser pulses** in conjunction with a **high resolution (~2 ps) streak camera** receiver system can resolve the temporal response fairly well.
- **Recently improved data rate** from the NASA 48-Inch Telescope Facility allows to examine this problem.
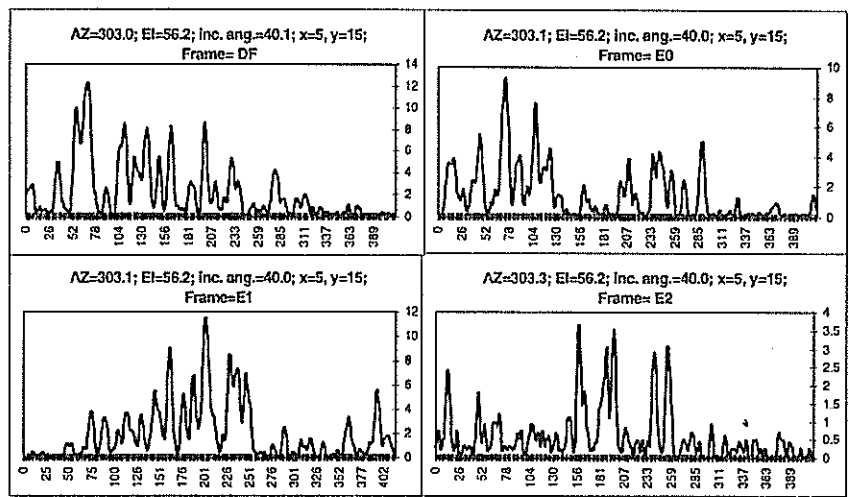
AlliedSignal
AEROSPACE
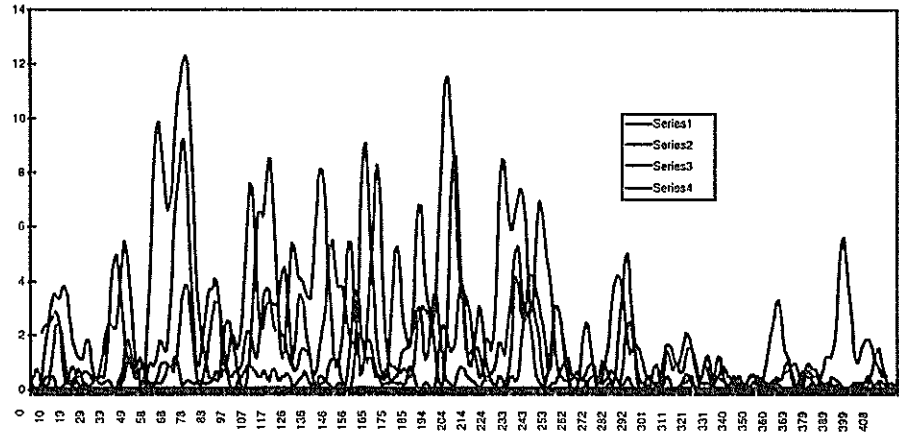
TOPEX: Experimental Measurement

d:\varghese\....\conference\shanghai\ Topx1031.ppt
3/17/97

13

AlliedSignal
AEROSPACE
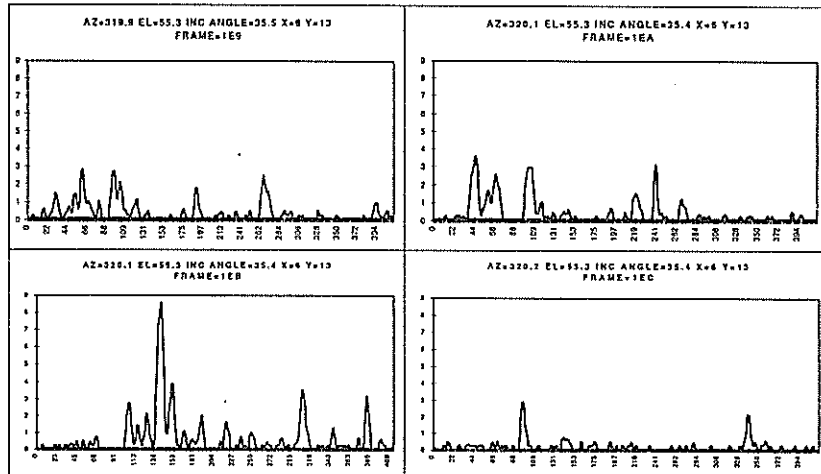
TOPEX TEMPORAL RESPONSE: Preliminary Results

- Preliminary results indicate that the shot-to-shot variations are significant
  - When the input laser pulsewidth is quite short such as 30 ps, the temporal overlap is quite small and hence the number of pulses contributing to the coherent interaction is small. This will naturally lead to large variations.
  - If the pulsewidth were larger (>150ps), there will be a substantial number of pulses contributing to the resulting pulse envelope and possibly less variations from shot-to-shot.
- A rigorous computational and measurement framework is being established to verify the on-orbit performance of the LRA.
- More experimental data is needed to examine and validate the model.

d:\varghese\....\conference\shanghai\ Topx1031.ppt
3/17/97

14

AlliedSignal
AEROSPACE

Refined mathematical model of satellite WPLTN-1-FIZEAU.

Eng.V.Burmistrov, Prof.V. Shargorodsky, Prof. V. Vassiliev, Dr.N.Soyuzova
Russian Institute for Space Device Engineering

Summary

Corrected results are presented of an analysis of the efficiency and accuracy parameters for the passive laser satellite WPLTN-1-Fizeau aimed for submillimeter-accuracy SLR technology demonstration. The satellite has been designed using the "one direction--one retroreflector" technology. The analysis has been done using a corrected model taking into account the slant beam incidence at the retroreflector, the mutual orientation of the velocity abberration direction and prism, as well as the reflected signal level used as weighting function.

The analysis has shown that the reflected signal level at the wavelenght of 0.532 μm in the case of the Fizeau effect presence will be 5 to 15 times (depending on the satellite angular position during observation) higher than in the case of its absence. The RMS difference between the satellite mass center and the measurement point defined by its design should not exceed 0.5 mm.

- For spherical passive spacecraft designed in a way that a few retroreflectors take part in reflection of laser light, as a rule major part of light is reflected by those retroreflectors on which light comes with angles close to normal. That is why optimization of width and shape of reflection pattern of retroreflectors of such spacecraft is usually performed for normal light incidence on a retroreflector.
- For satellites designed basing on principle "one direction-one retroreflector" each retroreflector serves some range of angles of light incidence on a satellite, in each such range all directions (including normal incidence) have the same probability. In this case optimization of retroreflector pattern should be done not for normal incidence, but in a way to provide maximum number of reflected signals within all field of view of a reflector.
- This consideration used for mathematical model of satellite WPLTN-1-FIZEAU designed basing on the principle "one direction-one retroreflector" and equipped with retroreflectors with reflection patterns optimal for Fizeau effect action, allowed to specify its energy and accuracy parameters both for classical interpretation of velocity aberration phenomenon, and for case of Fizeau effect influence.
- Energy efficiency of retroreflector within its field of view (1), which functionally depends on width and shape of reflection pattern is calculated to perform energy and accuracy estimations. Width and shape of reflection pattern, in their turn, are defined by size and direction of the beam inclination relative to velocity aberration vector.
- Systematic correction (3) and RMS of link of range measurements to the spacecraft's center of mass (4) are defined by averaging of weighted random values of systematic correction and squares of deviations within retroreflector's field of view. Normalized energy efficiency of retroreflector is used as weight function (2).
- As a main parameter for evaluation of correctness of selection of basic width and shape of reflection pattern there is used level of reflected signal averaged within

working field of view of the spacecraft (5). Maximization of this parameter by pre-defined accuracy, mass-dimension or other basic parameters can be a criterion for optimum design. It also can be a criterion for evaluation of different technical solutions or hypotheses, in particular this criterion is supposed to be used for testing of Fizeau effect influence on reflection of laser radiation from the spacecraft WPLTN-1-FIZEAU.

- We performed experimental studies of reflection patterns of retroreflectors with baffles from which it was seen that even with sloped light incidence (to $0°$) there can be considerable (doubled) widening of reflection patten in the direction of beams slope (fig.1, fig.2).

- For evaluation of degree of influence of Fizeau effect on quantity of signals reflected from the spacecraft WPLTN-1-FIZEAU, we calculated energy efficiency of retroreflectors depending on angle of beams slope, for case of Fizeau effect influence (solid line) and classical interpretation (dotted line) during range measurements at wavelength 0.532 μm. Dependencies are calculated for position of a spacecraft in zenith (velocity aberration is maximal) and at zenith dinstance $70°$ (velocity aberration is minimal) (fig.3, fig.4).

- Dependencies are calculated for case of beams slope in direct and orthogonal direction relative to velocity aberration vector. From them it is seen that at slope angles 5-8 degrees in the plane of velocity aberration vector, there is considerable increase of retroreflector's efficiency.

- Table 1 contains maximal and average level of reflected signal at wavelength 0.532 μm in absence and in presence of Fizeau effect. From analysis of given values one can make a decision that accounting increase of efficiency of retroreflector at sloped light incidence reduces difference of levels of reflected signal in case of presence or absence of Fizeau effect influence from 500-100 to 10-15 times. Accounting sloped light incidence for ranging at wavelength 1.54 μm does not lead to drastic changes of this ratio (table 2).

- Tables 3 and 4 contain averaged RMS errors and systematic corrections at wavelengths 0.532 and 1.54 μm. Accounting sloped light incidence leaded to insufficient increase of RMS error with classical interpretation of velocity aberration. Accounting sloped light incidence discovered slight dependence of systematic correction on velocity aberration value which depends on spacecraft zenith distance. This dependence needs to be taken into account during processing of laser ranging measurements of spacecraft WPLTN-1-FIZEAU.

BASIC PROPORTIONS

* Energy efficiency of retroreflector within its field of view:

$$S_{eff} = f(\Psi(\varepsilon,\alpha),\overline{\Theta},\alpha,\varepsilon) \tag{1}$$

where : $\overline{\Theta}$ - velocity aberration vector;

ε - angle of light incidence on retroreflector;

α - angle of light incidence relative to velocity aberration vector;

$\Psi(\varepsilon,\alpha)$ - retroreflector's pattern

* Normalized energy efficiency (weight function):

$$P = \frac{S_{eff}(\Psi(\varepsilon,\alpha),\overline{\Theta},\alpha,\varepsilon)}{\int\limits^{\Omega_r} S_{eff}(\Psi(\varepsilon,\alpha)\overline{\Theta},\alpha,\varepsilon)d\Omega} \tag{2}$$

where: $\Omega_r = f(\varepsilon,\alpha)$ - reteroreflector field of view.

* Averaged weighted systematic correction:

$$L = \int\limits^{\Omega_r} P(\Psi(\varepsilon,\alpha),\overline{\Theta},\alpha,\varepsilon)L(\varepsilon)d\Omega \tag{3}$$

where L(ε) - dependence of current value of systematic correction from the angle of light incidence on retroreflector

* Root mean square deviation of link of measurements to the spacecraft center of mass:

$$\sigma = \sqrt{\int\limits^{\Omega_r} P(\Psi(\varepsilon,\alpha),\overline{\Theta},\alpha,\varepsilon)(L - L(\varepsilon))^2 \, d\Omega} \tag{4}$$

* Average statistical level of signal reflected from a spacecraft:

$$n = \frac{\sum \Omega_r}{4\pi} \frac{1}{\Omega_r} n_0 \int\limits^{\Omega_r} S_{eff}(\Psi(\varepsilon,\alpha),\overline{\Theta},\alpha,\varepsilon)d\Omega \tag{5}$$
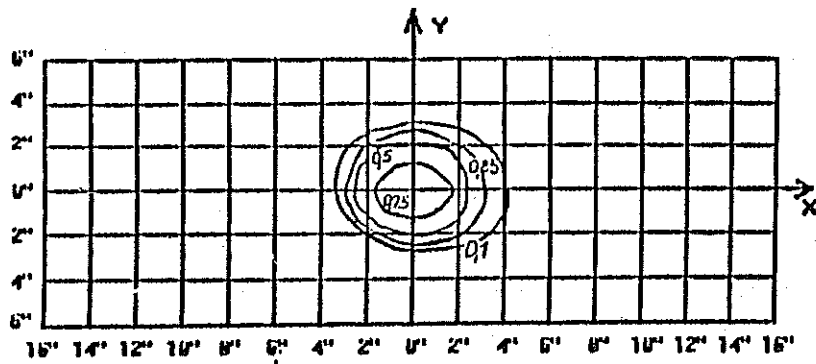
Fig.1 Reflection pattrn of a diffraction-limited retroreflector $D_{RR}=28$ mm at normal light incidence.
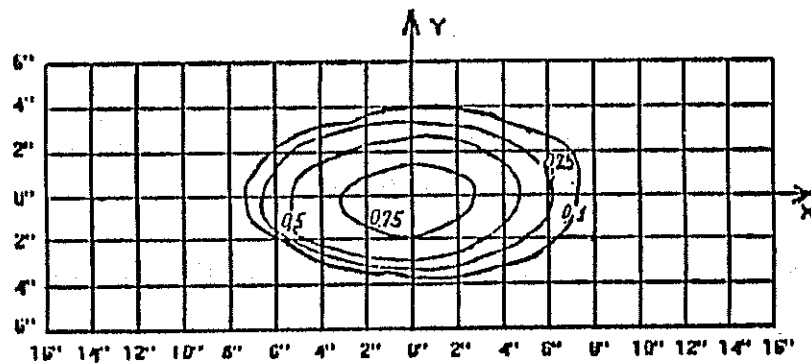

Fig.2. Reflection pattern of a diffraction-limited retroreflector with baffles H=26 mm, $D_{RR}=28$ mm with light incidence angle 10°.
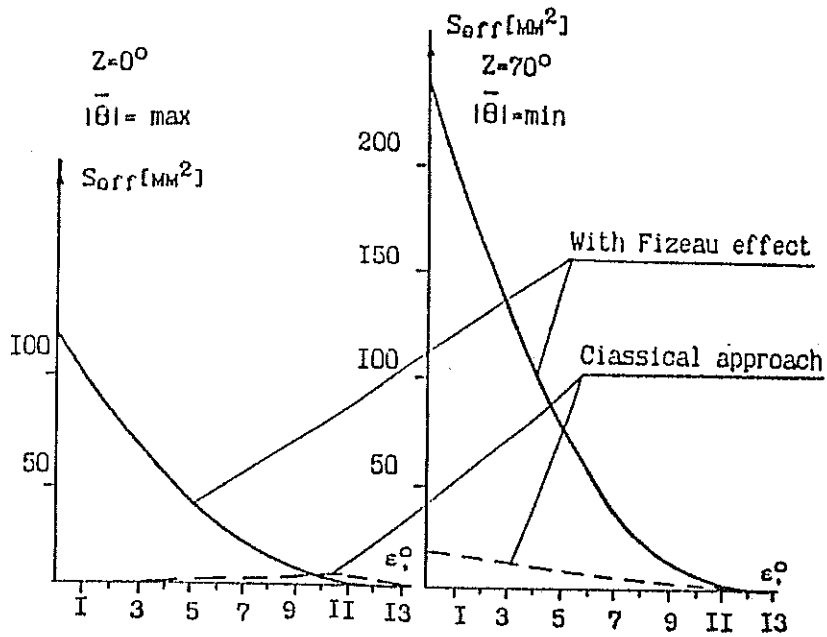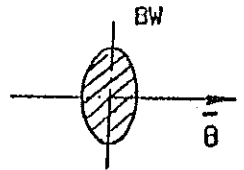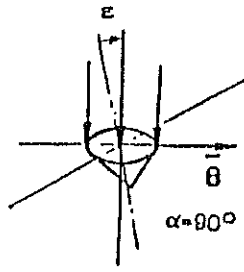
Fig.3. Energy efficiency of retroreflector with parallel direction of retroreflector's inclination relative to velocity aberration vector.
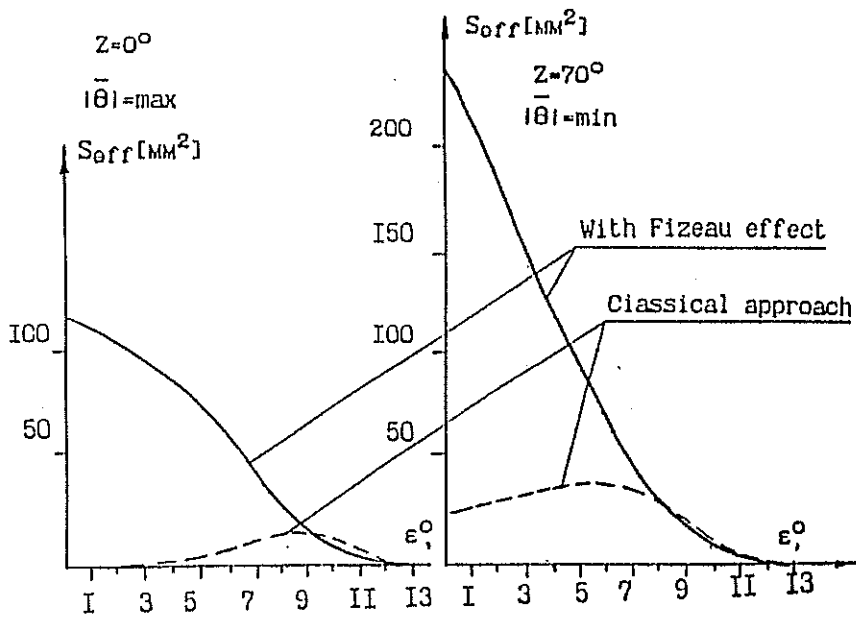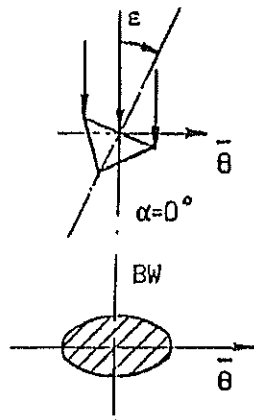
Fig.4. Energy efficiency of retroreflector with orthogonal direction of retroreflector's inclination relative to velocity aberration vector.

Energy potential of "WPLTN-1- FIZEAU" satellite during laser ranging at wavelength 0.532μm.

<div align="right">Table 1.</div>

Zenith distance, arc degrees	Compensation of velocity aberration				Classical velocity aberration			
	Zenith pass		Parameter pass		Zenith pass		Parameter pass	
	$n_s^{\bullet}$	$n_{S\,max}$	$n_s^{\bullet}$	$n_{S\,max}$	$n_s^{\bullet}$	$n_{S\,max}$	$n_s^{\bullet}$	$n_{S\,max}$
0	13.3	64.8	13.3	64.8	0.91	4.0	0.91	4.0
10	12.7	62.2	12.5	60.7	0.87	3.9	0.85	3.7
20	10.9	54.5	10.2	49.7	0.85	3.5	0.7	3.1
30	8.1	42.8	7.2	35.2	0.7	2.9	0.49	2.2
40	5.2	29.2	4.3	20.9	0.6	2.2	0.29	1.3
50	2.7	16.1	2.1	10.0	0.4	1.4	0.14	0.6
60	1.0	6.5	0.7	3.5	0.2	0.7	0.05	0.2
70	0.22	1.46	0.15	0.7	0.06	0.21	0.01	0.04

Energy potential of "WPLTN-1- FIZEAU" satellite during laser ranging at wavelength 1.54μm.

<div align="right">Table 2.</div>

Zenith distance, arc degrees	Compensation of velocity aberration				Classical velocity aberration			
	Zenith pass		Parameter pass		Zenith pass		Parameter pass	
	$n_s^{\bullet}$	$n_{S\,max}$	$n_s^{\bullet}$	$n_{S\,max}$	$n_s^{\bullet}$	$n_{S\,max}$	$n_s^{\bullet}$	$n_{S\,max}$
0	63.3	457.2	63.3	457.2	36.2	166.7	36.2	166.7
10	59.8	432.3	59.6	430.8	34.7	161.4	34.1	157.1
20	50.4	365.6	49.8	359.9	30.5	145.6	28.5	131.2
30	37.2	271.7	36.5	263.7	23.5	120.6	20.9	96.1
40	23.7	174.7	23.0	166.4	16.2	88.2	13.2	60.7
50	12.6	93.8	12.1	87.6	9.2	54.4	6.9	32.0
60	5.3	39.7	5.04	36.4	4.1	26.1	2.9	13.3
70	1.6	11.8	1.5	10.6	1.3	8.6	0.8	3.9

Accuracy characteristics of "WPLTN-1-FIZEAU" satellite during ranging at wavelength 0.532 μm.

Table 3

Zenith distance, arc degrees	Compensation of velocity aberration				Classical velocity aberration			
	Zenith pass		Parameter pass		Zenith pass		Parameter pass	
	δ	Δ_c	δ	Δ_c	δ	Δ_c	δ	Δ_c
0	0.429	62.574	0.429	62.574	0459	61.928	0.459	61.928
10	0.428	62.576	0.429	62.574	0.460	61.937	0.459	61.928
20	0.425	62.583	0.429	62.574	0.467	61.977	0.459	61.928
30	0.422	62.591	0.429	62.574	0.473	62.029	0.459	61.928
40	0.418	62.602	0.429	62.574	0.483	62.113	0.459	61.928
50	0.413	62.613	0.429	62.574	0.488	62.209	0.459	61.928
60	0.409	62.622	0.429	62.574	0.486	62.312	0.459	61.928
70	0.405	62.632	0.429	62.574	0.476	62.403	0.459	61.928

Accuracy characteristics of "WPLTN-1-FIZEAU" satellite during ranging at wavelength 1.54 μm.

Table 4

Zenith distance, arc degrees	Compensation of velocity aberration				Classical velocity aberration			
	Zenith pass		Parameter pass		Zenith pass		Parameter pass	
	δ	Δ_c	δ	Δ_c	δ	Δ_c	δ	Δ_c
0	0.3966	62.970	0.3966	62.970	0430	62.889	0.430	62.889
10	0.3965	62.970	0.3966	62.970	0.429	62.891	0.430	62.889
20	0.3961	62.971	0.3966	62.970	0.426	62.900	0.430	62.889
30	0.3956	62.972	0.3966	62.970	0.423	62.908	0.430	62.889
40	0.3938	62.974	0.3966	62.970	0.418	62.920	0.430	62.889
50	0.3942	62.975	0.3966	62.970	0.413	62.933	0.430	62.889
60	0.3936	62.976	0.3966	62.970	0.408	62.944	0.430	62.889
70	0.3930	62.978	0.3966	62.970	0.404	62.954	0.430	62.889

Study of retroreflectors with two-spot reflection pattern at sloped light incidence.

Eng.V.Burmistrov, Prof.V.Shargorodsky, Prof.V.Vassiliev, Dr.N.Soyuzova

Russian Institute for Space Device Engineering

Summary

Results are presented of experimental investigation of the two-lobe reflection pattern variations depending on the beam incidence angle for prism retroreflectors with a limited field of view in retroreflector systems using the technology "one direction--one retroreflector". As follows from the experimental data, with the increasing beam incidence angle the shape of the reflection pattern becomes unacceptably distorted, changing from a two-lobe one to a single-lobe one. Therefore by designing laser retroreflector systems with two-lobe retroreflectors the beam incidence angle at the retroreflector should not exceed 13 deg.

- Optical retroreflec tor antennas (ORA), designed basing on retroreflectors (RR) with two-spot reflection pattern (RP) used for compensation of classical velocity aberration, have 5-10 times higher energy efficiency. As it is known, ORA with such design was successfully tested on spacecraft METEOR-3 during in-flight laser testing of PRARE system.

- Upon request of Potsdam Geodesy Center (GFZ), we studied possibility of use of RR with two-spot RP on ORA consisting of four retroreflectors which GFZ plans to install on CHAMP spacecraft. Specific feature of this design is that in order to reduce cost, it is proposed to provide all field of view of ORA by minimal quantity (four) retroreflectors. With such design, retroreflectors are operating at considerable angles of light incidence- up to 45 arc degrees.

- We performed detailed measurements of change of two-spot reflection pattern with increasing angle of light incidence to RR. For the experiment there was selected a RP optimal for CHAMP orbit height with distance 13.7 arc seconds between center of spots at normal light incidence. We measured five reflection patterns for incidence angles 0, 13,20,30 and 40 degrees which are shown in fig. 1,2, 3, 4, 5, respectively.

- Analysis of measurements result showed that at big incidence angles two-spot reflection pattern turns into one-spot and at the distance of about 7 arc seconds from the center of RP efficiency of RR is:

at	3°	0.47
	20°	0.147
	30°	0.055
	40°	0.02

- This means that in design of ORA basing on RR with two-spot RR, one shall take measures so as number of reflectors is such that angle of light incidence on RR is not more than 13 arc degrees. With larger incidence angles reflection patterns becomes ineffective and, as a consequence, efficiency of ORA becomes intolerably small and insufficient for reliable registration of reflected signal in considerable part of satellite visibility zone.
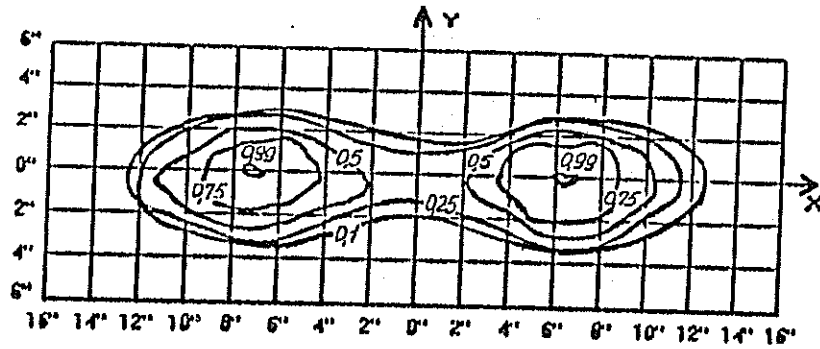
Fig.1. Retroreflector's reflection pattern at normal light incidence. Reflection efficiency in maximum is 1.00.
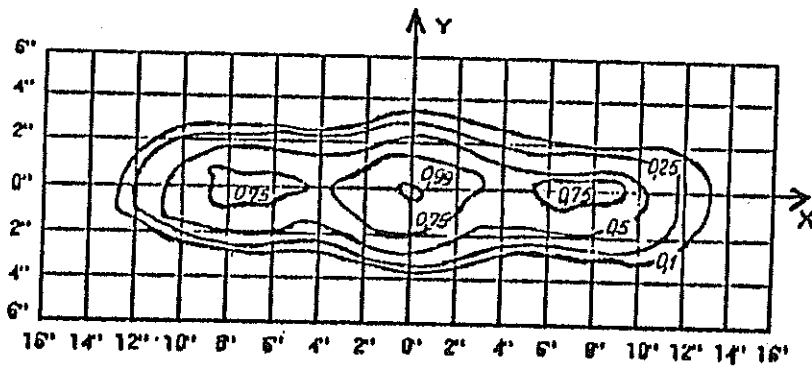
Fig.2. Retroreflector's reflection pattern at 13° light incidence. Reflection efficincy in maximum is 0.63.
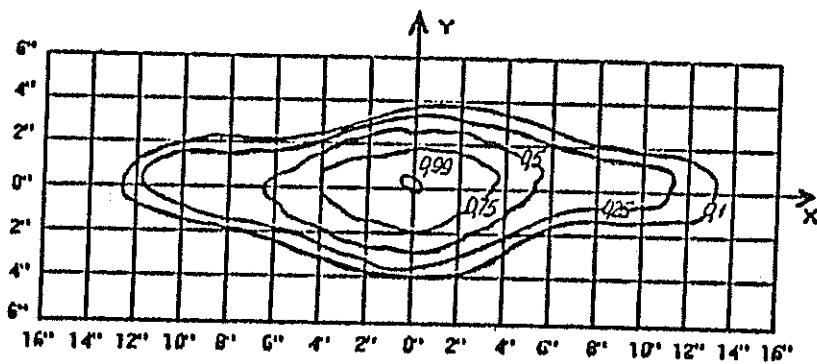
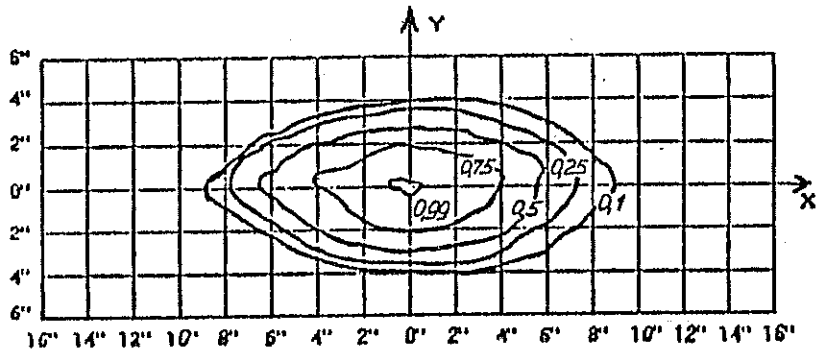Fig.3. Retroreflector's reflection pattern at 20° light incidence. Reflection efficiency in maximum is 0.42.

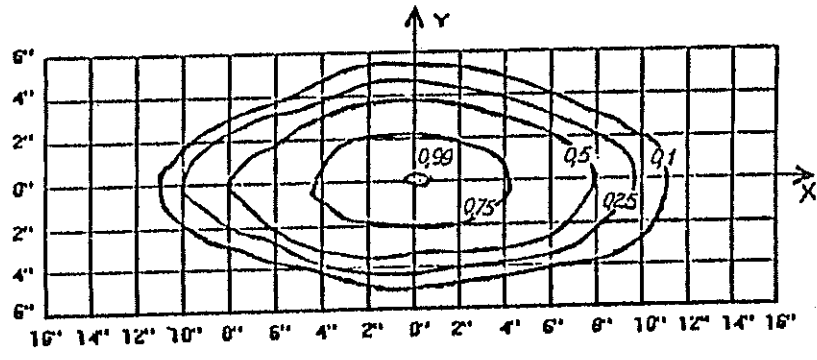Fig.4. Retroreflector's reflection pattern at 30° light incidence. Reflection efficiency in maximum is 0.22.

Fig.5. Retroreflector's reflection pattern at 40° light incidence. Reflection efficiency in maximum is 0.04.

THE POLARIZATION BEHAVIOUR OF CUBE CORNER RETROREFLECTORS USED IN SLR SATELLITES

M. Kasser, ESGT / CNAM, 18 Allée Jean Rostand, 91 025 EVRY Cedex, France
Fax : +331 69 36 74 21
B. Goupil, LOEMI / IGN, BP 68, 94 160 Saint-Mandé, France

INTRODUCTION

We have investigated new techniques to perform distance measurements between the SLR station and a satellite, and among them one requires to know the change of polarization of a laser beam due to the reflection on a cube corner retroreflector (CCR). This paper relates the results, both theoretical and experimental, that may help to understand the effect of CCR. The situation is considerably complicated by the fact that the CCR used in geodetic satellites have no reflecting coating on the back faces, so as to avoid CCR whose front face are far from the laser direction (typically more than 20E) of being active. In this case, the successive reflections on a dioptre not far from the limit angle induce a strong additional ellipticity (which is not the case with metallic coatings). Thus we have computed what happens for (i) a linear polarization and (ii) a circular polarization at various incidence angles, and we have checked some results with limited experimentations : The discrepancies are very limited, but we have not been able to find a good explanation for them.

POLARIZATION OF THE LIGHT AND TOTAL REFLEXION ON A DIOPTRE

If we consider the electric field **E** of an electromagnetic wave, **E** is perpendicular to the direction of propagation, and for its components E_x and E_y, a comprehensive way to describe the polarisation will be to use the 4 Stokes parameters (2) :

$$s_1 = E_{ox}^2 + E_{oy}^2$$

$$s_2 = E_{ox}^2 - E_{oy}^2$$

$$s_3 = 2 \, E_{ox} \, E_{oy} \, \cos(\Delta_y - \Delta_x)$$

$$s_4 = 2 \, E_{ox} \, E_{oy} \, \sin(\Delta_y - \Delta_x)$$

with :

$$E_x = E_{ox} \, . \, \cos(\omega t - \Delta_x)$$

$$E_y = E_{oy} \, . \, \sin(\omega t - \Delta_y)$$

The interaction with a dioptre may be modelled by the so-called Mueller matrix (ref. 1 et 2), acting on the Stokes parameters, the main computation problem being to check carefully the reference frame changes between each reflection. We have chosen to display the results on the Poincaré sphere, on which :

- The latitude angle is the Arctg of the ellipticity.

- The longitude is the orientation of the main axis of the ellipse.

For example the two circular polarisations are the two poles, and on the equator we find linear polarisations.
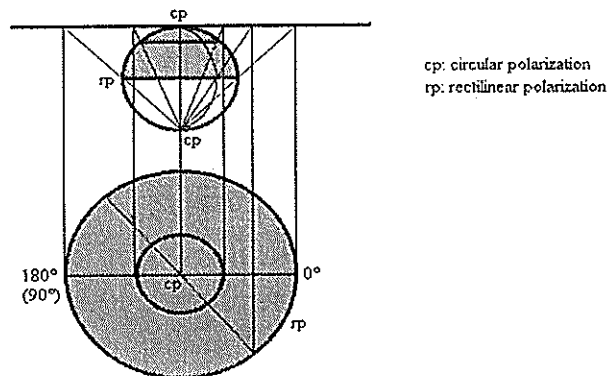

Figure 1 : Polar stereographic projection of the Poincaré sphere

The results of our computations are displayed using a polar stereographic projection, generally limited to the upper hemisphere : the largest circle represents the equator and thus, linear polarisations, and the central point represents the upper ("North") pole and thus a circular polarisation.

THEORETICAL COMPUTATIONS

We have first defined a reference frame linked to the RCC, each of the Ox, Oy and Oz axis being the intersection of two reflecting faces. The optical problems due to the crossing of the front dioptre have been neglected, as the incidence angles are low and the induced additional ellipticity seems very small.

The direction of the incident ray is provided through 2 angles :

   - The angle between the incidence plane, normal to the front .dioptre; and a reference plane (including Ox) also normal to the front dioptre : the azimuth.

   - The angle, within this incidence plane, between the incident ray and the normal to the front dioptre : the angle of incidence.

For each situation, we have six possible enchainments of faces, that are never commutative. The only simplifications of a systematic analysis of all directions are, in circular polarisation :

   - a 120E rotation on the azimuth reproduces the same pattern,

   - a symmetry relative to each of the three planes normal to the front dioptre and containing Ox, Oy or Oz provides a symmetric pattern.

The computations have been performed in C language, on a workstation, and some experiments have been performed in order to check the results. The one presented here (Fig. 3) is with a zero "incidence" and "azimuth" angles, in linear polarisation with the polarisation plane at 45E, 65E, 90E and 135E from the incidence plane. The experimental and theoretical curves (obtained by rotating a polarizing plate from 0 to 360E on the exit ray, the abscissa of the plot) show a small discrepancy that we could not explain completely, but which is not critical. The experimental device is the following (Fig. 2) :
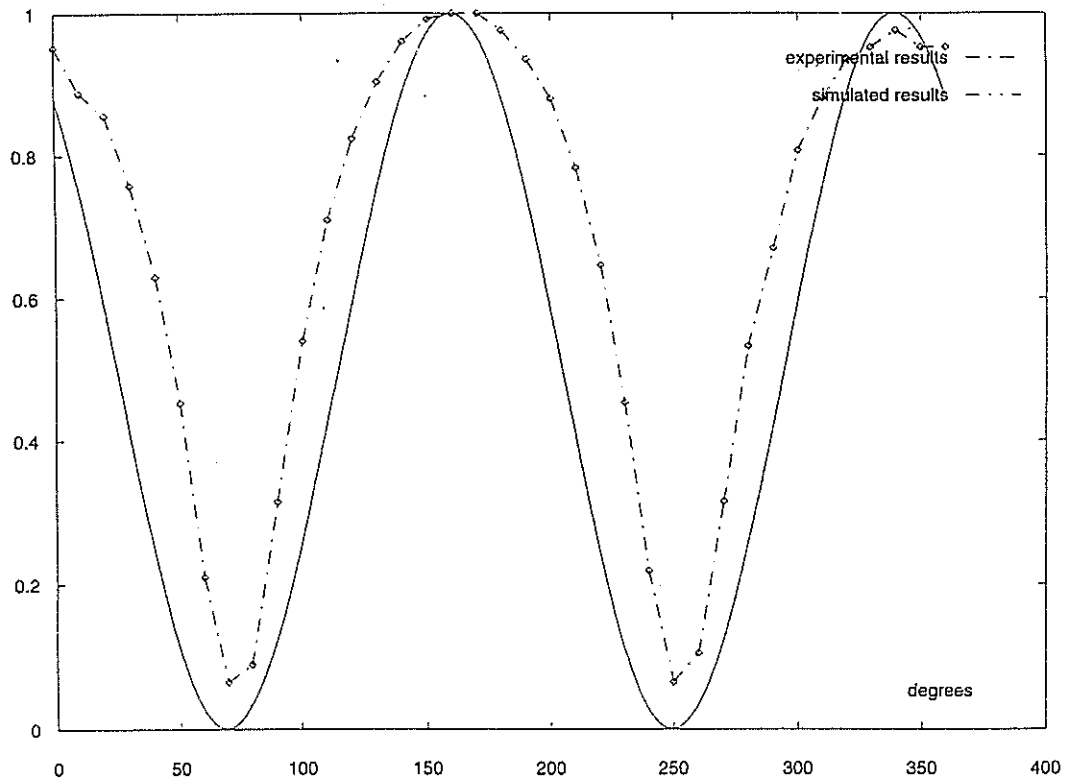
Figure 2 : Experimental device for a null incidence over the front plane of a glass CCR
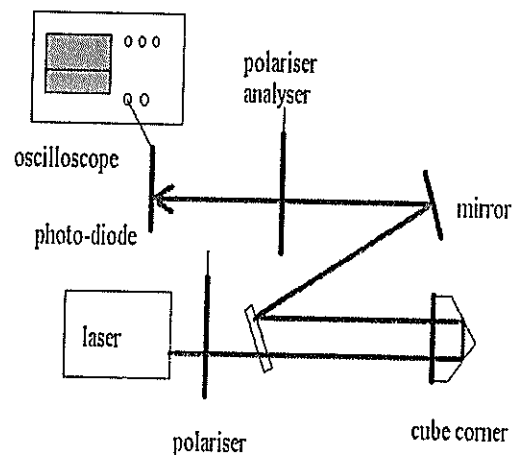
We present here the curves for 45° (Figure 3) :

reflexion in a cube corner, incidence 0, rectilinear polarization 45

RESULTS, AND CONCLUSIONS

Two series of results are proposed (next page), the first for an entering ray in circular polarisation, the second with linear polarisation. In each case the azimuth is given, the incidence angle varies from +13° to -13° (larger angles are useless because one of the reflections is no longer total).

The six enchainments of faces are always presented, but one has to remember that with SLR, in order to cancel the aberration due to the relative movement of the satellite and the station, all CCR are spoiled so that only one enchainment of faces is used at a time, for applications where the far field only is useful. But it is clear that in static applications, the six enchainments of faces produce a set of six different images where it generally does not exist any pair having exactly the same polarisation. This is an interesting optical situation as, on another hand, these six images are theoretically in the same wave plane.

When the incidence angle is low, the major conclusion is that **one enchainment of faces behaves not far from a quarter-wave plate**. But this is just a coarse approximation, and everyone may see that results vary very quickly in some geometric configurations.

We present here a large number of representations, under various situations. The main conclusion is that not metalled CCR are providing extremely complicated polarisation patterns in general. For SLR applications, we are lucky that only one enchainment of faces is simultaneously active. Nevertheless our results mean that it is not advisable to use laser modulation based upon polarisation modulation, as just a small variation of the incidence (which is impossible to control) creates strong modifications of the resulting polarisation.

Thus we propose to continue experiments with long laser pulses, modulated at a very high frequency, in a quasi-continuous mode, but with devices where polarisation of the return beam is not critical.
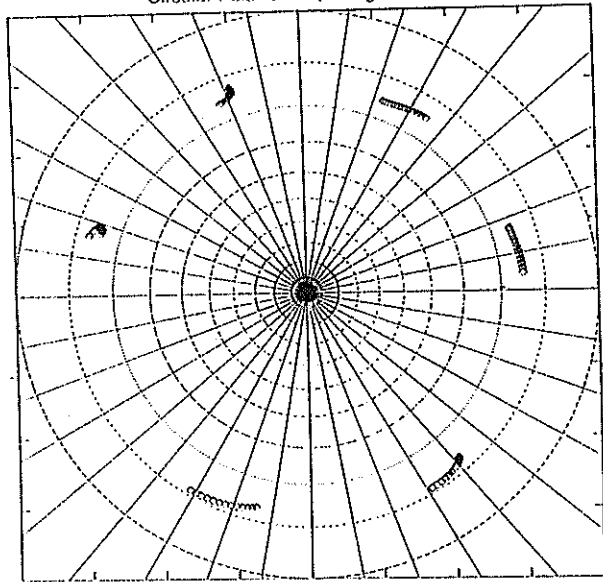

BIBLIOGRAPHY

(1)   **Born M., Wolf E., 1965**. Principles of optics, Pergamon press

(2)   **Clarke D., Grainger J.-F. 1971**. Polarised light and optical measurement, Pergamon press
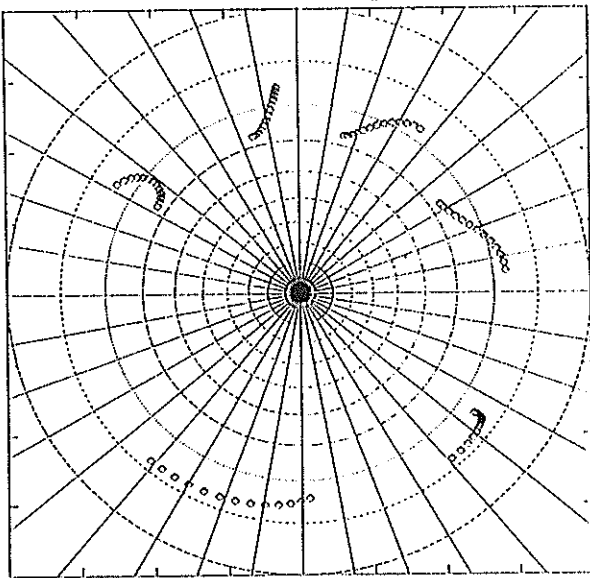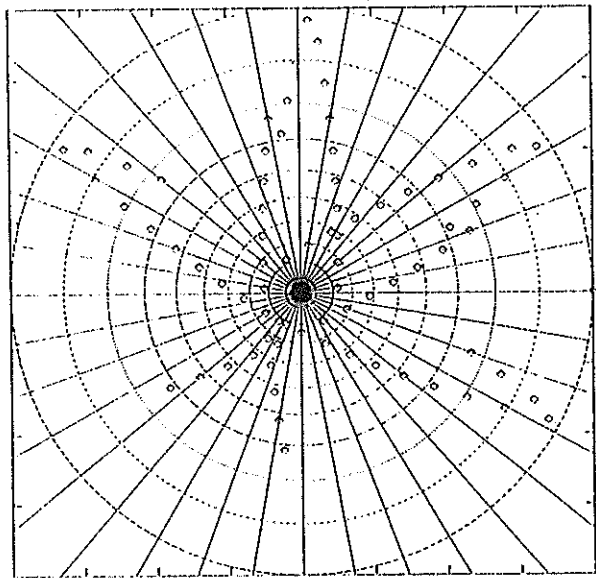
Circular Polarization, 0 deg. azimuth
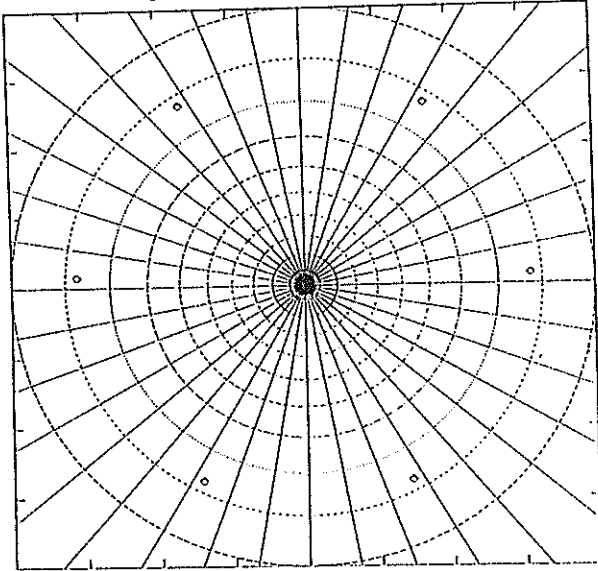
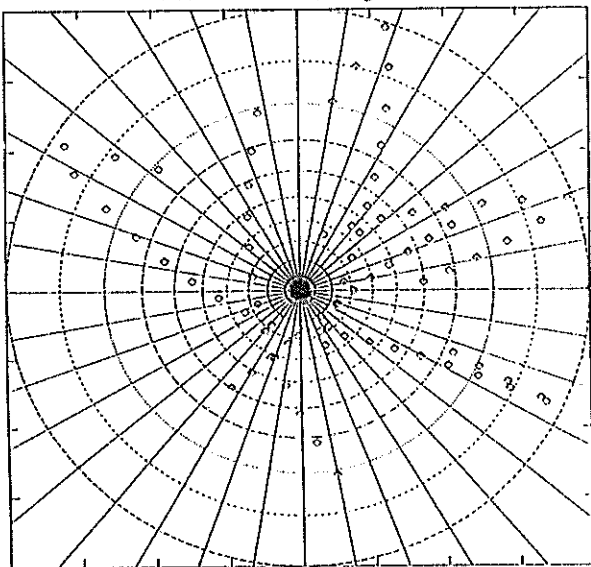Circular Polarization, 5 deg. azimuth
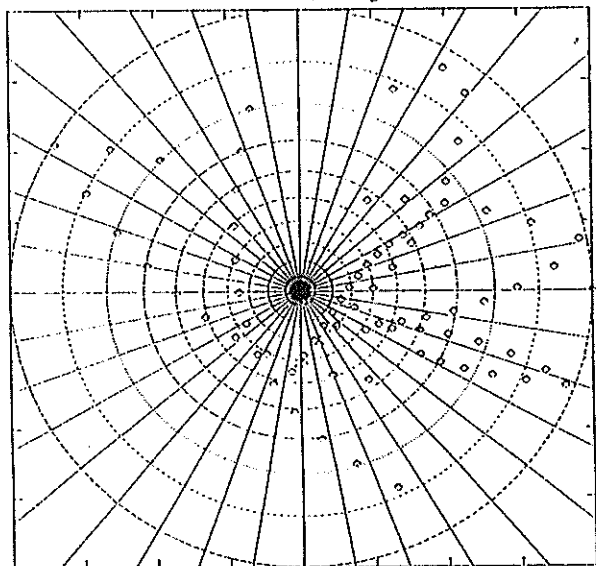
Circular Polarization, 10 deg. azimuth

Vertical Polarization, 0 deg. azimuth

Vertical Polarization, 5 deg. azimuth

Vertical Polarization, 10 deg. azimuth

EUROLAS Cluster Stations

Bias Workshop Results

G. Kirchner, F. Koidl
Institute for Space Research / Austrian Academy of Sciences
Observatory Lustbühel; A-8042 GRAZ / AUSTRIA

1.0 Introduction

During an EUROLAS meeting in spring 1996 at RGO, a small bias workshop in Graz was initiated, where
- all possible sources of SLR measurement biases should be discussed;
- tests and experiments should be initiated to detect/verify biases;
- methods should be suggested to ensure that all participating SLR stations deliver high quality, bias-free data products.

We tried to include all possible error sources, including calibration, start pulse detection, stop pulse detection, counters, air condition problems, meteorology, software etc.; this paper does not contain a complete list of all these items, but will show a few selected results only.

2.0 Meteorology

The most critical – and most difficult to calibrate – meteorological item is the barometric measurement; air temperature and humidity are of much less importance, or easy to verify. To enable an absolute calibration/comparison of barometric measurements, we suggested to send a calibrated, electronic barometer with remarkable accuracy and resolution on a round trip to the stations, for comparison with the local standards.

We organized a ParoScientific 740 Laboratory Standard – as a Demo device – from a German company (Althen), and sent it to RGO, Potsdam and Wettzell; all comparisons at these stations and in Graz resulted in maximum differences of below 0.1 hP.

Most stations use only one set of meteorolgical values, taken somewhere before or after a pass, which is applied then to all returns of the full pass; reaching now sub-cm accuracies, it is recommanded to take meteorological values more often (e.g. before AND after the pass) and to interpolate between these points for each range measurement.

Meteorological sensors should be read by computer only, to avoid observer errors; if possible, all meteorological values should be checked at least for plausibility, continuity etc.

3.0 Counters

Most counter problems can be detected easily with a MultiCounter system, as it is operational in Graz [1]; as a conclusion, we strongly recommand the use of at least a second counter for control/verification/improvement of the main counter.

As stated in [1], do not daisy-chain the external reference frequency for multiple counters; this might cause additional, hardly detectable biases.

Most counters have significant temperature problems (our HP5370A shows a drift of about 40 ps/°C of the cooling air; the cooling air temperature might be quite different from the

air condition temperature [1]); besides using counters in stabilized environment only, never switch off counters, to avoid warm-up problems, which might last for more than 1 hour.

4.0 Receiver

The main error source for SPAD systems is time walk due to different received energy; the best way to avoid this error is the use of time walk compensation circuits [2]; another way is to keep the return rate below the quantum efficiency (e.g. 20%); although this is an easy solution, it has some significant disadvantages:
- It reduces the amount of possible measurements by at least a factor of 5;
- Only the average return energy is at single photon-electron level; due to fluctuations there are still considerable multi photon-electrons present (although the major part of time walk will be cancelled out if calibration uses the same return energy);
- At single photon-electron level, the full satellite signature is present, and decreases single shot accuracy.

5.0 Calibration

It was recommanded to use short distance targets only (a few meters maximum) for calibration [3]; it is much easier to measure short distances to the mm-level or below; any meteorological influence is virtually eliminated (for a few 100 m target distance, this could be up to a few mm).

It was also recommanded to use at least 2 different targets, to avoid any specifics of a single target; any bias introduced by a single target could thus be detected easily; examples for such target specifics are target distance, one single, selected time only (Counter problems, HF-noise at that time etc.), direction dependence, fixed gate/return pulse relationships etc.

Any changes of the configuration between calibration and ranging should be avoided (like insertion of attenuation filters etc.).

6.0 Post-Processing Software Checks and Comparisons

Most of the EUROLAS stations use their own software for post-processing, Normal-Point calculations etc.; we wanted to make sure that these different software packages really produce the same results. Graz offered therefore to recalculate the Normal Points of various stations, using the Graz software, and compare the results with the NPs calculated at the stations (Fig. 1). If both calculations give similar numbers, this should be a good indication that both the stations software and the Graz software work correctly.

For all stations, we performed this comparisons for the raw data sets (as read from counters) and for MERIT-2 data sets; we have extended now also - on request - such comparisons for other stations outside EUROLAS, and we are offering such a quick check to anybody who is interested.

Fig. 2 shows a typical result of such a NP comparison with Potsdam Lageos data; the differences are typically far below 1 mm (6.6 ps), with no systematic offsets; due to complete diffferent methods (Graz uses e.g. polynomial fitting to residuals only, without any orbit analysis), the results cannot coincide exactly within the ps, but show that both methods deliver NP's coinciding to sub-mm. Slightly higher deviations at begin and end of the pass are usually due to small oscillations of polynomial fitting procedures of the Graz software.

Fig. 3 shows comparisons with RGO Normal Points; the slope is due to a difference of 40 ps between pre- and post-calibration: The RGO software uses the mean value, while the Graz software interpolates linearly between pre- and post-calibration for each return epoch. Besides this slope, the NP's coincide very well, except at begin and end, due to the Graz polynomial fitting procedures, and due to low number of points per NP here.

The MTLRS-1 data set (Fig. 4) shows the strong influence of the SPAD data skew; without any editing, the NP's coincide quite well, but the Peak-Minus-Mean of the data set is high (-8.9 mm); using a 2.2-sigma editing, this is reduced to -4.2 mm, but the mean values of the NP's are shifted now by more than -7 mm; to reduce this effect, it is important to handle both ranging and calibration data in exactly the same way; to eliminate it completely, the SPAD should be operated with higher Voltage above break (10 V instead of 2.5 V), using Time Walk Compensation Circuits; it is then possible to get Zero Peak-Minus-Mean [3]. MTLRS-1 will therefore consequently be upgraded with the full Graz Detection Package.

The Grasse Lageos-1 pass (Fig. 5) showed obvious problems; the NP differences were fluctuating randomly between +2 cm and -1 cm; the reason was an error in the Grasse software [4], which was detected and corrected; the comparison with the corrected data set shows that the error is eliminated completely now (Fig. 5).

References:

[1]   MultiCounter Operation at SLR Graz. G. Kirchner, F. Koidl; in these Proceedings.
[2]   Automatic SPAD Time Walk Compensation. G. Kirchner, F. Koidl; in these Proc.
[3]   Short Distance Calibration. G. Kirchner, F. Koidl; in these Proceedings.
[4]   F. Pierron, personal communication.
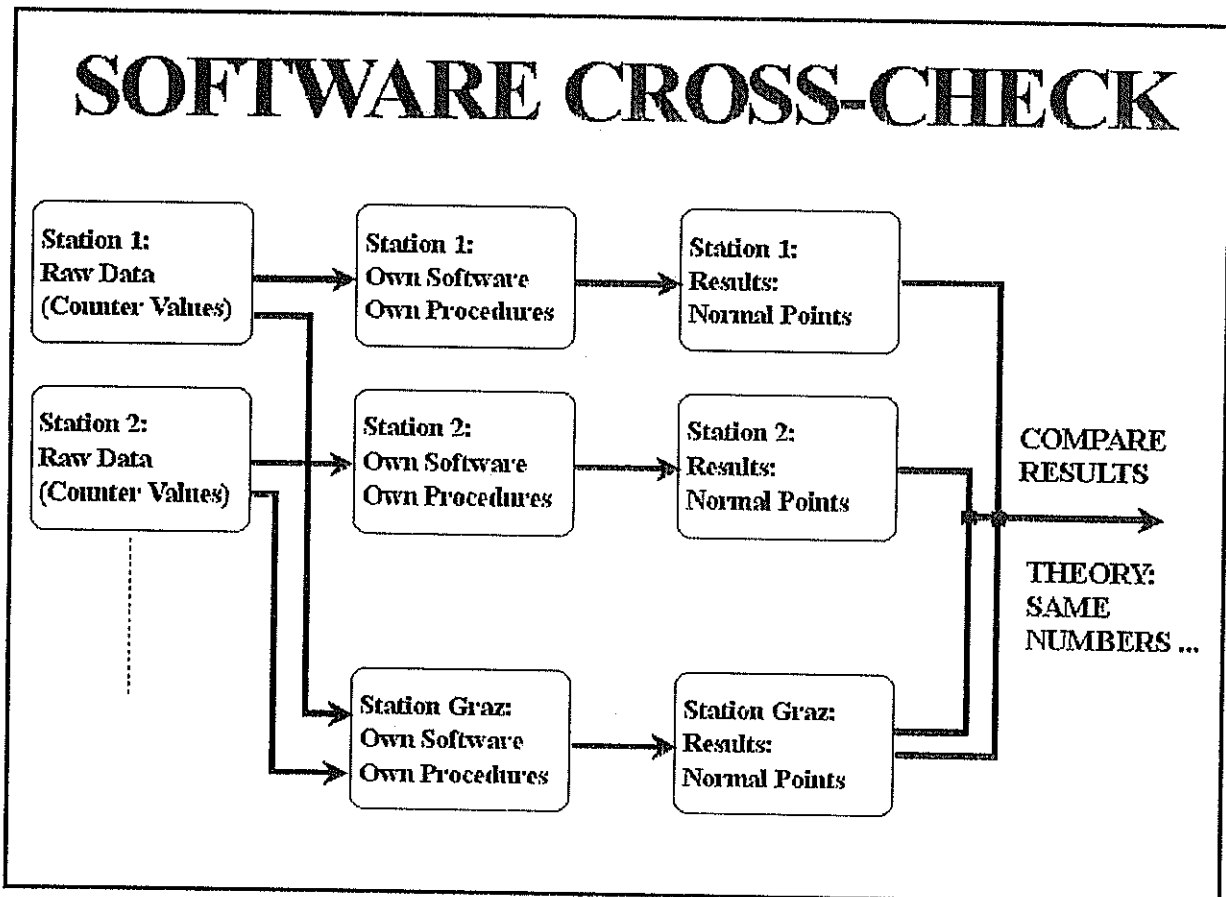
Fig. 1: Post-Processing Software Cross-Check Scheme
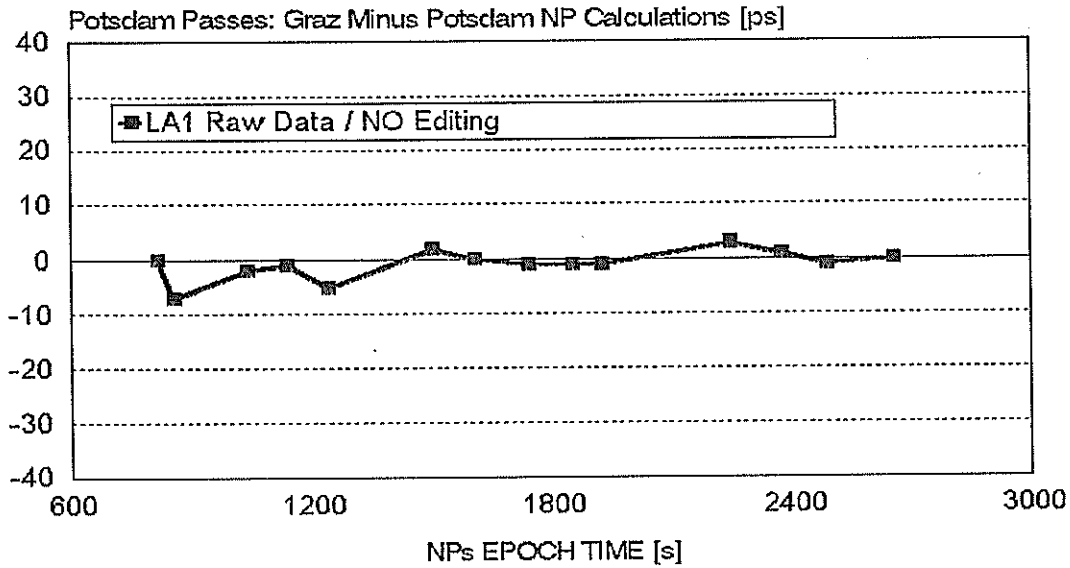
Fig. 2: Software Cross-Check: Potsdam LAGEOS-1 Raw Data
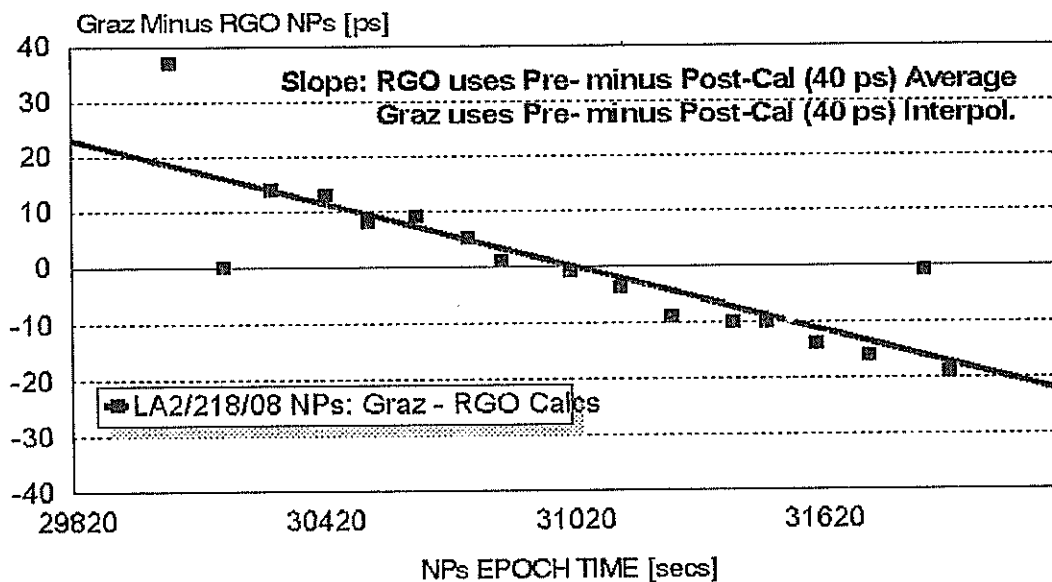
Fig. 3: Software Cross-Check: RGO LAGEOS-2 MERIT-2 Data
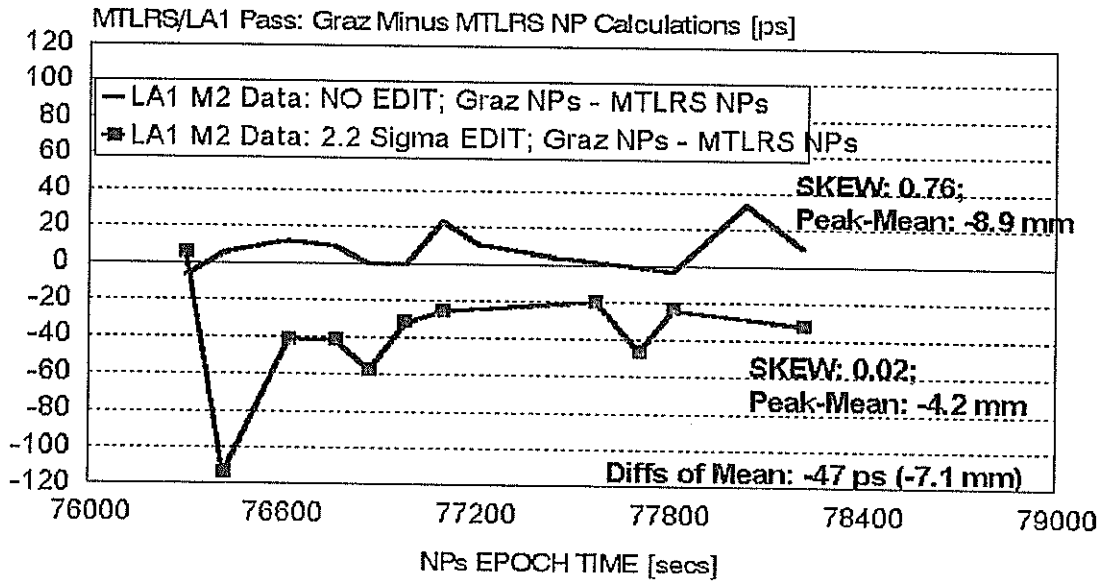
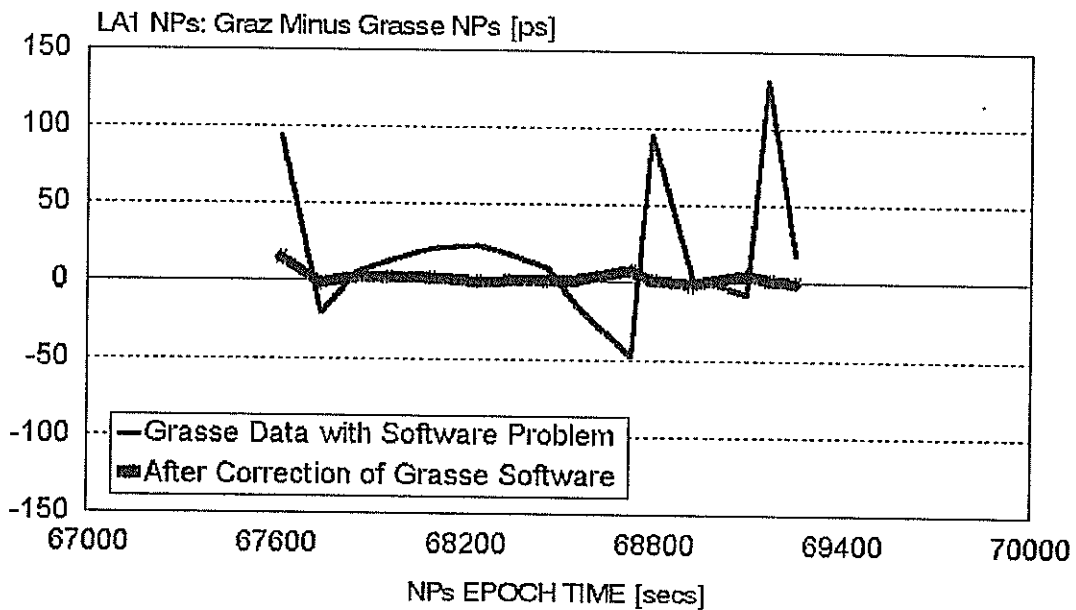Fig. 4: Software Cross-Check: MTLRS-1 LAGEOS-1 MERIT-2 Data

Fig. 5: Grasse LAGEOS-1 Raw Data, before / after Correction of Grasse Software

273

Detectors

and

Spectral Filters

The Performance Test of F4129f MCP-PMT in Changchun Station

Liu Zhi, Zhao You, Zhang Xinghua, Fan Cunbo
Changchun Artificial Satellite Observatory

The current paper presents the ranging results of both calibrating ground-target by using 3 different voltage dividers for F4129f MCP-PMT and ranging to satellites. The single shot range precision estimation is improved from 5-7cm (rms) to less than 3cm (rms).

1. Introduction

The single shot range precision of Changchun SLR was designed 5-7cm, and it has been this precision for many years. In order to follow the development of international SLR network, in 1994 we proposed a research plan to improve our SLR range precision, its target was: the single shot range precision to Lageos was better than 2cm. According to the situation of our SLR system, we chose the F4129 microchannel plate PMT, the product of ITT company, as photo-electronic detector, through more than one year test, we obtained the results of ranging to satellite.

The detector F4129 was the main device of this experiment, so we designed 3 kinds of voltage dividers which were suitable for F4129 device work ,and selected the best work condition for F4129 by ground target calibration. We chose voltage dividers and used it to range to satellites, the results of ranging to Lageos ware better than 2cm. The results of ranging to loworbit satellites were better than 2.5cm.

2. The Results of Ground Target Calibration

2.1 The principle diagram of calibration of ground target experiment

It is a simple and practicable way for us to select the best work condition of optic-electronic detector by calibration of ground target, simulating the strength of the satellite return signals, we drew up the calibration diagram, shown in Fig. 1.
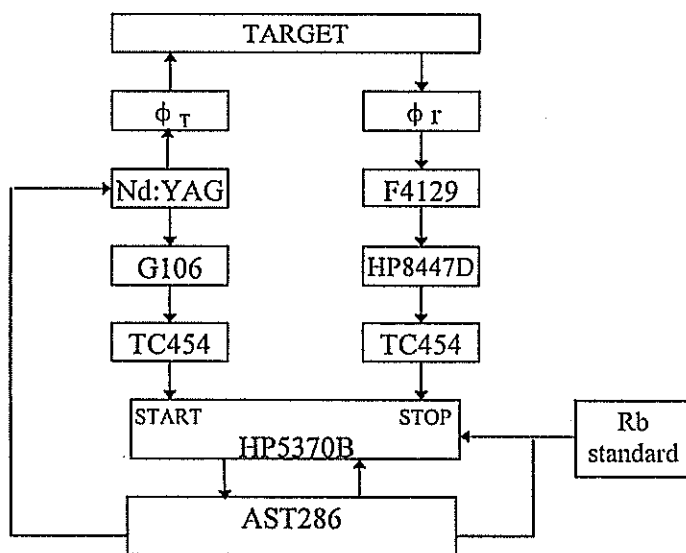

Fig.1 Scheme diagram of calibration

2.2 The structure and characteristics of 3 kinds of voltage divider

According to the characteristics of F4129, we designed 3 voltage dividers, whose structures and characteristics were as follows:

No.1 voltage divider:

    structure: Pi pole connected to ground, powered by positive and negative voltage

    characteristics: high gain

No.2 voltage divider:

    structure: A pole connected to ground, powered by high negative voltage

    characteristics: coupled directly, high gain

No.3 voltage divider:

    structure: Pi pole connected to ground, powered by positive and negative voltage

    characteristics: with negative feedback current, low gain

2.3 The condition for calibration ground target

The condition for calibration of ground target for 3 voltage dividers kept the same: the laser pulse width 220 ps; the laser output energy around 100 mj; the stability of rubidium standard 2×10^{-12} per day; the trigger level of 5370B counter -0.35v; the same constant fraction discriminator;

2.4 The results of calibration

The 3 voltage dividers were used to ground target calibration under above conditions, the results are shown in table 1, 2 and3. Table 4 is the calibration results of No.3 voltage divider simulating satellite dynamic echoes.

Table 1

OPE. Vol(v)	mean. (μs)	ξ (%)	rms (cm)	φ t	φ r	tem.(℃)
2900	8.588752	70	3.1	20	0.2	8
2950	8.588645	84	2.6	20	0.2	8
3000	8.588563	90	2.0	20	0.2	8
3100	8.588427	93	1.9	20	0.2	8
3200	8.588372	97	1.4	20	0.2	8

Table 2

OPE. Vol(v)	mean. (μs)	ξ (%)	rms (cm)	φ t	φ r	tem.(℃)
-2900	8.598611	20	4.0	20	0.2	10
-3000	8.589761	22	3.6	20	0.2	10
-3100	8.589214	30.1	3.0	20	0.2	10
-3200	8.588382	46.1	3.6	20	0.2	10

Table 3

OPE. Vol(v)	mean. (μs)	ξ (%)	rms (cm)	φ t	φ r	tem.(℃)
3100	8.589742	16	1.5	20	0.2	15
3100	8.589785	10	1.3	20	0.2	15
3200	8.589716	24.2	1.5	20	0.2	15
3200	8.589723	20.1	1.9	20	0.2	15
3300	8.589548	39.7	1.3	20	0.2	15
3300	8.589577	43.9	1.5	20	0.2	15

Table 4

OPE. Vol(v)	mean. (μs)	ξ (%)	rms (cm)	φt	φr	tem.(°C)
3200	8.582288	91.5	1.36	20	0.2	8
3200	8.582300	86.5	1.22	20	0.1	8
3200	8.582312	33.1	1.32	20	0.08	8
3200	8.582324	16.9	1.46	20×7	0.08	7
3200	8.582345	7.8	1.53	20×2	0.08	6

3. The Results of Satellite Ranging

According to the results shown in above tables, we selected No.3 voltage divider. In September 1995, we obtained some experimental data from satellites (in table 3). From table 3 we can see: the single shot range precision is better than 2cm to Lageos, and better than 2.5cm to loworbit satellites with No.3 voltage divider.

Table 3

LAGEOS-1		LAGEOS-2		ERS1		STARLETTE		AJISAI	
rms (cm)	obs	rms (cm)	obs	rms (cm)	obs	rms (cm)	obs	rms (cm)	obs
1.5	41	1.9	496	2.1	177	2.3	413	2.5	103
1.6	481	1.6	391			1.8	138		
		1.6	23						
		1.7	35						

4. Unsolved Problems

The gain and thermal noise problem of F4129 device

The data in table 3 show: the return rate of No.3 voltage divider is less than No.1 or No.2 voltage divider. When we use No.3 to satellite ranging, the work voltage of F4129 was close to its maximum work voltage; obviously, it is unacceptable for this device to work under its maximum voltage in long-term.

In order to improve the detector sensitivity, we tried to use two-stage amplifiers (HP8447D+HP8447E), but the noise increased, that is why we do not use it in our routine observation. We have ordered the pre-amplifier A-7 from No.13 Institute of Ministry of Electric Industry in China, its characteristics can meet our need. We hope the MCP-PMT receiver will be in operational in a few months.

References:

(1) ITT. Microchannel Plate Photomultiplier Tube Test Report Summary, 1991,1
(2) HP. 0.1-1300MHz Amplifier Operation and Service Manual
(3) The Products Manual of No.13 Institute of Ministry of Electronics Industry

Increasing System Sensitivity At LURE Observatory
or
How To Get GPS Data With A 400 mm (16 inch) Aperture Telescope

R. Zane, M. T. Maberry and D. J. O'Gara
University of Hawaii, Institute for Astronomy
LURE Observatory at Haleakala
P.O. Box 209
Kula, Maui, Hawaii, U.S.A.
E-Mail: zane@lure.ifa.hawaii.edu

Abstract: The overall system sensitivity was increased by modifying the Tennelec TC-454 discriminator to increase its input sensitivity and stability. An improved 532 NM narrow band filter with full width half maximum (FWHM) bandpass of 0.3 nm and 80% transmission was installed along with an adjustable field stop to regulate field of view. The resultant increase in system sensitivity allows regular acquisition of GPS satellites.

Introduction

Early attempts to increase system sensitivity involved using several different kinds of high speed pulse amplifiers to increase the pulse amplitude. No amplifiers were found which did not also introduce additional problems in the form of amplitude dependent phase shift or "time walk." It was also observed that amplification did not improve signal to noise ratio. It was then decided to approach the sensitivity problem by reducing losses, reducing noise while also increasing the input sensitivity of the TC-454 discriminator. Improvements were also made in the data acquisition software

Method

Constant Fraction Discriminators divide an input pulse into two components established by an attenuator network that has a fifty ohm impedance. One part is reduced by the fraction, F, while the other part is reduced by the fraction, (1-F). A typical value of F=0.2 is used in the Tennelec (Oxford Instruments) TC-454. In the TC-454, the fraction that is reduced by F is applied directly to the negative input of a fast, ECL, differential comparator (see schematic 4X038-S1). The fraction that is reduced by (1-F) is delayed slightly, so that its leading edge intersects the peak of the direct fraction, and applied to the positive input of the fast ECL differential comparator (see Figure 1). The difference appearing across the inputs of the comparator is shown in Figure 2. The comparator switches state when the difference passes through 0 volts. In principle the 0 volt crossing point is invariant in time as the input pulse amplitude changes. In practice, there are variations, both random and systematic, caused by noise, offsets in the comparator, and variations in the input pulse shape. Nonlinearities in the "timewalk" characteristic are especially noticeable for very low level pulses.

A Delayed Symmetry Discriminator applies the input pulse directly to the negative input of a fast ECL differential comparator. The same pulse is then delayed by the Full Width at Half Maximum (FWHM) of the input pulse and applied to the positive input of the differential comparator as shown in Figure 3. The difference appearing across the inputs

of the comparator is shown in Figure 4. The comparator switches state when the difference passes through zero volts. The zero volt crossing occurs at the Half Maximum point on the trailing edge of the direct pulse and at the Half Maximum point on the leading edge of the delayed pulse. The improved time stability and resolution of the DSD technique are due to the higher amplitude and faster rate of change of the differential voltage at the input to the comparator.

It has been found that a slight modification to the standard TC-454 allows operation of the TC-454 in the DSD mode. The circuit changes are detailed in schematic 4X038-S2. It has also been found that disabling the "Z" adjustment, so that "Z" is always 0 volts, results in less variation in the timewalk characteristic of the TC-454. This is due to the fact that small changes in the power supply voltages in the NIBin result in changes of about 1 mV on the "Z" bias. The return pulse out of the MCP Photomultiplier is typically around 1 NS FWHM. Pulses of this width are approaching the response limit of ECL comparator circuits. The ECL comparator integrated circuit used in the TC-454 discriminator is manufactured by four companies. The specified response times of the four circuits are as follows:

Manufacturer	Part No.	Response Time
1. MAXIM	MAX9687	1.9 NS
2. Signal Processing Technologies	SPT9687	2.3 NS
3. Analog Devices	AD9687	2.7 NS
4. GEC Plessey	SP9687	3.0 NS

The MAXIM comparator integrated circuit was tested and found to produce lower rms error than the GEC Plessey or the Analog Devices circuits. The Signal Processing Technologies version of the comparator was not tested.

The DSD modified TC-454 discriminator has been operated for the past 11 months with a single discriminator section used for the "start" pulse and a single discriminator section used for the "stop" pulse. The single discriminator mode of operation results in a savings of about -6db in losses due to a splitter and delay cable. The "stop" discriminator threshold has been set at minimum adjustment, "T"= -50MV, which produces a measured threshold of approximately -20 millivolts. Figures' 5A and 5B illustrate the results of a calibration using the DSD modified discriminator for both the "start" and "stop" pulses. The linear "time walk" characteristic in the calibration has been corrected with software (see "Real Time Correction of SLR Range Measurements for the Return Amplitude Induced Bias of the Multi-Channel Plate PMT/TC-454 DSD Discriminator Receive System, D. J. O'Gara, et al).

The receive optics were redesigned in order to increase the transmission of the return pulse while at the same time reducing the amount of optical noise(see 4X038-L1 and 4X038-L2). A variable field stop (2 to 30 mm) was added at the focal plane of the +225 mm F.L. focusing lens to allow control of the field of view. A +25 mm recollimating lens produces a collimated beam of about 1.75 mm diameter. A turning mirror, of high reflectivity, then redirects the beam into a Barr Associates 0.3 nm FWHM narrow band 532.08 filter. The narrow band filter is rotated to a tilt angle of about 3.5 degrees in order to optimize transmission at 532.00 NM. The filter has a peak transmission of approximately 80%.

Great care was taken to reduce electrical noise throughout the system by implementing good grounding and shielding techniques wherever possible. It was found that unused sections of the TC-454 discriminator needed to be gated off with a terminator because if the gates were left open the discriminators oscillated. The NIBIN containing the TC-454 was moved to a point directly beneath the receiver in order to reduce cable lengths. The output of the MCP was terminated directly into a 50 ohm pulse splitter. One output of the splitter was connected through 1 meter of coaxial cable directly to the stop discriminator (DSD modified). The other output was connected through a long coaxial cable to an amplifier driving another splitter to provide a return pulse for the digitizing display and the pulse energy digitizer (REM).

Conclusions

The reduction in system noise sources and decreased signal loss produced a substantial increase in signal to noise ratio of the "stop" pulse from the MCP photomultiplier. The improved sensitivity and linearity of the DSD modified TC-454 also allowed operation of the "stop" discriminator at a minimum threshold voltage setting. The previous dynamic range of "stop" pulse, as measured at the TC-454 input, ranged from a maximum of 4.5 V-NS to a minimum of 0.25 V-NS (18 to 1). The current dynamic range is from a maximum of 4.5 V-Ns to a minimum of 0.03 V-NS (150 to 1). The increased sensitivity permits regular acquisition of the GPS satellites.

CFD -Direct & Delayed Pulses

FIGURE 1

CFD - Difference Pulse
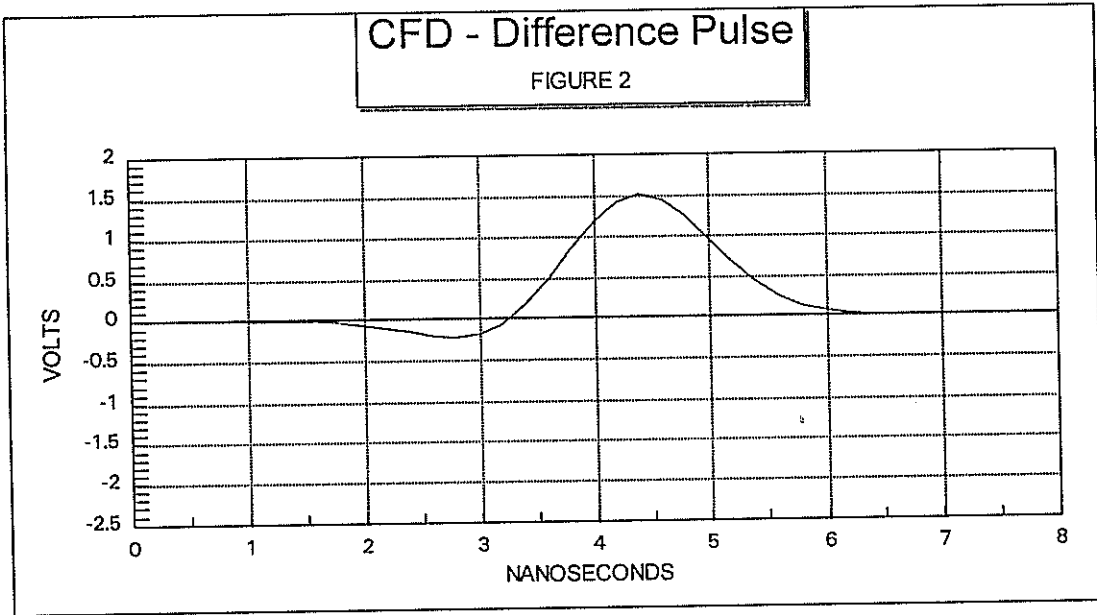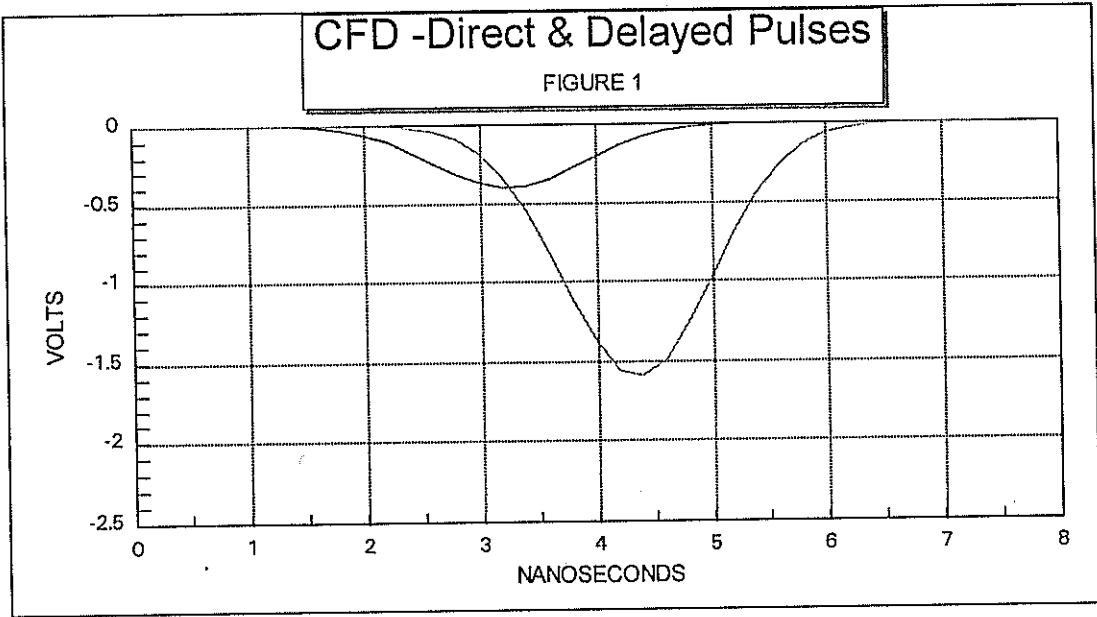
FIGURE 2

DSD - Direct & Delayed Pulses
FIGURE 3
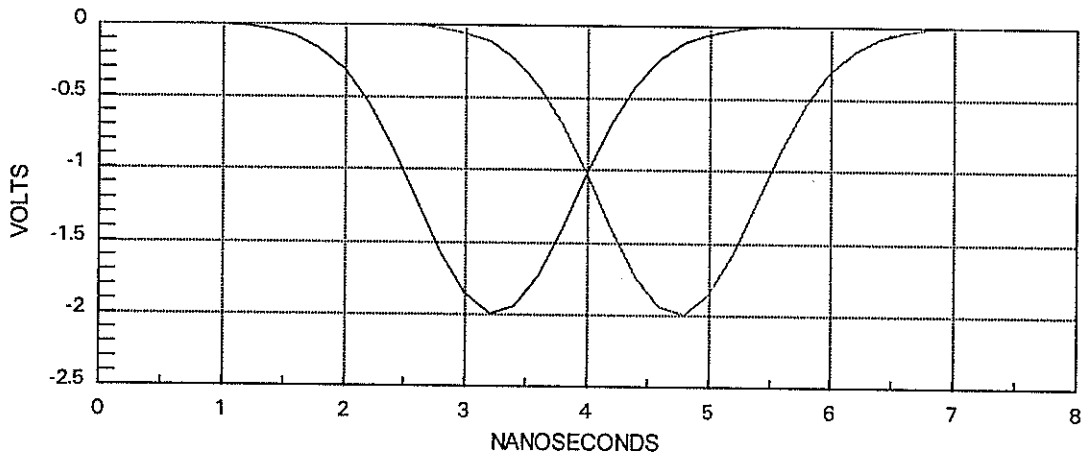
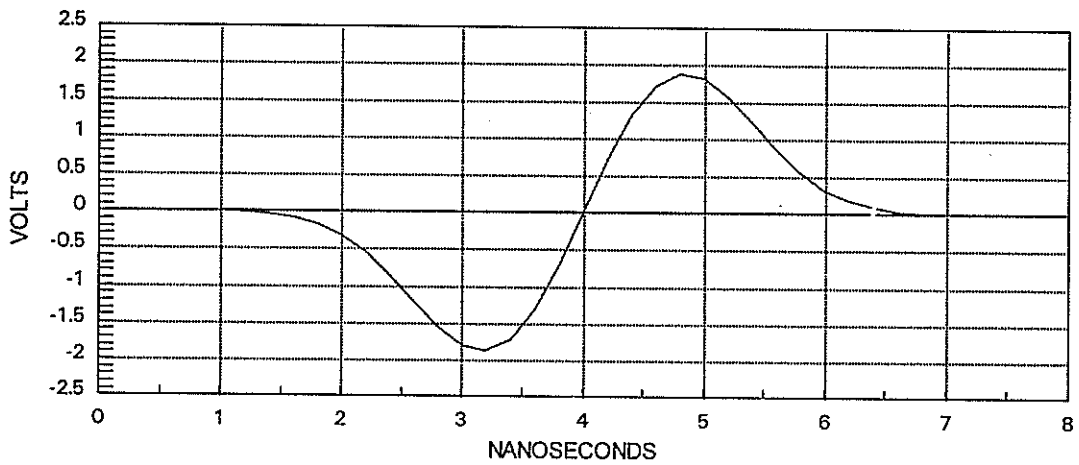

DSD - Difference Pulse
FIGURE 4

283

FIGURE: 5A
RESIDUAL VS REM# WITH LSQ FIT
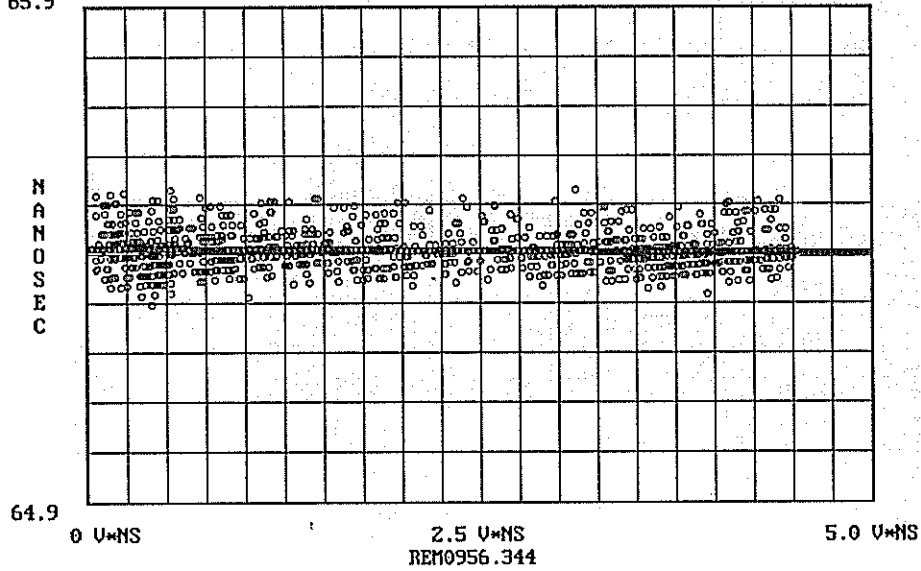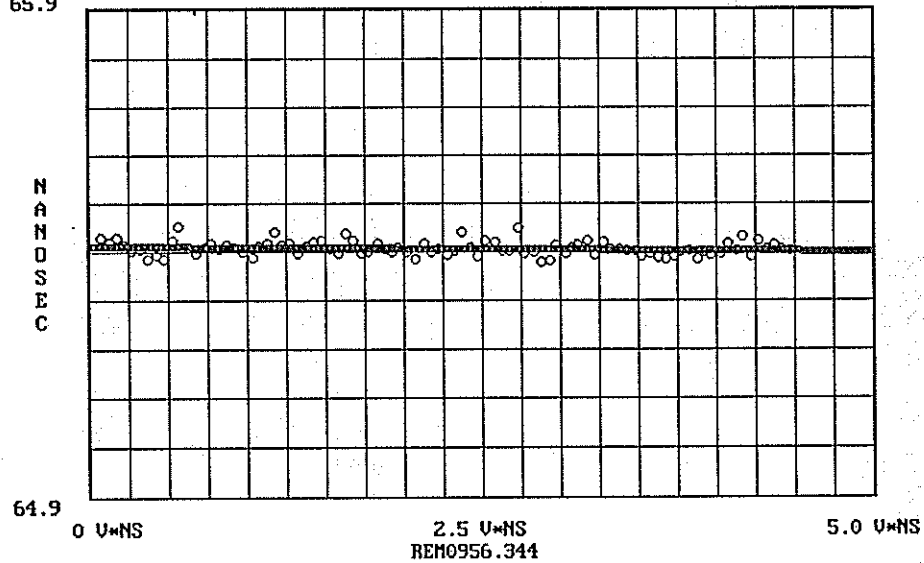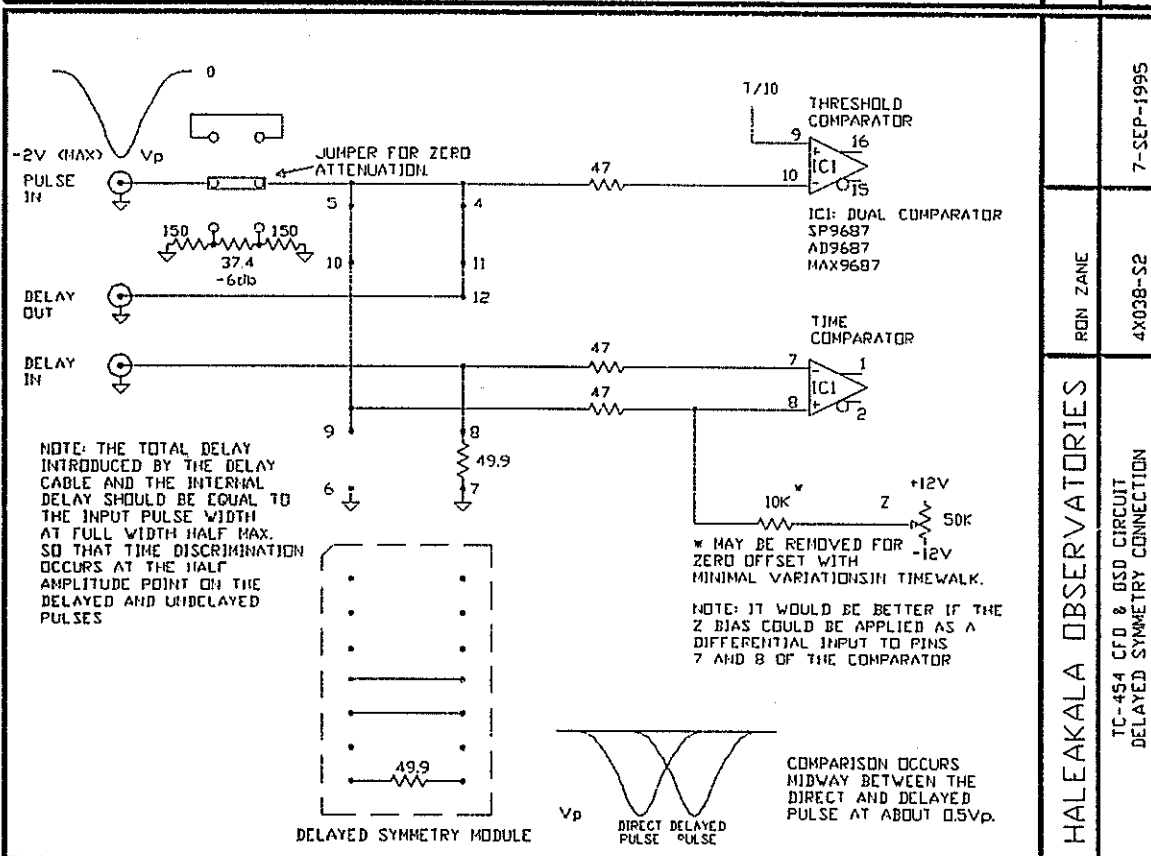INTERCEPT = 65.411 NS   SLOPE =-2 PS/V*NS   RMS = 6.27 MM

FIGURE: 5B
RESIDUAL VS REM# WITH LSQ FIT. MODULO 20
INTERCEPT = 65.411 NS   SLOPE =-2 PS/V*NS   RMS = 6.27 MM
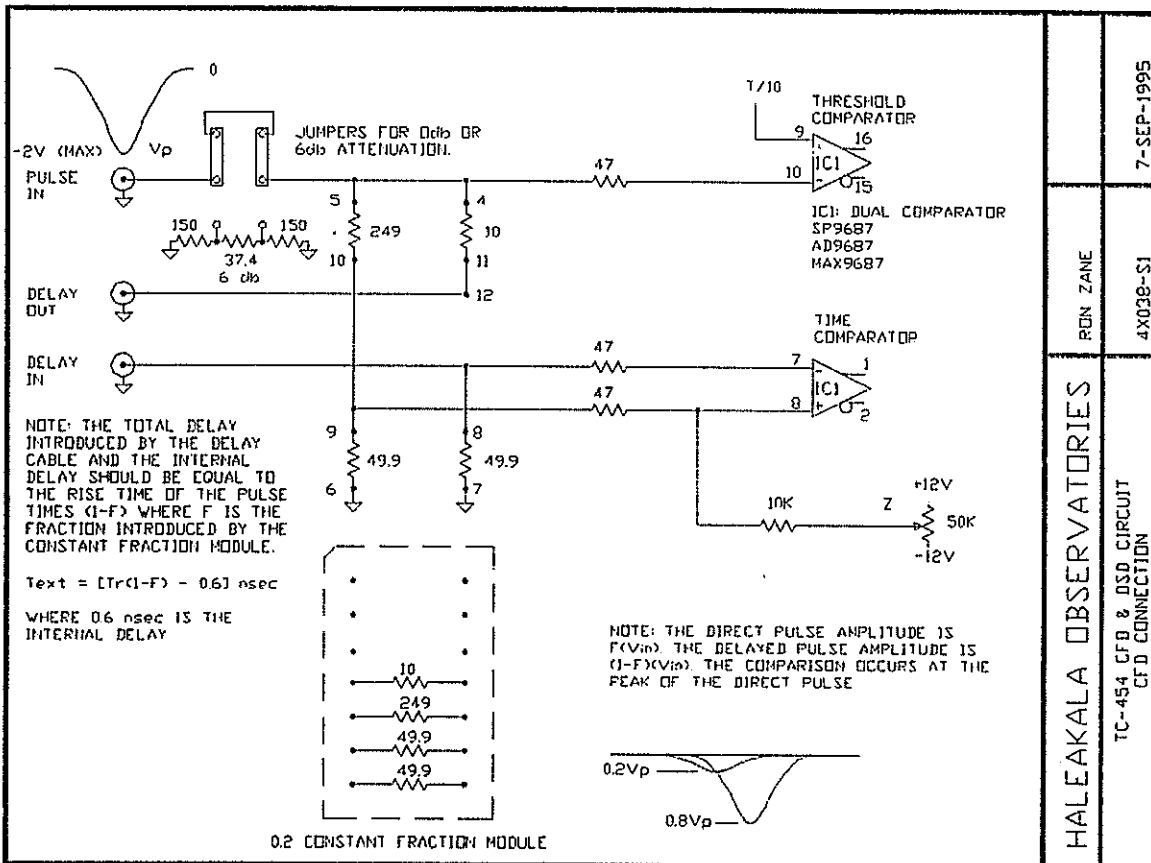
Top schematic

0

-2V (MAX) Vp

JUMPERS FOR 0db OR 6db ATTENUATION.

PULSE IN

7/10

THRESHOLD COMPARATOR

47

9   16
IC1
10   15

IC1: DUAL COMPARATOR
SP9687
AD9687
MAX9687

150   150
37.4
6 db

5   4
249   10
10   11
12

DELAY OUT

DELAY IN

TIME COMPARATOR

47

7   1
IC1
8   2

47

NOTE: THE TOTAL DELAY INTRODUCED BY THE DELAY CABLE AND THE INTERNAL DELAY SHOULD BE EQUAL TO THE RISE TIME OF THE PULSE TIMES (1-F) WHERE F IS THE FRACTION INTRODUCED BY THE CONSTANT FRACTION MODULE.

9   8
49.9   49.9
6   7

Text = [Tr(1-F) - 0.6] nsec

WHERE 0.6 nsec IS THE INTERNAL DELAY

+12V
10K   Z
50K
-12V

NOTE: THE DIRECT PULSE AMPLITUDE IS F(Vin). THE DELAYED PULSE AMPLITUDE IS (1-F)(Vin). THE COMPARISON OCCURS AT THE PEAK OF THE DIRECT PULSE

10
249
49.9
49.9

0.2 CONSTANT FRACTION MODULE

0.2Vp

0.8Vp

HALEAKALA OBSERVATORIES

RON ZANE

7-SEP-1995

4X038-S1

TC-454 CFD & QSD CIRCUIT
CFD CONNECTION

Bottom schematic

0

-2V (MAX) Vp

JUMPER FOR ZERO ATTENUATION.

PULSE IN

7/10

THRESHOLD COMPARATOR

47

9   16
IC1
10   15

IC1: DUAL COMPARATOR
SP9687
AD9687
MAX9687

150   150
37.4
-6db

5   4
10   11
12

DELAY OUT

DELAY IN

TIME COMPARATOR

47

7   1
IC1
8   2

47

9   8
49.9
6   7

NOTE: THE TOTAL DELAY INTRODUCED BY THE DELAY CABLE AND THE INTERNAL DELAY SHOULD BE EQUAL TO THE INPUT PULSE WIDTH AT FULL WIDTH HALF MAX. SO THAT TIME DISCRIMINATION OCCURS AT THE HALF AMPLITUDE POINT ON THE DELAYED AND UNDELAYED PULSES

+12V
10K   Z
50K
-12V

* MAY BE REMOVED FOR ZERO OFFSET WITH MINIMAL VARIATIONS IN TIMEWALK.

NOTE: IT WOULD BE BETTER IF THE Z BIAS COULD BE APPLIED AS A DIFFERENTIAL INPUT TO PINS 7 AND 8 OF THE COMPARATOR

49.9

DELAYED SYMMETRY MODULE

Vp

DIRECT   DELAYED
PULSE   PULSE

COMPARISON OCCURS MIDWAY BETWEEN THE DIRECT AND DELAYED PULSE AT ABOUT 0.5Vp.

HALEAKALA OBSERVATORIES

RON ZANE

7-SEP-1995

4X038-S2

TC-454 CFD & QSD CIRCUIT
DELAYED SYMMETRY CONNECTION

LURE OBSERVATORY SLR SYSTEM TRANSMIT OPTICS

DICHROIC BEAM SPLITTER

400 MM APERTURE ACHROMAT

100 MM DIAM. TRANSMIT BEAM. DIVERGENCE FROM 10 TO 160 uR.

27 INCH FLAT MIRROR 'LUNASTAT' ALTITUDE-AZIMUTH MOUNT DRIVEN BY COMPUTER

MOVEABLE DIVERGER LENS F.L. = -390 MM DIAM. = 50 MM

TURNING MIRROR

'HOLEY' MIRROR (10 MM HOLE)

6 ND FILTER INSERTION POINT

ND-YAG LASER

FOCUSSING LENS F.L. = 225 MM DIAM. = 80 MM

50 MM ENTRANCE APERTURE.

0 TO 2 ND AND 0 TO 4 ND VARIABLE ATTENUATORS.

VARIABLE FIELD STOP 2 TO 30 MM

0.3 NM LASER LINE FILTER, 25 MM DIAM. 80% TRANSMISSION

RECOLLIMATING LENS. F.L. = 25 MM DIAM. = 25.4 MM

TO STOP DISCRIMINATOR

TO REM AND DIGITIZER

RON ZANE | 6-OCT-1996

4X038-L1

TURNING MIRROR

MCP

SPLITTER

LURE OBSERVATORY SLR SYSTEM RECEIVE OPTICS

DICHROIC BEAM SPLITTER

400 MM APERTURE ACHROMAT

27 INCH FLAT MIRROR 'LUNASTAT' ALTITUDE-AZIMUTH MOUNT DRIVEN BY COMPUTER

MOVEABLE DIVERGER LENS F.L. = -390 MM DIAM. = 50 MM

40 MM DIAMETER COLLIMATED RETURN

TURNING MIRROR

'HOLEY' MIRROR (10 MM HOLE)

6 ND FILTER INSERTION POINT

ND-YAG LASER

FOCUSSING LENS F.L. = 225 MM DIAM. = 80 MM

50 MM ENTRANCE APERTURE.

0 TO 2 ND AND 0 TO 4 ND VARIABLE ATTENUATORS.

VARIABLE FIELD STOP 2 TO 30 MM

0.3 NM LASER LINE FILTER, 25 MM DIAM. 80% TRANSMISSION

RECOLLIMATING LENS. F.L. = 25 MM DIAM. = 25.4 MM

TO STOP DISCRIMINATOR

TO REM AND DIGITIZER

RON ZANE | 6-OCT-1996

4X038-L2

TURNING MIRROR

MCP

SPLITTER

286

SPAD DETECTORS FOR RANGING
WITH SUB-MILLIMETER BIAS

I.Prochazka, K.Hamal

Czech Technical University, Brehova 7
15 19 Prague 1, Czech Republic
fax +42 2 85762252, prochazk@mbox.cesnet.cz

B.Greene

Electro Optics Systems, PtyLtd, Queanbeyan,NSW, Australia

The SPAD detectors have proven to be the effective detectors for satellite laser ranging, principally because of the low bias obtainable in a single photo electron mode. The low bias property of the SPAD is a crucial feature, as bias reduction is the highest priority in global SLR. It is possible to obtain sub-millimeter bias in a SLR system using SPAD provided the return rate is low, under the standard ranging conditions not exceeding 10%.

However, the low return rate imposes some limitations on station performance also. In particular synchronous SLR data is valid only for occasions [shots] when four stations acquire a target simultaneously. It is obvious, that to obtain a realistic synchronous ranging data rate, the relatively high return rates at each station is needed. In addition, for non-synchronous SLR it is also an advantage to acquire a high number of valid return within a satellite pass, so that tracking efficiency is optimized.

Various techniques for operating a SPAD detector with a high single shot resolution and a low bias is discussed. The design of the new generation SPAD detectors which can be operated in low bias mode even at high return rate is given. The proposed devices have the advantage that they may be operated as a conventional SPAD, they use the same satellite optical depth models as for the conventional SPADs [ie it is backwards compatible] and raw , uncorrected, data is available for the corrected device.

GOALS
Ranging on SPAD with sub-millimeter bias

- LOW DETECTOR INDUCED RANGE BIAS

- SUB-MILLIMETER BASELINE ACCURACY

- SINGLE SHOT RESOLUTION (rms)
  < 4 millimeters on terrestrial
  < 5 millimeters on satellite

- SYSTEM TEMPORAL STABILITY
  < 4 psec / hour half peak to peak

- PRODUCTIVITY AND DATA QUALITY
  dark count
  data rate (synchron. ranging)
  data distribution

I.Prochazka, K.Hamal, B.Greene, Shanghai,'96

RANGING ON SPAD JITTER STATUS QUO

application	site (laser)	calib. / ERS-1
SLR	RGO (100 psec)	9 mm / 10-12 mm
	SALRO (100 psec)	9 mm / 10-12 mm
	Helwan 2 (35 psec)	8 mm / 10 mm
	Graz old (35 psec)	8 mm / 10 mm
indoor	Prague (30 psec)	* 4 mm
spectroscopy	Berlin (fsec)	* 3 mm

Single photon ranging limit, 3V above
* FWHM = 2.4 * RMS

I.Prochazka, K.Hamal, B.Greene, Shanghai'96

SPAD TIMING RESOLUTION LIMITS

- voltage above break
  2.5 ..5 (11) Volts above break

- temperature
  +22 . -90 Centigrades

- data distribution
  new data processing procedures
  rms = fwhm / 2.4

- signal strenght dependence

I.Prochazka, K.Hamal, Prague, July '96

RANGING JITTER REDUCTION - POSSIBLE SOLUTIONS

- VERY LOW ECHO RETURN RATE
  The single photoelectron echoes may be guaranteed
  by an extremely low echo return rate, 2 % or less.

- TIME WALK COMPENSATION
  A fast analog circuit is used to monitor echo signal
  strength and to adjust the detector propagation delay
  to compensate for the time walk effect.

- SINGLE PHOTOELECTRON ECHOES SELECTION
  The echo signal strength is monitored, the multi PE
  echoes are ignored.

- SIGNAL STRENGTH MONITORING
  The echo signal strength is monitored, the time walk
  is software compensated

Under normal conditions, the echo
signal strength is fluctuating typ. 1 : 100

I.Prochazka, K.Hamal, B.Greene, Shanghai '96

SPAD parameters vers. bias above break
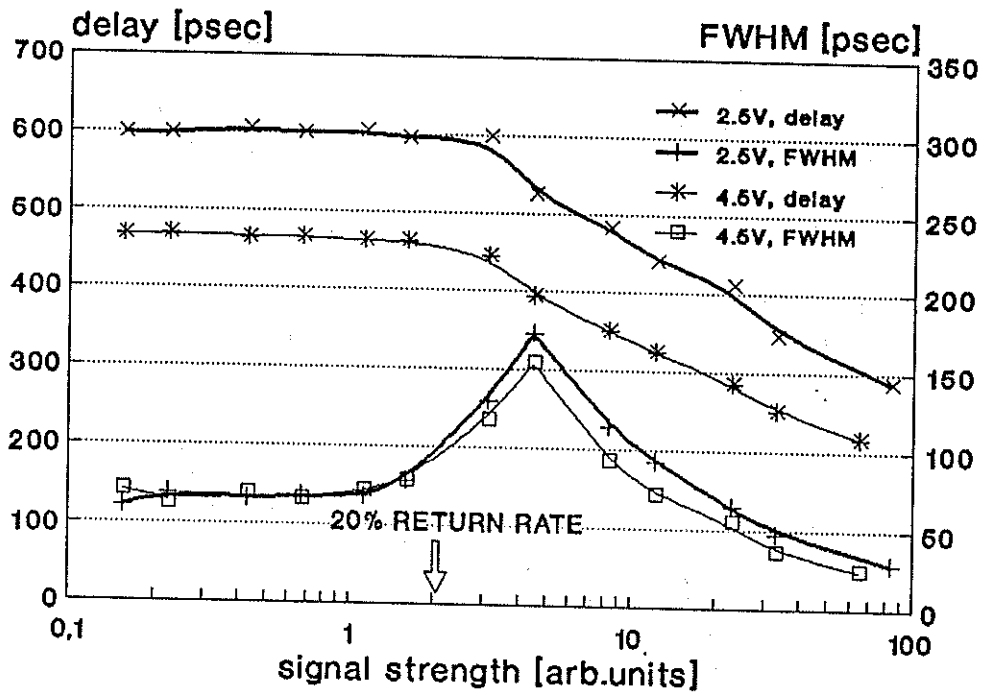## Cooled 200um chip,30ps electr.32ps laser

total FWHM [psec] sensitivity/dark [a.u.]

rel.sensitivity

dark count

timing FWHM

voltage above break [V]
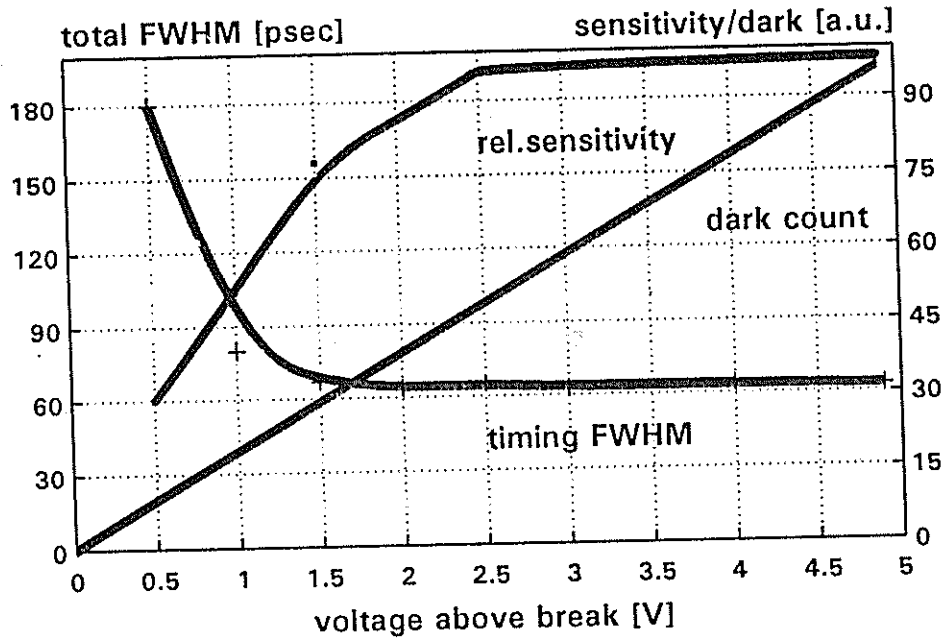
I.Prochazka, January, 95

SPAD timing jitter vers.cooling
Chip SN 23790,200um, comparator KP
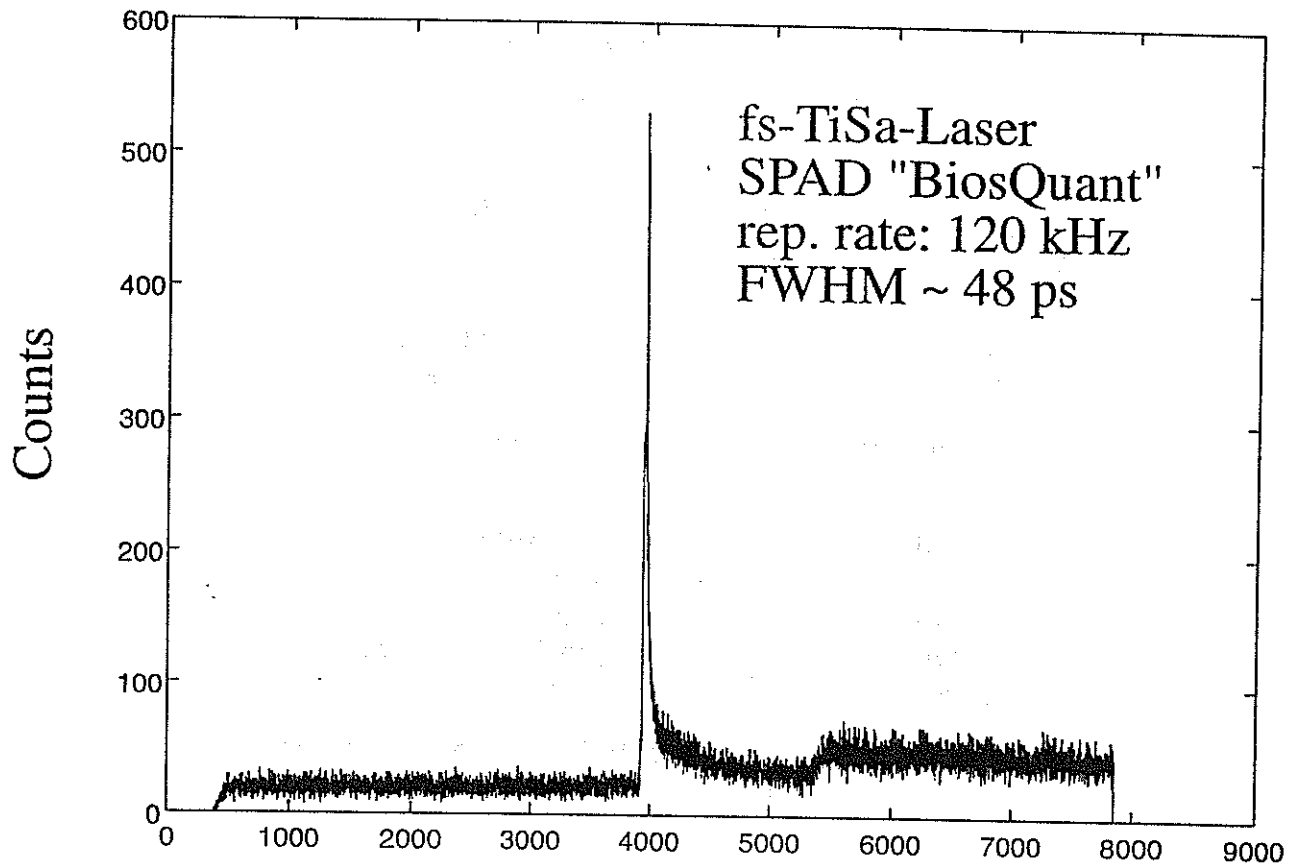## Electronics&laser contrib. deconvoluted

Timing resolution FWHM [psec] jitter [psec]

+23 Centig.

-80 Centig.

Bias above the break
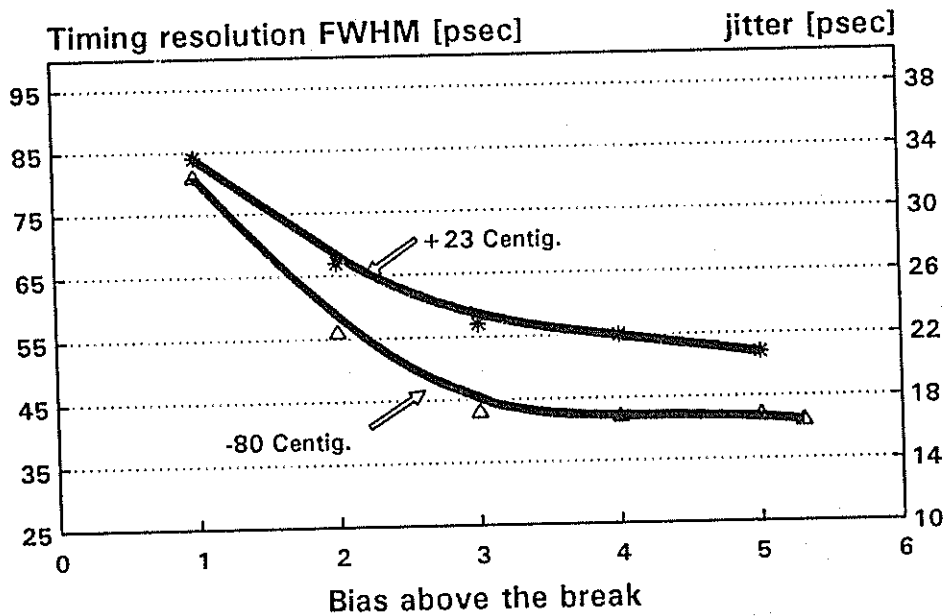
I.Prochazka, Prague,April 6,1995

SPAD dynamical range test

fs-TiSa-Laser
SPAD "BiosQuant"
rep. rate: 120 kHz
FWHM ~ 48 ps

J.Blazej, I.Prochazka, Prague June 1996

POSSIBLE SOLUTIONS COMPARISON

advantages   limitations

LOW RETURN RATE /RGO
* simple,NO additional hardware   * low return rate
* minimal range bias   * synchron.ranging
* satellite signature solved   data rate -> 0 %
* high timing stability

TIME WALK COMPENSATION /Graz
* existing hardware   * timing stability ?
* RMS < 4/5 mm demonstrated   * range biases to be solved
* return rate -> 99%   * sat.signature to be solved

SINGLE PE ECHOES SELECT./Prague
* minimal range bias   * hardware under development
* satellite signature solved   (40 psec gate)
* high timing stability   * return rate < 20%
* return rate -> 20%   * others ?

SIGNAL STRENGTH MONITORING /EOS
* single/multi PE timing   * harware under development
  information available   (2 psec timing)
* return rate -> 99%   * others ?

I.Prochazka, K.Hamal, B.Greene, Shanghai '96

CONCLUSION
SPAD detectors for ranging with sub-mm bias

* At the existing /non synchronous/ SLR systems
  sub-mm range biases are achievable using SPAD at
  strictly single photoelectron signal levels.

* The single shot resolution < 5 mm RMS is acheivable
  on standard SPADs 3V above at data rates < 2 %.

* Tha data rate 10% is the best trade off between
  normal point precision, single shot RMS, bias (RGO)

* For the single / multiple photoelectron ranging
  systems on SPAD, three schemes are investigated :
  a/ analog compensation of a time walk.
  b/ hardware selection of single PE echoes,only.
  c/ signal strength monitoring and delay correction.

* More experience from the field is needed before the
  schemes a/-c/ may be generally applied.

I.Prochazka,K.Hamal,B.Greene, Shanghai '96

Automatic SPAD Time Walk Compensation

G. Kirchner, F. Koidl
Institute for Space Research / Austrian Academy of Sciences
Observatory Lustbühel; A-8042 GRAZ / AUSTRIA

1.0 Introduction

SPADs introduce measurable timewalk effects for varying SPAD input energy; [1]; this effect mainly depends on SPAD type, SPAD operating conditions (voltage above break), SPAD input energy, and laser pulse width; for the Graz SLR system (100 μm Prague SPAD, 10 V above break, 35-ps-laser, few mJ only per SemiTrain pulse) the worst case time walk can reach up to 200 ps when ranging with collimated beam to low satellites (which we have avoided anyway in the past!).

2.0 Measuring Avalanche Pulse Rise Time Differences
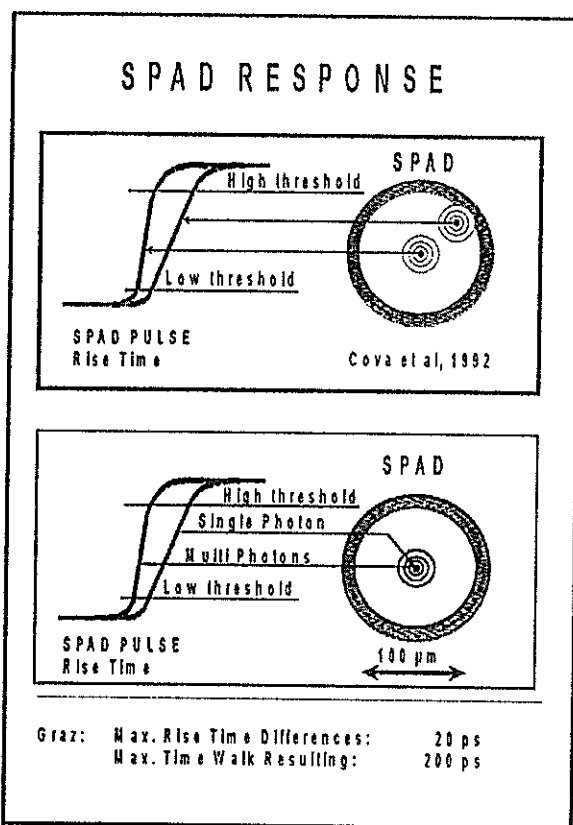
Fig. 1: SPAD Response dependence

In [2], some of the avalanche dynamics of silicon SPADs are explained; as a result, it is shown that the avalanche rise times vary slightly with different locations of the avalanche seed point; in addition, we have seen that this rise time also varies with input energy (Fig.1).

We have verified this already some time ago, and published the results in [3]; we used 2 fast comparators; one triggers near the start of the leading edge (about 10% of maximum amplitude) of the avalanche pulse (which itself is not easily accessible); the second triggers at a higher threshold (about 90% of maximum amplitude). Any differences in the measured delay between the two comparators thus are due to avalanche rise time differences.

The results show that the 200 ps time walk is correlated with a 20 ps rise time difference of the SPAD avalanche pulse.

3.0 Time Walk Compensation

Assuming a linear connection between rise time change and time walk effect, we built a circuit which measures these rise time differences, and uses them to compensate automatically the time walk; the main problem is that - positive - rise time differences of 1 ps have to be translated

into - negative - time shifts of 10 ps, while any jitter in the measurement of rise time differences will also be amplified by the same factor of 10; this requires careful selection of circuit design, electronic component selection, PCB layout (e.g. full SMD technique) etc.

The circuits use ultrafast comparators (e.g. AD96687BR) for pulse discrimination, pulse forming and pulse time shifting (Fig.2); the electronics proved to be very stable, adding no measurable jitter to the system; but initial adjustment may be somewhat tricky and time-consuming. After verifying the proper operation and the stability, we installed the final version of the circuit at end of Feb. 1996 into the standard channel of SLR Graz, where it is running now for 9 months of routine ranging, without any need for re-adjustment.
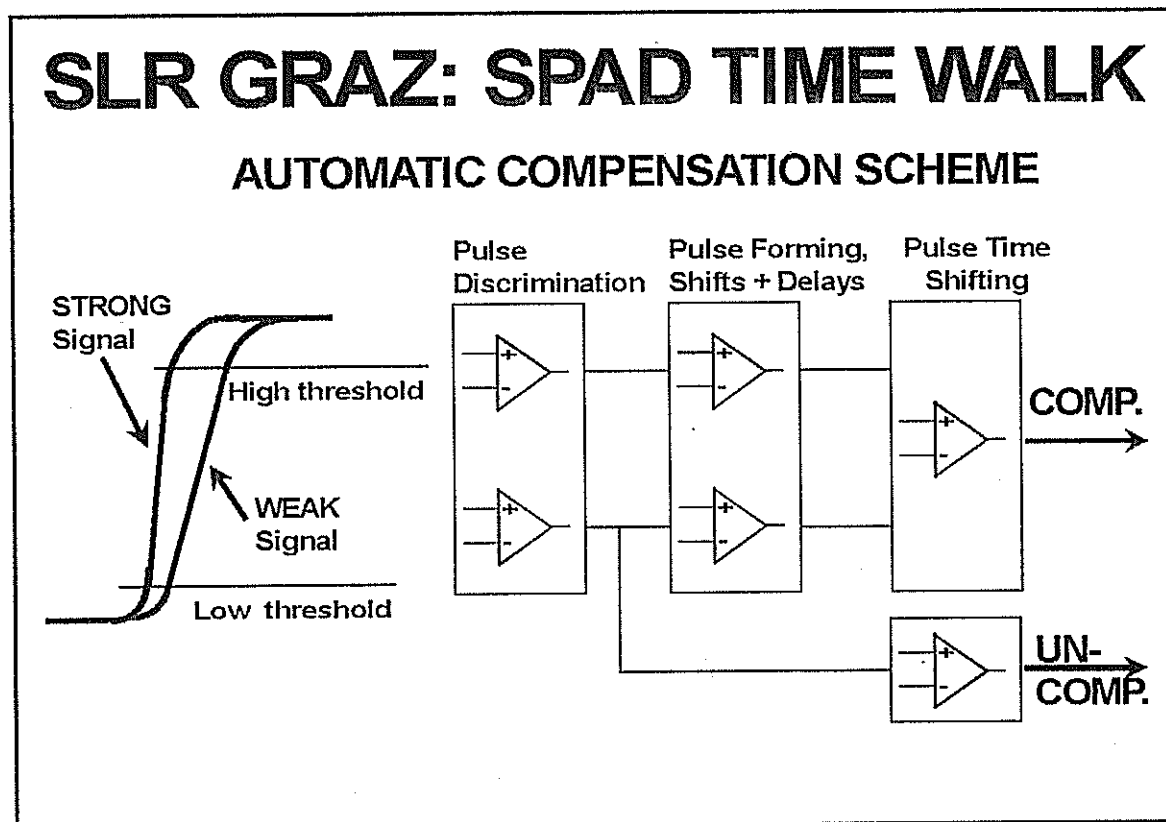
Fig.2: SPAD Time Walk Compensation Schematics

4.0 Results and Plans

The circuit now compensates the major part of the time walk effects (Fig. 3) of the SPAD (and the laser pulse rise time) during routine ranging of SLR station Graz; it reduces all possible time walk effects considerably (from Centimeters to Millimeters); e.g. for LAGEOS, the remaining time walk effects are below 2 mm; as return energy is kept within the tolerable limits by the automatic tracking software, the same results appear also for lower satellites.

There is not only no measurable contribution of the discrimination electronics to the overall system jitter; in contrast to that, the circuit improves significantly the system jitter, because the return signals from satellites and calibration targets always have significant random fluctuations,

which had resulted up to now in time walk and therefore jitter; this jitter source is eliminated now completely by the time walk compensation circuit.
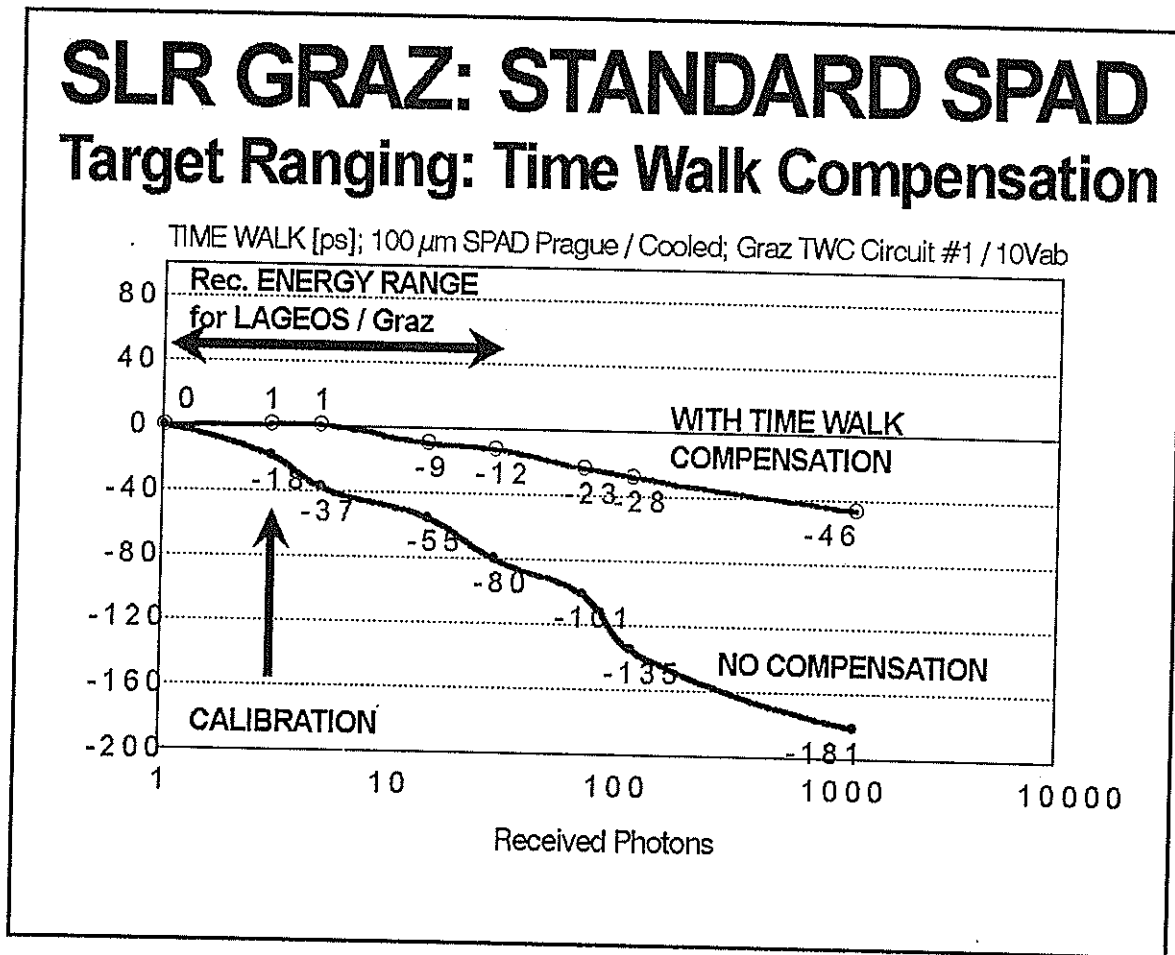

Fig 3: Graz Standard SPAD: Time Walk Compensation

The system now allows full use of a 100% return rate, which is desirable anyway for many obvious reasons, and is necessary also for our planned multi-color measurements. To keep return energy in the range allowed by the time walk compensation circuit, the automatic tracking program [4] identifies not only all valid returns, but checks also for pre-pulses (due to leakage of the pulse selector) indicating higher return signal level; the automatic tracking routines immediately perform some slight offset pointing in such a case, thus keeping return energy - reliably and independent from any observer action - within the tolerable limits [4].

To test the circuit under different conditions, a common project was initiated with the groups in Prague and Potsdam; Prague assembled a 200-μm SPAD, with 2-stage Peltier cooling, optics and housing; Graz built, integrated and adjusted the complete time walk compensation circuit, which also operates the SPAD at 10 Volts above break; adjustment was performed using the Graz laser (35 ps pulse width, similar to the Potsdam laser); for test and comparison purpose, an additional uncompensated output (Fig. 2) was added. Slightly different adjustments for this Potsdam setup were tested in Graz (Fig. 4), showing again possible time walk reduction to below ±1 mm for a range from 1 to more than 100 photons; or to below ±4 mm for a range from 1 to more than 1000 photons (limited by increasing pre-pulse numbers).
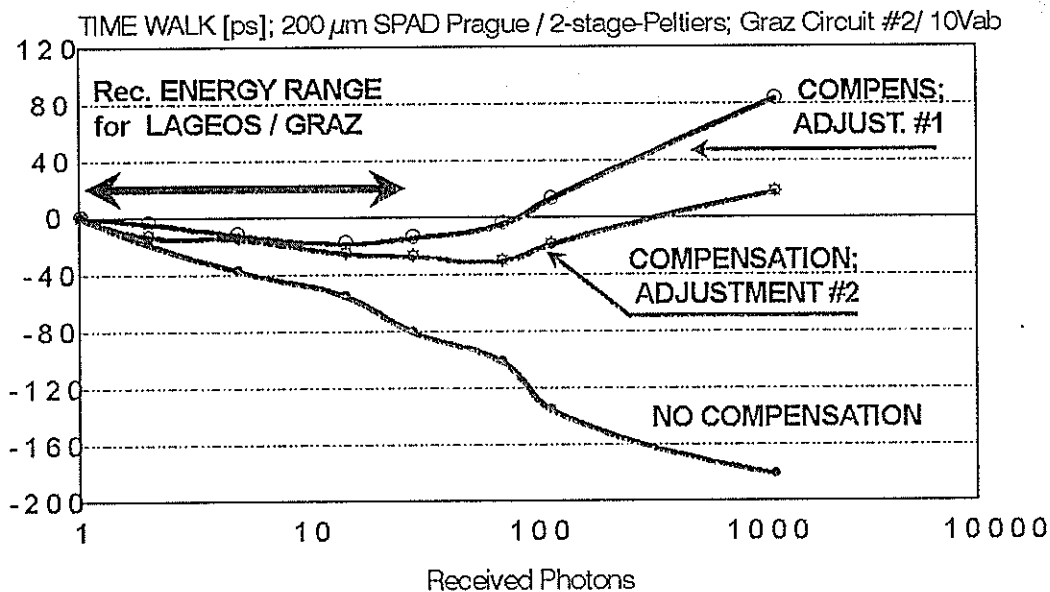
Fig. 4: SPAD Time Walk Compensation, Potsdam Test

The tests in Potsdam to the calibration target gave the same results, demonstrating the possible transfer of the technology to other SPAD stations. The unit is still in Potsdam, to make some more tests - including to satellites ₊, and will be made available than also for other interested groups for tests. In the mean time, we try to implement further improvements (e.g. faster comparators, now available).

We intend also to build such circuits for other types of APDs. In addition, we have started now to develop a circuit which just measures the rise time differences, makes it available to the computer, and will allow time walk compensation by software, as published by [5] in Shanghai.

References:

[1]   Determination of Satellite Signatures and Time Walk Effects in Graz. G. Kirchner, F. Koidl; 9th International Workshop on Laser Ranging Instrumentation, Canberra, 1994; Proceedings, p. 107

[2]   Tracking Capabilities of SPADs for Laser Ranging. Cova et al.;
       8th International Workshop on Laser Ranging Instrumentation, Annapolis, 1992

[3]   Proceedings of Annual Eurolas Meeting; G. Kirchner, F. Koidl; Munich, 3/1995; p 73

[4]   Automatic Tracking Software at SLR Graz; G. Kirchner, F. Koidl; in these proceedings

[5]   SPAD Detectors for Ranging with Sub-Millimetre Bias; K. Hamal, I. Prochazka, B. Greene; in these proceedings

Large-aperture germanium detector package for picosecond photon counting in the 0.5–1.6-μm range

I. Prochazka and K. Hamal

Czech Technical University, Brehova 7, 115 19 Prague 1, Czech Republic

B. Greene

Electro Optics Systems, Pty. Ltd., Queanbeyan, NSW, Australia

H. Kunimori

Communication Research Laboratory, 4-2-1 Nukui-Kitamachi, Koganei, 184 Tokyo, Japan

We report the design, construction, and parameters of a detector package based on a germanium avalanche photodiode operated in the Geiger mode cooled to 77 K. The new design of the active quenching circuit, proper diode structure, and cryogenic cooling setup permitted us to increase the detector's active area to 0.1-mm diameter while maintaining an acceptable dark-count rate, timing resolution, and photon-counting sensitivity at 1.54 μm. The active-area size and the compact design of the detector package permitted its application in satellite laser ranging at 0.532- and 1.543-μm wavelengths, yielding subcentimeter ranging precision. © 1996 Optical Society of America

The large-aperture germanium detector package is of general interest for several applications: time-resolved spectroscopy, laser-induced fluorescence, optical-time-domain reflectometry, laser ranging, and others aimed at developing a large-aperture single-photon counter for the near-infrared region. At present the most promising technique for detecting a single photon by use of a solid-state detector is the use of an avalanche photodiode (APD) operated in the Geiger mode. In this operation mode the diode is biased above its breakdown voltage; no current flows until an avalanche is triggered by an incoming photon or a thermally generated carrier. The current pulse rise time marks the photon's arrival time. An external electrical circuit, either passive or active, is used to quench the avalanche and to reapply the bias to the diode.[1]

Our previous research and development in the field of single-photon avalanche diodes resulted in a large-aperture silicon-APD-based detector package with an active quenching circuit, well adjusted for the applications mentioned above.[2] Recent developments have produced an APD with an active area 200 μm in diameter, a timing resolution of 44 ps FWHM, and a dark-count rate below 10 kHz. The APD is cooled by a three-stage thermoelectrical cooler enclosed in a vacuum package. These silicon-based APD's have been used to detect single photons in the near-infrared range up to 1.55 μm.[3] However, the quantum efficiency of such detectors at 1550 nm (10^{-4}–10^{-6}) is not considered adequate for most applications. We have made several attempts to increase the residual quantum efficiency of the silicon APD in the near infrared by replacing the silicon with GeSi as a starting material; although research continues, the results are not encouraging.

There are now two alternatives: germanium- and InGaAs-based diodes for photon counting in the near-infrared region for fiber optics at 1.3 and 1.55 μm, for spectroscopy and for laser ranging in the so-called 1.54-μm eye-safe window. The germanium detector-based on a commercially available APD of 30–50-μm diameter shows interesting results.[4,5] On the other hand, several applications including laser ranging require an active-area diameter of not less than 100 μm, as the small detector area limits the field of view of the system receiver. For example, a satellite laser ranging station using a 1.5-m-diameter telescope and a 100-μm diameter detector has a field of view of the entire receiver of 8 arcsec. This is the ultimate minimum for satellite laser ranging and optical communication applications as well.

InGaAs diodes manufactured by EG&G Judson, 100 μm in diameter at a 1.55-μm wavelength, have been tested for relative sensitivity, timing resolution, and dark-count rate at temperatures from 300 to 77 K. Photon-counting operation was achieved at temperatures below 240 K. The detector performance was not satisfactory for ranging applications, as the timing resolution was not better than 600 ps and the quantum efficiency did not exceed several percent at 1.55 μm.

Germanium has been the favored semiconductor material for APD structures for near-infrared detection. The typical spectral responsivity curve of a germanium APD is shown in Fig. 1. The solid curve represents the EG&G Judson data sheet; the dashed line is the extrapolation. There is strong demand for a single detector to detect photons in the spectral range 0.5–1.6 μm. Photon-counting detector parameters of interest are timing resolution, sensitivity, and dark count; all these depend on the diode bias above its breakdown. In general, photon-counting sensitivity increases with the bias above the breakdown and saturates at a certain level. The dark-count rate rises with the bias above the breakdown. The timing resolution improves with
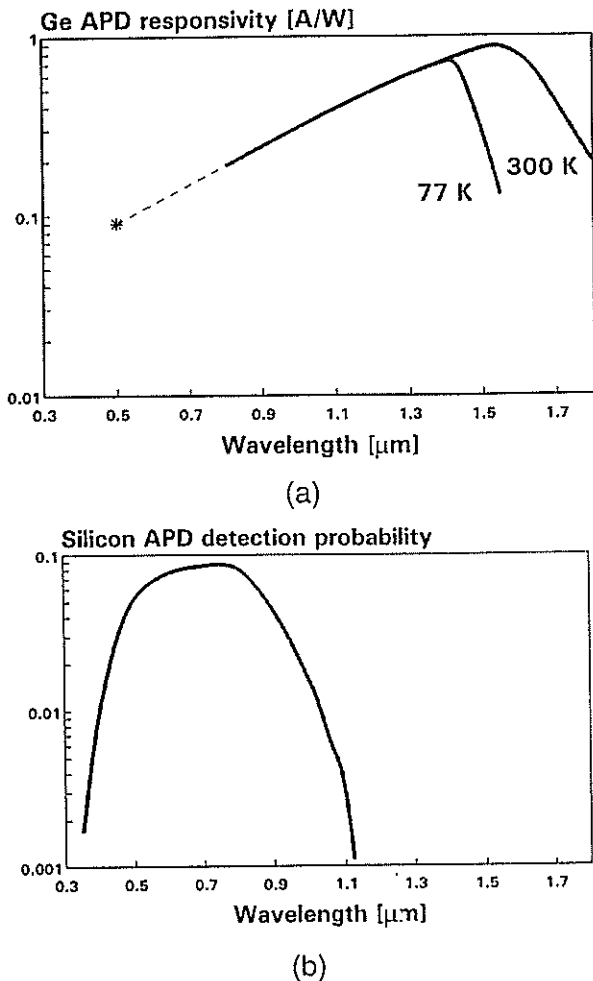
(a)

(b)

Fig. 1. Spectral responsivity of germanium- and silicon based APD's. (a) Solid curves, germanium APD data from the EG&G Judson infrared detector data sheet (EG&G, Montgomeryville, Pa., 1994); dashed line, extrapolation toward shorter wavelengths. (b) Silicon APD data from Ref. 2.

the bias above the breakdown voltage and saturates at several volts above the break. Therefore each application requires a compromise among these three parameters for a given detector configuration.

In developing the germanium-based single-photon avalanche diode we also examined photodiodes manufactured by NEC, EG&G Judson, and Hamamatsu. For photon-counting operation in the Geiger regime these diodes have to be cooled to 77 K. To optimize the germanium APD operation we modified the existing active quenching scheme to reduce the time during which the current is flowing through the diode. The circuit allows the APD to operate in the Geiger mode when biased to 3 V above the breakdown voltage. To cool the APD we designed a novel cryostat, which permits the incoming light to be focused onto the diode's active area, using optics with a focal ratio equal to unity. The cryostat is compact and fieldable, operates in any orientation, and has a liquid-nitrogen refill interval of 14 days.

To measure the photon-counting timing resolution of the detector we applied a time-correlated

photon-counting technique consisting of a Hamamatsu PLP01 laser diode pulser at 0.8-μm wavelength, a time-to-amplitude converter, and a multichannel pulse amplitude analyzer card in a personal computer. The timing resolution of the electronics chain is 30 ps FWHM, and the laser pulse duration is 32 ps FWHM. An example of the waveform of the laser
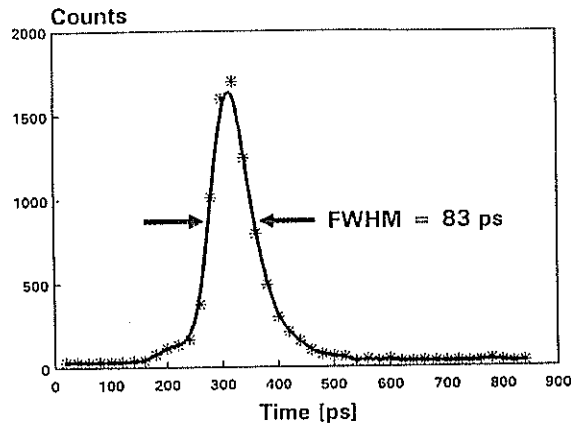

Fig. 2. Waveform of a 32-ps optical pulse from a laser diode. The APD was biased 1.7 V above the break voltage; the timing electronics contribution FWHM was 30 ps.
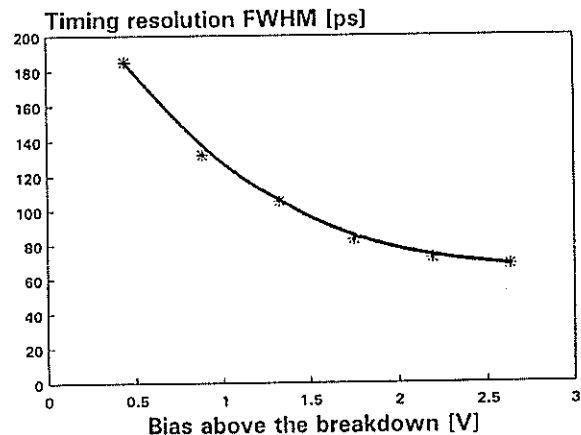

Fig. 3. Timing resolution of the germanium photon counter versus bias above the breakdown voltage.
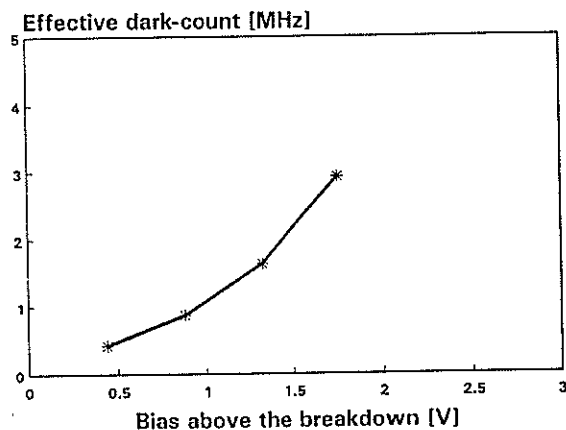

Fig. 4. Effective dark-count rate of the detector package versus APD bias above the break voltage. The APD was operated in an active quenching mode gated with a 10-Hz repetition rate.
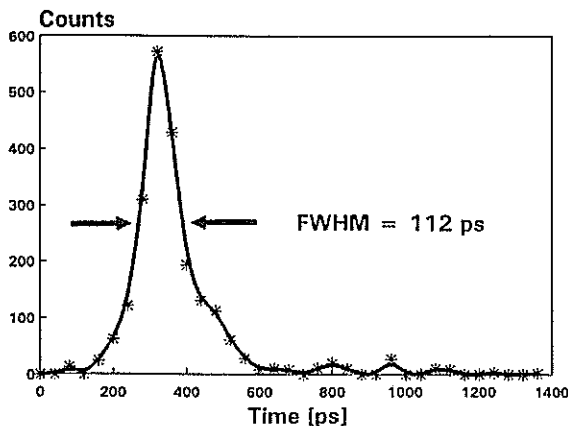
Fig. 5. Single-photon laser ranging to the ground target at 1.54-μm wavelength. The APD was biased 2 V above the breakdown voltage, the laser FWHM was 30 ps, and the ranging electronics contribution was 70 ps FWHM.
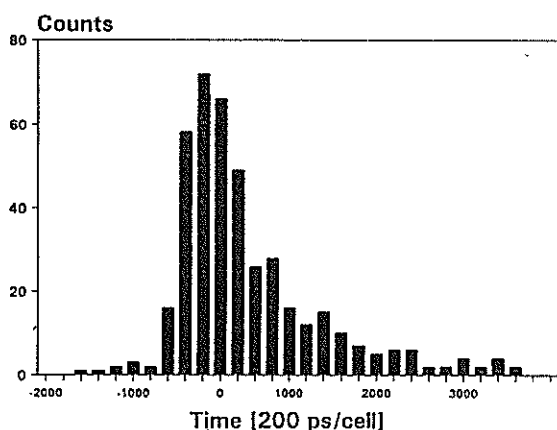

Fig. 6. Single-photon laser ranging to the Ajisai satellite at 1.54 μm. The APD was biased 0.6 V above the breakdown voltage, and the satellite distance was 2000 km. The returned signal is spread in time by the satellite geometry.

diode recorded with the 100-μm Ge APD biased 1.7 V above its breakdown is shown in Fig. 2. Deconvoluting the contributions of the laser pulse duration and the timing electronics yields an intrinsic timing resolution of the photon counter of 70 ps FWHM, which according to our knowledge is the best value of timing resolution reported so far for a 100-μm-diameter germanium photon counter. Figure 3 is a plot of the dependence of the timing resolution on the APD bias above the breakdown voltage. The dependence of the effective dark-count rate on the diode bias above the breakdown is shown in Fig. 4. The APD was operated in an active quenching mode and gated at a 10-Hz repetition rate. The effective dark-count rate is evaluated as an inverse value to the mean time for which the diode can be biased above the breakdown voltage before the avalanche is triggered when the detector is kept in darkness.

The detector package has been used for laser ranging at a wavelength of 1.54 μm.[6] This wavelength is in a laser range of special interest because it does

fit into the 1.54-μm eye-safe window. Using a 30-ps pulse duration laser and a ranging electronics resolution of 75 ps FWHM, we obtained the distribution of measured values shown in Fig. 5, resulting in subcentimeter range precision when we ranged the ground targets. What is to our knowledge the first eye-safe satellite laser ranging using the germanium photon counter was achieved at the Satellite Laser Station of the Communication Research Laboratory, Tokyo. A histogram of range residuals is shown in Fig. 6. For the data the APD was biased 0.6 V above its breakdown voltage and the satellite distance was 2000 km. The returned signal is spread in time because of the satellite geometry. With the same experimental arrangement at the same time, the result was obtained at a wavelength of 0.532 μm.[6] The quantum efficiency of 15% at the 0.53-μm wavelength was estimated by comparison with a silicon-based detector package of known quantum efficiency in a photon-counting experiment. The quantum efficiency at 1.54 μm was estimated by comparison with that at 0.532 μm by use of the energy budget link of the entire laser ranging system. Considering the transmitted energies at both wavelengths and the returned photon-count rate at both wavelengths, we concluded that the quantum efficiency of the germanium-APD-based detector package has a quantum efficiency of 15% at a wavelength of 1.54 μm.

Our setup arrangement, consisting of the germanium APD chip, the active quenching circuit, and the cryostat permits, operation of the single-photon counter with an active-area diameter up to 100 μm, yielding a picosecond timing resolution and maintaining an acceptable dark-count rate. The detector package permits multiple color satellite laser ranging at wavelength of 0.53 and 1.54 μm with an estimated quantum efficiency of 15% at both wavelengths.

References

1. S. Cova, IEEE J. Quantum Electron. **QE-19,** 630 (1983).
2. I. Prochazka, K. Hamal, B. Sopko, J. Ricka, and M. Hoebel, Inst. Phys. Conf. Ser. **126,** 147 (1991).
3. B. Sopko, J. Pavlu, I. Prochazka, and I. Macha, "Detection of near IR radiation by SiGe material," in *Proceedings of the 20th European Solid State Device Research Conference,* W. Ecleston, ed. (IOP Publishing, Bristol, UK, 1990), pp. 413–416.
4. A. Lacaita, P. A. Francese, F. Zappa, and S. Cova, Appl. Opt. **33,** 6902 (1994).
5. P. C. M. Owens, J. G. Rarity, P. R. Tapster, D. Knight, and P. D. Townsted, Appl. Opt. **33,** 6895 (1994).
6. H. Kunimori, B. Greene, J. Guilfoyle, K. Hamal, I. Prochazka, G. Kirchner, and F. Koidl, "Subcentimeter eyesafe ranging," in *Proceedings of the Pacific Rim Conference on Lasers and Electro Optics* (1995), pp. 17–18.
7. H. Kunimori, B. Greene, K. Hamal, and I. Prochazka, "Centimeter eyesafe satellite laser ranging using Raman shifted Nd:YAG laser and germanium photon counter," (to be published).

Ge SPAD quantum efficiency
Active quenching, 2.5 V above
New chip : no ring, 100 um, 77 K

detection probability

wavelength [um]

J.Prochazka, J.Blazej, November '98
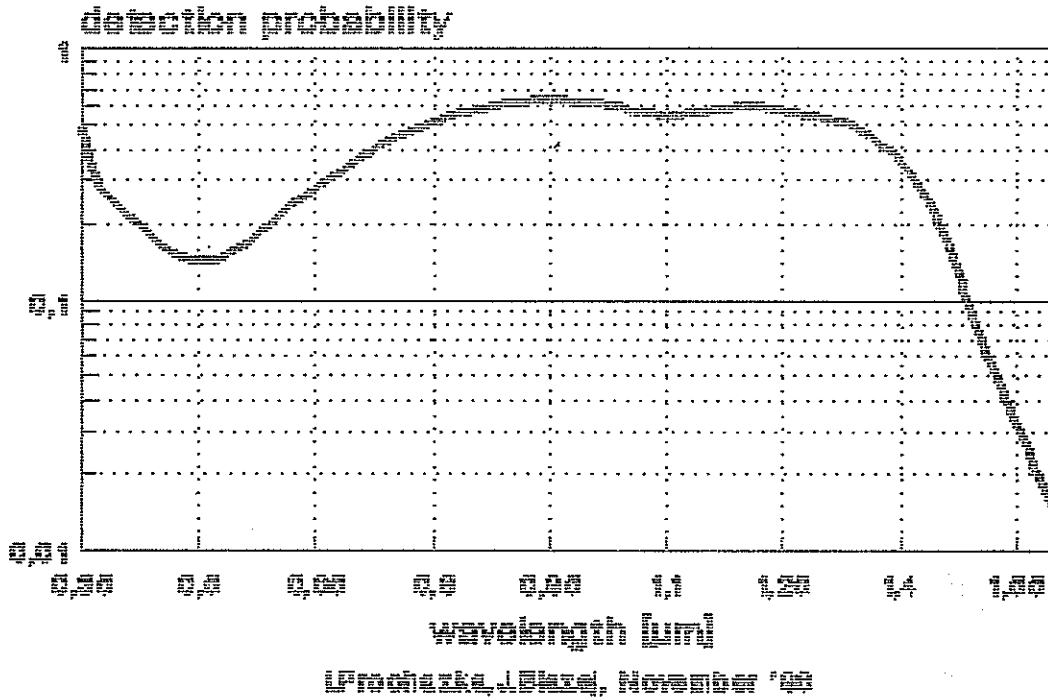
Testing Ge- APS's for Ranging Applications in a Cryogenic Environment

Ulrich Schreiber, Christian Schötz
Forschungseinrichtung Satellitengeodäsie
Fundamentalstation Wettzell
D - 93444 Kötzting
Germany

Karl Heinz Haufe
Institut für Angewandte Geodäsie
Fundamentalstation Wettzell
D-93444 Kötzting
Germany

Abstract

The technology for a ranging station that is based on frequency doubled Nd:YAG-lasers is well developed in every aspect. However, when it comes to dualcolor ranging, or to working in the infrared domain, there are still many open questions with respect to suitable detection devices and the propagation properties of the atmosphere. The fact that the infrared tracking channel often seems to be more sensitive than the usually used visible channel ($\lambda = 532nm$) and that there is a growing interest in ranging systems that work in the "eyesafe"- region around ($\lambda = 1.54\mu m$) stimulated some experiments on germanium avalanche photodiodes in geiger mode. Due to the low gap energy of germanium, these diodes develop a very high noise count rate, which is in the order of a few GHz. To reduce the noise a cryogenic operating environment is required. The goal of this work reported here was to establish test conditions for the diodes which are closely orientated to real ranging demands.

1. INTRODUCTION

The operation of silicon avalanche photo diodes put to the geiger mode in laser ranging has been well established [1, 2, 3] over the last ten years. The ease of use, their high sensitivity and ruggedness are widely appreciated. Many SLR stations are using this type of detector for their routine work now. In addition to these qualities, they also show sensitivity over a broader spectral range than conventional photomultipliers. This enabled satellite ranging on the fundamental frequency of Nd:YAG lasers [4, 5]. However their quantum efficiency is fairly low at $\lambda = 1.06\mu m$ and is negligible at $\lambda = 1.5\mu m$. Since the gap energy in germanium is considerably lower than in silicon, there is a high sensitivity to be expected from this type of diode in the infrared wavelength domain. On the other side this means an enormous increase in thermally induced noise recordings. This can be partly overcome by cooling the germanium diode under test to temperatures around 10 Kelvin.

2. EXPERIMENTAL SETUP

The germanium avalanche diode under test was placed in a little cryogenic chamber, which allows for a temperature setting between 10 K and room temperature. A window was placed at one side of this chamber, so that short light pulses illuminate the diode, causing a signal induced breakdown of the geiger voltage, which in turn was used as a stop signal on a time interval counter. The start pulse was derived from a frequency generator as a trigger source, running on a frequency of 10 Hz. This ensures that the results obtained are comparable to real ranging. The jitter of the Hamamatsu pulser with respect to the trigger input is of the order of a few picoseconds. However this is not an issue in this type of experiment, since the work presented here focuses mainly on the behaviour of the intrinsic noise of the various tested diodes, relative to the detection of low light level laser pulses. It was made sure that no unwanted background light caused false readings during the experiments. Figure 1 outlines the block diagram of the experimental setup.

Under room temperature conditions it usually takes only about 1 ns for a voltage break down to occur in a germanium avalanche diode. For a well behaved satellite a rangegate of 200 ns is sufficiently large for ranging. Therefore the experiment had set a delay of 170 ns between "gate on" at the detector and the occurence of the laser pulse. The influence of the cooling on the intrinsic noise of a germanium detector could therefore be studied in detail. Figure 2 illustrates the timing arrangement of this experiment. A sample experiment was run to verify the principle of operation and test the setup. The result is shown in Figure 3. The slight deviation from a gaussian distribution is characteristic for a detection based on avalanche diodes. The overall rms was estimated to yield 88 ps and the rate of valid detections is approximately 25 %.

3. INVESTIGATING THE PROPERTIES OF TWO DIFFERENT GERMANIUM DIODES

The sensitivity and scatter of a geiger mode operated avalanche diode is strongly determined by the degree to which the gate voltage, exceeds the breakdown threshold. Increasing the gate voltage leads to higher sensitivity and higher accuracy for the measurement. However, it also increases the probability for an intrinsic noise event. So in the first experiment the gate voltage was varied over the complete working range and the mean time between gate on and the occurence of a noise breakdown was taken from the histogram of the noise. There were two different detectors available for the experiments. One was made by Hamamatsu (type B2834-01) the active chipsize being 100 μm in diameter, while the other was manufactured by Siemens (tpye SRD 00512Z) having a chipsize of only 40 μm across. One has to bear this in mind, when their behaviour is compared. Figure 4 and 5 show the result obtained. All the measurements were taken at a temperature of 10 K. The Hamamatsu diode, operated at a geiger voltage of 3 volts above break down allows a gate width of roughly 200 ns, which is the practical limit for a known good satellite. The far better situation for the Siemens diode of nearly 800 ns at the same level of the geiger voltage has been attributed to smaller size of the active chip area, as mentioned above.

The other important parameter is the detection probability of a laser pulse, again depending on the geiger voltage. Detection probability in this context means the probability of

recording a laser pulse instead of a noise event. The intensity of the pulser signal was high enough so that it can be disregarded in this context. The result of these measurements are shown in figures 6 and 7. In both cases there is a roughly 60 % chance of detecting the signal instead of recording a noise event, when the gate voltage is set to 3 V. This is far from optimum performance for ranging applications but nonetheless it demonstrates the feasibility of the usage of these detectors. Again these measurements were taken at a temperature of 10 K. The timewalk in dependence of the geiger voltage was analysed in the next set of measurements. Since the observed timewalk was small and not significantly dependent on the applied gate, there are no extra plots given in this paper.

In the next set of experiments the behaviour of the thermal noise with respect to the detector temperature was analysed. The gate voltage was set to 3 V above breakdown for this purpose. Once again the probability of recording a valid pulser signal over a noise event was taken as the parameter of interest. Figures 8 and 9 show the result. For both diodes there is a weak temperature dependence in the detection probability of a laser pulse in the temperature range of 10 K to 50 K. However above this upper limit there is a strong increase in the detection of noise events. Above 100 K there is almost no probability of detecting a laser echo which arrives more than 170 ns after the gate was switched on. Both diagrams show roughly the same behaviour. It would be expected that the noise probability would be dependent upon the chip size. However there are obviously other effects masking such behaviour.

In order to characterise germanium diodes with respect to their spectral sensitivity another set of experiments have been carried out. The parameters temperature (10 K) and voltage above breakdown (3 V) were held constant, while measurements were taken at different settings of neutral density filters, which were placed in front of the detector. Figures 10 and 11 show the result. In this case one can see that the Hamamatsu detector is obviously superior to the Siemens diode. This again is attributed to the larger chip of the B2834-01. Unfortunately it is not possible to obtain the sensitivity of the germanium diode for the application in the infrared wavelength domain, since the pulser is operating on $\lambda = 0.776 \mu m$. On the other hand both detectors were treated in the same way, so that their relative difference in sensitivity can be compared. From figure 10 one can see, that at a level of four optical densities the single photon domain is obviously reached. Towards higher optical densities one can find a strict proportional relationship between the number of valid signal recordings and the applied attenuation of the pulse source. The Siemens diode appears to be far less sensitive. It is assumed that this is due to the smaller sensitive area, since the light pulse was not focused onto the detector, but applied as a collimated beam.

The variation of timewalk of a detector with respect to the receive signal intensity is one of the important parameters, which has also been investigated. In figure 12 and 13 one can see the respective behaviour of the two diodes, as the signal amplitude is decreased. The measurements yield a timewalk of nearly 1 ns for the diode B2834-01 over 5 magnitudes in intensity, while the detector SRD00512Z shows 200 ps over 3 magnitudes. The rms of the histogram taken over the pulser events is below 90 ps in all cases. When exposed to a high signal level, values of less than 40 ps were obtained. This is caused by a change of the multiplication factor for the avalanche growth process. This parameter is intensity

dependent and this behaviour is well known from the application of silicon avalanche diodes.

4. CONCLUSIONS

At the WLRS in Wettzell a laboratory system has been set up which allows the analysis of sensitive detectors capable of single photon detection. This experiment can be operated completely independent of the routine tracking system. A cryogenic chamber has been added, in order to allow the investigation of the properties of germanium diodes as sensitive detectors in the infrared wavelength domain. The construction of the chamber is such that it can also be operated as part of the WLRS. All relevant parameters for a tracking application were investigated for two different types of germanium diodes, as they became available. Their general properties are close to those of silicon diodes, however the intrinsic noise of the germanium avalanche diodes places additional demands on the tracking experiment. The cryo chamber was found to be completely adequate to meet these requirements. The major differences between the two specimens under test were found with respect to sensitivity and the amount of intrinsic noise. This was attributed to the different size of the semiconductor chip between the two diodes.

5. ACKNOWLEDGEMENTS

References

[1] A. W. Lightstone, R. J. McIntyre; "Avalanche Photodiodes for Single Photon Detection", *IEEE Trans. Electron Devices*, **ED-28**, 1210 (1981)

[2] U. Schreiber, K. H. Haufe, J. F. Manging, J. M. Torre and Chr. Veillet; "Operating the APD SP 114 at the LLR Station in Grasse", *Lidar Techniques for Remote Sensing, Chr. Werner, Editor*, Proc. SPIE 2310, **2**, (1994)

[3] I. Prochazka, K. Hamal; "Recent Achievements in Solid State Detector Technology for Laser Ranging", *Proceedings Of 9th International Workshop on Laser Ranging Instrumentation*, Canberra, 1994

[4] U. Schreiber, St. Riepl; "Measuring atmospheric dispersion employing avalanche photo diodes", *Lidar Techniques for Remote Sensing, Chr. Werner, Editor*, Proc. SPIE 2310, **25**, (1994)

[5] Ch. Veillet, E. Bois, J. E. Chabaudie, C. Dumoulin, D. Feraudy, M. Glentzlin, J. F. Mangin, J. PhamVan, J. M. Torre; "The Cerga Lunar Laser Ranging Station", *Proceedings Of 7th International Workshop on Laser Ranging Instrumentation*, Matera, 1989
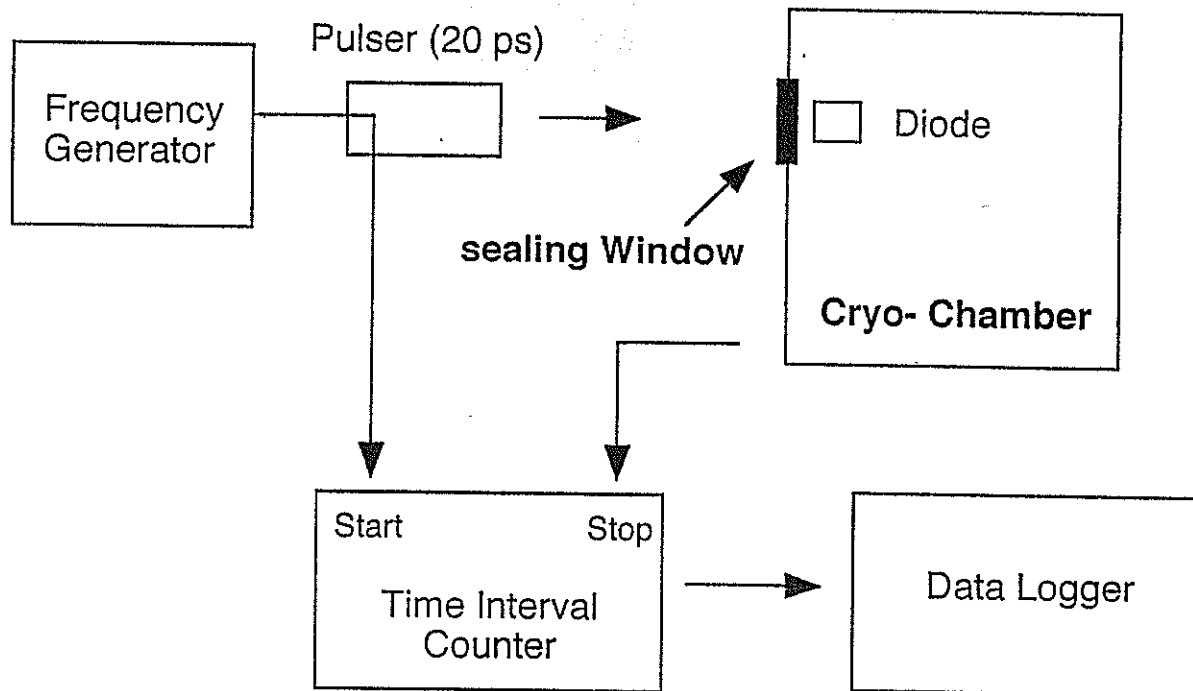
Figure 1: The block diagram of the experimental setup. The diode was placed inside the cryogenic chamber, while the signal source and the time interval counter were set up for an indoor ranging experiment
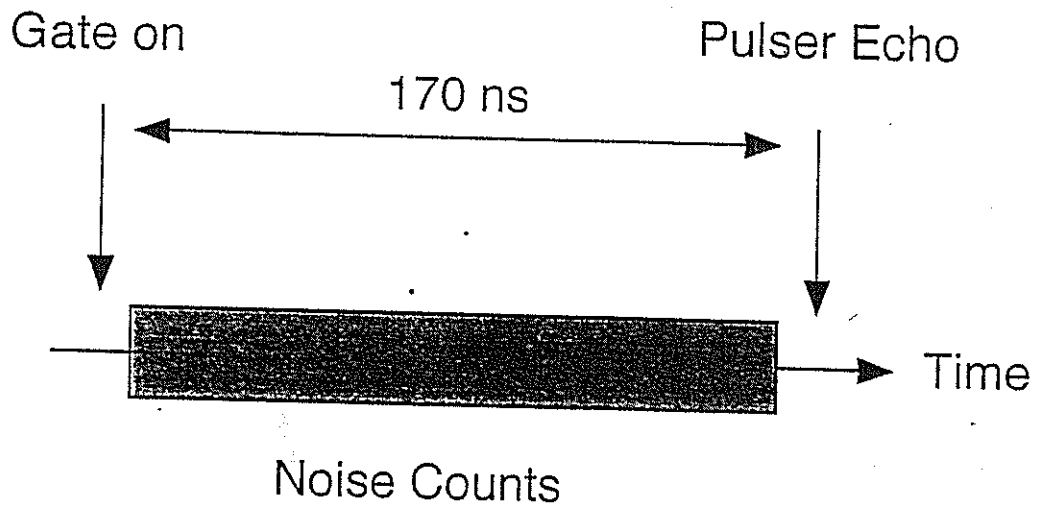
Figure 2: The simplified timing diagram of the discribed experiment. A period of 170 ps was set before the laser pulse hits the diode. This allows the effect of cooling on the diode to be studied
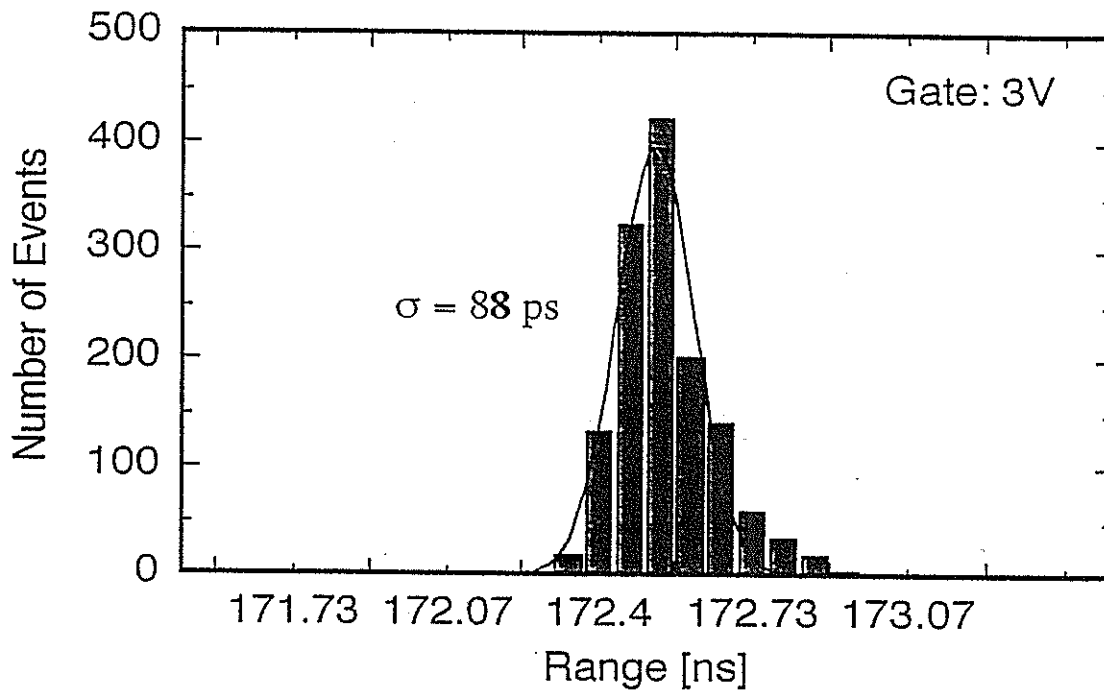

Figure 3: Histogram of a test ranging run for a typical germanium avalanche diode. The obtained overall rms was 88 ps. The detection rate is close to 25%
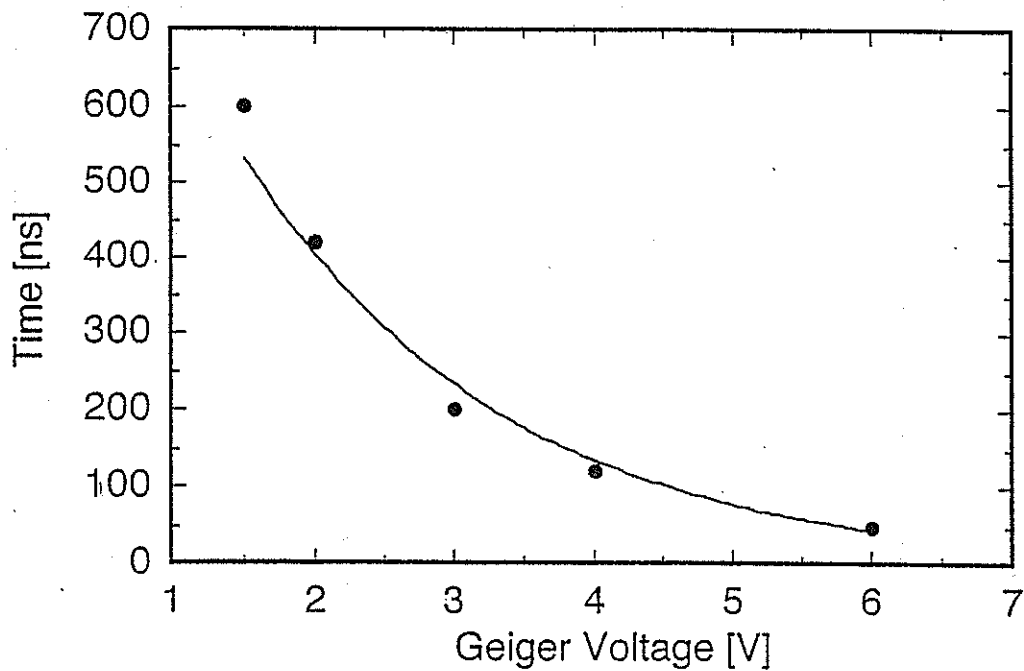
Figure 4: The average time between "Gate On" and a noise "Breakdown" over the Geiger pulse voltage for the diode B2S34-01. A geiger voltage of 3 V seems to be the highest reasonable value. The temperature is 10 K
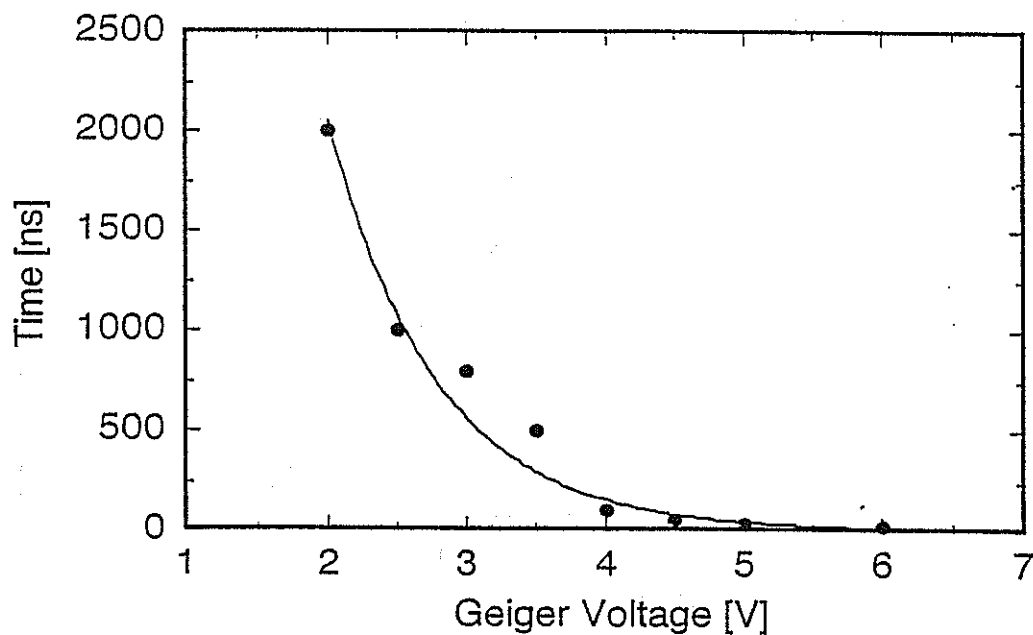

Figure 5: The average time between "Gate On" and a noise "Breakdown" over the Geiger pulse voltage for the diode SRD 00512Z. A geiger voltage of 3 V seems to be a good operating value. The temperature is 10 K
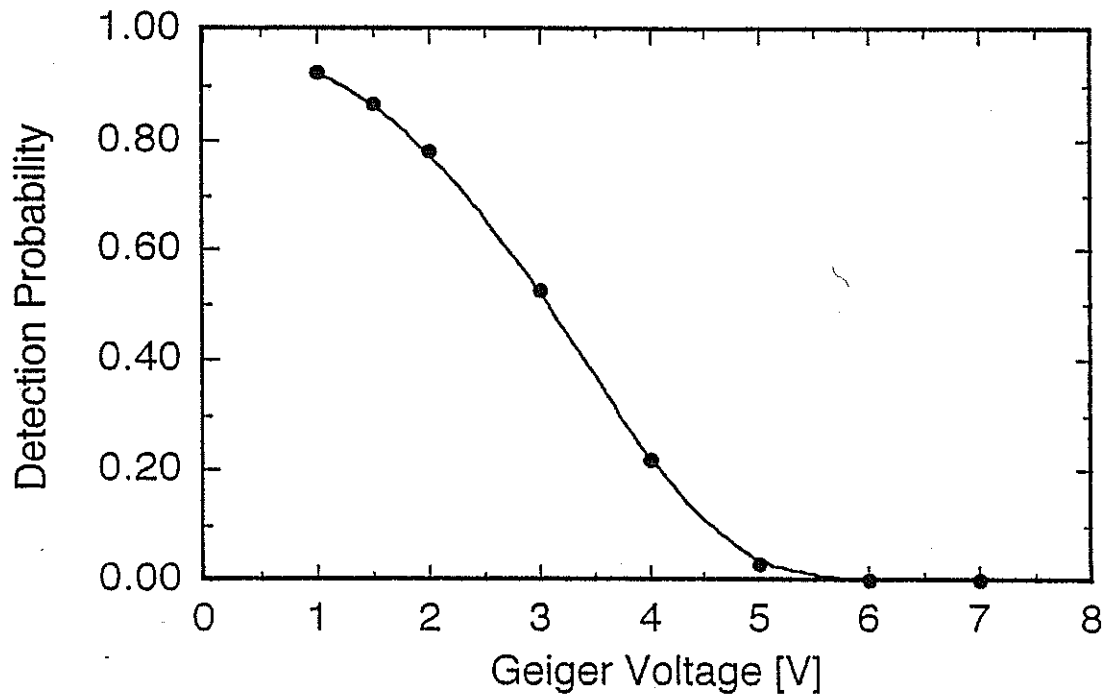
Figure 6: The probability of recording a signal instead of a noise event over the Geiger pulse voltage for the diode B2834-01. A geiger voltage of 3 V seems to be a good operating value. The temperature is 10 K
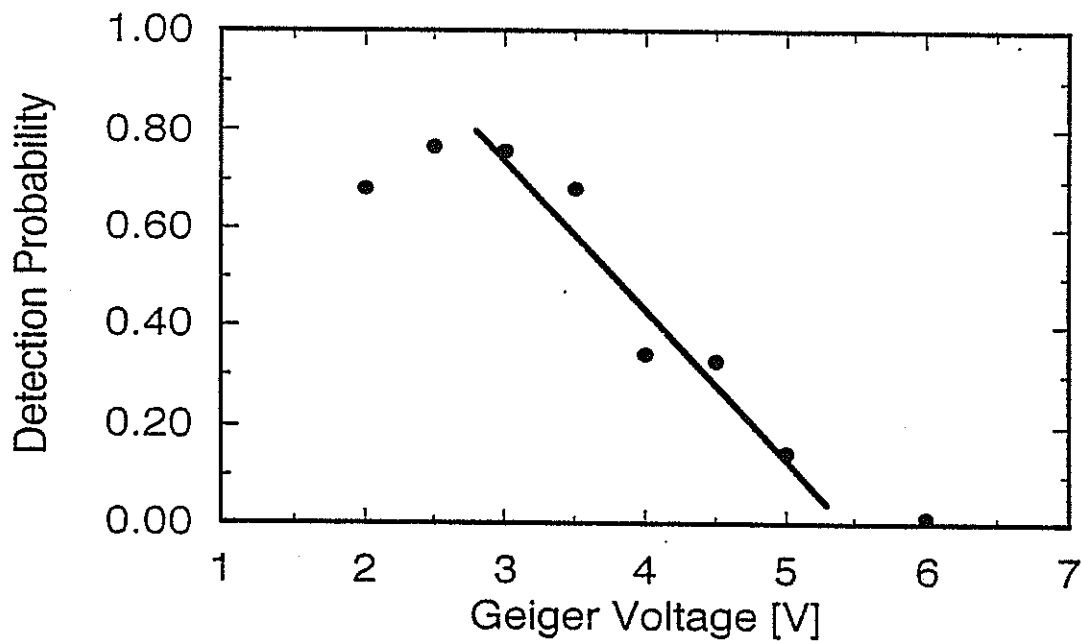

Figure 7: The probability of recording a signal instead of a noise event over the Geiger pulse voltage for the diode SRD 00512Z. A geiger voltage of 3 V seems to be a good operating value. The temperature is 10 K
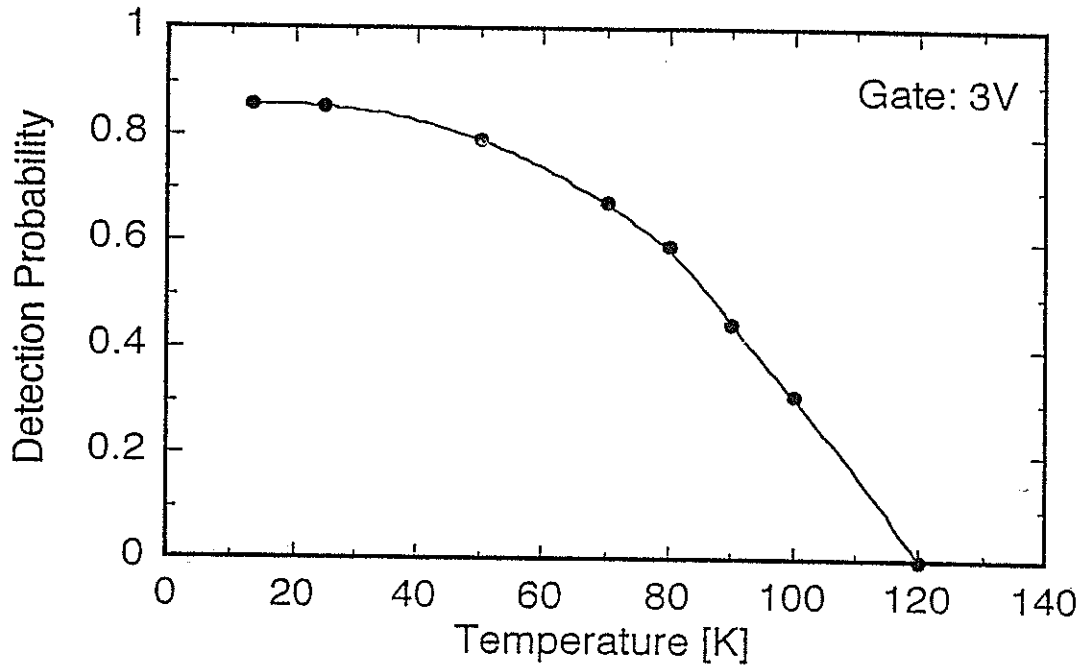
Figure 8: The probability of recording a signal instead of a noise event over the detector temperature for the diode B2834-01. A geiger voltage of 3 V was applied. Above 50 K there is a strong increase of the noise
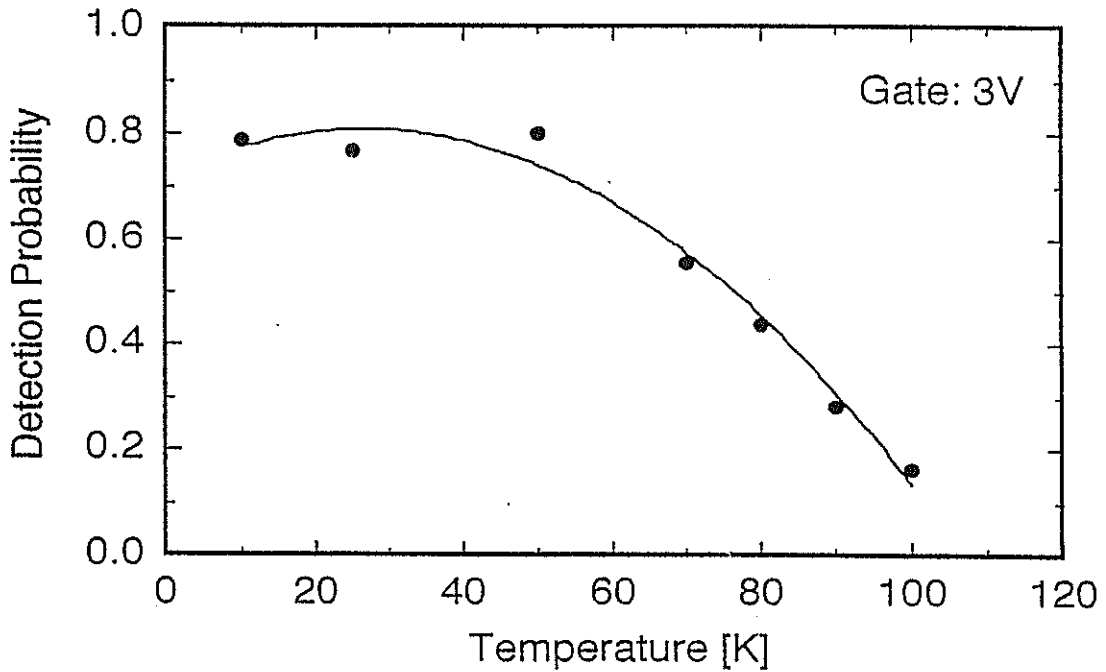
Figure 9: The probability of recording a signal insted of a noise event over the detector temperature for the diode SRD 00512Z. A geiger voltage of 3 V was applied. Above 50 K there is a strong increase of the noise
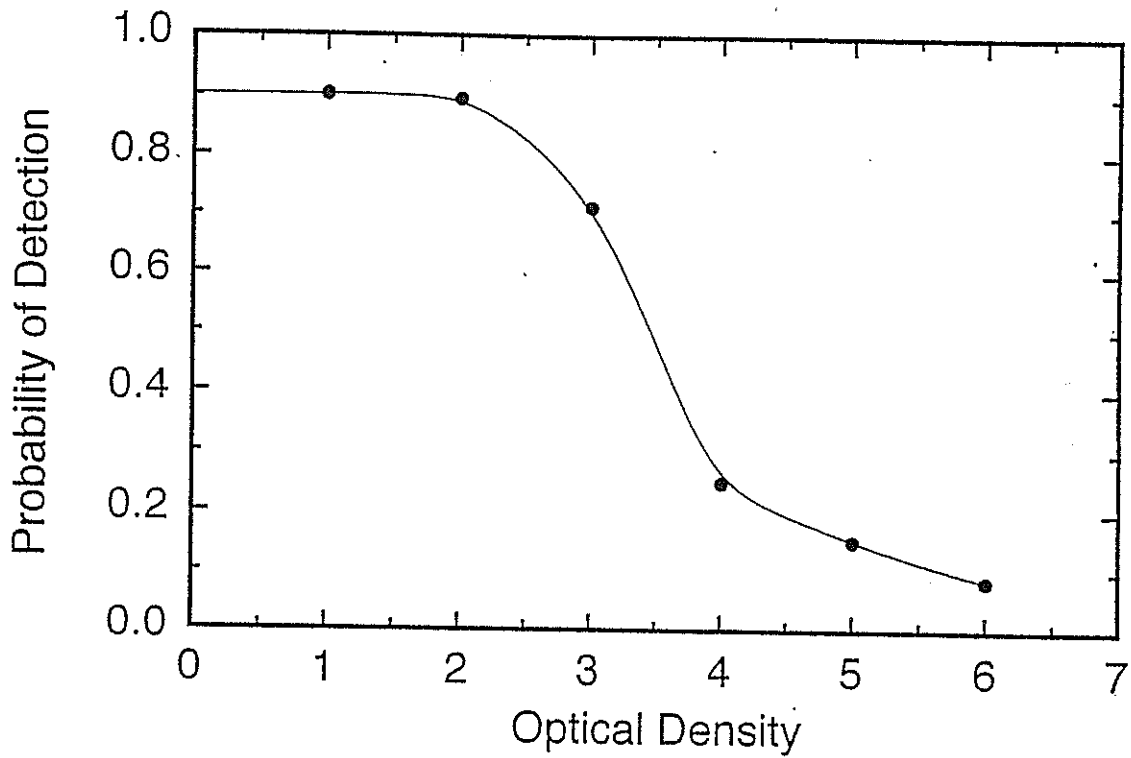
Figure 10: The spectral sensitivity of the diode B2834-01 at $\lambda = 0.776\mu m$. A geiger voltage of 3 V and a temperature of 10 K was applied to the detector
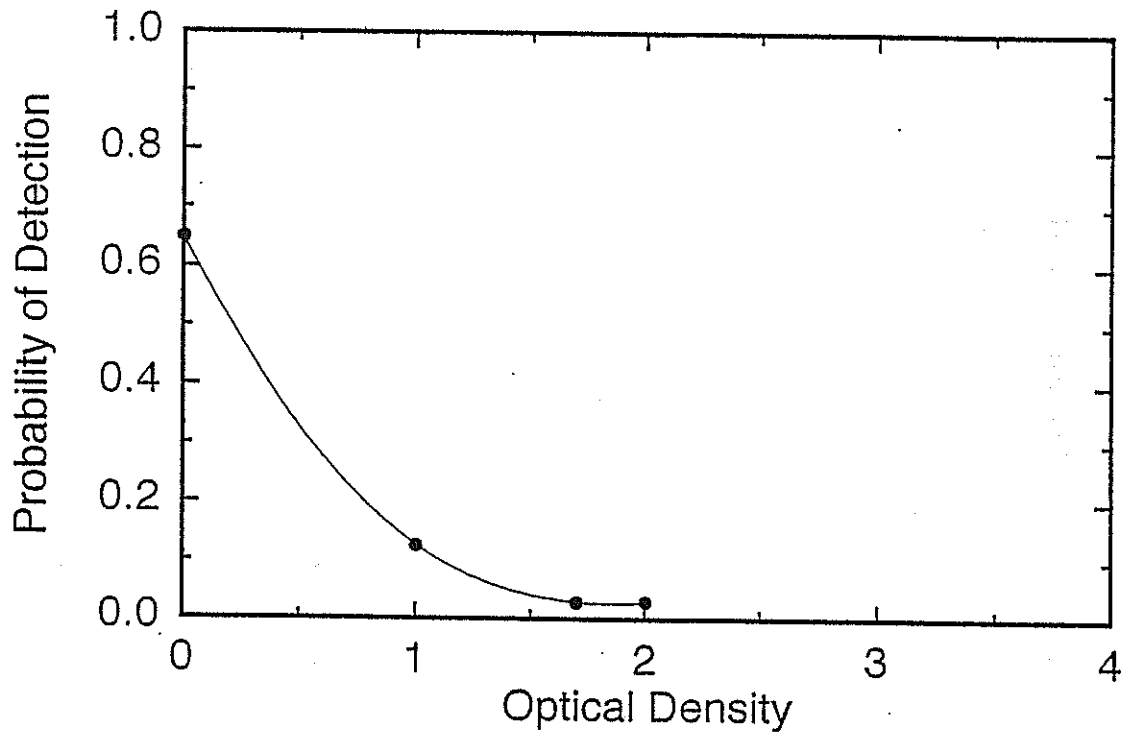
Figure 11: The spectral sensitivity of the diode SRD 00512Z at $\lambda = 0.776\mu m$. A geiger voltage of 3 V and a temperature of 10 K was applied to the detector

Figure 12: The experienced timewalk of the diode B2834-01 under various signal intensities. A geiger voltage of 3 V and a temperature of 10 K was applied to the detector

Figure 13: The experienced timewalk of the diode SRD 00512Z under various signal intensities. A geiger voltage of 3 V and a temperature of 10 K was applied to the detector

Effects of Common Gating Schemes on SPAD/APD Bias.

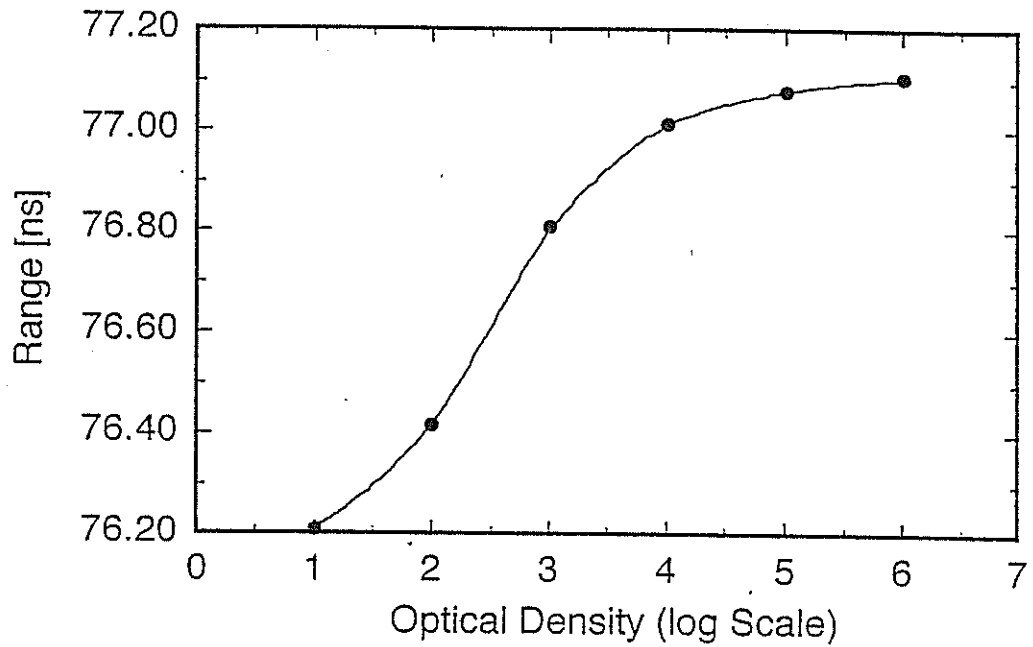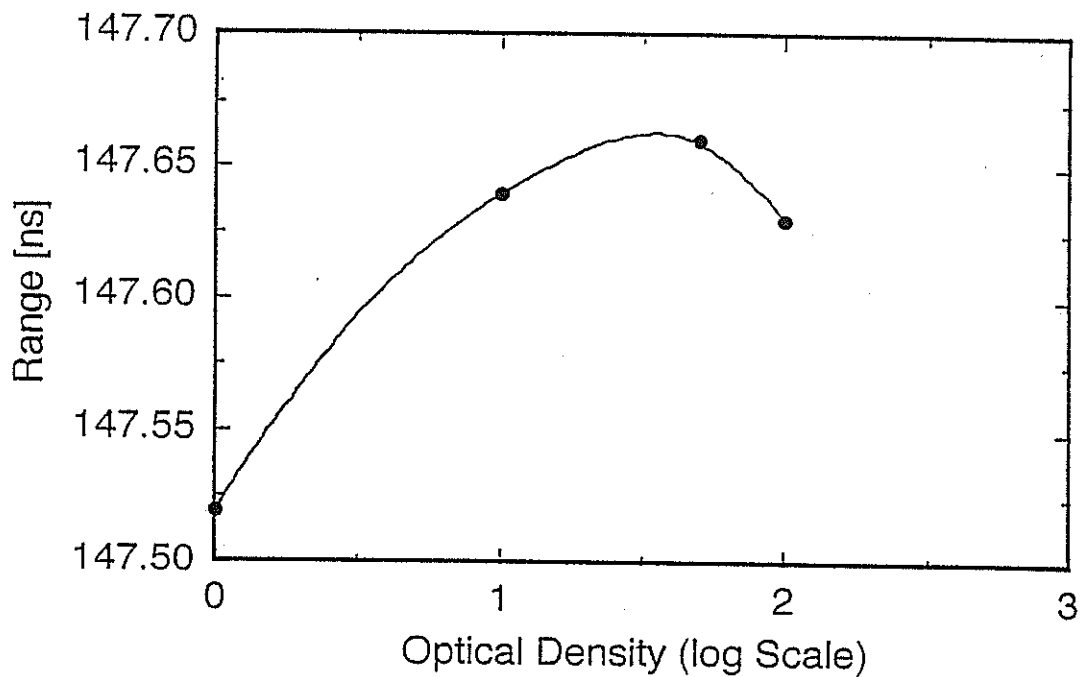Suzanne Jackson

Orroral Observatory

Australian Surveying & Land Information Group.

Phone: +61 6 235 7111.   Fax: +61 6 235 7103.   Email: suzyj@auslig.gov.au

Abstract:

Through our use of APD detectors at single-photon level over the last two years, we have noticed that different gating schemes in use in the SLR community can contribute significant biases to the data received. Our use of extremely short range calibrations, necessitating narrow gate pulses for calibration data has highlighted many of the traps in APD/SPAD use. This paper discusses some of the contributors to these biases, and how best to avoid them.

1. Introduction:

Considerable effort has been put into gaining a thorough understanding of the signal strength dependent time walk inherent to all APDs [1, 2]. It is now common practice to ensure that APDs are run in a single photon per return regime, or else more recently to gather data on the number of received photons using either a separate MCP or avalanche rise time so that this walk may be compensated out[3].

Less well known, it seems, is the effect that asymmetric calibration/satellite gates have on time bias.

Sharing a common aperture for transmit and receive has many advantages, such as improved transmit beam collimation and most effective use of available aperture. This technique also allows real-time calibration data to be gathered simply by placing a retro-reflector within the telescope tube. Unfortunately on the Orroral telescope[4], the calibration retro-reflector is not the only source of receive energy. The use of refractive optics in the common transmit/receive path, with their associated on-axis reflections, provides a number of other signal sources, any of which will trigger a gated APD.
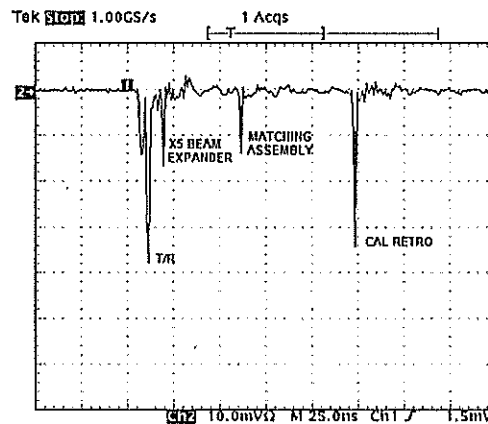

Figure 1: OTDR Plot of Orroral Common T/R Path.

The waveform in Figure 1 illustrates the time and amplitude relationship of return sources from telescope refractive optics. The waveform was captured by monitoring the MCP output with a 1GS/s digital oscilloscope. Of particular concern is the reflection from the Coudé matching

optics. This signal source is only three times weaker than the calibration retros, yet occurs just 65nsec before.

In order to ensure that only calibration returns trigger the APD, it is necessary to position the gate leading edge such that the APD is biased on in the interval between the matching assembly returns and the real calibration returns.

The necessary gate asymmetry has been found to introduce range biases, due to instabilities in the HV bias voltage at the start of the gate. Several gating schemes have thus been trialed at Orroral, in order to improve the gate switching speed, whilst ensuring stable bias for a reasonable gate period without increasing APD dissipation.

2. Relationship between APD voltage and response time:

Examination of the physics of geiger mode operation makes it clear that the response time of an APD is dependent on the excess bias voltage above the diodes breakdown voltage. As the electric field in the depletion layer becomes stronger with increased bias, avalanche events have more energy, and thus liberate more charge carriers in a given time. The avalanche spreads through the active area faster, leading to a faster time response at higher bias voltage, with correspondingly reduced jitter.
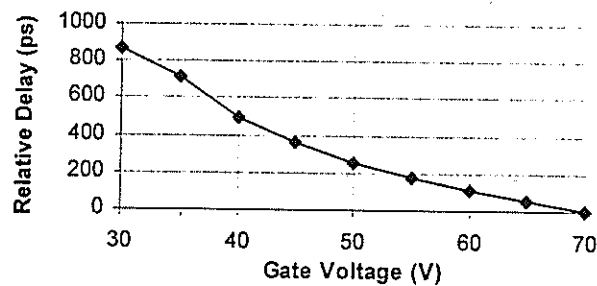

Figure 2: Relationship Between SSO-230 Gate Voltage and Delay.

The plot of delay versus gate voltage shown in Figure 2 was taken with the current Orroral APD, a Silicon Sensor SSO-230, cooled to -40°C with the HV bias set to -135V, 10V below breakdown. A gated passive quenching circuit was employed, with the gate leading edge positioned 200ns before the returns. At a typical operating gate voltage of 50V, there is a 22ps/V dependence between gate voltage and delay.

This figure illustrates that it is crucial to ensure that the bias voltage is the same for both calibration returns and satellite returns. On a system utilising real-time calibration data, where calibration and satellite gates are necessarily asymmetric, the bias driver plays an important role in ensuring that bias levels are consistent for the duration of the gate.

It should also be noted that varying the temperature of the diode has a corresponding effect on response time, as the breakdown voltage changes with temperature. Given a coefficient for breakdown of 600mV/°C [5], we get a variation of 13ps/°C at 50V gate. It is thus also important to ensure that the temperature of the APD is the same for calibration returns and satellite returns, just as with bias voltage. Indeed, in a system where calibration returns are gathered every shot, the possibility of range dependent time bias, due to the diode being cooled for a longer period on long ranges, exists where the diode cooling has a small time constant. This effect is minimised by ensuring that an avalanche event causes minimal dissipation within the APD.

313

3. Common gating schemes:

Numerous circuits have been devised to allow operation of APDs in the geiger mode. They are presented in order of complexity.
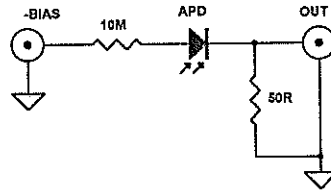
3.1 Ungated passively quenched.

Figure 3: Ungated Passively Quenched Circuit.

The biasing technique depicted in Figure 3 is common when APDs are used for simple photon counting applications.

When an avalanche event occurs, current is drawn from the bias supply, through the 10M series resistor. The bias voltage on the APD collapses, quenching the avalanche. The quenching time here is dependant on the time constant of the diode capacitance (typically a few pF) and the series resistance. Unfortunately, there is a corresponding reset time, after the avalanche has been quenched.

The likelihood of receiving a photon within the quench/reset time is quite high for all but the most noise-free APDs. The bias is not constant during this time, so the sensitivity and response speed is very unpredictable, making this type of bias circuit impractical for satellite ranging.

3.2 Gated passively quenched.

In order to make the passively quenched design work with noisy APDs, it is necessary to gate the device. This is usually done by reducing the bias voltage to less than the APD breakdown voltage, and capacitively coupling a low impedance, fast gate pulse to bring the voltage across the APD (the algebraic sum of the bias supply and the gate supply) to above the breakdown voltage. Avalanche quenching still occurs due to the collapse of the high impedance bias input, as for the ungated passively quenched circuit, but now the gate coupling capacitor adds to the diode capacitance to increase the quenching time constant (see Figure 4).
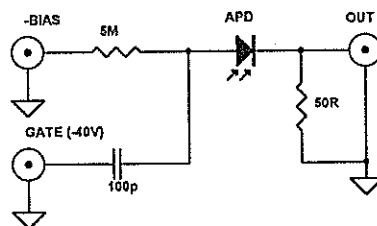
Figure 4: Gated Passively Quenched Circuit.

The advantage with this circuit over the ungated one is that we can be reasonably sure that the APD voltage will remain constant for a time after the gate pulse is applied. The important considerations here are the gate leading edge time, as this dictates the time between the start of the gate and the time when the APD voltage is stable, and also the fact that the voltage will 'bleed off' over the gate time through the resistor to the bias supply. For the circuit in Figure 4, with the bias supply set to 10V below the APD breakdown, and a 20us 50V gate, the reduction in APD voltage is given by:

$$\Delta V = V(1 - e^{-t/RC}) = 50\left(1 - e^{-20E^{-6}/500E^{-6}}\right) = 2.0V$$

Referring again to figure 2, this bias change represents a 43ps shift in time delay. Increasing the value of the gate coupling capacitor reduces this effect, but at the expense of increased dissipation in the APD due to a corresponding increase in the quench time constant, and increased gate ramp up time. At Orroral, we are currently using a compromise of 220pF gate coupling capacitor, and 10M HV series resistance, for a delay change of 5ps over a 10us 50V gate.
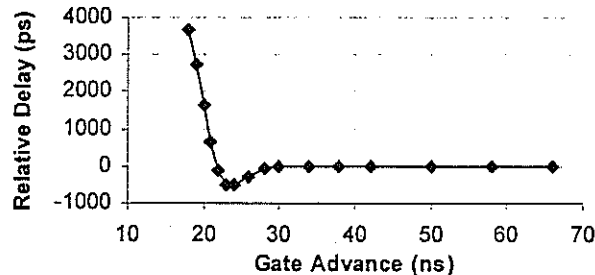
Figure 5: Delay vs Gate Advance for Gated Passively Quenched SSO-230

Figure 5 shows the actual measured bias with the gate edge placed close to the return. The gate on time is extremely short, being only 30ns or so. No returns were evident for the first 18ns. The bias has settled down (within 10ps) after 40ns, and remains stable all the way to 5us (the limit for ground ranging). This graph was created by firing at the ground target (1.1Km distant), using a HP5359A time synthesiser to generate a gate from the start detector output.

An important point to note with this circuit (and the actively quenched circuits) is that a portion of the change in bias at the APD will be capacitively coupled to the output. It is important to disable the output comparator or discriminator during 'the gate switch-on period, in order to stop the circuit from triggering on the leading edge of the gate.

To summarise, long gates must be avoided, even if the detector has a low enough noise count. There is a temptation to reduce the value of the HV series resistor, but this decreases the time constant of the bias discharge. Increasing the value of the gate coupling capacitor has a detrimental effect on APD dissipation, due to increased quenching time constant. The gate must be active a reasonable time before the return (say 50ns), to allow the bias to settle.

3.3 Actively quenched with 'Class A' bias driver.

To guarantee a constant bias voltage with long gates, whilst minimising APD dissipation, it is advantageous to actively control the bias voltage with a low impedance driver, as depicted in Figure 6.

Here the APD is driven by a relatively low impedance (10K) directly to the final bias voltage. In order to quench the avalanche, a transistor is employed to sink current from the bias source, thus reducing the APD voltage below breakdown. The quenching transistor is driven by the output of a flip flop, which is set by the avalanche event (detected by a fast comparator) and reset by the gate edge. By utilising a fast comparator, flip-flop, and quenching transistor, we are able to quench the avalanche in well under 100ns, limiting APD dissipation to acceptable levels.
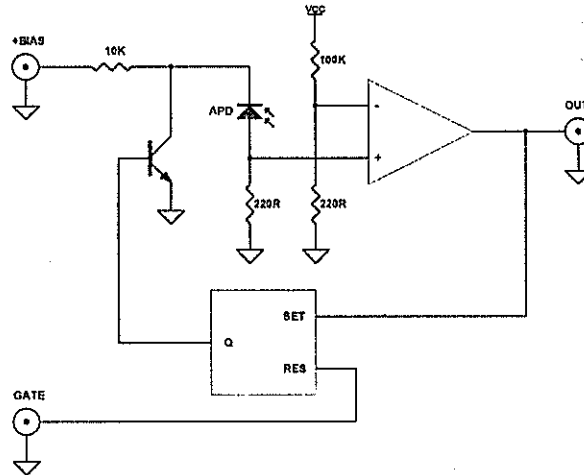
Figure 6: Actively Quenched 'Class A' Circuit.

Although this circuit appears significantly more complex than the passively quenched versions, the presence of the avalanche comparator on-board negates the need for an external discriminator.

This circuit exacerbates the problem with slow ramp up of APD bias at the start of the gate because of the 10K resistor sourcing current into the APD and quenching transistor capacitance. Reducing the value of the source resistor increases power dissipation in the quenching circuitry, and also increases the power requirements placed on the bias supply.

In summary, charging time constant is dependent on diode/transistor capacitance and bias series resistance. Decreasing charging resistance improves gate on time at the expense of extra dissipation in the quenching transistor and bias supply. Bias voltage is constant until the detector · is triggered, however, so noise count is the only limiting factor on gate duration with this circuit. APD dissipation is dependent on the propagation delay of the comparator, flip-flop, and driving transistor.

3.4 Actively quenched with 'Class A-B' bias driver.

The slow ramp up times experienced by the simple class-A bias driver may be improved by adding a buffer stage to the driver, so that it can source current as well.
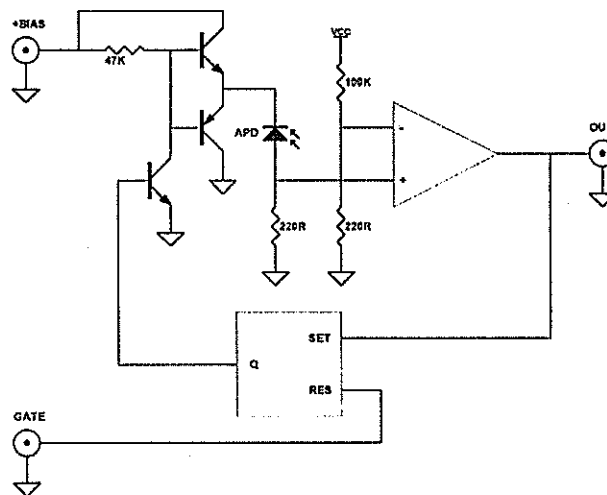
Figure 7: Actively Quenched 'Class A-B' Circuit.

Gate on time is reduced to a few tens of nanoseconds (dependant on the quenching circuit transistor speed and the quenching voltage difference), as with the passively quenched circuit. Bias current requirements are reduced over that of the class-A circuit. Note however that gate on times will not be as fast as for the passively quenched circuit, as bipolar transistor switch-off times are longer than switch-on times.

The APD bias voltage is now driven rapidly and accurately to the full supplied bias, and maintained until an avalanche event triggers the quenching circuit.

To summarise, Charging time constant is dependent on speed of bias driving transistors, diode capacitance, and decoupling. The power supply for the bias need only supply a few milliamps of current. As with the gated passive design, it is still important to activate the gate (say) 100ns or so before the return is expected, to ensure that the bias voltage has stabilised. After this point, bias voltage is constant until the detector is triggered. As with the class A circuit, APD dissipation is dependent on the propagation delay of the comparator, flip-flop, and bias driver transistors.

4. Conclusion:

There are numerous issues affecting the performance of APD/SPAD photon detectors when used for satellite laser ranging, beyond the simple multi-photon timewalk.

Gating circuitry, in particular the type of gating circuit used and the time relationship between the gate edge and the received photon, plays a considerable role in determining the overall accuracy of SLR measurements made with APD/SPAD detectors. Improper gating can contribute centimetre level errors to otherwise good data. It is of critical importance to ensure that calibration and satellite data are captured under identical conditions, in terms of receive energy, bias voltage, and temperature.

When faced with other constraints, such as the need to tightly gate calibration return sources on the Orroral telescope, the gating circuit must be carefully optimised to avoid biases.

5. Acknowledgment:

6. References:

1. Appleby, G. Gibbs, P. "Monitoring Potential Range Biases in Single Photon SLR Systems", Proc. Ninth International Workshop on Laser Ranging Instrumentation, Canberra, Australia, November 1994.

2. Schreiber, U. Maier, W. Haufe, K. H. and Kriegel, B. "Properties of Avalanche Photo Diodes", Proc. Ninth International Workshop on Laser Ranging Instrumentation, Canberra, Australia, November 1994.

3. Greene, B. Private communications, 1996.

4. Luck, J. McK. "Performance of the Upgraded Orroral Laser Ranging System", Proc. Eighth International Workshop on Laser Ranging Instrumentation, Annapolis, USA, May 1994.

5. Product Datasheet, SSO-AD230H-TO8PELT, Silicon Sensor GmbH Berlin.

Lsaer Technology

Development

Cr:LiSAF / Ti:Sapphire based solid state Laser System

for Two Color Satellite Laser Ranging

Peter Sperber, Armin Böer
Institut für Angewandte Geodäsie
Fundamentalstation Wettzell
D-93444 Kötzting
Germany

Eugen Pop
Astronomical Institute
University Berne
Sidlerstr. 5
CH-3012 Berne
Switzerland

Frederic Estable, Luc Vigroux
B.M. Industries
CE 2901
F-91029 Evry
France

Franck Falcoz
Institut d'Optique
Univ. Paris Sud
Cedex BP 147
F-91403 Orsay Cedex
France

Abstract: This paper is reporting on a diode pumped ps-Cr:LiSAF laser seeding a Ti:Sapphire regenerative and multipass amplifier.

This system produces pulses with 20 - 100 ps with an energy of about 100 mJ at 846/847 nm, combining the optimum wavelength for two color satellite ranging with the transmission of the atmosphere and the detection probability of high accuracy single photon detectors.

1. Introduction

During the last years Satellite Laser Ranging (SLR) using picosecond Nd:YAG Lasers achieved an accuracy of better than one cm. At this level of accuracy more emphasis has to be placed on the influence of satellite geometry and the atmospheric dispersion, causing errors up to a few cm /1,2,3/. The control and refinement of these models can be done with multiple wavelength ranging, measuring the Differential Time Interval between two wavelengths /4,5/. Taking into account the difference in the refractive index, the atmospheric transmission and the sensitivity of single photon detectors, best results are expected with wavelengths around 425 nm and in the near Infrared.

To fulfill all the requirements for a two color satellite laser ranging system in terms of peak power, pulse width, wavelength and repetition rate an all solid state Laser System based on a diode pumped ps Cr:LiSAF Oscillator and Nd:YAG pumped Ti:Sapphire amplifiers was designed and realized under contracts of B.M. Industries with the University Berne and the Institut für Angewandte Geodäsie.

2. System overview

2.1. Chromium LiSAF

Discovered in 1989, the Chromium:LiSAF crystal consists of a $LiSrAlF_6$ matrix doped with Cr^{3+} ions /6/. Like other solid state crystal, as Titanium Sapphire, this new material exhibits a large band off fluorescence in the near infrared between 800 and 1000 nm (see figure 1). The main advantage of this crystal is its absorption band between 600 and 700 nm (see figure 2) which is overlapping the emission wavelength of GaAlInP red diodes (at 670 nm). The Cr^{3+}:LiSAF is therefore an ideal candidate for tunable all solid state diodepumped lasers.

2.2. Titanium:Sapphire

It consists of a Sapphire matrix (Al_2O_3) doped with Titanium ions Ti^{3+} /6/. Titanium:Sapphire offers a very large band of fluorescence in the near infrared between 650 and 1100 nm (see figure 3). The absorption band is lying from 400 to 600 nm (see figure 4). This allows to pump this crystal with a source like Argon ion laser or Nd:YAG laser.

Figure 1: Shape of the emission spectrum of Cr^{3+}:LiSAF on the polarisation parallel to the c-axis

Figure 2: Shape of the absorption spectrum of Cr^{3+}:LiSAF on the polarisation parallel to the c-axis
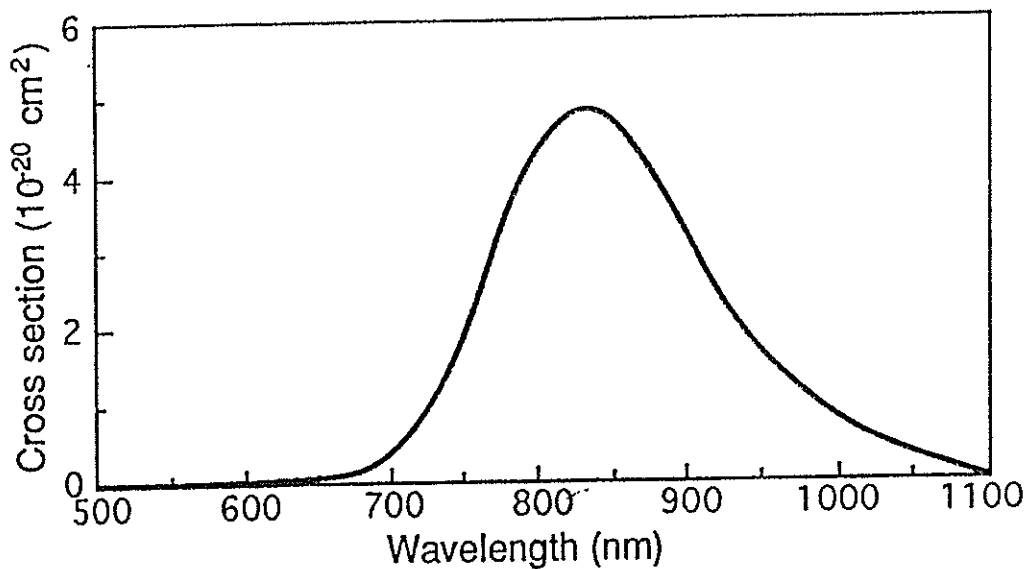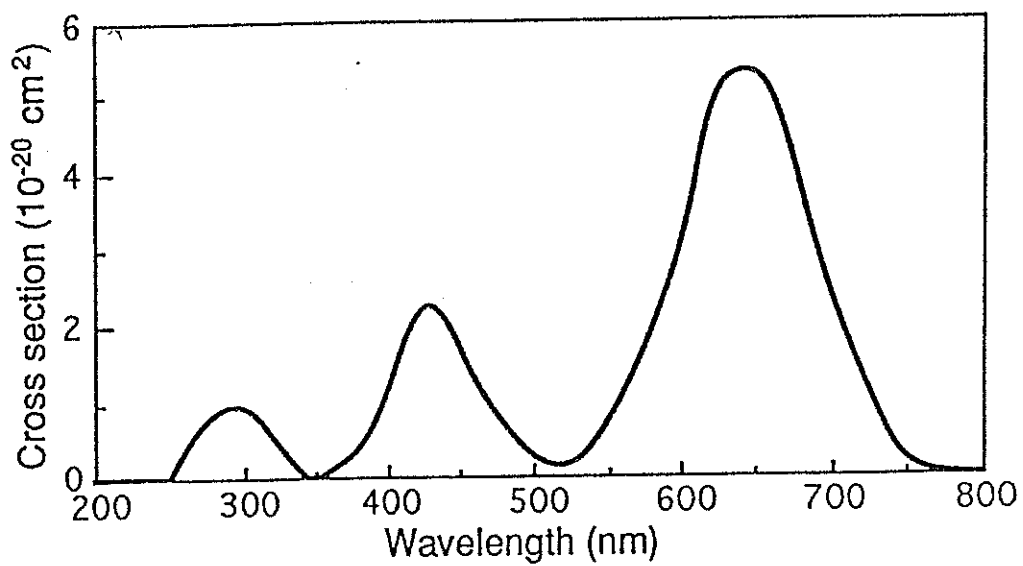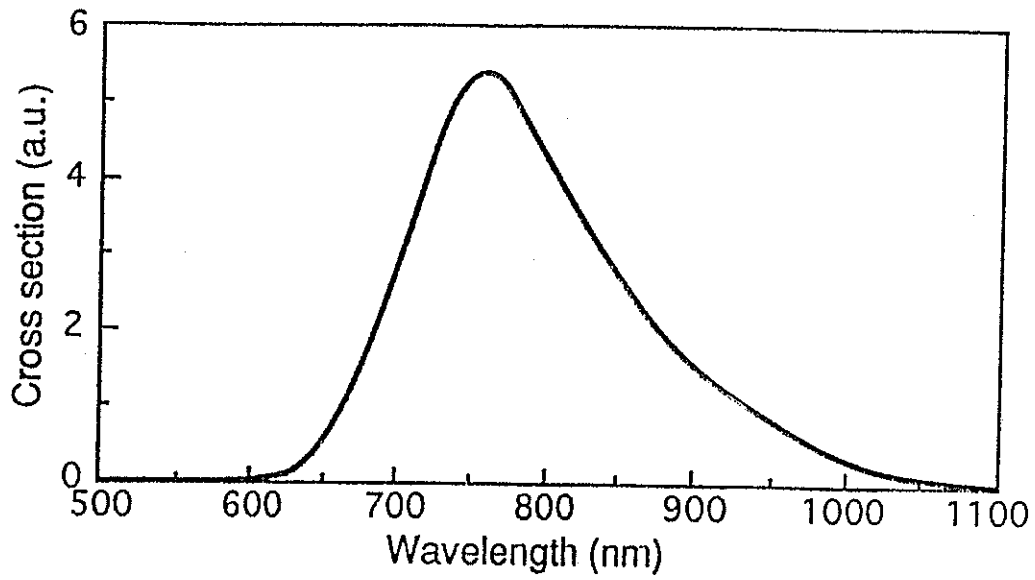
Figure 3: Shape of the emission spectrum of $Ti^{3+}:Al_2O_3$ on the polarisation parallel to the c-axis
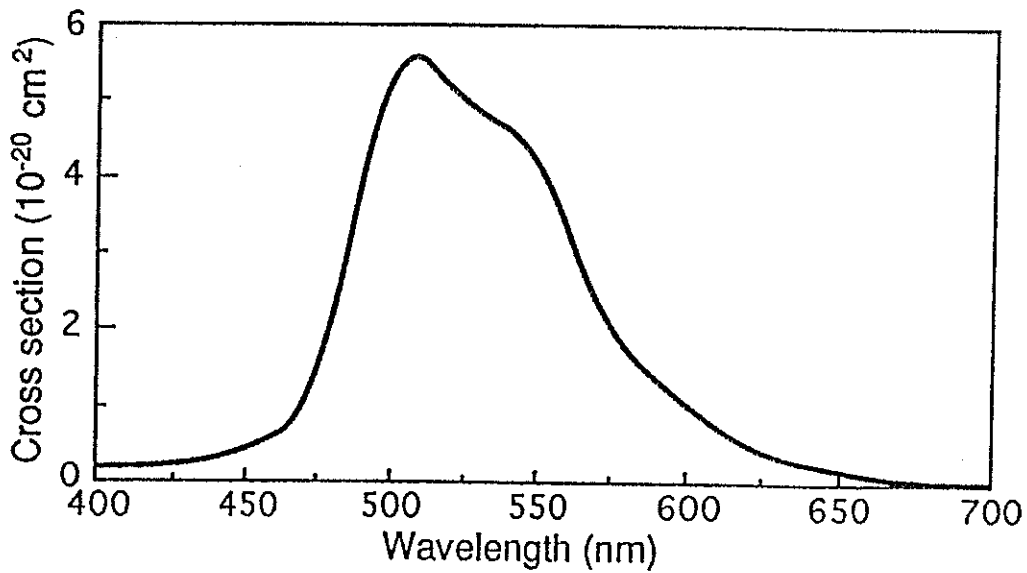
Figure 4: Shape of the absorption spectrum of $Ti^{3+}:Al_2O_3$ on the polarisation parallel to the c-axis

2.3. General Description

The Chromium:LiSAF-Titanium:Sapphire system consists of a Cr:LiSAF oscillator, an optical path selector, a regenerative amplifier, two multipass amplifiers and a second harmonic generator (see the general setup in figure 5). The "pump distributor" is used to split the pump beam in order to supply the different amplifiers.

The oscillator use Chromium:LiSAF as gain medium to generate a picosecond pulse train. The cw mode locking effect is achieved by using an acousto-optic modulator. The output wavelength can be tuned with the intra-cavity birefringent filter.
The optical path selector consists of a Faraday rotator with a half wave plate between two polarisers. This device rotates the polarisation of 90° in one direction, but does not change the polarisation in the other direction. It is used to send the beam from the oscillator to the regenerative amplifier at the first pass, and from the regenerative amplifier to the multipass amplifiers at the second pass.
The regenerative amplifier is used to increase the energy of the pulse to the milliJoule level. It consists of a resonator with Titanium:Sapphire as gain medium. The pulse is seeded and dumped out of the cavity by using a double step Pockels cell device. The repetition rate of the output train is fixed by the repetition rate of the Nd:YAG laser.
Two multipass amplifiers allow to increase the energy of the pulse. Different high reflection mirrors are used to make several passes into the Titanium:Sapphire crystals. The multipass preamplifier is pumped by the same Nd:YAG laser than the regenerative amplifier. The other Nd:YAG output is exclusively used by the main multipass amplifier.
The second harmonic generation is achieved by a non linear crystal with high conversion efficiency. The two wavelengths are separated and recombined by dichroic mirrors.
All the mechanical components are directly set on an optical table provided with covers.

Two similar systems are actually operational at the Astronomical Institute of University Berne and at the Institut für Angewandte Geodäsie in Wettzell. The general specifications of the systems are listed in Table 1. (If the specifications of the two systems are slightly different, the number for the Bernese system is marked by *.
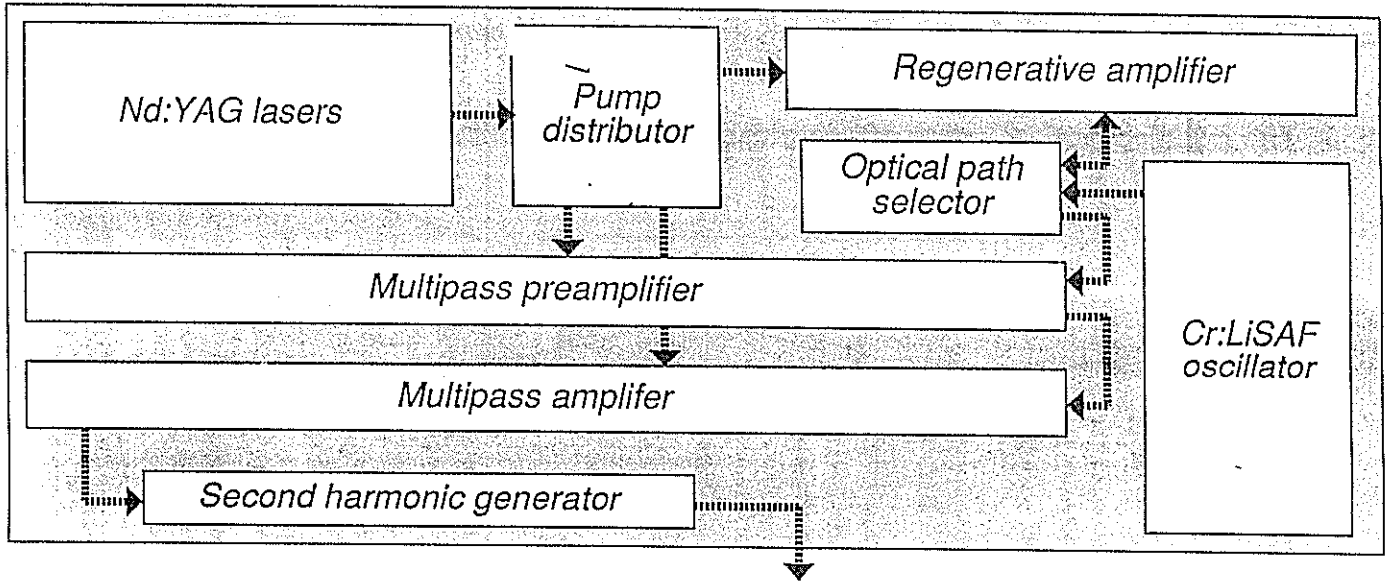
Figure 5: General Setup of the Cr:LiSAF/Ti:Sapphire Laser System

Oscillator	cw-modelocked diode pumped CR:LiSAF
Amplifier	Nd:YAG pumped Ti:Sapphire regenerative amplifier Two Nd:YAG pumped Ti:Sapphire multipass amplifiers
Wavelength	847/846* and 423.5/423* nm
Spectral width	< 0.5 Angström
Pulse duration	50/100* ps
Pulse energy	30/50* mJ
Repetition rate	10 Hz
Spatial mode	TEM 00
Divergence	< 1.5 mrad

Table 1: General system specifications

3.   Optical Setup

To get the best flexibility for future improvements, the laser system is setup from several standard parts that can be exchanged independently. This philosophy also makes the adjustment of the whole system quite easy as each part can be adjusted separately, the optical interfaces between the different parts are clearly defined.

The detailed optical setup of the pulse generation is shown in Figure 6.
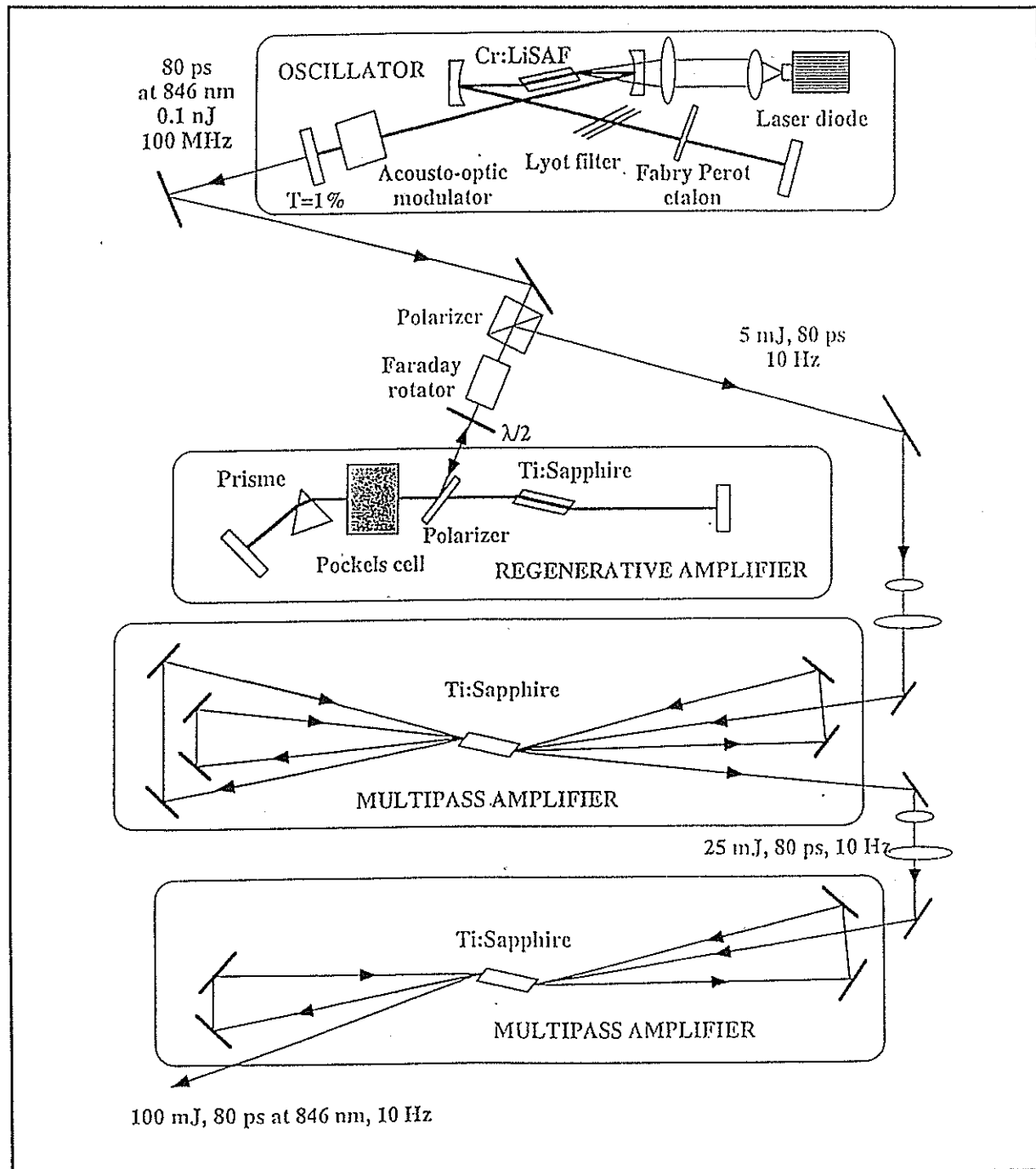
Figure 6: Detailed optical setup of the Laser System

3.1. Cr:LiSAF Oscillator

The oscillator is an actively mode-locked, diodepumped Cr:LiSAF-laser. A single stripe GAALJnP laser diode (400 mw cw at 670 nm) pumps a 5 mm long Brewster cut LiSAF crystal. The cavity consists of four mirrors, two concave mirrors (150 mm radius of curvature) around the crystal, a plane high reflector end mirror and a plane output coupler with 1% transmission between 800 and 900 nm. For the adjustment of the wavelength and the reduction of the spectrum width, a three-plate birefringent filter is used. In this case, pulses as short as 15 ps with a bandwidth of 0.06 nm around 850 nm have been obtained, indicating, that the pulses are transform limited. With different etalons, the pulse width can be adjusted between 50 ps and 200 ps. The average output power is around 15 mW at 100 MHz repetition rate corresponding to an energy per pulse of 0.1 nJ.
The output specifications of the oscillator are summarized in Table 2.

Cr:LiSAF oscillator	
Active medium	Cr^{3+}:LiSAF
Typical output power of oscillator	> 5 mW
Tuning range	820 - 900 nm
Operating wavelength	847/846* nm
Spectral width	< 0.5 Å
Repetition rate	100 MHz
Spatial mode	TEM_{00}
Polarisation	Linear horizontal
Pulse duration	variable 60/100* ps

Table 2:   Specifications of the oscillator

3.2. Regenerative amplifier

Through an optical path selector, the pulses from the oscillator are switched into an regenerative Ti:Sapphire amplifier pumped at 10 Hz by a Q-switched frequency-doubled Nd:YAG laser. At moderate pulse durations of 50 ps or higher the peak power in the amplifier is still low enough to avoid the classical Chirped Pulse Amplification (CPA) Technic. Therefor the setup is quite simple. The only additional element needed is a prism in the cavity to reduce the width of the free running spectrum and to match the central wavelength to that of the oscillator. The pump energy is about 50 mJ and the output energy at 846/847 nm is 5 mJ. The detailed specifications are summarized in Table 3.

Regenerative amplifier	
Active medium	Titanium: Sapphire ($Ti^{3+}:Al_2O_3$)
Tuning range	750 to 850 nm
Operating wavelength	847/846*nm
Repetition rate	10 Hz
Pump energy	40 mJ
Output energy (1)	> 2 mJ at 10 Hz
Spatial mode	TEM_{00}
Beam divergence	< 1.5 mrad
Pulse duration (FWHM) (2)	50 - 100 ps
Output polarisation	Linear vertical

(1)   Measured just at the output of the regenerative oscillator.
       The cavity is then unseeded.
(2)   For the seeded cavity only. This specification depends on the
       oscillator specifications.

Table 3:   Specifications of the regenerative amplifier

3.3.   Multipass Amplifiers

To increase the pulse energy to the required 60 mJ - 100 mJ two multipass amplifiers are used. The beam is expanded to avoid nonlinear effects in the amplifier crystals. The crystals of the two amplifiers are pumped from both sides to keep the pump fluence under 1.5 J/cm². After the first four pass amplifier an output energy of about 25 mJ is obtained for a pump energy of 150 mJ.

In the second (three pass) amplifier an output energy of 100 mJ is obtained. An independent Nd:YAG laser producing 350 mJ in the green is used to pump this amplifier. The use of two pump lasers gives the possibility to adjust the time delay between the two pump pulses and to optimize the pump arrival time in the second multipass amplifier. So we could take into account the build up time of the gain in the regenerative amplifier. Table 4 show the detailed specifications of the multipass amplifier chain.

Multipass preamplifier	
Active medium	Titanium:Sapphire
tuning range	750 to 850 nm
Operating wavelength	847/846* nm
Repetition rate	10 Hz
Pass number	4
Pump energy	200 mJ
Input energy	> 2 mJ
Output energy	> 25 mJ
Typical average power	> 250 mW at 10 Hz
Spatial mode	Single transverse
Beam divergence	< 1 mrad
Pulse duration (2)	50 - 100 ps
Output polarisation	Linear horizontal
Multipass amplifier	
Active medium	Titanium:Sapphire
Tuning range	750 to 850 nm
Operating wavelength	847/846* nm
Repetition rate	10 Hz
Pass number	3
Pump energy	400 mJ
Input energy	> 25 mJ
Output energy	> 65 mJ
Typical average power	> 650 mW at 10 Hz
Spatial mode	Single transverse
Beam divergence	< 1 mrad
Pulse duration (2)	50 - 100 ps
Output polarisation	Linear horizontal

(2)   Specification depends on the oscillator specifications

Table 4:   Specifications of the multipass amplifier chain

3.4. Second harmonic generation

The optical setup of the second harmonic generation is shown in Figure 7. A BBO type 1 crystal with a conversion rate of app. 50% generates pulses of 30 mJ at 846/847 nm and 423/423.5 nm. The wavelengths are split and each pulse can be independently attenuated to optimize the relative return level of both wavelengths during ranging. A lens telescope is used to adjust the different divergence of the two beams before recombining the two wavelengths into one beam.
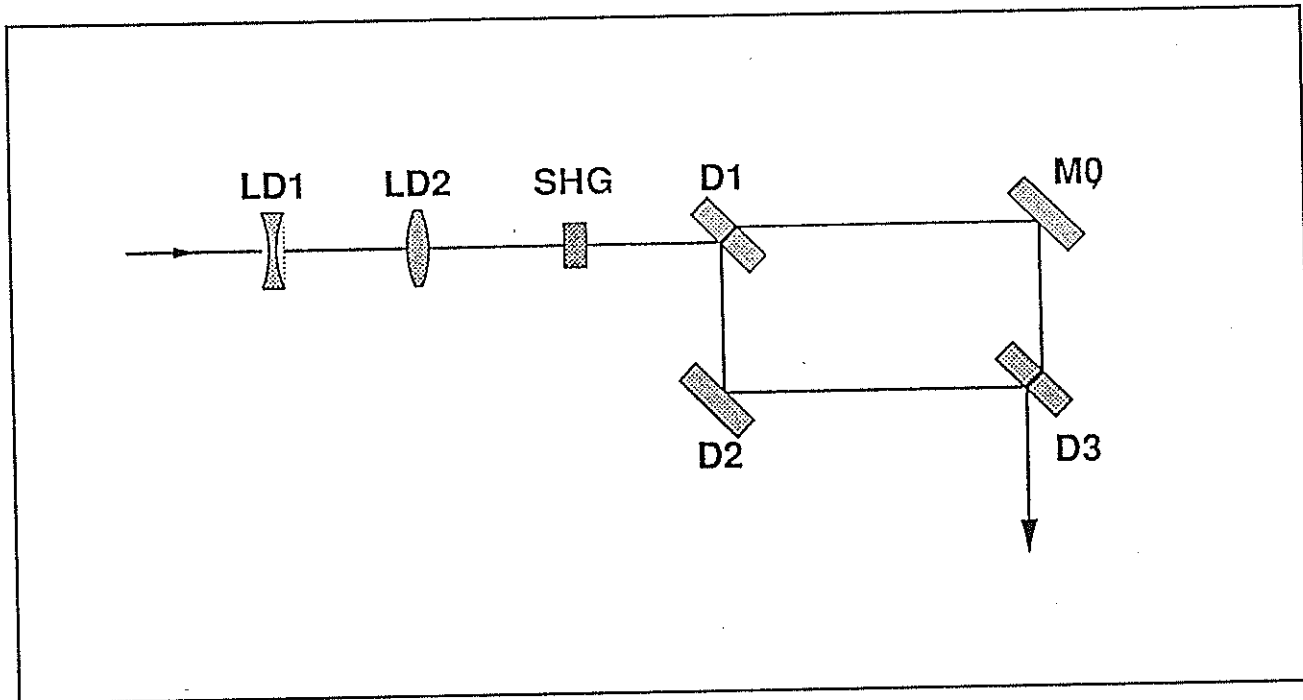
Figure 7: Optical setup of the Second Harmonic Generation

3.5. Pump laser

The Ti:Sapphire amplifier chain is pumped by a q-switched Nd:YAG laser with two independent channels (Figure 8). Channel one is used to pump the regenerative amplifier (50 mJ) and the first multipass amplifier (150 - 200 mJ).

The whole energy of channel two (400 mJ) can be used to pump the second multipass amplifier. With this pump energy an output energy of 100 mJ at 846/847 nm is available. At pulse durations below 100 ps the pump energy and therefor the output energy of the amplifier has to be reduced by slight misalignment of the Quarterwaveplate to prevent damage of the optical components in the multipass amplifier.

The specifications of the pump laser are listed in Table 5.
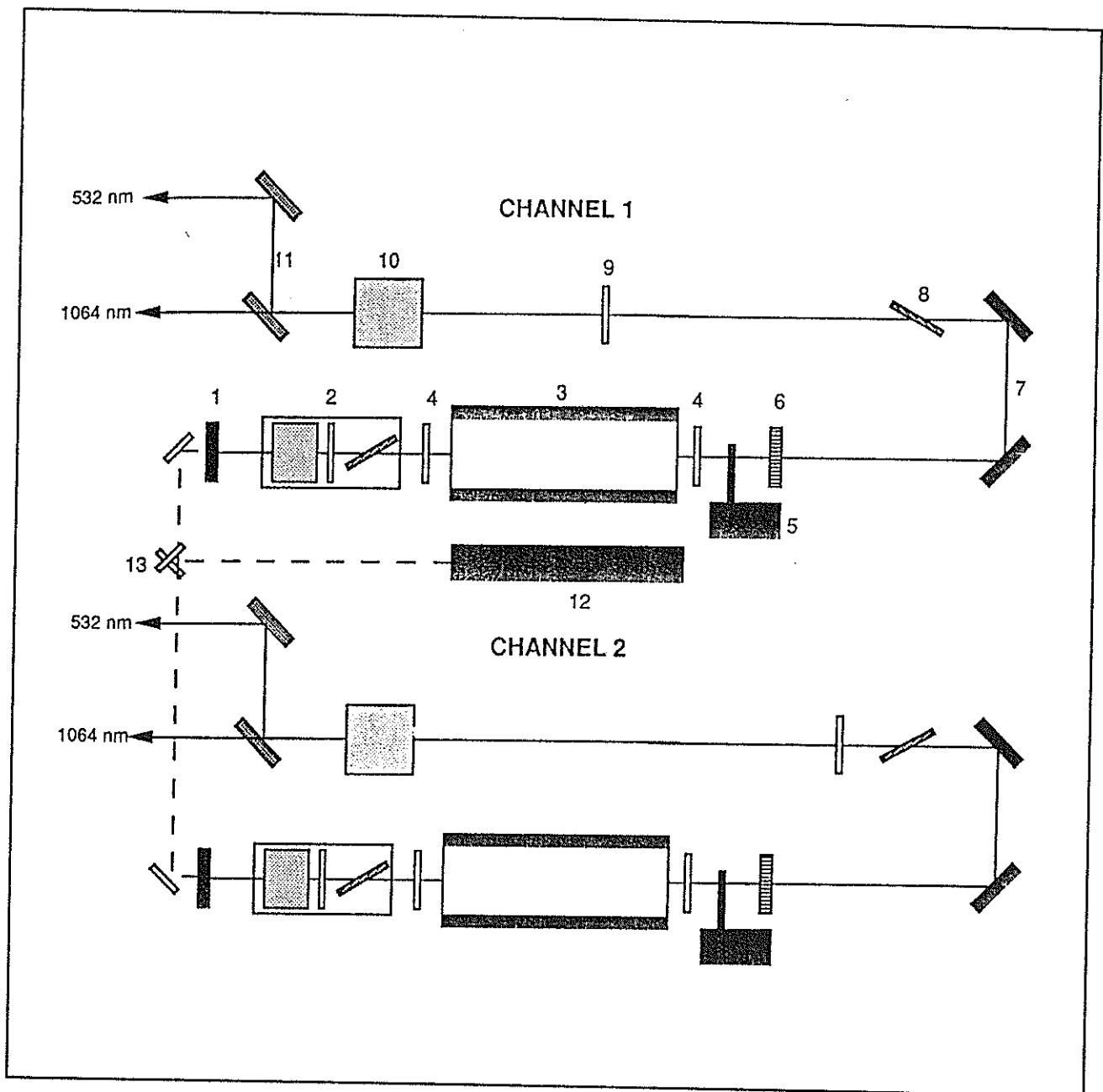
Oscillator 1&2:

1. High reflective mirror; 2. Electro-Optic Q-switch; 3. Pumping structure
4. Compensating quarter-wave plate; 5. Intracavity beam shutter;
6. Graded reflective output coupler; 7. Deflecting mirror
Second Harmonic Generation 1&2:
8. Polariser at 1064 nm; 9. Quarter-wave plate at 1064 nm;
10. Temperature regulated frequency doubler; 11. Dichroic mirror 532 nm
Micellaneous:
12. He-Ne Laser; 13. Silvered mirrors; 14. Control photodiode

Figure 8: Layout of the Nd:YAG Pump Laser

Nd:YAG pump laser	Model: 5000 D.NS 10
Typical output power on channel 1	> 450 mJ @ 1064 nm > 240 mJ @ 532 nm
Typical output power on channel 2	> 850 mJ @ 1064 nm > 400 mJ @ 532 nm
Repetition rate	10 Hz
Pulse duration (FWHM)	~ 7 ns
Beam diameter on channel 1	7 mm
Beam diameter on channel 2	9 mm
Spatial mode	Single transverse
Beam divergence	< 0.5 mrad
Polarisation	Linear vertical
Spectral width	~ 1 cm^{-1}

Table 5:   Specification of the pump laser

4.   Summary

In this paper we described a very flexible and modular laser system generating ps-pulses at wavelengths which are optimal for two colour satellite laser ranging. The laser is an all solid state system working already very reliable at the two new state-of-the-art SLR Systems in Zimmerwald and Wettzell (TIGO).

References:
/1/   Degnan I. I., Millimetre Accuracy Satellite Laser Ranging: A Review, Geodynamics Series Vol. 25, Contributions of Space Geodesy to Geodynamics, American Geophysical Union, Washington (1993), 125
/2/   Neubert R., An Analytical Model of Satellite Signature Effects, Australian Government Publishing Service, Proceedings of the 9th International Workshop on Laser Ranging Instrumentation, Canberra (1994) 82
/3/   Appleby G. M., Satellite Signatures in SLR Observations, NASA Conference Proceeding 3214, 8th International Workshop on Laser Ranging Instrumentation, Annapolis (1992) 2-1
/4/   Kirchner G., Koidl F., Hamal K., Prochazka I., Multiple Wavelength Ranging in Graz, Australian Government Publishing Service, Proceedings of the 9th International Workshop on Laser Ranging Instrumentation, Canberra (1994) 609

/5/   Schreiber U., Maier W., Riepl S., Measuring atmospheric dispersion employ-
        ing avalanche photodiodes, in Lidar Techniques for Remote Sensing, Christi-
        an Werner, Editor, SPIE 2310, 2 - 10, (1994)
/6/   W. Koechner, Solid State Laser Engineering, Springer series in Optical
        Science, Vol. 1, Fourth Edition, p. 66ff, (1996)

OPTIMAL DESIGN OF PASSIVELY Q-SWITCHED MICROLASER TRANSMITTERS FOR SATELLITE LASER RANGING

John J. Degnan
NASA Goddard Space Flight Center
Greenbelt, MD 20771 USA

ABSTRACT

The workhorse for third generation satellite laser ranging systems has been the modelocked Nd:YAG laser which produces pulsewidths measured in tens to hundreds of picoseconds. These systems are typically large (> 1 m long), complex, and require relatively sophisticated modulation and switching electronics, passive or active thermal control of the resonator length, and, in some cases, the use of limited lifetime dyes and carcinogenic solvents. Their complexity and reliance on inexpensive but short-lived flashlamps for pumping, with their attendant high voltage power supplies and ionozation circuits, further ensures a high level of maintenance by onsite personnel.

Recently, tiny Q-switched Nd-based microlasers, having lengths on the order of a millimeter and pumped by a single laser diode, have been demonstrated. These devices have operated at multikilohertz rates with pulsewidths as short as 115 picoseconds and single pulse output energies up to several tens of microjoules. Microlasers have been Q-switched via both active (e.g electro-optic) and passive (e. g. saturable absorber) means and generate more stable and temporally smooth profiles than many modelocked systems. Various passive diode-pumped multipass amplifier schemes have been devised for amplifying the microlaser output to millijoule levels without resorting to the use of fast switching or pulse selection devices. Thus, microlasers make ideal transmitters for the eyesafe SLR 2000 system and are a natural and inexpensive alternative to modelocked oscillators and/or regenerative amplifiers in higher power systems.

At GSFC, we have studied the manner in which both active and passive Q-switched lasers can be optimized for maximum efficiency (and coincidentally for minimum pulsewidth) and have examined the effects of thermalization among Stark sublevels and lower multiplet relaxation on pulse temporal profiles. More recently, we have begun to experimentally characterize the saturation properties of passive absorbers, such as chromium-doped YAG and Lithium Fluoride commonly used to Q-switch Nd-based lasers, as a function of pulsewidth. These theoretical and experimental efforts are combined in the present paper to derive optimum designs for an all diode-pumped SLR 2000 transmitter with the following characteristics: pulse energy ≥ 100 µJ at 532 nm, repetition rate ≥ 2 KHz, and pulsewidth ≤ 140 picoseconds.

1. INTRODUCTION

The workhorse for third generation satellite laser ranging systems has been the modelocked Nd:YAG laser which can produce pulsewidths measured in tens to hundreds of picoseconds. These systems are typically large (> 1 m long), complex, and require relatively sophisticated modulation and high voltage switching electronics, passive or active thermal control of the resonator length, and, in some cases, the use of limited lifetime modelocking dyes and carcinogenic solvents. Their complexity and reliance on inexpensive but short-lived flashlamps for pumping, with their attendant high voltage power supplies and ionization circuits, further ensures a high level of maintenance by onsite personnel. Field lasers typically generate 100 mJ of energy per pulse at repetition rates of 5 to 10 Hz for the frequency doubled wavelength at 532 nm. This corresponds to an average green power output of only 0.5 to 1.0 Watts although single pulse peak powers are typically in the Gigawatt range.

Recently, tiny Q-switched Nd-based microlasers, having lengths on the order of a millimeter and pumped by a single laser diode, have been demonstrated. These tiny oscillators have operated at multikilohertz rates with pulsewidths as short as 115 picoseconds in active Q-switching mode using a resonant end reflector and have produced single pulse output energies up to several tens of microjoules [1]. Microlasers have also been switched via passive saturable absorbers and generate more stable and temporally smooth profiles than many modelocked systems [2,3] although they have not yet achieved the very short pulsewidths on the order of 10 picoseconds available from modelocked systems. In some cases, the gain and saturable absorber media can be doped into the same host crystsal, such as Neodymium and Chromium ions, and optical coatings deposited on both ends to form a single element, monolithic laser [3]. Furthermore, various passive diode-pumped multipass amplifier schemes have been devised for amplifying the microlaser output to millijoule levels without resorting to the use of active regenerative amplifiers which require nanosecond rate switching or pulse selection devices [4]. One can therefore design a laser ranging transmitter which operates off a single DC voltage by using a combination of CW diode pumping for both the oscillator and amplifier, passive Q-switching by saturable absorbers, and passive multipass amplifier configurations. Since the resulting transmitter would produce average powers comparable to that of current field SLR systems (≤ 1 Watt) , but at much lower pulse energies and multikilohertz rates, the photon detection rate would also be similar. By allowing the low energy pulse train from the microlaser transmitter to fill the transmit/receive telescope aperture (<50 cm diameter), one can also meet current eye safety standards while maintaining average power levels comparable to current systems. Thus, microlasers make ideal transmitters for the eyesafe SLR 2000 system [5] and are a natural and very inexpensive alternative to modelocked oscillators and/or regenerative amplifiers in seeding higher power systems.

The author has previously studied the manner in which both actively [6] and passively [7] Q-switched lasers can be designed for maximum energy efficiency (and coincidentally for minimum pulsewidth in most cases of interest) and has further examined the effects of thermalization among Stark sublevels and lower multiplet relaxation on Q-switched laser energy and pulse temporal profiles [8]. More recently, Xiao and Bass [9] have demonstrated the manner in which excited state absorption, which occurs in some saturable absorbers, can be accomodated in Degnan's passive Q-switch optimization process. More recently, we have begun to experimentally characterize the saturation properties of passive absorbers, such as chromium-doped YAG and Lithium Fluoride commonly used to Q-switch Nd-based lasers, as a function of pulsewidth [10]. These theoretical and preliminary experimental efforts are combined in the present paper to derive optimum designs for an all diode-pumped SLR 2000 transmitter with the following characteristics: pulse energy ≥100 μJ at 532 nm, repetition rate ≥ 2 KHz, and pulsewidth ≤ 140 picoseconds.

2. OPTIMIZATION EQUATIONS FOR A CW-PUMPED, PASSIVELY Q-SWITCHED SYSTEM

Using Eqs. (21), (35), (36) and (38) in [7], one can show that, in order to optimize the output energy of a CW-pumped, passively Q-switched laser, the following three equations

$$z = \frac{\left(1 - e^{-\alpha\rho} - \alpha\rho\right)^2}{\left(1 - e^{-\alpha\rho} - \alpha\rho\right)\left(1 - e^{-\alpha\rho} - \alpha\rho e^{-\rho}\right) - \alpha\left(1 - e^{-\rho} - \rho\right)\left(1 - e^{-\alpha\rho} - \alpha\rho e^{-\alpha\rho}\right)}$$

(1a)

$$z = z_{cw} \frac{1 - \exp\left(-\tau_c / \tau_a\right)}{1 - \delta \exp\left(-\tau_c / \tau_a\right)} \equiv z_{cw} F$$

(1b)

$$\delta = 1 - \frac{f_a}{\gamma}\left(1 - e^{-\rho}\right)$$

(1c)

must be solved simultaneously for the parameters z, δ, and ρ where

$$z = \frac{2\sigma n_i l}{L} = \frac{2\ln(G_o)}{L}$$

(2a)

$$\rho = \ln\left(\frac{n_i}{n_f}\right)$$

(2b)

and δ is the fraction of the original inversion remaining from the previous Q-switch cycle as determined from a steady state analysis.

Alternatively, equations (1a) through (1c) can be combined to yield a single transcendental equation for the value of ρ in the optimized case, i.e.

$$z_{cw} = \frac{\left(1 - e^{-\alpha\rho} - \alpha\rho\right)^2 \left[1 + \frac{f_a}{\gamma} \frac{\left(1 - e^{-\rho}\right)}{\exp\left(\tau_c / \tau_a\right) - 1}\right]}{\left(1 - e^{-\alpha\rho} - \alpha\rho\right)\left(1 - e^{-\alpha\rho} - \alpha\rho e^{-\rho}\right) - \alpha\left(1 - e^{-\rho} - \rho\right)\left(1 - e^{-\alpha\rho} - \alpha\rho e^{-\alpha\rho}\right)}$$

(3)

Parameters appearing in (3) , which are assumed to be known or estimated apriori, are:

$z_{cw} = 2 \sigma n_{cw} l/L = 2 \ln(G_o)/L$ where G_o is the roundtrip CW small signal power gain in the absence of Q-switching, L is the dissipative roundtrip optical loss (which excludes the mirror transmission and saturable absorption loss), σ is the spectroscopic stimulated emission cross-section; n_{cw} is the population inversion density produced by the CW pump, and l is the gain length.

$$\alpha = \frac{F_{sat}^{amp}}{F_{sat}^{abs}} = \text{the ratio of the saturation fluences for the amplifying and absorbing media}$$

τ_a = upper laser multiplet relaxation time = 230 μsec for Nd:YAG

τ_c = desired Q-switch cycle time (inverse of repetition rate) = 500 μsec for SLR 2000 at 2 KHz

f_a = fractional Boltzmann population of laser Stark sublevel within the upper multiplet = .41 for Nd:YAG

γ = inversion reduction factor[6] where $f_a \leq \gamma \leq 2$ and takes on the upper value (2) when all thermalization and terminal level relaxation processes are slow relative to the resonator photon decay time and the lower value (f_a) when the processes are all relatively fast [8]. We have assumed a value of $f_a + f_b = 0.6$ for these Nd:YAG calculations which implies thermalization among Stark sublevels is fast but lower multiplet relaxation is slow compared to the resonator photon decay time.

By substituting (1c) in (1b), the quantity F, which represents the amount the initial Q-switch gain is reduced from its CW value due to the pulse repetition rate, can be written in the form

$$F = \left[1 + \frac{f_a}{\gamma} \frac{\left(1 - e^{-\rho}\right)}{\exp(\tau_c / \tau_a) - 1} \right]^{-1} \tag{4}$$

and computed once ρ is computed from (3). One can then use equations (22), (23), and (30) in [7] to compute the optimum unsaturated absorber transmission (T_{opt}), the optimum mirror reflectivity (R_{opt}), and the optimized laser output energy (E_{opt}). For our CW-pumped case, these equations can be written in a somewhat more transparent form, i.e.

$$T_{opt} = \exp\left[-\sigma n_{cw} l F \frac{\alpha \left(1 - e^{-\rho} - \rho\right)}{\left(1 - e^{-\alpha\rho} - \alpha\rho\right)} \right] \tag{5a}$$

$$R_{opt} = \exp\left[-\left(2\sigma n_{cw} l F + 2 \ln(T_{opt}) - L\right) \right] \tag{5b}$$

$$E_{opt} = \frac{h\nu A \rho}{2\sigma\gamma} \ln\left(\frac{1}{R_{opt}}\right) \tag{5c}$$

and computed sequentially in the order the equations are given. In (5c), A is the effective beam area in the gain medium and hv is the laser photon energy. The time averaged output power of the energy-optimized, CW-pumped microlaser is in turn given by

$$P_{ave} = \frac{E_{opt}}{\tau_c} = \frac{h\nu A \rho}{2\sigma\gamma\tau_c} \ln\left(\frac{1}{R_{opt}}\right) \tag{6}$$

337

One can also derive an expression for the laser pulsewidth using (32) in [7] which is given by

$$\tau = \frac{t_r}{\left[L - \ln\left(R_{opt}\right)\right]} \cdot \frac{1 - e^{-\rho} + \frac{\ln\left(T_{opt}\right)}{\alpha \sigma n_{cw} IF}\left(1 - e^{-\alpha\rho}\right)}{1 - \frac{g_t(\alpha,\rho)}{2\sigma n_{cw} IF} + \frac{\ln\left(T_{opt}\right)}{\alpha\sigma n_{cw} IF}\left(1 - \left[\frac{g_t(\alpha,\rho)}{2\sigma n_{cw} IF}\right]^{\alpha}\right) + \frac{L - \ln\left(R_{opt}\right)}{2\sigma n_{cw} IF}\ln\left[\frac{g_t(\alpha,\rho)}{2\sigma n_{cw} IF}\right]}$$

(7a)

where the roundtrip threshold gain, $g_t(\alpha,\rho)$, is obtained from an iterative solution of the equation [7]

$$g_t(\alpha,\rho) = \left[L - \ln\left(R_{opt}\right)\right] - 2\ln\left(T_{opt}\right)\left[\frac{g_t(\alpha,\rho)}{2\sigma n_{cw} IF}\right]^{\alpha}$$

(7b)

3. CW DIODE END-PUMPING OF A MICROLASER

Since our design goal is a short pulse comparable to that used in current centimeter accuracy SLR systems (<140 psec at 532 nm), the length of the microlaser must be kept fairly short, and therefore end-pumping by a single diode or fiber-coupled diode array is the only viable approach. Longer rods favor increased pump efficiencies which results in higher small signal gains, higher output energies, and higher average powers. However, the beneficial effects of higher gain on reducing laser pulsewidth are more than offset by an increase in the resonator roundtrip transit time. Thus, pulsewidth must be traded off against other important parameters such as pulse energy, peak power, or average power.

In order to begin our computation of the parameters for the optimized laser, we must compute the quantity z_{cw} appearing in Eqs. (1b) and (3) as a function of the diode pump intensity. For a CW-pumped laser, this is given by

$$z_{cw} = \frac{2\sigma n_{cw} l}{L} = \frac{2\sigma T_p \eta_p f_a \tau_a \eta_a I_p}{h\nu_p L}$$

(8)

where I_p is the CW pump intensity, $h\nu_p$ is the pump photon energy (= 2.46 x 10^{-19} J at 808 nm), η_p is the efficiency with which the energy deposited in the pump bands gets deposited into the upper laser multiplet (believed to be $\cong 1$ for the $^4F_{3/2}$ level in Nd:YAG), T_p is the transmission of the entrance face at the pump wavelength, and η_a is the fraction of the optical pump power entering the laser medium which is absorbed. The latter is given by the expression

$$\eta_a = \left[1 - \left(1 - R_p\right)e^{-\alpha_p l} - R_p e^{-2\alpha_p l}\right]$$

(9)

where, α_p is the pump absorption coefficient (~4.5/cm for Nd:YAG at a pump wavelength of 808 nm) and R_p is the reflectivity of the rod exit face at the pump wavelength. For one way pumping, the back face of the rod is AR-coated for the pump and laser wavelengths so that $R_p \cong 0$ whereas, for ideal two-way pumping, $R_p \cong 1$. In reality, the reflectivity of the pump wavelength must be traded off against the transmission at the laser wavelength which contributes to the dissipative loss, L, so that $R_p < 1$.

4. NUMERICAL RESULTS FOR A MONOLITHIC Nd³⁺;Cr⁴⁺:YAG CRYSTAL

We now use our theoretical expressions (3) through (7) to study the laser properties of a "monolithic" YAG crytal which is simultaneously doped with the ions producing gain (Nd^{3+}) and ions producing saturable absorption (Cr^{4+}) [3]. Since short pulses are our goal, use of a monolithic structure results in the simplest and shortest passively Q-switched laser resonator possible. In performing our numerical computations, we will assuime the following values for previously undefined parameters: $T_p=1$, $L=.02$, $R_p=1$, $F_{sat}^{amp} = 480$ mJ/cm² [7], $F_{sat}^{abs} = 179$ mJ/cm² [10]. We allow the length of the laser rod, l, to vary between 1 and 5 mm and assume that the optimum absorber doping for maximum laser efficiency can be accomodated within this crystal length. Figures 1 and 2 show plots of the optimum mirror reflectivity, optimum absorber transmission, and laser pulsewidth as a function of the CW diode pump intensity for different crystal lengths. The CW pump intensity was allowed to vary between 0 and 20 Watts/mm². The pulse energy curves are plotted against the same parameters for a total diode pump power of 1.2 Watts corresponding to the output of a Spectra Diode Labs Model SDL-2372-P3 diode laser which provides a high brightness beam in a 100 μm diameter spot via fiber optic coupling.
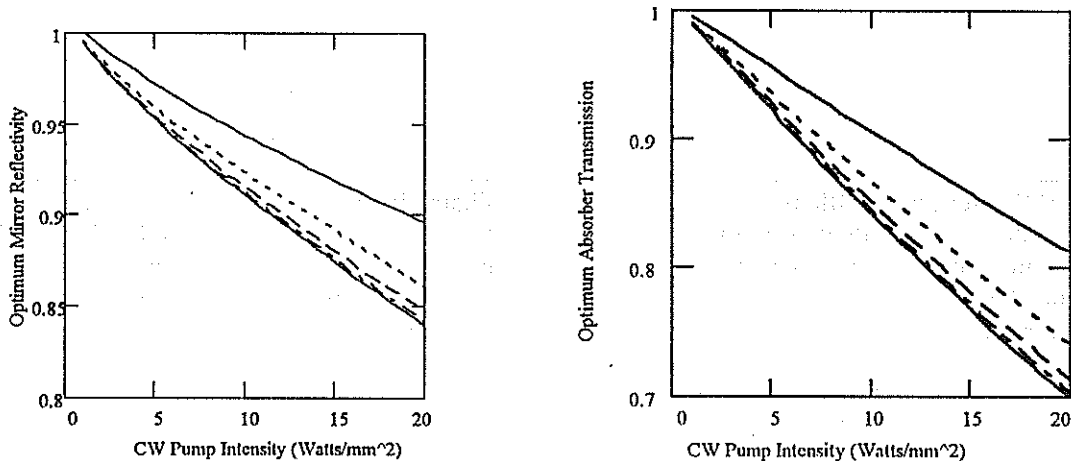
Figure 1: Optimum mirror reflectivity and absorber transmission as a function of CW pump intensity and rod length in 1mm increments. The top curve corresponds to a rod length of 1 mm and the bottom curve to a length of 5mm.

5. PASSIVE MULTIPASS AMPLIFIER

Coyle [4] has described a clever passive multipass amplifier design based on a rectangular slab shown in Figure 4. The slab is pumped on up to four sides by linear diode arrays. Typical cm long commercial arrays each produce up to 20 Watts of CW power.

One can define an amplifier "cell size", a, such that the length and width of the amplifier are equal to L = na and W = ma respectively where n and m are integers. One corner of the amplifier slab can be polished off to serve as an entrance face ,i.e. the entrance cell is cut in half along its diagonal and perpendicular to the beam.Thus, the beam size must be less than $\sqrt{2}a$ to fit within the entrance face. In addition, the beam size should be less than the width of the pumped volume in the slab. Once inside the slab, the beam will reflect internally off the sides of the amplifier at a 45° angle until it encounters another corner. This corner can be polished off (exit cell halved) to serve as an exit face.

339
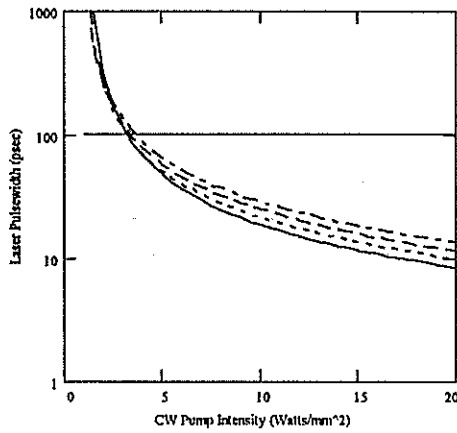
Figure 2: FWHM laser pulsewidth as a function of CW diode pump intensity and rod length in 1 mm increments. Bottom curve corresponds to a length of 1 mm and top curve to a length of 5 mm.
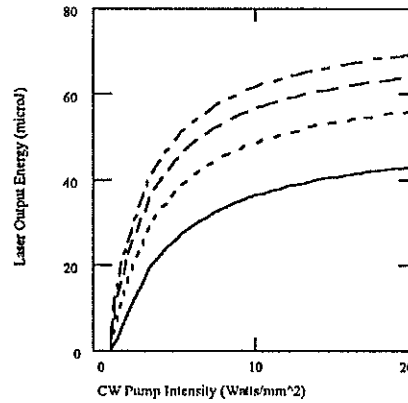
Figure 3: Laser pulse energy as a function of CW diode pump intensity and rod length in 1 mm increments for a total input power of 1.2 Watts. Bottom curve corresponds to a length of 1 mm and top curve to a length of 5 mm.

If m and n are chosen to have no common factors, one can show from a simple graph paper analysis that the effective multipass gain length before encountering a corner is given by

$$l_{eff} = \sqrt{2}a(mn - 1) = \sqrt{2}\left(\frac{LW}{a} - 1\right) \tag{10}$$

where $\sqrt{2}a$ is the diagonal length of a single "cell" and (mn-1) is the number of cell diagonals traversed before encountering a corner (one cell is lost by halving the entrance and exit cells to create the entrance and exit faces). Furthermore, the beam undergoes a number of 45° reflections inside the amplifier given by

$$n_r = m + n + 2 \tag{11}$$

so that the net multipass power gain in the amplifier is

$$G_{net} = \exp\left(\sigma n_{cw} l_{eff}\right) R_{45°}^{n_r} \tag{12}$$

where $R_{45°}$ is the reflectivity of the amplifier face at 45° incidence.

If the integers m and n are odd, the beam exits the amplifier from the corner opposite to the entrance face. If one integer is odd and the other even, the entrance and exit corners are adjacent to each other and lie on the same even numbered side.

If m and n have a common factor f, graphical analysis shows that the beam encounters a corner more quickly, and the effective gain length is reduced to

SLR 2000 LASER TRANSMITTER

Diode Laser Pump

Focusing Lens

Monolithic Passively Q-Switched Microlaser

Collimating Lens

Laser Out

Frequency Doubler

Polarizer

Rod Lens

Linear Diode Array (20Watts)

Multipass Amplifier (7x11)

Linear Diode Array (20Watts)

Rod Lens

$\frac{\lambda}{4}$ Plate

100% Reflector

1 cm

341
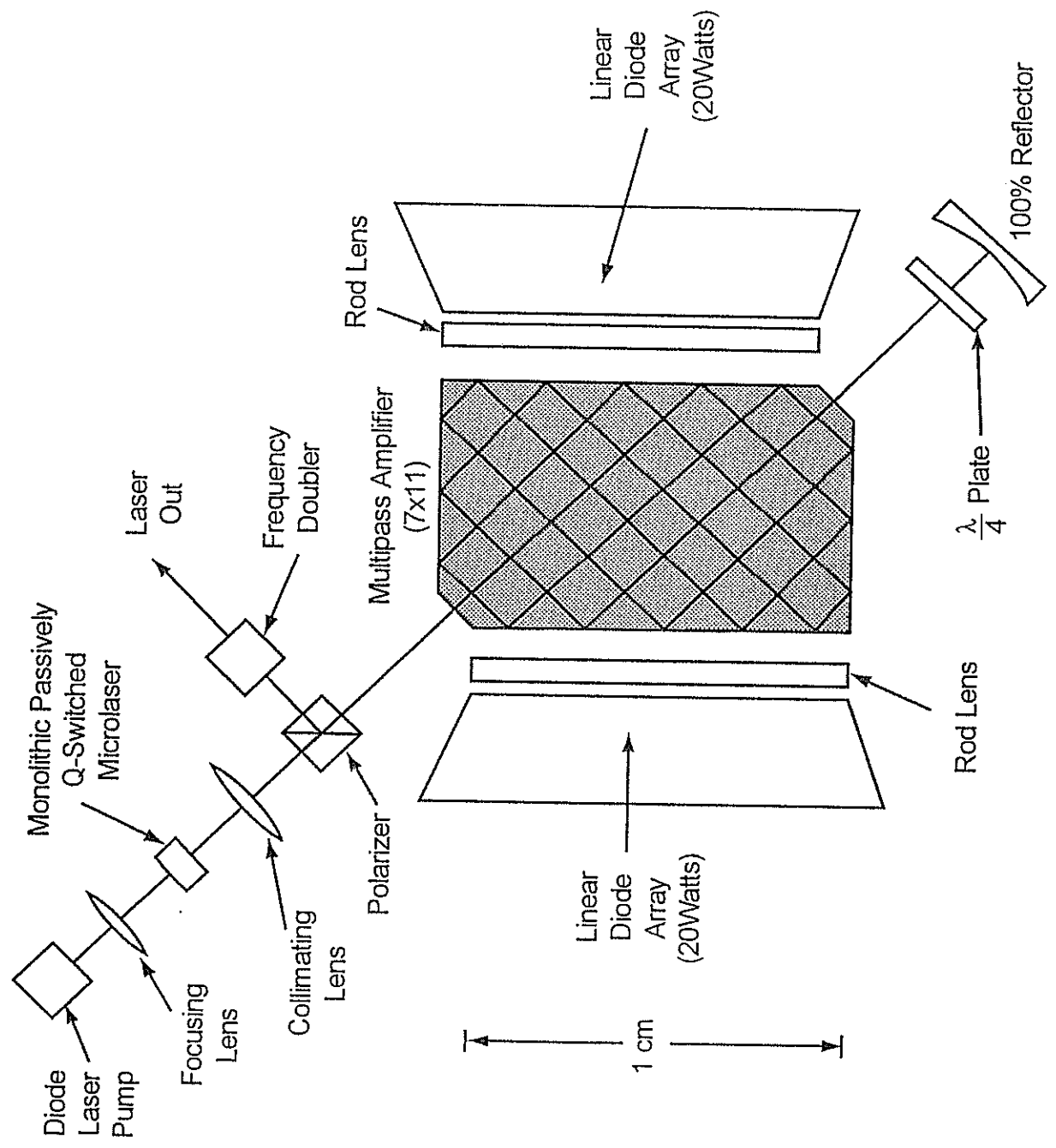
$$l_{eff} = \sqrt{2}a\left(\frac{mn}{f} - 1\right) = \sqrt{2}\left(\frac{LW}{fa} - 1\right) \qquad (13)$$

and this represents a "bad" design.

If L and W are both on the order of a cm (corresponding to a standard laser diode array length) and a is on the order of a mm (a typical slab pump width [4]) , then, from (12), the effective multipass gain length, on a single pass through the amplifier, can be as large as 14 cm. Placing a mirror at the exit face, as in the SLR2000 transmitter block diagram in Figure 4, allows the multipass amplifier to be used in a double-pass configuration, resulting in an effective gain length of 28 cm. Our computations show that such a configuration, pumped by two linear diode arrays, each producing 20 watts of CW power, can produce a double-pass small signal power gain of 16 if the diode pump light is focused into a typical 1.2 mm width. Thus, a 25 μJ pulse from the oscillator can be amplified to 400 μJ, which is more than adequate for SLR2000. Significant additional gain can be achieved, if necessary, by adding arrays to the two remaining unpumped sides of the amplifier as in [4], roughly squaring the small signal gain.

6. CONCLUSIONS

A comprehensive theoretical model has been developed for the passively Q-switched microlaser which (1) can be fit well to existing experimental data, (2) is useful in estimating unknown parameters, and (3) can guide prototype hardware design. Furthermore, a simple model for a totally passive CW laser diode-pumped multipass amplifier has been developed. This compact amplifier, with a ~1cm by 1 cm by 1mm pumped volume, produces gains much higher than can be achieved in a conventional single or double pass configuration pumped by the same diode power. Our calculations predict a maximum single pass gain of 4 and a maximum double pass gain of 16 for a slab multipass amplifier pumped by two 20 watt laser diode arrays, and this can be increased substantially by adding additional arrays. The resulting oscillator/amplifier design has no high speed pulsing or switching circuits and should easily achieve the laser energy, pulsewidth, and repetition rate goals of SLR2000.

REFERENCES

1. Zayhowski, J. and C. Dill III, "Coupled-Cavity Electro-optically Q-switched ND:YVO$_4$ Microchip Lasers", Optics Letters, 20, pp. 716-718, April, 1995.

2. Zayhowski, J. and C. Dill III, "Diode Pumped Passively Q-switched Picosecond Microchip Lasers", Optics Letters, 19, p. 1427-1430, 1994.

3. S. Li, S. Zhou, P. Wang, Y. C. Chen, and K. K. Lee, , "Self Q-switched Diode End-Pumped Cr, Nd: YAG with Polarized Output", Optics Letters, 18, pp. 203-204, February 1993.

4. Coyle, D. B., "Design of a High Gain Laser Diode Array Pumped Nd:YAG Alternating Precessive Slab (APS) Amplifier", IEEE J. Quantum Electronics, 27, pp. 2327-2331, October, 1991.

5. Degnan, J. , J. McGarry, T. Zagwodzki, P. Titterton, H. Sweeney, H. Donovan, M. Perry, B. Conklin, W. Decker, J. Cheek, A. Mallama, P. Dunn, and R. Ricklefs; "SLR2000: An Inexpensive, Fully Automated, Eyesafe Satellite Laser Ranging System", these proceedings.

6. Degnan, J. J. , "Theory of the Optimally Coupled Q-switched Laser", IEEE J. Quantum Electronics, 25, pp. 214-220, February, 1989.

7. Degnan, J. J., "Optimization of Passively Q-switched Lasers", IEEE J. Quantum Electronics, 31, pp. 1890-1901, November, 1995.

8. Degnan, J. J., D. B. Coyle, and R. B. Kay, "Effects of Thermalization on Q-switched Laser Parameters", IEEE J. Quantum Electronics, accepted with revisions.

9. Xiao G., and M. Bass, "A Generalized Model for Passively Q-switched Lasers Including Excited State Absorption in the Saturable Absorber", IEEE J. Quantum Electronics, 33, pp. 41-44, January 1997.

10. Gompers S. and J. Degnan, unpublished

EYE SAFE RAMAN LASER

K.Hamal, J.Blazej, I.Prochazka

Czech Technical University, Brehova 7
115 19 Prague 1, Czech Republic
fax +42 2 85762252, prochazk@mbox.cesnet.cz

To build the eye safe transmitter we were using the Raman cell filled by methane shifting the 1.064 micrometer Nd:YAG laser pulses to 1.54 micrometer wavelength. We examined the Raman process at 30, 60, 100 and 200 picoseconds long laser pulses using the active passive mode locked laser at methane pressure ranging from 5 to 11 Bars (the indoor experiment in Prague) and the active active mode locked laser at 180 picoseconds and 40 Bars (CRL Tokyo). The conversion efficiency varies from 5 to 10 percent. Using the CCD we tested the Raman beam structure. The beam divergence is generally 1.2 times smaller than the incoming 1.06 μm beam, the fluctuations from shot to shot are within the same value. Using the streak camera we measured the temporal structure, the Raman pulse duration was approximately 1.5 times shorter then the pumping pulse, however for longer pulse and higher pumping above the Raman threshold the pulse shape deterioration is pronounced and consequently influencing the overall single shot jitter of the laser ranging system. Testing the energy we found out that the Raman energy fluctuations increase by a factor 5 in comparison to 1.06 μm pump. In Tokyo SLR, using 10 milliJoules of 1.54 μm energy, all satellites up to 20 000 kilometers have been ranged.

Optical block scheme

K.Hamal,J.Blazej,I.Prochazka, Shanghai '96

345
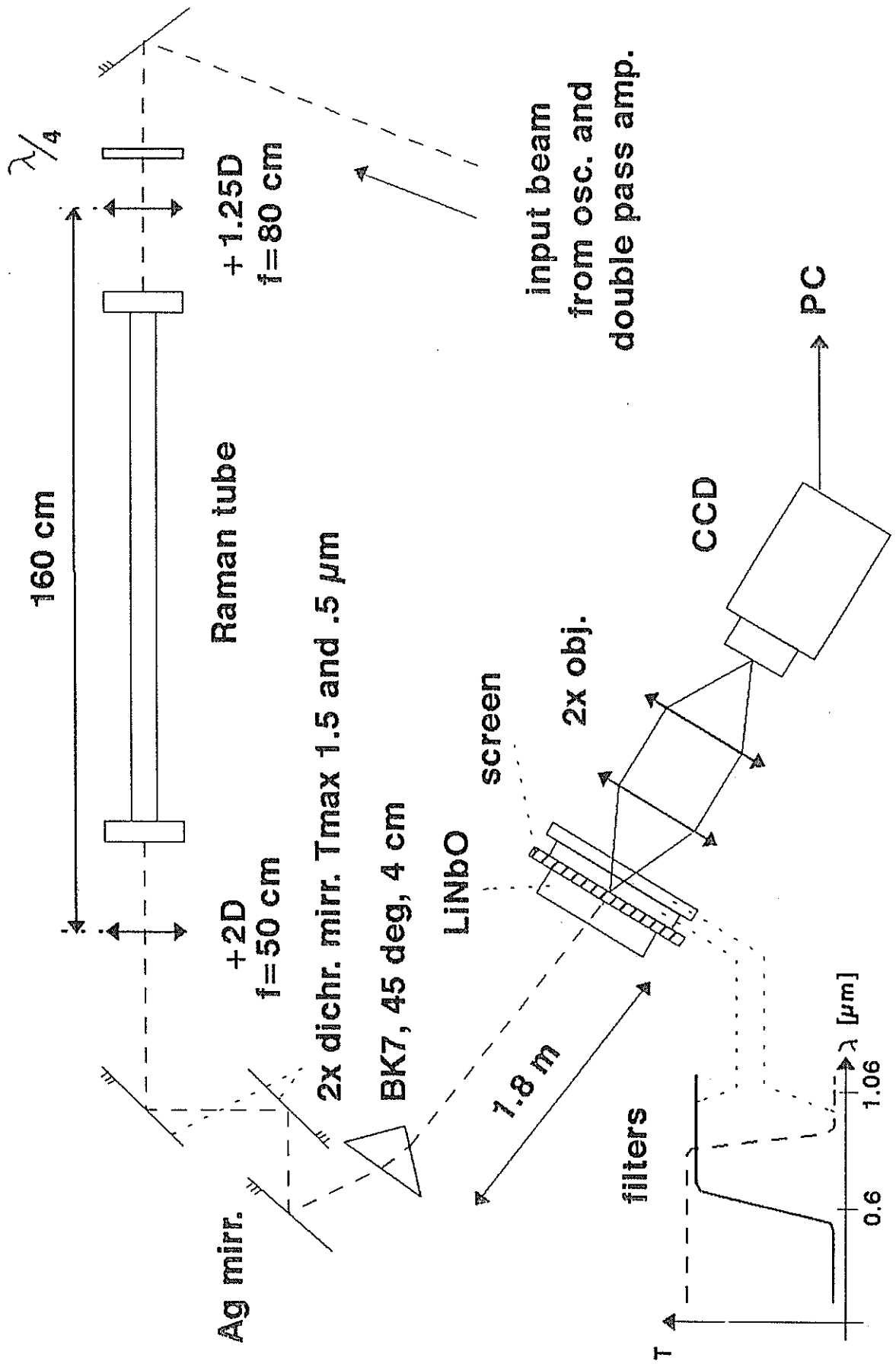
Eye Safe Raman Laser
Raman scattering in methane
Energy conversion
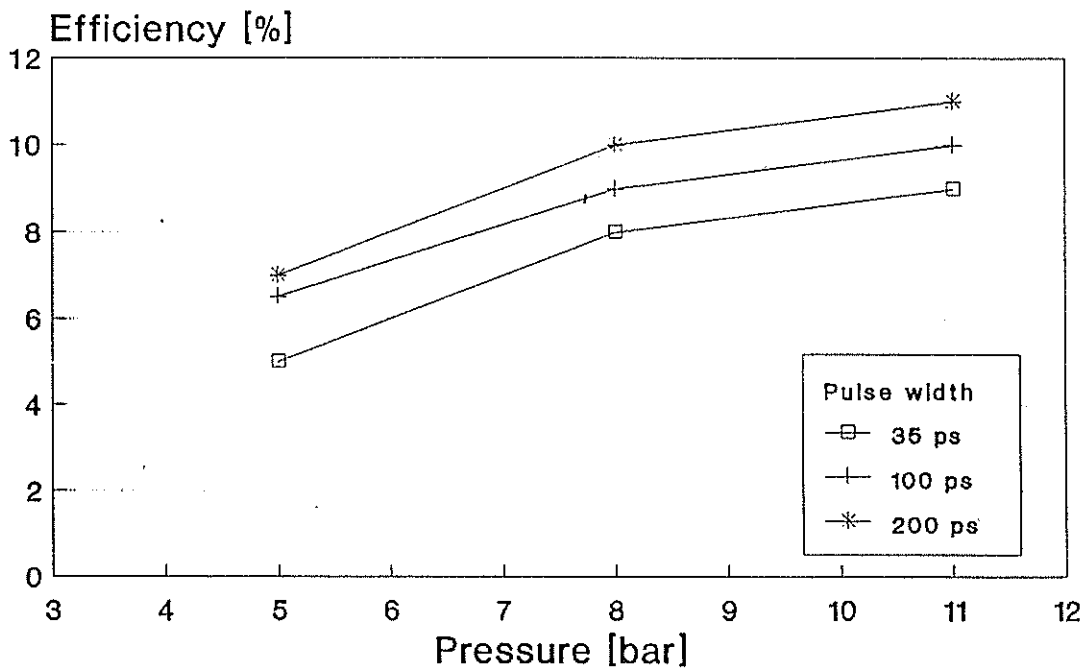
K.Hamal,J.Blazej,I.Prochazka, Shanghai '96

Eye Safe Raman Laser
Energy output stability

1.06 pumpe output
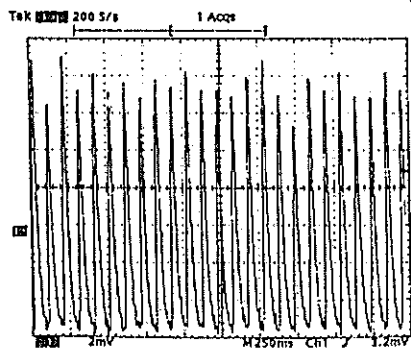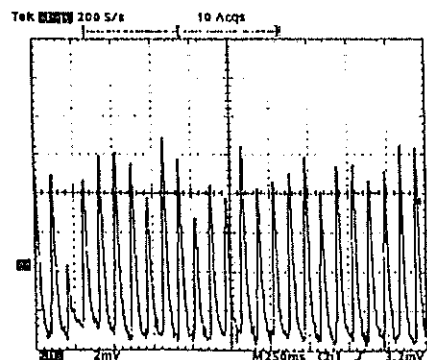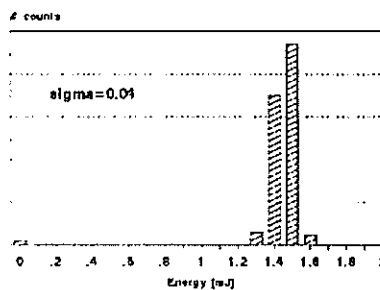
1.54 Raman tube output
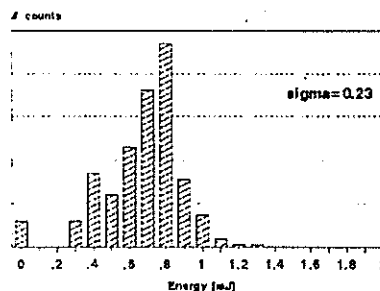
K.Hamal,J.Blažej,I.Procházka, Shanghai '96

Eye Safe Raman Laser
Spatial structure
methane 8 bar, 12 mJ, 35 psec

1.06 um

1.54 um
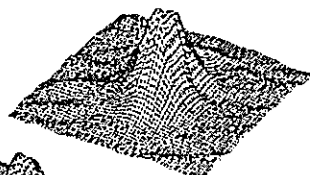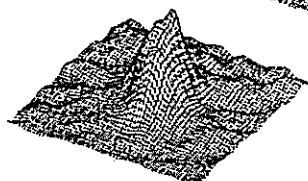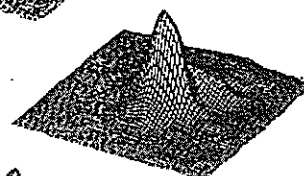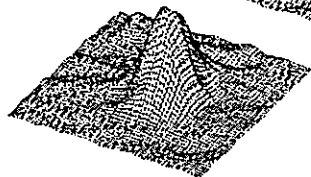
Eye Safe Raman Laser
Spatial fluctuation - superposition of 30 shots
methane 8 bar, 12 mJ, 35 psec

1.06   1.6 mrad

1.54   1.3 mrad

RAMAN LASER TEMPORAL PROFILE
Raman Stokes 1540 nm, 1.7 kV
Streak record

| 最大スケール= | 9950 | マーカ1 = | 244.944ps | -40cnt | 半値幅= | 72.9 |
| | 2000cnt/Div | マーカ2 = | 653.185ps | 781cnt | 面積 = | 2281 |

0.0ps 100.0ps 200.0ps 300.0ps 400.0ps 500.0ps 600.0ps 700.0ps 800.0ps 900.0ps
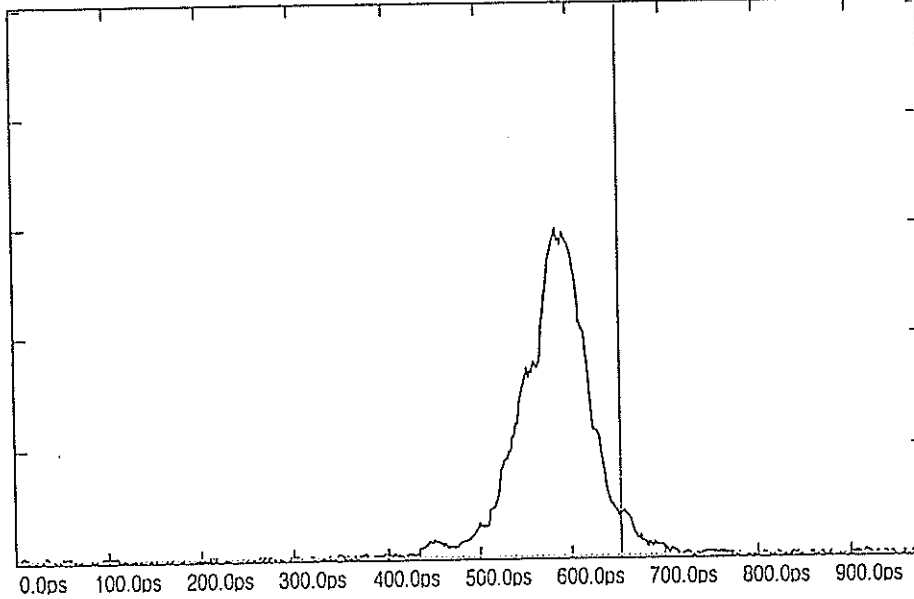
CRL Tokyo, January 20- February 11,'95

RAMAN LASER TEMPORAL PROFILE
Fundamantal 1064 nm, depleted, 1.4kVpump
Streak record

| 最大スケール= | 4950 | マーカ1 = | 244.944ps | 210cnt | 半値幅= | 40.9 |
| | 1000cnt/Div | マーカ2 = | 653.185ps | 35cnt | 面積 = | 1640 |
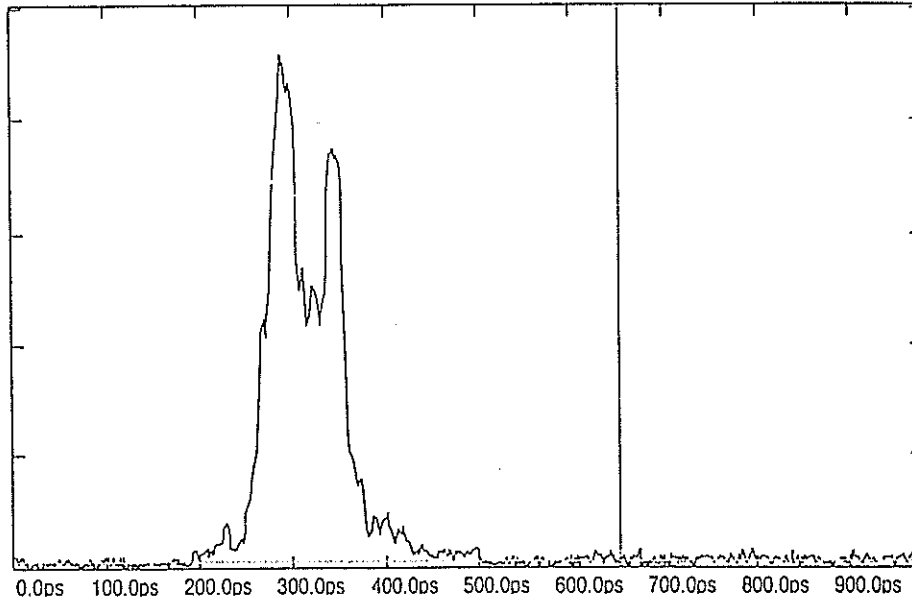
0.0ps 100.0ps 200.0ps 300.0ps 400.0ps 500.0ps 600.0ps 700.0ps 800.0ps 900.0ps

CRL Tokyo, January 20- February 11,'95

348

A Compact Modified SFUR Passively Mode-Locked Nd: YAG Laser for Satellite Ranging

Sun Zhan'ao, Yang Xiangchun, Zhu Xiaolei, Wu Zhaoqing

(Shanghai Institute of Optics and Fine Mechanics, Academia Sinica, China)

Yang Fumin, Chen Wanzhen, Xiao Chikun

(Shanghai Observatory, Academia Sinica, China)

Abstract

A compact frequency doubled Nd:YAG laser for satellite ranging is presented. In this system, a self-filtering unstable resonator (SFUR) in new modified configuration and linear colliding pulse mode-locked (CPM) scheme have been adopted. The typical parameters are:

Wavelength	532 nm
Single pulse energy	≥ 30 mJ
Pulse duration	20 – 50 ps
Repetition rate	1 – 5 pps
Laser dimensions (main body)	$132 \times 32 \times 25$ cm

Using this system, the Lageos satellite laser ranging have been performed successfully. Up to date, at Shanghai Observatory fixed station and Wuhan transportable laser ranging station the laser has been operating over one year.

I. Theory and optical scheme of the laser system

For our new modified SFUR, the recollimating mirror is replaced by a flat mirror which allows a shorter cavity for the same magnification. In this case, a slightly displaced position,.

$\Delta = L_1 - f_1$ with respect to the f_1 focal plane is needed. The aperture a is as follow:

$$a = [\, 0.61\,(\, 2 - L_1\, /\, f_1)\, L_1\,]^{\,1/2}$$

In this configuration, the output beam is divergent. The magnification of the cavity is

$$M = -\,(\, 2\, L_2 + \Delta\,)\, /\, f_1$$

M as a parameter, according to [1], has the following expressions:

$$\Delta = -\, f_1\, /\, M$$

$$L_1 = (1 - 1\, /\, M)\, f_1$$

[1] IEEE J. QE – 24 (8): (1988) 1543 – 1547

$$f_2 = d - M (1 - 1 / M^2) f_1$$

For our new modified SFUR, $d = 0$, then, f is the radius of curvature of the laser beam reaching the aperture. The concave mirror with a pinhole is taken as self-filtering component, also used for compensate the pure geometrical divergence. So, the redius of curvature of the concave mirror $R = 2 f$.

(1) Mirror $R_1 = 500$ mm   H.R. at 1.064 μm

(2) Concave mirror, $R \cong 3000$ mm, aperture $d \cong 1$ mm

(1) and (2) consist a self-filtering and collimating output coupler system.

II. Experimental and Observational Results

1. The pulse width of the output was measured by a Hamamatsu streak camera (Figure).

2. The new laser has been operational at Shanghai SLR station since October, 1995.

About 600 passes returns from many satellites, such as Lageos 1、2, Etalon 1、2, Glonass 63、67, have been obtained. The stability of the laser is quite good.

III. Future Plans

1. Cr^{4+}, Nd^{3+} YAG, self-Q switched supershort cavity,

pulse duration $t = 100$ ps

repetition rate   10 Hz

2. Diode pumping mode-locked laser (DPL)

pulse duration   20-30 ps

repetition rate   1 Kz
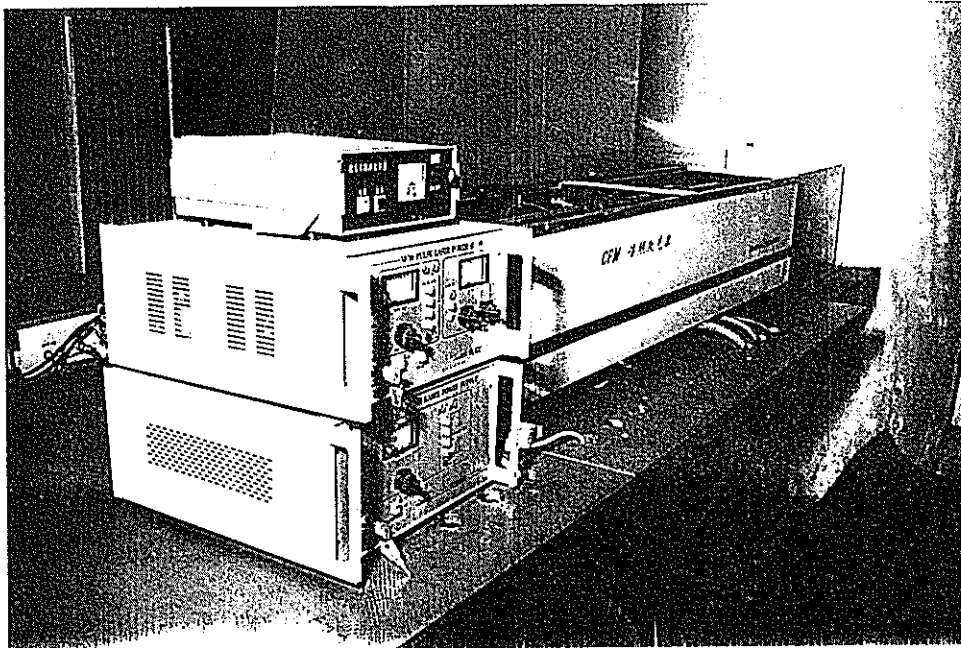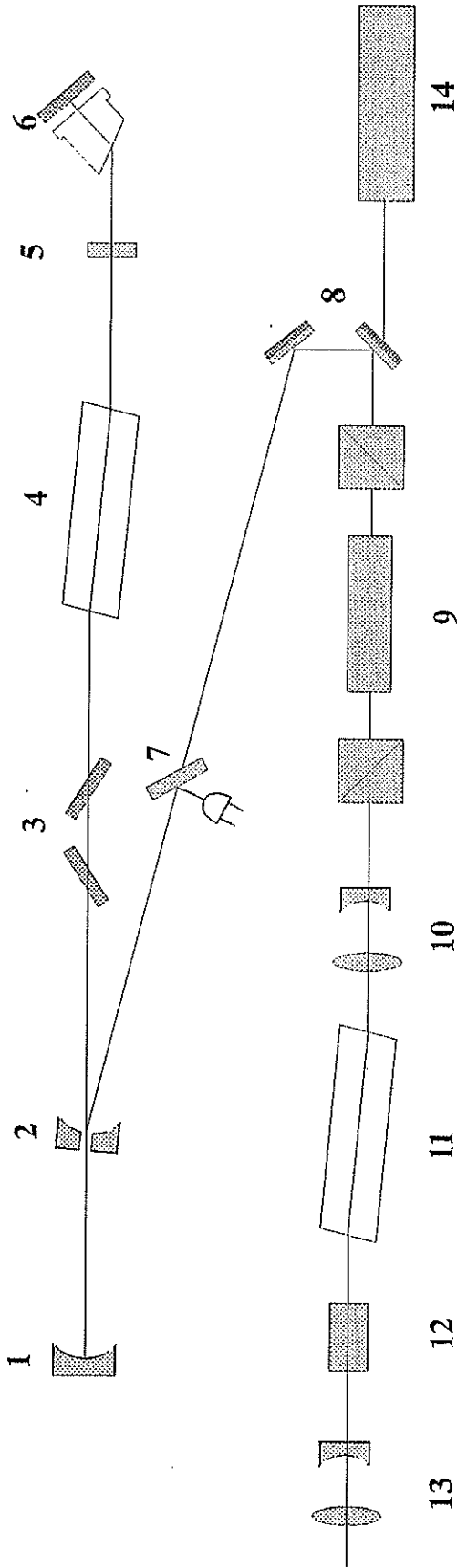
1. HR Concave Mirror (R= -500mm)
2. Pinhole and Coupling HR Concave Mirror
3. Polarizers
4. Oscillator Nd:YAG rod
   ϕ 6 × 90 mm
5. F-P
6. Dye Cell and HR Mirror
7. Sampling Plate

8. Bending Mirrors
9. LiNO3 Semi-train pulses selector
10. 1.5x Beam Expander
11. Amplifier Nd:YAG rod
    ϕ 9 × 125mm
12. KDP SHG
13. 1.5x Beam Expander
14. He-Ne Laser

Optical Layout of SFUR Nd:YAG Laser System at Shanghai

(Made by SIOM,   Installed in October1995,   The same laser for CTLRS)

kHz Lasers for Satellite Ranging

Yue Gao, Ben Greene, Yanjie Wang

Electro Optic Systems Pty Limited (EOS), Queanbeyan, NSW, Australia

Abstract

The design process for KSP laser with a maximum repetition rate of 1 kHz and final laser performance are presented.

1. INTRODUCTION:

Modern SLR has a wide range of performance requirements which impact the laser specification and design. eye safe, automated, and accurate tracking of multiple satellites requires a total systems design approach which can impose severe constraints on the lasers.

The requirement for low bias (hence SPAD detection) results in pressure for very short pulses (few pico-seconds) to provide precision and thus timely normal points. However, high satellites require high pulse energy, mitigating against ultra short pulses.

Satellite traffic density and data production efficiency considerations suggest high repetition rates. In addition, data yield optimisation shows that for any given average power, the repetition rate should be as high as SNR will allow. Finally, millimetre accurate satellites will have a rotation rate which requires kHz ranging rates to accurately resolve range to better than 0.5 mm.

2. SYSTEM DESIGN AND PERFORMANCE

2.1 SELECTION OF GAIN MEDIUM

Trade-off study between different gain media, Nd^{3+}: YAG, Nd^{3+}: YLF, Nd^{3+}: YVO, and Ti^{3+}: sapphire was conducted. The second harmonic generation (SHG) and third harmonic generation (THG) of Nd^{3+}: YAG at 532 and 355 nm are nearly as good as 423 nm and 846 nm generated by Ti^{3+}: sapphire laser for two colour satellite laser ranging. Other factors considered include the maximum energy that the gain medium can handle, the maximum available size, cost, how easily the output wavelength can be converted into the eye safe wavelength region. As a result, Nd:YAG is used as the gain medium, with an emission wavelength of 1.064 μm.

2.2 SYSTEM DESCRIPTION

The laser system consists of an aircraft detection and a satellite ranging sub-systems.

Satellite laser ranging raises significant safety issues since the laser energy used to track satellites presents a significant hazard. The hazard to personnel, in some modes, is significant at distances of kilometres. Thus there is a possibility of hitting an aircraft or helicopter and causing temporary reduction in vision and possibly permanent damage to the eyes. The possibility of eye damage can be eliminated by preceding every ranging pulse with the transmission of a laser pulse at the 'eye-safe' wavelength of 1.57 μm. This pre-ranging pulse leads the ranging pulse by 300 micro-second and presents no hazard at the exit aperture of the ranging telescope. If a reflection of any of the energy of the pre-ranging pulse is detected, the interlock system blocks firing of the following satellite ranging pulse.

The aircraft detection laser comprises a nano-second Nd:YAG laser and an Optical Parametric Oscillator (OPO) which is able to convert non-eye safe pulses at 1.064 μm into nano-second pulses at 1.57 μm which is eye safe according to Laser Safety Standard ANSI Z136.1 (1993).

The satellite ranging sub-system comprises a diode pumped mode-locked laser oscillator, a diode pumped regenerative amplifier, two power amplifiers, a second harmonic generator (SHG) and a third harmonic generator (THG), if applicable, and generates pico-second pulses.

The laser table layout is shown in Figure 1.
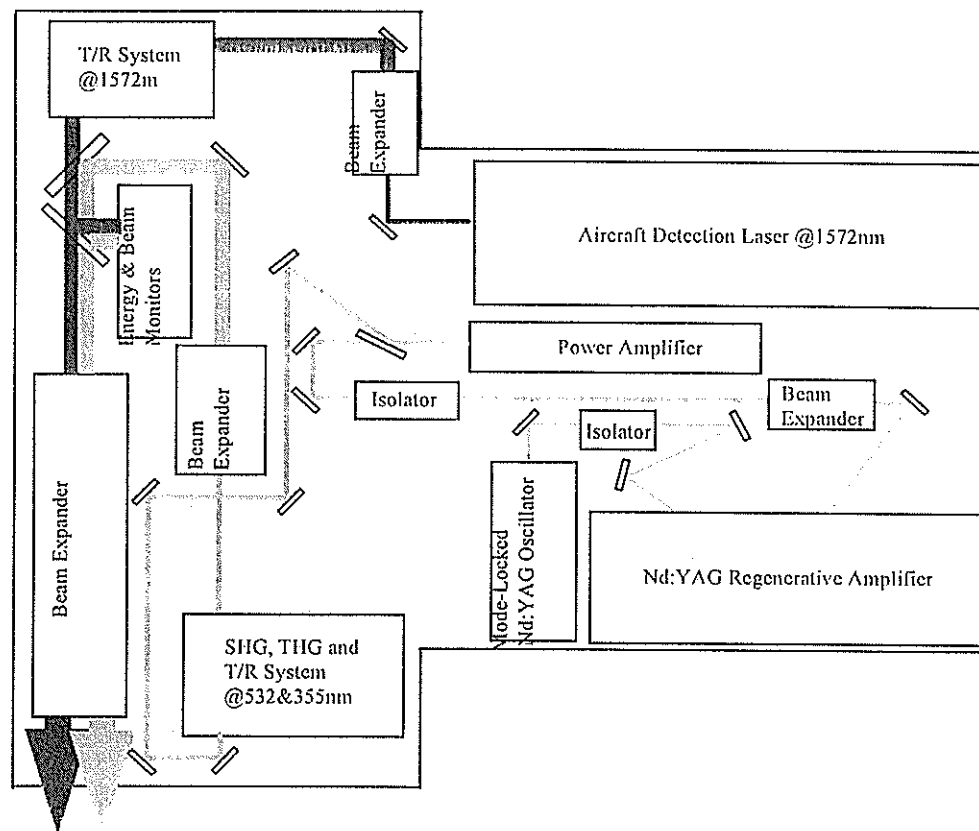
Figure 1. Laser Table Layout

The second harmonic at 532 nm of the Nd:YAG is used as the main wavelength for satellite laser ranging in eye safe and non-eye safe modes. The satellite ranging sub-system allows multi-wavelength output utilising second harmonic at 532 nm and third harmonic at 355 nm.

The laser system is automatically controlled. Changing the repetition rate and energy level, and monitoring of the laser beam quality and energy at 1.57 μm, 532 nm are automated. The temperature of the key laser elements are continuously monitored.

A security system is able to activate a shutdown or recovery of the laser system. Interlocks are provided at the access to the laser area and in the laser system. In case un-authorised personnel enter the laser area the laser system will be shutdown and stay in stand-by mode until security status is clarified.

2.3 SATELLITE RANGING SUB-SYSTEM OPERATING MODES

The sub-system has two operation modes for satellite ranging:

- Reduced transmitted power mode which could be essentially eye safe according to ANSI Z136.1 (1993).

- Full power mode which might not be eye safe

353

The sub-system is capable of being switched from eye safe to non-eye safe full power mode to maintain data acquisition if weather conditions deteriorate.

2.3.1 Reduced Transmitted Power Mode

In this mode only the oscillator and regenerative amplifier operate and the beam will pass through the power amplifiers while the power amplifiers remain idle. The satellite ranging sub-system is able to produce pulse energy in the range of 50 to 500 μJ at 532 nm and at repetition rates up to 1000 Hz. The energy output will be set so that when converted through a second harmonic generator, the output is in the eye safe range. The design of the regenerative amplifier was one of the challenges at the beginning of the design process in terms of whether a single output pulse and the desired output energy can be achieved at all the specified repetition rates, whilst maintaining good beam quality.

Figure 2 shows the beam profile of the regenerative amplifier output before the beam passes through the power amplifier. Beam profiles with a good Gaussian fit were obtained at 10, 20, 50, 100 and 1000 Hz.
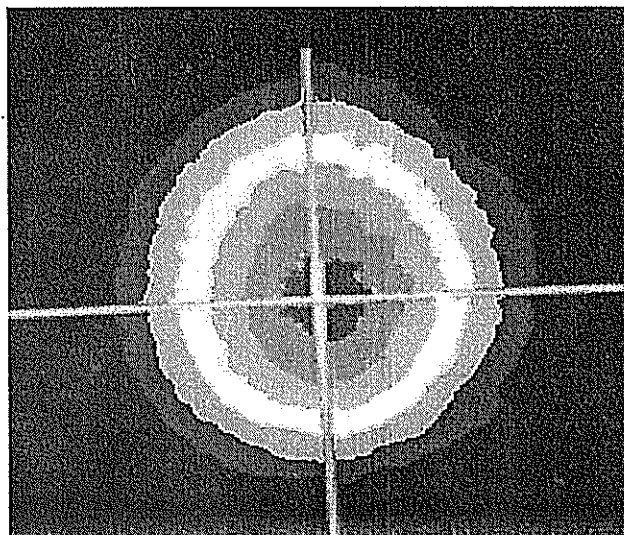
Figure 2. Beam profile of regenerative amplifier output at 10Hz

As shown in Figure 3 the output pulses measured at 10, 100, 500, and 1000 Hz are clean single pulses.
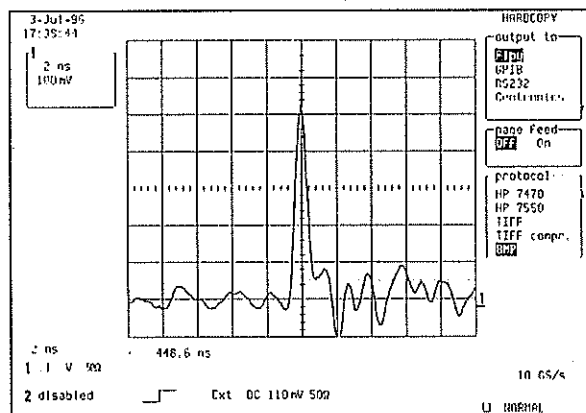
Rep rate: 10 Hz
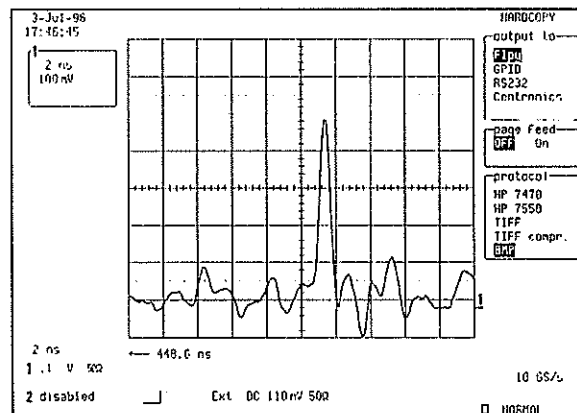
Rep rate: 500 Hz
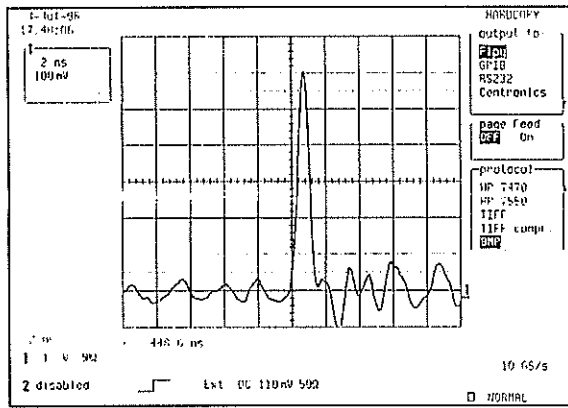
Rep rate: 100 Hz
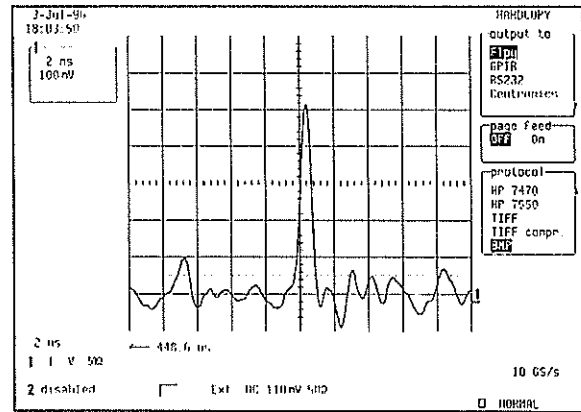
Rep rate: 1000 Hz

Figure 3 Regenerative Amplifier Output Pulses at 10, 100, 500 and 1000 Hz

The pulse width of the regenerative amplifier output was measured using an autocorrelator and is basically the same as the pulse width of the mode-locked oscillator.

It should be mentioned that air turbulence plays an important role in the performance of the regenerative amplifier at a repetition rate higher than 50 Hz. Both the beam quality and energy stability deteriorate when the ambient air turbulence increases. This effect is also very significant to the power amplifier output.

Table 1 shows the design specification and results achieved in the reduced transmitted power mode.

	Design Specification	Results Achieved
Pulse Energy (μJ)	50-500	60-150
Pulse Width (ps)	< 30	< 30
Pulse Repetition Rate (Hz)	10, 20, 50, 100 and 1000	10, 20, 50, 100, and 1000
Mode Structure	> 60% Gaussian fit	> 60% Gaussian fit

Table 1. The design specification and results achieved in the reduced transmitted power mode

The beam profile measured after the beam passes through the power amplifier while it remains idle is shown in Figure 4. Very even energy distribution is obtained.
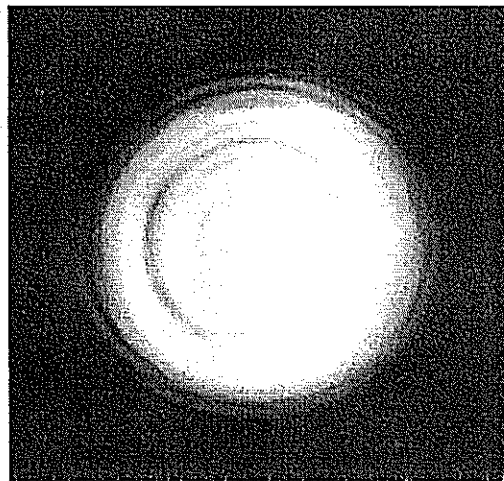
Figure 4. Beam profile after the power amplifiers

355

2.3.2 Full Power Mode

In this mode the oscillator, regenerative amplifier and power amplifiers operate and the satellite ranging sub-system will produce maximum pulse energy up to 50 mJ at 532 nm after the Second Harmonic Generator (SHG).

The maximum pulse energy at 532 nm is 25 mJ after the Third Harmonic Generator (THG), if applicable. The energy output at 355 nm will be greater than 7 mJ. In this mode the output energies at 532 nm and 355 nm are controlled from the computer. The repetition rate is variable from 10 to 100 Hz in 4 discrete steps at 10, 20, 50 and 100 Hz. The design specification and results achieved are in Table 2.

	Design Specification	Results Achieved
Maximum Pulse Energy (mJ)	≥ 50 @ 532 nm after SHG	≥ 57 @ 532 nm after SHG
	≥ 25 @ 532 nm after THG	≥ 37 @ 532 nm after THG
	≥ 7 @ 355 nm after THG	≥ 10.7 @ 355 nm after THG
Pulse Width (ps)	< 30	< 30
Pulse repetition rate (Hz)	10, 20, 50, 100	10, 20, 50, 100

Table 2. Design specification and results achieved in full power mode

The design of the power amplifier was the second challenge in the design process in terms of whether a good beam quality can be achieved at all the specified repetition rates, since the thermal lensing effect is very significant in this case. As shown in Figure 5, the beam profiles of power amplifiers output measured at 10, 20, 50, and 100 Hz are consistent.

Beam profile of power amplifier output at **10Hz, 70 mJ**

Beam profile of power amplifier output at **20Hz, 70 mJ**

Beam profile of power amplifier output at **50Hz, 70 mJ**

Beam profile of power amplifier output at **100Hz, 30 mJ**
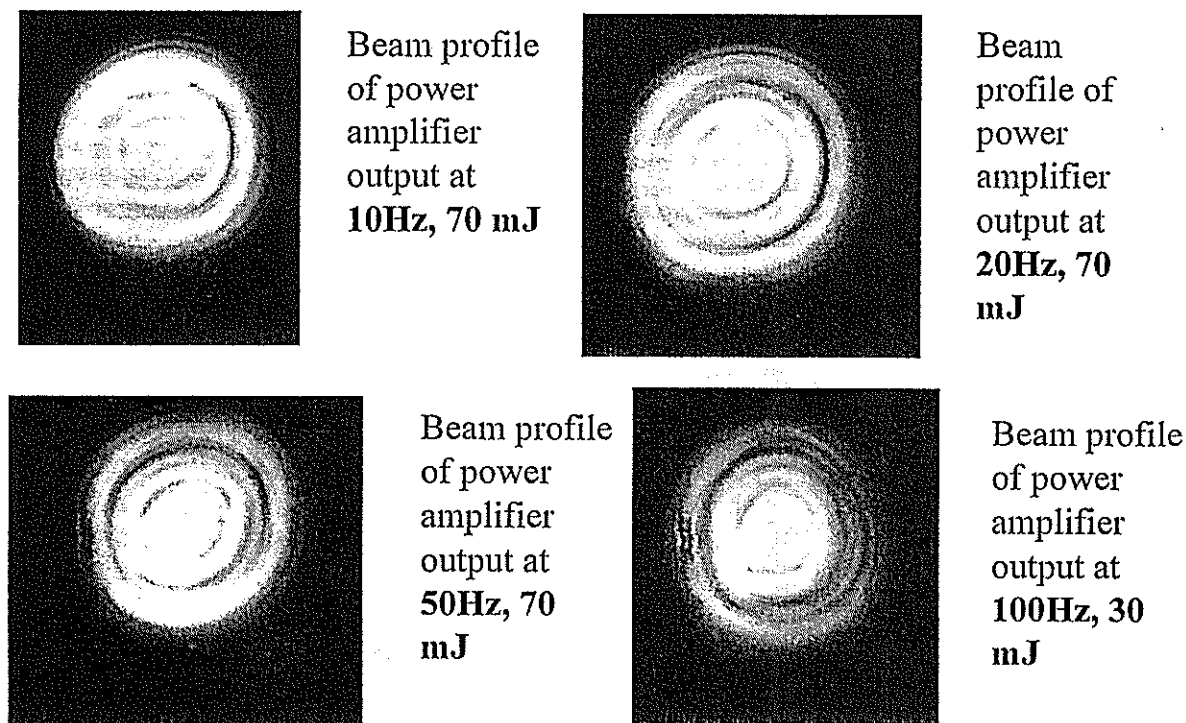
Figure 5. The beam profiles achieved at different repetition rates in full power mode

2.4 AIRCRAFT DETECTION LASER

A repetition rate variable nano-second Nd:YAG laser and an efficient OPO are the two key components of the aircraft detection laser system. Consistent beam quality over a wide range of pulse repetition rates is necessary because the satellite ranging laser is designed to operate at repetition rates between 10 Hz and 1 kHz. Sufficient conversion of pulse energy at a wavelength of 1.06 μm to 1.57 μm by the OPO can ensure that all the necessary altitude at which the aircraft may fly can be covered.

As shown in Table 3, all the design specifications have been achieved.

	Design Specification	Results Achieved
Maximum Pulse Energy at 1.57 μm (mJ)	30	31
Energy Stability (shot to shot)	5%	1.1%
Pulse Width (ns)	2.7 ± 0.2	2.7 ± 0.2
Pulse Repetition rate (Hz)	10, 20, 50, 100	10, 20, 50, 100
Mode Structure	Top hat	Top hat

Table 3. Aircraft detection laser design specification and results achieved

Figure 6 shows the beam profile of OPO output at 1.57 μm. Ideal 'top hat' beam profile is achieved.
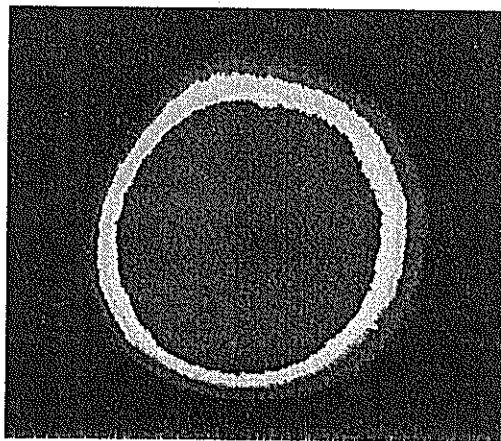
Figure 6. Beam profile of optical parametric oscillator (OPO) output at 10Hz

The pulse width of the OPO signal pulse is basically the same as that of the pump pulse, as shown in Figure 7. A sharp leading edge is obtained with the OPO signal pulse which is very good for ranging.

In conclusion, all the major design specifications have been achieved for kHz satellite ranging.

Figure 7. OPO pump and signal pulses
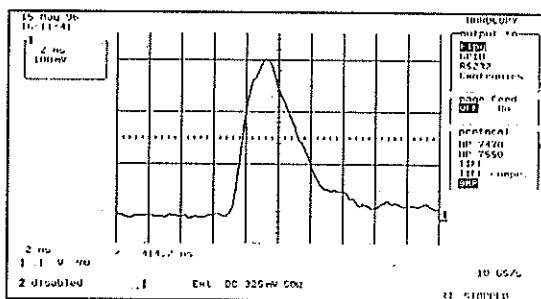
The OPO pump pulse
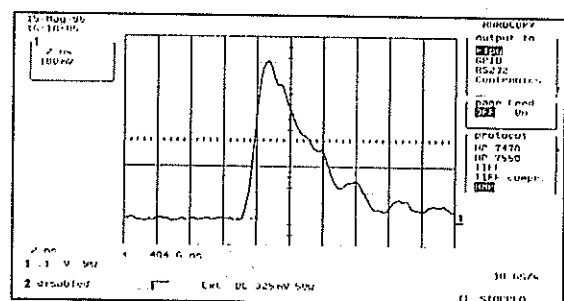
The OPO signal pulse

Eyesafe Systems

AlliedSignal
AEROSPACE

Integration of the SLR Radar into the Geophysical Laboratory

H. Donovan, T. Varghese, R. Allshouse,
D. Patterson, R. Suvall, J. Miller

NASA SLR Program
AlliedSignal Aerospace
AlliedSignal Technical Services Corporation
Lanham, Maryland, 20706, USA

J. Degnan

NASA Goddard Space Flight Center
Geosciences Technology Offices

AlliedSignal
AEROSPACE
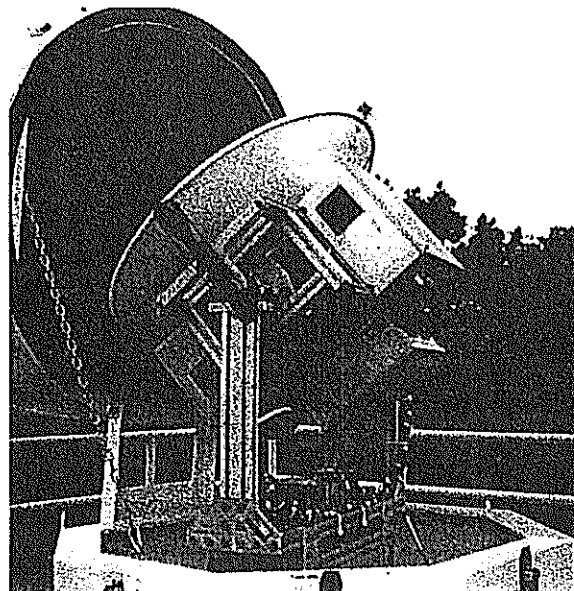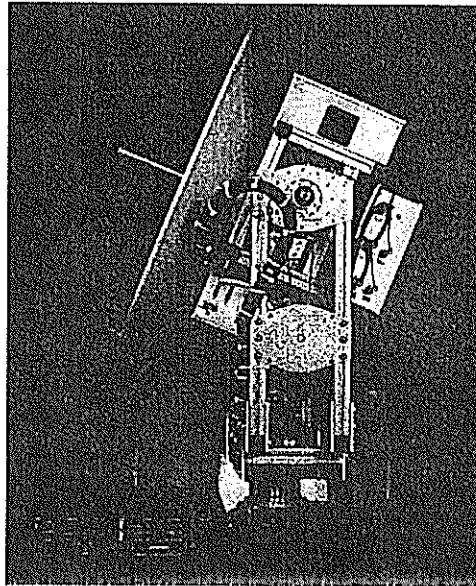
SLR Radar

SLR Radar

The SLR Radar System

The SLR Radar System provides a means of detecting aircraft before they intersect a transmitted laser beam. Once an aircraft is detected, a control signal is issued which can be used to disable the transmitted laser beam. The aircraft detection capabilities of the SLR Radar are from a quarter of a mile to more than twenty-five miles which covers the ocular hazard distances typically found in current laser ranging systems.

Key Points
- Field proven system
- Very low maintenance
- Adaptable to a variety of interface schemes
- Decreased station operational staffing requirements

SLR Radar Features

High Reliability

- The radar transmitter and receiver are commercial units which have been modified for automated operational functions to obtain optimum receiver tuning and gain.

- The radar is mounted on an ruggedized pedestal constructed of light weight T-slotted extruded aluminum. Pedestal drive is simplified through the use of DC torquer motors with integral tachometers coupled to harmonic drives.

Low Maintenance

- Use of highly reliable components and placing the radar inside an environmentally controlled radome greatly reduces the need for maintenance. Also, mean-time-to-repair is low as the result of inbuilt software diagnostic programs which can detect faults down to the field replaceable board level. Finally, these programs can be accessed remotely via modem for direct factory support or for system monitoring.

AlliedSignal
AEROSPACE

SLR Radar Features

Universal Interface

- The microprocessor based Data Translator Board allows the Radar Local Controller to accept a variety of position signals which can be converted for slaving the radar to the host telescope. The DTB can accept parallel or serial protocol and perform coordinate conversions and/or error corrections. The DTB is:

  -TTL compatible
  -Able to support 33 bits of parallel data per axis
  -Supports RS-232 protocol, asynchronous or synchronous
  -Coordinate conversions from BCD or other based systems
  -Minimum of one tenth of one degree position accuracy required from host

SLR Radar Specifications

Power Requirements	
•Voltage, Frequency	100/220VAC,50 - 60 Hz
•Phase	Single Phase
•Power	Consumption 100W
Signal Interfacing	
•Interunit	FSK, RS-232C
•Input from Host	RS-232C, Binary, BCD
RF Characteristics	
•Center Frequency	9410 MHz =/-30 MHz
•Peak Power Output	4kW (2.1 watts CW)
•PRF	750 Hz
•Pulse Width	700nsec
IF Amplifier	
•Center Frequency	60 MHz
•Bandwidth	3 MHz at -3 dB
•Overall Noise Figure	<6dB
Antenna	
•Diameter	33 inches
•Gain @ 9.4GHZ	36.5 dB
•Beam Width @ 3 dB	2.8 degrees
•First Side Lobe	-23 dB @ 12 degrees
•Second Side Lobe	-30 dB @ 20 degrees
Pedestal	
•Azimuth Rotation	Unlimited
•Elevation Rotation	0 to 180 degrees
•Position Resolution	0.09 degrees (both axis)

The Effects of SLR Radar Emissions Upon Radio Astronomy Observatories

Quantitative analysis has shown:

- SLR Radar isotropic radiation emissions are well below the ITU VLBA guidelines for near and far distances

- SLR Radar isotropic directional emissions lie outside the allocated band for VLBA radio astronomy

Radio Astronomy Allocations
Within VLBA Bands

VLBA Band	Radio Astronomy Allocated Band	Allocation Status	Sharing Services R.A. Lines, etc.
312 - 342 MHz	322 - 328.6 MHz	P	Fixed, Mobile Deuterium line
596 - 626 MHz	608 - 614 MHz	P S	Region 2 Regions 1, 3 except African Broad-casting Area (Alloc. band was U.S. TV Ch. 37)
1350 - 1750 MHz	1400 - 1427 MHz	P (Pas)	Hydrogen line
	1610.6 - 1613.8 MHz	P	Mobile Sat. Serv. Radio-determination Sat. Serv., OH line
	1660 - 1670 MHz	P	Fixed, Mobile, Mol. Sat., OH line
	1718.8 - 1722.2 MHz	S	Fixed, Mobile, OH line
2150 - 2350 MHz	None		2290 - 2300 MHz Space Res., Deep Sp., Sp.-to-Earth
4600 - 5100 MHz	4800 - 4990 MHz	S	Fixed, Mobile, OO line
	4990 - 5000 MHz	P	Fixed, Mobile
8000 - 8800	None		8400 - 8500 MHz, Space Res., Sp.-to-Earth
10.2 - 11.2 GHz	10.6 - 10.68 GHz	P	Fixed, Mobile
	10.68 - 10.7 GHz	P (Pas)	
12.0 - 15.4 GHz	14.47 - 14.5 GHz	S	Fixed, Fixed Sat., Mobile H₂CO line
	15.35 - 15.4 GHz	P (Pas)	
21.7 - 24.1 GHz	22.21 - 22.5 GHz	P	Fixed, Mobile, B line
	23.6 - 24.0 GHz	P (Pas)	NH lines
41.0 - 45.0 GHz	42.5 - 43.5 GHz	P	Fixed, Fixed Sat., Mobile SIO lines

"P" Primary Allocation; "S" Secondary Allocation; "Pas" Passive Band

ITU Guidelines vs SLR Radar
Spurious Emission
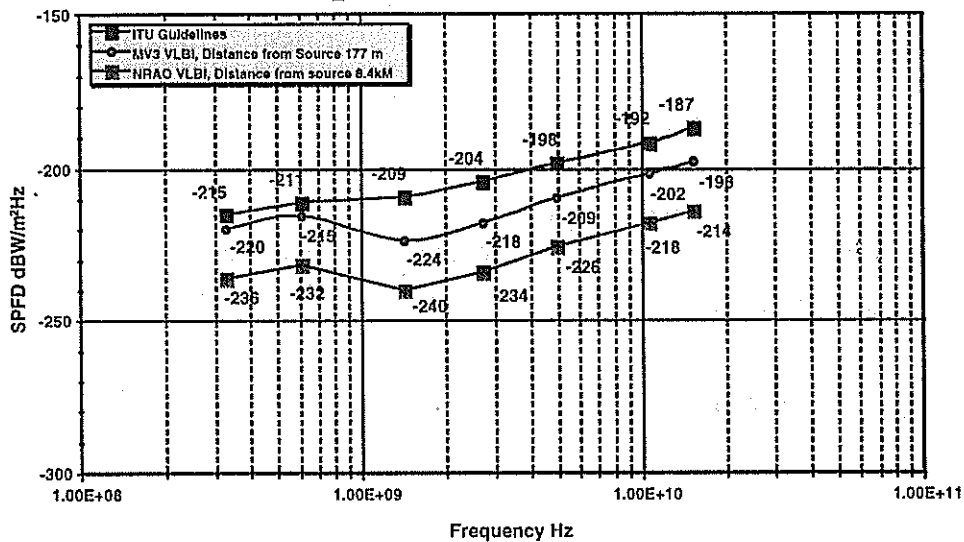
SLR Radar Isotropic Spectral Emissions
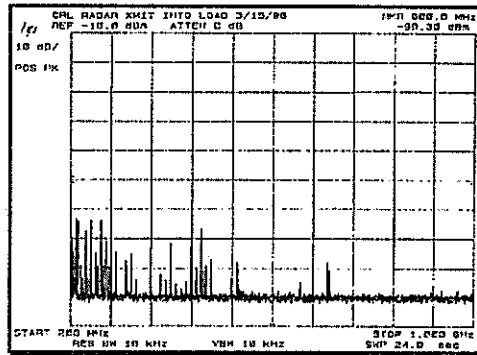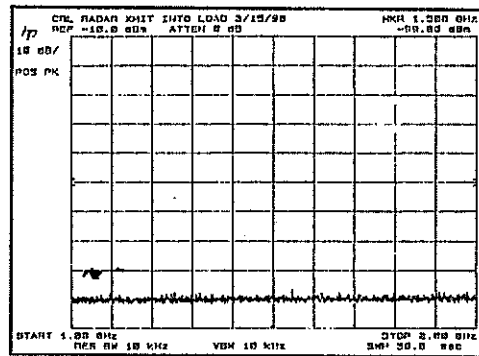
1GHz to 2GHz

200MHz to 1GHz

SLR Radar Isotropic Spectral Emissions

4GHz to 6GHz

2GHz to 4GHz

![NASA logo] **AlliedSignal** AEROSPACE
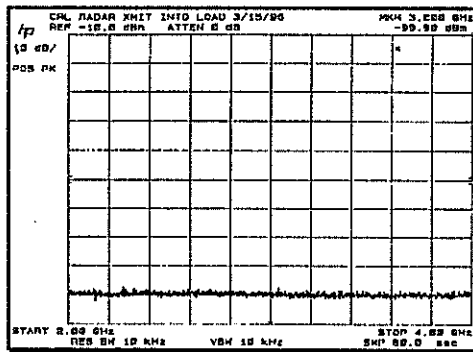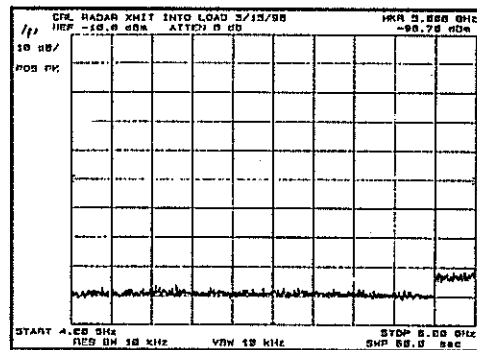
SLR Radar Isotropic Spectral Emissions
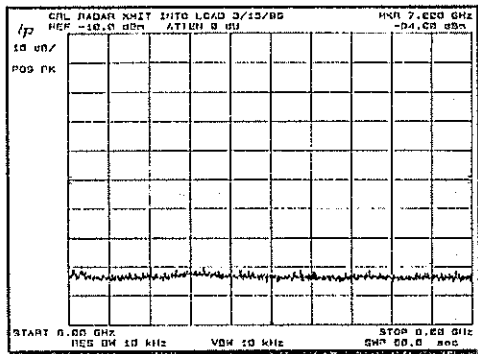
6GHz to 8GHz

8GHz to 10GHz
⇩

![NASA logo] **AlliedSignal** AEROSPACE
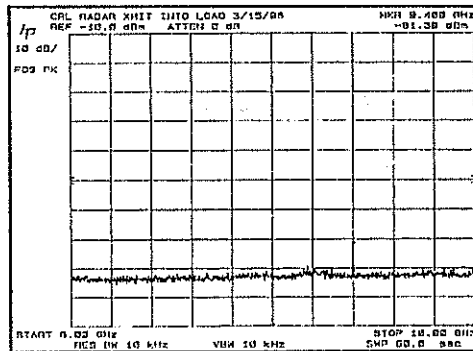
SLR Radar Isotropic Spectral Emissions
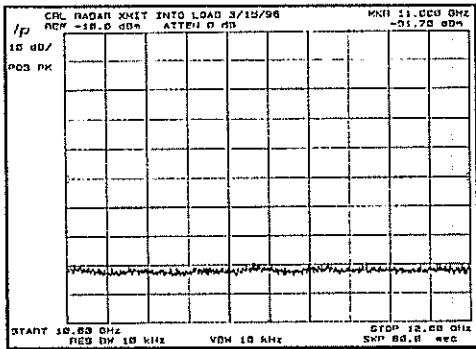
10GHz to 12GHz

12GHz to 14GHz
⇩
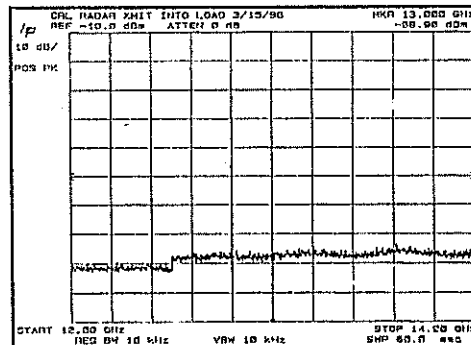
SLR2000: AN INEXPENSIVE, FULLY AUTOMATED, EYESAFE SATELLITE LASER RANGING SYSTEM

John Degnan, Jan McGarry, Thomas Zagwodzki
NASA Goddard Space Flight Center

Paul Titterton, Harold Sweeney
EOO, Inc.

Howard Donovan, Michael Perry, Brion Conklin, Winfield Decker
AlliedSignal Technical Services Corporation (ATSC)

Jack Cheek, Anthony Mallama, Peter Dunn
Hughes STX

Randall Ricklefs
University of Texas

ABSTRACT

SLR2000 is an autonomous, unmanned satellite laser ranging station with an expected single shot range precision of about one centimeter and a normal point precision better than 3 mm. The system will provide continuous 24 hour tracking coverage and reduce capitalization, operating and maintenance costs by an order of magnitude relative to current outlays. Computer simulations have predicted a daylight tracking capability to GPS and lower satellites with telescope apertures under 50 cm and have demonstrated the ability of our current autotracking algorithm to extract mean signal strengths as small as 0.0001 photoelectrons per pulse from noise.

The dominant cost driver in present SLR systems is the onsite and central infrastructure manpower required to operate the system, to service and maintain the complex subsystems (most notably the laser), and to ensure that the transmitted laser beam is not a hazard to onsite personnel or overflying aircraft. In designing the SLR2000 system, preference was given to simple hardware over complex, to commercially available hardware over custom, and to passive techniques over active resulting in the prototype design described here. This general approach should allow long intervals between maintenance visits and the "outsourcing" of key central engineering functions on an "as needed" basis. In unassembled "kit" form, the per system hardware costs for SLR2000 are expected to be less than $300K. A fully assembled and tested field system should be reproducible for about $500K per system in quantities of eight or more.

SLR2000 consists of seven major subsystems: (1) Time and Frequency Reference Unit; (2) Optical Head; (3) Tracking Mount;(4) Correlation Range Receiver; (5) Meteorological Station; (6) Environmental Shelter with Azimuth Tracking Dome; and (7) System Controller. The Optical Head in turn consists of a 40 cm aperture telescope and associated transmit/receive optics, a Q-switched microlaser operating at 2KHz, a start detector, a quadrant stop detector, a CCD camera for automated star calibrations, and spectral and spatial filters. The current design status of each of these subsystems is addressed in the present paper.

1. INTRODUCTION

The feasibility of a fully autonomous, satellite laser ranging system operating at visible wavelengths with eyesafe energies (on the order of 100 μJ for a 30 to 40 cm telescope aperture) and high repetition rates (on the order of 2 KHZ) was first postulated by Degnan[1], and some early concepts and analyses were described at the last SLR Workshop in Canberra [2,3]. The present paper gives a progress report on the engineering design of the overall SLR2000 system, while four companion papers in these proceedings describe in more detail the microlaser transmitter[4], the correlation range receiver algorithms and analysis [5], the results of recent system simulations [6], and the feasibility of SLR2000 ranging over interplanetary distances to an asynchronous laser transponder incorporating many of the SLR2000 subsystems [7]. The simulations, which are based on realistic models of the hardware and atmospheric channel, suggest that ranging to GPS in daylight is feasible with a telescope aperture as small as 40 cm[5,6].

When designing an autonomous and inexpensive system such as SLR2000, it is necessary to make certain assumptions regarding the environment into which it will be placed. Specifying an environment which is unrealistically isolated and forbidding will only drive up the fabrication and operational costs. The typical SLR2000 site is anticipated to have: (1) generally good weather and visibility; (2) good site stability with access to bedrock; and (3) easy access to basic services such as stable commercial power, communications (telephone, Internet), transportation (airports), "industrial level" security (i.e. limited personnel access), and janitorial/custodial services.

To keep construction and maintenance costs at a minimum, we have also adopted the following design philosophies:

> (1) Use off the shelf commercial components wherever possible; this allows rapid component replacement and "outsourcing" of engineering support;

> (2) Use TLRS-size telescopes; this constrains the cost of the optical tracking mount and telescope;

> (3) For low maintenance and failsafe reliability, use passive techniques and components rather than active ones (e.g. eyesafe beams vs active radars, passive T/R switches, passively Q-switched lasers and passive multipass amplifiers).

Adherence to these fundamental assumptions and design philosophies have led to the SLR2000 design described here.

2. MAJOR SUBSYSTEMS

SLR2000 is composed of the following seven major subsystems:

> Time and Frequency Reference Unit
> Optical Head
> Tracking Mount
> Correlation Range Receiver
> Meteorological Station
> Environmental Shelter with Azimuth Tracking Dome
> System Controller

In the following subsections, the status of each subsystem will be described.

2.1 Time and Frequency Reference Unit

The Hewlett Packard Model HP58503A GPS Time and Frequency Reference Receiver has been selected to serve as the station clock and frequency reference. The unit consists of a GPS-disciplined Quartz crystal oscillator and provides clock outputs at both 1 Hz and 10 MHz.

The one pps output has a pulse-to-pulse jitter of less than 750 psec with only one GPS satellite in view. Its time accuracy, when locked to GPS, is specified at less than 110 nsec with respect to UTC (i.e. the master clock at the US Naval Observatory in Washington, DC). In the prolonged absence of a GPS signal (unlocked), the accumulated time error is less than 8.6 μsec in 24 hours. The 10 MHz output has a Root Allen Variance, when locked to GPS, of 1.5×10^{-11} for a 100 msec sample time typical of artificial satellite laser ranging. Thus, ranging errors introduced by variations in the clock frequency will be submillimeter for all satellites up to and including the highest satellites, GPS, GLONASS, and ETALON.

2.2 Optical Head

The optical head consists of the telescope, a passive transmit/receive switch , a Q-switched microlaser operating at 2KHz, a start diode, a quadrant stop detector with bias supply and gating circuit, a CCD camera for automated star calibrations, and spectral and spatial filters. The outgoing single pulse energy is maximized, within eye hazard constraints, by filling the available telescope aperture with the transmit beam and by using a passive wavelength-dependent transmit/receive switch to separate the transmitted and received beams.

A block diagram of the preliminary optical head design is shown in Figure 1. A 2KHz pulse train from the Nd:YAG microlaser transmitter (21), described in a companion paper in these proceedings [4], is transmitted through a dichroic mirror (16) which passes infrared radiation at 1064 nm and reflects the frequency doubled green radiation at 532 nm. The low energy pulse train is focused by a lens (14) into a doubling crystal (15) and the resulting green radiation at 532 nm is magnified and recollimated by a second lens. After passing through a second dichroic beamsplitter (10), which is coated to pass the majority of the 532 nm radiation, a final diverging lens (8) matches the outgoing green beam to the focal length of the telescope primary for further magnification and collimation of the outgoing transmitter beam. The position of the diverging lens (8) is adjustable under computer control and can be used to correct for thermally induced variations in system focus. The outgoing reflections of the transmit beam off the two beamsplitters are used to monitor the infrared (23) and green (25) energies from the laser and doubling crystal respectively. Filter (24) blocks 1064 nm light from entering the green detector. The green radiation reflected from the satellite retraces the same optical path until it is reflected by the dichroic beamsplitter (16) into the quadrant detector (20) after first passing through a narrowband spectral filter (17), an imaging lens (18), and a variable spatial filter (19). Thus, the combination of dichroic mirror (16) and doubling crystal (15) provides a passive, wavelength-dependent transmit/receive switch [8] which is independent of polarization and allows the entire telescope primary (2) to be used simultaneously by both the transmitter and receiver.

During star calibrations, collimated starlight reflects off dichroic beamsplitter (10), passes through a broadband filter (11) centered on the 532 nm laser wavelength, and is focused by a lens (12) onto a 324 x 242 pixel Electrim Model EDC-1000M CCD array (13) which in turn measures the position of the star and provides pointing error information to the system computer for periodic mount modelling and pointing verification. It is also used to periodically check and

verify accurate system focus by minimizing the star spot diameter. The star calibration optical train provides a field of view of approximately two arcminutes.

The quadrant stop detector lies behind the focal plane so that the incoming reflected laser energy and background noise is spread over the four quadrants, allowing estimation of the position of the satellite in the receiver field of view by the correlation range receiver as described in Subsection 2.4.3.
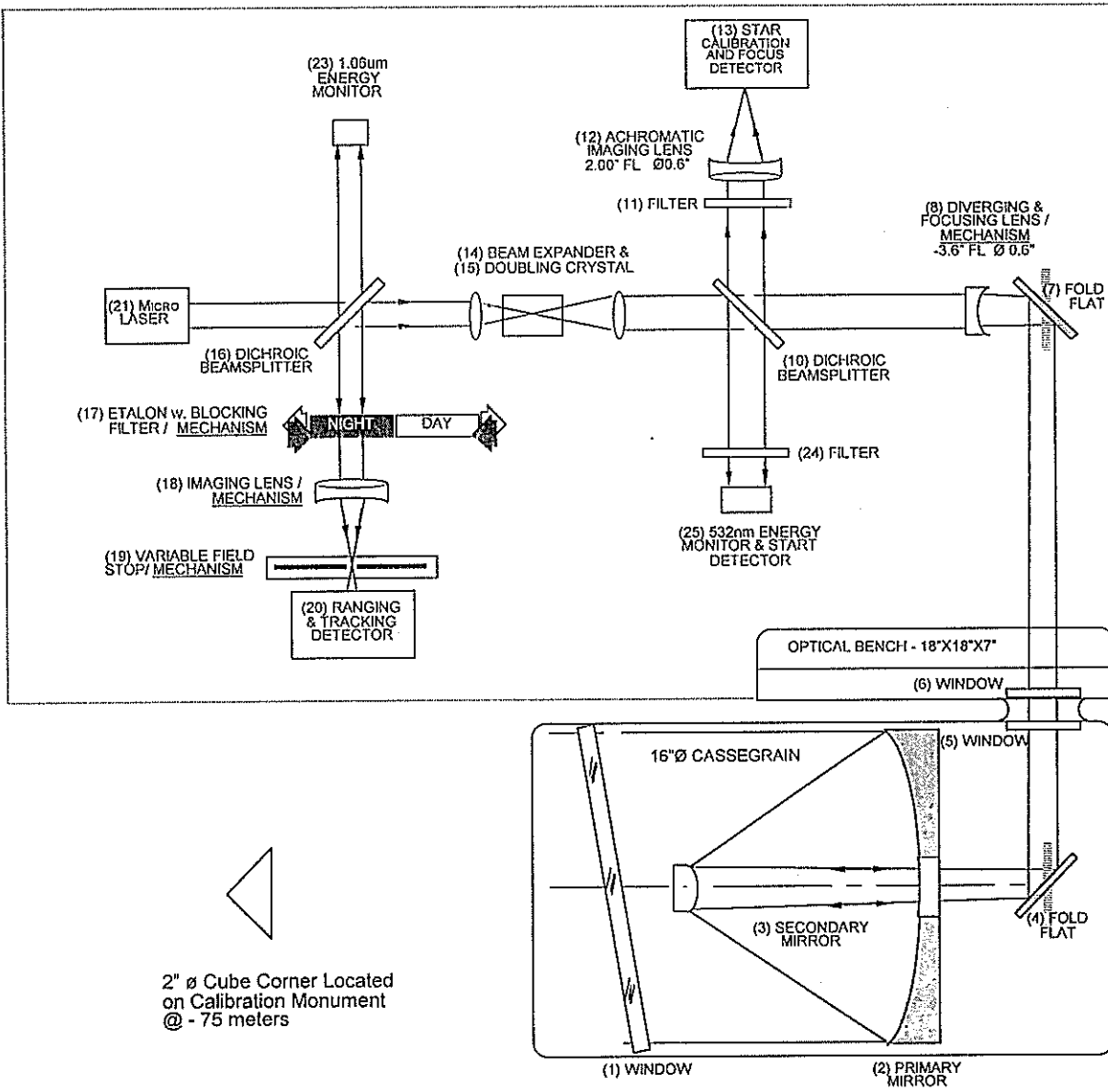
Figure 1: Preliminary block diagram of the SLR2000 optical head.

2.3 Tracking Mount

The optical head will be mounted in one of the Aerotech Model AOM360-D series of tracking mounts, to be selected upon completion of the optical head preliminary design. The latter mounts can accommodate loads up to 50 cm in diameter and are driven by direct-drive DC torque motors. The absence of gear trains and other drive mechanisms eliminates position error contributions due to mechanical hysteresis and backlash. The mount has a high axis positioning accuracy of one

arcsecond, a bidirectional repeatability to one arcsecond, and a low axis wobble, also at the one arcsecond level. Orthogonality of the axes is good to 3 arcseconds, but this error can be taken out with star calibrations and mount modelling. Thermal stability is 0.4 arseconds/°C. The use of Inductosyns, rather than optical encoders, for angle sensing allows electrical cables to be passed from the environmental shelter to the optical head through the center of the azimuth and elevation drive bases. The mount will be equipped with military style electrical connectors and bearing seals to provide additional environmental protection over and above that provided by the dome.

2.4 Correlation Range Receiver (CRR)

The correlation range receiver performs several critical functions which include: (1) precise time of flight (TOF) measurements; (2) the discrimination of signal from noise; and (3) the generation of subarcsecond pointing corrections. The power of the CRR is that it carries out these functions simultaneously using all of the ranging signal available to it. Like the microlaser transmitter, the CRR must operate at KHz rates. To fully understand the design and operation of the CRR, one must first describe the manner in which the TOF measurement is made under these high repetition rate conditions.
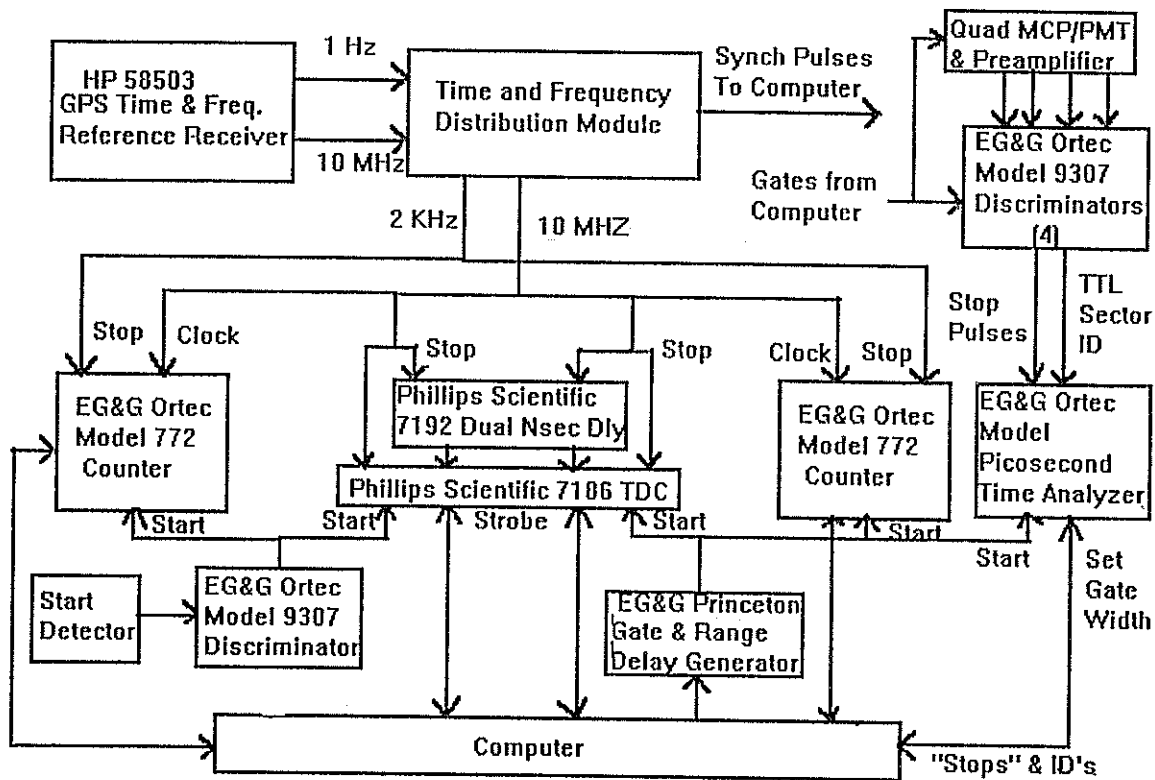
Figure 2: A correlation range receiver configuration designed using commercially available nuclear timing instrumentation.

2.4.1 CRR Time-of-Flight Measurement

Figure 2 shows a baseline design for the CRR which is built up entirely from NIM/CAMAC nuclear timing instrumentation commercially available from three companies: EG&G Ortec, EG&G Princeton and Phillips Scientific. The timing is centered around the nominal 2 KHz fire rate of the microlaser transmitter as illustrated by the timing diagram in Figure 3. The 10 MHz output of the HP Time and Frequency Reference Receiver is used to generate a 2 KHz train of

synchronized clock pulses. Within each 500 μsec fire interval, there will be one "start" pulse and potentially one "stop" pulse plus noise counts. Since each fire interval corresponds to a one-way distance interval of 75 Km, the stop pulse occurring during satellite ranging in the (n+m)th interval originates from the "start" pulse occurring in some earlier (nth) interval. The (n+m)th 2 KHz clock pulse starts the "start" counter for that interval. The arrival of the (n+m)th "start" pulse stops the "start" counter and starts a time to digital converter (TDC) which is then stopped by the next 10 MHz clock pulse. Thus, the temporal position of the "start" laser pulse within the fire interval is determined by adding the "start" counter and "start" TDC vernier outputs. Similarly, the range gate from the EG&G Princeton Research Gate and Time Delay Generator starts a second "stop" counter, a second "stop" TDC, and an EG&G Model 9308 Picosecond Time Analyzer (PTA). The "stop" TDC is stopped by the next 10 MHz clock pulse and the "stop" counter is stopped by the next 2 KHz clock pulse. Adding the outputs of the second TDC vernier and the "stop" counter gives the time interval between the range gate and the (n+m+1)th 2 KHz clock pulse. The PTA is capable of recording multiple events separated by at least 50 nsec and gives the temporal positions of any signal or noise counts occurring within the range window relative to the range gate. The width of the PTA range window is programmable down to a minimum of 80 nsec. The time resolution of the PTA is the window divided by 64,000 or about 1.2 psec for its narrowest window setting. Thus, all "events" occurring within each 500 μsec fire interval are well-positioned with respect to the 2 KHz clock pulses which bound that interval.
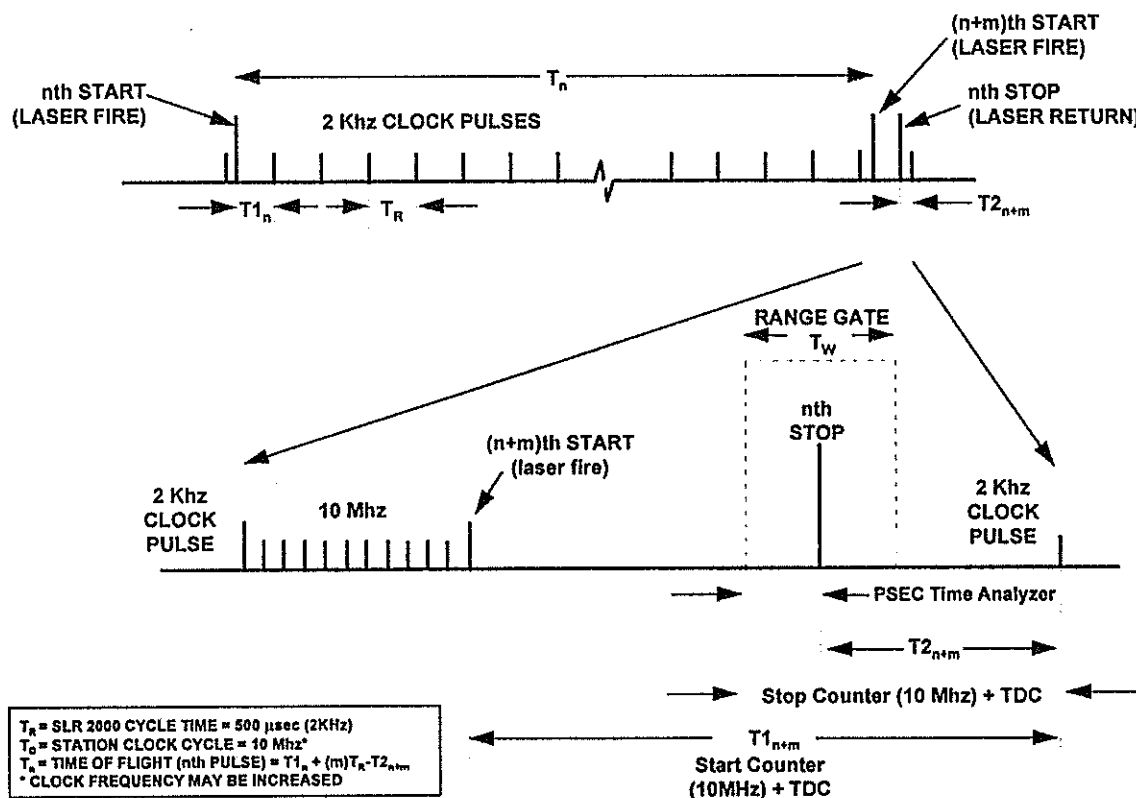
Figure 3: SLR2000 Timing Diagram

To compute the range to the satellite as measured by the nth start pulse, one must now use the following formula (see Figure 3)

$$T_n = T1_n + mT_R - T2_{n+m}$$

where TI_n is the interval between the nth clock pulse and the nth start pulse as measured by the "start" counter and "start" TDC, $T_R = 500$ μsec is the fire interval between 2 KHz clock pulses, $T2_{n+m}$ is the interval between the (n+m)th signal arrival time and the (n+m+1)th clock pulse as measured by the "stop" counter, "stop" TDC, and PTA, and m is the number of intervening 2 KHz clock cycles between a "start" pulse and its corresponding "stop" pulse and can be computed a priori from our approximate knowledge of the station and satellite positions.

We are looking into possible enhancements which would improve the timing precision of the baseline CRR, such as multiplying the 10 MHz to higher clock frequencies (~100 MHz) or modifying the event timer developed by ATSC for the Matera Laser Ranging Observatory [9] to perform all of the CRR functions.

2.4.2 Post-Detection Poisson Filtering of CRR Range Data

The timing outputs (starts, stops, and noise events) from the CCR are transferred to the SLR2000 ranging computer which assigns them to "time bins" in accordance with satellite-dependent algorithms described in detail in [5] and simulated in [6]. Signal counts from the satellite would be bunched in a narrow time interval whereas dark current or background noise counts would be spread over the full width of the range gate. Put simply, the ranging computer looks at the number of counts in each time bin to identify the probable presence of the signal, applies an iterative filter, computes an updated range and time bias, and gradually reduces the range gate width to decrease the number of noise counts in future frames.

SLR 2000:
Simultaneous Ranging And Angular Tracking
In Photon Counting Mode
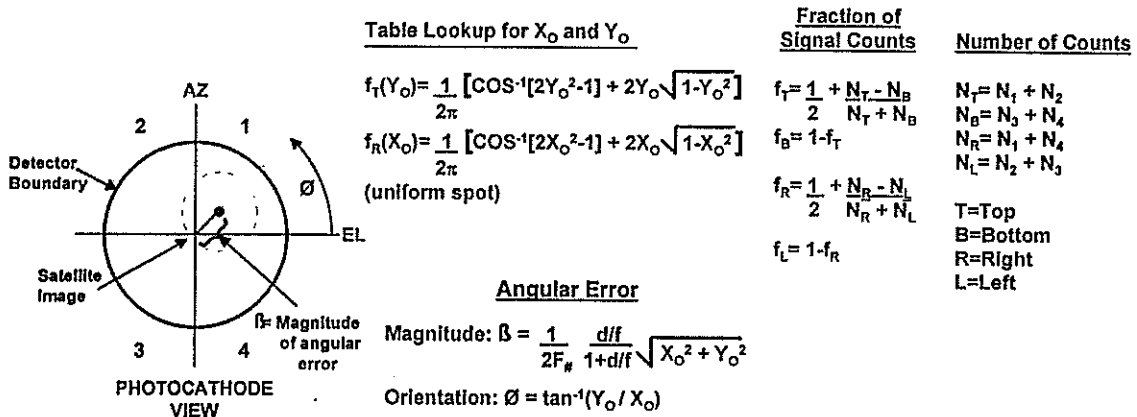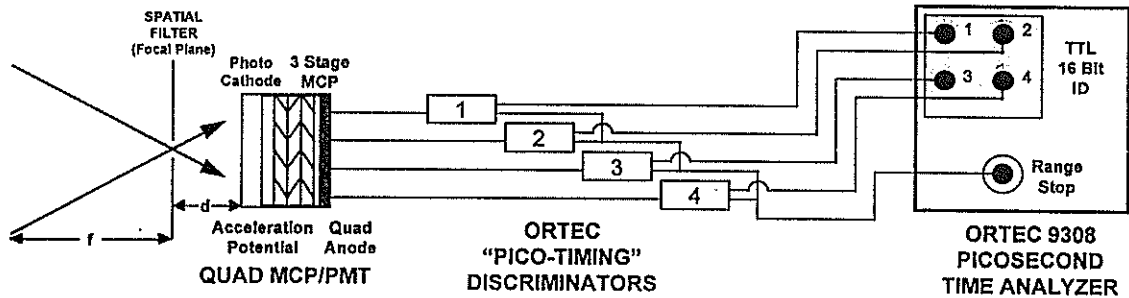
Figure 4: Correcting pointing error in the photon counting mode using the correlation range receiver.

2.4.3 CRR Derivation of Subarcsecond Pointing Error

As mentioned in Section 2.2, the stop detector is placed behind the telescope focal plane so that the satellite image is enlarged and distributed over the four quadrants as in Figure 4. Following a photon event in one of the quadrants, the corresponding anode produces an electronic pulse which is input to one of four EG&G Ortec Model 9307 "Pico-timing Discriminators". The latter device produces both a fast ECL logic "stop" pulse, which is summed with the other three discriminator channels and input to the PTA timing circuitry, and a second TTL logic pulse, which is input to a second circuit in the PTA and identifies which of the four quadrants the timing signal came from. One would expect, on average, that noise counts would be equally distributed among the four quadrants whereas, if there were a small pointing error, signal counts would pile up preferentially in one or more quadrants. Following the filtering of noise counts based on time of arrival by the postdetection Poisson filter, a subarcsecond pointing angle correction can be computed by adding or subtracting the residual counts in each quadrant using the algorithms summarized in Figure 4.

2.5 Meteorological Station

The meteorological subsystem measures pressure, temperature, and relative humidity with the requisite accuracy for millimeter ranging. In order to protect the system from the external environment and extend component lifetimes, the meteorological subsystem also monitors: (1) wind speed and direction ; (2) the presence, type, and accumulation of various forms of precipitation (rain, snow, etc.); (3) local visibility out to 50Km; and (4) cloud cover.

The meteorological station consists of four principal parts, three of which are commercially available:

(1) Paroscientific MET3-1477-001 Pressure, Temperature, and Relative Humidity Monitor

Pressure: Range 800 to 1100 mbar; Accuracy ~0.1 mbar; Stability < 0.1 mbar/year
Temperature: Range -40 to 70°C; Accuracy < 0.5°C; Stability < 0.1°C/year
Relative Humidity: Range 0 to 100%; Accuracy ±2%, Stability<1%/year

(2) Vaisala FD12P Precipitation and Visibility Sensor

The FDP12 consists of an optical transmitter, receiver, controller, and a capacitive rain sensor. It utilizes an optical forward-scatter sensor that not only sees fog but also distinguishes between precipitation particles. An ambient temperature sensor is included to increase the reliability of precipitation type assessment. The unit measures visibility optically from 10 m to 50 Km and the
type, intensity, and accumulation of precipitation.

(3) Belfort 200 Wind Monitor

Wind speed is sensed by an 18 cm diameter helicoid propellor. A six pole permanent magnet attached to the shaft induces a sinusoidal AC signal in a stationary coil with a frequency proportional to the wind speed. Wind direction is sensed by rotation of the sensor on its vertical shaft Vane position is transmitted by a 10K ohm conductive potentiometer. With a reference voltage applied to the potentiometer, an analog voltage proportional to azimuth angle is produced as output.

Wind Speed: Range 0 to 135 mph; ±0.6 mph
Wind Direction: Range 0 to 360°; Accuracy ±3°

(4) Cloud Sensor

Presently we are looking at two very distinct options for detecting clouds. One approach is to add a crude lidar channel to the receiver to monitor the laser backscatter from clouds, but this requires the system dome to be open and the laser ranging system to be operating. A potentially more attractive option is to have a CCD camera outside the dome view the hemispherical sky from a convex mirror. In daylight, the sky would be viewed alternately through blue and green filters (blue sky = clear) whereas, at night, approximate cloud cover would be inferred from the presence or absence of low magnitude stars. In both cases, the image would be used in determining whether or not to open the dome, and, if partially clear, which parts of the sky should be avoided in scheduling satellite tracks.

2.6 Environmental Shelter with Azimuth Tracking Dome

The Aerotech tracking mount will be positioned (three-points of contact) and leveled, using two attached differential leveling bubbles, on a central concrete monument. A mount model, updated by frequent star calibrations, further defines and maintains the system orientation and alignment. The telescope and calibration targets will be more than 2 meters off the ground, making access by unauthorized personnel difficult.
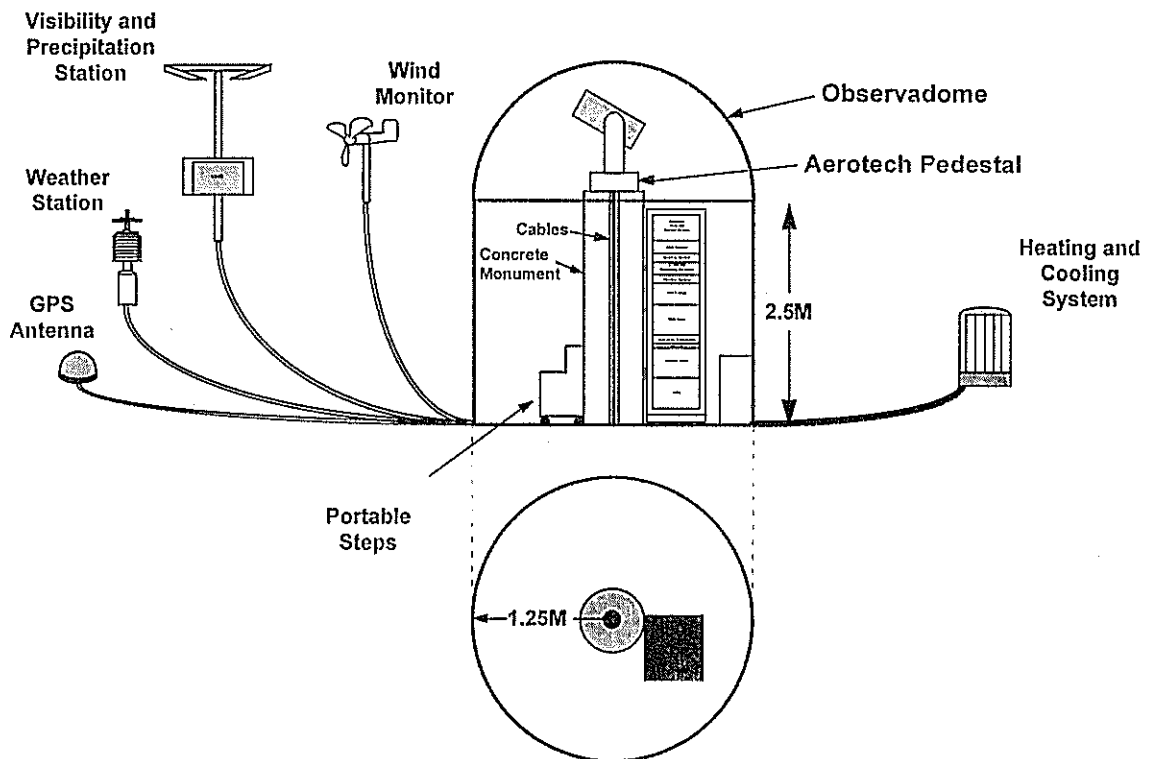
Figure 5: SLR2000 field installation concept.

The central monument sits inside an environmental shelter and a protective astronomical dome as in Figure 5. The interior of the environmental shelter is maintained at nominal room temperature (≅23°C) by an external heat pump. This stabilizes the timing electronics, provides a source of heated dry air for preventing condensation on the optics, helps to stabilize the temperature of

certain elements in the optical head, and provides a comfortable workplace for visiting maintenance personnel. To allow the optical head and tracking mount to follow the external ambient temperature and thereby minimize thermal gradients in the optical head during system operation, the heated (or cooled) "electronics room" is thermally isolated from the dome area by a removable "ceiling". A technician can gain access to the optical head and tracking mount by removing the "ceiling" and using a set of portable steps permanently stored in the shelter. Diagnostic tests can be performed onsite by plugging a laptop computer into the central computer system. Internet and telephone communications are also provided in the shelter. A modem provides a backup means of communicating with the system when the Internet is inaccessible.

The 2.5 meter dome is built by Observadome™ and has a motorized slit (shutter) and azimuth drive. Both are under computer control and the dome azimuth drive is slaved to the Aerotech tracking mount azimuth.

Electrical signal and power cables are passed from the electronics rack through the center of the Aerotech azimuth stage Inductosyn , through one arm of the mount yoke, and through the elevation Inductosyn in order to power the optical head and tracking mount and to extract the ranging, star calibration, and housekeeping signals. Small hoses bearing filtered, heated (or cooled) dry air from the electronics room can also pass through the same path as necessary to prevent condensation on optics and to provide a heat exchange medium for temperature-sensitive elements in the optical head (e.g. diode pump lasers, spectral filters, etc) .

It is expected that the shelter will be equipped with additional inexpensive security devices for automatically detecting and reporting threats to system security, via Internet and/or recorded phone messages. These might include motion and intrusion sensors and surveillance cameras for detecting and reporting unauthorized personnel in the vicinity, thermal sensors for detecting heat pump failure, etc.

2.7 System Controller

The SLR2000 computer consists of three Pentium-based processors, two in a VME backplane and the third in a PC/ISA crate. The VME bus was chosen for its higher bus speed (40MB/sec), while the ISA bus was needed to handle specialized interface cards for the camera, Picosecond Time Analyzer, and mount. The ISA computer functions simply as an Input/Output processor, passing data to and from the VME computers via shared memory. The VME processors perform all of the decision making, data analysis, and external communication. One of these processors, called the "Pseudo-Operator", performs the functions of a human operator, making decisions on whether the weather permits opening the dome and tracking, which satellite should be tracked, and whether the returns in the ranging window are signal or noise. The Pseudo-Operator also monitors the system temperatures and voltages, and acts to protect the system if it detects system health or safety problems. The second VME processor, called the Analysis CPU, computes the Normal Point data from the raw tracking/ranging data and sends this data out to a central archive. This processor also gets predictions for the system, and converts it to the appropriate format. Information is communicated between the two VME processors via file and memory sharing. Both processors are expected to be running the Lynx Real-Time Operating System.

Human interaction with the SLR2000 system requires communicating with the Analysis CPU through the internet. A laptop PC running a special software package will allow personnel to monitor the operation of the system via graphical displays, get information from the system to analyze off-line, run diagnostic tests, and change system parameters.

3. SUMMARY

SLR2000 is an autonomous, unmanned satellite laser ranging station with an expected single shot range precision of about one centimeter and a normal point precision better than 3 mm. The system will provide continuous 24 hour tracking coverage for all satellites up to and including GPS and will reduce capitalization, operating and maintenance costs by an order of magnitude relative to recent outlays. The dominant cost driver in present SLR systems is the onsite and central infrastructure manpower required to operate the system, to service and maintain the complex subsystems (notably the laser), and to ensure that the transmitted laser beam is not a hazard to onsite personnel or overflying aircraft. In designing the SLR2000 system, preference was given to simple hardware over complex, to commercially available hardware over custom, and to passive techniques over active resulting in the prototype design described here. This general approach should allow long intervals between maintenance visits and the "outsourcing" of key central engineering functions on an "as needed" basis. In unassembled "kit" form, the per system hardware costs for SLR2000 are expected to be roughly $300K. A fully assembled and tested field system, including shelter and monument, should be reproducible for about $500K per system in quantities of eight or more.

REFERENCES

1. Degnan, J.J., "SLR2000" in Satellite Laser Ranging in the 1990's : Report of the 1994 Belmont Workshop, NASA Conference Publication 3283, pp. 101-106, 1994.

2. Degnan, J. J. , "SLR2000: An Autonomous and Eyesafe Satellite Laser Ranging Station", Proc. Ninth International Workshop on Laser Ranging Instrumentation, pp. 312-323, Canberra, Australia, November, 1994.

3. McGarry, J. , J. J. Degnan, P. Titterton, H. Sweeney, B. P. Conklin, and P. J. Dunn, "Automated Tracking for Advanced Satellite Laser Ranging Systems", Proc. Spring SPIE Meeting, SPIE Vol. 2739, pp. 89-103, Orlando, FL, April 10-11, 1996.

4. Degnan, J. J., "Optimal Design of Q-switched Microlaser Transmitters for SLR", these proceedings.

5. Titterton, P., and H. E. Sweeney, "Correlation Processing Approach for Eyesafe SLR2000", these proceedings

6. McGarry, J., "SLR2000 Performance Simulations", these proceedings

7. Degnan, J. J. , "Compact Laser Transponders for Interplanetary Ranging and Time Transfer", these proceedings

8. Hamal, K. and B, Greene,"Second Harmonic Generator T/R Switch" , these proceedings.

9. Selden, M., C. Steggerda, R. Stringfellow, D. McClure, C. B. Clark, and G. Bianco, "Instrument Development and Calibration for the Matera Laser Ranging System ", these proceedings.

Correlation Processing Approach for Eyesafe SLR 2000*

Paul J. Titterton and Harold E. Sweeney
EOO, Inc.
269 North Mathilda Avenue, Sunnyvale, CA 94086-4830
(408) 738-5390; FAX: (408) 738-5399. e-mail: EOOInc@aol.Com
*Supported in part by NASA Goddard Space Flight Center

The SLR 2000 design, discussed in the Canberra meeting two years ago, employs a high PRF / low energy-per-pulse 532 nm transmitter beam which is expanded to fill a large aperture. The system is also designed to be capable of fully unattended operation. The following table summarizes the top level electro-optical parameters for the SLR-2000, as presently configured.

Transmitter Side	Receiver Side
Wavelength: 532 nm	Filter Bandpass : 1.2 Å (50% throughput) [B_{opt}]
Energy Per Pulse: 207 µjoule [$E_p\gamma_t$]	Quantum Efficiency: 40 % [η]
Pulse Repetition Frequency: 2000 Hz	Total Dark Counts: < 10^4 /second @ 20 °C
Pulsewidth: 140 psec	Resolution: < 100 psec
Transmitter Aperture: 50 cm diam. [D_t]	Receiver Aperture: 50 cm diam. [D_r]
Optical Transmission: > 80 % [γ_t]	Optical Transmission: > 30 % [γ_r]
Half Angle Beamwidth: 20 µrad [θ_t]	Half Angle Beamwidth: 20 µrad [θ_r]
Power Distribution - At Aperture: Top Hat - Far Field: Airy Disc	Field-of-View : Sharp Edged Uniform Sensitivity
Pointing Jitter: < 5 µradians (nominal)	Boresight with Transmitter: < 5 µradians
Pointing Offset: < 5 µradians (nominal)	Special: Quadrant Detector

System eye safety is based on ANSI Z136.1-1993, Section 8.2, Table 5 and the accompanying Errata Sheet. The governing equation is

$$C_\# MPE = \frac{E_p\gamma_t}{\pi D_t^2 \big/ 4} \qquad (1)$$

for $C_\#$ = Multiple pulse correction to the allowable single pulse MPE

$= \left[PRF(Exposure\,Duration)\right]^{-\frac{1}{4}}$,for PRF = laser pulse repetition frequency (Hz),

MPE = Maximum Permissible single pulse/single exposure energy density,

$C_\# = \left[PRF(0.25)\right]^{-\frac{1}{4}}$ (in the green, for short pulses) = 0.2115 for PRF = 2000 Hz,

MPE = 5 (10^{-7}) joules/cm^2 (in the green for short pulses).
Evaluating Equation 1 we find in general that

$$E_p\gamma_t = 8.305\left(10^{-8}\right)D_t^2 \qquad \text{joules.} \qquad (2)$$

The 50 cm aperture case is used in the baseline SLR-2000 configuration, and corresponds to the 207 µjoule value for energy per pulse at the aperture.

The range equation (cf. Bibliography) is

$$n_{pe}^s = \eta \left(\frac{E_p \gamma_t}{h\nu} \right) \tau_a \tau_{c\ell} \left(\frac{\sigma}{\pi \theta_t^2 \gamma_{turb}^2 R^2} \right) \tau_{c\ell} \tau_a \gamma_r \left(\frac{A_r}{\pi R^2} \right) \overline{G} \qquad (3)$$

for n_{pe}^s = signal photo-electrons (pe's) per pulse; $h\nu$ = energy per photon; τ_a = one-way clear atmosphere path transmission; τ_{cl} = one-way cirrus cloud path transmission; σ = satellite optical cross-section; γ_{turb} = impact of atmospheric turbulence on beam divergence; R = range from ground station to target; $A_r = \pi D_r^2 / 4$; $\overline{G}$ = normalized impact of transmitter truncation and beam shape at the satellite = 0.5.

The elevation angle dependence of the parameters and the optical cross sections are shown in the following table for the Starlette, LAGEOS and ETALON satellites. (The cross sections are ~ 80% of typical values, which provides performance margin.) Equation 3 is evaluated for these parameters in the following figure.

Elevation Angle (Degrees)	Range to Starlette(km)	Range to LAGEOS (km)	Range to ETALON (km)	τ_a	τ_{cl}	γ_{turb}
20	2034	8532	22861	0.75	0.12	1.6
30	1626	7776	21783	0.84	0.36	1.4
40	1362	7164	21006	0.87	0.53	1.27
50	1188	6687	20360	0.89	0.65	1.14
60	1074	6333	19854	0.90	0.72	1.07
70	1002	6089	19491	0.911	0.75	1.03
80	963	5947	19273	0.915	0.77	1.01
90	960	5900	19200	0.92	0.78	1.00
σ (10^6 m^2)	0.52	5.7	48			

Signal Photo-electrons per Pulse vs Elevation Angle
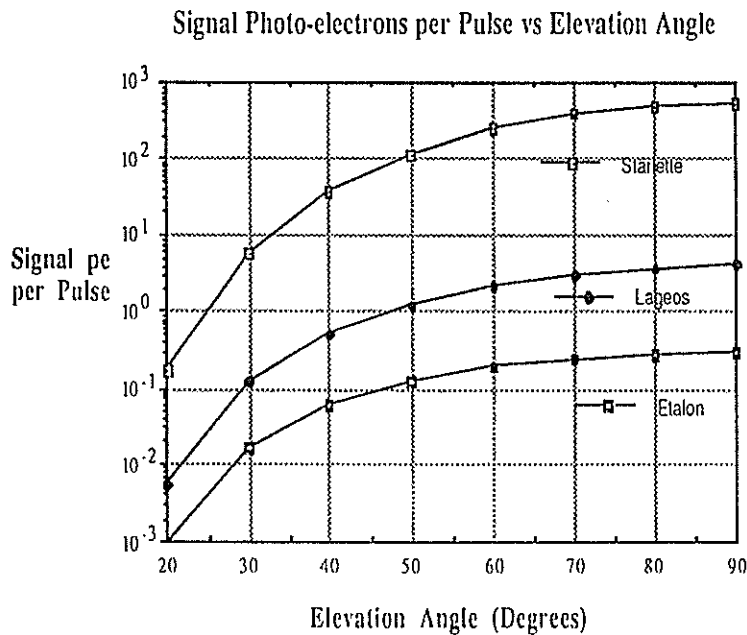
During initial acquisition (at the lowest elevation angles), the signal levels per pulse are very small: 0.159 /Starlette /20°, 0.0054 /LAGEOS /20°, and 0.00165 / ETALON / ~ 22°.

There are three functions which the system must perform at these low signal levels: acquisition, ranging, and tracking/pointing during ranging. The assumed requirements during acquisition are shown in the next table --- the basic acquisition requirement is to narrow the initial range, angle and time uncertainties.

Initial Uncertainties	Starlette	LAGEOS	ETALON	Desired Performance
Angle (μrad)	± 100 x ± 80	± 80 x ± 80	± 80 x ± 80	± 5
Range (nsec)	± 100	± 100	± 100	± 5
Range Rate(nsec/sec)	~ 300	~ 10	~ 1	Target Specific
Time to acquire (sec)	< 10	< 120	< 300	

Ranging must occur with the requirements shown in the next table.

	Starlette	LAGEOS	ETALON
Normal point Precision	~ mm	~ mm	~ mm
Time per Normal Point (sec)	30	120	300

During ranging, slow system pointing errors often occur, and so the final functional requirement is to develop a pointing error from the characteristics of the returned light, and update the pointing angles to enable correcting for these errors.

To meet these requirements at very low signal levels, we use the relative temporal location of the signal pulses over many intervals. The concept is illustrated in the following figure. The basic insight is that signal pulses will reside in time correlated "bins" within the gates, while noise counts will be randomly distributed.
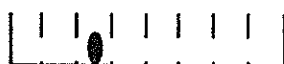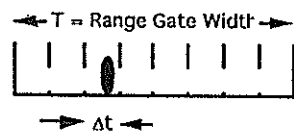
n_{bin} = # of pulse resolution intervals per gate,

N_{pe}^s = mean # of signal pe after K gates

K = # of gates before detection decision;
Frame = K range gates

$$T = n_{bin}(\Delta t) \quad \text{and} \quad N_{pe}^s = K\left(n_{pe}^s\right)$$

We assume that both n_{pe}^s and N_{pe}^s are Poisson distributed. The probability that signal photo-electrons will be detected in corresponding time bins in separate range gates is

$$P_K(\geq 3) = 1 - \left(1 + N_{pe}^s + \frac{\left(N_{pe}^s\right)^2}{2!}\right) e^{-N_{pe}^s} \text{, k (\# of pe correlations)} \geq 3 . \quad (4)$$

Equation 4, and corresponding ones for k=2 and 4, are evaluated in the following figure.

Correlated Detection Probabilities vs Mean Number of Detected Photo-electrons per Frame

Probability of Correlated Detection vs Number of Signal pe after K Range Gates
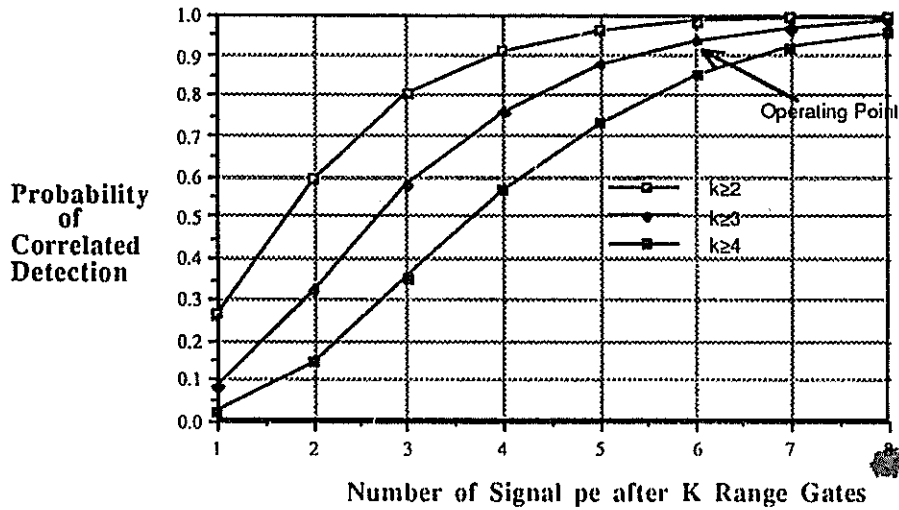
After an average of 6 signal photo-electrons are detected, k ≥ 3 correlation detection provides ~ 94% probability of signal acquisition. The corresponding times required to accumulate the 6 signal photo-electrons are shown in the next figure.

Time to achieve a Mean Photo-electron count ≥ 6 in ≥ 3 pulses vs Elevation Angle

Time to Detect ≥ 6 Signal pe in ≥ 3 pulses (seconds) vs Elevation Angle
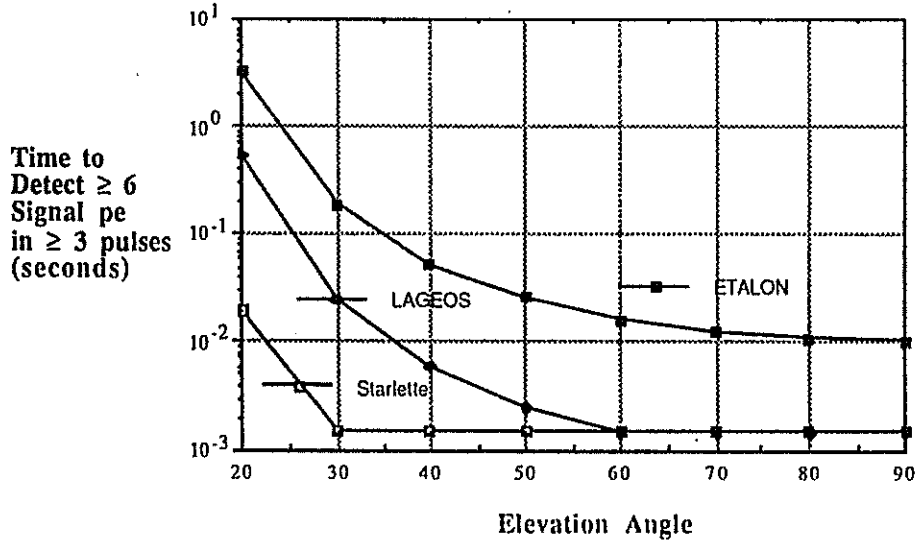
This figure is interpreted as the time it should take to acquire these satellites, which is a function of elevation angle. The times are: 0.0189 seconds / Starlette / 20°; 0.532 seconds / LAGEOS / 20°; 1.818 seconds / ETALON / 22°. During this same time noise counts occur. Using the formulation in the bibliography, and the parameters in the initial table in this paper, we find for the assumed quadrant photo-detector:

381

Clear Daytime Optical Background, pe's per range gate:	0.0278 Total
	0.00695 per quadrant
Dark Counts: 10^4 / second , pe's per range gate:	0.0020 Total
	0.0005 per quadrant
Signal Backscatter:	Prevented by Appropriate Receiver Blanking
	Programmably vary Laser Firing Time to Prevent "Collisions"

Net Noise Photo-electron rate:	Day	14.9 / second / quadrant
	Night	1 / second / quadrant

To analyze the probability of false acquisition, we define m = # of noise photo-electrons present in a Frame and n_{bin} = # of time bins per range gate. The probability that these noise photo-electrons will lead to a (false) correlation is given by

$$P_{FAQ} = 1 - \left\{ e^{-\frac{m}{n_{bin}}} \sum_{j=0}^{k-1} \frac{\left(\frac{m}{n_{bin}}\right)^j}{j!} \right\}^{n_{bin}} \quad (5)$$

m = [noise pe rate] x [time to detect 6 signal pe]

n_{bin} = [(range rate uncertainty) x (time to detect 6 signal pe) $]^{-1}$ x [range gate width].

Equation 5 is evaluated for a single ± 20 μradian beam at minimum elevation angle, k ≥ 3, and a 200 nsec gate in the following table.

		Time for 6 signal pe (sec)	Range Rate Uncertainty (nsec/sec)	m	Bin Width (nsec)	n_{bin}	PFalseAcq
Starlette	Day	0.0189	300	0.282	5.67	35	0.025 %
20°	Night	0.0189	300	0.0192	5.67	35	< 0.00001 %
LAGEOS	Day	0.532	10	7.93	5.32	38	4.75 %
20°	Night	0.532	10	0.53	5.32	38	0.0017 %
ETALON	Day	1.818	1	27.1	1.818	110	20.4 %
~22°	Night	1.818	1	1.82	1.818	110	0.0082 %

For Daytime ETALON, the SLR 2000 system parameters and k ≥ 3 correlation detection will find the signal ~ 94% of the time that it is present, and falsely identify noise counts as signal ~ 20% of the time when the signal is absent, for a single ± 20 μradian spot. The total time to acquire includes the effect of scanning the ± 20 μradian beam over the full angular uncertainty, including the effect of spot overlap and revisit, both included in an overhead factor. The resulting times are shown in the next table.

		Initial Angular Uncertainty (μradians)	Time per Spot (seconds)	Approximate Overhead	# of Spots	Maximum Acquisition Time (seconds)	Required Acquisition Time (seconds)
Starlette	Day	± 100 x ± 80	0.0189	33%	27	0.51	< 10
	Night	± 100 x ± 80	0.0189	33%	27	0.51	< 10
LAGEOS	Day	± 80 x ± 80	0.532	50%	24	12.55	< 120
	Night	± 80 x ± 80	0.532	33 %	21	11.17	< 120
ETALON	Day	± 80 x ± 80	1.818	100 %	32	58.2	< 300
	Night	± 80 x ± 80	1.818	33%	21	38.2	< 300

Before ranging, we center the spot on the quadrant to enable tracking, narrow the range gate to 10 nsec, and narrow the time bins to 100 psec . The resulting ranging performance, maintaining k ≥ 3 correlation to correctly identify 100 psec time bins, and defining precision per measurement point: $\left(\dfrac{c\Delta t}{2}\right) \approx 15$ mm, is given in the next table.

Satellite	Elevation Angle (Degrees)	# of Measurement Points per Normal Point	Approximate Precision (15 mm ÷ $\sqrt{\text{# of meas. pts}}$)
Starlette	20	1580	0.38 mm
	90	20,000	0.10 mm
LAGEOS	20	225	1.0 mm
	90	20,000	0.10 mm
ETALON	~ 22	165	1.17 mm
	90	30,000	0.087 mm

Tracking is achieved by using the quadrant signal to provide "slow" pointing updates. Signal counts per quadrant are accumulated until an adequate SNR exists.

$$SNR_{opt} = \frac{n_{pe}^{s}}{\left[n_{pe}^{s} + n_{pe}^{n}\right]^{1/2}} \rightarrow SNR_{opt} = \frac{\dot{n}_{pe}^{s} T_s}{\left[\dot{n}_{pe}^{s} T_s + \dot{n}_{pe}^{n} T_s\right]^{1/2}} = \frac{\dot{n}_{pe}^{s}}{\left[\dot{n}_{pe}^{s} + \dot{n}_{pe}^{n}\right]^{1/2}} T_s^{1/2} \qquad (6)$$

for T_S = measurement time. For a 10 nsec range gate, signal spot centered on the quadrant, and a $SNR_{quadrant}$ = 10 dB, tracking performance is shown in the next table.

Satellite	Elevation Angle	T_S (seconds)	Angular Motion per Update (milli-degrees)
Starlette	20°	0.127	15
(Daytime)	90°	0.0005	0.22
LAGEOS	20°	4.73	156
(Daytime)	90°	0.005	0.28
ETALON	~ 22°	23.1	230
(Daytime)	90°	0.22	2.53

For realistic system parameters, correlation detection provides :

Satellite Acquisition Probability	≥ 90 %
Initial Acquisition Times:	Starlette ~ 0.5 seconds at 20°
(Daytime)	LAGEOS ~ 13 seconds at 20°
	ETALON ~ 60 seconds at ~ 22°
Ranging Precision per Normal Point:	Starlette ~ 0.4 mm at 20°
(Daytime)	LAGEOS ~ 1 mm at 20°
	ETALON ~ 1.2 mm at ~ 22°
Tracking/Pointing Update Rate:	Starlette ~ every 15 milli-deg at 20°
(Daytime)	LAGEOS ~ every 156 milli-deg at 20°
	ETALON ~ every 230 milli-deg at ~ 22°

Bibliography

J. J. Degnan, Millimeter Accuracy Satellite Laser Ranging: A Review, Geodynamics Series Volume 25, Contributions of Space Geodesy to Geodynamics: Technology, 1993.

J.J. Degnan, "SLR 2000" in "Satellite Laser Ranging in the 1990's", Proceedings of the Belmont Workshop, Elkridge, MD, NASA Conference Publication 3283, Ed. J.J. Degnan, pp. 101-106, February 1-2, 1994.

J.J. Degnan, SLR 2000: An Autonomous and Eyesafe Satellite Laser Ranging System, Ninth International Workshop on Laser Ranging Instrumentation, Canberra 1994, J. McK. Luck Ed., Volume 1, pps. 312-323.

J.F. McGarry, B. Conklin, W. Bane, R. Eichlinger, P. Seery and R.L. Ricketts, Tracking Satellites with the Totally Automated SLR2000 System, Ninth International Workshop on Laser Ranging Instrumentation, Canberra 1994, J. McK. Luck Ed., Volume 2, pps. 717-725.

P. Titterton and H. Sweeney, SLR 2000 Design and Processing Approach Sensitivity, EOO Report 94-003, Dec. 15, 1994. GSFC PO# S-44974-Z.

P. Titterton, H. Sweeney and T. Driscoll, SLR 2000 Analytical Study of 1060 nm Aided Acquisition and Tracking, EOO Report 95-007, Nov. 1, 1995, GSFC PO# S-61158-Z.

J.F. McGarry, J.J. Degnan, P.J. Titterton, H.E. Sweeney, B.P. Conklin and P.J. Dunn, Automated tracking for advanced satellite laser ranging systems, Paper 2739-08 in Acquisition, Tracking and Pointing X, Proceeding of the SPIE Volume 2739, M.K, Mastern and L.A. Stockum Editors, 10-11 Apr. 1996, pps. 89-103.

J. J. Degnan, J.F. McGarry, T. Zagwodski, P. Titterton, H. Sweeney, H. Donovan, M. Perry, B. Conklin, W. Decker, J. Cheek, T. Mallama and R. Rickleffs, An inexpensive, fully automated, eyesafe satellite laser ranging system, Tenth International Workshop on Laser Ranging, Shanghai, 1996, these Proceedings.

J. McGarry, SLR2000 performance simulations, Tenth International Workshop on Laser Ranging, Shanghai, 1996, these Proceedings.

SLR2000 PERFORMANCE SIMULATIONS
Presented in the Eyesafe Systems Session of the
Tenth International Workshop on Laser Ranging Instrumentation
November 11-15, 1996

Jan McGarry
NASA/Goddard Space Flight Center
Greenbelt, Maryland 20771 USA

The SLR2000 Simulator is a software package designed to allow testing of new tracking and ranging algorithms prior to the actual hardware development of NASA's next generation of Satellite Laser Ranging Systems, called SLR2000. The simulator is written in FORTRAN, currently runs in the HPUX environment, and models relevant errors in the receiver system, tracking mount, weather sensors, station location, system timing, predictions, and others. Recent work includes adding a new signal to noise algorithm, improving the tracking mount model, and developing an acquisition search algorithm. As a consequence of this work, we feel that the simulation results now provide a more realistic example of SLR2000 performance. Simulations of SLR2000 tracking and ranging performance will be presented.

Introduction

SLR2000 is a low cost, totally autonomous, eyesafe satellite laser ranging system currently being developed at NASA's Goddard Space Flight Center. The eye safety constraint implies a low transmit energy (200 microjoules), narrow laser divergence (+-4 arcseconds), and a rapid fire rate (2kHz). Algorithms to distinguish signal from noise must be developed since the system will be operating in a very low signal to noise environment. The operator functions must also be replaced by algorithms to perform such tasks as scheduling passes, acquiring and tracking satellites, and determining if the weather permits ranging. Lastly, the predictions must be made more accurate in order to improve pointing (for the narrower laser divergence) and to reduce the slope of the range errors in the ranging window (for the signal to noise algorithm to succeed).

The performance of SLR2000 depends heavily on the design and development of these improved models and algorithms. The simulator allows us to test the design of the algorithms, see how these algorithms affect performance prior to development of the hardware, and work in a controlled environment where absolute truth is known and can be used to judge performance.

For a more detailed description of the SLR2000 system see the paper[1] by John Degnan in this Proceedings. For a theoretical analysis of the potential acquisition, tracking and ranging performance of SLR2000 see Paul Titterton's paper[2] also in this Proceedings.
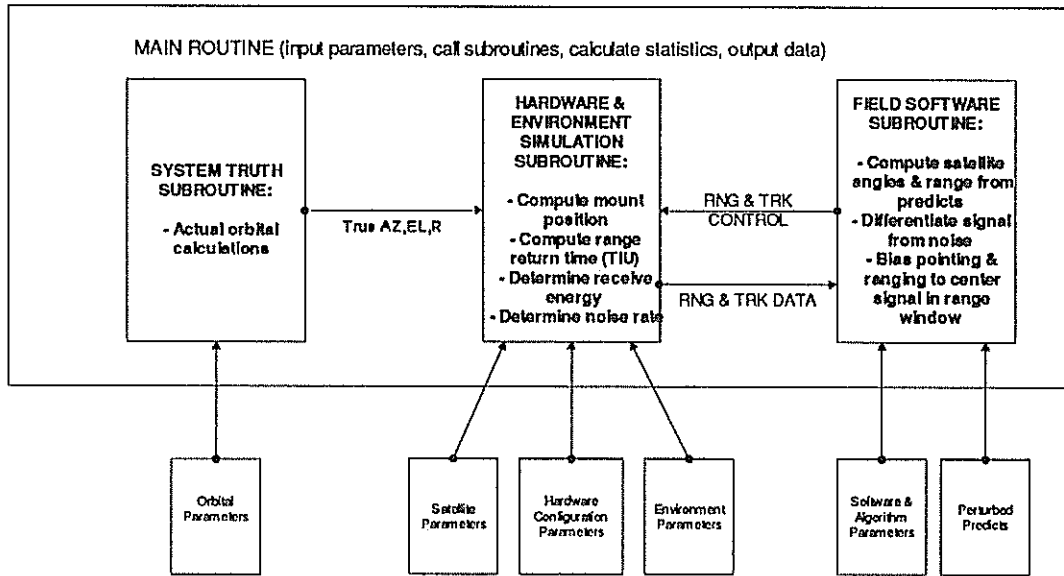
Figure 1: SLR2000 Simulator Design
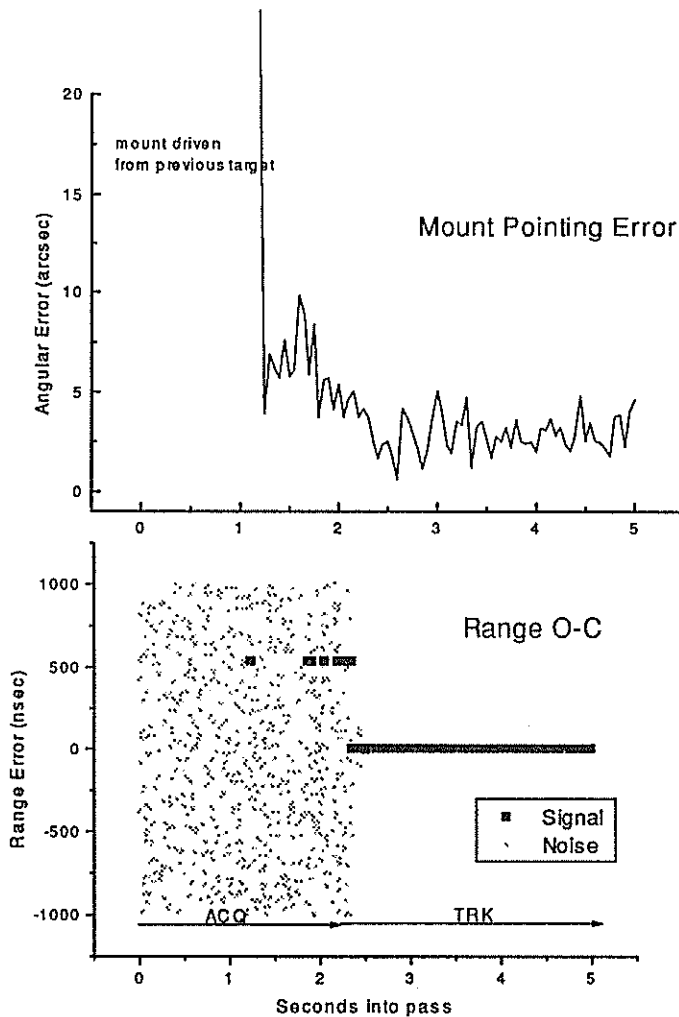
Figure 2: STARLETTE Daylight Pass

Simulator Description

The simulator models the ground instrumentation, the satellite orbit, the environment and the field software to produce a virtual SLR2000 system. The field software interacts with the hardware as in a real station to read in data and control the instrumentation. The System Truth, which includes where the satellite actually is, what the sky clarity is like, what time of day it is, and how the atmosphere is affecting the signal strength, is maintained to allow determination of actual system performance. The hardware readings are essentially System Truth perturbed by various random measurement errors and biases. The field software has no access to System Truth to ensure integrity of the testing process. Figure 1 illustrates this design. Recent enhancements include the addition of an angular search during acquisition, a model for a quadrant detector, moving clouds, and an improved tracking mount model. Listed below are some of the functions modeled in the simulator.

SLR2000 SIMULATOR HARDWARE FUNCTIONS / ERRORS MODELED

► POINTING SYSTEM
- Bias of mount system (error in mount model and mount wobble)
- Random jitter
- Mount drive at 2kHz with limits on acceleration & velocity
- Actual mount pointing kept separate from encoder readings

► RECEIVER TIMING
- Detector modeled:
  Photomultiplier or photon-counting Avalanche Photodiode.
- Time Interval Unit error modeled as random Gaussian noise
- Computation of background noise above threshold
- System delay bias applied

► RECEIVER ENERGY
- Fixed transmitter energy
- Gaussian pulse (spatial and temporal)
- Computation of transmitter gain as function of laser divergence
- Attenuation of energy with system and atmospheric transmission
- Satellite treated as single cube with given cross-section
- Moving cloud cover

► STATION READINGS
- Station location biases
- Weather sensor offsets
- System timing bias

► QUADRANT DETECTOR
- Simple model determines proportion of signal in each
   quadrant as function of pointing error
- Noise rate is divided equally between the 4 quadrants
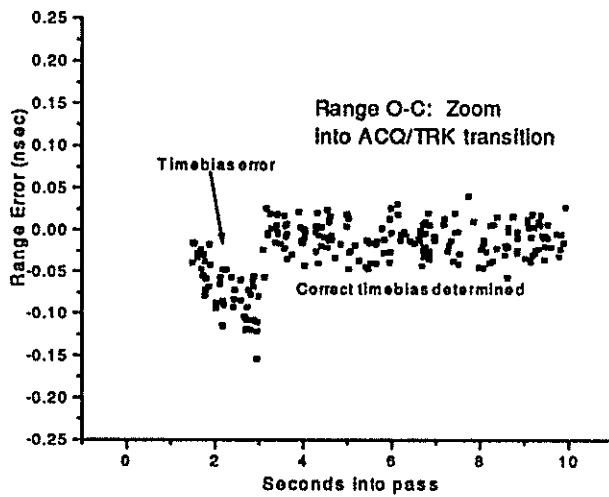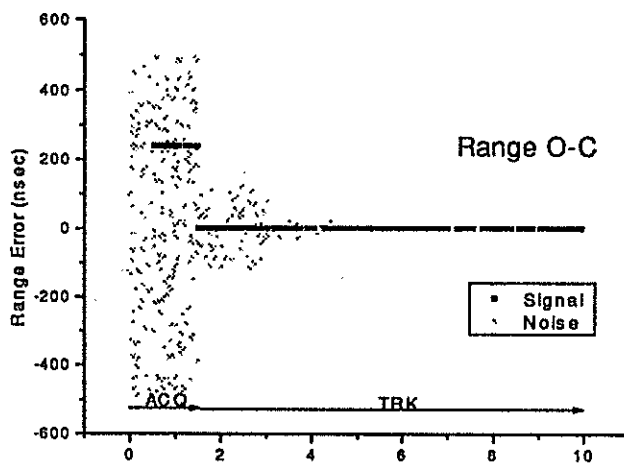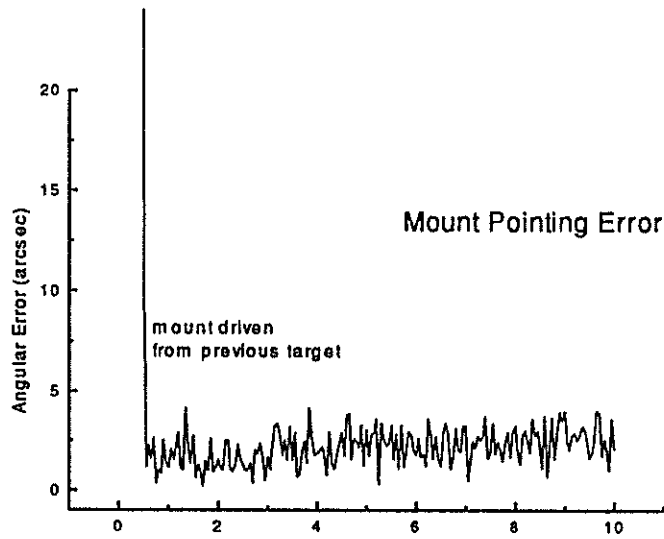
Figure 3: LAGEOS Daylight Pass

SLR2000 SIMULATOR ORBIT & FIELD SOFTWARE FUNCTIONS MODELED

- ► SYSTEM TRUTH
  - Orbital update using GEM10 and Texas Integrator
  - Sun position calculated and used in optical background determination
  - Environment truth maintained

- ► SOFTWARE POINTING COMPUTATIONS
  - Polynomial used to update satellite position (NASA SLR Network method)
  - Output to mount drive at 100Hz
  - Quadrant Detector output used as angular correction

- ► ALGORITHM COMPUTATIONS
  - EOO algorithm[2] used to detect Signal from Noise
  - Time and Range Bias computed from Signal
  - Angular Search used to find target (spiral scan)

The simulator is written in FORTRAN and contains approximately 4,000 lines of code. It currently runs under HPUX, but since there are few system unique calls, the simulator should be easily portable, and our plans are to convert it for Windows95. The simulator has more than 70 different variables that can be modified; each must currently be changed by editing the appropriate input file. A few of the possible parameters that can be changed, along with the values used in the Simulator Results section, are listed in Table 1. Future Windows95 versions will contain a graphical menu front end for helping the user configure the simulator and run it. There are also many possible outputs to select from, including mount errors, range O-C plots, and autotracking decisions. All of these are currently output as ASCII files which must be graphed post-run via an independent plotting package. This will also be changed in future versions, where results will be plotted from the simulator's graphical user interface.

Table 1: Important Simulator Parameters

Parameter	Value used in Simulations
Quantum Efficiency	0.40
Energy /pulse at aperture(μJ)	200
One way path transmission	0.75 @ 90° elev. and 0.12 @ 20° elev.
Optical Cross-section (m^2)	0.65(10^6) for STARLETTE 7 (10^6) for LAGEOS 20 (10^6) for GPS35
Receiver Optics Transmission	0.12
Receiver Area (m^2)	0.196 for 50 cm diam.
Transmitter half-angle beamwidth (arcsec)	4
Optical Bandpass filter (Å)	1.2
Solid angle FOV (sterad)	1.81 (10^{-9})
Background spectral radiance (watts/m^2-ster-Å)	1.46 (10^{-3}) day and 1.46 (10^{-8}) night
Dark current density (amps/cm^2)	10^{-15} (◊ background rate = 7000/sec for 1.2cm diameter cathode)
Mount jitter (arcsec)	0.5
Mount wobble / model error (arcsec)	4

Simulator Results

Figures 2 - 4 show simulations of the SLR2000 system acquiring STARLETTE, LAGEOS and GPS. The plots show Observed minus Calculated ranging data (O-C) in the range window along with the corresponding mount errors. The errors are graphed versus seconds into the pass. The darker range returns are the signal and the light gray returns represent noise. In all cases the simulator correctly finds the signal, corrects the pointing, range and time biases to center the satellite returns in the quadrant detector, and centers the signal in the range window. As the signal is acquired, the field software also closes down the range window. The mount errors shown include the time to close on the start of the pass from another mount position, the errors in the commands due to errors in the prediction polynomials, and the mount jitter and wobble. The polynomials used are those from the current NASA SLR Network and while accurate enough for the MOBLAS systems which have +-10 arcsecond beam divergences and 100 millijoule laser energies, they are not accurate enough for SLR2000 requirements and will not be used in the actual system.

Figure 2 shows a STARLETTE acquisition at 20 degrees elevation with a slant range of around 2,000km. Figure 3 is a LAGEOS pass being acquired at 20 degrees with a slant range of around 8,500km. This figure also zooms into the range window to show the timebias correction being applied (the slope of the range error being zeroed). Figure 4 shows GPS being acquired at 30 degrees elevation with a slant range of around 23,500km. All results are for a 50 centimeter telescope with parameters shown in Table 1 above. It should be emphasized that in these simulations the algorithm does not mistake noise for signal, even in the GPS case with a 1 microsecond range window. Previous simulations, using a 30cm telescope, showed false acquisitions for daylight GPS.[3] This agrees with theory which gives the probability of false acquisition for this telescope aperture to be nearly 100%. For the 50 centimeter telescope the probability of false acquisition is less than 20%.

Conclusions

Simulations of SLR2000 performance agree with the analytical conclusion that a low energy, 50cm telescope system with a quadrant detector, will be able to acquire and track, during daylight, all of the satellites currently tracked by the NASA Network from STARLETTE out to GPS.
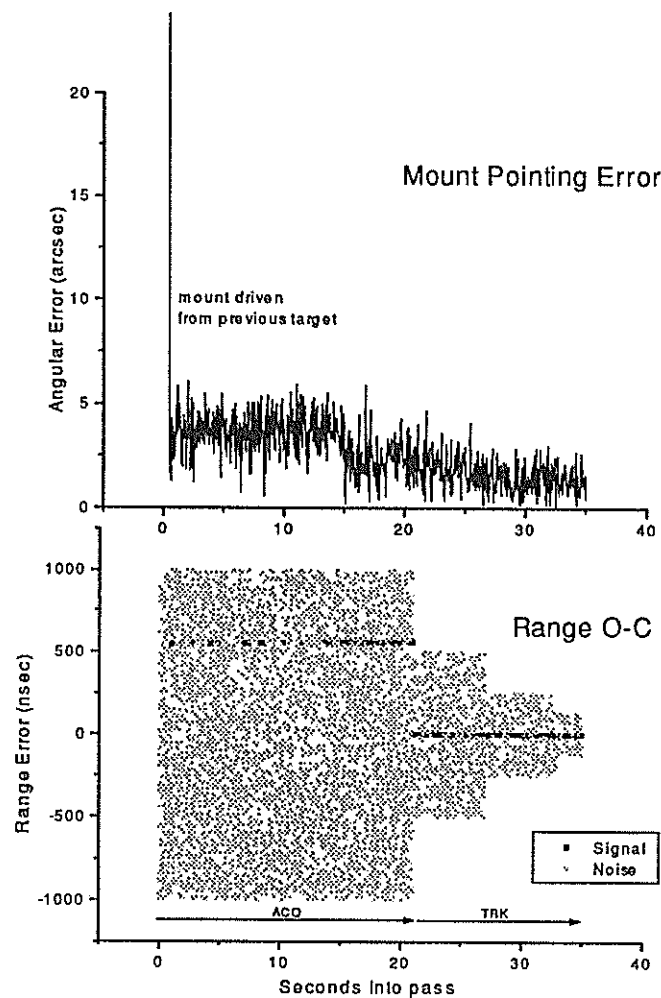
Figure 4: GPS Daylight Ranging

References
1. Degnan, John, Jan McGarry, Thomas Zagwodzki, Paul Titterton, Harold Sweeney, et al, "SLR2000: An Inexpensive, Fully Automated, Satellite Laser Ranging System," in this Proceedings.
2. Titterton, Paul, and Harold Sweeney," Correlation Processing Approach for Eyesafe SLR 2000," in this Proceedings.
3. McGarry, Jan.F, John J. Degnan, Paul Titterton, Harold Sweeney, Brion P.Conklin, Peter J. Dunn, "Automated tracking for advanced satellite laser ranging systems", in the proceedings from Acquisition, Tracking, and Pointing X, Vol. 2739, SPIE Aerosense, Orlando, April 1996.

Centimeter Eyesafe Satellite Laser Ranging

Using Raman Shifted Nd:YAG Laser and Germaniumm Photon Counter

B.Greene

Electro Optic Systems Pty Limited, Queanbeyan, NSW, Australia

H.Kunimori

Communication Research Laboratory, Nukui-kita, Tokyo, Japan

K.Hamal, I.Prochazka

Czech Technical University, Brehova 7,115 19 Prague, Czech Republic

Abstract

Centimeter eyesafe satellite laser ranging has been performed to a wide range of satellites using a Raman shifted picosecond Nd:YAG laser operating at 1543 nanometers and a novel Germanium single photon detector. The ranging has been accomplished for retroreflector equipped satellites up to an altitude of 30,000 kilometers, establishing link parameters through the atmosphere for this wavelength for the first time. The experiment paves the way for deployment of high power eyesafe lasers in space applications.

1. INTRODUCTION

Satellite laser ranging (SLR) is performed routinely by a global network of around 40 active stations. The precision of these stations is now at the centimetre level, and further improvements are anticipated in the future. SLR data has made major contributions to science in the past 3 decades in applications including geodynamics, crustal deformation, earth rotation, environmental studies, oceanography, relativity, and cosmology.

The technique of SLR involves satellites equipped with retroreflectors, tracked by ground laser stations equipped with a picosecond laser, tracking telescope, detector, and a timing system. Laser transmitters used up to now operate in the wavelength range 355 to 1064 nanometers, with pulse energies far above the eye safe (Maximum Permissasble Exposure) levels. The high power laser pulses transmitted by the station can represent a serious eye damage hazard to aircraft passengers and crew, and to the SLR station operators. The need for ground calibration extends this risk to people in the local area of the station.

To reduce the risk to acceptable levels, a strong set of safety guidelines are in force at most stations. Over billions of laser pulses sent into space, there has never been any injury from a pulse transmitted from an SLR station. However, as air traffic increases and is globally less regulated, as the tracking program multiplies in intensity, and as pressure is applied for reductions in operating costs, there is a clear need to render the SLR operations intrinsically harmless to humans.

An eyesafe SLR station is defined as one for which the emitted laser beam intensity is below statutory MPE levels. This can be achieved by reducing the transmiited energy of existing lasers (operating at 532 nm) by (typically) several orders of magnitude, which correspondingly reduces data yield and makes the tracking of high satellites (above 10,000 km) problematic. An alternative approach is to operate the laser

at another wavelength within the eye safety window near 1540 nanometers [1], where reductions in laser pulse energy to meet MPE criteria are not necessary.

This second approach has the potential to allow all traditional SLR applications to be maintained, and even expanded. The approach has been inhibited by several technical obstacles and uncertainties:

- the lack of a reliable picosecond laser source with (at least) millijoule pulses;

- the lack of a picosecond detector with suitable characteristics;

- uncertainty over the response of existing laser satellites to 1.5 um radiation; and

- uncertainty over the effect of various atmospheric conditions on link budgets at this wavelength.

Provided these difficulties and uncertaintanties could be overcome, the cost, productivity, and range of application of SLR systems and technology would be enhanced by migrating the operating wavelength to around 1.5 micron.

2. EYESAFE SLR DESIGN

The experiment was performed by adding a second (1.54 um) wavelength capability to a standard 532 nm SLR system (EOS SLR Version 3d) installed at CRL. Figure 1 shows the exerimental arrangement [2].

The 1.5 meter aperture tracking telescope is used to transmit the laser pulse to the satellite and to collect the returned signal. The same telescope aperture is used for both transmit and receive, by means of an optical switch comprising a rotating mirror synchronized to the laser firing.

The SLR system is capable of routinely tracking all satellites of scientific interest, and has an instrumental accuracy (ie excluding atmospheric dispersion correction) of around 1 mm at any range. using the Si SPAD (Single Photoelectron Avalanche Diode).

Routine SLR operations are normally carried out by transmitting 70 mJ in 150 ps (FWHM) of 532 nm radiation, and using the Si SPAD detector. This configuration typically gives a single shot precision of 15 mm. For this experiment, modifications were made to allow a second laser pulse at 1543 nm to be transmitted synchronously with the original beam, and to provide a second receiver channel at 1543 nm. No modifications were need to the SLR operating system, as it allows multiple satellite returns to be taken from two detectors.

The receiver was modified by adding a dichroic beamsplitter to create a second optical path to the Ge SPAD. The dichroic is placed so as to utilise the existing spatial filter. A bandpass filter and 532 nm block are also added to the 1543 nm channel. The use of a common spatial filter to which both detectors are aligned ensures that the satellite will be in the field of both detectors simultaneously.

The experiment requires at least 1 mJ of 1543 nm energy for useful data over a variety of atmospheric conditions and for various satellites. Considering the present picosecond laser technologies, the two principal alternatives to develop the laser transmitter are optical parametric techniques based on non-linear solid state devices (OPO/OPG/OPA), or Raman Shifted Laser (RSL). Preliminary experiments at SLR stations in Graz, Austria and Tokyo, Japan [4] were based on a RSL configuration which was further developed and applied here. For this experiment Raman stimulated emission provided 6 mJ of 1543 nm energy in 160 ps, using 50 mJ input energy at 1064 nm focussed into a Raman tube filled to 30 Bar with methane. The final beam divergence at the telescope was 10 microradians.

For this experiment, a Germanium SPAD (Ge SPAD) operated in Geiger mode with active quenching and gating [5] was developed. To reach the single photon sensitivity and subcentimeter precision the

photodiode is pulse biased above the break voltage. A similar detector (Si SPAD [3]) is in routine use at many SLR stations for 400 - 1064 nanometer wavelength SLR.

The Ge SPAD and electronics are housed in a custom-designed cryostat, allowing the detector to operate at 77K. The cryostat is a high-vacuum insulation design, allowing several days between liquid Nitrogen refills.

Detector performance was calibrated using calibration facilities at the Czech Technical University in Prague. The experimental Ge SPAD was determined to have the following characteristics:

- active area diameter   0.1 millimeter

- single photon timing jitter   32 picoseconds rms

- quantum efficiency   15% at 532 and 1543 nanometers

- dark count rate   1 Mhz.

Using ground target calibration facilities at SLR Station Graz (Austria), and ranging at 1543 nanometers using 30 picosecond pulse duration laser, these measurements were confirmed.

3. EYESAFE SLR RESULTS

The eyesafe SLR system described above was developed and installed at CRL between June 1994 and January 1996. SLR at 1543 nanometer range was achieved on January 11, 1996. The retroreflector equipped satellites Topex, Starlette, Ajisai, Lageos 1, Lageos 2, Etalon, and Glonas at distances 1000 - 20,000 kilometers have been ranged routinely since January 1996. Figures 2a and 2b show typical results from Lageos 2 and Ajisai respectively. The atmospheric dispersion effect can be noticed on Figure 2, as optical signals at different wavelengths experience different optical thickness of the atmosphere.

The Lageos satellite elevation above the horizon varied from 60 to 70 degrees during the pass on Fig. 2a and the Ajisai satellite elevation in Fig. 2b changed from 63 degrees down to 20 degrees.

The ranging precision was tested on a satellite with minimal target depth (Starlette) yielding 25 millimeters single shot precision, as expected for this initial configuration.

4. DISCUSSION AND CONCLUSIONS

- The respective signal return rates at 532 nm and 1543 nm are comparable, after consideration is given to output pulse energy, detector efficiency, detector area, and beam divergence.

- The calibrated response of the detector is 45 ps RMS per detected photon. However the observed satellite ranging precision was 165 ps [25 millimeters] RMS for a single shot, due to the laser pulse of 160 ps FWHM [which adds up to 90 ps RMS of uncertainty to the timing process] and Raman jitter. The pulse transmition epoch is referred to the Raman pump 1064 nm pulse, and therefore the overall ranging precision at 1543 nm is affected by the fluctuations in Raman generation process, which appears at different epochs relative to the 1064 nm pump pulse. Raman generation epoch fluctuations will reach a significant proportion of the pump pulse duration of 200 picoseconds.

- The results prove the feasibility of eyesafe SLR in the 1543 nanometer eyesafe window.

- The observed relative link budgets for 532 nm and 1543 nm for 2-way atmospheric transmission generally agree with predictions based on atmospheric transmission models, although more data is required over a wider variety of conditions to allow the separate model elements to be validated.

397

- The use of Raman techniques for reliable picosecond pulse generation over many millions of shots has been demonstrated. However operational limitations of the Raman technique, such as epoch jitter and conversion efficiency for picosecond pulses and parasitic anti-stokes conversion, remain to be overcome.

- The novel Ge SPAD detector can resolve sinlge photon events with 100 ps resolution. This detector is likely to find widespead use in photon counting over a broad spectral range.

- The response of existing retroreflectors in space to 1543 nm radiation has been established. None of the retroreflectors used were designed for or tested at this wavelength prior to launch, and the satellite response before this experiment has been unknown. It has been shown that the cross section for all satellites at 1543 nm is at least similar to the 532 nm cross section.

- As it has been demonstrated that SLR can be conducted within eye safety standards, unmanned and automated systems are now possible. This will expand the range of applications and the flexibilty of deployment of SLR and its derivative techniques.

- Routine two wavelength ranging measurements with picosecond accuracy [6] will contribute to the existing atmospheric refraction model verification and possible refining in the near infrared range.

5. Acknowledgements

References

[1]   American National Standard: Z 136.1-1993

       Japanese Industrial Standard: JIS C6802-1991

       European Community Standard: EN60825:1991

[2]   Kunimori H., Imamura K., Taka-hashi F., Itabe T., Aruga T., Yamamoto A., "New Development of Satellite Laser Ranging System for Highly Precise Space and Time measurements", Journal of Communication Research Laboratory, Vol.38, No.2, pp303-317, July 1991.

[3]   Prochazka I., Hamal K., Kirchner G., Sopko B., "Photodiode for Subcentimeter Satellite Laser Ranging Operating at the Room Temperature", Technical Digest Series, Proceedings of the Conference on Lasers and Electro Optics, CLEO '90, Optical Society of America, pp 138, 1990.

[4]   Kunimori H., Greene B., Guilfoyle J., Hamal K., Prochazka I., Kirchner G., Koidl F., "Subcentimeter eyesafe ranging", Technical Digest Series, Proceedings of the CLEO Pacific Rim '95 Conference, Tokyo, pp 17-18,1995.

[5]   Prochazka I., Hamal K., Greene B., Kunimori H.,' Large aperture Germanium detector package for picosecond photon counting in 0.5 to 1.6 um range', to be published in Optics Letters.

[6]   Prochazka, I. Hamal K., Kirchner G., Koidl F., "Atmospheric optical density measurement using multiple wavelengths picosecond satellite laser ranging", Proc. of the Conference on Lasers and Electro Optics CLEO'94, Teschnical Digest Series, Optical Society of America, paper CWQ3.
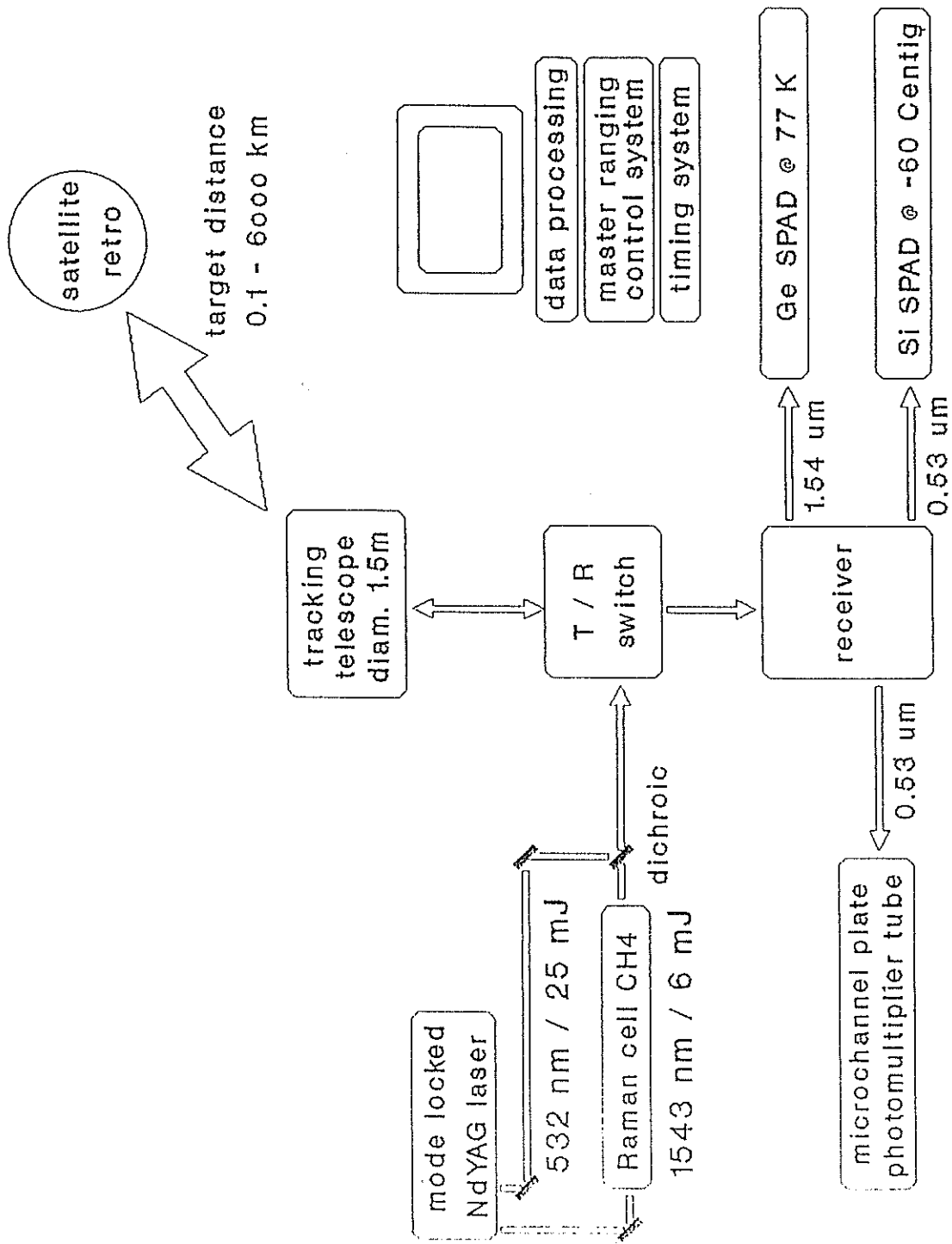
Figure 1: Satellite laser ranging station block diagram.
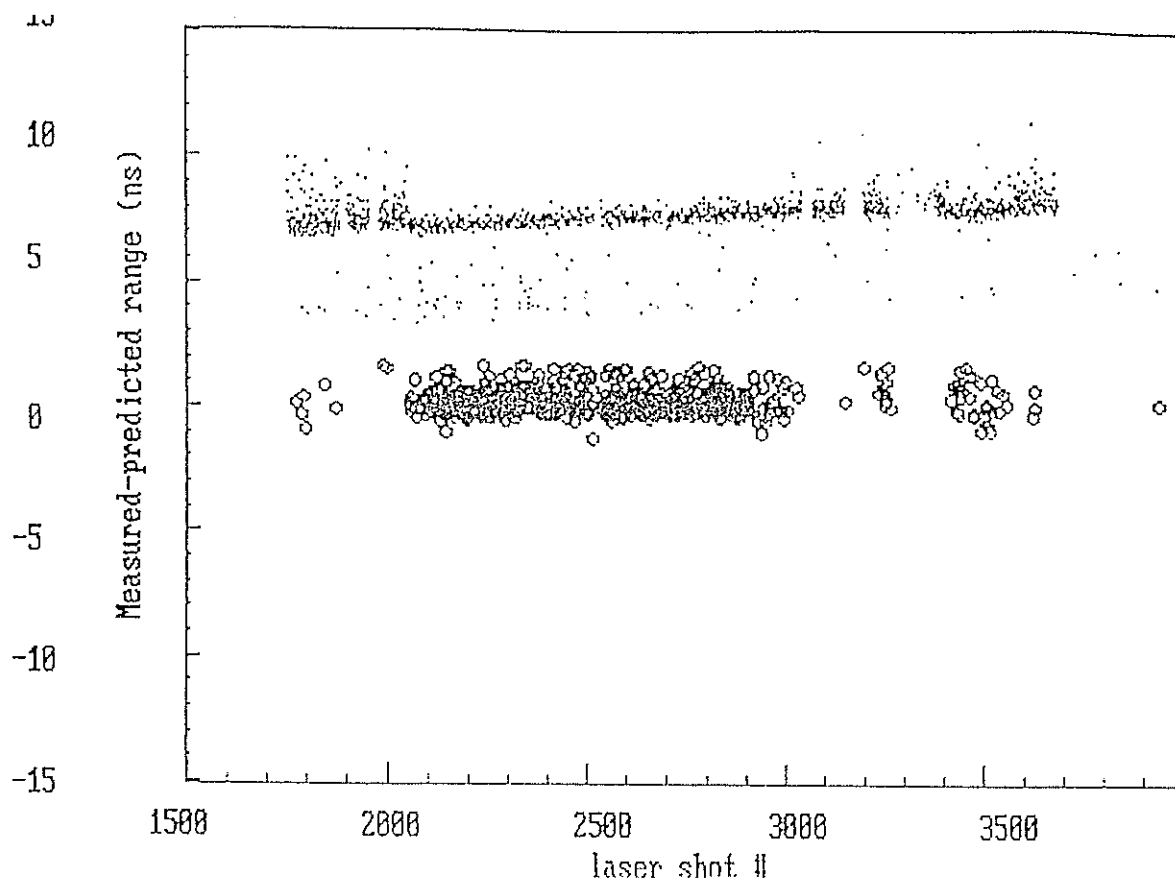
Figure 2a: Satellite Ranging Results, 532 nm [upper trace] and 1543 nm [lower trace]. Lageos 2 satellite, mean distance 6000 km,
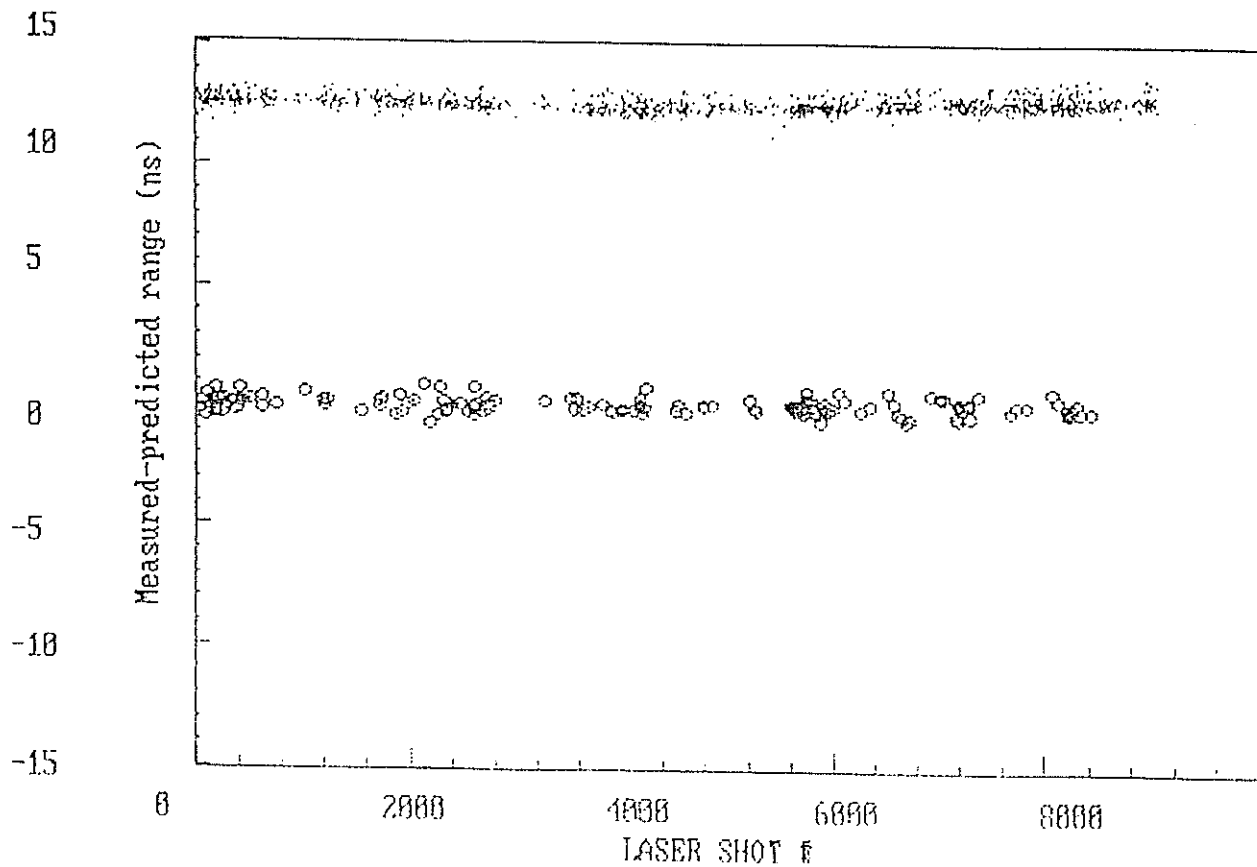
Figure 2b: Satellite Ranging Results, 532 nm [upper trace] and 1543 nm [lower trace]. Ajisai satellite, mean distance 2000 km.

401

Timing Devices

and

Calibration

Instrumentation Development and Calibration for the Matera Laser Ranging Observatory

Tenth International Workshop on Laser Ranging

Shanghai Observatory, Chinese Academy of Sciences

November 11-15, 1996

AlliedSignal Technical Services Corp.
Charles Steggerda, C. Bart Clarke, J. Michael Heinick, David McClure,
Michael Selden, Ray Stringfellow,

Italian Space Agency (ASI)
Dr. Giuseppe Bianco

Abstract

Three instruments are being developed for use with the Matera Laser Ranging Observatory (MLRO). These are: an event timer with picosecond resolution and less than 5 picosecond RMS jitter (after calibration), an eight-channel range gate generator with 20 picosecond resolution, and an eight-channel peak amplitude measurement device with 1 GHz bandwidth for each channel. These have been integrated with a calibration assembly to form the heart of the MLRO data measurement system. Initial results from testing of the event timer and range-gate generator will be described here. The peak amplitude detector prototype is still under development and no test data are yet available; however, its design properties will also be described here.

The MLRO system design required three instruments with performance not commercially available. These were an event timer with picosecond level resolution and accuracy to support time interval measurements to most SLR / LLR targets, a multi-channel range gate generator capable of providing range gate and simulation signals that can change dynamically at a high rate, and a multi-channel peak amplitude measurement device to allow for real-time laser diagnostics and modeling of amplitude-dependent systematic errors.

Event Timer

The event timer project was started in 1995. The development has been divided into two main phases: 1) the prototype development phase, which focused on developing a single-vernier prototype unit, and 2) the commercial instrument phase, currently in progress, which will result in a commercial-quality unit capable of supporting from one to four parallel verniers. Phase two will be completed by late spring 1997.
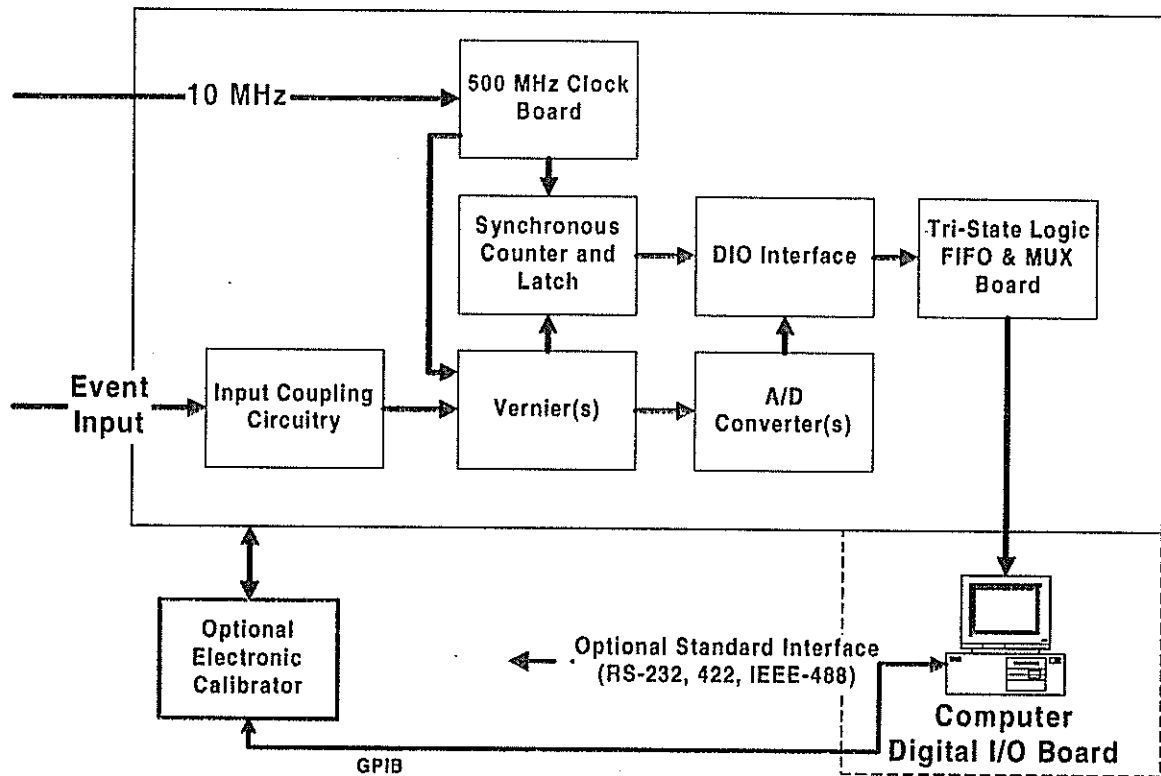
Figure 1: Event Timer Block Diagram

Event Timer Functional Description

A block diagram depicting the event timer as it will be offered in Figure 1. The event timer has been designed using predominantly ECL logic. It requires a high-quality 10 MHz input from a Cesium, Rubidium, or disciplined quartz standard. The event timer uses this input frequency to develop its internal 500 MHz clock. The internal clock drives a 26-bit synchronous counter resulting in a coarse count of 2 ns.

When an input event is received by the event timer, the vernier sweep is started and a synchronizer circuit is activated to select out the second 500 MHz pulse after the event. The selected 500 MHz pulse is used to sample the sweep for the A/D converter and to latch the count of the 26-bit synchronous counter. The resultant data from the two measurements provides ephemeris data with a resolution (for one vernier) less than 2 ps. The measurements are stored in 512-deep FIFO storage to be read by the computer. The system is capable of reading data at a 10 MHz rate until the FIFOs overflow. The speed of data flow is thus dependent on the computer I/O transfer speed, which is currently in the multi-kHz rate. Each vernier provides a measurement for each event, thus for 4 verniers the resultant resolution is 500 femtoseconds.

The event timer and its software are designed to allow for calibration of the small non-linearity of the vernier sweep. The MLRO system is equipped with an optical calibration and diagnostic assembly capable of modeling and testing the small non-linearity of the event timer vernier sweep. An electronic calibration assembly will be available (as an option) with the event timer to allow for automated calibrations.

Event Timer Features and Characteristics

Clock Speed (Internal)	500 MHz, 2 Nanosecond course counter
Channels	1 This is a single-stop event timer which uses the same electronics to measure each event. It can measure events in bursts of up to a 10 MHz rate.
Resolution	Better than 2ps per vernier, for a 4-vernier event timer the resolution is 500 femtoseconds.
Dead-Time	100 Nanoseconds (Minimum time between events measured)
RMS Jitter	Conservatively <10 picoseconds / vernier, however the vernier is capable of measurements of 3 to 4 picoseconds RMS jitter per vernier if calibration is provided. For a 4-vernier event timer we expect to see a 2-fold improvement of this number.
FIFO Depth	512 events can be stored internally to the event timer before being read by the computer.
Interface	Application-Dependent (Parallel I/O, IEEE-488, or RS-232)
Software	Measurement, Calibration, and Diagnostic software available for UNIX, MS Windows.

Event Timer Testing

The event timer testing has taken place in several stages using several techniques in both synchronous and asynchronous modes.

Electronic Pulse Test
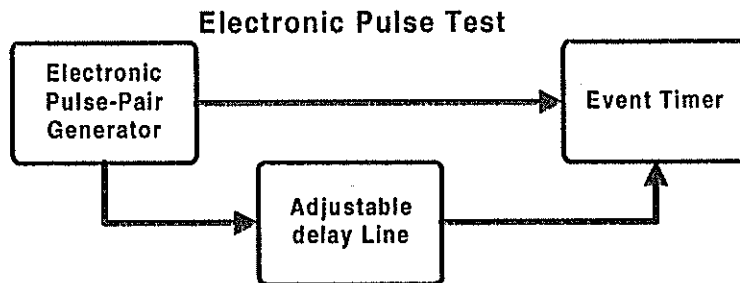
Figure 2: Event Timer Electronic Signal Testing

Electronic Signal Testing

The electronic signal testing is done in a synchronous fashion. One of the 500 MHz ECL clock signals is transmitted through an adjustable electronic delay line under computer control. A number of samples are taken at the various delay-line positions (delay-values). These allow us to map the linearity of the sweep signal over the 2 nanosecond dynamic range used for the measurement and to determine the single-event measurement jitter. This technique is the simplest test used and is especially effective for mapping the sweep linearity since it involves no external error sources.
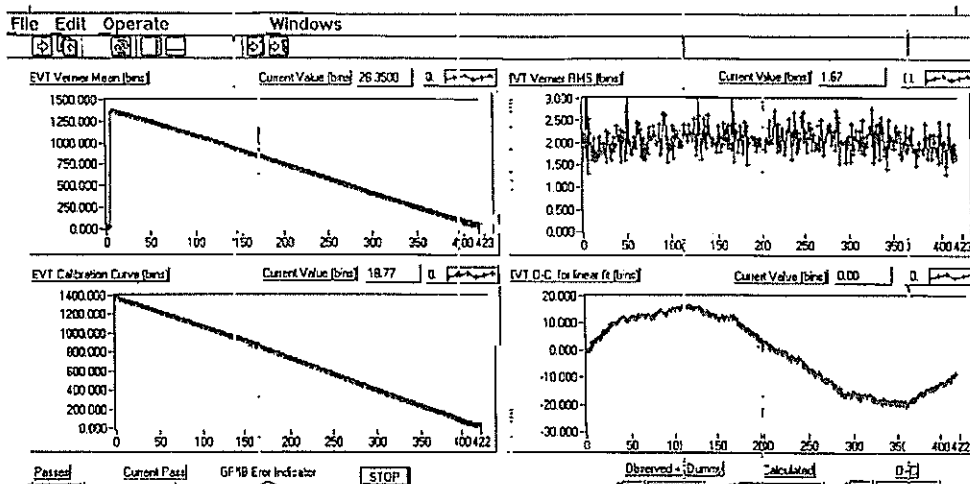
Figure 3: Event Timer Vernier Calibration Screen-Dump

The salient features of Figure 3 are the calibration offset and the RMS jitter. The lower right-hand panel displays the offset of the vernier measurement from the calculated range. The y-axis units are "bins" which represent a single bin-change of the vernier A/D converter truncated by the software (about 2 picoseconds). The upper right-hand panel displays the RMS jitter of the same data described in the offset plot. Forty samples were taken at each point along the curve and there is no data filtering -not even 3-sigma.
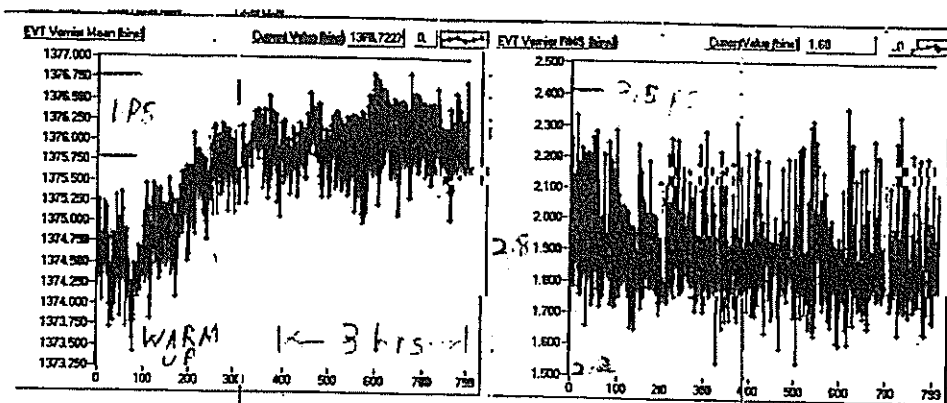
Figure 4 Screen-Dump from Event Timer Warm-up Stability Test

Figure 4 is a plot of the data acquired during a warm-up stability test. The most important features of this plot are the range stability plot (on the left) and the RMS jitter plot (on the right). For this test, the range measured was held constant and the event timer was switched-on from a cold start. The data were acquired over a six-hour period and 500 samples were taken for each plotted data point. The left-hand plot shows an increase in measured range as the event timer was warmed-up over a three-hour period. The total change in the measured value was less than 3 picoseconds. After the first three hours (the warm-up period) the measured range was stable. A hand-drawn pair of lines on the plot provides a scale factor of 1 picosecond. The right-hand panel shows the RMS jitter of each of the 500-point samples. Hand drawn figures indicates the scale where the y-axis

407

value is 2.2 picoseconds and 3.5 picoseconds. The average RMS value was less than 3 picoseconds for the test.
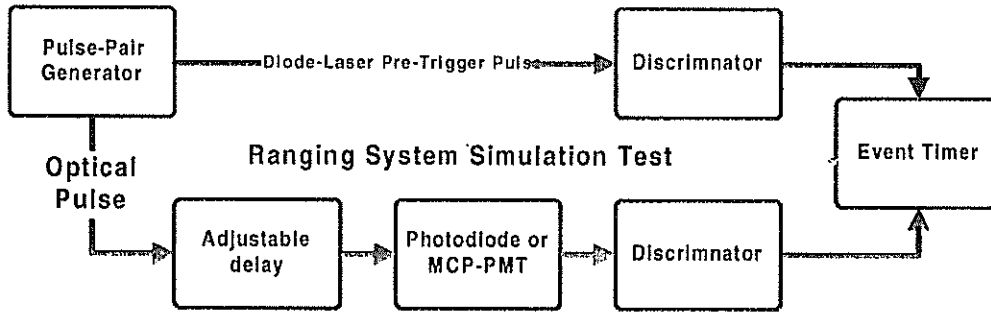
Figure 5: Optical Test Set-up

Optical Signal Testing

Optical signal testing is asynchronous and closely simulates the mode of operation experienced during laser ranging. A diode laser is used to provide a pair of pulses. The first pulse is generated by the diode laser electronics and is used to fire the diode laser. This pre-trigger signal (a simulated "start" event) was processed through a tennelec (Oxford) discriminator to provide an input signal consistent with the expected "stop" event; it was then coupled to the event timer. The diode laser optical pulse was sent through a computer-controlled optical delay, then coupled to an optical detector. The detector output signal was processed by a second discriminator channel, then coupled to the event timer. The Diode laser contributes 5 picoseconds of RMS jitter and the discriminator contributes about 7 picoseconds RMS jitter.
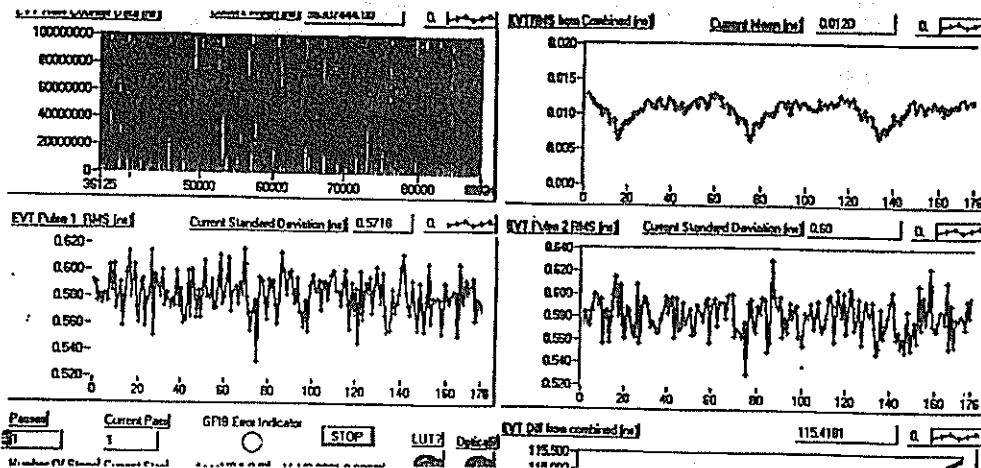
Figure 6 Event Timer Asynchronous Optical Test

Figure 6 shows an event timer test using an optical diagnostic cycle. For this test, the optical calibrator provides a series of different ranges under computer control and the event timer is used to measure the changing range. Each point represents one position and

500 samples. The most important panel of this screen-dump is the upper right-hand plot which shows the RMS jitter for the entire measurement system. For this test a rough (obsolete) calibration file was used and the resulting episodic pattern of the RMS jitter (between 6 ps and 12 ps) is a result of an obsolete calibration. The RMS jitter on this plot achieves a minimum when the point of the vernier sampled for the start signal is identical as the point sampled for the stop signal. Under these conditions (2 nanoseconds - or 1 clock-cycle apart) there is no calibration required to achieve maximum accuracy. This panel is representative of one of the types of diagnostics available for the event timer. This test provides data to show when it is necessary to recalibrate the event timer. A decision to recalibrate is based on a pre-determined threshold of error tolerance.
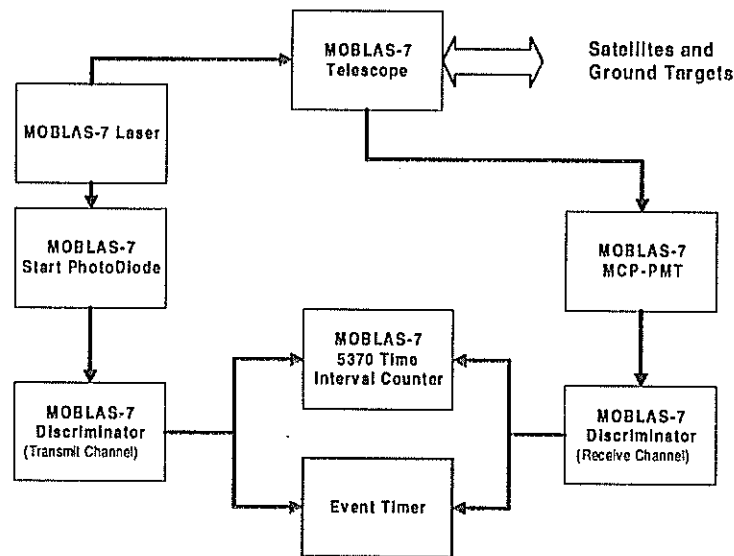
Figure 7 Event Timer SLR Testing

Satellite Laser Ranging Testing

Regardless of successful results from laboratory testing, the true test of an instrument or system is how it behaves in actual operations, rather than laboratory simulations. To provide a good understanding of the event timer performance, we placed the prototype into MOBLAS-7 as illustrated in Figure 7 and connected it in parallel with the operational HP5370 time interval unit. A number of satellite passes and ground target data were collected over a period of a week (on a periodic non-dedicated basis). Throughout the tests no calibration data were applied to the event timer; no corrects were made for systematic non-linearity of the vernier sweep circuit. A pure linear sweep was assumed through the sweep interval.

A summary of the results for the event timer SLR testing is shown in Figure 8. The event timer resulted in a 30% to 40% improvement in the overall single-shot RMS jitter for those satellites that were tracked. This feature can also be seen in Figure 9, which shows a comparison of the data scatter between the HP5370 and the event timer using single-shot residual plots for a LAGEOS-1 pass. The MOBLAS-7 counter data showed a 9 mm RMS jitter while the event timer measured a 5 mm RMS jitter. Figure 10 shows that the event

timer and the HP-5370 agree on the value of the range measurement. The scatter of the data is limited by the HP-5370 random error (jitter). Although there was also a significant improvement for ground target data, the overall improvement was masked by the MOBLAS-7 operational procedures. The operators deliberately vary the amplitude of the receive signal using an adjustable neutral-density filter wheel to simulate the full range of signal amplitudes experienced during ranging. This operational procedure results in a variable range dependent on the received amplitude. However, when the calibration data were divided into time-sequenced segments, the improvements became more evident.
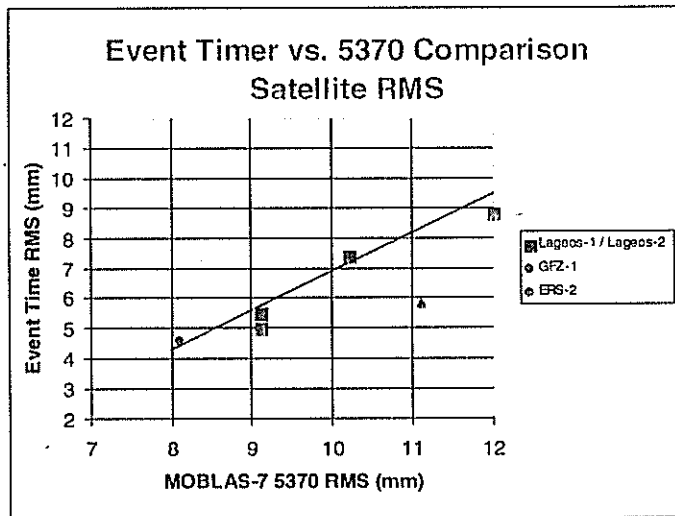
Figure 8 Summary of Satellite Laser Ranging Results
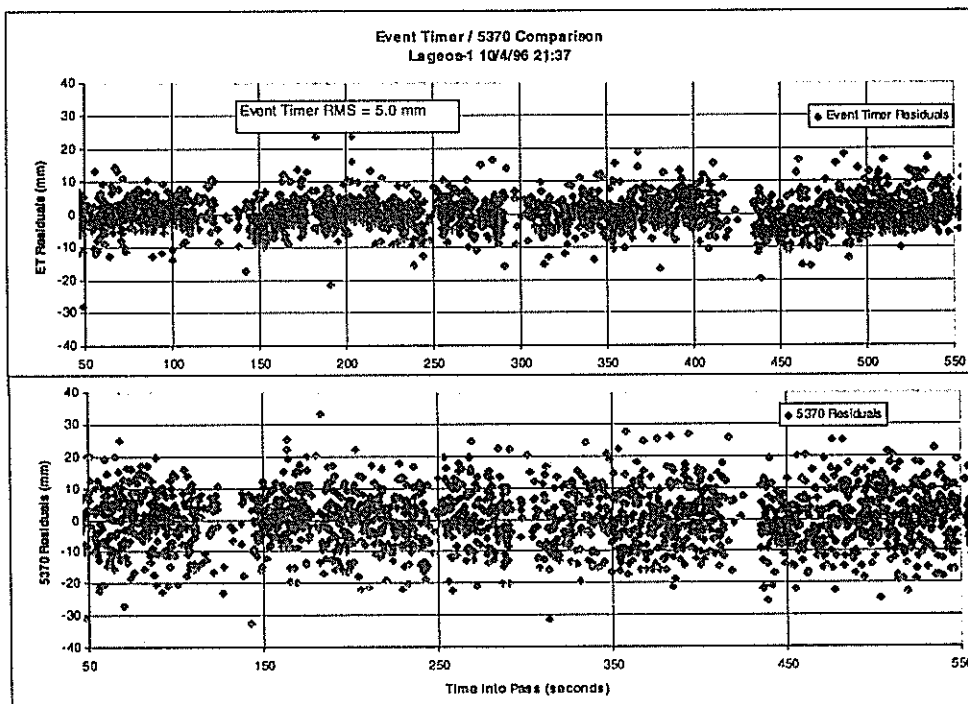
Figure 9 Shot-for-shot comparison of HP5370 and Event Timer SLR data for a LAGEOS-1 pass
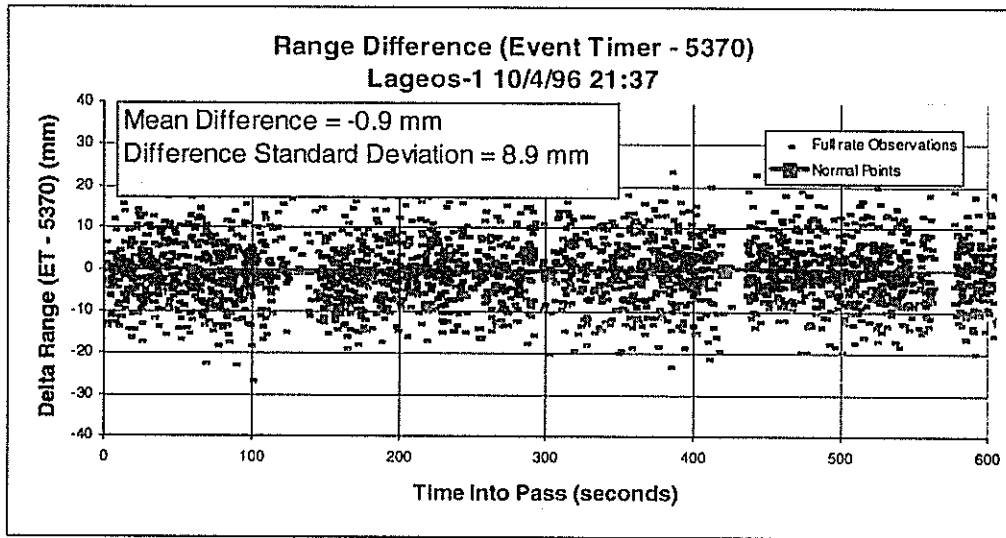
Figure 10 Plot of the bias range between the HP5370 and the event timer

Range-Gate Generator (RGG)

The range-gate generator has been developed to provide signals for gating and simulation. The MLRO will be equipped with two RGG units. A block diagram of the RGG is illustrated in Figure 11. The unit is provided a 10 MHz clock and a beginning-of-frame signal. Data for the next frame is loaded from the computer during the current frame. When the frame-clock signal is received by the RGG unit, the data is latched to the counter and verniers and the various channels each count until they reach their assigned time delay for 1) the start-of-pulse then 2) the stop-of-pulse. This allows for eight independent pulse delays and widths each frame from each RGG unit. The computer software determines which channels must receive start and/or stop signals each frame. This method allows for gating and simulations with ranges and widths varying each shot up to Multi Mega-Hertz frame-rates, only limited by the speed of the computer and its digital interface.
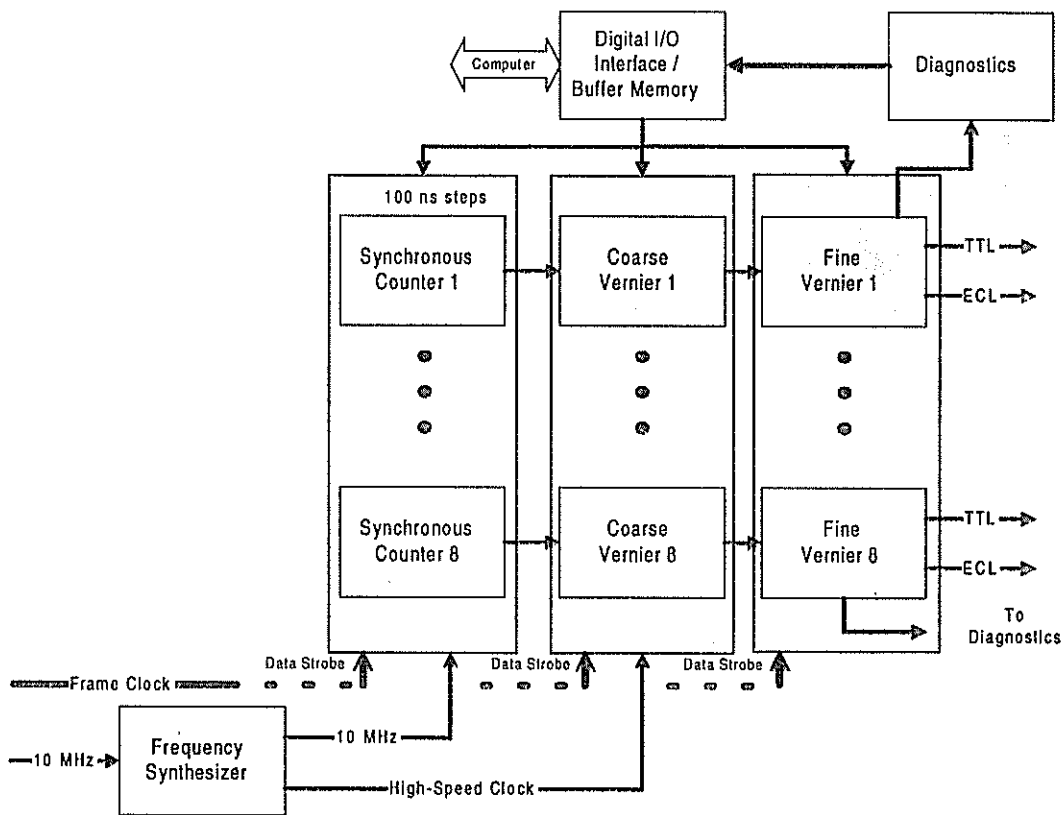
Figure 11: Range-Gate Generator Block Diagram

The RGG unit is equipped with an internal diagnostic circuit to check for the functionality of each channel upon request by the computer. Each of the vernier channels outputs both a TTL and ECL pulse each frame. The user may select which pulse is needed for a particular channel. The RGG

Range-Gate Generator Characteristics

Clock Speed (Internal)	250 MHz
Channels	8 Independent Channels with independently variable range and pulse width.
Resolution	20 picoseconds (leading edge), 500 ps (trailing edge)
Range	20 ns to Infinity (under computer control)
Output Levels	TTL, ECL
Maximum Repetition Rate	10 MHz (or limited by computer interface)
RMS Jitter	< 50 ps
Interface	Parallel Digital I/O, Can be provided with a PC for standard interfaces
Software	Measurement, Calibration, and Diagnostic software

Peak Amplitude Detector

The peak amplitude detector (PAD) is being developed to allow the MLRO system to calibrate and model amplitude-dependent systematic errors in the ranging data. In addition

to improving the data accuracy, the PAD will support real-time diagnostics of the laser and transmit/receive optics alignment.

The PAD is designed contains eight channels, each with a 1 GHz bandwidth. Each channel will measure the peak amplitude of a pulse with eight-bit resolution. The channels will be periodically calibrated using a 1 GHz waveform digitizer. Each channel also contains flags to indicate over-range and under-range values. The PAD is currently in the prototype development stage.

Summary

Three instruments are being developed for use with the Matera Laser Ranging Observatory (MLRO). These are: an event timer with picosecond resolution and less than 5 picosecond RMS jitter, an eight-channel range gate generator with 20 picosecond resolution, and an eight-channel peak amplitude measurement device with 1 GHz bandwidth for each channel. As part of the development process ATSC is thoroughly testing each unit to ensure that the instruments indisputably meet or exceed their design goals. These instruments are being designed to permit an increase in the accuracy, and reliability of the system while allowing for an increase in the laser repetition rate to support multi-kHz ranging.

MultiCounter Operation at SLR Graz

G. Kirchner, F. Koidl
Institute for Space Research / Austrian Academy of Sciences
Observatory Lustbühel; A-8042 GRAZ / AUSTRIA

1.0 Introduction

In the process of measuring distances to satellites with lasers, we found that at the moment the Time Interval Counter is the weakest point; the jitter contribution to the overall measurement jitter is the highest of all single elements, and there are essential bias problems hidden in counter non-linearities and counter temperature drifts, which are difficult and tricky to detect with a single counter. We therefore added additional SR620 counters - we were happy to have access to 3 pieces - to our HP5370A, operating them all in parallel (Fig. 1).

2.0 Hardware Setup for MultiCounter Operation

Instead of using only our old HP5370A counter to measure the time of flight of the laser pulse, we added up to 3 additional SR620's, connected just parallel to the HP5370A; all of them are thus measuring the same time interval (Fig. 1). All counters are supplied with identical start and stop pulses, which are generated with ultrafast comparators; this also ensures constant pulses (duration, amplitude, risetime etc.) for the counter inputs.
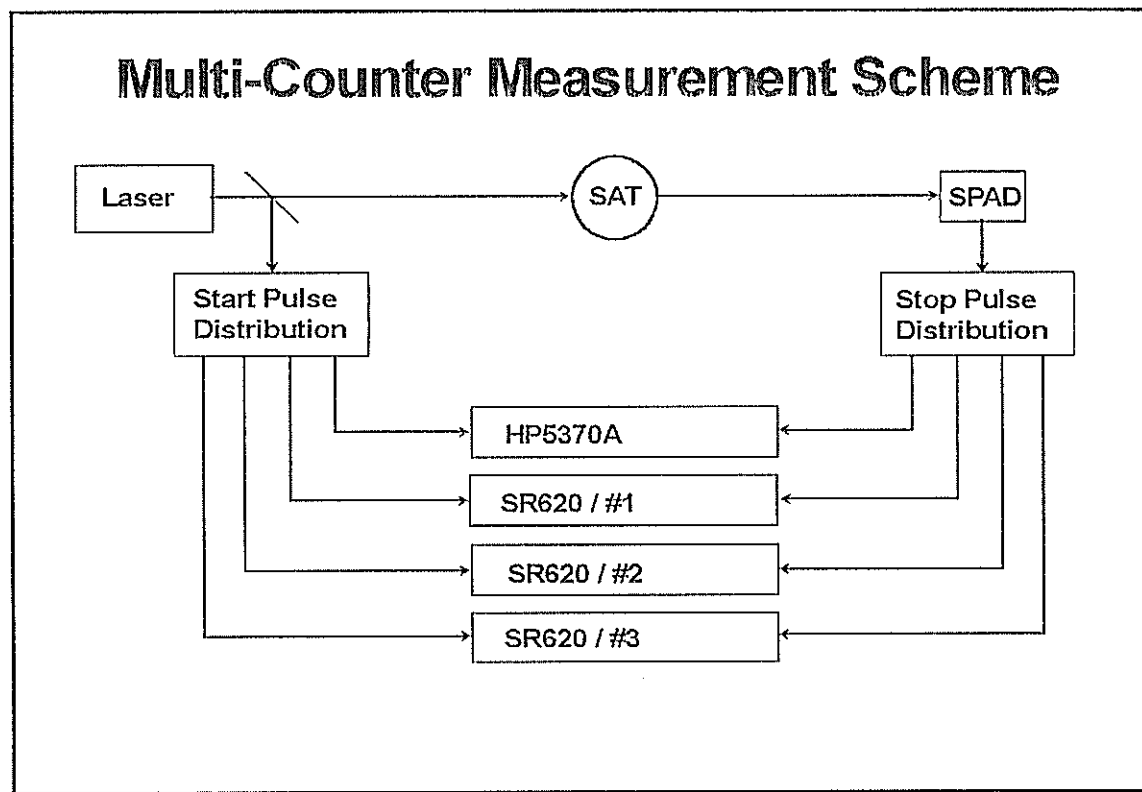
Fig. 1: Hardware Scheme for MultiCounter Operation

Although all counters get similar signals, and are measuring the same time interval, the results are different: the offsets between the counters are in the order of some Nanoseconds, due to non-identical trigger levels, different sensitivity of inputs etc.; this is no problem for Single-Counter-Operation (it is part of the calibration), but has to be handled with multiple counters. In addition, these offsets are not constant; their values are changing due to different temperature effects, cable or setup changes etc. We therefore decided to evaluate all relevant counter offsets automatically during calibration, ranging and post-processing.

In calibration, the result of all 4 counters are stored for each shot; after getting the desired number of valid target returns (usually 500), the differences between the HP5370A and the SR620's are calculated for each shot, averaged, and smoothed (iterative Sigma elimination); with the resulting mean offsets of the Stanford's with respect to the HP5370A, all Stanford results are corrected; for each shot, we then calculate the mean value of all counters; these values are then used for evaluation of the calibration constant.

One of the counters (SR620/#1) showed a typical non-linearity of almost 150 ps in a limited range (Fig.2); if the routine calibration would be done with this counter only and in this range, the calibration would result in a - difficult to detect - bias of more than 2 cm.

Due to such non-linearity problems, it would also be dangerous to use only valid target returns for counter offset determination; we therefore use ALL recorded points, including the intrinsic noise stops of the SPAD (covering a range of up to some ten μs), for this counter offset determination procedure.
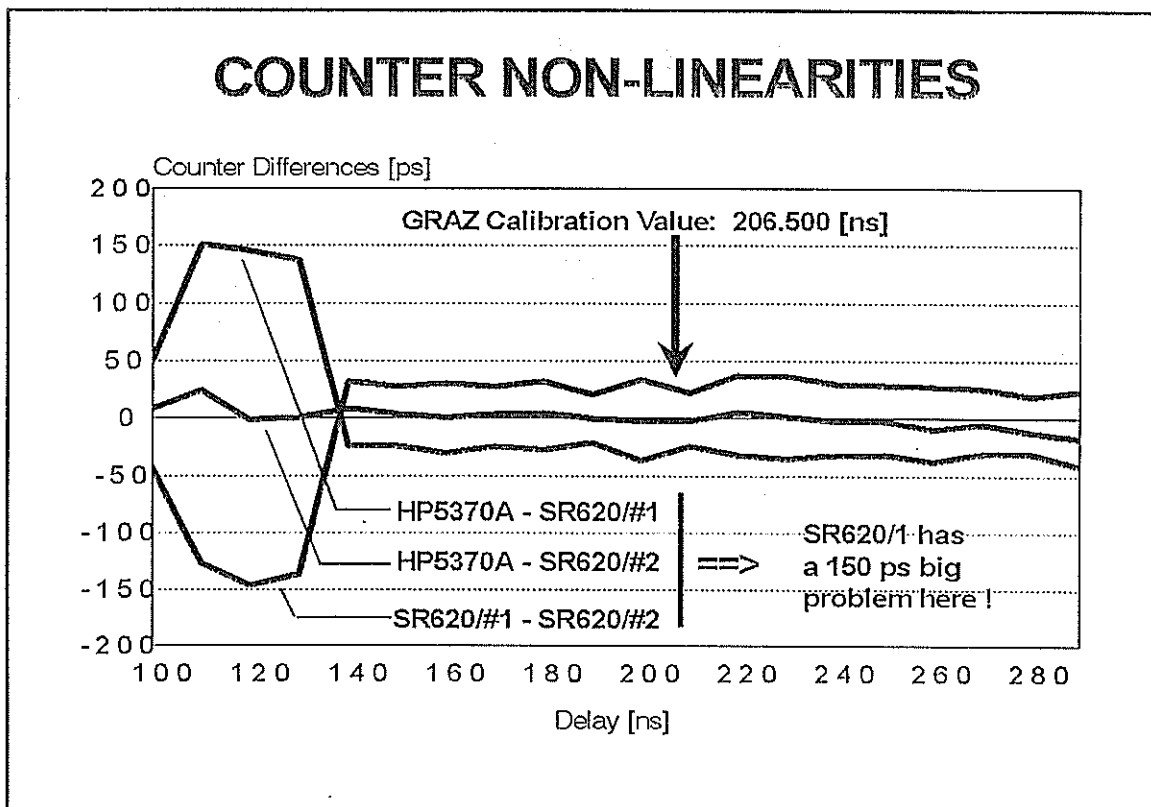
Fig. 2: Non-Linearity of SR620/#1

All counter offsets and corresponding RMS are stored and kept in log files for later access, checks, and comparison with similar counter offsets calculated during post-processing.

During actual ranging, the readings of all 4 counters are just stored on disk, without doing any calculations, offset determination etc. To form the residuals required for the real-time-display, return identification etc., it is sufficient to use the result of one counter only.

In post-processing, the program mainly performs the same sequence for counter offset determination, as in the calibration program: It reads all stored counter values, determines all offsets of the Stanford's to the HP5370A, averages and smoothes them, and subtracts these offsets from each single Stanford reading; then, for each return, the mean of all counters is calculated, which is then used for all post-processing. Due to the wide spread of measured time intervals (over the full range of each satellite pass), any non-linearities are more or less eliminated, and have almost Zero influence on offset determination.

As in the whole Graz software, theMultiCounter operation is made as flexible and easy to handle as possible; the number of counters to be used for any program is defined in an ASCII setup file; this makes it easy to add or remove additional counters. For each counter, there is also an ASCII setup file, where all specific programming codes are defined; thus it is easy to change/optimize e.g. trigger levels etc.

4.0 Experiences and Results with MultiCounter Operation

As example of another single counter problem, which was easily identified with the MultiCounter
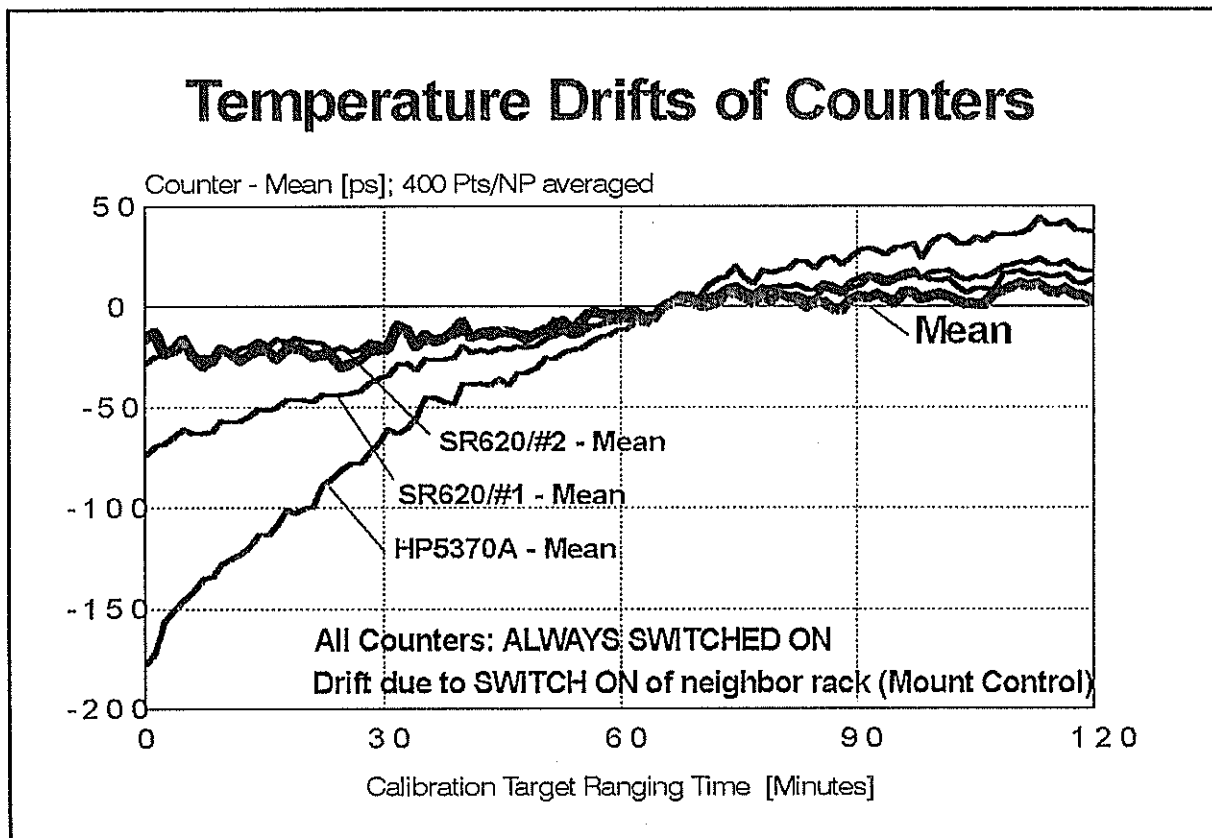
Fig. 3: Temperature drift of HP5370A, identified with MultiCounter Operation

operation, Fig. 3 shows a temperature problem of our HP5370A; although operated in an air-conditioned environment, the switching ON/OFF of the neighbored mount electronics rack at begin and end of ranging sessions caused a slow change of the counters cooling air temperature of up to 4° C (within 1 or 2 hours); this caused a corresponding drift of about 200 ps (more than 3 cm in range!) of the HP5370A measurements; although the major part of such a drift is eliminated by pre-/post calibrations, small portions of this error always remain, and are in general highly undesirable.

Another - more tricky to detect - problem was identified also with the MultiCounter system; as mentioned above, all counter offsets - evaluated in calibration and ranging/post-processing - are stored in log files; as there is no change in setup between calibration and ranging to all satellites, all corresponding counter offsets should give the same values; however, there appeared a significant difference between low satellites and LAGEOS (Fig. 4).
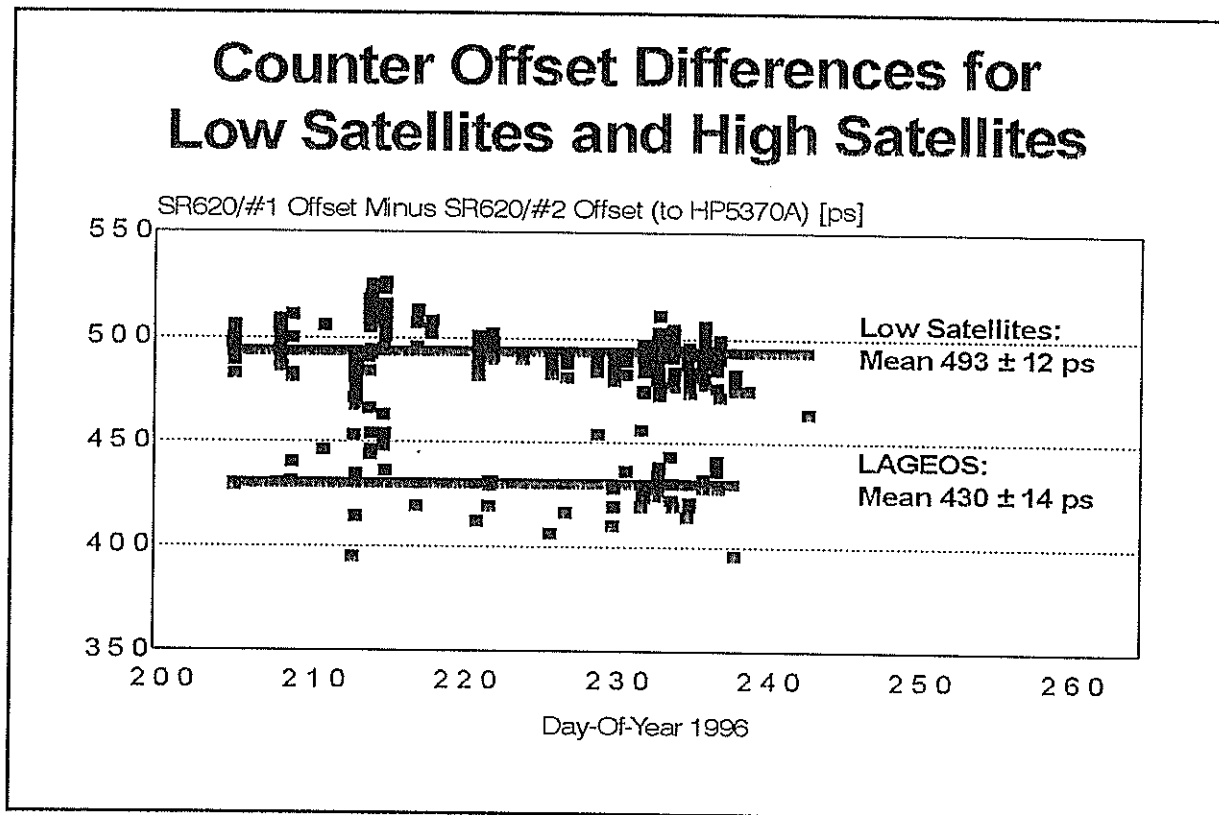
Fig. 4: Counter Offset Differences for different satellites: Should be the same ....

After some more tests we found the reason (although not the explanation): We always used some form of daisy-chaining to supply the external 10-Mhz frequency to the counters; with the single counter system (HP5370A only) of last years, we supplied our range gate generator (HP5359) with the external 10 Mhz, and used its output (its internal quartz oscillator, slaved to the external reference) as external frequency source for our HP5370A. With the MultiCounter system (up to 4 counters), we supplied the first counter with the external 10 Mhz, using its slaved quartz oscillator output for the next counter, and so on. This caused a variable bias in the whole LAGEOS range (38 to 60 ms) of up to more than 2 cm, for the first counter; for the second

417

counter, the effect was smaller; for the next counters, it disappeared; for the low satellites range (5 to 15 ms), these effects were much smaller.

Realizing these problems (although we still do not have an explanation), we started to supply each counter with its own, independent, external frequency source (October 1996); as a preliminary result, the SLR Graz range bias, as published by the University of Texas, changed significantly [1]: Before October 1996, it was unstable, and ranging from -20 to -30 mm; since October 1996, it is more or less fixed at -13 mm, with weekly variations of less than ± 2 mm.

In conclusion, we found the following advantages of using multiple counters to measure the time-of-flight:

- Any possible biases caused by a single counter are detectable, can be minimized or can be avoided completely with a MultiCounter system;
- The improvement in Single Shot RMS is significant (Fig. 5); including our Automatic Time Walk Compensation Circuit, we get now below 5 mm RMS from ERS-2;
- Compared to the total cost of the SLR station, or to the cost of currently developped epoch timers, the cost of MultiCounter operation is relatively low, fully scalable, and helps to avoid or at least to minimize all - possibly undetectable - bias problems;
- Due to a flexible software, it is easy to install or remove - borrowed - additional counters.
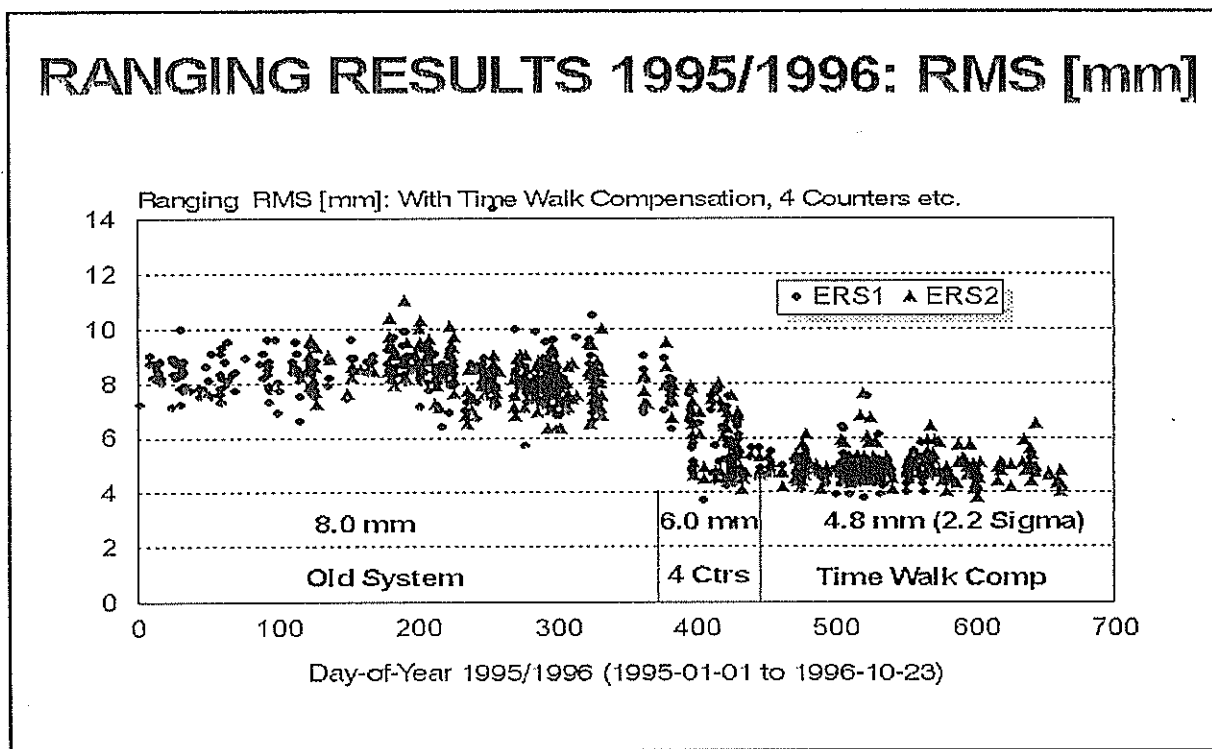
Fig. 5: Single Shot RMS Improvement of ERS-Ranging, using MultiCounters etc.

References:

[1]   EUROLAS Cluster Stations: Bias Workshop Results. G. Kirchner, F. Koidl; in these Proceedings.

Femtosecond Timing of Electronic Pulses for SLR

Ben Greene, Leigh Dahl,
Electro Optic Systems Pty Limited, Australia
Josef Kölbl
Electro Optic Systems Gmbh, Germany

Abstract

A system methodology for the electronic timing of pulses with 100 femtosecond resolution and 300 femtosecond accuracy is presented. The calibration and timing systems to achieve such performance are also discussed.

1. INTRODUCTION

Advanced technology componentry provides significant benefits to the performance of electronic timing systems. Electro Optic Systems (EOS) has developed new products which supersede the traditional timing systems and their architectures, and these are now being incorporated into our Satellite Laser Ranging systems such as the Keystone network in operation in Japan. Work is currently being undertaken which should take the performance of such timing systems below the picosecond threshold before the turn of the century. Timing system development at EOS has achieved the performance levels shown in Table 1.0. Current developments will soon produce systems for electronic timing of pulses with 100 femtosecond resolution and 300 femtosecond accuracy.

		1985	1990	1995
Precision	(ps)	40	20	10
Accuracy	(ps)	6	2	2
Stability	(ps/hr)	5	1	1

Table 1.0 : Progress in Electronic Timing Systems

Although the terms referred to in the table above are commonly used by the SLR community, it is important that they are clearly understood. The **accuracy** of a laser ranging measurement is the *absolute correctness of a measurement* which is an error term defining the difference between the true range and the measurement obtained. The **precision** is a parameter describing the error distribution of a set of samples, usually the standard deviation of a Gaussian distribution. It is used specifically to define the distribution of individual measurements relative to their mean and is dependant on the measurement resolution and stability. The measurement accuracy of the single sample will comprise of the summation of the random errors described by the system precision plus the systematic range biases. The system bias will be produced from a combination of a number of system error sources with finite stabilities, and these will produce a deviation from an accurate value. The "jitter" of a timing pulse is a reflection of the signal noise, and this parameter can be quantified from an analysis of the standard deviation of a signal's delay measurement. A list of the timing terms used in SLR is documented in the Appendix .

A timing system measurement precision can be improved by obtaining more samples, but this compromises the effective data rate of the system. To achieve the desired accuracy in realtime, the precision of the measurement must also improve down to picoseconds. Timing systems performance of this order, and simultaneous developments in the design of next generation

satellites, atmospheric modelling techniques and data analysis will give significant benefits to earth science and geodesy.

The following graph shows the predicted development path over the next three years ("System 2").

Femtosecond Timing of Electronic Pulses

Each of the electronic component elements in an electronic timing system have defined trigger level or threshold settings that are not infinitely stable, whether TTL, CMOS, ECL, or NIM. The noise on each threshold will contribute to the overall system jitter. As well as noise these thresholds are affected by environmental changes such as temperature, so it is desirable to minimise the uncertainty of these trigger thresholds by:

- minimising the number of critical path components ie. thresholds.
- reducing component noise by decoupling, regulation and filtering
- and maintaining fast risetimes on the transitions thereby reducing the probability time distribution of the uncertainty period.

This must be achieved without impacting on the performance through unwanted side effects such as increased RF noise levels. As well as the threshold noise any electronic circuit will have a noise produced from the resistive elements. These are well characterised as shot, Johnson, and flicker noise. The discussions and equations for calculating the noise from such sources is well documented in texts describing electronic design theory.

There are other causes of a signal jitter besides that of the threshold and signal noise. For example, the simultaneous switching of a circuit's outputs which induce a "ground- bounce" on the component and introduce an indeterminate offset in the resultant waveform. Metastability is another problem in logic design which is produced when asynchronous timing signals are presented to synchronous logic inputs. Other issues which must be considered are signal line reflections due to finite impedance matching tolerances, any impedance discontinuity in a circuit (such as Printed Circuit Board PCB tracking), signal under and/or overshot, cross talk, and electromagnetic interference.

Following examination of the issues identified above, the design engineer can set about to reduce the contributors of limited system performance, through application of RF and high-speed design techniques. The techniques which should be employed in system design include:

- the use of low impedance PCB grounding achievable with multilayer PCBs
- the use of differential signal drivers whenever possible
- controls on PCB design and fabrication to ensure the controlled matching of signal line impedances
- the use of low ohmic impedances hence a reduction in resistive noises
- the exclusive use of system components with low noise figures
- employing fast transitions and slew rates to minimise the jitter probability function

Miniaturisation in fabrication processes which lead to an integration and subsequent reduction in the size of the design also improve timing system performance. This is because medium scale integration (MSI) device designs do not achieve matched line impedance terminations without finite tolerances. They also have longer signal propagation delays and higher skew, which limits bandwidth and are subject to larger temperature dependencies. If the rise-time t_r of a pulse is less than twice the propagation delay of a track t_{PD}, then the track has to be terminated with the characteristic impedance of the line according to the transmission line theory:

$$t_r \leq 2 \cdot t_{PD}$$

As an example, consider the following: when transmitting a pulse with 100 ps rise-time the design requires a matched termination at the receiver end when it is transmitted along a PCB track as

421

short as 7.5 millimetres of length (for typical FR4 PCB material with $\varepsilon_r \approx 4$). Hence, circuit integration technologies should be employed in both the analogue and digital domains through high density programmable gate arrays, multichip modules (MCM), flipchip and, full-custom application specific integrated circuits (ASICs). This digital integration permits an increase in the clock frequency at the same time reducing the dynamic range of the analogue vernier component of the timing systems. Hybrid analogue design techniques not only reduces propagation delay and skew but allows for laser trimming of discrete components. ASIC and analogue hybrid technology does require an engineering investment, but by observing such issues and using general components with tight tolerances performance improvements can still be made.

The sources of signal jitter can be identified and categorised into different types, such as: synchronous modulated, asynchronous modulated, cycle to cycle, input/output, long term, and systematic jitter. Increases in the precision of the electronic timing modules can be achieved by reducing system noise from signal and thresholds and maintaining the rise and fall times in all electronic pulses. By using the maximum circuit bandwidth available for the transmission of these signals the probability of distribution of trigger uncertainty is reduced. The SLR range measurement error consisting of the measurement precision plus the systematic bias, can be reduced by minimising the electronic pulse jitter.

2.2 MEASUREMENT TECHNIQUES FOR QUANTIFYING CIRCUIT JITTER.

High bandwidth digitising and sampling oscilloscopes can be used to quantify the jitter inherent in an electronic circuit by using a test signal source which is repetitive in nature. These instruments use sequential repetitive or random repetitive sampling techniques to acquire the jitter histogram of the pulse. There are a number of vendors marketing equipment in the order of 10 Gsamples per second, for example LeCroy with the Model 9362, HP with the 54750, and Tektronix's CSA803. Jitter analysis equipment can also by utilised from the optical and RF communications fields. One such device is from the US company Wavecrest who have a dedicated jitter and pulse analyser (Models DTS2070 and DTS2075) for the time and frequency domain. This type of instrument is designed with the internal trigger jitter requirements which otherwise limit the measurement accuracy.

The time interval counters from Stanford Research Systems (SR620, SR625) which are commonly used in the SLR community also incorporate features to measure signal jitter. The internal jitter of the SR620 when used in time interval measurement mode with a signal risetime of 500ps is in the order of 20ps rms. Any such jitter measurement must also be analysed in terms of the statistical processes under which it was made and for any timing system be referenced appropriately back to the circuit input. This last point is important as the test signal used will also have a finite jitter which is not a part of the timing system under test and may vary from that used in ranging systems ie. Rubidium, Caesium or other high stability oscillator source.

3. Timing Circuit Calibration methodology

	Stability	Precision	Accuracy	Continuum
Passive Cable	✓	✓		✓
Optical Delay	✓	✓	✓	✓
Electronic Delay	✓	✓	✓	✓

Table 3.0 : Calibration Systems for Electronic Timing

There are a number of calibration methods which can be used to calibrate electronic timing systems, and some of these are shown in Table 3.0. It is important to address terms like stability, precision (see jitter above), accuracy and continuum in calibration. Stability is defined as the repeatability of controlled delays over a specified time interval. The stability of passive cable delays for instance, is poor due to changing following connector mating cycles. When implemented correctly all three calibration techniques can be made to produce continuum delays, which means the adjustable calibrator reference delays are never subject to discontinuities.

3.1 THE OPTICAL CALIBRATOR TECHNIQUE

The optical calibration setup is traceable to the International Standard (the speed of light as defined by the metric standard), but must be implemented in the correct manner to attain these performance requirements. The following diagram demonstrates the basic concept of the optical calibration setup implemented in our developments:
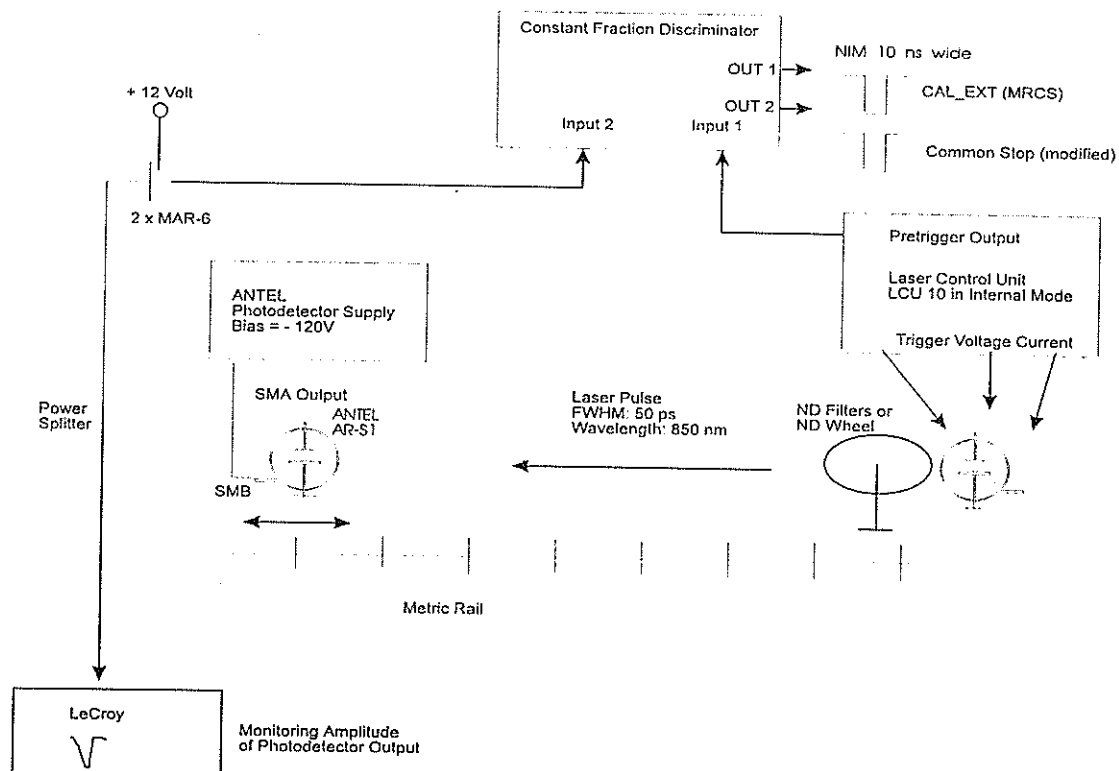
In this example, a picosecond laser is used to produce short laser pulses (FWHM 50 ps) at a repetition rate of about 1 kHz. The wavelength used is 850 nm. A standard silicon photodetector is placed on a movable micrometer screw along a metric rail. The maximum distance must be sufficient to cover the operating dynamic range of the timing system.

The problems we encountered in the early development of this setup included a change in the output amplitude of the detector diode along the rail. This introduced a time error which was reduced by the constant fraction discriminator but not eliminated. The adjustable natural density filter wheel was then introduced to keep the photons seen by the detector diode at the same amount. The result being that the output of the photodetector diode will stay at a constant voltage

along the rail. The output was monitored by the oscilloscope for verification. The jitter between start and stop pulse with the original configuration was typically less than 20 ps rms. Calibrating the timing system down to 1 ps is then a statistical process achieved by acquiring at least 400 samples.

3.2 THE ELECTRONIC CALIBRATOR TECHNIQUE

Electronic calibrators are less expensive to produce, easier and faster to set up and operate, and allow calibration as the routine rather than the exception. Full automation of calibration procedures eliminates human error. Nevertheless, each electronic calibrator has to be calibrated against the International Standard.

First generation electronic calibrators employed were based on a programmable controlled crystal oscillator driven by a stable reference frequency. The implementation of such a system is based on programming the oscillator to produce precise time delays which are then offered into the timing system through electronic switches. These calibration pulses are provided via the same path to the timing system as that used by the real detectors for symmetric ranging systems.

Second generation calibrators are based on charge controlled switch devices. Delays from a few picoseconds to over 10 nanoseconds, adjustable in hundreds of femtosecond steps, have been shown to be possible with this system. The time jitter associated with these type of electronic calibrators is typically less than 5 ps rms. In the process of developing electronic calibrators and an optical calibration setup it is extremely important to consider ultra-low noise design and RF design techniques.

4. SUMMARY

Using such design principles and methodologies we shall be able to improve the performance of the SLR timing system beyond the state of the art currently available in commercial timing instrumentation. Subpicosecond accuracies are attainable due to advances to the technology available and by following the design methodologies outlined. As can be seen in the following screen capture from the Keystone system the 10 ps (one-sigma un-filtered) timing system precision has already been achieved.
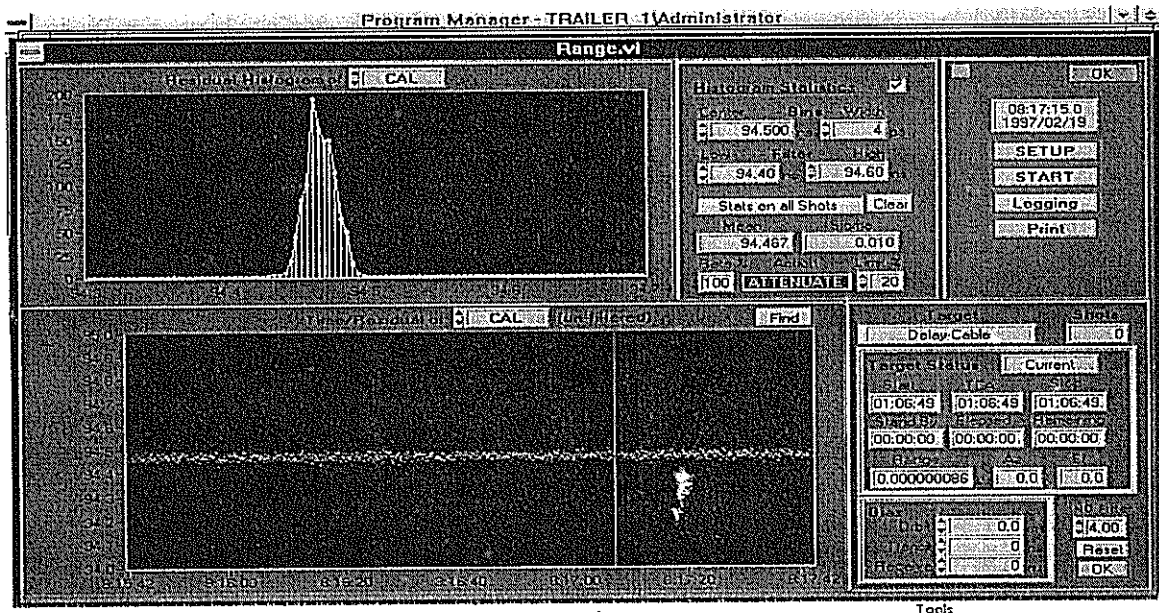
5. APPENDIX : DEFINITION OF TERMS

ACCURACY

A quantative term for the measurement to the true value of a parameter within declared probability limits. Range measurement accuracy is the measurement error. That is the difference between the true range and the measured range to within a specified measurement tolerance.

RESOLUTION

Range measurement resolution is the minimum differential measurement which can be made irrespective of accuracy or precision. Resolution is the difference between two adjacent measurement points or the smallest element in a measurement reading.

PRECISION

Range measurement precision is the standard deviation of the measurement about the true measurement or the root mean square variation of measurement.

SENSITIVITY

Sensitivity is the measure of the dependency of one parameter on another or the ratio of particular output parameter to corresponding input change

STABILITY

Repeatablity of a process over a certain time otherwise the variation of measured output under specified constraints.

JITTER

Jitter is a random displacement of a signal from its true location in time. These displacements can occur in amplitude, phase, and pulse width, and are generally categorised as either deterministic or random. This term applies to the time of an event often start and stop times which the uncertainty of rise and fall times may then affect.

BIAS

Offset to a quiescent point (ie zero voltage) or in SLR bias can be used to describe systematic deviation from an accurate value. Particularly common in statistical estimates of parameters

DETERMINISTIC

Deterministic means non-random ie determined or initiated by a known or controlled event. This refers to an action or event. ie it is determined or initiated by a known or controlled event

SYMMETRIC RANGING

Measurement of related events (T1 T2) via the same optical and semiconductor (vernier) path to cancel systematic errors.

WLRS Timing System Aspects

Ulrich Schreiber
Forschungseinrichtung Satellitengeodäsie
Fundamentalstation Wettzell
D - 93444 Kötzting
Germany

Karl Heinz Haufe, Nikolaus Brandl, Reiner Dassing,
Günther Herold, Günther Pochert, Dieter Feil
Institut für Angewandte Geodäsie
Fundamentalstation Wettzell
D-93444 Kötzting
Germany

Abstract

One of the most crucial elements in a laser ranging station is the timing system. It determines the achievable resolution in the time of flight measurement of the laser pulse in general. However, quite often the timing system is responsible for small scale systematic errors in the range measurements. These errors can be the cause of persisting bias effects for a station. Therefore the properties of the timing system [1] of the WLRS (Wettzell Laser Ranging System) have been studied in detail. This paper discusses some of its characteristics.

1. DESIGN OF THE EVENT TIMER

The 5 MHz output of a hydrogen maser source is multiplied to 50 MHz and fed to the master ranging controller. This clock signal represents a stable coarse epoch of 20 ns granularity. The fine epoch, which interpolates between these intervals is generated on the occurance of a stop event. The estimation of this fine epoch is based on the charged capacitor principle, where the short timespan between the recorded event and the next clock signal is used to charge a capacitor. This capacitor is discharged at a constant rate over a far longer time interval (approx. 2000 times longer) afterwards, so that the time of the electrical discharge is easy to measure. This means that time is proportional to the voltage on the capacitor and the timer must have a very linear relationship between time and voltage. The WLRS uses 3 time to digital converters (LeCroy 2229) for this purpose and their respective non linearity was found to be below 10 ps over the entire operating range.

Since the WLRS uses a realtime calibration along with the range measurement, it is an absolute necessity to have the same electrical path for both signal sources, down to the level of individual circuit components. This demand results from the effect, that the travel

426

time of say the rising edge of an electrical signal through the timer circuit is of the order of roughly a hundred nanoseconds, while differences in the timing of events are significant at the level of less than 10 ps.

2. CALIBRATION AND STABILITY

For ranging operation, it is absolutely mandatory to perform a precise calibration of these fine epoch timing devices now and again. This is preferably done by using an optical rail, where increments in the time of flight are achieved by increasing the distance between the pulse laser and the detection device, as a retroreflector is pushed along a rail. Figure 1 sketches the principle of the optical setup. The high energy laserpulse passes through a wedged window on its way towards the telescope. The return from one of the antireflection coated window surfaces is guided along a rail, where it bounces back from a corner reflector. The returning light passes through the window again and passes a diffusing window, before it is detected by an avalanche diode, operated in linear mode. Even under non saturated conditions this diode responds with a very sharp risetime of less than 200 ps. The repeatability of a measurement was shown to be less than the resolution of the timing unit, once the diffusive window was inserted. Without this window there were numerous miscounts obviously due to spurious contributions from the laser signal.

Usually this calibration of the slope of the fine epoch generator is very stable, so there is no requirement for frequent updates. On the other hand one finds significant variations in the time of flight measurement for a geometrically constant reference path. This can be as much as 4 cm over a period of a few weeks, down to a few mm within an hour. The cause of this is temperature variations in the ranging electronics. Ideally all the timer electronics should be temperature stabilized to the level of a tenth of a degree over a few days. Since there are a number of heat dissipating units inherently part of the timer, the temperature level is not very well maintained. Figure 2 shows the behaviour of the temperature on the sensitive part of the timing board of the Master Control Ranging unit. One can see changes in the temperature of the electronics of up to 3 degrees within less than 20 hours. The duty cycles of the airconditioning system are also clearly visible in this time series. Since the timer is built such that it frequently performs a new slope calibration of the verniers by the use of internal electronic delay lines, a similiar temperature dependence was expected. Figure 3 shows how the observed variations in the temperature affect the calibration of the time to digital converters. Taking into account, that the shown calibration runs are only taken during two time intervals of the temperature sequence of figure 2 marked with A and B on the plots, a very strong correlation is evident. For example, calibration run A yielded an offset of $0.0001 \frac{ns}{count}$, which corresponds to change in the range measurement of 130 ps. A comparison between a number of these internal calibrations and some intermediately done absolute optical calibrations showed that these changes can be basically related to the temperature behaviour of the internal delay line electronics. Therefore the internal calibration feature was disabled.

Since the temperature dependence of the signal transit time through electronic components is a general problem, similiar behaviour was found for two crucial sections within the event timer. These sections are the time to digital converters for the fine epoch and the control circuit, which directs the detection signal to its respective receive channel. A sudden

increase in temperature of about 3 degrees was introduced to the respective circuits. A drastic effect of far more than 100 ps were found for both as one can see from figure 4 and figure 5.

The effect on the range measurements however is not as dramatic as discribed above, since it affects both calibration and range. On the other side it causes a floating value for the (constant) calibration measurement from pass to pass, which in turn makes a clear diagnosis of the system's operational state impossible. A general remedy for the addressed problems for the given event timer can not be made easily, since all the timing related components are made from individual logic circuits, which are mixed with non critical logic on the same circuit board. A sufficiently stable temperature control could not be realised, due to high heat dissipation of many of the electronic parts. In order to keep the probability of instrument introduced biases low on the WLRS, a normal point binwise correction for the ranges was implemented.

References

[1] Electro Optic Systems Pty Ltd.; "Design manual of the Wettzell Laser Ranging System", (1988)
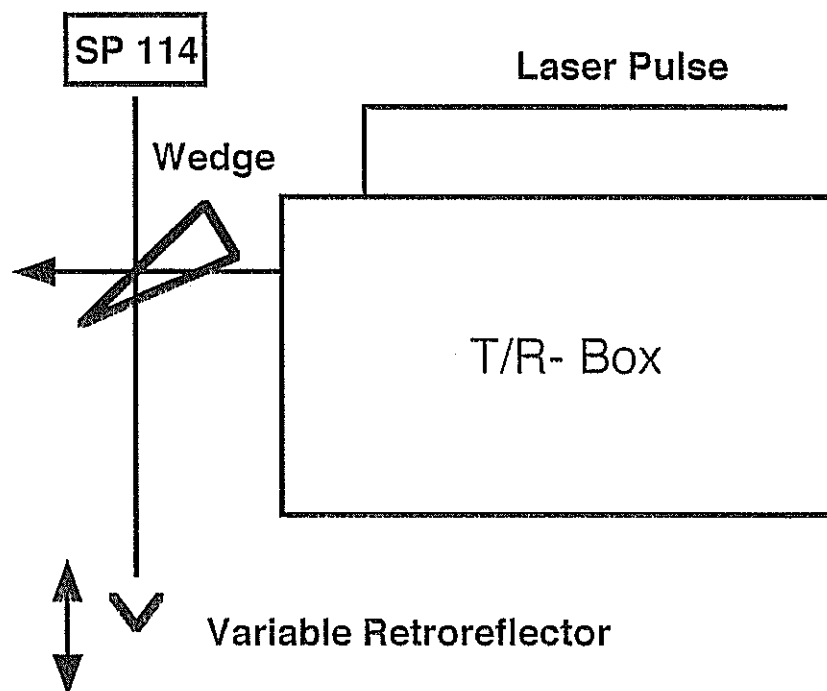
Figure 1: The principle of the optical setup of the calibration of the time to digital converters
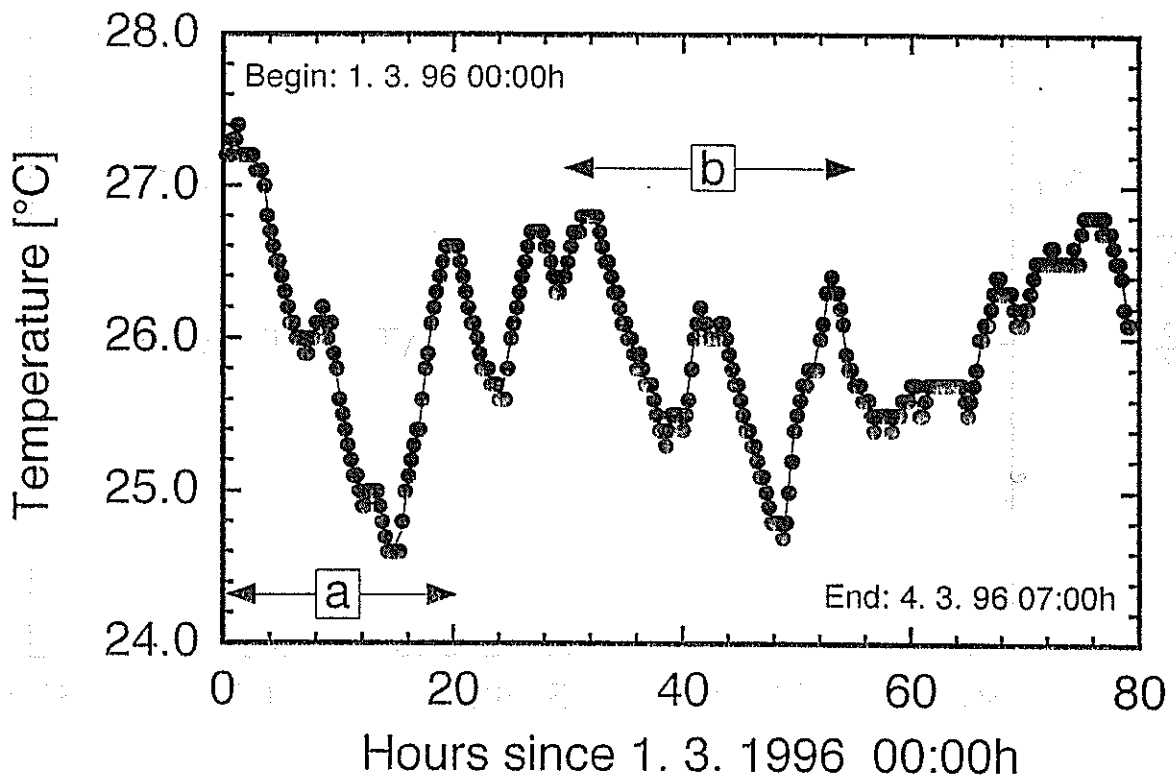
Figure 2: Temperature variation on the Master Ranging Controller board under normal ranging conditions over a weekend
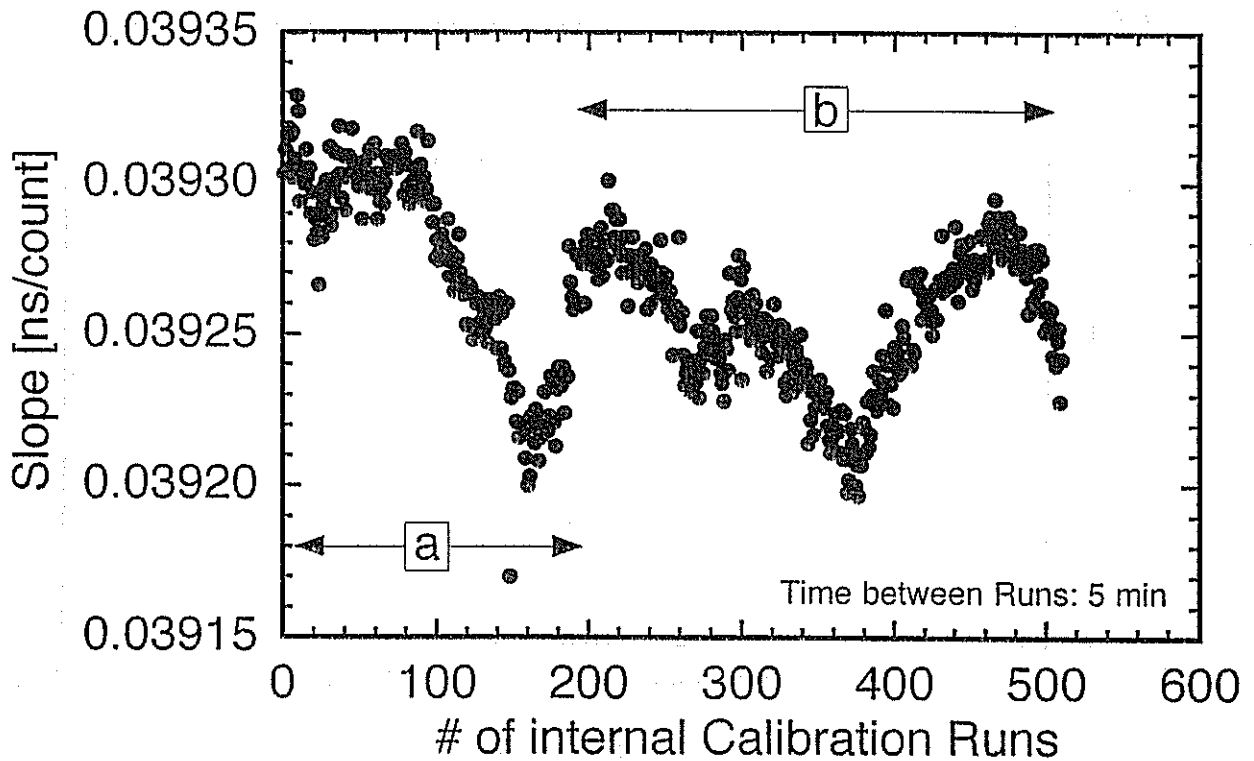
Figure 3: The effect of temperature variations on the slope calibration of the MRCS event timer. On average there are 1300 counts to a fine epoch. Therefore one has a change of roughly 130 ps due to 3 degrees of change in the ambient temperature
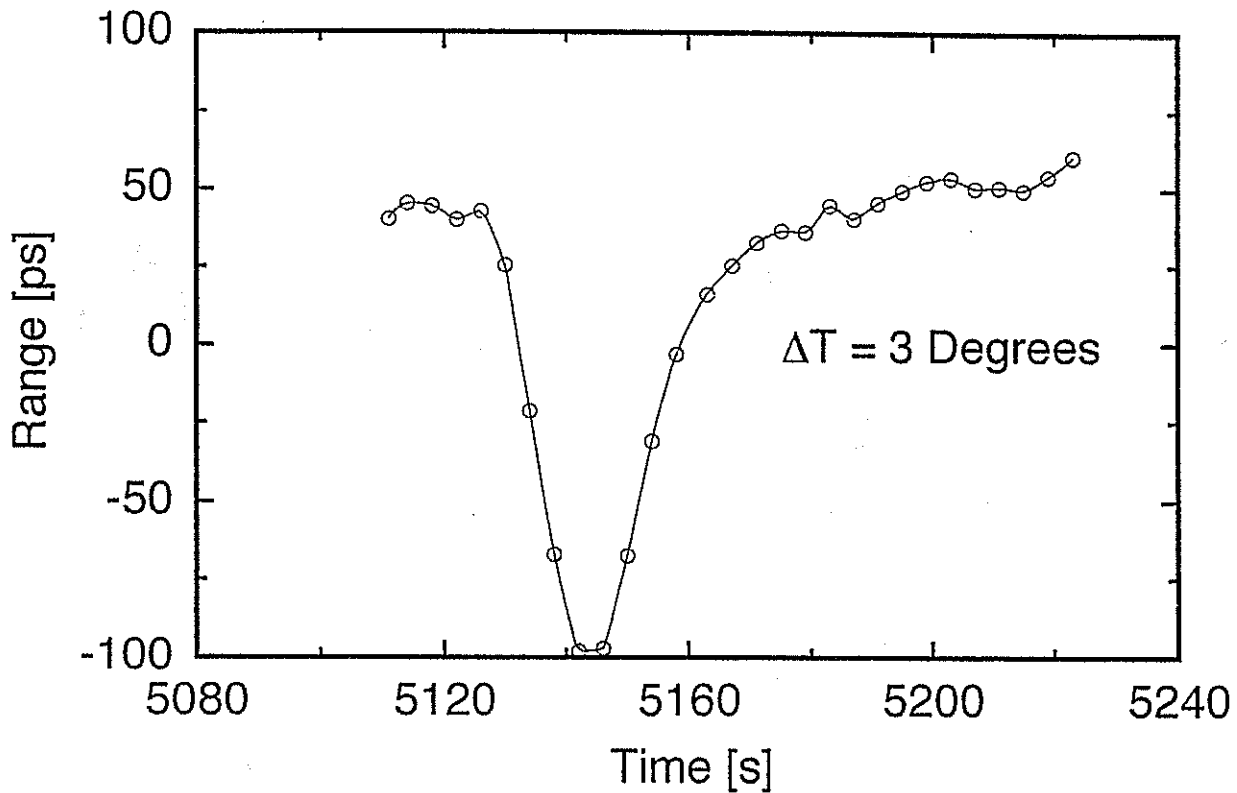
Figure 4: Variation in the range measurement for a constant range under the application of a temperature change of 3 degrees to a LeCroy 2229 unit over a short period of time
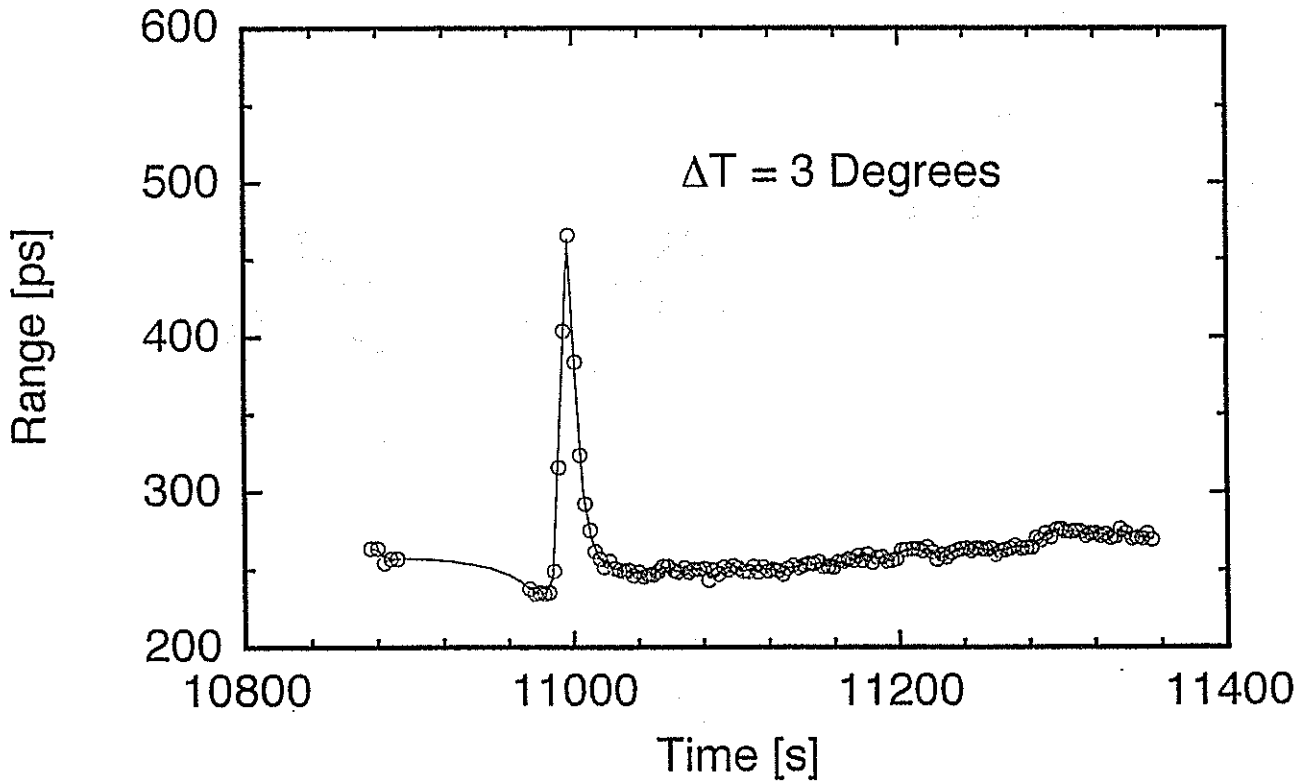
Figure 5: Variation in the range measurement for a constant range under the application of a temperature change of 3 degrees to the signal control unit of the MRCS over a short period of time

Short Distance Calibration

G. Kirchner, F. Koidl
Institute for Space Research / Austrian Academy of Sciences
Observatory Lustbühel; A-8042 GRAZ / AUSTRIA

1.0 Introduction

The target used for external calibration at SLR Graz during the last 16 years was a simple flat plate, located in a distance of almost 400 m; the transmitted laser beam was attenuated by insertion of 2 mirrors into the transmit path; although easy and convenient for routine operation, we realized many disadvantages, potential hazards for range biases, and inherent accuracy problems. To avoid all possible drawbacks, a new, very-short-distance, external target was designed, build and installed within the laser dome. The total error sum due to the new target is now below 1 mm, and its contribution to measurement jitter now is close to Zero.

2.0 Disadvantages of the old system

Approaching ranging results of below 5 mm single shot RMS for ERS satellites, and below 1 mm Normal Point RMS for LAGEOS, such a simple target became totally inadequate:

- The distance, dictated by the transmit/receive parallax, is difficult to measure to Sub-mm;
- Due to the necessary effort, re-measurements were rare, and not accurate enough;
- The influence of meteorological uncertainties could be up to 2 mm;
- Tilting of the attenuation mirrors could cause errors of up to 2 mm;
- Misalignment of the flat plate caused biases (up to 3 mm), and increased the jitter;
- The target was not accessible in bad weather conditions;
- Due to the long atmospheric path, the target was not acceptable for MultiColor Calibration.

3.0 Design of the new target

A new target was designed (Fig. 1, 2) which now fulfills the following specifications:
- The distance is very short (about half a meter in front of the telescope); this allows very accurate distance measurements, which are also easy to repeat and to check;
- The short distance eliminates any meteorological uncertainties; it allows also calibration and tests even when there is rain or fog outside (everything is within the dome);
- The optical path is identical for calibration and ranging; there are no filters etc. inserted;
- There are no restrictions for MultiColor Calibration;
- We tried to avoid any possibility to add bias or jitter by the target;
- Changes of target position / distance are indicated by a low-cost CCD to sub-mm accuracy.

Due to the short distance, and due to the location of the target within the dome, the laser has to be attenuated BEFORE leaving the laser room, to avoid heavy backscatter in the dome, which would create serious problems for any Single-Photon Detector; this is done by changing the delay time of the laser amplifier flashlamps relative to the oscillator flashlamps (done automatically by

the real-time PC); due to the location of the start pulse detector before the amplifiers, this does not affect the timing at all.

GRAZ SHORT DISTANCE CAL TARGET

1742.3 mm

DIFFUSOR PLATE

Receive-

0.1 %

99.9 % PRISM,
AR-COATED

Transmit-

Telescope

CAL TABLE
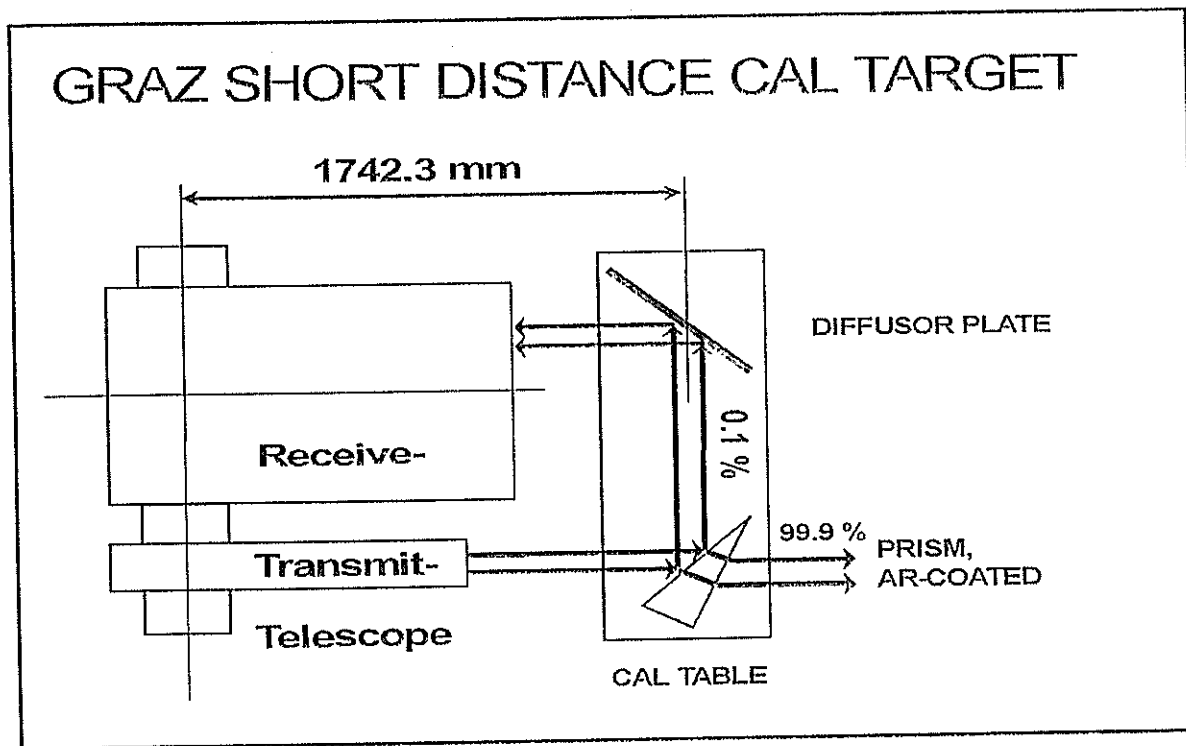
Fig. 1: The new short distance calibration target .....

Also due to the short distance, the standard gate pulse - derived from the standard start pulse for ranging operation - would arrive too late at the SPAD unit to gate it. Thus we use a separate gate pulse detector for generation of the calibration gate pulse, which detects the pre-pulses of the mode-locked train about 300 ns before the actual laser pulse. Because this gate pulse is slightly fluctuating relative to the actual laser pulse - due to the uncertainty of detecting one out of many rather small pre-pulses - the position of the calibration return pulse within the calibration range gate is also fluctuating slightly; this eliminates automatically any possible bias problems related to a fixed position of return pulse within the cal range gate, or would indicate it at least by increasing the jitter.

1742.3mm

Calibr.
Table

Receive

Transmit

CCD

Concrete Pillar

Fig. 2: ..... is mounted on the telescope pillar

The target itself consists of a prism and a diffusor (Fig. 1) to redirect the beam into the receiver; both items are aligned for perpendicularity - using auxiliary penta prisms etc. - and to keep all parts of the calibration beam in the same horizontal plane, avoiding any geometrically induced biases and jitter.

The prism is AR-coated for 532 nm to reduce the reflected energy to 0.1%; the AR-coating is chosen for higher reflection for the 683 and 435 nm, to compensate here for lower energies. The use of the prism avoids any secondary reflections. The diffusor is just a flat piece of black anodized aluminium, to attenuate the laser once more.

The beam is additionally attenuated by using the standard small Field-of-View for day-light ranging; small changes of this FOV allow fine adjustment of the received energy, giving return rates between 1% and 100%. Significant higher - or also lower - received energies (for tests only) can be easily selected by manually changing the laser amplifier delays.

The whole target is mounted on the same concrete pillar as the telescope mount (Fig. 2); in this way the relative distance between mount and target is fixed. To protect the target, its mounting rod is enclosed by an additional protective rod.

The position, distance and alignment of the whole target is checked with a CCD camera down to the sub-mm range: A small hole in the diffussor directs a portion of the calibration beam to a small auxiliary mirror, which reflects this beam - with an angle of 45° - down to a CCD at the bottom of the telescope mount. Thus even sub-mm movements of the target, its distance or its position relative to the telescope are visible as big offsets on the TV screen.
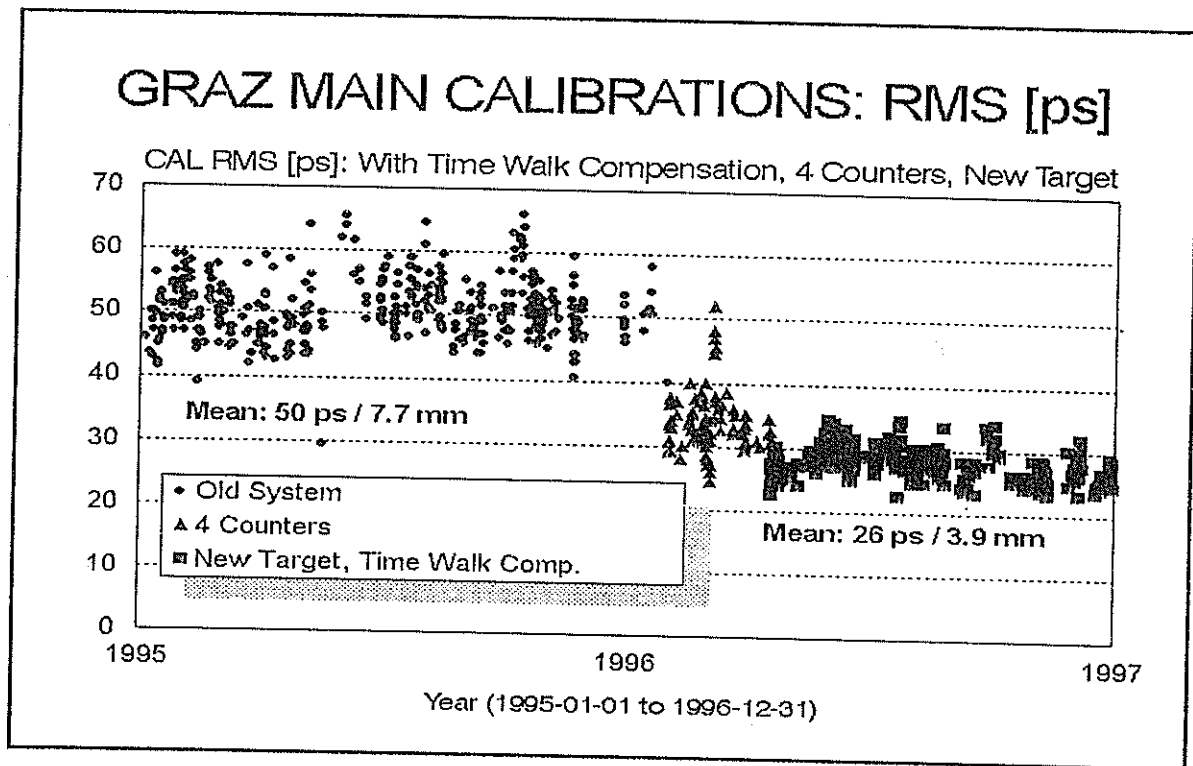
Fig. 3: Single Shot RMS Improvements

4.0 Results

The new calibration path was measured multiple times. using different persons, methods, scales etc.; resulting in a corresponding target distance of 1742.3 ± 0.3 mm. The single shot RMS of the routine calibrations to the new target now is below 4 mm (Fig. 3), which is also due to the use of up to 4 counters parallel, Time Walk Compensation for the SPAD etc.

At the same time - April 1996 - the calibration procedure was changed; before this time we used pre- and post-calibrations for each single pass; now we make more extensive calibrations (at least 500 returns) whenever a time slot between satellite passes allows, but at least once each hour; all results (calibration values, meteorology values, counter offsets etc.) are stored in a main calibration file; during post-processing, all relevant values are interpolated linearly for the epoch of each return (Fig. 4).
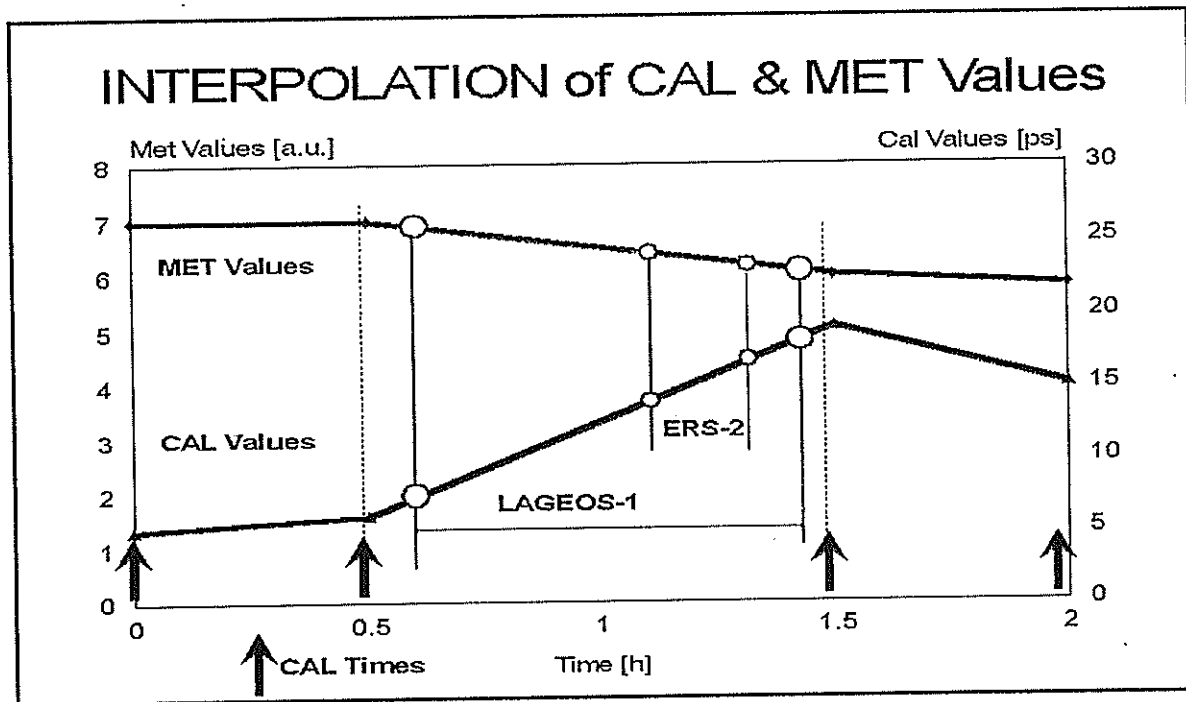
Fig. 4: Calibration Procedure / Sequence
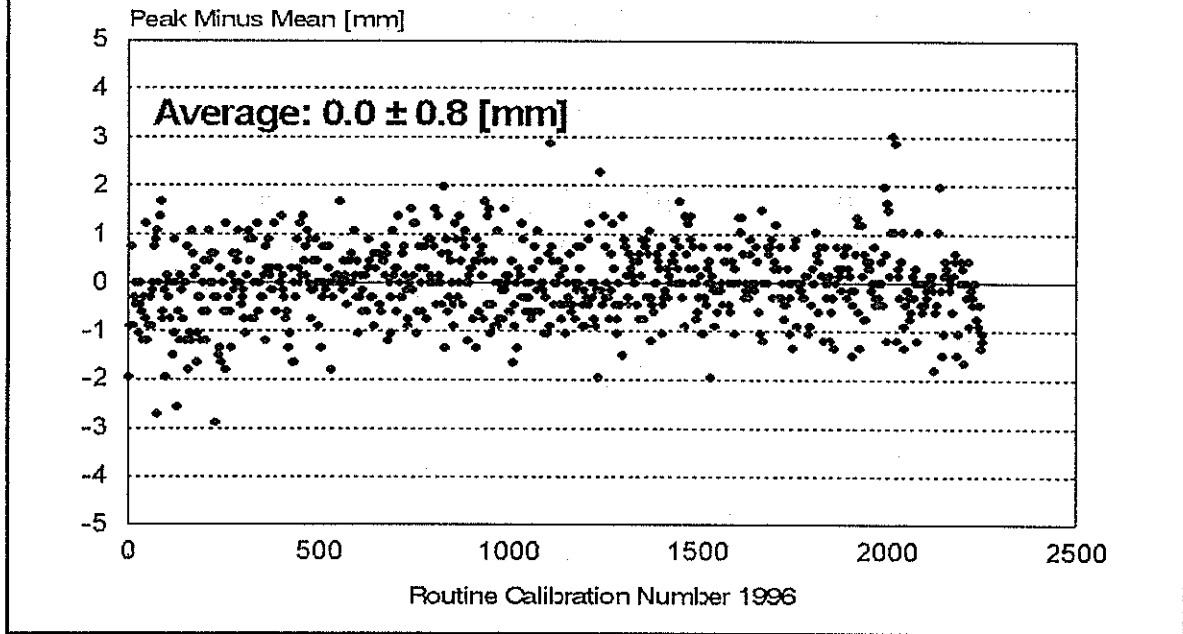
Fig. 5: Peak-Minus-Mean of Calibration Runs

The sum of all improvements (very short distance cal target, SPAD Time Walk Compensation, SPAD gating with 10 V above Break, MultiCounter Operation) now gives a very symmetric distribution of the returns from the target (in spite of the inherent tail of SPAD return distribution); this can be seen in the Peak-Minus-Mean Statistics (Fig. 5) of the routine 1996 calibration runs:: There is no skew, and average Peak-Minus- Mean is Zero.

435

PORTABLE SLR CALIBRATION STANDARD

I. Prochazka, K.Hamal

Czech Technical University, Brehova 7
115 19 Prague 1, Czech Republic
fax +42 2 85762252, prochazk@mbox.cesnet.cz

H. Kunimori

Communication Research Laboratory, Tokyo, Japan

B. Greene

Electro Optics Systems, PtyLtd, Queanbeyan,NSW, Australia

Range bias is the key issue facing SLR in the next years. Since system standardization will not overcome this problem fully in the foreseeable future, there is a need for a means of calibrating the individual SLR system for range and time biases. The most rigorous calibration would involve a complete SLR portable standard, which would collocate with the system under test. A more economical approach allows the laser and telescope of the system under test to be used.

We are presenting a concept and design of a portable calibration standard for Keystone Project satellite laser ranging systems. It consists of the reference time interval counter, epoch counter, independent standards of frequency and epoch, meteorological sensors, control electronics and software package. All the crucial parts are enclosed in an air-tight box maintaining the temperature within 50 milli Kelvins. The only inputs to the Standard are the Start and Stop signals of the SLR under test. Due to the Keystone Project SLR systems design ['zero offset calibration scheme' among others] the Portable Calibration Standard will be able to identify most of the biases in the SLR system under test. The range and time bias resolution is 1 millimeter / 100 nanoseconds respectively on a single satellite pass basis. The Standard is enclosed in a hand transportable box, it may be easily and quickly relocated within the SLR network.

PORTABLE CALIBRATION STANDARD
PHILOSOPHY

- Range bias is the key issue facing SLR.

- There is a need for a means of calibrating the individual SLR systems for range and time biases.

- The most rigorous test procedure is a collocation with an independent SLR system.

- A more economical aproach allows the laser, telescope and detectors of the system under test to be used.

Prochazka.Hamal,Greene,Kunimori, Shanghai '96

PORTABLE CALIBRATION STANDARD
CONCEPT

- Independent – ranging hardware (start/stop NIM inp.)
  - epoch & frequency reference
  - noise reduction, data processing SW
  - meteo sensor (pressure)
  - temperature control
  - RF protection
  - AC power filtering
  - grounding

- Compact design, hand transportable

- One calibration standard rotated regularly through KSP SLR systems will form an independent ranging refference.

Prague. February '96

PORTABLE CALIBRATION STANDARD
PARAMETERS

Time of flight	Stanford Research SR620
Epoch & frequency ref.	GPS Hewlett Packard
Climabox	airtight, +/- 0.05 K
Control	notebook size PC
Air pressure sensor	0.01 mB
Dimensions	50 x 40 x 30 cm
Mass, power	25 kg , 200 W
Setup time / warm up	1 hour / 1 day

Prague, February '96

PORTABLE CALIBRATION STANDARD
PARAMETERS 2

Time of flight resolution	25 psec RMS /SR620/
Frequency accuracy	10E-12 /GPS/
Laser fire epoch resolution	100 nsec
Epoch reference	110 nsec /HP-GPS/
Measuring repetition rate	10 - 5 Hz low satellites/GPS
Control	notebook size PC
Prediction	Integration IRVs time bias on-site update
Data analysis	noise filtering, data reduction normal points, full rate..
Data comparison	Range and time biases frequency, epoch, meteo

Prague, February '96

PORTABLE CALIBRATION STANDARD
ACCURACY

RANGE
resolution / single shot   ‹ 10 mm RMS
stability   0.5 mm / hour
frequency   10E-12 /GPS/

RANGE BIAS
resolution / pass   ‹ 1 mm
stability   0.5 mm / hour

EPOCH
resolution / single shot   100 nsec
refference   110 nsec /GPS/

TIME BIAS
resolution / pass   ‹ 50 nsec

Prague, February '96

Portable Calibration Standard (PCS)
CONCLUSION

- Portable Calibration Standard is a powerful tool
  to identify most of range and time bias sources
  introduced by   – ranging machine
                 – calibration
                 – on-site data processing
                 – operator error

- Due to high mobility, short setup time and shot
  by shot comparison scheme, the result is available
  within days at any SPAD based SLR site.

- Considering the existing and foreseen SLR network
  status and the SLR data quality requirements,
  the Portable Calibration Standard seems to be
  worth considering as an option to a true collocation.

Prochazka,Hamal,Greene,Kunimori '96

439

SLR bias sources
Ranging machine contribution

source		identification
Frequency & epoch		PCS
Calibration	survey	minicollocation
	mount ecc.	minicol.partially
	correlated RF	PCS partially
		minicol.partially
	stability	PCS
Signal strength/time walk		low rate / SPAD
Instrumental errors		PCS
Data processing		PCS
Meteo data		PCS
Operator errors		PCS

Prochazka,Hamal,Greene,Kunimori '96

PORTABLE CALIBRATION STANDARD
DESIGN OBJECTIVES

- Determination of range and time biases
  of the satellite laser ranging system.

- Identification of contributors to these biases.

- Alternative to the collocation using the mobile
  SLR system :
  - simple deployment to the site
  - short setup time
  - fast 'feedback' on site
  - shot by shot comparison available
  - based on proved technology HW/SW

Prague, February '96

PORTABLE CALIBRATION STANDARD

METEO

GPS time & frequency

CLIMA box +/- 0.05 K

RF shield

1 pps 10MHz

PCE

SR620

SLR system under test

START STOP

notebook

GND

AC pwr

MERIT2 / NPT output data

Data comparison

MERIT2 / NPT output data

RESULT
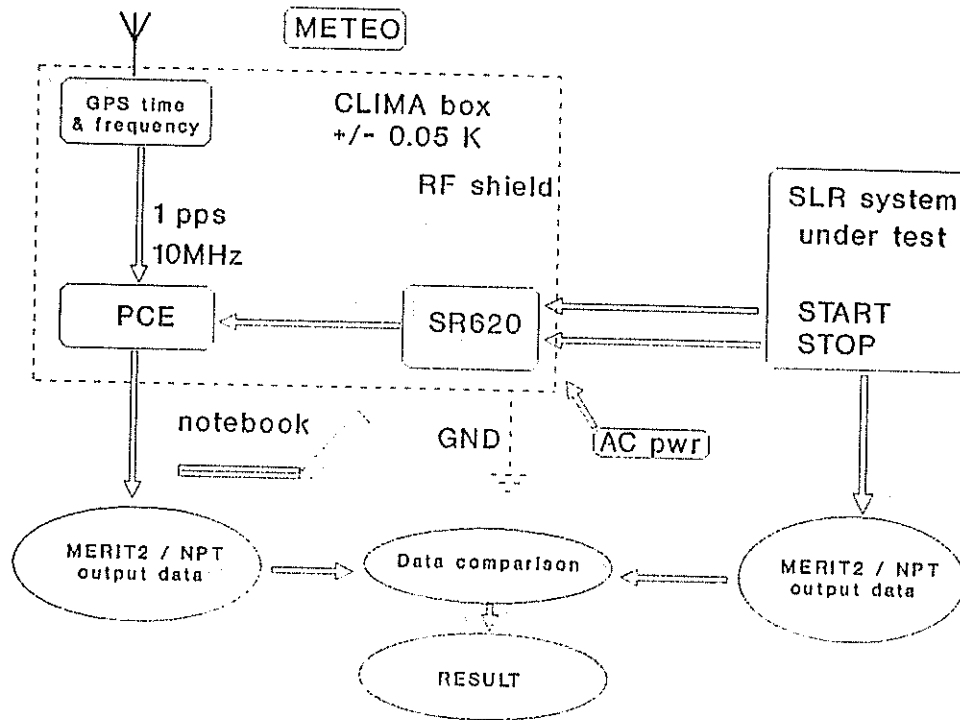
Prague, February '96

CLIMABOX TEMPERATURE CONTROL
Device mainframe temperature
Dissipated 100 W, ambient +20.. +24C

device temperature [Centig]

SR620 drift 5psec/Centig.

time [min]

J..Blazej, I.Prochazka, Shanghai '96

441
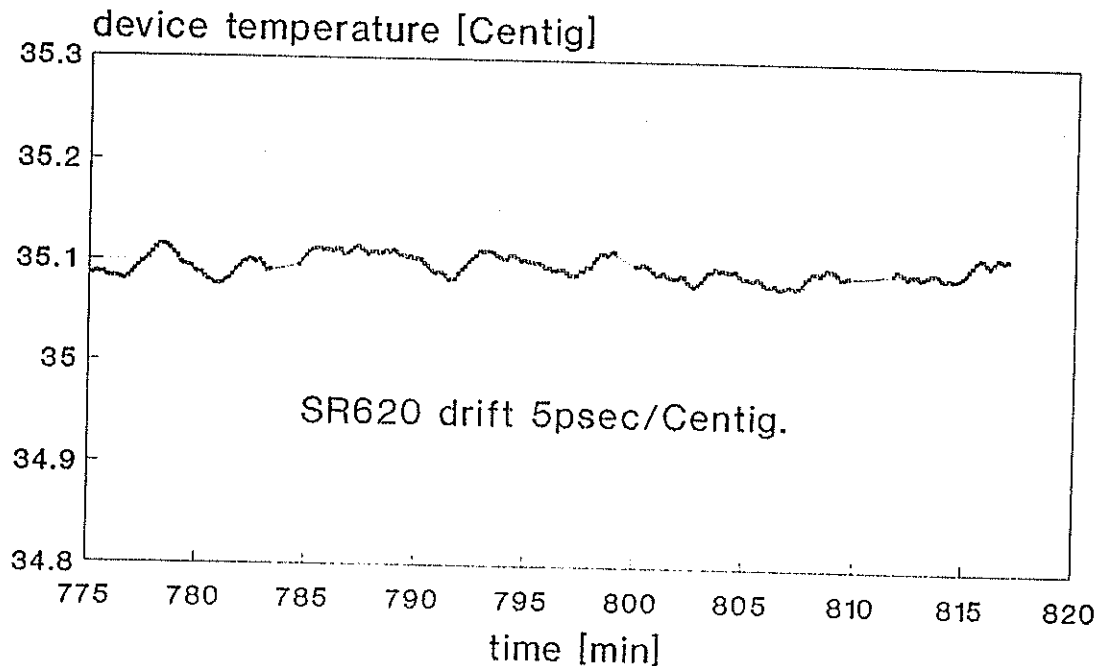
CALIBRATION SETUP FOR HELWAN STATION
TWO DETECTORS COMPARISON EXPERIMENT

M.Tawadros

National Research Institute of Astronomy and Geophysics
Helwan, Egypt
fax +20 2 782683

I.Prochazka, M.Cech, K.Hamal, H.Jelinkova, A. Novotny

Czech Technical University, Brehova 7
115 19 Prague 1, Czech Republic
fax +42 2 85762252, prochazk@mbox.cesnet.cz

The Helwan Satellite Laser Station is been upgraded under the joint effort of the National Research Institute of Astronomy and Geophysics, Egypt and the Czech Technical University. Among others, the additional guiding / receiving telescope 280 mm in diameter equipped with the solid state detector SPAD have been added to the existing system. Due to the optical setup of the new receiver and detector, the new calibration target and procedure had to be developed. To guarantee the satellite ranging data continuity and to preserve the low range bias of the station, both receivers and detectors were operated simultaneously. Due to the single photon ranging, both the detector output signals could be combined into the single ranging electronics, the echoes corresponding to different detectors were identified by their delays. Completing a satellite laser ranging pass, the appropriate calibration constants are applied to corresponding echoes. The range bias of the new receiver/detector/calibration setup versus the original one is evaluated by a simple substraction of measured ranges. The first results based on limited number of low satellites passes indicate the range bias +18+/-10 mm. It is expected, that the comparison scheme will be operated for the entire 1997 laser ranging mission to tune the new calibration procedure.

HELWAN 2 SATELLITE LASER STATION

Mount, DC motors, encoders, guiding telescope
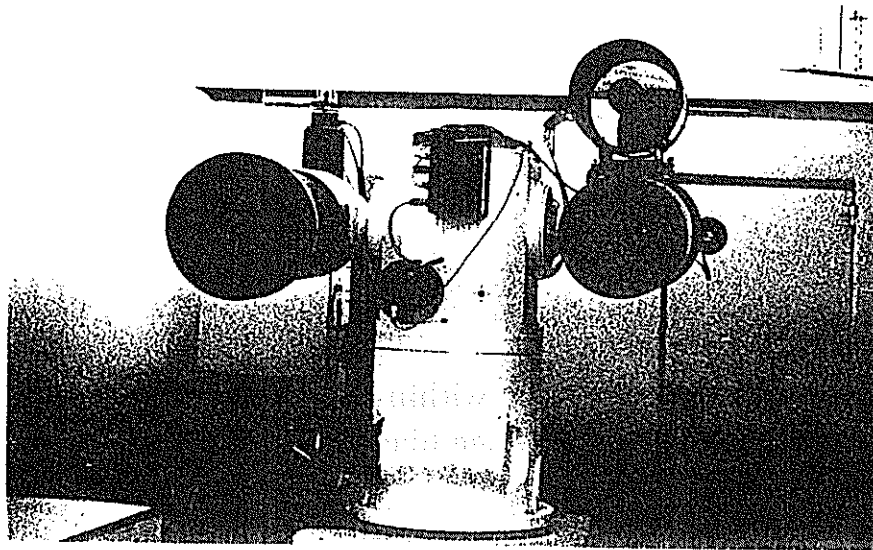
New receiver package, CCD guiding system (right)
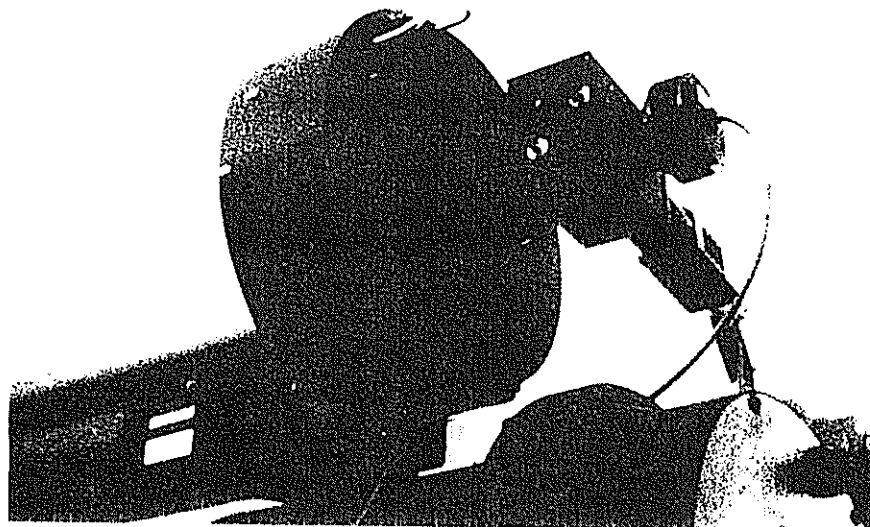
Helwan, September 12, 1995

O-C (ns)

Helwan 96 0 17 7501001.
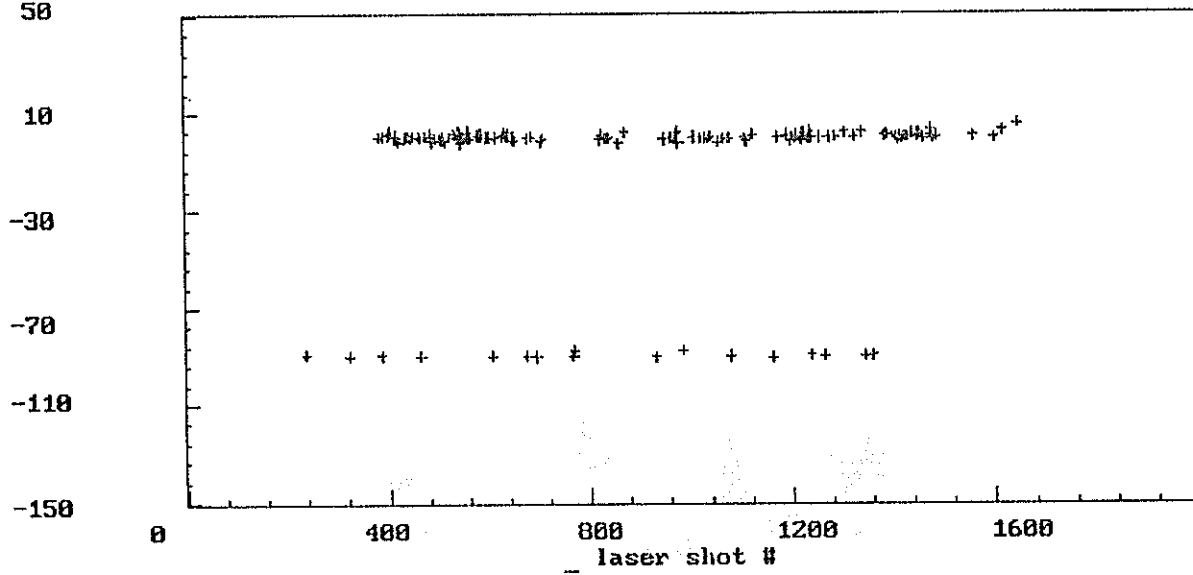
Starlette ranging, the first pulse within the semitrain selected, only.
Data used for range bias evaluation.

O-C (us)

Helwan 95 9 18 9207002.
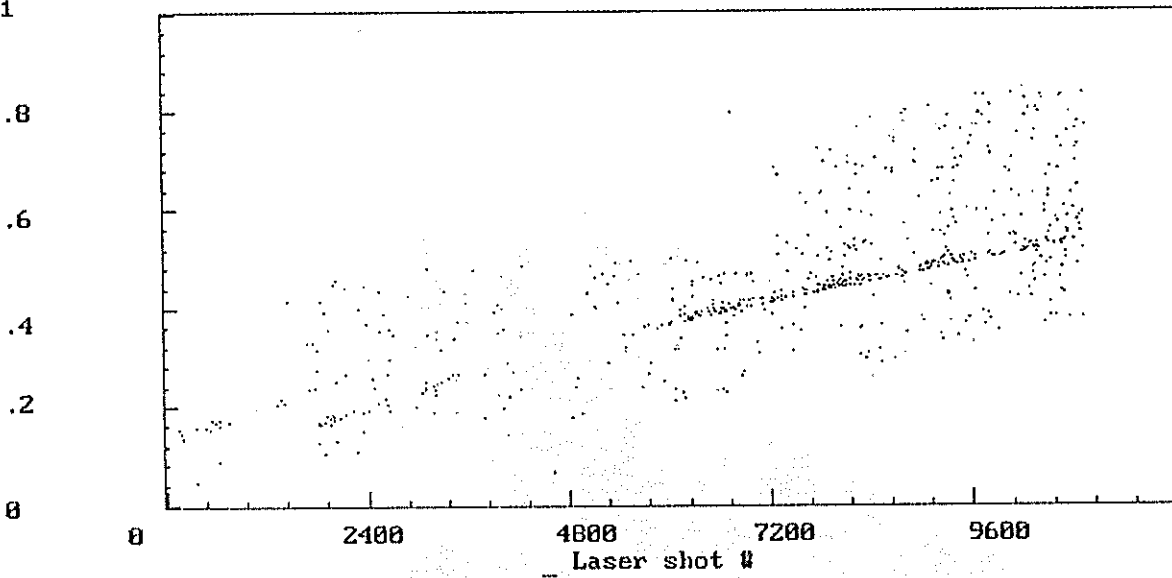
Lageos 2 ranging, due to optical axes alignment problem, the SPAD
data rate is elevation dependent. Note the dark count contribution of
SPAD and the ratio of return rate of both detectors. The average
data rate for well aligned SPAD was about 7x the PMT.

Multiwavelength Ranging

/

Streak Cameras

STREAK CAMERA
and
Two Color Laser Ranging

JEAN GAIGNEBET, JEAN-LOUIS HATAT, JEAN-LOUIS ONETO
OCA/CERGA, AVENUE COPERNIC - 06130 GRASSE - FRANCE

Goals of Two Color Laser Ranging (TCLR)

TCLR is able to measure *in situ* the index correction caused by the double crossing of the atmosphere with an accuracy of 5 mm shot by shot. This correction could be considered a white noise only for very long integration time. This time has yet to be determined.

The discrepancy between the two color measurement and the existing models for a given epoch, fixed meteorological conditions and in a limited solid angle, could be considered as constant. This upper limit of this angle has to be defined by stations with a shot by shot ability to perform TCLR. My feeling is that a value has to be measured at least each 5° along the satellite track (geocentric angle).

Two Color Laser Ranging

TCLR is by essence a multiphoton process. It could be implemented along two different concepts.

◊ **Single photon counting (SPC).** The differential flight time is computed by difference of the flight times obtained in each color, averaging a great number of relatively inaccurate measures. One have to keep in mind that :

  • As the precision is increasing, a multiphoton event has a greater bias effect on the average value. To maintain a true SPC operation the ratio of returns over shots as to be kept very low. It could be in the 1 % range.

  • The differential value has to be accurate within a few picoseconds. Reaching this level with individual measures at a shot by shot noise of 20 to 50 ps implies hundreds or thousands of detected returns.

Combining this two remarks, we see that the two color correction can be obtained only each 10^4 to 10^5 shots. Obviously the method is adequate only for very long passes on very high satellites with already very weak link budgets. As LLR is limited to true SPC operation this field is constrained to this approach.

◊ **Mutiphoton record (MPR).** The differential flight time of each shot is deduced from the record of the arrival time of each photon in multiphoton collected light pulses. Today the equipment to implement the concept is limited to Streak Cameras (SC). We will see that with the pulsewidth optimized, without pulse processing, the number of photons is in the order of a few hundreds per wavelength for a single corner cube target.

Streak Camera limitation.

A Streak Camera is a time to space transformer. Statistically a photon extracts an electron from a photocathode. After acceleration of this electron and its deflection by two electrodes, it reaches a phosphor screen where it could be seen (Fig. 1). The position of the light spot is related to the arrival time of the photon on the photocathode. As in any detection device, the electron emitted from the photocathode is quite slow (a few eV), with spread energy and direction. An electrostatic field (kV.mm^{-1}) accelerates it and imposes a velocity parallel to it. This electrostatic field is limited by the breakdown field of the vacuum. As the energy of the photon reaches one keV, the speed is such that the jitter of the travel time of the electron during its flight is negligible versus the initial time spread. This intrinsic limit caused by the process of the detection itself is in the order of 2 ps RMS (narrower than for a SPAD 5 ps).
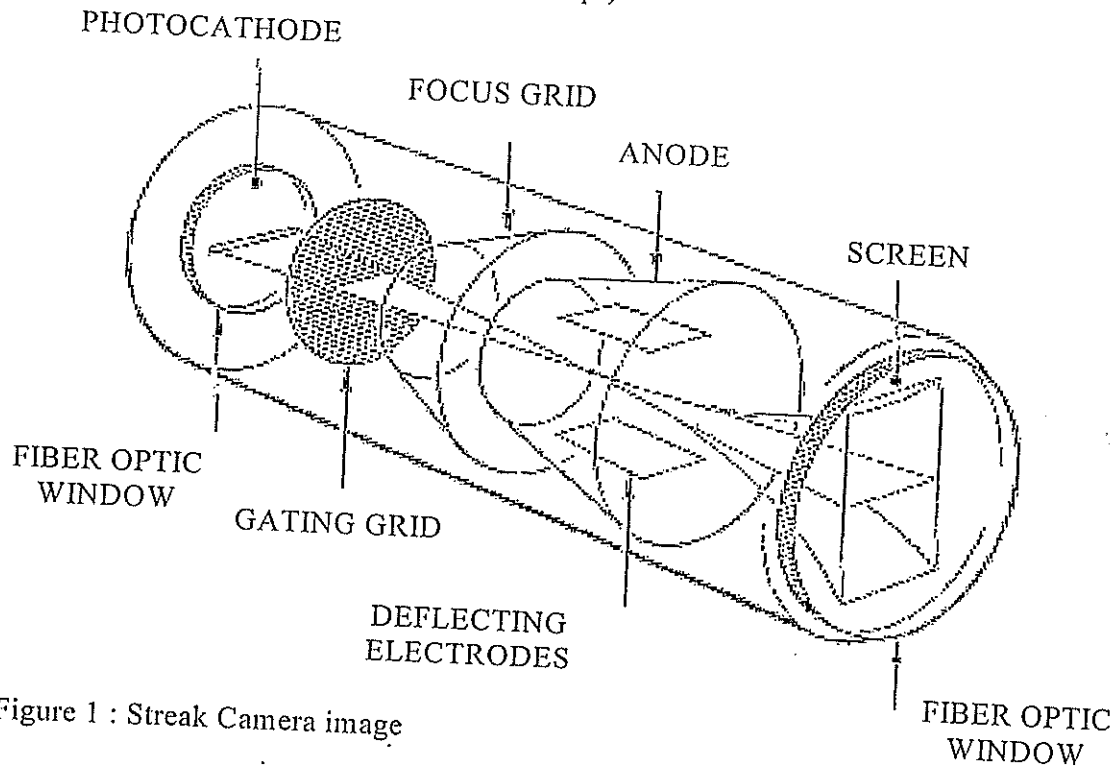
Figure 1 : Streak Camera image

The following formula explicits the effect of the Streak Camera timing errors, and laser pulsewidth on the range measurement.

$$\sigma^2{}_D = \frac{(0.15)^2}{N} A^2 \left(\frac{\sigma_0^2 + \sigma_{\lambda_1}^2}{n_{\lambda_1} Q_{e\lambda_1}} + \frac{\sigma_0^2 + \sigma_{\lambda_2}^2}{n_{\lambda_2} Q_{e\lambda_2}} + \sigma_s^2 \right)$$

where

σ_D (mm)	= error on the distance correction
σ_{λ_i}	= 0.4242 the FWHM λ_i pulselength
σ_0	= intrinsic resolution (2 ps)
n_{λ_i}	= incident number of photon @ λ_i
$Q_{e\lambda_i}$	= photocathode quantum efficiency @ λ_i
N	= number of measures
σ_s	= camera readout errors
A	= sensitivity factor of the two color measurement (9 to 40)

447

Some remarks could be made :

- σ_S is smaller than σ_0 so σ_S^2 could be neglected.

- $\dfrac{\sigma_0^2 + \sigma_{\lambda_1}^2}{n\lambda_1 + Q_{c\lambda_1}}$ is the same order of magnitude as $\dfrac{\sigma_0^2 + \sigma_{\lambda_2}^2}{n\lambda_2 + Q_{c\lambda_2}}$.

The formula could then be approached by the simplified one :

$$\sigma_D^2 \approx \frac{(0.15)^2}{N} A^2 \left(2\, \frac{\sigma_0^2 + \sigma_\lambda^2}{n\lambda\, Q_{c\lambda}} \right)$$

In order to reduce σ_D one has to minimize $\dfrac{\sigma_0^2 + \sigma_\lambda^2}{n\lambda\, Q_{c\lambda}}$. As σ_0 is a fixed value, two

possibilities remain :

◊ Decrease of σ_λ :

If one decreases the emitted pulselength, the received one decreases to a minimum then increases again. This effect is caused by the dispersion induced by the bandwidth of the narrow pulse. For straightforward emission-reception schemes, the minimum received pulselength is around 14 ps (10 ps emitted, 10 ps broadening by dispersion). The number of photons needed to reach a defined accuracy is $\dfrac{2^2 + 14^2}{2^2 + 2^2} = 25$ times greater than the number needed for a 2 ps pulse. By pulse processing (chirp and pulse compression) it is possible to go down to received pulses in the ps region. If one designs a SC with a subpicosecond intrinsic resolution, the number of photons in each color, needed for a given accuracy, could be reduced by a factor of 200 versus the best systems available today.

◊ Increase of $n\lambda\, Q_{c\lambda}$

This is an increase of the link budget. Any of its elements is concerned :

- laser energy
- emission divergence
- retroreflector efficiency
- collector area
- filter transmission
- detector quantum efficiency

Subpicosecond timing devices.

Today the intrinsic limit of a SC is at the detection interface (photocathode). Getting down under this limit is bypassing this bottleneck. Out of a few possible principles, two are already tested.

◊ **Statistical event timer**

Electro-optic crystal coupled with an analyzing polarizer (Fig. 2)
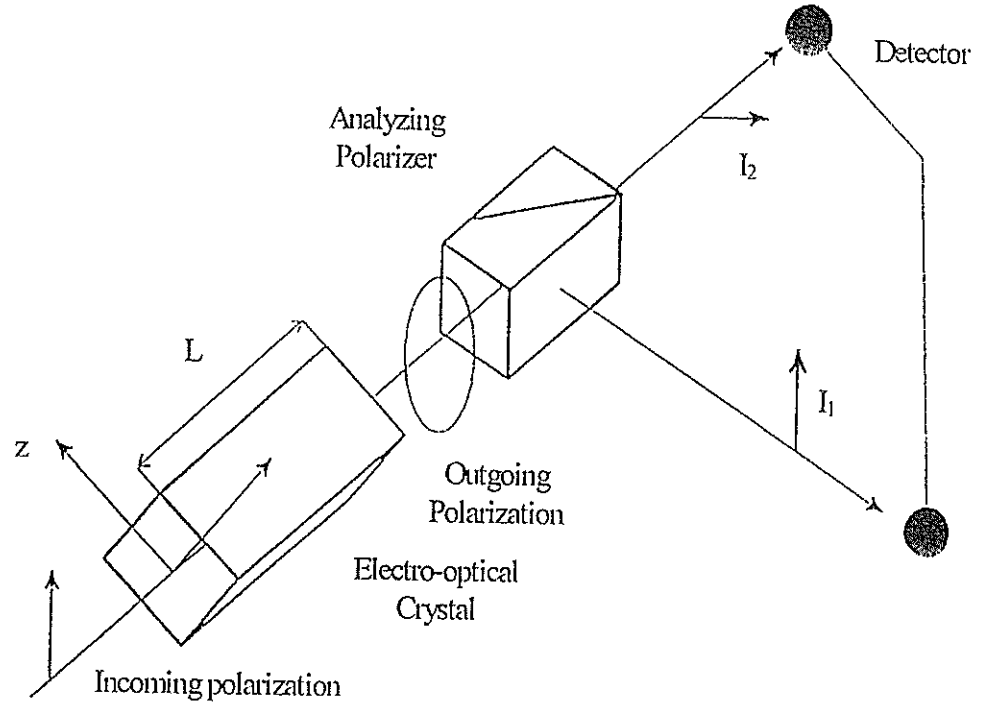
Figure 2 : Statistical event timer

The vertically polarized light pulse crosses the electro-optic crystal. A sinusoidal modulating voltage changes the crystal indexes and therefore the polarization state of the outgoing light pulse. An analyzing polarizer, here a Glan prism divides the outgoing light pulse in two components respectively polarized horizontally and vertically. The number of photons I_1 and I_2 allows to determine the polarization status of the crystal at the crossing moment and to determine this moment related to the sinusoidal modulation voltage.

Obviously this event timer is a multiphoton device and thus to be used in pair outphased by $\dfrac{\pi}{2}$ to avoid ambiguity. Around 500 photons are needed for a 50 ps time uncertainty. As such this kind of event timer could be used as an emission timing device where the number of photons could be very important.

The variations of the mirror reflectivity (electro-optic crystal and analyzer) could be achieved by other means.

As an example the ratio between the straight beam and the deflected one changes periodically as the fringes appear and disappear in an acousto-optic modulation. An event timer could be conceived around such devices.

◊ **Optical sweep**

The system could be described as a streak camera without the detection stage and the temporal dispersion of this photon to electron conversion. The propagating optical beam itself is deflected with a direct space to time relation. This deflection could be done by a prism whose indexes change with an electric field (Fig. 3). Already some crystals present this electro-optical sensitivity as lithium niobate ($LiNbO_3$) or strontium and barium niobate (SBN). Up to now the sensitivity is rather low ($\frac{\delta n}{n} \approx 10^{-3}$ kV.mm^{-1}).
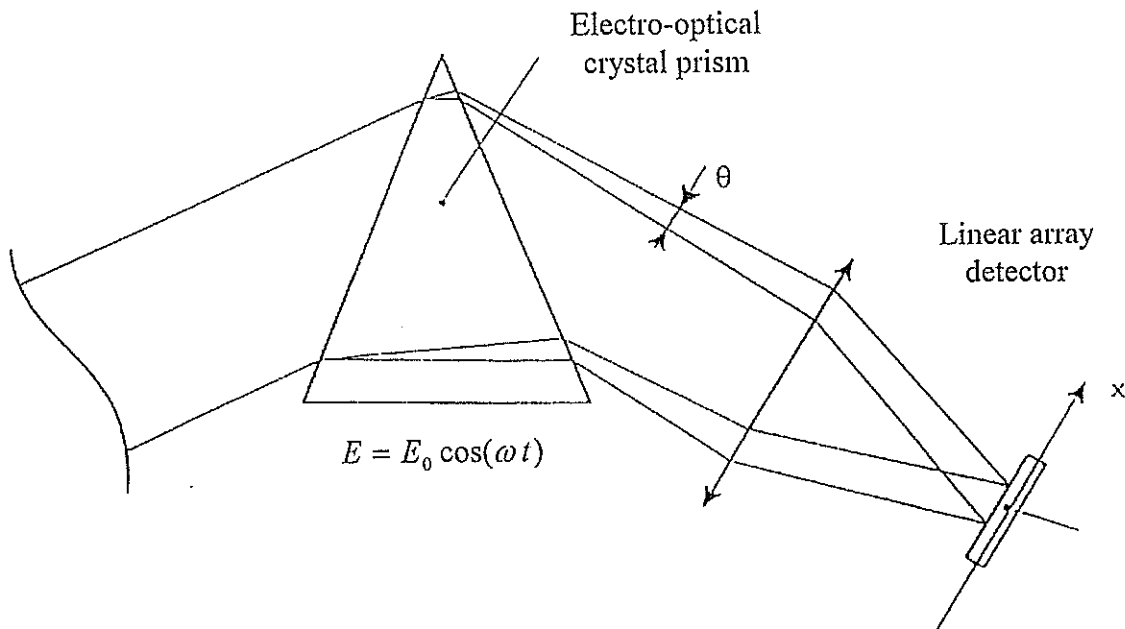
Figure 3 : Electro-optical Streak Camera

Conclusion

Two color laser ranging being a multiphoton process and needing a very high differential timing accuracy, very few stations are able to implement it.

Reducing the number of photons to achieve a good index correction is needed.
Two ways to achieve this are foreseen :
◊ Enhance the accuracy of the timing device
◊ Use the information potentially provided by each received photon.

The Circular Streak Camera Experiment of the WLRS

Stefan Riepl, Ulrich Schreiber
Forschungseinrichtung Satellitengeodäsie
Fundamentalstation Wettzell
D - 93444 Kötzting, Germany

Wolfgang Schlüter
Institut für Angewandte Geodäsie
Fundamentalstation Wettzell
D - 93444 Kötzting, Germany

Abstract

The Circular Streak Camera Experiment at Wettzell is nearing routine operation. By means of synchronizing the deflection voltage of the streak camera with the mode locking frequency of the Nd:YAG laser and locking both to a stable frequency standard, the streak camera represents a complete timing system allowing simultanous measurement of absolute pseudo ranges with an ambiguity of roughly $1m$ in the infrared and green wavelength domain. In addition to that the laser can be operated in semi train mode compensating the shortcomings of the relative insensitive S1–Photocathode, by integration of succeeding pulses. In order to calibrate the device, ranging to a local ground target was carried out. It is shown that a standard deviation of about 10 ps can be reached operating the device in multi photon mode, despite the fact that the laser is operated with 200 ps FWHM pulses. The analysis of the satellite laser ranging experiments show that this high precision can be reached as well in the earth to space propagation channel. Receiving the backscattered intensity distribution over time, the optical impulse response of the satellite can be reconstructed by further analysis of the data. Moreover, looking at the shot by shot detected signal strength in both wavelengths, atmospheric propagation and transmittance characteristics can be derived via time series analyses, showing agreement with theoretical results of electromagnetic wave propagation in turbulent media.

1 INTRODUCTION

There have been several attempts [5] [2] [1] to utilize streak cameras in satellite laser ranging in order to derive the atmospheric correction. As their time resolution can

be pushed beyond 1 ps, these devices seem to offer a good approach to improve the accuracy of laser ranging instrumentation. One major drawback of the up to now published techniques is that this precision is not obtained for the absolute range information but only for the range differences of two simultaneously emitted laser pulses of different wavelength. This drawback forbids the evaluation of streak camera measured differential ranges in terms of atmospheric delay corrections, assuming equal intensity distributions at both wavelengths, which doesn't hold for cross atmospheric propagation due to turbulence induced scintillation. The experimental setup allows both, the determination of absolute ranges, as well as the detection of range differences between laser pulses of the fundamental (1064 nm) and second harmonic (532 nm) Nd:YAG frequencies. Figure 1 illustrates the principle of operation. On the right hand side there is a schematic representation of an active and passive q-switched oscillator, emitting pulse trains of nominal 200 *ps* FWHM pulses. The driving frequency of the acoustooptic modelocker is generated by a synthesizer which is synchronized to a frequency standard. As a result the temporal separation of any two pulses is precisely an integer multiple of the reciprocal driving frequency. The streak camera sweep frequency is derived from the same synthesizer in order to synchronize the detector unit with the laser output pulses. The laser pulse train passes the slicer and several amplifiers and is frequency doubled before it is transmitted from the 75cm aperture WLRS telescope. After reflection by a target the laser pulses are collected by the same telescope and guided along the receive path. After passing the spatial filter the laser pulses are imaged onto the streak camera cathode. The resulting photoelectrons are deflected in two dimensions while being accelerated from photocathode to the microchannel plate. This plate emits secondary electrons that are detected at the phosphor screen by a CCD array. If t denotes the round trip time of a laser pulse, then the angular location Φ (see figure 1) can be expressed in terms of the driving frequency F by

$$\Phi = 2\pi t \bmod T, \quad T = \frac{1}{F}. \tag{1}$$

Expressing t in terms of a whole number N and the sweep period T, i. e.

$$t = T(N + \frac{\Phi}{2\pi}), \tag{2}$$

the round trip time can be measured by determination of N and Φ. In case of satellite ranging N is of the order of one million. So for round trip time measurements of 5 ps accuracy, the driving frequency of 140 MHz has to be known to 0.1 Hz. This requirement is met by the equipment. To moderate the drawback of the relative insensitive S1 photo cathode of the streak camera, the laser can be operated in semi train mode. This gives four times the intensity as operation in single pulse mode. The temporal spacing of the laser pulses equals exactly the sweep period of the streak camera. Therefore the succeeding pulses are imaged onto the same angular location

Φ on the phosphor screen, if the optical path can be considered as constant within 50 ns. This holds for all earth orbiting satellites.

2   RANGING TO GROUND TARGET

In order to test and calibrate the device with respect to the reference point of the telescope, ranging to a local ground target was performed. Figure 2 shows a histogram of detected peak locations. The abscissa is plotted in units of picoseconds, with an arbitrary origin. The ordinate shows the number of events in each bin. An event is obtained by averaging the CCD signal, which is proportional to the time varying intensity given by a laser pulse. An accuracy of 14 ps is obtained, although the laser pulses are 200 ps FWHM. However this timing performance is only reached when the intensity of the detected signal is quite high, i.e. the device is operated in multi photon mode. This is because the pulse shape of the laser is reproduced quite well, thus allowing a good determination of the centre of the pulse. The achievable accuracy, dependent on intensity, can be written as

$$\delta t = \sqrt{\delta t_i^2 + (\delta t_l e^{-\frac{I\eta}{a}})^2}, \tag{3}$$

where δt_i refers to the intrinsic resolution of the streak camera, i.e. beam spread inside the tube etc., δt_l is the FWHM of the laser pulse, I its intensity, η the cathode's quantum efficiency and an empirical constant a which equals 2 in this case. From equation 3 one can see that a downgrade of the intensity to the detector's single photon mode ($I\eta = 1$) results in a loss of accuracy. This is shown in figure 3. The standard deviation is spread by a factor 8 in contrast to figure 2, but the RMS is still half as much as the laser pulse half width. Therefore it is assumed that reducing the laser pulse half width to 30 ps ensures an accuracy of 15 ps in single photon mode, as δt_i is always much smaller than the contribution of the laser to the error budget.

3   STREAK CAMERA SATELLITE RANGING

When ranging to satellites the effect of speckle patterns must be considered. In case of ground target ranging, the propagation distance is not large enough to develop proper phase fluctuations and the image is relative undistorted. When ranging to satellites two effects related to the turbulent atmosphere must be considered:

- The transmission of a laser pulse with homogenous intensity distribution results in a speckle structured intensity distribution at the location of the satellite (see

453

TATARSKI [10]). The mean diameter of a speckle is of the order of a Fresnel zone

$$d_0 = \sqrt{\lambda L}, \tag{4}$$

where λ denotes the wavelength and L the propagation distance. Thus the intensity distribution has a random spatial modulation resulting in a wavelength dependent intensity scintillation of the backscattered laser light.

- Imaging a laser beam reflected by a satellite results in a speckle pattern comparable to those you get by imaging unresolved stars with short exposure time (see DAINTY [11]). The turbulent atmosphere introduces phase fluctuations in the electromagnetic phase fronts of the laser beam, which results in spatially spread images according to the current seeing conditions. The wavelength dependence of phase fluctuations is given in STROHBEHN [7]

$$D_S(\rho) \doteq 1.46 \frac{4\pi^2}{\lambda^2} C_n^2 L_{tur} \rho^{\frac{5}{3}}, \tag{5}$$

where C_n denotes the refractive index structure constant, L_{tur} the propagation distance in turbulence and ρ corresponds to the separation between two points where the phase is evaluated. This also results in a random speckle pattern where one can find a characteristic size of the speckles, which is known to be of the order of a diffraction limited image of a point source (see DAINTY [11]).

In summary one can conclude that the satellite backscattered intensity is not necessarily correlated for two different wavelengths. Furthermore one has to bear in mind, that the satellite image, generated by laser illumination, is random spatially spread. Rigorous spatial filtering as suitable for high resolution streak cameras will lead to large attenuation of the transmitted intensity. So one ends up with a trade off between speckle induced pulse broadening and less representative pulse shape reconstruction due to a lower photoelectron level arising from spatial filtering. Keeping in mind that the spatial frequency of the satellite speckle image is higher for shorter wavelengths one introduces an additional wavelength dependent effect on the transmitted intensity by spatial filtering.

As experimental evidence, figure 4 shows a sample plot of a two color laser pulse reflected by satellite STELLA. The field of view was chosen wider than the seeing limit (5 arc seconds for Wettzell) so that there is no discrimination of the spread image intensity. The solid line shows the intensity as measured by the streak camera, the dashed line is a fit of the theoretical impulse response. The pulse on the left hand side refers to the infrared wavelength and shows good agreement with the theoretical impulse response, whereas the laser echo in the green wavelength on the right hand side shows a total different shape. The convolution theorem, as applied in speckle interferometry (DAINTY [11]), provides theoretical proof that speckle images of unresolved

stars can be deconvolved resulting in a nearly diffraction limited image. Given that the undistorted satellite image refers to an object intensity $O(\rho)$, which is a function of the two dimensional vector ρ in the image plane. Then a distorted short exposed image of the object taken at time t_n can be expressed as a function of intensity

$$I_{t_n}(\rho') = \int O(\rho)G_{t_n}(\rho',\rho)d\rho, \tag{6}$$

where G_{t_n} denotes the point spread function, which characterizes the random turbulent state of the atmosphere at time t_n and the imaging capability of the optical system. The latter is not discussed here. To apply this formalism to streak camera satellite laser ranging it is convenient to formulate the problem for a one dimensional object intensity. This is reasonable because the streak camera output is one dimensional too, representing a temporal intensity profile. By averaging over the spatial dimension being perpendicular to the deflection direction, validates the object intensity transformation from space to time according to

$$O(\rho) = O(tc) = o(t) \tag{7}$$
$$G_{t_n}(\rho',\rho) = G_{t_n}(t'c,tc) = g_{t_n}(t',t) \tag{8}$$

where c denotes the speed of light in vacuum. This leads to a temporal intensity distribution

$$i_{t_n}(t''') = \int\int\int o(t)p(t',t)s(t'',t')g_{t_n}(t''',t'')dtdt'dt'', \tag{9}$$

where convolution functions for the satellite temporal impulse response $s(t'',t')$ and for the laser pulse shape $p(t',t)$ have been added. In this case the streak camera is not able to resolve the spatial object intensity $O(\rho)$ of the satellite, now mapped onto a temporal scale by $o(t)$. So one can express $o(t)$ in terms of an infinitely narrow delta function leading to the simplified equation

$$i_{t_n}(t'') = \int\int p(t)s(t',t)g_{t_n}(t'',t')dtdt'. \tag{10}$$

Following REINECKE [4] a fourier transform to equation 10 is applied, which yields

$$\begin{aligned} \tilde{i}_{t_n}(f) &= \int\int\int p(t)s(t',t)g_{t_n}(t'',t')e^{-2\pi i f t''}dtdt'dt'' \\ &= \int\int\int p(t)e^{-2\pi i f t}s(t',t)e^{-2\pi i f(t'-t)}g_{t_n}(t',t)e^{-2\pi i f(t''-t')}dtd(t'-t)d(t''-t') \\ &= \tilde{p}(f)\tilde{s}(f)\tilde{g}_{t_n}(f). \end{aligned} \tag{11}$$

The point spread function is a random function of time. So its power spectrum approaches a time independent value when averaged over enough samples. For n samples taken at times t_n the intensity power spectrum is

$$\sum_n |\tilde{i}_{t_n}(f)|^2 = |\tilde{s}(f)|^2|\tilde{p}(f)|^2\sum_n |\tilde{g}_{t_n}(f)|^2. \tag{12}$$

So with a known laser pulse shape $p(t)$, a given satellite impulse response function $s(t)$ and their Fourier transforms respectively, one can calculate the power spectrum of the point spread function by

$$\sum_n |\tilde{g}_{t_n}(f)|^2 = \frac{\sum_n |\tilde{i}_{t_n}(f)|^2}{|\tilde{s}(f)|^2|\tilde{p}(f)|^2}. \tag{13}$$

This makes the study of the wavelength dependence of point spread functions feasible. The ability to measure the point spread function presents the opportunity of constructing an adaptive filter which may be applied in the time domain, removing noise and the effects introduced by the turbulent atmosphere.

4 RESULTS OF STREAK CAMERA SATELLITE RANGING

Because the streak camera is only capable of detecting modulo ranges with a one way ambiguity of roughly $1m$, a simultaneous additional range measurement is required to resolve this Ambiguity. This consists of a very sensitive avalanche photo diode [6], which is illuminated by the light leakage of a mirror in the optical receive path. The data gathered by this device was utilized to calculate the whole number part N of the ranges.

Due to the effect of image spread mentioned above the spatial filter was adjusted wider than the seeing limit. In the first experiments with satellites a centroid detection technique was used to locate satellite echoes in time. This was done by averaging the video signal, obtained by the streak-camera, over an area where the amplitude of the signal exceeds a threshold. Recovering the round trip time according to equation 2, one obtains the complete range information as shown in figure 5. For the correction of the atmospheric path delay caused by dispersion, the model of MARINI and MURRAY [3] was applied. The ordinate shows the residual ranges which remain after fitting the data to the satellite orbit, whereas the abscissa represents the elevation of the telescope in degrees. The plot shows the data corrected for the green wavelength, so the ranges measured in this wavelength domain are distributed around zero. The dashed curve refers to the path delay between green and infrared, according to the model of Marini and Murray. One can see that this model fits the infrared observations of the lower track quite well.

To analyze the distribution of collected returns more clearly, figure 6 shows two histograms over the residuals of figure 5, one corresponding to green the other to infrared data. The returns of the green wavelength show a higher standard deviation than those obtained in the infrared. This may be due to the speckle effect stated above,

as this measurement was taken with a wide field of view, and the speckle influences the green wavelength detection more than the infrared. The standard deviation in the infrared wavelength measurements nearly equals that obtained with the ground target experiment in single photon mode, shown in figure 3. For higher intensities an excellent resolution for satellite measurements could be obtained, which is comparable to that shown in figure 2.

5 SATELLITE IMPULSE RESPONSE RECONSTRUCTION

To reconstruct the satellite impulse response function of satellites by streak camera imaging, the same procedure as described above is used. The only difference is that record complete frames of intensity distributions is recorded, representing the backscattered intensity versa time within one ambiguity interval. After the removal of the streak sweep nonlinearity and the telescope invariant point correction, the frames are corrected due to the laser pulse time of flight, so that averaging the measured intensity distributions yield the satellite backscattered intensity. Averaging is applied for several reasons:

- Firstly the photoelectron level at the streak camera was found to be insufficient to reconstruct the response function of the satellite for every shot. Satellite ranging with the streak camera is still performed in single photon mode resulting in sharp peaked single photoelectron events rather than a continuous response function.

- The path delay of laser pulses reflected from different retroreflectors at the satellite causes interference of the electromagntic field at the receiver. This is the well known effect of target speckle (see DEGNAN[12]) and is due to the coherent nature of laser radiation. Introducing a diversity of satellite orientations, i.e. sampling the response function over a variety of path delay realizations, one approaches the incoherent response function.

- Due to the discrete satellite retroreflector distribution one can only find satisfying results when averaging over different satellite orientations. This permits the comparison of the measurement with the incoherent response function introduced by DEGNAN [12].

To check out the capability of measuring satellite impulse responses with the streak camera two rather different targets, AJISAI and STARLETTE were chosen. While AJISAI is about $2.2m$ in diameter STARLETTE is only $0.24m$, so there must be

Satellite	FWHM of Impulseresponse [ps]	
	1064nm	532nm
STARLETTE	245	258
AJISAI	483	403

Table 1: *Measured FWHM of impulse responses for the given wavelengths.*

a significant difference in the observed response function. Figure 7 shows the calculated incoherent impulse response function [12] for both satellites as well as the measured impulse response, averaged over all returns of one satellite pass. According to the calculation for the FWHM of AJISAI 564ps are expected, whereas STARLETTE should lead to a much sharper response of 266ps FWHM. This tendency is found in the observation for both wavelengths and is summarized in table 1. Due to the cut off effect because of the noise floor the measured values are below the ones predicted by theory. To investigate the spatial image spread caused by atmospheric turbulence as mentioned in section 3 with respect to the transmitted wavelength, the recorded streak image frames were Fourier transformed and averaged yielding the average power spectrum of the distorted intensity distribution $\sum_n |\tilde{it}_n(f)|^2$ as described by equation 12. The power spectra obtained were divided by the estimated power spectrum $|\tilde{s}(f)|^2|\tilde{p}(f)|^2$, namely the convolution of laser pulse shape and satellite response function, giving the power spectrum of the point spread function $\tilde{g}(f)$ for both wavelengths. The result is plotted in figure 8 as a function of normalized frequency for the same pass of STARLETTE as the average intensity was shown in figure 7. There is only negligible power in the low frequency domain corresponding to the frequencies occupied by the actual signal. Around 0.07 parts of the sampling frequency there is a significant peak for both wavelengths. This indicates the induction of higher frequency components in the measured intensity distribution by the point spread function. Moving up the frequency scale one can observe in principle an identical behaviour in both wavelengths, but there is a trend to higher power for higher frequencies in the 532nm wavelength domain.

6   INTENSITY TIME SERIES ANALYSIS

To characterize the transmittance properties of the atmosphere in terms of a turbulent medium the data obtained by the streak camera was subjected to further analysis. By averaging the intensity detected in each time channel where the satellite return was expected for every shot and wavelength, time series of satellite backscattered intensities are obtained for the time span of the satellite pass.

Figure 9 shows such a histogram of measured intensities. The probabilty $p(I)$ of measuring intensity I is given after GRACHERA [8] by the equation

$$p(I) = \frac{1}{\sigma_I \sqrt{2\pi}} \exp \left[-(\ln(\frac{I}{<I>}) + \frac{\sigma_I^2}{2})^2 (2\sigma^2)^{-1} \right], \tag{14}$$

where σ_I refers to the normalized intensity variance. The dotted line in figure 9 represents equation 14 with mean and variance applied from the measurements taken. The model fits the observation quite well indicating that the atmosphere can be understood as a weak turbulent medium, i.e. $\sigma_I \ll 1$. For strong turbulence equation 14 should approach a Rayleigh probability distribution. Figure 9 was obtained from infrared data.

The treatment of the data obtained in the green channel lead almost to identical results with respect to the intensity probability distribution. However there are differences to be found looking at the time series. ISHIMARU [9] found an asymptotic solution for the power spectrum of the logarithmic intensity fluctuations in terms of the wind speed transversal to the optical path. The result for the low and high frequency limit is

$$\lim_{f \to 0} W_\chi = 0.8506 \frac{C_n^2}{V} k^{2/3} L^{7/3} \tag{15}$$

$$\lim_{f \to \infty} W_\chi = 2.192 \frac{C_n^2}{V} k^{2/3} L^{7/3} (\frac{f}{f_0})^{-8/3}, \tag{16}$$

where L denotes the path length in turbulence, C_n the refractive index structure constant and k the wave vector. In both limits there is a proportionality to the transversal wind speed V which acts as a transport mechanism causing the scintillation in intensity by shifting the turbulent cells across the beam path. In the presented case this turbulent transport is not due to the transversal wind velocity alone, but to the movement of the satellite tracking laser beam as well. In the high frequency limit, there is an additional dependence on the wind speed incurred by the factor

$$f_0 = \frac{V\sqrt{kL}}{2\pi}. \tag{17}$$

This factor governs the frequency dependence of the power spectrum beginning at a certain cutoff, which is related to the transversal wind speed, or turbulent transport, as well. On the right hand side of figure 10 there is an illustration of the frequency dependence of equation 15 indicating a decay proportional to

$$\lim_{f \to \infty} W(f) \propto f^{-8/3}. \tag{18}$$

On the left side there is a spectrum derived from satellite backscattered logarithmic intensities, where this behaviour can be found as well. According to equation 17 the

cutoff frequency at which the decay of power starts is a function of the transmitted wavelength. To provide experimental evidence figure 11 shows spectra of intensity time series obtained in the infrared and green channel. The wavelength dependent cutoff frequencies are marked by two arrows. As predicted by theory the cutoff frequency for $1064nm$ is lower than that for $532nm$. From the evaluation of two color satellite laser ranging point of view this indicates a higher variability of detectable intensity for shorter wavelengths. To analyze the correlation characteristics of intensity fluctuations of two different operating wavelengths it is convenient to derive the cross spectrum of these quantities (ISHIMARU [9])

$$Corr(\ln(I(\lambda_1)), \ln(I(\lambda_2), \tau) = \int\limits_{-\infty}^{\infty} \ln(I(\lambda_1, t)) \ln(I(\lambda_2, t + \tau)) dt \qquad (19)$$

and its Fourier transform respectively, the latter being called the coherence function

$$FT[Corr(\ln(I(\lambda_1)), \ln(I(\lambda_2)), \tau)] = \ln(I(\lambda_1, f)) \ln(I(\lambda_2, f))^*. \qquad (20)$$

Figure 12 shows the coherence function of the operating wavelengths obtained from a satellite pass of AJISAI. Again there is a sharp drop off in the area of $0.2Hz$. This is associated now with the loss of coherence of intensity fluctuations of the transmitted wavelengths. In other words, stable intensity relations between the two wavelengths can only be achieved if one averages for a time at least as large as the period associated with the cutoff frequency, i.e. 5 seconds in this case. The comparison of the correlation function obtained from two color measurements of satellites with different diameters allows an interpretation concerning the Fresnel zone mentioned in section 3. Figure 13 shows correlation functions of intensity fluctuations in different wavelengths obtained from STARLETTE and AJISAI passes. The correlation function is plotted versa the lag, labeled as τ in equation 19. The main fact which can be deduced from these measurements is that the detected intensities do not correlate for different wavelengths (correlation coefficients around 0.001). However it is quite astonishing why the correlation coefficients obtained from STARLETTE and AJISAI differ in sign for small lags around zero. For a satellite orbiting at a height of about $1000km$ the Fresnel zone is of the order of $1m$. So one finds that STARLETTE, being $0.24m$ in diameter, lies always within one Fresnel zone, wheras AJISAI, $2.1m$ in diameter, covers more than one Fresnel zone. This leads to the conclusion, that the observed effect can be interpreted in terms of aperture averaging at the satellite. Large diameter satellites are more suitable for two color laser ranging, giving better chances of simultaneous detection in different wavelength domains.

7 ACKNOWLEDGMENTS

References

[1] H. Hamal and I. Prochatzka, "Modular Streak Camera for Laser Ranging",*SPIE 1358,55*

[2] Th. Varghese, Chr. Clarke, Th. Oldham, M. Selden, Streak Camera Based SLR Receiver For Two Color Atmospheric Measurements, *Proceedings of 8th International Workshop on Laser Ranging Instrumentation*, (1992)

[3] J. W. Marini,"Correction of satellite tracking data for an arbitrary tropospheric profile", *Radio Science 7, 223-231*, (1972)

[4] M.Reinecke, H.Ruder: *Speckle Interferometrie*, Sterne u. Weltraum, 7, 246–255 (1977)

[5] U. Schreiber, S. Riepl, "Measuring atmospheric dispersion employing avalanche photo diodes", *Lidar Techniques for Remote Sensing, Chr. Werner, Editor, Proc. SPIE 2310, 2*,(1994)

[6] U. Schreiber, K. H. Haufe, J. F. Mangin, J. M. Torre and C. Veillet, "Operating the APD SP114 at the LLR station in Grasse", *Lidar Techniques for Remote Sensing, Chr. Werner, Editor, Proc. SPIE 2310,25*,(1994)

[7] J.W.Strohbehn, Editor, "Laser Beam Propagation in the Atmosphere", *Springer Verlag Berlin*,(1978)

[8] M.E.Grachera: *Similarity Relations and Their Experimental Verification*, in Laser Beam Propagation in the Atmosphere, Topics in Applied Physics, (J.W.Strohbehn, Editor), 25, Springer Verlag, Berlin, Heidelberg, New York 1978

[9] A.Ishimaru: *The Beam Wave Case and Remote Sensing*, in Laser Beam Propagation in the Atmosphere, Topics in Applied Physics. 25, Springer Verlag, Berlin, Heidelberg, New York 1978

[10] V.I.Tatarski: *The Effects of the Turbulent Atmosphere on Wave Propagation*, Israel Program for Scientific Translations Ltd., Keter Press, Jerusalem (1971)

[11] J.C Dainty: *Laser Speckle and Related Phenomena*, Spinger–Verlag, Berlin, Heidelberg, New York (1975)

[12] J.J. Degnan: *Millimeter Accuracy Satellite Laser Ranging: A Review*. Geodynamics Series 25
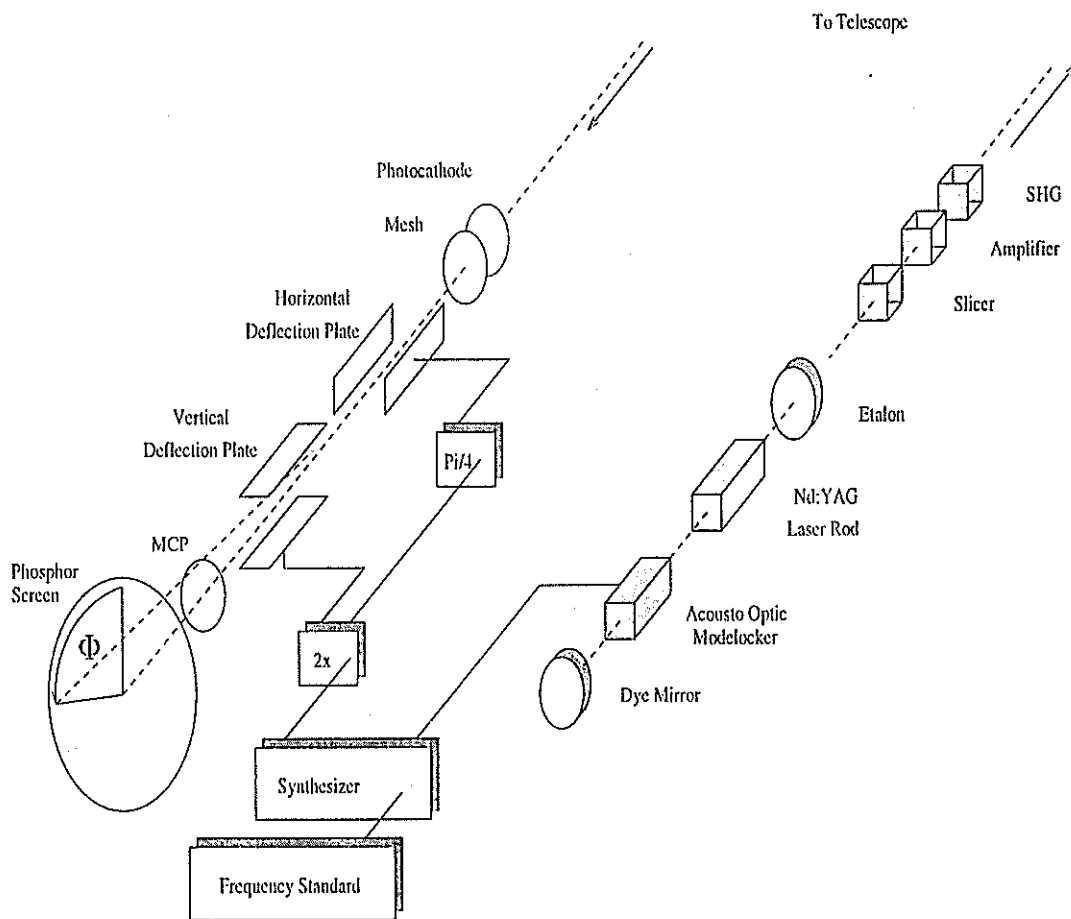
Figure 1: Experimental setup of satellite modulo ranging. The modulo range is measured in terms of the angular location Φ of photo electron traces on the phosphor screen of the streak camera.
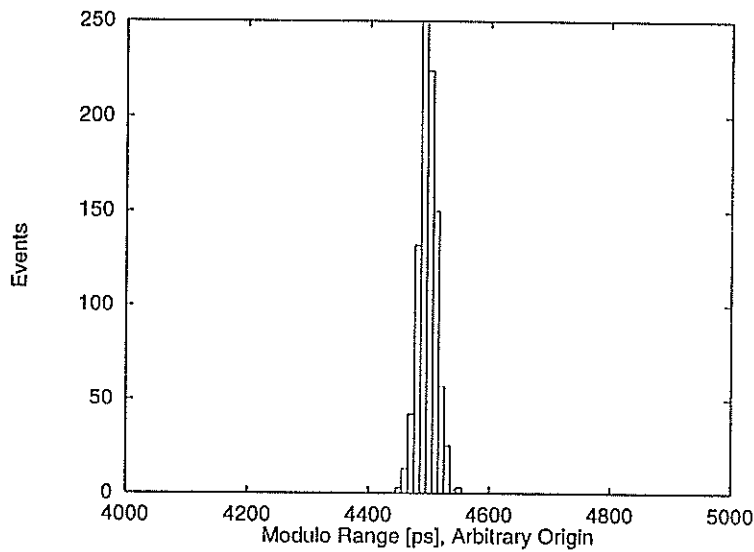
Figure 2: Histogram of 1064 nm ground target echoes. The device was operated in multi photon mode. A RMS of 14 ps was obtained.
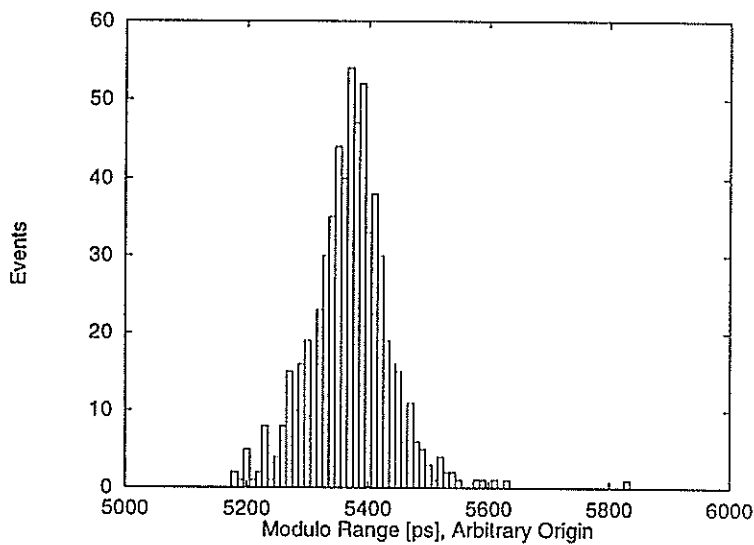
Figure 3: Histogram of 1064 nm ground target echos. The device was operated in single photon mode. A RMS of 90 ps was obtained.
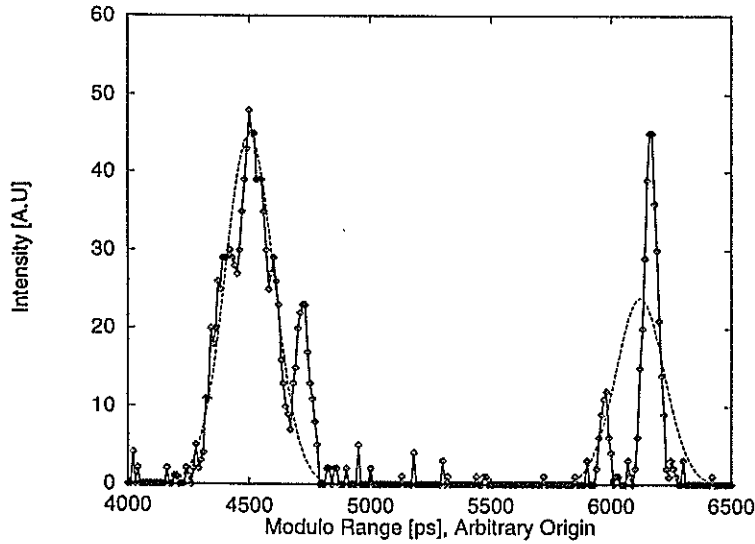
Figure 4: Dual color signal reflected from satellite STELLA. The solid line shows the infrared laser pulse on the left and the green laser pulse on the right side. The dashed line is the theoretical pulse response normalized to the intensity detected in each channel.
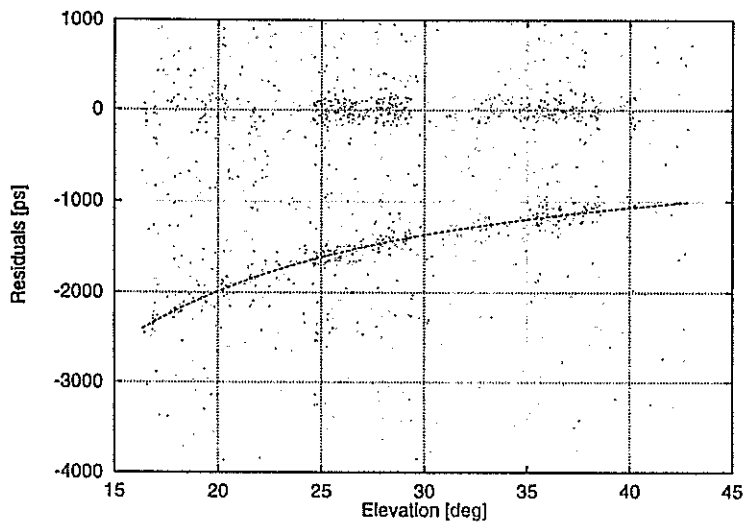
Figure 5: Range residuals obtained from ERS1 as a function of elevation. The upper trace corresponds to 532 nm, the lower trace to 1064 nm echoes. The dashed line indicates the dispersive delay predicted from surface meteorological data.
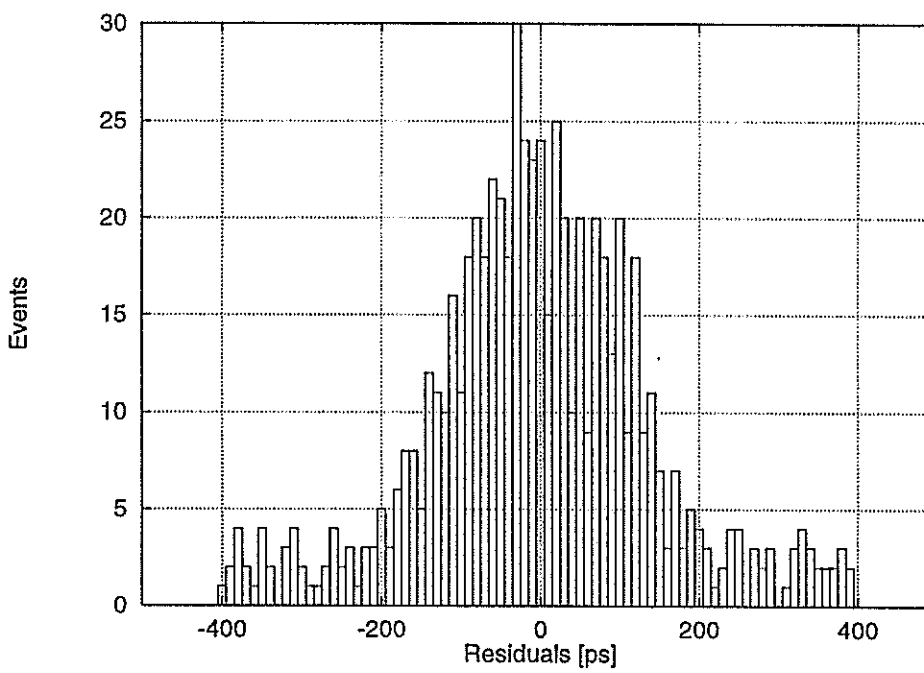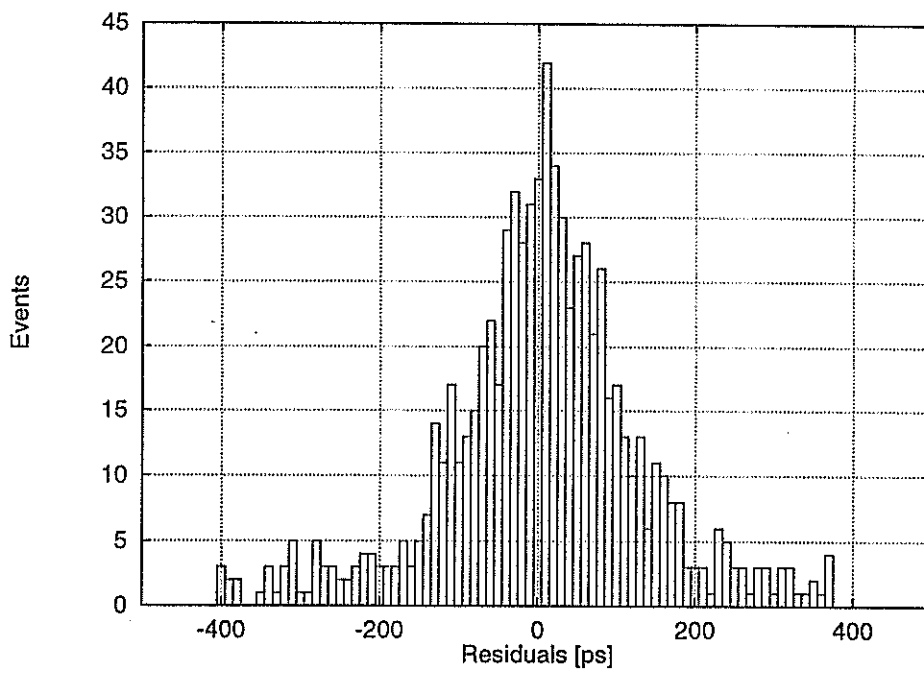
Figure 6: Residual histogram of 1064 nm (top) and 532 nm (bottom) echos, reflected by satellite ERS1
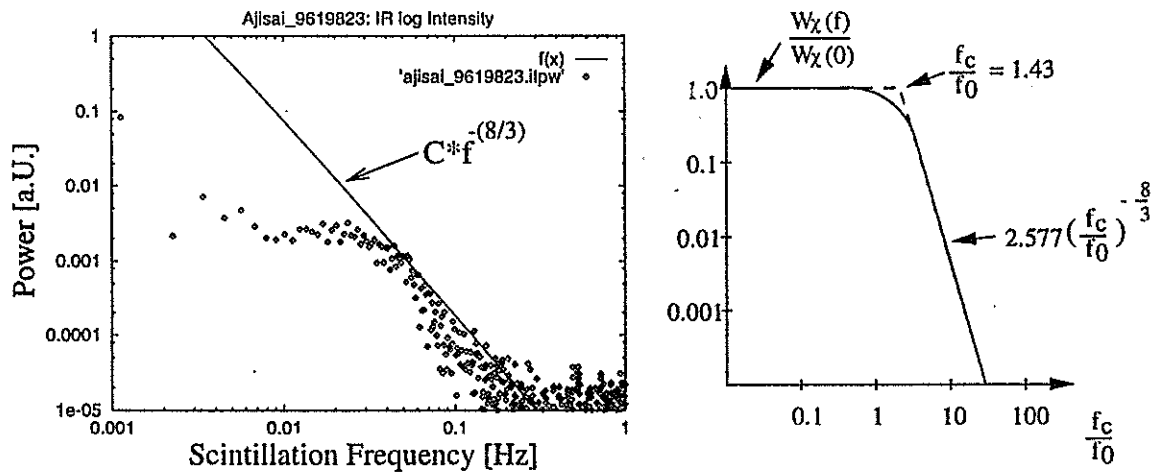
Figure 10: Frequency behaviour of the log intensity power spectrum: The left plot is obtained from measuring satellite backscattered intensities, whereas the right plot illustrates the theoretical frequency behaviour derived by ISHIMARU [9].
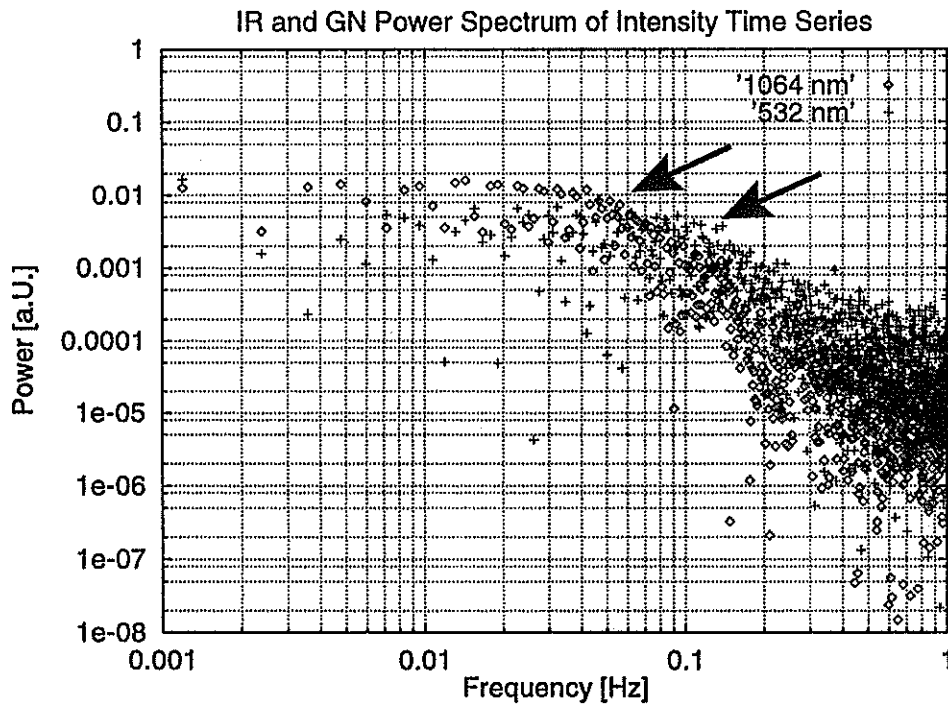
Figure 11: Power spectra of intensity fluctuations obtained from two color measurement to satellite AJISAI in the infrared and green wavelength domain. The arrows indicate the wavelength dependent cutoff where the power starts to decay with frequency.
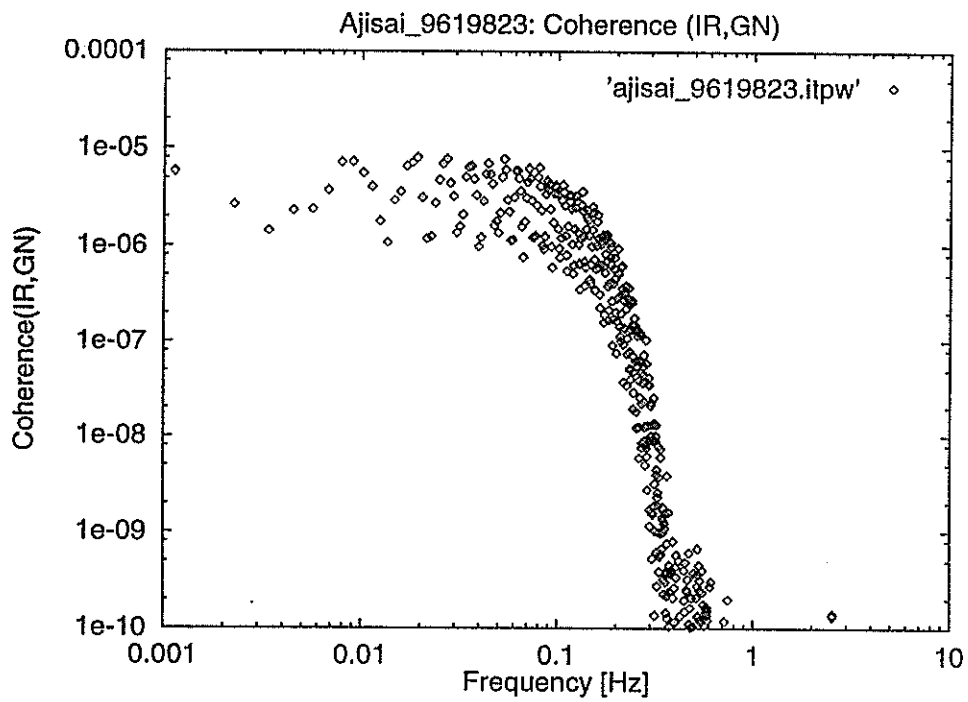
Figure 12: Coherence function of intensity fluctuations obtained from two color intensity time series measured during an AJISAI pass.
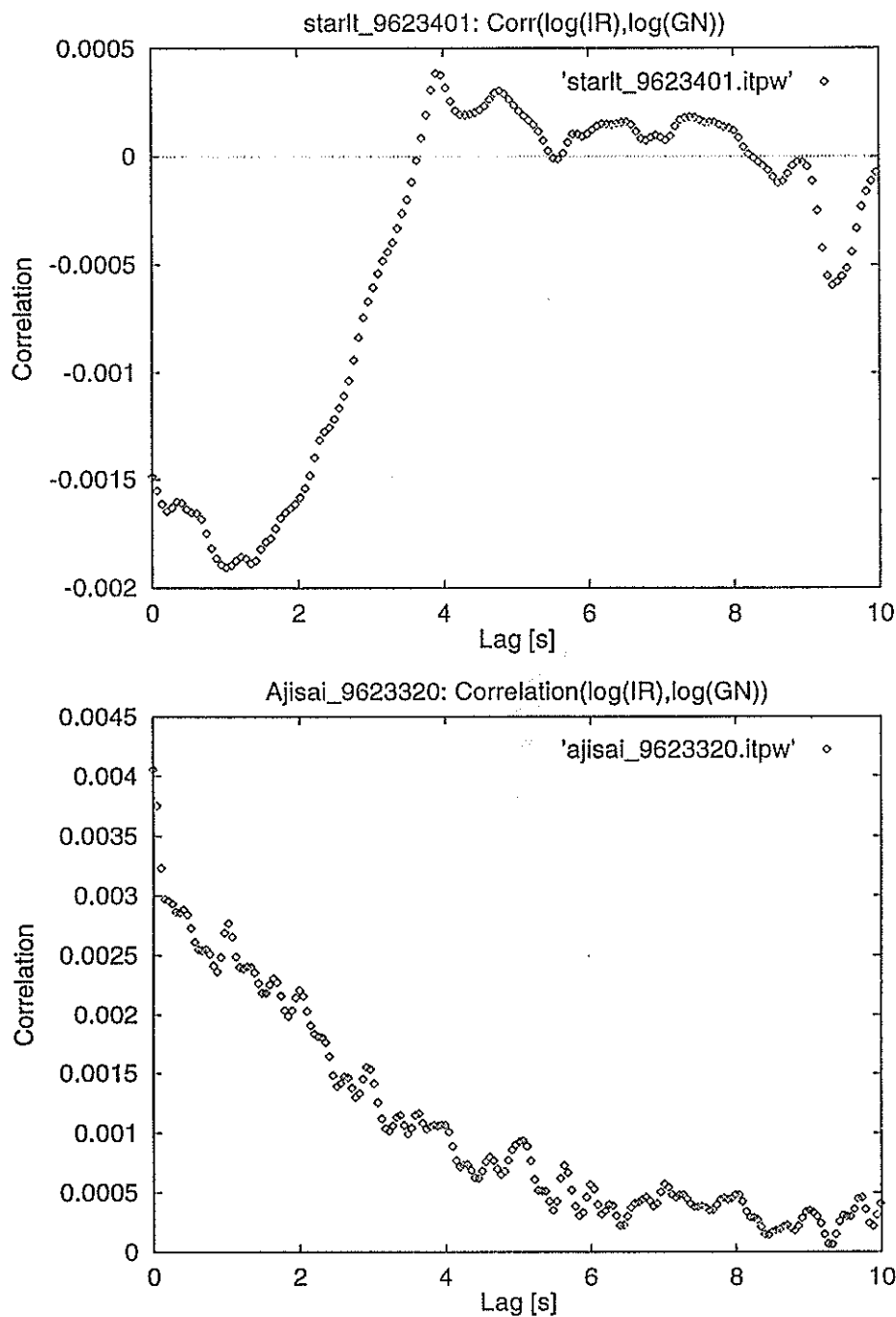
Figure 13: Correlation of intensity fluctuations of different wavelengths obtained from two color measurements to satellites of differing diameters. STARLETTE shows a slightly negative correlation at lag 0, whereas AJISAI shows a slightly positive correlation. This may be interpreted in terms of the Fresnel zone size (see text).

Water Vapour Correction of Two-Colour SLR

Reinhart Neubert

GeoForschungsZentrum Potsdam, Div.1: Kinematics and Dynamics of the Earth
Telegrafenberg A17, D-14473 Potsdam, Germany
Tel.: (49)-331-288-1153, Fax.: (49)-331-288-1111, e-mail: neub@gfz-potsdam.de

Introduction

The dispersion method to determine the atmospheric delay for SLR is now near to become practicable. At this stage we want to return to a principal systematic error source: the water vapour content of the atmosphere. As pointed out by Greene and Herring [1] using ray tracing calculations, insufficient knowledge of the atmospheric water vapour content may cause an error of more than 6 millimeters. This could partially explain the systematic effects observed in two-colour SLR by Schreiber et al. [2].

In this paper we first estimate analytically the influence of water vapour on the two-colour SLR results. In the remaining part we discuss the status of different remote sensing techniques for atmospheric water vapour.

Estimation of the influence of water vapour on SLR

For simplicity we regard the range correction $R(\lambda)$ for the zenith only:

$$R(\lambda) = \int_0^H (n-1)dh = f_d(\lambda) \cdot M_d + f_w(\lambda) \cdot M_w$$

Eq.1

where:

$$M_d = \int_0^H \rho_d(h)dh \qquad ; \qquad M_w = \int_0^H \rho_w(h)dh$$

Eq.2

are the total air masses of the dry and water vapour component, respectively. The integrals are taken from the station level to the satellite. The dimension and order of magnitude of the quantities are given in Tab.1:

Table 1: Approximate numerical values for the refractivities and air masses

Quantity	$f_d(0.53\mu m)$	$f_w(0.53\mu m)$	Md	Mw	fd Md	fw Mw
Unit	m³/kg	m³/kg	kg/m²	kg/m²	mm	mm
Numerical value	0.0002362	0.0003275	10 000	30 (very variabel)	2362	9.8

It can be seen that at optical frequencies the contribution of the water vapour to the zenith delay is about one centimeter only.

As has been shown by Saastamoinen [3], the total air mass M=Md + Mw can be estimated with high accuracy from the surface pressure using the fact that the atmosphere is near to hydrostatic equilibrium:

$$M = p / g_m \quad ; \quad g_m = \frac{\int_0^\infty g(h) \cdot \rho(h) dh}{\int_0^\infty \rho(h) dh}$$

Eq.3

where p is the total pressure and g_m is the mean gravity computed from the height-dependent gravity g(h) using the air density as a weighting function. Thus, regarding the total air mass as a known quantity, it is useful to rewrite Eq.1 into the form:

$$R(\lambda) = f_d(\lambda) \cdot M + (f_w(\lambda) - f_d(\lambda)) \cdot M_w$$

Eq.4

Eq.4 is the kernel of the commonly used Marini-Murray formula [4]. The water vapour term in Eq.4 is proportional to the difference of the refractivities of water and dry air. This explaines the rather weak dependence of the Marini-Murray correction from humidity.
The first term in Eq.4 is called the hydrostatic term. Sometimes it is referred to as the dry component, although it contains a large part of the water vapour contribution.

The main idea of the dispersion method in optical distance measurement is to determine the refraction correction from measurements at different wavelengths directly becoming free from any assumption on the distribution of the atmospheric density. From two-colour ranging we can determine the range correction if the water vapour content is known. Adding a third optical or near infrared wavelength permits the dry and wet components to be separated, theoretically. However, the required range resolution of the three-colour method is too high to be realistic.

Introducing two wavelengths into Eq.1, we can derive the following relation by eliminating M_d

$$R(\lambda_1) = F(\lambda_1, \lambda_2) \cdot (R(\lambda_1) - R(\lambda_2)) + G(\lambda_1, \lambda_2) \cdot f_w(\lambda_1) \cdot M_w$$

Eq.5

where:

$$F(\lambda_1, \lambda_2) = \frac{f_d(\lambda_1)}{(f_d(\lambda_1) - f_d(\lambda_2))} \quad ; \quad G(\lambda_1, \lambda_2) = 1 - \frac{f_d(\lambda_1)}{f_w(\lambda_1)} \cdot \frac{f_w(\lambda_1) - f_w(\lambda_2)}{f_d(\lambda_1) - f_d(\lambda_2)}$$

Eq.6

The first term in Eq.5 is the most important and depends on the differential range only. The sensitivity factor F is of the order 10 to 20 depending on the wavelength pair used. For high accuracy a small F-number is essential. The second term in Eq.5 describes the influence of the water vapour. The water vapour mass M_w must be known from some independent source with a precision depending on the sensitivity factor G (Eq.6). This factor is very weakly depending on the choice of the wavelength pair (Fig1).
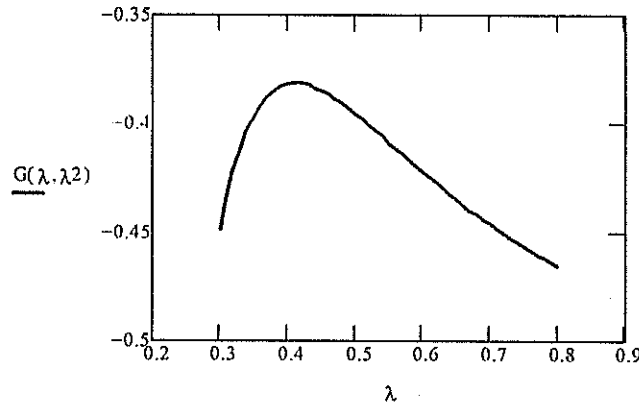
Fig.1: The sensitivity factor G versus the short wavelength (nm), if the 2nd wavelength is fixed at 1.06 μm.

If the fundamental and 2nd harmonic of Nd-YAG is used, G is about -0.4. The negative sign of G means that the range correction will be overestimated if the water vapour correction is neglected.

It migth be interesting to look at the influence of water vapour on the Marini-Murray correction, based on surface data and the assumption of hydrostatic equilibrium. For this purpose we rewrite Eq.4 :

$$R(\lambda) = f_d(\lambda) \cdot M + G'(\lambda) \cdot f_w(\lambda) \cdot M_w \qquad \text{where} \quad G'(\lambda) = \frac{f_w(\lambda) - f_d(\lambda)}{f_w(\lambda)}$$

Eq.7

This form is fully analogous to Eq.5. The water sensitivity factor G' in Eq.7 is again nearly independent from the wavelength and for the 2nd harmonic of Nd-YAG equal to 0.28. The positive sign of G' means that the hydrostatic term in Eq.5 or 7 is underestimating the range correction (this is because the refractivity of water vapour is higher than the refractivity of dry air). The conclusion of this comparison is: two-wavelength ranging is sligthly more dependent on the water vapour than the Marini-Murray formula. If the water vapour mass according to Table 1 (30 kg/m²) is adopted, we calculate the water correction term in Eq.7 to be 2.7 mm. Therefore, very rough estimates of the water mass are sufficient to be comparable with other model errors of the Marini-Murray formula.

Main aim of two-colour SLR is to obtain the range correction with higher accuracy than possible with the hydrostatic model using the surface pressure. It is believed that from surface pressure the zenith range correction can be obtained with an error of less than 1 cm. To justify the effort connected with two-colour ranging, we set the accuracy requirement of the water vapour correction to 1 mm. This corresponds to the knowledge of the water vapour mass with an error of 7.6 kg/m² or less. It is quite a low accuracy, but not reliably obtained using surface data only.

How we can get the water vapour mass?

There is a lot of efficient techniques available now achieving the accuracy requirement for SLR. One of the most promising sources is GPS. It has been shown that from the GPS residuals the water vapour content can be retrieved with sufficient accuracy [5..7]. The main reason for this is the high refractivity of water vapour for radio waves. The idea can be described as follows: The

zenith range correction can be treated as an unknown parameter in the least square analysis of the GPS data. This gives reasonably accurate estimates if some conditions are fulfilled: simultaneous tracking of many satellites at different elevations, inclusion of sufficient well-distributed GPS receivers, careful modelling of all instrumental effects (e.g. antenna phase center variations). The angular dependence of the atmospheric delay has to be modelled. It is assumed to be independent from azimuth in general. Introducing now surface weather data (mainly pressure), the dry and wet components of the atmospheric delay can be separated.

It has been demonstrated by comparison with other techniques that the GPS-derived water vapour masses are usually accurate within 10 per cent. As an example, we show some results obtained during a test campaign in May/June 1994 [8]. In this field test two GPS receivers, two microwave radiometers as well as a new high resolution solar spectrometer were included. The two microwave radiometers were kindly made available by B.Bürki from ETH Zürich. The measurements were taken simultaneously at GFZ Potsdam and the research campus Berlin-Adlershof. Fig.2 shows the comparison between GPS and the water vapour radiometers at both sites.
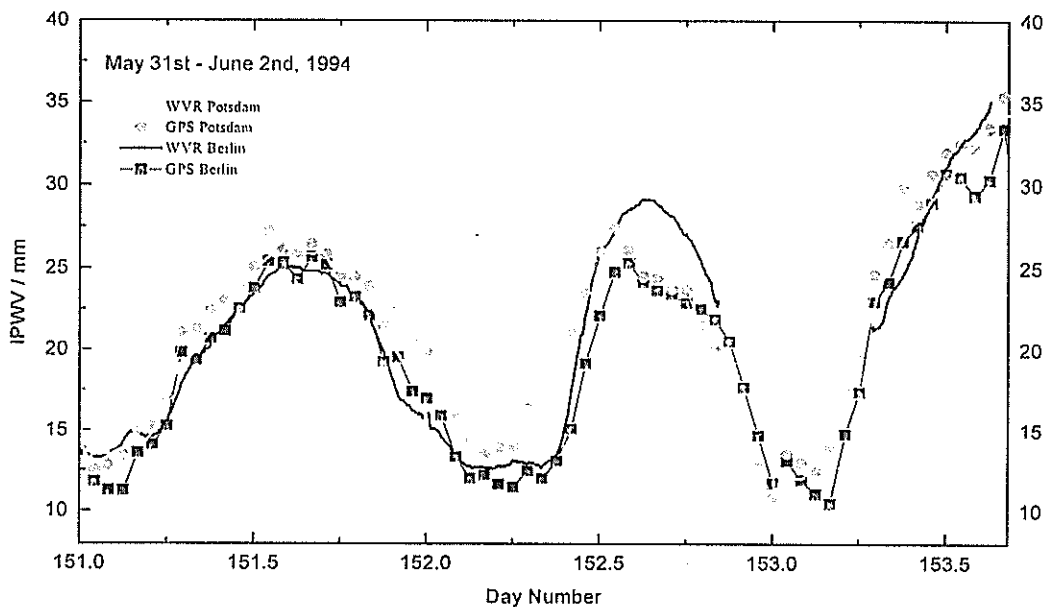
Fig.2: Integrated water vapour above the two test sites from May 31st until June 2nd estimated from GPS and measured by water vapor radiometers (WVR), from [8]

In Fig.2 the integrated precipitable water (IPW) in mm is given. This quantity is numerically identical with the columnar water vapour mass in kg/m^2. It can be seen that the deviations between both methods are smaller than the error limit of the radiometers (5%) in general, except for Berlin at day number 152.7. This isolated discrepancy could be attributed to the GPS method referring to the results of high resolution solar spectroscopy. This method which could be developed to a benchmark, consists in the observation of well isolated vibrational-rotational absorption lines of water vapour. This test has been done in cooperation with the Laboratorium fuer spektroskopische Methoden der Umweltanalytik, Berlin-Adlershof, using a double echelle spectrograph described in [9]. An example absorption spectrum is shown in Fig.3. The advantage of using high resolution in contrast to the commonly used broadband solar photometry is that there is no overlap with absorption from other atmospheric gases and that the background can be assumed to be constant within the small wavelength range. This allows simple models to be used

to retrieve the water vapour content from the spectra. The only parameters required are the laboratory-measured spectroscopic constants of the individual lines.
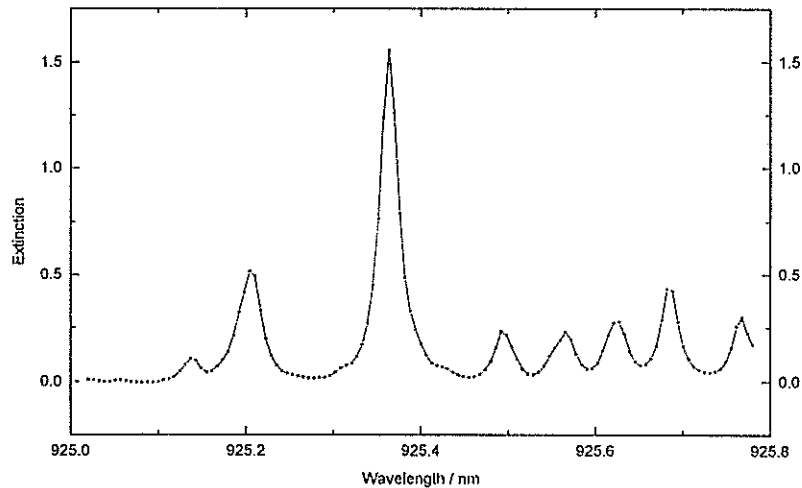
Fig.3: Typical absorption spectrum of water vapour in a small near infrared window of 1 nm width, (from [8])
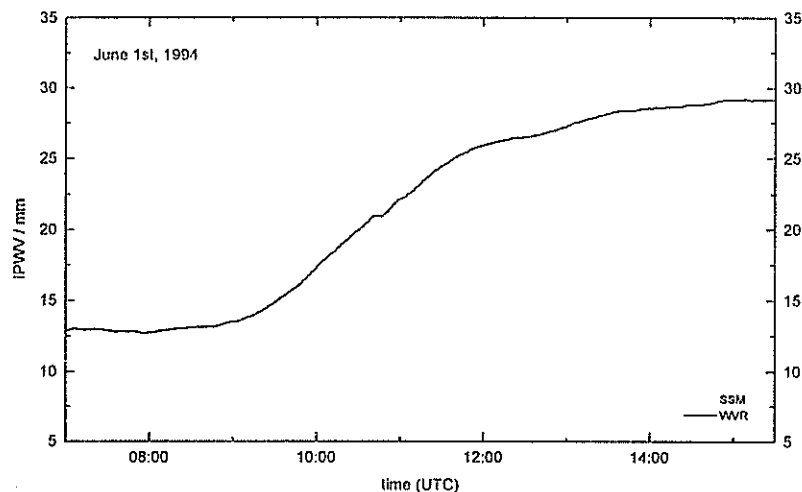
Fig. 4: Integrated water vapour for June 1st, 1994 measured by a water vapour radiometer (WVR) and a solar

spectrometer (SSM) in Berlin-Adlershof , (from [8])

The last Fig.4 shows a comparison between the microwave radiometer and the optical spectrometer for June 1st in Adlershof. The differences are within the error limits of the radiometer. On this day GPS is giving significantly lower values (Fig.2). Because of the good agreement of the other methods it is believed that the deviation is due to the GPS method in this example. Fig.4 is interesting because of the strong change of the water vapour content within a few hours. In this case the weather data measured at the surface did not indicate a significant change of the water vapour. This demonstrates clearly that the surface data are insufficient for estimating the integrated water vapour content reliably.

Conclusion

- two-colour SLR measurements need to be corrected for water vapour
- surface weather data are not sufficient to do this correction
- a cost-effective and sufficiently accurate method for water vapour determination is GPS-meteorology
- high resolution optical absorption spectroscopy can be used as a benchmark to calibrate/control the GPS method and/or microwave radiometry

References

[1] B.A.Greene, T.A.Herring: Multiple Wavelength Laser Ranging, Proc. 6th Workshop on Laser Ranging Instrumentation, Antibes, Sept.22-26, 1986, p.581

[2] U.Schreiber, W.Maier, S.Riepl, K.H.Haufe: Measuring Atmospheric Dispersion Employing Avalanche Photo Diodes, Proc. 9th Workshop on Laser Ranging Instrumentation, Canberra Nov. 7-11, 1994, p.615

[3] J.Saastamoinen: Contributions to the Theory of Refraction, Bull. Geod. 105, p.279, 1972

[4] J.W.Marini, C.W.Murray jr.: Correction of Laser range Tracking Data for Atmospheric Refraction at Elevations above 10 Degrees , NASA Techn. Report X-591-73-531, 1973

[5] M.Bevis, S.Businger,T.A.Herring, Ch.Rocken, R.A.Anthes, R.H.Ware: GPS Meteorology: Remote Sensing of Atmospheric Water Vapor Using the Global Positioning System, JGR Vol.97, 1992, pp.15787-15801

[6] M.Bevis, S.Businger: GPS Meteorology and the International GPS Service, in: IGS Workshop 'Special Topics', Potsdam, May 1995

[7] G.Gendt: Estimation of tropospheric water vapor content by ground-based GPS receivers in: Field Campaign LINEX 96/1 : Water Vapor Observation with different Remote Sensing Techniques from April 15th to May 13th at Meteorological Observatory Lindenberg, Deutscher Wetterdienst, Arbeitsergebnisse Nr.39, Offenbach 1996

[8] B.Sierk, B.Bürki, H.Becker-Roß, S.Florek, R.Neubert, H.-G.Kahle: Tropospheric Water Vapour Derived from Radiometer, Solar Spectrometer and GPS Measurements, submitted to JGR

[9] H.Becker-Ross, S.Florek: High-resolution Spectrometer for Atomic Spectrometry, J. Anal. At. Spectrom., Vol. 10, p. 145, 1995

Acknowledgement

ATMOSPHERIC DISPERSION MONITORING
USING 0.53 um AND 1.54 um SATELLITE LASER RANGING

B.Greene
Electro Optic Systems, Pty.Ltd., Queabeyan, NSW, Australia

H.Kunimori
Communication Research Laboratory, Tokyo, Japan

K.Hamal, I.Prochazka
Czech Technical University, Prague, Czech Republic

Several attempts have been made to contribute to the existing atmospheric dispersion and optical signal propagation delay models using picosecond high precision multiple wavelength Satellite Laser Ranging (SLR) in visible region [1]. We are reporting, to our knowledge for the first time, on the two wavelengths SLR in visible at 0.53 um and in the near infrared at 1.54 um.

The SLR Observatory in Tokyo, Japan employs 1.5 meter aperture telescope. The NdYAG laser delivering 200 mJ in 140 picosecond pulses at 1.064 um is split in two beams; a second harmonic generator transmites 30 mJ at 0.53 um, the second one entering the Raman cell filled by Methane delivers 6 mJ at 1.54 um. The receiver package consists of two detectors. The Silicon based Single Photon Avalanche Diode (SPAD) detects the signal at 0.53 um. The Germanium based SPAD cooled to 77K detects the reflected signal at 1.54 um. The detectors quantum efficiency estimate is 15 % at each wavelength, their output signals in NIM form are registered in Picosecond Timing System with 10 picoseconds resolution and processed in Master Ranging Control System. The single shot temporal resolution of the entire laser ranging chain is limited by the laser pulse duration to 100 psec. The results of laser ranging to several satellites equipped by retroreflectors and orbiting at the altitudes 1 000 to 20 000 km are summarized on Figure 1, where the two wavelengths time interval is plotted as a function of satellite elevation above the horizon. The solid curve represents the Marini Murray model [2]. No discrepancy has been detected on the present resolution.

Figure 1 The 0.53 um and 1.54 um wavelength differential delay versus elevation above the horizon basen on ranging to Topex, Lageos2 and Ajisai satellite. Solid line Marini Murray model.

[1] I.Prochazka,K.Hamal,G.Kirchner, Technical Digest of the Conference on Lasers and Electro Optics CLEO'94, Anaheim, CA, May 1994,55 (1994)

[2] J.B.Abshire, App.Opt. Vol.19, 3436-3440 (1980)

GOALS
Subcentimeter eye safe laser ranging

- subcentimer satellite laser ranging

- eye safe operation 1.54 um

- two wavelength operation 0.53 & 1.54 um

- single photon detection

- prerequisite for system automation

KunimoriGreeneGuilfoyleHamalProchazkaKirchnerKoidl

Eyesafe Laser Ranging
ENERGY BUDGET LINK

	0.53 : 1.54
laser energy (mJ)	35 : 5
beam divergence	1 : 1
receiver FOV (arcsec)	12^2 : 8^2
detector QE (%)	15 : 5
T/R optics	1 : 2
photon energy	3 : 1
total machine	7 : 1
satellite cross sect.	
atmospheric transm.	
satellite ranging	8 : 1

Kunimori, Greene, Hamal, Prochazka, '96

SECOND HARMONIC BASED T/R SWITCH

K.Hamal

Czech Technical University, Brehova 7
115 19 Prague 1, Czech Republic
fax +42 2 85762252, prochazk@mbox.cesnet.cz

B. Greene

Electro Optics Systems, PtyLtd, Queanbeyan,NSW, Australia

There are several schemes to realize a Transmit / Receive (T/R) for the coaxial SLR Coude optics, in particular the rotating disc, aperture sharing etc. Reffering to the invention presented at the workshop in Antibes, 1986, the second harmonic based T/R switch consists of the second harmonic generator and the fundamental/second harmonic dichroic mirror. The transmitted laser beam at the fundamental wavelength (1.064um) passes the dichroic mirror and the second harmonic generator to the telescope. The reflected beam from a target (0.53 um) passing the harmonic generator with negligible losses is reflected by the dicroic mirror to the receiver package. There are no moving parts, no time synchronization is needed. The minimal range distance is zero. In the particular application for the Keystone Project, the KTP crystal 10x10x3 millimeters and Silicon SPAD detector have been used. The T/R switch has been tested ranging to the target at the T/R switch output, retroreflector located inside the main telescope and to the calibration piers at various distances. The T/R switch box for Keystone is constructed to allow three color ranging at 0.53,0.35 and 1.54 micrometers simultaneously.

479

Indoor calibratiom, Kashima

BEXP x2 FRONT FACE REFLECTION 09-17-1996 04:36:09

Data file T5   coll. # 1

31   Cell width   .04   Tic =   0.400000
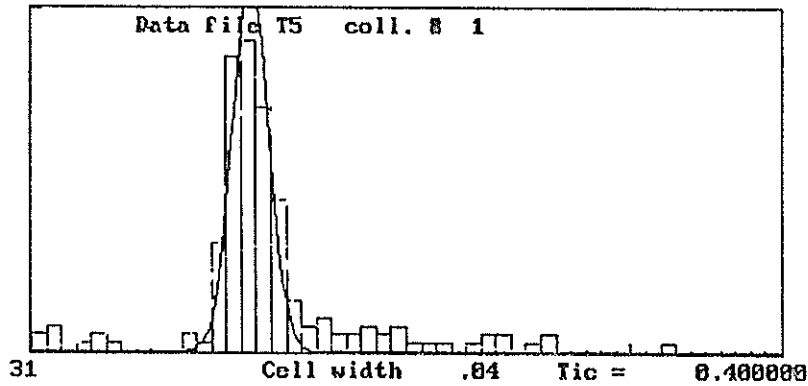
Limits	Criter.		MEAN	SIGMA	PT #
	31.000 /	33.000	31.633671	0.228239	181
	3 * SIGMA		31.597706	0.074174	151
	2.5*SIGMA		31.580030	0.054093	140
	2.0*SIGMA		31.583683	0.047358	131

Terrestrial ranging 'south pier',Kashima

4X ND + 1 A DETUNED 09-17-1996 07:45:51

Data file T15   coll. # 1

235.6   Cell width   .04   Tic =   0.320001
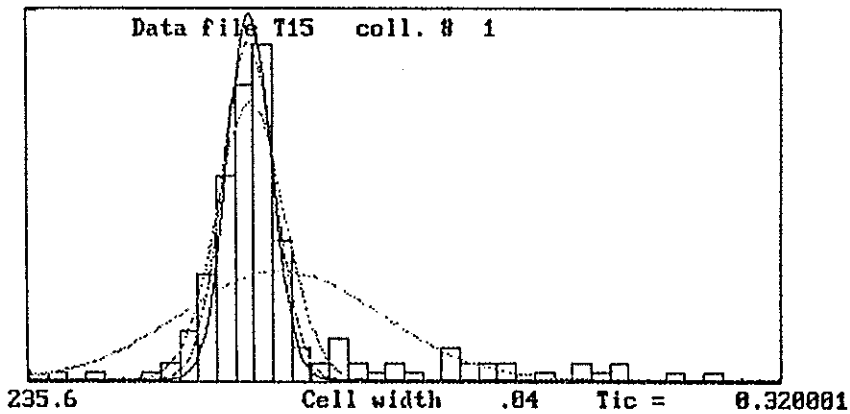
Limits	Criter.		MEAN	SIGMA	PT #
	235.600 /	237.200	236.137978	0.213180	178
	3 * SIGMA		236.071564	0.072128	153
	2.5*SIGMA		236.067642	0.055178	142
	2.0*SIGMA		236.069397	0.047269	132

System Automation and Operational Software

An assessment of the IRV model for the GPS satellites

A.T. Sinclair

Royal Greenwich Observatory, Madingley Road, Cambridge CB3 0EZ, England.

1. Introduction

The IRV format, coordinate system and force model were adopted by the Center for Space Research (CSR), University of Texas, in about 1982 as a means of providing predicted positions of Lageos for the SLR stations. They adapted the IRV system from a system previously in use at NASA. The IRV system has now been adopted for all SLR satellites, but using a higher degree and order for the lower satellites. In a paper presented at the Laser Ranging Workshop in Canberra in 1994, this author showed that the IRV model was rather inadequate for very low and very high satellites. That paper concentrated particularly on the problems for low satellites. In this paper we consider in more detail the problems for the GPS satellites, in view of the important contribution that SLR can make by providing a completely independent check on the accuracy of the precise IGS orbits.

2. Deficiencies of the IRV force model

The IRV force model is fairly basic, in order to reduce the computer time needed by the on-site numerical integration program, which is used for generating the predicted orbit. With the computer power now available this has become a minor consideration. However for most satellites in use for SLR it still serves it purpose adequately, and so it has been retained, as it would be big job to carry out any changes through the wide variety of software implementations that are in use throughout the SLR network. The IRV model is described in the Newsletter of the SLR Subcommission of the CSTG, June 1995, pp 33-36.

The technique of forming IRVs is to generate a precise orbit over a period of perhaps 2 weeks, by fitting an orbit integrated using an elaborate and precise force model to SLR data or some other data (e.g., the phases of the GPS broadcast signals or the GPS broadcast elements), and then run this orbit ahead over the prediction period, of perhaps several months. The simpler IRV orbit is then fitted to the precise orbit over periods of one day, resulting in a series of initial positions and velocities at 0 hours of each day of the prediction period. Thus an SLR station can take the position and velocity for the current day, and need only run its integrator for at most perhaps a little over 24 hours, if a pass happens to start near midnight (UT) and continue into the next day.

The simple IRV orbit will of course not give a perfect fit to the precise orbit, but for most of the SLR satellites the errors are only a few metres, which are of no consequence. The GPS satellites suffer a fairly large solar radiation pressure force which is not included in the IRV force model. Figure 1 shows a typical plot of the resulting errors of the IRV orbit, which can reach about 50 metres along-track and 40 metres radially. (The errors are discontinuous at the end of each day, but in these plots the discontinuities have been joined by a straight line.) The along-track error causes an angular displacement of the GPS satellite of less than 1 arcsec, which is of no consequence whatever from the point of view of pointing an SLR telescope at the satellite. For such high satellites the along-track error has a much reduced effect on the range, by a factor of 10 or more. Hence the range errors of the IRV orbit can be up to a little over 40 metres, requiring a

Figure 1 GPS36. Residuals of IRV orbit (1—day spans) from the precise orbit.
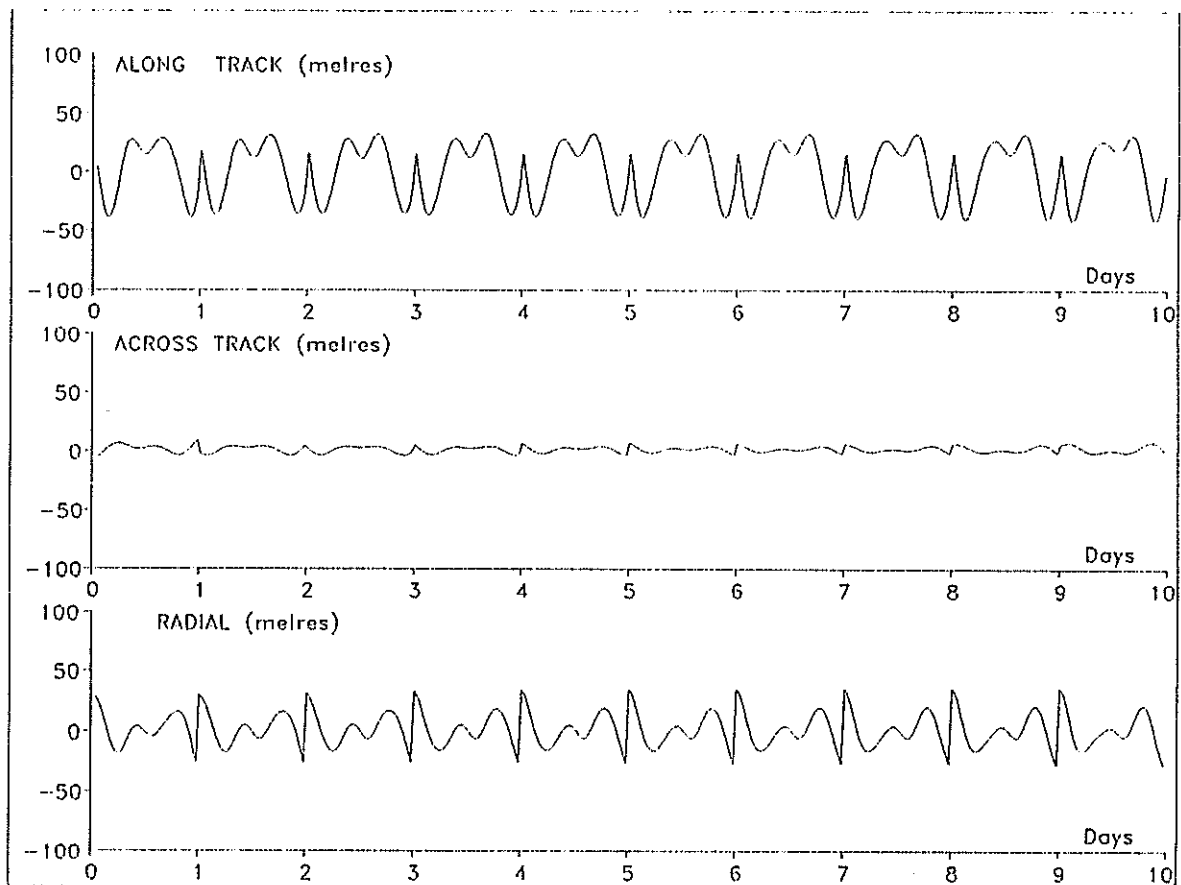
Figure 2 GPS36. Residuals of IRV orbit (1/4 day spans) from the precise orbit.

483
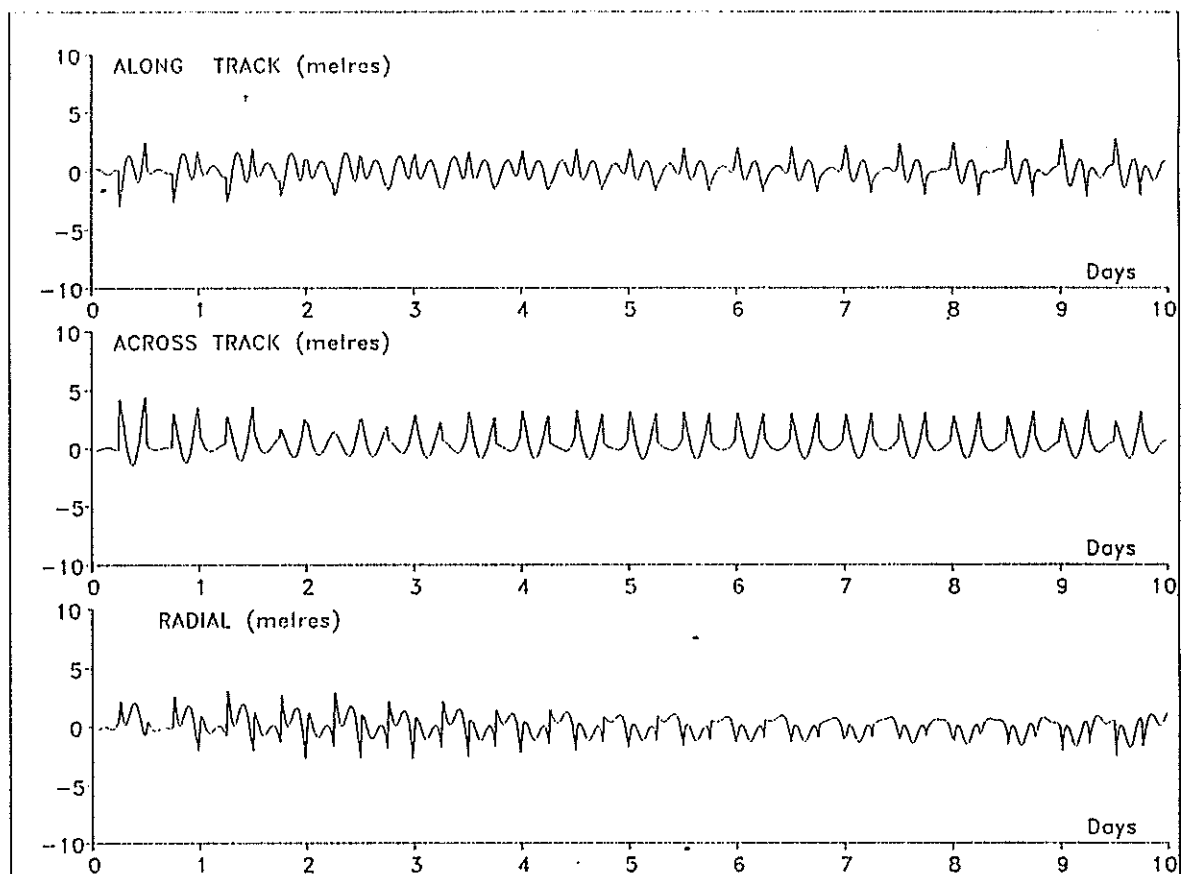
Figure 3 GPS36. Time biases determined from SLR data. Sept 1–19. Using IRVs of 1/4 day span.
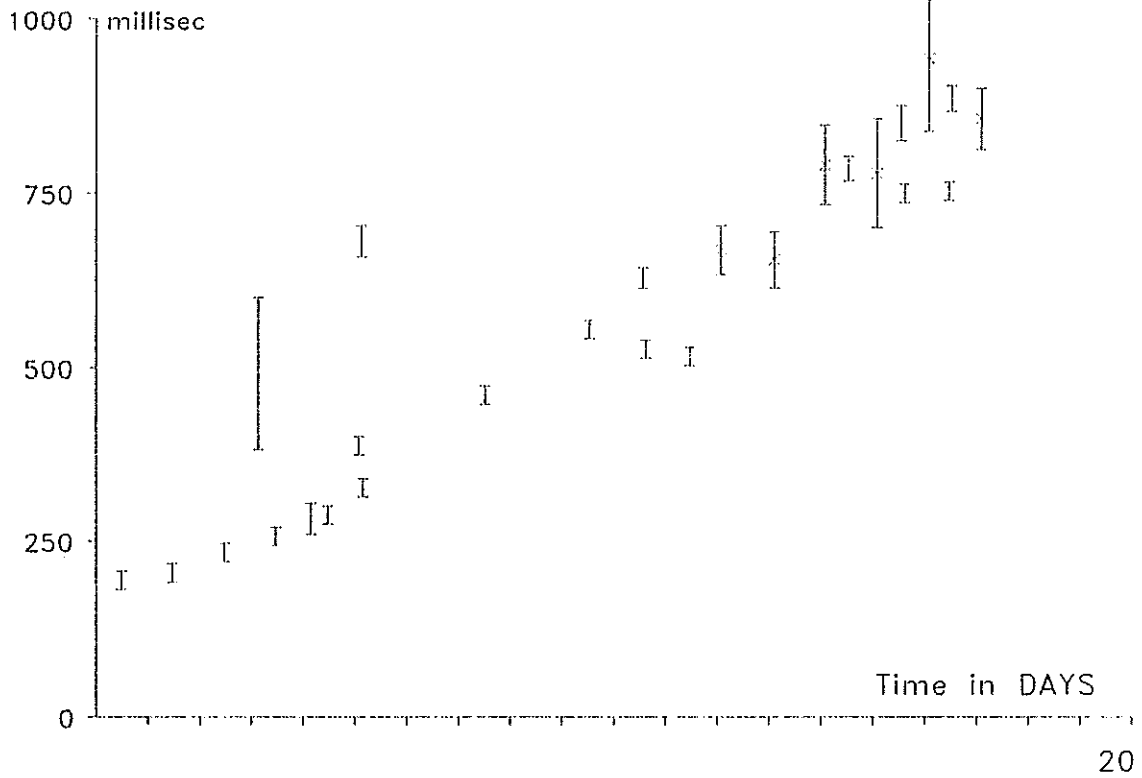
Figure 4 GPS36. Time bias of IRVs determined by comparison with the broadcast elements. Sept 1–19.
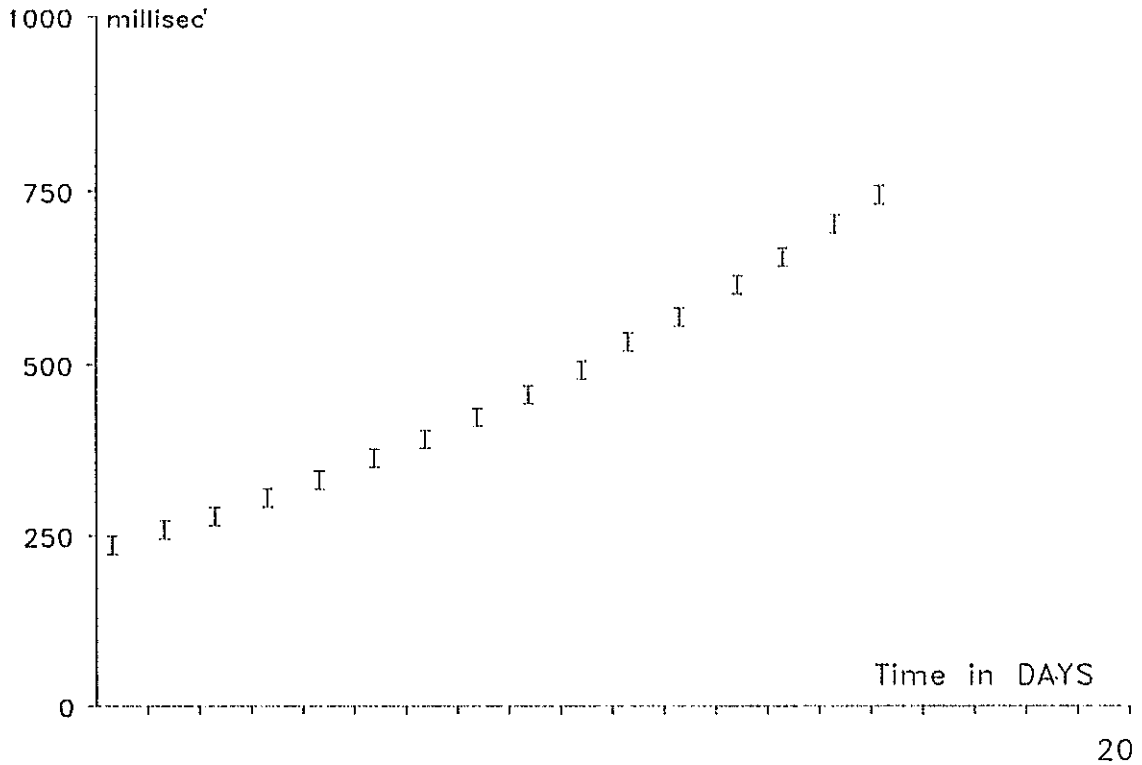
range gate of about ± 300 ns around the predicted range. This is more than is desirable for such high satellites, in view of their very weak return signal.

In a paper presented at the Canberra Workshop (1994) this author examined several possible methods of overcoming the deficiencies of the IRV force model for low and high satellites, and concluded that a method that is simple to implement by the stations is to reduced the span over which the IRV orbit is fitted to the precise orbit. For the GPS satellites it is effective to fit over quarter-day spans, and so there will be four sets of IRVs for each day, and all the station has to do is to select the set for the quarter of the day in which it starts tracking the pass, and use this set in exactly the same way as it would use a normal set of IRVs. Figure 2 shows typical residuals of quarter-day IRVs from the precise orbit for GPS36. The residuals are much reduced, and give range differences from the precise orbit less than about 10 metres.

Of course this error of misfit of the IRV orbit to the precise orbit is only one part of the error of the predictions. There is also the larger contribution due to the degradation of the predicted orbit compared with the actual orbit. We consider this in the next section.

3. Time bias corrections

All predicted orbits deteriorate with time, with the error being primarily along-track. It has been found to be a successful scheme to determine from SLR passes as they are obtained the current along-track error, expressed as a time-bias, to fit a low order polynomial through these values, and to use this for predicting the time bias for subsequent passes. It is more convenient for the stations to use a single set of IRVs for several weeks rather than changing it frequently, perhaps as often as daily. Also it appears to be rather more successful to use a set of IRVs with a well-determined time bias history, even if the time bias is large, rather than frequent changes to new sets of IRVs, which no doubt have small time biases, but with no knowledge of the rate of change.

There are several problems with this scheme as applied to GPS satellites. For these high satellites the range measurements are only weakly dependent on the along-track error, and hence give a poor determination of the along-track error. Also the misfit error of the IRVs discussed above contributes to the difference of the range measurement from the prediction, and hence adds more scatter to the along-track error that is deduced from the range measurement. Figure 3 shows the typical scatter of time bias values for a set of IRVs for GPS36, derived from the SLR tracking data alone.

For the GPS satellites there are other sources of orbit information in addition to the SLR data. The broadcast elements give the positions of the satellites to about 5 metres accuracy. Figure 4 shows the time biases the IRVs of GPS 36 over the same time period as in Figure 3, but derived each day from the broadcast elements received by the ROGUE GPS receiver at Herstmonceux. It is seen that the overall trend is much the same as derived from the SLR data, but with considerably reduced scatter. A single GPS receiver only receives the elements that are valid for the part of the orbit in view by that receiver, and this can produce a small bias in the values determined for the time biases. However the effect is not too serious, and does not seem justify the effort of setting up an automatic system to obtain the elements from another receiver. In this way the time biases of the IRVs of GPS35 and GPS36 are determined at Herstmonceux shortly after 0^h UT each day, for both the IRVs sets produced by RGO and by ATSC, and time bias polynomials derived from these values are placed in the RGO ftp directory.

Figure 5 shows the actual range residuals that would have been obtained by the SLR stations, using the IRVs with the time bias correction derived from the broadcast elements. The range residuals reach nearly 50 metres, and so a range gate of at least ± 350 ns would be needed.

The IRVs used for this plot and for deriving the time bias polynomial used the quarter-day spans. If the standard 1-day spans are used then the range residuals are only slightly worse, perhaps reaching 60 metres. The reason for this rather insignificant improvement of the quarter-day IRVs is that the precise predicted orbit itself develops an error signature compared with the actual orbit that cannot all be absorbed by an along-track correction. Figure 6 shows this typical error signature, with the along-track component removed, after a prediction span of 31 days. Clearly, improving the fit of the IRV orbit to the precise orbit will not help a lot if the precise orbit itself has significant errors that are not absorbed by the along-track correction.

Thus the main limitation of the present system is the use of a long time span of one or two months for the predicted orbit, and in order to improve it is necessary to restrict the predictions to shorter time spans ahead.

4. Predictions derived from GPS precise orbits

There are a number of analysis groups that routinely generate precise orbits for the GPS satellites from the received phases of the broadcast coded signals. These orbits form one of the products of the International Geophysical Service (IGS). Some of these groups also form predicted orbits, valid for the current day and the next day or so. These predicted orbits are accurate to probably better than a metre, and would in effect be perfect predictions for the purpose of SLR tracking. These orbits are in the form of rectangular coordinates referred to the Greenwich meridian and true equator of date. The best thing that a station could do would be to use these directly in its prediction software, if it could manage to do so. An alternative is to fit the IRV orbit model to these predicted orbits, so that the IRVs can be used in the normal software at the stations. Inevitably this will degrade the accuracy of the predictions, due to the misfit of the IRV model. As was discussed in Section 2, this misfit can cause range residuals of up to 40 metres using the standard IRVs fitted over one-day spans. This is not significantly better than what is being achieved by the present system of long prediction spans with time bias corrections. Thus to be worthwhile it is also necessary to improve the fit of the IRVs, and as we have discussed, an easy way of implementing this is to use fit spans of a quarter-day.

The Center of Orbit Determination in Europe (CODE), at the Astronomical Institute of the University of Bern, generates several predicted orbit products, and at my request and also that of Erricos Pavlis, who was working along similar lines on behalf of the NASA stations, CODE now generate a predicted orbit spanning 72 hours, valid for the current day and the following two days, and this is placed in their ftp directory by about 17:00 each day. At RGO these are used to form IRVs for the current day and the following two days. These are fitted over 8-hour spans, starting at 0^h, 6^h, 12^h and 18^h of each day , with the 2-hour overlap being to permit tracking of a pass to continue without deterioration of accuracy if it should cross a quarter-day point. Each set of IRVs gives the position and velocity at 0^h, and so is used in exactly the same way as normal IRVs. Figure 7 shows the range residuals that would have been obtained by SLR stations tracking GPS35 for several passes in October 1996. The final pass shown, and two other outlying points, are all bad data, as has been verified by a precise orbit fit. The residuals of the good data are all less than 10 metres.

Figure 5 GPS36. Residuals of SLR data from IRVs, with time bias polynomial applied.
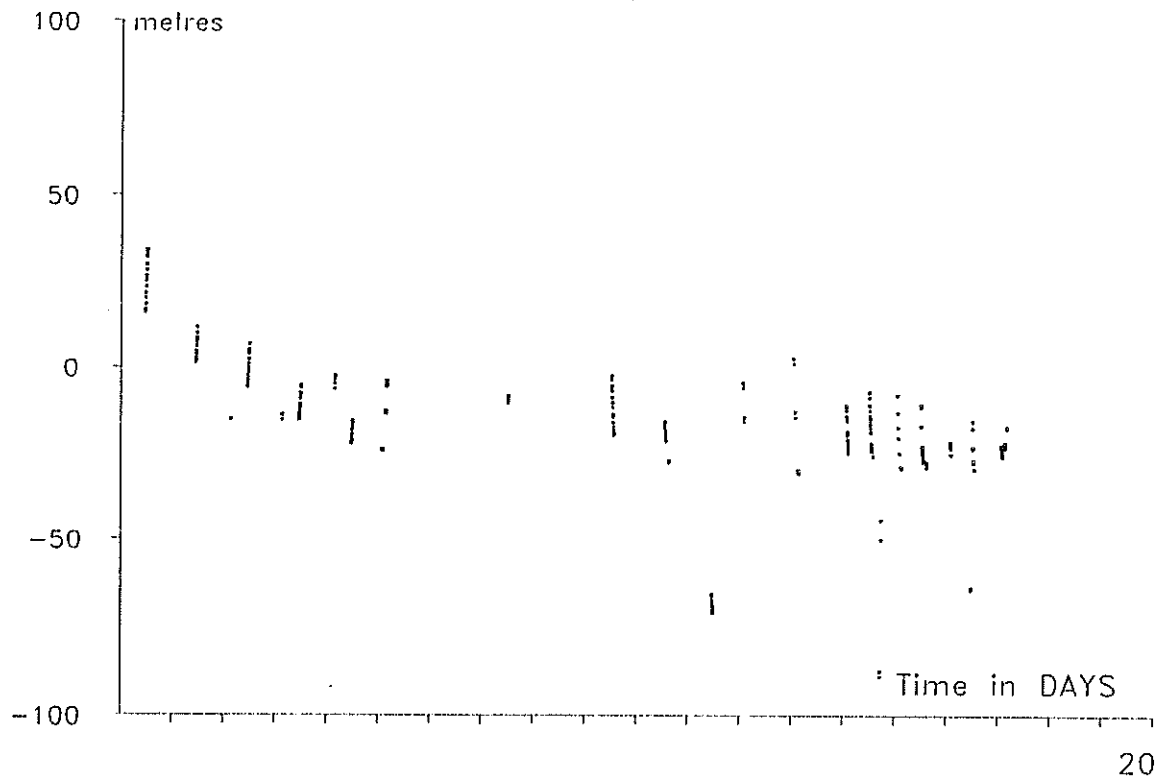
Figure 6 GPS36. Comparison of predicted orbit (with time bias applied) with the actual orbit after 31 days.
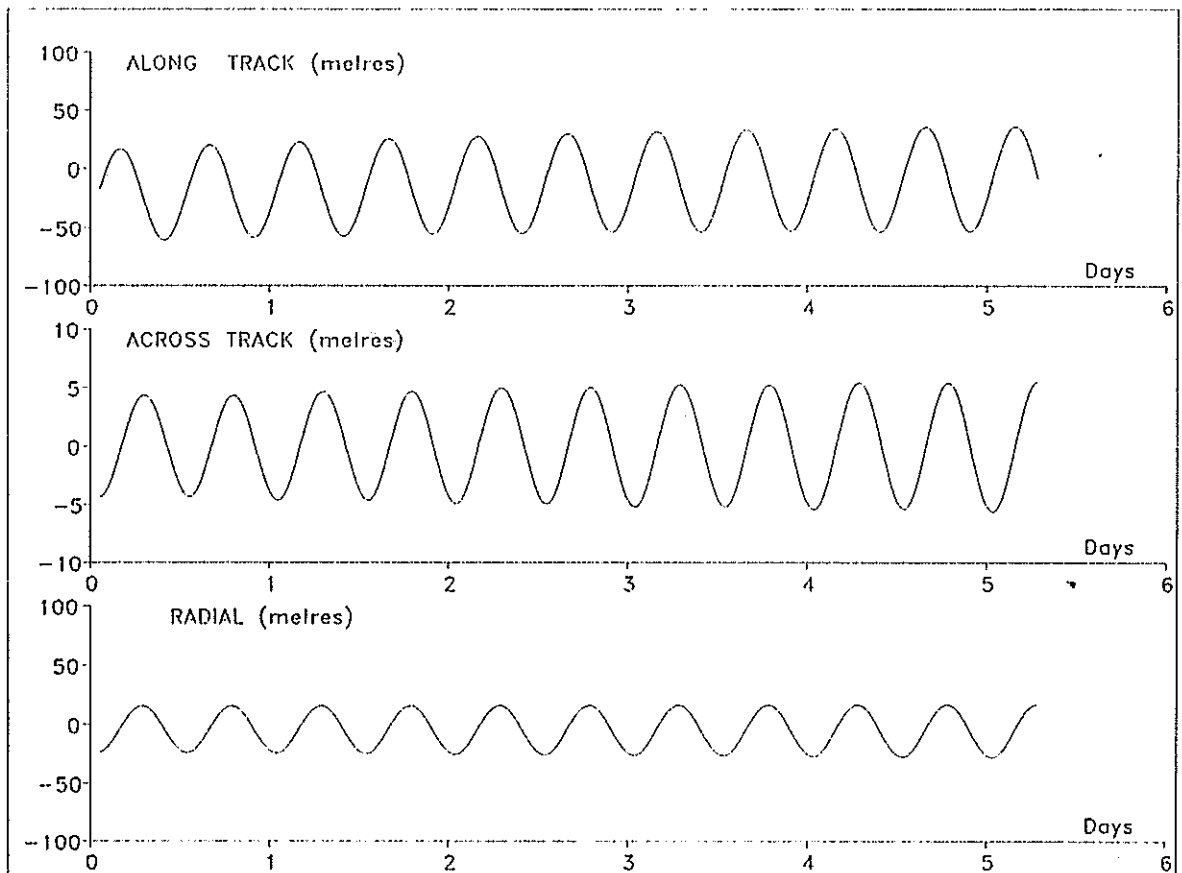
Figure 7   GPS35. Residuals of SLR data from IRVs based on CODE predicted orbit. 1996 Oct 17-25.
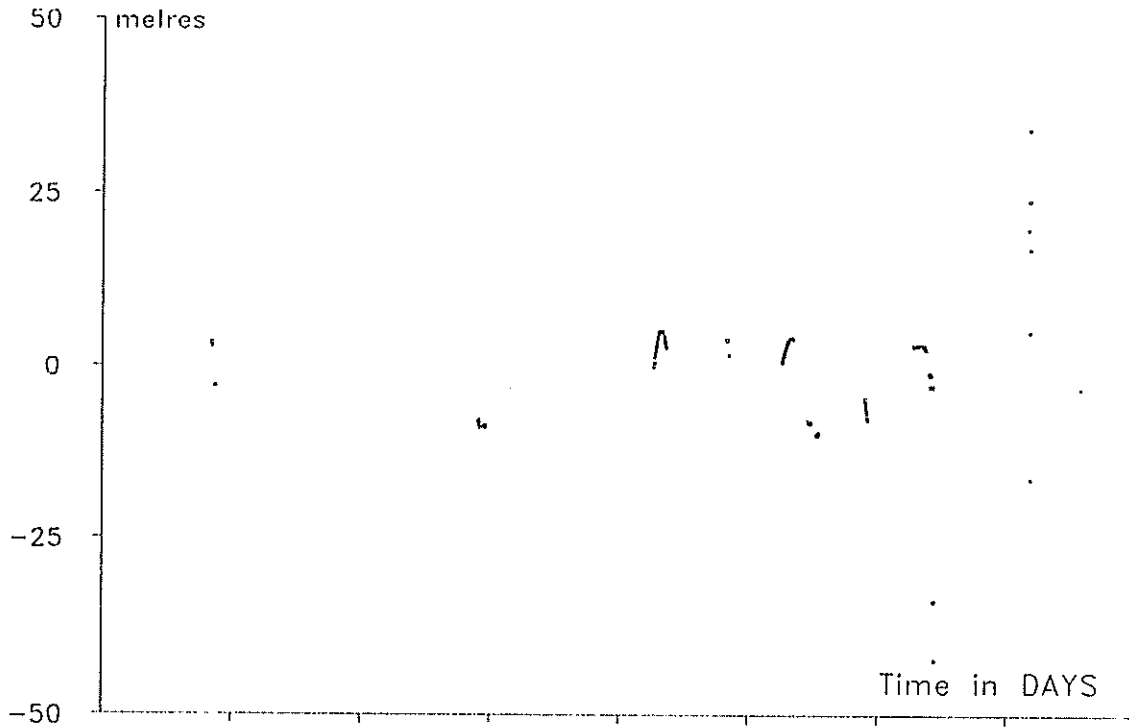
5. Conclusions

The present SLR prediction system for GPS satellites of using IRVs fitted over one-day spans, and running the predicted orbits ahead for a month or so, with time-bias corrections determined daily from the broadcast elements, is fairly close to the best that can be done using such long prediction spans. This system gives a negligible pointing error of less than 1 arcsec, but requires a range gate width of about ± 450 ns.

Improvement can be made by using predictions over a short time span, and the best short term predictions available are those generated using GPS data as contributions to the IGS. The best way to use these would be directly, but if they are used indirectly using the IRV system then is necessary to improve the misfit error of the IRV model, such as by using fits over quarter-day spans.

The GFZ/D-PAF Orbit Prediction System with Emphasis on the Low Flyer GFZ-1

Z. Chen, R. König
GeoForschungsZentrum Potsdam (GFZ),
Div.I: Kinematics and Dynamics of the Earth,
GFZ/D-PAF c/o DLR, Oberpfaffenhofen, Germany

Abstract: Since July 1991, the GFZ/D-PAF orbit prediction system provides regular orbit predictions for several satellites to the SLR community. During this five years practice many improvements towards automatisation and quality have been achieved in the system. The orbit prediction accuracy is increasing continuously. A short report about the orbit prediction quality for ERS-2 as well as for the completed ERS-1 and Meteor-3 tracking campaigns is given.

The launch of GFZ-1 in April 1995 has challenged the orbit prediction system to be capable in handling extremely low flying satellites. A drag function in addition to the tuned IRVs was designed and introduced to the SLR community to account for the missing drag model in the SLR station integrators. Although the modelling of the Earth's gravity field and of the surface forces in GFZ-1 precise orbit determination is quite difficult, the quality of GFZ-1 orbit predictions is sufficient for tracking purposes; experiences made in the last one and a half years are reported. The dependence of the orbit prediction quality on the solar activity and its predictions is investigated. Also demonstrated are the benefits of concentrations of laser stations (f.i. in Europe) for such difficult missions in case of poor weather periods for the maintenance of the acquisition loop.

1. Introduction

Since the launch of ERS-1 in July 1991, the GFZ/D-PAF orbit prediction system provides orbit predictions for several satellites to the SLR community. The orbit predictions consist of tuned IRVs, SAO-elements, the time bias functions, and the drag functions. The time bias function accounting for the along-track errors of the orbit predictions was introduced to ERS-1 for the first time, meanwhile it is well established. The drag function was dedicated to GFZ-1 to account for along-track error residuals due to the missing drag model in the station integrator which are not covered by IRV tuning.

During five years of experience many improvements have been achieved in the system. The accuracy of orbit predictions has been increasing continuously enabling the prolongation of orbit prediction lengths. For satellites at altitudes like that of ERS-1/-2 or higher, the orbit prediction generation runs fully automatically. For new tracking campaigns, the acquisition loop can be installed within a few days. For the low flyer GFZ-1, orbiting at the lowest altitude ever in SLR history, orbit predictions in appropriate quality for tracking have been generated and distributed for one and a half years.

The following chapter 2 deals with the quality of orbit predictions for the ERS-2 and for the completed ERS-1 and Meteor-3 tracking campaigns. The generation of GFZ-1 orbit predictions

which is more complicated will be discussed in chapter 3. A brief survey of these missions may be found in *Kramer* [1992]. Finally, a conclusion is given in chapter 4.

2. Quality of Orbit Predictions for ERS-1/-2 and Meteor-3

The ERS-1 laser tracking campaign started on July 17th, 1991, and terminated on July 28th, 1996. During the five years 20,201 laser passes from 69 stations have been acquired. The generation of ERS-1 orbit predictions is described in *König* [1989]. *Figure 1* displays the along-track errors of ERS-1 orbit predictions including time bias function updates. The vertical dashed lines in *Figure 1* indicate orbit manoeuvre events. The major part of large inaccuracies can be found after the manoeuvres due to under- or overperformance of the manouevres. In the first 250 days the accuracy was heavily affected by frequent manoeuvres and also by large solar and geomagnetic activity. The overall along-track error can be assessed at about 12 ms for the whole tracking campaign or at about 5-6 ms after the initial 8 months period of high solar and geomagnetic activity.
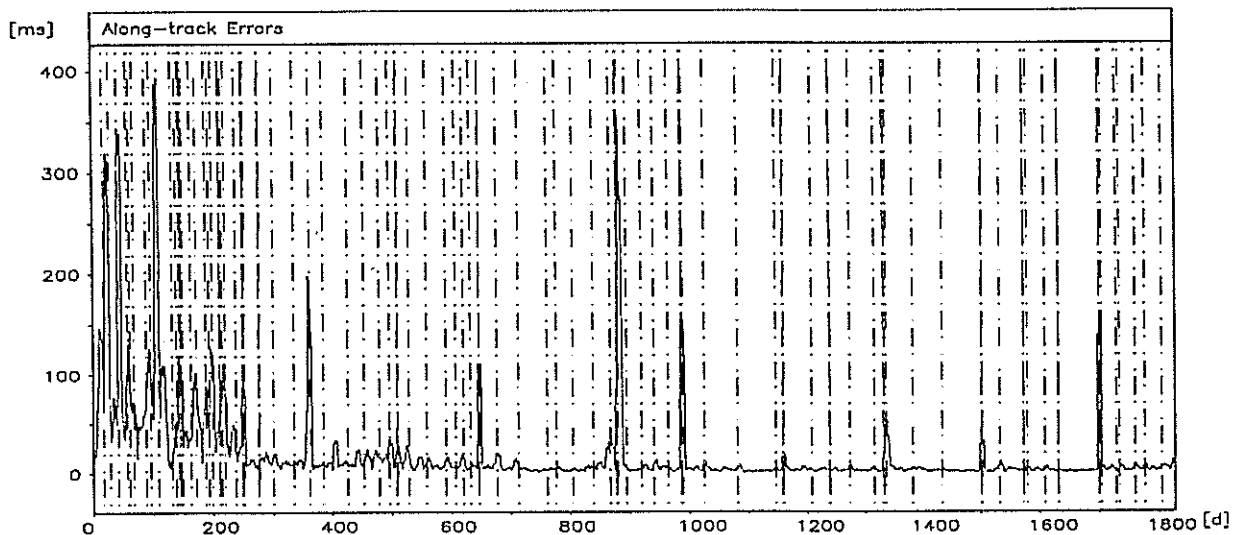
Figure 1: ERS-1 Orbit Prediction Accuracy in Along-Track Direction (91/07/17 - 96/07/27).

The steady accuracy improvements are traced back to the following facts:

- the improvements in the modelling of Earth's gravity field and of surface forces,
- the decline of the solar and geomagnetic activity as shown in *Figure 2*,
- software upgrades for precise orbit determination.

Due to the increasing accuracy, the prediction period could be expanded from 1 week at the beginning to 3 weeks at the end of the tracking campaign.

The ERS-2 satellite was launched on April 21st, 1995. The procedure of orbit prediction generation is the same as for ERS-1. Since the launch 7,200 passes from 42 stations have been acquired. The quality of the orbit predictions is very similar to ERS-1 during their common operation phase. Since the along-track error development is small in general, each

orbit prediction can be maintained for about 3 to 4 weeks if no manoeuvre happens. It is also sufficient to update the along-track error estimate by 1 to 2 time bias functions per week. However, it could become necessary to increase the frequency of orbit prediction updates again, when solar and geomagnetic activity move into their cyclic maximum expected for the year 2001.
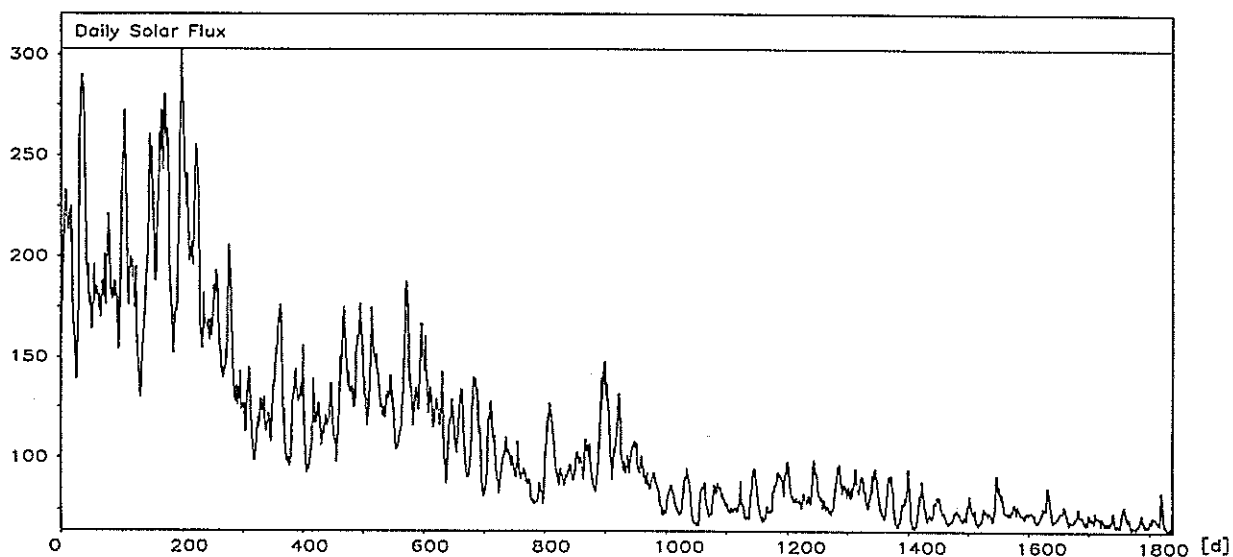
Figure 2a: Solar Activity (91/07/17 - 96/07/27).
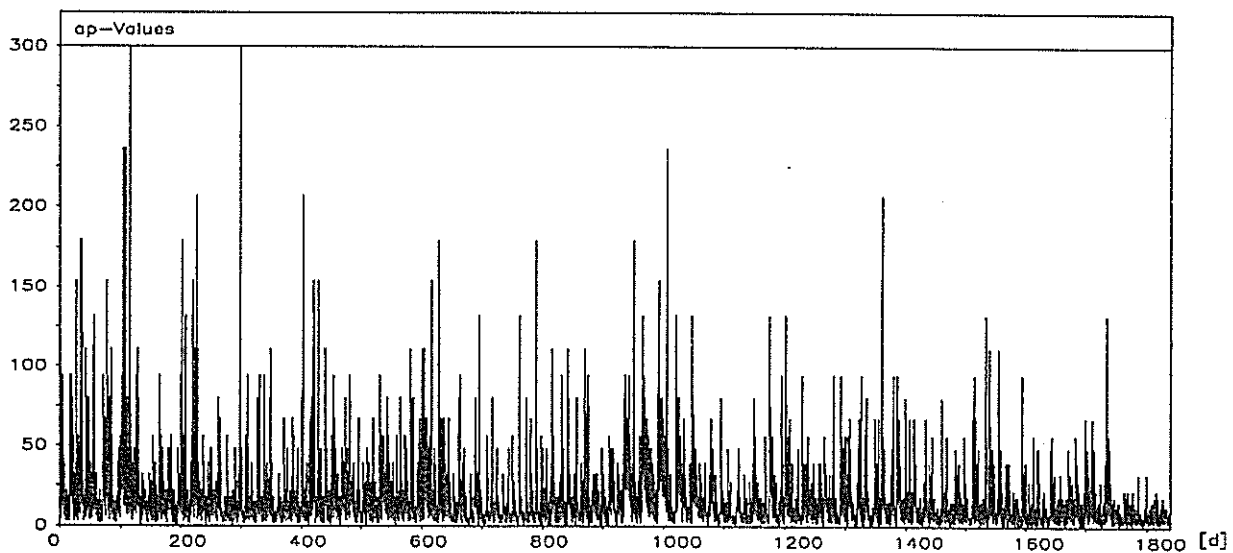
Figure 2b: Geomagnetic a_p Indices (91/07/17 -96/07/27).

The Meteor-3 laser tracking campaign in support of the PRARE validation covered the period from January 1994 to October 1995. Due to the relative high altitude of the spacecraft, the orbit prediction generation could be carried out in a more relaxed way than in case of ERS-1/-2. Typically orbit predictions were released after 3 weeks and time bias functions at weekly frequency. The along-track errors of the orbit predictions including time bias function updates

remained in general below 10 ms.

3. GFZ-1 Orbit Predictions

GFZ-1 is a pure laser satellite orbiting since April 19th, 1995. The primary mission goal is to improve Earth's gravity field models. Therefore a very low altitude, even the lowest altitude orbit ever flown by geodetic missions, was chosen for GFZ-1. *Dow* [1996] reports to the United Nations on the usefulness of new targets including GFZ-1 for the development of new gravity field models.

GFZ-1 is a very fast moving target. For a tracking station, its apparent angular velocity is about twice as large as for ERS-1/-2. With decreasing orbital altitude and increasing solar activity, the drag pertubations exerted on GFZ-1 will dynamically increase in the course of the 4 years mission. This will put more stringent demands on acquisition procedures in the future. More details about GFZ-1 orbit perturbations and prediction problems can be found in *König, Chen* [1994] and *Reigber, König* [1994]. *König et al.* [1996] give an extended report on various mission aspects.

GFZ-1 data analysis is exclusively based on laser tracking data. Since the launch more than 2,733 laser passes have been acquired. *Figure* 3 displays the number of tracking passes per week. Obviously the tracking record is highly correlated with Northern daylight or nighttime tracking phases, because

- most GFZ-1 tracking stations are located on the Northern hemisphere,
- GFZ-1 visibility changes with an approximately monthly period from daytime to nighttime; Daytime acquisition phases for the Northern hemisphere concur with nighttime phases for the Southern hemisphere and vice versa,
- particular, during sparse tracking periods usually concurrent with Northern daylight phases, orbit prediction accuracy degrades preventing quick acquisition in blind tracking mode.

The GFZ-1 orbit predictions are generally derived from laser tracking data. Only in case of lack of tracking data, the orbit predictions are based on AFIT (Air Force Institute of Technology, Massachusetts) twoline-elements. GFZ-1 orbit predictions consist of tuned IRVs, SAO-elements, time bias functions, and drag functions. The drag function [*Chen, König, 1995*] in addition to the tuned IRVs was designed and introduced to the SLR community in time before the GFZ-1 tracking campaign commenced. By using the drag function, the daily deviation in along-track direction of the integrated orbit based on the tuned IRVs can be reduced from about 22 ms to approximately 7 ms in these days of low solar activity. In the upcoming high solar activity phase, the application of the drag function will become indispensable.

It was found that using 1-2 days worths of laser tracking data for orbit predictions yields better orbit prediction qualities than 3-4 days worths of data do. This may be deduced from a corruption of atmospheric density scaling by older data. Nevertheless, the along-track orbit
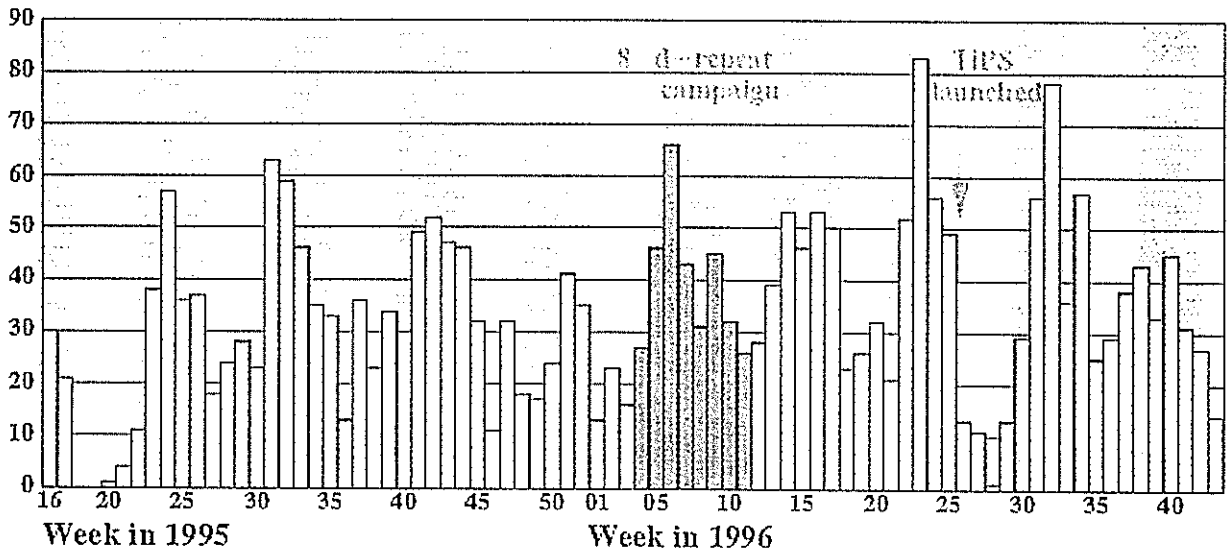
Figure 3: Acquired GFZ-1 SLR Passes per Week.

prediction errors rise very fast (see Table 1). Therefore orbit predictions are generated twice per week in order to keep the orbit prediction accuracy at a sufficient level.

	1d	2d	3d	4d
Time Bias [ms] Development	20 ± 20	73 ± 70	152 ± 119	207 ± 144

Table 1: Along-Track Error Development of GFZ-1 Orbit Predictions (95/04/21 - 96/10/14)

GFZ-1 orbit predictions have been updated by time bias functions once per day, if necessary and possible twice per day. The time bias functions are determined not only from recent tracking data, but also from orbit comparisons using recent 1-2 day tracking data and updated solar and geomagnetic activity parameters. This method is useful because

- very short passes at low elevations yield instable time bias estimates,
- the GFZ-1 orbit responds very quickly to changes in solar and geomagnetic activity.

The assessment from both methods gives more confidence in the time bias function which is finally delivered to the SLR community. However, in periods when only sparse tracking data are available, both methods may yield very different, even opposite trends for the time bias development. In such a case, a definitive decision does not come easy.

Figure 4 displays the along-track errors of GFZ-1 orbit predictions including time bias function updates since launch. Extremly large errors occured mostly during operation downtimes. In general the along-track errors size at the level of 20-25 ms during the first two

days and at 45 ms after 3 to 4 days as depicted in Table 2.

	1d	2d	3d	4d
along-track errors [ms]	± 20	± 25	± 44	± 46

Table 2: Accuracy of GFZ-1 Orbit Predictions Including Time Bias Function Updates (95/04/21 - 96/10/14).

In general the accuracy seems to be appropriate for daylight ranging. It should be stressed here that the drag function must be applied by the stations, because its extreme values reach up to 50 ms.

Along-track Errors [ms]
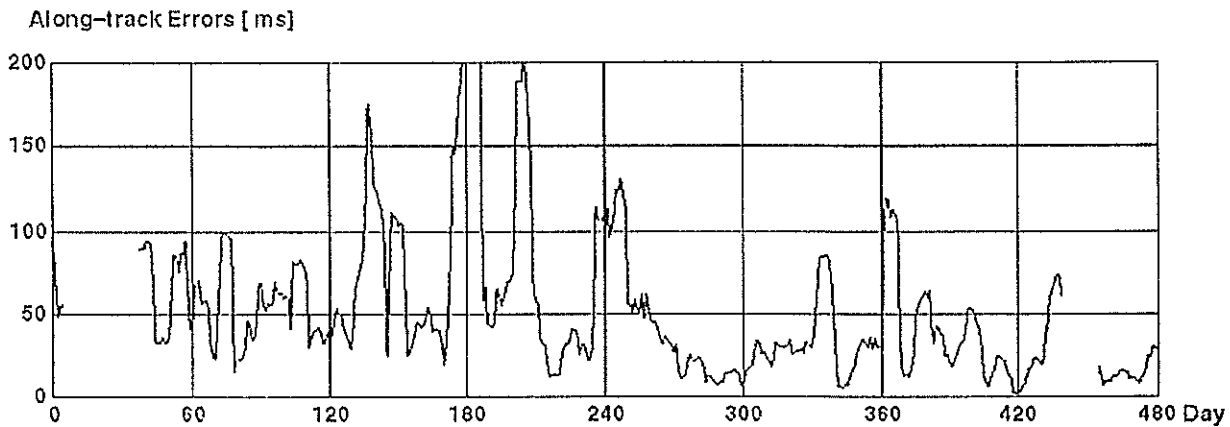
Figure 4: Accuracy of GFZ-1 Orbit Predictions from Laser Tracking (7 day moving mean, 95/04/20 - 96/10/17).

Figure 4 shows two large gaps in May 1995 and in July 1996. In May 1995, the satellite went into its first daylight visibility phase on the Northern hemisphere. Due to missing tracking support from the Southern hemisphere at that time and due to the rather new and demanding acquisition requirements, the tracking record went to zero. The orbit predictions had to be derived from AFIT twoline-elements. Tracking commenced again in June as the satellite moved back to nighttime visibility on the Northern hemisphere.

In the beginning of July 1996 very poor weather governed whole Europe. Due to unknown reasons GFZ-1 was not acquired in other parts of the world. So the orbit predictions had to be generated from AFIT twoline-elements again. The accuracy of GFZ-1 orbit predictions based on twoline-elements is much poorer than from laser tracking data deduction. The along-track errors range from 100 - 200 ms to 1 s. Also the radial and cross-track errors may reach hundreds of meters. Daylight tracking in view of this poor quality becomes immense difficult.

The quality of GFZ-1 orbit predictions is highly dependent on the quick transfer of Q/L data from the tracking stations to the data analysis center. Some European SLR stations route the GFZ-1 Q/L data immediately after acquisition directly to GFZ/D-PAF. At CDDIS a special facility was set up to allow hourly access of GFZ-1 Q/L data from some NASA stations . So all in all a considerable amount of GFZ-1 Q/L data can be analyzed within a few hours after acquisition.

One of the dominant factors for the limited quality of GFZ-1 orbit predictions originates from the uncertainties of the atmospheric models. Therefore the influences of solar and geomagnetic activity predictions on GFZ-1 orbit predictions in July and August 1995 were investigated. During the investigation period, the geomagnetic and solar activities are part of the low phase of the solar cycle. The accuracies of the activity predictions are good enough for orbit predictions for satellites at higher altitudes like ERS-1/-2. For GFZ-1, serious problems in orbit prediction accuracy result. GFZ-1 orbit predictions are extremly sensitive to fluctuations of the geomagnetic a_p indices and to the prediction errors of the a_p values and of the solar flux. Any peaks in the a_p series as well as small errors can give rise to large time bias deviations. A practical way to keep the time bias within certain limits is to keep the orbit prediction period short and to update the predictions as frequent as possible.

Figure 5 displays the GFZ-1 tracking record separately in three regional groups: Europe, North America, and Southern hemisphere plus Pacific. The geographic distribution of GFZ-1 passes is quite varying. More than half of all passes were tracked by a few European stations, at a level of about 3 passes per day. About 1 pass per day was acquired from North America or from the Southern hemisphere plus Pacific. Tracking from Asia came quite sporadically. The concentration of tracking passes from Europe turned out beneficial for such a difficult mission like GFZ-1. During sparse tracking phases (may be due to daylight ranging or due to bad weather conditions) a continental cluster of stations trying to range nearly simultaneously at the same target helps to increase the possibility that one of the stations can acquire the satellite. Thus at least the acquisition loop can be maintained. In general the European stations contribute to a better timely coverage of the observation of GFZ-1's orbital motion. However, from the viewpoint of precise orbit determination and Earth's gravity field modelling, it is highly desirable that the tracking records from other parts of the world would increase to 2-3 passes per day. All stations capable of GFZ-1 tracking are kindly asked to consider the possibility of putting highest priority on GFZ-1 tracking whenever feasible.

4. Conclusions

ERS-2 high quality orbit predictions are nowadays generated automatically. In contrast, GFZ-1 orbit predicition generation still needs large personal engagement. However, GFZ-1 orbit prediction accuracy is increasing thanks to the installation of fast data transfer procedures, due to frequent orbit analyses and due to improvements in analysis techniques. The accuracy in along-track direction remains sufficient for daylight ranging as long as a minimum of about 2 passes per day are acquired. To meet the daylight ranging accuracy requirements the drag function must be applied by the stations. The most important factor for keeping the orbit prediction accuracy at a high level, is the fast and continuous flow of tracking data, especially during the Northern daylight tracking phases. From the viewpoint of precise orbit and gravity

No. of Passes
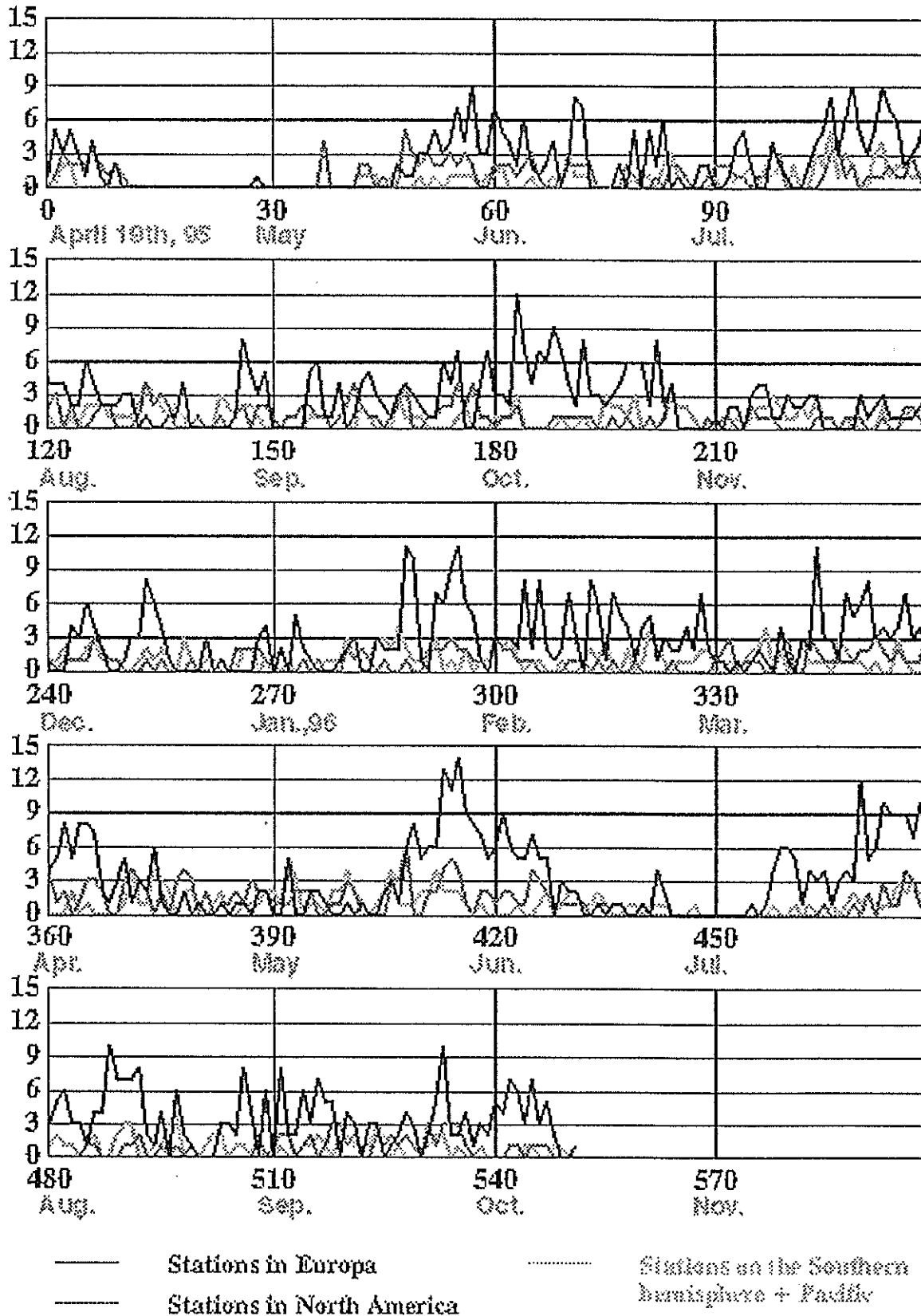
Figure 5: Distribution of GFZ-1 Laser Passes in three regional Groups.

field restitution, a more geographically balanced and a more timely continuous distribution of the tracking data would be desirable.

References

Chen, Z., and R. König: *Drag function for GFZ-1 IRVs*. In: Sinclair, A.T. (Ed.), Proceedings of Annual Eurolas Meeting, Munich, March 1995, pp. 85-88, Royal Greenwich Observatory, Cambridge, 1995

Dow, J.M.: *COSPAR Report to UN for 1996*. ESA/ESOC, 1996.

König, R.: *Predictions for ERS-1*. In: Veillet, C. (Ed.), Proceedings of 7th International Workshop on Laser Ranging Instrumentation, pp. 385-392, Grasse, 1989

König, R., Bode, A., Chen, Z., Grunwaldt, L., Neubert, R., Reigber, Ch., Schwintzer, P.: *The GFZ-1 Mission: Design, Operations and First Results*. In: Scientific Technical Report STR96/09, GeoForschungsZentrum Potsdam, Germany, 1996.

König, R., and Z. Chen: *Probable Qualities of GFZ-1 Orbit Predictions*. In: Proceedings of 9th International Workshop on Laser Ranging Instrumentation, Canberra 1994, in print.

Kramer, H.J.: *Earth Observation Remote Sensing, Survey of Missions and Sensors*. Springer, Berlin, 1992.

Reigber, Ch., and R. König: *Gravity and Atmosphere Aspects by the Low Altitude Target GFZ-1*. In: Proceedings of 9th International Workshop on Laser Ranging Instrumentation, Canberra 1994, in print

Matera Laser Ranging Observatory System

Tenth International Workshop on Laser Ranging

Shanghai Observatory, Chinese Academy of Sciences

November 11-15, 1996

AlliedSignal Technical Services Corp.
Michael Selden

Italian Space Agency (ASI)
Dr. Giuseppe Bianco

Abstract:

The Matera Laser Ranging Observatory (MLRO) system is being developed by AlliedSignal Technical Services Corporation for the Agenzia Spaziale Italiana. (ASI). The contract began at the beginning of 1994 and is entering the integration phase of its development. A brief system description and a report of progress will be discussed.

Introduction

This paper is divided into three parts. The first section will discuss the MLRO system characteristics and some of its features. The second section will discuss the current status of the major subsystems and the overall stage of the system development. The third section will describe some of the measures which have been taken to improve both the quality of the delivered product and the overall engineering process. ATSC and the ASI have worked closely together to ensure there is a clear understanding of the system requirements, its design, and to make the development process as open as possible to create a partnership relationship with the goal of producing the finest system possible.

System Characteristics and Features

The MLRO is a no-compromise, multi-mission system designed to perform satellite / lunar laser ranging while supporting advance (experimental) development as well as astronomical applications. It is designed to facilitate highly-automated calibrations, diagnostics and verification testing to ensure that the system will continue to operate at a high performance level. The MLRO is expected to not only meet, but exceed its specifications. A diagram showing the MLRO subsystems is illustrated in Figure 1.

Many Various T/R OpticsAssemblies
Transmit/Receive switch
Alignment Mirrors
Laser Beam Diagnostics
Intensified Imaging (GenIII, Gated)
Transmit Divergence Control
Adjustable Receive FOV
Automated Signal Control Mechanisms
Optical Range Calibration Assembly
Beam Block and Fixed Attenuation
Transmit Detection
Receive Detection
Wide-FOV camera
Medium FOV camera

Telescope / Mount

Laser

Meteorology

Safety

Control and Processing

Aircraft

Human

Instrumentation

Transmit / Receive Optics

Transmit / Receive Electronics

Detectors

Imaging

Gating — ATSC Developed

Event Timer — ATSC Developed

Peak Amplitude Measurement — ATSC Developed

Discriminator

Signal Control & Conditioning

Calibration and Simulations

Figure 1: Primary MLRO Subsystems and Assemblies

The MLRO employs a multi-photoelectron approach to SLR. It is a large-aperture system with an MCP-PMT detection approach using a 100 milli-Joule per pulse transmit energy at a 10 Hz repetition rate. It has been designed to accommodate a two-color ranging upgrade and can be easily adapted to accommodate a multi-kHz repetition rate if desired.

Telescope

The MLRO telescope is a 1.5 meter astronomical-quality telescope (manufactured to ATSC-specification by Contraves USA). The primary mirror exhibits a $\lambda/66$ wavefront error and the secondary exhibits a $\lambda/88$ wavefront error. The system uses a full-aperture, common transmit/receive approach and will have an internal calibration target attached to the end of the telescope for real-time system delay measurements. The telescope encoder system resolution is 0.03 arcsecond and the repeatability was measured at the sub-arcsecond level. A picture of the telescope is illustrated in Figure 2.
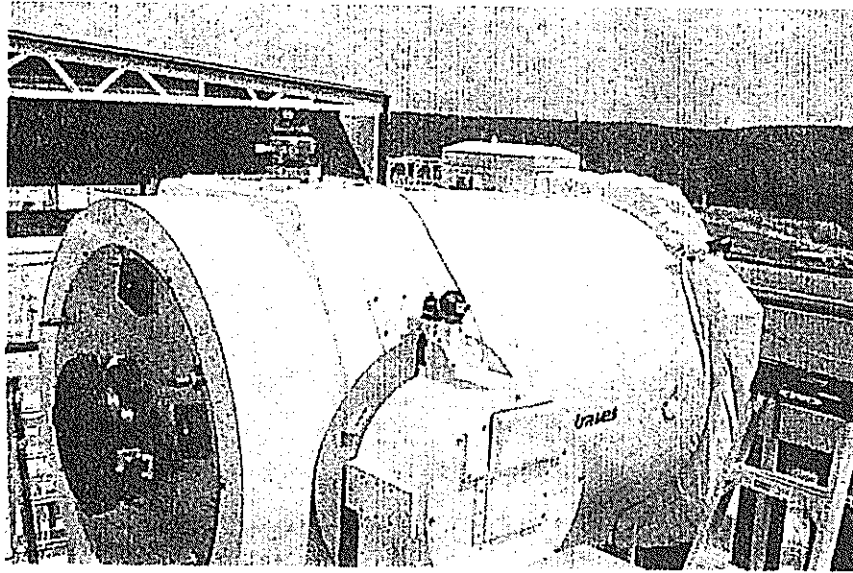
Figure 2: MLRO Telescope installed in the STALAS building at GGAO

Laser

The MLRO laser is a hybrid using a Lightwave CW mode-locked laser to produce a 100 MHz pulse train from which a pulse may be selected. This pulse is switched into a Continuum regenerative amplifier, then switched-out at a precisely-determined time. The output pulse travels through two power amplifiers. The resultant pulse is < 50 ps duration with 100 mJ energy. A picture illustrating the laser is presented in Figure 3.
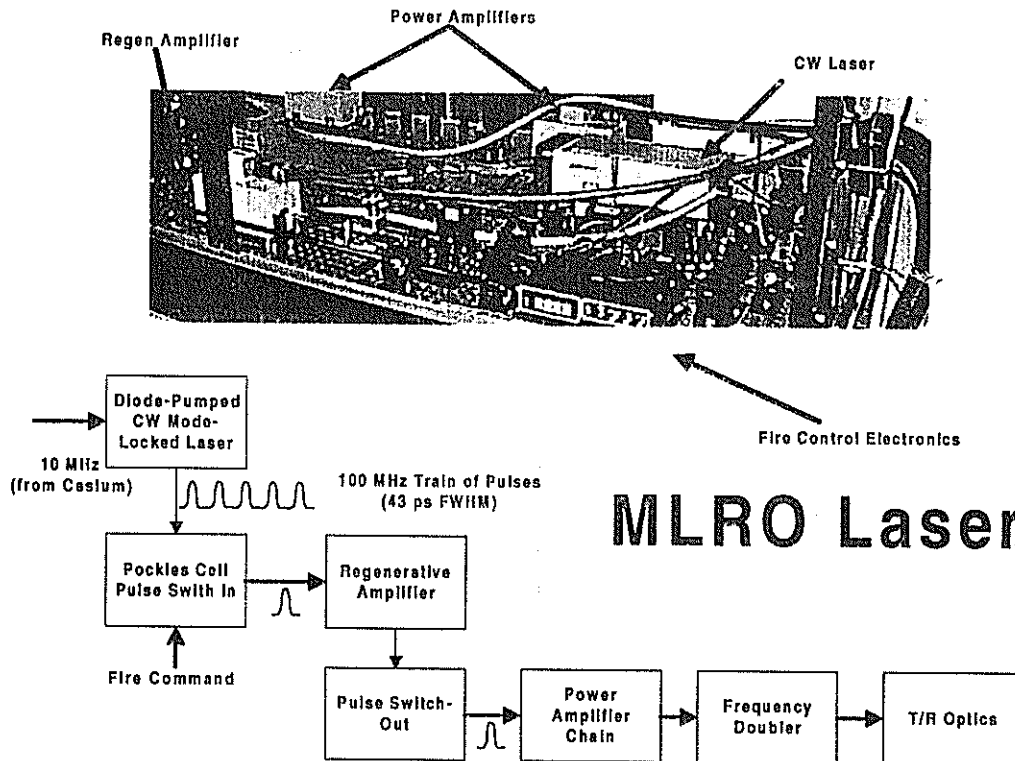
Figure 3: MLRO Laser

Meteorology

The meteorology subsystem measures the barometric pressure, temperature, relative humidity, wind speed, and wind direction and provides this information to the computer.

Safety

The safety subsystem includes the aircraft detection assembly, the instrumentation safety and health monitoring assembly and the interlock and human safety assemblies. These are designed to increase the safe operation of the system while also ensuring that the equipment does not experience harmful conditions. A picture of the ATSC-developed aircraft detection assembly is illustrated in Figure 4.
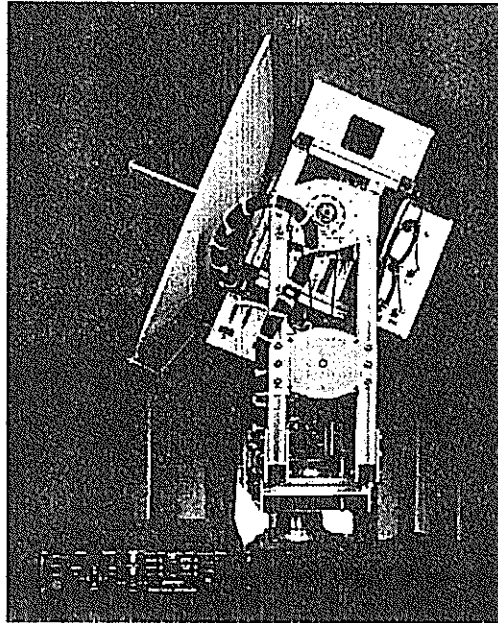
Figure 4: Aircraft Detection Assembly, protective weather enclosure not shown

Control and Processing

The control and processing subsystem consists of five powerful RISC-processor computers. Three real-time VME-based processors, and two HP UNIX workstations make up the subsystem. A drawing depicting the MLRO computing and control configuration is illustrated in the MLRO software paper within these proceedings.

Transmit / Receive Optics

The transmit/Receive optics subsystem contains a large number of assemblies. This subsystem couples the light between the laser, detectors, and telescope. The subsystem has been designed to allow for automated and semi-automated alignments and beam adjustments.

Transmit / Receive Electronics

It features a three GHz microchannel plate photomultiplier tube detector, coupled to an improved Oxford (Tennelec) discriminator for signal detection. These signals are input to the ATSC-developed event timer to determine time interval measurement. Amplitude

information is captured by an ATSC-developed amplitude measurement device, and gating is performed using an ATSC-developed range-gate generator. The subsystem has been designed to employ all of the best techniques developed over the past ten years to yield a highly-precise measurement of range. Some of the assemblies are discussed in more detail in another paper within these proceedings.

Development Process and Status

The MLRO subsystem development phase is nearing its completion. Subsystem development incorporates a number of grouped-functions as illustrated in Figure 5.
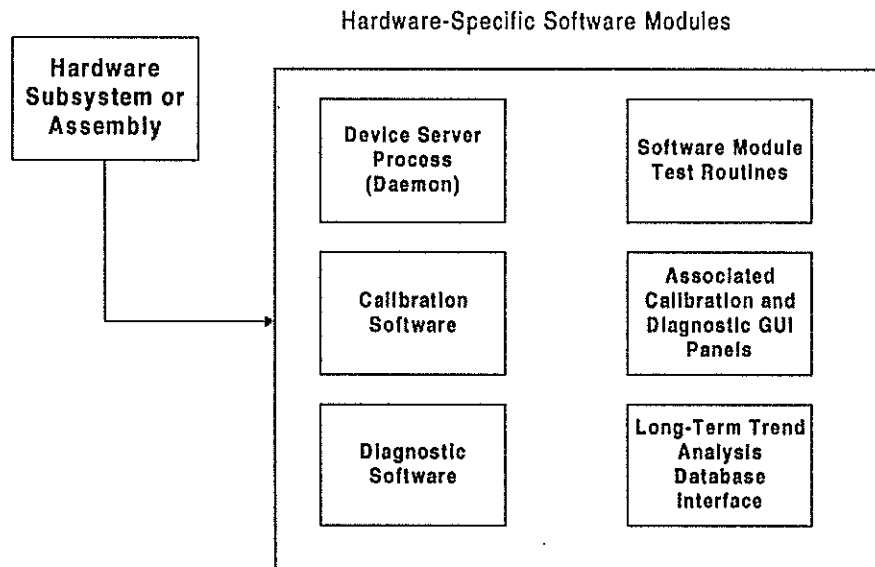
Figure 5: MLRO Subsystem Development

As a subsystem is developed its real-time daemon (device control software), calibration software, diagnostic software, associated GUI applications, and software test routines (to test the software) are developed. Additionally, the parameters which will be included in the system long-term trend analysis application are identified. This trend analysis will be useful to the ASI in monitoring, not only system performance, but also subsystem, assembly, and module-level performance.

Most of the primary subsystem development projects are complete. There are some exceptions to this but, the MLRO is now in the system integration phase. Due to facility-related problems, the MLRO has not yet conducted ranging activities, but the satellite returns are expected by March 1 1997.

Quality and Engineering Improvement Measures

ATSC and the ASI have taken steps to ensure a high-quality system. These include a very detailed and extensive design and design review process, the use of modern engineering modeling and manufacturing tools to improve the electronics, optical, and mechanical design of the system. The establishment and adherence to a modern software development model to ensure that the code is maintainable and upgradable, and extensive testing

throughout the development process was used to ensure that the specifications are met or exceeded.

As an example, the T/R optics subsystem was designed using a ray-tracing application which is used by both ATSC and the ASI. This allowed us to exchange and analyze critical design information on the optical properties. The mechanics of the subsystem were completely designed using the three-dimensional solid modeling package "ProEngineer". This allowed us to check for tolerances, clearances and to manage the quality-control of the manufacturing process very closely. The cabling and wiring diagrams have been developed using the "ProCabling" module which can verify cable stress factors as well as mass and thermal properties.

Our goal has been to produce a system with commercial-quality properties that would compete with the quality of a product produced by a company like Hewlett-Packard, while maintaining a close working relationship between the ASI and ATSC to allow for customization of the products.

Summary

The MLRO system has been designed and is being developed to offer the highest performance possible with a maximum upgrade flexibility and un-paralleled manufacturing and documentation quality. This project is scheduled to be complete in early 1998.

X WINDOW BASED GRAPHICAL USER INTERFACE FOR A LASER RANGING CONTROL SYSTEM

Jacek W. Offierski

Delft University of Technology
Faculty of Geodetic Engineering
Satellite Geodesy Group
Thijsseweg 11
2629 JA DELFT
The Netherlands

and

Marcel J. Heijink

Delft University of Technology
Central Electronic and Engineering Division
Mekelweg 6
2628 CD DELFT
The Netherlands

Abstract

This paper is a short description of the software structure of the Transportable Integrate Geodetic Observatory (**TIGO**) which has been developed in collaboration with TNO Institute of Applied Physics (TPD-TNO) for the Institute for Applied Geodesy (IfAG) in Germany. The modern Graphical User Interface (**GUI**), that is used in this implementation, offers a wide range of flexibility and a user friendly environment. Only GUI's based on Window systems can offer such a wide range of user-friendly and user-intuitive functionality. The applied GUI has the potential to minimize training time for new observers and was implemented on the X Window system (UNIX) using the OSF/Motif widget library. The described configuration provides also remote access capability. Its high level structure and modular construction are sufficiently flexible for future enhancements and replacement of any software module.

Introduction

In all modern measurement techniques, development – which is the engine of scientific progress – requires continues upgrading of each appliance. In Satellite Ranging Systems (**SLR**) the main trends in instrumentation are accuracy, efficiency and working costs. The application of new

software techniques is an important factor in this trend.. However, software elements like satellite prediction, result data screening, etc., are subject to improvement and contain some problems to solve. Particularly. the software that is responsible for the overall co-ordination of sub-tasks, must follow modern trends in software design.

Basic trends in this kind of software, are the application of parallelism and a user-friendly interface. In general, we can divide the software into a part that has a close relationship with the hardware, the Real Time Control Systems (RTCS) [Offierski, 1994], and a part that has a close relationship with the observer, the Off-line System (OLS). Parallelism plays a crucial role in both software parts.

There is no reason to involve the observer directly by tasks such as prediction calculation, ranging data screening (inside possible capabilities) or receiving and sending data. All routine tasks can be efficiently handled by the OLS in a transparent way according to assigned goals and priorities, set by experienced users. The main task of the observer is focusing at support of the RTCS and taking the strategic decisions.

Another trend should be the possibility for remote login on the SLR instrument (e.g. from home), with the aid of an accessible network, on every place on Earth. The described OLS implementation tries to reach all these goals.

Fig.1.Structure of the off-line system consisting of a number of parallel tasks
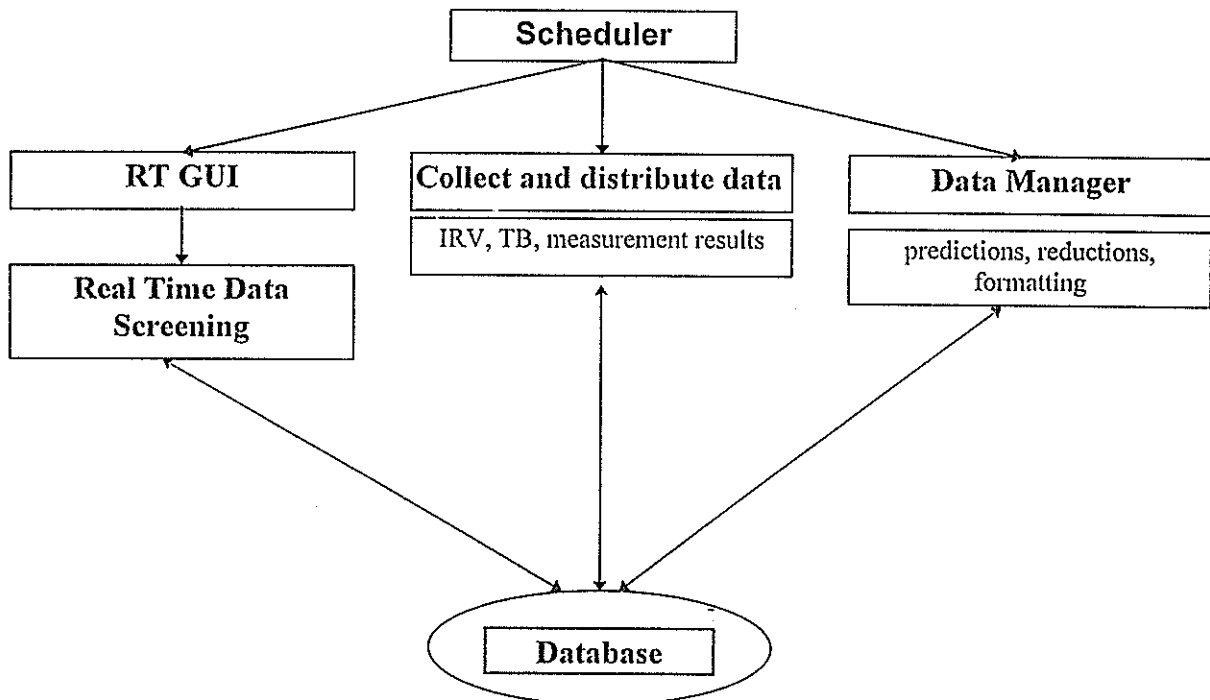
Scheduler

On the top of each parallel working task there is one general process (daemon) which takes control of all data streams from and to the component. It can start (or kill) a selected task with a requested priority level. Tasks can be executed at determined time moments, periodically or as the results of an event. A typical task that must happen in determined time is satellite tracking. Scheduler does not perform this task itself but calls the Real Time Graphic User Interface (RT-GUI) which is responsible for this. An example of a periodical task is the calculation of long-term predictions for satellites (Alerts). Other periodical tasks for this system are levelling and calibration of the 'calibration system'. Typical events that can trigger tasks are user interference (e.g. all tasks that belong to positioning like Star observation), incoming data (IRV or TB), readiness of result data to send or the necessity to make pre- and post- calibration.

Summarising this task:

- Execute tasks at determined time moments (ranging),
- Periodically execute tasks (for example levelling, calibration or collect data),
- Execute tasks on events (user interference, pre- and post- calibration, auto screening).

Collect and distribute data

This task is activated whenever an operation on data must be performed (incoming data available or data ready to send). The arriving data is uploaded to an external accessible FTP input directory. Any modification of the contents of this input directory starts this task. The first step of this task is checking the data for errors, then the data is reformatted to an internal format by independent programs. Independent reformatting has the advantage of being able to add different formats in the future. Finally, the reformatted data is stored in the database.

Also run-time changes in the **OLS** parameters, made by experienced users, can wake up this task. If the **OLS** itself has data to send, the data is put on a selected output directory. The FTP daemon will then automatically send the results to Data Centres.

Summarising this task:

- Error checking,
- Reformatting and storage in the Database,
- Sending results.

Database Management Task (DMT)

All the data that is managed by the **SLR** resides in a number of physical system databases. The system **DMT** are all typical relational databases. Each database contains a number of fields containing system information as well as information associated with the forms of the GUI.

Individual fields and forms can be replaced or changed by the user. It is even possible to completely redefine each database. The consequences of a new form definition or the replacement or introduction of new fields are just re-indexing. All operations on a database are subject to a recovery mechanism. The user has access to all data in a database. However, some of the data cannot be modified, e.g. observation results. Only special prepared programs are allowed to make modifications to such data. A single program, the **DTM** program, is used to maintain, configure and manipulate all system databases.

Currently defined databases include:

1. Satellite database,
2. Site database,
3. Time Bias (TB) database,
4. IRV database,
5. Ranging results database,
6. Calibration results database
7. Star observation results database
8. Ground markers result database.

This list can be extend.

Summarising this task:

■ Application of conventional database technology,

■ Expandable user defined databases,

■ User defined forms.

Real Time Graphic User Interface (RT-GUI)

The main task for **RT-GUI** is to communicate with the **RTCS** in a near synchronous way. Communication is establish with the TCP/IP protocol. The communication between the **RT-GUI** and **RTCS** uses a point-to-point binary data protocol, which makes intrusions from outside almost impossible. The RTCS has its own IP identification number which gives the possibility to

507

communicate with it from different computers. The communication can be traced for maintenance purposes.

The second important function of **RT-GUI** is the visualisation of **RTCS** status information in a form that enables the observer to take the proper decisions (for example correction on wavelengths, position, etc.).

The next function that makes this task the most important task, is the User Interaction that enables the user to carry out his decision's. This interactive process is essential for successfully making measurements.

The **RT-GUI** task can run in two modes: either automatic or manual. During automatic mode, the **RT-GUI** task takes all decisions itself according to pre-determined decision algorithms. In this mode, the only allowed user interference is switching to manual mode. It is also possible to connect external programs with the **RT-GUI** in a modular way to expand on the decision algorithm. This provides an opportunity, together with Real Time Data Screening (**RTDS**), to build a completely automatic system.

Summarising this task:

- Communication with the **RTCS**,
- Visualisation of the **RTCS** status,
- Interaction with the observer,
- Automatic tracking procedure.

Real Time Data Screening (RTDS)

At in current systems, only weak screening algorithms are used. The screening algorithm implemented in the **OLS** software offers the observer almost automatic data screening. Searching for a predicted signal pattern gives a high success / failure rate in the automatic distinction of signal from noise. The used algorithm is sensitive for non-random noise characteristics. The algorithm can communicate directly with the **RT-GUI** and is able to compensate the Time Bias. The results of the data screening can be visualised in different graphical representations (e.g. histogram) and be used by the observer for interpretation.

One of the basic functions of the **RTDS** is interactive graphical data selection. This task has also the ability to connect an external program module. This connection capability is made for future developments in data filtering algorithms.

Summarising this task:

- Near automatic signal from noise separation,
- TB determination for direct use.
- Accuracy calculation for system tuning,
- Interactive graphical data selection.

Data Manager

Almost every **SLR OLS** module contains a number of standard tasks. The described system implements those tasks as a collection of independent and separated programs. There are just a few programs needed to cover all required tasks:

1. Calculate Satellite and Stars predictions. These predictions are necessary to exploit the system.
2. Reduce astronomical measurement results for the position or mount model determination.
3. Formatting to Merit-II format (which is the selected format for external data exchange). Conversion between internal format and the Merit-II format.
4. Generation of Normal Points (NP) from the Merit-II format [Seeber, 1993].The algorithm is based on the 'Herstmonceux' recommendations [Kolenkiewicz, 1986].
5. The calibration results data management module offers the possibility to graphically represent the system calibrations. Long term drifts or accidental jumps in the calibration data can very easily be spotted.
6. For all satellite passes at the actual measure site, the long term visualisation of observation results can be displayed.

Conclusions

- The UNIX pre-emptive multitasking, multi-user and multithreading operating system seems to be the best choice for the modern **OLS** software for a **SLR** system.
- The modular construction of the **OLS** software gives extreme flexibility to include different modules in the future or replace current modules by improved ones.
- The X Window system provides the possibility to fully operate and control the SLR system from a remote site.

List of abbreviations

DMT	Database Management Task,
IRV	Inter Range Vectors,
FTP	File Transfer Protocol,
GUI	Graphical User Interface,
NP	Normal Points,
OLS	Off-line System software,
OSF/Motif	Standard widget set,
RTCS	Real Time Control System,
RTDS	Real Time Data Screening,
RT-GUI	Real Time Graphical User Interface,
SLR	Satellite Laser Ranging system,
TB	Time Bias,
TCP/IP	Transport Control Protocol / Internet Protocol,
TIGO	Transportable Integrate Geodetic Observatory,
UNIX	an Operating System,

References

1. Kolenkiewicz, R., P.J. Dunn, R.J. Eanes and R. Jonson, 'Comparison of LAGEOS satellite laser ranging normal points'. *Sixth international workshop on laser ranging instrumentation*, Antibes - Juan les Pins, 1986.

2. Offierski J., 'Parallel aspects of Laser Ranging Control'. *Ninth International Workshop on Laser Ranging Instrumentation*, Canberra - Australian Publishing Service, 1996.

3. Seeber, G., *Satellite Geodes; foundations, methods, and applications*. Berlin: De Gruyter, 1993.

4. E. Vermaat, J.W.Offierski, 'TIGO-SLR Control System'. *Ninth International Workshop on Laser Ranging Instrumentation*, Canberra - Australian Publishing Service, 1996.

Real-Time Correction of SLR Range Measurements for the Return Amplitude Induced Bias of the Multi-Channel Plate PMT/TC-454 DSD Discriminator Receive System

O'Gara, D.J., Zane, R., Maberry, M.T.

University of Hawai'i, Institute for Astronomy

LURE Observatory at Haleakala

PO Box 209

Maui, Hawai'i, USA

E-Mail: ogara@lure.ifa.hawaii.edu

Abstract: The receive system used at LURE introduces a recoverable bias (0-35mm) into the range measurement. This bias can be estimated by fitting a set of calibration residuals and their associated receive energy measurements to a straight line model. This model is updated on a daily basis by analyzing scheduled calibration runs taken during the previous 24 hours of operation. Range measurements (calibration and satellite) are then corrected for this bias real time by the ranging system software.

Introduction

By analyzing the effects of return energy on the range measurements to a calibration cube at LURE, it was shown that the range varied linearly with the received energy (commonly called time walk). A high energy return generally produces a range measurement that is early when compared to a low energy return. Figure 1 illustrates this by plotting the un-corrected range measurement residuals of a calibration (nanoseconds) against the relative received energy (REM).

In the LURE ranging system, this bias is attributable to the Multi-Channel Plate photo multiplier tube /TC-454 DSD discriminator receive subsystem. (See "Increasing System Sensitivity at LURE Observatory", Zane,et.al., these proceedings). The variation of this time walk was shown to be small over periods of months (Measurements made over a months time showed a slope of -57 femtoseconds/REM with a standard deviation of ~5 femtoseconds/REM). It was decided that a method to correct for the bias during data collection should be implemented.

Method

The amplitude dependent range bias can be determined by investigating the effect of return energy on the range measured during calibration. By subjecting sets of calibration range measurements to a least squares fit analysis (as in Figure 1.) it was shown that the

range was biased as a function of the REM. By removing this bias from all range measurements, the effect of the system time walk can be minimized. Figure 2 is the same data as in figure 1, but with the calculated time walk removed from the measurements.

On a daily basis, each calibration file that was taken the previous day is subjected to a linear least squares fit analysis. The independent variable is taken to be the relative receive energy
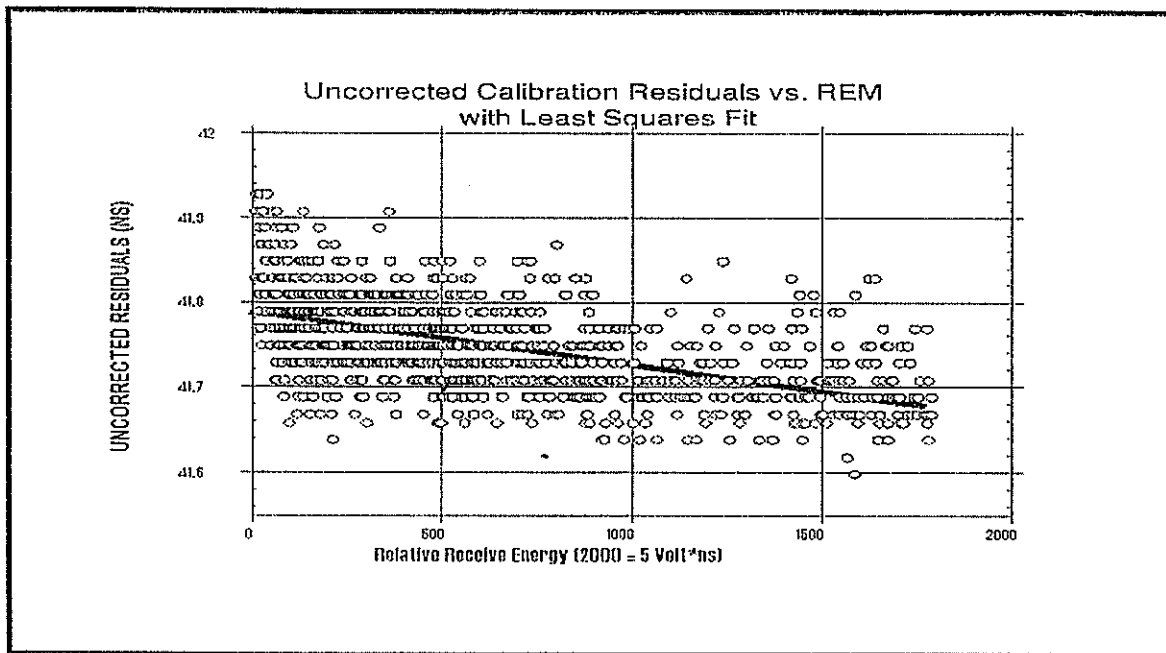
Figure 1.
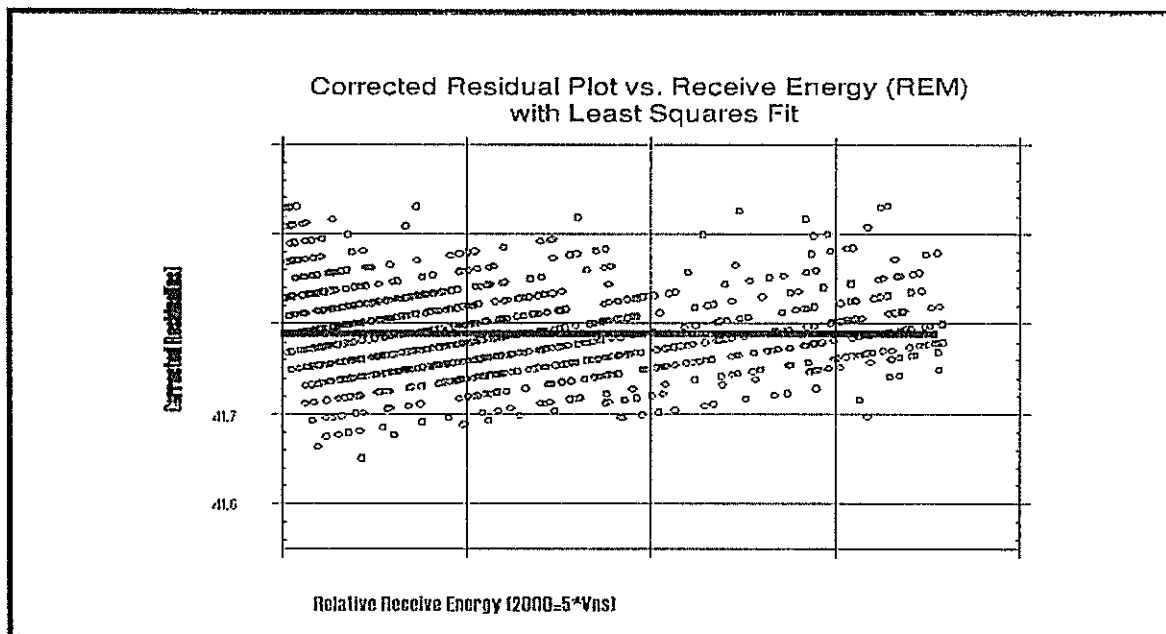
Figure 2.

(REM) number, with the calibration range residual (Observed Range - Calculated Range) being taken as the dependent variable. A FORTRAN program was written that takes as input raw calibrations files, and produce as output the model parameters and the update to the bias correction.

The resulting slope of each straight line fit is first divided by a damping value. This number is then added to the bias correction that is kept in a system data base file. A damping value is divided into the individual slope values to allow daily updates to the bias correction without a single "outlier" causing an abrupt change. Since all data is taken using the best known bias correction, the slope of subsequent calibrations will be the deviation from this correction. Thus, to update the system bias correction, simply add in the slope as determined by analysis of the individual calibrations.

This bias correction is used to correct range measurements in real time. The real time ranging system at LURE will read in the bias correction from a system data base file at start up. During operations, the raw target range is corrected before it is recorded to disk, using the expression:

Corrected Range = Raw Range - (Relative Receive Energy * Bias Correction)

This correction is done to both satellite data and calibration data.

The bias correction can be initialized to zero, or an initial bias correction can be determined by taking a calibration and entering the slope of this calibration as a starting value. At LURE, the initial bias was determined from a month long experiment. This experiment involved analysis of all calibrations (with bias included in the range measurements) taken during that period. An average bias from this experiment was used as a starting correction bias.

Conclusions

The time walk bias is a function of the returned energy. The targets that return the highest average energy benefit the most from this procedure. For example, the average correction for LAGEOS is approximately 2.5 mm, while for TOPEX/Poseidon, it is about 7.0 mm.

The process of maintaining the bias correction at LURE is entirely automated and requires no action by the operators. The analysis process is started automatically by the controller computer at 0:00 UT every day. The least squares fit analysis parameters and the bias correction used for each UT day are stored on disk. These data can be monitored for anomalies and are archived as a part of system history.

This process is currently implemented at LURE on a DEC PDP/11 running RSX-11/M OS.

COMBINED DIGITAL TRACKING SYSTEM

K.Hamal, I.Prochazka

Czech Technical University, Brehova 7
115 19 Prague 1, Czech Republic
fax +42 2 85762252, prochazk@mbox.cesnet.cz

The Combined Digital Tracking System for SLR consists of two CCD based subsystems. The Coude CCD is coupled to the main beam path via the dichroic. The Field of View (FOV) limited by the vignetting to 1 arcminute allows fully automated star tracking for the mount flexure model construction with arcsecond resolution and satellite tracking, as well. The wide FOV subsystem consists of the 8 inch or 11 inch telescope, variable focal reducing optics, laser blocking filter and CCD. The FOV is 3 - 12 arcminutes. The camera control electronics and the software package enables automatic guiding (lock on target), if desirable.

The Peltier cooled CCD has 164x192 pixels, 8 bits. The image integrating time up to 12 sec facilitates a considerably high sensitivity. The newly developed software package permits to operate under Windows NT or Windows 95 up to 4 CCD cameras on a single PC among other real time applications simultaneously. Due to an efficient video data compression plus image processing the transmitted data volume is reduced down to kilobits per frame.

The resolution of the Coude CCD at Tokyo 1.5 meter telescope is 1.5 arcseconds per pixel and at the Keystones telescopes 2 seconds of arc. The wide FOV subsystem allows to track all satellites up to 20 000 km range proved at Helwan SLR rather polluted atmosphere.

OBJECTIVES
Combined Digital Tracking system

- VISUAL GUIDING / all laser satellites

- Satellite image / laser beam / paralax

- MOUNT FLEX AUTOMATION / remote control

- Image data processing: low data flow rate

- WINDOWS NT platform

- Multiple camera control/image on one PC

- Calibration pier

K.Hamal,B.Greene, Shanghai '96

Combined Digital Tracking Subsystem (CDT)

- The CDT subsystem is dedicated for the coaxial (transmiter/reciver setup in Coude) SLR station

- The CDT consists of two CCD sensors, one subsidiary telescope, one focussing optics, PC+ software.

- The wide FOV subsidiary telescope/CCD is providing:
  - visual guiding/tracking of satellites (low, satellites, Lageos, Etalon, Glonass, GPS) on the displayed laser beam

- The narrow FOV CCD in Coude is providing :
  - star tracking for mount flex, autotrack option
  - telescope optics alignment tool

K.Hamal,I.Prochazka,Keystone, Nov. 27,'95

WIDE FOV SUBSYSTEM
Combined Digital Tracking system

Telescope	C8, D=200mm, f/D=10
Focal reducer	adjustable 2-4 x
CCD camera	ST-4, 2.5 x 2.5 mm 192x164, 14x16um
FOV (reducer 3x)	12 x 12 arcminutes 17 arcmin diagonal
Resolution	5 arcsec / pixel
Capability up to 10 sec.integration	up to Etalon, GPS in good conditions

I.Prochazka,K.Hamal, Keystone,November '95

WIDE FIELD OF VIEW TELESCOPE
Digital Guiding & Ranging Subsystem

600

400

F.R.

CCD

TELESCOPE

240

140

shutter

laser
block.

BASEPLATE

CCD control

220x150x60

DC 12V power

RS232C

control

CCD control to camera 2.5 m max.

Baseplate Al 380x100x8 to interface the telescope
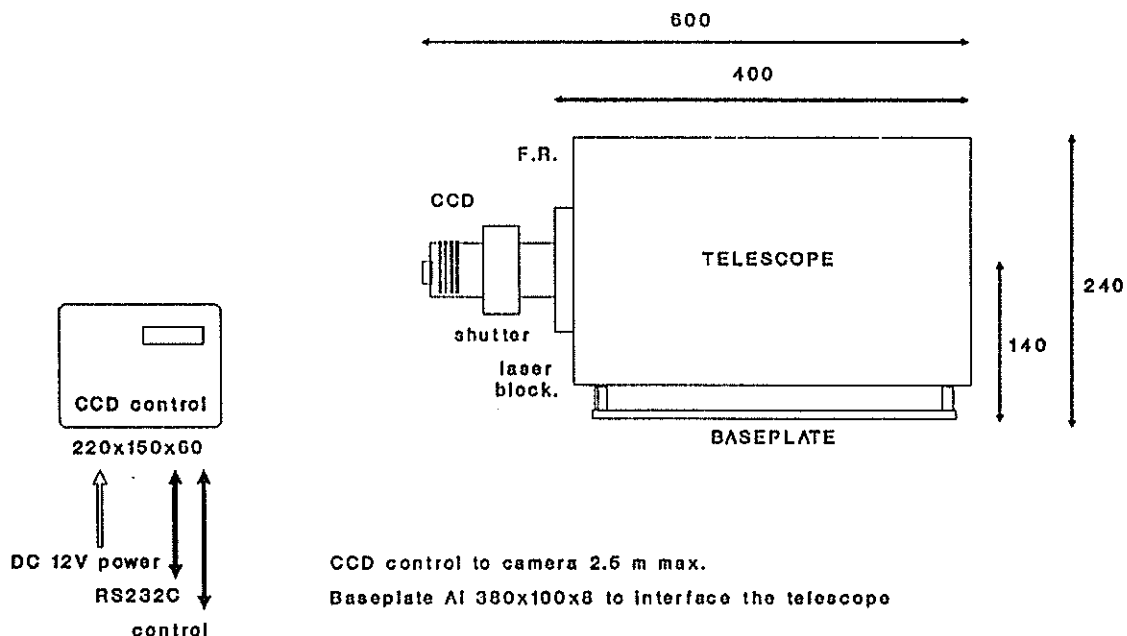
Hamal,Prochazka, Shanghai '96

NARROW FOV SUBSYSTEM
Combined Digital Tracking system

Coupling to main T/R telescope	via dichroic directing 600~1000 nm to CCD
CCD camera	ST-4, 2.5 x 2.5 mm 192x164, 14x16 um
Field of view	1 arcmin limited by vigneting
Camera optics	f = 56 mm Dmin = 37 mm f/D = 1.5
Pixel size (KSP)	2.0 arcsec / pixel
Tracking resolution	‹ 1 arcsec

I.Prochazka,K.Hamal,Keystone,Dec.6,'95

CCD in Coude block scheme
Combined Digital Tracking System
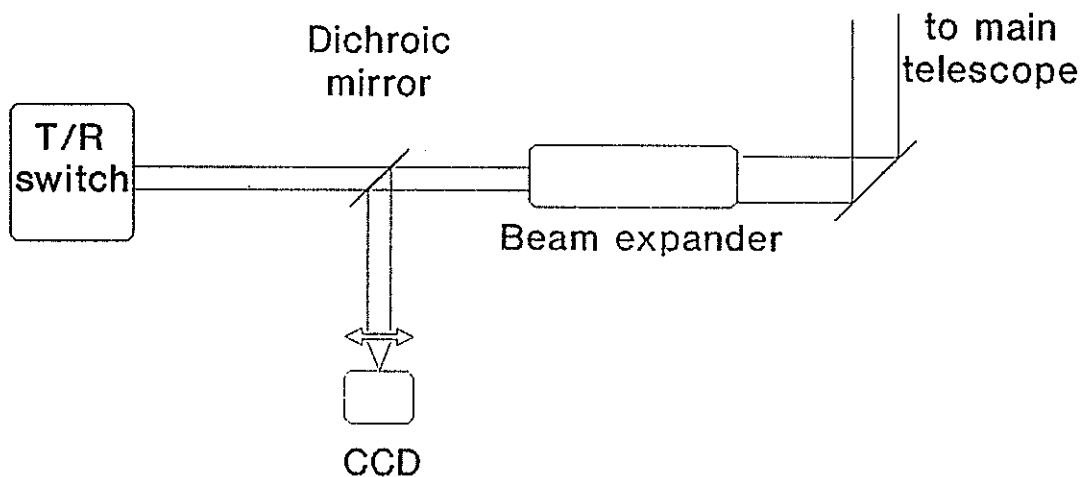
K.Hamal,I.Prochazka, Shanghai '96

HELWAN 2 SATELLITE LASER STATION
Visual guiding on CCD star tracker

LAgeos 47 deg medium sky ret.rate 50%

Contrast
Background:155
Range   : 3

Unsmoothed
Unzoomed
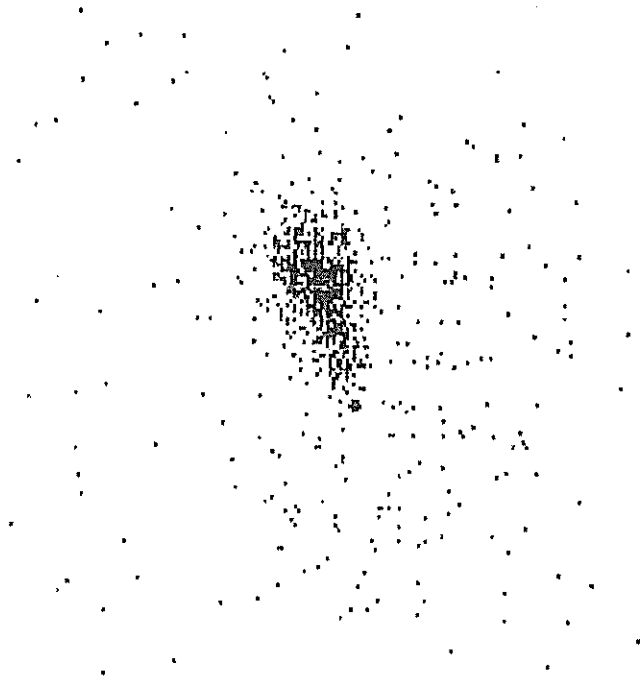
etalon 2 37 deg laser beam 99% dichr

Contrast
Background:170
Range   : 15

Unsmoothed
Unzoomed
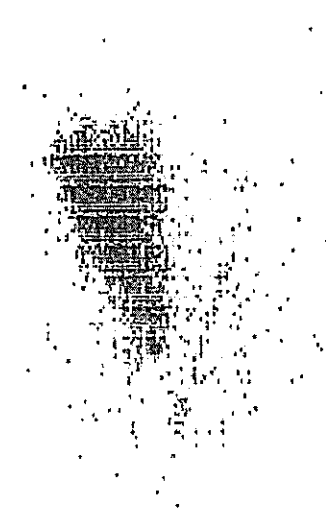
Helwan, September ;95

SATELLITE TRACKING IN GRAZ
Digital tracking system

TOPEX

GPS

topex + beam 10Hz , echoes

GPS + laser, 4 sec. Graz, 35 deg.elevation
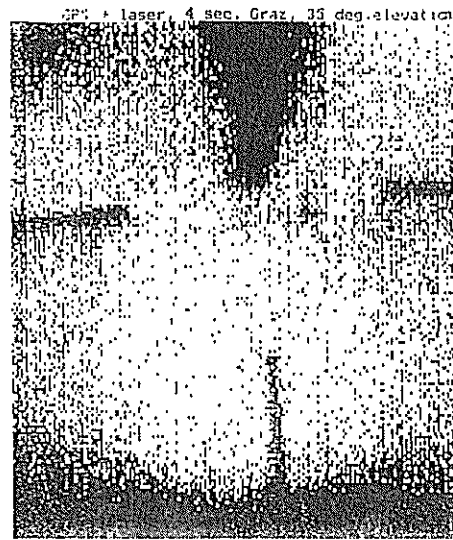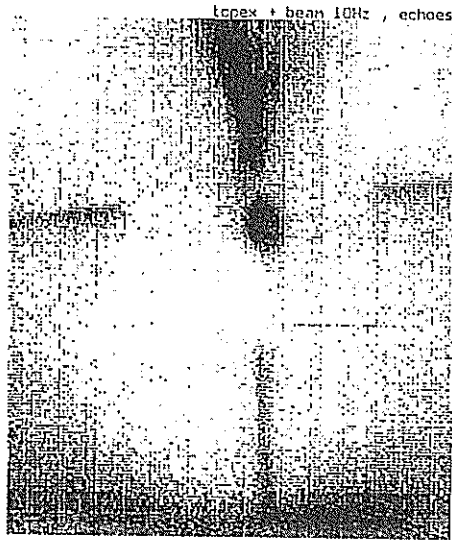
10th Workshop, Shanghai '96

SATELLITE TRACKING IN HELWAN
Digital tracking system

LAGEOS

ETALON

Lageos C11 in Helwan 4 sec poor visibility
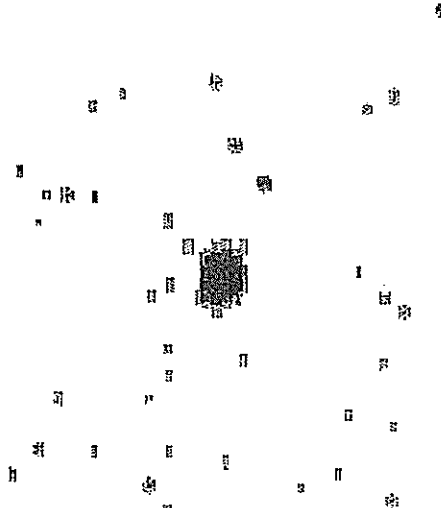
Etalon C11 Helwan 4 sec.exposure
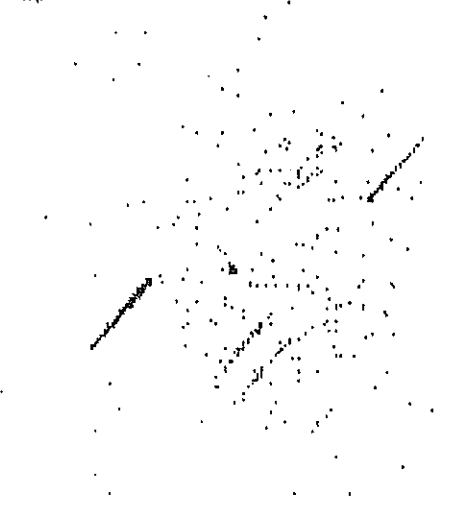
10th Workshop, Shanghai '96

LAGEOS tracked on C8 wide FOV camera, 6 seconds exposure, zoomed, gain level settings 0,55
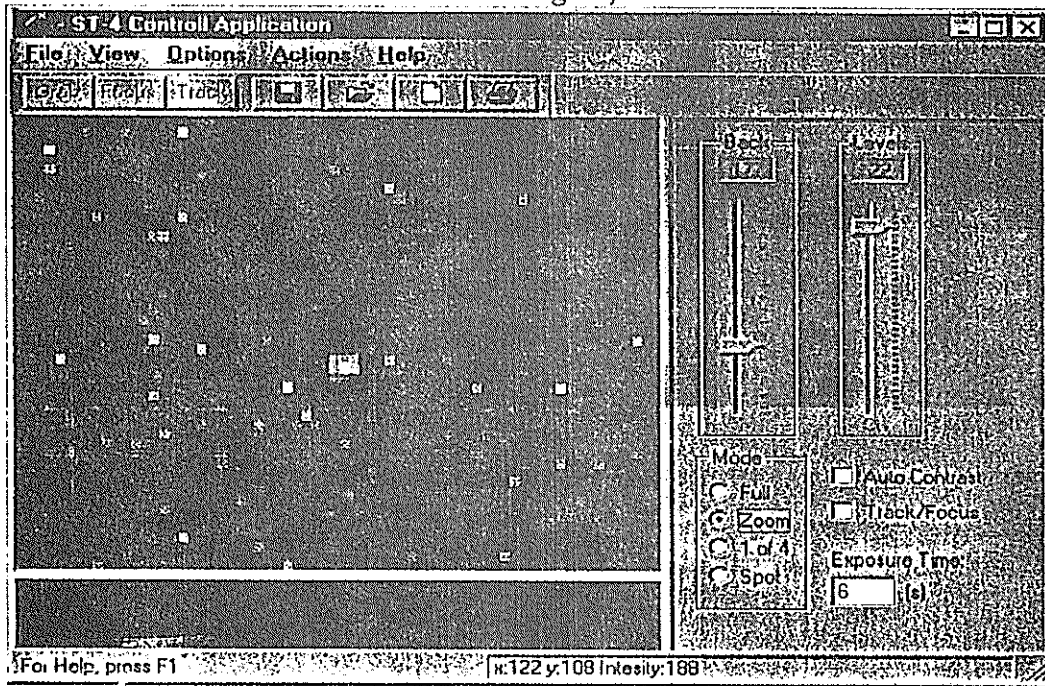
Laser beam on the LAGEOS C8, settings as above
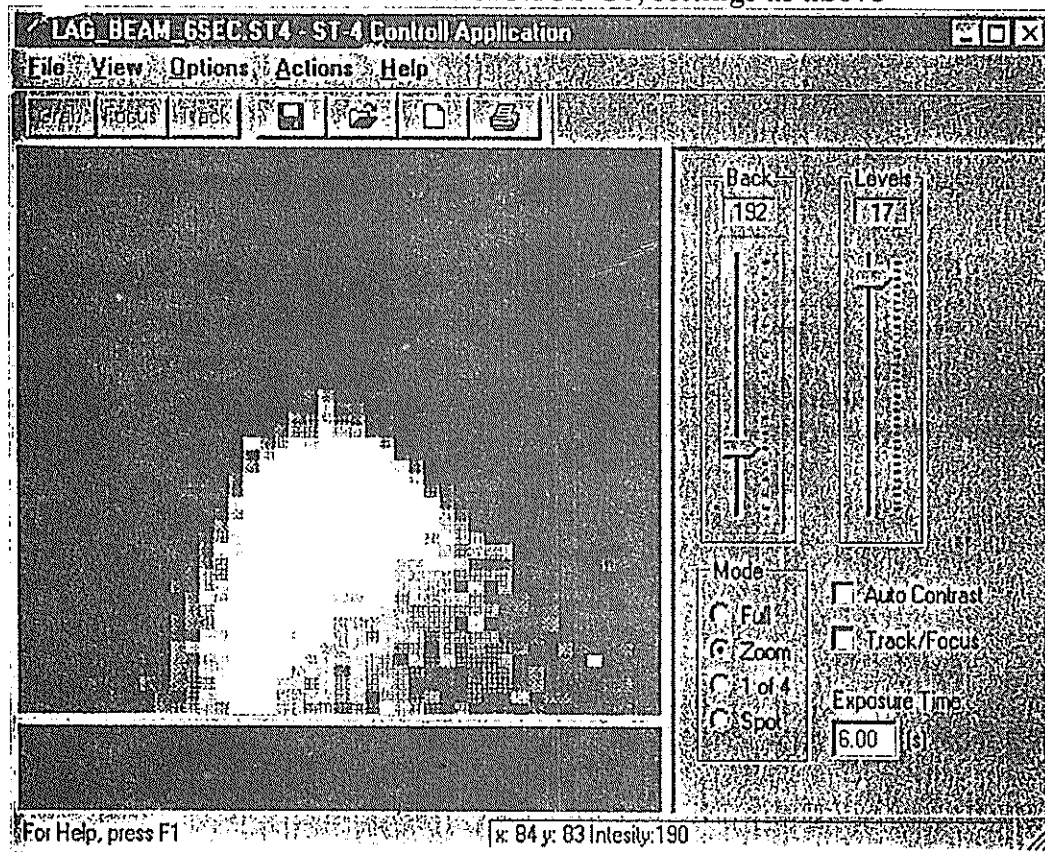
The Coude camera star image
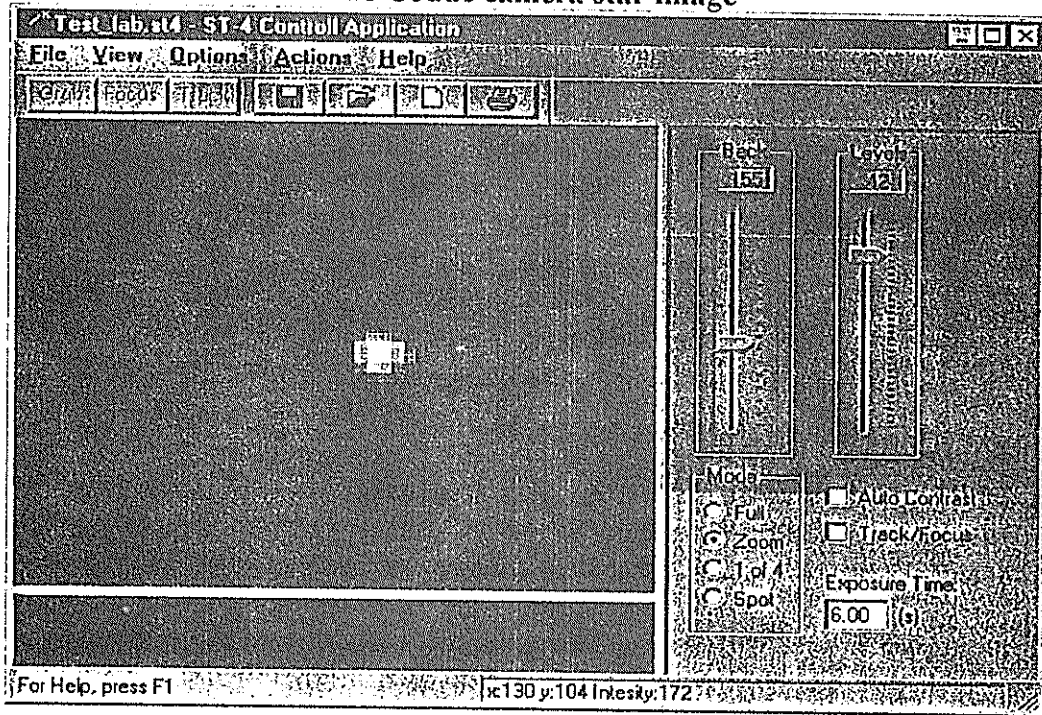
The Coude camera, star image demonstrating the secondary mirror alignment.
The main telescope was slightly defocussed,
in optimum alignment, the ring is symmetrically illuminated.
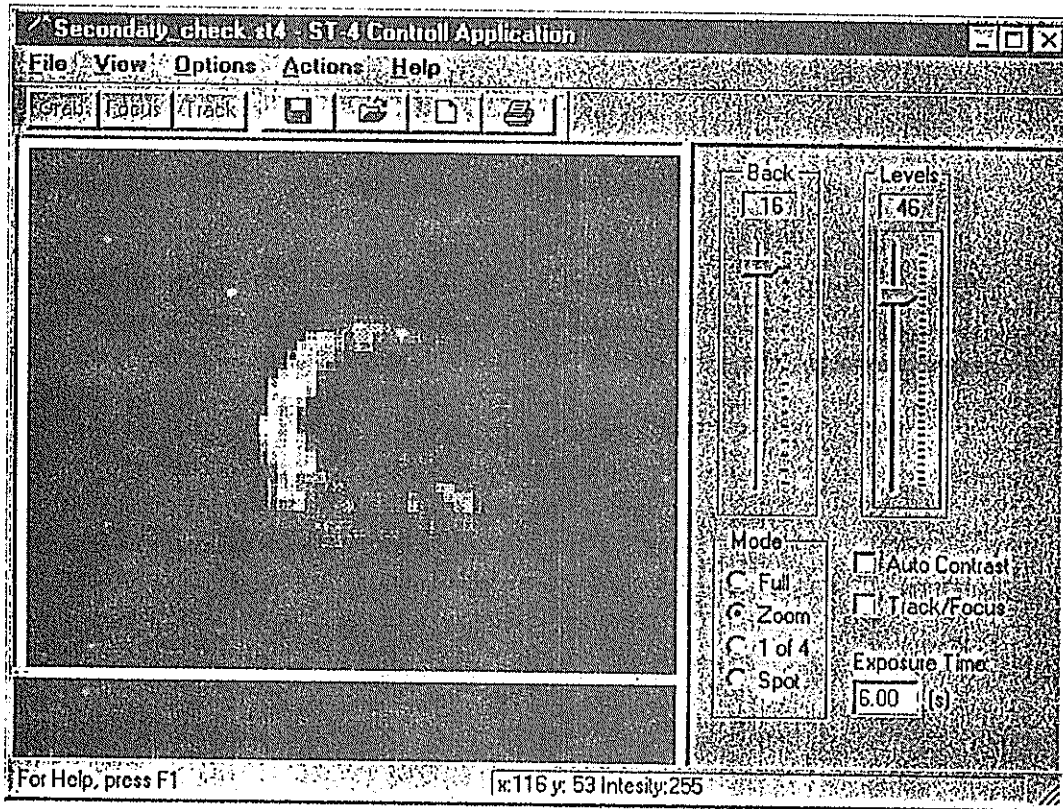
AUTOMATION OF THE BOROWIEC SLR

S.SCHILLAK, J.BARTOSZAK, E.BUTKIEWICZ

SPACE RESEARCH CENTRE
OF POLISH ACADEMY OF SCIENCES
BOROWIEC ASTROGEODYNAMICAL OBSERVATORY
62-035 KÓRNIK, POLAND
tel: +48-61-170-187
fax: +48-61-170-219
e-mail: sch@cbk.poznan.pl

ABSTRACT. The need for automation of the SLR systems arises fro two main reasons: faster pre- and post-observation operations induced by increasing number of laser satellites and assurance of single operator or full automatic operation because of prolonged observational activity and higher operational costs. The achievement of those two goals is the subject of intense effort at the Borowiec SLR station. The paper gives an exemple of satellite pass starting from the calculation of predictions and ending with sending the normal points to EDC. The process of automation will begin with automatic calculation of predictions for one day (or night) for all satellites at a step of 1 second (IRA program). The next stage will be a replacement of two men crew by a single operator. Then a CCD camera will work as an eye of an observer, small engines will be applied for remote control of the position of the beam, neutral filters and diaphragm, sensors will be used for read out of meteorological data. The third stage will be automation of analysis of the results after the pass (AOP program). At present we are at the stage when the operator's task is to choose the calibration set, eliminate the noise points by using a mouse and finally, accept the results before they are sent. The time of data processing has been significantly shortened and amounts now to about two minutes from the end of observation to sending the results as normal points.

The automation of SLR systems is necessary for obtaining a large number of results of observations and essential reduction of the cost of their obtaining. At present a large number of stations work with a single operator, however, still many stations, especially those equipped in separate transmitting and receiving systems need two person staff. In the second case the number of observers is increased or the number of observation days is limited. This is the case in Borowiec station whose construction, coming from the early 80s, poses serious problems as far as introduction of single man operation is concerned. In 1996 The Borowiec station entered the APO project aiming at introduction of a single person crew and reduction of the operator tasks. The main aim of the project whose realisation was planned for 3 years, was minimisation of the tasks to be performed by the operator during an observation. This process includes automation of the preparation of predictions, the hardware and software related to observation in the real time, results processing, their check and sending to EDC.

1. Prediction

The work on automation of ephemeries preparation has been already completed and includes:

- automatic read out of IRV data from the e-mail and attachment of these new data to the IRV string of each satellite,

- prior to the first observation automatic calculation of ephemeries for all satellites predicted in the observation program at Borowiec for a given night at a step of 1 second, and saving the data in the catalogue of ephemeris (IRA program); the operation does not require operator's intervention and takes only several seconds.

2. Observation of a satellite and calibration.

The main objective related to automation of hardware was installation of a CCD camera on a tracking telescope and little engines controlling the movement of the output prism of the Coude system. This solution permits correction of the position of the laser beam relative to the centre of the field of view by the operator at the controlling computer. The next task will be construction and installation of a packet for remote control of the neutral filters and diaphragm for calibration purposes and release and hold of the shutter. The following tasks will be installation of the meteorological data sensors and an automatic radar system for protection against the aircrafts.

The aim of the automation of the controlling software is elimination of all possible actions which require operator's intervention. A block diagram of the program controlling satellite tracking is given in Fig. 1. The exclamation marks are used to indicate the tasks requiring operator's intervention. These tasks and the ways of their elimination are listed below.
Pre-observation process:
- ephemeris; choice of the ephemeris from the list for a given night, made by the operator;
the program should be supplemented with automatic elimination of the overlapping satellite passes taking into account their priority (in the IRA program) then, for a given satellite, the program may start automatically,
- pass parameters; a change of pass parameters for a given satellite, mainly the filter and diaphragm for calibration, and introduction of time bias;
the filter and the diaphragm can be set automatically during calibration on the basis of the amplitude of the return signal or the percentage of good measurements for a given satellite, time bias should be introduced automatically during the ephemeris calculation (in the IRA program) and its corrections should be made during the observation,
- meteo; read out of the pressure, humidity and temperature;
the intended introduction of sensors will eliminate this problem,
- pre-pass calibration; the program requires the operator to decide about pointing the telescope to the target and beginning of the calibration, when the filter level and diaphragm are incorrect, the calibration process is terminated and begun again once the filter and diaphragm are correct;
setting of the telescope and beginning of the calibration can be conducted automatically at a certain time (a number of seconds) before the observation start; the filter and diaphragm could be selected automatically on the basis of the amplitude of the return signal or a percentage of good measurements for a given satellite,
- read keyboard; change of parameters directly before the observation starts;
in practice very rarely conducted mainly to introduce the time bias.
Observation:
- Fig. 2 presents the view of the controlling computer screen during an observation; the upper part presents the gate window with the O-C values in meters, on the right hand side there are the input points, the middle of the bottom part shows the deviation of the telescope position from the ephemeris position (a black square) which can be moved during an observation at an arbitrary step, the large circle has a diameter of 2.5 arcmin, the small one - 30 arcsec, the left hand bottom part shows the data which can be changed via keyboard during an observation; laser switch on/off, model of the telescope delay, gate window, step at which the telescope position is changed, time bias, corrections of the cross, azimuth and altitude; the right hand bottom part displays the results, that is the current number of the ephemeris point (with a step

STR - SATELLITE TRACKING PROGRAM
BOROWIEC SLR STATION

Fig. 1

LAGEOS-2   Start: 1996 8 22   00:23:22   A= 175   H= 40   NO : NO 1978 pom.

```
 100 -
  80 -
  60 -
  40 -
  20 -
   0 -
 -20 -
 -40 -
 -60 -
 -80 -
-100 -
```

LASER	L		ON			Nr efem.: 1157
MODEL	M	.	ON			Result: -32
GATE	O	=	100	m		
STEP	Q	=	4			
TIME	T	=	-20	ms		Azim: 237
CROSS	C	=	0			Elev: 56
AZIM	A	=	4			# Points: 678
ELEV	E	=	-8			End time: 10:34
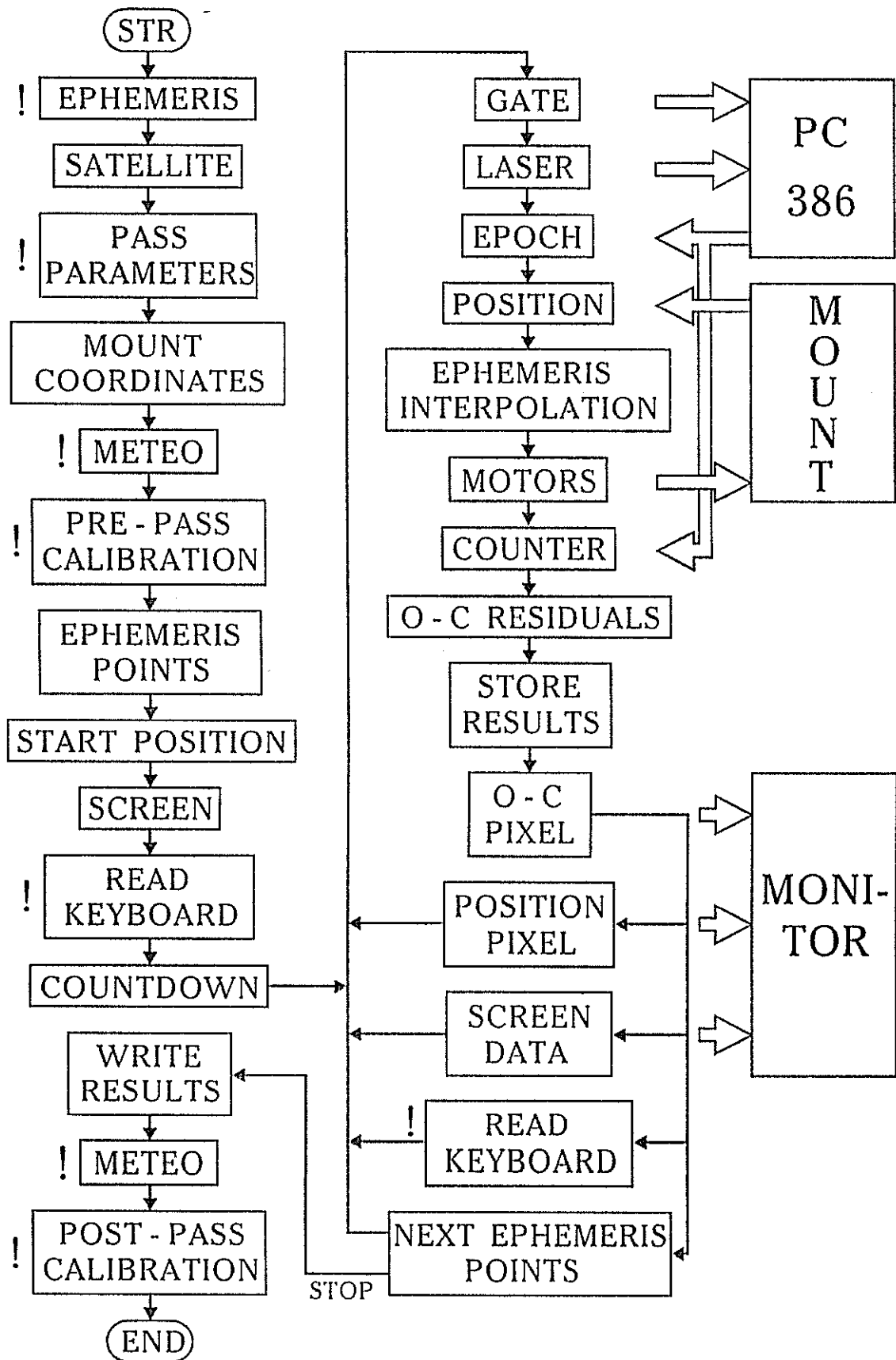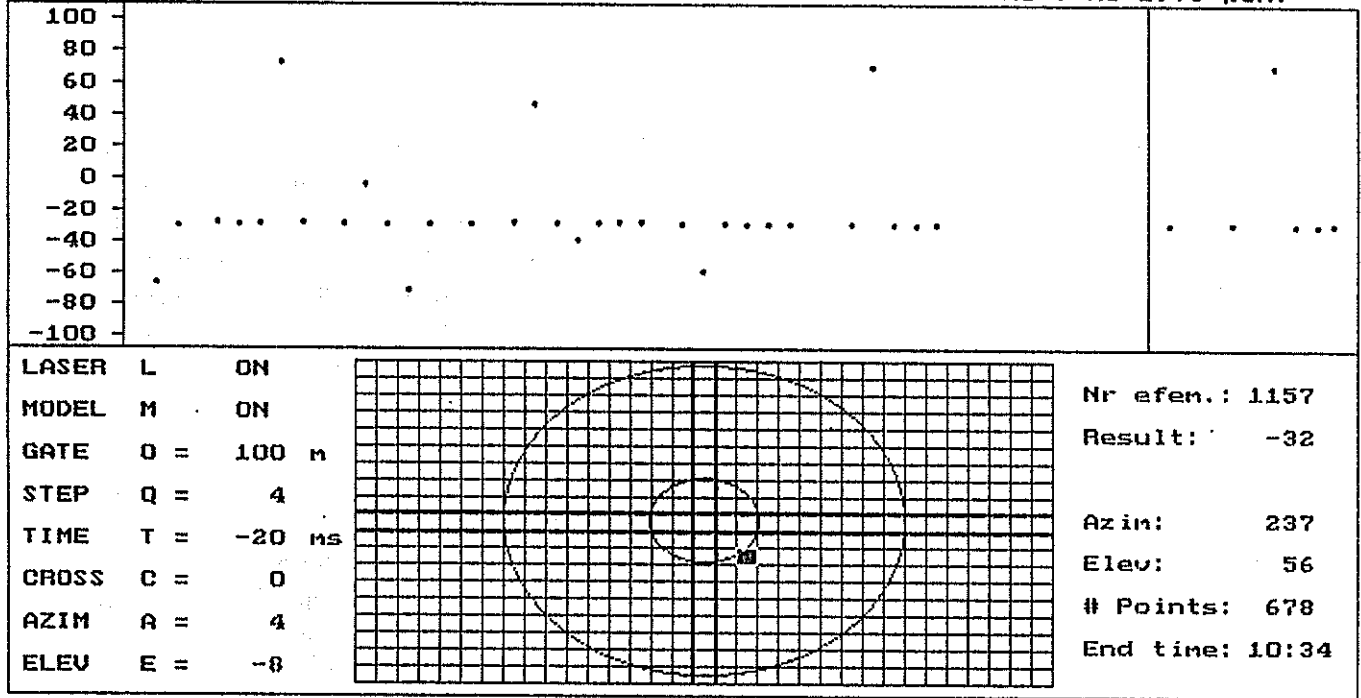
Fig. 2

of a second), O-C result in meters (when there is one within 2 seconds) or the number of points in the gate window appearing within 2 seconds, the current position of the telescope, the number of points which have appeared in the gate window so far, and the time till the end of the observation,

- read keyboard; all operations connected with finding a satellite and its tracking are made through the keyboard of the controlling computer, automation of these processes will probably be the most difficult, at present there are a few options of approaching the problem;

- at a low level of noise typical of the Borowiec system the searching for a satellite and keeping its track can be conducted automatically on the basis of the number of points in the gate window within 2 seconds, a significant increase of the number of these points indicates that the satellite has been hit, the system will automatically look for the greatest number of points by a stepwise adjustment of the telescope position with a step of the half beam divergence,

- at a high level of noise, good points can be found following the point by point analysis according to one of the geometrical methods, however, then a very fast computer is required,

- at a very high level of noise, the dark curve of returns against the background of the noise points can be found with the help of the graphical analysis of the picture through the use of a video card, however, this method requires an additional computer supporting the system,

- on the basis of the first good measurements the program can calculate the corrected value of the time bias which permits a reduction of the gate window and the number of noise points,

- control of the position of the laser beam related to the inaccuracies of the Coude system carried out by a video card on a separate computer, the computer will analyse the position of the laser beam end, if the beam is deviated too much from the centre of the field of view, its

position will be automatically corrected by the servo engines driving the output prism, preliminary tests have confirmed the possibility of applying this solution.

Post-observation process:

- meteo; the solution proposed is the same as in the pre-observation process,
- post-pass calibration; the choice of the filter and diaphragm should be adjusted to the average amplitude of the return signals or the percentage of good measurements during the satellite pass, if there are significant differences between the results pre- and post-pass calibrations in the mean, RMS or the level of sensitivity, the calibration performed before the observation should not be taken into account (this is a consequence of specific weather conditions in Borowiec where frequent fogs prevent from a correct choice of the filter and diaphragm for the pre-pass calibration, at present this is left up to the operator's decision), the other problems will be solved as indicated for the pre-pass calibration.

3. Results processing.

The processing of results including their control and formatting is carried out by the AOP program which ensures fast and almost fully automatic performance of all necessary operations: elimination of noise pulses, determination of range bias and time bias, polynomial smoothing, rejection of points according to the 2.5 sigma criterion, presentation of the distribution of deviations with determination of RMS, skewness and kurtosis, generation of normal points and assessment of their precision, graphic presentation of residuals (Fig, 3), analysis of the results of calibrations, saving the results in the inner catalogue of Borowiec, formatting of the results in the normal points quick-look format and their sending. The time the program takes to perform all these tasks from the end of the observation to sending of the results to EDC for about 1000 points is of about 2 minutes. At any time after processing the basic information about a given observation can be retrieved and printed: log sheet, distribution of deviations, graphic presentation of residuals (Fig. 3), results and assessment of the precision of normal points. A block diagram of the AOP program is shown in Fig. 4, where the exclamation mark indicates the tasks which require operator's intervention. These tasks and the proposed ways of elimination of operator's actions are listed below:

- calibration data, the choice of a calibration for a given pass;
automatic choice can be carried out on the basis of the mean amplitude of the return signal or the percentage of good results,
- noise points elimination; at present performed by using a mouse;
this process can be carried out by the point by point analysis according to one of the geometrical or filtration methods,
- store results; at present a decision on acceptance of results is made by operator;
an additional program is necessary to control basic data on the results of observations and calibrations,
- e-mail to EDC; operator's decision on sending data to EUROLAS DATA CENTER;
requires automation of the process of data sending by e-mail, the decision on sending the results will be made as indicated above.

Realisation of the above presented tasks will permit almost full automation of the Borowiec SLR. Unfortunately, complete elimination of operator's involvement is impossible mainly because of the need to set the system on and off, control its work and response to highly unstable weather in Borowiec (decision to open or close the roof, to carry an observation out or break it).

STATION: BOROWIEC   SATELLITE: TOPEX   1996-06-21 21:59:30 3410 POINTS
TIME BIAS:-31.7ms   RANGE BIAS: 24.1m

O - C RESIDUALS
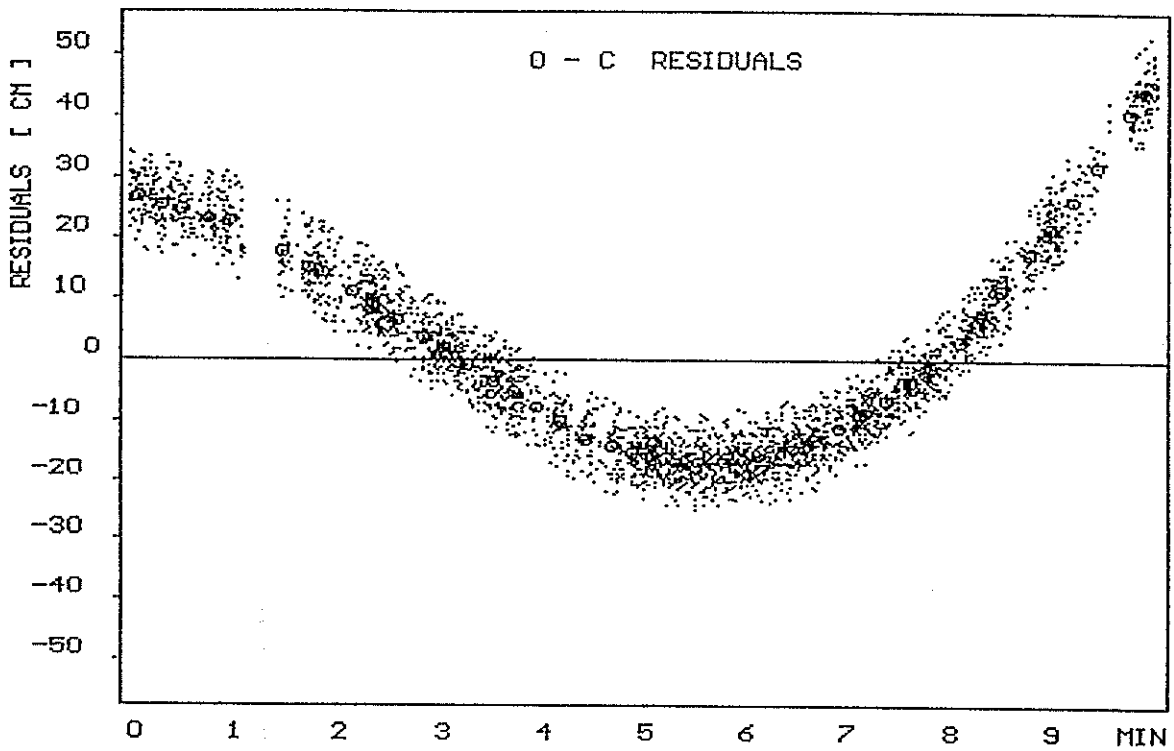
STATION: BOROWIEC   SATELLITE: TOPEX   1996-06-21 21:59:30 3410 POINTS
TIME BIAS:-31.7ms   RANGE BIAS: 24.1m   STEP OF POLY: 8   RMS: 3.42cm

SINGLE POINTS (dots) => NORMAL POINTS (circles)
3.42 cm => 0.32 cm
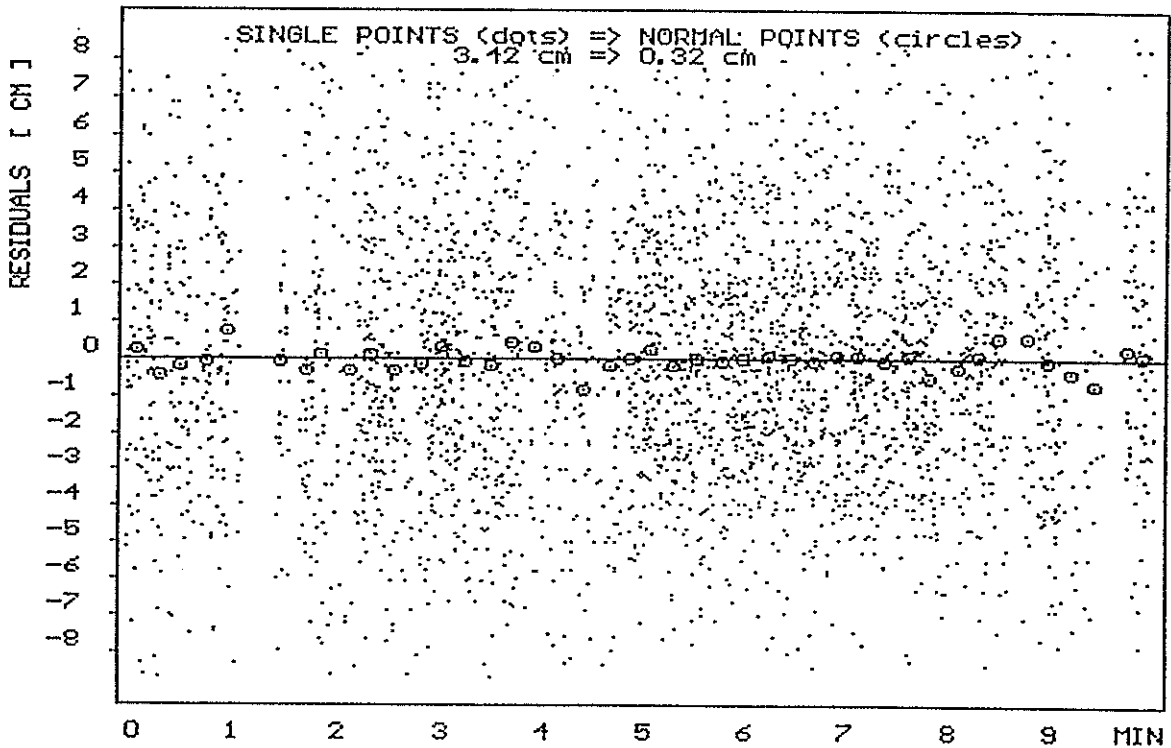
Fig. 3

AOP
POST-PASS DATA HANDLING PROGRAM
BOROWIEC SLR STATION
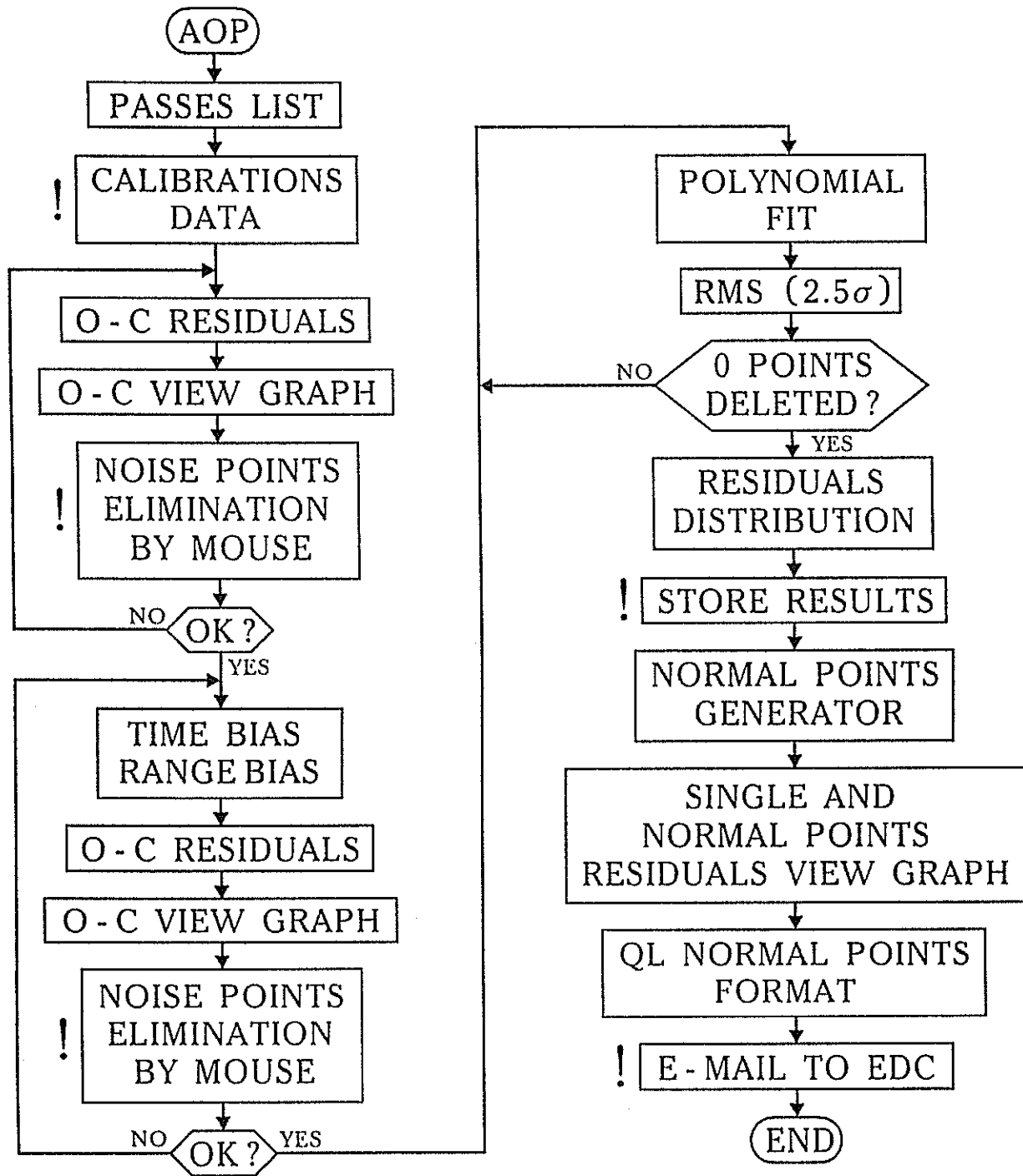
Fig. 4

UPGRADING THE NASA SATELLITE LASER RANGING NETWORK FOR THE 21ST CENTURY and THE SINGLE OPERATOR AUTOMATION PROJECT

Presented in the System Automation and Operational Software Session of the Tenth International Workshop on Laser Ranging Instrumentation
November 11-15, 1996

John Bosworth, <u>David Carter</u>, John Degnan, Jan McGarry
NASA Goddard Space Flight Center
Greenbelt, Maryland 20771 USA

Winfield Decker
AlliedSignal Technical Services Corporation (ATSC)
Lanham, Maryland 20706 USA

The NASA Satellite Laser Ranging (SLR) Network has been preparing for the 21st century by upgrading and planning the redistribution of its systems. NASA intends to relocate two of its MOBLAS systems to Tahiti, French Polynesia and South Africa, respectively. The purpose of the redistribution of the NASA MOBLAS systems is to improve the geographical distribution of the global SLR network. The upgrading program for the MOBLAS systems included several automation projects. The objectives of these projects were to improve productivity and make the MOBLAS systems more cost efficient while enhancing the quality as we approach the 21st Century. The automation program included the Mount Observer Automation (MOA), MOBLAS Upgrade Project (MUP), the High Sensitivity Laser Receiver (HSLR), and the Single Operator Automation Project (SOAP). The MOA, MUP, and HSLR have been discussed at previous conferences, therefore, the details of SOAP will be presented.

Introduction

The NASA SLR Network consist of five MOBLAS systems, two University systems, and a Transportable Laser Ranging System (TLRS). These systems are located across the United States in Maryland, Texas, California, and Hawaii. NASA also have systems located in Arequipa, Peru and Yarragadee, Australia. In order to provide better geographical coverage particularly in the southern hemisphere, NASA intends to relocate MOBLAS-8 (Quincy, California) and MOBLAS-6 (Greenbelt, Maryland) to Tahiti, French Polynesia and South Africa, respectively. The MOBLAS transfer to Tahiti is a joint effort among NASA, CNES, and the French University of the Pacific (UFP). The SLR site will be located on the campus of UFP. GPS, DORIS, and PRARE systems will also be located at the site. The MOBLAS system is scheduled to be transferred to Tahiti during July/August 1997. The discussions concerning the transfer of a MOBLAS to South Africa is in preliminary stages.

Over the past few years, NASA has been involved with an upgrading program for the MOBLAS systems. The program consist of four major upgrades: the Mount Observer Automation (MOA), MOBLAS Upgrade Project (MUP), High Sensitivity Laser Receiver (HSLR), and the Single Operator Automation Project (SOAP). The purpose of the MOA was to eliminate the necessity of a mount observer by replacing the observer with a radar and several automated processes. The purpose of the MUP was to enable future automation by the centralization of ranging and processing functions, upgrading of the computer platform, standardization of the hardware and software, and upgrading of the software and troubleshooting infrastructure. The purpose of the HSLR was to enhance the detection capabilities of the NASA MOBLAS systems on low optical link satellites such as GPS, GLONASS, and Etalon.

Single Operator Automation Project (SOAP)

SOAP was conceived to enable the NASA MOBLAS stations to operate effectively and safely with one operator per tracking shift. A single operator per shift will enable an increased level of satellite tracking support by making more effective utilization of personnel resources. SOAP builds on the other automation projects (i.e. Data system automation, MOA, and MUP), and is the culmination of a series of engineering projects designed to automate the functions of the mount observer and streamline processes for the console operator.

The MOBLAS systems currently operate with two crew member per 9-hour tracking shift. For SOAP to be implemented, detailed examinations on the engineering, maintenance, personnel, and safety issues, as well as operating procedures had to occur. Methods were developed to address the engineering and safety constraints associated with current operations. This was accomplished through field HP380 software enhancements, modifications to field operating procedures, additional operator training, and operator certification (see Figure 1). A strong emphasis was placed on crew safety especially with the remote locations of some of the NASA sites. With these modifications, SOAP will be able to provide 24 hour per day, seven days per week operations using 4 operators. This will double the temporal coverage over the previous two shift operations.

The final design approval for SOAP took place in June 1996. The installation and testing of the prototype occurred at MOBLAS-7 in July 1996. The installation of SOAP at MOBLAS-4 is scheduled to be completed in November 1996. The MOBLAS-8 installation will occur in January 1997, followed by the installation in MOBLAS-5 and MOBLAS-6 which are expected to be completed in the first quarter of 1997. The development, testing, and installation will occur on a parallel schedule for HOLLAS and MLRS.

Summary

NASA's upgrading program for the MOBLAS systems will be completely implemented in 1997. The benefits of these automation projects are that it reduces the cost of operations, increases the data volume, and enhances the safety of the MOBLAS operations. The MOBLAS-8 system will be transferred to Tahiti by August 1997 and detailed discussions will begin concerning transferring a system to South Africa. This will lead NASA into building and deploying "SLR2000"[1] systems in the 21st century.

References

[1] 1. Degnan, John, Jan McGarry, Thomas Zagwodzki, Paul Titterton, Harold Sweeney, et al, "SLR2000: An Inexpensive, Fully Automated, Satellite Laser Ranging System," in this Proceedings.

SINGLE OPERATOR AUTOMATION PROJECT (SOAP)

- HARDWARE / SOFTWARE ENHANCEMENTS
  - IMPROVED AUTOMATION OF STATION DATA REPORTING FUNCTIONS
  - INTERNET CAMERAS TO ALLOW VISUAL CONTACT BETWEEN STATIONS

- MODIFICATIONS TO FIELD OPERATING PROCEDURES
  - EMPOWERED EACH OPERATOR TO DECIDE THAT UNSAFE TRAVEL CONDITIONS WILL CANCEL OPERATIONS
  - PROHIBITED SPECIFIC TYPES OF MAINTENANCE UNLESS AT LEAST 2 PEOPLE ARE PRESENT (HIGH VOLTAGE)
  - PROVIDED CELLULAR TELEPHONE FOR EMERGENCY USE
  - ESTABLISHED COMMUNICATION SYSTEM TO MAINTAIN CONTACT WITH OPERATORS ON PRE-DETERMINED SCHEDULE

- OPERATOR TRAINING AND CERTIFICATION
  - ALL OPERTORS TRAINED FOR HIGHER LEVEL CERTIFICATION
  - FORMAL TRAINING IMPLEMENTED PRIOR TO START OF OPERATIONS
  - TYPES OF MAINTENANCE THAT CAN BE PERFORMED BY INDIVIDUALS SPECIFICALLY DEFINED

Figure 1

Automated Quality Control of NASA SLR Data

Van S. Husson
AlliedSignal Technical Services Corporation
NASA SLR Program
7515 Mission Dr.
Lanham, Md 20706

1.1.1 Introduction

This is an update to a paper that was previously published [*Husson et al.*, 1994] in the proceeding of the previous SLR workshop held in Canberra, Australia. The purpose of Automated Quality Control (AQC) is to quickly identify any data problems so that the cause can be identified and corrected as soon as possible to prevent more bad data from being taken. Therefore, AQC results needs to be readily available to the people who can take corrective action. In the current NASA network, this place is still at the system where we still have operators. The operators are the first line of defense in identifying data problems using information provided by AQC coupled with other routine evaluations of the sub-systems.

1.1.2 History

In the early and mid 1980's, the NASA SLR network hardware was upgraded and standardized with 200 picosecond pulsed non-mode locked Quantel lasers, Micro-Channel Plate Photo-Multiplier Tubes (MCPPMT), cascaded Tennelec discriminators, and stable short range calibration targets [*Husson*, 1992]. Before and after these system upgrades, extensive testing of the different sub-systems were performed in the laboratory. Collocation testing (see Figure 1) were used as a verification test of the complete system. These hardware upgrades coupled with improvements in NASA/ATSC data analysis and processing techniques improved the NASA SLR data precision and accuracy from the 10cm level in 1980 to the sub-cm level by the mid to late 1980's.

AlliedSignal Technical Services (ATSC), formerly Bendix Field Engineering Corporation, has been responsible for NASA SLR Network data processing, analysis, and quality control since the late 1970's. All through the 1980's, ATSC had 4-6 people at it's central facility who's primary responsibility was to perform these data related functions. Full-rate data was primarily used for system performance evaluation. The biggest problem with full-rate data analysis was the delay (up to 1 month) between the time the data was taken to when it was analyzed. Data problems could and did go undetected for a month. Most of this delay (2-3 weeks) was caused by the full-rate data shipment process. Full-rate data was stored on 9-track magnetic tapes and was forwarded only once per week to the central facility via regular postal mail. After the data was received at central facility, another week was needed for the data processing and data evaluation.

By the late 1980's, weekly long-arc analysis reports of quicklook data, produced by both the University of Texas and the University of Delft, were distributed to the global SLR community. Quicklook data was sampled full-rate data sent immediately after the data was taken. Quicklook data was not quality controlled at that time and because of that quicklook data quality was inferior to full-rate data quality. In the late 1980's, 5-10 cm problems were detectable in the Texas and Delft analysis and ATSC became reliant upon these reports as a redundant gross level quality control check. By the end of the 1980's, sampled data was being replaced with normal point data.

NASA/ATSC Collocation Results
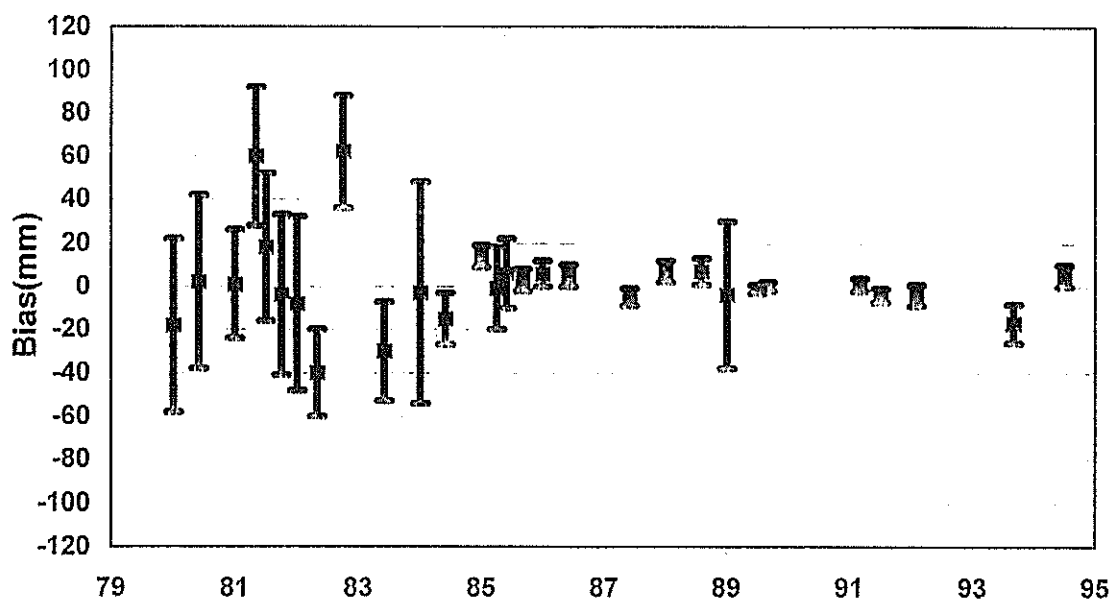
Figure 1. Collocation Results

By the early 1990's, we were faced with a huge technical challenge. NASA only had funds to support a single person quality control operation, NASA SLR data quality was to be maintained, management of full-rate data was to be phased out, and at the same time new SLR satellite missions had to be supported that would cause a dramatic (4-5 fold) increase in NASA SLR data quantity. AQC was mandatory to our survival.

1.1.3 Pre-requisites

The pre-requisites for development of AQC is a comprehensive understanding of system performance at the sub-system and overall system level [Pearlman, 1984].

1.1.4 Requirements

One initial requirement of AQC was to identify 95% of the NASA SLR data problems. NASA was willing to take some risk and could accept a 5% data loss. Problem data that was repairable in the past would now either have to be thrown away or if possible be documented (i.e. provide range bias, time bias, or barometric offset information) [Husson, 1992]. It took about 2 years to develop a quality control algorithm, benchmark it's effectiveness, automate it, and migrate it from the central facility to the field systems.

1.1.5 Algorithm Development and Benchmarking

Over 50 years of ATSC data analysis experience was used to develop the first LAGEOS quality control model. The algorithm was based on LAGEOS only, because LAGEOS was the primary target, had a very stable orbit, and the only satellite who's data was analyzed on a routine basis. The Center for Space Research (CSR) Weekly LAGEOS Reports and collocation analysis results

were used in determining the final quality of the data. Problem data was defined as any data having a known systematic error above the 1-2 centimeter (cm) level. This was and still is the smallest error detectable using LAGEOS long arc analysis techniques. Other satellites were eventually added to the algorithm.

Five years of NASA SLR LAGEOS-1 and LAGEOS-2 (1988 - 1993) data, consisting of a total of 11,167 passes, were used to benchmark this model. During the algorithm development and benchmarking, it was discovered that the basic pass-by-pass processing statistics (i.e. satellite RMS, calibration RMS, and calibration shift), that are computed in the generation of normal points, would become the critical performance statistics. These statistics already existed in the CSTG normal point format. This fact was critical to the success and ease of implementation of the algorithm, because full-rate data was being phased out and quicklook data was being transitioned from sampled data to normal point data. Another interesting discovery was that there should be two levels of quality control, a gross level and a fine level. Data should be verified first at the gross level, if it passed at the gross level, then it should be verified at the fine level. Below are the 2 levels in the algorithm:

1.1.5.1 Gross Level

```
If LAGEOS RMS > 5 cm or
       if combined calib. RMS > 5 cm or
              if (calib. shift > 5 cm and combined calib. RMS < 5 cm) Then
                     DATA IS BAD
```

Note: calib. is an abbreviation for calibration

All data that did not pass the gross level was bad and should be edited. However, certain NASA SLR system problems (i.e. excessive laser multi-pulsing), which would cause the data to flunk the gross level check, were and are repairable by manual intervention in the full-rate data and normal point generation process.

1.1.5.2 Fine Level

```
Else

If LAGEOS RMS > 1 cm or
       if combined calib. RMS > 0.8 cm or
              if (calib. shift > 0.5 cm and combined calib. RMS < 0.8 cm)
Then
                     DATA IS OK, BUT SHOULD BE CLOSELY MONITORED
End if
```

Data that passed the gross level check, but failed the fine check was still very usable data (i.e. accurate), but it's precision was slightly degraded. If degraded precision continued for an extended period of time (i.e. a few days), then a investigation should be initiated into the potential source of the problem.

1.1.5.3 Benchmark Results

The exact same algorithm could be used for each NASA SLR system, due to many of the standardized components in our network.

The AQC is still not a replacement for other sub-system performance checks done routinely as part of normal NASA SLR system operations. These other sub-system performance evaluations include daily monitoring of station time through use of GPS receivers to the 1 microsecond level; daily monitoring of barometric performance by comparing dual station barometers to the 1 millibar level; monthly monitoring of the timing frequency to one part in 10^{-12}; monthly multi-target ranging closure to the sub-cm level; and periodic checks of the station key processing parameters. If these sub-systems checks reveal a problem, data precision would usually not be effected, but data accuracy would be adversely effected. The good news is if thorough station performance records are maintained, the data can be corrected.

The benchmark results revealed that 15 percent of the total benchmark dataset had significant problems, but only 5 percent would be detectable by the AQC algorithm. The other ten percent of the data, had errors that would not manifest itself in either an abnormal satellite RMS, calibration shift, or calibration RMS. But, these problems, which effect accuracy and not precision are detectable through the sub-system tests mentioned above.

There are some other interesting benchmark discoveries. The root cause of the problem can be narrowed based on the values of the quality control statistics. For instance, if the satellite RMS or calibration RMS > 1-2 times nominal values, then the problem is usually in the receive electronics (i.e. MCPPMT, discriminators, time interval unit). If the satellite RMS or calibration RMS is between 20-40 cm, then the problem is usually laser related. If the satellite RMS or calibration RMS > 40 cm and if the pass was daytime, then low signal to background noise ratio is the cause.

1.1.6 Conclusions

Global SLR data quality control needs to be migrated to the stations as much as possible. To be successful in doing this, a complete understanding of the performance of every sub-system, including the system as a whole is required. We have demonstrated that AQC can be done and be effective, but many years of hard work were involved in getting to where we are today.
Standardization within the NASA SLR network was a key to the AQC success.
AQC needs to be readily accessible to the people that maintain the system. With recent advancements in computer networking technology (i.e. INTERNET), AQC can be done in near real time virtually anywhere (i.e. a centralized facility or in the field).

The AQC algorithm needs to be closely monitored for it's effectiveness, especially after any system hardware, software, or procedural changes or after tracking of a new satellite. AQC has been very crucial in maintaining NASA SLR data integrity in the 1990's and is a requirement of SLR2000.

1.1.7 Current Status

The AQC algorithm originally was used to flag data, not to edit data. We have since realized this is a severe weakness and on January 28, 1997, we now edit any NASA SLR data that flunks the gross level check as part of our automated global normal point data management operation.

1.1.8 Acknowledgments

1.1.9 References

Husson V, "Historical MOBLAS System Characterization", Proceedings of the Eighth International Workshop on Laser Ranging Implementation, Annapolis, Md, May 1992.

Husson V, Horvath J, and Su G, "NASA Automated Quality Control", Proceedings of the Ninth International Workshop on Laser Ranging Implementation, Canberra, Australia, Nov 1994.

Pearlman M, "Laser System Characterization", Smithsonian Astrophysical Observatory, Proceedings of the Fifth International Workshop on Laser Ranging

Automated and Remotely Operated SLR Systems

Christopher Moore, Jeff Cotter, Iztok Fras, Ben Greene, Adrian Loeff, Tim May

Electro Optic Systems Pty Limited (EOS) Queanbeyan NSW Australia 2620

Abstract

The Keystone SLR Project aims to continuously measure and monitor the geodetic positions of the invariant points of a number of sites around Tokyo to provide local crustal deformation information and to provide accurate predictions of the trajectories of selected satellites. The SLR systems at each site are required to provide highly reliable routine observations and be controlled by automatic processes supported by relatively unskilled operators from a central site. These requirements place a high demand on the hardware and software systems being developed for Keystone. This paper presents on overview of the software systems being developed to support this program.

1. INTRODUCTION AND BACKGROUND

The Keystone system requires hardware and software systems for four fixed SLR observation stations, located at Koganei, Kashima, Miura, and Tateyama, all within 200 km of Tokyo, and one mobile SLR facility which can be deployed much further afield. All of these stations are to be controlled from a central station. Figures 1 and 2 illustrates the software related facilities of the central network control station and a typical remote station respectively. The fixed stations are to be connected by a 128 KBytes per second wide area network and all stations connected by the low bandwidth public switching telephone network.
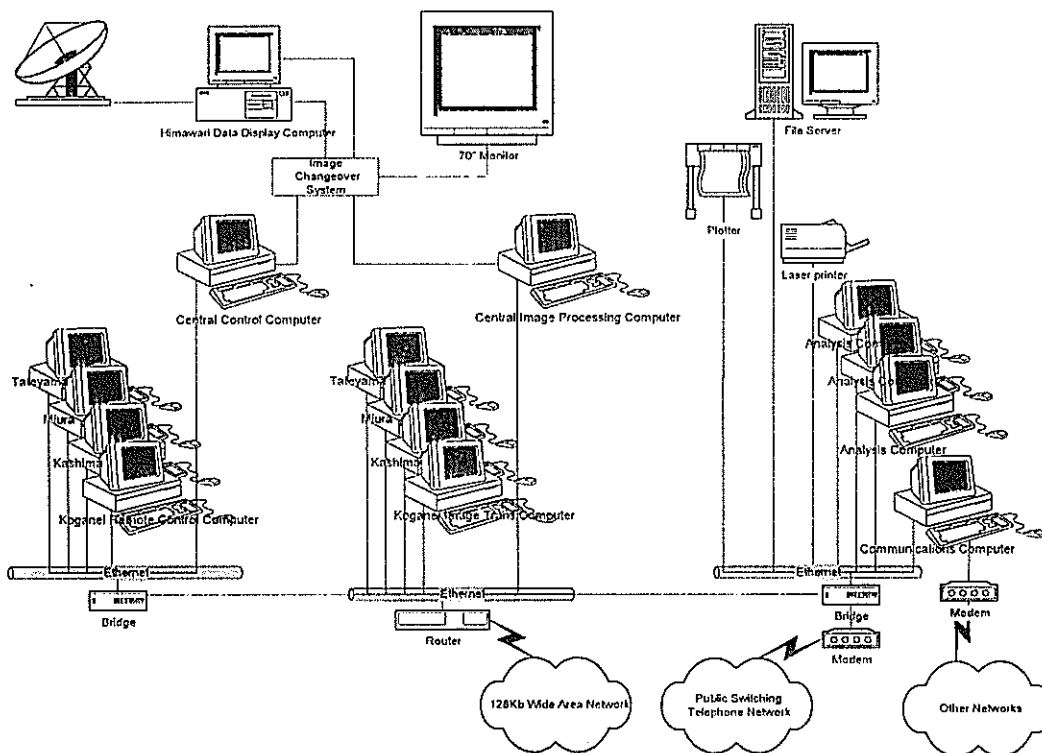
Figure 1 - Schematic of the Central Control facility
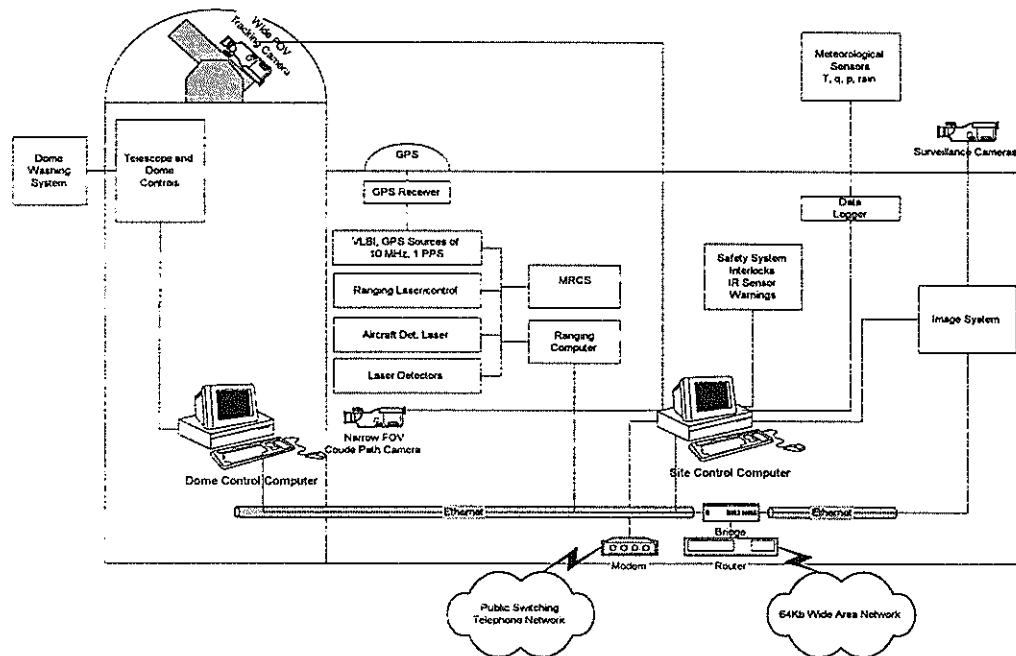
Figure 2 - Schematic of a Remote Station

The system supports three modes of control. One mode of operation will consist of control and monitoring of all network sites under the control of a single operator at the central station. The second mode allows single operators at the central station to be allocated to specific remote sites and undertake control of those sites separately from one another. The third mode allows operators at each station to control local operations independently from the central station.

All of the major software functions are being developed to support the requirement that the network of Keystone stations be operated automatically and remotely. These functions include:

- mission planning, i.e. the development of mission schedules and trajectory predictions;
- laser, dome and telescope systems control during SLR operations;
- performance of system testing and calibration; and
- data collection, analysis and archival.

2. SYSTEM ARCHITECTURE

The Keystone system is based on standard commercial Pentium PCs running under Windows NT. The central control facility computing resources, illustrated in Figure 1, consist of three groups of computers. One group provides a central control computer, and a number of remote site computers for the operational control and data monitoring of one or more sites. Another group provides for surveillance monitoring while the third group consists of computers dedicated to data analysis and data management and archiving.

539

Computing resources for each remote station consists of three computers as illustrated in Figure 2. The ranging computer, which is a dedicated VXI rack mounted Pentium microprocessor, controls laser and the master ranging control systems (MRCS), The dome control computer is dedicated to the control and monitoring of telescope, dome and associated equipment. The third computer provides general processing for the site, including user displays, data handing, intersite communications, operations scheduling and management of tests and calibration processes. This approach is designed to ensure high real time performance of the laser ranging subsystems yet allow applications to perform sophisticated automated and remote control operations.

Keystone software applications are developed in C++ with graphical user interfaces developed under Microsoft's 32 bit Windows NT. This approach allows the high performance requirements to be met, yet allow development to make use of the wide range of commercially available development products and hence minimise costs.

3. REMOTE CONTROL

To support the management of multiple sites, especially by a single central controller, it is important to use the power and flexibility of Windows style graphical user interfaces (GUIs). Figure 3 illustrates a "hierarchy" of related windows GUIs that are being developed for the Keystone project. It illustrates that from a top level "program manager" layer, an SLR application can be executed that allows control and monitoring of one or more remote stations, and other SLR applications can be launched, e.g. mission planning and engineering diagnostic tools.
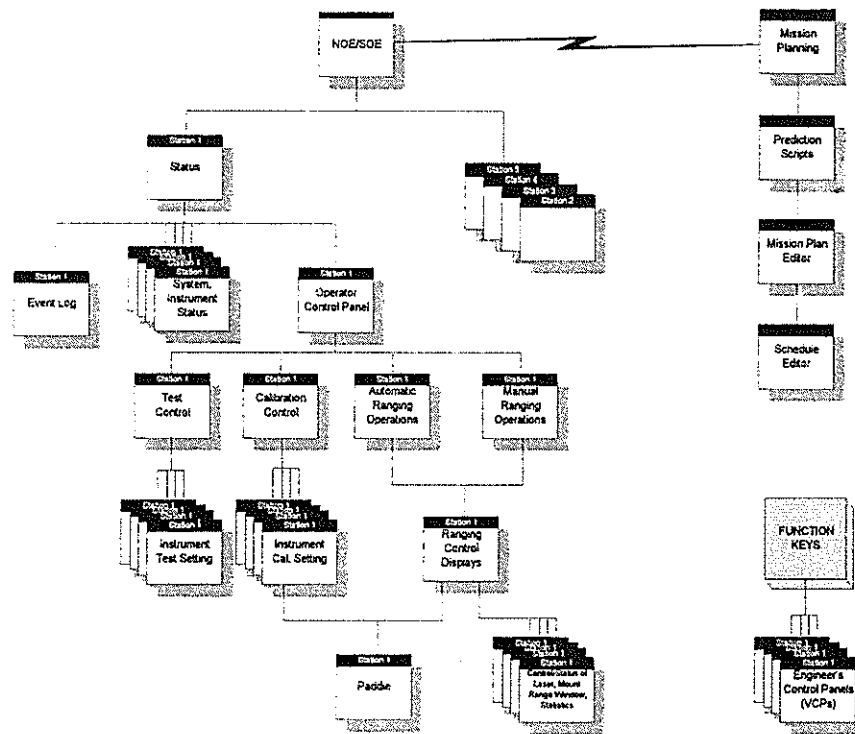
Figure 3 - Overview of KSP Operations Screens

To provide both local and remote management of a site, the general approach taken has been to provide upper level GUIs that allow site selection and monitoring - a function that is available to both local and remote operators, and to provide control screens at lower levels in the hierarchy for one operator authorised to have control. Note that the GUIs presented in this paper are schematics of conceptual displays only; and any data shown do not represent actual nor representative data.

3.1 STATUS MONITORING

Figure 4 illustrates the top level screen in which the status of all network sites is displayed in forms suitable for unskilled operators, but which can be expanded to suit the needs of more skilled operators. For example, it is possible for a network station to observe whatever operations are being performed by a selected remote site. If any problem or fault is reported by a remote station, more detailed status information can be readily accessed for that station. Such a display is illustrated in Figure 5.
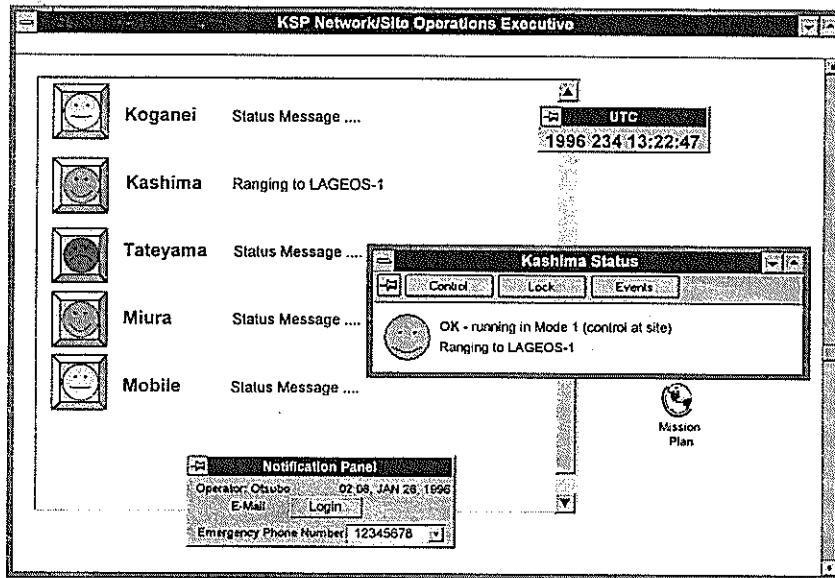
Figure 4 - Schematic of Top Level Operations Main Window
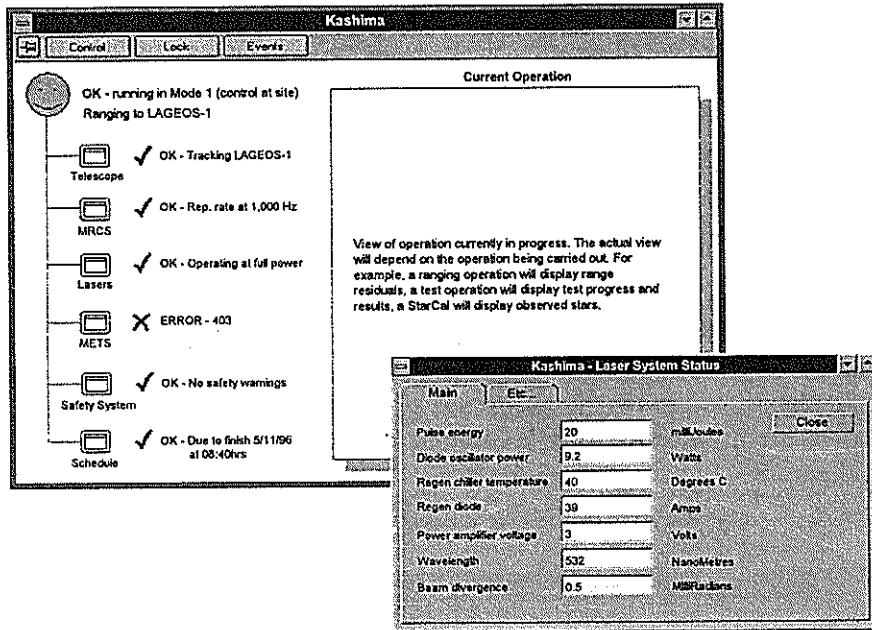
Figure 5 - Schematic of the detailed status screen

To allow local and remote control of sites, the software is designed to support all manual controls necessary for SLR operations once an operator gains the appropriate authorisation. Manual operations include the ability to conduct system and subsystem tests and calibrations, and the ability to manually select a satellite and initiate ranging operations. GUIs for such manual operations are illustrated in Figure 6 for the manual control testing and Figure 7 for ranging operations.

4. AUTOMATED OPERATIONS

The key characteristic of the Keystone system will be its ability to perform automatic SLR operations and maintain a reliable observation program with a minimum of operator attendance.
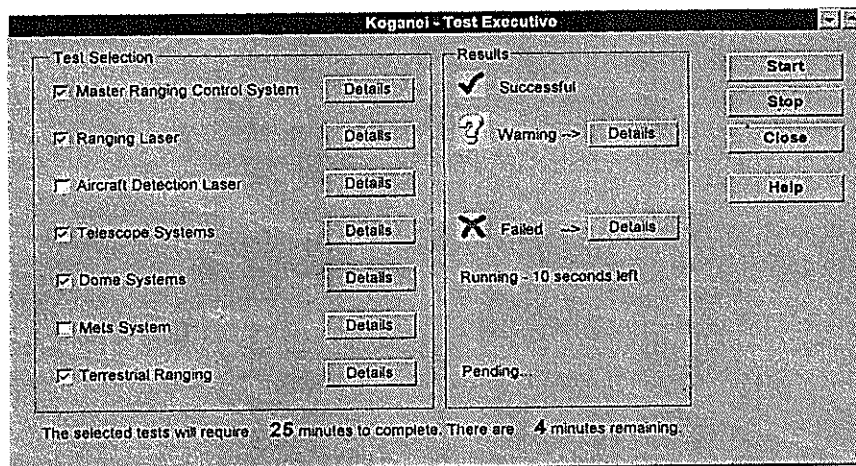
Figure 6 - Schematic of Test Control Screen
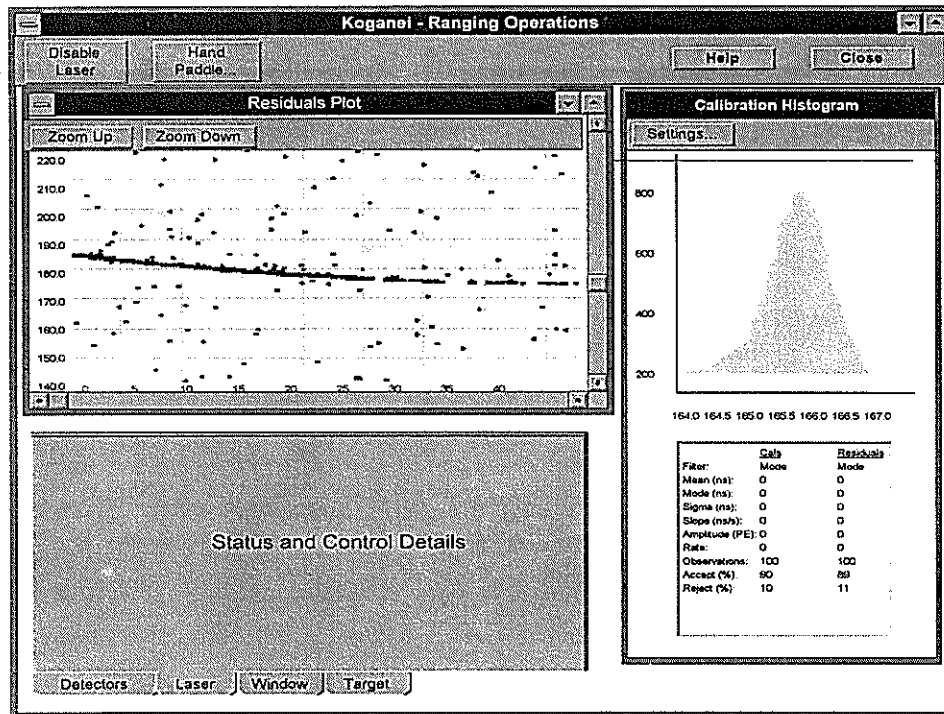
Figure 7 - Schematic of Ranging Operation Screen

Software related functions that support automated operations include:

- Automated and manual development of operating schedules

- Automated distribution of operating schedules to network sites

- Automatic performance of scheduled operations

- Automatic tracking

- Automated observation data management

- Automated data exchange between Keystone and external agencies.

Routine development of detailed operating schedules can be generated using a mission planning system, in which the tracking of selected satellites can be scheduled together with routine and automated calibration and test activities. This mission planning system will include an editor, illustrated in Figure 8, allowing selection of satellites for prioritised and dedicated SLR, or for selecting a number of satellites for interleaved observations.

To ensure as a high level of observation effectiveness, the system will support automatic acquisition and tracking, in which the software will have the ability to perform search patterns and adjust and optimise window widths and offsets, firing rates and laser power.
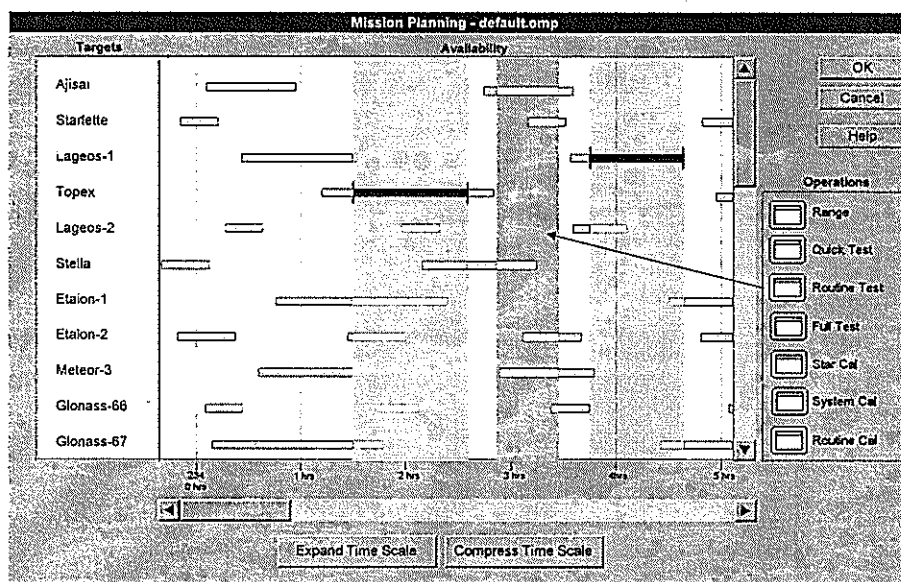
Figure 8 - Schematic of Mission Plan Editor

5. CONCLUSIONS

Software functionality needed to support the automated and remote operational requirements of the Keystone SLR Project has been summarised in this paper. Samples of the types of graphical user interfaces needed for this project have been presented. The ability to support, over a network containing multiple SLR stations:

- operator control at each local site

- operator control of one or more remote sites

- automated or unattended operation of one or more sites

places high demands on all systems, not least the software. The capability of current computing technologies, including advanced networking, file management, security and flexible graphical user interfaces executing on powerful processors, has made it possible to develop such a sophisticated system at a reasonable cost.

Development of software for the Keystone system will take remote and automatic operations of SLR stations to a new level of performance. This and other systems being developed by other groups suggest that this is just the first step in the evolution of advanced SLR software systems.

A method to improve the accuracy of low orbit satellite prediction[1]

Lin Qinchang[2]   Yang Fumin[3]   Tan Detong[3]

Tang Wenfang[3]   Zhang Zhongping[3]   Deng Youjun[2]

[2] (Guangzhou Satellite Station, Chinese Academy of Sciences,
Guangzhou   510640, China)
[3] (Shanghai Observatory, Chinese Academy of Sciences,
Shanghai   200030, China)

Abstract

In this method, the orbit elements a、i、Ω、$\xi = e \sin \omega$、$\eta = e \cos \omega$ and $\lambda = M + \omega$ derived from IRV data are taken as basic variables in numerical integration. By these elements the polynomial's degree of the interpolation can be decreased. The change of x-coordinate axis to Mean Equinox decreases the influence of the error of the predicted UT1-UTC. The usage of up date SLR data can improve the orbit elements of satellites. The order and degree of the Earth's spherical harmonic perturbation are extended to 20×20. The solar and lunar coordinates are improved to about 2', that can further improve the solar and lunar perturbations. The light pressure perturbation, the air drag perturbation, and the influences from the coordinate system and the polar motion transformation are also taken into account. The improved satellite prediction procedure would be available to the laser satellite observation at the daylight.

All computation programs are carried out at microcomputer 486/66 in Shanghai Observatory SLR station.

1. The necessary to improve the accuracy and fast computation of low orbit laser satellite prediction

Although the predicted accuracy of low orbit laser satellite prediction higher and higher, it is still very difficult to realize low orbit satellite laser ranging at the daylight. The succeeded echo ratio of SLR is no too high, even at night. One of the reason is that the accuracy of the low orbit laser satellite prediction is limited, at least, because following factors:

1) The error of the predicted values of   UT1-UTC, polar motion of the Earth, $F_{10.7}$, K_p, et al.

2) The error to compute various perturbations at satellite prediction.

3) The dynamic systematic errors of the tracking telescope of the SLR instrument.

We have investigated the dynamic systematic errors of the tracking telescope of the SLR instrument and detected the dynamic systematic errors of the tracking telescope of the SLR instrument at Shanghai Observatory. It is more urgent to improve the accuracy of the low orbit laser satellite prediction. Because if the precision of the low orbit laser satellite prediction is low, at least, following three situations often occur.

1) It increase the time to research the satellite and labor strength of the observers, and decrease the arc which could be laser range.

2) The regularity of the differences between observed and predicted values time-bias and ranging-bias is no enough good. These values have larger error. If it is used to improve the satellite prediction for following

several passes, it would derive the error of satellite prediction. These values are no sufficiently used.

3) It increased the trouble to separate the signal and noise after satellite laser ranging.

For the laser satellites are launched more and more, the number of the laser satellites moved around the Earth are reached about 20. There are about 40 passes opportunity to SLR. But only microcomputers would be used to most SLR stations. Therefore, it is necessary both to improve the precision and fast computation of low orbit laser satellite prediction.

2. To decrease the influence of the error of the predicted UT1-UTC to the laser satellite prediction

In order to decrease the influence of the error of the predicted UT1-UTC to laser satellite prediction, following rectangular coordinate system is adopted in our software system: the mass-center of the Earth is taken as the origin of the coordinate system; x axis is directed to the Mean Equinox; y axis also is located within the mean equator of the Earth and directed longitude 90 " measured eastward from the Mean Equinox; and z axis is directed the Mean North Polar of the Earth. This system is independent with UT1-UTC. Until to predict the satellite before observation, the most new predicted value of the UT1-UTC would be substituted following equation to compute the local sidereal time S of the station, thus, the influence of the error of the predicted value of UT1-UTC to satellite prediction would be decrease to least. Let

$$
\begin{aligned}
S = 1.7533685592333 &+ (628.33197068884 + (0.00000677071394 \\
&- 0.0000000045087672343T)T)T + 0.00007292115855306t \\
&+ (UT1-UTC) + \lambda + (x_p E + y_p D)C/B.
\end{aligned} \tag{1}
$$

Where, T is the Julian Century Number counted from 1.5 Jan. 2000 to UTC 0^h of the date to compute the satellite positions (36525 days as the time unit); t is the time counted from UTC 0^h of that day (second as the time unit); λ is the geocentric longitude of the station measured eastward from the meridian of Greenwich, x_p and y_p are two components of the polar motion of the Earth, and

$$
\begin{aligned}
B &= \cos \phi', \\
C &= \sin \phi', \\
D &= \cos \lambda, \\
E &= \sin \lambda.
\end{aligned} \tag{2}
$$

Where, ϕ' is the geocentric latitude of the station. Therefore, in this coordinate system, the error of the prediction value of UT1-UTC is no any influence upon satellite coordinates, and the influence on the compute the predicted station position would be decrease to least.

3. The computations of various perturbations on the satellites

In many SLR stations, among the computations of various perturbations on the satellites, only lower order and degree of the Earth's spherical harmonic and solar and lunar perturbations by coarse solar and lunar coordinates are computed. To improve the accuracy of predicted positions of the satellite, we computed following various perturbations.

1) The spherical harmonic perturbation of the Earth.

A method researched by us not only overflow in operation no occurs, moreover, even when the order and degree of the Earth's spherical harmonic are extended to 100×100 or more, but also the computing speed is higher than those of Cunningham's method and any other existing methods. When the order and degree of the Earth's spherical harmonic are extended to 20×20 by us, it is enough to satisfy the prediction to the low orbit laser satellite at the daylight.

2) Solar and lunar perturbations.

The accuracy to compute the solar and lunar coordinates is directly influence computing accuracy of the solar and lunar perturbations. Only microcomputers would be used to the satellite prediction in most stations. Although lunar ephemeris LE200 has high accuracy, but it is very difficult to be used to this kind of microcomputers. If several developments of triangle function is used to computed solar and lunar coordinates, we are afraid that the computed accuracy is no enough. We adopted following method to compute solar and lunar perturbations. Tens terms of developments of triangle function was used to computed solar and lunar coordinates, and the operation of triangular functions are transformed arithmetic operation as possible as. Thus, the operation speed is very high, and the accuracy to compute the solar and lunar coordinates are improve to about 2'. The accuracy to compute the solar and lunar perturbations would be improved.

3) The light pressure perturbation.

4) The air drag perturbation.

The computation of air drag perturbation on the low orbit laser satellite are not considered in many stations. Here not only the computation of air drag perturbation, but also the computation of air drag perturbation on the orbit plane of low orbit laser satellite derived by the rotation of the Earth are computed.

5) The coordinate system perturbation.

6) The polar motion perturbation.

4. The numerical integration

Many people adopted three rectangular coordinates and their three one-order variables as the basic variables to numerical integration. However, considered following factors, we adopt orbit elements as the basic variables.

1) Within same the duration of the period, the variance of the satellite's orbit elements is much slower than the compounds of their coordinates and velocity. If the orbit elements are adopted as basic variables to numerical integration, using lower degree of the polynomial, it can get higher accurate interpolated values during the interpolations. Therefore, it decreases the machine time used to interpolation.

2) Using the values of satellite's coordinate and velocity to numerical integration, if the initial coordinates just is in the most north (or south) of the orbit, the error of the start coordinates would bring bigger error to extrapolated orbit plane of the satellite. In the time, it increases the difficult to SLR at the daylight.

Adopting orbit elements a、i、Ω、$\xi = e \sin \omega$、$\eta = e \cos \omega$ and $\lambda = M + \omega$ as the basic variables to numerical integration, we use 4 degree Runge-Kutta method to numerical integration. It can be satisfy the demand for both to predicted accuracy for satellite laser ranging and to save the machine time at the same time. During numerical integration, further, we adopted the multi-step method and predicted-rectify method.

5. Interpolation

Adopted upper measure, we use 5 degree and 6 terms polynomial to interpolate the orbit elements which accuracy satisfied the demand. Interpolating is one part of a subroutine, and only several lines of the program. It

not has to be programmed to a special software, and decreases the trouble to operation.

6. The fast computation of the visual topocentric coordinate of the satellites

Following all computations are included in our software:

1) The transformation from the equatorial coordinate system of the satellite to the topocentric coordinate system of the station.

2) The computation to correct the rotation of the Earth UT1-UTC and the polar motion.

3) The correction of dynamic systematic errors of the tracking telescope of the SLR.

4) The correction of time delay of SLR system.

5) The satellite mass-center correction.

6) The corrections of azimuth, altitude and ranging derived by the atmosphere refraction, using the data of temperature, pressure et al. of the ground near station.

7) The correction of the satellite's position, using correction time-bias.

8) The primary selecting. To each SLR station, the time would be laser ranging is only tens minutes to every low orbit satellite for one day and night. To decrease the machine time to compute the topocentric coordinate of the satellites which is not have to compute, this software system would automatically select out the time when the satellite just arrives to the highest point of its visual arc. If the satellite's altitude on the ground is still lower the minimum predicted altitude at the time, this software would make that the predicted time will jump to the next time when the satellite just arrives to next the highest point of its visual arc. The stridden time interval may be 1 pass or several passes. Thus, the machine time to compute the visual topocentric coordinate of the satellites which is not have to be decrease minimum.

However, the used formulae are short. The method has be programmed to a software system and it need much less machine time.

7. Data procession and filter

The method of data procession adopted by us is included the filter. Because the data of SLR at daylight is including more noise, the filter method of this software system can separate the signal from the noise which is occupied 90 % of total data.

8. Initial orbit elements

In this software system, the method to determine initial orbit elements has two ways.

1) According the orbit elements which are before 1 month or 1 year, they be extrapolated to given time.

2) According three coordinate components and three velocity components in IRV data which are corresponded given time, the orbit elements a , e , i , M , ω and Ω are derived.

9. The orbit improvement

The method for orbit improvement of this software system can derive the corrected values which are any

combination of a、e、i、M、ω、Ω、$\ddot{M}$ and $\dddot{M}$, using SLR data

10. Application

Among the software system, the filter is programmed to a signal software, others are programmed to another software. Used filter software, the signal are separated from the observed data. Later software also has some filter function and has several computed schemes. If the computed schemes need be changed, it is only replace a figure in a datum file. Operating the microcomputer just once, it would carry out all computation, including initial orbit elements, data procession and filter, the computations of various perturbations on the satellites, the numerical integration, the orbit improvement, interpolation and the fast computation of the visual topocentric coordinate of the satellites.

Although the software system would improve the predicted accuracy of laser satellite, the operation speed is very fast. Using microcomputer 486/66 in SLR station Shanghai Observatory, it is only 10 second of machine time to perform 1 day numerical integration for low orbit laser satellite, and much less that 1 second of machine time to other auxiliary computation.

RGO Predictions and Time Bias Functions

Roger Wood

Satellite Laser Ranger Group
Herstmonceux Castle, Hailsham
East Sussex, BN27 1RP, UK

Abstract *The RGO's Space Geodesy Group in Cambridge computes Inter-Range Vectors (IRVs) for 8 satellites widely observed by the SLR network. The SLR Group at Herstmonceux produces time bias functions (TBFs) with respect to the RGC predictions for these satellites; and also for a further 9 satellites with respect to IRVs produced by other groups. IRVs and TBFs are publicly available at the RGO's web site, by anonymous FTP from Cambridge or, on request, by email from Herstmonceux. This paper describes what is available for which satellites, how the data are produced, the frequency with which they are updated and how to access them.*

Introduction

The requirement for good predicted orbits is self-evident. The additional benefits of having the very best estimate of time bias trends with respect to a particular orbit are threefold: ease of satellite acquisition; improved tracking of the satellite without offsetting; and better noise elimination by using a narrow range gate. The RGO group aims to provide high accuracy IRVs which give good predictions for several weeks supplemented by TBFs based on the most recent data and made available to all stations as quickly as possible.

RGO Predictions

Satellites: The satellites treated fall into two groups according to the origin of the basic data for computing orbits:

A Ajisai, Glonass 63, Glonass 67, Starlette, Stella and Topex;

B GPS 35 and GPS 36.

Basic data:

A normal point data from the worldwide SLR network retrieved from the CDDIS data bank;

B broadcast elements from the GPS satellites themselves using the data from the GPS Rogue receiver at Herstmonceux.

Method: For each satellite the basic data for an interval of 2 to 3 weeks are used to generate a precise orbit. This precise orbit is then projected forward for a period of 4 to 6 weeks and used to form daily IRVs.

Updating: New sets of IRVs are formed at roughly monthly intervals or sooner if a satellite such as Topex is manoeuvred or (very rarely) if the time bias trends are not smooth enough to be fitted by simple polynomials.

Filenames: Each filename consists of a 3-character satellite identifier and the date of formation, *e.g.* Stella IRVs produced on 1996 November 7 would be stored in file `ste_9611.07`.

Table 1: *Satellite identifiers for RGO predictions*

aji Ajisai	g63 Glonass 63	g67 Glonass 67	gpa GPS 35
gpb GPS 36	ste Stella	str Starlette	top Topex

Special notes for GPS IRVs: Using the broadcast data from the GPS satellites has the twin advantages that data are gathered every day, whatever the weather, and continuously over much longer arcs than are generally observed with SLR.

In addition, Andrew Sinclair has recently been developing techniques to utilise the highly accurate orbits produced each day at AIUB using GPS data from all around the world. Every afternoon the AIUB orbit data are FTPd to Cambridge as soon as they are available, converted to IRVs at 6 hourly intervals (rather than the usual daily intervals) for that day and the two following days, and then deposited in the RGO anonymous FTP account for general use. These IRVs are computed afresh every day and can therefore be used with zero time bias, which is why they do not appear in RGO TBF files. They are expected to provide the best possible IRV predictions for SLR with only minimal changes to existing prediction software. The best solution of all would be to use the GPS XYZ data directly in place of the XYZ generated by the IRV integrator.

Table 2: *Identifiers for RGO predictions based on daily Swiss GPS orbits*

spa GPS 35	spb GPS 36

RGO Time Bias Functions

Satellites: Adeos, Ajisai, ERS–2, Etalon 1 and 2, GFZ–1, Glonass 63 and 67, GPS 35 and 36, Lageos 1 and 2, No ton, Ralph, Starlette, Stella, Topex.

Basic data: Time biases for individual passes are derived from:

- Herstmonceux observations for all satellites;
- observations from all stations for all satellites retrieved as normal points from CDDIS;
- timebias values supplied from GFZ for ERS–2 and GFZ–1;
- for GFZ–1 only, normal points exchanged *immediately* after each successful pass between a few participating stations.

The time biases are referred to the most recent IRV set for the satellite from ATSC, GFZ, NASDA, RGO or Texas, as appropriate.

Method: For each satellite simple polynomials of first, second and third order in time are fitted through the available data and the one which is judged to give the best extrapolation of future trends is chosen for inclusion in the published file of TBFs.

Updating: TBFs are updated continuously as observations are reduced at Herstmonceux, day and night, and as data from other sources become available. Results are deposited in Cambridge every hour and emailed to anyone who requests them twice a day at 0800 and again at 1700 UT.

Filenames: The format is identical to that described above for IRVs but the prefix tbf is used to designate time bias functions *e.g.* tbf_9611.07.

Table 3: *Satellite identifiers for RGO Time Bias Functions*

ade	Adeos	aji	Ajisai	erb	ERS–2	eta	Etalon 1
etb	Etalon 2	gfa	GFZ–1	g63	Glonass 63	g67	Glonass 67
gpa	GPS 35	gpb	GPS 36	lga	Lageos 1	lgb	Lageos 2
nor	Norton	ral	Ralph	ste	Stella	str	Starlette
top	Topex						

Contents: TBF files are designed to give a compact, easy to use, one line per satellite summary of TB information for all current satellites. Each line contains:

- the 3-character identifier for the satellite;
- the starting Modified Julian Date (MJD) for the function, T_0;
- four polynomial coefficients, C_0, C_1, C_2, C_3;
- a code indicating the origin of the IRVs to which the TBs are referred;
- the identifier for the IRV set used.

Thus a typical entry is:

```
AJI 50390.00 61.222458 1.588192 -0.214656 0.000000 RGO AJI037
```

At MJD T, and writing $t = T - T_0$, the timebias in milliseconds is computed from

$$C_0 + C_1 t + C_2 t^2 + C_3 t^3$$

Special notes for GPS TBFs: For GPS 35 and 36 only TBFs are computed for IRVs from ATSC as well as RGO. In order to differentiate between the functions alternative TBF identifiers are, somewhat arbitrarily, assigned.

Table 4: *Identifiers for RGO TBFs using ATSC IRVs*

gqa	GPS 35	gqb	GPS 36

Access and Distribution

World Wide Web: All IRV and TBF data are available on the Royal Greenwich Observatory's Cambridge web site via the Space Geodesy pages.

Web site address: http://www.ast.cam.ac.uk/RGO

Anonymous FTP: All IRV and TBF files are also available from the RGO's Cambridge anonymous FTP account.

Address: ftp.ast.cam.ac.uk or 131.111.69.186

Directory: /pub/slrirv/current

Filenames: according to the date of deposit—see above for details.

Email: Anyone who would like to be added to the distribution list and receive twice daily updates to the time bias files by email should contact Roger Wood at the address below.

Contacts:

Roger Wood SLR Herstmonceux
    Telephone: +44 (1323) 833888
    Internet: slr@gxvf.rgo.ac.uk

Graham Appleby RGO Cambridge
    Telephone: +44 (1223) 374737
    Internet: gma@ast.cam.ac.uk

Automatic Ranging Software in Graz

G. Kirchner, F. Koidl
Institute for Space Research / Austrian Academy of Sciences
Observatory Lustbühel; A-8042 GRAZ / AUSTRIA

1.0 Introduction

About 2 years ago, we switched from the old HP1000 computer to a PC control system for all real-time ranging operations and calibrations in Graz; the simple PC (486/66mhz) has some standard interface cards added (GPIB, Digital I/O, Analog IN etc.). For this system, we wrote a complete new tracking / ranging software, and implemented fully automatic return detection/identification within the noise, automatic SemiTrain track identification, automatic range gate setting, automatic tracking optimization etc. Except an initial search phase (which will be implemented later, when we have time available), most passes are tracked, controlled and optimized fully automatically, ensuring maximum number of returns, keeping return energy within desired limits, and allowing our untrained students - after 1 night training - to enjoy their coffee during actual tracking ...

2.0 General Methods

For all real-time programs, we use LAHEY 16-Bit Fortran, which is in general much more suitable for real-time applications than 32-Bit versions; we use 32-Bit Versions for post-processing and data handling programs only.

Both main real-time programs used in Graz (Ranging and Calibration) are written as simple sequential programs, running under DOS (or in any DOS window), with a 10-Hz loop; no multi-tasking environment etc. is used. The programs are extremely structured, and very easy to maintain / improve / change. Although these programs handle all real-time operations, control / program / read all instruments, handle SemiTrain and MultiCounter (up to 4 different counters) procedures, and implements fully automatic tracking features, the source code of each program is only about 6000 lines (about 25% of that are comments!), which gives quite reasonably sized EXE-files of about 250 kB, leaving lot of space for future extensions. We have tested that at the moment even the simple 486-PC (66 Mhz) is still running at a small percentage of its capabilities, again leaving enough spare for the future.

To create a real time scale with sufficient resolution and accuracy, we use one of the available internal counters on the general Analog/Digital I/O Card in the PC slot; the counter is synchronized to and driven by an external 1 kHz derivate of our 10 Mhz standard frequency; this counter can be read by the PC within some µs, giving a real time clock with fast access, with the accuracy of our external time source, and with a 1 ms resolution.

3.0 Return Identification

Operating the SPAD at 10 V above break, it delivers noise rates of 400 to more than 2000 kHz, depending on cooling, day/night conditions etc.; besides limiting our maximum useful range gate to about 500 to 1000 ns, it is difficult to find returns of satellites with low return signals, e.g.

GPS etc, within this noise, without any assistance from the software.

To identify returns within the noise, we assume always a well known time bias for the satellite (due to the necessary small range gate, we HAVE to know it anyway; as it can be changed also in real time, it is easy to identify and set the correct satellite time bias down to sub-ms level); this ideally gives a flat, straight line of residuals. Of course we use all possible ways for accurate time bias predictions: All time bias functions arriving via e-mail (from RGO, GFZ-Potsdam, and now the standardized Time Bias Function File), as well as the automatically stored/updated values of our own last observations.

During tracking, any new residual is compared with the last 100 residuals, taking into account also the fixed SemiTrain distance of 8759 ps; if the new residual coincides with more than 3 previous residuals (we use a 250 ps coincidence limit at the moment), the new residual is identified as a valid return, gets a corresponding flag, is plotted in a different color and produces a special beep for easy acoustic identification.

The necessary calculations are simple (a small subroutine with 25 lines) and extremly fast, because they use only simple comparisons and coincidence number counting.

This method, although quite simple, proved to be much faster - especially in low return rate situations - than any trained observer; it also detects returns under conditions were it would be impossible or at least very difficult for observers (low return rate, high noise etc.); for higher return rates, it identifies valid returns within about 0.5 to 1 s (in our 10 Hz system).

There is - mainly during very noisy daylight sessions - a small probability that some noise points are identified as valid returns; but this probability is below 1% in worst case, and never disturbs any of the following procedures which depend on correctly identified satellite returns.

4.0 SemiTrain Track Number Identification

The last residuals are also used to identify the track number of the SemiTrain to which the new residual belongs; this is done by filling the last residuals of valid returns into bins of SemiTrain width, and identifying the bin with the maximum number of residuals; these residuals are than assigned to track #1 of the SemiTrain; as the SemiTrain distance is known, the correct SemiTrain track number can be assigned now easily to all other residuals, including the new one. The identified, valid residuals of different SemiTrain tracks may be plotted in different colors - according to their SemiTrain track number - on the real-time screen.

In addition, as soon as the track #1 of the SemiTrain is known, it is easy to identify also any pre-train returns (identified returns BEFORE track #1), which are due to small leakage of the Nd:YAG laser pulse selector, and may appear for low satellites with strong return signals (indicating too high received energy). This pre-train identification is used in the AutoTrack routines for immediate offset pointing to keep the return energy within the tolerable range for the SPAD Time Walk Compensation Unit [1] (see below).

5.0 Automatic Range Gate Setting and Shifting

As soon as the first track of the SemiTrain is identified, it is easy to use these residuals to control automatically all range gate parameters: The range gate is shifted so that all returns of track #1 always appear between 50 to 70 ns from range gate begin; this ensures that any influence from range gate setting (ringing etc.) has disappeared safely, while the time between range gate begin and returns is minimized (to minimize noise stops before actual returns). The range gate

width is also reduced automatically to about 200 ns, which allows space for roughly the first 15 tracks of the SemiTrain.

This AutoGate is set ON automatically as soon as the first few returns are identified; this is indicated by changing the range gate bar color on the real-time display (into blue, which is the standard color indicator for all our automatic processes).

The range gate follows any slopes of the residuals, regardless if due to incorrect time bias settings, time bias changes by the operator etc., as long as there are any identified residuals. If there are no identified returns for some time (e.g. due to clouds), the range gate parameters are just kept constant, until new returns are identified again.

Mark Points	X-Limits Min/Max	Y-Limits Min/Max	XMinMax: PASS RETS	BW/Color	

| 14.2° | | LA201416 | 51.8° | | LAGEOS-2 | 15.6° |
| 11105 Points: | | | Time Bias: | 51.7 ms; | Range Bias: | 11.7 m |
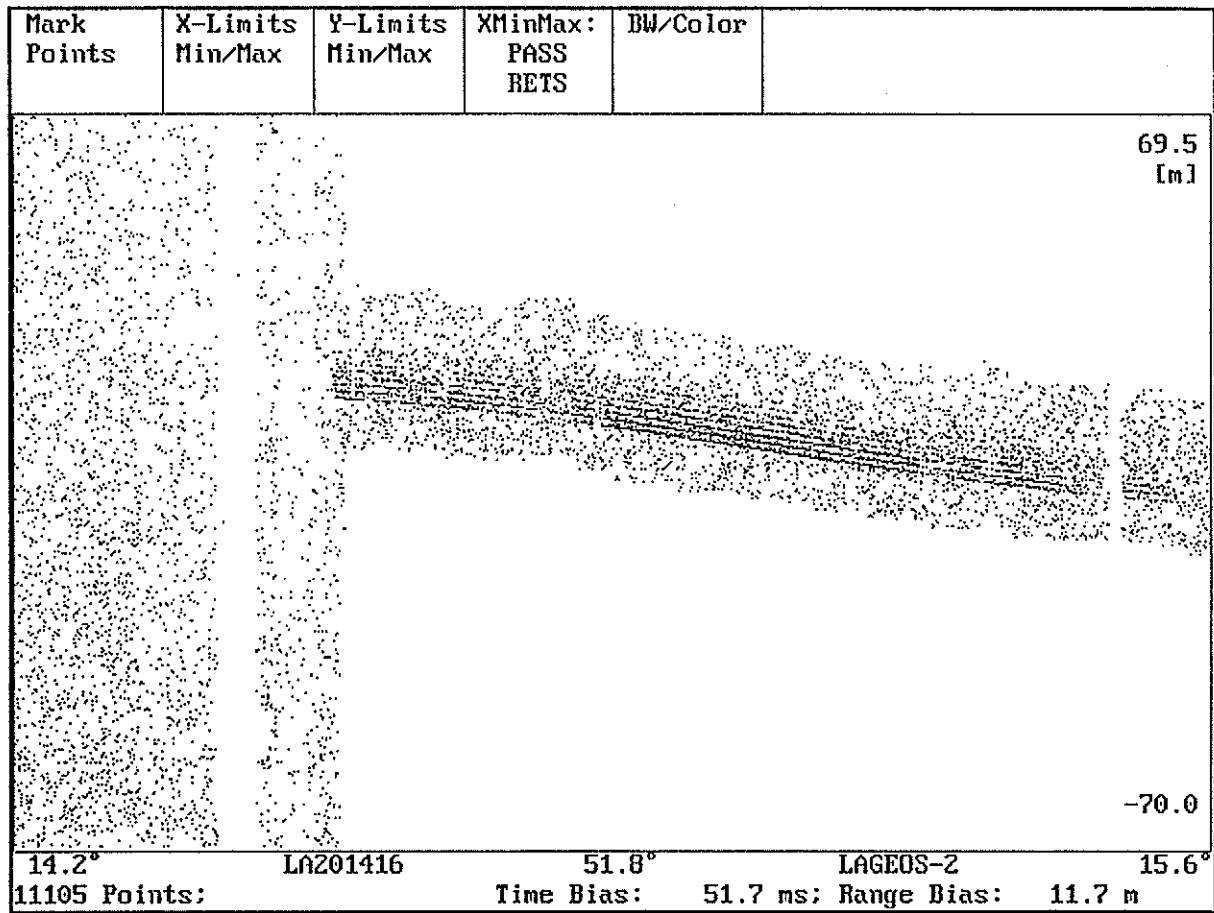
Fig. 1: Lageos-2 Post-Processing: Shows Return AutoDetection, and how AutoGate follows the Identified Residuals

The AutoGate can be switched OFF/ON or overwritten at any time also by manual input of the observers (via keyboard, function keys etc.).

6.0 Automatic Tracking Optimization

6.1 Weighted Return Rate Figure

The AutoTrack routines use these identified return residuals to calculate their own return rate figure, with each identified return weighted according to which SemiTrain track number it is assigned; returns in the first tracks are weighted higher, so that the return rate figure is maximized if as many returns as possible (or all) appear in the first SemiTrain track.

All AutoTrack routines try to maximize this weighted return rate figure; thus the systems optimization goal always is to have one single track only; this is easily reached for all lower satellites, and is achieved for LAGEOS in good weather conditions; but with the few mJ laser in the small Graz station, it will remain a goal for GPS-35 and GPS-36 anyway ...

6.2 Gradient Search for Maximum Return Rate

Usually, any tracking system moves the mount/telescope system according to the predicted satellite orbit; most systems allow the introduction of small offsets (along-track, azimuth/elevation offsets etc.) by operator inputs; the feed-back is usually some type of real-time display showing the returns, their amount, their position etc.

As all this feed-back information is now available to the software, it can be used to optimize any tracking offsets automatically in order to get maximum number of returns. The AutoTrack routines check the identified return rate figure per time unit, and perform a gradient search around the present position, changing slightly all tracking offsets always in those directions where the identified return rate figure increases.

To optimize the search for the various satellites, we assign all satellites to different, random categories according to their tracking requirements. Each category defines its own parameters for the search, like high/low limits for the time span to check for identified returns, high/low limits for azimuth/elevation offset step sizes, high/low limits to stop (no identified returns, or near 100% identified returns) or reassume (sufficient return rate figure again) the gradient search etc. All these parameters are increased or decreased dynamically by the software during actual tracking, according to the actual return rate: Thus the satellite is acquired fast (lower time spans, higher az/el step sizes) at begin, while settling down to optimize slowly and in small steps as soon as return rate figure is approaching higher values.

6.3 Gradient Search: Handling of Various Special Situations

The gradient search is started automatically as soon as there are some returns identified (the same minimum limits are used as for the automatic start of the AutoGate); to indicate this to the observer, the tracking offset indicator on the real time display changes it color into blue.

As soon as the software identifies too many pre-trains (more than the small amount, which is tolerable, indicating a still acceptable return energy for our Time Walk Compensation Circuit [1]), the AutoTrack routines perform immediately a slight offset pointing, increasing the offset until pre-train returns disappear. This ensures that the tolerable return energy levels are not exceeded, independent of - and much faster than - any observer action.

In case of clouds, the return rate figure decreases rapidly, and approaches Zero; this leads quickly to an increase in speed and steps of search in the vicinity, of course now without any success; in such a case, the systems returns to the average offsets of the last identified returns, waiting there for any new identified returns. For low satellites in daylight ranging (where we can observe the clouds with a small, low-cost video camera), the system re-starts already to identify returns (and consequently re-startsAutoGate / AutoTrack), when it is approaching the end or the

edge of the cloud (ranging through thin cloud layers), somewhat before any observer would even start to try getting echoes ...

At the end of each pass (or when the observer exits), all actual parameters, offset values, time bias etc. are stored on disk. If the same pass is re-started, all these actual parameters are used automatically; this ensures fast satellite re-acquisition, allowing efficient switching back and forth between the same passes (interleaved pass ranging). If the next pass of the same satellite is started within 24 hours, some selected parameters (Time Bias etc.) are also used automatically by the system.

As with the AutoGate, also the AutoTrack can be switched ON/OFF by manual observer inputs via keyboard; in addition, when AutoTrack is ON, the observer still has the full set of keyboard commands available for any tracking offsets (most of that is done simply with the keyboard arrow keys), which are just added to the AutoTrack offsets; this allows any desired operator assistance or correction to all AutoTrack features when deired.

7.0 Results and Conclusions

The automatic ranging software, operational in Graz now since almost 2 years - with improvements added according to our experience -, has a lot of advantages:

- It increases significantly the system output, by optimizing all tracking procedures;
- For most satellites, Graz gets the highest data density (returns per Normal Point);
- This is done almost independently of any observer action;
- New observers are able to do the best possible observations after a one-night training;
- Return signal level is kept automatically within required limits;
- The software is easy to change, extremely flexible, and poses no limits on our PC-486/66;
- Any additions can be made easily; e.g. adding or changing counters is done in minutes;
- Future extentions will include automatical initial search (which will use also the - averaged - 'experience' of the last passes, stored on disk), and direct switching from satellite to satellite for interleaved pass ranging (at the moment the telescope goes back to Zero position after each Pass Exit, which takes some additional seconds);
- The only tasks remaining for the observer at the moment are: Rotating the dome, scheduling the passes, starting - if necessary - some initial search, and correcting any Coudé path mispointing by tilting the remotly controlled last Coudé mirror.

With the additions planned, the system should be able to run fully automatically, although unfortunately we will not be allowed to use that really (one person is required always due to aircraft safety regulations).

Reference:

[1]   Automatic SPAD Time Walk Compensation. G. Kirchner, F. Koidl; in these Proc.

Data Analysis

and

Models

Analysis of HTLRS Data
at Marine Fiducial Points in Japan

Masayuki Fujita and Arata Sengoku

Hydrographic Department of Japan
5-3-1, Tsukiji, Chuo-ku, Tokyo 104, Japan
e-mail : mfuji@cue.jhd.go.jp

Abstract

The Hydrographic Department of Japan (JHD) has operated a mobile SLR station (HTLRS) since 1988 in the framework of the marine geodetic control project. In 1996, it has completed a first observation cycle at 14 marine fiducial points distributed at major off-lying islands and at some coastal areas in Japan.

The AJISAI data at all the HTLRS sites were analyzed with global data. The used software is GEODYN-II developed by NASA. The reference fixed stations are GSFC (Maryland, USA) and Haleakala (Hawaii, USA), for which the coordinates of the ITRF93 with its velocity field are adopted as a priori values. The rms of the resulted range residuals for the HTLRS data are 5-10cm, which is comparable to those of all the global stations.

The stability of the solutions for the baseline vectors between the HTLRS sites and Simosato, the stationary SLR station in central Japan, was examined by comparing the solution with those obtained under different estimation conditions. As a result, followings are concluded; (1) the estimated baseline vector can be determined within 1cm as far as the coordinates of both the HTLRS sites and Simosato remain as estimated parameters; (2) it can be well determined by a single arc analysis; (3) it can be determined within 1cm when the frequencies of estimations of the empirical acceleration and the drag coefficient are less than 3 days; (4) the estimation does not depend on the frequency of estimation of the solar radiation pressure coefficient; (5) the estimation does not depend on the selection of the atmospheric density model if the drag coefficient is appropriately estimated.

1. Introduction

The Hydrographic Department of Japan has been carrying out Satellite Laser Ranging (SLR) observations aiming at establishing the marine geodetic control network in Japan. In this project, a stationary observation by a fixed type laser ranging station has been continued at Simosato Hydrographic Observatory in Wakayama Prefecture, central Japan, since 1982, while a mobile type station, called HTLRS, has been operated at marine fiducial points since 1988, where 2-3 months campaign observations have been made.

The HTLRS sites were set at 14 sites located in major off-lying islands and some coastal areas as a backbone of the marine geodetic control network. It has completed its first round at all 14 fiducial points with Tyosi in 1996. A significant amount of ranging data of AJISAI were obtained for all the sites, whereas there were limited data acquired for LAGEOS-1,2 etc. at limited sites. The project for second round observations at some of these points has just started in order to monitor the variation of baseline from Simosato.

In this study, we demonstrate the result of analysis for all 14 HTLRS sites by using the software GEODYN-II developed by NASA and discuss the precision of baseline estimation between the HTLRS sites and Simosato.
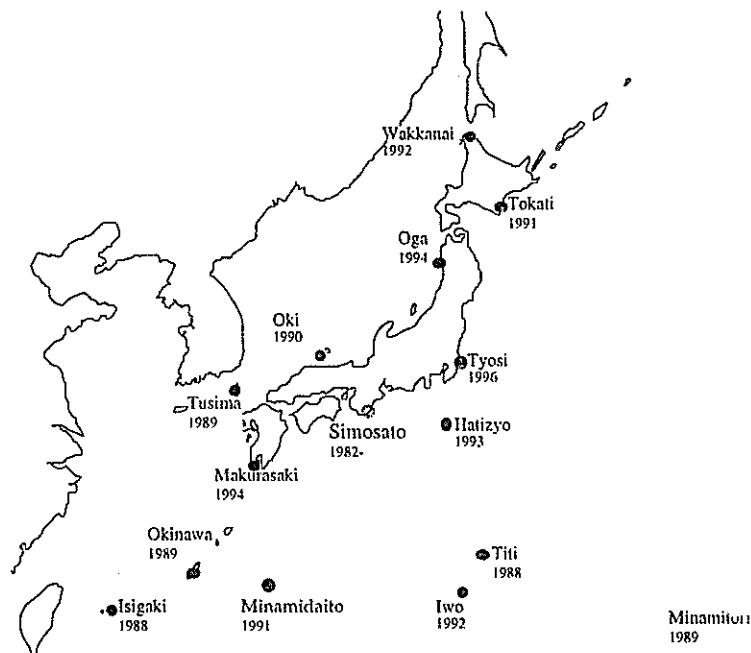
Figure 1. Map showing HTLRS sites

2. Data and analysis

Figure 1 shows the distribution of observation sites for Simosato and the HTLRS sites. The baseline lengths between Simosato and the HTLRS sites are about 360km for Hatizyo at the shortest and about 2020km for Minamitori at the longest.

Used data are global normal points of AJISAI. Table 1 lists the observation period and the number of passes at the HTLRS sites and Simosato. It also gives the abbreviation for each HTLRS site appearing in the later figures.

The software used for these analyses is GEODYN-II (Eddy et al., 1986). A single arc method, in which initial elements of the satellite are solved once at the start epoch, was applied to the analysis. As parameters as to non-gravitational forces on the satellite, we estimated 3-day atmospheric coefficient, 3-day once-per-revolution empirical accelerations in the cross-track and radial components, and 30-day radiation pressure coefficient.

An applied gravitational potential model is the JGM2 (Nerem et al., 1994) and atmospheric density model is MSIS86 (Hedin, 1987). Earth rotation parameters are fixed to the final values

Table 1. Data summary

Site name	(Abbrev.)	Start epoch (yymmdd, 0)	End epoch (yymmdd, 0)	Number of passes HTLRS	Simo
Titi	(TT)	880121	880228	34	98
Isigaki	(IS)	880724	880903	27	28
Minamitori	(MT)	890115	890317	41	49
Okinawa	(ON)	890709	890820	44	43
Tusima	(TS)	891007	891118	50	40
Oki	(OK)	900917	901024	27	26
Minamidaito	(MD)	910113	910204	12	39
Tokati	(TK)	910826	911025	21	54
Iwo	(IW)	920122	920314	25	35
Wakkanai	(WK)	920907	921013	24	26
Hatizyo	(HT)	930203	930311	19	75
Makurasaki	(MK)	940128	940311	11	58
Oga	(OG)	940814	940921	18	60
Tyosi	(TY)	960110	960307	62	80

appearing on IERS Bulletine B. An anisotropic reflection model (Sengoku, 1995) is applied.

The reference stations whose coordinates are fixed are Maryland(NASA/GSFC) and Hawaii(Haleakala Observatory). Applied coordinates as fixed values are ITRF93 with its velocity field (Boucher et al., 1994). Since the ITRF93 coordinates are given at the epoch 1993.0, the station positions are moved to the observation epoch by use of the velocity field.

A priori data sigmas given are 10cm for all stations, which implies that there is no weight difference between the stations.

3. Result

Table 2 shows estimated rectangular coordinates of the HTLRS sites together with their formal errors and residual rms' for the HTLRS sites and all the global stations. Table 3 shows 3 components of baseline vectors between Simosato and the HTLRS sites and baseline lengths with their formal errors. These values are evaluated at the start epoch of each observation.

Residual rms' of the HTLRS data are 5-10cm, which are comparable to those of all the global data. No correlation was found between observation periods and the resulted residuals. The formal errors for the HTLRS coordinates are 2-4cm.

Table 2. Estimated rectangular coordinates of HTLRS sites. Unit is in m.

Site	X		Y		Z		Residual RMS HTLRS	all
TT	-4491072.311	0.020	3481527.911	0.022	2887392.004	0.020	0.046	0.066
IS	-3265753.798	0.021	4810000.840	0.020	2614265.635	0.020	0.052	0.058
MT	-5227190.039	0.018	2551882.337	0.023	2607609.849	0.017	0.120	0.148
ON	-3505323.669	0.019	4532740.991	0.018	2792253.157	0.017	0.076	0.094
TS	-3344473.916	0.016	4087076.263	0.016	3564512.521	0.015	0.106	0.122
OK	-3536204.424	0.019	3749974.186	0.025	3744418.415	0.016	0.052	0.062
MD	-3786331.517	0.024	4320316.193	0.023	2761964.083	0.025	0.052	0.062
TK	-3788457.912	0.014	2820917.951	0.014	4271798.281	0.014	0.090	0.088
IW	-4522801.801	0.012	3622640.405	0.013	2656232.056	0.012	0.092	0.106
WK	-3522929.119	0.010	2779243.479	0.012	4517637.339	0.012	0.086	0.074
HT	-4087880.318	0.017	3451764.241	0.015	3460902.383	0.013	0.048	0.058
MK	-3528449.724	0.026	4162495.219	0.020	3291166.953	0.022	0.080	0.058
OG	-3731492.594	0.018	3164405.340	0.017	4078228.570	0.014	0.054	0.054
TY	-4021278.003	0.014	3273585.521	0.015	3701666.336	0.012	0.072	0.060

Table 3. Estimated baseline vectors and lengths between HTLRS sites and Simosato. Unit is in m.

Site	dx		dy		dz		Baseline	
TT	-668684.107	0.024	-217835.704	0.025	-620181.329	0.024	937665.031	0.024
IS	556634.604	0.025	1110637.339	0.025	-893307.650	0.023	1530148.993	0.025
MT	-1404801.736	0.021	-1147481.190	0.022	-899963.364	0.020	2024874.084	0.021
ON	317064.645	0.019	833377.421	0.019	-715320.022	0.018	1143123.199	0.019
TS	477914.434	0.018	387712.729	0.018	56939.226	0.017	618033.528	0.018
OK	286183.853	0.023	50610.564	0.027	236845.192	0.017	374911.019	0.022
MD	36056.891	0.024	620952.630	0.022	-745609.074	0.025	970986.694	0.028
TK	33930.497	0.015	-878445.590	0.016	764225.078	0.014	1164842.437	0.017
IW	-700413.429	0.013	-76723.168	0.014	-851341.157	0.012	1105100.530	0.014
WK	299459.315	0.014	-920120.075	0.016	1010064.141	0.014	1398758.880	0.018
HT	-265491.958	0.017	-247599.336	0.015	-46670.814	0.013	366018.545	0.017
MK	293938.656	0.027	463131.639	0.021	-216406.249	0.022	589680.010	0.019
OG	90895.741	0.020	-534958.250	0.018	570655.396	0.015	787457.901	0.019
TY	-198889.697	0.016	-425778.026	0.016	194093.246	0.015	508444.911	0.016
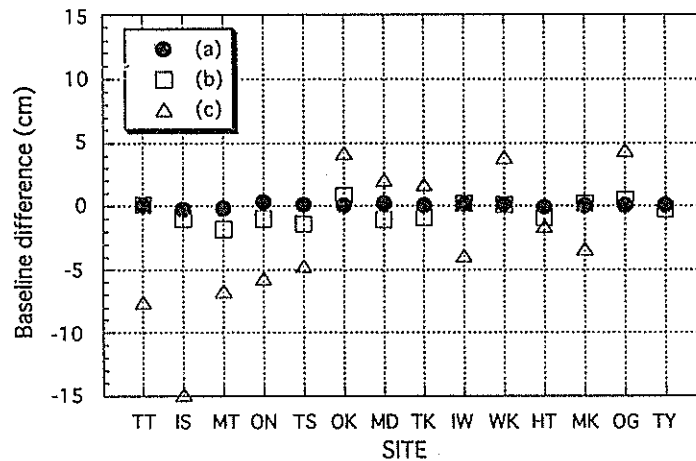
Figure 2. Comparison of estimated baseline lengths between Simosato and the HTLRS sites for the different fixed stations. Plotted are the baseline differences from the reference case.

4. Stability examinations

In the following, we examine the stability of the solutions by comparing with those obtained under different estimation conditions.

A. Different fixed stations

First, we examine differences of estimated baseline solutions depending on the different combination of fixed stations for all the HTLRS sites.

In the above analysis, we selected Maryland and Hawaii as fixed stations (reference case). Here we change the combination of fixed stations for the following 3 cases:

      (a) Maryland (GSFC) and Greenwich (RGO),
      (b) All but HTLRS sites and Simosato,
      (c) All but HTLRS sites.

Figure 2 shows the differences of estimated baseline lengths from those obtained for the reference case. The agreement is especially good for (a) and the difference does not exceed 1-2mm. As clearly shown from these comparison, the baseline estimation is significantly affected by whether Simosato is estimated or not, but not affected so much by whether other global stations are estimated or not.

B. Estimation frequency of arc parameters

Next, we examine the variation of estimated baseline vectors due to the estimation frequency of arc parameters, such as satellite elements and non-gravitational force parameters, for Titi sima and Tyosi results.

Table 4 shows the comparison of the estimated results between single and multi arc (every 3 days) analyses. The values are fractional parts of the estimated baseline vectors and lengths. This shows that the differences between these two conditions are insignificant.

Figure 3 shows the variation of estimated baseline lengths against the frequency of estimation of non-gravitational force parameters, plotted as a difference from the most frequent case for each parameter. As seen from the figure, the differences are within 1cm when the general

Table 4. Comparison between estimated baseline vectors for single and every 3-day arc for Titi and Tyosi. Unit is in m.

Condition		dx	dy	dz	Baseline	Residual	
						HTLRS	ALL
Tit	single*	0.107	0.704	0.329	0.031	0.046	0.066
	3-day	0.110	0.692	0.348	0.042	0.030	0.054
Tyo	single*	0.697	0.026	0.246	0.911	0.072	0.060
	3-day	0.682	0.025	0.253	0.906	0.070	0.060
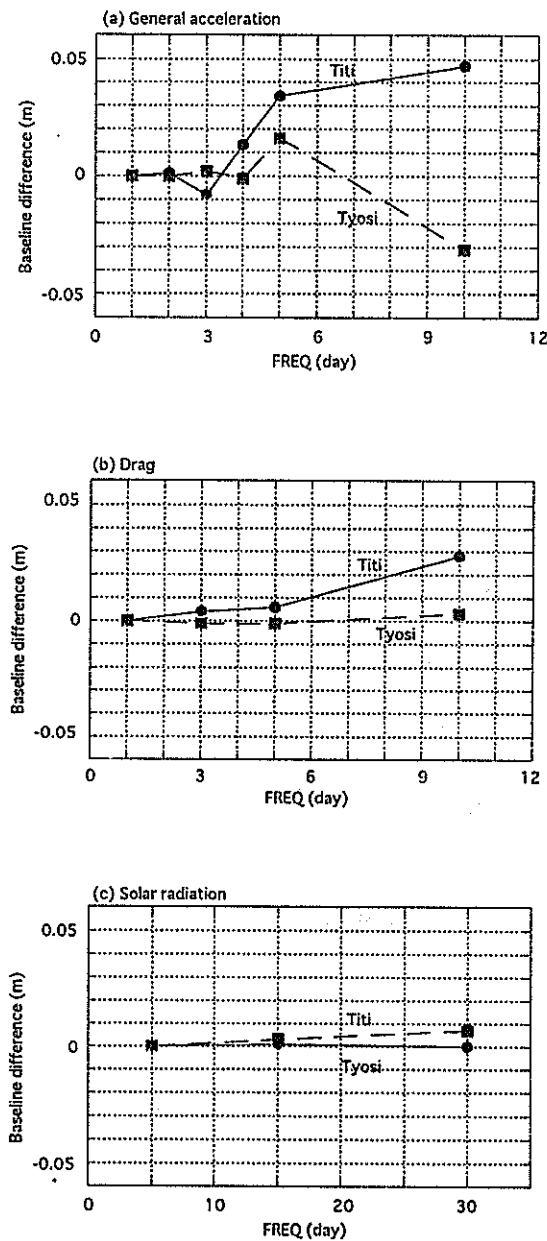
Figure 3. Variation of estimated baseline lengths against the frequency of estimation of non-gravitational force parameters for Titi and Tyosi: (a) general acceleration; (b) drag coefficient; (c) solar radiation pressure coefficient.

564

Table 5. Comparison between estimated baseline vectors for different atmospheric density models for Titi and Tyosi. Unit is in m.

Condition		dx	dy	dz	Baseline	Residual	
						HTLRS	ALL
Tit	MSIS*	0.107	0.704	0.329	0.031	0.046	0.066
	DTM	0.108	0.696	0.333	0.032	0.042	0.064
	JAC	0.102	0.684	0.336	0.027	0.044	0.066
Tyo	MSIS*	0.697	0.026	0.246	0.911	0.072	0.060
	DTM	0.697	0.026	0.247	0.911	0.072	0.060
	JAC	0.698	0.026	0.246	0.911	0.072	0.060

difference depending on the estimation frequency of the solar radiation pressure coefficient is quite insignificant.

C. Atmospheric density model

Finally, we compare the results for different atmospheric density models: MSIS86, DTM (Barlier et al., 1978), Jacchia71 (Jacchia, 1971). Table 5 shows the comparison of the results from these 3 models in the same way as Table 4. The table shows that the difference between the results for these 3 models is quite insignificant.

5. Conclusions

We analysed AJISAI data at all the HTLRS sites with global data. The rms of the resulted range residuals for the HTLRS data are 5-10cm, which is comparable to those of all the global stations.

The stability of the solutions for the baseline vectors between the HTLRS sites and Simosato was examined by comparing the solution with those obtained under different estimation conditions. As a result, followings are concluded;

(1) the estimated baseline vector can be determined within 1cm as far as the coordinates of both the HTLRS sites and Simosato remain as estimated parameters,

(2) it can be well determined by a single arc analysis,

(3) it can be determined within 1cm when the frequencies of estimations of the empirical acceleration and the drag coefficient are less than 3 days

(4) the estimation does not depend on the frequency of estimation of the solar radiation pressure coefficient,

(5) the estimation does not depend on the selection of the atmospheric density model if the drag coefficient is appropriately estimated.

References

Barlier, F., Berger, C., Falin, J., Kockarts, G., Thuillier, G.: Atmospheric Model Based on Satellite Drag Data, *Ann. Geophys.*, **34**, 9-24, (1978).

Boucher, C., Altamimi, Z., Duhem, L. : Results ans Analysis of the ITRF93, IERS TECHNICAL NOTE, **18**, (1994).

Eddy, W.F., McCarthy, J.J., Pavlis, D.E., Marshall, J.A., Luthke, S.B., Tsaoussi, L.S., Leung, G., Williams, D.A. : GEODYN-II System Operations Manual, Vol.1-5, *Contractor Report, ST Syst.Corp., Lanham, Md.,* (1990)

Hedin, A.E., MSIS-86 Thermospheric Model, *J.Geophys.Res.*, **92**, 4649-4662, (1987).

Jacchia, L.G., Revised Static Models of the Thermosphere and Exosphere with Empirical Temperature Profiles, *Special Report 332, smithsonian Institution Astrophysical Observatory (SAO), Cambridge, MA,* (1971).

Nerem, R.S., Lerch, F.J., Marshall, J.A., Pavlis, E.C., Putmey, B.H., Tapley, B.D., Eanes, R.J.,

Nerem, R.S., Lerch, F.J., Marshall, J.A., Pavlis, E.C., Putney, B.H., Tapley, B.D., Eanes, R.J., Ries, J.C., Schutz, B.E., Shum, C.K., Watkins, M.M., Klosko, S.M., Chan, J.C., Luthcke, S.B., Patel, G.B., Pavlis, N.K., Williamson, R.G., Rapp, R.H., Biancale, R., Nouel, F.: Gravity Model Development for TOPEX/POSEIDON: Joint Gravity Models 1 and 2, *J.Geophys.Res.*, **99**, 24421-24447, (1994).

Sengoku, A., Cheng, M.K., Schutz, B.E.: Anisotropic Reflection Effect on Satellite, Ajisai, *Jour. Geod.*, **70**, 140-145, (1995).

NEW MAPPING FUNCTION OF THE TROPOSPHERIC REFRACTION IN SLR

Haojian YAN and Chugang FENG

Shanghai Observatory, 200030 Shanghai, P.R. China

Electronic Mail: yhj@center.shao.ac.cn

Abstract. Based on the generator function method proposed by Yan & Ping (1995), the mapping function of refractive delay at optical frequencies has been introduced in this paper. The improved frequency-related mapping function, associated with the effect of wavelength on the zenith delay, has theoretically achieved an accuracy better than $0.3cm$ at $5°$ elevation for wide ground meteorological conditions and keeps convergent at an elevation angle near to horizon. Some related correction terms are also considered for high accurate laser ranging measurements at low elevation observations. The purpose of this research is mainly aimed to the low elevation objects and polychrome laser techniques in the future.

Key words: SLR - Tropospheric Refraction

1 Introduction

The accuracy of the Satellite Laser Range (SLR) has been greatly improved from decimeters to about one centimeter or better in recent decades. The correction formula of the tropospheric refraction nowadays hired in SLR has been used for more than twenty years since it was deduced by Marini and Murray (1973), meanwhile the change of the tropospheric refraction expression in Very Long Baseline Interferometry (VLBI) was made from Chao's (1970) to CfA2.2 (Davis et al. 1985) or those of Herring (1992). Recent developments of space techniques have led to a situation of that their main errors are in some extent related to the influence of atmospheric refraction. In the case of VLBI or GPS (Global Positioning System) measurement differencing, the signals received at two separated stations are differentiated. But SLR is used to precisely and directly measure the distance from a receiver point on the Earth to satellite on orbit. The laser beams suffer the effects of refraction and scattering when through atmosphere near the Earth. Atmospheric refraction increases the optical path length, which is considered as the direct results of radio wave distance measurement, by a magnitude of about two to decades meters that depends mainly on the elevation of observation. It was proved both practically and theoretically that Marini-Murray formula keeps the accuracy about centimeters at elevation above $10°$, and the accuracies become worse seriously when the elevations are down below $10°$. Developing a formula of SLR refraction correction below $10°$ might have a potential interest in future development of space techniques.

If the accuracy of millimeters is considered, some corrections, which are neglected in the nowadays used formula, may become significant especially for lower height spacecrafts at low elevation. The dispersive characteristic of optical signal of SLR is the first factor to be considered in the improved continued fraction mapping function proposed by Yan & Ping (1995).

The extra correction terms involve the influencies coming from the height and latitude of site, the height of spacecraft.

2 Atmospheric Refraction Correction

The tropospheric refractive delay $\Delta\sigma$ of the optical signal through atmosphere is defined as the difference between the optical and geometric distances from laser site P to satellite S:

$$\Delta\sigma = \int_P^S n_g d\ell - \int_P^S dx , \qquad (1)$$

where ℓ is the path of signal and x the straight line connecting site and satellite, n_g is the group refractive index of atmosphere which has relation with the group refractivity N_g (Marini & Murray 1973; Gardner & Rowlett 1976):

$$10^6(n_g - 1) = N_g = 82.4148 f(\lambda)\frac{P}{T} - 11.268\frac{e}{T} , \qquad (2)$$

in which λ is the wavelength of radiation in microns, P is the total atmospheric pressure in millibars, T is the temperature in Kelvin, e is the partial pressure of water vapor in millibars, and:

$$f(\lambda) = 0.94075 + \frac{0.01598}{\lambda^2} + \frac{0.0002224}{\lambda^4} , \qquad (3)$$

here for YAG laser with the relation

$$f(0.5320) = 1 .$$

3 Expressions of Refractive Delay

The tropospheric delay $\Delta\sigma$ is written as (Yan & Ping 1995):

$$\Delta\sigma = \Delta\sigma_z \cdot m , \qquad (4)$$

where $\Delta\sigma_z$ is the zenith delay and m is defined the mapping function. Using the perfect gas law, the law of partial pressure, and the hydrostatic equation, it is not difficult to write the zenith delay as:

$$\begin{aligned}\Delta\sigma_z &= \Delta\sigma_z^{YAG} f(\lambda) \\ &= \frac{f(\lambda)}{W(\phi, h_0)}(0.0024178P_0 + 0.00014586e_0) ,\end{aligned} \qquad (5)$$

in which P_0 is the atmospheric pressure in millibars taken at the laser site, e_0 is the water vapor partial pressure in millibars at the laser site, h_0 is the elevation of the station in kilometers, ϕ is the latitude of station. The term

$$W(\phi, h_0) = 1 - 0.00266 \cos 2\phi - 0.00028 h_0 \qquad (6)$$

is the correction of the zenith delay related to the latitude and height of the station (Saastamoinen 1972).

The water vapor partial pressure e_0 can be calculated from the relative humidity R_h (in percent) by Magnus experimental formula

$$e = \frac{R_h}{100}(6.11)10^{\frac{7.5(T-273.15)}{237.3+(T-273.15)}} \ . \tag{7}$$

In research of refraction correction, the mapping function has gotten more attention than the zenith delay. The expression of the mapping function nowadays adopted in laser ranging techniques was based on expansion of integrand in atmospheric refraction integral (Marini & Murray 1973). It was proved that the formula obtained by expansion method of integrand could not be available for observation elevation lower than $10°$ even if troublesome correction terms were included. The quadratic atmospheric profile hired in Marini & Murray formula could introduce some error in the mapping function. From the generator function theory of atmospheric refraction integration, a new continued fraction form of the mapping function was proposed, which was deduced from the expansion of the complementary error function (Yan & Ping 1995). This form of the mapping function can get higher accuracy and wider elevation coverage than those previous used. We take the atmospheric pressure, temperature and humidity as the required meteorological parameters in our presentation. Some other geophysical and meteorological parameters are usually not available in normal SLR observation data and so as to be taken constants: the tropospheric temperature lapse rate $\beta = -6.°5K\ km^{-1}$, the height of the tropopause $h_t = 11.132km$. Another important fact in laser techniques is the dispersion of air at optical frequencies, a frequency-relative mapping function is therefore appropriate for SLR technique.

The new mapping function is then generally written as:

$$m(E_0) = \cfrac{1}{\sin E_0 + \cfrac{D_1}{I^2 \csc E_0 + \cfrac{D_2}{\sin E_0 + \cfrac{D_3}{I^2 \csc E_0 + D_4}}}} \ , \tag{8}$$

in which

$$E_0 = 90° - \xi_0$$

is defined the *proper elevation* of observation which is coincident with the true elevation for an object at infinity, r_0 is the radius of the Earth, and the effective height of atmosphere H can be written as a vertical integral of the refractivity N:

$$H = \frac{1}{N_{g0}} \int_{h_0}^{\infty} N_g(h)\ dh \ , \tag{9}$$

where N_{g0} is the value of the refractive obtained on the ground, and the parameter

$$I = \sqrt{\frac{r_0}{2H}} \tan E_0 \tag{10}$$

is named the *normalized effective zenith argument*.

If the standard atmosphere model (Davis et al. 1985) is used, which is proved nearer to the true atmosphere (Allen 1973) than the quadratic profile used by Marini & Murray (1973), the coefficients D_i in Eq.(8) are listed:

$$D_1 = 0.463184 + 3.019 \times 10^{-5}(P_o - 1013.25)$$
$$-1.222 \times 10^{-4}(T_o' - 15) + 1.1 \times 10^{-6}(T_o' - 15)^2$$
$$-9.122 \times 10^{-3}(\lambda - 0.532) + 2.74 \times 10^{-2}(\lambda - 0.532)^2$$

$$D_2 = 0.828752 + 1.905 \times 10^{-5}(P_o - 1013.25)$$
$$+5.203 \times 10^{-4}(T_o' - 15) + 0.6 \times 10^{-6}(T_o' - 15)^2$$
$$-5.887 \times 10^{-3}(\lambda - 0.532) + 1.82 \times 10^{-2}(\lambda - 0.532)^2$$

$$D_3 = 2.53662 + 0.9095 \times 10^{-4}(P_o - 1013.25)$$
$$+3.869 \times 10^{-3}(T_o' - 15) + 0.3 \times 10^{-6}(T_o' - 15)^2$$
$$-2.787 \times 10^{-2}(\lambda - 0.532) + 8.76 \times 10^{-2}(\lambda - 0.532)^2$$

$$D_4 = 47.1584 + 1.377 \times 10^{-3}(P_o - 1013.25)$$
$$-3.584 \times 10^{-2}(T_o' - 15) + 1.1 \times 10^{-4}(T_o' - 15)^2$$
$$-4.291 \times 10^{-1}(\lambda - 0.532) + 1.34 \times (\lambda - 0.532)^2 ,$$

$$(11)$$

in which P_o in millibars, e_o in millibars, and T_o in Celsius are the corresponding values on ground, λ the wavelength in micron. Because the permanent dipole term of the refractivity is no longer significant in optical wavelength, the influences of the wet partial on the coefficients D_i of the mapping function have been greatly weakened and we can ignore their influences in above expression only introducing a negligible error to our results.

In comparison with the integrals along the path of signals the theoretical accuracy of the new model is proved better than $0.1cm$ above 10° elevation and $0.3cm$ above 5° elevation for wide meteorological conditions.

4 Correction of Finite Distance Object

In Fig.1, $\vec{SP}$ is the direction pointed from satellite S to observer P, $\vec{SQ}$ is the direction along the tangent to the light trajectory of the path of signal between S and P, and Q is the intersection point with the vertical Z-axis, which is named the *equivalent point* of observation. We call $\vec{QS}$ the *proper direction*, and $\vec{PS}$ the *true direction* which can accurately calculated from satellite ephemeris and the geophysical parameters. We can further define ξ_0 the *proper zenith distance*, and $\angle ZPS$ the *true zenith distance*, respectively. From above sections, it is found that the angular argument in the mapping function is physically the proper zenith distance. Only for the observation of an infinite object, the proper direction coincides with the true direction. If the heights of the satellites with laser reflectors cover from several hundreds to thousand kilometers, it might be reasonable to consider a distance correction for lower height satellites (Marini 1972), which comes from the difference between the true and the proper zenith distances.

For a spherically symmetrical atmospheric model Snell's law holds (Woolard and Clemence 1966):

$$n \cdot r \cdot \sin z = n_0 \cdot r_0 \cdot \sin z_0 = r_s \sin z_s , \qquad (12)$$

where r is the geocentric distance, z the arrival zenith taken on the path of light, r_0 and z_0 are the corresponding values taken at station, r_s and z_s the values at the field point taken on the orbit of satellite, and here it is assumed that

$$n(r_s) = 1 .$$

From Eq.(12), see Fig.1, the *equivalent height QP* (Murray 1973) or the *vertical proper displacement of the atmospheric refraction* (simply called the *proper displacement*) for the observer at P is obtained (Yan et al. 1992); (Yan, 1996):

$$QP = \left(\frac{n_0 \sin z_0}{\sin \xi_0} - 1\right) r_0 . \tag{13}$$

The angle between the proper direction and the true direction $\Delta\theta$ is readily represented by:

$$\Delta\theta = \frac{QP \sin \xi_0}{x} = \frac{r_0}{x}(n_0 \sin z_0 - \sin z_0 - \cos z_0 \, \Delta z_0) . \tag{14}$$

In above equation, the astronomical refraction for a finite distance object Δz_0 is further related to the proper zenith distance ξ_0 and the mapping function of the astronomical refraction m^* (Yan & Ping 1995):

$$\Delta z_0 = 10^{-6} N_{g0} \sin \xi_0 m^*(\xi_0) , \tag{15}$$

where m^* can also be formulated by an improved continued fraction form:

$$m^*(\xi_0) = \cfrac{1}{\cos \xi_0 + \cfrac{0.578710}{I^2 \sec \xi_0 + \cfrac{1.30248}{\cos \xi_0 + \cfrac{13.2497}{I^2 \sec \xi_0 + 173.423}}}} . \tag{16}$$

In order to get an accurate proper zenith distance ξ_0, an iteration algorithm can be used. Then the proper zenith distance is readily obtained by Fig.1

$$\xi_0 = (90^o - E) + \Delta\theta , \tag{17}$$

here the true elevation E of object can be accurately calculated from the ephemeris and the geophysical parameters.

5   Discussion

The numerical comparisons between the tropospheric delays of the model presented in this paper and that of (Marini & Murray 1973) have been made. Fig.2 gives the differences between these two model for different meteorological conditions.

After summerizing above sections we have following conclusions:
a. The atmospheric profile of SLR refraction correction used in our model has been renewed from the quadratic refractivity (Marini & Murray 1973; Gardner & Rowlett 1976) to the standard model (Allen 1973; Davis et al. 1985).
b. The generator function method of atmospheric refractive integral (Yan and Ping 1995) and the improved continued fraction form of the mapping function is applied to facility at optical

frequency in this paper. In such a way we offer a possibility to calculate the refraction correction of SLR observations with high accuracy at elevations of few degrees. The new mapping function has an unit when the observation is made in the zenith direction. The simulative computation results show the fact that Marini-Murray's formulas have several millimeters discrepancies above $10°$ elevation and becomes worse very rapidly when the elevation is keeping decreasing.

c. The angle argument in our mapping function is related to the proper elevation of observation for a finite distance object. The object distance correction of the mapping function is represented as the difference between the proper and the true elevations of object. This term might be considerable for satellites with height of several hundreds kilometers or less and to be observed at lower elevation angles. Fig.3 shows the range corrections of the objects with the heights of $960km$, $425km$ and $5900km$, respectively.

d. At optical frequencies, the operation frequency is most important factor in the parameters of the mapping function. Fig.4 represents the influences of laser beam frequency on the mapping function. This term will be of interest in multi-frequencies observation consideration of laser ranging.

References

Allen, C.W. 1973: *Astrophysical Quantities*, 3d ed., The Athlone Press, Chap.6, 114-120.

Chao, C.C., 1970: A preliminary estimation of tropospheric influence on the range and range rate data during the closest approach of the MM71 Mars Mission. *JPL Tech. Memo 391-129.*

Davis, J.L., T.A. Herring, I.I. Shapiro, A.E.E. Rogers and G. Elgered, 1985: Geodesy by radio interferometry: effects of atmospheric modeling errors on estimates of baseline length. *Radio Science,* 20, 1593-1607.

Gardner, C.S. and J.R. Rowlett, 1976: Atmospheric refraction errors in laser ranging system. *RRL Pub. No.477,* University Illinois, Urbana, Illinois.

Herring, T.A.; 1992. Modeling Atmospheric Delay in the Analysis of Space Geodetic Data, in "Refraction of Transatmospheric Signals in Geodesy", Proc. of the Symp. Hague, May 19-22, Netherlands Geodetic Commission Publications on Geodesy, New Series No36.

Marini, J.W., 1972: Correction of satellite tracking data for an arbitrary tropospheric profile. *Radio Science,* 7, 223-231.

Marini, J.W. and C.W. Murray, 1973: Correction of laser range tracking data for atmospheric refraction at elevation above 10 degrees. *NASA Tech. Rep. X-591-73-351.*

Murray, C.A., 1983: *Vectorial Astrometry,* Adam Hilger Ltd, Chap.7.

Owens, J.C., 1967: Optical refractive index of air: dependence on pressure, temperature and composition. *Appl. Opt.,* 6, 51-58.

Saastamoinen, J., 1972a, 1972b, 1973: contributions to the theory of atmospheric refraction. *Bull. Geod.,* V105-107, 279-298, 383-397, 13-34.

Woolard, E.W. and G.M. Clemence, 1966: *Spherical Astronomy,* Academic Press, Landon and New York, Chap.5.

Yan, H.J., K. Sauermann and E. Groten, 1992: The ray bending corrections in tropospheric refraction. in "6th International Geodetic Symposium on Satellite Positioning", March 17-20, 1992, The Ohio State University, Columbus, Vol.1, 291-301.

Yan, H.J. and J.S. Ping, 1995: The generator function method of the tropospheric refraction corrections. *A.J.* 110, 934-939.

Yan, H.J., 1996; A new expression for astronomical refraction, A.J.112, 1312-1316.

Fig.1 Geometry of a finite distance object

full line: P=1013.25mbar, T=15C

dashed line: P=1023mbar, T=0C

dotted line: P=1003mbar, T=28C

Fig.2 Comparison between new and Marini-Murray models

dashed line: height of object=425km
dotted line: height of object=5900km
full line: height of object=960km
P=1013.25mbar, T=15C
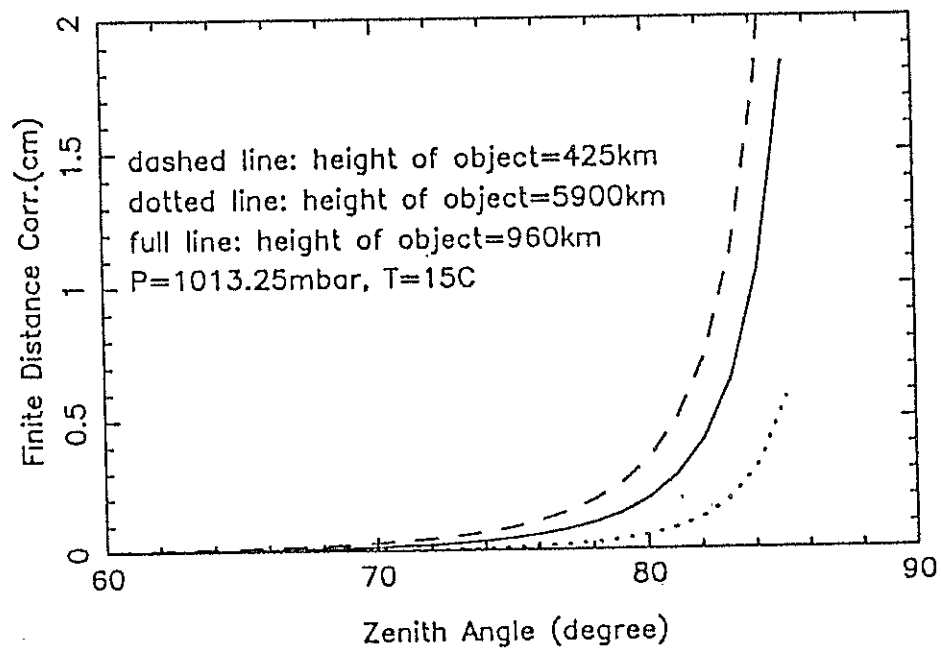
Fig.3 Corrections of finite distance objects

dashed line: Wave Length=0.355
full line: Wave Length=0.6943
P=1013.25mbar, T=15C
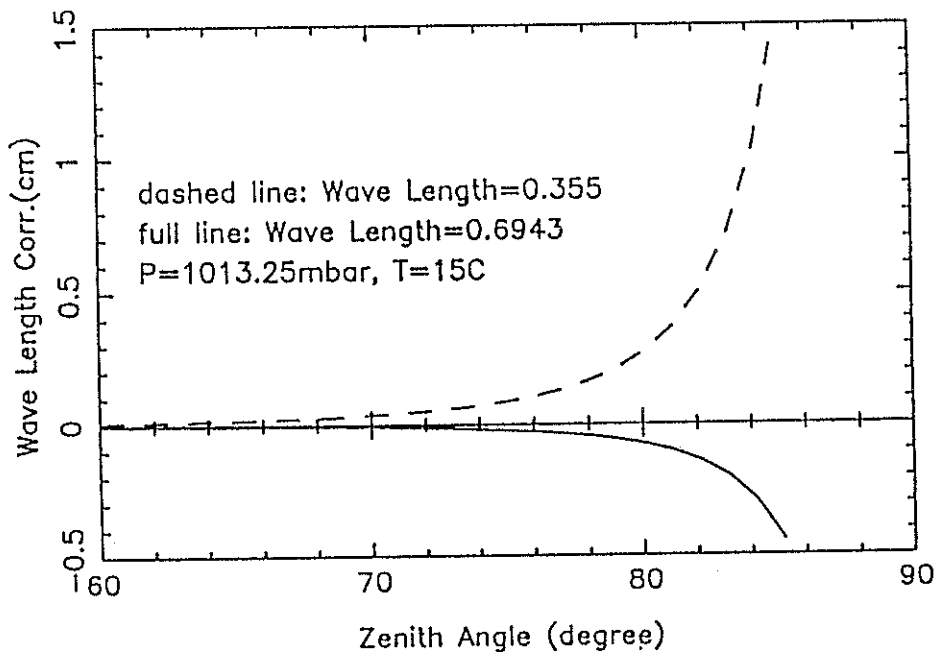
Fig.4 Frequency corrections in mapping function

The Question of SLR Measuring Error Distribution

Wu jie

National University of Defense Technology, China

wj@at.nudt.edu.cn

Li Zhengxin, Zhang Zhongping, Yang Fumin, Tan Detong

Shanghai Observatory, Academia Sinica

Abstract

The actual distribution of SLR measuring error is discussed in this paper. Through the analysis of 22 pass SLR data of Shanghai Observatory, it appeals that the standard model of error distribution (Normal distribution) is not always suitable for SLR measuring error. Instead of the conventional normal distribution, p-norm distribution is put in use, and adaptive least p-norm (ALp) estimation is put forward for SLR data preprocessing. The preliminary result shows that the ALp estimation is more reliable and efficient than the classical least square estimation.

1. Introduction

Each observation unavoidably include error in it. Measuring error obey Normal distribution, this is the simple hypothesis which we generally make in practice. But the hypothesis is not always suitable. In the case of SLR, because of highly automatic data collection and unavoidable external effect, there will be amount of gross errors (noise) in measuring data. It is then unsuitable to use only Normal distribution to describe SLR measuring errors. If the gross errors be deleted, will the measuring errors of remained observations obey Normal distribution ? No, they will not. Neubert, etc. (1995) indicate that: the distribution of SLR measuring error is related to laser pulse width, response function of satellite reflectors, and detector, the distribution density function is very complicated. The purpose of Neubert's research is to find out a 'reference point', and to calculate the center of mass correction. But the problem of how to get reliable estimation of real measuring error from practical measuring data (especially the data including amount of gross errors), is not researched. It is suggested in this paper that: to describe SLR measuring error with p-norm distribution family, and to estimate parameters in data preprocessing with ALp method. Preliminary result indicate that p-norm distribution family is suitable for SLR measuring error, ALp estimation of parameters are more precise and reliable than least square estimation.

2. P-norm distribution and SLR error statistics

2.1 P-norm distribution

The density function of p-norm distribution is (Sun Haiyan 1993)

$$f(x) = \frac{1}{\sqrt{2}\Gamma(1/p)b} \cdot \exp\{-(\frac{\sqrt{2}}{p}\frac{|x|}{b})^p\} \quad .....(1)$$

where x is the value of random variable, $\Gamma()$ means gama function, p,b are parameters of the distribution. P-norm distribution family (with different p) include Laplace distribution (p=1), Normal distribution (p=2), uniform distribution (p=∞) and so on.

2.2 SLR error statistics

Let's research the distribution of SLR measuring error with the example of a SLR data pass of Shanghai Observatory. regarding the difference between laser ranging and calculated distance as a new observation, and then conducting polynomial imitation (with iteration of gross error rejecting), the imitation parameters and residuals of all observations are obtained at last. These residuals are regarded as the real value of SLR measuring errors, and to be researched. Figure 2 gives out the histograms, p-norm distribution density curves, and Normal distribution curves of the residuals at different steps of gross error rejecting.

Summary
(1) SLR measuring errors as a whole obey Laplace distribution (p=1), not Normal distribution.
(2) After each step of gross error rejecting, p-norm distribution (with different p) is always suitable to describe SLR measuring errors (p-norm curves approach histograms), but Normal distribution is suitable only in special case (fig.2 (22-5,6)).
(3) The p of p-norm distribution will continually increase if so called 'gross errors' are continually rejected. the p will tend to be infinite when 'gross errors' are over rejected. In this case, the remained residuals obviously will not represent the normal SLR measuring error. We suggest that:
Stop gross error rejection if p just greater than 1, and then regard the remained residuals as 'normal' SLR measuring errors.

Table 1 gives out p-norm distribution parameter values of 'normal' SLR measuring errors of 22 pass at shanghai Observatory.
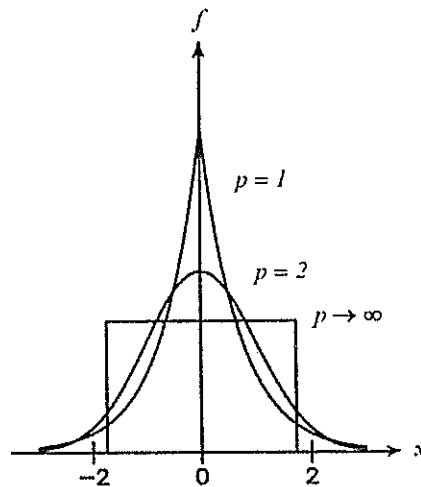
Fig.1 p-norm distribution density function

	Tab.1 'normal' SLR measuring errors statistics				Tab.2 Statistics of the remained residuals (3.0 σ rejection)						

Tab.1 'normal' SLR measuring errors statistics

No.	n/n_0	p	σ(m)©
1	0.20	1.4	0.09
2	0.32	1.3	0.05
3	0.44	1.2	0.05
4	0.43	1.3	0.04
5	0.42	1.4	0.06
6	0.49	1.2	0.07
7	0.51	1.3	0.05
8	0.45	1.7	0.06
9	0.55	1.6	0.05
10	0.48	1.0	0.07
11	0.24	1.3	0.06
12	0.33	1.4	0.06
13	0.49	1.7	0.03
14	0.83	1.8	0.04
15	0.71	1.5	0.04
16	0.53	2.1	0.04
17	0.51	1.6	0.04
18	0.83	1.8	0.05
19	0.74	1.3	0.06
20	0.83	1.9	0.05
21	0.73	1.5	0.05
22	0.57	2.0	0.04

annotations: p means the parameter of p-norm distribution, σ indicates precision, n/n_0 means the ratio of remained residuals number to total.

Tab.2 Statistics of the remained residuals (3.0 σ rejection)

No.	ALp method				LS method		
	n/n_0	p	σ(m)	IT	n/n_0	σ(m)	IT
1	0.20	1.6	0.079	8	0.99	99.530	1
2	0.32	1.3	0.056	3	0.31	0.049	12
3	0.43	1.1	0.044	3	0.44	0.047	6
4	0.45	1.3	0.041	3	0.45	0.040	6
5	0.43	1.8	0.066	3	0.43	0.069	6
6	0.46	1.4	0.056	3	0.47	0.059	9
7	0.52	1.2	0.054	3	0.53	0.059	8
8	0.46	1.2	0.060	3	0.79	0.782	2
9	0.55	1.4	0.049	2	0.78	0.492	3
10	0.47	1.2	0.069	4	0.68	0.501	7
11	0.24	1.3	0.058	6	0.45	0.900	12
12	0.34	1.2	0.064	3	0.57	0.746	7
13	0.49	1.4	0.035	2	0.49	0.036	11
14	0.83	1.7	0.045	1	0.83	0.043	3
15	0.72	1.1	0.050	1	0.71	0.043	3
16	0.53	2.0	0.037	2	0.54	0.040	4
17	0.52	1.9	0.038	3	0.44	0.046	10
18	0.83	1.8	0.048	1	0.82	0.046	3
19	0.71	1.9	0.048	2	0.73	0.055	7
20	0.84	1.5	0.050	1	0.83	0.046	4
21	0.73	1.6	0.045	1	0.73	0.048	3
22	0.57	1.9	0.039	2	0.58	0.045	3

annotations: n/n_0 means the ratio of remained observation number to the total, p means adaptive p (distribution parameter), σ the precision of residuals, IT means iteration number of gross error rejection.

3. ALp estimation and SLR data preprocessing

Adaptive least p-norm (ALp) estimation is the most probable estimation of parameters when measuring error obey p-norm distribution with p unknown (Wu Jie 1995,1996).

3.1 ALp estimation principle
ALp estimation of parameters X are the solution of equations as below

$$\begin{cases} \begin{cases} \Sigma |v_i|^p = \min \\ V = AX - l \end{cases} \\ \Phi = \ln f(v_i, p, b) = \max \end{cases} \quad \ldots\ldots (2)$$

where { means a body of iteration, V a vector of observation residuals, v_i the i'th element of V, A a constant matrix, X the unknown parameter vector to be estimated, f( ), p, b as in equation

(1), p also to be called as adaptive p. Wu Jie (1996) put forward a method to find the solution of equation (2) in detail. ALp estimation has the main properties (Wu Jie 1995,1996):

(1) Robustness. When there are amount of gross errors in the data, adaptive p will tend to be 1, ALp estimation becomes L1 estimation(least the sum of absolute residuals). L1 estimation is robust (Huber 1981). so be ALp estimation.

(2) Most probability (asymptotic efficiency). ALp estimation is derived with the condition under which probability function be maximal. So that ALp estimation is the most probable estimation, and asymptotic efficient too.

3.2 Preprocessing of SLR data

Since SLR measuring error obey p-norm distribution with p unknown, then ALp method should be used so as to obtain the most efficient parameter estimation. Observations of the 22 pass in table 1 are preprocessed again with ALp and LS (least square) method , and without screen edition. In the preprocessing, gross errors be treated with 3.0σ rejection (σ means the precision of remained residuals), and the rejection stop when adaptive $p>1$ in ALp, or every residuals beneath the 3.0σ boundary in LS. Observation equation is as below

$$r_i = a_0 + a_1\dot{\rho}_i + a_2 t_i +......+a_N t_i^{N-1} \quad ......(3)$$

where r_i (the difference between laser ranging and calculated distance) means the new observation at epoch time t_i, $\dot{\rho}_i$ means the velocity at radial direction, t_i the observing epoch time, $a_0,......,a_N$ means imitation parameters to be estimated. In this equation, a_0,a_1 are estimated at the same time with $a_2,......,a_N$ together, the purpose is to reduce the model error of observation equation. If $\dot{\rho}_i$ item and t_i item are strongly related, the equation should be adapted as below

$$r_i = a_0 + a_1 t_i +......+a_N t_i^{N} \quad ......(4)$$

The preprocessing results are displayed in table 2 and figure 3.

Summary:

(1) ALp estimation of imitate parameters is reliable, LS estimation is not (fig.3(1b) ,LS imitate curve be out of the plot boundary). ALp estimation is theoretically robust, LS unrobust , so that there must be the result.

(2) If screen edition be made (initially delete gross errors),LS estimation will generally be correct, but still different from ALp estimation. Such as showed in figure 3 (3b), LS curve and ALp curve (V=0, unplotted) have difference of 1-2 centimeters, while ALp curve is more reliable at first look.

(3) When parameter estimation are correct, the iteration number of gross error rejecting (IT) in ALp method is much less than LS method (2nd, 3rd,.. in table 2, and (2a),(3a) in figure 3). This result is also because of the robustness of ALp estimation.
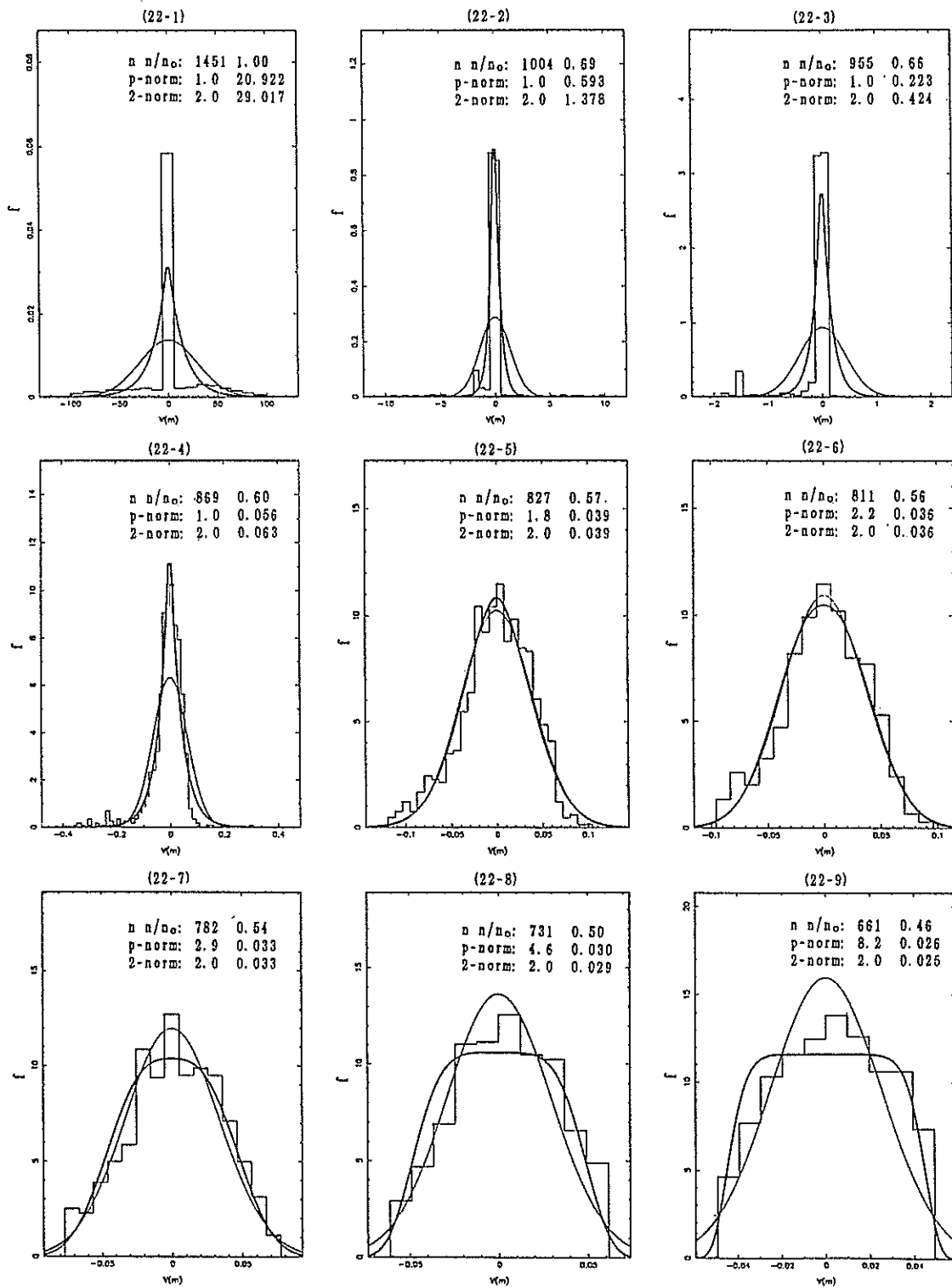
Fig.2 residual statistics of a SLR data pass

annotations:

[1] n means the number of remained residuals, n_0 the total, p-norm: p σ, p means p-norm
distribution parameter, σ means precision.

[2] stress line means p-norm distribution density curve, light line the Normal, ladder-shaped
line the histogram.
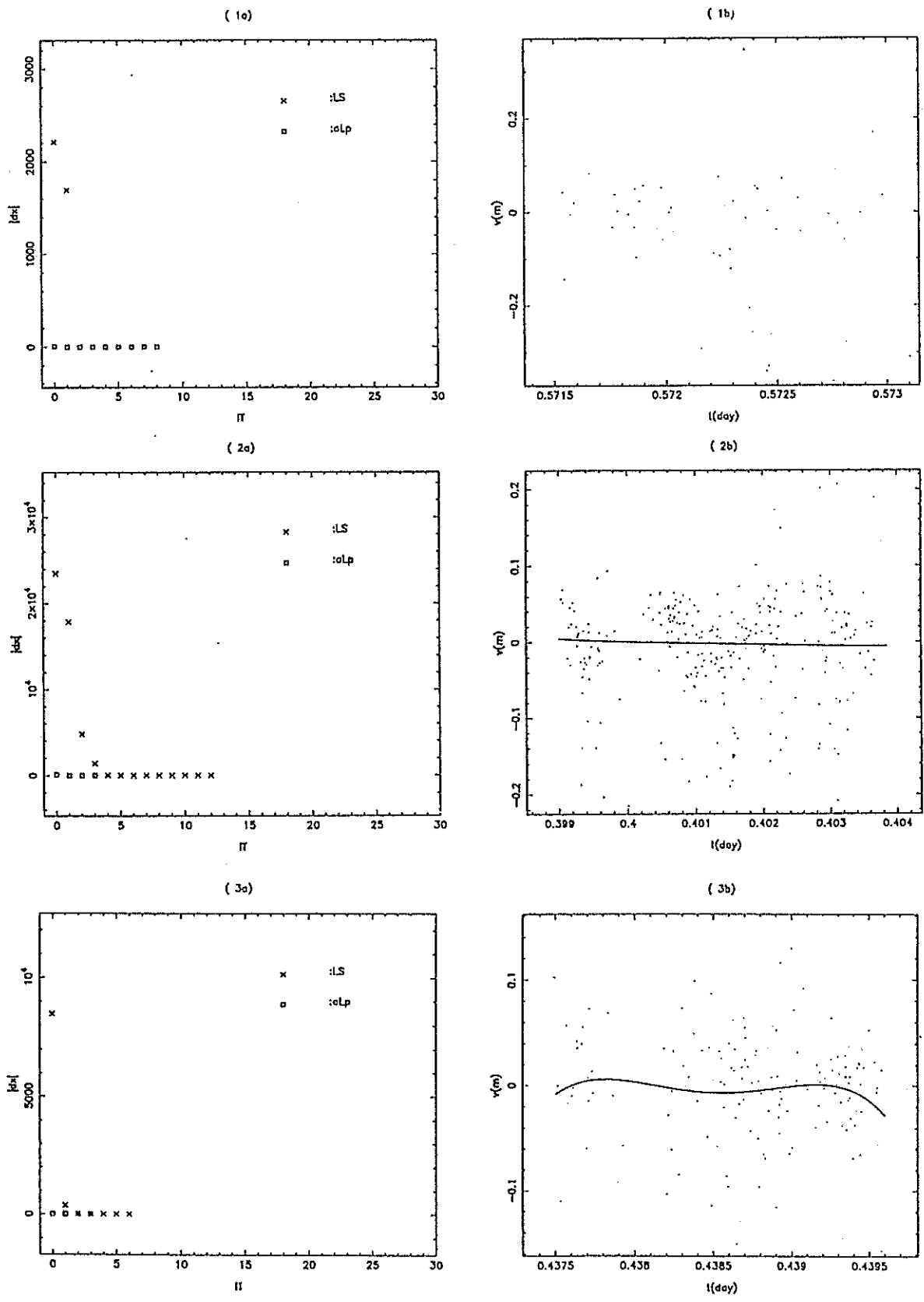
Fig.3 SLR preprocessing result (3.0 rejection)

annotations:

(1) (ia),(ib) means the result of i'th pass, i=1,2,3.

(2) in plot (ia), IT means the iteration number of gross error rejection, $|dx|$ means the modulus of parameter error vector (ALp estimation as the real).

(3) in plot (ib), t means the observing time, V means the residuals in ALp method, dot '.' stand for observation. ALp imitation curve is just horizontal axis (v=0, unplotted), LS imitation curve be plotted.

4. Conclusions

(1) SLR measuring error in whole obey Laplace distribution(including amount of gross errors).
(2) When gross errors are not deleted completely (such as in screening), the remained SLR measuring errors obey p-norm distribution with different p values. If so called 'gross errors' be over deleted, the adaptive p will tend to be ∞. We suggest that:
Stop gross error rejecting just when adaptive p>1, and regard each remained observation as a normal one.
(3) In SLR preprocessing, ALp method is more efficient and reliable than LS method.
(4) Most of normal observations are remained in ALp method. The ' normal point' data derived from imitation parameters correspond to the mean of normal SLR measuring errors, and then the 'center of mass' correction will be constant, for example 242.7 mm for Lageos (summary 1995). The 'normal point' data in LS method with tight gross error rejection (2.0σ or 1.0σ) will correspond to the distribution peak of normal SLR measuring errors (summary 1995). This method perhaps has defects as below:
  (a) Observations be over deleted, useful information is not utilized completely.
  (b) The center of mass correction is not constant, for example 7 mm variation for Lageos.

5. Subject for research

The p-norm distribution should be asymmetriclized, so as to fit in with SLR measuring error in practice more favorably, and then to get estimation of imitation parameters more efficiently and reliably.

References
[1] Huber, P.J., Robust Statistics, John Willey&Sons, 1981.
[2] Neubert, R., Satellite signature model: Application to Lageos and Topex, Proceedings of Annual Eurolas Meeting, Munich, March 1995.
[3] Sinclair, A.T., Data screening and peak location, same as [2].
[4] Summary of technical session on 'Satellite signatures and Centre-of Mass Corrections', same as [2].
[5] Sun Haiyan, Unified model of error distribution, Journal of Wuhan Surveying Technology university, China, Vol.18, No.3, p.49-56, 1993.
[6] Wu Jie, Li Zhengxin, etc., Adaptive Lp estimation and its applying in photographic astrometry, ACTA ASTRONOMIC SINICA, Vol.37, No.2, p.132-139, 1996.
[7] Wu Jie, Adaptive Least p-norm estimation and its application in astronomy and geodesy, doctor thesis of Shanghai Observatory of Academia Sinica, 1996.
[8] Yang Fumin, etc., Space geodesy, press of Chinese geological University, 1990.

Full-rate vs. Normal points:
two ways of managing SLR data

R.Devoti, M.Fermi, V.Luceri, P.Rutigliano and C.Sciarretta
nuovo **telespazio** s.p.o. CGS-Matera, Roma

G.Bianco
Centro di Geodesia Spaziale, Matera

Introduction

The huge quantity of SLR data became, at the beginning of the eighties, an urgent problem to avoid highly expensive analyses. The use of compression procedures that aggregate the data avoiding redundancy without losing information was willingly accepted by the scientific community; almost all analyses were performed, since then on, using the so-called normal points instead of full-rate data.

The decision, taken in December 1996 at the CSTG/Eurolas meeting in Berne, to cease also the archiving of the SLR full-rate data for all satellites raised the necessity to test once again the assumption that the normal points, or better the field generated normal points (FGNP), are completely equivalent to the full-rate data in terms of achievable results and information content.

For the result comparison, a set of tests has been addressed to check if the normal points can reproduce a satellite orbit obtained using the full-rate data. The attention has been focused on the orbit of the satellites because its precise determination permits to establish an accurate reference frame for the estimation of geodetic parameters. This kind of tests, already performed in the past on Lageos normal points, have been extended to other satellites with different orbital and physical characteristics.

The check on the respective information content has been directed toward the statistical analysis of the pass residuals going into the details of their distribution.

Orbit comparison

These tests consist in the comparison of the satellite orbits determined processing full-rate and normal points separately, with the same force model and arc structure, for all 1993; for all the arcs the set of station position has been kept fixed.

Among the geodetic satellites of the available constellation, we have chosen three satellites at different altitudes and with different sizes: Starlette, Ajisai and Lageos. Their physical characteristics, some information on their orbit and the analysis setup are shown in fig.1.

For each of them, the comparison of the orbits is performed by comparing the state vectors, estimated using GeodynII, at the beginning of each arc looking at the semi-major axis and at the relative satellite positions in the radial, cross-track and along-track directions.

In the first set of tests, the orbit determination is done weighting the data at 1, both for full-rate and normal points, as we were used to do for Lageos. The results of the comparison of the satellite positions in the radial and cross-track directions show that there is no significant difference in the estimates using the two types of data and this is valid for all the three satellites; in the case of the semi-major axis and the along-track component of the difference vectors, the results differ from satellite to satellite.

Satellite info	Analysis setup
LAGEOS - I Diameter 0.6 m Mean height 5900 Km Orbit inclination 109.84° CCR 426	**15 days arc** No estimation of global parameters Estimated arc parameters : - ephemerides at the begin of each arc - solar reflectivity coefficient - constant along track acceleration - once-per-rev acceleration
AJISAI Diameter 2.15 m Mean height 1500 Km Orbit inclination 50° CCR 1436 Mirrors 318	**10 days arc** No estimation of global parameters Estimated arc parameters : - ephemerides at the begin of each arc - solar reflectivity coefficient - daily CD coefficient - once-per-rev acceleration
STARLETTE Diameter 0.36 m Mean height 960 Km Orbit inclination 49.83° CCR 60	**5 days arc** No estimation of global parameters Estimated arc parameters : - ephemerides at the begin of each arc - solar reflectivity coefficient - daily CD coefficient - once-per-rev acceleration

Fig. 1

For Lageos, the weighted mean of the differences is very low and always within the associated sigma (0.1±0.0 mm for s.m.a., 1.8±1.4 cm for the along-track); for Starlette, nothing significant for the semi-major axis but a 6 cm weighted mean for the along-track component (fig.3: bullets); for Ajisai, the differences in the semi-major axis (fig.2: bullets) point out a bias of about 5 mm, the NP estimates longer than the FR one, and those in the along-track component (fig.3: bullets) a large bias of 20 cm.

Further analysis has been performed to understand the meaning of the results and the way to manage the data to avoid discrepancies.

One possible explanation has been found in the use of the same unitary weight for the normal points that alters the network balance defined by the full-rate data; substituting the FR with the NP with equal weights, we change the contribution of each station to the solution and also the influence of the range biases often present in their data. The situation is critical for Ajisai because many stations have higher biases in the data acquired from this satellite.
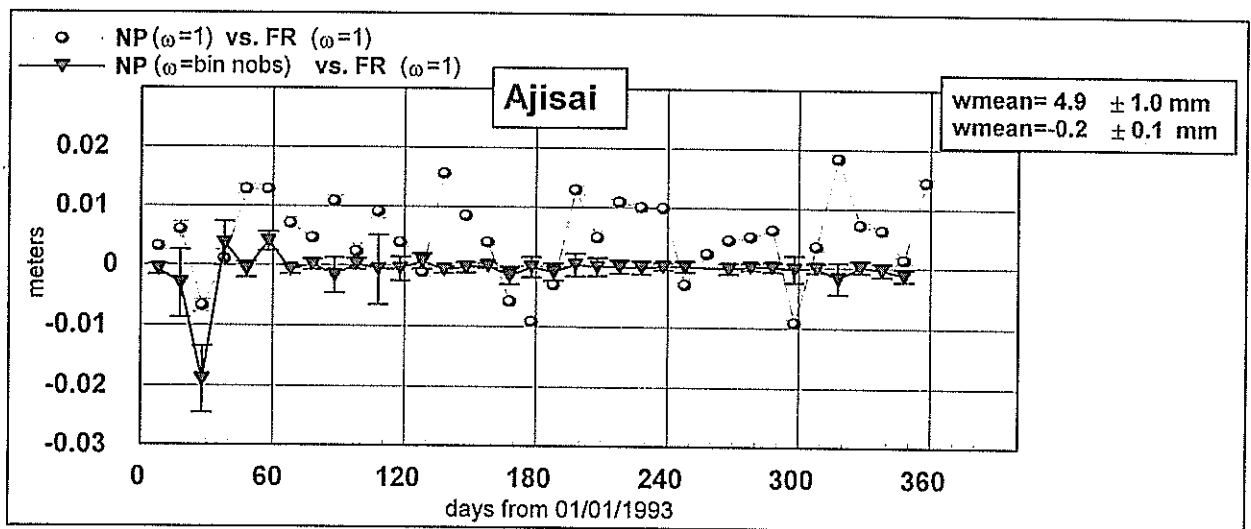
Fig. 2 - Comparison of semi-major axis
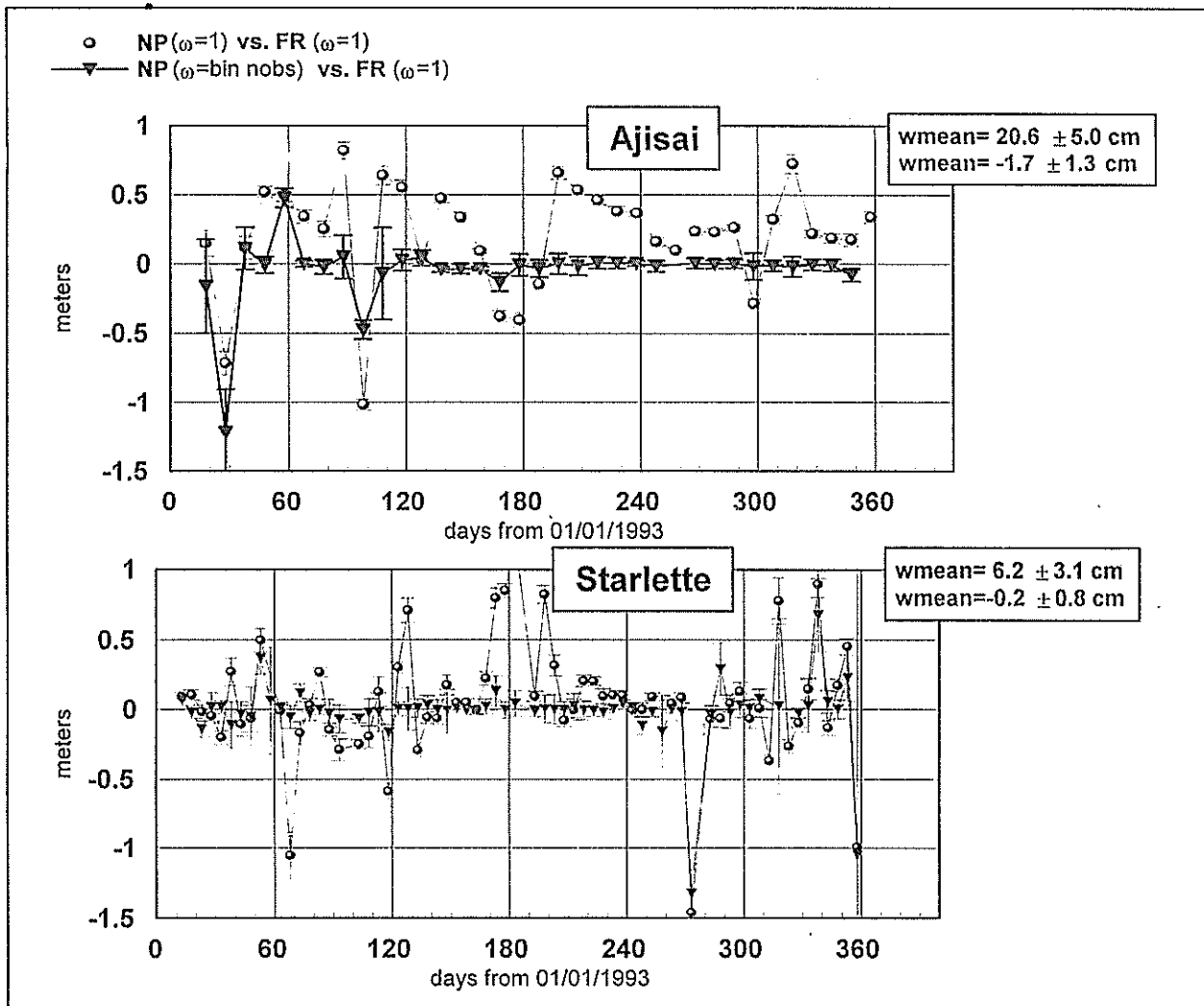
Fig.3 - Comparison of along-track components

For this reason, in the second set of tests, the NP have been weighted at n, where n is the number of observations in each bin, to reproduce the real situation and the results (fig.2, fig.3: triangles) clearly show that the biases disappear. More or less similar results are obtained when weighting the data at *1/bin variance* or, better, *n/bin variance* which is the best weight to give each normal point information on the number of the observations in a bin and on the dispersion of the bin residuals.

Future tests will check if the estimation of the station biases, during the orbit determination process, can overcome the problem.

Residual analysis

During the orbit determination process, the range residuals were computed and the analysis we are going to describe is based on the investigation of the distribution of these measurements residuals.

The procedure of normal points construction assumes that the range residuals have a gaussian distribution and this is true for most passes of Lageos; we have seen that this is not valid for Ajisai and Starlette.
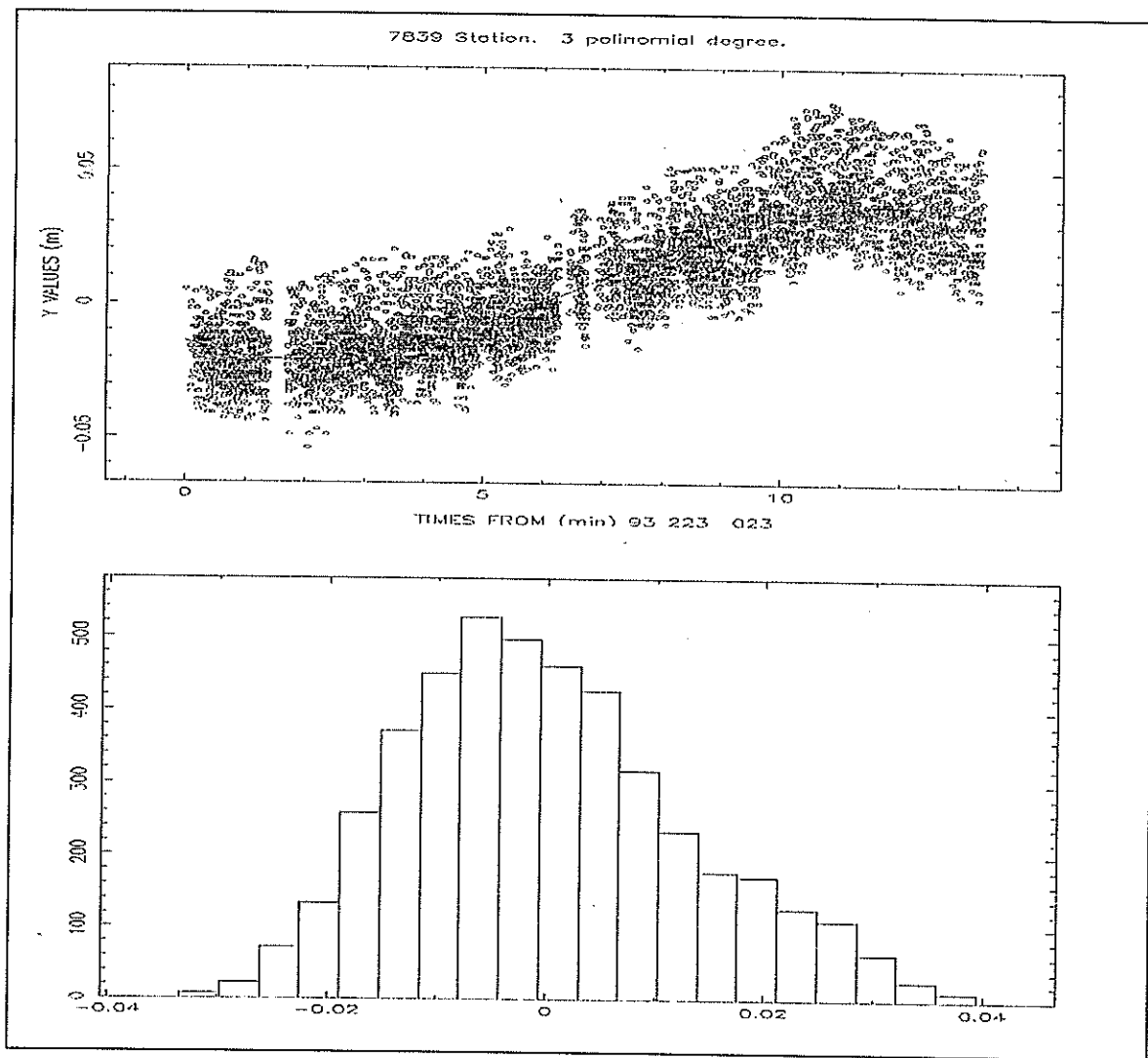
Fig.4

A typical Ajisai pass is shown in fig.4; the top of the figure is the plot of the orbit residuals with their fitting polynomial, the bottom is the histogram of the fit residuals. In the residual plot, the cloud of points along the pass, above the denser cluster below, indicates that the range of a large number of observations is longer than the real one. This situation is clearly pointed out in the residuals distributions. As you can see, it shows a strong tail (positive skewness: skewness is zero in a gaussian distribution) and the consequence is that the residuals is moved away from the peak of the distribution toward the tail itself.

The figure refers to an entire pass but we have checked that the bins of a skewed pass, when the number of observations is sufficiently high to permit this check, have a similar distribution. Since each normal point is computed using the mean of the residuals not the peak, in case of skewed passes we compute biased normal points and the bias is not recoverable without the full-rate data.

The value of the skewness depends on the satellite and station characteristics; the single-photon stations have a very high number of skewed passes, above all for Ajisai, probably due also to a target depth signature in the collected data.

Fig. 5 shows a pass analysis for Graz. For each pass we have computed the values of skewness and kurtosis, normalizing them with their sigmas, and performed the gaussianity test. The value of the normalized skewness and kurtosis is significative when it is higher than 3 (real value greater than 3σ) and we have found a value of about 10 in the case of Graz. The gaussianity test, which includes tests on the kurtosis, reveals that the percentage of non-gaussian passes is almost 90%. For some stations the situation is much better, for others worse.

In any case useful information coming out from the analysis of the data distribution is lost within the normal points.
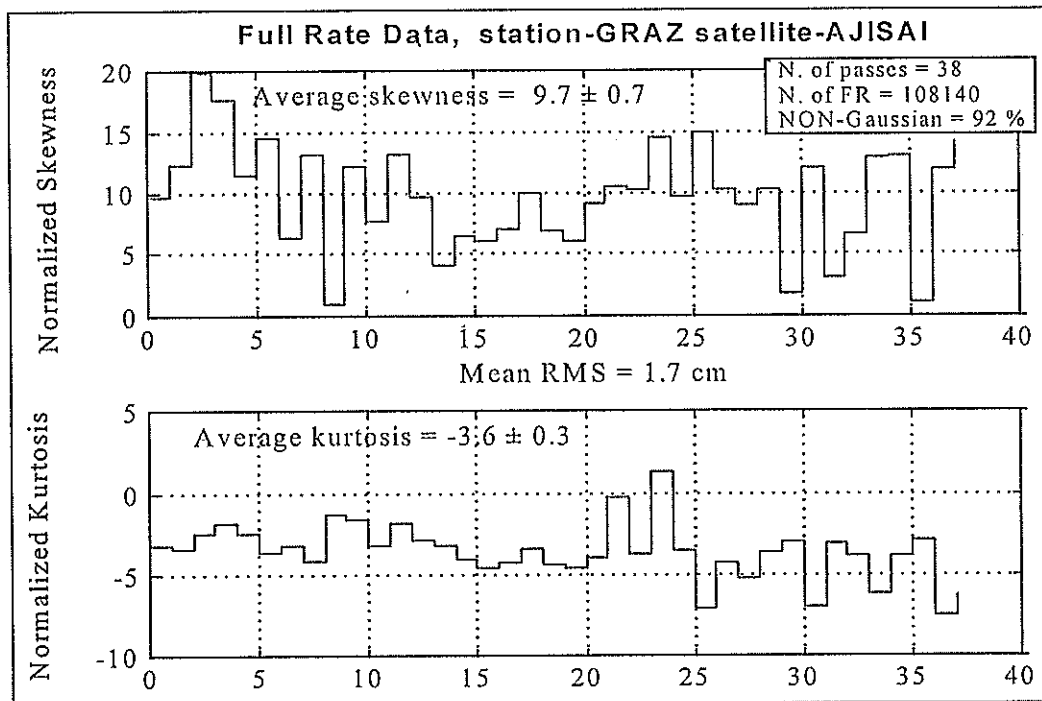
Fig.5

Conclusions

The SLR normal points are fundamental for the scientific analysis permitting to save computer and time resources but they cannot always be analysed as they were full-rate data, they need to be carefully used to achieve the same results.

The normal points will continue to be the primary type of data for analyses, however, on the other hand, the discontinuation of the full-rate archiving could be the source of future worries.

Some problems may have origin in the normal point construction phase:

- the passes with skewness could generate biased NP
- some information (e.g. pass distribution) could be lost
- future possible changes in the NP construction could not be applied to old data

others in the analysis phase:

- present and future analysis areas could need FR data
- different SLR analysis approaches (e.g. geometrical or semi-dynamical) could be compromised.

This decision is a point of no return, the risk is high and we hope that each station will continue to archive its own data anyway.

Fast computing the spherical harmonic perturbation on artificial satellite and the recurrence relations of the coefficients of the Earth's gravity[1]

Lin Qinchang

(Guangzhou Satellite Station,
Chinese Academy of Sciences,
Guangzhou 510640, China)

Lin Yuan

(Computer Sciences Department,
Zhongshan University,
Guangzhou 510275, China)

Abstract

A new method of fast computing the spherical harmonic perturbation on artificial satellite and the recurrence relations of the coefficients of the Earth's gravity is given in this paper. The method increases the computation speed in comparison with Cunningham's method and other existing methods, and has no overflow in operation occurs even the order and degree of the Earth's spherical harmonic are extended to 100×100 or more. The method satisfies for the accurate application of the SLR, GPS and LLR.

This method has been programmed and used in practice. For all computations of perturbations, it needs only 10 seconds in 486/66 for 1440 steps of numerical integration.

1. Introduction

The Earth's gravitational potential can be expressed as

$$V = \sum_{n=0}^{\infty} \sum_{m=0}^{n} \frac{R_{\oplus}^{n} P_{n}^{m}(\sin\phi)}{r^{n+1}}(C_{n,m}\cos m\lambda + S_{n,m}\sin m\lambda), \tag{1}$$

where $R_{\oplus}$ is the equatorial radius of the Earth; $C_{n,m}$ and $S_{n,m}$ are Earth's spherical harmonic coefficients; P_{n}^{m} is associated Legendre polynomial; and r, ϕ and λ are, the satellite's geocentric distance, the geocentric latitude and the longitude measured eastward from the meridian of Greenwich, respectively.

Up till now, among the numerical methods to compute the spherical harmonic perturbation on artificial satellite, the computation speed of Cunningham's method is the fastest. On theory, his method can be used to compute any number of zonal and tesseral terms in the Earth's gravitational potential. However, during running programs based on this method, it is easy for overflow to occur. For example, Cunningham used following equations. Define

$$V_{n,m} = \frac{P_{n}^{m}(\sin\phi)(\cos m\lambda + i\sin m\lambda)}{r^{n+1}}, \tag{2}$$

then the Earth's gravitational potential can be transformed into

---

$$V = \mathrm{Re}\left(\sum_{n=0}^{\infty} \sum_{m=0}^{n} R_{\oplus}^{n} (C_{n,m} - iS_{n,m})V_{n,m}\right), \tag{3}$$

where $i = \sqrt{-1}$ is the imaginary number unit; Re expresses to take the real part.

The recurrence relations among the Earth's gravitational potential $V_{n,m}$ were given in Cunningham's method. The computation of the perturbations of various orders and degrees is convenient and fast. However, the main disadvantage of his method is that the coefficients of $V_{n,n}$ rapidly increase as n increases. And other $V_{n,m}$ must be determined with $V_{n,n}$. From

$$V_{0,0} = \frac{1}{r} \tag{4}$$

derive out

$$V_{n,n} = (2n-1)\frac{(x+iy)}{r^2}V_{n-1,n-1} \tag{5}$$

Some of $V_{n,n}$ are listed as following.

. . . .

$$r^{57}V_{28,28} = 8.7 \times 10^{36}(x+iy)^{28},$$

$$r^{59}V_{29,29} = 8.7 \times 10^{38}(x+iy)^{29},$$

. . . .

$$r^{121}V_{60,60} = 7.0 \times 10^{98}(x+iy)^{60},$$

$$r^{123}V_{61,61} = 8.4 \times 10^{100}(x+iy)^{61},$$

$$r^{125}V_{62,62} = 1.0 \times 10^{103}(x+iy)^{62},$$

where x, y and z in Equation (11) are the satellite's rectangular coordinates.

$$x = r\cos\phi\cos\lambda,$$
$$y = r\cos\phi\sin\lambda, \tag{6}$$
$$z = r\sin\phi.$$

It can be found out that the tendency of the coefficients of $V_{n,n}$ increases more and more rapidly as n increases. With improvement of the observational accuracy of the satellite, higher order and degree perturbation of the Earth's spherical harmonic must be considered. But for example, the coefficient of $V_{29,29}$ reaches 5.0×10^{38}. Further, the coefficient of $V_{62,62}$ has exceeded 1.0×10^{103}.

In order to prevent from the overflow, in practice on computation with computer, normalized $\overline{P}_n^m$ have been adopted to replace the P_n^m by many people.

$$\overline{P_m^m}(\mu) = \frac{P_n^m(\mu)}{N_n^m},$$

$$N_n^m = \frac{1}{\sqrt{(2n+1)\dfrac{(n-m)!}{(n+m)!}\delta}}. \qquad \delta = \begin{cases} 1 & m = 0, \\ 2 & m \neq 0. \end{cases} \tag{7}$$

And the all coefficients of $C_{n,m}$ and $S_{n,m}$ are multiplied by the module N_n^m. However, when the n and m increase, $(n+m)!$ also rapidly increases. As a sample, when $n=m=35$, $(n+m)!$ is larger than 10^{100}. If the Equation (5) is directly used to compute, the opportunity of overflow in operation is even more than with $V_{n,n}$. When that method is programmed, it is possible to avoid the overflow in operation with the great effort. But there is no doubt that, using the normalized method, the operational machine time will increase further.

2. The Earth's gravitational potential

For both to prevent from the overflow in operation and to save the machine time at the same time, the fast computing the spherical harmonic perturbation on artificial satellite and the recurrence relations of the coefficients of the Earth's gravity would given in this paper. Let

$$L_{0,0} = V_{0,0}, \qquad L_{n,m} = \frac{(n-m)!}{(2n-1)!!}V_{n,m}, \tag{8}$$

where, $(2n-1)!!=1 \cdot 3 \cdot 5 \cdots (2n-1)$. From

$$L_{0,0} = \frac{1}{r}, \tag{9}$$

we get

$$L_{n+1,n+1} = \frac{x+iy}{r^2}L_{n,n}. \tag{10}$$

And using Equation (10), we get

$$L_{n+1,m} = \frac{zL_{n,m}}{r^2}, \qquad n = m,$$

$$L_{n+1,m} = \frac{zL_{n,m}}{r^2} - \frac{n^2-m^2}{4n^2-1}\frac{L_{n-1,m}}{r^2}, \quad n > m. \tag{11}$$

3. Derivatives

In practice of our method on computer, following equations would be adopted. Define

$$G_{n,m} = \frac{(2n+1)!!}{2(n-m)!} C_{n,m}, \qquad H_{n,m} = \frac{(2n+1)!!}{2(n-m)!} S_{n,m}, \qquad m > 0,$$

$$G_{n,0} = \frac{(2n+1)!!}{n!} C_{n,0},$$

(12)

where, $G_{n,m}$ and $H_{n,m}$ are the program constants to replace spherical harmonic coefficients $C_{n,m}$ and $S_{n,m}$. Then Equation (3) can be transformed into

$$V = \mathrm{Re}(\sum_{n=0}^{\infty} \sum_{m=0}^{n} R_{\oplus}^{n} (G_{n,m} - iH_{n,m}) U_{n,m}).$$

(13)

The derivatives of $U_{n,m}$ are

$$\frac{\partial U_{n,m}}{\partial x} = -L_{n+1,m+1} + L_{n+1,m-1}, \qquad m > 0; \qquad \frac{\partial U_{n,0}}{\partial x} = \mathrm{Re}(-L_{n+1,1});$$

$$\frac{\partial U_{n,m}}{\partial y} = i(L_{n+1,m+1} + L_{n+1,m-1}), \qquad m > 0; \qquad \frac{\partial U_{n,0}}{\partial y} = I_m(-L_{n+1,1});$$

(14)

$$\frac{\partial U_{n,m}}{\partial z} = -2L_{n+1,m}, \qquad m > 0; \qquad \frac{\partial U_{n,0}}{\partial z} = -L_{n+1,0};$$

where, I_m expresses to take the image part.

4. The recurrence relations, using $C_{n,m}$ and $S_{n,m}$

If we only have $C_{n,m}$ and $S_{n,m}$, let the ratio $K_{n,m}$ as following:

$$K_{n,m} = \frac{G_{n,m}}{C_{n,m}} = \frac{H_{n,m}}{S_{n,m}} = \frac{(2n+1)!!}{\delta(n-m)!}.$$

(15)

1) The recurrence relations of zonal terms coefficients
When m=0, δ =1, it corresponds computation of zonal terms coefficients.

$$K_{n,0} = \frac{(2n+1)!!}{n!}.$$

(16)

From

$$K_{0,0} = 1,$$

derive out

$$K_{n,0} = \frac{2n+1}{n} K_{n-1,0}, \qquad n > 1.$$

(17)

2) The recurrence relations of tesseral terms coefficients
When m>0, δ =2, it corresponds computation of tesseral terms coefficients. From

$$K_{1,1} = 1.5, \tag{18}$$

derive out

$$K_{n,1} = \frac{2n+1}{n-1} K_{n-1,1}, \qquad n > 1, \tag{19}$$

and

$$K_{n,m} = \frac{n-m+1}{n-m} K_{n,m-1}, \qquad m > 2. \tag{20}$$

5. The recurrence relations, using $\overline{C}_{n,m}$ and $\overline{S}_{n,m}$

Sometimes, the spherical harmonic coefficients of the Earth would be normalized. In the case, following recurrence relations would be used. The definitions of normalized $\overline{C}_{n,m}$ and $\overline{S}_{n,m}$ are:

$$\overline{C}_{n,m} = C_{n,m} N_n^m, \qquad \overline{S}_{n,m} = S_{n,m} N_n^m, \tag{21}$$

where, the definition of N_n^m is in Equation (7). We get the ratio

$$K_{n,m} = \frac{G_{n,m}}{\overline{C}_{n,m}} = \frac{H_{n,m}}{\overline{S}_{n,m}} = \frac{(2n+1)!!}{\delta(n-m)!}. \tag{22}$$

Thus,

$$K_{n,m} = (2n+1)!! \sqrt{\frac{2n+1}{\delta(n-m)!(n+m)!}}. \tag{23}$$

1) The recurrence relations of zonal terms coefficients
When m=0, δ =1, it corresponds computation of zonal terms coefficients.

$$K_{n,0} = \frac{(2n+1)!!}{n!} \sqrt{2n+1}. \tag{24}$$

From

$$K_{0,0} = 1, \tag{25}$$

derive out

$$K_{n,0} = \frac{2n+1}{n} \sqrt{\frac{2n+1}{2n-1}} K_{n-1,0}, \qquad n > 1. \tag{26}$$

2) The recurrence relations of tesseral terms coefficients
When m>0, δ =2, it corresponds computation of tesseral terms coefficients. From

$$K_{1,1} = 1.5\sqrt{3} \qquad\qquad (27)$$

derive out

$$K_{n,1} = (2n+1)\sqrt{\frac{2n+1}{(n^2-1)(2n-1)}}K_{n-1,1}, \qquad n>1, \qquad (28)$$

and

$$K_{n,m} = \sqrt{\frac{n-m+1}{n+m}}K_{n,m-1}, \qquad m>2. \qquad (29)$$

6. Practice on computer

.In practical computations, the values of $G_{n,m}$ and $H_{n,m}$ are independent of the satellite's coordinates, and they are the same for all satellites. Therefore, Equations (15) to (29) only need to compute once. Derived the ratio $K_{n,m}$ and $\overline{K}_{n,m}$, $G_{n,m}$ and $H_{n,m}$ are derived at once. As a constant file, $G_{n,m}$ and $H_{n,m}$ are stored in the computer and can be used to any Earth's satellites. The another feature of $G_{n,m}$ and $H_{n,m}$ is that their variable spans are much less than $V_{n,m}$. The reason is that as n increases, (2n+1)!! increases, but the values of $C_{n,m}$ and $S_{n,m}$ decrease. In fact, every value of $G_{n,m}$ or $H_{n,m}$ is a big figure multiplied a small one. Therefore, the possibility of the overflow becomes much less on the computer. The method satisfies for the accurate application of the SLR, GPS and LLR.

The gravitational potential and its derivatives have been programmed. For computing the order and degree of the Earth's spherical harmonic perturbation to 20 × 20, including all other computations of perturbations, it needs only 10 seconds in 486/66 for 1440 steps of numerical integration. Thus, the accuracy to compute the spherical harmonic perturbation on artificial satellite is improved, and machine time is saved.

Work organization and some results of the data analysis on satellite laser location at Russian Mission Control Center

Glotov V.D. , Mitrikas V.V., Poliakov V.S., Pochukaev V.N.
Russian Mission Control Center, Moscow, Russia.

Abstract.

This paper describes briefly the work organization and some activity results of the Laser Operational-Analytical Center at Russian Mission Control Center (MCC). In particular, there are some examples of the SLR data quality analysis results for the Shanghai and Changchun stations and comparison of this results with other data analysis centers.

1. Laser Operational-Analytical Center "LOAC" was created at MCC in 1991 on the basis of ballistic service of Earth Artificial Satellite (EAS) orbit determination and has passed some stages in its development. Originally, the LOAC goals consisted of the ephemeride support of the domestic network' s laser stations, acquisition of measurement data from these stations at location by them of 2-3 specialized spacecraft (SC), data preprocessing and transferring to the international centers of the measurements analysis within the framework of work on introduction of Russian stations into world laser subsystem.

For period 1991-1994 yr. the methodical and software-mathematical means of the acquisition, storage and high-precision analysis of laser measurements were developed in MCC, LOAC hardware instrumentation is conducted by means of electronic communication and computer data processing, principles of interface with stations and Centers of a world laser network are fulfilled. Now LOAC (besides functions on maintenance of regular work of a domestic network of stations at location of 14-16 specialized EAS within the framework of realization of the international programs of ephemeride support, acquisition, storage, processing and transferring of the measurement information) is one of the four world operative centers of the laser data analysis, ensuring high-precision determination of Earth Rotation Parameters and the analysis of stations work quality in a mode of a regular service.

2. The software (SW)   -mathematical support of the LOAC, intended for processing of laser measurements, is realized on personal computers within the framework of operating system MS-DOS. Developed in MSS , the SW provides both as the solution of problems of technological and operative character : formation of normal points, express - analysis of data, storage of the information, preparation of the reports ,etc. `, and realization of the precision analysis of measurements of whole world network's stations at solution of multiparametrical problems of the parameter estimation . Both as   the models, recommended by the international standards and by the agreements (IERS Standards), and own original techniques of calculation realization - were used at SW development .

In particular, the accounting of a gravitational field of the Earth in various models , gravitational effect of planets, Sun and Moon, tides in solid Earth , oceanic tides, indirect influence of the Earth oblateness, direct solar pressure, nonmodelled empirical acceleration ,etc - is admitted in motion model. The lithosherical plates motion , coordinates displacement due to the pole motion, tides in solid Earth, deformation of rotation because of tides - is taken into account in model of ground stations

coordinates. Mentioned SW provides the opportunities of EAS orbits determination with residual errors within the level of units of centimeters, parameters of orientation of the Earth, coordinates and velocities of ground stations in earth coordinate frame , etc.

3. The fact, that LOAC, being in structure of a laser stations domestic network, has strongly come into the structure of a world laser subsystem and works successfully within the framework of world cooperation at realization of the Russian and international programs of a specialized EAS location and scientific analysis of received results - can be referred to main results of the LOAC work for period since 1991. Constant quality surveillance of measurements of the station's domestic network and analysis of available errors character, realized in LOAC, promoted to increase the measuring data accuracy and high stability of stations work during the realization of the programs of SC tracking, located by the world network , total - about 20 EAS.
Results of operative determination of parameters of the Earth orientation: pole coordinates and day duration , received by LOAC in mode of a regular service during the data processing of a laser ranging of the SC "LAGEOS-1" and "LAGEOS-2" by world network's stations (total about 50 stations), are sent in Central (Paris) and Operative (Washington) Bureau of the International Earth Rotation Service. Thus , the accuracy of received in 1996 results of Earth Rotation Parameters corresponds to the best world level, achieved by similar international centers of the data analysis: Texas and Delft Universities with average errors of pole coordinates determination , being equal to 1-3 centimeters on Earth surface .
Moreover , the series of scientific and applied researches on precision data processing on Satellite Laser Ranging , is conducted, as a result of which at 1996, in particular , the "Glonass-63" and "Glonass-67" high -precision orbit on semi-annual interval of tracking for these SC by world network's laser stations and model of EAS motion of the given class, ensuring the accuracy increase of SC orbit determination and forecasting in 3-8 times in comparison with similar regular model - was constructed .

GLOBAL LASER RANGING STATISTICS

January-October, 1996

SC	Maidanak (1864)	Komsomolsk (1868)	Mendeleevo (1870)	Katzively (1893)
GFZ-1	20	-	2	-
ERS-1	54	6	37	11
ERS-2	154	19	86	13
ADEOS	1	-	1	-
TOPEX	104	66	90	7
AJISAI	-	-	-	5
RALPH	10	-	-	-
NORTON	8	-	-	-
LAGEOS-1	141	54	-	31
LAGEOS-2	111	53	-	15
GPS-35	10	1	-	-
GPS-36	8	8	-	-
GLO-63	52	18	-	2
GLO-67	63	14	-	12
ETALON-1	37	10	-	3
ETALON-2	58	14	-	3
TOTAL	831	263	216	102

EOP Residuals analysis (MCC)

Xp(IERS) - Xp(CSR) ME = 5.9299e-04 RMS = 2.5398e-04
Xp(IERS) - Xp(MCC) ME = -1.6666e-05 RMS = 3.7086e-04

Residuals (")

Time (days)
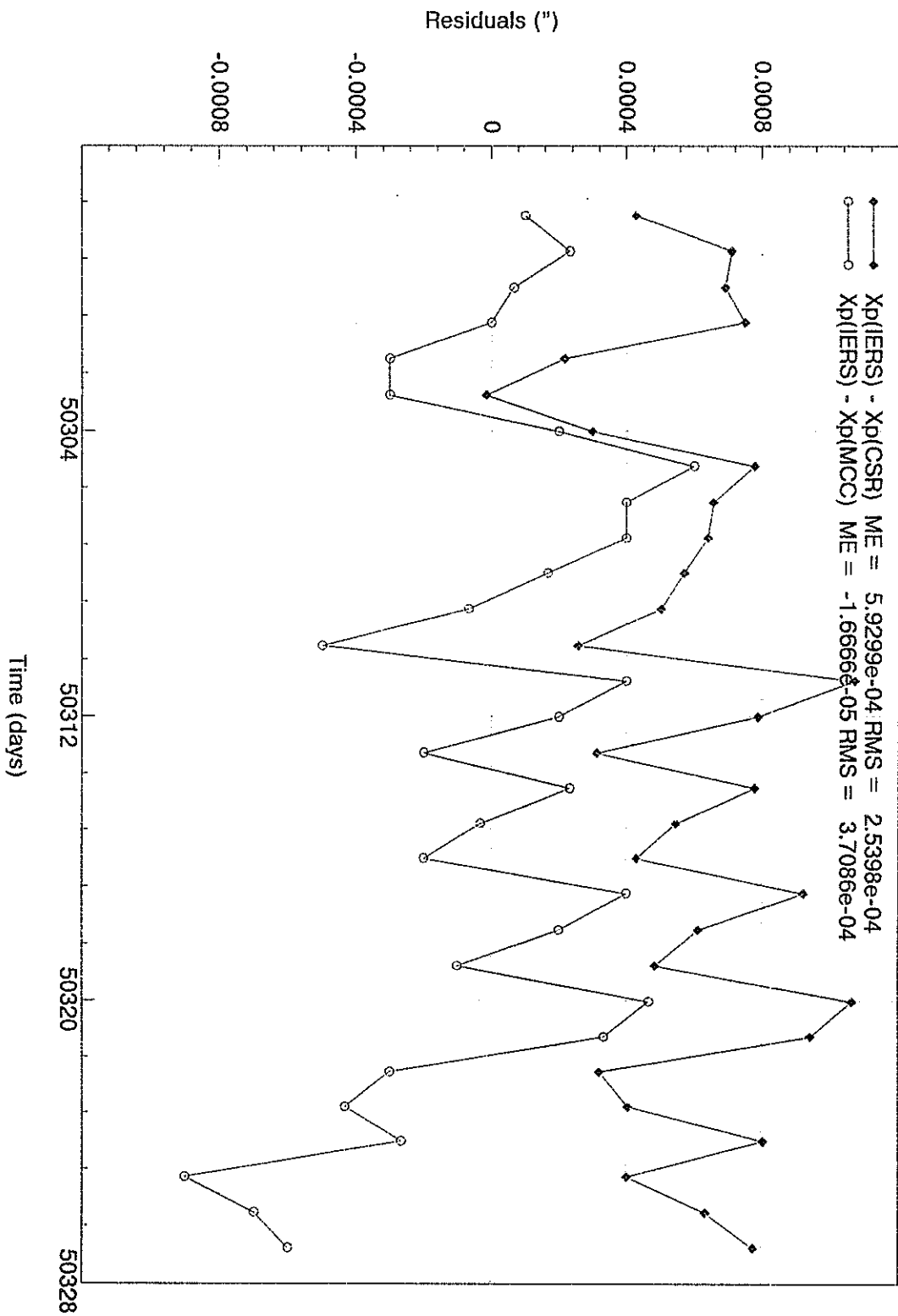
Cutting out Quicklook Residual Analysis Report (CSR)

STA ID	AVG PASS TIME YY/MM/DD HH:MM	SAT	GOOD OBS	RAW RMS (MM)	PREC EST (MM)	RANGE BIAS (MM)	TIME BIAS (US)	PASS DUR (MIN)	EDITED OBS	OBS	CALIB+ MEAN (MM)	CALIB SDEV (MM)	CALIB++ SHIFT (MM)	STPASS RMS (MM)
> (7837) Shanghai														
7837	96/10/02 13:37	L2	13	332	147	-64	-126	29	0	ALT	8127 E	45	0 P	30
> (7237) Changchun														
7237	96/10/04 10:18	L2	3	263	247	-90	0	3	0	ALT	22912 E	45	0 P	25
7237	96/10/09 12:32	L2	23	141	39	138	22	56	0	ALT	22946 E	45	0 P	64

Cutting out Quicklook Residual Analysis Report (MCC)

Shanghai (7837 NP)

DATA	T ini	T fin	SC	TTL	INC	ME mm	RMS mm	ORMS mm	ELEV deg	T C	P mm	H %	CALIB mm	TB us	RB mm	PRMS mm
02.10.96	13:21	13:50	L2	13	13	70	342	349	027-060	23	763	87	8127	-128	-20	318 (*)
02.10.96	13:21	13:50	L2	13	11	-31	10	34	027-060	23	763	87	8127	7	-27	8

Changchun (7237 NP)

DATA	T ini	T fin	SC	TTL	INC	ME mm	RMS mm	ORMS mm	ELEV deg	T C	P mm	H %	CALIB mm	TB us	RB mm	PRMS mm
04.10.96	10:17	10:20	L2	03	02	50	26	75	029-034	10	737	74	22911	0	50	26
09.10.96	12:09	13:04	L2	23	17	29	48	58	017-084	4	742	90	22946	32	52	29

(*) - no edited

Changchun Laser Station (7237)
Residuals from the orbit in meters
Date: October 9

Time from 0 hours in hh:mm:ss
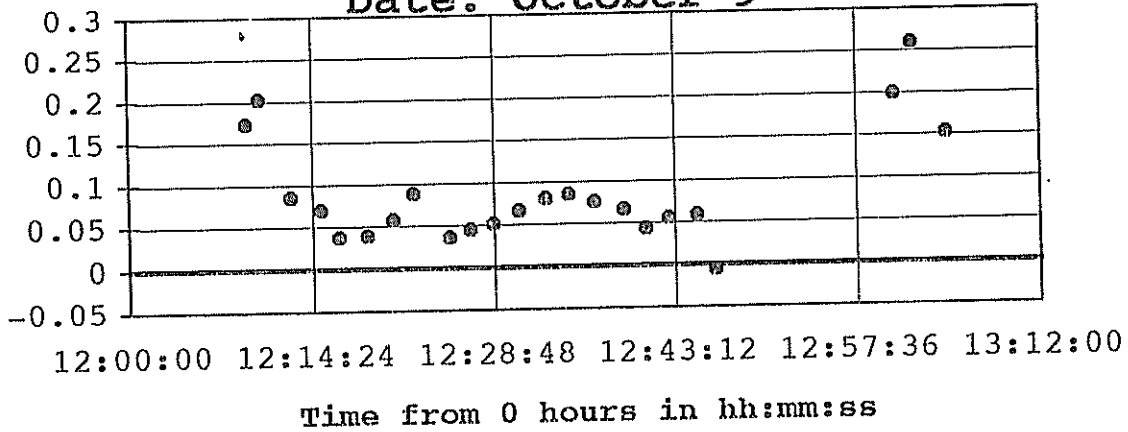
Shanghai Laser Station (7837)
Residuals from the orbit in meters
Date: October 2

Time from 0 hours in hh:mm:ss
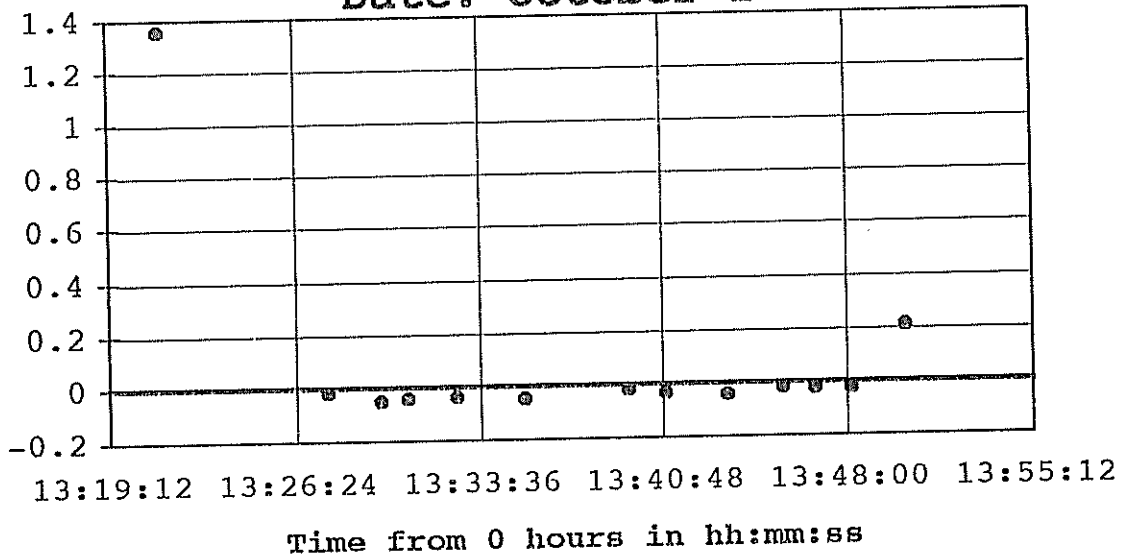
Residual Analysis Report
Shanghai (7837 NP)

DATA	T ini	T fin	SC	TTL	INC	ME	RMS	ORMS	ELEV	T	P	H	CALIB	TB	RB	PRMS
						mm	mm	mm	deg	C	mm	%	mm	us	mm	mm
02.10.96	13:21	13:50	L2	13	11	-31	10	34	27-60	23	763	87	8127	7	-27	8
02.10.96	16:07	16:23	L1	09	09	-18	7	21	31-42	22	763	85	8127	-3	-17	7
02.10.96	17:45	18:18	L2	18	18	-29	20	35	34-56	22	763	83	8127	5	-29	18
02.10.96	19:33	19:50	L1	10	10	-81	12	85	48-60	21	763	81	8125	-10	-80	8
04.10.96	13:45	14:24	L2	21	19	-25	18	32	19-56	21	764	80	8141	16	-34	7
04.10.96	13:45	14:24	L2	21	21	-25	18	32	19-56	21	764	80	8141	10	-30	12
04.10.96	16:45	17:12	L1	15	15	-21	17	28	34-57	20	764	84	8140	-10	-20	8
04.10.96	16:45	17:12	L1	15	15	-21	17	28	34-57	20	764	84	8140	-10	-20	8
04.10.96	17:57	18:32	L2	19	19	-22	22	33	32-61	20	764	84	8140	17	-21	7
04.10.96	17:57	18:32	L2	19	19	-22	22	33	32-61	20	764	84	8140	17	-21	7
09.10.96	12:37	12:50	L2	07	05	639	61	716	30-57	17	767	83	8122	239	186	29
18.10.96	15:39	15:58	L2	11	11	21	32	38	42-52	20	767	90	8259	-17	24	28
19.10.96	13:25	13:50	L2	14	14	52	14	57	28-47	18	770	73	8182	14	64	8
19.10.96	14:12	14:24	L1	07	07	60	14	68	22-28	18	770	75	8182	-10	68	12
19.10.96	17:17	17:32	L1	09	09	-14	12	20	25-65	16	770	81	8182	17	21	8
19.10.96	17:41	17:52	L2	07	07	21	8	24	37-65	16	760	81	8183	-14	-3	6
22.10.96	16:48	17:04	L1	10	10	-58	28	68	34-76	20	768	99	8259	21	-28	21

Discussion over Orbit Determination of Satellite Ajisai

Jiang Hu   Feng Chugang
Shanghai Observatory, the Chinese Academy of Sciences

Abstract

When we make researches on near-Earth satellite orbit determination, it is inevitable that we should be subject to meeting with some atmospheric models, such as exponential atmospheric model, DTM, CIRA86, J77,and so forth. As a noted, comparatively later established atmospheric model, J77 seems so conspicuous that it is usually taken into full considerations as far as air drag perturbation is concerned.

Here we are involved in a puzzle of calculation divergence resulting from introduction of J77 as an atmospheric model to deal with the precision orbit determination of the near-Earth satellite Ajisai, if a computer operating system named VAX3800 is utilized. Based on many simulating calculations and postanalyses we suppose that the essence of calculation divergence may be brought about by improperly adopting a default value of parameter ε in our software SHORDE for researches on satellite orbit determination and dynamical geodesy. Calculation shows that this parameter is dependent of, but not just equal to, the significant value of a specific computer operating system. After adjusting the parameter ε, we recalculate its orbital elements and find the results convergent. Finally we compare the results with those produced by some other atmospheric models, and comparisons indicate that our adjustment of parameter ε is rational, necessary and effective.

1. Introduction

J77 is one of the currently noted atmospheric models; it was presented by L.G., Jacchia with SAO (1977). His other similarly patterned models are · J65, J70, and J71(Jacchia,1965,1970,1971a,1971b). Those models constitute a family of Jacchia's.

J77 includes the basic static models and a set of formulae; the former offers temperature and density profiles for the relevant atmospheric constituents for specified exospheric temperature; the latter is used to calculate the exospheric temperature and the expected deviations from the static models as a result of all the recongnized kinds of thermospheric models. Like any other atmospheric models, J77 is by no means perfect. So far it has been proved that there is much to be desired in J77 (Tang, 1995).

2. Problem arising

when we do researched on atmospheric drag in order to further our study of precision orbit determiation of near Earth satellite Ajisai, it happens that RMS for observational data seems beyond explicitly reasonable explanation since the batch-moded calculation fails to work. Debuging the calculation process finds that divergence appears in certain integration phase of satellite motion equations. However the essentially original key cause lies elsewhere as is expected to be expounded in the coming section.

3. Solutions

Further scrutinization finds that the calculation divergence may as well be accounted for by direct use of a default value of parameter ε in our software for the study of satellite precision orbit determination and dynamical geodesy (Huan, 1985). ε is computer-dependent (Lafontaine and Hughes,1983), which can be empirically expressed as follows:

$$\varepsilon = f(\varepsilon_0)$$

where, as a variable, ε_0 is the significant figures available on the computer operating system Micro VAX3800 at Shanghai Astronomical Observatory.

In the default case, ε is chosen to be 10^{-14}. As demonstrated by the calculation, the results are divergent. Tracing into the resultant file given by our software, we find that the RMS for the observational data is nomalous. As a rule of thumb, we commence to doubt whether there is something wrong with some initial evaluations of constant parameters, especially ε.

when ε is set to be 10^{-13}, as shown by calculation, results remain divergent. If let ε be 10^{-12}, then calculation comes to be convergent. Certainly some other ε-dependent parameters have been adjusted during the cases of adopting different values of parameter ε. For the sake of conciseness and no redundancy, we have to omit those detailed references to the choices of ε-dependent parameters here.

4. Comparisons and Conclusion

In order to make a comparison, DTM model is employed to make data reduction from satellite Ajisai. Using both DTM and J77 Models, we have analyzed the data from Ajisai covering the period between Septemper 1st., 1995 and Septemper 20th., 1995. Multistage-multiarc method is taken into consideration (He, Zhu, and Feng, et al., 1989); the sub-subarc,subarc and the whole arc last respectively 5^d, 10^d, and 20^d. The data statistics are shown in figure 1; the adopted force models,reference system and measurement models are listed in table 1. The quantitative and qualitative results are respectively presented in table 2 and figure2.

From the comparison, we can see that after parameter-adjustment, RMS in the case of J77 agrees very well with that in the case of DTM. Therefore J77 is safe to apply in the atmospheric drag realm, especially in the case of the satellite Ajisai.

Table 1.

Force Models	Reference System	Measurement Models
GEM-T3 Earth gravity model	J2000.0 mean equator and mean equinox	Marini-Murray's atmosphere refractivity model
Lunisolar gravity model	IAU76 Precession model	Offset correction for centre of mass
Wahr solid tide model	IAU80 Nutation model	Displacement for stations by solid tide
Schwiderski Ocean tide model (2-6)	DE200/LE200	Displacement for station by ocean load
Solar radiation pressure and that of earth		
Atmospheric drag models		

Table 2.

Atmospheric Models / Arcs		J77 Model (m)	DTM Model (m)
Sub-sub arc1	*RMS*	0.274377	0.275961
Sub-sub arc2	*RMS*	0.320080	0.318562
Sub arc1	*RMS*	0.292065	0.292395
Sub-sub arc3	*RMS*	0.224982	0.226459
Sub-sub arc4	*RMS*	0.185197	0.187381
Sub arc2	*RMS*	0.201999	0.203859
Total arc	*RMS*	0.244969	0.246013
Required CPU Time		$16^h10^m24^s$	$14^h47^m16^s$

Identifying No. of Stations

Number of total observation data of stations
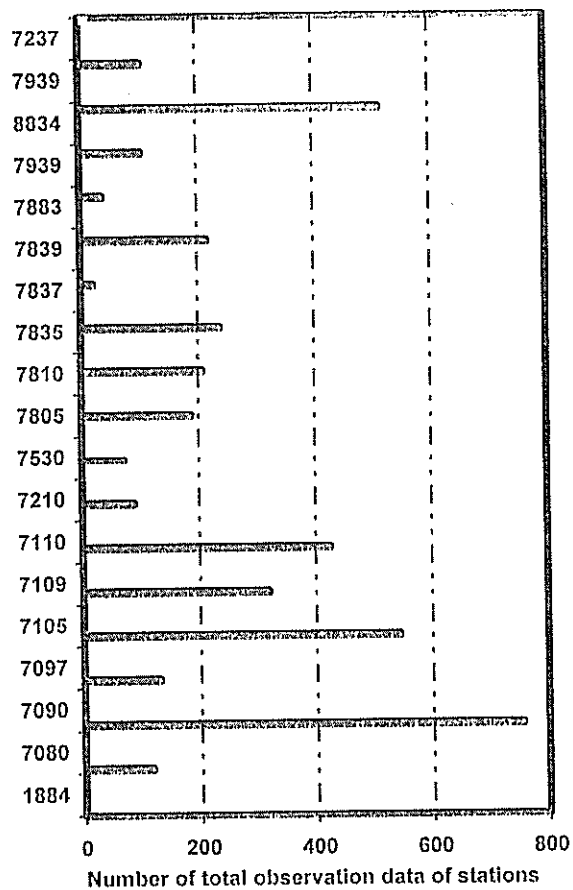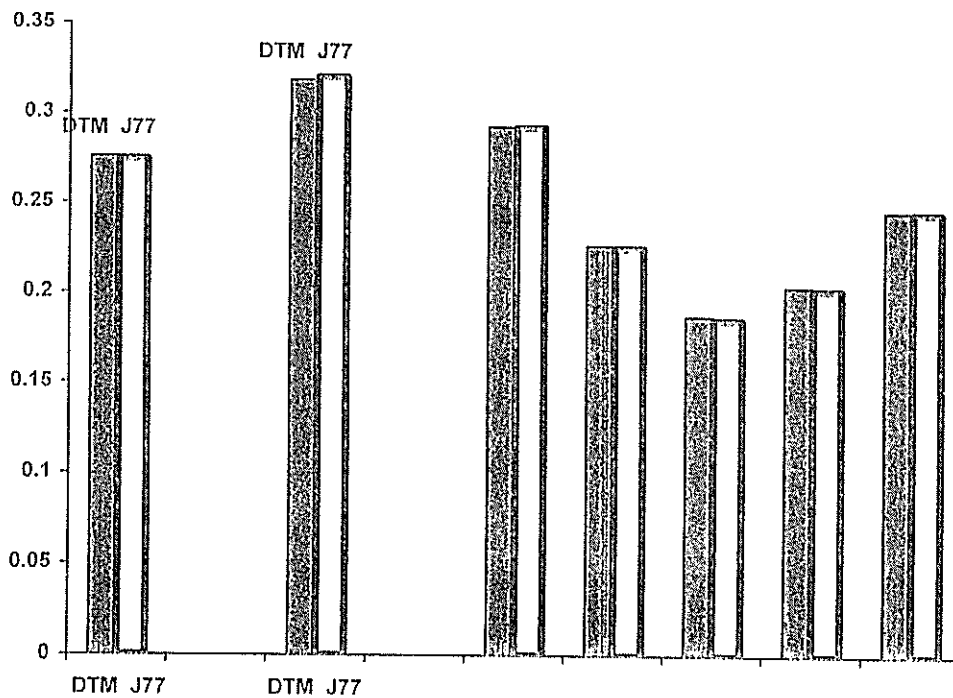
Figure 1.

Figure 2.

References:

Jacchia, L.,G., (1977), 'Thermospheric Temperature,Density, and Composition: New Models',Research in Space Science SAO Special Report No.375

Jacchia, L.,G., (1965), 'Static diffusion models of the upper atmosphere with empirical temperature profiles' Smithsonian Contr. Astrophys.,Vol.8,215-257

Jacchia, L.,G., (1970), 'New static models of the thermosphere and exosphere with empirical temperature profiles', Smithsonian Astrophys.Obs.Spec.Rep.,No.313,87

Jacchia, L.,G., (1971), 'Revised static models of the thermosphere and exosphere with empirical temperature profiles, Smithsonian Astrophys.Obs.Spec.Rep.,No.332,113

Tang, X.,S., (1995), ACTA Astronomica Sinica

Huan,C.,(1985). 'Determination of EOP from LAGEOS', Doctoral Thesis, Shanghai Astronomical Observatory,the Chines Academy of Sciences

Lafontaine, J.,D., P.,Hughes, (1983). 'An analytic version of Jacchia's 1977 model atmosphere', Celest. Mech. 29, 3-26

He Miaofu,Zhu Wenyao,Feng Chugang, et al.. (1989), 'SHORDE1 Program System and Application', Celest. Mech. 45,61-64

Late Coming Papers

Keystone SLR System

H. Kunimori, C. Miki, J. Amagai, H. Nojiri, T. Otsubo,
Communications Research Laboratory, 4-2-1 Nukui-kita Koganei Tokyo 184 Japan,

B. Greene,
Electro Optic Systems, 55A Monaro Street Queanbean NSW 2620, Australia, and
And
H.Izuha,
Hitachi, Ltd. , 216 Totsuka, Yokohama 244 Japan

1. Introduction

The Keystone Project (KSP) was initiated in 1993 by Communications Research Laboratory to establish four state-of-art geodetic fiducial sites around metropolitan Tokyo, monitoring site displacement very precisely by means of space geodetic techniques, Very Long Baseline Interferometer (VLBI) and Satellite Laser Ranging (SLR) systems. It aims to have any signs of major earthquakes with millimeter accuracy on baseline and heights of the stations, namely, Kashima, Koganei, Miura and Tateyama. Fig.1 shows a schematic geography of KSP stations and a picture of SLR observatory building at each site.

While VLBI observation started in 1994, the construction of SLR station started in 1995. It has incorporated a wide range of new technologies, including telescope, dome, laser, timing system, calibration system as well as automation and remote control system.

This paper describes concept of Keystone SLR system and some of new technologies utilized in KSP.

2. Design Concept

KSP SLR is designed to operate as not only four sets of SLR, but as a single instrument of all four or more SLR networking with each other. The major concept of KSP is categorized as follows:

- Accurate: Modern SLR has pursued ranging accuracy to 1 cm, mainly parameterized single shot precision. However, uncorrected range bias and its instability is much difficult to control in minimum, as they are reported in global orbit analysis often varying over a few cm. The concept lead into design in the system is (1) to provide picoseconds epoch timer and frequency source to ensure ultimate accuracy available, (2) to provide a redundant means to calibrate a system delay to check each other, by multiple reference targets and independent calibrators. We operate ranging in single color, leaving atmospheric correction on a conventional model, except Kashima station which will have a multiple wavelength ranging capability to asses atmospheric model error.

- High Yield and Automation: Since the Keystone demands the regular monitoring of site displacement with high temporal resolutions and the increasing number of missions/satellite for SLR in various fields, system has capability to continues observation with maximum efficiency and tolerance as long as weather permits. The station itself is designed as autonomous manner. Possibility of down time due to environment such as temperature and precipitation must be

minimized. Networking the multiple stations and control overall system from a center is important features in order to make a flexible expansion of the network.

- Eye-safe: The SLR, especially in urban area demands the operation in accordance of any kind of safety regulation. The typical laser used in SLR has mode-locked high power laser, with a class 3B or more, potentials of dangerous exposure in the beam out of the telescope. Keystone SLR adopted a infra-red aircraft detection laser, as a second laser superimposed in the ranging laser to prevent laser beam from contact to aircraft and local personnel.

3. Subsystem for Keystone SLR

3.1 Telescope and Dome

Figure 2 illustrates the Keystone SLR system including dome building and trailer box housing laser and electronics.

The KSP telescope and dome are designed for dedicated SLR with the mm accuracy and installed in a KSP observation tower. The telescope has a 75 cm primary mirror on Alt-AZ mount. A 15cm secondary mirror is on a spider structure sustained by on a dimension-temperature compensating tube (a schematic diagram in Fig.3). A drive speed specified 12deg/s for both axes. A Coude configuration optics lead a beam down through optical table where transmitting laser is located. Figure 4 is an example of interferometer response for the primary surface with 0.037 wavelength rms. Both the tracking camera on the secondary 20cm diameter telescope on the main and on the Coude path end enable us to automatic acquisition of the target.

The KSP dome is fully sealed and optical interface is a ranging window made of high quality glass. In the observation tower, temperature and Humidity of the room is controlled by air-conditioner to +/- 2 degrees C and 50 %, respectively. Because of no possibility of weather intrusion, it reduces mechanical corrosion in dome, and to be fail-safe under power fail conditions and stabilize temperature, lower humidity and dust proof which are crucial to telescope optics performance in an automatic operation in a long run.

3.2 Laser optics and Electronics

All the optics and electronics except for telescope and dome needed in SLR is set in a temperature controlled trailer box dimensioned by 7.5m x 2.4m x 2.2m. It aims that each trailer box can be exchanged by spare box when repair is needed and multiple boxes can be collocated at an observation tower with common telescope for test and calibration at the same time.

A diode-pumped laser oscillator followed by regen amplifier and main amplifiers is used for stable operation with high performance of laser pulse and energy and for longer mean time between maintenance break. Figure 5 illustrates the optical layout on the table. Laser has multiple operation mode in pulse energy and repetition rate which enable us to scale a variety of targets from low orbit satellite to geosynchronous satellite in the standard receiving condition.

The second laser which produce a 1.5 micron wavelength which has 10^5 greater MPE(Maximum

Permissible Exposure) than visible light. is used to detect aircraft or any other target before the main laser pulse emission. If the first pulse detect target in the beam, second (SLR) laser will interlocked immediately.

Ranging electronics consists of receivers (a single photon avalanche diode and Micro Channel Plate photo multiplier), an picosecond epoch timing unit, a GPS timing receiver. We can use frequency and timing signal from Hydrogen maser used for VLBI by switch.

Any status and operational parameters to affect the system accuracy and automation performance can be monitored and recorded by computer.

3.3 Network and Software

Koganei has a function of control and monitoring of all the Keystone stations using a dedicated 128 kbps communication network.

The central station delivers the schedule and orbit information. Each station observes satellites automatically and send the observation data and instrument status. An operator at Koganei station can override any command to initiate and stop observation by monitoring weather information, alarm status as well as video information from multiple cameras in the station. Fig.6 shows a block scheme of the control and monitoring of Keystone network. Analysis center is also located at Koganei, where all the orbital prediction and determination and baseline analysis are conducted by commercial GEODYNE-II based CRL analyzer working on three Windows NT based high performance PCs. If any one of the station is successful to acquire a satellite, the orbit correction is transferred to the rest of station through the network.

4. Installation and Schedule

The project commenced in October 1995 with contracts for delivery 4 complete SLR stations and one mobile system. They were designed, manufactured and delivered in March 1996, and are starting integration firstly at Kashima and Koganei. After link establishment at the stations, the accuracy validation phase will be started in early 1977. Nominal operation date of four station will be in the middle of 1997.

Fig.1   Map of Tokyo Metropolitan Area and delivered SLR systems.
Fig.2   Keystone SLR view including dome building and trailer box housing laser and electronics.
Fig.3   Schematic view of Keystone telescope with dimensions.
Fig.4   An example of interferometer response for the 75cm primary surface
Fig.5   The optical layout on the Keystone SLR laser and T/R system
Fig.6   The block scheme of the control and monitoring center of Keystone network.

The Crustal Deformation Monitoring of the Tokyo Metropolitan Area

Fig.1

Map of Tokyo Metropolitan Area and delivered SLR systems

Fig.2
Keystone SLR view including dome building and trailer box housing laser and electronics

Fig.3
Schematic view of Keystone telescope with dimensions

Fig.4
An example of interferometer response for the 75cm primary surface

ENERGY METER

BEAM ANALYSER

CAMERA

BEAM EXPANDER

HARMONIC GENERATORS,
TR & DETECTORS
λ<1.3um

AUTO COLLIMATOR

OSCILLATOR

REGEN AMPLIFIER

DETECTOR
λ>1.3um

DIVERGENCE
CONTROLLER

OPO

POWER AMPLIFIER 2

POWER AMPLIFIER 1

AIRCRAFT DETECTION
LASER

1000

2400

1300

2000

Fig.5
The optical layout on the Keystone SLR laser and T/R system

612

Central control computer

Intra-station LAN

File server

Intra-station LAN

Analysis computer

Intra-station LAN

Remote control computer

Observation control instructions from central station to observatory stations

Central station

Observatory station

Raw data and status of observation and image data for environmental monitoring from observatory stations to contral station

Observation computers

Observation for ranging

Fig.6

The block scheme of the control and monitoring center of Keystone network

Preliminary Report on ADEOS/RIS Laser Tracking Experiments

H.Kunimori, T. Gotoh, H. Nojiri,

Communications Research Laboratory, 4-2-1 Nukuikita Koganei Tokyo 184 Japan.

M. Sawabe, M. Ogawa, and M. Maeda,

National Space Development Agency, 2-1-1 Sengen, Tsukuba-City Ibaraki 305, Japan.

* Poster presented in the session Target design, signature and biases

1. Introduction

Advanced Earth Observing Satellite(ADEOS) was launched in August, 1996. ADEOS is carrying CCR(Corner Cube Reflector) called RIS(Laser Reflector In Space). RIS provided by Environment Agency is a hollow cube-corner retroreflector with an effective diameter of 0.5m [1]. Main mission of the RIS is to measure the absorption spectrum of a small amount ingredient, such as ozone, methane and nitrogen oxide, in the atmosphere.

Because the RIS is a single-element corner cube with a large aperture, there will be no jitters in the reflection, and the reflection from the RIS will be much brighter than that from other targets for satellite laser ranging. In addition, by its clean spectrum response the RIS is an ideal test target for multiple wavelength satellite laser ranging experiments.

With the requirement from future Japanese earth observation satellites, it is necessary to determine the position of the satellite more accurately than the present and the high accuracy trajectory prediction is necessary for the observation operation of RIS, as well.

NASDA is determining the satellite orbit at present based on range and range rate (R&RR) between the ground stations and the satellite obtained by radio wave link where the precision of the measurement of range by S-band radio wave is about 1 m . However, the delay due to temperature drift in transponders or to ionosphere, uncertainly will easily reach tens of meter, respectively. The orbit determination accuracy by R&RR becomes about 1(km) for Geostationary satellites, about 150(m) for satellites in the Low earth orbit. As for orbit determination by SLR or by GPS, higher accuracy will be expected, as in Figure 1.

2. Data communication system

The Communications Research Laboratory (CRL) has developed a data center for the distribution and archiving of SLR data of ADEOS/RIS, and NASDA carries out generation of orbital information as a research phase. NASA's support in prediction of orbit is requested to confirm the accuracy of the prediction by CRL/NASDA. Figure 2 illustrates the data communication system in ADEOS/RIS network.

The Laser ranging data obtained by international SLR stations is once gathered at the CRL through Internet. with checking the quality of those data, CRL transmits them to the Tracking & Control Center, TACC of NASDA via Earth Observation Center, EOC of NASDA. Data handling is operated automatically. TACC generates three types of orbit information, namely TIRV, Time bias and orbit determination result report. Those kinds of orbit information are transmitted to the SLR stations' networks through the course that is the same as the reception course of SLR data.

3. Pre-launch test with AJISAI and ERS2

Since the launch of ADEOS in August, mission check out has been performed for 3 month, and we have been obtaining RIS SLR data since October 30, 1996.

Before the ADEOS/RIS experiments. we performed pre-experiments using other satellites with laser reflector, AJISAI and ERS2. Figure 3 shows 19 SLR stations used for pre-launch analysis. The SLR stations exist mainly in the middle latitudes such as Asia, Europe, and north and south America.

We also show the models used for these analyses in Fig.4 . Basically, we apply the IERS Standards 1992 .

As shown in Fig. 5, when we perform long-arc orbit, we use 3.5 day data arcs, which have 0.5 days overlap. For AJISAI, we performed 10 cases of orbit determination, and for ERS-2, 8 cases. Figure 6 show the difference in orbit position and velocity during overlapped period. The difference in AJISAI is about 3-9(m), whereas in ERS-2, 10-60(m) . This is supposed to be the influence of the air drag, which is not successfully modeled yet and comes out more strongly to ERS-2 with lower altitude.

On the other hand, in the short-arc orbit determination, for each orbit determination, we use 1 pass data that include data obtained by plural SLR stations as shown in lower in Fig.5. The data arc is approximately 5 - 10 minute each. Fig.7 shows the deference between observed value and calculated value, and standard deviation. Total O-C for short-arc determination is an order of magnitude smaller than that of for long-arc determination. The residuals in the cases using fewer stations are smaller, but its standard deviations of determined positions are larger. This is because there is less geometric restriction.

4. Preliminary ADEOS/RIS experiment

We have received 23 passes data since October 30 before November 6.

We performed orbit determination using long-arc data, in the same manner as AJISAI and ERS-2. During the overlapped period, the differences in orbit position are 5 to 15 m, and the differences in velocity are 2 to 11 mm/sec. Figure 8 shows the comparison of our TIRV with NASA TIRV. Discrepancy is about several hundreds meters and millimeters/seconds in position and velocities, respectively.   It is good enough accuracy for tracking purpose, however, further analysis is needed since we have not received the detailed information about NASA TIRV yet. We would like to continue this analysis with cooperation of other analysis center.

5. Future Plan

We are going to continue these SLR experiments for the duration of the ADEOS mission period, and to improve the accuracy of orbit determination and prediction by improving force models and measurement models.

As for force models, we are planning to improve space craft shape model that is related to modeling of air drag, to adopt more precise Geopotential model, such as JGM-3, and so on.   As for measurement models, we are planning to apply the precise center of mass correction and so on.

We suppose the results of this experiment system will contribute to make a basis of high accuracy trajectory determination system in the future.

References

[1] ADEOS/RIS Tracking Standards, published by RITAG, July, 1996.

RITAG: ADEOS/RIS Tracking Support Coordination Group. National Institute for Environmental Study, Communications Research Laboratory and National space Development Agency of Japan.

Fig.1

S/C Orbit determination Accuracy

Method	LEO	GEO	Luner Mission
S-band Range & Range Rate	150m	1km	～km
Satellite Laser Ranging	～cm	1m	-
On board GPS	100m	-	-
Differential GPS using code	10 ～1m	-	-
Differential GPS using phase	10～1cm	-	-

NASDA

Fig.2

ADEOS/RIS Network

Telemetory Range&RangeRate

ADEOS

Laser Ranging

Mission Data

Internet

NASDA Tracking & Control Center (TACC)

DATA Circuit

NASDA Earth Observation Center(EOC)

DATA Circuit

Communications Research Labolatory(CRL)

International SLR Stations

Maritime Safety Agency

CRL Stations

Kashima, Koganei,Miura, Inuishi

SLR Data

Orbital Information
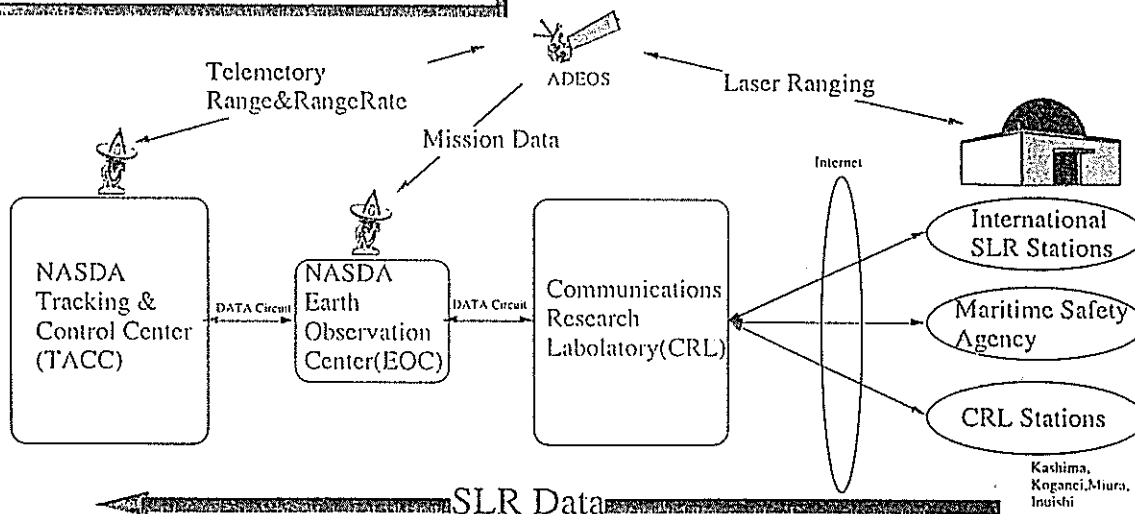
· TIRV
· Orbit determination result report
· time bias function

NASDA

Fig.3

Stations

Fig.4
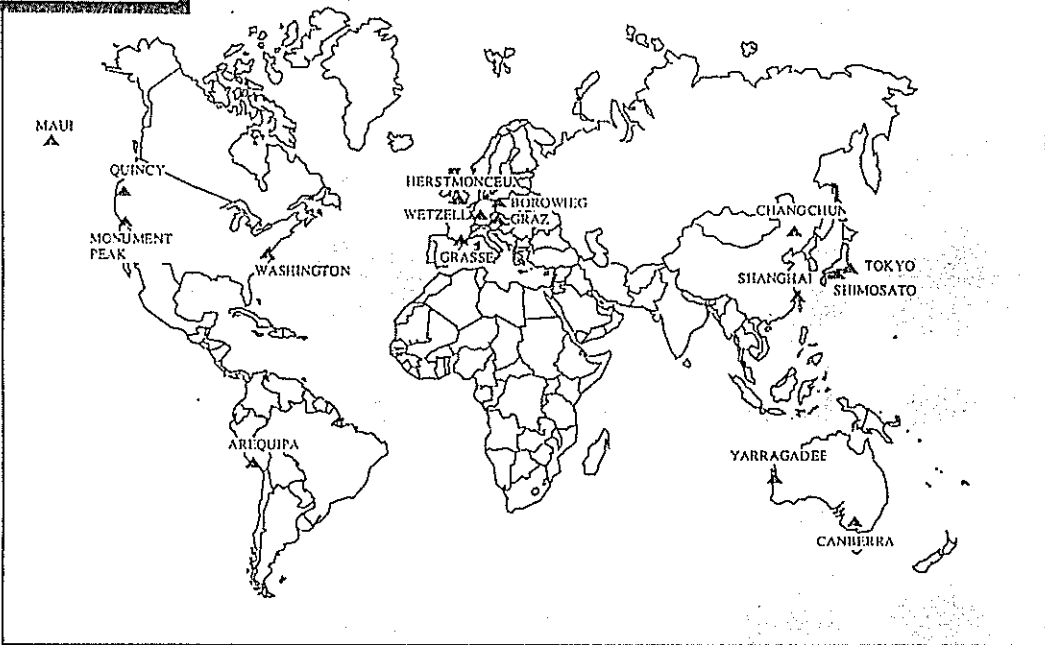
Software Model

Inertial	Mean equator and equinox of 2000.0
Geopotential Model	GEM-T3 to degree and order 36
Atmospheric density model	Jacchia-Nicolet
Tropospheric refraction	Marini and Murray model

(Mainly According to IERS Standard)

Fig.5
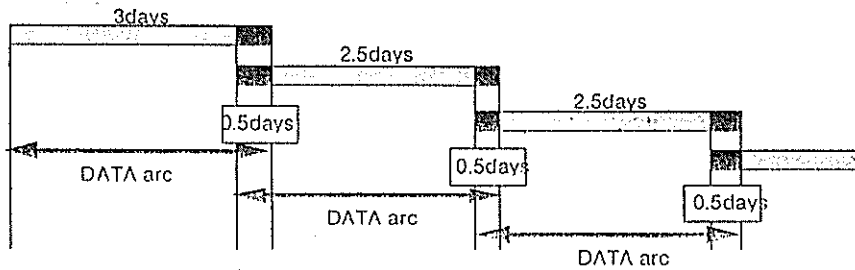
Orbit determination using LONG-Arc data

Orbit determination using SHORT-Arc data

NASDA

Fig.6
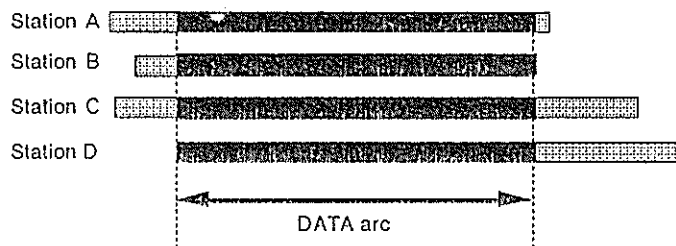
Orbit determination using LONG-Arc data

AJISAI

Arc No.	Overlap	Stations	Pass	Difference in position(m)			Difference in Velocity(mm/s)		
				X	Y	Z	VX	VY	VZ
1 – 2	96/5/02 0h · 12h	5	6	‹2	‹5	‹3	‹2	‹2	‹3
2 – 3	96/5/05 0h · 12h	2	4	‹1	‹8	‹3	‹6	‹1	‹3
3 – 4	96/5/08 0h · 12h	3	6	‹2	‹3	‹3	‹2	‹2	‹2
4 – 5	96/5/11 0h · 12h	5	7	‹2	‹8	‹3	‹6	‹2	‹3
5 – 6	96/5/14 0h · 12h	4	7	‹2	‹8	‹5	‹6	‹2	‹5
6 – 7	96/5/17 0h · 12h	3	4	‹2	‹9	‹1	‹7	‹2	‹1
7 – 8	96/5/20 0h · 12h	4	5	‹2	‹7	‹2	‹5	‹2	‹2
8 – 9	96/5/23 0h · 12h	7	11	‹2	‹7	‹2	‹5	‹2	‹2
9 – 1 0	96/5/26 0h · 12h	3	4	‹2	‹7	‹4	‹5	‹2	‹4

ERS-2

Arc No.	Overlap	Stations	Pass	Difference in position(m)			Difference in Velocity(mm/s)		
				X	Y	Z	VX	VY	VZ
1 – 2	96 8/01 0h · 12h	1	1	‹5	‹60	‹5	‹60	‹10	‹10
2 – 3	96 8/04 0h · 12h	5	6	‹5	‹50	‹5	‹50	‹10	‹10
3 – 4	96 8/07 0h · 12h	7	8	‹3	‹10	‹3	‹10	‹3	‹3
4 – 5	96 8/10 0h · 12h	3	3	‹3	‹25	‹3	‹25	‹8	‹3
5 – 6	96 8/13 0h · 12h	2	2	‹5	‹25	‹5	‹25	‹5	‹5
6 – 7	96 8/16 0h · 12h	4	6	‹1	‹15	‹5	‹15	‹1	‹5
7 – 8	96 8/19 0h · 12h	3	3	‹3	‹25	‹3	‹25	‹3	‹3

NASDA

Fig.7

Orbit determination using SHORT-Arc data

AJISAI

CASE No	Residual in orbit determination (m)				Total O-C RMS (m)	Standard Deviation	
	960521-2024 BOROWIEC	960521-2025 GRAZ	960521-2031 WETTZELL	960521-2023 HERSTMONCEUX		Orbit Position (m)	Orbit Velocity (mm/s)
1	0.1052	0.0039	0.0082	0.0143	0.0610	0.272	0.123
2	0.0307	0.0035		0.0150	0.0210	0.438	0.154
3	0.0525		0.0072	0.0225	0.0370	0.549	0.352
4		0.0040	0.0078	0.0142	0.0090	0.296	0.124
5	0.0912	0.0041	0.0085		0.0600	0.522	0.239
6	0.0146			0.0109	0.0130	1.240	1.130
7		0.0035		0.0145	0.0100	1.320	1.260
8			0.0067	0.0108	0.0090	1.870	1.210
9	0.0299	0.0035			0.0230	0.563	0.477
10	0.0123		0.0064		0.0110	0.636	0.585
11		0.0035	0.0067		0.0050	0.654	0.363
Long-Arc	0.0691	0.1038	0.1588	0.1370			

ERS-2

CASE No	Residual in orbit determination (m)				Total O-C RMS (m)	Standard Deviation	
	960521-2024 BOROWIEC	960521-2025 GRAZ	960521-2031 WETTZELL	960521-2023 HERSTMONCEUX		Orbit Position (m)	Orbit Velocity (mm/s)
1	0.1900	0.0023	0.0215		0.1100	1.860	2.000
2	0.0402	0.0018			0.0270	0.339	0.384
3	0.0429		0.0029		0.0320	0.926	0.738
4		0.0019	0.0035		0.0030	1.560	1.510
Long-Arc	0.3057	0.1729	0.1599				

Fig.8

ADEOS/RIS Experiments

- Received 23 data ('96.10.30-'96.11.7)

- Orbit determination using Long-Arc data

Overlap	Stations	Pass	Difference in Position (m)			Difference in Velocity (mm/s)		
			X	Y	Z	VX	VY	VZ
96-11-02 0h - 12h	1	1	<5	<5	<15	<8	<5	<9

- Comparison with NASA TIRV

Epoch	Difference in Position (m)				Difference in Velocity (mm/s)			
	ΔX	ΔY	ΔZ	ΔR	ΔVX	ΔVY	ΔVZ	ΔV
96-11-4 0h	2.180	16.164	-61.211	63.347	63	22	6	68
96-11-7 0h	-135.653	-54.320	-65.509	160.137	59	66	-149	173
96-11-10 0h	-203.195	-158.936	244.547	355.460	-246	-80	-266	371
96-11-13 0h	209.263	39.047	432.479	482.031	-374	-267	200	501
96-11-16 0h	459.677	319.222	-36.910	560.864	100	-56	568	579

Synchronous Satellite Laser Ranging
for Millimeter Baselines

T. Herring

Massachusetts Institute of Technology, USA

H. Kunimori

Communications Research Laboratory, Japan

B. Greene

Electro Optic Systems Pty Limited, Australia

Abstract

We propose a synchronous Satellite Laser Ranging which in principle leaves only the ranging system accuracy as the limiting effect on baseline accuracy. Initial simulations for the Japanese Keystone Project network are provided using by Kalman filter formulated simulator and demonstrated to determine baselines and heights to a few mm per day over 150 km baselines using at least 5 SLR stations operating synchronously and with careful station location.

1 Introduction

SLR has a wide range of applications, including the determination of station coordinates and baselines for geodetic monitoring. SLR baseline now routinely achieve a precision of several centimeters, but a limiting factor is often the uncertainty, or error, in the determination of the orbits of the satellites used. The orbit uncertainty will always be worse than uncertainty of the range measurements to the satellites.

Short arc analysis techniques were designed to reduce the orbit error contamination of the baseline integrity by utilizing the geometry of at least two SLR stations which range quasi-simultaneously to a satellite. However, these techniques, although producing better results than those which ignore geometry, have never completely removed the effect of satellite orbit error from the baseline.

Synchronous ranging uses additional constraints on the measurement geometry to completely remove any effects of orbit error from the baseline, or relative coordinates, solution, if it hits simultaneously the same position. Synchronous ranging in principle this leaves only the ranging system accuracy as the limiting effect on baseline accuracy. Figure 1 shows a concept of synchronous ranging and number of parameters to be solved for in a single arc. Modern systems have a precision and accuracy in absence of atmosphere of better than one millimeter, synchronous ranging can preserve this into a baseline.

Initial simulations for the synchronous ranging applied to the Japanese Keystone Project [1] network are outlined. Keystone SLR system has operating mode which capable to synchronize a

laser firing timing at satellite with a precision of 5 ns.

2 Synchronous SLR Simulator

The simulator for synchronous satellite laser ranging (SSLR) system is developed based on Kalman Filter formulation. At each measurement epoch, the position of satellite being observed is assumed to have position errors with standard deviation of 1km. The a priori uncertainty in station position is assumed to 1m. These standard deviations are sufficiently large that they have no impact on the final answers. Measurements are made to this satellite with assumed random noise +/- 1mm for the range measurements. Such measurements are assumed to be made every 30 seconds that a satellite is visible. In the Kalman filter, station positions and the instantaneous satellite position are estimated.

Figure 2 is a map showing the locations of sites used. In addition to the four Keystone sites, three additional simulation sites SI01, SI02 and SI03 as shown in the map. Provided four or more stations make measurement simultaneously, the system of equations can be solved within an arbitrary rotation and translation of the station coordinate frame. The distances between the sites are uniquely determined, but to establish station coordinates we fixed the position of one site, two coordinates of another site and one coordinate of a final site. The first three of the constraints resolve the translation rank deficiency and the latter three constraints remove the rotational rank deficiency. These constraints have not effect on the standard deviation of the baseline length estimates.

In the simulator, we assumed measurements were made to satellites with the same inclination and semi-major axes as Lageos-1, Lageos-2, Starlette, and Ajisai. The longitudes of the nodes of these satellites were set to arbitrary values. The measurement scenario was set such that when more than one satellite was visible, a satellite would be observed for 5 minutes and then another satellite would be observed. All visible satellites are cycled through in this fashion.

All the results should really be scaled by the effective range noise to the satellite. This error budget would include any ranging errors, atmospheric errors, and the definition of the point being measured on the satellite.

3. Results

Figure 3 shows a set of baseline sigma derived from simulator at the end of 24 hours using all seven sites. Baseline length less than 200 km represent combinations of Keystone sites and all have formal errors less than 1mm. However, if we dropped the all external sites SI01, SI02 and SI03, making a network of four sites, the baselines sigma results are around a few tens of milimeters or more, as the geometry of network is so poor. Figure 4 shows an example how the coordinates of site Miura is badly conversing in 24 hours. We tested to put each of external station included in solution and see how the baseline sigmas are improving, and found that if you put one station SI01, at the westward of Tokyo, the baseline sigmas are a converging the best to a few milimeters for Keystone stations.

We note it is sacrificing a bit of accuracy of baseline for those of combination to the outlier station. The baseline sigma of all combination and coordinates conversion in Miura of this particular case are shown in Figure 5 and Figure 6, respectively.

4. Conclusions

We simulated the synchronous SLR on Keystone network. Using at least 5 SLR stations including Keystone stations operating synchronously and with careful station location, it is possible to determine baselines and heights to a few mm per day within 150 km baseline length. If more outlying stations are used we determine baselines and heights to 1 mm per day. The network can be extended to longer baselines by adding "outlier" stations which are not resolved to the same precision, indicating that in Keystone SLR network, synchronous SLR will have potentials to determine baselines and heights to 1-3 mm on a daily basis, if a mobile system is deployed as an "outlier".

References

[1] H.Kunimori and et al , Keystone SLR system, Tenth International workshop on Laser Ranging Instrumentation, Shanghai, 1996, in this issue.
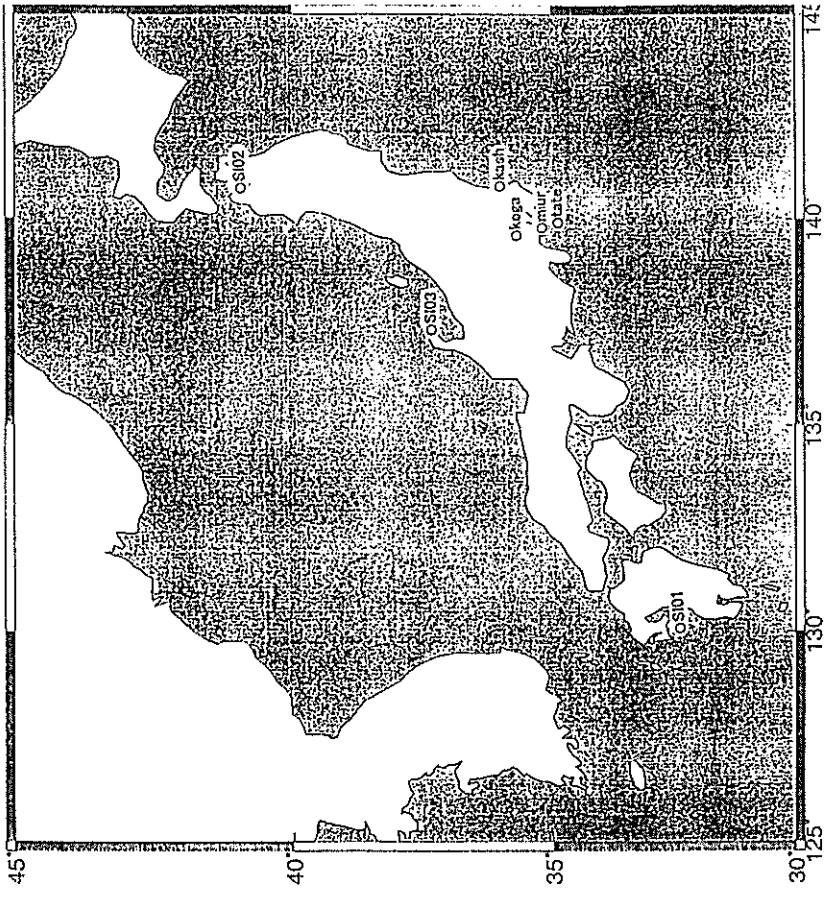
Figure 2   Locations of simulation sites including Keystone
network   (Koganei, Kashima, Miura and Tateyama)
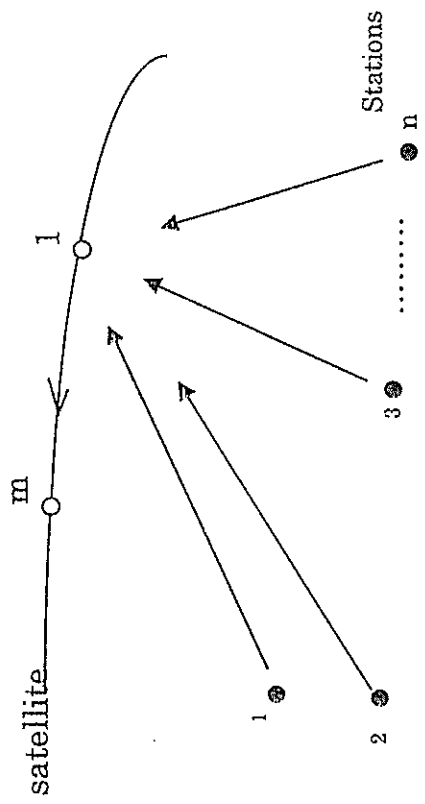
n Stations   m Observations
UNKNOWNS   3m + 3n
OBSERVATIONS   mn
Therefore   n > 3   ie   n = 4
Minimum number of stations for simple linear equations
solve for the unknowns

Fig.1 Concept of Synchronous SLR
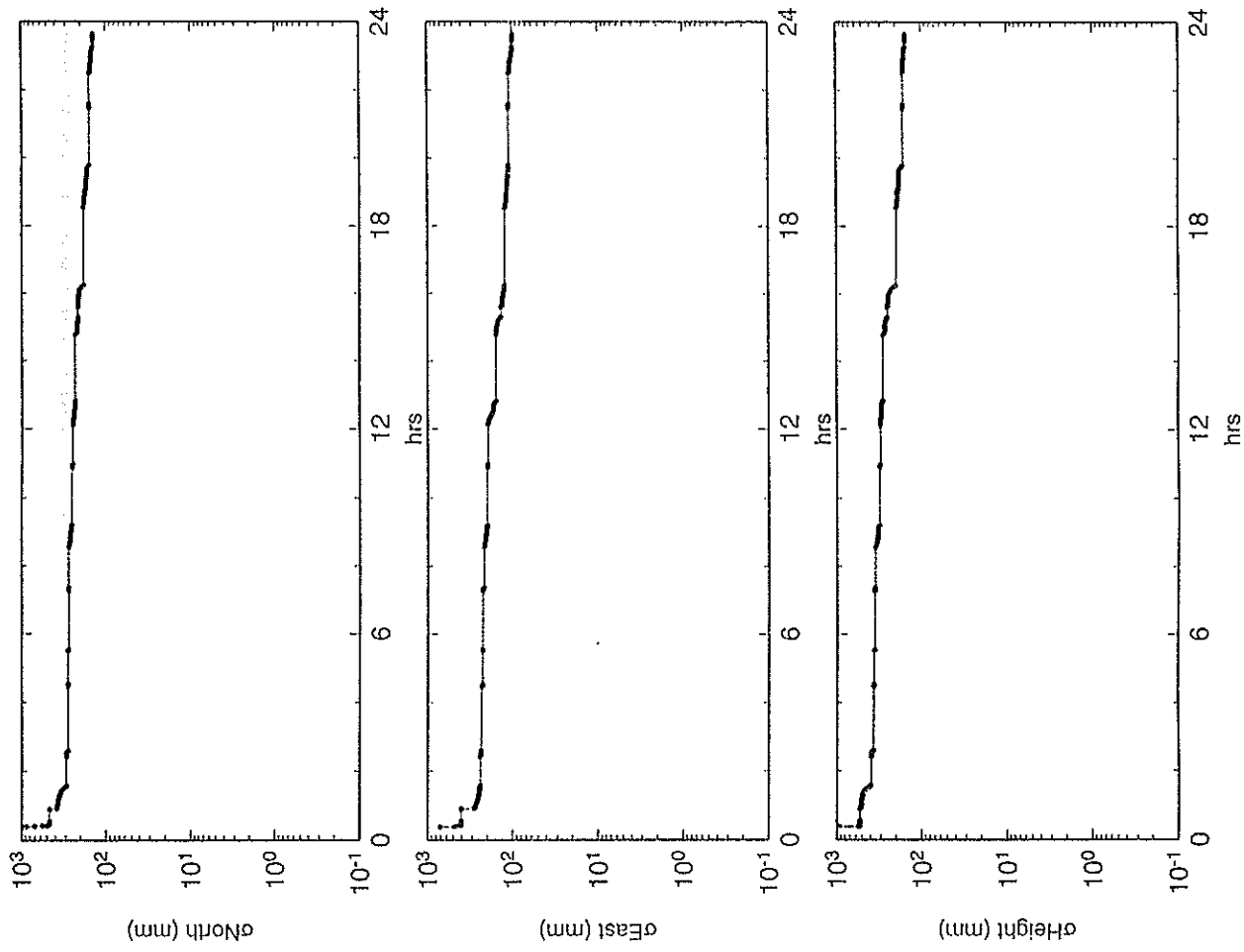
Figure 4 The coordinates (North, East and Height) of Miura conversion within 24 hours by 4 sites simulation
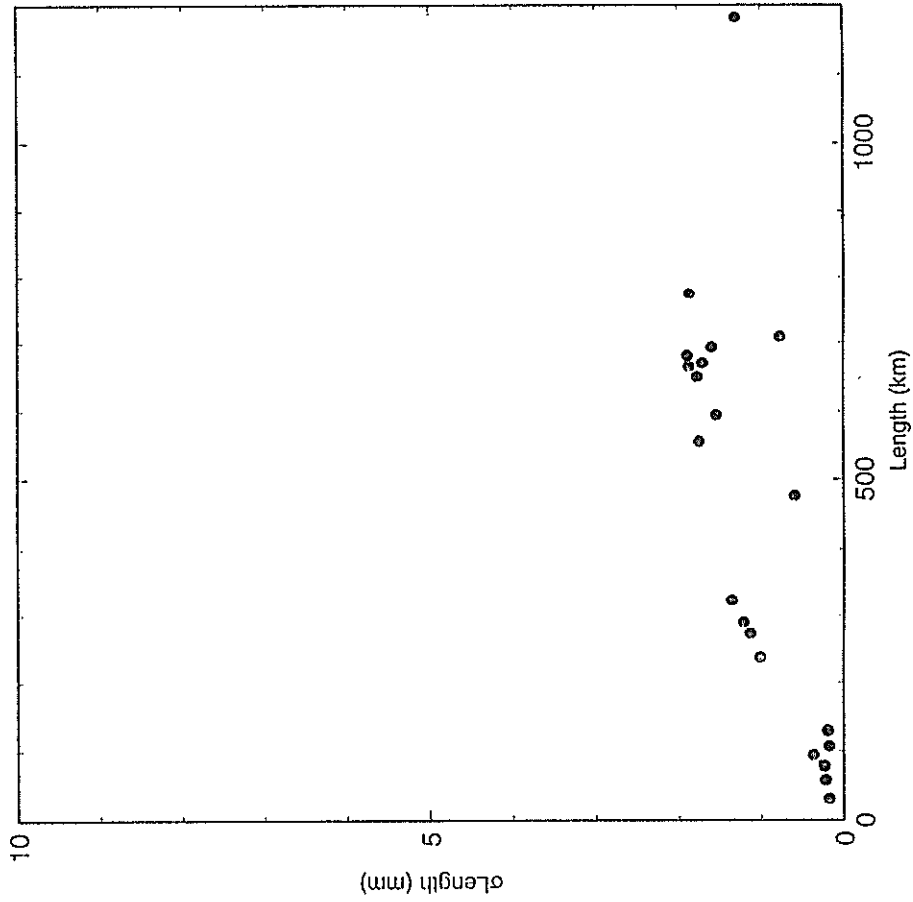
Figure 3 The baseline sigma derived from simulator at the end of 24 hours using all seven sites

Figure 6 The coordinates (North, East and Height) of Miura conversion within 24 hours by 5 sites (Keystone plus SIó1 site) simulation

Figure 5 The baseline sigma derived from simulator at the end of 24 hours using Keystone sites plus SI01 site.

Session Summaries

and

Resolutions

Science Achievements and Applications
Chairperson: Richard Eanes

Science Achievements

- Temporal variations of the gravity field, geocenter, earth orientation
- Lunar science: relativity, lunar "geophysics", orbital evolution
- Station positioning: horizontal motions, monthly vertical with 10 mm accuracy
- mean gravity field: excellent and improving
- Non-gravitational force modeling

Applications

- Solar system ranging with transponders
- Airborne wide angle ranging for vertical
- Environmental monitoring with LIDAR
- CW Laser ranging
- New target opportunities

Laser Ranging Performance Evaluation

Chairperson: Michael Pearlman

The Session on Laser Ranging Performance Evaluation was organized to give us the opportunity to examine a broad range of issues regarding network performance, including:

How do our customers evaluate our data products? Are we satisfying their needs?
How do the Operations and Analysis Centers evaluate our performance?
Do the Analysis Centers all get the same results?
How do the stations evaluate their own performance?
How can we improve our network effectiveness? How do we know what we have?
What should we expect from the global SLR network and the individual stations within the network?

The session was divided into six sections:

1. Applications, Data Usage, and Requirements (Mike Pearlman),
2. Performance Evaluation by the Data Q/C Operations Centers (Van Husson),
3. Performance Evaluation by the Analysis Centers (Peter Dunn),
4. Performance Evaluation at the Field Stations
5. Baselining Station Performance (Tom Varghese), and
6. Performance Expectation (Mike Pearlman).

The papers that follow in this section address these topics. We have asked the authors to consolidate material where possible.

New Fixed Station

Chairperson: Hiroo Kunimori

NEW STATION since Canberra 1994 Nov.

STARTING OPERATION

- USAF Starfire NRL   (US)

NEW FEATURES and UPGRADE since Canberra

- Changchun (Mount Encoder)   (China)
- Katsively   (Ukraine)
- Borowiec   (Poland)
- Metsahovi   (Finland)

NEW STATION WILL COME OUT and BE STARTING OBSERVATION BEFORE 11-TH WORKSHOP

- Zimmerwald   1997-   (Switzerland)
- Matera MLRO   1997-   (Italy)
- Keystone SLR   1997-   (Japan)

New Mobile Systems

Chairperson: Ulrich Schreiber

6 new stations

- most of them are operational
- very different design

3 dB gain

over the last workshop

Lunar Laser Ranging

Chairperson: Peter Shelus

The lunar laser ranging community has enjoyed a remarkable amount of success during the past several years, both in its ability to increase the quantity and quality of its observations as well as in the amount of science analysis that has been performed. A paper, specifically dealing with LLR-derived science, can be found elsewhere in these Workshop proceedings. A second paper, assessing the adequacy of the quality and quantity of LLR data for the science that needs to be done, can also be found elsewhere in these proceedings. Papers specific to the LLR technique can be found here.

For the past decade or so we have been moving steadily into an era in which there has been a dramatic decrease in the amount of resources being made available to the laser ranging community. At the same time the number of targets that require laser ranging observations has been growing just as dramatically. This is not only true for LLR/SLR, it is also true for the microwave space geodetic techniques, for VLBI, and for GPS. It is clear that we must strive to make the most efficient use of whatever resources exist.

For LLR, the appropriate scientific community has defined several specific data requirements and observing strategies to support a number of actual experiments. Some of these experiments include the generation of Earth orientation parameters as well as support for interplanetary spacecraft navigation, Solar System ephemeris generation, lunar interior studies, relativity, and gravitational physics. The observing requirements for these LLR-based experiments include sequential multi-reflector series of observations during short intervals of time, more extensive observational coverage at the full Moon and new Moon phases, and the generation of routine sub-cm LLR data.

As can be seen in the reports of this LLR session, the routinely operating, LLR-capable stations are the MLRS at the University of Texas's McDonald Observatory near Fort Davis, Texas in the USA and OCA at the Observatoire de le Cote d'Azur near Grasse, France. Both of these stations are obtaining reasonable amounts of LLR data, while they use the appropriate observational strategies that are defined by the analysts. Both stations are pushing hard to obtain sub-cm data and better lunar phase coverage. However, weather, equipment and funding drop-outs can be devastating to a two-station network.

Therefore, there is a demonstrated need for additional laser ranging stations in the world-wide network that are LLR-capable. As we look at the situation around the world we have glimmers of hope for LLR from the MLRO station in Italy, the Wettzell station in Germany, the Orroral station in Australia, the SALRO station in Saudi Arabia, and a possible LLR-capable station in Kunming, China. Are there others?

In summary, we would like to have more laser ranging stations be LLR-capable because, in a situation with severely limited resources, the building and maintaining of a lunar-only network is impossible. It should be noted that a modest 0.75-m aperture system with epoch timing and a reasonable laser (i.e., 10 Hz repetition rate, 100 millijoule/pulse, 200 psec pulse-length) should be sufficient. The sharing of modest observational requirements across a greater number of LLR-capable stations would place very little observing pressure on any one station. The Moon should be viewed as just another laser ranging target for the laser ranging community.

Target Design, Signature and Biases

Chairperson: Andrew Sinclair

BIASES

J.Luck: effect of signal strength on calibration:

-action taken at Orroral.

S.Schillak: contributions to error budget of SLR:

- signal strength effects on data distribution.

SIGNATURE

T.Otsubo: theoretical determination of satellite signature effect for Ajisai

- good agreement with observed.

e.g. RGO Theory: 29 mm (CoM corrn for Mean)

Observed: 22 mm (Mean-Peak)

TARGET DESIGN

R.Neubert: design of Champ retro -low signature

- 2 colour

B.Greene: new design of satellite - low signature

Shargorodsky et al: mathematical model of WPLTN-1 (Fizeau)

2-spot reflection pattern retros.

Kasser et al: polarisation effects of retros.

- Themes are:

  - reducing signature

  - understanding signature

  - improving reflection efficiency

OTHERS:

Tips,

Laser beam propagation in LLR

Detectors and Spectral Filters

Chairperson: Georg Kirchner

MCP / Microchannel Plates

- Improvements on operational MCP's have been reported from Changchun, Hawai, Star Fire Optical Range, concerning:

    - Sensitivity: To get Single Photons from GPS-36 / GPS-36
    - Accuracy.

CFD / Constant Fraction Discriminators

- Improvements have been made also in

    - Sensitivity: To get Single Photons from GPS-36 / GPS-36
    - Accuracy.

- Time Walk Compensation is achieved now by Hardware and Software.

SPAD / Single Photon Avalanche Detector / Silicon:

- Main improvements on Time Walk Compensation:

    - Some ways have been shown how to compensate/eliminate Time Walk;
    - Circuits for TW Compensation are already operational;
    - Circuits are adapted now for different stations;

- SPAD gating techniques are well established now.

SPAD / Germanium:

- Developments driven by Eye-Safe Requirements;
- Already used now for ranging up to ETALONs;
- Single-Photon Sensitivity for $\lambda = 0.35 \ldots 1.54$ has been demonstrated already;
- Is the only detector for SP sensitivity for this wavelength range.

Laser Technology Development

Chairperson: Karel Hamal

STATUS

LASER	WAVE	ENERGY	REP.	FWHM	RANGE	SITE
	nm	mJ	Hz	psec		
TiSAPPHIRE	846	50	10	50	sat.	Bern
(two color)	423	50	10	50	ground	TIGO
YAG/SHG	532	50	100	15-30	sat.	Keystone
YAG/THG	355	10	100	15-30		Japan
YAG/OPG	1547	5	100	15-30		
YAG/SHG	532	.1 - .5	1000	15-30	ground	
YAG/SHG	532	.2	2000	140		NASA
(uLASER)						SLR2000
RAMAN	1540	5	10	80	sat.	Tokyo
eyesafe	532	35	10	160	sat.	CRL
YAG/SHG	532	30	5	50-100	sat.	Shanghai
(semitrain)						

Eyesafe Systems

Chairperson: Ivan Prochazka

- The review of the eyesafe operations of the SLR has been given: operating on the energy levels below the maximum permitted explosure limit ('micro Joule mode'), operating within an eyesafe wavelength window near 1540 nm or surveying the laser propagation direction using an independent radar operating in microwave or eyesafe wavelength region prior to the ranging laser emission.

- The description of the SLR2000 system operating in a micro Joule mode: project status, correlation processing approach and performance simulation has been presented.

- The first routine ranging of a SLR system operating in an eyesafe window 1540 nm in Tokyo, Japan has been described.

Timing Devices and Calibration

Chairperson: John Luck

Six papers were presented. The session finished within two picoseconds of its allotted time.

The main thrust of the Timing Systems section was the drive to break through the 2 picosecond barrier in resolution, stability and accuracy. Important factors reported include:

- tight control, compensation and calibration of temperature fluctuations within the verniers and their surroundings
- selection and tolerancing of components
- achieving very fast rise-time through high bandwidth components
- averaging multiple verniers or counters
- calibration by variable optical path lengths.

Cautions were sounded about anomalies over very short ranges, and instabilities over long ranges, in counters of the SR620 and HP5370 types, and the need for long warmup times. The developmental models include their own computers, and imminent in one model. Absolute biases still exist, although the ranging method cancels them.

The System Calibration section contained a report from Graz on a very short range target achieved by feeding the transmitted pulse back to the receiver as it leaves the telescope. The path lengths can be measured with 0.1 mm accuracy, and meteorological effects including rain are insignificant. Careful attention to attenuating the received signal and detector triggering methods are needed; and skewness in the detected signal has been eliminated. It has not yet been demonstrated that range bias has been eliminated.

A Portable Calibration Standard was described, which calibrates all parts of a ranging system after the discriminators and provides diagnostic information on other sub-systems. It is an almost complete ranging system itself apart from telescope, laser and detector, and includes predictions software, high precision meteorological sensors, and GPS-disciplined oscillator/time reference. It operated by plugging into spare discriminator channels at the host station during ranging and has less than 1 mm range bias and 10 mm single shot resolution. It does not claim to replace co-location completely, but is a compact adjunct.

Multiwavelength Ranging/Streak Cameras

Chairperson: Jean Gaignebet

Even if Multiwavelength ranging is by essence a multiphoton process, this session is at the crossing of two concepts.

Single photon counting (SPC) with SPAD and electronic timers.

Differential flight time accuracy is obtained by averaging a great number of records· on each color (very seldom simultaneously) and as SPC means a low ratio of returns (1/100 now) a tremendous amount of shots is needed.
The only field where is may be adequate is for very long passes (LLR).

Multiphoton Record (MPR)

Direct measurement of differential flight times with a streak camera and a great number of photoelectrons (some 10^2). Shot by shot atmospheric index correction around 5 mm (exactness of the range) is possible.

Reduction of the number of photon via :

>   New SC concepts
>   Pulse processing (Stretching and compression).

-------- - ------

Many stations, even single wavelength ones, are far from operating on a true SPC mode and are developing smart "Bricolage" to correct for the multiphoton events.

IT MAY BE TIME TO TAKE ADVANTAGE OF THE POTENTIAL INFORMATION OF EACH PHOTON AND LEARN HOW TO EXTRACT IT.

System Automation and Operational Software

Chairperson: Jan Mcgarry

- **PREDICTIONS**
    - GPS: IGS daily orbit (good ~1m) - 4/day IRVs Available from RGO
    - GFZ-1 Drag must be applied to IRV for accuracy
        - Need: 2-3 passed/day (N.Am, S.Hem, Asia)

- **OPERATIONAL SOFTWARE**
    - Multi-processor
    - Internet for communication
    - Windows displays - emphasis on user friendly
    - Remote control, automation are goals

- **AUTOMATION**
    - Goals: reduce cost + increase data yield
    - Processing power onsite now capable
    - Single operator goal at many existing stations
    - Full automation + remote control at new systems
    - Keystone: entire network automated
    - CCD's can effectively be used to aid tracking
    - Data corrections done automatically onsite (R/T)

- **DATA QUALITY**
    - Q/C can effectively be done automatically onsite without orbit (CAL RMS, CAL SHIFT, SAT RMS)
    - More (good) SLR tracks of GPS needed (so SLR can Q/C GPS, not vice-versa)

Data Analysis and Models

Chairperson: Vincenza Luceri

The issues presented in this session can be grouped in these major areas:

- efforts towards the estimation of regional baselines, on one hand, by collecting and analysing data of a dense and local network, on the other, by developing new methods to increase the baseline precision

- attention to the problems of tropospheric correction, station biases and residual distribution and their effects on the analysis results

- implementation of algorithms to save computer and time resources and solve technical problems during the orbit determination process

RESOLUTIONS

1. Recognising the increasing prominence of data processing and analysis, and of quality control of their products, in the deliberations of the Workshop, the participants of the Tenth Workshop RECOMMEND that the word "INSTRUMENTATION" in the Workshop title be deleted. The next Workshop title will be 11th INTERNATIONAL WORKSHOP ON LASER RANGING.

2. Recognising the synergy between the Workshops and the SLR/LLR Subcommission of CSTG, the desire by CSTG to encourage such Workshops and meetings among all its Subcommissions, the desirability of having the Workshops recognised as official activities of internationally accredited organisations such as IAG and COSPAR, and potential economies of organisational effort, the participants of the Tenth Workshop RECOMMEND that the International Workshops on Laser Ranging invite the CSTG SLR/LLR Subcommission to recognise the Workshops as an official activity.

3. This Workshop commends Russia on its new mission ZEYA, and encourages it to continue the development and launch of innovative satellite designs, and RECOMMENDS that the CSTG sub-committee seriously consider the tracking of ZEYA.

4. The participants of the Tenth International Workshop on Laser Ranging Instrumentation express our sincere appreciation and warmest thanks to Shanghai Observatory of the Chinese Academy of Sciences for organising and hosting this wonderful workshop, and particularly recognise the hard work of the Local Organising Committee cheerfully led by Yang Fumin.